Oxidative Medicine and Cellular Longevity

Characterization of Food Varieties Bioactive Compounds and their Health Promising Effects

Lead Guest Editor: Tarique Hussain
Guest Editors: Jing Wang, Yehui Duan, and Muhammad Saleem Kalhoro

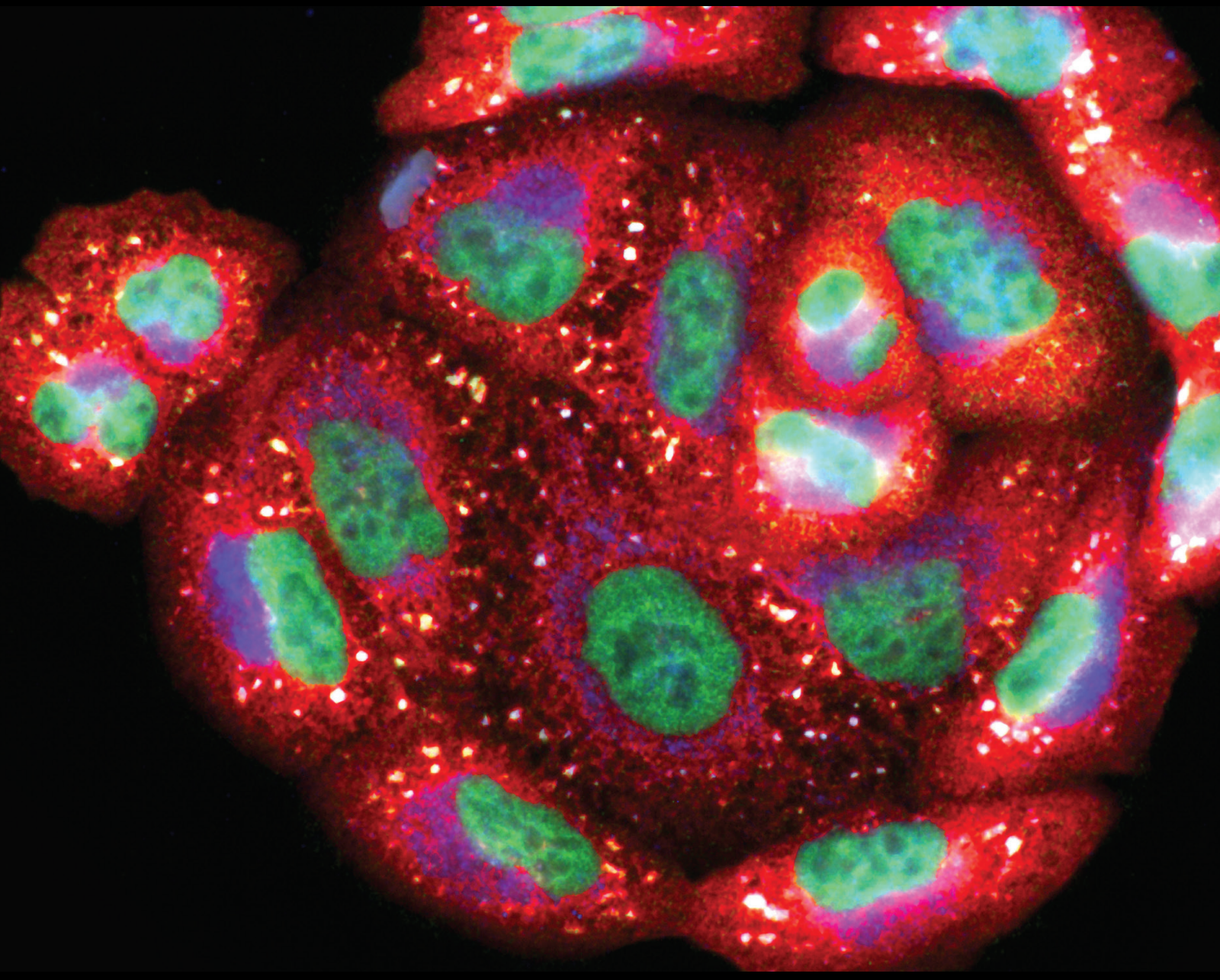

Characterization of Food Varieties Bioactive Compounds and their Health Promising Effects

Oxidative Medicine and Cellular Longevity

Characterization of Food Varieties Bioactive Compounds and their Health Promising Effects

Lead Guest Editor: Tarique Hussain
Guest Editors: Jing Wang, Yehui Duan, and Muhammad Saleem Kalhoro

Contents

Contents

Hindawi
Oxidative Medicine and Cellular Longevity
Volume 2023, Article ID 7675183, 23 pages
https://doi.org/10.1155/2023/7675183

Review Article

Effects of Herbs and Derived Natural Products on Lipopolysaccharide-Induced Toxicity: A Literature Review

Majid Kianmehr,[1] **Mohammad Behdadfard**,[2] **Mahdiyeh Hedayati-Moghadam**,[3] **and Mohammad Reza Khazdair**[4]

[1]*Esfarayen Faculty of Medical Sciences, Esfarayen, Iran*
[2]*Student Research Committee, Birjand University of Medical Sciences, Birjand, Iran*
[3]*Department of Physiology, School of Medicine, Jiroft University of Medical Sciences, Jiroft, Iran*
[4]*Cardiovascular Diseases Research Center, Birjand University of Medical Sciences, Birjand, Iran*

Correspondence should be addressed to Mohammad Reza Khazdair; m.khazdair@yahoo.com

Received 3 August 2022; Revised 13 November 2022; Accepted 17 March 2023; Published 17 April 2023

Academic Editor: Muhammad Saleem Kalhoro

Introduction. Oxidative stress (OS) during inflammation can increase inflammatory responses and damage tissue. Lipopolysaccharide (LPS) can induce oxidative stress and inflammation in several organs. Natural products have several biological activities including anti-inflammatory, antioxidant, and immunoregulatory properties. The aims of the study are to study the possible therapeutic effects of natural products on LPS inducing toxicity on the nervous system, lung, liver, and immune system. *Methods*. The *in vitro* and *in vivo* research articles that were published in the last 5 years were included in the current study. The keywords included "lipopolysaccharide," "toxicity," "natural products," and "plant extract" were searched in different databases such as Scopus, PubMed, and Google Scholar until October 2021. *Results*. The results of most studies indicated that some medicinal herbs and their potent natural products can help to prevent, treat, and manage LPS-induced toxicity. Medicinal herbs and plant-derived natural products showed promising effects on managing and treating oxidative stress, inflammation, and immunomodulation by several mechanisms. *Conclusion*. However, these findings provide information about natural products for the prevention and treatment of LPS-induced toxicity, but the scientific validation of natural products requires more evidence on animal models to replace modern commercial medicine.

1. Introduction

Lipopolysaccharide (LPS) is a central component of the outer membrane in Gram-negative bacteria which causes inflammation [1]. LPS is a glycolipid in the outer membrane that provides an effective permeability barrier against deleterious molecules such as antibiotics. The LPS molecule has a tripartite structure including (i) lipid A, the hydrophobic moiety that anchors LPS to the outer membrane, (ii) core oligosaccharide, which contributes to maintaining the integrity of the outer membrane with together lipid A, and (iii) O antigen (O antigen polysaccharide), which consist of a polymer made of repeating oligosaccharide units and connected to the core in direct contact with the external milieu [2].

Systemic administration of LPS could induce disorder in several organs [3, 4]. The degeneration of the proinflammatory mediators was increased due to LPS via nuclear factor kappa-light-chain-enhancer of activated B cells (NF-κB) pathways [5]. LPS also mediated immune response due to the activation of Toll-like-receptor 4 (TLR4) [6]. LPS/TLR4 signaling induces the production of the proinflammatory cytokine [5]. So, the changes in proinflammatory mediator levels in the serum are important indicators of the immune response due to LPS administration [7]. LPS also declined the density of nicotinic acetylcholine receptors of the α7 subtype (α7 nAChRs) in the brain as well as reduced nucleated cell numbers in the hippocampus and striatum in mice [8].

It was reported that LPS-treated animals induced liver and heart toxicities by activation of NF-κB and toxic

mediators generated by the activated macrophages (proinflammatory molecules and cytokines releases) and activation of reactive nitrogen and oxygen species (RNS and ROS) including superoxide and nitric oxide (NO) radicals [9, 10]. LPS could stimulate ROS pathways by a mediated protein-tyrosine kinase (PTK), protein kinases (PK), and mitogen-activated protein kinase (MAPK) [11].

Administration of LPS also causes lung damage through several inflammatory mechanisms [12]. Oxidative stress (OS) and inflammation are important components of lung diseases, including pulmonary fibrosis, asthma, and acute lung injury (ALI) [13]. The imbalance between cellular antioxidative capacity and ROS formation occurred in OS. It was reported that the interplay between OS and inflammation resulted in the progression of several disorders [14] which have an important function in ALI induced by LPS. Also, OS causes the recruitment of inflammatory cells including macrophages and T lymphocyte-mediated production of proinflammatory mediators such as interferon-gamma (IFN-γ), interleukin (IL)-1b, and IL-12, that lead to inflammation [15]. LPS signaling is highly relevant to the pathophysiology of many chronic inflammatory diseases. LPS influences a range of cell types and physiological processes such as the immune system, neural system, lung, liver, and cardiovascular system [16].

Recent studies suggest that the use of natural products as antioxidant and anti-inflammatory agents has beneficial effects in ameliorating responses to inflammatory insults of LPS-induced toxicity [17]. Then, it is logical that inhibition of inflammation and OS is an effective strategy to reduce LPS-induced tissue damage.

It has been reported that almost 7,000 active natural compounds have been derived from medicinal herbs [18]. The major advantage of herbal drugs (active natural compounds derived from herbs) is the lower side effects compared to chemically synthesized drugs [19]. Phytomedicine, due to its antioxidant, anti-inflammatory, and immunoregulatory effects, was used for the treatment of various diseases [20–22]. The effect of thymoquinone (TQ), the main component of *Nigella sativa* seeds, on LPS-induced lung injury in rats significantly improved lung pathological changes and the levels of cytokines (TGF-β1, INF-γ, PGE2, and IL-4) in bronchoalveolar lavage fluid (BALF) compared to the LPS-treated group [23]. The effects of hydroethanol extract *Zataria multiflora* on learning and memory capacity in LPS-challenged rats also remarkably reduced IL-6, malondialdehyde (MDA), and nitric oxide (NO) metabolite concentrations, but increased thiol content, superoxide dismutase (SOD), and catalase (CAT) activities [24].

The aim of this study was to review the evidence on the role of herbs and derived natural products in the treatment or reducing the adverse effects of LPS-induced toxicity on different organs.

2. Method

The information of this study was obtained by searching the keywords such as "lipopolysaccharide", "natural products", "medicinal plant", and "toxicity" in different online databases including Google Scholar, PubMed, Science Direct, and Scopus as follows: (TITLE-ABS-KEY (lipopolysaccharide) AND TITLE-ABS-KEY (induced AND inflammation) AND TITLE-ABS-KEY (natural AND products)) in Scopus: 406 ((lipopolysaccharide [Title/Abstract]) AND (inflammation [Title/Abstract])) AND (natural products [Title/Abstract]), Pubmed: 87.

3. Effects of Natural Products on LPS-Induced Neuroinflammation

3.1. In Vitro Studies. Neuroinflammation accompanies and often precedes the development of neurodegenerative diseases including Parkinson's and Alzheimer's diseases (AD) and might be one of the pathogenic factors for neurodegeneration [25].

Pretreatment of rat brain microglia cells exposed by LPS with crocin (20 μM) and crocetin (20 μM) separately, markedly decreased hyperproduction of NO, tumor necrosis factor-α (TNF-α) and interleukin (IL)-1β. Also, crocin and crocetin (20 and 40 μM) could inhibit the LPS-induced activity of NF-κB [26]. Microglia activation has a critical role in the pathology of neurodegenerative disorders in considering the close correlation of excessive microglia activation with the secretion of proinflammatory mediators and neurotoxic factors [27]. A study by Liu et al. [28] showed a significant reduction of TNFα and NO levels in neuron-glia cells pretreated with the extract of *Tripterygium wilfordii* (a Chinese herb) due to improvement of microglia function [29]. Tripchlorolide (1.25–10 nM), extracted from *Tripterygium wilfordii*, was able to increase cell survival via inhibition of inflammatory enzymes including cyclooxygenase-2 (COX-2) and inducible nitric oxide synthase (iNOS). Tripchlorolide suppressed the production of TNF-α, IL-1b, prostaglandin E2 (PGE2), NO, and intracellular superoxide anion in LPS-stimulated neuro-2A cells and primary cortical neurons [30].

LPS with activation of inflammatory mechanisms in the substantia nigra (a midbrain dopaminergic nucleus) and degeneration of motor neurons are used for induction of Parkinson's disease models. Administration of myricetin (12.5, 25, and 50 micromoles (μM)) as lipophenolic compounds extracted from red wine on a murine microglia cell line (BV-2) exposed to LPS reduced mRNA and the protein levels of the TNF-α, IL-1β, and IL-6 in the cells [28].

Usage of isoflavone, Biochanin A (1.25, 2.5, 5 μM) mainly found in red clover (a flowering plant) for 21 days in rat primary microglia exposed to LPS decreased the levels of NO, TNF-α, ROS, and IL-1b in microglial culture [31].

Licochalcone A, a flavonoid isolated from licorice roots, changed neuroglia inflammatory circuits in BV-2 cells by inhibiting phosphorylation of NF-κB p65 and Ras-dependent extracellular signal-regulated kinase (ERK1/2) [32].

LPS also could induce NO production via an increase of activity of iNOS and p38 mitogen-activated protein kinase (MAPK) signaling pathway. Silymarin, a milk thistle polyphenolic flavonoid, decreased levels of TNF-α and NO in mesencephalic LPS-stimulated mixed neuron–glia cultures.

Silymarin treatment also inhibited NF-κB activation and superoxide generation with any change in the p38 MAPK signaling pathway [33].

3.2. In Vivo Studies. The result of the Morris water maze and passive avoidance (based on negative reinforcement and used to study memory) showed that administration of a monoterpenoid phenol (carvacrol) improved memory and learning disturbances as well as brain tissue inflammation and OS in LPS-exposed rats. Intraperitoneal (IP) injection of carvacrol (25, 50, and 100 mg/kg, IP) 30 min before LPS administration significantly reduced NO, IL-6, and malondialdehyde (MDA) level and increased catalase (CAT) and superoxide dismutase (SOD) activity, as well as total thiol content in brain tissue of rats, inoculated with LPS [34]. Lee et al. (showed daily administration of carvacrol (25-100 mg/kg, IP) for 21 days in neuroinflammation induced by LPS reduced the expression of IL-1β, TNF-α, and COX-2 in the brain of rats. In addition, carvacrol decreased the expression of TLR4 mRNA and increased the mRNA expression of brain-derived neurotrophic factor (BDNF) [35].

Gypenosides (the main active components of Gynostemma species) as anti-inflammatory agents was useful for the treatment of neuropsychiatric disease, such as anxiety. Treatment with gypenosides (25-100 mg/kg), for 21 days improved behavior test results in rats with chronic inflammation induced by intracerebroventricularly (ICV) injection of LPS. Gypenosides administration increased the percentage of open arm entries and time spent in the plus maze test that commonly used behavioral assays to evaluate anxiety-related behavior in rodents. Furthermore, a decrease in brain proinflammatory mediators level including NF-κB, IL-6, and IL-1β as well as low expression of TLR4 and BDNF mRNA in LPS- injected rats caused by gypenosides [36].

Treatment with aqueous *Clinacanthus nutans* extract (500 and 1000 mg/kg) for 14 days resulted in a significant alteration in neuroinflammation metabolite biomarkers in LPS-injected rats. Improvement in the metabolism of isoleucine, leucine, valine, and pyruvate as well as regulation of metabolic pathway glycolysis, gluconeogenesis, and TCA cycle was done by *Clinacanthus nutans* oral treatment [37]. Neuroinflammation and OS have main roles in the pathogenesis of Alzheimer's disease. LPS also due to inducing inflammation and the OS process could induce memory loss. Choi et al. reported the memory impairment induced by LPS could be ameliorated by properties of antioxidant, antiamyloidogenic, and anti-inflammatory effects of *Euphausia superba* [38] and *Nannochloropsis oceanica (N. oceanica)* [39]. Results of both studies showed administration of *Euphausia superba* (*E. superba*) oil (80 mg/kg/day), for 30 days and *N. oceanica* (50, 100 mg/kg), for 4 weeks, separately improved cognitive impairment in IP administration of LPS in mice via down expression of COX-2 and iNOS as well as decrease the level of MDA. Furthermore, *E. superba* oil and *N. oceanica* extract prevented amyloidogenesis by suppressing p50 and p65 translocation into the nuclei of brain cells. In addition, *E. superba* oil and *N. oceanica* extract inhibited amyloid protein precursor (APP) and β-site APP cleaving enzyme (BACE1) expression in brain cells of LPS-injected mice. The APP and BACE1 have main roles in the generation of amyloid beta, an insoluble peptide that accumulated in the brain of neurodegenerative disorders [38, 39].

Kong et al. showed the LPS induced neurotoxicity and neuroinflammation in mice hippocampus, HT22 cells, and BV-2 cells via activation of C-Jun NH2 terminal kinase (JNK), WDFY1/TLR3, and NF-κB signaling cascades. Treatment with a glycoside isolated from *Forsythiae fructus* (Forsythoside B), prevented LPS function in the activation of inflammatory mechanisms [40].

In vitro and *in vivo* experiments showed a sesquiterpene lactone, isolated from *Centipeda minima,* 6-Oangeloylplenolin (0.5–4 μM), has anti-inflammatory and anti-oxidative properties in cell line and mice associated with LPS induced neuroinflammation and stimulated secretion of TNF-α, IL-1β, NO, and PGE2 in BV2 and primary microglial cells. This study also showed 6-Oangeloylplenolin could improve synaptic connections and function of neurons and neuroglial in the central nervous system due to attenuate of LPS-induced NF-κB activation. Pretreatment of mice with 6-Oangeloylplenolin (5-20 mg/kg, IP) for 7 days before LPS injection prevented cytokine secretion via inhibition of the NF-κB signaling pathway and downregulation of inflammatory enzymes in brain cells [41]. LPS with activation of inflammatory mechanisms in substantia nigra and degeneration of motor neurons was used for induction of Parkinson models. Treatment of LPS-induced Parkinson model rat with myricetin, ameliorated rat's motor dysfunction. In addition, the downregulation of microglial inflammatory mediator expression due to MAPK and NF-κB pathways suppressed by myricetin caused to compensate for LPS-induced reduction in dopaminergic neurons number [28].

The usage of biochanin A (an O-methylated isoflavone) for 21 days improved the results of behavioral tests in Parkinson's disease model rats induced by LPS. Biochanin A could protect dopaminergic neurons via inhibition of cytokine secretion such as TNF-α, IL-1b, and IL-6 and suppress of ERK, JNK, and p38 phosphorylation and block MAPK signaling pathway in Parkinson's disease rats. Results of *in vitro* study also showed the levels of NO, TNF-α, ROS, and IL-1b decreased in supernatants of microglial culture by biochanin A treatment [31]. LPS with an increase of microglial activity, a decrease in dopamine uptake, and tyrosine hydroxylase activity could induce Parkinson's disease. Treatment with a phenol chalconoid extracted from the roots of Glycyrrhiza species, Licochalcone A (1.25, 2.5, and 5 mg/kg, IP), attenuated behavioral deficits in female Wistar rats that have been injected LPS to substantia nigra [32].

An animal study showed *Polygala tenuifolia* which has anti-inflammatory and antioxidant properties could protect dopaminergic neurons against the progression of Parkinson's disease. Usage of tenuigenin (300 mg/kg, 14 weeks), an active component of *Polygala tenuifolia*, prevented LPS-induced microglia activity and increased dopamine content in the striatum of LPS-injected rats. Furthermore, tenuigenin was able to decrease the levels of TNF-α and IL-1b in the substantia nigra pars [42]. Upregulation of TLR4 is associated with initiating the immune response in the microglia resulting in

neuronal death and apoptosis. LPS could induce expression of TLR4 in the microglial following an ischemia stroke. Induction of TLR4 caused increased cytokines production via increased activity of proinflammatory pathway mediators such as NF-κB, MyD88, ERK1/2, JNK, p38, and MAPK. Treatment with active component extracted from Flos *Carthami tinctorii* (Hydroxysafflor yellow A), by downregulation TLR4 pathway-mediated signaling components and also upregulation of BDNF, alleviated LPS-induced neuroinflammation in microglia as well as degeneration in neurons [43]. The results of various *in vitro* and *in vivo* studies indicated that some medicinal herbs and plant ingredients showed neuroprotective effects by anti-inflammatory and antioxidant properties in LPS-induced neurotoxicity. The effects of medicinal plants and plant ingredients on LPS-induced neuroinflammation were summarized in Table 1 and Figure 1.

4. Effects of Natural Products on LPS-Induced Lung Injury

4.1. In Vitro Studies. Procyanidin B2 (PCB2) is a multifunctional natural dietary phytochemical at doses (5, 10, and 20 mM) that inhibited activation of NF-κB and reduced expression and release of TNFα and IL-1β in LPS-treated human alveolar epithelial cells (AECs). PCB2 also prevented LPS-induced NLR family pyrin domain containing 3 (NLRP3) inflammasome activation and reduced ROS generation in human vascular endothelial cells. PCB2 enhanced Bcl-2 expression while inhibiting LPS-induced Bax and active caspase-3 production. The researchers found that in LPS-treated human AECs, PCB2 inhibited the activation of the NF-κB and NLRP3 inflammasomes, suggesting that it may have therapeutic potential for acute lung injury (ALI) [44].

Lately, the effect of Lonicerin (LCR) has been examined on the nontumorigenic human lung epithelial cell line (BEAS-2B). LCR (0 to 160 μM) significantly decreased the production of TNF-α, IL1, and IL6. LCR pretreatment significantly reduced the number of p-NF-κB expressing cells compared to LPS-treated cells. According to studies, LPS elevated the expression of caspase-3 and poly (ADP-ribose) polymerase (PARP), which was considerably controlled by LCR pretreatment. In BEAS-2B cells, LCR also reversed the impact of LPS on the expression of Bax and B-cell lymphoma 2 (Bcl-2). Pretreatment with LCR might prevent LPS from activating the apoptotic pathway [45].

4.2. In Vivo Studies. Methanol extract of *Spiraea prunifolia* (SP) leaves which were examined on NCI-H292 cells in a mouse model (0, 10, 25, 50, and 100 μg/mL) decreased IL-1β, IL-6, and the levels of TNF-α in the bronchoalveolar lavage fluid (BALF). In LPS-induced ALI mice, SP dramatically reduced the phosphorylation of MAPKs and NFκB. SP therapy increased Nrf2 elevated antioxidant enzymes and reduced ROS-mediated OS in LPS-induced ALI. Treatment with SP showed a considerable reduction in ROS generation and a large increase in glutathione (GSH) and 2,2-diphenyl-picrylhydrazyl (DPPH) radical scavenging activities. SP decreased lipid peroxidation by activating nuclear factor erythroid 2–related factor 2 (Nrf2) and upregulating antioxidant enzymes such as heme oxygenase 1 (HO-1) and NAD(P)H dehydrogenase (quinone 1) (NQO1). SP's capacity to stimulate Nrf2 activation and decrease the phosphorylation of MAPKs and NF-κB was associated with the ability to suppress airway inflammation [46].

According to Mo et al., S-allylmercaptocysteine (SAMC) can reduce LPS-induced ALI in mice by reduction of inflammation via NF-κB and Nrf2 pathways. According to their findings, TNF-α, IL-1β, and IL-6 levels were reduced after treatment with SAMC (10, 30, and 60 mg/kg, IG). Also, treatment with SAMC enhanced the levels of SOD and GSH while inhibiting the generation of MDA. SAMC treatment considerably reduced inflammatory cell infiltration and decreased the notable elevation of metropolitan planning organization (MPO), COX2, and iNOS caused by LPS. The administration of SAMC reduced the infiltration of LPS-induced inflammatory cells such as macrophages and neutrophils, revealing that SAMC might effectively cure LPS-induced ALI [47].

Robustaflavone-4′-dimethyl ether (RDE) from *Selaginella uncinata* suppressed FLT3 (a member of the type III receptor tyrosine kinase) activation by interacting with a generation of inflammatory cytokines and preventing neutrophil activation in ALI mice. RDE (50, 100, and 200 mg/kg, intragastric (IG)) reduced neutrophil-endothelial cell contacts and even neutrophil infiltration in lung tissues and serum levels of IL-6 and TNF-α and adhesion molecules, showing that RDE suppressed LPS-induced neutrophil stimulation. MPO activation was reduced by RDE administration in a dose-dependent manner. These findings showed that RDE could suppress FLT3 expression, then inhibit the LPS-induced AKT (Protein kinase B) and MAPK pathways. In a dose-dependent way, RDE may reverse the elevated levels of P-selectin, IL-6, TNF-α, and intercellular adhesion molecule 1 (ICAM-1) caused by LPS stimulation and ameliorate lung pathologic characteristics [48].

Wang et al. showed that LPS significantly activated the COX2/NLRP3/NF-κB pathway in lung tissues. Per os (PO) or oral administration of eriodictyol (20, 40, and 80 mg/kg, PO) in ALI induced by LPS in mice significantly suppressed the COX2/NLRP3/NF-κB pathway. eriodictyol also inhibited the release of PGE2, TNF-α, IL-6, and IL-1 into BALF, which were generated by LPS. The levels of MPO and MDA, total cells, and neutrophils were significantly reduced by eriodictyol. Moreover, the histopathologic lesions decreased in the eriodictyol groups. Meanwhile, in the LPS group, SOD activity was observed to be decreased, but eriodictyol considerably enhanced SOD levels. eriodictyol also improved lung pathological abnormalities and reduced the W/D ratio. The effect of eriodictyol on ALI was proven to be mediated through decreasing the inflammatory response. The suppression of COX2/NLRP3-mediated NF-κB signaling by eriodictyol causes a reduction in inflammatory cytokine production [49].

The anti-inflammatory effect of a standardized extract of *Euphorbia cuneata* (EC) against LPS-induced ALI in mice was evaluated. Total and differential cell counts were decreased by EC. Treatment with EC (25 and 50 mg/kg, PO) significantly increased CAT, SOD, and GSH while significantly decreasing

Table 1: Effects of natural products on LPS-induced neuroinflammation.

Natural product	Doses and administration	Study design	Effects	Ref.
Crocin Crocetin	20 μM 40 μM	Rat brain microglial cells	↓ NO production ↓ TNF-α production ↓ IL-1β production ↓ NF-κB activity	[26]
Tripterygium wilfordii	—	Neuron-glia cells	↓ Level TNFα and NO	[29]
Myricetin (extracted from red wine)	12.5, 25, 50 μM	BV-2 murine microglia cell line	↓ Levels of the TNF-α, IL-1β and IL-6 mRNA ↓ Levels of the TNF-α, IL-1β and IL-6 proteins Suppression of MAPK and NF-κB pathways	[28]
Biochanin	1.25, 2.5, 5 μM	Rat primary microglia	↓ Levels of NO, TNF-a, ROS, and IL-1b	[31]
Tripchlorolide (extract of *Tripterygium wilfordii*)	1.25–10 nM	Primary cortical neurons and neuro-2A cells	Inhibition of iNOS and COX-2 ↓ Production of TNF-a, IL-1b, NO, PGE2, superoxide anion	[30]
Licochalcone A (a flavonoid isolated from licorice roots)	0.625, 1.25, and 2.5 μg/ml	BV-2 cells	Inhibiting phosphorylation of NF-KB p65 and ERK1/2 ↓ Production of NO and PGE2 ↓ Expression of iNOS and COX-2. ↓ Production of TNF-α, IL-1β, IL-6 Prevention of degeneration of dopaminergic neurons	[32]
Silymarin (a milk thistle polyphenolic flavonoid)	10, 20, 40, 60, 80, and 100 μM	Mixed mesencephalic neuron–glia cultures	↓ Levels of TNF-α and NO ↓ Expression levels of iNOS protein and mRNA Inhibition of NF-κB ↓ Superoxide generation	[33]
Carvacrol	25, 50, and 100 mg/kg, IP	Rats	↓ NO, IL-6 and MDA level ↑ CAT, SOD activity ↑ Total thiol content	[34]
Carvacrol	25, 50, and 100 mg/kg, IP	Rats	↓ IL-1β, TNF-α, TLR4, and COX-2 expression ↑ BDNF expression	[35]
Gypenosides	25, 50, and 100 mg/kg, ICV	Rats	↓ NF-κB, IL-6, IL-1β level ↓ TLR4 and BDNF expression	[36]
Aqueous *Clinacanthus nutans* extract	500 and 1000 mg/kg, oral gavage	Rats	Improvment in metabolism of isoleucine, leucine, valine and pyruvate Regulation of metabolic pathway glycolysis, gluconeogenesis, and TCA cycle	[37]
Euphausia superba oil	80 mg/kg/day, feeding (rodent chow supplemented with 5 wt % of *Euphausia superba* oil)	Mice	↓ Expression of COX-2 and iNOS ↓ Level of MDA Suppress of translocation of p50 and p65 into the nuclei ↓ APP expression ↓ BACE1 expression	[38]
Nannochloropsis oceanica	50, 100 mg/kg, Administration of ethanol extract in drinking water	Mice	↓ Expression of COX-2 and iNOS ↓ Level of MDA Suppress of translocation of p50 and p65 into the nuclei ↓ APP expression ↓ BACE1 expression	[39]
Forsythoside B	1 and 2.5 μM	BV-2 cells and HT22 cells	Inhibition of JNK, WDFY1/TLR3, and NF-κB pathway	[40]

Table 1: Continued.

Natural product	Doses and administration	Study design	Effects	Ref.
Forsythoside B	400 mg/kg, intragastrically	C57 mice	Inhibition of JNK, WDFY1/TLR3, and NF-κB pathway	[40]
6-Oangeloylplenolin (isolated from *Centipeda minima*)	5–20 mg·kg, IP	Mice	↓ Expression levels of TNF-α and IL-1β ↓ Protein levels of iNOS, COX-2, phospho-NF-κB p65, NF-κB p65, phospho-IκB-α, and IκB-α	[41]
6-Oangeloylplenolin (isolated from *Centipeda minima*)	0.5–4 μM	BV2 and primary microglial cells	↓ Protein levels of NF-κB p65, phospho-NF-κB p65, IκB-α, and phospho-IκB-α ↓ Expression of iNOS and COX-2 ↓ Concentration of NO and PGE2 ↓ Expression of NOX-2 and NOX-4	[41]
Myricetin (extracted from red wine)	2.5, 5, 10 mg/kg, IP	Rats	↓ Number of Iba-1-positive cells ↓ Levels of the Iba-1 protein ↓ Expression of TNF-α, IL-1β, and IL-6	[28]
Biochanin	12.5, 25, 50 mg/kg, IP	Rats	↓ Secretion IL-1b, IL-6, and TNF-α Suppress of ERK, JNK, p38 phosphorylation Block of MAPK signaling pathway	[31]
Licochalcone A (a flavonoid isolated from licorice roots)	1.25, 2.5, and 5 mg/kg, IP	Rats	↓ Expression of iNOS, COX-2, TNF-α, IL-6, and IL-1 β in the substantia nigra pars compacta region	[32]
Tenuigenin (an active component of *Polygala tenuifolia)*	300 mg/kg	Rats	Prevention of degeneration of dopaminergic neurons. ↓ TNF-α and IL-1b levels in the substantia nigra pars compacta and blood	[42]
Hydroxysafflor yellow A (a component extracted from Flos *Carthami tinctorii)*	50 and 100 μM	Cortical neuron and microglial cells	↓ TLR4 expression in the microglia ↓ The numbers of apoptotic neurons ↓ Levels of the cleaved caspase-3 protein in the neurons ↓ Expression, phosphorylation, and nuclear translocation of MyD88, NF-κB p65 in the microglia ↓ Levels of the MyD88 protein in the neurons ↓ p-ERK1/2, p-JNK, and p-p38 expression in the microglia ↓ TNF-a, IL-1b, and NO levels in the microglia ↑ Expression of BDNF in the microglia	[43]

ICAM-1: intercellular adhesion molecule-1; VCAM-1: vascular cell adhesion molecule-1; MPO: myeloperoxidase; CAT: catalase; SOD: superoxide dismutase; ROS: reactive oxygen species; TLR4: Toll-like Receptor 4; MDA: malondialdehyde; COX2: cyclooxygenase-2; GSH: glutathione; MCP-1: monocyte chemoattractant protein-1; W/D: wet/dry; NF-κB: nuclear factor-kappa B; lactate dehydrogenase; KC: keratinocyte-derived chemokine; 4-HNE: 4-hydroxynonena; C+R+I: chlorogenic acid+rosmarinic acid+isofraxidin; PMNs: polymorphonuclear leukocytes; AECs: alveolar epithelial cells; iNOS: inducible nitric oxide synthase; PMVECs: pulmonary microvascular endothelial cells; MAPKs: mitogen-activated protein kinases; JNK: Jc-Jun-NH2 terminal kinase; GRP78: glucose-regulated protein 78; p-IRE1α: phosphorylated inositol-requiring enzyme 1α; TXNIP: thioredoxin interaction protein; IRE1α: inositol-requiring enzyme 1α; GSH-Px: glutathione peroxidase; ICV: intracerebroventricularly; IP: intraperitoneal injection. Per os (PO) or Oral administration; IV: intravenous; IG: intragastric.

MDA and 4-hydroxynonena (4-HNE) compared with the LPS-treated group. The capacity of EC to decrease NF-κB and COX activation revealed its anti-inflammatory properties. In comparison to the untreated LPS group, EC administration reduced the W/D ratio, total protein, and LDH activity. EC was also found to have antioxidant properties as it reduced lipid peroxidation. EC also reduced infiltration of inflammatory cell, lung edema, and histological changes, in addition to suppressing inflammatory mediator production (TNF-α, IL-8, IL-4). Overall, the study showed that EC has a protective effect against LPS-induced ALI, which might relate to its t anti-inflammatory and antioxidant properties [50]. The ethanol extract of *Trichilia martiana* C. DC. (TMEE) in LPS-induced ALI male C57BL/6 N mice in the LPS-treated group elevated TNF-α level in the LPS group, but TMEE administration (5, 10, 20, and 40 g/ml, PO) significantly decreased this, suggesting that TMEE modulates LPS-induced macrophage influx and TNF-α expression. Following TMEE therapy, the amount of IκB activation was

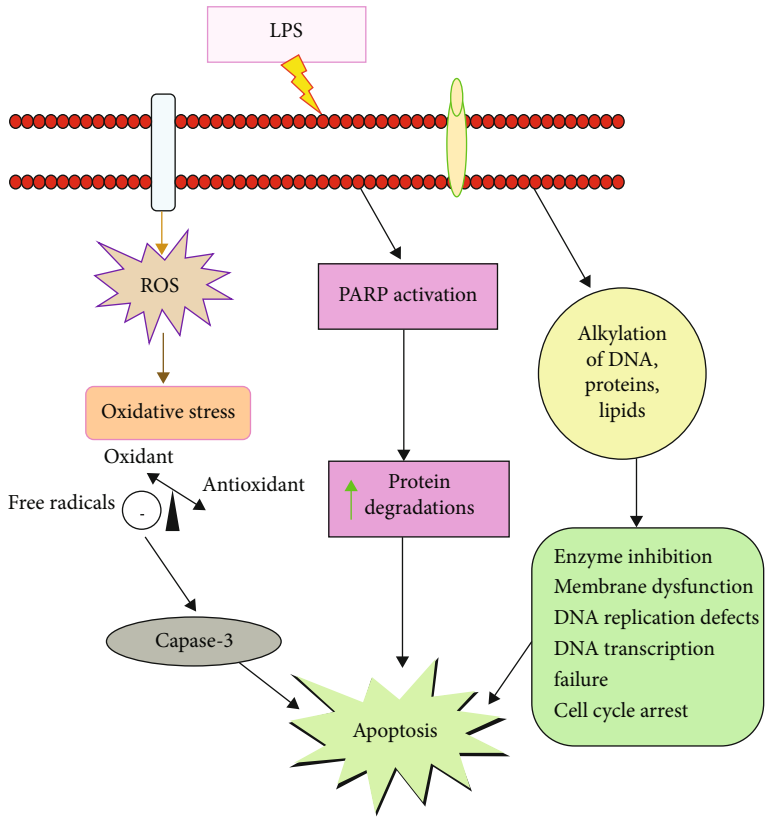

Figure 1: Lipopolysaccharide- (LPS-) induced neurotoxicity. Reactive oxygen species (ROS). Poly (ADP-ribose) polymerase (PARP).

dramatically reduced. TMEE also dramatically decreased the upregulation of ERK and JNK in LPS-induced ALI animals. The findings showed that TMEE-induced HO-1 production was linked to a reduction in the inflammatory response caused by LPS. The downregulation of MAPKs (particularly ERK and JNK)/NF-B signaling pathways and the activation of HO-1 appear to be linked to TMEE's actions [51].

Treatment of induced ALI mice with nanoemulsions containing pequi oil (pequi-NE) (20 mg/kg, PO) decreased the levels of IL-1, TNF-α, IL-6, monocyte chemoattractant protein-1 (MCP-1), and keratinocyte-derived chemokine (KC). The migration of leukocytes and neutrophils into the lungs is reduced by pequi-NE. Treatment with pequi-NE lowered MPO levels and recovered activation of catalase to saline control level. MDA levels dramatically reduced after treatment with pequi-NE. The results suggested that using nanoemulsions containing pequi oil to treat mice with ALI/ARDS (acute respiratory distress syndrome) caused by LPS has anti-inflammatory and antioxidant properties. The findings imply that pequi-NE might be used to treat pulmonary inflammatory diseases as an alternative therapeutic method [52].

The ethanolic extract of *Glycyrrhiza glabra* (*G. glabra*) (200 and 300 mg/kg, PO) significantly reduced total cell count and inflammatory cell migration, reduced the W/D weight ratio, reduced the total protein content, reduced the expression of TNF-α, IL-1, and IL-6, improved SOD activity, and significantly protected the lung injury in LPS-induced ALI female mice. *G. glabra* also reduced neutrophil infiltration in the lungs of ALI mice [53].

The potential of *Thalictrum minus* L. (TML) protecting mice against LPS-induced ALI in C57 male mice was shown. The findings indicated that TML (10, 20, and 40 mg/kg, PO) decreased the lung W/D weight ratio and reduced inflammatory cell tissue infiltration, which revealed that TML could help treat pulmonary edema. TML significantly reduced LPS-induced inflammatory cytokines such as TNF-α and IL-1, decreased NO, and elevated SOD, and effectively alleviated LPS-induced increases in total protein, leukocytes, and macrophages, according to the researchers. Bax and LC3II expressions were notably decreased, whereas Bcl-2 protein levels were elevated. TML protected against LPS-induced ALI through regulating AMPK-Nrf2/KEAP (AMP-activated protein kinase) and MAPKs p38-NLRP3/caspase1 signaling pathways and suppressing apoptosis and autophagy [54].

The results of a study on male BALB/c albino mice showed that tovophyllin A (TA) protects mice from LPS-induced ALI, which may be due to anti-inflammatory and antioxidant characteristics. Differential and total inflammatory cell counts, protein content, LDH (lactate dehydrogenase) activity, and the lung W/D ratio were all reduced by TA (50 or 100 mg/kg, PO) in LPS-induced mice. TNF-α, IL-1, and IL-6 levels lowered by TA. Moreover, TA improved lung lesions and enhanced antioxidant levels such as GSH and SOD [55].

According to earlier researches on male BALB/c mice, peiminine (1, 3, and 5 mg/kg, IP) reduced LPS-induced inflammatory cell aggregation and decreased MPO activity. Peiminine has been shown to reduce the generation of

inflammatory cells, macrophages, and neutrophils. Additionally, peiminine therapy reduced histopathological alterations and TNF-α, IL-1, and IL-6 expression. During peiminine therapy, the lung W/D ratio was clearly lower. The findings showed that peiminine decreases inflammatory response injury to the body and even the risk of pulmonary edema. Peiminine might reduce ALI caused by LPS by blocking the PI3K/AKT/NF-κB signaling pathway [56].

Administration of *Nigella sativa* (NS) extract on LPS-exposed male Wistar rats decreased IFN-γ, PGE2, and transforming growth factor beta-1 (TGF-β1) but increased IL-4 levels. Treatment with NS extract (100-400 mg/kg, IP) inhibits the synthesis of IL-6, TNF-α, and NO. In rats exposed to LPS, NS therapy enhanced the total WBC count (eosinophils, neutrophils, basophils, monocytes). Administration of NS decreased the generation of MDA and increased thiol level and also serum SOD and CAT activity. NS therapy also improved pathogenic abnormalities in the lungs [57].

Administration of narciclasine (2 mg/kg, IP) in the LPS-induced rats protected lung injury via interdiction effect on apoptosis, excessive inflammation, and OS. Narciclasine treatment also attenuated pathological injury and pulmonary edema and suppressed the secretion of IL-6, IL-1β, TNF-α, and MCP-1 as well as reduced the expression of intercellular adhesion molecule-1 (ICAM-1) and vascular cell adhesion molecule 1 (VCAM-1) in neonatal ALI rats. Besides that, narciclasine inhibited nuclear translocation of NF-κB and activation of the TLR4/NF-κB/Cox2 signaling pathway. Overall, narciclasine protected against lung damage by inhibiting excessive inflammation, OS, and apoptosis [58]. Chrysin (CHR) (3 mg/kg, IT) may have therapeutic potential for relieving LPS-induced ALI in mice by blocking the Inositol-requiring enzyme 1/thioredoxin interaction protein/NLRP3 (IRE1/TXNIP/NLRP3) pathway and thus decreasing inflammatory cytokine release. CHR pretreatment reduced MPO synthesis and levels of IL-1β, IL-6, and TNF-α, which reduced inflammation. Furthermore, CHR increased antioxidant capacity by enhancing SOD and glutathione peroxidase activity (GSH-Px). CHR also decreased lung edema and vascular leakage as well as the expression of TXNIP, NLRP3, and cleaved caspase-1 [59].

Zhang et al. revealed that ergosterone (15 and 30 mg/kg, PO) reduced the damage caused by the LPS model in ALI model mice by inhibiting the NLRP3 signaling pathway. The findings showed that ergosterone pretreatment reduced the W/D ratio, IL-1, IL-6, TNF-α, NO, and MDA levels in lung tissues while also notably increasing SOD levels. Furthermore, ergosterone reduced the activation of NLRP3 caused by LPS. The findings suggest that ergosterone protects against ALI caused by LPS, and it may suppress the NLRP3 signaling pathway's activation. Ergosterone pretreatment not only decreased OS but also improved pulmonary impairment and reduced lung edema [60]. Ferulic acid (FA) (25-100 mg/kg, IG) in LPS-treated lungs in mice significantly reduced the production of TNF-α, IL-1, and IL-6. Treatment with FA or dexamethasone (DEX) substantially reduced the LPS-induced lung W/D weight ratio and histopathological abnormalities. The invasion of total neutrophils and macrophages in the BALF of mice damaged by LPS was reduced by FA. The study showed that FA therapy could significantly reduce cell infiltration and protect against ALI caused by LPS. FA decreased pulmonary edema, activation of MPO, and monocyte chemoattractant protein-1 (MCP1) level in LPS-injured mice. The mechanisms of FA's protection against LPS-induced ALI were related to the reduction of inflammatory response via the inhibition of the TLR4/NF-κB signaling pathway [61].

Fucoxanthin's anti-inflammatory properties have recently been expanded in mice. Through activating the Nrf2-mediated pathway, fucoxanthin (10 mg/kg, IV) notably reduced inflammatory responses in LPS-induced ALI mice. LPS induced upregulation of IL-6, IL-10, iNOS, COX-2, TNF-α, and IL-1β that was reduced by fucoxanthin via the AMPK/NF-κB signaling pathway. TLR4/MyD88/NF-κB signaling was inhibited by fucoxanthin, which binds directly to TLR4. Based on discoveries, fucoxanthin can considerably suppress LPS-induced inflammatory mediators [62].

Under *in vivo* condition, LCR pretreatment reduced the production of IL-6, IL-1β, and TNF-α, by controlling the activation of TLR4, myeloid differentiation factor 2 (MD2), and p-NF-κB. Pretreatment with LCR (10, 20, and 30 mg/kg, IP) significantly reduced stimulated caspase-3 and PARP cleavage in the lungs of mice. Administration of LCR improved histologic changes and reduced inflammatory cell infiltration. As a result, LCR could be a new promising treatment option for ALI based on the anti-inflammatory and antiapoptotic effects [45].

Dehydrodieugenol B can reduce lung edema, inflammatory cells, IL-6 and IL-1β levels, inflammatory cell infiltration, iNOS, an inhibitor of metalloprotease-1 (TIMP-1), matrix metalloproteinase-9 (MMP-9), and collagen content and expression. Treatments decreased the number of total inflammatory cells, according to the findings. Dehydrodieugenol B (20-60 mg/kg/weight) prevented pulmonary remodeling in an animal model of ALI by reducing inflammatory cells, lung edema, IL-6 and IL-1β levels, iNOS, and collagen content and expression. Dehydrodieugenol B showed anti-inflammatory and antioxidant properties by reducing OS and inhibiting JNK [63]. It has been reported that three kinds of bioactive components in *Sarcandra glabra* (rosmarinic acid+isofraxidin+chlorogenic acid) in different doses (5 to 50 mg/kg) reduced LPS-induced phosphorylated NF-κB protein expression. Also, pretreatment with three components reduced MPO but increased SOD activation and HO-1 expression. Three components inhibited the production ofIL-1β, IL6, and TNF-α and reduced the production of iNOS and COX-2 proteins. They also reduced inflammatory response by blocking macrophage activation, resulting in lower IL-6, NO, and TNF-α secretion [64].

The effects of Salviplenoid A (SA) in the LPS-induced ALI mice model blocked expression of activated Nrf2 and nuclear factor of kappa light polypeptide gene enhancer in B-cells inhibitor, alpha (IκB-α) phosphorylation in a dose-dependent manner. The amount of COX-2 protein in LPS-induced ALI animals was significantly elevated, which was potently reduced by administration of SA (10-40 mg/kg, IP). In the presence of SA, the levels of HO-1 mRNA

increased significantly as compared to the untreated group [65].

Treatment with thymol (20-80 mg/kg, IP) 1 h after administration of LPS reduced alveolar wall thickness and lung edema, and increased the level of infiltrated inflammatory cells in mice. Thymol also inhibited the production of IL-6, IL-1β, and TNF-α, in the BALF of mice. In addition, thymol reduced MDA content and MPO activity in the lung tissue. Thymol also significantly inhibited LPS-induced NF-κB activation [66]. Pretreatment with carvacrol (20-80 mg/kg) decreased the lung wet/dry weight ratio in LPS-induced ALI in mice and significantly decreased total and different WBC similar to dexamethasone (5 mg/kg). Carvacrol also reduced inflammatory infiltration, focal area of fibrosis, and production of IL-1β, IL-6, and TNF-α in the BALF of mice [67].

The effect of hordenine (Hor) (10 mg/kg) on LPS-induced ALI inhibited the levels of IL-1β, IL-6, and TNF-α in the BALF and IL-1β, IL-6, iNOS, Cox2, and MPO mRNA expression levels in the lung tissues of ALI mouse model. Pretreatment with Hor significantly decreased the increased COX-2, iNOS, IL-6, and TNF-α levels and promoted the expression of arginase one (Arg-1), chitinase-3-like-3, and mannose receptor (CD206). Hor also reduced ALI by inhibiting the phosphorylation of phosphorylated protein kinase (AKT), NF-κB, and mitogen-activated protein kinase (MAPK), [68].

The effects of munronoid I, which is extracted and purified from *Munronia sinica* on LPS-induced inflammation in mice showed administration of munronoid I (10 mg/kg, IV) significantly inhibited LPS-induced infiltration of inflammatory cells, scored of lung tissue damage, and also the production of IL-1β and IL-6 in BALF of ALI mice [69]. The effects of medicinal herbs and natural products on LPS-Induced lung inflammation are shown in Table 2 and Figure 2.

5. Effects of Natural Products on LPS-Induced Hepatotoxicity

5.1. In Vitro Studies. The findings of the RT-qPCR and ELISA tests demonstrated that Mangiferin (MF), a glucosylxanthone remarkably reduced LPS-induced mRNA and protein level of TNF-α. Additionally, reporter gene analysis revealed that MF dramatically reduced LPS-enhanced NF-κB and activator protein-1 (AP-1) activity. The expression of LPS-induced TLR4 in Kupffer cells (KCs) was also downregulated by MF, according to flow cytometry data. Furthermore, the findings suggested that eme oxygenase-1 (HO-1) may downregulate the TLR4 signaling pathway, therefore regulating the anti-inflammatory action of MF in KCs [70]). The findings show that apigenin (2.5, 5, 10, and 20 μM) can protect against D-galactosamine (D-GalN)/LPS-treated hepatocellular damage via increasing translocation of Nrf2 nucleus, which increases the protein expression of peroxisome proliferator–activated receptor γ (PPAR), CAT, and SOD amounts, and so inhibits the inflammatory reaction. The MDA content was reduced in the apigenin-treated groups. The IκB-α and PPAR proteins expression was enhanced in the hepatocytes after treatment with apigenin. Apigenin therapy may similarly reduce the amount of TNF-α. To summarize, the current findings show that apigenin protects against D-GalN/LPS-enhanced liver damage [71].

In LPS-induced HepG2 cells, researchers discovered that limonin (10, 25, and 50 μM) increased cell survival *in vitro*. Hepatotoxicity induced via LPS was reduced by limonin. On the other hand, limonin suppressed the production of ROS in cells caused by LPS. The results demonstrated that LPS increased NOD-like receptor protein 3 (NLRP3) protein expression in HepG2 cells but limonin administration significantly reduced. In the presence of LPS, limonin reduced the proportion of cas-1, as well as IL-1β, in HepG2 cells. As a result of their evidence, limonin appears to have the potential to be a future medicine to treat liver damage [72].

5.2. In Vivo Studies. LPS-induced liver damage in mice was reduced by pretreatment with an ethanol extract of *Illicium henryi* (EEIH). EEIH (1.25-5.0 mg/kg, IP) dramatically reduced expression of IL-1β, IL-6, TNF-α, and COX-2 in LPS-induced ALI, through downregulating of TLR4 mRNA expression and suppressing NF-κB phosphorylation. Additionally, EEIH significantly lowered the rate of nitrosative stress and liver oxidative in LPS-treated mice by lowering NO and iNOS values, upregulating Nrf2, and increasing GSH and SOD values. The blood values of alanine transaminase (ALT) and aspartate aminotransferase (AST) and MPO activity in the liver in LPS-induced mice were significantly reduced after pretreatment with EEIH. The findings showed that EEIH defends mice against ALI by decreasing the TLR4/NF-κB signaling pathways and lowering the inflammatory reaction [73].

The effects of kaempferol on the ALF-induced mouse were investigated. The terminal deoxynucleotidyl transferase dUTP nick end labeling (TUNEL) assay revealed that in D-GalN/LPS-induced liver damage, the quantity of hepatocyte apoptosis had dramatically increased but kaempferol pretreatment reduced them. In the ALF-induced mouse model, kaempferol (2.5-40 mg/kg, IV) pretreatment decreased the mRNA and protein rates of C/EBP-homologous protein (CHOP), a modulator for reticulum stress- (ER stress-) induced apoptosis, according to RT-PCR and western blotting studies. Finally, kaempferol protects the mouse from ALF by inhibiting apoptotic hepatocytes through modulating the CHOP-glucose-regulated/binding immunoglobulin protein 78- (Grp78-) ER stress pathways. As a result, kaempferol may be effective in the treatment of ALF [74].

Chicoric acid (CA) was studied in the context of acute liver damage caused by LPS and d-GalN. According to the findings, CA (50 mg/kg) lowered aspartate aminotransferase (AST), alanine aminotransferase (ALT), and ROS in serum and reduced mortality caused by LPS/d-GalN. The amount of GSH in the liver elevated after treatment with CA. To reduce inflammation, CA may inhibit mitogen-activated protein kinases (MAPKs) and NF-κB. Meanwhile, the findings showed that CA activated the Nrf2 pathway by raising AMP-activated protein kinase (AMPK) levels. The CA suppressed the NLRP3 and ASC, so the rate of cas-1 was reduced in the treatment group. CA therapy significantly enhanced the protein levels of autophagy genes [75].

Table 2: Effects of natural products on LPS-induced lung inflammation.

Natural product	Doses	Study design	Effects	Ref.
Procyanidin B2	5, 10, 20 mM	Alveolar epithelial cells (AECs)	↓ Annexin V ↓ NLRP3, ↓ NF-kB ↓ ROS ↓ TNF-α, ↓ IL-1β ↓ Bax, ↓ caspase-3 ↑ Bcl-2	[44]
Lonicerin	From 0 to160 μM	BEAS-2B cell line	↓ IL-6, ↓ TNF-α, ↓ IL1β ↓ TLR4, ↓ MD2, ↓ p-NF-κB ↓ Caspase-3, ↓ PARP	[45]
Spiraea prunifolia	50 , 100 mg/kg, PO.	NCI-H292 cells in mouse model	↓ Lipid Peroxidation ↓ IL-1β, ↓ IL-6, ↓ TNF-α ↓ MAPKs, ↓ NF-κB ↓ OS, ↓ ROS, ↓DPPH radicals, ↓ GSH ↑ Nrf2, ↑ HO-1, ↑ NQO1	[46]
S-allylmercaptocysteine	10, 30, and 60 mg/kg, IG.	Male BALB/c mice	↓ Macrophages, ↓ Neutrophils ↓ TNF-α, ↓ IL-1β, ↓ IL-6 ↓OS, ↓ MPO ↓ NF-κB activation ↓ MDA, ↓ iNOS, ↓ COX2 ↓ Nrf2 pathway ↑ SOD, ↑ GSH	[47]
Robustaflavone-4′-dimethyl ether	50, 100, and 200 mg/kg, IG.	ICR mice	↓ FLT3 ↓ AKT, ↓MAPK ↓ Neutrophils, ↓ MPO ↓ IL-6, ↓ TNF-α ↓ P-selectin, ↓ ICAM-1	[48]
Eriodictyol	20, 40, and 80 mg/kg, PO.	Male BALB/c mice	↓ Macrophages, ↓ Neutrophils ↓ MPO, ↓ MDA ↓ COX-2, ↓ NLRP3, ↓ NF-κB ↓ PGE2, ↓ IL-6, ↓ TNF-α, ↓ IL-1β ↑ SOD, ↑ W/D ratio	[49]
Trichilia martiana C. DC.	5, 10, 20, and 40 μg/ml, PO.	Male C57BL/6N mice	↓ Macrophages ↓ TNF-α ↓ IκB, ↓ ERK, ↓ JNK ↑ HO-1	[51]
Pequi (*Caryocar brasiliense* Cambess)	20 mg/kg, PO.	Male ALI mice	↓ Leukocytes, ↓ Neutrophils ↓ TNF-α, ↓ IL-1, ↓ IL-6 ↓ MCP-1, ↓ KC ↓ MPO, ↓ MDA	[52]
Glycyrrhiza glabra	200, 300 mg/kg, PO.	Female mice	↓ Cell migration ↓ W/D ↓ Lung edema ↓ Protein content ↓ TNF-α , IL-1β, and IL-6 ↑ SOD activity	[53]
Thalictrum minus L.	10, 20, 40 mg/kg, PO.	C57 male mice	↓ W/D weight ratio ↓ Total protein ↓ NO, ↓ TNF-α, ↓ IL-1β ↓ MAPKs, ↓ p38-NLRP3, ↓ Caspase-1 ↓ COX2 ↓ Bax, ↓ LC3II, ↑ Phosphorylation of AMPK ↑ Bcl-2, ↑ Nrf2 ↑ SOD	[54]
Tovophyllin A	50 or 100 mg/kg, PO.	Male BALB/c albino mice	↓ LDH activity, ↓ Total protein, ↓ W/D ratio	[55]

Table 2: Continued.

Natural product	Doses	Study design	Effects	Ref.
Peiminine	1, 3, 5 mg/kg, IP.	Male BALB/c mice	↓ Inflammatory cells ↓ Lung lesions ↓ TNF-α, ↓ IL-6, ↓ IL-1β ↑ GSH, ↑ SOD ↓ W/D ratio ↓ TNF-α, ↓ IL-1β, ↓ IL-6 ↓ Neutrophils, ↓ Macrophages. ↓ MPO ↓ NF-κB, ↓ PI3K, ↓ AKT	[56]
Euphorbia cuneata	25 and 50 mg/kg, PO.	Male Balb/c albino mice	↓ W/D ratio ↓ Total protein ↓ TNF-α, ↓ IL-8, ↓ IL-4 ↓ LDH ↓ Neutrophils, ↓ Macrophage, ↓ Lymphocyte ↓ MDA, ↓ 4-HNE ↓ NF-κB , ↓ COX ↓ Lipid peroxidation ↑ CAT, ↑ SOD, ↑ GSH	[50]
Nigella sativa	100, 200, 400 mg/kg, IP.	Male Wistar rats	↓ Eosinophils, ↓ Neutrophils, ↓ Basophils, ↓ Monocytes ↓ INFγ, ↓ TGF-β1, ↓ PGE2, ↓ NO, ↓ IL-6 ↓ MDA ↑ IL-4, ↑ CAT, ↑ SOD ↑ Thiol level	[57]
Narciclasine	2 mg/kg, IP.	Neonatal rats	↓ TNF-α, ↓ IL-6, ↓ IL-1β, ↓ MCP-1 ↓ ICAM-1, ↓ VCAM-1 ↓ ROS, ↓ Cell apoptosis ↓ TLR4, ↓ MyD88, ↓ COX2 ↓ p-IκBβ	[58]
Chrysin	3 mg/kg, IT.	Male ICR mice	↓ MPO ↓ IL-1β, ↓ IL-6, ↓ TNF-α ↓ GRP78, ↓ p-IRE1α ↓ IRE1α, ↓ TXNIP, ↓ NLRP3 ↑ SOD, ↑ GSH-Px	[59]
Ergosterone	15 and 30 mg/kg, PO.	ALI model mice	↓ W/D ratio ↓ Pulmonary edema ↓ TNF-α, ↓ IL-1, ↓ IL-6, ↓ NO ↓ P-selectin, ↓ ICAM-1 ↓ MDA, ↓ NLRP3 ↑ SOD	[60]
Ferulic acid	25, 50, 100 mg/kg, IG.	Female BALB/c mice	↓ Cells infiltration ↓ Neutrophils, ↓ Macrophages ↓ Lung edema ↓ W/D ratio ↓ MPO, ↓ MCP-1 ↓ TNF-α, ↓ IL-1β, ↓ IL-6 ↓ TLR4, ↓ NF-κB	[61]
Fucoxanthin	10 mg/kg, IV.	ALI model mice	↓ COX-2, ↓ iNOS, ↓ IL-10, ↓ IL-6 ↓ TNF-α, ↓ IL-1β ↓ NF-κB ↓ TLR4, ↓ MyD88 ↑ Nrf2 p	[62]
Lonicerin	10, 20, and 30 mg/kg, IP.	Male C57BL/6 mice	↓ W/D weight ratio ↓ Total protein ↓ PMNs, ↓ Macrophages ↓ IL-6, ↓ TNF-α, ↓ IL-1β	[45]

Table 2: Continued.

Natural product	Doses	Study design	Effects	Ref.
Dehydrodieugenol B	20, 30, and 60 mg/kg/ weight	Male BALB/C mice	↓ TLR4, ↓ MD2, ↓ p-NF-κB ↓ Bax, ↓ Bcl-2 ↓ Caspase-3, ↓ PARP ↓ Lung edema, ↓ Inflammatory cells, ↓ IL-6, ↓ IL-1 β ↓ iNOS, ↓ MMP-9, ↓ TIMP-1 ↓ JNK	[63]
chlorogenic acid+rosmarinic acid+isofraxidin	5 to 50 mg/kg, IP.	Female and male BALB/c mice	↓ Inflammatory cell ↓ TNF-α, ↓ iNOS, ↓ COX-2, ↓ IL-6 ↓ W/D ratio ↓ MPO, ↓ NFκB p65 ↓ OS, ↓ NO ↑ SOD, ↑ HO-1	[64]
Salviplenoid A	10, 20, and 40 mg/kg, IP.	Male BALB/c mice	↓ TNF-α, ↓ IL-6, ↓ IL-8, ↓ IFN-γ ↓ COX-2 ↓ Eosinophils ↑ Nrf2, ↑ HO-1, ↑ GCLC	[65]
Thymol	20-80 mg/kg, IP.	Male BALB/c mice	↓ Histopathological changes, ↓ IL-6, ↓ TNF-α, ↓ IL-1β ↓ MPO ↓ MDA ↓ NF-κB activation	[66]
Carvacrol	20, 40, or 80 mg/kg, IP.	Male BALB/c mice	↓ Inflammatory cell ↓ TNF-α, ↓ IL-6 ↓ W/D ratio ↓ IL-1β	[67]
Hordenine	10 mg/kg	ALI mouse model	↓ Inflammatory cell ↓ TNF-α, ↓ iNOS, ↓ COX-2, ↓ IL-6 ↓ IL-1β ↓ NF-κB	[68]
Munronoid I	10 mg/kg, IV.	ALI mouse model	↓ Inflammatory cell ↓ TNF-α, ↓ IL-6 ↓ IL-1β ↓ Scored of lung tissue damage	[69]

ICAM-1: intercellular adhesion molecule-1; VCAM-1: vascular cell adhesion molecule-1; MPO: myeloperoxidase; CAT: catalase; SOD: superoxide dismutase; ROS: reactive oxygen species; TLR4: Toll-like Receptor 4; MDA: malondialdehyde; COX2: cyclooxygenase-2; GSH: glutathione; MCP-1: monocyte chemoattractant protein-1; W/D: wet/dry; NF-κB: nuclear factor-kappa B; LDH: lactate dehydrogenase; KC: keratinocyte-derived chemokine; 4-HNE: 4-hydroxynonena; C+R+I: chlorogenic acid+rosmarinic acid+isofraxidin; PMNs: polymorphonuclear leukocytes; AECs: alveolar epithelial cells; iNOS: inducible nitric oxide synthase; PMVECs: pulmonary microvascular endothelial cells; MAPKs: mitogen-activated protein kinases; JNK: Jc-Jun-NH2 terminal kinase; GRP78: glucose-regulated protein 78, p-IRE1α: phosphorylated inositol-requiring enzyme 1α; TXNIP: thioredoxin interaction protein; αIRE1α: inositol-requiring enzyme 1; GSH-Px: glutathione peroxidase.

It was reported that myricetin (Myr) (25-100 mg/kg, IP) protected fulminant hepatitis (FH) in mice against LPS/D-GalN-induced by reducing mortality, lowering serum AST and ALT levels, and reducing histological alterations, inflammation (IL-1β, IL-6, and TNF-α), OS, and liver apoptosis. Furthermore, in mice with LPS/D-GalN-induced FH, Myr could effectively moderate multiple signaling pathways, not only regulation of P53 protein and caspase-3/9, NF-κB activation, and MAPK and inhibition of TLR4 but also a raise in Nrf2 and HO-1 expression, ACC, and AMPK phosphorylation. Administration of Myr could suppress NLRP3 inflammasome in mouse-induced FH [76].

In LPS-treated mice, limonin (50 and 100 mg/kg, PO) decreased serum AST and ALT activity and LDH generation while increasing hepatic GSH levels and suppressing IL-1β maturation. In addition, histological analysis of the liver demonstrated that limonin prevents liver failure induced by LPS. They also found that limonin reduced LPS-induced hepatotoxicity by suppressing pyroptosis through the gasdermin D/NLRP3 pathways. In conclusion, this research identified the method by which limonin reduced LPS-induced liver injury and showed that limonin might be a good candidate treatment for hepatotoxicity. [72] In LPS/D-GalN-induced mice, administration of mangiferin (MF) (30-150 mg/kg, PO) increased survival and lowered serum ALT and AST activities. MF inhibited LPS-induced TNF-α generation by inhibiting the NF-κB/TLR4 pathways. MF therapy dramatically increased the expression and activation of HO-1 in hepatic tissues. The experiment found a possible preventive drug for LPS/D-GalN-enhanced acute liver damage [70].

Sae-tan et al. discovered that treatment with MSWE (150 mg/kg, PO) reduced the expression of iNOS in LPS-

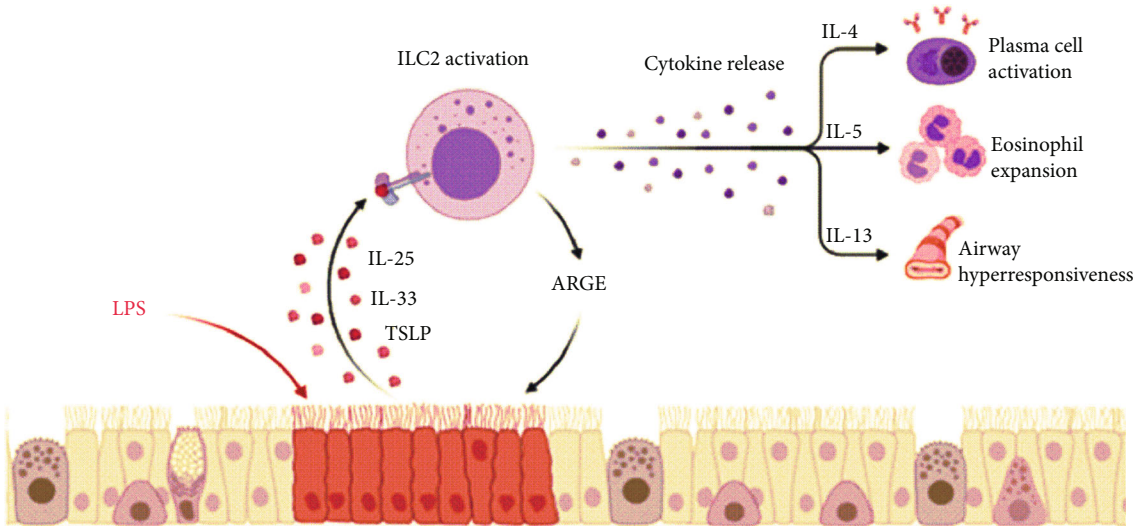

Figure 2: Lipopolysaccharide- (LPS-) induced lung inflammation. Thymic stromal lymphopoietin (TSLP). Innate lymphoid cells (ILC2). Amphiregulin (AREG).

enhanced ALI mice *in vivo* studies. Expression of inflammatory cytokines such as IL1b and infiltration of macrophages had similarly reduced in the livers. TLR4 mRNA expression was shown to be considerably reduced in MSWE-treated group mice compared to the LPS group. Pretreatment with MSWE caused reduced levels of Emr1. This article showed that MSWE might be useful in the treatment of a variety of inflammatory illnesses [77]. Treatment with diosgenin (50 mg/kg, PO) might significantly decrease AST, alkaline phosphatase (ALP), and ALT concentrations in the blood. In addition, when compared to the LPS/D-Gal-treated group, hepatic rates of IL-6, IL-1β, MDA, ROS, NF-κB, TNF-α, and TRL4 dramatically reduced, while the Nrf2 rate and activity of SOD improved. Furthermore, after diosgenin delivery, MPO activity, a sign of neutrophil infiltration, is reduced. In conclusion, diosgenin reduced inflammatory responses, OS, and liver damage indices, and it is considered a treatment for liver damage [78].

The NLRP3 inflammasome and the NLR family have recently been found to reduce the degree of LPS/GaIN-enhanced liver injury in mice. Shiitake mushroom-derived ELNs (S-ELNs) (1×10^{10}/g, IP) showed to suppress activation of NLRP3 and inhibit inflammasome generation in primary macrophages. After treatment with S-ELN, the increased blood AST and ALT rates caused by GalN/LPS reduced. S-ELNs also reduced IL-18 and -6 secretion, as well as gene of IL-1β production. In summary, S-ELN treated mice indicated to prevent ALI caused by GalN/LPS. As a result, S-ELNs, which have been discovered as strong NLRP3 inflammasome inhibitors, demonstrated a potential effect on ALI [79].

Administration of S-allyl cysteine (SAC) (25 and 100 mg/kg, PO) in the DGal/LPS induced mice group reduced AST, ALT, and ALP and partially reduced ROS and MDA, as well as inflammation-related biomarkers such as ferric reducing antioxidant power (FRAP), MDA, liver ROS, cas-1, COX-2, TLR4, NF-κB, TNF-α, NLRP3, IL-6 and -1β, and MPO function. Furthermore, SAC was able to improve apoptotic indicators such as DNA fragmentation and cas-3. In conclusion, SAC protects the liver against DGal/LPS by reducing the inflammatory response, OS, apoptotic cells, and infiltration of neutrophils, which is mainly due to the inhibition of NLRP3/NFB/TLR4 signaling [80]. Pretreatment with *Pulicaria petiolaris* (PP) (50 and 100 mg/kg, PO) resulted in a considerable decrease in LDH, AST, ALP, ALT, and CK-MB. It was discovered that pretreatment with PP considerably decreased the increased MDA concentration. Administration with PP significantly raised GSH levels and activities of SOD. Pretreatment with PP reduced NF-κB p65 activity. The amounts of IL-6 and TNF-α dramatically reduced after pretreatment with PP. These findings implied that PP reduces LPS-enhanced oxidative injury to the liver by acting as an anti-inflammatory and antioxidative [81].

Apocynin pretreatment (300 mg/kg, IP) reduced the increase of ROS, thiobarbituric acid reactive substances (TBARS) compounds, and protein carbonyl content caused by D-Gal/LPS. Further, pretreatment with apocynin decreased the number of TUNEL-positive cells, decreased histological abnormalities, suppressed the generation of TNF-α, prevented the activation of the caspase downstream, and decreased mortality caused by D-Gal/LPS. Remarkably, therapy with apocynin reduced D-Gal/LPS-induced OS, apoptosis of hepatic cells, and liver damage while boosting survival. Gal/LPS-treated activation of the late-stage proapoptotic AMPK/JNK pathway was prevented by apocynin administration. These findings imply that NOX-derived ROS may be a late-stage deleterious component in D-Gal/LPS-enhanced ALI through activating the proapoptotic JNK/AMPK pathway. Apocynin may be effective in the pharmacological treatment of ALI caused by inflammation [82]. *Beta vulgaris* ethanol extract (BVEE) effectively reduced blood AST, ALT, and gamma-glutamyl transpeptidase (γ-GTP) levels in a rat hepatotoxicity model caused by LPS and alcohol. The elevated mRNA levels of cytochrome P450 2E1 (CYP2E1), TUNEL MAPK1, 3, α-Smooth muscle actin (α-SMA), and NF-κB in the BVEE (200 and

400 mg/kg, PO) treated group had dramatically reduced. These findings suggested that BVEE might protect against hepatotoxicity by modifying several indications of liver damage caused by LPS or alcohol [83].

Curcumin (CUR) administration (200 mg/kg) resulted in a decrease in LDH, AST, and ALT activities. Furthermore, LPS/DCL caused a considerable reduction in liver GSH level and SOD activity, which was considerably restored in rats supplemented with CUR. MDA and NO levels were dramatically lowered in the livers of CUR-treated rats. CUR also decreased serum CRP, liver IL-6, TNF-α, NF-κB, TLR4, JNK, and p38 expression while upregulating HO1. Finally, CUR protected rats against LPS/DCL-induced liver damage by reducing inflammation, TLR4 signaling, and OS while increasing HO-1. As a result, in LPS/DCL-induced rats, CUR inhibited the development and severity of liver damage while also improving liver function [84].

Administration of apilarnil (API) (0.2, 0.4, and 0.8 g/kg, PO) dramatically reduced tissue damage in LPS-induced groups. The findings showed that the API treatment group had decreased in the number of TUNEL-positive cells but the LPS-induced group had risen. The LPS-treated group raised xanthine oxidase (XOD), transcobalamin 1 (TCN1), and MDA rates while reducing CAT and SOD rates; however, API treatment inversed these effects. The LPS-induced group showed elevating in NF-κB, TLR4, high mobility group box 1 (HMGB1), iNOS, IL-1β, IL-6, and TNF-α expression; however, API treatment mitigated this increment. Finally, apilarnil is considered to protect rats from LPS-induced liver injury by blocking the NF-κB/TLR4/HMGB-1 pathways [85].

Administration of heptamethoxy flavone (HMF) (500 mg/kg) reduced serum ALT, ALP, AST, and MDA levels in ALI-induced rats. The antioxidant enzyme values were considerably higher in the HMF group. Furthermore, administration with HMF caused decreased rates of cas-3 and -9, Bax, Bcl-2, TNF-a, IL-b, and NF-jB in the HMF-treated rats. These findings significantly suggest that HMF might be useful for the development of a hepatoprotective medication to treat ALI [86]. Researchers found that esculetin (40 mg/kg, PO) reduced OS and myeloperoxidase activity, amount of AST, ALP, and ALT, and hepatic levels of IL-1β, IL-6, TNF-α, NF-κB, and TLR4. Furthermore, esculetin reduced hepatic tissue damage after an LPS/D-Gal exposure. Esculetin has hepatoprotective properties against ALF and can prevent liver damage by reducing oxidative load, neutrophil infiltration, and inflammation [87].

According to the findings, *Platycodon grandiflorus* polysaccharides (PGPSt) (100 and 200 mg/kg, IG) dramatically lowered SOD, ALT, and AST activities. TNF-α, IL-1β, IL-6, and MDA amounts were reduced by PGPSt, although GSH expression was elevated. Apoptosis of hepatocytes is inhibited by PGPSt, which could be due to suppression of Bax and cas3, and overexpression of Bcl-2. Furthermore, western blot investigations demonstrated that PGPSt inhibited the synthesis of NF-κB p65, p-P38, and TRL4 proteins. In mice, PGPSt protected them against LPS/D-GalN-induced ALI. In conclusion, the findings showed that PGPSt is an efficient therapeutic medication that increases the production of antiapoptotic proteins, lowers inflammatory mediators, and reduces OS, and might be applied to treat ALI in the future [88]. In LPS-induced mice, treatment with apigenin and myricetin (myricetin and apigenin, 100 and 200 mg/kg, PO) increased total protein levels, decreased serum levels of ALP, AST, ALT, CRP, γ-GT, direct and total bilirubin rates, MDA, NOx, and liver MPO activity. The liver structure damaged by LPS treatment was significantly restored by apigenin and myricetin treatment. Pretreatment with myricetin and apigenin decreased liver damage indicators, OS, and inflammatory events, suggesting that these flavonoids may have hepatoprotective properties in ALI [89].

Pretreatment with *Lepidium sativum* (LS) (50 mg/kg) significantly reduced serum ALT and AST rates in the LPS-induced mice. The results showed a rise in TNF-α protein rates in the liver of mice administered with LS. The inflammatory mediator generation of IL-6, IL-10, IL-4, TGF-β, and IFN-γ was also reduced after administration with LS. Treatment with LPS may cause abnormalities such as sinusoid congestion, neutrophil infiltrations, necrosis, and hepatocellular decay, whereas LS therapy reduced these effects. These data suggest that LS has considerable hepatoprotective properties in ALI induced by LPS in mice [90].

Treatment with *Galaxaura oblongata* (*G. oblongata*) (200 mg/kg, IP) extract in LPS-induced mice notably reduced serum cytokines, such as LPO, NF-κB, and MPO, and ameliorated apoptosis of the liver by suppressing the protein tyrosine kinase (PTK), which could be because of antioxidative properties of G. oblongata extract. The MDA level was suppressed in G. oblongata therapy. The marine extract of G. oblongata was shown to protect mice from acute liver damage in the research [91].

Treatment with aminoguanidine (AG) (50, 100, and 150 mg/kg, IP) reduced LPS-enhanced liver toxicity by lowering MDA, NO, and IL-6 rates while enhancing total thiols, CAT, and SOD activity. Regarding the preventive role of AG seen in this investigation, AG appears that could reduce the elevated NO rates caused by iNOS activation in LPS-enhanced hepatotoxicity. When compared to the LPS group, AG injection improved serum albumin. In the present article, AG reduced NO, MDA, and OS metabolite levels while boosting total thiol group levels, as well as SOD and CAT activity in liver tissue in AG-treated groups [92]. The effects of medicinal herbs and natural products on LPS-Induced hepatotoxicity are shown in Table 3 and Figure 3.

6. Effects of Natural Products on LPS-Induced Immunomodulation

The *in vitro* anti-inflammatory activity of the ethyl acetate fraction of *Agarum cribrosum* in LPS-stimulated macrophage cell line (RAW264.7 cells) reduced the NO production. The expression of IL-1, IL-6, COX-2, and TNF-α was significantly suppressed by *A. cribrosum* fractions (5, 10, and 20 μg/mL). The anti-inflammatory activity was also confirmed by studying its effects on proinflammatory signaling pathways. The suppression of NF-κB p-65 inhibited the activation of NF-κB and MAPKs. As a result, trifuhalol A (a

Table 3: Effects of natural products on LPS-induced hepatotoxicity.

Natural product	Doses	Study design	Effects	Ref.
Mangiferin	—	*In vitro,* liver-resident Kupffer cells	↓ TNF-α, ↓ NF-κB, ↓ AP-1 ↓ TLR4, ↓ HO-1	[70]
Apigenin	2.5, 5, 10, and 20 μM	*In vitro,* rat BRL hepatocytes	↓ MDA, ↓ TNF-α ↑ Nrf2, ↑ PPAR, ↑ IκB-α	[71]
Limonin	10, 25, and 50 μM	*In vitro,* HepG2 cells	↓ ROS, ↓ NLRP3, ↓ cas-1 ↓ IL-1β	[72]
Ethanol extract of *Illicium henryi* (EEIH)	1.25, 2.5, and 5.0 mg/kg, IP.	Male BALB/c mice	↓ IL-1β, ↓ IL-6, ↓ TNF-α, ↓ COX-2 ↓ TLR4, ↓ NF-κB, ↓ NO, ↓ iNOS ↓ ALT, ↓ SLT, ↓ MPO ↑ Nrf2, ↑ GSH, ↑ SOD	[73]
Kaempferol	2.5, 5, 10, 20, and 40 mg/kg, IV.	Male wild-type mice	↓ CHOP, ↓ Grp78, ↓ ER stress	[74]
Chicoric acid (CA)	50 mg/kg	Male C57BL/6 mice	↓ AST, ↓ ALT, ↓ ROS ↓ MAPKs, ↓ NF-κB, ↓ NLRP3 ↓ Cas-1, ↓ ASC ↑ GSH, ↑ Nrf2, ↑ AMPK	[75]
Myricetin (Myr)	25, 50, or 100 mg/kg, IP.	Male C57BL/6 mice	↓ AST, ↓ ALT, ↓ OS ↓ IL-6, ↓ IL-1β, ↓ TNF-α ↓ Cas-3, ↓ Cas-9 ↓ TLR4, ↓ NF-κB, ↓ MAPK ↑ Nrf2, ↑ HO-1, ↑ ACC	[76]
Limonin	50 and 100 mg/kg, PO.	C57BL/6 mice	↓ AST, ↓ ALT, ↓ LDH ↓ IL-1β, ↓ Pyroptosis ↑ GSH	[72]
Mangiferin (MF)	30, 100, or 150 mg/kg, PO.	BALB/c mice	↓ ALT, ↓ AST, ↓ TNF-α ↓ NF-κB, ↓ TLR4 ↑ HO-1	[70]
Mungbean seed coat water extract (MSWE)	150 mg/kg, PO.	Male ICR mice	↓ iNOS, ↓ IL1b, ↓ TLR4 ↓ Emr1	[77]
Diosgenin	50 mg/kg, PO.	Male C57BL/6 mice	↓ AST, ↓ ALP, ↓ ALT ↓ IL-6, ↓ IL-1β, ↓ MDA, ↓ ROS, ↓ NF-κB, ↓ TNF-α, ↓ TRL4, ↓ MPO, ↓ OS ↑ Nrf2, ↑ SOD	[78]
Shiitake mushroom-derived ELNs (S-ELNs)	1×10^{10}/g, IP.	C57BL/6 J mice	↓ NLRP3, ↓ AST, ↓ ALT ↓ IL-18, ↓ IL-6, ↓ IL-1β	[79]
Ganoderma lucidum (G. lucidum)	5, 10, and 20 mg/kg	Female BALB/c mice	↓ MyD88, ↓ TLR4, ↓ NF-κB, ↓ MAPK ↓ p38, ↓ JNK, ↓ ErK1/2 ↓ IL-6, ↓ TNF-α, ↓ AST, ↓ALT	[104]
S-allyl cysteine (SAC)	25 and 100 mg/kg, PO.	Male C57BL/6 mice	↓ AST, ↓ ALT, ↓ ALP ↓ ROS, ↓ MDA, ↓ OS ↓ FRAP, ↓ MDA, ↓ ROS ↓ cas-1, ↓ cox-2, ↓ TLR4, ↓ NF-κB, ↓ TNF-α, ↓ NLRP3, ↓ IL-6, ↓ IL-1β, ↓ MPO, ↓neutrophils ↑cas-3	[80]
Pulicaria petiolaris (PP)	50 and 100 mg/kg, PO.	Male Swiss albino mice	↓ AST, ↓ ALP, ↓ ALT ↓ MDA, ↓ NF-κB, ↓ IL-6, ↓ TNF-α	[81]

Table 3: Continued.

Natural product	Doses	Study design	Effects	Ref.
Apocynin	300 mg/kg, IP.	Male BALB/c mice	↓ LDH, ↓ CK-MB ↑ GSH, ↑ SOD ↓ ROS, ↓ TBARS ↓ TNF-α, ↓ OS, ↓ mortality ↓ AMPK, ↓ JNK	[82]
Beta vulgaris ethanol extract (BVEE)	200 and 400 mg/kg, PO.	Male Sprague–Dawley rats	↓ AST, ↓ ALT, ↓ γ-GTP ↓ CYP2E1, ↓ MAPK1, ↓ MAPK3 ↓ α-SMA, ↓ NF-κB ↑ NO	[83]
Curcumin (CUR)	200 mg/kg suspended in 1% CMC	Male albino Wistar rats	↓ LDH, ↓ AST, ↓ ALT ↓ GSH, ↓ SOD, ↓ MDA, ↓ NO ↓ CRP, ↓ IL-6, ↓ TNF-α, ↓ TLR4 ↓ NF-κB, ↓ JNK, ↓ p38, ↓ OS ↑ HO-1	[84]
Apilarnil (API)	0.2, 0.4, and 0.8 g/kg, PO.	Sprague-Dawley rats	↓ XOD, ↓ TCN1, ↓ MDA ↓ NF-κB, ↓ TLR4, ↓ HMGB-1 ↓ iNOS, ↓ IL-6, ↓ IL-1β, ↓ TNF-α ↑ CAT, ↑ SOD	[85]
Heptamethoxyflavone (HMF)	500 mg/kg	Male albino adult rats	↓ ALT, ↓ ALP, ↓ AST ↓ MDA, ↓ Cas-3, ↓ Cas-9 ↓ Bax, ↓ Bcl-2, ↓ TNF-a ↓ IL-b, ↓ NF-jB	[86]
Esculetin	40 mg/kg, PO.	Male C57BL/6 mice	↓ IL-6, ↓ IL-1β, ↓ TNF-α, ↓ NF-κB ↓ TLR4, ↓ neutrophils, ↓ OS ↓ AST, ↓ ALP, ↓ ALT	[87]
Platycodon grandiflorus polysaccharides (PGPSt)	100 and 200 mg/kg, IG.	SPF-BALB/c mice	↓ SOD, ↓ ALT, ↓ AST ↓ TNF-α, ↓ IL-1β, ↓ IL-6 ↓ Bax, ↓ Cas-3, ↓ MDA ↑ GSH	[88]
Apigenin and myricetin	Myricetin and apigenin 100 and 200 mg/kg, PO.	Male Balb/c mice	↓ ALP, ↓ AST, ↓ ALT ↓ CRP, ↓ γ-GT, ↓ PGE2 ↓ TNF-a, ↓ MDA, ↓ NO ↓ MPO, ↓ ↓ IL-6, ↓ IL-1 ↓ Bilirubin, ↓ COX-2, ↓ iNOS ↓ NF-κB, ↓ IKK, ↓ OS ↑ Total protein	[89]
Lepidium sativum (LS)	50 mg/kg	Male mice	↓ ALT, ↓ AST, ↓ TNF-α ↓ IL-6, ↓ IL-10, ↓ IL-4 ↓ TGF-β, ↓ IFN-γ, ↓ Neutrophils	[90]
Galaxaura oblongata (*G. oblongata*)	200 mg/kg, PO.	BALB/C mice	↓ LPO, ↓ NF-κB, ↓ MPO ↓ PTK, ↓ MDA	[91]
Aminoguanidine (AG)	50, 100, and 150 mg/kg, PO.	Wistar rats	↓ MDA, ↓ NO, ↓ IL-6 ↓ NO, ↓ OS ↑ Total thiols, ↑ CAT, ↑ SOD	[92]

TNF-α: tumor necrosis factor-α; Nrf-2: nuclear factor erythroid 2-related factor 2; PPAR: peroxisome proliferator–activated receptor γ; CAT: catalase; SOD: superoxide dismutase; NF-κB: nuclear factor-κB; TLR4: Toll-like receptor 4; NLRP3: NOD-like receptor protein 3; Grp78: glucose-regulated/binding immunoglobulin protein 78; CHOP: C/EBP-homologous protein; ER stress: reticulum stress; AST: aspartate aminotransferase; ALT: alanine aminotransferase; ALP: alkaline phosphatase; MAPKs: mitogen-activated protein kinases; AMPK: AMP-activated protein kinase; HO-1: heme oxygenase-1; ACC: acetyl-CoA carboxylase; CK-MB: creatine kinase-MB; LDH: lactate dehydrogenase; TBARS: thiobarbituric acid reactive substances; HMGB-1: high-mobility group box protein 1; TCN-1: testican 1; OS: oxidative stress; CAS: caspase; IKK: inhibitor of nuclear factor kappa-B kinase; COX-2: cyclooxygenase 2; PTK: protein tyrosine kinase; LPO: lipid per oxidation; ICV: intracerebroventricularly, IP: intraperitoneal injection. Per os (PO) or oral administration; IV: intravenous; IG: intragastric.

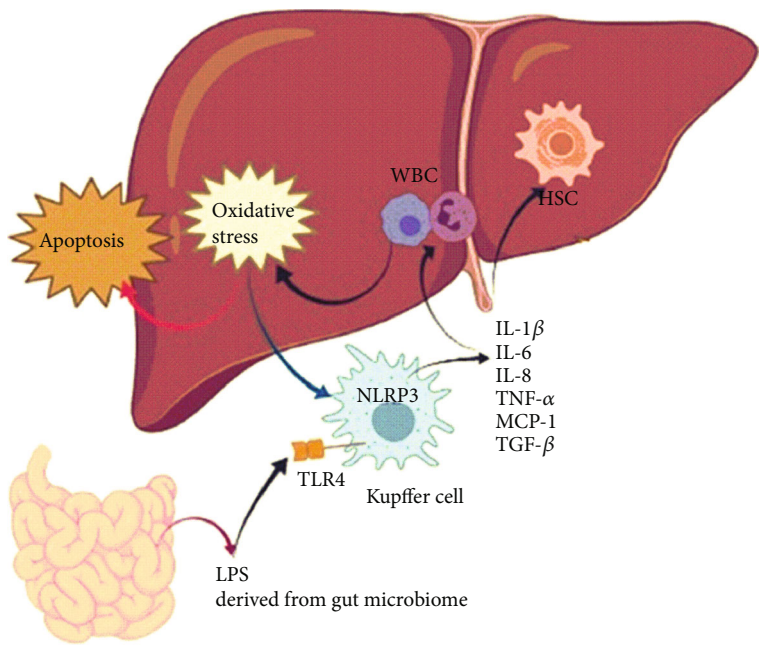

Figure 3: Lipopolysaccharide- (LPS-) induced hepatotoxicity. Toll-like receptor 4 (TLR4). Transforming growth factor beta (TGF-β). Monocyte chemo-attractant protein-1 (MCP-1).

phlorotannin extracted from *Agarum cribrosum*) can be used in the prevention or treatment of inflammation [93].

Recently, LPS-induced RAW macrophages were used to test the efficacy of tamarind extract. The effect of tamarind extract on the generation of NO in RAW macrophages was investigated. LPS-unstimulated macrophages (control) produced the least amount of NO, whereas the LPS-stimulated group produced more. The generation of NO was reduced in the presence of tamarind (3.175 to 150 μg/mL) extract at the dosages examined. LPS-stimulated RAW macrophages significantly increased iNOS gene expression. iNOS levels were considerably reduced in the presence of tamarind extract at different dosages, compared to LPS treatment alone. The aqueous fruit pulp extract's inhibitory action on NO generation and iNOS gene expression make it an excellent anti-inflammatory treatment in situations when NO production is in excess [94]. Essential oils of *Amomum aromaticum* (0.1 μg/ml to 100 μg/ml) decreased NO production in LPS-induced RAW264.7 Cells (*In vitro*) by preventing expressions of COX-2 and iNOS [95].

Crocetin improved cell cytotoxicity and suppressed MCP-1 and the expression of IL-8 through blocking nuclear factor-kappaB p65 (NF-κB p65) activity after LPS-induced inflammatory responses in Human umbilical vein endothelial cells (HUVEC) cells. Furthermore, crocetin inhibited immune cell infiltration, adhesion molecules expression, and ameliorated dysfunction endothelium [96]. These results indicated that crocetin showed protective effects on induced vascular injury by reduction of inflammation.

It was shown that quercetin as an immunoregulatory agent dependently impaired the high production of chemokines and cytokines in LPS-stimulated dendritic cells (DCs). Generation of cytokines such as IL-1 β, TNF-α, IL-1 α, IL-6, IL-10, IL-12 p70, and chemokines such as MCP-1, macrophage inflammatory protein (MIP)-1 a, and MIP-1 b significantly decreased by quercetin treatment (6.25, 12.5, 50, and 100 μg/ml) in LPS-stimulated DCs. Quercetin also significantly suppressed the increased expression of CD40, CD80, and CD86 in the DCs [97].

The effect of *Portulaca oleracea* ethanol extract (50-200 μg/ml) against LPS-induced inflammation in RAW 264.7 cells was examined. Results of this study showed this extract could inhibit the production of NO, IL-1β, TNF-α, and IL-6 in the cells. *P. oleracea* extracts inhibited the phosphorylation of ERK1/2, JNK, and activation of NF-κB in the cells [98]. Treatment with 250 μg/ml of a polysaccharide fraction purified from *P. oleracea* (POL-P3b) upregulated the expression of CD80, CD83, and CD86 in DCs. Also, the production of TNF-α, IL-12, and to a lesser extent IL-10 were upregulated by POL-P3b. In addition, POL-P3b increased the expression of TLR-4 in DCs [99].

Administration of thymoquinone (10 μM) on LPS-activated mast cells restored LPS-induced changes at mRNA and protein levels of IL-5 and IL-13 but did not affect IL-10 production. Thymoquinone also inhibited GATA transcription factor binding at the IL-5 promoter induced by LPS stimulation [100]. Treatment with thymoquinone (1-20 μM) also significantly inhibited LPS-induced IL-12, IL-10, and TNF-α release from DCs and suppressed LPS-induced phosphorylation of Protein kinase B (PKB)/Akt and ERK1/2 but induced caspase-3 and caspase-8 activity in DCs [101].

The effects of linalool on LPS-induced inflammation in both *in vivo* and *in vitro* were evaluated. Linalool (25 mg/kg, IP) inhibited the phosphorylation of inhibitor alpha gene (IjBa) protein, JNK, p38, and extracellular signal-regulated

Table 4: Effects of natural products on LPS-induced immunomodulation.

Natural product	Doses and administration	Study design	Effects	Ref.
Agarum cribrosum	5, 10 and 20 μg/mL	RAW264.7 cells	↓ NO production ↓ TNF-α, ↓ IL-6, ↓ IL-1β, ↓ COX2 ↓ NF-κB p65, ↓ MAPKs	[93]
Tamarindus indica	3.175 to 150 μg/mL	RAW 264.7 macrophages	↓ NO production ↓ iNOS	[94]
Amomum Aromaticum	From 0.1 μg/ml to 100 μg/ml	Murine macrophage RAW264.7 cells	↓ NO production ↓ TNFα, ↓ IL-1β, ↓IL-6 ↓ Cox-2, ↓ iNOS	[95]
Dehydrodieugenol B	10, 20, 30, and 60 μg/mL	RAW 264.7 macrophages	↓ NO, ↓ IL-1β, ↓ IL-6	[63]
Sarcandra glabra	C+R+I: 0.03, 0.06, and 0.06 mmol	RAW 264.7 macrophages	↓ IL-6, ↓ TNF-α ↓ MAPK, ↓ NF-κB ↓ IκB, ↓ COX-2, ↓ iNOS ↓ P-p38, ↓ P-JNK, ↓ P-ERK	[64]
Salviplenoid A	—	RAW 264.7 murine macrophage	↓ NO, ↓ TNF-α ↓ NF-κB	[65]
Munronoid I	12.5 μM, 25 μM, 50 μM	Mouse peritoneal macrophages	↓ COX-2, ↓ iNOS, ↓ IL-1β, ↓ TNF-α	[69]
Crocetin (saffron)	—	HUVEC	↓ MCP-1 expression ↓ IL-8 expression ↓ NF-κB p65 activity ↓ Immune cells infiltration ↓ Adhesion molecules expression	[96]
Quercetin	6.25, 12.5, 50, and 100 μg/ml	Dendritic cells	↓ Generation of TNF-α, IL-1 α, IL-1 β, IL-6, IL-10, IL-12 p70 ↓ Generation of MCP-1, MIP-1α, and MIP-1 b Suppress of expression of CD40, CD80, and CD86	[97]
Portulaca oleracea ethanol extract	50, 100, and 200 μg/ml	RAW 264.7 cells	↓ Production of NO, TNF-α, IL-1β and IL-6 ↓ Phosphorylation of ERK1/2, JNK ↓ Activation of NF-κB	[98]
POL-P3b (a polysaccharide fraction purified from *P. oleracea*)	250 μg/ml	Dendritic cells	↑ Expression of CD80, CD83, CD86, and MHC class II molecules ↑ Production of IL-12, TNF-α, and IL-10 ↑ Expression of TLR-4	[99]
Thymoquinone	10 μM	Mast cells	↓ Levels of IL-5 and IL-13 mRNA ↓ Levels of IL-5 and IL-13 protein Inhibition of GATA transcription factor binding at the IL-5 promoter	[100]
Thymoquinone	1-20 μM	Dendritic cells	↓ Release of IL-10, IL-12, and TNF-α Suppress of phosphorylation of PKB/Akt, and ERK1/2 Induction of caspase-3 and caspase-8 activity	[101]
Linalool		RAW 264.7 cells	Inhibition of phosphorylation of IkBα protein, p38, c-JNK, and ERK ↓ Level of IL-6, TNF-α	[102]
Linalool	25 mg/kg, IP.	*In vivo*, mice	↓ Level of IL-6, TNF-α in the BALF	[102]
Aqueous extract of *Curcuma longa*	0.5, 4, 20, 100, 500	Mouse splenocytes and mouse macrophages	↑ Level of NO, IL-12, IL-10, IL-6, IL-2, TNF-α, IFN-γ, and MCP-1 in non-LPS-stimulated cells ↓ Production of IL-12 and PGE2 in LPS-stimulated cells	[103]

MCP-1: monocyte chemoattractant protein-1; IL-8: interleukin-8; NF-κB p65: nuclear factor-kappa B p65; HUVEC: human umbilical vein endothelial cell; NO: nitric oxide; TNF-α: tumor necrosis factor-α; IL-1β: interleukin-1β; MDA: malondialdehyde, CAT: catalase; SOD: superoxide dismutase; TLR4: Toll-like receptor 4; BDNF: brain-derived neurotrophic factor; TCA: tricarboxylic acid; ICV: intracerebroventricularly; IP: intraperitoneal injection; COX-2: cyclooxygenase-2; APP: amyloid protein precursor; BACE1: β-site APP cleaving enzyme; MMP-3: matrix metalloproteinase 3; JNK: C-Jun NH2-terminal kinase; PGE2: Prostaglandin E2; Iba-1: ionized calcium binding adaptor molecule-1; MAPK: mitogen-activated protein kinases; ERK: Ras-dependent extracellular signal-regulated kinase; ROS: reactive oxygen species; MyD 88: myeloid differentiation factor 88; MIP-1α: macrophage inflammatory protein-1α; MHC: major histocompatibility complex; PKB/Akt: protein kinase B/serine-threonine kinase; IkBα protein: ubiquitination-inducible multiprotein.

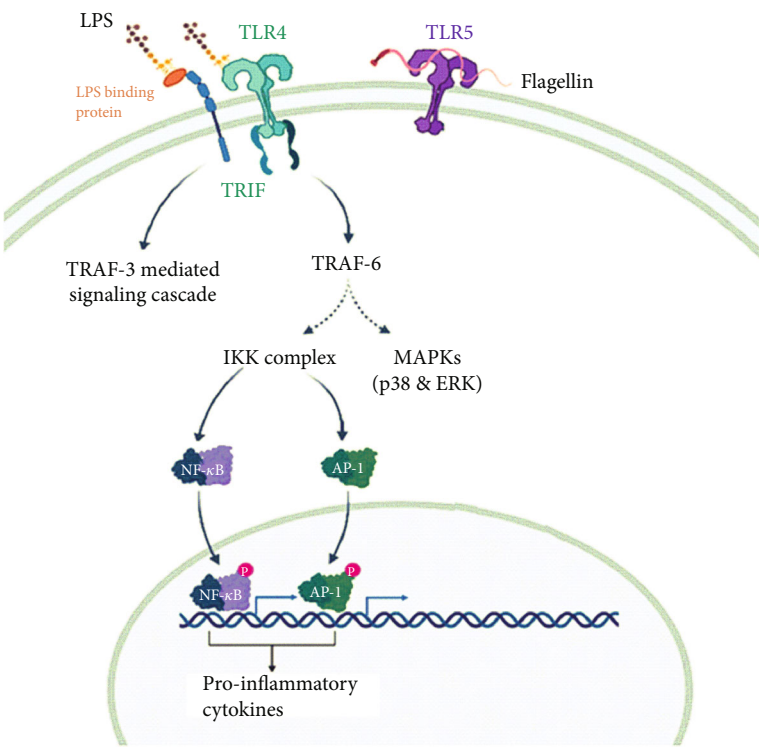

Figure 4: Lipopolysaccharide- (LPS-) induced immunomodulation. Lipopolysaccharides (LPS). Nuclear transcription factor-kappa B (NFκB). Toll-like receptor 4 (TLR4). The mitogen activated protein kinases (MAPKs). Janus kinase-signal transducers and activators of transcription (JAK-STAT).

kinase in LPS-stimulated RAW 264.7 cells. Linalool also significantly reduced the production of inflammatory cytokines in the BALF of mice with LPS-induced lung injury and attenuated histopathological changes of lung tissues compared to the LPS group [102].

The extract of *Curcuma longa* significantly increased the level of NO, IL-2, IL-6, IL-12, IL-10, IFN-γ TNF-α, and MCP-1 in non-LPS stimulated mouse splenocytes and mouse macrophages. This extract also inhibited the production of PGE2 and IL-12 in LPS-stimulated cells [103]. The effects of medicinal herbs and natural products on LPS-Induced immunomodulation are shown in Table 4 and Figure 4.

7. Conclusion

In vitro and *in vivo* studies reported that the possible potential therapeutic effects of herbal medicine and natural products on LPS-induced toxicity in different organs. The preventive or prophylactic effects of natural products on LPS-induced toxicity may be due to their anti-inflammatory, antioxidant, and immunomodulatory properties. Therefore, the results of the current review study suggested the therapeutic effect of natural products on inflammation and oxidative stress pathway. However, these findings provide information about natural products for the prevention and treatment of LPS-induced toxicity, but the scientific validation of these compounds requires clinical trials and evidence on animal models for replacing modern commercial medicine.

Data Availability

Data used to support the findings of this review are included within the article.

Conflicts of Interest

The authors have no conflicts of interest to declare for this study.

Authors' Contributions

MK, MB, and MHM searched the literature and helped in the preparation of the manuscript. MRK contributed to the study design and critically revised the manuscript. All authors read and approved the final version of the manuscript.

References

[1] L. Qin, X. Wu, M. L. Block et al., "Systemic LPS causes chronic neuroinflammation and progressive neurodegeneration," *Glia*, vol. 55, no. 5, pp. 453–462, 2007.

[2] C. Whitfield and M. S. Trent, "Biosynthesis and export of bacterial lipopolysaccharides," *Annual Review of Biochemistry*, vol. 83, no. 1, pp. 99–128, 2014.

[3] E. P. Ingenito, R. Mora, M. Cullivan et al., "Decreased surfactant protein-B expression and surfactant dysfunction in a murine model of acute lung injury," *American Journal of Respiratory Cell and Molecular Biology*, vol. 25, no. 1, pp. 35–44, 2001.

[4] X. Zhang, H. Huang, T. Yang et al., "Chlorogenic acid protects mice against lipopolysaccharide-induced acute lung injury," *Injury*, vol. 41, no. 7, pp. 746–752, 2010.

[5] A. Płóciennikowska, A. Hromada-Judycka, K. Borzęcka, and K. Kwiatkowska, "Co-operation of TLR4 and raft proteins in LPS-induced pro-inflammatory signaling," *Cellular and Molecular Life Sciences*, vol. 72, no. 3, pp. 557–581, 2015.

[6] D. Tamandl, M. Bahrami, B. Wessner et al., "Modulation of toll-like receptor 4 expression on human monocytes by tumor necrosis factor and interleukin-6: tumor necrosis factor evokes lipopolysaccharide hyporesponsiveness, whereas interleukin-6 enhances lipopolysaccharide activity," *Shock*, vol. 20, no. 3, pp. 224–229, 2003.

[7] I. Sozen and A. Arici, "Interactions of cytokines, growth factors, and the extracellular matrix in the cellular biology of uterine leiomyomata," *Fertility and Sterility*, vol. 78, no. 1, pp. 1–12, 2002.

[8] O. Lykhmus, L. Voytenko, L. Koval et al., "*A*7 nicotinic acetylcholine receptor-specific antibody induces inflammation and amyloid β42 accumulation in the mouse brain to impair memory," *PLoS One*, vol. 10, no. 3, article e0122706, 2015.

[9] Z. Jiang, Y. Meng, L. Bo, C. Wang, J. Bian, and X. Deng, "Sophocarpine attenuates LPS-induced liver injury and improves survival of mice through suppressing oxidative stress, inflammation, and apoptosis," *Mediators of Inflammation*, vol. 2018, Article ID 5871431, 12 pages, 2018.

[10] L. Xianchu, Z. Lan, L. Ming, and M. Yanzhi, "Protective effects of rutin on lipopolysaccharide-induced heart injury in mice," *The Journal of Toxicological Sciences*, vol. 43, no. 5, pp. 329–337, 2018.

[11] H.-Y. Hsu and M.-H. Wen, "Lipopolysaccharide-mediated reactive oxygen species and signal transduction in the regulation of interleukin-1 gene expression," *Journal of Biological Chemistry*, vol. 277, no. 25, pp. 22131–22139, 2002.

[12] S. E. Orfanos, A. Kotanidou, C. Glynos et al., "Angiopoietin-2 is increased in severe sepsis: correlation with inflammatory mediators," *Critical Care Medicine*, vol. 35, no. 1, pp. 199–206, 2007.

[13] P. Di Rosanna and C. Salvatore, "Reactive oxygen species, inflammation, and lung diseases," *Current Pharmaceutical Design*, vol. 18, no. 26, pp. 3889–3900, 2012.

[14] M. Mittal, M. R. Siddiqui, K. Tran, S. P. Reddy, and A. B. Malik, "Reactive oxygen species in inflammation and tissue injury," *Antioxidants & Redox Signaling*, vol. 20, no. 7, pp. 1126–1167, 2014.

[15] V. Cachofeiro, M. Goicochea, S. G. De Vinuesa, P. Oubiña, V. Lahera, and J. Luño, "Oxidative stress and inflammation, a link between chronic kidney disease and cardiovascular disease: new strategies to prevent cardiovascular risk in chronic kidney disease," *Kidney International*, vol. 74, pp. S4–S9, 2008.

[16] M. J. Page, D. B. Kell, and E. Pretorius, "The role of lipopolysaccharide-induced cell signalling in chronic inflammation," *Chronic Stress*, vol. 6, pp. 1–8, 2022.

[17] M. Larocca, A. M. Perna, A. Simonetti et al., "Antioxidant and anti-inflammatory effects of cauliflower leaf powder-enriched diet against LPS induced toxicity in rabbits," *Food & Function*, vol. 8, no. 9, pp. 3288–3296, 2017.

[18] A. Sofowora, E. Ogunbodede, and A. Onayade, "The role and place of medicinal plants in the strategies for disease prevention," *African journal of traditional, complementary, and alternative medicines: AJTCAM*, vol. 10, no. 5, pp. 210–229, 2013.

[19] A. Karimi, M. Majlesi, and M. Rafieian-Kopaei, "Herbal versus synthetic drugs; beliefs and facts," *Journal of nephropharmacology*, vol. 4, no. 1, pp. 27–30, 2015.

[20] P. A. Greenberger, "Therapy in the management of the rhinitis/asthma complex," *Allergy & Asthma Proceedings*, vol. 24, no. 6, 2033.

[21] S. G. Mortazavi Moghaddam, M. Kianmehr, and M. R. Khazdair, "The possible therapeutic effects of some medicinal plants for chronic cough in children," *Evidence-based Complementary and Alternative Medicine*, vol. 2020, Article ID 2149328, 15 pages, 2020.

[22] M. Kianmehr and M. R. Khazdair, "Possible therapeutic effects of *Crocus sativus* stigma and its petal flavonoid, kaempferol, on respiratory disorders," *Pharmaceutical Biology*, vol. 58, no. 1, pp. 1140–1149, 2020.

[23] M. Boskabady, M. R. Khazdair, R. Bargi et al., "Thymoquinone ameliorates lung inflammation and pathological changes observed in lipopolysaccharide-induced lung injury," *Evidence-based Complementary and Alternative Medicine*, vol. 2021, Article ID 6681729, 10 pages, 2021.

[24] Z. Arab, M. Hosseini, N. Marefati et al., "Neuroprotective and Memory Enhancing Effects of *Zataria Multiflora* in Lipopolysaccharide-Treated Rats," in *Veterinary Research Forum*, p. 101, Faculty of Veterinary Medicine, Urmia University, Urmia, Iran, 2022.

[25] V. Wee Yong, "Inflammation in neurological disorders: a help or a hindrance?," *The Neuroscientist*, vol. 16, no. 4, pp. 408–420, 2010.

[26] K. N. Nam, Y.-M. Park, H.-J. Jung et al., "Anti-inflammatory effects of crocin and crocetin in rat brain microglial cells," *European Journal of Pharmacology*, vol. 648, no. 1-3, pp. 110–116, 2010.

[27] B. Liu and J.-S. Hong, "Role of microglia in inflammation-mediated neurodegenerative diseases: mechanisms and strategies for therapeutic intervention," *Journal of Pharmacology and Experimental Therapeutics*, vol. 304, no. 1, pp. 1–7, 2003.

[28] B. Huang, J. Liu, D. Ma, G. Chen, W. Wang, and S. Fu, "Myricetin prevents dopaminergic neurons from undergoing neuroinflammation- mediated degeneration in a lipopolysaccharide-induced Parkinson's disease model," *Journal of Functional Foods*, vol. 45, pp. 452–461, 2018.

[29] Y. Liu, H.-L. Chen, and G. Yang, "Extract of *Tripterygium wilfordii* hook F protect dopaminergic neurons against lipopolysaccharide-induced inflammatory damage," *The American Journal of Chinese Medicine*, vol. 38, no. 4, pp. 801–814, 2010.

[30] X. D. Pan, X. C. Chen, Y. G. Zhu et al., "Neuroprotective role of tripchlorolide on inflammatory neurotoxicity induced by lipopolysaccharide-activated microglia," *Biochemical Pharmacology*, vol. 76, no. 3, pp. 362–372, 2008.

[31] J. Wang, W.-Y. Wu, H. Huang, W. Z. Li, H. Q. Chen, and Y. Y. Yin, "Biochanin a protects against lipopolysaccharide-induced damage of dopaminergic neurons both in vivo and in vitro via inhibition of microglial activation," *Neurotoxicity Research*, vol. 30, no. 3, pp. 486–498, 2016.

[32] B. Huang, J. Liu, C. Ju et al., "Licochalcone a prevents the loss of dopaminergic neurons by inhibiting microglial activation in lipopolysaccharide (LPS)-induced Parkinson's disease

models," *International Journal of Molecular Sciences*, vol. 18, no. 10, p. 2043, 2017.

[33] M. J. Wang, W. W. Lin, H. L. Chen et al., "Silymarin protects dopaminergic neurons against lipopolysaccharide-induced neurotoxicity by inhibiting microglia activation," *European Journal of Neuroscience*, vol. 16, no. 11, pp. 2103–2112, 2002.

[34] Z. Hakimi, H. Salmani, N. Marefati et al., "Protective effects of carvacrol on brain tissue inflammation and oxidative stress as well as learning and memory in lipopolysaccharide-challenged rats," *Neurotoxicity Research*, vol. 37, pp. 965–976, 2019.

[35] B. Lee, M. Yeom, I. Shim, H. Lee, and D. H. Hahm, "Inhibitory effect of carvacrol on lipopolysaccharide-induced memory impairment in rats," *The Korean Journal of Physiology & Pharmacology*, vol. 24, no. 1, pp. 27–37, 2020.

[36] B. Lee, I. Shim, H. Lee, and D. H. Hahm, "Gypenosides attenuate lipopolysaccharide-induced neuroinflammation and anxiety-like behaviors in rats," *Animal cells and systems*, vol. 22, no. 5, pp. 305–316, 2018.

[37] A. A. Azam, I. S. Ismail, M. F. Shaikh, K. Shaari, and F. Abas, "Effects of *Clinacanthus nutans* leaf extract on lipopolysaccharide-induced neuroinflammation in rats: a behavioral and 1H NMR-based metabolomics study," *Avicenna journal of phytomedicine*, vol. 9, no. 2, p. 164, 2019.

[38] J. Y. Choi, J. S. Jang, D. J. Son et al., "Antarctic krill oil diet protects against lipopolysaccharide-induced oxidative stress, neuroinflammation and cognitive impairment," *International Journal of Molecular Sciences*, vol. 18, no. 12, p. 2554, 2017.

[39] J. Y. Choi, C. J. Hwang, H. P. Lee, H. S. Kim, S. B. Han, and J. T. Hong, "Inhibitory effect of ethanol extract of *Nannochloropsis oceanica* on lipopolysaccharide-induced neuroinflammation, oxidative stress, amyloidogenesis and memory impairment," *Oncotarget*, vol. 8, no. 28, pp. 45517–45530, 2017.

[40] F. G. Kong, X. Jiang, R. Wang, S. Zhai, Y. Zhang, and D. Wang, "Forsythoside B attenuates memory impairment and neuroinflammation via inhibition on NF-κB signaling in Alzheimer's disease," *Journal of Neuroinflammation*, vol. 17, no. 1, pp. 1–15, 2020.

[41] Y. L. Zhou, Y. M. Yan, S. Y. Li et al., "6-O-angeloylplenolin exerts neuroprotection against lipopolysaccharide-induced neuroinflammation in vitro and in vivo," *Acta Pharmacologica Sinica*, vol. 41, no. 1, pp. 10–21, 2020.

[42] H. L. Yuan, B. Li, J. Xu et al., "Tenuigenin protects dopaminergic neurons from inflammation-mediated damage induced by the lipopolysaccharide," *CNS Neuroscience & Therapeutics*, vol. 18, no. 7, pp. 584–590, 2012.

[43] Y. Lv, Y. Qian, A. Ou-Yang, and L. Fu, "Hydroxysafflor yellow a attenuates neuron damage by suppressing the lipopolysaccharide-induced TLR4 pathway in activated microglial cells," *Cellular and Molecular Neurobiology*, vol. 36, no. 8, pp. 1241–1256, 2016.

[44] Y. Jiang, X. Wang, W. Yang, and S. Gui, "Procyanidin B2 suppresses lipopolysaccharides-induced inflammation and apoptosis in human type II alveolar epithelial cells and lung fibroblasts," *Journal of Interferon & Cytokine Research*, vol. 40, no. 1, pp. 54–63, 2019.

[45] L. Z. Gu and H. Sun, "Lonicerin prevents inflammation and apoptosis in LPS-induced acute lung injury," *Front Biosci (Landmark Ed)*, vol. 25, no. 3, pp. 480–497, 2020.

[46] B. W. Lee, J. H. Ha, H. G. Shin et al., "*Spiraea prunifolia var. simpliciflora* attenuates oxidative stress and inflammatory responses in a murine model of lipopolysaccharide-induced acute lung injury and TNF-α-stimulated NCI-H292 cells," *Antioxidants*, vol. 9, no. 3, p. 198, 2020.

[47] M. Mo, S. Li, Z. Dong et al., "S-allylmercaptocysteine ameliorates lipopolysaccharide-induced acute lung injury in mice by inhibiting inflammation and oxidative stress via nuclear factor kappa B and Keap1/Nrf2 pathways," *International Immunopharmacology*, vol. 1, no. 81, article 106273, 2020.

[48] X. N. Wu, Y. Yang, H. H. Zhang et al., "Robustaflavone-4'-dimethyl ether from *Selaginella uncinata* attenuated lipopolysaccharide-induced acute lung injury via inhibiting FLT3-mediated neutrophil activation," *International Immunopharmacology*, vol. 1, no. 82, article 106338, 2020.

[49] X. Wang, R. Deng, J. Dong, L. Huang, J. Li, and B. Zhang, "Eriodictyol ameliorates lipopolysaccharide-induced acute lung injury by suppressing the inflammatory COX-2/NLRP3/NF-κB pathway in mice," *Journal of Biochemical and Molecular Toxicology*, vol. 34, no. 3, article e22434, 2020.

[50] H. M. Abdallah, D. S. El-Agamy, S. R. Ibrahim et al., "*Euphorbia cuneata* represses LPS-induced acute lung injury in mice via its antioxidative and anti-inflammatory activities," *Plants*, vol. 9, p. 1620, 2020.

[51] J. W. Park, H. W. Ryu, H. I. Ahn et al., "The Anti-Inflammatory Effect of Trichilia martiana C. DC. in the Lipopolysaccharide-Stimulated Inflammatory Response in Macrophages and Airway Epithelial Cells and in LPS-Challenged Mice," *Journal of Microbiology and Biotechnology*, vol. 30, no. 11, pp. 1614–1625, 2020.

[52] D. de Sá Coutinho, J. Pires, H. Gomes et al., "Pequi (*Caryocar brasiliense* Cambess)-loaded nanoemulsion, orally delivered, modulates inflammation in LPS-induced acute lung injury in mice," *Pharmaceutics.*, vol. 12, no. 11, p. 1075, 2020.

[53] Y. Shen, N. Han, H. Chen, M. Zhang, and W. Cai, "Evaluation of lipopolysaccharide-induced acute lung injury attenuation in mice by Glycyrrhiza glabra," *Pharmacognosy Magazine*, vol. 16, no. 67, pp. 92–98, 2020.

[54] R. Badamjav, D. Sonom, Y. Wu et al., "The protective effects of *Thalictrum minus* L. on lipopolysaccharide-induced acute lung injury," *Journal of ethnopharmacology*, vol. 10, no. 248, article 112355, 2020.

[55] D. S. El-Agamy, G. A. Mohamed, N. Ahmed et al., "Protective anti-inflammatory activity of tovophyllin A against acute lung injury and its potential cytotoxicity to epithelial lung and breast carcinomas," *Inflammopharmacology*, vol. 28, pp. 153–163, 2020.

[56] B. Du, L. Cao, K. Wang et al., "Peiminine attenuates acute lung injury induced by LPS through inhibiting lipid rafts formation," *Inflammation*, vol. 43, pp. 1110–1119, 2020.

[57] A. Mokhtari-Zaer, F. Norouzi, V. R. Askari et al., "The protective effect of *Nigella sativa* extract on lung inflammation and oxidative stress induced by lipopolysaccharide in rats," *Journal of ethnopharmacology*, vol. 10, no. 253, article 112653, 2020.

[58] Q. Duan, Y. Jia, Y. Qin, Y. Jin, H. Hu, and J. Chen, "Narciclasine attenuates LPS-induced acute lung injury in neonatal rats through suppressing inflammation and oxidative stress," *Bioengineered*, vol. 11, no. 1, pp. 801–810, 2020.

[59] M. Chen, J. Li, X. Liu et al., "Chrysin prevents lipopolysaccharide-induced acute lung injury in mice by suppressing the IRE1α/TXNIP/NLRP3 pathway," *Pulmonary*

Pharmacology & Therapeutics, vol. 1, no. 68, article 102018, 2021.

[60] Y. Zhang, T. Zhao, H. Wang et al., "Effects of ergosterone on lipopolysaccharideinduced acute lung injury and nucleo side-binding oligomerization domain, leucine-rich repeats and pyrin domain containing protein 3 inflammatory signaling pathway in mice," *Materials Express.*, vol. 11, pp. 38–45, 2021.

[61] X. Wu, L. Lin, and H. Wu, "Ferulic acid alleviates lipopolysaccharide-induced acute lung injury through inhibiting TLR4/NF-κB signaling pathway," *Journal of Biochemical and Molecular Toxicology.*, vol. 35, no. 3, article e22664, 2021.

[62] X. Li, R. Huang, K. Liu et al., "Fucoxanthin attenuates LPS-induced acute lung injury via inhibition of the TLR4/MyD88 signaling axis," *Aging (Albany NY)*, vol. 13, no. 2, p. 2655, 2021.

[63] M. I. Bittencourt-Mernak, N. M. Pinheiro, R. C. da Silva et al., "Effects of Eugenol and Dehydrodieugenol B from *Nectandra leucantha* against Lipopolysaccharide (LPS)-Induced Experimental Acute Lung Inflammation," *Journal of natural products*, vol. 84, no. 8, pp. 2282–2294, 2021.

[64] C. P. Liu, J. X. Liu, J. Gu et al., "Combination effect of three main constituents from *sarcandra glabra* inhibits oxidative stress in the mice following acute lung injury: a role of MAPK-NF-κB pathway," *Frontiers in Pharmacology*, vol. 11, no. 11, article 580064, 2021.

[65] J. L. Huang, R. Z. Fan, Y. H. Zou, L. Zhang, S. Yin, and G. H. Tang, "Salviplenoid A from *Salvia plebeia* attenuates acute lung inflammation via modulating NF-κB and Nrf2 signaling pathways," *Phytotherapy Research*, vol. 35, no. 3, pp. 1559–1571, 2021.

[66] L. Yao, G. Hou, L. Wang, X. S. Zuo, and Z. Liu, "Protective effects of thymol on LPS-induced acute lung injury in mice," *Microbial Pathogenesis*, vol. 116, pp. 8–12, 2018.

[67] X. Feng and A. Jia, "Protective effect of carvacrol on acute lung injury induced by lipopolysaccharide in mice," *Inflammation*, vol. 37, no. 4, pp. 1091–1101, 2014.

[68] X. Zhang, L. Du, J. Zhang, C. Li, J. Zhang, and X. Lv, "Hordenine protects against lipopolysaccharide-induced acute lung injury by inhibiting inflammation," *Frontiers in Pharmacology*, vol. 12, article 712232, 2021.

[69] X. Ma, X. Li, Q. Di et al., "Natural molecule munronoid I attenuates LPS-induced acute lung injury by promoting the K48-linked ubiquitination and degradation of TAK1," *Biomedicine & Pharmacotherapy*, vol. 138, article 111543, 2021.

[70] S. Yang, G. Kuang, L. Zhang et al., "Mangiferin attenuates LPS/D-GalN-induced acute liver injury by promoting HO-1 in Kupffer cells," *Frontiers in Immunology*, vol. 11, p. 285, 2020.

[71] R. J. Zhou, Y. Zhao, K. Fan, and M. L. Xie, "Protective effect of apigenin on d-galactosamine/LPS-induced hepatocellular injury by increment of Nrf-2 nucleus translocation," *Naunyn-Schmiedeberg's Archives of Pharmacology*, vol. 393, no. 6, pp. 929–936, 2020.

[72] R. Yang, H. Yu, J. Chen et al., "Limonin attenuates LPS-induced hepatotoxicity by inhibiting pyroptosis via NLRP3/Gasdermin D signaling pathway," *Journal of Agricultural and Food Chemistry*, vol. 69, no. 3, pp. 982–991, 2021.

[73] M. S. Islam, H. Yu, L. Miao, Z. Liu, Y. He, and H. Sun, "Hepatoprotective effect of the ethanol extract of *Illicium henryi* against acute liver injury in mice induced by lipopolysaccharide," *Antioxidants (Basel)*, vol. 8, no. 10, 2019.

[74] H. Wang, L. Chen, X. Zhang et al., "Kaempferol protects mice from d-GalN/LPS-induced acute liver failure by regulating the ER stress-Grp78-CHOP signaling pathway," *Biomedicine & Pharmacotherapy*, vol. 111, pp. 468–475, 2019.

[75] Z. Li, H. Feng, L. Han et al., "Chicoric acid ameliorate inflammation and oxidative stress in Lipopolysaccharide and d-galactosamine induced acute liver injury," *Journal of Cellular and Molecular Medicine*, vol. 24, no. 5, pp. 3022–3033, 2020.

[76] H. Lv, B. An, Q. Yu, Y. Cao, Y. Liu, and S. Li, "The hepatoprotective effect of myricetin against lipopolysaccharide and D-galactosamine-induced fulminant hepatitis," *International Journal of Biological Macromolecules*, vol. 155, pp. 1092–1104, 2020.

[77] S. Sae-Tan, T. Kumrungsee, and N. Yanaka, "Mungbean seed coat water extract inhibits inflammation in LPS-induced acute liver injury mice and LPS-stimulated RAW 246.7 macrophages via the inhibition of TAK1/IκBα/NF-κB," *Journal of Food Science and Technology*, vol. 57, no. 7, pp. 2659–2668, 2020.

[78] S. M. Mohamadi-Zarch, T. Baluchnejadmojarad, D. Nourabadi, A. M. Khanizadeh, and M. Roghani, "Protective effect of diosgenin on LPS/D-Gal-induced acute liver failure in C57BL/6 mice," *Microbial pathogenesis*, vol. 1, no. 146, article 104243, 2020.

[79] B. Liu, Y. Lu, X. Chen et al., "Protective role of shiitake mushroom-derived exosome-like nanoparticles in D-galactosamine and lipopolysaccharide-induced acute liver injury in mice," *Nutrients*, vol. 12, no. 2, p. 477, 2020.

[80] A. M. Rousta, S. M. Mirahmadi, A. Shahmohammadi, S. Ramzi, T. Baluchnejadmojarad, and M. Roghani, "S-allyl cysteine, an active ingredient of garlic, attenuates acute liver dysfunction induced by lipopolysaccharide/d-galactosamine in mouse: Underlying mechanisms," *Journal of Biochemical and Molecular Toxicology*, vol. 34, no. 9, article e22518, 2020.

[81] N. Ahmed, D. S. El-Agamy, G. A. Mohammed, H. Abo-Haded, M. Elkablawy, and S. R. Ibrahim, "Suppression of LPS-induced hepato- and cardiotoxic effects by *Pulicaria petiolaris* via NF-κB dependent mechanism," *Cardiovascular Toxicology*, vol. 20, no. 2, pp. 121–129, 2020.

[82] X. Peng, Y. Yang, L. Tang et al., "Therapeutic benefits of apocynin in mice with lipopolysaccharide/D-galactosamine-induced acute liver injury via suppression of the late stage pro-apoptotic AMPK/JNK pathway," *Biomedicine & Pharmacotherapy*, vol. 125, article 110020, 2020.

[83] B. H. Kim, S. H. Jung, and S. Jung, "Beet root (Beta vulgaris) protects lipopolysaccharide and alcohol-induced liver damage in rat," *Toxicology Research*, vol. 36, no. 3, pp. 275–282, 2020.

[84] M. H. Al-Dossari, L. M. Fadda, H. A. Attia, I. H. Hasan, and A. M. Mahmoud, "Curcumin and selenium prevent lipopolysaccharide/diclofenac-induced liver injury by suppressing inflammation and oxidative stress," *Biological Trace Element Research*, vol. 196, no. 1, pp. 173–183, 2020.

[85] Z. Doğanyiğit, A. Okan, E. Kaymak, D. Pandır, and S. Silici, "Investigation of protective effects of apilarnil against lipopolysaccharide induced liver injury in rats via TLR 4/HMGB-1/ NF-κB pathway," *Biomedicine & Pharmacotherapy*, vol. 125, article 109967, 2020.

[86] Y. Swarnalatha, S. U. Sivakkumar, and S. Siddharthan, "Protective role of heptamethoxyflavone on LPS-induced hepatotoxicity," *Toxin Reviews*, vol. 41, no. 1, pp. 100–107, 2022.

[87] S. M. Mohamadi-Zarch, T. Baluchnejadmojarad, D. Nourabadi, S. Ramazi, M. Nazari-Serenjeh, and M. Roghani, "Esculetin Alleviates Acute Liver Failure following Lipopolysaccharide/D-Galactosamine in Male C57BL/6 Mice," *Iranian Journal of Medical Sciences*, vol. 46, no. 5, pp. 373–382, 2021.

[88] C. Qi, L. Li, G. Cheng et al., "*Platycodon grandiflorus* polysaccharide with anti-apoptosis, anti-oxidant and anti-inflammatory activity against LPS/D-GalN induced acute liver injury in mice," *Journal of Polymers and the Environment*, vol. 29, no. 12, pp. 4088–4097, 2021.

[89] M. Berköz, S. Ünal, F. Karayakar et al., "Prophylactic effect of myricetin and apigenin against lipopolysaccharide-induced acute liver injury," *Molecular Biology Reports*, vol. 48, no. 9, pp. 6363–6373, 2021.

[90] A. A. Sayed, A. M. Ali, and G. M. Bekhet, "The protective effect of garden cress *lepidium sativum* against lipopolysaccharide (LPS) induced hepatotoxicity in mice model," *Indian Journal of Animal Research*, vol. 55, no. 9, pp. 1065–1071, 2021.

[91] A. Nabil-Adam and M. A. Shreadah, "Red algae natural products for prevention of lipopolysaccharides (LPS)-induced liver and kidney inflammation and injuries," *Bioscience Reports*, vol. 41, no. 1, 2021.

[92] F. Beheshti, M. Hosseini, M. Taheri Sarvtin, A. Kamali, and A. Anaeigoudari, "Protective effect of aminoguanidine against lipopolysaccharide-induced hepatotoxicity and liver dysfunction in rat," *Drug and Chemical Toxicology*, vol. 44, no. 2, pp. 215–221, 2021.

[93] K. Phasanasophon and S. M. Kim, "Anti-inflammatory activity of the phlorotannin Trifuhalol A using LPS-stimulated RAW264.7 cells through NF-κB and MAPK Main signaling pathways," *Natural Product Communications*, vol. 14, no. 5, p. 1934578X19849798, 2019.

[94] M. M. Leya and R. Anitha, "Anti-inflammatory Effect of the Aqueous Fruit Pulp Extract of Tamarindus indica Linn in Lipopolysaccharide-Stimulated Macrophages," *Pharmacognosy Journal*, vol. 11, no. 4, 2019.

[95] N. H. Dang, L. T. Anh, and N. T. Dat, "Anti-inflammatory effects of essential oils of *Amomum aromaticum* fruits in lipopolysaccharide-stimulated RAW264. 7 cells," *Journal of Food Quality*, vol. 2020, Article ID 8831187, 5 pages, 2020.

[96] L. Song, C. Kang, Y. Sun, W. Huang, W. Liu, and Z. Qian, "Crocetin inhibits lipopolysaccharide-induced inflammatory response in human umbilical vein endothelial cells," *Cellular Physiology and Biochemistry*, vol. 40, no. 3-4, pp. 443–452, 2016.

[97] R.-Y. Huang, Y.-L. Yu, W.-C. Cheng, C. N. OuYang, E. Fu, and C. L. Chu, "Immunosuppressive effect of quercetin on dendritic cell activation and function," *The Journal of Immunology*, vol. 184, no. 12, pp. 6815–6821, 2010.

[98] S.-W. Seo, "The anti-inflammatory effect of Portulaca oleracea 70% EtOH extracts on lipopolysaccharide-induced inflammatory response in RAW 264.7 cells," *The Korea Journal of Herbology*, vol. 30, no. 6, pp. 33–38, 2015.

[99] R. Zhao, T. Zhang, H. Zhao, and Y. Cai, "Effects of *Portulaca oleracea* L. polysaccharides on phenotypic and functional maturation of murine bone marrow derived dendritic cells," *Nutrition and Cancer*, vol. 67, no. 6, pp. 987–993, 2015.

[100] M. El Gazzar, "Thymoquinone suppressses *in vitro* production of IL-5 and IL-13 by mast cells in response to lipopolysaccharide stimulation," *Inflammation Research*, vol. 56, no. 8, pp. 345–351, 2007.

[101] N. T. Xuan, E. Shumilina, S. M. Qadri, F. Götz, and F. Lang, "Effect of thymoquinone on mouse dendritic cells," *Cellular Physiology and Biochemistry*, vol. 25, no. 2-3, pp. 307–314, 2010.

[102] M. Huo, X. Cui, J. Xue et al., "Anti-inflammatory effects of linalool in RAW 264.7 macrophages and lipopolysaccharide-induced lung injury model," *Journal of Surgical Research*, vol. 180, no. 1, pp. e47–e54, 2013.

[103] C. V. Chandrasekaran, K. Sundarajan, J. R. Edwin, G. M. Gururaja, D. Mundkinajeddu, and A. Agarwal, "Immune-stimulatory and anti-inflammatory activities of *Curcuma longa* extract and its polysaccharide fraction," *Pharmacognosy Research*, vol. 5, no. 2, pp. 71–79, 2013.

[104] Z. Hu, R. Du, L. Xiu et al., "Protective effect of triterpenes of *Ganoderma lucidum* on lipopolysaccharide- induced inflammatory responses and acute liver injury," *Cytokine*, vol. 127, article 154917, 2020.

Hindawi
Oxidative Medicine and Cellular Longevity
Volume 2023, Article ID 9291417, 14 pages
https://doi.org/10.1155/2023/9291417

Research Article

Effect of Administration of an Equal Dose of Selected Dietary Chemicals on Nrf2 Nuclear Translocation in the Mouse Liver

Nadia Salem Alrawaiq,[1,2] **Ahmed Atia**,[1,3] **and Azman Abdullah**[1]

[1]*Department of Pharmacology, Faculty of Medicine, Universiti Kebangsaan Malaysia, Jalan Yaacob Latif, 56000 Cheras, Kuala Lumpur, Malaysia*
[2]*Department of Pharmacology, Faculty of Pharmacy, Sebha University, Sebha, Libya*
[3]*Department of Anaesthesia and Intensive Care, Faculty of Medical Technology, Tripoli University, Tripoli, Libya*

Correspondence should be addressed to Azman Abdullah; azman.abdullah@ppukm.ukm.edu.my

Received 4 August 2022; Revised 5 October 2022; Accepted 6 October 2022; Published 10 April 2023

Academic Editor: Daniel Dias Rufino Arcanjo

Certain dietary chemicals influenced the expression of chemopreventive genes through the Nrf2-Keap1 pathway. However, the difference in Nrf2 activation potency of these chemicals is not well studied. This study is aimed at determining the difference in the potency of liver Nrf2 nuclear translocation induced by the administration of equal doses of selected dietary chemicals in mice. Male ICR white mice were administered 50 mg/kg of sulforaphane, quercetin, curcumin, butylated hydroxyanisole, and indole-3-carbinol for 14 days. On day 15, the animals were sacrificed, and their livers were isolated. Liver nuclear extracts were prepared, and Nrf2 nuclear translocation was detected through Western blotting. To determine the implication of the Nrf2 nuclear translocation on the expression levels of several Nrf2-regulated genes, liver RNA was extracted for qPCR assay. Equal doses of sulforaphane, quercetin, curcumin, butylated hydroxyanisole, and indole-3-carbinol significantly induced the nuclear translocation of Nrf2 with different intensities and subsequently increased the expression of Nrf2-regulated genes with an almost similar pattern as the Nrf2 nuclear translocation intensities (sulforaphane > butylated hydroxyanisole = indole-3-carbinol > curcumin > quercetin). In conclusion, sulforaphane is the most potent dietary chemical that induces the Nrf2 translocation into the nuclear fraction in the mouse liver.

1. Introduction

Aerobic organisms are constantly producing reactive oxygen species (ROS), such as superoxide, hydrogen peroxide, and hydroxyl free radicals, as a natural by-product of oxygen metabolism. Free radicals are molecules with one or more unpaired electrons. Free radicals cause damage when they react with other molecules to find electrons to pair with their unpaired electrons. The other molecules then lost their electrons, causing them to become free radicals themselves, thus creating a chemical chain reaction of free radical production [1]. Oxidative stress is a condition that occurs when there is an imbalance between the production and accumulation of free radicals (reactive oxygen species) in the living system and the ability of the living system to detoxify these reactive products [2]. Oxidative stress in the body due to pollutants, xenobiotics, and certain foods can expedite the formation of free radicals. The free radical chain reaction may cause damage to cellular homeostasis due to its potential in causing alterations in the lipid, protein, and DNA structure. The damaged molecules may initiate mutation and growth of tumours [1]. Reactive oxygen species (ROS) play an essential role in cell signaling and homeostasis. However, high levels of ROS are responsible for various medical conditions, including ageing, cancer, inflammation, and chronic illnesses [1]. Therefore, exogenous antioxidants from the chemicals in foods have been used to prevent or repair the oxidative damage caused by ROS [3]. Another way to protect against oxidative damage is perhaps to increase the production of endogenous antioxidant/phase II detoxifying enzymes via the activation of the antioxidant signaling route [4].

Several dietary compounds are recognized as potential agents that interfere with disease processes. Certain vegetables and fruits, such as broccoli, blueberries, and cacao beans, are known to be especially highly protective as they contain excessive amounts of phytochemicals such as isothiocyanates, polyphenols, and flavonoids [5]. Upon entry to cells, these phytochemicals can directly hunt down free radicals and can also activate electrophilic stress signals that stimulate various cellular signaling pathways, such as the Keap1-Nrf2/ARE pathway which induces the expression of cytoprotective phase II proteins [4]. The nuclear erythroid 2-related factor 2 (Nrf2) is a transcription factor that protects against oxidative stress [6]. The Keap1-Nrf2 signaling pathway comprises the Kelch-like ECH-associating protein 1 (Keap1), Nrf2, and the antioxidant responsive element (ARE) cis-acting element. This pathway serves as a master oxidation-reduction system, which protects cells from injury and death [7].

In the absence of stress, Keap1 is an E3 ubiquitin ligase substrate adaptor that targets Nrf2 for rapid proteasomal degradation, which results in a limited cytoplasmic concentration of Nrf2 [8]. When exposed to electrophiles or oxidative stress, several highly reactive cysteine residues of Keap1 are modified to prevent it from targeting Nrf2 for proteasome degradation, resulting in rapid accumulation of Nrf2 proteins, which translocate into the nucleus and undergo dimerization with small musculoaponeurotic fibrosarcoma (sMaf) proteins, which are then able to target genes coding for a wide range of cytoprotective enzymes, such as antioxidant enzymes, that have ARE (antioxidant response elements) elements in their regulatory regions [9]. Intracellular endogenous antioxidant genes, such as NAD(P)H: quinone oxidoreductase-1 (NQO1), superoxide dismutase (SOD), heme oxygenase-1 (HO-1), glutathione s-transferases (GST), and γ-glutamylcysteine synthetase (γ-GCS) also called glutamate cysteine ligase (GCL), catalase(-CAT), etc., are increased to maintain homeostasis [10].

Nrf2 induced the expression of many detoxification phase II enzyme genes such as glutamate cysteine ligase catalytic subunit (GCLC), catalase (CAT), and glutathione peroxidase-1 (GPX1), which are reported in this study, and the function of these phase II enzymes is mainly to metabolize harmful carcinogens to inert metabolites, which could prevent the formation of cancer. This concept is known as cancer chemoprevention [11]. The expression of many phase II enzymes is regulated by the transcription factor Nrf2 [12]. Phase II enzymes are important for cellular defence by enhancing the removal of toxic metabolites and free radicals, thereby playing a possible protective role against the development of cancer and other diseases, which is an integral component of cancer chemoprevention [11]. The redox-sensitive transcription factor Nrf2 mediates cellular defence against chemical and oxidative stress. Oxidative, chemical, and electrophilic stresses lead to Nrf2 activation and nuclear translocation, which in turn upregulates the expression of several antioxidant defence genes and various phase II detoxifying enzymes, which detoxifies any potential carcinogen thus preventing the formation of cancer [11, 13, 14]. Therefore, in healthy mice (and most possibly in healthy individuals), activation of the Nrf2 pathway by administration of dietary supplements would upregulate the expression of antioxidant proteins and phase II detoxifying enzymes, thus potentially hindering any opportunity for cancer initiation.

Phytochemicals such as sulforaphane (SUL), curcumin (CUR), quercetin (QRC), and indole 3 carbinol (I3C) have been shown to activate the Nrf2 pathway in the livers of animals such as rats and mice [15–20] (Table 1). We have previously shown that the treatment of mice with equal dose (50 mg/kg body weight) of SUL, CUR, QRC, I3C, and BHA for 14 days resulted in different patterns of expression of phase II enzymes regulated by Nrf2 such as NQO1 and HO-1 in the liver [21, 22]. At a dose of 50 mg/kg body weight for 14 days, administration of SUL resulted in the highest NQO1 expressional level in the liver, followed by I3C and BHA (equal expression level), QRC, and CUR [21]. Also, at the same dose of 50 mg/kg, SUL administration resulted in the highest level of expression of HO-1 in the mouse liver, followed by I3C and BHA (equal expression level), CUR, and QRC (lowest expression) [22].

Sulforaphane is a potent Nrf2 inducer that could increase the expression of many cytoprotective enzymes. The central carbon of its electrophilic isothiocyanate group (–N=C=S) reacts with nitrogen-, sulfur-, and oxygen-based nucleophiles [23–25]. It is postulated that the central carbon of the isothiocyanate (–N=C=S) group of sulforaphane is highly electrophilic and reacts avidly with sulfhydryl groups. The highly electrophilic nature of the central carbon atom of the isothiocyanate (–N=C=S) group is likely to induce Nrf2 transcriptional activity through its modification of specific Keap1 cysteine thiols [24–26].

Curcumin exerts both direct and indirect antioxidant effects by scavenging ROS and inducing the expression of cytoprotective proteins in an Nrf2-dependent way [20]. ROS scavenging capacity of curcumin (direct antioxidant effect) is mainly attributed to its structure as a bis-α,β-unsaturated-diketone of the two ferulic acid units, connected through a methylene group. The direct scavenging of radicals and other reactive oxygen species is due to the presence of two phenolic functional groups and the β-diketo moiety in curcumin, which is known as the Michael acceptor group [27].

Quercetin is an example of a dietary chemical that requires electrophilic conversion for inducer activity. ROS (e.g., $O_2^{\cdot}$–) and reactive nitrogen species (RNS) (e.g., NO and ONOO–) are the primary targets of quercetin [28]. The presence of two pharmacophores within the quercetin molecule (characterized by the optimal configuration for free radical scavenging, i.e., the catechol group in the B ring and the OH group at position 3) configures quercetin antioxidant capacity. Quercetin is considered a weak electrophile due to the electron-donating effect of the 3-hydroxyl group and both aromatic rings. Quercetin is oxidized to a quinone when serving as an antioxidant, and such quinones react with thiols [29]. Quercetin is oxidized in the body to become a more electrophilic quinone methide [30]. Quinone methide is much more reactive toward thiolates. Therefore, researchers postulated that free radical-oxidized quercetin

Table 1: Dietary chemicals used in this study.

Dietary chemicals	Structure	Functional group	Source
Sulforaphane (SUL)	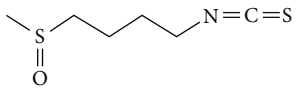	Isothiocyanate	Broccoli 
Curcumin (CUR)	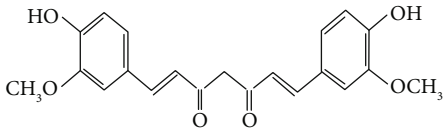	α,β-Unsaturated carbonyl (good Michael acceptor), 1,2-diphenol	Turmeric 
Quercetin (QRC)	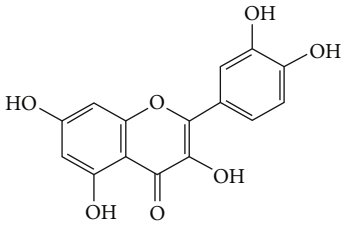	B ring *o*-dihydroxyl groups, the 4-oxo group in conjugation with the 2,3-alkene, and the 3-hydroxyl group	Onions, apples 
Butylated hydroxyanisole (BHA)	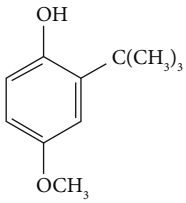	Methoxyphenol	Preservative in fats, foods, and cosmetics 
Indole-3-carbinol (I3C)	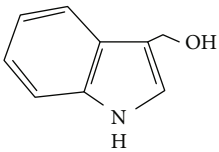	Indoles	Cabbage family 

reacts with thiols in Keap1, thus causing Nrf2 nuclear translocation and transcriptional regulation of antioxidant-responsive genes.

I3C and its metabolite 3,3′-diindolylmethane (DIM) cause Nrf2 induction and many other cancer chemopreventive effects [18]. DIM, a major metabolite of I3C, is primarily responsible for the chemopreventive activity of I3C [18]. Interestingly, DIM, but not I3C, was detected in human plasma samples following supplementation with I3C [31]. DIM was found to be more effective in inducing the Nrf2-Keap1 activity compared to I3C.

Commonly added as an additive to preserve oils and fats, butylated hydroxyanisole (BHA) is a synthetic phenolic antioxidant. BHA is widely used as an antioxidant and preservative in food, food packaging, and medicines (Table 1). It is subjected to O-dealkylation by cytochrome P450 isozymes in the liver to produce tert-butylhydroquinone (TBHQ) which further breaks down into tert-butylquinone (TBQ), which are prooxidants [32, 33]. The chemopreventive effect of BHA is mediated mainly by its reactive metabolites THBQ and TBQ. Its chemopreventive properties are attributed to its ability to activate Nrf2, which regulates the bodily processes of detoxification and protection against oxidative stress [34].

The transcription factor nuclear factor-κB (NF-κB) is responsible for the expression of various genes involved in multitude cellular processes such as apoptosis, cell cycle, angiogenesis, and metastasis. A large number of NF-κB target genes are involved in innate immune response, inflammation, and cancer, which includes cytokines, chemokines, proteases, NOS2, and COX2 [25]. In conditions related to oxidative stress, the presence of ROS can both activate and repress the NF-κB signaling in a phase- and context-dependent manner. The NF-κB pathway can have both anti- and prooxidant roles in the setting of oxidative stress [35].

Previous cellular-based and animal studies have indicated that SUL, CUR, QRC, I3C, and BHA are involved in the chemoprevention of liver malignancy [24, 34, 36–39].

It was also evident from the results of our lab that the administration of equal doses of different chemicals to mice resulted in different patterns of expressions of certain phase II enzymes regulated by Nrf2 in the liver. However, the reasons behind the difference in expressions are not clear. Therefore, this study is aimed at investigating whether the difference in phase II enzymes expression pattern is due to the difference in Nrf2 translocation into the nuclear fraction of the liver, despite the same dose of chemicals being administered to the animals [21, 22]. It would also be pertinent to investigate whether the different patterns of expression of phase II enzymes are influenced by the difference in the intensity of Nrf2 expression levels in the nuclear fractions of the liver induced by equal doses of dietary chemicals with different structural properties.

In most tissues, cells are exposed to frequent changes in levels of oxidative stress and inflammation. Oxidative stress and inflammation can trigger a multitude of cellular response through a variety of signaling pathways [40]. Nrf2 and NF-κB are the two key transcription factors that regulate cellular response to oxidative stress and inflammation, respectively. Pharmacological and genetic studies suggest that there is functional cross-talk between these two important pathways [41]. The deficiency of Nrf2 elevates the expression of NF-κB, leading to increased production of inflammatory factors [42]. Additionally, NF-κB could influence the expression of downstream target genes by regulating the transcription and activity of Nrf2. A large number of hepatoprotective reagents have been shown to activate the Nrf2-related gene expression and suppressed NF-κB expression [41]. Some phase II antioxidant genes possess binding sites for NF-κB in their regulatory element region [43–45]. With regard to these aspects, apart from Nrf2 nuclear translocation, we also investigated whether NF-κB is translocated into the liver nuclear fraction and affect the expression of our genes of interest.

2. Materials and Methods

2.1. Chemicals and Materials. Butylated hydroxyanisole (BHA), indole-3-carbinol (I3C), quercetin (QRC), curcumin (CUR), Tween 20, dimethylsulfoxide (DMSO), and sodium chloride were purchased from Sigma-Aldrich (Seelze, Germany). Sulforaphane (SUL) was purchased from Santa Cruz Biotechnology (Santa Cruz County, California, USA). TRIzol reagent was manufactured by Life Technologies (Carlsbad, California, USA). iScript cDNA synthesis kit, iQ SYBR Green supermix (2×) kit, and MJ Mini thermal cycler were purchased from Bio-Rad (Hercules, California, USA). Real-time PCR primers were synthesized by Vivantis Technologies (Oceanside, California, USA). Chemiluminescence Western blotting detection reagents were bought from Amersham (Uppsala, Sweden). Nitrocellulose membrane and Ponceau red dye absolute solution were purchased from Sigma-Aldrich (Seelze, Germany). Primary polyclonal rabbit anti-mouse β-actin antibody was purchased from Abcam Biotech (Cambridge, UK). Primary polyclonal rabbit anti-mouse Nrf2, primary polyclonal rabbit anti-mouse NF-κB-p50, primary polyclonal rabbit anti-mouse histone H3 antibodies, and RIPA lysis buffer were purchased from Santa Cruz Biotechnology (Dallas, Texas, USA). Anti-rabbit IgG peroxidase secondary antibody was purchased from Santa Cruz Biotechnology (Dallas, Texas, USA). All other chemicals were manufactured by Sigma-Aldrich unless otherwise stated.

2.2. Experimental Animals. Experimental animals used in this study were adult male ICR white mice obtained from the Universiti Kebangsaan Malaysia (UKM) Laboratory Animal Research Unit (LARU). Forty-two eight-week-old adult ICR male white mice (25-30 g) were used. Male mice were chosen in this study because their livers are larger than female mice. Furthermore, male mice are not subjected to oestrous cycles that can complicate the pharmacological studies of rodents. Most animal pharmacology/toxicology studies have been performed with male mice due to the fact that female mice undergo oestrous cycles that could create a tremendous amount of variability in experimental results [22]. The animals were treated after a period acclimatization of seven days at room temperature and relative humidity of 28.5°C and 50%, respectively. Mice were kept in conventional mouse cages at room temperature with a 12-hour light-dark cycle and fed with a standard pelletized diet (Gold Coin, Selangor, Malaysia) with tap water given ad libitum. The composition of the standard pelletized diet is given in Table 2. The standard pelletized food has been shown to be suitable for the growth of mice [46, 47]. The health of the animals was monitored daily by observing their behaviours and by measuring their body weight. Animals were maintained and handled according to the recommendations from the UKM Animal Ethics Committee (UKMAEC) which had approved the study design of the experiment (Approval Code: FP/FAR/2012/AZMAN/23-MAY/442-JUNE-2012-JUNE-2015).

2.3. Study Design. Forty-two male adult ICR white mice were divided into 7 groups (vehicle 1 control, vehicle 2 control, SUL, CUR, QRC, BHA, and I3C; $n = 6$ for each group). All chemicals were administered intraperitoneally at a dose of 50 mg/kg body weight for 14 days. Vehicle 1 (DMSO, Tween 20, and normal saline in the ratio of 0.05 : 0.1 : 0.85) was used to dissolve sulforaphane (SUL), curcumin (CUR), and quercetin (QRC) and was administered alone to the vehicle control 1 mouse group. Vehicle 2 (corn oil) which was used to dissolve butylated hydroxyanisole (BHA) and indole-3-carbinol (I3C) was administered alone to the vehicle control 2 mouse group. The chemicals were administered intraperitoneally (i.p.) at a dose of 50 mg/kg body weight for 14 consecutive days. In many previous studies (cited in Reference [22]), the dose of 50 mg/kg of several phytochemicals (SFN, indole-3-carbinol, quercetin, and curcumin) was effective in inducing several important antioxidant enzyme expressions. In a number of studies [21, 22, 48–50], two or more phytochemicals were given at a dose of 50 mg/kg in order to compare which phytochemical is more potent in producing positive health-protective effects. Therefore, the dose of 50 mg/kg was chosen in this current study because we wanted to observe which phytochemical is the most

Table 2: Composition of standard pelletized diet (Gold Coin, Malaysia).

Composition	Amount/percentage
Crude protein	20%
Crude fibre (max)	5.0%
Crude fat (min)	2.5%
Moisture (max)	13.0%
Calcium	0.7-1.4%
Phosphorus	0.6–1.0%
Nitrogen-free extract	49.0%
Vitamin A	10 M.I.U
Vitamin D_3	2.5 M.I.U
Vitamin E	15 g
Vitamin B_1, vitamin B_2, vitamin B_3, vitamin B_5, vitamin B_6, vitamin B_{12}, vitamin K, choline, Santoquin, microminerals	Trace amounts

potent in inducing Nrf2 translocation and subsequently Nrf2-regulated gene expression, at that particular dose. The other reason we chose to give the dietary chemicals in terms of mg/kg body weight is to mimic the drug dosage given to humans, which is usually in terms of mg/kg. The animals were sacrificed by cervical dislocation once the 14-day treatment period was completed. The mice were not subjected to fasting before being sacrificed. Their livers were subsequently isolated, cleaned, snapped frozen in liquid nitrogen, and stored at -70°C until further use.

2.4. Nuclear Extract Preparation. Nuclear extracts from mouse liver tissues were prepared according to a procedure previously described by Atia et al. with slight adjustments [13]. Briefly, 100 mg of liver tissue was homogenized in 1 ml of cold buffer A [50 mM NaCl, 10 mM Hepes pH 8, 1 mM EDTA, 0.5 mM sucrose, 0.5 mM spermidine, 0.15 mM spermine, and 0.2% Triton X-100 (v/v)] at 4°C. The resulting homogenate was incubated on ice for 10 min and was subsequently subjected to centrifugation at 2500 g for 5 min at 4°C. The resulting supernatant (cytosolic fraction) was transferred into new microcentrifuge tubes and kept in -80°C until further use. The pellet was suspended in 0.5 ml of buffer B [2.5 mM NaCl, 0.5 mM Hepes–KOH, 0.05 mM EDTA, 0.025 mM spermidine, 0.075 mM spermine, and 25% glycerol] followed by centrifugation for 3 min at 1200 g at 4°C. The supernatant was discarded, and the pellet was resuspended in 50 μl of cold buffer C [17.5 mM NaCl, 0.5 mM Hepes–KOH, 0.05 mM EDTA, 0.025 mM spermidine, 0.075 mM spermine, 25% glycerol, 0.4 mM PMSF, 4.5 μl protease inhibitor cocktail in DMSO, and 0.6 mM 2-mercaptoethanol]. The suspension was then incubated on ice for 30 min and was subsequently centrifuged for 5 min at 1200 g at 4°C. The resulting supernatant (nuclear extract) was transferred into new microcentrifuge tubes and kept in storage at −80°C until further use.

2.5. Determination of Nrf2 Nuclear Translocation by Western Blot Analysis. Hepatic Nrf2 nuclear translocation and the expression levels of other proteins of interest in the nuclear and cytoplasmic fractions of the liver were determined using a previously described immunoblotting method [51]. Briefly, 100 μg of liver protein (either from the nuclear or cytosolic fractions) was separated using 15% sodium dodecyl sulfate polyacrylamide gel (SDS-PAGE) electrophoresis. The proteins in the gel were then electrophoretically transferred to a nitrocellulose membrane. The membrane was then blocked at room temperature for 30 min using nonfat milk blocking solution. After blocking, the membrane was incubated with a primary antibody. The primary antibodies used in this experiment were those that recognized Nrf2, NF-κB, and histone H3. After several washing steps, the membrane was incubated for 1 hour with a suitable secondary antibody. After another series of washing steps, the membrane was incubated with a detection solution. Protein bands were visualized using the enhanced chemiluminescence method. The intensity of the protein bands was quantified, relative to the signals obtained for housekeeping protein (histone H3 for the nuclear fraction and β-actin for the cytoplasmic fraction), using ImageJ software.

2.6. RNA Extraction. For the determination of gene expression levels, total RNA was isolated from liver tissues using TRIzol reagent, according to the manufacturer's instructions. Isopropyl alcohol (Sigma, USA) was added during each extraction step to precipitate the total RNA. The extracted total RNA pellet was then washed with 75% ethanol and dried before being dissolved in RNase-free water. Total RNA was stored at -80°C immediately after isolation. The concentration and purity of the extracted RNA were determined by NanoDrop spectrophotometer 2000c (Thermo Scientific, USA) at a wavelength of 260 nm (OD260). RNA with RNA integrity number (RIN) ranging from 7 to 10 and absorbance ratio of A260 to A280 ranging from 1.5 to 2.0 was used for cDNA synthesis.

2.7. Reverse Transcription. cDNA synthesis was performed using the iScript cDNA synthesis kit according to the manufacturer's instructions. Briefly, a volume (containing 1 μg) of total RNA from each sample was added to a mixture of 4 μl of 5× iScript reaction mix, 1 μl of iScript reverse transcriptase, and a suitable volume of nuclease-free water (the final reaction mix volume is 20 μl). The final reaction mixture was kept at 25°C for 5 min and 42°C for 30 min and heated to 85°C for 5 min in a thermocycler (TC-412, Techne, Barloworld Scientific, UK). The cDNA was then used as a template for amplification by polymerase chain reaction (PCR).

2.8. Quantification of Glutamate Cysteine Ligase Catalytic Subunit (GCLC), Catalase (CAT), and Glutathione Peroxidase-1 (GPX1) Gene Expression by Quantitative Real-Time PCR (qPCR). Quantitative real-time PCR was performed on the MiniOpticon cycler (Bio-Rad, USA). The total reaction volume used was 20 μl, consisting of 1 μl of 10 μM forward primer and 1 μl of 10 μM reverse primer

Table 3: Oligonucleotide sequences used for real-time PCR reactions.

Gene	Primer sequences	Reference
GADPH	F: 5′-GTGGAGTCTACTGGTGTCTTCA-3′ R: 5′-TTGCTGACAATCTTGAGTGAGT-3′	Kong et al. [53]
GCLC	F: 5′-GCACGGCATCCTCCAGTTCCT-3′ R: 5′-TCGGATGGTTGGGGTTTGTCC-3′	Leung et al. [54]
CAT	F: 5′-GTGCGGACATTCTACACAAAGG-3′ R: 5′-GAACATTGCCGGCCACC-3′	Lu et al. [55]
GPX1	F: 5′-AGTCCACCGTGTATGCCTTCT-3′ R: 5′-GAGACGCGCGACATTCTCAATGA-3′	Nakamura et al. [56]

F: forward primer; R: reverse primer.

(500 nM final concentration of each primer), 10.0 μl of iQ™ SYBRTM Green Supermix (2×) (Bio-Rad, USA), 6.0 μl of nuclease-free water, and 2.0 μl of cDNA. Both forward and reverse primers for the genes of interest in this study were designed according to previous studies and synthesized by Vivantis Technologies (Oceanside, CA, USA). The primer sequences for our genes of interest are shown in Table 3. The thermocycling conditions were initiated at 95°C for 30 sec, followed by 40 PCR cycles of denaturation at 95°C for 15 sec and annealing/extension at 60°C for 30 sec. At the end of each cycle, a melting curve (dissociation stage) analysis was performed to determine the specificity of the primers and the purity of the final PCR product. All measurements were performed in triplicate, and no-template controls (NTC) were incorporated into the same set of PCR tubes to test for contamination by any assay reagents. Threshold cycles were determined for each gene, and quantification of templates was performed according to the relative standard curve method. The relative gene expression (DDCt) technique was used to analyze the real-time PCR data [52]. In short, the expression level of each target gene was given as a relative amount against GAPDH standard controls.

2.9. Statistical Analysis. Data are presented as the mean ± standard error of the mean (SEM). All values to be compared were analyzed for normality using the Shapiro-Wilk test. The Mann–Whitney test was used where nonparametric analysis was indicated. Statistical analysis was conducted using the SPSS software version 22. Results were considered statistically significant when P values were less than 0.05 ($P < 0.05$).

3. Results

3.1. Body Weight and Food Intake of Mice. The body weight and food intake of mice in each group were recorded every two days in order to investigate whether equal doses (50 mg/kg) of SUL, BHA, I3C, CUR, and QRC treatment affect the body weight gain and food intake in the control and treated mice. In the control and 50 mg/kg SUL-, BHA-, I3C-, CUR-, and QRC-treated mice, the body weight was significantly higher after 14 days of treatment compared to the first day of treatment for all groups. There was no significant difference between the groups in terms of body weight at the end of the treatment period (day 14) (Table 4). Daily food consumption was consistent throughout the study period and was not significantly different between groups (Table 4).

3.2. The Difference in Hepatic Nuclear Nrf2 Translocation Induced by Equal Doses of Different Dietary Chemicals. Treatment of mice with an equal dose (50 mg/kg) of dietary chemicals (SUL, BHA, I3C, CUR, and QRC) for 14 days significantly increased Nrf2 band intensity levels in the nuclear fraction of the liver compared to mice in the control groups (Figure 1(a)). This was complemented by low Nrf2 band intensity levels in the cytoplasmic fraction (Figure 1(b)), indicating that Nrf2 has translocated into the nuclear fraction. Quantitative analysis of the band intensity levels obtained for Nrf2 in the nuclear fraction, as optimized to that of histone H3 bands, revealed that SUL, BHA, I3C, CUR, and QRC treatment produced a significant induction of Nrf2 protein expression in the nuclear fraction, compared to the control groups (2.5-, 2.0-, 2.0-, 1.5-, and 1.3-fold, respectively, as compared to controls; $P < 0.05$) (Figure 1). In the cytoplasmic fraction, the Nrf2 bands of the treatment groups looked very faint, suggesting that Nrf2 has translocated into the nuclear fraction. Quantitative analysis of the band intensity levels obtained for Nrf2 in the cytoplasmic fraction, as optimized to that of β-actin bands, showed that the expression levels of Nrf2 in the SUL, BHA, I3C, CUR, and QRC groups are similar to the control groups (1.0-fold for all groups). The Nrf2 expression levels are also not significantly different from the control groups (Figure 1). The ratios of Nrf2 expression between the nuclear and cytoplasmic fractions for SUL, BHA, I3C, CUR, and QRC are 2.5-, 2.0-, 2.0-, 1.5-, and 1.3, respectively. Therefore, the potency of the dietary chemicals in inducing Nrf2 translocation was in the order of SUL > BHA = I3C > CUR > QRC. The results suggested that treatment with dietary chemicals (SUL, BHA, I3C, CUR, and QRC) led to the translocation of Nrf2 protein from the cytosol to the nucleus in mouse liver with differing potencies (Figure 1).

3.3. Administration of SUL, BHA, I3C, CUR, and QRC Did Not Affect NF-κB Nuclear Translocation. To further investigate whether or not another oxidative stress-sensitive

Table 4: Body weight and food intake of control and treated mice.

Groups	Body weight		Daily food intake
	Day 1 (g)	Day 14 (g)	(g/b.w./day)
VH1	26.25 ± 0.48	29.72 ± 0.52*	4.27 ± 1.18
VH2	26.60 ± 0.50	29.75 ± 0.43*	4.33 ± 0.16
SUL	27.23 ± 0.73	30.03 ± 0.65*	4.62 ± 1.20
CUR	26.32 ± 0.28	29.50 ± 0.34*	4.25 ± 1.38
QRC	26.55 ± 0.27	29.55 ± 0.33*	4.71 ± 0.19
BHA	27.53 ± 0.71	30.63 ± 0.57*	4.56 ± 1.93
I3C	26.47 ± 0.48	29.55 ± 0.47*	4.53 ± 0.03

Values are given as the mean ± SEM ($n = 6$ mice in each group). Asterisk (*) denotes significant difference in body weight at day 1 vs. day 14 (Mann–Whitney test; $P < 0.05$). SUL: sulforaphane-treated group; CUR: curcumin; QRC: quercetin; BHA: butylated hydroxyanisole; I3C: indole-3-carbinol; VH1: control group treated with vehicle 1; VH2: control group treated with vehicle 2.

transcription factor apart from Nrf2 was activated by administration of different dietary chemicals, Western blot assays for the detection of NF-κB expression were performed in the nuclear and cytoplasmic fractions derived from liver homogenates of mice treated with equal doses (50 mg/kg) of SUL, BHA, I3C, CUR, and QRC. Our results showed that there was no obvious NF-κB induction or translocation in the liver nuclear fraction. The NF-κB expression can only be prominently detected in the liver cytosolic fractions of mice in the control and treated groups, implying that the different dietary chemicals are not a trigger of NF-κB activation in the liver (Figure 2).

3.4. The Different Patterns of Nrf2 Nuclear Translocation Induced by Different Dietary Chemicals Are Functionally Relevant In Vivo. GCLC, GPX1, and CAT have been known to be regulated by Nrf2 [13, 57]. In this study, the effects of administration of equal doses of several dietary chemicals on GCLC, GPX1, and CAT gene expression were determined. As shown in Figures 3(a), 3(b), and 3(c), administration of equal doses (50 mg/kg) of SUL, BHA, I3C, CUR, and QRC to mice resulted in a significant increase in the fold change of liver gene expression levels of GCLC (3.5-, 2.8-, 2.8-, 2.6-, and 2.5-fold, respectively, as compared to controls; $P < 0.05$), GPX1 (2.6-, 2.3-, 2.3-, 1.9-, and 1.9-fold, respectively, as compared to controls; $P < 0.05$), and CAT (2.9-, 2.6-, 2.6-, 2.5-, and 2.5-fold, respectively, as compared to controls; $P < 0.05$). The GCLC, GPX1, and CAT-inducing potency of the chemicals was therefore in the order of SUL > BHA = I3C > CUR > QRC. Therefore, the order of relative expression level for each of the three genes (GCLC, GPX1, and CAT) follows the order of relative change of nuclear fraction of their transcription factor Nrf2. Thus, the different patterns of expression of Nrf2-regulated genes seen in the liver, even though the same dose of SUL, BHA, I3C, CUR, and QRC was administered to the animals, provided additional evidence that the dietary chemicals have different potencies in inducing stabilization and translocation of Nrf2 protein into the nuclear fraction.

4. Discussion

The effect of administration of equal doses (50 mg/kg) of SUL, BHA, I3C, CUR, and QRC to mice on liver Nrf2 nuclear translocation is the main objective of this study. In this study, healthy mice were used as the experimental model in order to mimic the situation whereby healthy humans are taking dietary supplements to find out whether there are any beneficial health effects seen in this case. If the extent of Nrf2 nuclear translocation is significantly increased and the gene expression of antioxidant proteins is significantly enhanced after administration of dietary chemicals in healthy mice, it strongly suggests that the dietary chemicals have the property of being chemoprotective if the mice encounter any disease or exposed to environmental and oxidative stress, which could be extrapolated back to humans. Subsequently, it was found that administration of equal doses (50 mg/kg) of SUL, CUR, QRC, BHA, and I3C to mice significantly induced the translocation of Nrf2 into the nuclear fraction of the liver with differing intensities. The differing intensities of Nrf2 translocation subsequently resulted in the different levels of expression of Nrf2-regulated genes (GCLC, GPX1, and CAT), but with a similar pattern as the Nrf2 nuclear translocation intensities (i.e., SUL > BHA = I3C > CUR > QRC) (Figures 1 and 3). The similar relative intensity values (i.e., the value of 1) of Nrf2 expression in the cytoplasmic fraction between controls and treatment samples indicated that the low expression levels of Nrf2 in the cytoplasmic fraction are similar throughout for controls and samples, as indicated by the faint Nrf2 bands compared to β-actin bands (Figure 1).

Even though we administered SUL, CUR, QRC, BHA, and I3C through intraperitoneal administration, the metabolism of the dietary chemicals in the liver should occur after intraperitoneal administration of the chemicals and not only exclusively after oral consumption [58]. Intraperitoneal administration was performed to lessen the complications in the absorptions of the various dietary chemicals. Therefore, the results of our studies should be valid because the dietary chemicals are all on equal footing when it comes to absorption, in the sense that the complexities arising from the poor absorption of the chemicals due to gastrointestinal absorption after oral consumption are eliminated by giving intraperitoneal absorption. After being administered intraperitoneally, the chemicals will enter the mesenteric blood vessels in the peritoneum, which eventually goes to the portal vein of the liver, and in the liver, the various dietary chemicals will be metabolized to their active metabolites [58]. It is most likely that in the liver, BHA will be metabolized to tert-butylhydroquinone (TBHQ) and tert-butylquinone (TBQ), whereas I3C will be metabolized to 3,3′-diindolylmethane (DIM), for example.

Certain chemicals with prooxidant properties alter the redox state of target cells directly through the generation of moderate amounts of reactive oxygen species (ROS) which disrupts the affinity between Nrf2 and Keap1, subsequently resulting in Nrf2 nuclear translocation. With this regard, the capability of dietary chemicals to induce Nrf2-regulated gene expression correlates well with their prooxidant

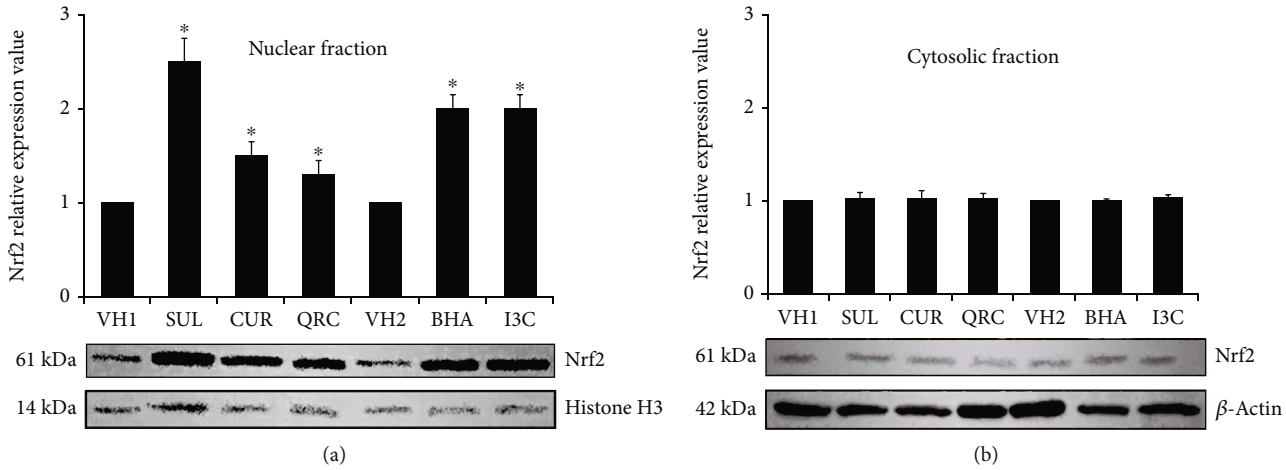

Figure 1: Administration of equal doses (50 mg/kg b.w.) of SUL, CUR, QRC, BHA, and I3C to mice for 14 days induces Nrf2 nuclear translocation in the liver *with different potencies*. (a) Nuclear fractions (100 μg) from each mouse were separated by electrophoresis, and the expressions of proteins were analyzed by Western blotting. Nrf2 is the protein of interest, while histone H3 is the housekeeping protein for the nuclear fraction. The bands for Nrf2 and histone H3 were densitometrically scanned, and the expression of nuclear Nrf2 (relative to histone) was determined as fold increase of the vehicle-treated (control) animals as shown in the bar chart above. (b) Cytoplasmic fractions (100 μg) from each mouse were separated by electrophoresis, and the expressions of proteins were analyzed by Western blotting. Nrf2 is the protein of interest, while β-actin is the housekeeping protein for the cytoplasmic fraction. The bands for Nrf2 and β-actin were densitometrically scanned, and the expression of Nrf2 in the nuclear fraction (relative to β-actin) was determined as fold increase of the vehicle-treated (control) animals as shown in the bar chart above. Values are expressed as the mean ± SEM ($n = 4$). Asterisk (∗) indicates a statistically significant difference from all control groups (vehicle 1 control and vehicle 2 control groups) after analysis using the Mann–Whitney test ($P < 0.05$). SUL: sulforaphane-treated group; CUR: curcumin-treated group; QRC: quercetin-treated group; BHA: butylated hydroxyanisole-treated group; I3C: indole 3 carbinol-treated group; VH1: control group treated with vehicle 1; VH2: control group treated with vehicle 2.

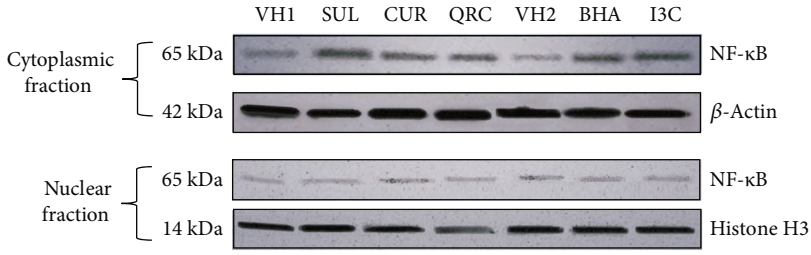

Figure 2: Administration of equal doses (50 mg/kg b.w.) of SUL, CUR, QRC, BHA, and I3C to mice for 14 days did not induce NF-κB nuclear translocation.

properties [10]. Such chemicals with prooxidant properties include tert-butylhydroquinone (TBHQ) and butylquinone (TBQ), which are phase I metabolites of BHA in the liver [32, 33]. These prooxidants oxidize Keap1 thiols and release Nrf2 from Keap1 binding. Nrf2 is then able to enter the nucleus and activates the expression of chemopreventive genes [59]. This suggests the important chemoprotective role of BHA against liver oxidative injury and liver cancer.

Sulforaphane most possibly activates Nrf2 via the formation of thionoacyl adducts with Keap1 to release Nrf2 [60]. Modification of the critical cysteine thiols (C38, C151, C368, C489, C77, C226, C319, and C434) of Keap1 resulted in Nrf2 being translocated to the nucleus and activates ARE-responsive genes [26]. Further detailed studies revealed that sulforaphane preferentially reacts with the thiol group of cysteine 151 on the surface of Keap1. Any mutation in cysteine 151 of Keap1 severely abolished the activity of sulforaphane [60]. The two Michael acceptor groups characterizing the curcumin can interact readily with cysteine sulfhydryl groups of Keap1 via Michael addition and change the conformation of Keap1-Nrf2 complex, thereby releasing Nrf2 and promoting its activity [61]. Curcumin had been shown to induce nuclear translocation of Nrf2 and upregulate the expression of cytoprotective enzymes in rats afflicted with acute liver injury, which implies its protective role in the chemoprevention of liver injury [61].

Quercetin promotes Nrf2 nuclear translocation, the binding activity of nuclear proteins to the ARE, and increased the Nrf2-mediated gene transcription [62, 63]. Quercetin upregulated Nrf2 translocation in rat intestinal epithelial IEC-6 cells. Quercetin administration increased Nrf2 nuclear translocation in broiler chickens (LPS-induced intestinal oxidative stress) and male Sprague-Dawley rats (cerebral ischemia-induced oxidative stress). The

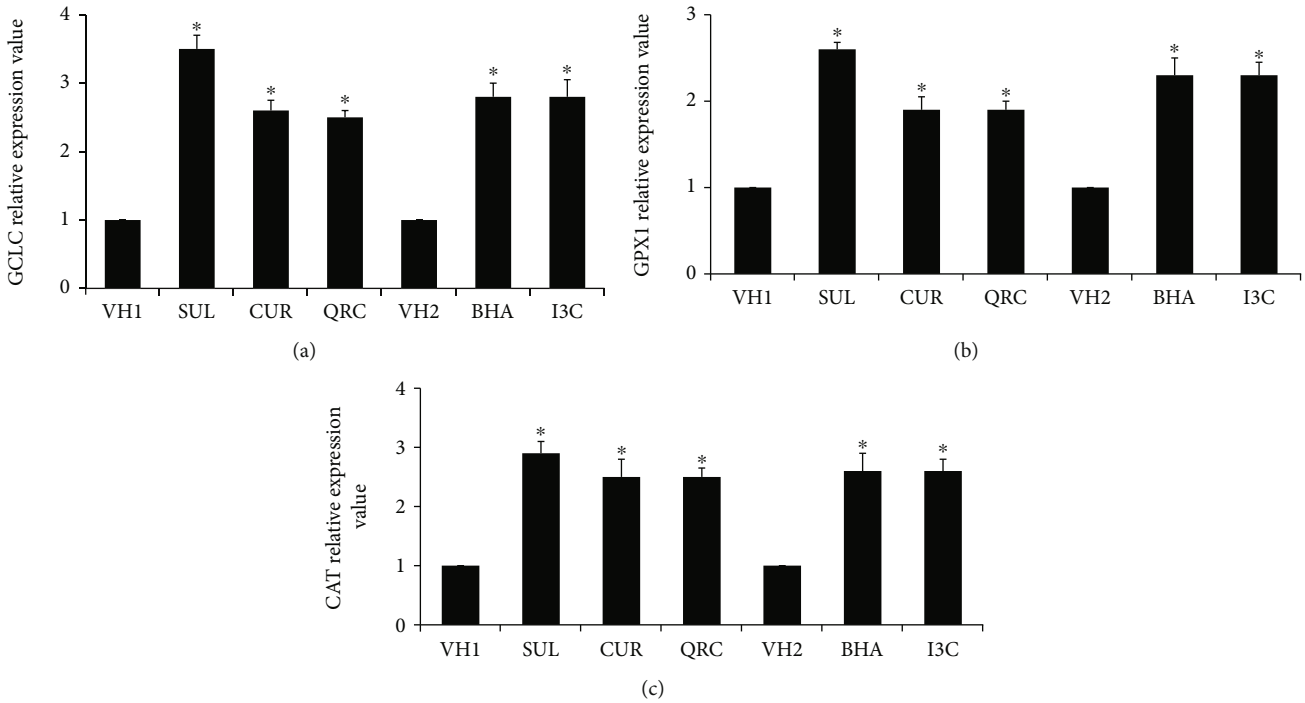

Figure 3: Effects of administration of 50 mg/kg SUL, CUR, QRC, BHA, and I3C for 14 days on (a) GCLC, (b) GPX1, and (c) CAT gene expressions in the livers of mice using RT-qPCR. GAPDH was designated as the reference gene. Data were represented as the mean ± SEM of six experiments, $n = 6$. Asterisk (∗) indicates a statistically significant difference compared to all control groups (vehicle 1 control and vehicle 2 control groups) after analysis using the Mann–Whitney test ($P < 0.05$). SUL: sulforaphane-treated group; CUR: curcumin-treated group; QRC: quercetin-treated group; BHA: butylated hydroxyanisole-treated group; I3C: indole 3 carbinol-treated group; VH1: control group treated with vehicle 1; VH2: control group treated with vehicle 2.

downstream activation of the Nrf2/ARE pathway upon Nrf2 nuclear translocation by quercetin has been demonstrated through the CAT gene overexpression (which is Nrf2-regulated) [62, 64]. Previous research has shown that quercetin increases the mRNA level of GCLC and stimulates the nuclear translocation of Nrf2 in neuronal cells [65]. There is also convincing evidence to show that quercetin can modestly increase Nrf2 nuclear translocation in human hepatocytes, possibly mediated by p38 and endoplasmic reticulum kinase [66]. These findings suggest that quercetin could play an important role in the chemoprotective actions against liver injury, disease, and malignancy. In the present study, I3C induced the translocation of Nrf2 into the nuclear fraction and increased the expression of several Nrf2-regulated genes in the mouse liver. Therefore, our result indicated that I3C possessed the ability to increase the expression of Nrf2-regulated genes. DIM (the major metabolite of I3C) induced Nrf2 transactivation and the expression of genes regulated by Nrf2 (γGCS, NQO1, and HO-1) [67]. DIM (and I3C) is a weaker Nrf2 agonist than SFN [67]. This result is similar to the result obtained in our present study.

Some of the Nrf2-regulated genes (such as HO-1 and GPX1) have binding sites for the oxidative stress-sensitive transcription factor nuclear factor-kappa-B (NF-κB) in their regulatory regions [43–45]. In this study, we investigated whether equal doses (50 mg/kg) of sulforaphane, curcumin, quercetin, BHA, and I3C induced the translocation of NF-κB into the nuclear fraction of the mouse liver with a similar pattern and intensity. The results of our study showed that equal doses of the aforementioned dietary chemicals inhibited the NF-κB translocation in the nuclear fraction (Figure 2).

Dietary glucosinolate derivatives inhibit NF-κB-mediated processes in vitro and in vivo. Glucosinolate derivatives (e.g., sulforaphane) are capable of inhibiting NF-κB-regulated pathways by blocking proinflammatory signals at various levels; however, the precise molecular mechanisms by which these interactions are exerted are still not clearly understood. Previous studies suggested that sulforaphane suppressed IKK/IkB phosphorylation, inhibited IκB and p65 NF-κB nuclear translocation, and downregulated the transcriptional activity of NF-κB, thus affecting the function of inflammatory mediators such as IL-6, iNOS, TNF-α, and COX-2 [24, 25, 68].

From the results of our study, it could be seen that curcumin was unable to induce NF-κB translocation into the nuclear fraction (Figure 2). This is in agreement with the results from previous studies which showed curcumin convincingly inhibited NF-κB activity in several cell types [69, 70]. The molecular mechanisms involved in the suppressive effects of flavonoids on NF-κB are currently unknown, but several possibilities have been postulated [71]. The flavonoid quercetin is one such agent and has been found to possess potent anti-inflammatory effects, due in part to its anti-NF-κB activity [72].

Our results indicated that butylated hydroxyanisole (BHA) caused inhibition of NF-κB protein (Figure 2). Our results agreed with previous findings showing that BHA

and its metabolite TBHQ suppressed NF-κB activation [73, 74]. Our present study indicates that I3C inhibited NF-κB protein expression. I3C and its metabolite DIM have been found to inhibit both inducible and constitutive NF-κB activation, suppressed the activation of IKK, and prevented the nuclear translocation of p65 NF-κB and NF-κB-dependent gene expression in myeloid and leukemia cells [75–77].

Since NF-κB nuclear translocation was inhibited in this study, it is therefore likely that the increased expression of phase II and antioxidant genes of interest in this study (GCLC, GPX1, and catalase) was most likely mediated by activation of Nrf2 observed in the mice administered with structurally diverse dietary chemicals (sulforaphane, curcumin, quercetin, BHA, and I3C), as indicated by an increased nuclear concentration of Nrf2 with different patterns according to each chemical characteristic. Indeed, studies have suggested that chemopreventive agents capable of inhibiting NF-κB translocation, especially those derived from dietary agents, hold great promise in the treatment and prevention of cancer [78].

Following the aforementioned discussion, it can be concluded that a panel of equal doses (50 mg/kg) of small molecules, mainly involving compounds belonging to different structural classes, e.g., α-β unsaturated carbonyls, isothiocyanates, flavonoid, and polyphenols, with differing oxidative or electrophilic properties, were found to activate Nrf2 at different potencies. The selection of small molecules was based on their electrophilic nature, as in the case of the α-β unsaturated carbonyl-containing compounds and isothiocyanates, or based on their potential chemical or enzymatic conversion to electrophiles, similar to that of the flavonoids and phenolic compounds (Table 1). Including other likely mechanisms such as phosphorylation of Nrf2, compounds in this study that were capable of activating Nrf2 are postulated to be those that can modify the Keap1 thiols or be converted to compounds capable of such modifications. The final result is the disruption of the Keap1-Nrf2 complex, most likely through interaction with the thiols present on Keap1. Further studies are needed to conclusively determine the detailed mechanisms of Nrf2 release from Keap1 binding. In our discussion above, we only postulated the possible mechanisms in which these dietary chemicals cause the release of Nrf2 from Keap1 binding. The verification of the postulated mechanisms in which the dietary chemicals react with Keap1 is beyond the scope of our study. Further studies are needed to conclusively determine the interaction mechanisms between the dietary chemicals and Keap1 that causes the release of Nrf2. However, our study is still novel in the sense that no previous study has measured the difference in the potency of different dietary chemicals in inducing Nrf2 translocation in the liver using in vivo mouse studies. Most other studies of similar nature have used either cells or cell lines [67].

Previous cellular-based and animal studies have indicated that SUL, CUR, QRC, I3C, and BHA are involved in the chemoprevention of liver malignancy [24, 34, 36–39]. Studies utilizing animal models and cell culture have indicated that SUL, CUR, QRC, I3C, and BHA are involved in the chemoprevention of liver malignancy [24, 34, 36–39]. SUL, CUR, QRC, I3C, and BHA have also been shown to activate the Nrf2 pathway in the livers of animals such as rats and mice [15–20]. However, no previous studies have been attempted to find which dietary chemical is the most potent in inducing Nrf2 translocation in the liver nuclear fraction in vivo, and therefore theoretically the most potent in the chemoprevention of liver malignancy. Our animal-based study has indeed shown that in the mouse liver, SUL is the most potent dietary chemical in inducing Nrf2 nuclear translocation, followed by BHA and I3C (equipotent), CUR, and QRC. Previously, SUL has been implicated in many cellular-based studies as one of the most potent naturally occurring inducers of phase II enzymes [67, 79], and this conclusion is further confirmed by our animal-based study. The electrophilic tuning ability of sulforaphane enables it to be the most efficient in enhancing Nrf2 activation compared to other dietary chemicals used in this current study [67]. However, it is still unclear whether the combination of SUL together with one or more of the other dietary chemicals (CUR, QRC, I3C, and BHA) would further increase Nrf2 activation and the induction of its downstream genes, thus providing superior cancer chemoprevention effect than SUL alone. Further studies are needed to confirm this possibility.

The different induction profiles of the downstream genes regulated by Nrf2 indicate the differences in the fundamental mechanism of actions of Nrf2, at least at the mRNA level. Some possible reasons for the variations could be (1) differences in the arrangements of the AREs existing in the promoters of Nrf2-regulated genes, (2) differences in the composition of the ARE binding complexes in terms of the identities and relative quantities of the proteins concerned, (3) the levels of expression of genes and proteins induced vary depending on the nature of chemicals that elicits the response, and (4) different chemicals might activate the MAPK/PKC pathways in different ways, all of which could affect Nrf2-ARE activation at various intensities or levels.

5. Conclusion

Our findings indicated equal doses (50 mg/kg) of SUL, CUR, QRC, BHA, and I3C induced liver Nrf2 nuclear translocation with different potencies. The results also showed that equal doses (50 mg/kg) of SUL, CUR, QRC, BHA, and I3C could elicit different patterns of Nrf2-dependent gene expression levels in the liver. Sulforaphane is the most potent Nrf2 inducer amongst the dietary chemicals studied. The diverse nature of Nrf2 activators implies that the activation of Nrf2 is perhaps due to the binding of electrophilic functional groups of the dietary chemicals to Keap1 thiols. Although Nrf2 activation is not the only mechanism of protection conferred by the dietary chemicals, it is perhaps one of the most important mechanisms involved. Therefore, increased dietary consumption of vegetables (e.g., broccoli, cabbages, and kale), fruits (e.g., apples, grapes, and berries), and spices (e.g., onions and turmeric) is potentially the most practical way to induce Nrf2 activation in the human body and to provide chemoprevention against liver malignancy through induction of phase II enzymes in the liver. In the

current study, we found that SUL is the most potent Nrf2 inducer, thus potentially and theoretically having the best cancer chemopreventive effect. However, the effect of the combination of SUL with other dietary chemicals has not been studied. It could be that the combination of SUL with one or more dietary chemicals would further enhance its cancer chemoprevention potency. Further studies are needed to confirm this possibility. Despite promising results in laboratory settings, the applicability of chemoprevention to human for any cancer has met with limited success largely due to inefficient systemic delivery and bioavailability of promising chemopreventive agents. We envision that nanoparticle-mediated delivery could be useful to limit the perceived toxicity and to enhance the bioavailability of the chemopreventive agents, and the concept of "nanochemoprevention" could be the way forward, where nanotechnology is incorporated for the enhancement of chemopreventive efficacy of agents. Neutraceutical-based supplements containing the dietary compounds used in this study, but formulated in such a way so as to have good oral absorption, should be the way forward for liver cancer chemoprevention. Clinical trials using nanoformulated potent Nrf2 activators in combination with standard treatments should be the focus of future research in liver cancer chemoprevention and treatment.

Data Availability

All data are available from the corresponding author under reasonable request.

Disclosure

The funders had no role in the design of the study; in the collection, analyses, or interpretation of data; in the writing of the manuscript; or in the decision to publish the results.

Conflicts of Interest

The authors declare no conflict of interest.

Acknowledgments

The authors would like to thank all the laboratory staff of the Pharmacology Department, Universiti Kebangsaan Malaysia (UKM), for their help and support throughout the length of this study. This research was funded by the Ministry of Higher Education Malaysia (grant number FRGS/1/2012/SKK03/UKM/02/2) and Universiti Kebangsaan Malaysia (UKM) (grant number UKM-GUP-2011-297).

References

[1] A. Abdullah, A. Atia, N. S. Alrawaiq, M. K. Yusof, and M. F. Rusli, "Palm Oil Tocotrienols in Cancer Chemoprevention and Treatment," in *Elaeis guineensis*, IntechOpen, 2021.

[2] G. Pizzino, N. Irrera, M. Cucinotta et al., "Oxidative Stress: Harms and Benefits for Human Health," *Oxidative Medicine and Cellular Longevity*, vol. 2017, Article ID 8416763, 13 pages, 2017.

[3] A. Galano, G. Mazzone, R. Alvarez-Diduk, T. Marino, J. R. Alvarez-Idaboy, and N. Russo, "Food antioxidants: chemical insights at the molecular level," *Annual Review of Food Science and Technology*, vol. 7, no. 1, pp. 335–352, 2016.

[4] J. H. Lee, T. O. Khor, L. Shu, Z. Y. Su, F. Fuentes, and A. N. T. Kong, "Dietary phytochemicals and cancer prevention: Nrf2 signaling, epigenetics, and cell death mechanisms in blocking cancer initiation and progression," *Pharmacology & Therapeutics*, vol. 137, no. 2, pp. 153–171, 2013.

[5] S. Patra, R. Nayak, S. Patro et al., "Chemical diversity of dietary phytochemicals and their mode of chemoprevention," *Biotechnology Reports (Amsterdam, Netherlands)*, vol. 30, article e00633, 2021.

[6] I. Bellezza, I. Giambanco, A. Minelli, and R. Donato, "Nrf2-Keap1 signaling in oxidative and reductive stress," *Biochimica et Biophysica Acta (BBA)-Molecular Cell Research*, vol. 1865, no. 5, pp. 721–733, 2018.

[7] S. Chirumbolo and G. Bjørklund, "Sulforaphane and 5-fluorouracil synergistically inducing autophagy in breast cancer: a possible role for the Nrf2-Keap1-ARE signaling?," *Food and Chemical Toxicology*, vol. 112, pp. 414-415, 2018.

[8] M. Yamamoto, T. W. Kensler, and H. Motohashi, "The KEAP1-NRF2 system: a thiol-based sensor-effector apparatus for maintaining redox homeostasis," *Physiological Reviews*, vol. 98, no. 3, pp. 1169–1203, 2018.

[9] N. Akino, O. Wada-Hiraike, H. Terao et al., "Activation of Nrf2 might reduce oxidative stress in human granulosa cells," *Molecular and Cellular Endocrinology*, vol. 470, pp. 96–104, 2018.

[10] Y. Zhou, Z. Jiang, H. Lu et al., "Recent advances of natural polyphenols activators for Keap1-Nrf2 signaling pathway," *Chemistry & Biodiversity*, vol. 16, no. 11, article e1900400, 2019.

[11] B. P. George, R. Chandran, and H. Abrahamse, "Role of phytochemicals in cancer chemoprevention: insights," *Antioxidants*, vol. 10, no. 9, p. 1455, 2021.

[12] V. Krajka-Kuźniak, J. Paluszczak, and W. Baer-Dubowska, "The Nrf2-ARE signaling pathway: an update on its regulation and possible role in cancer prevention and treatment," *Pharmacological Reports*, vol. 69, no. 3, pp. 393–402, 2017.

[13] A. Atia, N. S. Alrawaiq, and A. Abdullah, "Tocotrienols activate Nrf2 nuclear translocation and increase the antioxidant-related hepatoprotective mechanism in mice liver," *Current Pharmaceutical Biotechnology*, vol. 22, no. 8, pp. 1085–1098, 2021.

[14] B. Han, S. Li, Y. Lv et al., "Dietary melatonin attenuates chromium-induced lung injury via activating the Sirt1/Pgc-1α/Nrf2 pathway," *Food & Function*, vol. 10, no. 9, pp. 5555–5565, 2019.

[15] M. Iranshahy, M. Iranshahi, S. R. Abtahi, and G. Karimi, "The role of nuclear factor erythroid 2-related factor 2 in hepatoprotective activity of natural products: a review," *Food and Chemical Toxicology*, vol. 120, pp. 261–276, 2018.

[16] M. Russo, C. Spagnuolo, G. L. Russo et al., "Nrf2 targeting by sulforaphane: a potential therapy for cancer treatment," *Critical Reviews in Food Science and Nutrition*, vol. 58, no. 8, pp. 1391–1405, 2018.

[17] R. T. Ruhee, S. Ma, and K. Suzuki, "Protective effects of sulforaphane on exercise-induced organ damage via inducing antioxidant defense responses," *Antioxidants*, vol. 9, no. 2, p. 136, 2020.

[18] C. L.-L. Saw, M. Cintrón, T. Y. Wu et al., "Pharmacodynamics of dietary phytochemical indoles I3C and DIM: induction of Nrf2-mediated phase II drug metabolizing and antioxidant genes and synergism with isothiocyanates," *Biopharmaceutics & Drug Disposition*, vol. 32, no. 5, pp. 289–300, 2011.

[19] S. Lee, J. Lee, H. Lee, and J. Sung, "Relative protective activities of quercetin, quercetin-3-glucoside, and rutin in alcohol-induced liver injury," *Journal of Food Biochemistry*, vol. 43, no. 11, article e13002, 2019.

[20] M. H. Farzaei, M. Zobeiri, F. Parvizi et al., "Curcumin in liver diseases: a systematic review of the cellular mechanisms of oxidative stress and clinical perspective," *Nutrients*, vol. 10, no. 7, p. 855, 2018.

[21] N. S. Alrawaiq, A. Atia, and A. Abdullah, "The effect of administration of an equal dose of different classes of dietary chemicals on nqo1 expressional level in mice liver," *Pharmacophore*, vol. 8, no. 5, pp. 1–9, 2017.

[22] A. Abdullah, N. S. Alrawaiq, and A. Atia, "The effect of administration of an equal dose of different classes of phytochemicals on heme oxygenase-1 gene and protein expression in mice liver," *Asian Journal of Pharmaceutical and Clinical Research*, vol. 12, pp. 256–260, 2019.

[23] H. Liang and Q. Yuan, "Natural sulforaphane as a functional chemopreventive agent: including a review of isolation, purification and analysis methods," *Critical Reviews in Biotechnology*, vol. 32, no. 3, pp. 218–234, 2012.

[24] P. Soundararajan and J. S. Kim, "Anti-carcinogenic glucosinolates in cruciferous vegetables and their antagonistic effects on prevention of cancers," *Molecules*, vol. 23, no. 11, p. 2983, 2018.

[25] F. Fuentes, X. Paredes-Gonzalez, and A. N. T. Kong, "Dietary glucosinolates sulforaphane, phenethyl isothiocyanate, indole-3-carbinol/3,3'-diindolylmethane: antioxidative stress/inflammation, Nrf2, epigenetics/epigenomics and in vivo cancer chemopreventive efficacy," *Current pharmacology reports*, vol. 1, no. 3, pp. 179–196, 2015.

[26] C. Hu, A. L. Eggler, A. D. Mesecar, and R. B. van Breemen, "Modification of keap1 cysteine residues by sulforaphane," *Chemical Research in Toxicology*, vol. 24, no. 4, pp. 515–521, 2011.

[27] T. Ak and I. Gülçin, "Antioxidant and radical scavenging properties of curcumin," *Chemico-Biological Interactions*, vol. 174, no. 1, pp. 27–37, 2008.

[28] A. L. Eggler and S. N. Savinov, "Chemical and biological mechanisms of phytochemical activation of Nrf2 and importance in disease prevention," *Recent Advances in Phytochemistry*, vol. 43, pp. 121–155, 2013.

[29] A. W. Boots, G. R. M. M. Haenen, and A. Bast, "Health effects of quercetin: from antioxidant to nutraceutical," *European Journal of Pharmacology*, vol. 585, no. 2-3, pp. 325–337, 2008.

[30] H. Jacobs, M. Moalin, A. Bast, W. J. F. van der Vijgh, and G. R. M. M. Haenen, "An essential difference between the flavonoids monoHER and quercetin in their interplay with the endogenous antioxidant network," *PLoS One*, vol. 5, no. 11, article e13880, 2010.

[31] G. A. Reed, D. W. Arneson, W. C. Putnam et al., "Single-dose and multiple-dose administration of indole-3-carbinol to women: pharmacokinetics based on 3,3'-diindolylmethane," *Cancer Epidemiology, Biomarkers & Prevention*, vol. 15, no. 12, pp. 2477–2481, 2006.

[32] Y. Abiko, T. Miura, B. H. Phuc, Y. Shinkai, and Y. Kumagai, "Participation of covalent modification of Keap1 in the activation of Nrf2 by tert-butylbenzoquinone, an electrophilic metabolite of butylated hydroxyanisole," *Toxicology and Applied Pharmacology*, vol. 255, no. 1, pp. 32–39, 2011.

[33] A. T. Dinkova-Kostova and X. J. Wang, "Induction of the Keap1/Nrf2/ARE pathway by oxidizable diphenols," *Chemico-Biological Interactions*, vol. 192, no. 1-2, pp. 101–106, 2011.

[34] L. Luo, Y. Chen, D. Wu et al., "Butylated hydroxyanisole induces distinct expression patterns of Nrf2 and detoxification enzymes in the liver and small intestine of C57BL/6 mice," *Toxicology and Applied Pharmacology*, vol. 288, no. 3, pp. 339–348, 2015.

[35] K. Lingappan, "NF-κB in oxidative stress," *Current opinion in toxicology*, vol. 7, pp. 81–86, 2018.

[36] J. I. Okano, Y. Fujise, R. Abe, R. Imamoto, and Y. Murawaki, "Chemoprevention against hepatocellular carcinoma," *Clinical Journal of Gastroenterology*, vol. 4, no. 4, pp. 185–197, 2011.

[37] C. Gupta, D. N. Tripathi, A. Vikram, P. Ramarao, and G. B. Jena, "Quercetin inhibits diethylnitrosamine-induced hepatic preneoplastic lesions in rats," *Nutrition and Cancer*, vol. 63, no. 2, pp. 234–241, 2011.

[38] S. A. Darvesh, B. B. Aggarwal, and A. Bishayee, "Curcumin and liver cancer: a review," *Current Pharmaceutical Biotechnology*, vol. 13, no. 1, pp. 218–228, 2012.

[39] Y. Shukla, N. Kalra, S. Katiyar, I. A. Siddiqui, and A. Arora, "Chemopreventive effect of indole-3-carbinol on induction of preneoplastic altered hepatic foci," *Nutrition and Cancer*, vol. 50, no. 2, pp. 214–220, 2004.

[40] S. Li, P. Wu, B. Han et al., "Deltamethrin induces apoptosis in cerebrum neurons of quail via promoting endoplasmic reticulum stress and mitochondrial dysfunction," *Environmental Toxicology*, vol. 37, no. 8, pp. 2033–2043, 2022.

[41] M. Yan, W. Gao, L. Guo et al., "Dissecting the crosstalk between Nrf2 and NF-κB response pathways in drug-induced toxicity," *Frontiers in Cell and Developmental Biology*, vol. 9, 2021.

[42] X. Yang, Y. Fang, J. Hou et al., "The heart as a target for deltamethrin toxicity: inhibition of Nrf2/HO-1 pathway induces oxidative stress and results in inflammation and apoptosis," *Chemosphere*, vol. 300, article 134479, 2022.

[43] B. Chen, Z. Shen, D. Wu et al., "Glutathione peroxidase 1 promotes NSCLC resistance to cisplatin via ROS-induced activation of PI3K/AKT pathway," *BioMed Research International*, vol. 2019, Article ID 7640547, 12 pages, 2019.

[44] A. Jadhav, E. Torlakovic, and J. F. Ndisang, "Interaction among heme oxygenase, nuclear factor-kappaB, and transcription activating factors in cardiac hypertrophy in hypertension," *Hypertension*, vol. 52, no. 5, pp. 910–917, 2008.

[45] N. Sharma, E. J. Shin, D. T. Pham et al., "GPx-1-encoded adenoviral vector attenuates dopaminergic impairments induced by methamphetamine in GPx-1 knockout mice through modulation of NF-κB transcription factor," *Food and Chemical Toxicology*, vol. 154, article 112313, 2021.

[46] C. Choo, N. Y. Sulong, F. Man, and T. W. Wong, "Vitexin and isovitexin from the leaves of Ficus deltoidea with in-vivo α-glucosidase inhibition," *Journal of Ethnopharmacology*, vol. 142, no. 3, pp. 776–781, 2012.

[47] A. Atia, N. Alrawaiq, and A. Abdullah, "Food Consumption and Body Weight in Mice Treated with Palm Oil–Derived Tocotrienol Rich Fraction (TRF)," *International Journal of PharmTech Research*, vol. 9, no. 3, pp. 262–266, 2016.

[48] R. Domitrović, H. Jakovac, V. Vasiljev Marchesi et al., "Differential hepatoprotective mechanisms of rutin and quercetin in CCl_4-intoxicated BALB/cN mice," *Acta Pharmacologica Sinica*, vol. 33, no. 10, pp. 1260–1270, 2012.

[49] C. Girish, B. C. Koner, S. Jayanthi, K. Ramachandra Rao, B. Rajesh, and S. C. Pradhan, "Hepatoprotective activity of picroliv, curcumin and ellagic acid compared to silymarin on paracetamol induced liver toxicity in mice," *Fundamental & Clinical Pharmacology*, vol. 23, no. 6, pp. 735–745, 2009.

[50] G. H. Heeba, M. E. Mahmoud, and A. A. Hanafy, "Anti-inflammatory potential of curcumin and quercetin in rats: role of oxidative stress, heme oxygenase-1 and TNF-α," *Toxicology and Industrial Health*, vol. 30, pp. 551–560, 2014.

[51] A. Atia, N. Salem AlRawaiq, and A. Abdullah, "The effect of tocotrienol-rich fraction on the expression of glutathione S-transferase isoenzymes in mice liver," *Sains Malaysiana*, vol. 47, no. 11, pp. 2799–2809, 2018.

[52] K. J. Livak and T. D. Schmittgen, "Analysis of relative gene expression data using real-time quantitative PCR and the $2^{-\Delta\Delta C_T}$ method," *Methods*, vol. 25, no. 4, pp. 402–408, 2001.

[53] L. Kong, M. Tanito, Z. Huang et al., "Delay of photoreceptor degeneration in tubby mouse by sulforaphane," *Journal of Neurochemistry*, vol. 101, no. 4, pp. 1041–1052, 2007.

[54] L. Leung, M. Kwong, S. Hou, C. Lee, and J. Y. Chan, "Deficiency of the Nrf1 and Nrf2 transcription factors results in early embryonic lethality and severe oxidative stress," *The Journal of Biological Chemistry*, vol. 278, no. 48, pp. 48021–48029, 2003.

[55] H. Lu, V. Koshkin, E. M. Allister, A. V. Gyulkhandanyan, and M. B. Wheeler, "Molecular and metabolic evidence for mitochondrial defects associated with beta-cell dysfunction in a mouse model of type 2 diabetes," *Diabetes*, vol. 59, no. 2, pp. 448–459, 2010.

[56] B. N. Nakamura, G. Lawson, J. Y. Chan et al., "Knockout of the transcription factor NRF2 disrupts spermatogenesis in an age-dependent manner," *Free Radical Biology & Medicine*, vol. 49, no. 9, pp. 1368–1379, 2010.

[57] C. Tonelli, I. I. C. Chio, and D. A. Tuveson, "Transcriptional regulation by Nrf2," *Antioxidants & Redox Signaling*, vol. 29, no. 17, pp. 1727–1745, 2018.

[58] O. A. Almazroo, M. K. Miah, and R. Venkataramanan, "Drug metabolism in the liver," *Clinics in Liver Disease*, vol. 21, no. 1, pp. 1–20, 2017.

[59] T. Satoh, S. R. McKercher, and S. A. Lipton, "Nrf2/ARE-mediated antioxidant actions of pro-electrophilic drugs," *Free Radical Biology & Medicine*, vol. 65, pp. 645–657, 2013.

[60] T. W. Kensler, P. A. Egner, A. S. Agyeman et al., "Keap1-nrf2 signaling: a target for cancer prevention by sulforaphane," *Topics in Current Chemistry*, vol. 329, pp. 163–177, 2013.

[61] M. Rahban, M. Habibi-Rezaei, M. Mazaheri, L. Saso, and A. A. Moosavi-Movahedi, "Anti-viral potential and modulation of Nrf2 by curcumin: pharmacological implications," *Antioxidants*, vol. 9, no. 12, p. 1228, 2020.

[62] T. L. Suraweera, H. P. V. Rupasinghe, G. Dellaire, and Z. Xu, "Regulation of Nrf2/ARE pathway by dietary flavonoids: a friend or foe for cancer management?," *Antioxidants*, vol. 9, no. 10, p. 973, 2020.

[63] S. Tanigawa, M. Fujii, and D. X. Hou, "Action of Nrf2 and Keap1 in ARE-mediated NQO1 expression by quercetin," *Free Radical Biology & Medicine*, vol. 42, no. 11, pp. 1690–1703, 2007.

[64] L. Sun, G. Xu, Y. Dong, M. Li, L. Yang, and W. Lu, "Quercetin protects against lipopolysaccharide-induced intestinal oxidative stress in broiler chickens through activation of Nrf2 pathway," *Molecules*, vol. 25, no. 5, p. 1053, 2020.

[65] F. Arredondo, C. Echeverry, J. A. Abin-Carriquiry et al., "After cellular internalization, quercetin causes Nrf2 nuclear translocation, increases glutathione levels, and prevents neuronal death against an oxidative insult," *Free Radical Biology & Medicine*, vol. 49, no. 5, pp. 738–747, 2010.

[66] P. Yao, A. Nussler, L. Liu et al., "Quercetin protects human hepatocytes from ethanol-derived oxidative stress by inducing heme oxygenase-1 via the MAPK/Nrf2 pathways," *Journal of Hepatology*, vol. 47, no. 2, pp. 253–261, 2007.

[67] I. Ernst, C. Schuemann, A. E. Wagner, and G. Rimbach, "3,3'-Diindolylmethane but not indole-3-carbinol activates Nrf2 and induces Nrf2 target gene expression in cultured murine fibroblasts," *Free Radical Research*, vol. 45, no. 8, pp. 941–949, 2011.

[68] H. Wang, T. Oo Khor, L. Shu et al., "Plants vs. cancer: a review on natural phytochemicals in preventing and treating cancers and their druggability," *Anti-Cancer Agents in Medicinal Chemistry*, vol. 12, no. 10, pp. 1281–1305, 2012.

[69] H. Zhou, C. S. Beevers, and S. Huang, "The targets of curcumin," *Current Drug Targets*, vol. 12, no. 3, pp. 332–347, 2011.

[70] P. Liczbiński, J. Michałowicz, and B. Bukowska, "Molecular mechanism of curcumin action in signaling pathways: review of the latest research," *Phytotherapy Research*, vol. 34, no. 8, pp. 1992–2005, 2020.

[71] G. Martínez, M. R. Mijares, and J. B. de Sanctis, "Effects of flavonoids and its derivatives on immune cell responses," *Recent Patents on Inflammation & Allergy Drug Discovery*, vol. 13, no. 2, pp. 84–104, 2019.

[72] S. Ghafouri-Fard, H. Shoorei, A. Khanbabapour Sasi, M. Taheri, and S. A. Ayatollahi, "The impact of the phytotherapeutic agent quercetin on expression of genes and activity of signaling pathways," *Biomedicine & Pharmacotherapy*, vol. 141, article 111847, 2021.

[73] J. A. Blanchard, S. Barve, S. Joshi-Barve, R. Talwalker, and L. K. Gates, "Antioxidants inhibit cytokine production and suppress NF-kappaB activation in CAPAN-1 and CAPAN-2 cell lines," *Digestive Diseases and Sciences*, vol. 46, no. 12, pp. 2768–2772, 2001.

[74] J. Bai, X. J. Yu, K. L. Liu et al., "Tert-butylhydroquinone attenuates oxidative stress and inflammation in hypothalamic paraventricular nucleus in high salt-induced hypertension," *Toxicology Letters*, vol. 281, pp. 1–9, 2017.

[75] Y. Takada, M. Andreeff, and B. B. Aggarwal, "Indole-3-carbinol suppresses NF-kappaB and IkappaBalpha kinase activation, causing inhibition of expression of NF-kappaB-regulated antiapoptotic and metastatic gene products and enhancement of apoptosis in myeloid and leukemia cells," *Blood*, vol. 106, no. 2, pp. 641–649, 2005.

[76] F. H. Sarkar, Y. Li, Z. Wang, and D. Kong, "Cellular signaling perturbation by natural products," *Cellular Signalling*, vol. 21, no. 11, pp. 1541–1547, 2009.

[77] N. Saini, A. Akhtar, M. Chauhan, N. Dhingra, and S. Pilkhwal Sah, "Protective effect of indole-3-carbinol, an NF-κB inhibitor in experimental paradigm of Parkinson's disease: in silico and in vivo studies," *Brain, Behavior, and Immunity*, vol. 90, pp. 108–137, 2020.

[78] H. P. Glauert, "Role of NF-κB in hepatocarcinogenesis and its potential inhibition by dietary antioxidants," *Current Cancer Drug Targets*, vol. 12, no. 9, pp. 1160–1172, 2012.

[79] K. C. Wu, P. McDonald, J. Liu, and C. D. Klaassen, "Screening of natural compounds as activators of the keap1-nrf2 pathway," *Planta Medica*, vol. 80, no. 1, pp. 97–104, 2014.

Hindawi
Oxidative Medicine and Cellular Longevity
Volume 2023, Article ID 8475995, 10 pages
https://doi.org/10.1155/2023/8475995

Research Article

Antimicrobial Activities and Biopreservation Potential of Lactic Acid Bacteria (LAB) from Raw Buffalo (*Bubalus bubalis*) Milk

Muhammad Saleem Kalhoro,[1] **Anil Kumar Anal**,[1] **Dildar Hussain Kalhoro**,[2] **Tarique Hussain**,[3] **Ghulam Murtaza**,[4] **and Mazhar Hussain Mangi**[5]

[1]*Food Engineering and Bioprocess Technology, Department of Food, Agriculture & Bioresources, Asian Institute of Technology, P.O. Box 4, Pathumthani 12120, Thailand*
[2]*Department of Veterinary Microbiology, Faculty of Animal Husbandry and Veterinary Sciences, Sindh Agriculture University, Tandojam 70060, Pakistan*
[3]*Animal Sciences Division, Nuclear Institute for Agriculture and Biology (NIAB), P.O. Box 128, Jhang Road, Faisalabad, Pakistan*
[4]*Department of Animal Reproduction, Faculty of Animal Husbandry and Veterinary Sciences, Sindh Agriculture University, Tandojam 70060, Pakistan*
[5]*Key Laboratory of Animal Epidemiology and Zoonosis, Ministry of Agriculture, National Animal Transmissible Spongiform Encephalopathy Laboratory, College of Veterinary Medicine, China Agricultural University, Beijing 100193, China*

Correspondence should be addressed to Muhammad Saleem Kalhoro; saleemkalhoro@yahoo.com

Received 7 October 2022; Revised 7 December 2022; Accepted 23 January 2023; Published 7 February 2023

Academic Editor: Amjad Islam Aqib

The aim of this study was to investigate the antimicrobial and biopreservation potential of lactic acid bacteria. The potential probiotic culture inhibited the growth of gram-positive and gram-negative foodborne pathogens in agar spot assay with inhibition zones ranging from 10 to 21 mm in diameter. The strains showed coaggregation capabilities ranging from 7 to 71% with tested food pathogens including *Escherichia coli*, *Staphylococcus aureus*, *Listeria monocytogenes*, and *Salmonella enterica* subsp. *enterica* serovar Typhimurium. The effect of cell-free supernatants on the release of 260 nm absorbing material, especially nucleic acids, was evaluated and indicated the antagonistic activity on foodborne pathogens, the highest being *Lactobacillus paraplantarum* against *E. coli* (3.77) and *S. aureus* (3.86) after 60 min. The effect of cell-free supernatant (CFS) on the growth of pathogens showed that *Lactobacillus paraplantarum* 11 and *L. pentosus* 93 had the highest inhibitory activity against tested strains. The biopreservation assay indicated that the potential probiotic strains *Lactobacillus paraplantarum* 11 (BT), *Lactiplantibacillus plantarum* 19, *Lactobacillus pentosus* 42, *Limosilactobacillus fermentum* 60, *Lactobacillus pentosus* 93, and *Limosilactobacillus reuteri* 112 were effective in reducing the *Listeria monocytogenes* population in raw buffalo milk. Complete *Listeria monocytogenes* inhibition was observed after 6-8 days. This study showed that probiotic LAB from buffalo milk have antimicrobial and biopreservation potential; these strains have the potential to be utilized as biopreservative agents in food products.

1. Introduction

Food spoilage by microorganisms leads to significant economic losses as well as health problems [1]. Foodborne pathogens are a threat to food quality and result in several diseases and disorders such as respiratory infections, inflammatory diseases, intestinal disorders, and cancer [2]. In recent years, there has been growing interest in alternative natural ways to control food spoilage due to the harmful effects of artificial chemicals and antimicrobial resistance [3]. The prevention of food spoilage by using biopreservative agents such as probiotics and their antimicrobial compounds is a satisfactory alternative approach to prevent spoilage without altering the taste and smell of food products [4].

The lactic acid bacteria (LAB), considered potential probiotic candidates, are the diverse group of gram-positive, non-spore-forming, catalase and cytochrome oxidase negative, and nonmotile bacteria, which produce lactic acid as a product of fermentation [5, 6]. The basic criteria for the LAB strains to be used as probiotics include the following: (1) they should have GRAS status, (2) they should be resistant to low pH and high bile concentration and survive in gastrointestinal fluids, (3) they should have adhesion characteristics, (4) they should have antibacterial characteristics against enteric pathogens, and (5) they should survive and be viable during the processing and storage [7]. There are different sources of LAB such as fermented meat, fish, milk, cheese, and herbs [1, 8–11].

The LAB are associated with several health benefits such as improvement of gastrointestinal tract conditions, antibacterial and antifungal activities, antiallergic and antioxidant properties, and lowering cholesterol levels and immunomodulatory activities [12, 13]. The LAB produce their antimicrobial activity through the reduction of pathogen translocation, inhibition of pathogen adherence, and production of antimicrobial compounds [14]. Antimicrobial compounds produced by lactic acid bacteria include organic acids, hydrogen peroxide, diacetyl, and bacteriocins, which can inhibit the growth of bacteria as well as fungi [11, 14].

Increased outbreaks of foodborne diseases in recent years along with antimicrobial resistance of pathogens against commercial antibiotics [8] demand greater interest and need for natural alternative ways to control foodborne pathogens. Lactic acid bacteria and their antimicrobial metabolites can inhibit foodborne pathogens and act as natural biopreservatives. Very limited studies have been reported on biopreservative potential of the probiotics from buffalo milk and their antimicrobial metabolites [11, 13]. Therefore, the present study was undertaken to characterize the antimicrobial activity of probiotic LAB isolated from raw buffalo milk and to evaluate their biopreservation potential.

2. Materials and Methods

2.1. Indicator Pathogenic Strains. *Bacillus cereus* (ATCC 11778), *Bacillus subtilis* (*ATCC 6633*), *Escherichia coli* (ATCC 25922), *Enterococcus faecalis* (ATCC 19433), *Listeria monocytogenes* (*ATCC 19115*), *Listeria innocua* (ATCC 33090), *Salmonella enterica* subsp. *enterica* serovar Enteritidis (ATCC 13076), *Salmonella enterica* subsp. *enterica* serovar Typhimurium (ATCC 13311), *Shigella dysenteriae* (ATCC 11835), *Staphylococcus aureus* (*ATCC 25923*), and *Pseudomonas aeruginosa* (ATCC 27853) were used as pathogenic indicator strains.

2.2. Probiotic Strains. *Lactobacillus paraplantarum* 11 (BT), *Lactiplantibacillus plantarum* 19, *Lactobacillus pentosus* 42, *Limosilactobacillus fermentum* 60, *Lactobacillus pentosus* 93, and *Limosilactobacillus reuteri* 112, which were previously isolated from buffalo milk were used as probiotic strains in this study [11, 13]. The strains were preserved in 20% glycerol and resuscitated in MRS broth.

2.3. Antibacterial Activity of Live Probiotic Culture. Antibacterial activity against foodborne pathogens was evaluated through the agar spot method as a previously described method [15] with slight modifications. The cell culture of potential probiotic strains was spotted (5 μL) on MRS agar plates and incubated at 37°C for 48 h. The plates were overlaid with 10 mL of BHI soft agar (0.75% agar) which was previously inoculated with pathogens (10^4 CFU/mL). The diameter of the inhibition zone was measured after incubation at 37°C for 24 h.

2.4. Coculture of Isolated Probiotics with Test Foodborne Pathogens. The coculture of probiotic strains with foodborne pathogens was determined as the previously described method [16] with slight modifications. The cell culture (500 μL) of each potential probiotic and pathogenic strain was mixed (1 : 1) and incubated at 37°C for 24 h. The total plate count of indicator pathogenic strains was performed on selective agar medium (MacConkey agar for *E. coli* and Baird Parker agar for *Staphylococcus aureus*). The monoculture of pathogenic and probiotic strains was grown at 37°C for 24 h, and the total plate count was performed on selective medium, which was used as control.

2.5. Evaluation of Coaggregation of Isolated Probiotics with Test Pathogens. The coaggregation activity was evaluated as the previously described method [17] with slight modifications. Cell culture (500 μL) of probiotic and pathogenic strains were mixed and incubated at 37°C for 24 h. The absorbance (A600nm) of the mixture and each culture probiotic and pathogenic strain alone was measured through Uv-Vis spectrophotometer (UV-1800, Shimadzu, Japan).

The coaggregation percentage was calculated by the following equation:

$$[(\text{Apat} + \text{Aprobio})/2 - (\text{Amix})]/(\text{Apat} + \text{Aprobio})/2 \times 100\%, \quad (1)$$

where Apat = absorbance (A600nm) of pathogen, Aprobio = absorbance (A600nm) of probiotic, and Amix = absorbance (A600nm) of mixture.

2.6. Effect of Cell-Free Supernatant on Releasing the Cellular Materials. The effect of cell-free supernatant (CFS) on the release of cellular materials from pathogens (*E. coli* and *S. aureus*) was evaluated following the previously described method [18], with slight modifications. Overnight cultures of *E. coli* and *S. aureus* were washed twice and resuspended in sterile peptone water. The overnight culture of probiotic strains was centrifuged, and CFS was collected. The CFS (1.5 mL) of probiotic strains was mixed with pathogen culture (1.5 mL) and incubated at 37°C. The cell suspensions were centrifuged (10,000 rpm for 10 min 4°C) at 0, 30, and 60 min of intervals. The supernatant was taken to measure the absorbance at OD_{260} nm using the Uv-Vis spectrophotometer (UV-1800, Shimadzu, Japan). The control was prepared the same way without the addition of CFS.

Table 1: Antibacterial activity of LAB against pathogens.

Pathogenic bacteria	Probiotic strains					
	11	19	42	60	93	112
	Diameter of inhibition zone (mm)					
B. cereus	16.3 ± 0.5	15.0 ± 0.0	18.3 ± 0.5	15.3 ± 0.5	17.6 ± 0.5	14.0 ± 0.0
B. subtilis	15.3 ± 0.5	17.3 ± 0.5	16.3 ± 0.5	13.0 ± 0.0	14.3 ± 0.5	16.3 ± 0.5
E. coli	19.0 ± 0.0	17.0 ± 0.0	17.0 ± 0.0	16.6 ± 0.5	19.3 ± 0.5	18.3 ± 0.5
E. faecalis	17.0 ± 1.0	16.0 ± 1.0	19.3 ± 0.5	18.0 ± 0.0	17.0 ± 0.0	19.6 ± 0.5
L. monocytogenes	21.3 ± 0.5	19.0 ± 0.0	20.3 ± 0.5	18.3 ± 0.5	18.6 ± 0.5	17.3 ± 0.5
L. innocua	19.6 ± 0.5	19.3 ± 0.5	17.3 ± 0.5	17.6 ± 0.5	18.6 ± 0.5	19.3 ± 0.5
S. Enteritidis	20.3 ± 0.5	18.0 ± 1.0	18.3 ± 0.5	19.0 ± 1.0	20.6 ± 0.5	16.6 ± 0.5
S. Typhimurium	20.0 ± 0.0	17.0 ± 0.0	16.6 ± 0.0	18.0 ± 0.0	19.6 ± 0.5	18.3 ± 0.5
S. dysenteriae	16.6 ± 0.5	17.6 ± 0.5	16.6 ± 0.5	16.0 ± 1.0	17.3 ± 0.5	17.0 ± 1.0
S. aureus	17.3 ± 0.5	18.0 ± 0.0	20.3 ± 0.5	19.6 ± 0.5	20.0 ± 0.0	19.0 ± 1.0
P. aeruginosa	16.6 ± 0.5	15.3 ± 0.5	14.3 ± 0.5	10.0 ± 0.0	16.3 ± 0.5	15.3 ± 0.5

Mean ± SD of results from three replicates. *L. paraplantarum* (11), *L. plantarum* (19), *L. pentosus* (42), *L. fermentum* (60), *L. pentosus* (93), and *L. reuteri* (112).

2.7. Effect of CFS on Growth of Pathogens. The antibacterial activity of CFS on the growth of *S.* Typhimurium, *L. monocytogenes*, *E. coli*, and *S. aureus* was evaluated by following a previously described method [19] with slight modifications. The potential probiotic strains were centrifuged (10,000 rpm for 10 min 4°C), and CFS was collected and sterilized through 0.2 μm membrane filter (Sartorius, Minisart, Germany). The CFS (10 mL) of each LAB strain was mixed with 100 mL of cell culture of each pathogenic strain and incubated at 37°C for 24 h. The optical density ($OD_{600\,nm}$) was measured every 2 h through a Uv-Vis spectrophotometer (UV-1800, Shimadzu, Japan). The cell cultures of *S.* Typhimurium, *L. monocytogenes*, *E. coli*, and *S. aureus* without the addition of CFS were used as control.

2.8. Biopreservation Potentials of Probiotic LAB in Raw Milk. The biopreservation potential of probiotic LAB strains against *L. monocytogenes* in buffalo milk was performed following the previously described method [20] with slight modifications. Pasteurized buffalo milk (50 mL) samples were inoculated with 1 mL of *L. monocytogenes* and probiotic culture. The milk samples were stored for 10 days at 37°C. The samples were drawn every day, and the total plate count was performed on Listeria selective agar and MRS agar (HiMedia, India). The samples containing *L. monocytogenes* culture were used as control.

2.9. Statistical Analysis. Data are presented as the mean and standard deviation (mean ± SD) of three independent replicates. Statistical analysis was performed using the SPSS 23.0 program (SPSS Inc., Chicago, IL).

Table 2: Coculture of probiotic strains with *E. coli* and *Staphylococcus aureus* (growth in Log CFU/mL).

Isolate	LAB	*E. coli*
11	9.13 ± 0.05 (9.18 ± 0.06)	3* (9.39 ± 0.03)
19	9.11 ± 0.04 (9.30 ± 0.03)	3.82 ± 0.09 (9.40 ± 0.03)
42	9.33 ± 0.03 (9.41 ± 0.03)	4.01 ± 0.06 (9.35 ± 0.03)
60	9.02 ± 0.05 (9.21 ± 0.03)	3.74 ± 0.06 (9.41 ± 0.03)
93	9.34 ± 0.03 (9.41 ± 0.03)	3.71 ± 0.07 (9.40 ± 0.03)
112	9.05 ± 0.03 (9.10 ± 0.04)	4.17 ± 0.03 (9.40 ± 0.03)
Isolate	LAB	*S. aureus*
11	9.10 ± 0.05 (9.15 ± 0.05)	3* (9.30 ± 0.04)
19	9.19 ± 0.04 (9.22 ± 0.04)	3* (9.40 ± 0.03)
42	9.21 ± 0.04 (9.38 ± 0.03)	3.93 ± 0.05 (9.41 ± 0.03)
60	9.11 ± 0.04 (9.18 ± 0.03)	3.74 ± 0.06 (9.34 ± 0.03)
93	9.28 ± 0.03 (9.38 ± 0.03)	3* (9.34 ± 0.03)
112	9.08 ± 0.04 (9.18 ± 0.04)	3.93 ± 0.04 (9.41 ± 0.03)

Values in parentheses represent growth of controls. An asterisk (*) indicates less than 3 value. Mean ± SD of results from three replicates. *L. paraplantarum* 11, *L. plantarum* 19, *L. pentosus* 42, *L. fermentum* 60, *L. pentosus* 93, and *L. reuteri* 112.

3. Results and Discussion

Very limited studies have been reported on probiotics and their antimicrobial effects from buffalo milk and their antimicrobial effects on pathogens. In this study, the effect of live culture of probiotics and their CFS on the growth of pathogenic bacteria is observed. The probiotic culture was used as a biopreservative in order to improve the shelf life of fermented milk products. Purification and characterization of antimicrobial compounds were not performed as the major objective of this research was to use live LAB culture as an inhibitory substance. One isolate (*L. paraplantarum* BT-11) produced bacteriocin-like inhibitory substance (BLIS), which has been already reported by the main author [13]. Live culture of LAB and their CFS were used against both gram-positive and gram-negative pathogens in several experiments during this study including the biopreservation

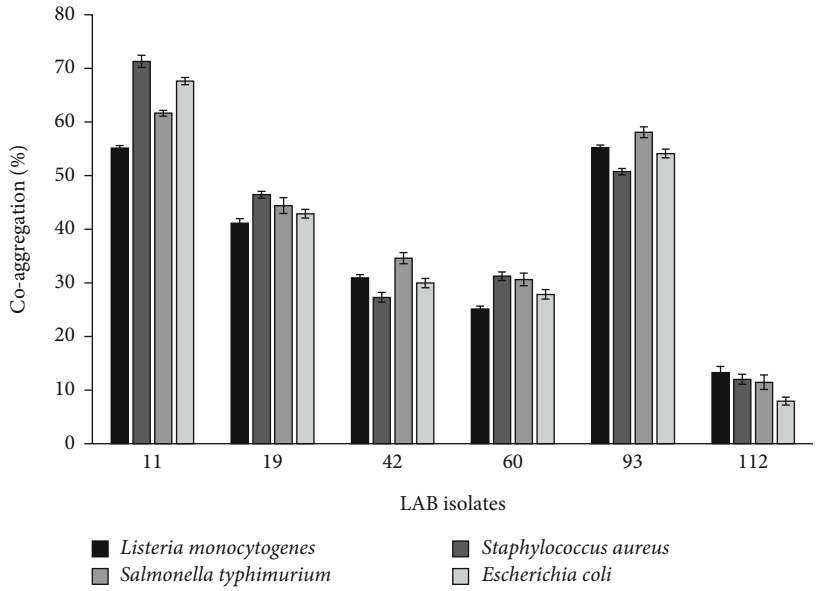

Figure 1: Coaggregation activity of *L. paraplantarum* 11, *L. plantarum* 19, *L. pentosus* 42, *L. fermentum* 60, *L. pentosus* 93, and *L. reuteri* 112 strains with pathogenic strains after incubation at 37°C for 24 h. Mean ± SD of three independent readings.

Table 3: Effect of CFS on 260 nm releasing material (nucleic acid) of *E. coli* at different time intervals.

Isolate	Time (min)	Control ($OD_{260\ nm}$)	Treatment ($OD_{260\ nm}$)
11	0	1.36	1.38
	30	1.36	2.90
	60	1.37	3.77
19	0	1.32	1.33
	30	1.34	2.25
	60	1.35	3.72
42	0	1.35	1.37
	30	1.36	2.66
	60	1.38	3.51
60	0	1.34	1.33
	30	1.37	2.85
	60	1.38	3.63
93	0	1.36	1.38
	30	1.37	2.39
	60	1.37	3.38
112	0	1.36	1.44
	30	1.38	2.48
	60	1.39	3.62

CFS = cell-free supernatant; control = *E. coli* culture; treatment = *E. coli* culture with LAB CFS. *L. paraplantarum* 11, *L. plantarum* 19, *L. pentosus* 42, *L. fermentum* 60, *L. pentosus* 93, and *L. reuteri* 112.

Table 4: Effect of CFS on 260 nm releasing material (nucleic acid) of *S. aureus* at different time intervals.

Isolate	Time (min)	Control ($OD_{260\ nm}$)	Treatment ($OD_{260\ nm}$)
11	0	1.42	1.46
	30	1.44	2.90
	60	1.46	3.86
19	0	1.45	1.47
	30	1.45	2.60
	60	1.47	3.43
42	0	1.44	1.48
	30	1.44	2.50
	60	1.47	3.74
60	0	1.45	1.46
	30	1.45	2.13
	60	1.46	3.60
93	0	1.42	1.44
	30	1.44	2.71
	60	1.45	3.69
112	0	1.43	1.49
	30	1.45	2.95
	60	1.46	3.72

CFS = cell-free supernatant; control = *S. aureus* culture; treatment = *S. aureus* culture with LAB CFS. *L. paraplantarum* (11), *L. plantarum* (19), *L. pentosus* (42), *L. fermentum* (60), *L. pentosus* (93), and *L. reuteri* (112).

test to further explore the inhibitory potential of probiotic LAB.

3.1. Antibacterial Activity of Live Cells. The antibacterial activity of live cells of LAB against foodborne pathogens is shown in Table 1. All probiotic strains displayed antagonistic activity against tested indicator pathogens in the agar spot assay. The live culture probiotic strains showed antagonistic activity against both gram-positive (*B cereus*, *B. subtilis*, *L. monocytogenes*, *L. innocua*, and *S. aureus*) and

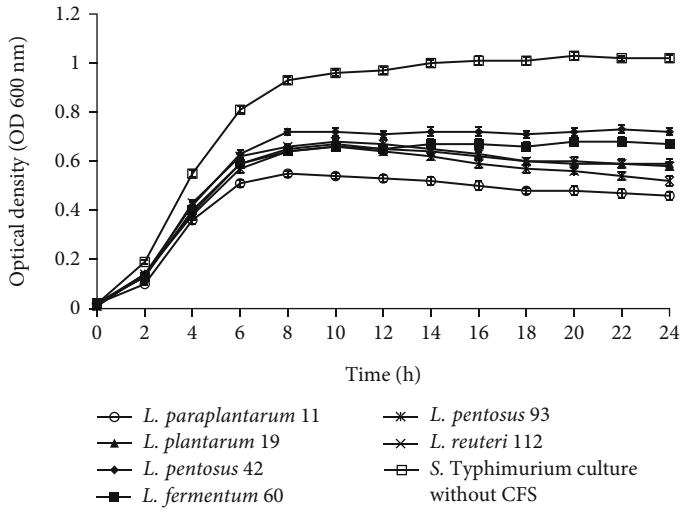

Figure 2: Effect of cell-free supernatant (CFS) of *L. paraplantarum* 11, *L. plantarum* 19, *L. pentosus* 42, *L. fermentum* 60, *L. pentosus* 93, and *L. reuteri* 112 on the growth of *S.* Typhimurium during 24 h incubation at 37°C. The *S.* Typhimurium culture without CFS was used as control. Mean ± SD of results from three replicates.

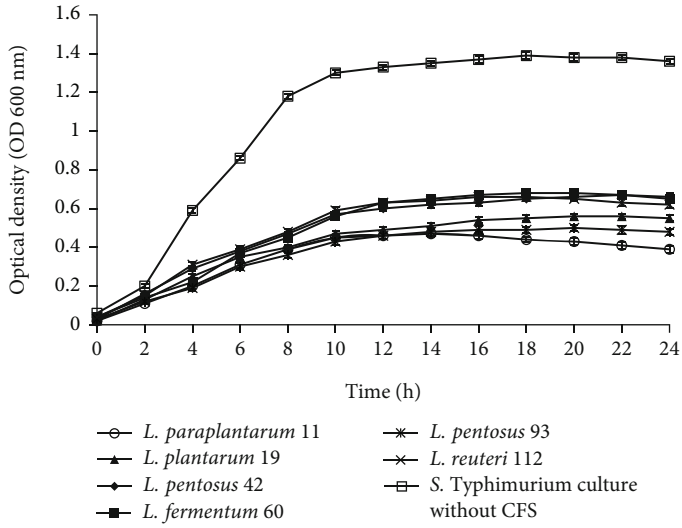

Figure 3: Effect of cell-free supernatant (CFS) of *L. paraplantarum* 11, *L. plantarum* 19, *L. pentosus* 42, *L. fermentum* 60, *L. pentosus* 93, and *L. reuteri* 112 on the growth of *L. monocytogenes* during 24 h incubation at 37°C. The *L. monocytogenes* culture without CFS was used as control. Mean ± SD of results from three replicates.

gram-negative (*E. coli*, *Enterococcus faecalis*, *S. Enteritidis*, *S.* Typhimurium, *Shigella dysenteriae*, and *P. aeruginosa*) pathogens. The inhibitory activity ranged from 10 to 21 mm. *L. paraplantarum* 11 (BLIS-producing strain) produced the highest antibacterial activity against *L. monocytogenes*.

The antagonistic activity of LAB or their antimicrobial compounds is an important characteristic of probiotics. The probiotic bacteria produce several compounds such as organic acids (lactic acid, acetic acid, and butyric acid), hydrogen peroxide, and bacteriocins or BLIS which shows the antagonistic activity against the pathogens [21]. Palachum et al. [10] reported antibacterial activity of live culture of probiotic strain *L. plantarum* WU-P19 against gram-positive and gram-negative pathogens. The antibacterial activity of the live cultures in the present study was higher than that reported by Monteagudo-Mera et al. [22].

3.2. Coculture with Pathogens. Table 2 represents the coculture of pathogens with probiotics. The survival of *E. coli* and *S. aureus* was 4.1 to less than 3 Log CFU/mL and 3.9 to less than 3 Log CFU/mL and 5 to 6 Log CFU/mL reduction in coculture with probiotic strains. Coculture studies of probiotics and pathogens help to understand the effects of probiotics on the growth of foodborne pathogens. Afolayan and Ayeni [16] reported 6 Log CFU/mL reduction of *E. coli* after coculture with *L. plantarum* and *L. fermentum*. In a similar study, Voravuthikunchai et al. [23] reported inhibitory activity of *L. reuteri* (L22) against MRSA with

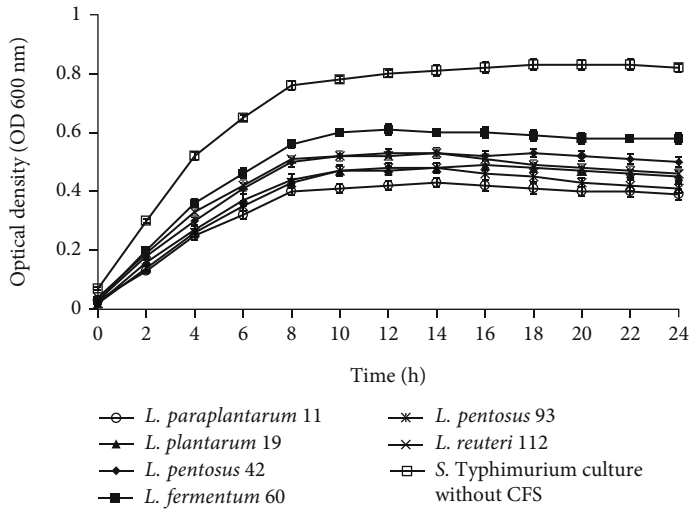

Figure 4: Effect of cell-free supernatant (CFS) of *L. paraplantarum* 11, *L. plantarum* 19, *L. pentosus* 42, *L. fermentum* 60, *L. pentosus* 93, and *L. reuteri* 112 on the growth of *E. coli* during 24 h incubation at 37°C. The *E. coli* culture without CFS was used as control. Mean ± SD of results from three replicates.

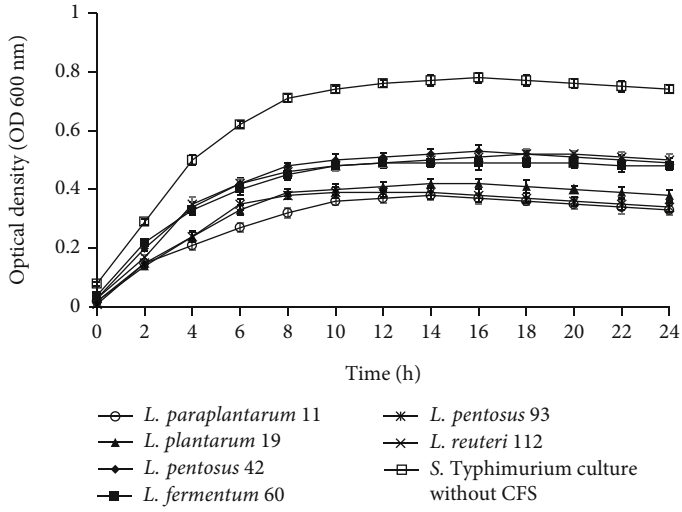

Figure 5: Effect of cell-free supernatant (CFS) of *L. paraplantarum* 11, *L. plantarum* 19, *L. pentosus* 42, *L. fermentum* 60, *L. pentosus* 93, and *L. reuteri* 112 on the growth of *S. aureus* during 24 h incubation at 37°C. The *S. aureus* culture without CFS was used as control. Mean ± SD of results from three replicates.

4 Log CFU/mL survival and complete inhibition of *S. aureus* after 24 h incubation in coculture experiment. Drago et al. [24] reported 4-5 and 6 Log CFU/mL reduction in the population of *E. coli* and *S.* Enteritidis, respectively, after coculture study with Lactobacilli strains. The difference in MRS medium, which contains complex proteins, may also affect the growth of strains in coculture studies [25].

3.3. Coaggregation with Pathogens. The coaggregation activity of probiotic LAB with *E. coli*, *S.* Typhimurium, *S. aureus*, and *L. monocytogenes* is shown in Figure 1. All probiotic isolates exhibited coaggregation with pathogens. *L. paraplantarum* (BT-11) showed the highest coaggregation percentage (71%) against *S. aureus* whereas the lowest coaggregation percentage (7%) was shown by *L. reuteri* (112) against *E. coli*. The coaggregation capability of probiotics with pathogens is a good indicator of their gut colonization property. Coaggregation with pathogens enhances the probiotic potential and cellular aggregation that promote the colonization of probiotic bacteria [26, 27]. Kumari et al. [28] reported the coaggregation ability of LAB strains isolated from fermented foods and beverages with *L. monocytogenes* (11-72%).

3.4. Effect of CFS on 260 nm Releasing Materials. The effect of CFS of LAB strains on the release of *E. coli* and *S. aureus* 260 nm absorbing material (DNA and RNA) is shown in Tables 3 and 4. The absorbance values increasing at an optical density of 260 nm with time indicate the cell death of indicator pathogenic strains while control for both strains

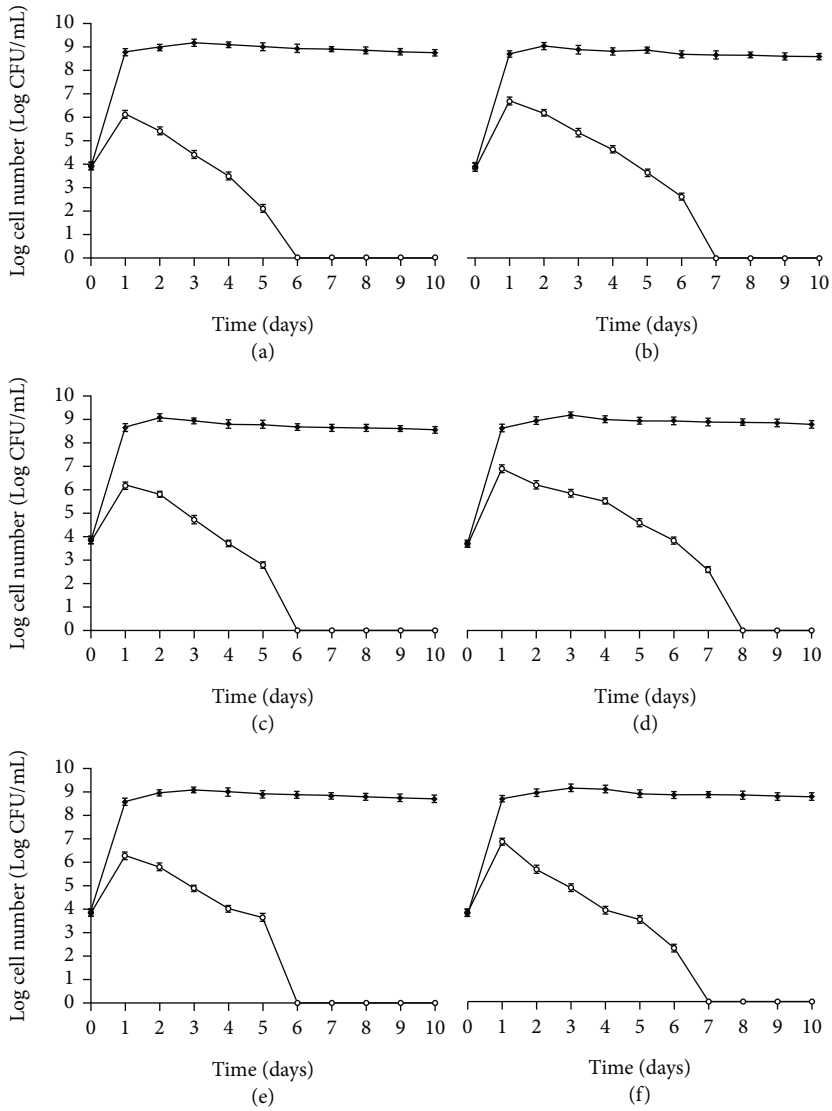

Figure 6: Biopreservation effect (0) of *L. paraplantarum* 11 (a), *L. plantarum* 19 (b), *L. pentosus 42* (c), *L. fermentum* 60 (d), *L. pentosus* 93 (e), and *L. reuteri* 112 (f) against *L. monocytogenes* in milk during 10 days of storage. The samples containing *L. monocytogenes* culture were used as control (black diamond). Mean ± SD of three independent readings.

remained the same. The release of the extracellular material indicates the integrity of the cell membrane; nucleotides (DNA, RNA) absorb ultraviolet light at 260 nm; therefore, they are termed 260 nm absorbing materials [29]. The release of 260 nm absorbing material (DNA and RNA) due to the CFS of probiotic strains leads to the loss of essential cell electrolytes and cell structure and integrity [8]. Different antimicrobial compounds are reported to produce their antagonistic activity through leakage of cytoplasm and its coagulation, which affects the functions and integrity of the affected cell leading to cell death [30]. Similar results regarding the loss of 260 nm absorbing materials of pathogens due to the antimicrobial compounds or LAB were also reported [8, 31, 32].

3.5. Effect of CFS on Growth of Foodborne Pathogens. Figures 2–5 illustrate the antibacterial activity of *L. paraplantarum* 11, *L. plantarum* 19, *L. pentosus* 42, *L. fermentum* 60, *L. pentosus* 93, and *L. reuteri* 112 on the growth of foodborne pathogens. The results show the reduction in the growth of pathogenic strains with the addition of CFS. All probiotic strains had a broad antimicrobial spectrum against the growth of gram-positive and gram-negative pathogens. The CFS of isolate *L. paraplantarum* 11 and *L. pentosus* 93 revealed the highest antibacterial activity against all indicator strains. The antimicrobial activity of CFS can be attributed to the presence of several antimicrobial compounds such as organic acids, hydrogen peroxide, reuterin, reutericyclin, bacteriocin, or BLIS. These results indicate the antimicrobial characteristics of potential probiotic strains and their potential to be used in several food and biomedical applications. Ahmadova et al. [33] reported bacteriostatic antibacterial effect of LAB strain *E. faecium* AQ71 from cheese against *L. monocytogenes* and bactericidal effect

against *Levilactobacillus brevis* while Khodaei and Sh [19] reported reduced growth of *P. aeruginosa* and *L. monocytogenes* after the addition of CFS of enterococci in a similar experiment.

3.6. Biopreservation in Milk. Figure 6 illustrates the antibacterial effects of six probiotic strains in raw buffalo milk against *L. monocytogenes*. The results show that the probiotic strains have a biopreservative effect on raw milk against *L. monocytogenes*. The growth of *L. monocytogenes* was gradually reduced with time as compared to the control. The probiotic LAB strains showed an antagonistic effect against *L. monocytogenes* in raw buffalo milk. No growth of *L. monocytogenes* was found after the 6th day (*L. paraplantarum* 11, *L. pentosus 42*, and *L. pentosus* 93), 7th day (*L. plantarum* 19, *L. reuteri* 112), and 8th day (*L. fermentum* 60).

In this study, the effect of live culture of potential probiotic LAB was performed as a challenge study. Live cultures of probiotic LAB were used to compare the effects of longer storage periods on the growth of LAB and pathogenic bacteria (in terms of Log CFU/mL) in milk. Fermented milk showed a reduction in the growth of pathogenic bacteria during the storage period. Lactic acid bacteria and their antimicrobial compounds are used as biopreservatives. One of the objectives of this study was to compare the increase in the growth of LAB and decrease in the growth of pathogens in fermented milk with longer storage periods; with CFS or purified compounds, this comparison was not possible; therefore, live cultures of LAB were used for the biopreservation purpose. Fernandes et al. [20] also reported a similar study of control of *L. monocytogenes* in raw milk through *L. plantarum* culture.

The LAB are most suitable candidates for biopreservation as they are naturally present in many food products and produce antimicrobial compounds against pathogens [34]. The probiotic strains isolated from the same source where they will be used as biopreservative agents are more preferred as they have adopted the rough environmental conditions of that food product and are more competitive than LAB strains from other sources [35].

Several studies have reported the biopreservation potential of LAB in foods against foodborne pathogens [36, 37]. *L. monocytogenes* growth was inhibited in whole milk with antimicrobial compounds produced by *Lactobacillus curvatus* [38]. Sriwattanachai et al. [39] reported food preservation potential and synergistic effect of *L. plantarum* CFS and essential oil. Akbar and Anal [40] reported complete inhibition of *S. aureus* in poultry meat with *L. lactis* culture.

4. Conclusion

A detailed study was conducted on the antimicrobial and biopreservation potential of probiotics from buffalo milk. Six probiotic LAB strains (*L. paraplantarum* 11, *L. plantarum* 19, *L. pentosus* 42, *L. fermentum* 60, *L. pentosus* 93, and *L. reuteri* 112) showed promising antibacterial and biopreservation potential. Live cultures of all strains were effective in reducing the growth of foodborne and spoilage-causing pathogens. The viable count of gram-positive and gram-negative pathogens was reduced in the coculture assay. The probiotic strains showed aggregation characteristics; the CFS had a significant effect on pathogens, which was reflected by the release of 260 nm absorbing material and reduced growth of pathogens. The live culture of probiotic strains showed biopreservative potential against *L. monocytogenes* in raw milk. Based on the results, the potential probiotic strains have the potential to be used as natural biopreservative agents against foodborne pathogens.

Data Availability

The data used to support the findings of this study are included within the article.

Conflicts of Interest

The authors declare that there is no conflict of interest.

Acknowledgments

The authors acknowledge the Higher Education Commission, Pakistan for providing scholarship (award letter: PD/OS-II/Batch-V/2013/10377) to pursue PhD to one of the authors, Mr. M. Saleem Kalhoro, at the Asian Institute of Technology, Thailand.

References

[1] Y. Hu, X. Liu, C. Shan et al., "Novel bacteriocin produced by *Lactobacillus alimentarius* FM- MM_4 from a traditional Chinese fermented meat Nanx Wudl: Purification, identification and antimicrobial characteristics," *Food Control*, vol. 77, pp. 290–297, 2017.

[2] R. Kumariya, A. K. Garsa, Y. S. Rajput, S. K. Sood, N. Akhtar, and S. Patel, "Bacteriocins: classification, synthesis, mechanism of action and resistance development in food spoilage causing bacteria," *Microbial Pathogenesis*, vol. 128, pp. 171–177, 2019.

[3] N. Nayyeri, M. R. Edalatian Dovom, M. B. Habibi Najafi, and M. Bahreini, "A preliminary study on antifungal activity of lactic acid bacteria isolated from different production stages of Lighvan cheese on *Penicillium expansum* and *Rhodotorula mucilaginosa*," *Journal of Food Measurement and Characterization*, vol. 11, no. 4, pp. 1734–1744, 2017.

[4] A. Galvez, R. L. Lopez, H. Abriouel, E. Valdivia, and N. B. Omar, "Application of bacteriocins in the control of foodborne pathogenic and spoilage bacteria," *Critical Reviews in Biotechnology*, vol. 28, no. 2, pp. 125–152, 2008.

[5] E. A. Pfeiler and T. R. Klaenhammer, "The genomics of lactic acid bacteria," *Trends in Microbiology*, vol. 15, no. 12, pp. 546–553, 2007.

[6] M. S. Bin Masalam, A. Bahieldin, M. G. Alharbi et al., "Isolation, molecular characterization and probiotic potential of lactic acid bacteria in Saudi raw and fermented milk," *Evidence-Based Complementary and Alternative Medicine*, vol. 2018, Article ID 7970463, 12 pages, 2018.

[7] Y. Feng, L. Qiao, R. Liu, H. Yao, and C. Gao, "Potential probiotic properties of lactic acid bacteria isolated from the intestinal mucosa of healthy piglets," *Annals of Microbiology*, vol. 67, no. 3, pp. 239–253, 2017.

[8] V. K. Bajpai, J. H. Han, I. A. Rather et al., "Characterization and antibacterial potential of lactic acid bacterium *Pediococcus pentosaceus* 4I1 isolated from freshwater fish *Zacco koreanus*," *Frontiers in Microbiology*, vol. 7, p. 2037, 2016.

[9] A. Ahmadova, S. D. Todorov, I. Hadji-Sfaxi et al., "Antimicrobial and antifungal activities of *Lactobacillus curvatus* strain isolated from homemade Azerbaijani cheese," *Anaerobe*, vol. 20, pp. 42–49, 2013.

[10] W. Palachum, Y. Chisti, and W. Choorit, "In-vitro assessment of probiotic potential of *Lactobacillus plantarum* WU-P19 isolated from a traditional fermented herb," *Annals of Microbiology*, vol. 68, no. 2, pp. 79–91, 2018.

[11] M. S. Kalhoro, L. T. Nguyen, and A. K. Anal, "Evaluation of probiotic potentials of the lactic acid bacteria (LAB) isolated from raw buffalo *(Bubalus bubalis*) milk," *Pakistan Veterinary Journal*, vol. 39, no. 3, pp. 395–400, 2019.

[12] E. S. Khalil, M. Y. Manap, S. Mustafa, M. Amid, A. M. Alhelli, and A. Aljoubori, "Probiotic characteristics of exopolysaccharides-producingLactobacillusisolated from some traditional Malaysian fermented foods," *CyTA-Journal of Food*, vol. 16, no. 1, pp. 287–298, 2018.

[13] M. S. Kalhoro, W. Visessanguan, L. T. Nguyen, and A. K. Anal, "Probiotic potential ofLactobacillus paraplantarumBT-11 isolated from raw buffalo (*Bubalus bubalis*) milk and characterization of bacteriocin-like inhibitory substance produced," *Journal of Food Processing Preservation*, vol. 43, no. 8, article e14015, 2019.

[14] W. Sirichokchatchawan, P. Pupa, P. Praechansri et al., "Autochthonous lactic acid bacteria isolated from pig faeces in Thailand show probiotic properties and antibacterial activity against enteric pathogenic bacteria," *Microbial Pathogenesis*, vol. 119, pp. 208–215, 2018.

[15] N. Hwanhlem, S. Buradaleng, S. Wattanachant, S. Benjakul, A. Tani, and S. Maneerat, "Isolation and screening of lactic acid bacteria from Thai traditional fermented fish (*Plasom*) and production of _Plasom_ from selected strains," *Food Control*, vol. 22, no. 3-4, pp. 401–407, 2011.

[16] A. Afolayan and F. Ayeni, "Antagonistic effects of three lactic acid bacterial strains isolated from Nigerian indigenous fermented Ogi onE. coliEKT004 in co-culture," *Acta Alimentaria*, vol. 46, no. 1, pp. 1–8, 2017.

[17] Y. Bao, Y. Zhang, H. Li et al., "In vitro screen of *Lactobacillus plantarum* as probiotic bacteria and their fermented characteristics in soymilk," *Annals of Microbiology*, vol. 62, no. 3, pp. 1311–1320, 2012.

[18] H. Liu, Y. du, X. Wang, and L. Sun, "Chitosan kills bacteria through cell membrane damage," *International Journal of Food Microbiology*, vol. 95, no. 2, pp. 147–155, 2004.

[19] M. Khodaei and S. N. Sh, "Isolation and molecular identification of bacteriocin-producing enterococci with broad antibacterial activity from traditional dairy products in Kerman province of Iran," *Korean Journal for Food Science of Animal Resources*, vol. 38, no. 1, p. 172, 2018.

[20] P. Fernandes, D. Loureiro, V. Monteiro et al., "*Lactobacillus plantarum* isolated from cheese: production and partial characterization of bacteriocin B391," *Annals of Microbiology*, vol. 67, no. 6, pp. 433–442, 2017.

[21] M. Ivey, M. Massel, and T. G. Phister, "Microbial interactions in food fermentations," *Annual Review of Food Science and Technology*, vol. 4, no. 1, pp. 141–162, 2013.

[22] A. Monteagudo-Mera, L. Rodríguez-Aparicio, J. Rúa et al., "In vitro evaluation of physiological probiotic properties of different lactic acid bacteria strains of dairy and human origin," *Journal of Functional Foods*, vol. 4, no. 2, pp. 531–541, 2012.

[23] S. P. Voravuthikunchai, S. Bilasoi, and O. Supamala, "Antagonistic activity against pathogenic bacteria by human vaginal lactobacilli," *Anaerobe*, vol. 12, no. 5-6, pp. 221–226, 2006.

[24] L. Drago, M. R. Gismondo, A. Lombardi, C. Haën, and L. Gozzini, "Inhibition of in vitro growth of enteropathogens by new *Lactobacillus* isolates of human intestinal origin," *FEMS Microbiology Letters*, vol. 153, no. 2, pp. 455–463, 1997.

[25] I. Starke, J. Zentek, and W. Vahjen, "Effects of the probiotic *Enterococcus faecium* NCIMB 10415 on selected lactic acid bacteria and enterobacteria in co-culture," *Beneficial Microbes*, vol. 6, no. 3, pp. 345–352, 2015.

[26] T. K. Sahoo, P. K. Jena, N. Nagar, A. K. Patel, and S. Seshadri, "In vitro evaluation of probiotic properties of lactic acid bacteria from the gut of *Labeo rohita* and *Catla catla*," *Probiotics and Antimicrobial Proteins*, vol. 7, no. 2, pp. 126–136, 2015.

[27] A. Abushelaibi, S. Al-Mahadin, K. El-Tarabily, N. P. Shah, and M. Ayyash, "Characterization of potential probiotic lactic acid bacteria isolated from camel milk," *LWT-Food Science Technology*, vol. 79, no, pp. 316–325, 2017.

[28] A. Kumari, K. Angmo, and T. C. Bhalla, "Probiotic attributes of indigenous Lactobacillus spp. isolated from traditional fermented foods and beverages of north-western Himalayas using in vitro screening and principal component analysis," *Journal of Food Science Technology*, vol. 53, no. 5, pp. 2463–2475, 2016.

[29] C. Z. Chen and S. L. Cooper, "Interactions between dendrimer biocides and bacterial membranes," *Biomaterials*, vol. 23, no. 16, pp. 3359–3368, 2002.

[30] J. K. Patra, H. Hwang, J. W. Choi, and K. H. Baek, "Bactericidal mechanism of bio-oil obtained from fast pyrolysis of Pinus densiflora against two foodborne pathogens, *Bacillus cereus* and *Listeria monocytogenes*," *Foodborne Pathogens and Disease*, vol. 12, no. 6, pp. 529–535, 2015.

[31] H.-L. Alakomi, E. Skyttä, M. Saarela, T. Mattila-Sandholm, K. Latva-Kala, and I. M. Helander, "Lactic acid permeabilizes gram-negative bacteria by disrupting the outer membrane," *Applied environmental microbiology*, vol. 66, no. 5, pp. 2001–2005, 2000.

[32] V. K. Bajpai, I. A. Rather, R. Majumder, F. H. Alshammari, G. J. Nam, and Y. H. Park, "Characterization and antibacterial mode of action of lactic acid bacterium *Leuconostoc mesenteroides* HJ69 from Kimchi," *Journal of Food Biochemistry*, vol. 41, no. 1, article e12290, 2017.

[33] A. Ahmadova, S. D. Todorov, Y. Choiset et al., "Evaluation of antimicrobial activity, probiotic properties and safety of wild strain *Enterococcus faecium* AQ71 isolated from Azerbaijani Motal cheese," *Food Control*, vol. 30, no. 2, pp. 631–641, 2013.

[34] Z. Yildirim, H. Bilgin, H. Isleroglu, K. Tokatli, D. Sahingil, and M. Yildirim, "Enterocin HZ produced by a wild *Enterococcus faecium* strain isolated from a traditional, starter-free pickled cheese," *Journal of Dairy Research*, vol. 81, no. 2, pp. 164–172, 2014.

[35] S. Ammor, G. Tauveron, E. Dufour, and I. Chevallier, "Antibacterial activity of lactic acid bacteria against spoilage and pathogenic bacteria isolated from the same meat small-scale facility: 1–screening and characterization of the antibacterial compounds," *Food Control*, vol. 17, no. 6, pp. 454–461, 2006.

[36] D. Cizeikiene, G. Juodeikiene, A. Paskevicius, and E. Bartkiene, "Antimicrobial activity of lactic acid bacteria against pathogenic and spoilage microorganism isolated from food and their control in wheat bread," *Food Control*, vol. 31, no. 2, pp. 539–545, 2013.

[37] H. Ahn, J. Kim, and W. J. Kim, "Isolation and characterization of bacteriocin-producing *Pediococcus acidilactici* HW01 from malt and its potential to control beer spoilage lactic acid bacteria," *Food Control*, vol. 80, pp. 59–66, 2017.

[38] H. A. Hartmann, T. Wilke, and R. Erdmann, "Efficacy of bacteriocin-containing cell-free culture supernatants from lactic acid bacteria to control *Listeria monocytogenes* in food," *International Journal of Food Microbiology*, vol. 146, no. 2, pp. 192–199, 2011.

[39] S. Sriwattanachai, M. B. Sadiq, and A. K. Anal, "Synergistic antifungal effects of thyme essential oil and *Lactobacillus plantarum* cell-free supernatant against *Penicillium* spp. and in situ effects," *Journal of Food Processing Preservation*, vol. 42, no. 1, article e13400, 2018.

[40] A. Akbar and A. K. Anal, "Occurrence of *Staphylococcus aureus* and evaluation of anti-staphylococcal activity of *Lactococcus lactis* subsp. *lactis* in ready-to-eat poultry meat," *Annals of Microbiology*, vol. 64, no. 1, pp. 131–138, 2014.

Hindawi
Oxidative Medicine and Cellular Longevity
Volume 2023, Article ID 2567333, 12 pages
https://doi.org/10.1155/2023/2567333

Research Article

Investigation of Anti-Inflammatory Properties, Phytochemical Constituents, Antioxidant, and Antimicrobial Potentials of the Whole Plant Ethanolic Extract of *Achillea santolinoides* subsp. *wilhelmsii* (K. Koch) Greuter of Balochistan

Ali Akbar,[1] **Zareen Gul**,[1,2] **Su Hlaing Chein**,[3] **and Muhammad Bilal Sadiq**[4]

[1]*Department of Microbiology, University of Balochistan, Quetta, Balochistan, Pakistan*
[2]*Department of Botany, University of Balochistan, Quetta, Balochistan, Pakistan*
[3]*Spectrum-Sustainable Development Knowledge, Yangon 11111, Myanmar*
[4]*School of Life Sciences, Forman Christian College (A Chartered University), Lahore, Pakistan*

Correspondence should be addressed to Ali Akbar; aliakbar.uob@gmail.com and Su Hlaing Chein; suhlaing.shc08@gmail.com

Received 29 July 2022; Revised 5 September 2022; Accepted 24 November 2022; Published 25 January 2023

Academic Editor: Yehui Duan

Medicinal plants are rich source of phytochemical constitutes and can be used to treat many human diseases. Infectious diseases have always been a major source of concern. Globally, the medicinal plant *Achillea wilhelmsii* locally known as Bohe Madran is extensively dispersed and widely used as traditional medicine. The aim of this present work is to investigate phytochemical constituents and antimicrobial, antioxidant, and anti-inflammatory properties of the whole plant ethanolic extract of *Achillea santolinoides* subsp. *wilhelmsii* (WEEAW) from Balochistan region. The total phenolic content was 14.81 ± 0.18 mg GAE/g of the extract whereas the total flavonoid content was 12.27 ± 0.12 mg QE/g of the extract. The antioxidant ability of the extract was analyzed by DPPH (2,2-diphenyl-1-picryl-hydrazyl) scavenging assay and FRAP (ferric reducing antioxidant power) assay in terms of concentration having 50% inhibition (IC_{50}). Results showed that IC_{50} value for DPPH% inhibition was 0.367 ± 0.82 mg/mL while FRAP assay represented with IC_{50} value of 0.485 ± 1.26 mg/mL. In antileishmanial bioassay, the extract was analyzed against Leishmania major and showed good activity with IC_{50} value of 7.02 ± 0.83 mg/mL. Antibacterial assay revealed that *Staphylococcus aureus* was highly sensitive with the diameter of inhibition zone (21.61 ± 1.09 mm) followed by *Salmonella typhi* (17.32 ± 0.15 mm), *Pseudomonas aeruginosa* (16.41 ± 0.63 mm), and *Escherichia coli* (15.30 ± 1.17 mm) while *Klebsiella pneumoniae* showed minimum inhibition (14.13 ± 0.49 mm). Antifungal activity was tested against *Aspergillus flavus* with 89% of inhibition zone and 77% against *Mucor mucedo* and *Aspergillus niger* with 74% of inhibition zone. The anti-inflammatory assay was carried out by inhibiting protein denaturation, proteinase inhibitory activity, and heat-induced hemolysis. The IC_{50} value for protein denaturation was 6.67 ± 1.25 mg/mL, proteinase inhibitory with IC_{50} value of 4.12 ± 0.69 mg/mL, and heat-induced hemolysis assay with IC_{50} value 4.53 ± 0.82 mg/mL by comparing to the standard drug aspirin having IC_{50} value 1.85 ± 0.54 mg/mL. Results of the current work showed that whole plant ethanolic extract of *Achillea wilhelmsii* exhibited substantial anti-inflammatory action, thus can be utilized as a traditional treatment. Furthermore, overall finding of this research suggested that the antioxidant potential of the plant aids to prevent free radical damage and reduce the incidence of chronic disease. More research is needed to find out more active compounds present in the extract that are responsible for their pharmacological effects.

1. Introduction

Medicinal plants naturally produce a variety of phytochemical constitutes as secondary metabolites which can be used to treat many human diseases. Additionally, plant secondary metabolites have a great potential for producing novel medications and have been successfully employed to treat chronic and infectious diseases [1]. The World Health

Organization (WHO) estimates that 80 percent of the world's population still relies on indigenous medications for basic healthcare due to their ease of access [2]. These plants have significant antibacterial, antifungal, anti-inflammatory, antioxidant, anticancer, and antidiabetic properties and used for the treatment of various infections [3]. The natural antimicrobial agents present in medicinal plants have strong resistance to the usual antibiotics and drugs. As an alternative, these plants provide a traditional substitute to produce traditional drugs with low cost and easily available for local communities. In the future, such plants may play a larger role in disease control [4].

Achillea wilhelmsii is a perennial herb commonly known as Bohe Madran and Zawal in Brahui and Pashto languages. The plant belongs to Asteraceae or Compositae family, and the genus *Achillea* comprises over 120 species worldwide [5]. The plant is widely distributed in Asia particularly in Pakistan, Iran, and India [6]. The word *Achillea* was derived from the Greek word Achilles, which means "hero," and was mostly used to cure various diseases during battles [7]. The plant is best known for its pleasant fragrant aroma and traditionally used for treating a variety of health problems by local community [8]. *Achillea wilhelmsii* contains various chemical constituents including alkamides, alkaloids, carvacrol, linalool, α- and β-pinene, borneol, sesquiterpenoids (wilhemsin and wilhelmsolide), monoterpenoids, caryophyllene, rutin, thujene, 1,4-cineol, and camphor [6]. It has been shown that *Achillea* contains bitter aromatic substances having imperative effects on nervous system and neurological diseases such as epilepsy, neurasthenia, and seizures [9]. Many research studies documented that fractions, extracts, pure chemical compounds, and essential oils derived from *Achillea* species have a wide range of biological functions such as cytotoxic, antidiabetic, antispasmodic, antianxiety, anticancer, anti-inflammatory, analgesic, antibacterial, anticholinesterase activities [10, 11]. The plant decoction is used to treat children's motion, jaundice stomach pain, and fever, whereas green tea made from young shoots is used to treat stomach complications [12]. Inflammation is a complicated biological response of bodily tissues to adverse stimuli such as infections, damaged cells, or irritants and is characterized in vascular tissues by redness, warmth, swelling, and discomfort. Acute inflammation is a short-term process characterized by pain, redness, immobility, swellings, heat, and loss of body functions. Available anti-inflammatory medicines alleviate symptoms, suppress enzyme activities, and come with complicated negative side effects [2]. Consequently, using anti-inflammatory drugs with fewer side effects is also crucial.

The in vitro analysis of phytochemical constituents, antibacterial, antifungal, anti-inflammatory, and antileishmanial potentials of the ethanolic extracts of *Achillea wilhelmsii* variety available in Quetta Balochistan has not been reported. Therefore, the plant was evaluated for its antibacterial, antifungal, antioxidants, antileishmanial, and anti-inflammatory potentials against different microorganisms using an in vitro assay.

2. Materials and Method

2.1. Plant Collection and Sample Preparation. *Achillea wilhelmsii* plants were collected from Quetta region Balochistan with the area coordinates 30.623926 N, 67.323998 E. The plant was collected and identified by the Botanist Zareen Gul Department of Botany University of Balochistan Quetta. One part of the collected plant was dried preserved and kept at the Food Microbiology and Bioprocess Technology Laboratory Department of Microbiology University of Balochistan for reference. The other part of the plant was washed with distilled water and dried for a few weeks in the shade at room temperature with controlled humidity. Using an electronic grinder, the dried plants were crushed into fine powder and stored in desiccators for future investigation.

2.2. Extraction of Bioactive Compounds by Maceration. For extraction, 200 g of fine ground powder was extracted using 2 L of 70% ethanol as the solvent in a 1 : 10 ratio for 24 hours, as indicated by Gul et al. [2]. The treatment was performed in a dark environment to avoid light exposure. The flask was shaken at regular intervals. The ethanolic mixture was filtered using Whatman filter paper no. 1. The *Achillea santolinoides* subsp. *wilhelmsii* (K. Koch) Greuter whole plant ethanolic extract (WEEAW) obtained was dried in a rotary evaporator at 65°C and used for further research.

2.3. Phytochemical Analysis. The WEEAW was subjected to determine the presence of different phytochemical constituents (alkaloids, steroids, tannins, saponins, flavonoids, glycosides, terpenoids, quinones, coumarin, carbohydrates, and phenolic compounds) using standard procedures as described by Akbar et al. [13].

2.4. Estimation of Total Phenolic Content. The total phenolic content (TPC) of the WEEAW was determined using the Folin-Ciocalteu reagent technique using gallic acid as a standard, and the results were represented in milligrams of gallic acid equivalents (mg GAE/g) of sample dried weight [14]. In brief, 0.5 mL (1 mg/mL) dried crude plant extract was appropriately combined with newly made (2 mL) Folin-Ciocalteu reagent. After 5 minutes at room temperature, the mixture was neutralized with 2 mL of 10% Na_2CO_3 and incubated for 30 minutes. The absorbance at 750 nm was calculated using a T60 UV-Visible Spectrophotometer (PG, UK) and a blank of 95% ethanol.

2.5. Total Flavonoid Content. Total flavonoid contents (TFC) of the WEEAW were determined by aluminum chloride colorimetric assay as explained by Sadiq et al. [15]. Quercetin was employed as a control, and the results were represented in milligrams of quercetin equivalents per gram of the sample (mg QE/g). Simply, 0.5 mL of the extract (1 mg/mL) was combined with 95 percent ethanol and 0.5 mL ($NaNO_2$ 5%) solution. After 5 minutes (10% w/v, 0.1 mL) of $AlCl_3.6H_2O$, 0.5 mL of 1 M NaOH and 2 mL of deionized water were added and incubated at 25°C for 40 minutes. Absorbance was measured at 415 nm against a blank using a T60 UV-Visible Spectrophotometer (PG, UK). The measurements

were done using a standard curve and varied amounts of quercetin.

2.6. DPPH Radical Scavenging Activity. The antioxidant activity of WEEAW was assessed based on the radical scavenging effect on (2,2-diphenyl-1-picryl-hydrazyl) DPPH free radical. From the stock solution, several doses (1-0.0625 mg/mL) of the extract were prepared, and 50 μL of the extract was mixed with 5 mL of freshly prepared DPPH (40 ppm in ethanol) solution. The reaction mixture was mixed and incubated at room temperature in the dark for 30 minutes. Ascorbic acid was utilized as a control. The decrease in absorbance at 517 nm was used to detect DPPH decolorization. As a blank and control, ethanol and DPPH solutions without plant extract were utilized [15].

The following equation was used for % inhibition calculation:

$$\%\text{inhibition of DPPH} = \frac{\text{AC} - \text{AS}}{\text{AC}} \times 100. \quad (1)$$

Here, AC is the absorbance of control (DPPH), and AS is the extract absorbance.

The relationship curve was created by graphing the scavenging activity against various extract concentrations and was expressed in mg/mL. The results were presented as IC_{50} values (concentration of sample required to scavenge 50 percent of free radicals).

2.7. Ferric Reducing Antioxidant Power (FRAP) Assay. For the reduction of ferric 2,4,6-tris(2-pyridyl)-1,3,5-triazine [Fe(III)TPTZ] to the ferrous complex, the procedure from Benzie and Strain [16] was followed with little modifications. Suspension of FRAP was prepared by adding acetate buffer (0.3 M) pH 3.6, $FeCl_3{\cdot}6H_2O$ (0.02 M), and TPTZ (0.01 M) in HCl (0.04 M), respectively. In the dark, acetate buffer (25 mL), TPTZ solution (2.5 mL), and ferric chloride hexahydrate solution (2.5 mL) were mixed and incubated for 30 minutes at 37°C. Briefly, 0.5 mL of (WEEAW) 1 mg/mL was mixed with 2 mL of FRAP suspension followed by incubation at 37°C for 30 min in the dark, and absorbance was read at 595 nm, and % reduction was determined by the following equation:

$$\text{FRAP\%reduction} = \frac{\text{AC} - \text{AS}}{\text{AC}} \times 100, \quad (2)$$

where AC is the absorbance of control and AS is the absorbance of the extract.

2.8. Antileishmanial Assay. To accomplish antileishmanial assay of WEEAW, the *L. major* (promastigotes) were grown in culture medium Novy–Mac Neal–Nicolle (NNN) supplemented with penicillin (100 U/mL) and streptomycin (100 μg/mL) followed by incubation at 37°C for 72 h. The log phase of promastigotes at 1×10^6 cells/mL was used, and the assay was performed by means of a 96-well plate method described by Gul et al. [2]. Briefly, stock solution (1 mg/mL) of the test sample was prepared in DMSO. Twofold serial dilutions of the samples were carried out at different concentrations (1, 0.5, 0.25, 0.125, and 0.0625 mg/mL), respectively. 10 μL of each dilution and 50 μL promastigotes log phase culture were dispensed to each well of 96-well plate. Glucantime (Meglumine antimonate) was employed as a reference medication and DMSO as negative control. The titer plate was incubated at 37°C for 72 h. Following the incubation period, 1 mL of DMSO was added to each well, and the percent mortality of the test and control medicines was evaluated using 20 L (5 mg/mL in phosphate buffer pH 7.2) of nitro blue tetrazolium (NBT) chloride solution. The absorbance at 630 nm was measured using a Microplate Reader (RT-6000), and the results were represented as a mean percent suppression in parasite population. The extract's IC_{50} values were computed using the linear regression approach, and the percent cell viability was obtained using the following formulas:

$$\%\text{cell viability} = \frac{A_{630}\text{of test sample}}{A_{630}\text{ of control}} \times 100,$$
$$\%\text{inhibition} = 100 - \%\text{viability}. \quad (3)$$

2.9. Antibacterial Activity. The antibacterial activity of WEEAW was determined by agar well diffusion method described by Gul et al. [2]. Freshly prepared Muller Hinton Agar (Oxoid UK) media were sterilized and inoculated with the 100 μL of target bacterial strains (*Escherichia coli*, *Pseudomonas aeruginosa*, *Salmonella typhi*, *Staphylococcus aureus*, and *Klebsiella pneumoniae*) in different flasks and poured into sterilized plates. Wells were made through 6 mm sterilized cork borers in agar plates followed by adding 100 μL of the extract (1 mg/mL) and kept for incubation for 24 hr at 37°C. The antibiotic doxycycline was employed as a positive control, whereas dimethyl sulfoxide (DMSO) was used as a negative control. The diameter of the clean zone around the wells was measured in millimeters (mm) to obtain the results.

2.10. Antifungal Activity. Antifungal activities of WEEAW were determined by the method of Gul et al. [2]. Freshly produced Potato Dextrose Agar (Oxoid UK) was mixed with 1 mL of the extract and placed into Petri plates. After solidification, 6 mm diameter wells were created into agar by cork borer, and the actively growing test fungi (*Aspergillus flavus*, *Aspergillus niger*, and *Mucor mucedo*) were poured into various wells and incubated at 37°C for 72 h. The positive control contained media containing organisms without extract, while the negative control was merely media. Fluconazole, an antifungal drug, was employed as a reference. After five days of incubation, the results of the growth inhibition of the target fungal species were recorded. The growth inhibition of target fungus was measured in millimeters (mm) in comparison to the negative control. The following equation was used to calculate the final findings:

$$\%\text{inhibition} = \frac{100 - \text{linear growth in test(mm)}}{\text{linear growth in control(mm)}} \times 100. \quad (4)$$

2.11. Anti-Inflammatory Activity Determination

2.11.1. Inhibition of Albumin Denaturation. Anti-inflammatory effect was assessed using the inhibition of albumin denaturation assay, as described by Yesmin et al. [17]. The reaction suspension (5 mL) contained 1 mL of the extract (1 mg/mL), 3.8 mL of phosphate buffered saline (PBS, pH 6.4), and 0.2 mL of aqueous solution containing 1 percent bovine albumin. After incubation for 15 minutes at 37°C in a water bath, the reaction mixture was heated to 70°C for 5 min. After cooling, the absorbance at 660 nm was measured using UV-VIS Spectrophotometer (T60 UK). Acetylsalicylic acid was used as the standard medicine, and phosphate buffer solution was used as the control. The following formula was used to compute the % inhibition of protein denaturation:

$$\%\text{inhibition of protein denaturation} = 100 \times \frac{1 - \text{A2}}{\text{A1}}, \quad (5)$$

where $A1$ is the absorption of the control sample and $A2$ is the absorption of the test sample.

2.11.2. Proteinase Inhibitory Activity. Proteinase inhibitory activity of WEEAW was measured according to the method described by Gunathilake et al. [18] to examine the in vitro anti-inflammatory action. The reaction suspension (2 mL) was made up of 0.06 mg trypsin, 1 mL of 20 mM Tris-HCl buffer (pH 7.4), and 1 mL of the extract. The mixture was incubated for 5 minutes at 37°C before adding 1 mL of 0.8 percent (w/v) casein and incubating for another 20 minutes before adding 2 mL of 70% perchloric acid and centrifuged. At 210 nm, the absorbance of the supernatant was measured using a phosphate buffer solution as a control and acetylsalicylic acid as a reference medication for the experiment. The percentage inhibition was calculated by using the following formula:

$$\%\text{proteinase inhibition} = \frac{(\text{Abs control} - \text{Abs sample}) \times 100}{\text{Abs control}}. \quad (6)$$

2.12. Heat-Induced Hemolysis Assay. Erythrocyte suspension was prepared following Gul et al. [2] with some modifications. A healthy individual's whole blood was obtained. To remove supernatants, the blood was centrifuged at 2000 × g for 5 min. The mixture was rinsed with an equivalent volume of normal saline (0.9 percent NaCl) and centrifuged for 5 minutes at 2000 × g. The procedure was performed three times, and the blood volume was calculated and reconstituted as a 10% (v/v) suspension with an isotonic buffer solution (10 mM sodium phosphate buffer pH 7.4). The buffer solution used (g/L) contained $NaH_2PO_4.2H_2O$ (0.2) g, Na_2HPO_4 (1.15) g, and NaCl (9.0) g.

Heat-induced hemolysis assay was carried out as described by Yesmin et al. [17] with some modifications. In brief, 0.06 mL of blood cell suspension and 0.06 mL of the extract were combined with 2.93 mL of phosphate buffer (pH 7.4) before being incubated in a water bath at 54°C for 20 minutes. The mixture was centrifuged again (2000 × g for 3 min), and the absorbance of the supernatant was measured at 540 nm using a microplate reader (T60 UV VIS Spectrophotometer). For the experiment, a phosphate buffer solution was utilized as a control, and acetylsalicylic acid was employed as a standard medication. The following equation was used to compute the % inhibition of hemolysis:

$$\text{Percentage inhibition of hemolysis} = \frac{(\text{Abs control} - \text{Abs sample}) \times 100}{\text{Abs control}}, \quad (7)$$

where $A1$ is the absorption of the control and $A2$ is the absorption of test sample.

2.13. Statistical Analysis. MS Excel 2010 software was used to compute the magnitude of the means, standard curve, and standard deviations. The findings are presented as the mean SD of three replicates. Linear regression method was used to measure the inhibitory concentrations (IC_{50}) value.

3. Results

3.1. Phytochemical Analysis. The phytochemical evaluation of WEEAW confirmed the presence of alkaloids, flavonoids, terpenoids, anthraquinones, saponins, tannins, coumarin, steroids, carbohydrates, and phlobatannins. However, cardiac glycoside and quinones were absent (Table 1). These investigations also revealed that *Achillea wilhelmsii* contains a diverse variety of phytochemical compounds.

3.2. Phenolic Contents. The TPCs of WEEAW were evaluated by using Folin-Ciocalteu method while gallic acid was used as a reference for standard. The TPCs of the extract were recorded 14.81 ± 0.18 mg GAE/g (Table 2).

3.3. Flavonoid Contents. The total flavonoid content was determined, and the results were computed using the calibration curve and represented as mg quercetin equivalents (QE) per gram of dry weight sample. Total flavonoid contents in extract were 12.27 ± 0.12 mg QE/g as presented in Table 2.

3.4. Quantitative Assay for DPPH Free Radical Scavenging Activity. In the presence of DPPH stable radical, the WEEAW hydrogen donating ability was determined, and its reducing potential was calculated based on their concentration indicating 50% inhibition (concentration of the extract needed to scavenge 50 percent DPPH free radicals). The results were obtained using a linear regression equation formed by the concentration of the extract versus their percent scavenging ability. According to the findings, the extract's radical scavenging activity increased with increasing concentration (Table 3 and Figure 1(a)). In current study, the DPPH radical scavenging activity was confirmed with IC_{50} (0.367 ± 0.82 mg/mL) in comparison with the standard ascorbic acid having IC_{50} (0.251 ± 0.91 mg/mL) as presented in Table 4.

Table 1: Phytochemical constituents of the whole plant ethanolic extract of *Achillea wilhelmsii*.

S. no	Phytochemical test	Results
1	Alkaloids	+ve
2	Cardiac glycosides	-ve
3	Tannins	+ve
4	Steroids	+ve
5	Terpenoids	+ve
6	Flavonoids	+ve
7	Saponins	+ve
8	Coumarin	+ve
9	Carbohydrates	+ve
10	Quinones	-ve
11	Anthraquinones	+ve
12	Phlobatannins	+ve

Note: +ve = present; -ve = absent.

Table 2: Total phenolic contents and total flavonoid contents of the whole plant ethanolic extract of *Achillea wilhelmsii*.

Sample	Total phenolic (mg GAE/g) ± SD	Total flavonoid (mg QE/g) ± SD
WEEAW	14.81 ± 0.18	12.27 ± 0.12

Note: results are expressed as mean ± SD for three readings.

Table 3: DPPH % inhibitions, FRAP % reduction, and antileishmanial assay of the whole plant ethanolic extract of *Achillea wilhelmsii* at different concentrations.

Concentrations in (mg/mL)	DPPH % inhibition assay	FRAP % reduction assay	Antileishmanial assay
1	82.21 ± 1.52	88.42 ± 0.81	59.23 ± 0.67
0.5	68.33 ± 1.21	70.15 ± 1.01	52.08 ± 0.18
0.25	44.26 ± 0.96	51.23 ± 0.54	45.54 ± 0.26
0.125	37.17 ± 1.03	43.08 ± 0.76	37.19 ± 0.20
0.0625	23.09 ± 1.25	21.81 ± 1.13	29.24 ± 0.62

3.5. Ferric Reducing Antioxidant Power Assay. WEEAW's antioxidant capacity was assessed using the ferric reducing antioxidant power (FRAP) assay. The results were expressed as the concentration providing 50% inhibition (IC_{50}), which is the concentration of the extract required to decrease Fe^{3+} to Fe^{2+}. The linear regression equation formed by the concentrations of the extracts versus their percent reduction ability yielded the findings. According to the obtained result, the extract has FRAP % reduction activity with IC_{50} (0.485 ± 1.26 mg/mL) as presented in Table 4. The higher IC_{50} value indicates lower antioxidant potential and same for ferric reducing activity. In comparison with the standard having IC_{50} value (0.314 ± 0.97 mg/mL), WEEAW showed relatively lower antioxidant potential. The current studies demonstrated that the extract's radical scavenging activity increased with increasing concentration, as mentioned in Table 3 and Figure 1(b).

3.6. Antileishmanial Assay. Antileishmanial assay was used to investigate the hidden potential of WEEAW against promastigotes (*Leishmania major*). Results have shown that different concentrations (1, 0.5, 0.25, and 0.125 mg/mL) of the extract exhibited a significant antileishmanial activity with substantial % inhibition having IC_{50} value (7.02 ± 0.83 mg/mL) compared with standard drug Glucantime IC_{50} (4.32 ± 0.63 mg/mL) as shown in Table 4. The % inhibition decreased with decrease in concentration as presented in Table 3 and Figure 2.

3.7. Antibacterial Activity. Antibacterial assay of WEEAW was evaluated against different bacterial strains. Results were presented in diameter of the inhibition zones (Table 5). Among Gram-negative and Gram-positive bacteria, *Staphylococcus aureus* was observed highly sensitive with the diameter of inhibition zone (21.61 ± 1.09 mm) followed by *Salmonella typhi* (17.32 ± 0.15 mm), *Pseudomonas aeruginosa* (16.41 ± 0.63 mm), and *Escherichia coli* (15.30 ± 1.17 mm) diameter of the inhibition zones, respectively. The extract was found active against all selected bacteria except Gram-negative *Klebsiella pneumoniae* that showed minimum inhibition (14.13 ± 0.49 mm).

3.8. Antifungal Activity. The percentage of inhibition zone was used to assess WEEAW's antifungal activity against three filamentous fungi (*A. flavus*, *A. niger*, and *M. mucedo*). When compared to the antifungal medication fluconazole, the extract demonstrated substantial antifungal action against fungus strains. The extract exhibited substantial antifungal action against Aspergillus flavus (89% inhibition) and *Mucor mucedo* (77% inhibition) but had a very minor effect on the growth of *A. niger* (74% inhibition). Fluconazole, an antifungal medication, inhibited *M. mucedo* by 98%, *A. niger* by 95 percent, and *A. flavus* by 94% (Figure 3 and Table 6).

3.9. In Vitro Anti-Inflammatory Assay. To examine the anti-inflammatory properties, WEEAW was subjected to preliminary analysis using known procedures. The results of in vitro anti-inflammatory activity for inhibition of protein denaturation, proteinase inhibition, and heat-induced hemolysis were presented in Table 7. Results of the current work revealed the effectiveness of the extract. Comparing results with reference drug aspirin IC_{50} value (1.85 ± 0.54 mg/mL), maximum % inhibition of the extract was observed for proteinase inhibition with lowest IC_{50} value (4.12 ± 0.69 mg/mL) followed by heat-induced hemolysis (4.53 ± 0.82 mg/mL). Minimum % inhibition was seen for inhibition of protein denaturation with highest IC_{50} value (6.67 ± 1.25 mg/mL), respectively. The highest activity was observed in concentration of (1 mg/mL), and the viability increased with decreased in concentration presented in Figure 4.

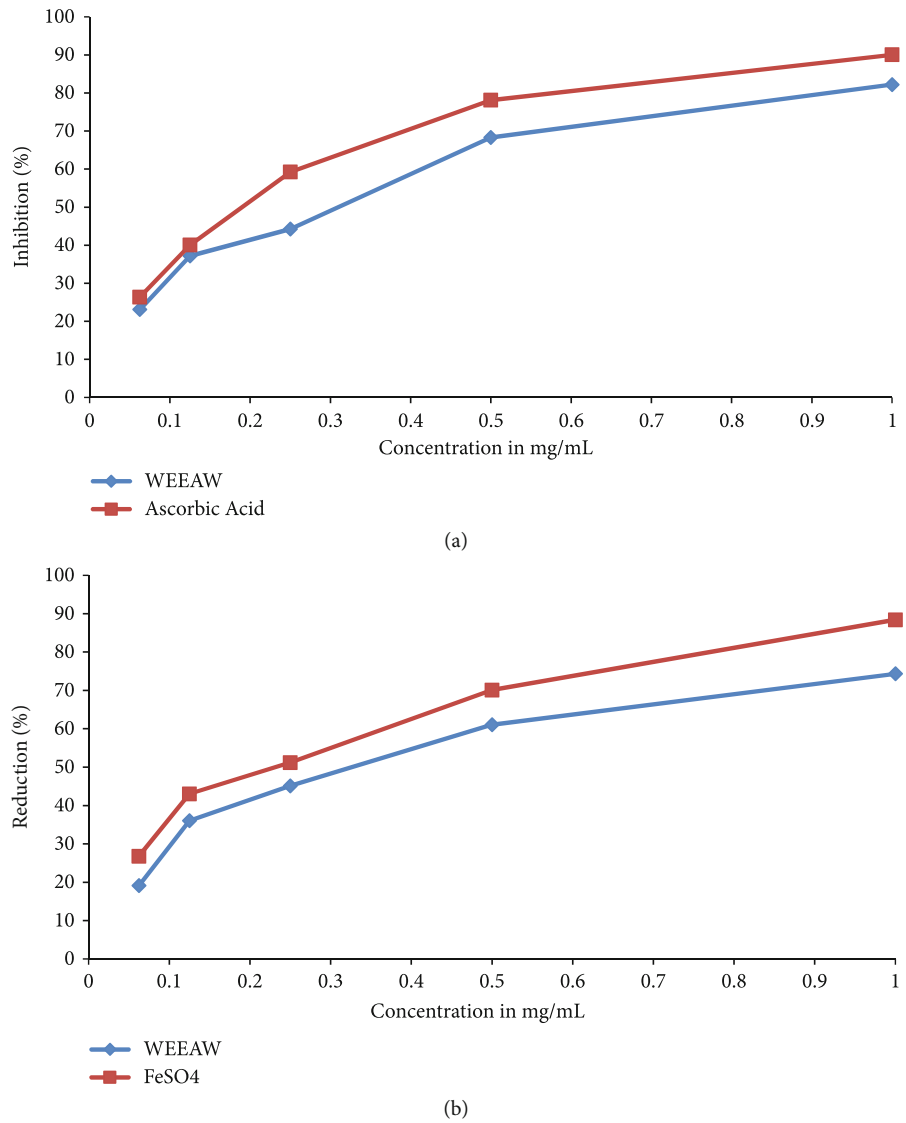

Figure 1: (a) Free radical scavenging activity (DPPH). (b) Ferrous reducing capacity (FRAP) of the whole plant ethanolic extract of *Achillea wilhelmsii*.

Table 4: Estimated IC_{50} values of the whole plant ethanolic extract of *Achillea wilhelmsii* and standards.

Assay	Samples	IC_{50} value (mg/mL)
DPPH	WEEAW	0.367 ± 0.82
	Ascorbic acid	0.251 ± 0.91
FRAP	WEEAW	0.485 ± 1.26
	$FeSO_4$	0.314 ± 0.97
Antileishmanial	WEEAW	7.02 ± 0.83
	Glucantime	4.32 ± 0.63

Note: ascorbic acid, $FeSO_4$, and Glucantime are used as a standards for the studies.

4. Discussion

Plants with high phytochemical constituents are beneficial to health because of their ability to reduce the risk of various ailments such as heart diseases, diabetes, and certain cancers [19]. The present study was conducted to evaluate the phytochemical constituents and antimicrobial and antioxidant activities of the whole plant ethanolic extract of *Achillea wilhelmsii* (WEEAW) from different regions of Balochistan. Alkaloids, tannins, phlobatannins, anthraquinones, saponins, flavonoids, phenolics, carbohydrates, coumarin, steroids, and terpenoids were discovered. All the chemicals found are physiologically active, with antibacterial, antifungal, antiviral, antiparasitic, and antioxidant properties. Alkaloids are anti-inflammatory and analgesic substances that serve to boost the immune system, relieve pain, and are used to treat snakebite, skin disorders, and asthma. Alkaloids provided the basic structure for the development of numerous

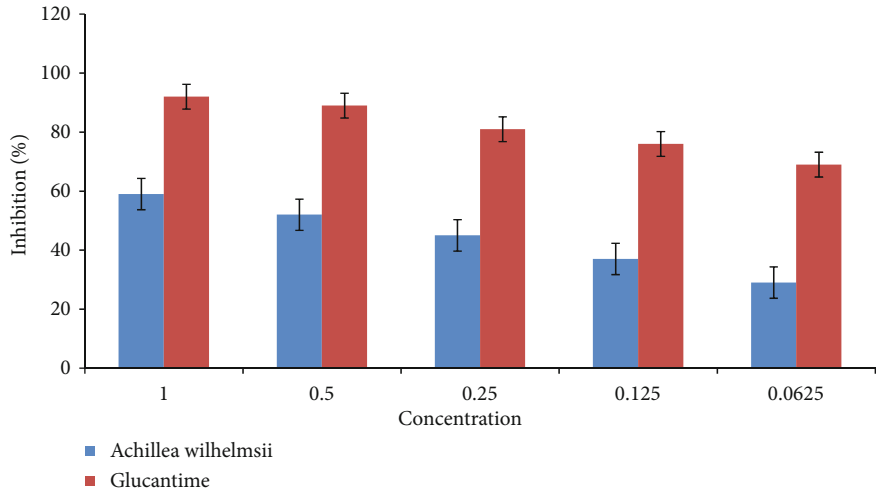

Figure 2: Antileishmanial activities of the whole plant ethanolic extract of *Achillea wilhelmsii* against promastigotes (*Leishmania major*). Bars represent the standard deviation of the mean.

Table 5: Antibacterial activity of the whole plant ethanolic extract of *Achillea wilhelmsii* with inhibitory zones.

	Diameter of zone of inhibition against target pathogens in millimeters (mm)				
Samples	*E. coli*	*K. pneumoniae*	*P. aeruginosa*	*S. aureus*	*S. Typhi*
WEEAW	15.30 ± 1.17	14.13 ± 0.49	16.41 ± 0.63	21.61 ± 1.09	17.32 ± 0.15
Doxycycline	20.61 ± 2.85	19.37 ± 2.48	12.62 ± 2.67	21.12 ± 1.41	14.60 ± 2.85
DMSO	0	0	0	0	0

Note: *E. coli* = *Escherichia coli*; *K. pneumoniae* = *Klebsiella pneumoniae*; *P. aeruginosa* = *Pseudomonas aeruginosa*; *S. aureus* = *Staphylococcus aureus*; *S. typhi* = *Salmonella typhi*.

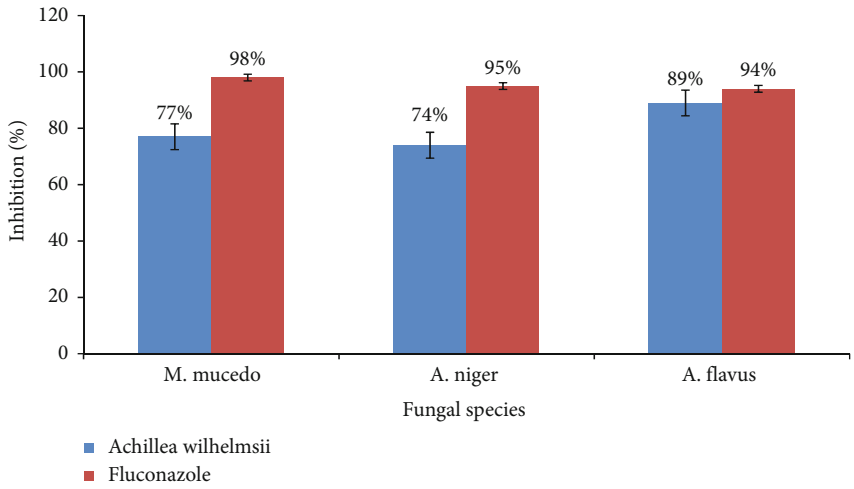

Figure 3: Antifungal activity of the whole plant ethanolic extract of *Achillea wilhelmsii* against fungal species *Mucor mucedo*, *Aspergillus niger*, and *Aspergillus flavus*. Bars represent the standard deviation of the mean.

antibiotics with a diverse actions [20]. Flavonoids have significant physiological impacts, including the ability to alter how the body responds to viral infection, allergies, and carcinogens. Literature also revealed the presence of several subgroups of terpenes in *Achillea* species [21]. Tannins also have antitumor and antidefensive activities, thus have ability to lower the blood pressure, speed up the blood coagulation, and lower the amount of lipid in serum [22]. Saponins have medicinal importance as it exhibits antioxidant, antimicrobial, antidiabetic, anticancer, anti-inflammatory, antispasmodic, and analgesic properties; hence, their presence in plant extract is a solid sign of its therapeutic usefulness [23]. An extensive range of secondary metabolites such as steroids, flavonoids, tannins, alkaloids, and terpenoids were

Table 6: Antifungal activity of the whole plant ethanolic extract of *Achillea wilhelmsii* against three fungal species.

ID	*M. mucedo*	*A. niger*	*A. flavus*
	Growth inhibition in percent		
WEEAW	77	74	89
Fluconazole	98	95	94

Note: percentage of inhibition: 0-39 = low; 40-59 = moderate; 60-69 = good; above 70 = significant activity.

found in *Achillea* species that has antimicrobial, antitumor, anti-inflammatory, antidiabetic, and antiradical potentials [24]. Current results of phytochemicals are in agreement with Serino et al. [6]. These findings imply the bioactive potential of *Achillea wilhelmsii*.

The phenolic content has been shown to have antibacterial, antioxidant, anti-inflammatory, and antidepressant properties. These compounds are deemed as active component of plants comprising good reducing potential due to which they act as good antioxidants. According to Raudone et al. [25], phenolic and flavonoid contents present in *Achillea wilhelmsii* were among particularly important group of metabolites because they contribute to substantial biological activity and may be related to antioxidant potential. In current study, the total phenolic contents of WEEAW were 14.81 ± 0.18 mg GAE/g. Previously, Fathi et al. [26] reported a higher TPC of *Achillea wilhelmsii* value 37.4 ± 0.3 mg GAE/g of the extract. According to the reported data of Jafari et al. [27], the total phenolic contents of *Achillea wilhelmsii* extract were 55.07 ± 0.295 mg GAE/g dry extract. Bashi et al. [28] documented that total phenolic contents of *Achillea wilhelmsii* methanolic extract value 17.18–59.61 mg GAE/g that were in agreement with the present findings. Recently, Şabanoğlu et al. [29] reported 119.4 ± 1.4 mg GAE/g extract of flower, 155.5 ± 8.7 mg GAE/g extract of leaves, and 136.4 ± 8.8 mg GAE/g extract for roots, respectively. The results of phenolic content were also in agreement with Asariha et al. [5]. Other study also revealed 104.66 mg GA/g of total phenolic contents for *Achillea santolina* by Yazdanparast et al. [30]. According to these findings, *Achillea* species appear to be a high source of phenolic acids and can be considered an auspicious natural antioxidant source [31]. Nevertheless, it has been illustrious that phenolic content assessed by spectrophotometry can be influenced by a variety of factors that comprise method of extraction, sampling treatment before processing, climatic condition, soil structure, and even plant age [32]. According to Sevindik et al. [33], *Achillea millefolium* petroleum ether extract resulted 85.72 ± 0.067 and methanolic extract with 77.78 ± 0.145 μg GAE/mg extract. According to the findings of Gharibi et al. [34], the total phenolic contents varied from 15.55 mg in *Achillea aucheri* to 60.65 mg tannic acid/g of dry product in *Achillea pachycephala*.

Flavonoid contents are known as good antioxidants having strong reducing potentials. These components also comprise antimicrobial, anti-inflammatory, anticancer, and antidepressant potentials [35]. Among the metabolite classes found in Achillea species, flavonoids are the most abundant natural compounds in extracts. They can be found as aglycones and glycosides. Jafari et al. [27] documented higher total flavonoid contents of *Achillea wilhelmsii* which were 39.14 ± 0.100 mg rutin equivalent/g dry extract as compared to present study. Additionally, lower flavonoid content 2.5 ± 0.1 mg quercetin equivalent/g of the extract was also reported by Fathi et al. [26]. Another study, conducted in Iran, illustrates that the total flavonoid contents in *Achillea wilhelmsii* range from 7.79 to 12.61 mg catechin equivalent/g sample in maceration and ultrasound-assisted extraction [28] and stated that *Achillea wilhelmsii* has a lower total flavonoid content than *Achillea biebersteinii*. Several research studies have also shown that increasing flavonoids in the diet reduces the risk of a variety of human diseases [5].

In the present study, WEEAW was seen to have greatest antioxidant activity with IC_{50} value of 0.367 ± 0.82 mg/mL compared with ascorbic acid as standard. Results are in agreement with available data of Şabanoğlu et al. [29] with IC_{50}1.500 ± 0.024, 0.812 ± 0.013, and 0.991 ± 0.017 mg/mL for flower, leaf, and root, respectively. Recently, Asariha et al. [5] reported that *Achillea wilhelmsii* GNPs and leaf infusion showed 58 and 68% of the scavenging effect at a concentration of 300 μg/mL, respectively. Previously, Fathi et al. [26] illustrated the DPPH radical scavenging activity of *Achillea wilhelmsii* with IC_{50}58.9 ± 2.7 μg/mL, and IC_{50} values for ascorbic acid, quercetin, and BHA were 3.7 ± 0.1, 3.9 ± 0.2, and 29.3 ± 5.9 μg/mL, respectively. Another study reported by Alfatemi et al. [36] showed the antioxidant activity of essential oil of *Achillea wilhelmsii* with EC_{50} of 0.01 mg/mL, and scavenging activity EC_{50} was 0.58 mg/mL. Previous researchers documented that the antioxidant activities of essential oils *Achillea* can be attributed to their phenolic contents [37]. Present results are also in accordance with Bashi et al. [28]. Furthermore, a research study conducted in Iran revealed that IC_{50} of *Achillea wilhelmsii* was 154.5 ± 1.01 μg/mL where the IC_{50} of BHT (standard) was calculated as 33.5 ± 0.16 μg/mL. Hence, these results showed that antioxidant capacity of *Achillea wilhelmsii* was 0.21 time more than BHT [27]. In addition, Gharibi et al. [34] also reported the antioxidant activity of three Iranian endemic *Achillea* species of *Achillea aucheri*, *Achillea kellalensis*, and *Achillea pachycephala* and documented the antioxidant activity by DPPH assay with IC_{50} (248–844 μg/mL) and stated that the variation for IC_{50} among species might be attributed to differences in polyphenolic compounds. Furthermore, the methods of extraction and time can highly affect the results of DPPH assay. Similarly, Barış et al. [31] reported the antiradical activities of *Achillea biebersteinii*, *Achillea aleppica*, and *Achillea aleppica* subsp. *zederbaueri* ethanol extract through DPPH scavenging assay were 85%, 81%, and 73% with IC_{50} values of 33, 33, and 32 μg/mL, respectively. Likewise, Sevindik et al. [33] stated that *Achillea millefolium* ethyl acetate extract showed 55.1 ± 1.168 and methanolic extract displayed 23.7% inhibition in DPPH radical at 40 μg/mL.

The reducing capacity of a sample identifies a considerable potential antioxidant activity. Hence, the FRAP assay is used to examine the reduction of ferric iron (Fe^{3+}) into ferrous iron (Fe^{2+}). The results of this study displayed that WEEAW possessed adequate antioxidant power with IC_{50}

Table 7: IC_{50} (mg/mL) of in vitro anti-inflammatory activity whole plant ethanolic extract of *Achillea wilhelmsii* (WEEAW).

Test samples	Conc. (mg/mL)	Inhibition of protein denaturation IC_{50} (mg/mL)	Proteinase inhibition IC_{50} (mg/mL)	Heat induced hemolysis IC_{50} (mg/mL)
WEEAW	1 0.5 0.25 0.125 0.0625	6.67 ± 1.25	4.12 ± 0.69	4.53 ± 0.82
Aspirin	1 0.5 0.25 0.125 0.0625	1.85 ± 0.54	1.85 ± 0.54	1.85 ± 0.54

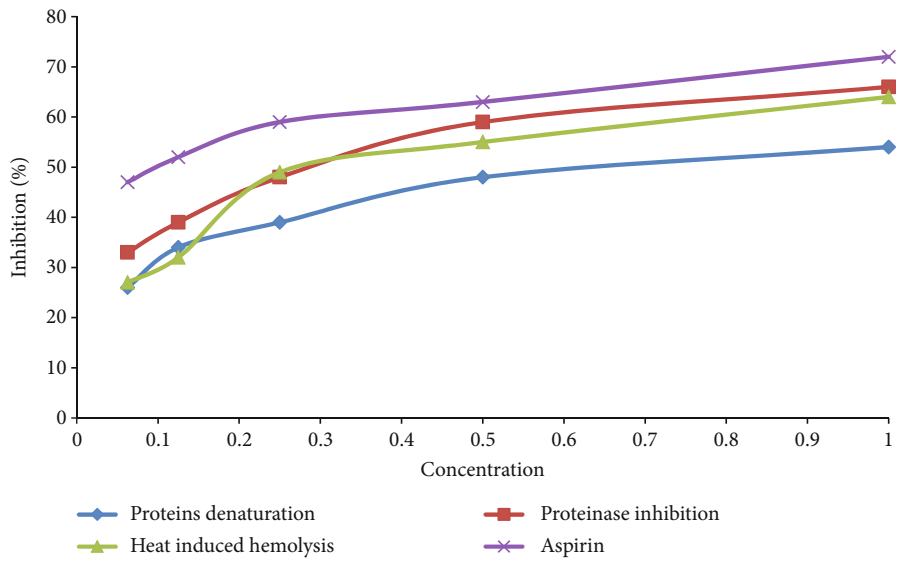

Figure 4: Anti-inflammatory activity of the whole plant ethanolic extract of *Achillea wilhelmsii*.

value of 0.485 ± 1.26 mg/mL. FRAP reducing power of *Achillea fragmentisma* methanol extract was recently studied. The results showed that plants gathered from two separate habitats had significantly higher reduction capacity in concentrations of 100 and 1000 μg/mL, with estimated IC50 values of 0.23 ± 0.02 g/L and 1.91 ± 0.05 g/L, respectively [38]. Likewise, Zengin et al. [39] demonstrated that methanolic extract of *A. biebersteinii* exhibited highest reducing power (196.12 mg TE/g extract). The methanolic extract of *Achillea coarctata* showed the moderate antioxidant activity with 1.74 mM/L FRAP value at 2 mg/mL compared with ascorbic acid which was 4.52 mm/L [40]. The higher the total phenolic and flavonoid contents, the higher will be the antioxidant potential. These ingredients are known to have antioxidant properties by either breaking the free radical chain or donating a hydrogen atom [29]. Alsohaili and Sulaiman [41] conducted a research study on essential oil of *Achillea tomentosa* and reported that the essential oil possessed lower ferric reducing power (EC 54.69 ± 4.69 μg/mL) compared to trolox (10.87 ± 3.34 μg/mL). Venditti et al. [42] analyzed *Achillea ligustica* All. composition and found that the flower and aerial parts contained secondary metabolites mainly sesquiterpenoids and flavonoid glucuronides. The crude extract obtained from aerial parts of *Achillea tenorii* was reported to be effective in α-glucosidase inhibition and antioxidant potential attributed to the presence of phenolic compounds [43]. The methanolic leave extract of *Achillea fragrantissima* was reported with antimicrobial and anticancer potential against various cancer cell lines [44].

Antileishmanial assay was used to investigate the hidden potential of ethanolic extract of *Achillea wilhelmsii* against *L. major*. The results confirmed that WEEAW exhibited a significant antileishmanial activity at different concentrations. Numerous antileishmanial investigations have already been conducted on the essential oil of *Achillea* species, including *Achillea wilhelmsii*. A result of a study conducted in Balochistan [8] revealed that whole plant n-hexane fraction

of *Achillea wilhelmsii* (WHFAW) has significant antileishmanial potential. The inhibitory concentration (IC_{50}) of the whole plant against *L. major* was found to be 58.27 ± 0.52 μg/mL. According to Darwish et al. [45], *Achillea* plant with concentration 100 μM showed antileishmanial action with 97.25% ± 1.63% inhibition and stated that various phytochemicals present in *Achillea* genus have antileishmanial properties. Moreover, Al-Sokari et al. [46] investigated antileishmanial action of 16 different medicinal plant including *Achillea biebersteinii*, against *L. amazonensis* where *Achillea biebersteinii* flowers displayed the most promising activity with inhibition% value of (IC_{50} = 26.9 ± 2.9 μg/mL). Countless research studies identified that plant containing chemical constituents naturally such as alkamides identified from *Achillea* species was shown to have antileishmanial properties [46].

Antibacterial assay of WEEAW was evaluated, and the results were presented in diameter of the inhibition zones (Table 5). Among Gram-negative and Gram-positive bacteria, *Staphylococcus aureus* was observed highly sensitive with the diameter of inhibition zone (21.61 ± 1.09 mm) followed by *Salmonella typhi*, *Pseudomonas aeruginosa*, and *Escherichia coli*, with the diameter of inhibition zone of 17.32 ± 0.15, 16.41 ± 0.63, and 15.30 ± 1.17 mm), respectively. While *Klebsiella pneumoniae* showed less sensitivity with the diameter of inhibition zone of (14.13 ± 0.49 mm). Previously, Amjad et al. [47] examine antibacterial activity of *Achillea wilhelmsii* against four pathogenic bacteria. The results revealed that the methanolic extract of *Achillea wilhelmsii* was the least efficient against *Pseudomonas aeruginosa* compared with other bacterial pathogens. Due to the differences in cell wall structure, Gram-positive bacteria are more sensitive than Gram-negative bacteria because their outer cell membrane acts as a barrier to different components, including antibiotics [48]. Some previous research studies found that *Achillea lingulata*, *Achillea millefolium*, and *Achillea clavennae* showed lower sensitivity to bacterial pathogens such as *S. enteritidis*, *E. coli*, *K. pneumoniae*, *P. aeruginosa*, and *S. aureus* [33]. The results of the previous studies revealed that the essential oils of *Achillea wilhelmsii* are rich in monoterpenes, such as borneol, myrtenol, camphor, and 1,8-cineole, and these constituents have potent antibacterial effects [37]. Additionally, this plant naturally contains phenolic components, sesquiterpenes, lactones, and flavonoids having antibacterial properties [28]. It has been recently reported that *Achillea fragmentisma* methanol extract demonstrated good antibacterial activity against Gram-positive clinical isolate (*Bacillus cereus*, *Staphylococcus epidermidis*, and *Staphylococcus aureus*), with antibacterial activity ranging from high to no activity (between 14.5 ± 0.5 and 6.0 ± 0.0 mm zone of inhibition), but no effect on Gram-negative bacteria *Escherichia coli* and *Klebsiella pneumoniae* [38].

Antifungal activity revealed that WEEAW exhibits potent antifungal activity against fungal strains. In the present study, *Aspergillus flavus* was observed highly sensitive with the percentage zone of inhibition (89%) followed by *Mucor mucedo* and *Aspergillus niger* with the percentage zone of inhibition 77% and 74% comparison with standard antifungal drug fluconazole with 98% zone of inhibition. Previously, Amjad et al. [49] reported that the methanolic extract of *Achillea wilhelmsii* C. Koch flowers has excellent antifungal activity against 20 Candida albicans strains. In contrast to the current work, Tajehmiri et al. [50] found that three fungal species *Aspergillus fumigatus*, *Aspergillus niger*, and *Aspergillus flavus* were susceptible to *A. wilhelmsii* extract. Antimicrobial activity of *Achillea wilhelmsii* extract was also investigated by Bashi et al. [28], and their findings showed no obvious inhibitory effect on *Aspergillus niger*. A research work conducted in Iran investigated the antifungal activities of essential oil of *Achillea biebersteinii* against five pathogenic fungi. The results illustrated the strong antifungal activities against all tested fungal species [51]. Thus, according to the preceding research, the presence of saponins, tannins, alkaloids, terpenes, carotenoids, and flavonoids caused antifungal potentials [28].

The plant extract was subjected to determine its in vitro anti-inflammatory capabilities by using known procedures as inhibition of protein denaturation, proteinase inhibition, and heat-induced hemolysis. Protein denaturation occurs in inflammatory disorders such as rheumatoid arthritis and diabetes, as well as in cancer, and is one of the main causes of inflammatory diseases. Inflammatory disorders might be minimized by preventing protein denaturation. Anti-inflammatory medications could benefit from chemical compounds that prevent protein denaturation. In arthritic condition, proteinase plays a crucial role. A serine proteinase is copiously found in the lysosomal granules of neutrophils. Previous literature documented that during inflammatory reactions, leukocyte proteinase plays a significant role in the development of tissue damage; hence, proteinase inhibitors provide significant protection. There have been a few studies on anti-inflammatory activities of *Achillea* species. However, literature demonstrated that *Achillea* is a well-known genus to have anti-inflammatory potential as it comprises phenolic, flavonoids, tannins, saponins, terpenoids, sesquiterpenes, diterpenes, lignans, essential oil, and rarely triterpenes [6]. Additionally, alkamides were also well known for their anti-inflammatory properties [52]. Similarly, sesquiterpenes and lactones prevent DNA binding of transcription factors which control evolution of inflammation more effectively [53]. Recently, Honari et al. [54] reported the strong anti-inflammatory effect of *Achillea wilhelmsii* from Iran. Current results were also supported by the previous documented data of in vivo anti-inflammatory activity of five *Achillea* species [52].

5. Conclusion

The findings of the present study illustrated that whole plant ethanolic extract of *Achillea wilhelmsii* (WEEAW) exhibited significant antioxidant, antibacterial, antileishmanial and anti-inflammatory activities. The outcome of these findings suggests that the extract has significant medicinal benefits and possesses promising biological potentials. However, more research studies are needed to explore the bioactive molecules responsible for their efficiency.

Data Availability

Most of the data is part of the manuscript, and the remaining data will be made available on reasonable request.

Conflicts of Interest

The authors declare that they have no conflicts of interest.

References

[1] S. Verma, "Medicinal plants with anti-inflammatory activity," *Journal of Phytopharmacology*, vol. 5, no. 4, pp. 157–159, 2016.

[2] Z. Gul, A. Akbar, and S. K. Leghari, "Elucidating therapeutic and biological potential of Berberis baluchistanica Ahrendt bark, leaf, and root extracts," *Frontiers in Microbiology*, vol. 13, pp. 823673–823673, 2022.

[3] M. S. Bari, L. Khandokar, E. Haque et al., "Ethnomedicinal uses, phytochemistry, and biological activities of plants of the genus *Gynura*," *Journal of Ethnopharmacology*, vol. 271, article 113834, 2021.

[4] T. Bibi, M. Ahmad, S. E. Edwards, N. M. Tareen, R. Jabeen, and I. Abdullah, "Ethnomedicinal uses of plants in the treatment of paediatric geohelminth infections in Kalat district of Northern Balochistan, Pakistan," *Journal of Ethnopharmacology*, vol. 183, pp. 176–186, 2016.

[5] M. Asariha, A. Chahardoli, N. Karimi et al., "Green synthesis and structural characterization of gold nanoparticles from Achillea wilhelmsii leaf infusion and in vitro evaluation," *Bulletin of Materials Science*, vol. 43, no. 1, pp. 1–10, 2020.

[6] E. Serino, A. Chahardoli, N. Badolati et al., "Salvigenin, a trimethoxylated flavone from *Achillea wilhelmsii* C. Koch, exerts combined lipid-lowering and mitochondrial stimulatory effects," *Antioxidants*, vol. 10, no. 7, p. 1042, 2021.

[7] Z. Aytac, H. Duman, and M. Ekici, "Two new *Achillea* L.(Asteraceae) species from Turkey," *Turkish Journal of Botany*, vol. 40, no. 4, pp. 373–379, 2016.

[8] J. K. Achakzai, M. Anwar Panezai, A. M. Kakar et al., "*In vitro* antileishmanial activity and GC-MS analysis of whole plant hexane fraction of *Achillea wilhelmsii* (WHFAW)," *Journal of Chemistry*, vol. 2019, Article ID 5734257, 26 pages, 2019.

[9] M. Hosseini, F. Harandizadeh, S. Niazamand, M. Soukhtanloo, and M. Mahmoudabady, "Antioxidant effect of *Achillea wilhelmsii* extract on pentylenetetrazole (seizure model)-induced oxidative brain damage in Wistar rats," *Indian Journal of Physiology and Pharmacology*, vol. 57, no. 4, pp. 418–424, 2013.

[10] H. Boutennoun, L. Boussouf, M. Kebieche, K. Al-Qaoud, and K. Madani, "*In vivo* analgesic, anti-inflammatory and antioxidant potentials of *Achillea odorata* from north Algeria," *South African Journal of Botany*, vol. 112, pp. 307–313, 2017.

[11] F. Chávez-Silva, L. Cerón-Romero, L. Arias-Durán et al., "Antidiabetic effect of *Achillea millefollium* through multitarget interactions: α-glucosidases inhibition, insulin sensitization and insulin secretagogue activities," *Journal of Ethnopharmacology*, vol. 212, pp. 1–7, 2018.

[12] U. Özgen, Y. Kaya, and P. Houghton, "Folk medicines in the villages of Ilıca District (Erzurum, Turkey)," *Turkish Journal of Biology*, vol. 36, no. 1, pp. 93–106, 2012.

[13] A. Akbar, I. Ali, N. U. Samiullah, S. A. Khan, Z. Rehman, and S. U. Rehman, "Functional, antioxidant, antimicrobial potential and food safety applications of curcuma longa and Cuminum cyminum," *Pakistan Journal of Botany*, vol. 51, no. 3, pp. 1129–1135, 2019.

[14] V. L. Singleton and J. A. Rossi, "Colorimetry of total phenolics with phosphomolybdic-phosphotungstic acid reagents," *American Journal of Enology and Viticulture*, vol. 16, no. 3, pp. 144–158, 1965.

[15] M. B. Sadiq, W. Hanpithakpong, J. Tarning, and A. K. Anal, "Screening of phytochemicals and *in vitro* evaluation of antibacterial and antioxidant activities of leaves, pods and bark extracts of *Acacia nilotica* (L.) Del.," *Industrial Crops and Products*, vol. 77, pp. 873–882, 2015.

[16] I. F. Benzie and J. J. Strain, "The ferric reducing ability of plasma (FRAP) as a measure of "antioxidant power": the FRAP assay," *Analytical Biochemistry*, vol. 239, no. 1, pp. 70–76, 1996.

[17] S. Yesmin, A. Paul, T. Naz et al., "Membrane stabilization as a mechanism of the anti-inflammatory activity of ethanolic root extract of Choi (Piper chaba)," *Clinical Phytoscience*, vol. 6, no. 1, pp. 1–10, 2020.

[18] K. Gunathilake, K. Ranaweera, and H. Rupasinghe, "Influence of boiling, steaming and frying of selected leafy vegetables on the in vitro anti-inflammation associated biological activities," *Plants*, vol. 7, no. 1, p. 22, 2018.

[19] M. Ahmed, M. Ji, P. Qin et al., "Phytochemical screening, total phenolic and flavonoids contents and antioxidant activities of *Citrullus colocynthis* L. and *Cannabis sativa* L," *Applied Ecology and Environmental Research*, vol. 17, no. 3, pp. 6961–6979, 2019.

[20] L. Othman, A. Sleiman, and R. M. Abdel-Massih, "Antimicrobial activity of polyphenols and alkaloids in Middle Eastern plants," *Frontiers in Microbiology*, vol. 10, p. 911, 2019.

[21] M. Strzępek-Gomółka, K. Gaweł-Bęben, and W. Kukula-Koch, "*Achillea* species as sources of active phytochemicals for dermatological and cosmetic applications," *Oxidative Medicine and Cellular Longevity*, vol. 2021, Article ID 6643827, 14 pages, 2021.

[22] I. Riaz, Y. Bibi, N. Ahmad, S. Nisa, and A. Qayyum, "Evaluation of nutritional, phytochemical, antioxidant and cytotoxic potential of Capsella bursa-pastoris, a wild vegetable from potohar region of Pakistan," *Kuwait Journal of Science*, vol. 48, no. 3, pp. 1–11, 2021.

[23] N. Ali, S. W. A. Shah, I. Shah, G. Ahmed, M. Ghias, and I. Khan, "Cytotoxic and anthelmintic potential of crude saponins isolated from *Achillea wilhelmsii* C. Koch and *Teucrium Stocksianum* boiss," *BMC Complementary and Alternative Medicine*, vol. 11, no. 1, pp. 1–7, 2011.

[24] L. Apel, P. Lorenz, S. Urban et al., "Phytochemical characterization of different yarrow species (*Achillea* sp.) and investigations into their antimicrobial activity," *Zeitschrift für Naturforschung C*, vol. 76, no. 1-2, pp. 55–65, 2021.

[25] L. Raudone, J. Radušiene, F. Seyis et al., "Distribution of phenolic compounds and antioxidant activity in plant parts and populations of seven underutilized wild *Achillea* species," *Plants*, vol. 11, no. 3, p. 447, 2022.

[26] H. Fathi, B. L. Aghaee, and M. A. Ebrahimzadeh, "Antioxidant activity and phenolic contents of *Achillea wilhemsii*," *Pharmacologyonline*, vol. 2, pp. 942–949, 2011.

[27] M. Jafari, K. M. Naeini, Z. Lorigooini, and R. Namjoo, "Oral acute and sub-acute toxic effects of hydroalcoholic *Terminalia chebula* Retz and *Achillea wilhelmsii* extracts in BALB/c mice," *Biomedicine*, vol. 9, no. 4, p. 25, 2019.

[28] D. S. Bashi, B. S. Fazly Bazzaz, A. Sahebkar, M. M. Karimkhani, and A. Ahmadi, "Investigation of optimal extraction, antioxidant, and antimicrobial activities of Achillea biebersteinii and A. wilhelmsii," *Pharmaceutical Biology*, vol. 50, no. 9, pp. 1168–1176, 2012.

[29] S. Şabanoğlu, A. Gökbulut, and M. L. Altun, "Characterization of phenolic compounds, total phenolic content and antioxidant activity of three Achillea species," *Journal of Research in Pharmacy*, vol. 23, no. 3, pp. 567–576, 2019.

[30] R. Yazdanparast, A. Ardestani, and S. Jamshidi, "Experimental diabetes treated with *Achillea santolina* : effect on pancreatic oxidative parameters," *Journal of Ethnopharmacology*, vol. 112, no. 1, pp. 13–18, 2007.

[31] D. Barış, M. Kızıl, Ç. Aytekin et al., "In vitro antimicrobial and antioxidant activity of ethanol extract of three Hypericum and three Achillea species from Turkey," *International Journal of Food Properties*, vol. 14, no. 2, pp. 339–355, 2011.

[32] R. Gharibi, H. Yeganeh, A. Rezapour-Lactoee, and Z. M. Hassan, "Stimulation of wound healing by electroactive, antibacterial, and antioxidant polyurethane/siloxane dressing membranes: in vitro and in vivo evaluations," *ACS Applied Materials & Interfaces*, vol. 7, no. 43, pp. 24296–24311, 2015.

[33] H. G. Sevindik, Z. Güvenalp, K. Ö. Yerdelen, H. Yuca, and L. Ö. Demirezer, "The discovery of potential anticholinesterase compounds from *Achillea millefolium* L.," *Industrial Crops and Products*, vol. 76, pp. 873–879, 2015.

[34] S. Gharibi, B. E. S. Tabatabaei, G. Saeidi, S. A. H. Goli, and M. Talebi, "Total phenolic content and antioxidant activity of three Iranian endemic *Achillea* species," *Industrial Crops and Products*, vol. 50, pp. 154–158, 2013.

[35] S. Aziz, A. Akbar, Z. Gul et al., "Functional potential and chemical profile analysis of propolis oil extracted from propolis of balochistan," *Journal of Food Quality*, vol. 2022, Article ID 4782813, 10 pages, 2022.

[36] S. M. H. Alfatemi, J. S. Rad, M. S. Rad, S. Mohsenzadeh, and J. A. T. da Silva, "Chemical composition, antioxidant activity and in vitro antibacterial activity of *Achillea wilhelmsii* C. Koch essential oil on methicillin-susceptible and methicillin-resistant *Staphylococcus aureus* spp," *3 Biotech*, vol. 5, no. 1, pp. 39–44, 2015.

[37] K. Saeidi, M. Moosavi, Z. Lorigooini, and F. Maggi, "Chemical characterization of the essential oil compositions and antioxidant activity from Iranian populations of *Achillea wilhelmsii* K.Koch," *Industrial Crops and Products*, vol. 112, pp. 274–280, 2018.

[38] E. R. Elsharkawy, S. M. Alghanem, and E. Elmorsy, "Effect of habitat variations on the chemical composition, antioxidant, and antimicrobial activities of *Achillea fragrantissima* (Forssk) Sch. Bip," *Biotechnology Reports*, vol. 29, article e00581, 2021.

[39] G. Zengin, A. Aktumsek, R. Ceylan et al., "Shedding light on the biological and chemical fingerprints of three *Achillea* species (A. *biebersteinii*, A. *millefolium* and A. *teretifolia*)," *Food & Function*, vol. 8, no. 3, pp. 1152–1165, 2017.

[40] S. Albayrak and N. Silahtarlıoğlu, "Determination of biological activities of essential oil and extract obtained from Achillea coarctata Poir," *Advances in Traditional Medicine*, vol. 20, no. 1, pp. 77–88, 2020.

[41] S. A. Alsohaili and S. F. Sulaiman, "Phytochemical constituents, antioxidant, antibacterial and enzyme inhibition activities of essential oil from the aerial part of *Achillea tomentosa* L. grown in Jordan," *Journal of the Chilean Chemical Society*, vol. 66, no. 1, pp. 5093–5097, 2021.

[42] A. Venditti, L. Guarcini, A. Bianco, S. Rosselli, M. Bruno, and F. Senatore, "Phytochemical analysis of *Achillea ligustica* all. From Lipari Island (Aeolian Islands)," *Natural Product Research*, vol. 30, no. 8, pp. 912–919, 2016.

[43] A. Venditti, F. Maggi, S. Vittori et al., "Antioxidant and α-glucosidase inhibitory activities of *Achillea tenorii*," *Pharmaceutical Biology*, vol. 53, no. 10, pp. 1505–1510, 2015.

[44] M. K. B. Break, K. M. Younes, S. Elkahoui et al., "*Achillea fragrantissima* (Forssk.) Sch. Bip. methanolic extract exerts potent antimicrobial activity and causes cancer cell death *via* induction of caspase-dependent apoptosis and S-phase arrest," *Natural Product Research*, vol. 36, 2022.

[45] A. G. G. Darwish, M. N. Samy, S. Sugimoto, K. Matsunami, and H. Otsuka, "In vitro antileishmanial activity of methanolic extracts for some selected medicinal plants," *Pharmacognosy Magazine*, vol. 15, no. 62, p. 34, 2019.

[46] S. S. Al-Sokari, N. A. A. Ali, L. Monzote, and M. A. Al-Fatimi, "Evaluation of Antileishmanial Activity of Albaha Medicinal Plants against *Leishmania amazonensis*," *BioMed research international*, vol. 2015, Article ID 938747, 6 pages, 2015.

[47] L. Amjad, M. Mohammadi-Sichani, and M. Mohammadi-Kamalabadi, "Potential activity of the *Achillea wilhelmsii* leaves on bacteria," *International Journal of Bioscience, Biochemistry and Bioinformatics*, vol. 1, no. 3, pp. 216–218, 2011.

[48] K. Klobucar and E. D. Brown, "New potentiators of ineffective antibiotics: targeting the gram-negative outer membrane to overcome intrinsic resistance," *Current Opinion in Chemical Biology*, vol. 66, article 102099, 2022.

[49] L. Amjad, K. Mousavidehmourdi, and M. Saghazadeh, "Antifungal potential of *Achillea wilhelmsii* flowers methanolic extract on different strains of Candida albicans," *International Journal of Biological and Medical Research*, vol. 3, no. 3, pp. 2107–2110, 2012.

[50] A. Tajehmiri, M. R. Rahmani, S. S. Moosavi, K. Davari, and S. S. Ebrahimi, "Antifungal effects of six herbal extracts against *Aspergillus* sp. and compared to amphotericin B and nystatin," *International Journal of Advanced and Applied Sciences*, vol. 5, no. 7, pp. 53–57, 2018.

[51] S. F. Mirahmadi and R. Norouzi, "Chemical composition, phenolic content, free radical scavenging and antifungal activities of *Achillea biebersteinii*," *Food Bioscience*, vol. 18, pp. 53–59, 2017.

[52] E. Küpeli, İ. Orhan, Ş. Küsmenoğlu, and E. Yeşilada, "Evaluation of anti-inflammatory and antinociceptive activity of five Anatolian *Achillea* species," *Turkish Journal of Pharmaceutical Sciences*, vol. 4, no. 2, pp. 89–99, 2007.

[53] D. Chaturvedi, *Sesquiterpene lactones: structural diversity and their biological activities, In-Opportunity, challanges and Scope of Natural Products in Medicinal Chemistry*, Research Signpost, Trivandrum, 2011.

[54] N. Honari, P. Shaban, S. Nasseri, and M. Hosseini, "Ethanolic extract of *Achillea wilhelmsii* C. Koch improves pulmonary function and inflammation in LPS-induced acute lung injury mice," *Journal of Complementary and Integrative Medicine*, vol. 19, no. 2, pp. 261–267, 2022.

Hindawi
Oxidative Medicine and Cellular Longevity
Volume 2022, Article ID 7660118, 22 pages
https://doi.org/10.1155/2022/7660118

Research Article

Autologous Bioactive Compound Concentrated Growth Factor Ameliorates Fistula Healing of Anal Fistula in a Pig Model and Promotes Proliferation and Migration of Human Skin Fibroblasts via Regulating the MEK/ERK Pathway

Xiufeng Zhang, Jianming Qiu, Houdong Wang, Zhenfeng Lu, Shuxian Shao, Jun He, and Zhong Shen

Department of Coloproctology, Hangzhou Third People's Hospital, Zhejiang, China

Correspondence should be addressed to Zhong Shen; shenzhong114@sina.com

Received 26 July 2022; Revised 20 August 2022; Accepted 23 August 2022; Published 14 October 2022

Academic Editor: Yehui Duan

Recent evidence suggested that autologous concentrated growth factor (CGF), a new bioactive compound from autologous blood is used widely as an ingenious biomaterial in tissue regeneration with anti-inflammatory properties. This study investigated whether CGF could be involved in the treatment of fistula healing in the anal fistula. For this purpose, the porcine anal fistula model was conducted using the rubber band ligation method and collected pig autogenic CGF to treat the fistulas. CGF treatment promoted fistula healing, which was reflected in the downregulation of inflammatory factors, upregulation of growth factors, and promoted epithelial-mesenchymal transition with increased collagen synthesis. Besides, 16S rRNA gene sequencing analysis of fistula tissues between the control and CGF groups showed that the microbial populations exhibiting significant differences were *VadinCA02*, *Blastomonas*, *Deinococcus*, *Devosia*, *Sphingomonas*, *Rubrobacteria*, and *GW_34*. CGF of volunteers were collected to process small interfering RNA- (siRNA-) ERK or siRNA-negative control transfected human skin fibroblasts (HSF). The results showed that CGF also promoted the proliferation and extracellular matrix-related functions in HSF, as well as activated the MEK/ERK pathway *in vitro* and *in vivo*. Finally, knockdown ERK reversed the effects of CGF in promoting wound healing in HSF. Collectively, our results suggest that the CGF as the bioactive compound from autologous blood exhibited great potential for repairing fistulas as well as promoting the proliferation and migration of human skin fibroblasts by triggering MEK/ERK signaling. These findings provided a fresh perspective for understanding the role of CGF in the management of fistulas.

1. Introduction

Anal fistula is a self-growing chronic inflammatory sinus around the rectum and anus [1]. Perianal pain is often accompanied by fever and listlessness, which seriously affects the quality of life of patients with anal fistula [1]. At present, the treatment of anal fistula is mainly surgery, but surgery inevitably causes anal sphincter injury to a certain extent [2]. In recent years, some biomaterial-based minimally invasive treatment methods for anal fistula, which promote the healing of the fistula by injecting biomaterials (bio-glue, anal fistula plug, acellular matrix, autologous or allogeneic mesenchymal stem cells, etc.) into the fistula, hardly cause any damage to the anal sphincter, but these biomaterials still have the disadvantage of the potential risk of allergic reaction with a high cost and have failed in a phase III pivotal trial [3, 4]. Therefore, finding new biological materials with high-cost performance, suitable for promotion and therapeutic effect are warranted.

Autologous platelet-rich plasma (PRP), a platelet concentrate extracted from autologous blood, contains a high concentration of growth factors, which can significantly accelerate wound healing [5]. In addition, PRP has been widely used in clinical practice in recent years due to its

simple preparation, high safety, and autologous origin, thus eliminating the rejection between tissues [6, 7]. Moreover, clinical trials have reported that PRP-filled fistula treatment is safe and has a certain cure rate [8, 9]. However, PRP is close to fluid in shape and is difficult to retain in the fistula for sufficient time to affect its role as a biological skeleton. Autologous concentrated growth factor (CGF) is the latest generation of platelet-rich product, which contains high concentrations of growth factors like PRP, but has a more solid structure than PRP [10]. These characteristics make CGF more suitable for the minimally invasive treatment of anal fistula in theory.

Fistula healing consists of three stages: an inflammatory response phase, a granulation phase, and a tissue remodeling phase [11]. In the first stage, white blood cells are recruited to produce a variety of inflammatory factors; in the second stage, recruited fibroblasts, vascular endothelial cells, and epithelial cells participate in angiogenesis and fiber proliferation to induce granulation tissue from the wound [12]; in the third stage, the ECM undergoes recombination, degradation, and resynthesis, with reduced water and blood vessels in the granulation tissue and the formation of scar tissue [13]. In these processes, various cytokines play an important role, including growth factors, inflammatory factors, and matrix metalloproteinases (MMPs) [14]. Among them, epidermal growth factor (EGF) is currently recognized as one of the most closely related cytokines to wound healing [15]. Also, it has been proven that EGF possessed a strong prodivisive activity on a variety of tissue-derived epithelial cells and promoted the migration of epithelial cells, endothelial cells, and fibroblasts [16]. MEK/ERK signaling pathway has been widely validated to be associated with the wound healing process [17, 18]. Extracellular signal-regulated kinases (ERK1/2), the downstream of MEK signaling pathway, are one of the components of the MAPK family [18]. Furthermore, it was found that ERK signaling pathway can promote the growth of granulation tissue in the wound by mediating the proliferation and migration of fibroblasts [19]. Of note, CGF contains a high concentration of EGF which has the ability to activate the ERK signaling pathway [20]. Therefore, we speculated that the injection of CGF into the fistula could activate the ERK signaling pathway. In this study, we sought to determine whether the MEK/ERK pathway was involved in the effect and molecular mechanism of CGF on human skin fibroblast proliferation and migration, as well as fistula healing in a pig model.

2. Materials and Methods

2.1. Animals and Ethics Statement. A total of 6 male landrace pigs (70-120 days old, 30 kg) were supplied by Wujiang Tianyu Biological Technology Co., Ltd. (Certificate no. SCXK (Su) 2021-0007) and housed in an environmentally controlled room (24°C, 12 h/12 h light/dark, and 50% humidity). Our research was approved by the Animal Ethical and Welfare Committee of Zhejiang Chinese Medical University (Approval number: IACUC-20211108-06, Hangzhou, China).

2.2. Construction of the Anal Fistula Animal Model. The pigs underwent anal fistula operation after adaptive feeding for one week. The anal fistula animal model was established as previously described with minor modification [21]. Before surgery, pigs were anesthetized by intramuscular injection of propofol (2 mg/kg). After tracheal intubation, 3% isoflurane (3 L/min) was administered to maintain anesthesia in the pigs. After the anesthesia was effective, routine disinfection was performed, and all the pigs were subjected to anoscopy, digital diagnosis, and anoscopy in the lateral decubitus position. A 0.5 cm incision was made at the lateral margin of the anus about 2 cm from the anus at 3, 9, and 12 o'clock of the lithotomy position (three fistulas were used as control, CGF, and model groups, respectively). A vascular clamp was used to penetrate the anal sphincter structure above the dentate line directly from the small incision. A vascular forceps were used to puncture the anorectal mucosa, and a rubber band was clamped from the anus to penetrate through the whole fistula tract and then exit the perianal incision. The rubber bands were fixed with thin wires to avoid falling off and blocking the anus, and the incision was fixed with a gauze bandage. The pigs were returned to the postoperative care unit until they awoke. After the operation, the vital signs of the animals were detected. The wounds of animals were observed daily, and their dressing changes were made.

2.3. Autologous CGF Preparation. 10 mL peripheral blood of landrace pig was drawn into a sterile anticoagulation tube and immediately centrifuged in a special machine (Medifuge CGF MF 200100 Silfradent SRL, Sofia, FC, Italy). The centrifugation procedures were as follows: 30s acceleration, 2700 rpm for 2 min, 2400 rpm for 4 min, 2700 rpm for 4 min, 3000 rpm for 3 min, and 36 s deceleration to stop. The middle layer of the centrifuged liquid was used for subsequent experiments.

2.4. Groups and Drug Treatment. Four weeks after the operation, the fistulas in the model group were collected for model verification, the fistulas in the control group were subjected to curettage and X-ray examination (X-ray equipment, Philips, Germany), while those in the CGF group were subjected to X-ray examination, curettage, and CGF injection (the fistula was filled, and the suture was performed at the external orifice). Six weeks after surgery, all the animals were further evaluated for fistula healing by B-mode ultrasonography, and the skin on the surface of the fistula was collected for histological staining and immunohistochemistry assays. Eight weeks after surgery, all animals were examined by B-mode ultrasound, and the fistulae were collected for histological staining, immunohistochemistry, enzyme-linked immunosorbent assay (ELISA), quantitative reverse transcription-polymerase chain reaction (qRT-PCR), and Western blot analyses, and the distribution of fistula flora was also identified by 16S DNA sequencing.

2.5. B-Mode Ultrasonography Analysis. A proper amount of ultrasonic coupling agent was applied to the anus and perianal skin of landrace pigs, and the ultrasonic probe of the

digital color ultrasonic diagnostic apparatus (G50, VINNO, China) was placed on the bare skin to observe the tissue morphology.

2.6. Histological Analysis. The tissues were fixed in the fixing solution (G1101, Servicebio, China) for more than 24 hours, and then the tissues were successively dehydrated and embedded. The wax block was placed in microtomes (RM2016, Leica, China) and cut into 4 μm slices, which were then baked in a 60°C oven. The paraffin sections were subsequently dewaxed and hydrated, followed by staining with hematoxylin (G1004, Servicebio, China). After being subjected to differentiation and bluing, the sections were stained with eosin (G1001, Servicebio, China) and subjected to dehydration and transparency treatment. Thereafter, the sections were sealed with neutral balsam (10004160, Sinopharm Chemical Reagent Co., Ltd., China) and were observed under microscopy (Nikon Eclipse E100, Nikon, Japan).

2.7. ELISA Assay. The tissue was homogenized and centrifuged, and the supernatant was collected as an ELISA sample. The contents of EGF, platelet-derived growth factor (PDGF), vascular endothelial growth factor (VEGF), angiotensin- (Ang-) II, insulin-like growth factor- (IGF-) 1 receptor (R), transforming growth factor- (TGF-) β1, IL-6, IL-12, IL-1β, and TNF-α were measured with ELISA kits (Meimian, China). In brief, the sample was added to an ELISA plate which was coated with antibodies. After incubating for 30 minutes at 37°C, the sample was reacted with an enzyme-labeled antibody for 30 minutes at 37°C. Subsequently, the substrate chromogenic solution was added to the ELISA plate for chromogenic reaction, and finally, the reaction was stopped by stopping solution. The optical density (OD) value was measured with a microplate reader (CMaxPlus, MD, China) at a wavelength of 450 nm.

2.8. Terminal Deoxynucleotidyl Transferase-Mediated Deoxyuridine Triphosphate Nick End Labeling (TUNEL) Staining. TUNEL staining was carried out with the help of the TUNEL Kit (G1507, Servicebio, China). In brief, paraffin sections were dewaxed, hydrated, and repaired with proteinase K solution. Then, the slices were incubated with Triton X-100 (G1204 Servicebio, China), and then with 3% hydrogen peroxide solution (216763, Merck, Germany). After that, the slices were reacted with TUNEL reaction solution and Streptavidin-HRP solution in turn, and then undergo DAB color development (G1212, Servicebio, China) and hematoxylin staining. After dehydration, transparentization, and mounting, the sections were finally observed under a microscope.

2.9. Western Blot Assay. Protein extraction was performed by RIPA lysis buffer (R0010, Solarbio, China), after which the protein concentration was quantified using a BCA protein kit (BI-WB005, SBJBIO, China). Afterwards, equal contents of protein (30 μg) were fractionated by SDS-PAGE and then transferred into PVDF membranes (Millipore, USA). After being blocked with 5% skim milk for 2 h, the membranes were incubated with primary antibodies at 4°C overnight. Then, the membranes were washed three times and incubated with secondary antibodies for 1 h at room temperature. The information on antibodies was shown in Table S1. Visualization of protein expression was conducted by ECL reagent (abs920, Absin, China) on eZwest Lite Auto Imaging System (Genscript, USA), and GAPDH or β-actin was selected as a loading control.

2.10. Immunohistochemistry and Immunofluorescence Staining. The paraffin sections were dewaxed, hydrated, and placed in citrate buffer (BL604A, Biosharp, China) and then heated by microwave for antigen repair. Thereafter, sections were soaked in a 3% hydrogen peroxide solution for immunohistochemistry. After being blocked by 3% BSA, the sections were incubated with primary antibodies including anti-EGF, anti-FSP1/A100A4, anti-CD34, anti-P-ERK, and antivimentin. The next day, the sections were incubated with secondary antibody or fluorescent secondary antibody at room temperature for 1 hour. For immunohistochemistry, the sections were developed by DAB and stained with hematoxylin, while for immunofluorescence, the sections were stained with DAPI (40728ES03, Yeasen, China). The sections were finally observed under a microscope or fluorescent microscope (NIKON ECLIPSE C1, Nikon, Japan).

2.11. Quantitative Reverse Transcription-Polymerase Chain Reaction (qRT-PCR). Total RNA was extracted by TRIzol reagent (Sangon Biotech, China), subsequent to which reverse transcription was conducted using First Strand cDNA Synthesis Kit (abs601510, Absin, China) for cDNA generation. After that, cDNA amplified in a Real-Time PCR System (7500, ThermoFisher, USA) was traced by SYBR Premix Ex Taq^{II} Mix (Takara, Japan). The relative expressions were normalized to GAPDH using $2^{-\Delta\Delta CT}$ approach [22]. The sequences of the primers are listed in Table S2.

2.12. 16S rRNA Sequencing. 16S rRNA sequencing was conducted as previously described [22]. In brief, the DNA was separated from the sample by DNA kit (EE101-11, Transgen, China), then quantified by NanoDrop (ND-ONE-W, Thermo Fisher, USA). The target fragment was amplified and the product was purified by magnetic beads (N411-01, Vazyme, China) and then quantified by Quant-iT PicoGreen dsDNA Assay Kit (P7589, Thermo Fisher, USA). Next, sequencing libraries were prepared using TruSeq Nano DNA LT Library Prep Kit (20015964, Illumina, USA) and sequenced on the Illumina MiSeq/NovaSeq platform. Sequencing raw data were stored in FASTQ format and subsequently denoised or clustered by DADA2 [23] or VSEARCH [24]. QIIME 2[25] software was used for annotation, evaluation of alpha diversity of microorganisms, and principal coordinate analysis (PCoA). The amplicon sequence variant (ASV)/operational taxonomic unit (OTU) plots were produced using either the Venn Diagram package or the plotrix package to analyze species differences. Marker and intergroup differences were analyzed by linear

discriminant analysis effect size (LEfSe), and metabolic pathways were analyzed by the KEGG and MetaCyc databases.

2.13. Cell Culture. Human skin fibroblasts (HSF) were purchased from Aybio (China) and cultivated in DMEM medium (SH30243.01, Hyclone, USA) with 10% fetal bovine serum (16140071, Gibco, USA) and 1% penicillin/streptomycin (15140148, Gibco, USA).

2.14. Transfection. HSF were seeded in 6-well plates (5×10^5 cells/well) and cultured for 24 hours. ERK-specific small interfering RNA (siRNA) and its corresponding negative control (NC) were synthesized by Sangon (siRNA-ERK#1: TGGCTA CGATGAGAACATGAACA; siRNA-ERK#2: GACCTTCAA CCTCTATTACTATG; siRNA-ERK#3: CTCCTTTCTCC GGCAAAACGATG). The transfection was conducted with the help of a transfection reagent (L3000001; Thermo Fisher Scientific, USA). In brief, the reagent and siRNA were, respectively, diluted in the serum-free medium and then mixed, which was later added to cells for 24 hours of incubation. The interference efficiency was determined by Western blot.

2.15. Preparation of Human CGF. Venous blood was drawn from 3 healthy volunteers into anticoagulation tubes for the preparation of CGF as described previously [26]. All volunteers signed informed consent. In brief, the centrifugation procedures were as follows: 2700 rpm/min for 2 min, 2400 rpm/min for 4 min, 2700 rpm/min for 4 min, and 3000 rpm/min for 3 min. The middle layer of the centrifuged liquid was used for subsequent experiments.

2.16. Grouping. The cell experiments were conducted in three parts. First, HSF was incubated with different concentrations of human CGF (0, 5, 10, 15, 20, 25, and 30%) for 8 hours, and then the appropriate CGF concentration was screened by cell counting kit 8 (CCK8). Next, HSF was incubated with selected concentrations of CGF (0, 10, 15, and 20%) for 8 hours and the cells were tested for biological behavior. Third, cells transfected with siRNA-ERK or siRNA-NC were incubated with CGF (20%) for 8 hours and then evaluated for biological behavior.

2.17. CCK-8 Assay. HSFs were seeded in a 96-well plate (5×10^3 cells/well) and cultured for 24 h. Next, cells were incubated with CCK-8 solution (HY-K0301, MCE, China) for 2 h, and a microplate reader was utilized to read the OD value at 450 nm.

2.18. Cell Proliferation Assay. Cell proliferation was determined by Yefluor 594 Edu Imaging Kits (40276ES60, Yeasen, China). Sterile coverslips were placed in 12-well plates and cells were subsequently inoculated in 12-well plates. EdU working solution was added to the cells and incubated for 4 h. The cells were fixed with 95% ethanol, washed with PBS, permeabilized with TritonX-100, and incubated with click reaction solution for 30 minutes. After that, the cells were stained with DAPI for 2 minutes and subsequently mounted. The image was photographed under a fluorescence microscope.

2.19. Scratch Assay. HSFs were seeded in a 6-well plate (5×10^5 cells/well) and cultured for 24 hours. Linear wounds across the monolayer of cells were made by a pipette tip. After washing with phosphate-buffered saline (PBS, E607008, Sangon, China), the cells were cultured in the incubator for 24 hours. The scratch closure area was photographed at 0 and 24 hours using a microscope.

2.20. Statistical Analysis. The measurement data were presented as mean ± standard deviation. The measurement data conforming to normal distribution and homogeneity test of variance were analyzed using one-way ANOVA. LSD analysis was used for further pairwise comparison between groups. Dunnett's T3 test or independent sample t-test was used for heterogeneity of variance. Kruskal-Wallis H test was used for the measurement data does not conform to normal distribution. The statistical analysis was implemented with SPSS 16.0 software, with $P < 0.05$ considering statistical significance.

3. Results

3.1. CGF Treatment Promoted the Healing of Pig Fistula. Figures 1(a)–1(i) showed the process of anal fistula animal model construction and CGF treatment. Two and four weeks after CGF treatment, the pig fistula was examined by B-mode ultrasound. As shown in Figure 1(j), after two weeks of CGF treatment, a relatively broad lumen was visible in the fistula tissue of the control group, while the lumen in the fistula tissue of the CGF group was narrower than that of the control group and showed signs of healing. After four weeks of treatment with CGF, partial healing of the fistula was observed in the control group, but the hollow part was still clearly visible. The fistulas in the CGF group almost healed, and an elongated tube could be faintly seen.

In addition, we also evaluated the pathological changes of fistula tissue by H&E staining (Figure 1(k)). Four weeks after CGF treatment, in the control group, cicatrix repair was dominant in porcine fistula tissue wounds, and a small amount of granulation tissue was formed, accompanied by a large number of inflammatory cell infiltration, and no new capillary formation was observed. The wounds of porcine fistula tissue in the CGF group were repaired, and the inflammatory cell infiltration was reduced. The fibroblasts were mature and arranged neatly, and the distribution of new capillaries was visible.

3.2. CGF Increased Expressions of Angiogenesis-Related Factors and Inhibited Inflammatory and Apoptosis Levels in Granulation Tissue. Wound blood supply and inflammatory response played an important role in wound healing, so we assessed the levels of angiogenesis-related factors and inflammatory factors in each group after 4 weeks of CGF treatment. We found that after treatment with CGF, the levels of angiogenesis-related factors (EGF, PDGF, VEGF, Ang-II, IGF-1R, and TGF-β1) in central granulation tissue of fistula wound were increased (Figure 2(a), $P < 0.05$), while the levels of inflammatory factors (IL-6, IL-12, IL-1β, and TNF-α) were decreased (Figure 2(b), $P < 0.05$). In addition,

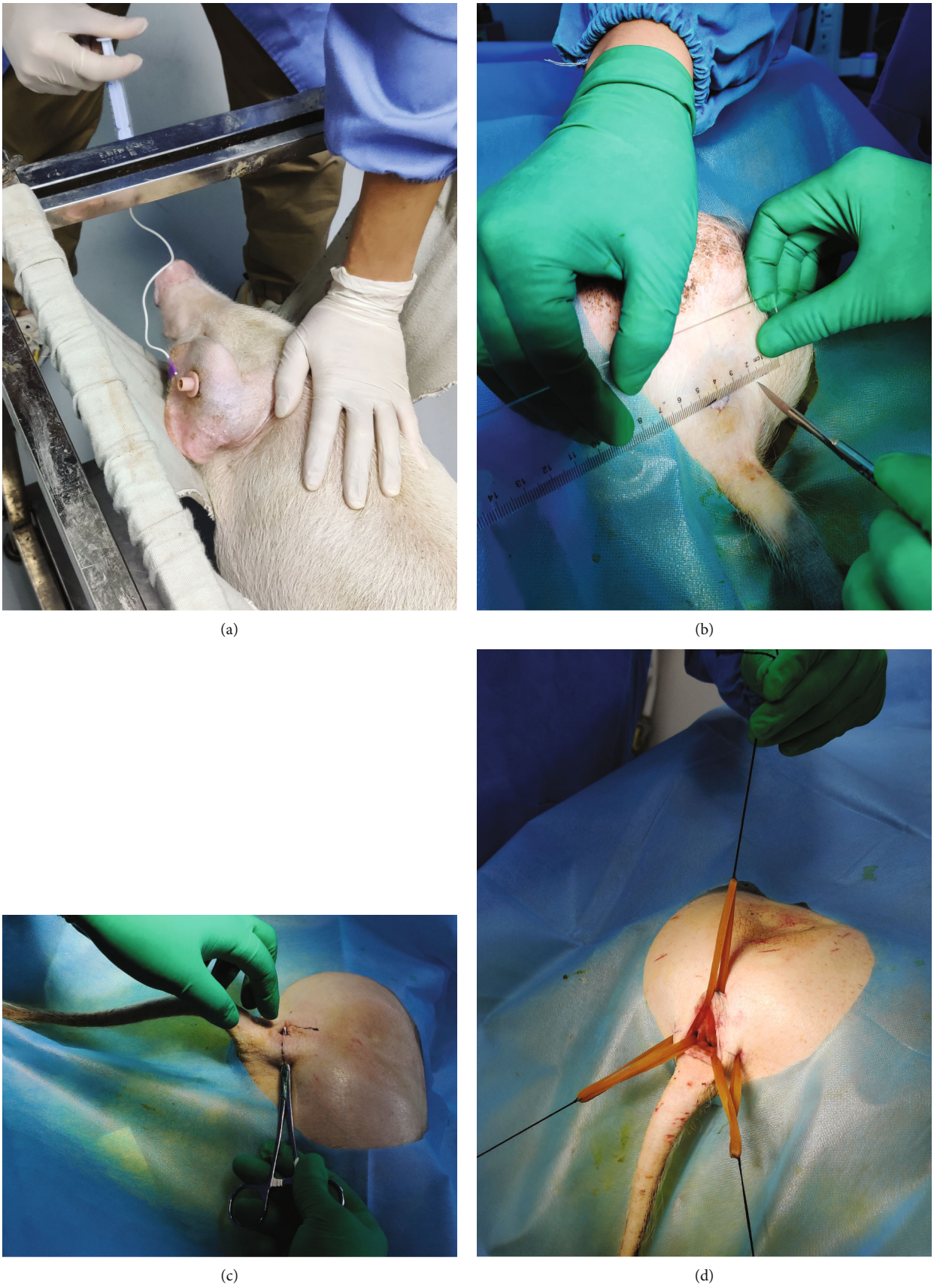

(a) (b) (c) (d)

Figure 1: Continued.

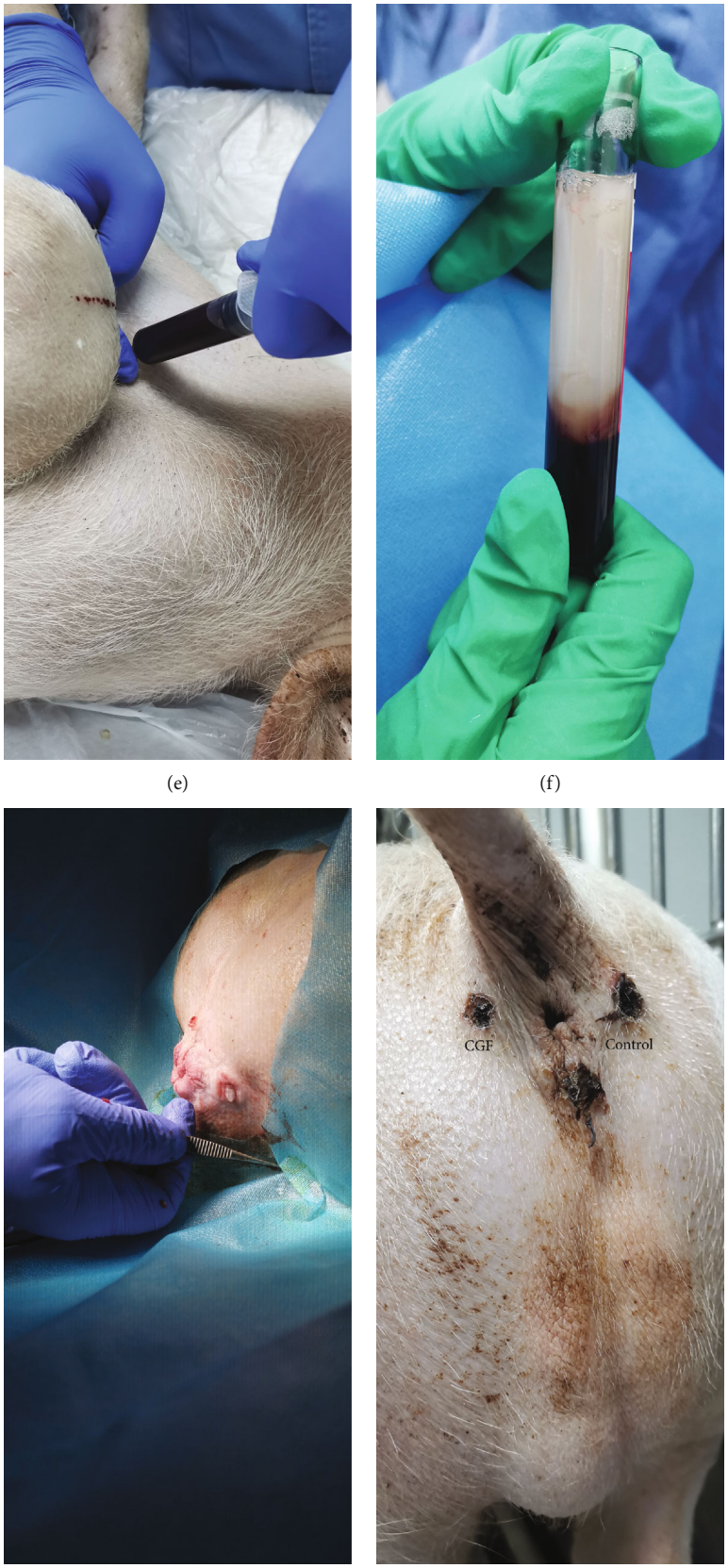

(e) (f)

(g) (h)

Figure 1: Continued.

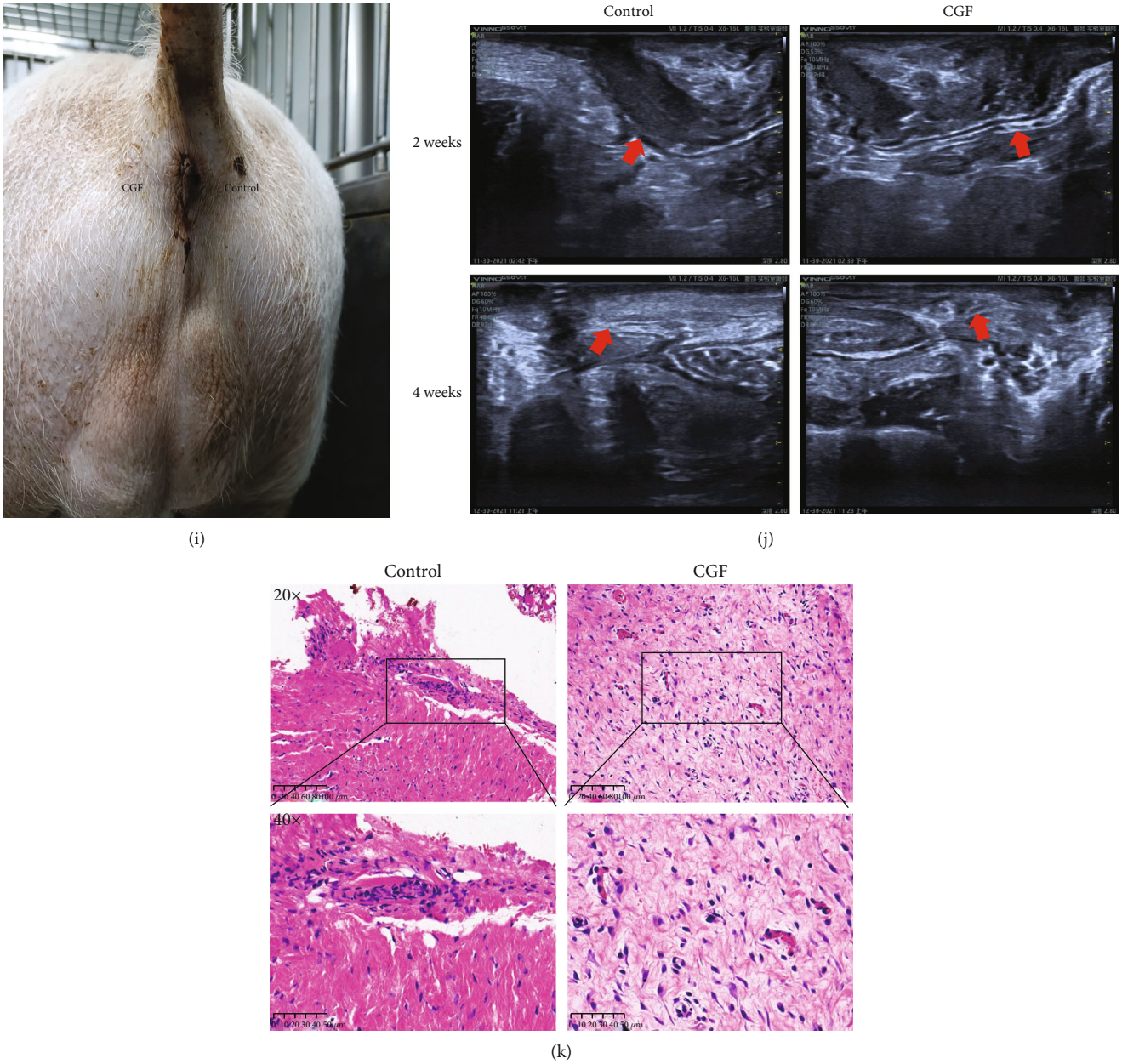

Figure 1: Porcine anal fistulae model creation process using rubber ligation surgery and treatment. (a) The marginal ear vessels injection with propofol at 2 mg/kg. (b) A 2 cm minimal incision was made in the anus at 3, 9, and 12 o'clock positions, and ligated rubber was used. (c) Directly cross through the anal rectal mucosa with the hemostatic clamp. (d) Rubber ligation was fixed to the fistula. (e) 10 ml blood sample was corrected from the pig. (f) Concentrated growth factor (CGF) was prepared from the pig itself. (g) CGF was used to treat the fistula at the 9 o'clock position. (h) CGF treatment for 2 weeks. (i) CGF treatment for 4 weeks. (j) B-mode ultrasound diagnosis imaging evaluation of created fistulas. (k) Posttreatment specimens of anal fistulae were stained with H&E and visualized at 20× and 40×.

the TUNEL staining of central granulation tissue of fistula wound unveiled that CGF treatment reduced the apoptosis rate (Figure 3(a), $P < 0.01$). Besides, the results of Western blot showed that CGF suppressed the expression levels of Bax and cleaved caspase-3 and fostered the levels of Bcl-2 in central granulation tissue of fistula wound (Figure 3(b), $P < 0.01$).

3.3. CGF Promoted Fibroblast Activation and ECM Accumulation by Activating MEK/ERK Pathway. We found that CGF treatment increased the expression of EGF, FSP1 (interstitial cell marker), CD34 (neovascular endothelial cell marker), and p-ERK in central granulation tissue of fistula wound (Figures 4(a) and 4(b)). Furthermore, qRT-CPR and Western blot experiments showed that factors related to the growth, proliferation, and differentiation of fibroblasts (PDGF, VEGF, TGF-β1, PNCA, and α-SMA) and genes related to the improvement of ECM function (COL1A1, COL3A1, TIMP-1, and C-fos) were upregulated by CGF, while the expression of MMP-3, a gene that inhibited ECM function, was downregulated by CGF (Figures 5(a)–5(c), $P < 0.05$). Our results also found that CGF also promoted

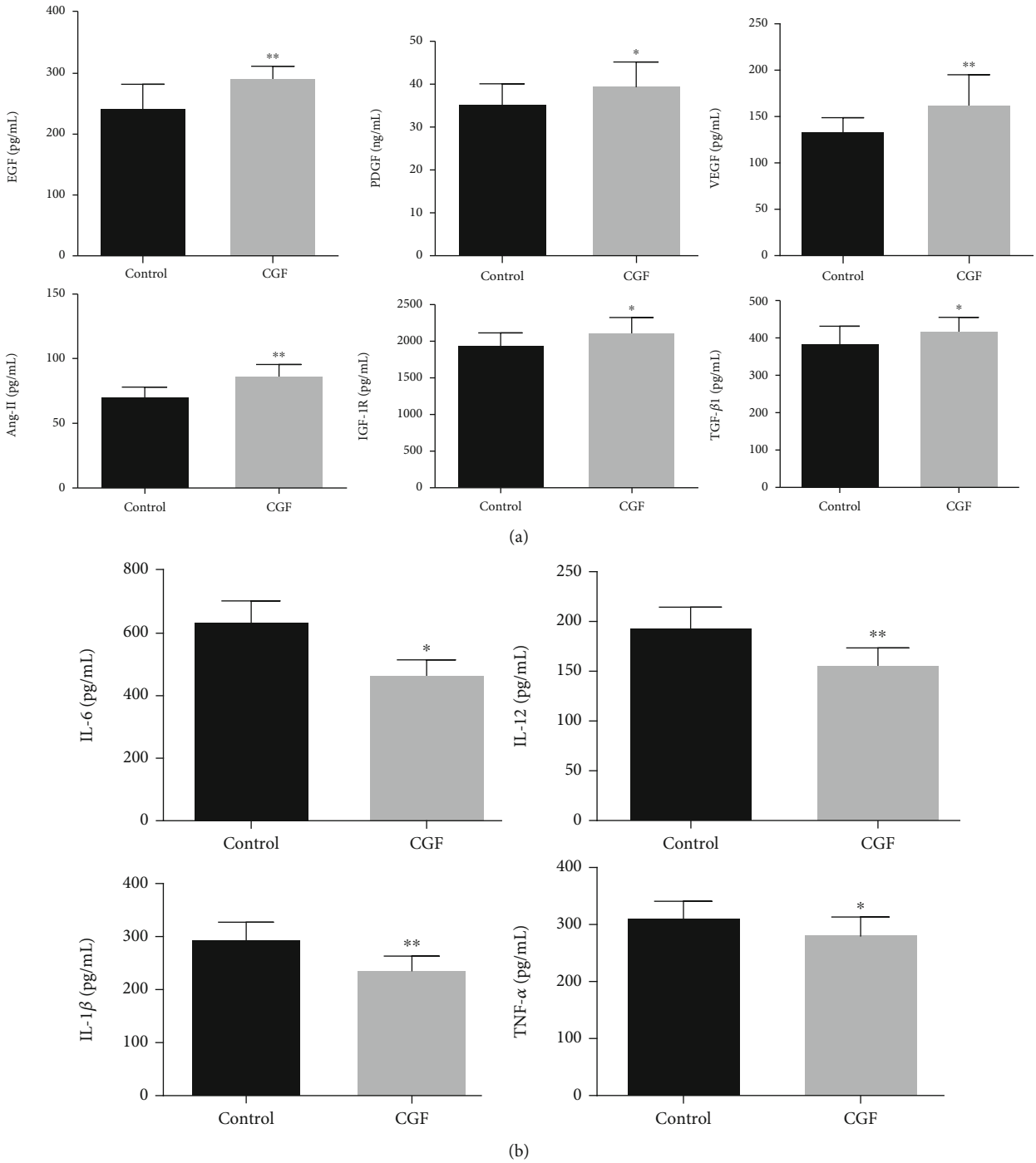

Figure 2: Effect of CGF on levels of vascular growth and inflammation-related factors in specimens of anal fistulae of pigs. (a) Levels of vascular growth-related factors EGF, PDGF, VEGF, Ang-II, IGF-1R, and TGF-β1 in specimens of anal fistulae were measured using ELISA assays. (b) Levels of inflammation-related factors IL-6, IL-12, IL-1β, and TNF-α were measured using ELISA assays. $^{*}P < 0.05$, $^{**}P < 0.01$ vs. control group.

vimentin but inhibited the expression of E-cadherin, indicating that the way of epithelial cells transform into fibroblasts for wound repair through EMT would be promoted by CGF (Figures 5(b)–5(c)). Meanwhile, CGF also promoted the expression of p-MEK1/2 and p-ERK1/2, which meant that CGF promoted the growth of fibroblasts by activating the MEK/ERK pathway (Figure 5(c)).

3.4. Analysis of 16S rRNA Sequencing. To evaluate the effects of CGF on the porcine fistula microbiota, 16S rRNA sequencing was conducted on fistula samples. We assessed the alpha diversity between samples using 7 indices. Chao1 and Observed species characterized the richness of microorganisms. Simpson and Shannon indices indicated species diversity. Pielou_e indicated species evenness, Faith_PD

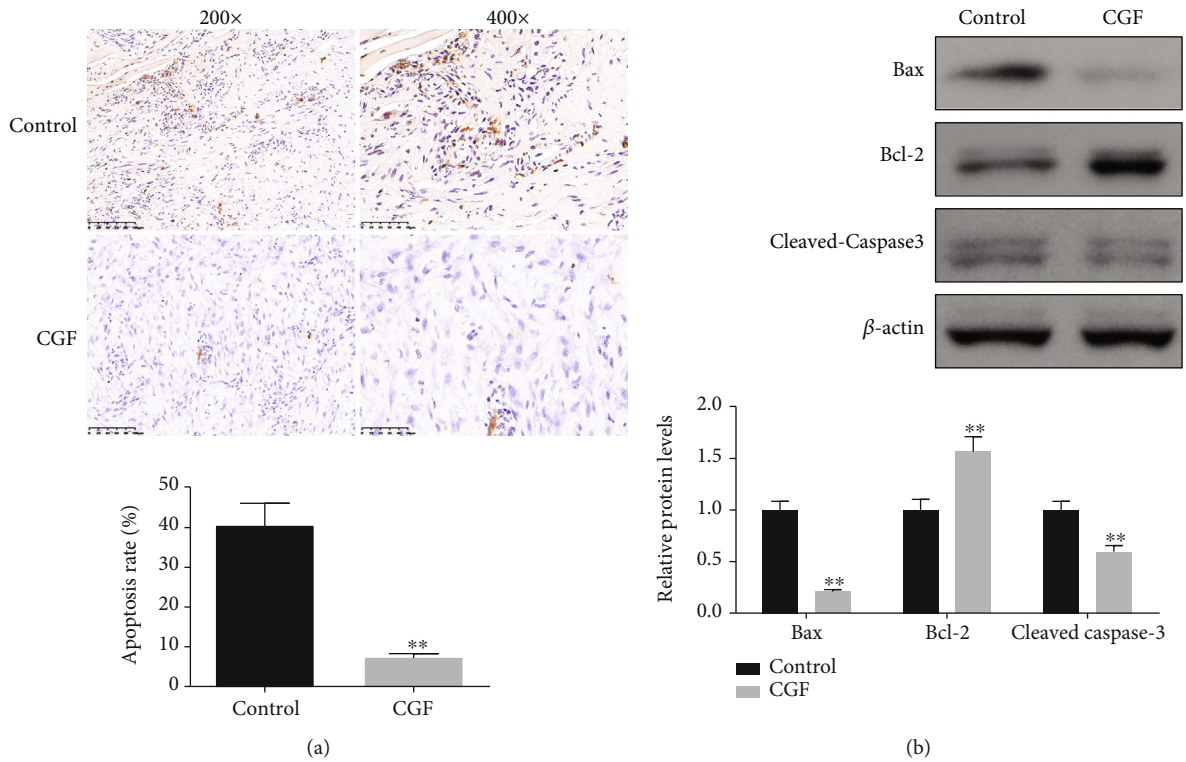

Figure 3: Effect of CGF on cell apoptosis of fistula tissues in pigs. (a) Cell apoptosis of fistula tissues was measured using TUNEL assay (scare bar = 50 μm). (b) Protein expression levels of Bax, Bcl-2, and cleaved caspase-3 were detected by Western blot assay. $^{*}P < 0.05$, $^{**}P < 0.01$ vs. control group.

indicated diversity based on evolution, and Goods_coverage indicated coverage. As shown in Figure 6(a), there are no significant differences in alpha diversity between the two groups ($P > 0.05$). Subsequently, PCoA was used to explore β diversity, and it can be seen that the two groups of samples were clearly distinguished (Figure 6(b) and 6(c)). To further analyze which species caused these differences, we counted the abundance of the corresponding ASV/OTU in each area at the level of phylum and genus and displayed it with a histogram (Figure 7(a)). The LEfSe analysis was then used to analyze significantly different species, with Figure 7(b) showing the predominant flora in the sham and CGF groups. According to the results of LEfSe, the microbial communities or species structures of different groups at different levels were shown by the cladogram. Seven different genera were identified in the fistula microbiota of the sham and CGF groups (LEfSe LDA > 2 and $P < 0.05$). *VadinCA02* and *Blastomonas* were increased in the sham group, whereas *Deinococcus*, *Devosia*, *Sphingomonas*, *Rubrobacteria*, and *GW_34* were increased in the CGF group (Figure 7(c)). The metabolic pathway analysis of the flora was carried out through the KEGG database and the MetaCyc databases. As illustrated in Figures 8(a) and 8(b), we found that the microbes were associated with amino acid and carbohydrate metabolism or biosynthesis, cofactor, prosthetic group, electron carrier, and vitamin biosynthesis, as well as nucleoside and nucleotide biosynthesis were more abundant in the CGF group. Furthermore, the CGF group had a higher abundance of microbes that participated in cell motility, translation, as well as replication, and repair.

3.5. CGF Promoted Cell Proliferation and Migration of HSF by Triggering the MEK/ERK Pathway. To further validate the role of CGF in fistula wound healing, we conducted an in vitro experiment in which HSF was cultured with CGF extracted from the venous blood of healthy volunteers. CGF (5%, 10%, 15%, and 20%) promoted the viability of HSF, while CGF at concentrations above 20% (25% and 30%) was less effective at promoting cell viability than CGF at 20% (Figure 9(a), $P < 0.01$). Therefore, we selected 10%, 15%, and 20% CGF for follow-up experiments. Through phenotypic experiments, we determined that these three concentrations of CGF promoted the proliferation and migration of HSF (Figures 9(b) and 9(c), $P < 0.01$). Moreover, CGF can also regulate the expression of ECM function-related, EMT-related, and MEK/ERK pathway-related proteins in HSF, as shown in the fact that CGF resulted in the increase of COL1A1, COL3A1, TIMP-1, C-fos, vimentin, p-MEK1/2/MEK1/2, and p-ERK1/2/ERK1/2 as well as the decrease of MMP-3 and E-cadherin (Figures 9(d) and 9(e), $P < 0.05$).

3.6. Knockdown ERK Reversed the Effects of CGF on Cell Proliferation and Migration in HSF. Since the ERK pathway was closely related to wound healing [27], we used siRNA-ERK to assess whether the role of CGF in

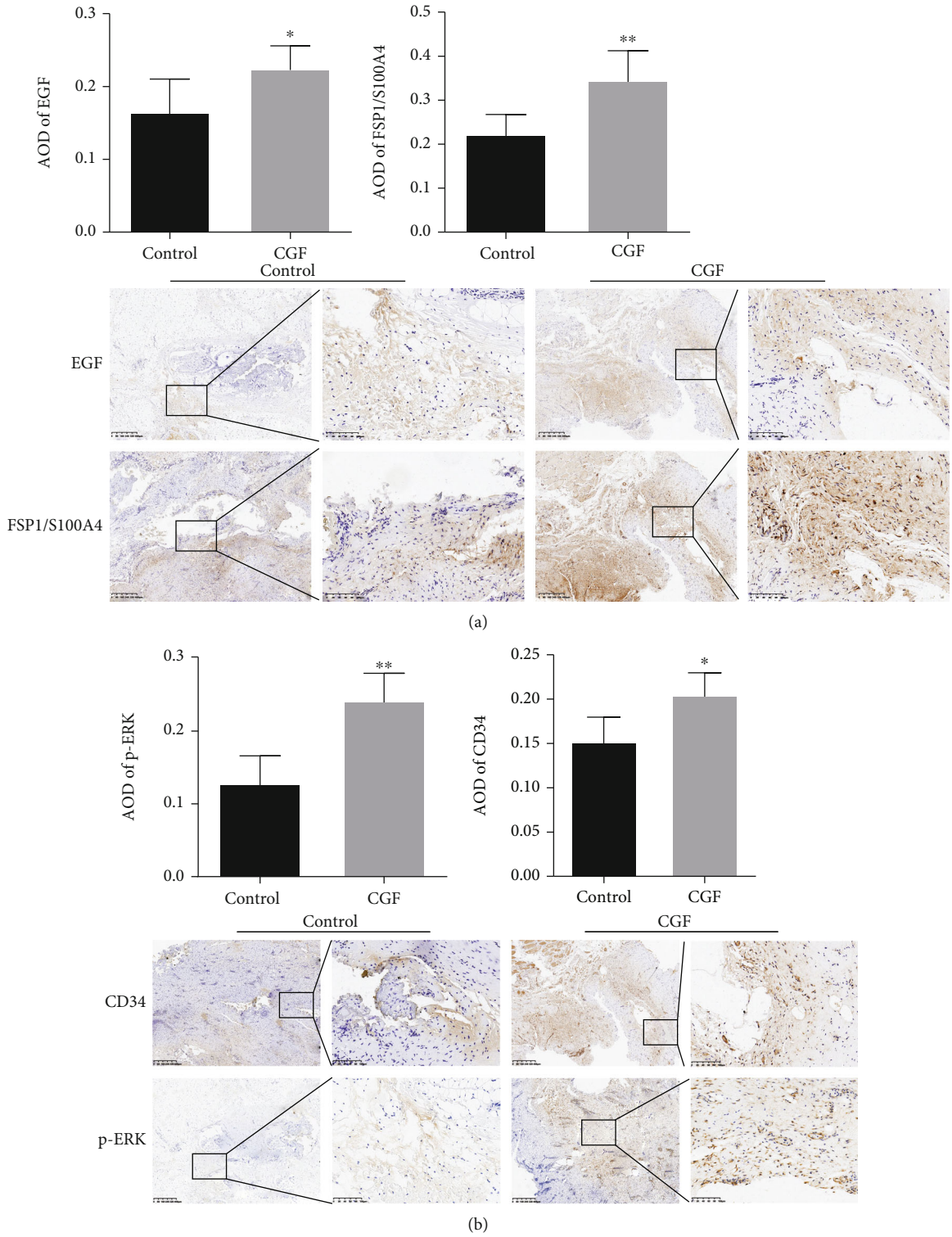

Figure 4: Effect of CGF on EGF, FSP1/S100A4, CD34, and p-ERK levels in fistula tissues of pigs. (a) EGF, FSP1/S100A4, (b) CD34, and p-ERK protein content in tissue samples were examined by IHC analysis. $^{*}P < 0.05$, $^{**}P < 0.01$ vs. control group.

promoting wound healing was mediated by regulating the ERK pathway. We designed three siRNA-ERKs, among which the inhibition effect of siRNA-ERK#3 was the most significant (Figure 10(a), $P < 0.05$). Therefore, siRNA-ERK#3 was selected for subsequent experiments. Interestingly, we found that siRNA-ERK reversed the promotion effect of 20% CGF on the viability, proliferation, and migration of HSF (Figures 10(b)–10(d), $P < 0.05$). Furthermore, the regulation of 20% CGF on ECM function-related, EMT-related, and MEK/ERK pathway-related proteins were also reversed by siRNA ERK (Figures 10(e) and 10(f), $P < 0.05$).

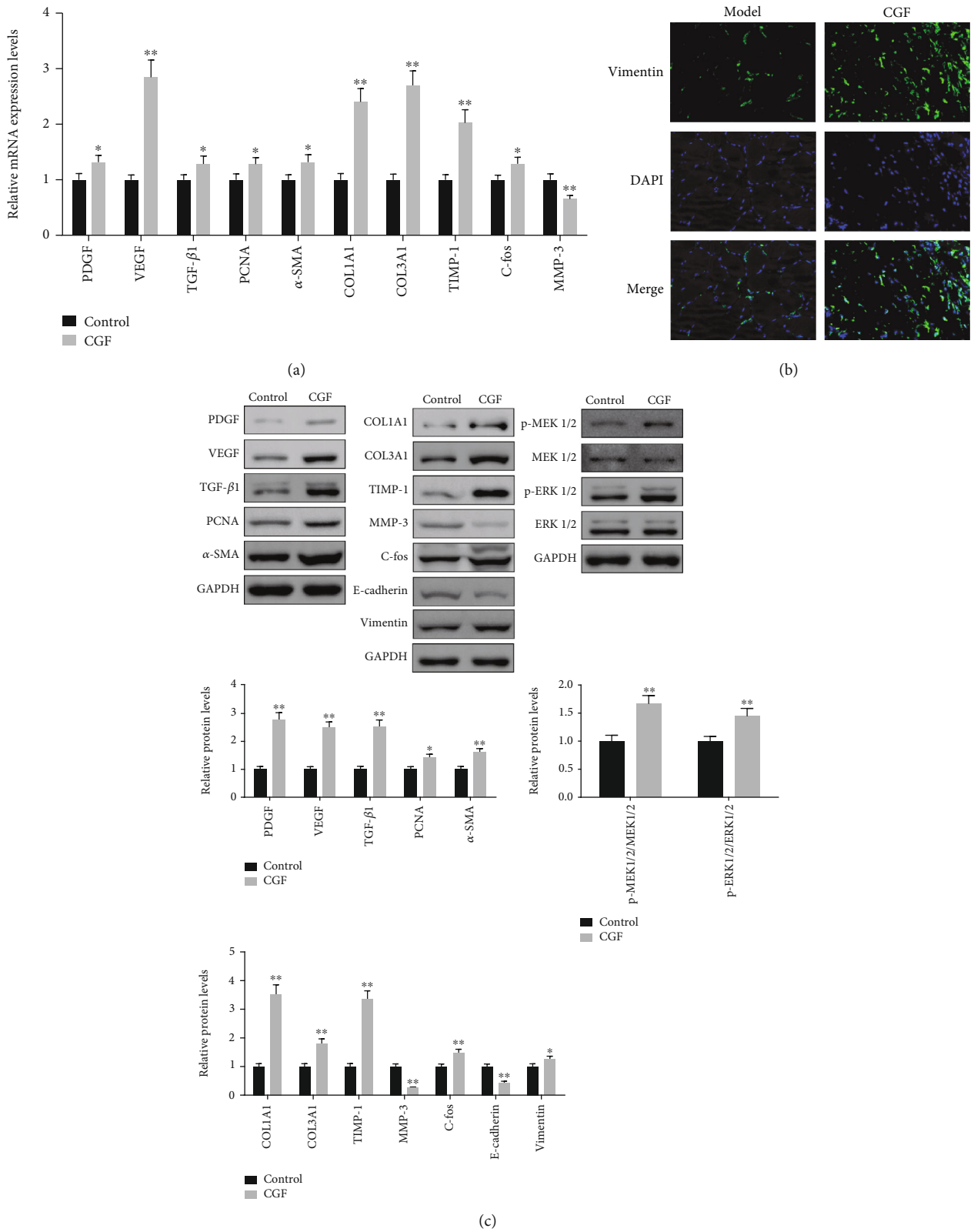

Figure 5: Effect of CGF on levels of healing-growth factors in fistula tissues of pigs. (a) The expression of PDGF, VEGF, TGF-β1, PCNA, α-SMA, Col1A1, Col3A1, TIMP-1, C-fos, and MMP-3 mRNA in tissue samples as examined by real-time PCR. (b) The protein levels of Vimentin were determined by immunofluorescence experiments. (c) The protein levels of PDGF, VEGF, TGF-β1, PCNA, α-SMA, Col1A1, Col3A1, TIMP-1, C-fos, E-cadherin, Vimentin, p-MEK1/2, MEK1/2, p-ERK1/2, and ERK1/2 were determined by immunoblotting. $^{*}P < 0.05$, $^{**}P < 0.01$ vs. control group.

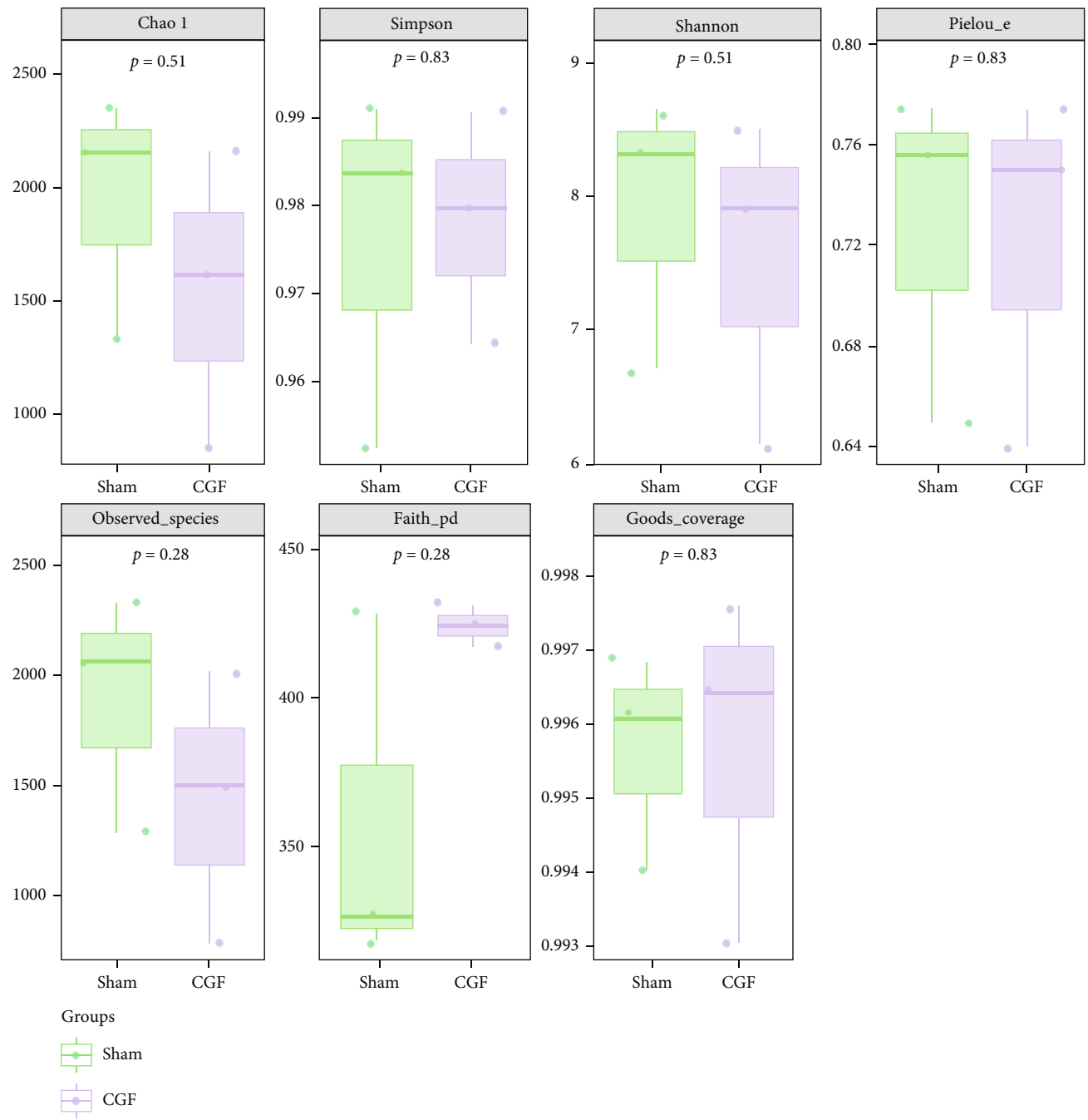

(a)

Figure 6: Continued.

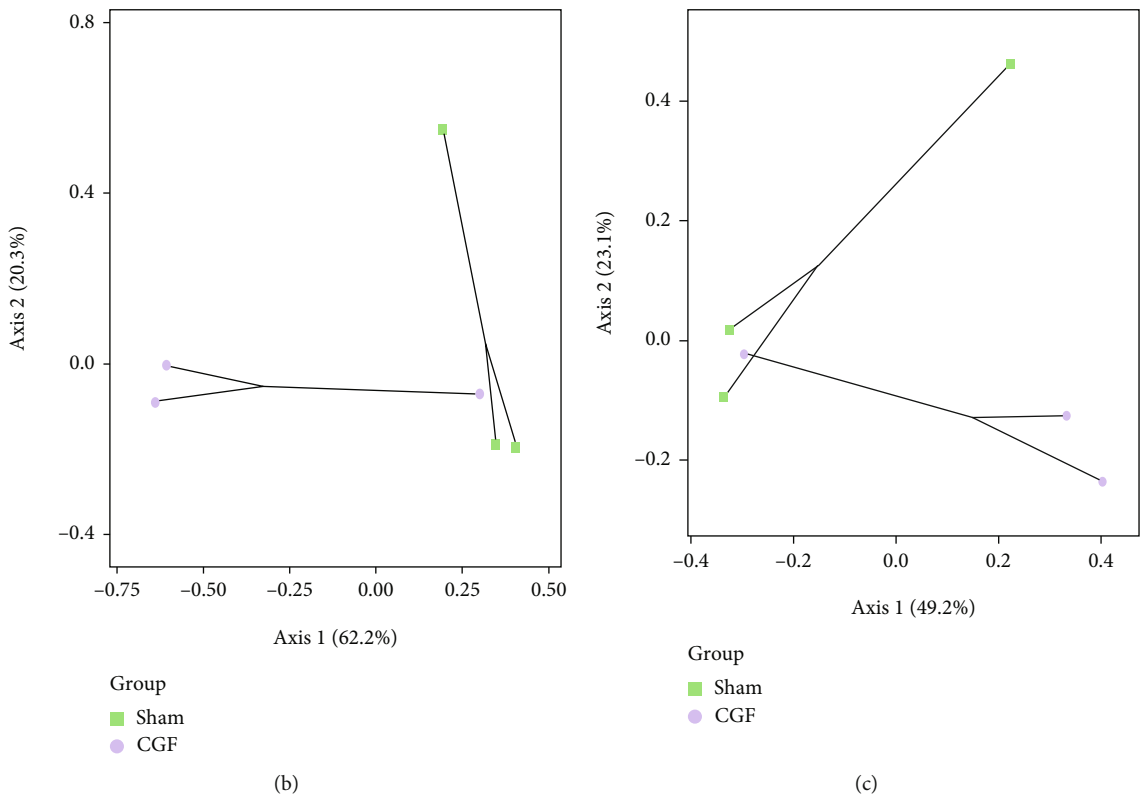

Figure 6: Gut microbial diversity in fistula tissues of pigs. (a) Alpha diversity was evaluated based on the Chao1, Simpson, Shannon, Pielou_e, Observed species, Faith_pd, and Goods_coverage indices of the OTU levels. Principal coordinates analysis of beta diversity was based on the weighted UniFrac (b) and Bray-Curtis (c) analyses of the OTU levels.

4. Discussion

In this study, we reported the role of CGF in promoting wound healing in anal fistulas, consistent with previous reports that CGF promotes chronic wound healing [28]. As the anal fistula model established by small animals failed to explain the pathogenesis and related mechanisms of the anal fistula, we constructed the landrace pigs anal fistula model and then observed the effects of CGF treatment on the secretion of inflammatory factors, angiogenesis, fibroblast activation, ECM degradation, activation of the ERK pathway, and microbial population in pig fistula tissues to clarify the mechanism of CGF treatment for anal fistula healing.

Studies have reported that inflammatory factors and growth factors participated in wound healing. Specifically, overexpression of inflammatory factors, such as IL-6, IL-12, IL-1β, and TNF-α, causes slow wound healing by affecting fibroblast apoptosis and collagen expression. Growth factors, such as EGF, PDGF, VEGF, IGF-1R, TGF-β1, and Ang-II, promote the division and proliferation of fibroblasts and endothelial cells which migrate to the wound by inducing functional vascular growth, thereby improving the speed of wound healing [29]. Previous studies have proved that CGF contains high concentrations of growth factors and rich CD34 positive cells and can reduce the secretion of inflammatory factors, which were beneficial to wound healing [30, 31]. Consistently, our results found that CGF upregulated the expression of growth factors and downregulated the expression of inflammatory factors in porcine fistula, indicating that CGF can promote fistula healing by promoting angiogenesis and limiting the inflammatory response.

Fibroblasts, vascular endothelial cells, and epithelial cells are required to participate in the process of wound healing [32]. Epithelial cells differentiate into new fibroblasts through EMT, which express the mesenchymal marker FSP1 and can migrate to wounds to enhance ECM function by promoting collagen synthesis [33]. Fibroblasts then differentiate into myofibroblasts, which promote wound closure through α-SMA-mediated contraction [33–35]. Bonazza et al. reported that CGF can stimulate the growth and proliferation of fibroblasts and vascular endothelial cells [36]. Similarly, we found that CGF elevated the expressions of PCNA and C-fos associated with cell proliferation and inhibited the apoptosis-related protein in granulation tissue or HSF. In addition, Lei et al. pointed out that CGF could promote the migration of gingival mesenchymal stem cells and increase the expression of collagen, thus promoting gingival regeneration [37]. Shao et al. reported that a CGF-rich fibrin scaffold could promote collagen deposition and accelerate the healing of skin defects by promoting the secretion of type I and type III collagen, increasing the expression of TIMP-1 (MMP inhibitor) and inhibiting MMPs [38]. Consistent with the previous studies, our results have demonstrated that CGF promotes HSF migration, increases the protein levels of COL1A1, COL3A1, and TIMP-1 and inhibits the protein level of MMP-3. Although there is no

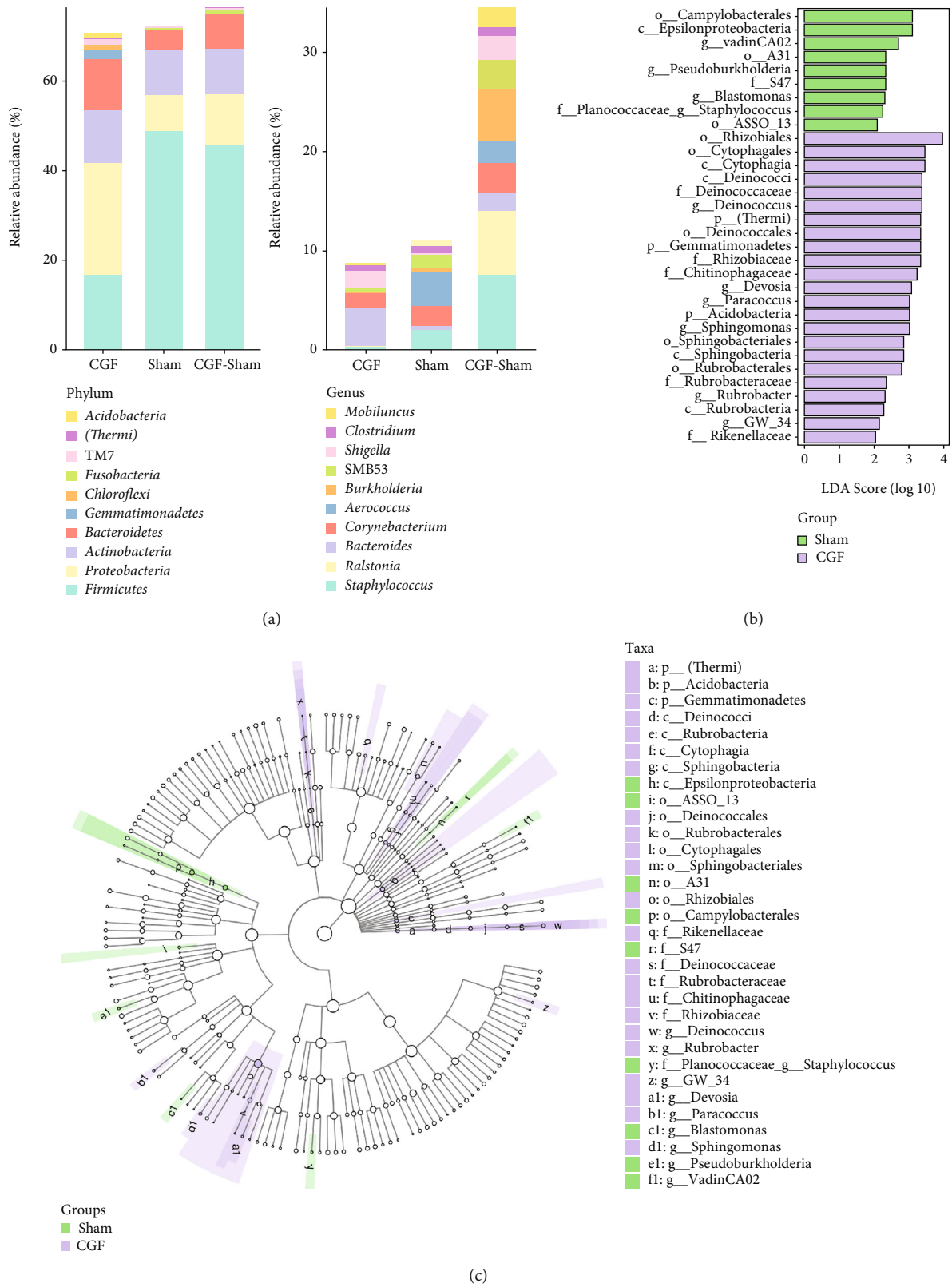

Figure 7: Composition of microbial communities from fistula tissues assessed by 16S rRNA gene sequencing. (a) Percent of community abundance on phylum level and genus level. *y*-axis represents relative abundance (%), *x*-axis represents each sample in the CGF group and sham group, and each taxonomic category is shown with a different color. CGF: CGF group, sham: control group. (b) Cladogram generated from the LEfSe analysis indicating the phylogenetic distribution from phylum to genus of the microbiota of CGF-treated pigs. (c) Histogram of LDA scores to identify differentially abundant bacterial genera between CGF-treated and control pigs.

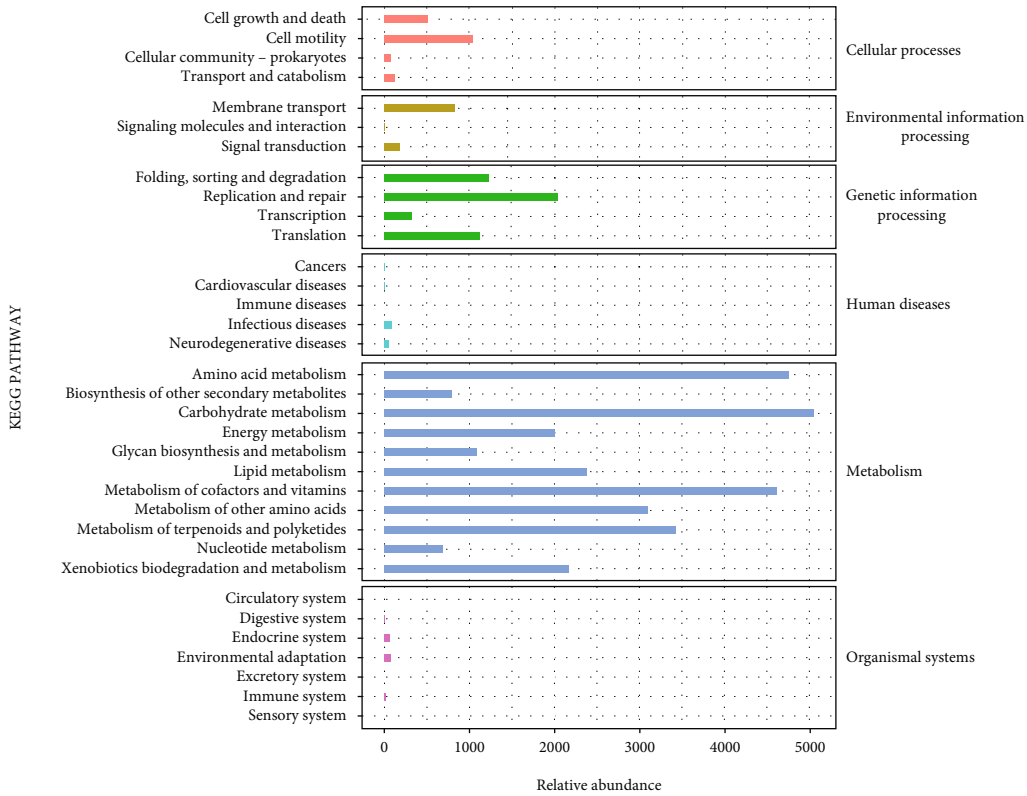

(a)

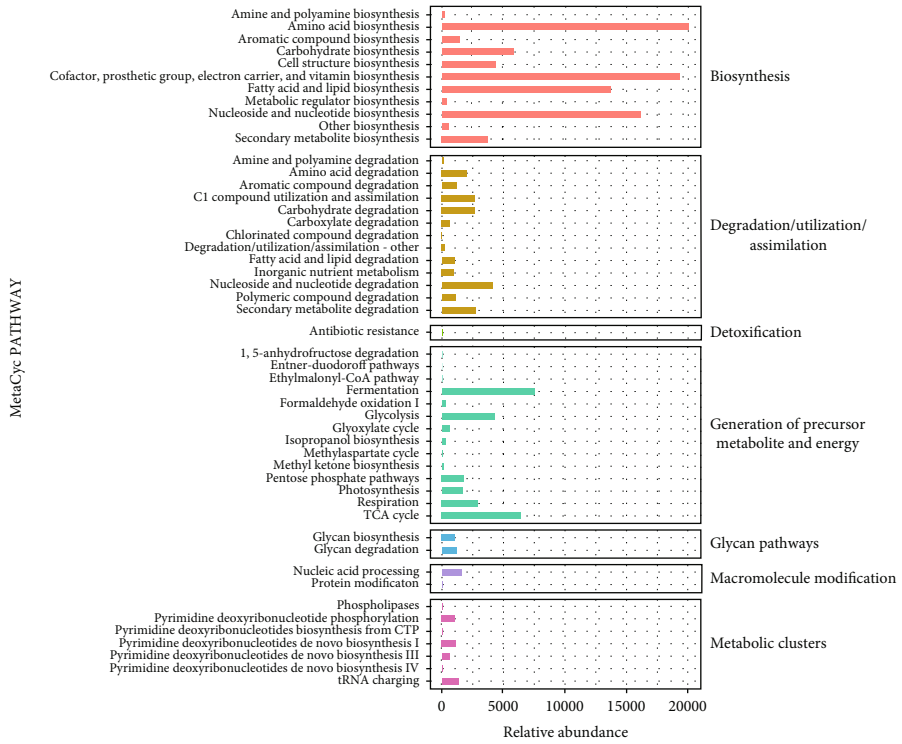

(b)

Figure 8: PICRUST2 analysis of the therapeutic role of CGF in fistula tissues of pigs. Phylogenetic Investigation of Communities by Reconstruction of Unobserved States (PICRUST2) based on 16S rRNA sequencing data was used to predict KEGG pathways (a) and metabolic pathway (b) of microbial communities.

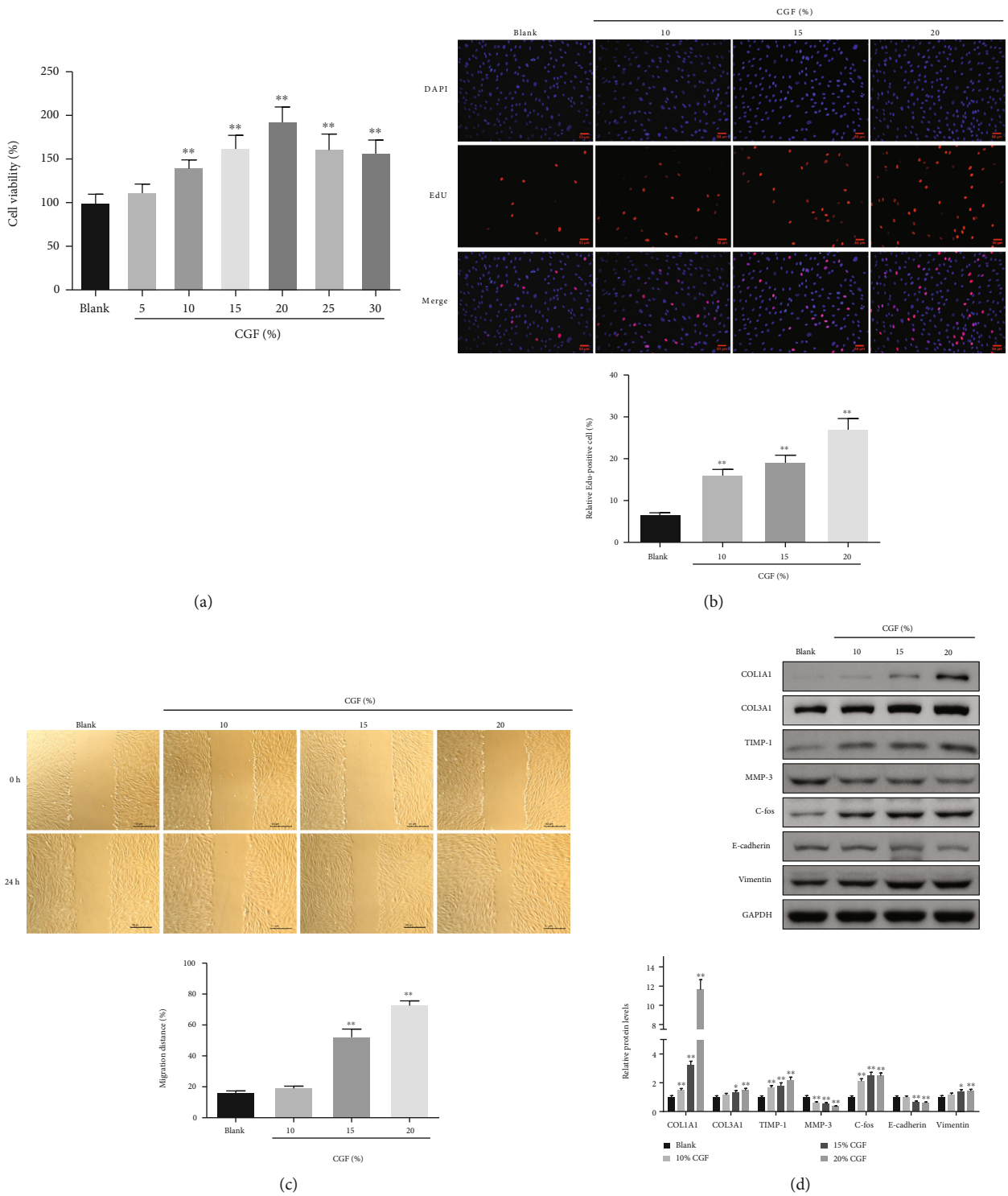

Figure 9: Continued.

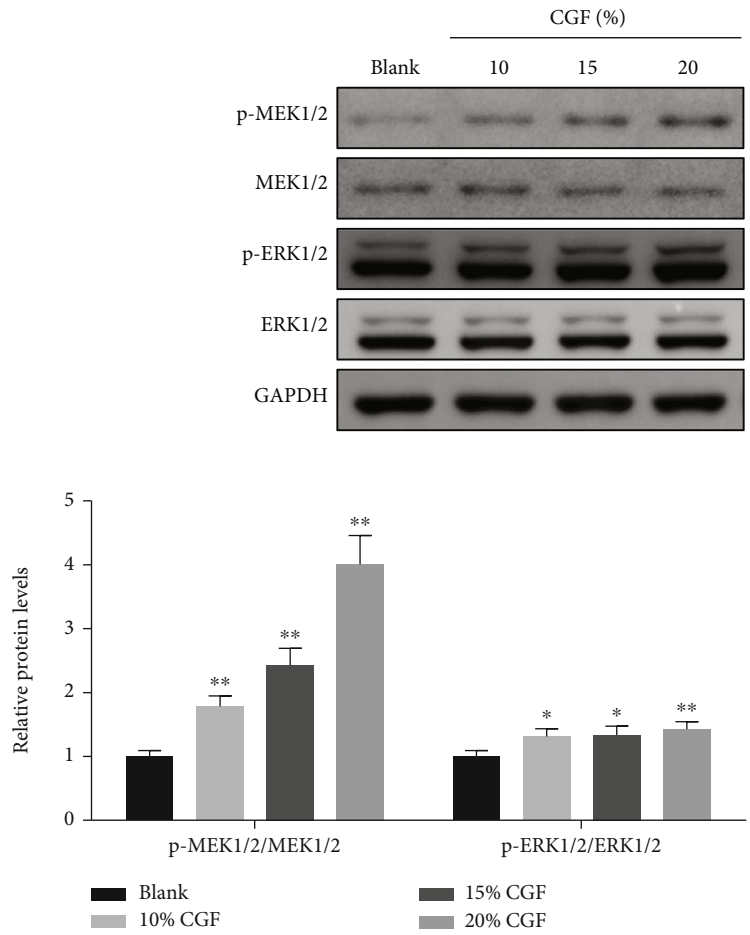

(e)

Figure 9: Effect of CGF on cell proliferation and migration ability by activating MEK/ERK signaling in HSF cells. (a) The effect of CGF on cell death in HSF cells at different dosages. (b) EdU assays of HSF cells treated with CGF were performed to evaluate cell proliferative ability. (c) Wound healing assays were performed in HSF cells treated with CGF at different dosages. (d, e) The protein levels of Col1A1, Col3A1, TIMP-1, MMP-3, C-fos, E-cadherin, vimentin, p-MEK1/2, MEK1/2, p-ERK1/2, and ERK1/2 to be measured after treatment of CGF in HSF cells by Western blot. $^{*}P < 0.05$, $^{**}P < 0.01$ vs. blank group.

direct evidence that CGF regulates cell EMT, platelet-derived biomaterials have been proved to improve bone injury by promoting EMT and enhancing the migratory ability of embryonic fibroblasts [39]. In this study, CGF, also a platelet-derived biomaterial, was able to promote vimentin expression and inhibit E-cadherin expression in granulation tissue and HSF, indicating that CGF accelerated wound healing by promoting the EMT process. Taken together, this evidence shows that CGF can enhance tissue repair by promoting fibroblast activation and inhibiting ECM degradation.

Growing evidence suggests that MEK/ERK pathway can induce cell proliferation and survival according to the various specific extracellular stimuli. CGF contains a large amount of EGF, and the binding of EGF to EGFR will lead to the activation of the downstream MEK/ERK pathway involved in the regulation of cell proliferation and metastasis [39, 40]. Furthermore, the pharmacological mechanism of some drugs for wound healing is associated with the activation of the MEK/ERK pathway [41, 42]. In particular, Yang et al. reported that plant extracts promoted wound healing of anal fistula by activating the MEK/ERK pathway [43]. Evidence has also shown that PRP can accelerate the repair of damaged musculoskeletal tissues by activating the ERK pathway [44]. In the present study, we found that p-MEK1/2 and p-ERK1/2 expressions were markedly upregulated in fistula tissues. Moreover, CGF treatment significantly promoted the proliferation and migration of HSF. Of note, ERK1 and ERK2, the bonafide substrates of MEK1/2, are supposed as the focal point of the MEK/ERK pathway to activate or inactivate a variety of proteins via phosphorylation in different subcellular compartments for inducing cell proliferation or cell cycle arrest [45]. Based on this, we knocked down the expression of ERK1/2 expression in CGF-treated HSF and assessed its effect on cell viability, proliferation, and migration. Our results suggest that the effect of CGF on proliferation and migration of HSF was reversed by ERK knockdown, which indicated that the effect of CGF on fistula healing was realized by activating the ERK pathway.

We analyzed the effect of CGF treatment on microbiota groups using 16S rRNA sequencing. After treatment with

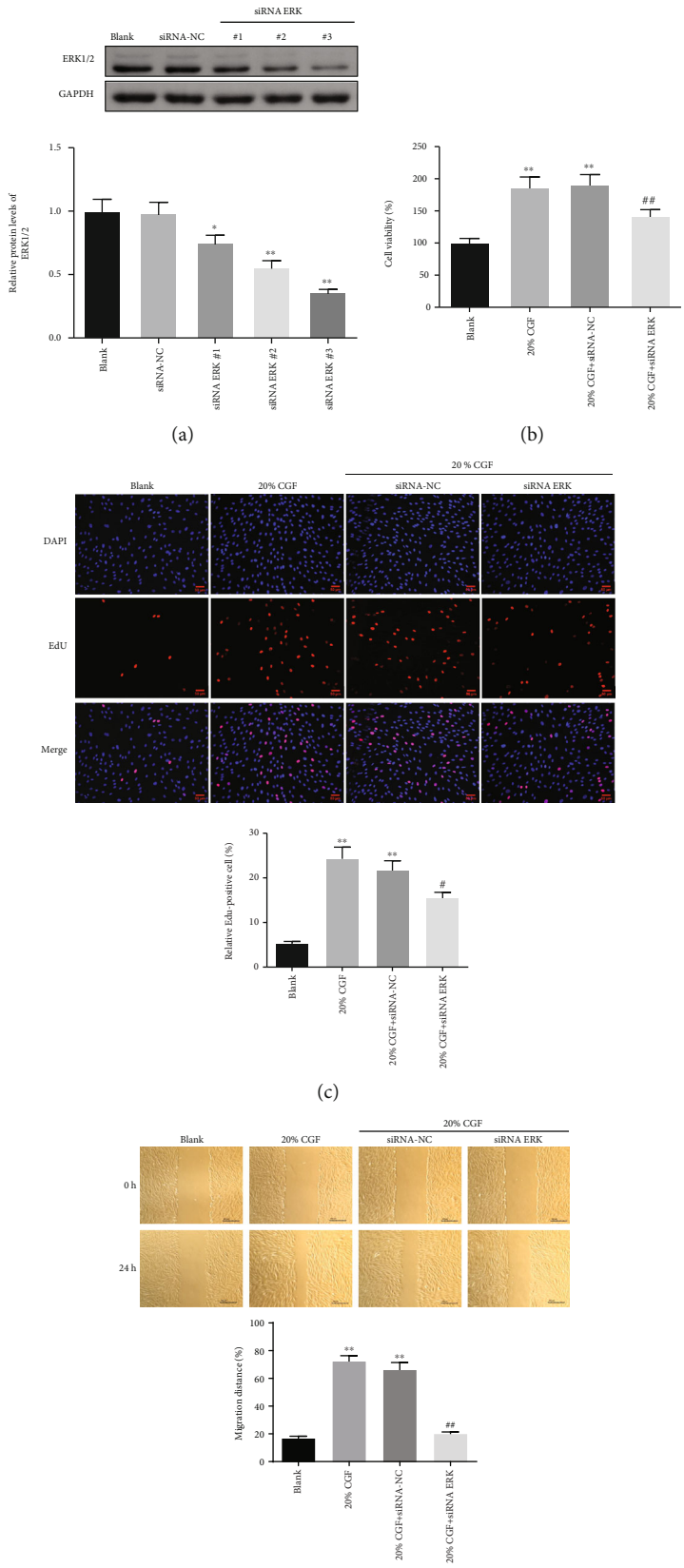

Figure 10: Continued.

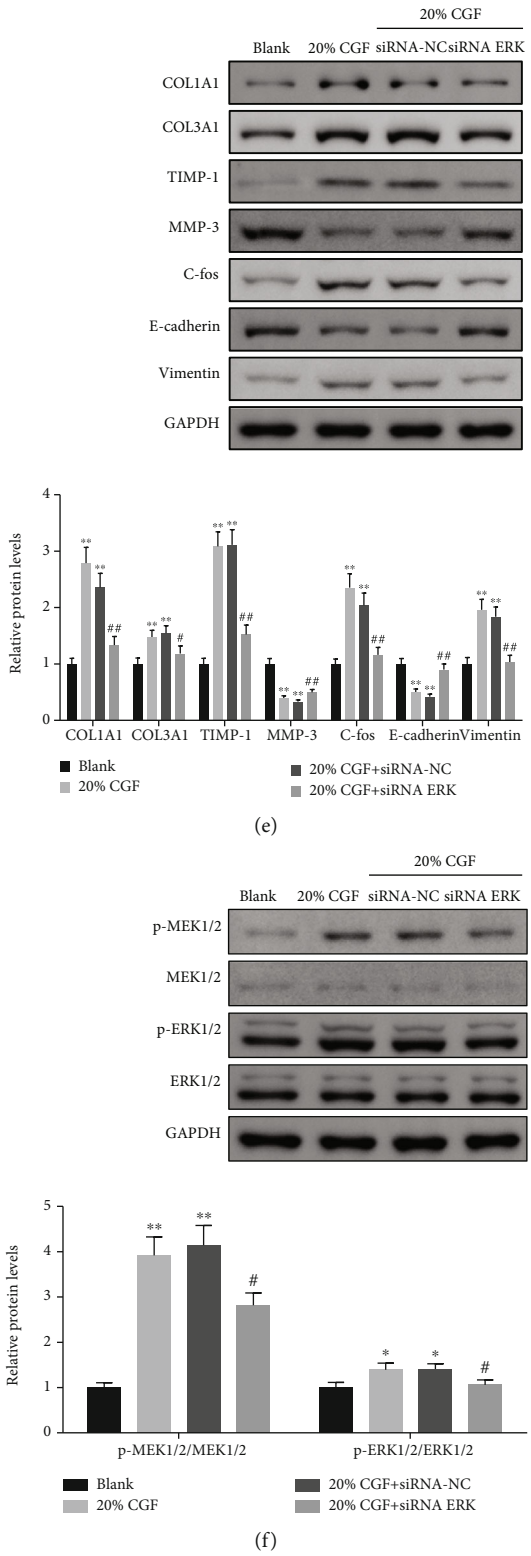

Figure 10: Knock-down of ERK effectively reverses CGF-induced activation of cell proliferation and migration ability in HSF cells. (a) Expression of ERK1/2 was confirmed by Western blot in HSF cells transfected with siRNA-NC or siRNA-ERK. (b, c) Cell proliferation was determined in 20% CGF-treated HSF cells following transfection with siRNA-ERK. (d) Cell migration assays were performed in 20% CGF-treated HSF cells following transfection with siRNA-ERK using wound healing assays. (e, f) The protein levels of Col1A1, Col3A1, TIMP-1, MMP-3, C-fos, E-cadherin, vimentin, p-MEK1/2, MEK1/2, p-ERK1/2, and ERK1/2 were detected in 20% CGF-treated HSF cells following transfection with siRNA-ERK by using Western blot assays. $^{*}P < 0.05$, $^{**}P < 0.01$ vs. blank group; $^{\#}P < 0.05$, $^{\#\#}P < 0.01$ vs. 20% CGF+siRNA-NC group.

CGF, there was no significant change in species diversity, but microbial communities were significantly changed, as reflected in the increase of *Bacteroidetes* and *Bacteroides* and a decrease in *Firmicutes* and *Staphylococcus*. In particular, *Deinococcus*, *Devosia*, *Sphingomonas*, *Rubrobacteria*, and *GW_34* were increased in the CGF group. Previous studies have reported that the increase of *Bacteroidetes* and the decrease of *Firmicutes* are beneficial to intestinal health [46]. *Bacteroides* are generally beneficial in the intestine, whereas *Staphylococcus* promotes infection [47, 48]. Interestingly, Wang et al. found that *Bacteroides spp* that positively correlated with the progress of colitis was significantly increased in the gut, which decreased in the *Prunella vulgaris*- (PVH-) treated dextran sulfate sodium- (DSS-) induced acute colitis rats [49]. Altogether, our results show that the changes in the fistula microbiota may be related to the severity of fistula healing in anal fistula pigs. In addition, the KEGG and MetaCyc databases analyses revealed that these microbial communities may affect fistula healing through the metabolic and biosynthetic pathways of amino acid, carbohydrate, cofactors, and vitamins in this study. Therefore, the current results indicated that CGF treatment has created a healthy intestinal environment by changing the fistula microbial community. There are some limitations to the current study, including relatively small sample size and lacking clinical experiments. Also, the differential fistula microbes were obtained based on the 16S rRNA sequencing analysis. However, their role in fistula healing remains unclear. Therefore, CGF could be used for clinical therapy still needs a large number of clinical trials to be confirmed.

In conclusion, our research showed that CGF stimulated the MEK/ERK signaling pathway to suppress the inflammatory response, increase angiogenesis, fibroblast activation, and ECM function, as well as to control the microbiological environment of the fistula, so aiding in fistula repair. These results offer a theoretical foundation for the clinical use of CGF in minimally invasive anal fistula surgery.

Data Availability

The datasets used and/or analyzed during the current study are available from the corresponding author on reasonable request.

Conflicts of Interest

The authors declare that they have no competing interests.

Authors' Contributions

XFZ, JMQ, HDW, and ZS designed the study. XFZ, JMQ, ZFL, SXS, and JH performed the sampling process. XFZ performed the data analysis and wrote the manuscript. JMQ and ZS revised the manuscript. All authors have read and approved the final manuscript. Xiufeng Zhang and Jianming Qiu contributed equally to this work.

Acknowledgments

This work was supported by grants from the Public Welfare Program Foundation from the Science and Technology Bureau of Zhejiang Province (grant number: LGF20H030002), the General Program Foundation from the Science and Technology Bureau of Hangzhou City (grant number: 20171226Y17), and the General Program Foundation from the Hangzhou City Health Bureau (grant number: 20210250).

Supplementary Materials

Supplementary 1. Supplementary Table S1: Antibodies used in this study.

Supplementary 2. Supplementary Table S2: Primers used in this study.

References

[1] T. Yamamoto, P. G. Kotze, A. Spinelli, and R. Panaccione, "Fistula-associated anal carcinoma in Crohn's disease," *Expert Review of Gastroenterology & Hepatology*, vol. 12, no. 9, pp. 917–925, 2018.

[2] Z. Mei, Q. Wang, Y. Zhang et al., "Risk factors for recurrence after anal fistula surgery: a meta-analysis," *International Journal of Surgery*, vol. 69, pp. 153–164, 2019.

[3] H. Guadalajara, R. Sanz-Baro, J. M. Ramirez, M. Leon, M. Garcia-Arranz, and D. Garcia-Olmo, "New Perspectives in the Treatment of Anal Fistulas," in *Anal Fistula and Abscess. Coloproctology*, C. Ratto, A. Parello, F. Litta, V. Simone, and P. Campennì, Eds., Springer, Cham, 2022.

[4] N. Lopez, S. Ramamoorthy, and W. J. Sandborn, "Recent advances in the management of perianal fistulizing Crohn's disease: lessons for the clinic," *Expert Review of Gastroenterology & Hepatology*, vol. 13, no. 6, pp. 563–577, 2019.

[5] P. Everts, K. Onishi, P. Jayaram, J. F. Lana, and K. Mautner, "Platelet-rich plasma: new performance understandings and therapeutic considerations in 2020," *International Journal of Molecular Sciences*, vol. 21, no. 20, p. 7794, 2020.

[6] J. Xu, L. Gou, P. Zhang, H. Li, and S. Qiu, "Platelet-rich plasma and regenerative dentistry," *Australian Dental Journal*, vol. 65, no. 2, pp. 131–142, 2020.

[7] P. A. Everts, A. van Erp, A. DeSimone, D. S. Cohen, and R. D. Gardner, "Platelet rich plasma in orthopedic surgical medicine," *Platelets*, vol. 32, no. 2, pp. 163–174, 2021.

[8] F. de la Portilla, A. Jiménez-Salido, A. Araujo-Miguez et al., "Autologous platelet-rich plasma in the treatment of perianal fistula in Crohn's disease," *Journal of Gastrointestinal Surgery*, vol. 24, no. 12, pp. 2814–2821, 2020.

[9] J. Cwaliński, J. Hermann, J. Paszkowski, and T. Banasiewicz, "Assessment of recurrent anal fistulas treatment with platelet-rich plasma," *Arquivos de Gastroenterologia*, vol. 58, no. 2, pp. 185–189, 2021.

[10] L. F. Rodella, G. Favero, R. Boninsegna et al., "Growth factors, CD34 positive cells, and fibrin network analysis in concentrated growth factors fraction," *Microscopy Research and Technique*, vol. 74, no. 8, pp. 772–777, 2011.

[11] G. S. Sica, S. Di Carlo, G. Tema et al., "Treatment of peri-anal fistula in Crohn's disease," *World Journal of Gastroenterology*, vol. 20, no. 37, pp. 13205–13210, 2014.

[12] B. Pariente, S. Hu, D. Bettenworth et al., "Treatments for Crohn's disease-associated bowel damage: a systematic review," *Clinical Gastroenterology and Hepatology*, vol. 17, no. 5, pp. 847–856, 2019.

[13] S. Werner, T. Krieg, and H. Smola, "Keratinocyte-fibroblast interactions in wound healing," *The Journal of Investigative Dermatology*, vol. 127, no. 5, pp. 998–1008, 2007.

[14] P. Rousselle, M. Montmasson, and C. Garnier, "Extracellular matrix contribution to skin wound re-epithelialization," *Matrix Biology*, vol. 75-76, pp. 12–26, 2019.

[15] P. Viaña-Mendieta, M. L. Sánchez, and J. Benavides, "Rational selection of bioactive principles for wound healing applications: growth factors and antioxidants," *International Wound Journal*, vol. 19, no. 1, pp. 100–113, 2022.

[16] D. Yoon, D. Yoon, H. J. Cha, J. S. Lee, and W. Chun, "Enhancement of wound healing efficiency mediated by artificial dermis functionalized with EGF or NRG1," *Biomedical Materials*, vol. 13, no. 4, 2018.

[17] L. Pan, X. Zhang, and Q. Gao, "Histatin-1 alleviates high-glucose injury to skin keratinocytes through MAPK signaling pathway," *Journal of Cosmetic Dermatology*, 2022.

[18] Y. J. Guo, W. W. Pan, S. B. Liu, Z. F. Shen, Y. Xu, and L. L. Hu, "ERK/MAPK signalling pathway and tumorigenesis," *Experimental and Therapeutic Medicine*, vol. 19, no. 3, pp. 1997–2007, 2020.

[19] P. H. Wang, B. S. Huang, H. C. Horng, C. C. Yeh, and Y. J. Chen, "Wound healing," *Journal of the Chinese Medical Association*, vol. 81, no. 2, pp. 94–101, 2018.

[20] M. Balli, F. Vitali, A. Janiszewski et al., "Autologous micrograft accelerates endogenous wound healing response through ERK-induced cell migration," *Cell Death and Differentiation*, vol. 27, no. 5, pp. 1520–1538, 2020.

[21] B. Li, H. Tang, X. Bian et al., "Calcium silicate accelerates cutaneous wound healing with enhanced re-epithelialization through EGF/EGFR/ERK-mediated promotion of epidermal stem cell functions," *Burns & Trauma*, vol. 9, 2021.

[22] M. M. Ba-Bai-Ke-Re, A. Ti-Jiang, H. Chen, X. Liu, and Y. H. Wang, "Experimental porcine model of complex fistula-in-ano," *World Journal of Gastroenterology*, vol. 23, no. 10, pp. 1828–1835, 2017.

[23] W. Peng, P. Yi, J. Yang et al., "Association of gut microbiota composition and function with a senescence-accelerated mouse model of Alzheimer's Disease using 16S rRNA gene and metagenomic sequencing analysis," *Aging*, vol. 10, no. 12, pp. 4054–4065, 2018.

[24] B. J. Callahan, P. J. McMurdie, M. J. Rosen, A. W. Han, A. J. Johnson, and S. P. Holmes, "DADA2: high-resolution sample inference from Illumina amplicon data," *Nature Methods*, vol. 13, no. 7, pp. 581–583, 2016.

[25] T. Rognes, T. Flouri, B. Nichols, C. Quince, and F. Mahé, "VSEARCH: a versatile open source tool for metagenomics," *PeerJ*, vol. 4, article e2584, 2016.

[26] M. Hall and R. G. Beiko, "16S rRNA gene analysis with QIIME2," in *Methods in Molecular Biology*, vol. 1849, pp. 113–129, Humana Press, New York, NY, 2018.

[27] M. Zhang, T. Zhang, Y. Tang, G. Ren, Y. Zhang, and X. Ren, "Concentrated growth factor inhibits UVA-induced photoaging in human dermal fibroblasts via the MAPK/AP-1 pathway," *Bioscience Reports*, vol. 40, no. 7, article BSR20193566, 2020.

[28] E. Hirata and E. Kiyokawa, "ERK activity imaging during migration of living cells in vitro and in vivo," *International Journal of Molecular Sciences*, vol. 20, no. 3, p. 679, 2019.

[29] C. H. Kao, "Use of concentrate growth factors gel or membrane in chronic wound healing: description of 18 cases," *International Wound Journal*, vol. 17, no. 1, pp. 158–166, 2020.

[30] N. X. Landén, D. Li, and M. Ståhle, "Transition from inflammation to proliferation: a critical step during wound healing," *Cellular and Molecular Life Sciences*, vol. 73, no. 20, pp. 3861–3885, 2016.

[31] H. Masuki, T. Okudera, T. Watanebe et al., "Growth factor and pro-inflammatory cytokine contents in platelet-rich plasma (PRP), plasma rich in growth factors (PRGF), advanced platelet-rich fibrin (A-PRF), and concentrated growth factors (CGF)," *International Journal of Implant Dentistry*, vol. 2, no. 1, p. 19, 2016.

[32] H. Luo, W. Liu, Y. Zhou et al., "Concentrated growth factor regulates the macrophage-mediated immune response," *Regenerative Biomaterials*, vol. 8, no. 6, article rbab049, 2021.

[33] M. Rodrigues, N. Kosaric, C. A. Bonham, and G. C. Gurtner, "Wound healing: a cellular perspective," *Physiological Reviews*, vol. 99, no. 1, pp. 665–706, 2019.

[34] G. D. Marconi, L. Fonticoli, T. S. Rajan et al., "Epithelial-mesenchymal transition (EMT): the type-2 EMT in wound healing, tissue regeneration and organ fibrosis," *Cells*, vol. 10, no. 7, p. 1587, 2021.

[35] R. C. de Oliveira and S. E. Wilson, "Fibrocytes, wound healing, and corneal fibrosis," *Investigative Ophthalmology & Visual Science*, vol. 61, no. 2, p. 28, 2020.

[36] V. Bonazza, E. Borsani, B. Buffoli et al., "In vitro treatment with concentrated growth factors (CGF) and sodium orthosilicate positively affects cell renewal in three different human cell lines," *Cell Biology International*, vol. 42, no. 3, pp. 353–364, 2018.

[37] L. Qi, L. Liu, Y. Hu et al., "Concentrated growth factor promotes gingival regeneration through the AKT/Wnt/β-catenin and YAP signaling pathways," *Artif Cells Nanomed Biotechnol.*, vol. 48, no. 1, pp. 920–932, 2020.

[38] Z. Shao, C. Lyu, L. Teng et al., "An injectable fibrin scaffold rich in growth factors for skin repair," *BioMed Research International*, vol. 2021, Article ID 8094932, 13 pages, 2021.

[39] Y. R. Chou, W. C. Lo, N. K. Dubey et al., "Platelet-derived biomaterials-mediated improvement of bone injury through migratory ability of embryonic fibroblasts: in vitro and in vivo evidence," *Aging*, vol. 13, no. 3, pp. 3605–3617, 2021.

[40] P. Wee and Z. Wang, "Epidermal growth factor receptor cell proliferation signaling pathways," *Cancers*, vol. 9, no. 5, p. 52, 2017.

[41] X. Q. Shi, G. Chen, J. Q. Tan et al., "Total alkaloid fraction of *Leonurus japonicus* Houtt. Promotes angiogenesis and wound healing through SRC/MEK/ERK signaling pathway," *Journal of Ethnopharmacology*, vol. 295, article 115396, 2022.

[42] J. Li, L. Chen, J. Xu et al., "Effects of _*Periploca forrestii*_ Schltr on wound healing by Src meditated Mek/Erk and PI3K/Akt signals," *Journal of Ethnopharmacology*, vol. 237, pp. 116–127, 2019.

[43] D. Yang, J. H. Xu, and R. J. Shi, "Root extractive fromDaphne genkwabenefits in wound healing of anal fistula through up-regulation of collagen genes in human skin fibroblasts," *Bioscience Reports*, vol. 37, no. 2, article BSR20170182, 2017.

[44] M. J. McClure, N. M. Clark, Z. Schwartz, and B. D. Boyan, "Platelet-rich plasma and alignment enhance myogenin via

ERK mitogen activated protein kinase signaling," *Biomedical Materials*, vol. 13, no. 5, article 055009, 2018.

[45] P. K. Wu, A. Becker, and J. I. Park, "Growth inhibitory signaling of the Raf/MEK/ERK pathway," *International Journal of Molecular Sciences*, vol. 21, no. 15, p. 5436, 2020.

[46] Y. Zhang, K. Yu, H. Chen, Y. Su, and W. Zhu, "Caecal infusion of the short-chain fatty acid propionate affects the microbiota and expression of inflammatory cytokines in the colon in a fistula pig model," *Microbial Biotechnology*, vol. 11, no. 5, pp. 859–868, 2018.

[47] H. Zafar and M. H. Saier Jr., "Gut *Bacteroides* species in health and disease," *Gut Microbes*, vol. 13, no. 1, pp. 1–20, 2021.

[48] K. Lisowska-Łysiak, R. Lauterbach, J. Międzobrodzki, and M. Kosecka-Strojek, "Epidemiology and pathogenesis ofStaphylococcusBloodstream infections in humans: a review," *Polish Journal of Microbiology*, vol. 70, no. 1, pp. 13–23, 2021.

[49] K. Wang, Z. Wan, A. Ou et al., "Monofloral honey from a medical plant, *Prunella Vulgaris*, protected against dextran sulfate sodium-induced ulcerative colitis via modulating gut microbial populations in rats," *Food & Function*, vol. 10, no. 7, pp. 3828–3838, 2019.

Hindawi
Oxidative Medicine and Cellular Longevity
Volume 2022, Article ID 6360133, 11 pages
https://doi.org/10.1155/2022/6360133

Research Article

SIRT6 Prevents Glucocorticoid-Induced Osteonecrosis of the Femoral Head in Rats

Lun Fang,[1] **Gang Zhang**,[2] **Yadi Wu**,[1,2] **Zhongzhe Li**,[1] **Shan Gao**,[3] **and Lu Zhou**[1,2]

[1]*Institute of Sports Medicine, Shandong First Medical University & Shandong Academy Medical Sciences, Taian, 271016 Shandong Province, China*
[2]*Department of Orthopedics, The Second Affiliated Hospital of Shandong First Medical University, Taian, 271000 Shandong Province, China*
[3]*School of Pharmaceutical Science, Shandong First Medical University & Shandong Academy Medical Sciences, Taian, 271016 Shandong Province, China*

Correspondence should be addressed to Shan Gao; gaoshan@sdfmu.edu.cn and Lu Zhou; zhoulu@sdfmu.edu.cn

Received 6 September 2022; Accepted 27 September 2022; Published 13 October 2022

Academic Editor: Tarique Hussain

Objective. Glucocorticoid-induced osteonecrosis of the femoral head is one of the most common causes of nontraumatic osteonecrosis of the femoral head, but its exact pathogenesis remains unclear. The aim of this study was to investigate the role of SIRT6 in the maintenance of bone tissue morphology and structure, intravascular lipid metabolism, and its potential molecular mechanism in glucocorticoid-induced osteonecrosis of the femoral head. *Methods*. SIRT6 adenovirus was transfected into GIONFH in rats. The microstructure of rat bone was observed by micro-CT and histological staining, and the expression of bone formation-related proteins and angiogenesis-related factors was determined through western blot and immunohistochemistry. Alkaline phosphatase activity, alizarin red staining, and the expression levels of Runx2 and osteocalcin were used to evaluate the osteogenic potential. And *in vitro* tube formation assay and immunofluorescence were used to detect the ability of endothelial cell angiogenesis. *Results*. Dexamethasone significantly inhibited osteoblast differentiation, affected bone formation, and destroyed microvessel formation, increased the intracellular Fe^{2+} and ROS levels and induced the occurrence of ferroptosis. SIRT6 can inhibit ferroptosis and restore the ability of bone formation and angiogenesis. *Conclusion*. SIRT6 can inhibit the occurrence of ferroptosis, reduce the damage of vascular endothelium, and promote osteogenic differentiation, so as to prevent the occurrence of osteonecrosis of the femoral head.

1. Introduction

Nontraumatic osteonecrosis of the femoral head, a disease characterized by chronic pain and limited mobility of the hip, is the most common reason of hip replacement in young adults [1, 2]. Glucocorticoid-induced osteonecrosis of the femoral head (GIONFH) is caused by the massive use of glucocorticoids, and its prevalence accounts for the first place of nontraumatic osteonecrosis of the femoral head. The massive use of glucocorticoids will cause many pathophysiological changes in vivo, such as metabolic disorders, elevated blood glucose, and coagulation dysfunction, so that the blood is in a hypercoagulable state, which makes the local formation of thrombosis in the femoral head, leading to ischemic osteonecrosis of the femoral head [3, 4]. The excessive use of hormones leads to the decrease of osteogenic differentiation and the increase of lipogenic differentiation, thus blocking the blood supply of the femoral head, leading to the collapse of local bone tissue, which is the main factor leading to its necrosis [5]. According to previous studies, the pathogenesis of GIONFH can be summarized in two aspects: (1) impaired blood supply of femoral head and (2) diminished osteogenic activity. And some studies

have found that strengthening angiogenesis and osteogenesis is the key to prevent GIONFH or provide early treatment of GIONFH [6].

Silent information regulatory protein (Sirtuin) is an evolutionary conserved protein that regulates key physiological processes such as apoptosis, metabolism, energy balance, mitochondrial function, and aging [7]. SIRT6, as a member of the Sirtuin family, has both NAD^+-dependent histone deacetylase activity and ADP-ribosyltransferase activity [8]. SIRT6 has deacetylase activity against histone H3K9Ac and acts as a transcription factor hypoxia-inducible factor 1α, c-Jun, and nuclear factor κB (NF-*K*b), deacetylating histone H3K9Ac at its target promoter and downregulating the expression of its target genes [9]. With the development of research, more and more biological functions of SIRT6 have been discovered, including delaying cellular senescence, regulating lipid metabolism, antirheumatism, and reversing myocardial hypertrophy. However, there is no study on the protection of vascular endothelial cells by SIRT6 to prevent or treat related vascular injurious necrosis diseases at home and abroad.

SIRT6 plays an important role in osteogenic differentiation and angiogenesis. This study was aimed at investigating the role of SIRT6 in the maintenance of bone tissue morphological structure, intravascular lipid metabolism, and its potential molecular mechanism in GIONFH, providing a theoretical basis for the clinical treatment of GIONFH.

2. Materials and Methods

2.1. Animals and GIONFH Models. A total of 75 male SD rats were randomly divided into the following five groups: normal control group (NC), hypoxia model control group (con), adenoviral function control group (LacZ), SIRT6 overexpression group (Ad-SIRT6), and SIRT6 mutation group (Mt-SIRT6). The femoral head necrosis model was created by intramuscular injection of 10 mg/kg dexamethasone sodium phosphate once every three days for 8 weeks; the blank control group was injected with saline [10]. LacZ, SIRT6, and SIRT6 mutant adenoviruses were injected into the tail vein of rats in the LacZ group and SIRT6 mutation group on the day before the start of modeling, respectively, to increase or decrease the corresponding protein levels. Adenovirus was used to increase the protein content of the SIRT6 gene, and LacZ virus was used as a functional control virus of adenovirus to detect the safety and identify adenovirus. SIRT6 mutant viruses do not possess deacetylase activity and only retain ADP-ribosyltransferase activity [11].

2.2. Microcomputed Tomography (Micro-CT). When the GIONFH model was completed in SD rats, the femurs were collected from the rats immediately after euthanasia. The structure of the femoral head and cortical area was examined by microcomputed tomography. The following parameters were measured for the assessment of bone quality: trabecular bone volume/total volume (BV/TV), trabecular thickness (Tb. Th, mm), trabecular number (Tb. N, 1/mm), and trabecular separation (Tb. Sp, mm).

2.3. Histological Staining. Femurs were fixed in 10% buffered formalin and decalcified using 10% EDTA decalcification solution (pH 7.2–7.4) for 4 weeks, and fresh decalcification solution was replaced once every two days. After decalcification was completed and embedded in paraffin, the tissues were sectioned longitudinally [12]. Hematoxylin-eosin (HE) staining and safranin-O staining were then performed.

2.4. Immunohistochemical Staining. DAKO EnVision System (DAKO, Denmark) was used to perform Immunohistochemical staining, which uses horseradish peroxidase-conjugated dextran polymers. Then, the paraffin samples were warmed for 30 min at 55°C. Following deparaffinization, tissue sections were treated with in 0.01 M sodium citrate buffer (pH 6.0) and immunostained with CD31 and VEGF antibody using a microwave antigen retrieval procedure.

2.5. Cell Culture. Mouse preosteoblastic MC3T3-E1 cells (ATCC company) and human umbilical vein vascular endothelial cells HUVEC (Otwo Biotech (Shenzhen) Inc.) were used for the study. They were cultured with DMEM high-glucose medium containing 10% FBS, in which 100 μg/ml streptomycin and 100 U/ml penicillin (Lot. P1400; Solarbio) were added and placed in an incubator with 5% CO_2 and at 37°C.

2.6. Cell Model. To mimic culturing cells under ischemic conditions, we placed the cell culture in an Oxoid anaerobic tank with an Oxoid AnaeroGen anaerobic packet (cat.no. HBYY001; hopebio). The anaerobic bacterial sac in the sealed tank rapidly absorbs the oxygen in the atmosphere and produces CO_2, and the oxygen concentration decreases to less than 1% within 1 h.

2.7. Cell Transfection and Grouping. Logarithmically growing MC3T3-E1 and HUVEC cells were seeded into 6-well plates and transfected when the cells were confluent to 30%–50%. LacZ adenovirus, SIRT6 adenovirus, and SIRT6 gene mutant adenovirus were added to serum-free and antibiotic-free medium, and fresh complete medium was replaced after 6 hours of transfection. Untreated cells were also used as the normal control group. After 24 hours of culture, the expression of SIRT6 in the cells was detected by western blot.

2.8. Alkaline Phosphatase (ALP) Staining and Alizarin Red (ARS) Staining. MC3T3-E1 cells were seeded in 6-well plates. When the cells reached 80% confluence, hypoxia treatment was performed, osteogenic induction medium (complete medium containing 10 mM β-sodium glycerophosphate (cat.no. A56289; OKA)) and 50 μg/ml ascorbic acid were added to induce differentiation into mature osteoblasts [13], and fresh osteogenic induction medium was replaced every other day. The activity of alkaline phosphatase was measured by ALP staining kit (cat.no. D001-2; Jiancheng Biochemical) after 7 days' induction. Osteogenic differentiation was induced 21 days, and the mineralized nodule formation of MC3T3-E1 was determined using alizarin red solution (cat.no. C1452; Solarbio). Then, they were stained with 1% ARS for 5 min at 37°C. The cells were then washed with distilled water to remove excess dye and finally

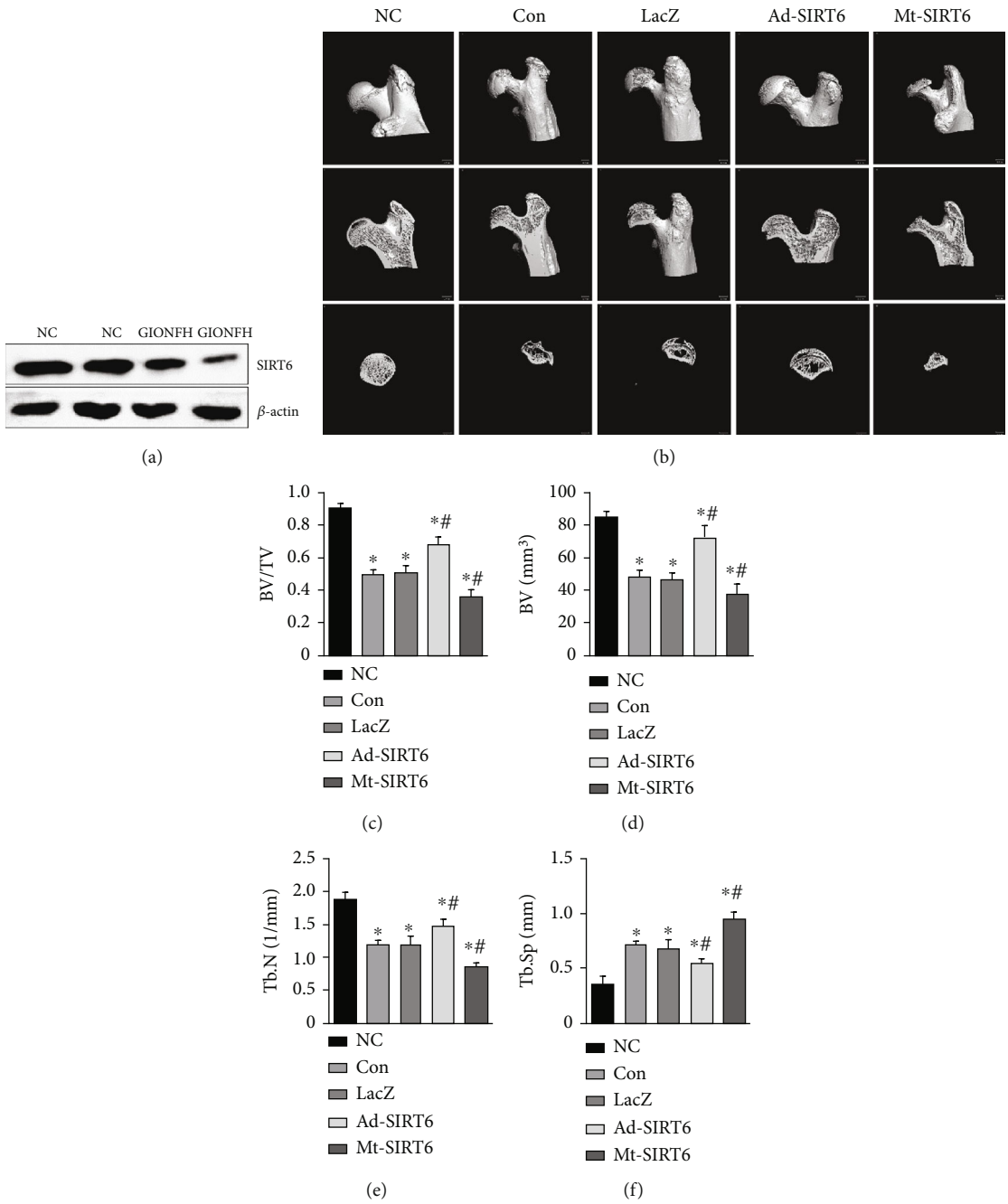

Figure 1: SIRT6 prevents disruption of femoral head microarchitecture. (a) The expression of SIRT6 was detected in the femoral head region of GIONFH by western blot. (b) Micro-CT scan image of the femoral head. (c–f) Bone parameters, including BV, BV/TV, Tb. N, and Tb. Sp. $^{*}P < 0.05$ versus the NC group; $^{\#}P < 0.05$ versus the model group.

placed under a light microscope to observe and photograph the stained matrix.

2.9. Tube Formation In Vitro. Matrigel (cat.no. 0827045, ABW) was diluted with an equal volume of DMEM and added to a 96-well plate for plating, 50 μl of Matrigel was added to each well, and the cells were seeded in a 96-well plate. HUVEC cells were observed for the formation of tube-like structures under a microscope.

2.10. Immunofluorescence. Cells were fixed with 4% paraformaldehyde for 30 min and blocked with 3% BSA for 30 min. Anti-VEGF antibody dilutions were incubated overnight. PBS was washed three times, and secondary antibodies were incubated for 1 h in the dark. DAPI was stained in the nucleus for 5 min. They were observed and photographed under a fluorescence microscope.

2.11. Assay of Ferrous Iron. Cells were collected and disrupted with ultrasonic waves. Centrifuge at 12,000 rpm for

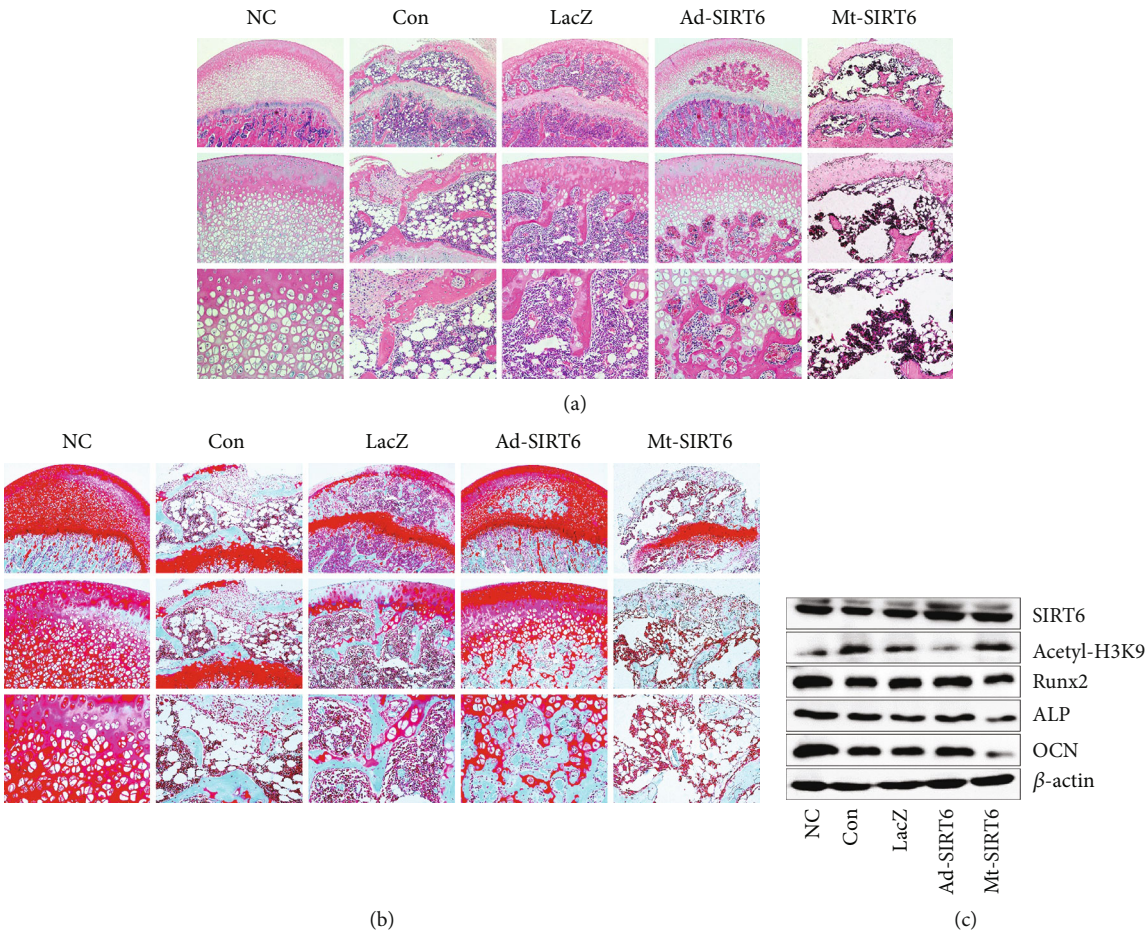

Figure 2: SIRT6 reduces the destruction of the femoral head structure by dexamethasone. (a) Representative images of HE staining of the femoral head. (b) Representative images of safranin-O staining of the femoral head. (c) Western blot was used to detect the expression of bone-related proteins.

10 min at 4°C, and take the supernatant. Add 1,10-phenanthroline (cat.no. 320056; Sigma-Aldrich), mix well, and place for 60 min. The absorbance was measured at 506 nm.

2.12. Determination of Glutathione (GSH). The cells were collected by centrifugation, and the samples were subjected to repeated rapid freezing and thawing, and the supernatant was used for the determination of GSH. Intracellular total GSH levels were measured following the operating instructions of the GSH assay kit (cat.no. S0055; Beyotime).

2.13. Determination of Malondialdehyde (MDA). MDA content was measured by MDA assay kit (cat.no. S0131S; Beyotime). Cells were disrupted by ultrasound, and the supernatant was taken. The collected supernatant was added to thiobarbituric acid. The absorbance was read at 532 nm. The MDA level indicates the ratio to the absorbance value of the normal control group.

2.14. Reactive Oxygen Species (ROS) Assay. ROS level was measured using Dihydroethidium (cat.no. S0063; Beyotime). Cells were seeded in 6-well plates and transfected. After 12 hours of hypoxia, 10 μM Dihydroethidium was added and incubated with an incubator for 30 min, and the mean fluorescence intensity was measured by flow cytometry.

2.15. Western Blot. Total protein was extracted from the femoral heads and cells of each group with RIPA lysate, and protein concentration was determined with Coomassie brilliant blue. Protein samples of 30 μg were transferred to PVDF (Polyvinylidene Difluoride) membranes after polyacrylamide gel electrophoresis. 5% skimmed milk was blocked for 1 h at room temperature, incubated overnight with primary antibodies for SIRT6 (1 : 1000; cat.no. 12486; Cell Signaling Technology, Inc.), HIF-1α (1 : 1000; cat.no. 14179; Cell Signaling Technology, Inc.), Acetyl-H3K9 (1 : 1000; cat.no. ab10812; Abcam), Runx2 (1 : 1000; cat.no. 12556; Cell Signaling Technology, Inc.), ALP (1 : 1000; cat.no. ab229126; Abcam), osteocalcin (OCN; 1 : 1000; cat.no. ab93876; Abcam), CD31 (1 : 1000; cat.no. 3528; Cell Signaling Technology, Inc.), VEGF (1 : 1000; cat.no. 9698; Cell Signaling Technology, Inc.), transferrin receptor (TFRC; 1 : 1000; cat.no. ab214039; Abcam), divalent metal transporter-1 (DMT1; 1 : 1000; cat.no. ab55735; Abcam), SLC7A11 (1 : 1000; cat.no. ab175186; Abcam), GPX4 (1 : 1000; cat.no. 59735; Cell Signaling Technology, Inc.), and β-actin (1 : 5000; cat.no. AB0035; Abways Technology), and the next

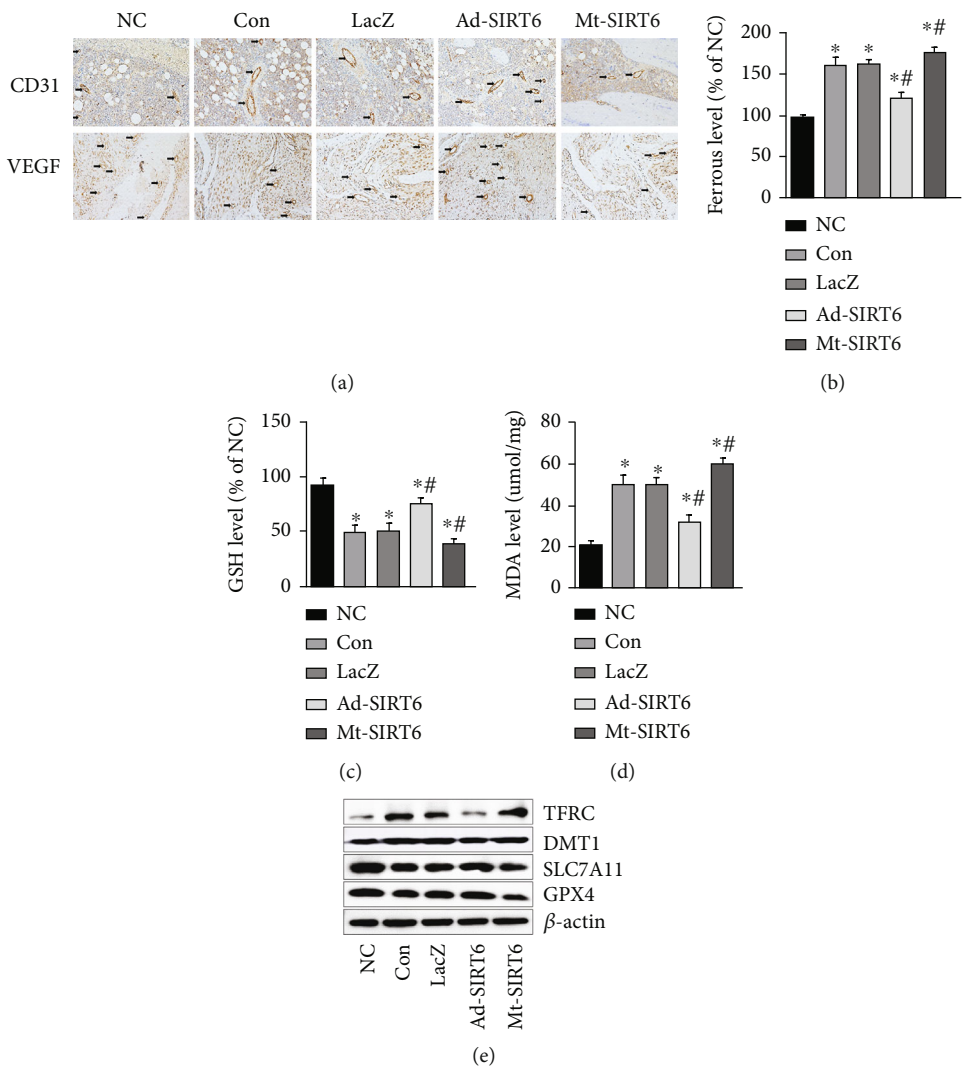

Figure 3: SIRT6 promotes angiogenesis to prevent ONFH by inhibiting ferroptosis. (a) Immunohistochemical staining for CD31 and VEGF-associated antigens and vascular density in the femoral head. (b) Serum ferrous iron levels in rats with GIONFH. (c) Serum GSH levels. (d) Serum lipid peroxidation product MDA levels. (e) Expression of ferritin and ferroptosis-related proteins in the femoral head. $^{*}P < 0.05$ versus the NC group; $^{\#}P < 0.05$ versus the model group.

day, secondary antibody was added and incubated for 1 h at room temperature for development. β-Actin was used as a reference.

2.16. Statistical Analysis. All the above tests were repeated three times. GraphPad Prism 6.02 software was used for statistical analysis of data. Independent sample t-test was used to compare mean values of two samples. ANOVA was used to compare mean values in multiple groups. $P \leq 0.05$ was considered statistically significant.

3. Results

3.1. SIRT6 Reduces the Destruction of the Femoral Head by Dexamethasone. In order to verify the changes of SIRT6 during the development of GIONFH, the changes of SIRT6 protein expression levels in the femoral head of normal and GIONFH model rats were compared by western blot. The expression of SIRT6 in the osteonecrosis area of the femoral head decreased in GIONFH rats (Figure 1(a)). According to the results of micro-CT scanning, it was found that dexamethasone caused the destruction of the bone surface structure of the femoral head in rats. It was rough, and there were a large number of cavities in the bone (Figure 1(b)). Bone mineral density and bone parameters BV and BV/TV decreased. After injection of SIRT6-overexpressing adenovirus, compared with the model control group, the surface of the femoral head was smooth, the structure of the femoral head was intact, the internal structure of the femoral head showed no significant abnormality, and BV and BV/TV were improved (Figures 1(c)–1(f)).

The results showed that the cartilage layer of the femoral head became thinner, the bone arrangement was sparse and disordered, and the number of empty lacunae increased in the model group and adenovirus functional control group. These

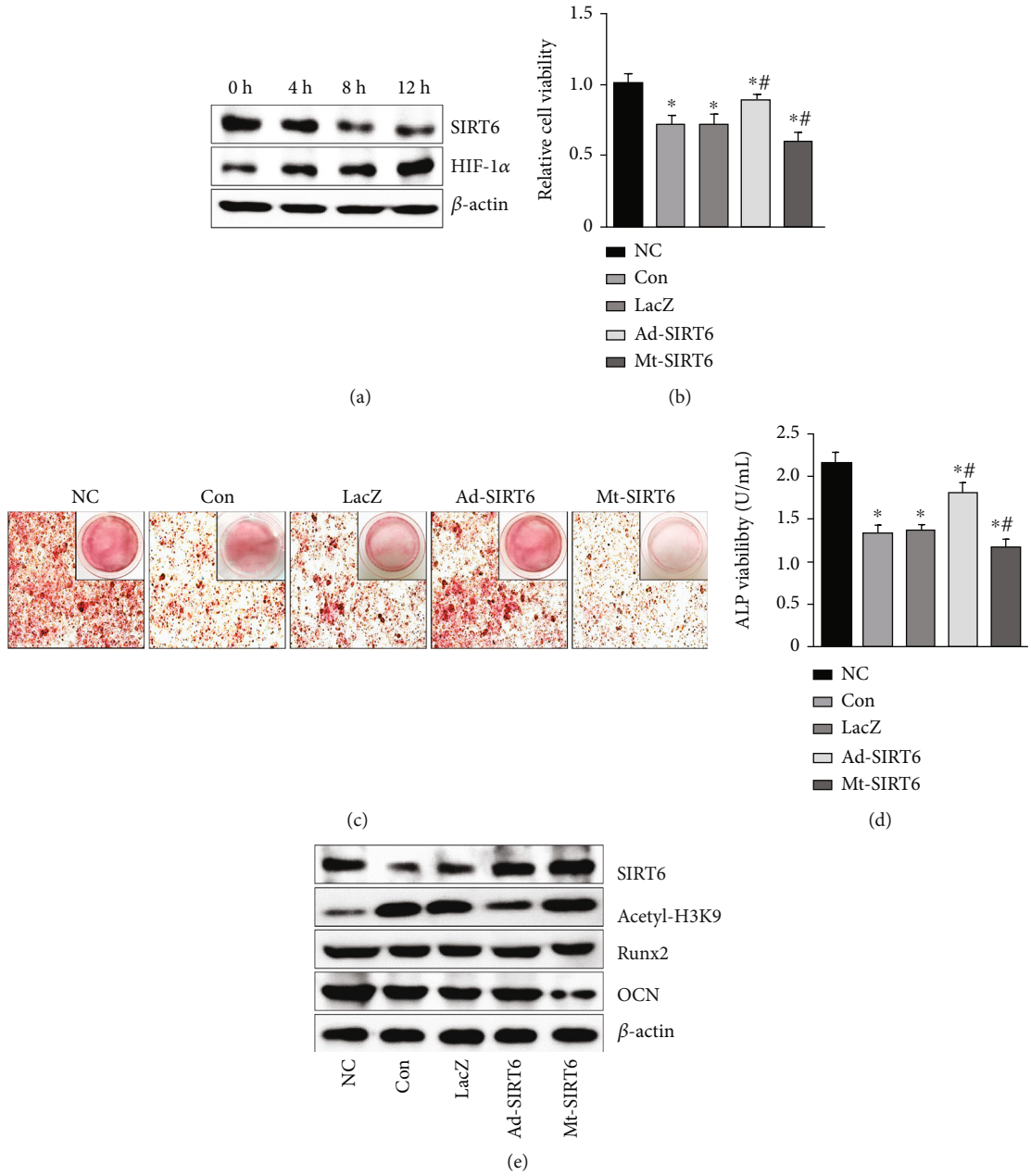

Figure 4: SIRT6 promoted osteogenic differentiation in vitro. (a) The expression level of SIRT6 in MC3T3-E1 cells after hypoxia was detected by western blot. (b) MTT assay was performed to examine the viability of MC3T3-E1 cells after hypoxia treatment. (c) The effect of SIRT6 on bone-related proteins in MC3T3-E1 cells after hypoxia. (d) ALP staining was used to detect ALP activity in MC3T3-E1 cells that induced osteogenic differentiation after 7 days. (e) The formation of mineralized nodules was detected by ARS staining in osteogenic differentiation induced 21 days in MC3T3-E1 cells. $^{*}P < 0.05$ versus the NC group; $^{\#}P < 0.05$ versus the model group.

results could be reversed after SIRT6 overexpression treatment (Figures 2(a) and 2(b)). Relevant studies have found that SIRT6 mainly exerts various biological functions through its deacetylase function. SIRT6 mutation adenoviruses do not possess deacetylase activity and only retain ADP-ribosyltransferase activity. SIRT6 overexpression inhibited acetylation of histone H3 lysine 9 in the femoral head, whereas this effect was reversed after treatment with mutant SIRT6. In addition, further aggravation of femoral head destruction was observed in the SIRT6 mutation group. Meanwhile, the rat femoral head protein was extracted, and SIRT6 increased the expression levels of ALP, Runx2, and OCN and inhibited the expression of these proteins after SIRT6 mutation (Figure 2(c)).

3.2. SIRT6 Promotes Angiogenesis to Prevent ONFH by Inhibiting Ferroptosis. In the early stage of GIONFH, intravascular pressure rises and vascular endothelium is mostly damaged. And related studies have found that SIRT6 has a role

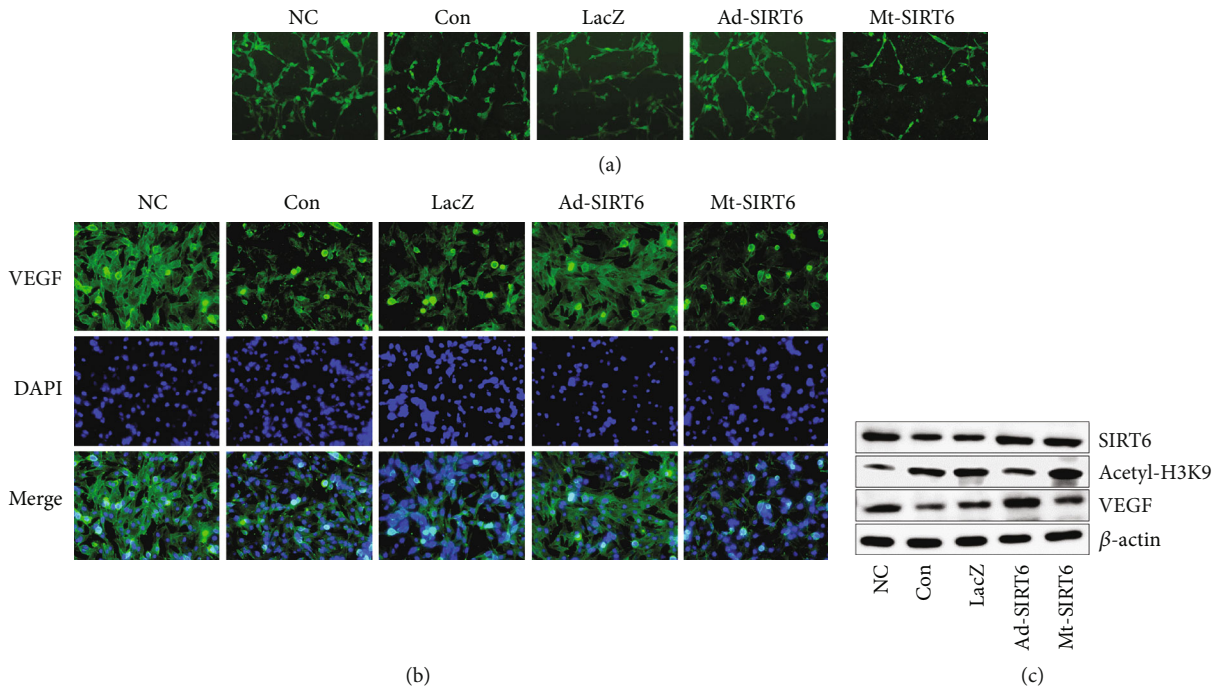

Figure 5: SIRT6 promotes angiogenesis. (a) SIRT6 promoted HUVEC to form a uterine-like structure as detected by tube formation assay in vitro. (b) Effect of SIRT6 on angiogenesis-related protein VEGF in HUVEC cells. (c) Immunofluorescence staining of HUVEC cells following interference with SIRT6.

in protecting vascular endothelial cells and promoting angiogenesis [14, 15]. To verify the effect of SIRT6 on angiogenesis in rat femoral head, antibodies against CD31 and VEGF were selected for immunohistochemical staining (Figure 3(a)). The expression of CD31 and VEGF in the femoral head was decreased, the microvascular structure was destroyed, and there were few intact microvessels after dexamethasone administration. SIRT6 overexpression showed more CD31- and VEGF-positive cells, increased vascular density, and basically intact microvascular structure. What is more, the serum iron and ferritin levels of the model were higher than those of the normal control group (Figures 3(b)–3(d)). Protein was extracted from the femoral head (Figure 3(e)). A significant decrease in SLC7A11 and GPX4 expression was observed. And the contents of GSH and MDA also showed corresponding fluctuations. These results indicate that ferroptosis may have occurred in GIONFH.

3.3. SIRT6 Promotes Osteoblast Differentiation In Vitro. Since the phenomenon of decreased SIRT6 expression levels in a rat model of GIONFH was found, whether SIRT6 was associated with osteoblast differentiation was further assessed *in vitro*. To mimic the in vitro ischemic environment, we subjected the cells to hypoxia. First, cells were subjected to hypoxia treatment for different periods of time to determine the most appropriate oxidative stress stimulation conditions. The expression level of SIRT6 decreased after hypoxia treatment in MC3T3-E1 cells, and the SIRT6 expression level became lower with prolonged hypoxia (Figure 4(a)). The viability of osteoblasts was decreased after hypoxia by MTT assay, partially restored after SIRT6 overexpression (Figures 4(b) and 4(c)). MC3T3-E1 cells treated with hypoxia had decreased ALP activity and decreased mineralized nodule formation compared with the normal group (Figure 4(d)). Alkaline phosphatase is a marker of the early stage of osteogenic differentiation, while the formation of calcium nodules is a marker of the later stage of osteogenic differentiation [16]. The expression of Runx2 and OCN was decreased in hypoxia-treated cells, indicating that hypoxia impaired osteoblast function (Figure 4(e)). The osteogenic function of MC3T3-E1 cells was further inhibited after SIRT6 gene mutation. SIRT6 overexpression protected the ALP activity and mineralization properties of MC3T3-E1 cells against hypoxia, and the expression of Runx2 and OCN was elevated. These results indicate that SIRT6 is essential for osteogenic differentiation.

3.4. SIRT6 Promotes Angiogenesis In Vitro. The results showed that endothelial cells in the SIRT6 overexpression group differentiated into complete annular vessel-like structures, while vessel-like structures were incomplete or sparse in the SIRT6 mutation group (Figures 5(a) and 5(b)). Western blot results showed that hypoxia decreased the expression VEGF in HUVEC cells, and SIRT6 could improve the results (Figure 5(c)). Immunofluorescence showed the same results.

3.5. SIRT6 Inhibits Ferroptosis in GIONFH. To further verify whether ferroptosis was activated in osteonecrosis of the femoral head, firstly, HUVEC cells were placed in a hypoxic environment and analyzed by MTT that hypoxia significantly reduced cell viability (Figure 6(a)). To analyze whether the decrease in cell viability was due to the occurrence of ferroptosis, we examined relevant measures of ferroptosis. The results showed that hypoxia could increase the consumption of glutathione and the content of malondialdehyde and increase the

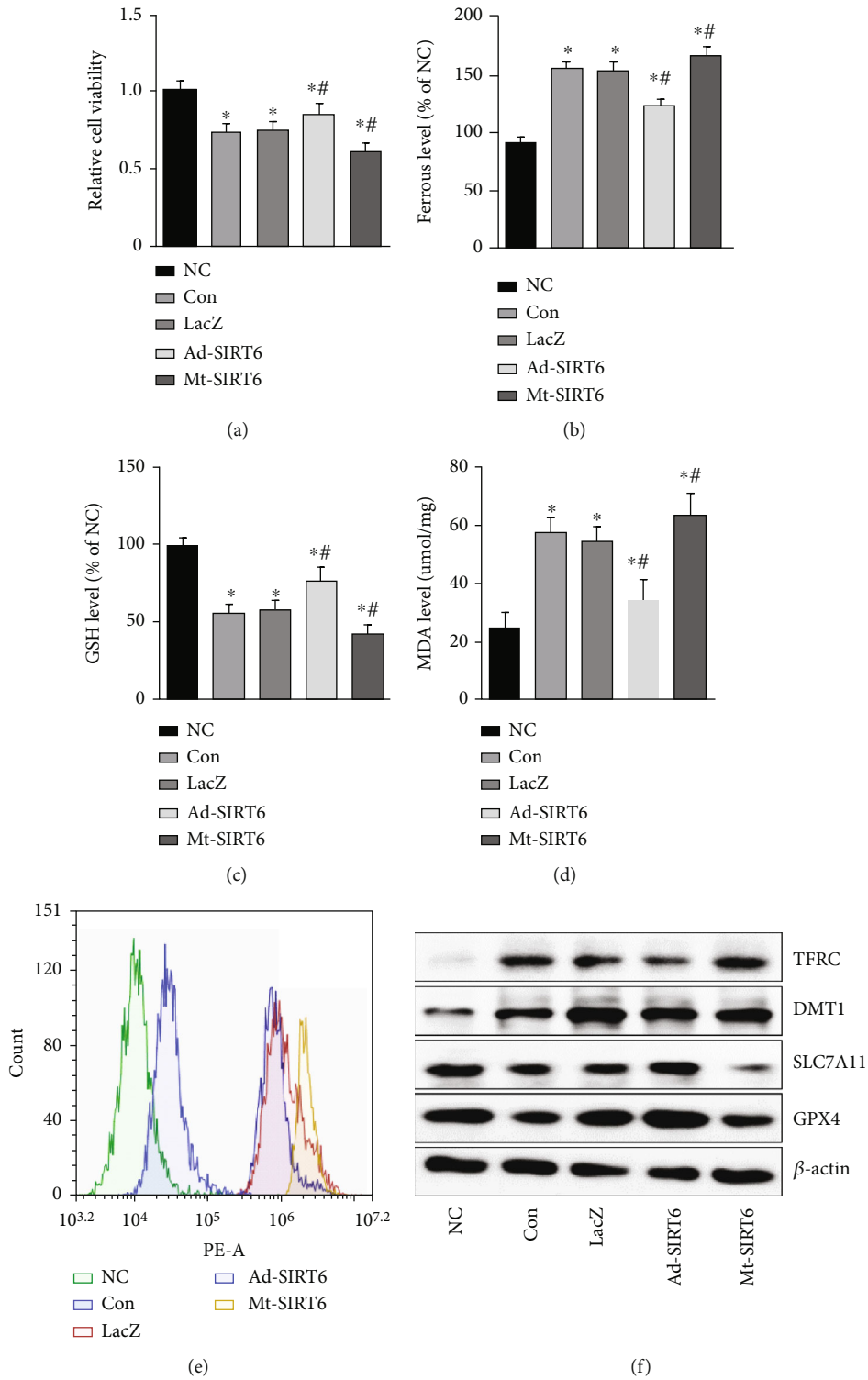

Figure 6: SIRT6 inhibits ferroptosis to prevent the development of osteonecrosis of the femoral head. (a) MTT assay was used to examine the viability of HUVEC cells after hypoxia. (b) Ferrous iron levels in HUVEC. (c) The content of GSH in HUVEC cells after interfering SIRT6. (d) The content of MDA in HUVEC cells. (e) Flow cytometry analysis of ROS levels. (f) The expression levels of ferroptosis-related proteins in HUVEC cells. $^{*}P < 0.05$ versus the NC group; $^{\#}P < 0.05$ versus the model group.

level of ROS in HUVEC cells (Figures 6(b)–6(e)). Hypoxia resulted in a decrease in the intracellular GPX4 and SLC7A11 expression levels. These results were exacerbated by the SIRT6 mutation group. However, SIRT6 overexpression could reverse the decrease of GPX4, SLC7A11, and GSH and reduce intracellular MDA and ROS accumulation (Figure 6(f)).

4. Discussion

This study verified the role of SIRT6 in GIONFH. This study found that dexamethasone downregulated SIRT6 expression, induced high ROS levels, and impaired osteogenesis and angiogenesis. Overexpression of SIRT6 can protect the activity of osteoblasts, promote osteoblastic differentiation, and reduce the damage of vascular endothelium, thereby preventing the occurrence of osteonecrosis of the femoral head.

Dexamethasone was applied to establish the GIONFH model in this study. This study found that the model group showed severe destruction of the bone structure in the subchondral bone area, necrosis of the surrounding bone marrow cells, and a large number of hollow lacunae. SIRT6 plays a key role in regulating bone formation and bone resorption. In this study, the effect of SIRT6 on GIONFH in rats was evaluated by micro-CT and histopathology and found that SIRT6 significantly improved the bone mass of the femoral head in glucocorticoid-induced rats, increased the number of trabecular, and decreased the separation of trabecular. New studies have found that Sirt6 Tg mice are resistant to the release of inflammatory factors and the progression of osteocyte death, bone resorption, and osteoarthritis after ischemic surgery, while osteoblast/osteocyte-specific SIRT6 knockout mice show severe bone loss and deformity [17]. SIRT6 could improve the viability of MC3T3-E1 cells in a femoral head necrosis model induced by hypoxia in vitro. Hypoxia also blocked osteoblast differentiation, while SIRT6 could improve the differentiation ability of osteoblasts injured by hypoxia, mainly reflected in increased ALP activity and increased number of calcified nodules. BMSCs from Sirt6 knockout mice had significantly lower alkaline phosphatase expression, reduced calcium nodule formation, and decreased osteogenic differentiation ability at the late stage of osteogenic differentiation, while Sirt6 knockout promoted the proliferation and differentiation of osteoclasts [18]. Western blot results also showed elevated expression of osteogenesis-related markers Runx2 and OCN after SIRT6 overexpression. The findings are consistent with previous findings that interference with SIRT6 can inhibit bone differentiation and affect osteogenesis [19, 20]. Therefore, these results suggest that SIRT6 may promote bone formation by elevating osteoblast viability and differentiation, thereby inhibiting osteonecrosis of the femoral head.

Massive use of glucocorticoid causes damage to vascular endothelial cells, triggering intravascular coagulation. Ischemia and osteonecrosis are the core pathological mechanisms of osteonecrosis of the femoral head. The expression of CD31, a key protein for angiogenesis, was downregulated. SIRT6 plays an important role in delaying endothelial cell senescence and protecting endothelial cell function [21, 22]. It was also demonstrated that SIRT6 could promote the generation of local blood vessels in the GIONFH model rat, and CD31 protein levels were markedly upregulated in bone tissue. Vascular endothelial cells, as the most important structural components in blood vessels, play a significant effect on maintaining the function of blood vessels and ensuring the normal blood supply of tissues. Hypoxia reduced the viability and angiogenic ability of HUVEC by MTT assay and tube formation assay in vitro. SIRT6 overexpression alleviated the damage of HUVEC induced by hypoxia and played a protective role. Previous studies have found that SIRT6 reduces the senescence of endothelial cells by reducing DNA damage and improving telomere function and maintains its ability to proliferate and form tubes in vitro [23]. CD31 is mainly expressed in vascular endothelial cells and is recognized as one of the classical markers of vascular endothelial cells [24]. VEGF is a hallmark regulator of angiogenesis. Hypoxia can downregulate the expression of CD31 and VEGF, while was upregulated after SIRT6 overexpression, which further indicated that SIRT6 could promote angiogenesis.

Ferroptosis is a new form of regulatory cell death. Abnormal intracellular iron metabolism, especially iron excess, leads to the continuous production of reactive oxygen species, which form and accumulate a large number of iron-dependent lipid peroxides in turn, which triggers ferroptosis. Several studies have shown that GC triggers ferroptosis [25]. First, in this study, we found that there was iron accumulation in GIONFH and that TFRC and DMT1 expression levels were increased. TFRC and DMT1 mediate the accumulation and transport of ferrous iron, leading to ferroptosis [26]. GPX4 inactivation is a feature of ferroptosis, and the activity of GPX4 depends on the supply of GSH, which is weakened by the rapid depletion of GSH. Hypoxia leads to inhibition of GPX4 activity in endothelial cells and that GSH concentration also decreases. However, SIRT6 increased not only GSH levels but also GPX4 expression levels. And the intracellular SLC7A11 expression level was also decreased after hypoxia treatment. SLC7A11 is a subunit of the XC-system and has a variety of functions, including the import of extracellular cysteine for glutathione biosynthesis, reactive oxygen species interpretation, and antioxidant activity [27]. SLC7A11 and GPX4 play a key role in preventing iron death mediated by lipid peroxidation. Inhibition of SLC7A11 and GPX4 interrupts intracellular GSH metabolism and promotes lipid peroxidation and subsequent ferroptosis [28]. Ferroptosis is also closely related to lipid peroxidation as well as the increase of reactive oxygen species. In addition, MDA is a marker of lipid peroxidation products [29]. Upregulation of SIRT6 can decrease the levels of intracellular MDA and ROS in vascular endothelial cells. However, current studies on the role of SIRT6 in ferroptosis are still limited. Recently, it has been demonstrated that sodium hydrogen sulfide can enhance SIRT6 expression and inhibit ferroptosis in the frontal cortex of diabetic mice [30]. Consistent with their findings, SIRT6 overexpression inhibited ferroptosis in vascular endothelial cells in this study. These results demonstrate that overexpression of SIRT6 can reverse hypoxia-induced ferroptosis.

5. Conclusion

In summary, SIRT6 can inhibit the occurrence of ferroptosis, reduce the damage of vascular endothelium, and promote osteogenic differentiation, thereby preventing the occurrence of osteonecrosis of the femoral head. Our study provides a theoretical basis for SIRT6 as a potential target for GIONFH therapy.

Data Availability

The datasets during the current study are available from the corresponding authors on reasonable request.

Conflicts of Interest

The authors declare that there are no competing interests regarding the publication of this paper.

Authors' Contributions

Lun Fang and Gang Zhang contributed equally to this work. Shan Gao and Lu Zhou are cocorresponding authors.

Acknowledgments

This work was supported by the Natural Science Foundation of Shandong Province, China (grant no. ZR2019MH120), and Academic promotion programme of Shandong First Medical University (grant no. 2019QL011).

References

[1] A. Cohen-Rosenblum and Q. Cui, "Osteonecrosis of the femoral head," *The Orthopedic Clinics of North America*, vol. 50, no. 2, pp. 139–149, 2019.

[2] M. A. Mont, H. S. Salem, N. S. Piuzzi, S. B. Goodman, and L. C. Jones, "Nontraumatic osteonecrosis of the femoral head: where do we stand today?: a 5-year update," *The Journal of Bone and Joint Surgery. American Volume*, vol. 102, no. 12, pp. 1084–1099, 2020.

[3] J. Xu, H. Gong, S. Lu, M. J. Deasey, and Q. Cui, "Animal models of steroid-induced osteonecrosis of the femoral head-a comprehensive research review up to 2018," *International Orthopaedics*, vol. 42, no. 7, pp. 1729–1737, 2018.

[4] A. Wang, M. Ren, and J. Wang, "The pathogenesis of steroid-induced osteonecrosis of the femoral head: a systematic review of the literature," *Gene*, vol. 671, pp. 103–109, 2018.

[5] J. Li, Z. Ge, W. Ji, N. Yuan, and K. Wang, "The proosteogenic and proangiogenic effects of small extracellular vesicles derived from bone marrow mesenchymal stem cells are attenuated in steroid-induced osteonecrosis of the femoral head," *BioMed Research International*, vol. 2020, Article ID 4176926, 2020.

[6] R. Zuo, L. Kong, M. Wang et al., "Exosomes derived from human CD34(+) stem cells transfected with miR-26a prevent glucocorticoid-induced osteonecrosis of the femoral head by promoting angiogenesis and osteogenesis," *Stem Cell Research & Therapy*, vol. 10, no. 1, p. 321, 2019.

[7] M. C. Haigis and D. A. Sinclair, "Mammalian sirtuins: biological insights and disease relevance," *Annual Review of Pathology*, vol. 5, no. 1, pp. 253–295, 2010.

[8] R. I. Khan, S. S. R. Nirzhor, and R. Akter, "A review of the recent advances made with SIRT6 and its implications on aging related processes, Major Human Diseases, and Possible Therapeutic Targets," *Biomolecules*, vol. 8, no. 3, 2018.

[9] X. Saiyang, W. Deng, and T. Qizhu, "Sirtuin 6: a potential therapeutic target for cardiovascular diseases," *Pharmacological Research*, vol. 163, article 105214, 2021.

[10] L. Chen, B. Z. Wang, J. Xie et al., "Therapeutic effect of SIRT3 on glucocorticoid-induced osteonecrosis of the femoral head via intracellular oxidative suppression," *Free Radical Biology & Medicine*, vol. 176, pp. 228–240, 2021.

[11] J. A. Collins, M. Kapustina, J. A. Bolduc et al., "Sirtuin 6 (SIRT6) regulates redox homeostasis and signaling events in human articular chondrocytes," *Free Radical Biology & Medicine*, vol. 166, pp. 90–103, 2021.

[12] L. Zhou, S. J. Yoon, K. Y. Jang et al., "COMP-angiopoietin1 potentiates the effects of bone morphogenic protein-2 on ischemic necrosis of the femoral head in rats," *PLoS One*, vol. 9, no. 10, article e110593, 2014.

[13] J. Gao, Z. Feng, X. Wang et al., "SIRT3/SOD2 maintains osteoblast differentiation and bone formation by regulating mitochondrial stress," *Cell Death and Differentiation*, vol. 25, no. 2, pp. 229–240, 2018.

[14] Y. Gao, H. Zhu, Q. Wang, Y. Feng, and C. Zhang, "Inhibition of PERK signaling prevents against glucocorticoid-induced endotheliocyte apoptosis and osteonecrosis of the femoral head," *International Journal of Biological Sciences*, vol. 16, no. 4, pp. 543–552, 2020.

[15] J. Guo, Z. Wang, J. Wu et al., "Endothelial SIRT6 is vital to prevent hypertension and associated cardiorenal injury through targeting Nkx3.2-GATA5 signaling," *Circulation Research*, vol. 124, no. 10, pp. 1448–1461, 2019.

[16] M. Ruh, M. P. Stemmler, I. Frisch et al., "The EMT transcription factor ZEB1 blocks osteoblastic differentiation in bone development and osteosarcoma," *The Journal of Pathology*, vol. 254, no. 2, pp. 199–211, 2021.

[17] Z. Zhang, Y. Song, S. I. Wang et al., "Osteoblasts/osteocytes sirtuin6 is vital to preventing ischemic osteonecrosis through targeting VDR-RANKL signaling," *Journal of Bone and Mineral Research*, vol. 36, no. 3, pp. 579–590, 2021.

[18] Y. J. Moon, Z. Zhang, I. H. Bang et al., "Sirtuin 6 in preosteoclasts suppresses age- and estrogen deficiency-related bone loss by stabilizing estrogen receptor α," *Cell Death and Differentiation*, vol. 26, no. 11, pp. 2358–2370, 2019.

[19] F. Xiao, Y. Zhou, Y. Liu, M. Xie, and G. Guo, "Inhibitory effect of Sirtuin6 (SIRT6) on osteogenic differentiation of bone marrow mesenchymal stem cells," *Medical Science Monitor*, vol. 25, pp. 8412–8421, 2019.

[20] J. Xiao, S. Qin, W. Li et al., "Osteogenic differentiation of rat bone mesenchymal stem cells modulated by MiR-186 via SIRT6," *Life Sciences*, vol. 253, article 117660, 2020.

[21] Z. Yang, Y. Huang, L. Zhu et al., "SIRT6 promotes angiogenesis and hemorrhage of carotid plaque via regulating HIF-1α and reactive oxygen species," *Cell Death & Disease*, vol. 12, no. 1, p. 77, 2021.

[22] Y. Yang, T. Tian, Y. Wang, Z. Li, K. Xing, and G. Tian, "SIRT6 protects vascular endothelial cells from angiotensin II-induced apoptosis and oxidative stress by promoting the activation of Nrf2/ARE signaling," *European Journal of Pharmacology*, vol. 859, p. 172516, 2019.

[23] W. Grabowska, E. Sikora, and A. Bielak-Zmijewska, "Sirtuins, a promising target in slowing down the ageing process," *Biogerontology*, vol. 18, no. 4, pp. 447–476, 2017.

[24] A. F. Ajayi and S. B. Olaleye, "Immunohistochemical studies of age-related changes in cell proliferation and angiogenesis during the healing of acetic acid-induced gastric ulcers in rats," *The Scientific World Journal*, vol. 2020, Article ID 3506207, 10 pages, 2020.

[25] J. Lu, J. Yang, Y. Zheng, X. Chen, and S. Fang, "Extracellular vesicles from endothelial progenitor cells prevent steroid-induced osteoporosis by suppressing the ferroptotic pathway in mouse osteoblasts based on bioinformatics evidence," *Scientific Reports*, vol. 9, no. 1, p. 16130, 2019.

[26] J. Y. Cao and S. J. Dixon, "Mechanisms of ferroptosis," *Cellular and Molecular Life Sciences*, vol. 73, no. 11-12, pp. 2195–2209, 2016.

[27] H. Ma, X. Wang, W. Zhang et al., "Melatonin suppresses ferroptosis induced by high glucose via activation of the Nrf2/HO-1 signaling pathway in type 2 diabetic osteoporosis," *Oxidative Medicine and Cellular Longevity*, vol. 2020, Article ID 9067610, 18 pages, 2020.

[28] L. Liu, R. Liu, Y. Liu et al., "Cystine-glutamate antiporter xCT as a therapeutic target for cancer," *Cell Biochemistry and Function*, vol. 39, no. 2, pp. 174–179, 2021.

[29] B. R. Stockwell, J. P. Friedmann Angeli, H. Bayir et al., "Ferroptosis: a regulated cell death nexus linking metabolism, redox biology, and disease," *Cell*, vol. 171, no. 2, pp. 273–285, 2017.

[30] Y. Wang, S. Wang, Y. Xin et al., "Hydrogen sulfide alleviates the anxiety-like and depressive-like behaviors of type 1 diabetic mice via inhibiting inflammation and ferroptosis," *Life Sciences*, vol. 278, article 119551, 2021.

Hindawi
Oxidative Medicine and Cellular Longevity
Volume 2022, Article ID 4972622, 16 pages
https://doi.org/10.1155/2022/4972622

Research Article

Nuclear and Morphological Alterations in Erythrocytes, Antioxidant Enzymes, and Genetic Disparities Induced by Brackish Water in Mrigal Carp (*Cirrhinus mrigala*)

Ghulam Ali Raza,[1] Abdul Ghaffar,[1] Riaz Hussain,[2] Adil Jamal,[3] Zulfiqar Ahmad,[4] Bahaeldeen Babiker Mohamed,[5] and Abdullah S. M. Aljohani[6]

[1]*Department of Zoology, Islamia University of Bahawalpur, 63100, Pakistan*
[2]*Department of Pathology, Faculty of Veterinary Sciences, Islamia University of Bahawalpur, 63100, Pakistan*
[3]*Sciences and Research, College of Nursing, Umm Al Qura University, 715 Makkah, Saudi Arabia*
[4]*Department of Food Science and Technology, Faculty of Agriculture and Environment, The Islamia University of Bahawalpur, 63100, Pakistan*
[5]*Institute of Environment Natural Resources, The National Centre of Research, Khartoum, Sudan*
[6]*Department of Veterinary Medicine, College of Agriculture and Veterinary Medicine, Qassim University, Buraydah, Saudi Arabia*

Correspondence should be addressed to Riaz Hussain; dr.riaz.hussain@iub.edu.pk
and Bahaeldeen Babiker Mohamed; bahaeldeen.elhag@ncr.gov.sd

Received 1 July 2022; Revised 7 September 2022; Accepted 24 September 2022; Published 11 October 2022

Academic Editor: Muhammad Saleem Kalhoro

Salinization of aquatic ecosystem, abrupt climate change, and anthropogenic activities cause adverse impact on agricultural land/soil as well as the aquaculture industry. This experimental study was designed to evaluate different biomarkers of oxidative stress, antioxidant enzymes, and genotoxic potential of diverse salinities of brackish water on freshwater fish. A total of 84 fresh water mrigal carp (*Cirrhinus mrigala*) were randomly segregated and maintained in four groups (T0, T1, T2, and T3) in a glass aquarium under similar laboratory conditions at various salinity levels (0, 3, 5, and 7 parts per thousand) to determine the pathological influence of brackish water. All the fish in groups T1, T2, and T3 were exposed to various salinity levels of brackish water for a period of 90 days while the fish of group T0 served as the control group. The experimental fish reared in different groups T1, T2, and T3 displayed various physical and behavioral ailments. The results revealed significantly augmented quantity of different oxidative stress indicators including reactive oxygen species (ROS) and thiobarbituric acid reactive substance (TBARS) in different visceral tissues (kidneys, liver, and gills) of exposed fish. Different antioxidant enzymes such as reduced glutathione (GSH), peroxidase (POD), superoxide dismutase (SOD), and catalase (CAT) along with total proteins were remarkably reduced in the kidneys, gills, and liver tissues. Results showed significantly increased values of different nuclear abnormalities (erythrocyte with micronucleus, erythrocyte with condensed nucleus, and erythrocyte with lobed nucleus) and morphological changes (pear shaped erythrocyte, spindle-shaped erythrocytes, and spherocyte) in red blood cells of experimental fish. The results on genotoxic effects exhibited significantly increased DNA damage in isolated cells of liver, kidneys, and gills of exposed fish. The findings of our experimental research suggested that brackish water causes adverse toxicological impacts on different visceral tissues of fresh water fish at higher salinity level through disruption and disorder of physiological and biochemical markers.

1. Introduction

Aquaculture is considered the most important source of proteins for human as well as other terrestrial animals. The sustainable production and utilization of nutritive foods has become crucial due to rapid growth of human population. Fish and different other aquaculture species play important role to control malnutrition across the globe. Due to extensive growth of human population, if food supply and security cannot be maintained, it may lead to numerous problems regarding utilization of nutritive foods. Therefore, optimum production and health of aquaculture has become necessary due to the increase pressure of human population in various developing countries [1]. Studies have investigated that global aquaculture supplies huge amount of proteins in terms of growing different kinds of fish in a very short period by providing a healthy and perfect habitat [2–4].

An ever-increasing human population, water scarcity, land acquisition costs, and the indiscriminate use of pharmaceuticals and variety of chemicals are putting pressure on the aquaculture industry [5]. Physiological functions, growth performance, and immunological modulation in fish farming are the key factors influenced by water having high salinity [6]. Saltiness is one of the most important feature characteristics in determining osmoregulatory stress level in different species of freshwater fish. It is observed that investigation of adverse effects of water having high salinity is important to maintain the process of osmoregulation and ionic concentration in various tissues (gill, kidney, and gut) of fish for optimum biological functions and growth [7].

When compared to freshwater, brackish water has high salinity levels but is less salty than seawater [8]. There are a variety of sources of brackish water, including groundwater (naturally salinized aquifers), rivers, wastewater (including those produced by hydraulic fracturing, human activities, and industrial operations) and irrigation return flow [9]. The runoff of various salt deposits such as halite or gypsum is found in sedimentary rocks, as well as discharges from industrial effluents containing dissolved salts and leachates from saline soils ultimately lead to formation of brackish water [10, 11]. Salinity is believed to have an impact on around one-third of the world's cultivable land [12].

Understanding of optimum salinity for specific species of fish and other species can contribute in expansion of aquaculture productions by utilizing wide range of culturing environments including resources of brackish water. Rearing of both freshwater and marine fish species in water having inadequate salinity levels can directly affects the physiology of fish causing poor growth, increased mortality, low immune response, and disease resistance [13].

However, prior to establishing aquaculture operations in these places, it is critical to pick suitable fish species that are tolerant to saline environments. This is mostly due to the fact that greater salinity of water can operate as a significant stressor in both wild and farmed environments [14]. Furthermore, salinity has the ability to influence the metabolism of fish, which in turn has an impact on the survival, growth, feed intake, and even the geographic spread of fish species [15, 16].

Blood is commonly regarded as an effective stress indicator for revealing the potential harmful stress and health status of fish [17–19]. It is recorded that the monitoring and determination of hematological profile of fish is of vital, useful, and reliable tool for the estimation of different pathological ailments induced by various environmental pollutants both in aquatic and terrestrial animals. In addition, studies have highlighted that determination of variations in different biochemical profile including enzymes and proteins is of vital importance to assess the physiological ailments in aquatic organisms [17, 20–23]. The red blood cells of fish and other animals are directly exposed to different environmental contaminants when they enter into the blood and are reliable biomarkers for the early screening of pathophysiological effects employed by all kind of drugs and other pollutants [18, 20–23]. The toxic effects induced by various pollutants can induce physiological stress leading to induction of different genotoxic abnormalities and development of morphological nuclear changes in erythrocytes of exposed aquatic animals [17, 24]. Studies have recorded that investigation of morphological features of red blood cells are frequently utilized in toxicity testing and in determination of health condition of fish [17, 18].

Reactive oxygen species (ROS) generate oxidative stress when they be more than the body's antioxidant capacity, as they do under conditions of environmental stress [25]. ROS generation is tightly linked to variations in salinity, resulting in oxidative stress in fish [26, 27]. It has been recorded that ROS are extensively generated in the body during an aerobic condition and at different physiological disorders creating oxidative eustress [17, 21, 22]. Moreover, different antioxidant enzymes including both enzymatic and nonenzymatic play crucial and vital role in maintaining the redox status and oxidative stress balance by providing defense against free radicals [17, 22]. Different antioxidant enzymes (SOD, CAT, and GSH) prevent induction of oxidative stress in different tissues of the animals including aquatic life and are frequently used to estimate the risk of various environmental contaminants in [17, 21]. It has been recorded that increased salinity level induces different physiological disorders via oxidative stress and alterations in concentrations of hormones in plasma, abnormal energy metabolism, and electrolyte imbalance in different animal species [28]. In addition, different investigations have indicated that increased level of salinity results disorders regarding intake of O_2 leading to abnormalities in respiration which can be transformed to oxidative stress and lower the antioxidant defense [29].

As a result, it is vital to investigate the specific stresses associated with brackish water salinity. So, the objective of this study is to examine the erythrocytic morphological and nuclear alterations, genotoxic potential, oxidative stress, and status of antioxidant enzymes in visceral tissues of mrigal carp reared in brackish water.

2. Methodology

2.1. Fish Handling. The recent research was conducted in laboratories of the Department of Zoology and Department

of Pathology, Islamia University of Bahawalpur. A total of 84 mrigal fish with approximately similar body weight (160-180 g), size, and free from any external and internal parasitic infections were obtained from private hatchery located at district Bahawalpur. All the Fish were carried to laboratory in oxygen rich plastic sacks and were kept in glass aquaria under similar laboratory conditions. Aerators were installed in all the glass aquaria to ensure availability of sufficient oxygen for experimental organisms. After a period of 15 days of acclimatization, all the fish were indiscriminately picked and placed in four groups. A total of 21 fish were placed in each group. All of the fish were fed standard fish feed with enough proteins (25 percent). All experimental procedures were according to the rules issued by the office of the directorate of research and bioethics committee of Islamia University Bahawalpur concerning the use and welfare of laboratory organisms. On a daily basis, all waste material (fish excretions) and residual feed were filtered and removed from each aquarium. Different physical and chemical properties of study water were determined on weekly basis, and the average values were computed at days 30, 60, and 90 of the trial. All the chemicals used in our trial were obtained from Sigma-Aldrich (USA) and Merck (Germany).

2.2. Collection of Water. The brackish water used in present research was collected from Derawer Fort (Cholistan desert) District Bahawalpur, Punjab, Pakistan. Derawer fort is a well-known historical place being in Cholistan desert and lies between latitudes 28.76° N and longitudes 71.33° E (Figure 1). Brackish water having salinity level of 7.2 parts per thousand (ppt) was collected and diluted to 3.00 ppt, 5.00 ppt, and 7.00 ppt by adding fresh water (Table 1), whereas fresh water (0 ppt) was obtained from the laboratory, Department of Zoology, Islamia University of Bahawalpur.

2.3. Experimental Design. After two weeks of acclimatization, all the active fish, without any obvious clinical ailments and free from any external and internal parasitic infection, were blindly picked and placed into four equal groups (T0, T1, T2, and T3). Fish kept in groups (T1, T2, and T3) were exposed to brackish water having different salinity levels (3.00 ppt, 5.00 ppt, and 7.00 ppt). The fish present in group T0 served as control group (0 ppt). All of the fish were closely observed on a regular basis by visual examination for any obvious physical or behavioral alterations.

2.4. Blood Sampling and Genotoxicity Evaluation. By using 26 gauge sterile hypodermic needle, blood sample (2 mL) was obtained from the caudal vein of each fish at days 30, 60, and 90 of the trial [30]. After that, blood films were made on glass slides from fresh blood without any anticoagulant. All the blood films were then dried, fixed with 100% alcohol, and stained using Giemsa solution. All the blood films were observed under computer-assisted light microscope to record the nuclear and morphological disparities in erythrocytes. A total of 1500 erythrocytes from each fish were observed with the help of computer-assisted light microscope using immersion lens [30]. The severity of genotoxic effects of study water in visceral organs (kidneys, liver, and gills) was determined by using single-cell gel electrophoresis or comet essay [31, 32]. For this purpose, visceral organs (kidneys, liver, and gills) were removed after dissection and placed in chilled normal saline solution. After that, about 0.2 g tissue from each organ (kidneys, liver, and gills) was homogenized and centrifuged separately for separation of cells. DNA damage in isolated cells was determined by using a comet assay [31]. Briefly, thin smear of low melting point (1%) along with normal point (1%) agarose liquified in Milli-Q water was created on frosted slides. Isolated cells of each tissue were suspended in agarose of low melting point [31]. After preparing the slides, they were lysed in cold buffer solution. For electrophoresis, the slides were placed in a horizontal tank with a chilled electrophoretic solution. The electrophoresis (25 volts) was conducted for a period of 30 minutes [33]. After the electrophoresis, the prepared slides were neutralized by placing in an ice-cold 0.4 M Tris buffer (pH 7.5) [34]. Eventually, ethidium bromide was applied for staining, and frequency of DNA damage in different tissues was estimated by using a fluorescent microscope (Euromex Ox Spare LED; SL.5510) at 400x. A total of 500 cells/fish/slides were examined, and frequency of DNA damage (%) was calculated [34].

Figure 1: Geographical location of brackish water of selected site (Derawer Fort) of District Bahawalpur, Punjab, Pakistan.

Table 1: Physico-chemical properties of water in various salinity.

Parameters	Salinity levels			
	T0	T1	T2	T3
Electrical conductivity (mS/cm)	5.73	30.7	82.8	104.6
Water temperature (°C)	26.8	27.2	26.2	28.1
Total dissolved solids (mg/L)	172.7	195.7	212.7	228.4
Dissolved oxygen (mg/L)	6.97	7.11	7.33	7.38
pH	7.5	7.7	7.9	8.1
Total hardness (mg/L)	291.45	515.62	711.8	1036.4
Chlorides (mg/L)	48.6	472.3	758.5	1037.7
Magnesium (mg/L)	72.63	112.7	197.4	242.9
Calcium (mg/L)	44.56	59.5	77.3	104.8
Potassium (mg/L)	3.36	27.6	33.8	38.9
Sulphates (mg/L)	7.87	12.6	15.7	17.4
Sodium (mg/L)	43.86	211.5	387.3	667.9
Total alkalinity ($CaCO_3$ mg/L)	273.89	321.5	335.8	360.3

T: treatments; T0: 0.00.00 ppt; T1: 3.00 ppt; T2: 5.00 ppt; T3: 7.00 ppt.

Table 2: Frequency of different morphological and nuclear changes in erythrocytes of mrigal carp (*Cirrhinus mrigala*) due to brackish water of different salinity regimes.

Parameters/days	Groups (brackish water of different salinities)			
	T0 (0.0 ppt)	T1 (3.0 ppt)	T2 (5.0 ppt)	T3 (7.0 ppt)
Erythrocytes with lobed nucleus (%)				
30	1.33 ± 0.17	1.39 ± 0.18	1.43 ± 0.18	1.46 ± 0.13
60	1.35 ± 0.09	1.41 ± 0.11	2.36 ± 0.22*	2.92 ± 0.24*
90	1.34 ± 0.13	1.44 ± 0.15	2.87 ± 0.21*	3.64 ± 0.18*
Erythrocytes with blebbed nucleus (%)				
30	1.25 ± 0.10	1.30 ± 0.22	1.31 ± 0.13	1.32 ± 0.17
60	1.25 ± 0.11	1.31 ± 0.21	2.20 ± 0.35*	2.31 ± 0.29*
90	1.26 ± 0.14	1.32 ± 0.44	2.44 ± 0.11*	2.88 ± 0.58*
Erythrocytes with vacuolated nucleus (%)				
30	2.35 ± 0.25	2.37 ± 0.18	2.41 ± 0.17	2.42 ± 0.25
60	2.36 ± 0.23	2.39 ± 0.18	3.11 ± 0.31*	3.66 ± 0.30*
90	2.39 ± 0.28	2.40 ± 0.39	3.43 ± 0.26*	4.3 ± 0.25*
Erythrocytes with notched nucleus (%)				
30	1.78 ± 0.15	1.81 ± 0.18	1.82 ± 0.83	1.84 ± 0.21
60	1.79 ± 0.17	1.83 ± 0.15	2.65 ± 0.34*	3.14 ± 0.26*
90	1.80 ± 0.18	1.85 ± 0.13	3.13 ± 0.17*	3.82 ± 0.24*
Binucleated erythrocytes (%)				
30	1.64 ± 0.32	1.66 ± 0.28	1.68 ± 0.35	1.72 ± 0.25
60	1.69 ± 0.32	1.68 ± 0.28	2.42 ± 0.27*	2.93 ± 0.17*
90	1.71 ± 0.22	1.75 ± 0.35	2.91 ± 0.22*	3.53 ± 0.21*
Pear-shaped erythrocytes (%)				
30	2.90 ± 0.48	2.92 ± 0.32	2.95 ± 0.29	2.99 ± 0.25
60	2.84 ± 0.62	2.95 ± 0.28	3.90 ± 0.21*	4.51 ± 0.24*
90	2.89 ± 0.65	2.97 ± 0.35	4.28 ± 0.22*	5.12 ± 0.23*
Erythrocytes with micronucleus (%)				
30	1.75 ± 0.34	1.77 ± 0.17	1.80 ± 0.22	1.82 ± 0.25
60	1.76 ± 0.38	1.79 ± 0.17	2.68 ± 0.21*	3.09 ± 0.28*
90	1.74 ± 0.41	1.82 ± 0.21	3.16 ± 0.17*	3.78 ± 0.25*
Erythrocytes with condensed nucleus (%)				
30	2.13 ± 1.12	2.15 ± 0.26	2.18 ± 0.25	2.21 ± 0.56
60	2.09 ± 0.61	2.16 ± 0.22	3.08 ± 0.31*	3.54 ± 0.32*
90	2.16 ± 0.82	2.21 ± 0.25	3.56 ± 0.18*	4.17 ± 0.29*
Spindle-shaped erythrocytes (%)				
30	1.42 ± 0.21	1.46 ± 0.22	1.47 ± 0.25	1.50 ± 0.27
60	1.47 ± 0.26	1.48 ± 0.33	2.37 ± 0.021*	2.94 ± 0.025*
90	1.46 ± 0.22	1.51 ± 0.26	2.81 ± 0.26*	3.64 ± 0.34*
Spherocytes (%)				
30	1.93 ± 0.25	1.95 ± 0.21	1.97 ± 0.26	1.98 ± 0.17
60	1.94 ± 0.13	1.96 ± 0.29	2.91 ± 0.25*	3.49 ± 0.25*
90	1.96 ± 0.26	1.99 ± 0.28	3.41 ± 0.22*	4.18 ± 0.26*

Values (mean ± SE) containing asterisks (*) in each row differ significantly ($p < 0.05$) different to normal group.

2.5. Tissue Preparation and Biochemical Analysis. Fish was dissected at days 30, 60, and 90 of the experiment for separation of different visceral organs (kidneys, gills, and liver) for biochemical evaluation. All the collected tissues were placed in cold saline solution for estimation of thiobarbituric acid reactive substance (TBARS), reactive oxygen species

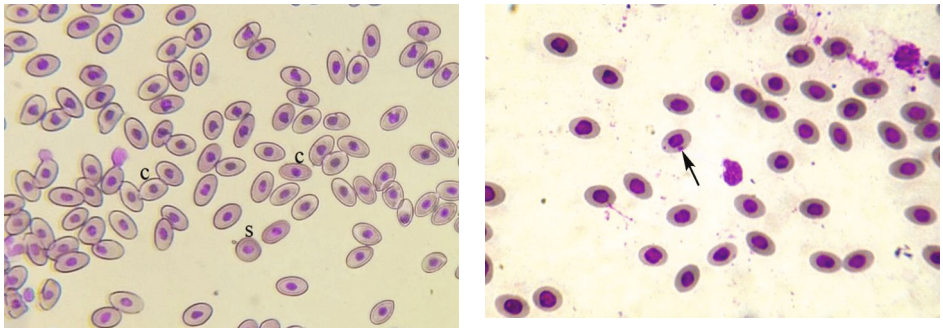

(a) (b)

Figure 2: Photomicrograph of blood smear of fish placed in group T3 at day 90 of trial showing (a) erythrocyte with condensed nucleus (c) and spherocyte (s) and (b) showing erythrocyte with micronucleus (arrows). Giemsa stain: ×1000.

(ROS), reduced glutathione (GSH), total proteins, and various antioxidant enzymes catalase (CAT), peroxidase (POD), and superoxide dismutase (SOD) [34]. Various biochemical markers, such as reactive oxygen species [35] and thiobarbituric reactive substance [36], along with reduced glutathione [37], were estimated in the kidneys, gills, and liver of each fish using UV spectrophotometer (Libra S60; Biochrom, UK). The status of antioxidant enzymes including peroxidase [38], superoxide dismutase [39], and catalase [38] in the liver, gills, and kidneys was determined following the procedures as described in the previous published literature.

2.6. Statistical Analysis. All the collected data is presented as a mean standard deviation. Variance of one-way analysis was used in IBM SPSS statistical programmer (version no. 20) to conduct statistical analysis because the data in each group was normally distributed. A post hoc Tukey's test with significance threshold of 0.05 was used to evaluate the variance in mean values (mean ± SE) of erythrocytic nuclear and morphological disparities, oxidative stress, and antioxidant enzymes, along with genotoxic potential in visceral organs of control and experimental groups. Pearson's correlation analysis was performed to know the association between different variables of the liver, kidneys, and gills of experimental fish.

3. Results

No mortalities were recorded in fish kept in various treatment groups (T1, T2, and T3) having different salinity levels of brackish water throughout the study. Mild to moderate abnormal swimming, lack of coordination, air gulping, swimming in isolation, and lie down on single side were visually observed in experimental fish exposed to brackish water of high salinity (T2) after day 60 of the trial. Different severe physical disorders such as increased swimming, protrusion of eyes, loss of stability, increased opercular movements, breathing on surface of water, and mucous discharge from mouth and gills were observed in fish of group T3 after day 60 of experiment. The intensity of several behavioral and clinical indications in fish exposed to brackish water increased in a time-dependent manner.

3.1. Morphological and Nuclear Irregularities in Erythrocytes. The results of the current study revealed that the frequency of various nuclear and morphological abnormalities in erythrocytes of fish exposed to increasing salinity levels of brackish water was remarkably increased in comparison to normal fish. The prevalence of different morphological anomalies in erythrocytes was significantly high in fish exposed to 5.00 ppt and 7.00 ppt salinity of brackish water at days 60 and 90 of current study. The percentage of erythrocytes with lobed nuclei, erythrocytes with blebbed nuclei, erythrocytes with vacuolated nuclei, erythrocytes with notched nuclei, and erythrocytes with binucleus was considerably high in mrigal carp exposed to 5.00 ppt and 7.00 ppt salinity at days 60 and 90 of the experiment comparing to control group (Table 2). On days 60 and 90 of the current study, fish exposed to 5.00 ppt and 7.00 ppt salinity of brackish water had also significantly higher percentage of erythrocytes with micronucleus (Figure 1) along with erythrocytes with condensed nucleus than untreated control fish (Table 2). Increased percentile rate of erythrocytes having spindle shape and spherocytes (Figure 2) was recorded in mrigal carp exposed to 5.00 ppt and 7.00 ppt salinity of brackish water at days 60 and 90 of the trial (Table 2).

3.2. Oxidative Stress and Status of Antioxidant Enzymes. The current study revealed that the quantity of ROS in isolated hepatocytes of fish exposed to 5.00 ppt and 7.00 ppt salinity of brackish water increased significantly at days 60 and 90, while the contents of TBARS in isolated hepatocytes of mrigal carp treated with 7.00 ppt salinity of brackish water was significantly higher at days 60 and 90 of trial. The contents of TBARS in isolated hepatocytes of mrigal carp treated with 5.00 ppt was considerably high at day 90 of the trial (Table 3). The contents of total proteins along with reduced glutathione in isolated hepatocytes of mrigal carp reared in brackish water having 7.00 ppt salinity was prominently diminished at days 60 and 90 of the trial (Table 3), while quantity of reduced glutathione and total proteins in isolated hepatocytes of mrigal carp in 5.00 ppt salinity was significantly decreased at day 90 of the trial (Table 3). When compared to untreated mrigal carp, the quantity of SOD, CAT, and POD in isolated hepatocytes of treated fish exposed to

Table 3: GSH contents, total proteins, and quantity of antioxidant enzymes in the liver of fish exposed to different salinities of brackish water.

Parameters/days	Groups (different salinities of brackish water)			
	T0 (0.0 ppt)	T1 (3.0 ppt)	T2 (5.0 ppt)	T3 (7.0 ppt)
Liver				
Reactive oxygen species (ROS) contents (optical density)				
30	0.13 ± 0.03	0.14 ± 0.02	0.15 ± 0.01	0.16 ± 0.04
60	0.14 ± 0.04	0.15 ± 0.04	0.21 ± 0.03*	0.23 ± 0.03*
90	0.15 ± 0.02	0.16 ± 0.01	0.24 ± 0.02*	0.27 ± 0.02*
Thiobarbituric acid reactive substances (TBARS) contents (nmol/TBARS formed/mg protein/min)				
30	24.3 ± 0.42	25.6 ± 0.40	25.8 ± 0.60	26.4 ± 0.23
60	24.5 ± 0.45	25.9 ± 0.25	27.2 ± 0.26	29.6 ± 0.51*
90	24.4 ± 0.10	26.3 ± 0.28	30.7 ± 0.73*	31.8 ± 0.47*
Reduced glutathione GSH (μmol/g tissue)				
30	5.55 ± 0.02	5.48 ± 0.01	5.44 ± 0.01	5.36 ± 0.02
60	5.58 ± 0.01	5.43 ± 0.09	5.36 ± 0.01	4.01 ± 0.01*
90	5.61 ± 0.25	5.31 ± 0.14	4.05 ± 0.03*	3.92 ± 0.04*
Total proteins (μg/mg tissue)				
30	6.29 ± 0.02	6.21 ± 0.01	6.11 ± 0.01	6.04 ± .03
60	6.30 ± 0.01	6.14 ± 0.03	5.96 ± 0.03	4.59 ± 0.01*
90	6.33 ± 0.03	6.04 ± 0.02	4.55 ± 0.04*	4.48 ± 0.27*
Superoxide dismutase SOD (units/mg protein)				
30	11.3 ± 0.05	11.1 ± 0.06	10.8 ± 0.03	10.7 ± 0.05
60	11.5 ± 0.04	10.8 ± 0.03	8.73 ± 0.05*	8.61 ± 0.02*
90	11.6 ± 0.02	10.3 ± 0.02	7.8 ± 0.10*	7.1 ± 0.23*
Catalase CAT (units/min)				
30	6.46 ± 0.03	6.43 ± 0.01	6.40 ± 0.02	6.38 ± 0.03
60	6.43 ± 0.02	6.39 ± 0.01	4.81 ± 0.01*	4.78 ± 0.02*
90	6.40 ± 0.02	6.35 ± 0.02	4.68 ± 0.05*	4.46 ± 0.01*
Peroxidase POD (units/min)				
30	4.62 ± 0.05	4.48 ± 0.04	4.44 ± 0.05	4.37 ± 0.01
60	4.64 ± .05	4.42 ± 0.03	3.40 ± 0.03*	3.31 ± .01*
90	4.60 ± .01	4.38 ± 0.01	3.27 ± 0.01*	3.17 ± 0.05*

Values (mean ± SE) containing asterisks (*) in each row differ significantly ($p < 0.05$) different to normal group.

5.00 ppt and 7.00 ppt salinity of brackish water was significantly lowered at days 60 and 90 of the trial (Table 3).

At days 60 and 90 of the trial, the contents of ROS in isolated kidneys of fish exposed to 7.00 ppt salinity of brackish water was considerably increased, while the contents of ROS in isolated kidney cells of fish exposed to 5.00 ppt was significantly increased at day 90 of the experiment (Table 4), while the contents of TBARS in isolated kidneys of fish exposed to 7.00 ppt salinity was significantly increased at days 60 and 90 of the current study (Table 4). The contents of total proteins and reduced glutathione were decreased considerably in isolated kidney of fish exposed to 5.00 ppt and 7.00 ppt salinity of brackish water at day 90 of the trial (Table 4). The values of SOD were decreased in isolated kidneys of fish exposed to 7.00 ppt salinity at days 60 and 90 of the trial, while the values of SOD decreased at 5.00 ppt salinity at day 90 of the trail (Table 4). At day 90 of the trail, the contents of CAT and POD decreased in isolated kidney of fish exposed to 5.00 ppt and 77.00 ppt salinity of brackish water (Table 4).

The values of ROS in isolated gill tissues of fish exposed to 5.00 ppt and 7.00 ppt were significantly increased at days 60 and 90 of the trial, while contents of TBARS gill of fish were increased significantly when exposed to 5.00 ppt salinity at 90 days of the trail and 7.00 ppt salinity at days 60 and 90 of the trial (Table 5). The contents of GSH were decreased in isolated gills of fish exposed to 5.00 ppt and 7.00 ppt salinity of brackish water at days 60 and 90 of the current study (Table 5). At days 60 and 90 of the trial, total proteins in isolated gill of fish exposed to 7.00 ppt were significantly decreased (Table 5). The contents of total proteins decreased considerably in the gills of mrigal carp reared in brackish water having 5.00 ppt salinity at day 90 of the

Table 4: Oxidative stress parameters, GSH contents, and total proteins along with quantity of various antioxidant enzymes in the kidneys of fish exposed to different salinities of brackish water.

Parameters/days	Groups (different salinities of brackish water)			
	T0 (0.0 ppt)	T1 (3.0 ppt)	T2 (5.0 ppt)	T3 (7.0 ppt)
Kidney				
Reactive oxygen species (ROS) contents (optical density)				
30	0.28 ± 0.02	0.30 ± 0.02	0.31 ± 0.03	0.33 ± 0.01
60	0.29 ± 0.01	0.32 ± 0.01	0.33 ± 0.01	0.39 ± 0.04*
90	0.31 ± 0.04	0.34 ± 0.03	0.38 ± 0.02*	0.42 ± 0.03*
Thiobarbituric reactive substances (TBARS) contents (nmol/TBARS formed/mg protein/min)				
30	32.6 ± 0.29	33.7 ± 0.60	34.2 ± 0.85	35.7 ± 0.42
60	32.9 ± 0.63	34.1 ± 0.24	35.8 ± 0.32	37.4 ± 0.21*
90	33.5 ± 0.29	34.8 ± 0.43	36.5 ± 0.35	38.4 ± 0.27*
Reduced glutathione GSH (μmol/g tissue)				
30	4.33 ± 0.06	4.27 ± 0.05	4.24 ± 0.03	4.20 ± 0.01
60	4.32 ± 0.01	4.20 ± 0.03	4.17 ± 0.04	4.11 ± 0.03
90	4.38 ± 0.03	4.18 ± 0.02	3.72 ± 0.06*	3.65 ± 0.02*
Total proteins (μg/mg tissue)				
30	5.63 ± 0.03	5.57 ± 0.05	5.51 ± 0.02	5.46 ± 0.04
60	5.65 ± 0.25	5.50 ± 0.03	5.43 ± 0.01	5.35 ± 0.07
90	5.66 ± .01	5.44 ± 0.02	3.98 ± 0.03*	3.62 ± 0.02*
Superoxide dismutase SOD (units/mg proteins)				
30	12.4 ± 0.25	12.0 ± 0.16	11.7 ± 0.17	11.3 ± 0.02
60	12.6 ± 0.06	11.9 ± 0.03	11.5 ± 0.11	10.13 ± 0.05*
90	12.9 ± 0.13	11.6 ± 0.03	10.17 ± 0.02*	10.01 ± 0.04*
Catalase CAT (units/min)				
30	4.18 ± 0.04	4.02 ± 0.02	3.94 ± 0.04	3.87 ± 0.01
60	4.16 ± 0.01	3.97 ± 0.01	3.88 ± 0.04	3.76 ± 0.02
90	4.13 ± 0.03	3.88 ± 0.03	3.22 ± 0.03*	3.11 ± 0.01*
Peroxidase POD (units/min)				
30	3.87 ± 0.03	3.79 ± 0.01	3.70 ± 0.02	3.63 ± 0.05
60	3.83 ± 0.02	3.74 ± 0.01	3.61 ± 0.02	3.42 ± 0.01
90	3.76 ± 0.23	3.67 ± 0.02	2.36 ± 0.02*	2.18 ± 0.03*

Values (mean ± SE) containing asterisks (*) in each row differ significantly ($p < 0.05$) different to normal group.

experiment. The concentrations of antioxidant enzyme like SOD, CAT, and POD in isolated gills decreased significantly at days 60 and 90 of the trail in fish exposed to 5.00 ppt and 7.00 ppt salinity of brackish water (Table 5).

3.3. Genotoxic Potential. Results on the DNA damage determined by comet assay (Figure 3) showed significantly increased frequency of DNA damage in various visceral organs of treated fish at days 60 and 90 in isolated cells of the hepatocytes, gills, and kidneys. At days 60 and 90 of the experiment, the frequency of genotoxic potential in isolated gill cells of mrigal carp exposed to 7.00 ppt salinity increased dramatically. The results recorded that the DNA damage was increased significantly at day 90 of the experiment in mrigal carp exposed to 5.00 ppt salinity of brackish water (Figure 4). The frequency of mutagenic potential in isolated hepatocytes and kidney cells at days 60 and 90 in fish exposed to brackish water having 7.00 ppt salinity was significantly high than the fish of control group. The frequency of DNA damage was also higher in fish exposed to brackish water having 5.00 ppt at day 90 of the experiment.

3.4. Correlation Analysis of Studied Variables. The results on Pearson's correlation analysis showed correlation between study variables of the kidneys, liver, and gills of fish reared in brackish water at different sampling days. The results exhibited that total proteins in the kidneys of fish at day 60 has correlation of 0.7 with superoxide dismutase. Weak correlation was observed between DNA damage (COM) by comet assay with other variables. Reactive oxygen species and TBARS at sampling day 30, DNA damage by comet assay, TBARS, and ROS at day 60, while ROS, TBARS, and

Table 5: Oxidative stress parameters, GSH contents, and total proteins along with quantity of various antioxidant enzymes in the gills of mrigal fish exposed to different salinities of brackish water.

Parameters/days	Groups (different salinities of brackish water)			
	T0 (0.0 ppt)	T1 (3.0 ppt)	T2 (5.0 ppt)	T3 (7.0 ppt)
Gills				
Reactive oxygen species (ROS) contents (optical density)				
30	0.15 ± 0.02	0.16 ± 0.03	0.18 ± 0.04	0.19 ± 0.03
60	0.16 ± 0.04	0.17 ± 0.01	0.22 ± 0.03*	0.26 ± 0.01*
90	0.16 ± 0.01	0.19 ± 0.04	0.23 ± 0.05*	0.29 ± 0.04*
Thiobarbituric acid reactive substances (TBARS) contents (nmol/TBARS formed/mg protein/mg)				
30	34.0 ± 0.47	35.4 ± 0.45	36.9 ± 0.39	37.2 ± 0.23
60	34.3 ± 0.23	36.1 ± 0.29	39.3 ± 0.21	41.5 ± 0.20*
90	34.5 ± 0.28	37.2 ± 0.40	41.8 ± 0.59*	43.3 ± 0.37*
Reduced glutathione GSH (μmol/g tissue)				
30	1.36 ± 0.05	1.23 ± 0.02	1.21 ± 0.04	1.17 ± 0.02
60	1.37 ± 0.03	1.21 ± 0.01	1.04 ± 0.06*	1.03 ± 0.03*
90	1.37 ± 0.04	1.14 ± 0.03	1.01 ± 0.03*	0.96 ± 0.01*
Total proteins (μg/mg tissue)				
30	5.39 ± 0.03	5.34 ± 0.10	5.29 ± 0.04	5.18 ± 0.26
60	5.37 ± 0.14	5.30 ± 0.08	4.14 ± 0.02	3.81 ± 0.04*
90	5.35 ± 0.02	5.27 ± 0.02	3.87 ± 0.03*	3.78 ± 0.12*
Superoxide dismutase SOD (units/mg proteins)				
30	8.65 ± 0.04	8.53 ± 0.01	8.44 ± 0.01	8.32 ± 0.01
60	8.64 ± 0.04	8.49 ± 0.03	6.41 ± 0.02*	6.25 ± 0.02*
90	8.64 ± 0.09	8.42 ± 0.05	6.15 ± 0.04*	6.11 ± 0.05*
Catalase CAT (units/min)				
30	2.81 ± 0.02	2.72 ± 0.03	2.64 ± 0.01	2.62 ± 0.02
60	2.85 ± 0.03	2.69 ± 0.02	2.17 ± 0.02*	2.07 ± 0.01*
90	2.84 ± 0.03	2.61 ± 0.05	2.15 ± 0.25*	2.04 ± 0.04*
Peroxidase POD (units/min)				
30	0.31 ± 0.01	0.29 ± 0.01	0.27 ± 0.01	0.26 ± 0.02
60	0.32 ± 0.03	0.28 ± 0.02	0.26 ± 0.03*	0.25 ± 0.04*
90	0.33 ± 0.05	0.27 ± 0.04	0.23 ± 0.06*	0.21 ± 0.07*

Values (mean ± SE) containing asterisks (*) in each row differ significantly ($p < 0.05$) different to normal group.

DNA damage by comet assay at day 90 have significant negative correlation. The variables POD, TP, SOD, GSH, and CAT at day 30, variables SOD, POD, CAT, and GSH at day 60, and variables SOD, POD, CAT, GSH, and TP at day 90 of trial have significant positive correlation (Figure 5). The results on Pearson's correlation analysis for different variables of liver showed weak correlation between frequency of DNA damage at sampling day 30 and all other variables. The results indicated that total proteins (TP), POD, CAT, SOD, and GSH at sampling day 30, TP, CAT, POD, and SOD at sampling day 60, and POD, CAT, SOD, GSH, and TP have significant positive correlation. Results indicated that ROS and TBARS at day 30, percentile rate of DNA damage, TBARS, and ROS at day 60, and TBARS, percentile rate of DNA damage, and ROS at sampling day 90 have negative correlation (Figure 6). The results on Pearson's correlation analysis for different variables of gills showed weak correlation between frequency of DNA damage at sampling day 30 and all other variables. The results indicated that different variables such as CAT, SOD, GSH, and POD at day 30, GSH, CAT, SOD, and TP at day 60, and SOD, TP, POD, POD, CAT, and GSH at day 90 of trial have significant positive correlation. Results showed that variable including ROS and TBARS at day 30, percentile rate of DNA damage (COM), ROS and TBARS at day 60, and ROS, TBARS, and COM at day 90 of trial have negative correlation (Figure 7).

4. Discussion

In brackish and marine water, salinity is an essential physical feature that is employed as a water tracer. It denotes the

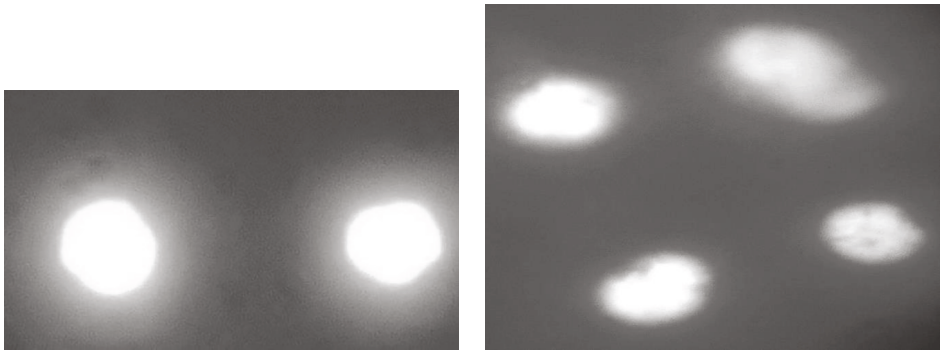

(a) (b)

Figure 3: Comet assay or single cell gel electrophoresis exhibiting normal cells (a) and DNA damage in isolated cells of fish kept in group T3 at day 90 of trial. Ethidium bromide stain: 400x.

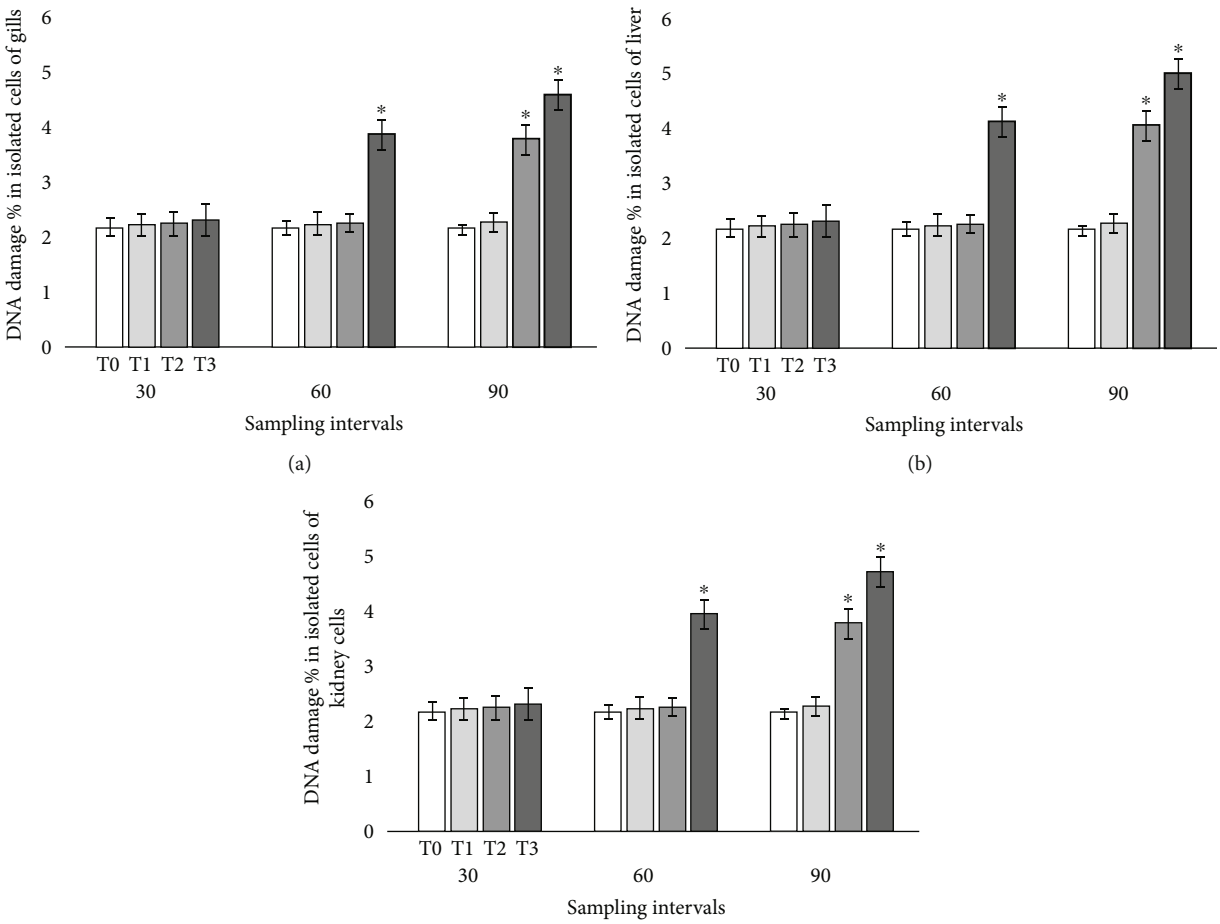

Figure 4: Photograph exhibiting frequency of DNA damage in isolated cells of gill (a), liver (b), and kidneys (c) of fish reared in brackish water. Bars show mean ± SE, and asterisks on bars show significant difference at ($p < 0.05$).

overall concentration of dissolved inorganic ions and salts. Salinization is a natural rise in soluble salts over an optimal level. Salinity is a vital environmental component for all aquatic organisms including fish. Abrupt change in the salinity of habitat water generates salinity stress by interfering with physiological homeostasis and normal biological activities of the exposed animals. The majority of wetlands is degraded due to salinization which ultimately leads to an imbalance in the ecosystem and impacts the biodiversity [40]. Salinization is principally caused by glacial/interglacial cycles, catchment weathering, salt content in rain (acquired by evaporation), and sea spray [40, 41]. Moreover,

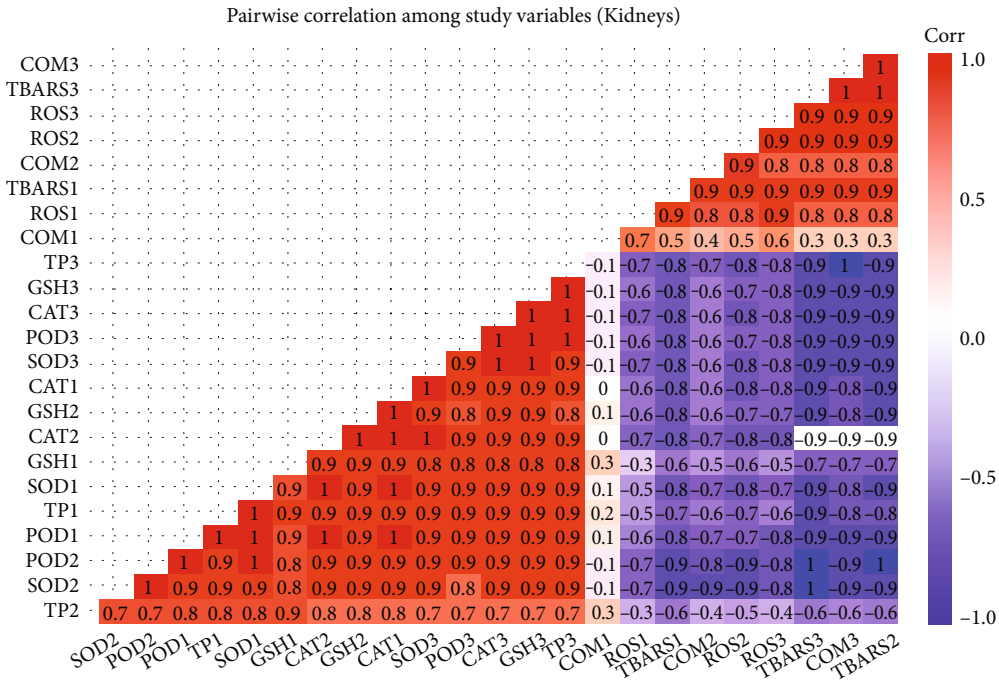

Figure 5: Photograph shows correlation between study variables of kidneys at different levels of sampling days. The values of correlation ranged from -1 to +1. The absolute values between 0 and 0.2, 0.2 and 0.4, 0.4 and 0.6, 0.6 and 0.8, and 0.8 and 1 indicate very week, week, moderate, strong, and very strong relationship, respectively. The last digit of each variable indicates sampling points which are 1 (day 30), 2 (day 60), and 3 (day 90).

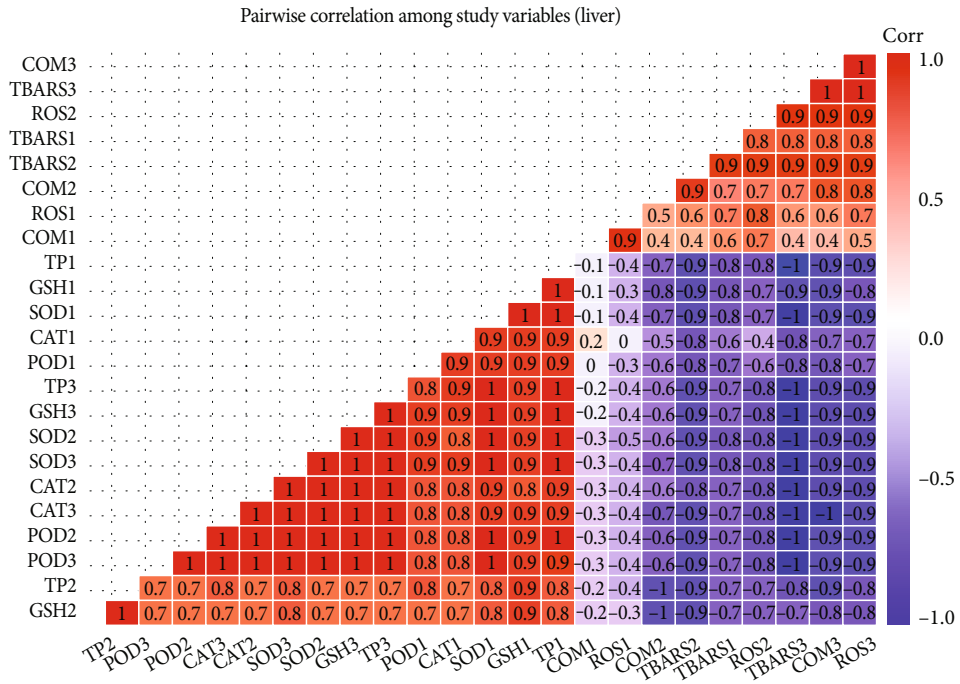

Figure 6: Photograph shows correlation between study variables of liver at different levels of sampling days. The values of correlation ranged from -1 to +1. The absolute values between 0 and 0.2, 0.2 and 0.4, 0.4 and 0.6, 0.6 and 0.8, and 0.8 and 1 indicate very week, week, moderate, strong, and very strong relationship, respectively. The last digit of each variable indicates sampling points which are 1 (day 30), 2 (day 60), and 3 (day 90).

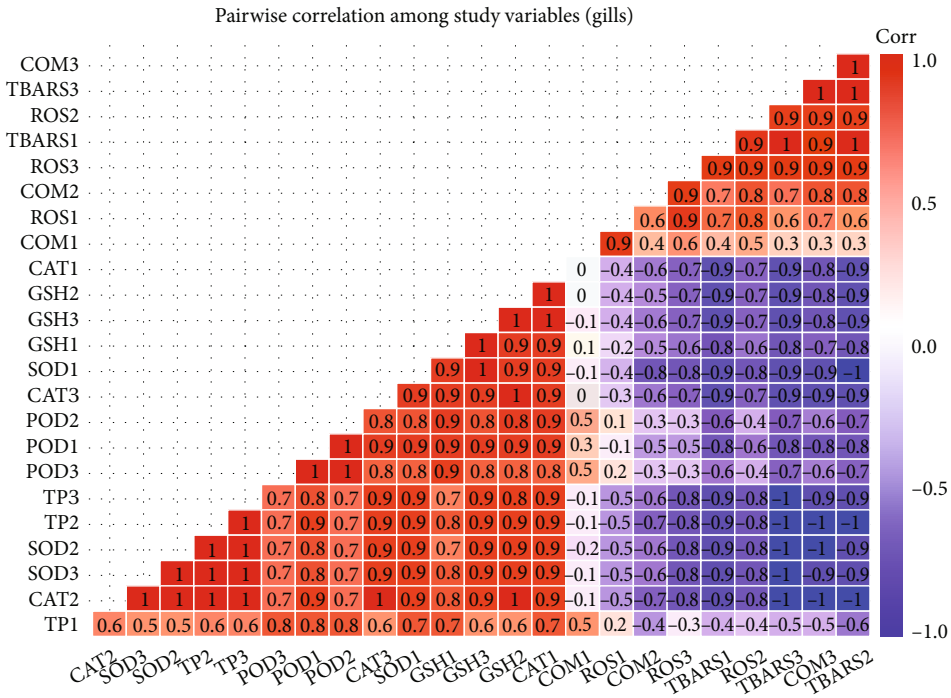

Figure 7: Photograph shows correlation between study variables of gills at different levels of sampling days. The values of correlation ranged from -1 to +1. The absolute values between 0 and 0.2, 0.2 and 0.4, 0.4 and 0.6, 0.6 and 0.8, and 0.8 and 1 indicate very week, week, moderate, strong, and very strong relationship, respectively. The last digit of each variable indicates sampling points which are 1 (day 30), 2 (day 60), and 3 (day 90).

salinization occurs as a result of anthropogenic activity such as urban drainage inflow, vegetation clearing, intense irrigation, river management, sea level rise caused by global warming, and mining activities. It has been recorded that salinization results in biodiversity loss and environmental imbalance [42, 43].

After prolonged exposure to different salinities, mrigal carp displayed several behavioral abnormalities including abnormal swimming pattern, gill motion, and convulsions. The severity of these anomalies increased in fish reared in brackish water in a time- and concentration-dependent manner. Formerly, different physical anomalous-like abnormal swimming pattern, gill motion, and convulsions in *Pangasionodon hypophthalmus* [44] at higher salinities have been observed. Abnormal swimming pattern has been detected in Indian major carp, *Catla catla* [45], *Oryzias latipes* [46], and *Cyprinus carpio* [47]. Previously, disorders of convulsions were detected in *Channa punctatus* reared in water at high level of salinity [48].

Nuclear and morphological abnormalities in red blood cells of fish and other avian species are regarded as reliable biomarkers which provide an overview of genetic alterations and cytotoxicity induced by different natural and synthetic environmental pollutants [34]. It has been recorded that estimation of morphological and genetic disparities in erythrocytes are effective indicators of oxidative stress [49]. The current study recorded significantly higher frequency of different nuclear and morphological alterations including erythrocytes with lobed nuclei, erythrocytes with blebbed nuclei, erythrocytes with vacuolated nuclei, erythrocytes with notched nuclei, erythrocytes with micronuclei, erythrocytes with condensed nucleus, and binucleated erythrocytes along with different morphological changes such as pear-shaped erythrocytes and spherocytes in exposed fish. As far as we know, no information related to erythrocytic morphological and nuclear changes in mrigal carp reared in brackish water is available. According to previous studies, it has been recorded that erythrocytes are the best indicators of oxidative stress showing almost all morphological and nuclear alterations in animals exposed to various toxicants [50–52]. Increased intracellular generation of reactive oxygen and nitrogenous species might be the cause of these cellular alterations [53, 54]. In our study, increased percentage of erythrocyte with micronuclei and lobed nuclei might be owing to an excess of caspase-activated DNase, which is accountable for the cleavage of cytoskeletal (gelsolin, fodrin, and vimentin), nuclear, and aneuploid proteins, as well as oxidative damage to the mitochondrion [55, 56]. Furthermore, different studies have observed different morphological and nuclear alterations in erythrocytes of various species of fish (*Cyprinus carpio* and *Labeo rohita*) and other avian species in response to oxidative stress [30, 51, 52, 57–61]. The increase lipid peroxidation product causes increased permeability and decreased symmetry of the membrane of red blood cells resulting in increased osmotic fragility and abnormalities in the surface of erythrocytes [20, 23].

Antioxidant enzymes including GSH, SOD, CAT, and POD along with oxidative stress (TBARS and ROS) parameters are well-known indicators of inflammatory reactions and effective tools for monitoring of tissues from free radical

injuries [32, 60, 62, 63]. These parameters are frequently measured to assess toxicological consequences of various hazardous environmental and synthetic compounds [64, 65]. Our study results exhibited significantly increased contents of oxidative stress biomarkers including reactive oxygen species (ROS) and thiobarbituric reactive substance in different visceral tissues like gills, liver, and kidneys of mrigal carp reared in brackish water. Published data has indicated that exposure to different toxicants induces rapid generation of reactive oxygen species in target and nontarget animals [34]. The generation of reactive oxygen species (ROS) initiates the lipid peroxidation process which ultimately leads to induction of abnormalities in cellular membranes of various cells of exposed tissues causing severe damage to these tissues and formation of thiobarbituric reactive substance [61, 66]. Previously, it has been recorded that salinity is the major threshold for increased production of ROS and TBARS in *Dicentrarchus labrax* [67], *Catla catla* [68], and Esturine fish [69]. In our study, elevated levels of oxidative stress parameters in mrigal carp reared in brackish water of various salinities might be related to the depletion and misbalancing of antioxidant enzymes. Furthermore, the elevated contents of oxidative stress parameters might be attributed to tissue damage and abnormal mechanism of oxidative phosphorylation [61]. Our research indicated that contents of GSH and total proteins were decreased in tissues including gills, liver, and kidneys of mrigal carp reared in brackish water. Previously, no information could be found regarding the lower contents of GSH and total proteins in various tissues of mrigal fish due to brackish water. The decreased levels of GSH and total proteins in current study might be due to dysfunction of tissues and increased consumption of energy to eliminate the oxidative stress. Several contaminants have previously been linked to protein deprivation in the liver, gills, and kidneys of numerous fish such as *Labeo rohita*, *Channa punctatus*, *Mystus vittatus*, and *Oreochromis spilurus* [66, 70, 71]. The contents of different antioxidant enzymes including reduced glutathione, superoxide dismutase, catalase, and peroxidase in different visceral tissues (gills, liver, and kidneys) were significantly lowered in mrigal fish reared in brackish water. Previously, it has been recorded that the contents of GSH, SOD, CAT, and POD were decreased in *Cyprinus carpio* reared in water of various salinities [72]. In previous published literature, it has been recorded that the increased contents of oxidative stress parameters and reduced contents of antioxidant enzymes in tissues of visceral organs of treated fish are interlinked [66, 72, 73]. Moreover, lower contents of antioxidant enzymes in tissues (liver, gills, and kidneys) of cat fish [74], reduced glutathione in the liver of Delta smelt [75], Jundiara fish [76], and lower values of reduced glutathione and superoxide dismutase in plasma of gold fish [77] due to various toxicants have been recorded. In contrast to our results, increased contents of superoxide dismutase, peroxidase, reduced glutathione, and catalase in different species of fish including Nile tilapia [78], *Catla catla* [68], *Anoplopoma fimbria* [27], and *Clarias gariepinus* [79] reared in water having higher salinity have been recorded.

In our research, the results on comet assay under alkaline conditions displayed high frequency of DNA damage in isolated cells of the kidneys, gills, and liver of Mrigal fish reared in brackish water. It has been determined that comet assay is a sensitive, appropriate, reliable, and frequently used approach for assessing DNA damage in various tissues of aquatic and terrestrial species [30, 32, 60, 66, 80]. Previously, no report is available in published literature regarding DNA damage in various tissues of freshwater fish reared in brackish water. Our study investigated significantly increased DNA damage in mrigal carp reared brackish water. The increased frequency of DNA damage in multiple tissues of Mrigal fish might be due to increase production of free radicals leading to oxidative stress. Furthermore, genotoxic effects can be primarily linked to oxidative stress [17, 62, 81] and lipid peroxidation which might be the source genotoxicity [20–23]. Various previous reports have indicated that the production of free radicals along with oxidative stress are the primary causes of genotoxicity in different tissues of animals [31, 32, 59, 60, 66]. Moreover, DNA damage in various visceral organs (liver, kidneys, and gills) of mrigal fish might be linked to genetic mutations generated by brackish water causing abnormal physiological disorders in different tissues and abnormal functions of various proteins resulting in dysfunctioning of mitochondrion and breakdown of nuclear proteins. The results of this experimental study suggested that brackish water causes adverse toxicological problems on blood and various visceral tissues of mrigal carp (*Cirrhinus mrigala*). Exposure of mrigal carp to brackish water at 5.00 ppt and 7.00 ppt induces genotoxic effects in isolated cells of the liver, kidneys, and gills. Furthermore, the results of our study indicated that brackish water even having low salinity levels reduces different antioxidant biomarkers and increases oxidative stress biomarkers in multiple visceral organs of fresh water fish mrigal carp when reared for long duration.

Data Availability

All the data related to the study is mentioned in the manuscript.

Disclosure

This experimental research was carried out at the laboratories of Department of Zoology and Department of Pathology, Faculty of Veterinary and Animal Sciences, The Islamia University Bahawalpur, Pakistan. The current research was part of the PhD thesis and was approved by the Board of Study (Department of Zoology) and Directorate of Advanced Studies and Research Board Islamia University of Bahawalpur Pakistan.

Conflicts of Interest

All the authors declare no conflict of interest regarding the publication of the current research paper.

Authors' Contributions

Riaz Hussain and Abdul Ghaffar designed study and planned the experiment. Ghulam Ali Raza and Riaz Hussain conducted the research trial, collected the data, and wrote the early and final draft of the manuscript. Adil Jamal, Zulfiqar Ahmed, Abdullah S.M. Aljohani, and Bahaeldeen Babiker Mohamed performed statistical analysis and interpretation of results.

Acknowledgments

The authors give credit to Dr. Tariq Abbas (Associate Professor, Department of Epidemiology, Cholistan University of Veterinary and Animal Sciences, Bahawalpur, Pakistan) for his statistical analysis. We acknowledge the funds provided by the Punjab Agriculture Research Board (PARB) for this research under the research grant no. 689 entitled "Saline and Brackish water Aquaculture: Survival, Rearing, and Growth Performance of different age groups of fresh water Fish species in Saline and Brackish Water of Cholistan."

References

[1] FAO, *World food and agriculture—statistical yearbook 2020*, Food and Agriculture Organization of the United Nations, Rome, 2020.

[2] B. O'Neill, F. De Raedemaecker, D. McGrath, and D. Brophy, "An experimental investigation of salinity effects on growth, development and condition in the European flounder (Platichthys flesus. L.)," *Journal of Experimental Marine Biology and Ecology*, vol. 410, pp. 39–44, 2011.

[3] J. Pérez-Robles, A. D. Re, I. Giffard-Mena, and F. Díaz, "Interactive effects of salinity on oxygen consumption, ammonium excretion, osmoregulation and Na+/K+-ATPase expression in the bullseye puffer (Sphoeroides annulatus, Jenyns 1842)," *Aquaculture Research*, vol. 43, no. 9, pp. 1372–1383, 2012.

[4] F. Fazio, S. Marafioti, F. Arfuso, G. Piccione, and C. Faggio, "Influence of different salinity on haematological and biochemical parameters of the widely cultured mullet, Mugil cephalus," *Marine and Freshwater Behaviour and Physiology*, vol. 46, no. 4, pp. 211–218, 2013.

[5] S. K. Das, C. Sarkhel, A. Mandal, and R. Dinda, "Piscicides in tropical freshwater aquaculture–an overview," *Indian Journal of Animal Health*, vol. 56, no. 1, pp. 11–30, 2107.

[6] Y. Fang, V. K. Chan, C. W. Hines, K. T. Stiller, J. G. Richards, and C. J. Brauner, "The effects of salinity and photoperiod on aerobic scope, hypoxia tolerance and swimming performance of coho salmon (Oncorhynchus kisutch) reared in recirculating aquaculture systems," *Comparative Biochemistry and Physiology Part A: Molecular and Integrative Physiology*, vol. 231, pp. 82–90, 2019.

[7] H. A. Al-Hilali and M. S. Al-Khshali, "Effect of water salinity on some blood parameters of common carp (Cyprinus carpio)," *International Journal of Applied Agricultural Sciences*, vol. 2, no. 1, pp. 17–20, 2016.

[8] D. E. Sachit and J. N. Veenstra, "Analysis of reverse osmosis membrane performance during desalination of simulated brackish surface waters," *Journal of Membrane Science*, vol. 453, pp. 136–154, 2014.

[9] E. Jones, M. Qadir, M. T. van Vliet, V. Smakhtin, and S. M. Kang, "The state of desalination and brine production: a global outlook," *Science of the Total Environment*, vol. 657, pp. 1343–1356, 2019.

[10] G. Cucci, G. Lacolla, M. A. Mastro, and G. Caranfa, "Leaching effect of rainfall on soil under four-year saline water irrigation," *Soil and Water Research*, vol. 11, no. 3, pp. 181–189, 2016.

[11] J. Morillo, J. Usero, D. Rosado, H. el Bakouri, A. Riaza, and F. J. Bernaola, "Comparative study of brine management technologies for desalination plants," *Desalination*, vol. 336, pp. 32–49, 2014.

[12] S. Singh, I. Jahan, A. Sharma, and V. K. Misra, "Research paper inland saline aquaculture–a hope for farmers," *International Journal of Global Science Research*, vol. 4, no. 2, pp. 577–593, 2017.

[13] S. Küçük, "The effects of salinity on growth of goldfish, Carassius auratus and crucian carp, Carassius carassius," *African Journal of Biotechnology*, vol. 12, no. 16, pp. 2082–2087, 2013.

[14] M. Islam, D. A. Ahsan, S. C. Mandal, and A. Hossain, "Effects of salinity changes on growth performance and survival of rohu fingerlings, Labeo rohita (Hamilton, 1822)," *Journal of Coastal Development*, vol. 17, no. 1, p. 379, 2014.

[15] M. S. Akhtar, A. K. Pal, N. P. Sahu, A. Ciji, D. K. Meena, and P. das, "Physiological responses of dietary tryptophan fed Labeo rohita to temperature and salinity stress," *Journal of Animal Physiology and Animal Nutrition*, vol. 97, no. 6, pp. 1075–1083, 2013.

[16] M. S. Mubarik, A. Ismail, S. M. Hussain et al., "Survival, growth and body composition of Cyprinus carpio under different levels of temperature and salinity," *International Journal of Biosciences*, vol. 6, no. 10, pp. 132–141, 2015.

[17] A. Ghaffar, R. Hussain, N. Ahmad et al., "Evaluation of hemato-biochemical, antioxidant enzymes as biochemical biomarkers and genotoxic potential of glyphosate in freshwater fish (Labeo rohita)," *Chemistry and Ecology*, vol. 37, no. 7, pp. 646–667, 2021.

[18] M. M. Khatun, G. M. Mostakim, M. Moniruzzaman, U. O. Rahman, and M. S. Islam, "Distortion of micronuclei and other peripheral erythrocytes caused by fenitrothion and their recovery assemblage in zebrafish," *Toxicology Reports*, vol. 8, pp. 415–421, 2021.

[19] C. Kavitha, A. Malarvizhi, S. S. Kumaran, and M. Ramesh, "Toxicological effects of arsenate exposure on hematological, biochemical and liver transaminases activity in an Indian major carp, Catla catla," *Food and Chemical Toxicology*, vol. 48, no. 10, pp. 2848–2854, 2010.

[20] R. Hussain, I. Khan, A. Jamal, B. B. Mohamed, and A. Khan, "Evaluation of hematological, oxidative stress, and antioxidant profile in cattle infected with brucellosis in Southern Punjab, Pakistan," *BioMed Research International*, vol. 2022, Article ID 7140909, 10 pages, 2022.

[21] Y. Mahmood, R. Hussain, A. Ghaffar et al., "Acetochlor affects bighead carp (Aristichthys nobilis) by producing oxidative stress, lowering tissue proteins, and inducing genotoxicity," *BioMed Research International*, vol. 2022, Article ID 9140060, 12 pages, 2022.

[22] X. Li, S. Naseem, R. Hussain, A. Ghaffar, K. Li, and A. Khan, "Evaluation of DNA Damage, Biomarkers of Oxidative Stress, and Status of Antioxidant Enzymes in Freshwater Fish (Labeo rohita) Exposed to Pyriproxyfen," *Oxidative Medicine and Cellular Longevity*, vol. 2022, Article ID 5859266, 13 pages, 2022.

[23] Z. A. Bhutta, M. F. E. A. Kulyar, I. S. Jahanzaib, S. Shabbir, P. Boruah, and A. Bello, "Evaluation of hematological, antioxidant enzymes and oxidative stress parameters in buffaloes infected with babesiosis," *Continental Veterinary Journal*, vol. 2, pp. 29–34, 2022.

[24] M. Al-Emran, N. A. Hasan, M. P. Khan et al., "Alterations in hematological parameters and the structure of peripheral erythrocytes in Nile tilapia (Oreochromis niloticus) exposed to profenofos," *Environmental Science and Pollution Research*, vol. 29, no. 19, pp. 29049–29061, 2022.

[25] J. H. Kim, H. J. Park, I. K. Hwang et al., "Toxic effects of juvenile sablefish, Anoplopoma fimbria by ammonia exposure at different water temperature," *Environmental Toxicology and Pharmacology*, vol. 54, pp. 169–176, 2017.

[26] F. Yin, S. Peng, P. Sun, and Z. Shi, "Effects of low salinity on antioxidant enzymes activities in kidney and muscle of juvenile silver pomfret Pampus argenteus," *Acta Ecologica Sinica*, vol. 31, no. 1, pp. 55–60, 2011.

[27] J. H. Kim, H. J. Park, K. W. Kim et al., "Growth performance, oxidative stress, and non-specific immune responses in juvenile sablefish, Anoplopoma fimbria, by changes of water temperature and salinity," *Fish Physiology and Biochemistry*, vol. 43, no. 5, pp. 1421–1431, 2017.

[28] C. Y. Choi, K. W. An, and M. I. An, "Molecular characterization and mRNA expression of glutathione peroxidase and glutathione S-transferase during osmotic stress in olive flounder (Paralichthys olivaceus)," *Comparative Biochemistry and Physiology Part A: Molecular and Integrative Physiology*, vol. 149, no. 3, pp. 330–337, 2008.

[29] B. Paital and G. B. N. Chainy, "Antioxidant defenses and oxidative stress parameters in tissues of mud crab (Scylla serrata) with reference to changing salinity," *Comparative Biochemistry and Physiology Part C: Toxicology and Pharmacology*, vol. 151, no. 1, pp. 142–151, 2010.

[30] A. Ghaffar, R. Hussain, G. Abbas et al., "Assessment of genotoxic and pathologic potentials of fipronil insecticide in Labeo rohita (Hamilton, 1822)," *Toxin Reviews*, vol. 40, no. 4, pp. 1289–1300, 2019.

[31] R. Hussain, F. Mahmood, M. Z. Khan, A. Khan, and F. Muhammad, "Pathological and genotoxic effects of atrazine in male Japanese quail (Coturnix japonica)," *Ecotoxicology*, vol. 20, no. 1, pp. 1–8, 2011.

[32] Y. Mahmood, A. Ghaffar, and R. Hussain, "New insights into hemato-biochemical and histopathological effects of acetochlor in bighead carp (Aristichthys nobilis)," *Pakistan Veterinary Journal*, vol. 41, no. 4, pp. 538–544, 2021.

[33] N. P. Singh, M. T. McCoy, R. R. Tice, and E. L. Schneider, "A simple technique for quantitation of low levels of DNA damage in individual cells," *Experimental Cell Research*, vol. 175, no. 1, pp. 184–191, 1988.

[34] R. Akram, R. Iqbal, R. Hussain, F. Jabeen, and M. Ali, "Evaluation of oxidative stress, antioxidant enzymes and genotoxic potential of bisphenol A in fresh water bighead carp (Aristichthys nobils) fish at low concentrations," *Environmental Pollution*, vol. 268, p. 115896, 2021.

[35] I. Hayashi, Y. Morishita, K. Imai, M. Nakamura, K. Nakachi, and T. Hayashi, "High-throughput spectrophotometric assay of reactive oxygen species in serum," *Mutation Research/Genetic Toxicology and Environmental Mutagenesis*, vol. 631, no. 1, pp. 55–61, 2007.

[36] M. Iqbal, S. Sharma, H. Rezazadeh, N. Hasan, M. Abdulla, and M. Athar, "Glutathione metabolizing enzymes and oxidative stress in ferric nitrilotriacetate mediated hepatic injury," *Redox Report*, vol. 2, no. 6, pp. 385–391, 1996.

[37] D. J. Jollow, J. R. Mitchell, N. Zampaglione, and J. R. Gillette, "Bromobenzene-induced liver necrosis. Protective role of glutathione and evidence for 3,4-bromobenzene oxide as the hepatotoxic metabolite," *Pharmacology*, vol. 11, no. 3, pp. 151–169, 1974.

[38] B. Chance and A. Maehly, "136 Assay of catalases and peroxidases," *Methods in Enzymology*, vol. 2, pp. 764–775, 1955.

[39] P. Kakkar, B. Das, and P. Viswanathan, "A modified spectrophotometric assay of superoxide dismutase," *Indian Journal of Biochemistry and Biophysics (IJBB)*, vol. 21, no. 2, pp. 130–132, 1984.

[40] E. R. Herbert, P. Boon, A. J. Burgin et al., "A global perspective on wetland salinization: ecological consequences of a growing threat to freshwater wetlands," *Ecosphere*, vol. 6, no. 10, pp. 1–43, 2015.

[41] A. L. Herczeg, S. Dogramaci, and F. W. J. Leaney, "Origin of dissolved salts in a large, semi-arid groundwater system: Murray Basin, Australia," *Marine and Freshwater Research*, vol. 52, no. 1, pp. 41–52, 2001.

[42] C. G. Palmer, W. J. Muller, A. K. Gordon et al., "The development of a toxicity database using freshwater macroinvertebrates, and its application to the protection of south African water resources," *South African Journal of Science*, vol. 100, no. 11, pp. 643–650, 2004.

[43] M. Cañedo-Argüelles and M. Rieradevall, "Disturbance caused by freshwater releases of different magnitude on the aquatic macroinvertebrate communities of two coastal lagoons," *Estuarine, Coastal and Shelf Science*, vol. 88, no. 2, pp. 190–198, 2010.

[44] F. Hossain, S. M. Islam, M. S. Islam, and M. Shahjahan, "Behavioral and histo-pathological indices of striped catfish (Pangasionodon hypophthalmus) exposed to different salinities," *Aquaculture Reports*, vol. 23, p. 101038, 2022.

[45] R. T. Selvi and M. Ilavazhahan, "Histopathological changes in gill tissue of the fish Catla catla exposed to sublethal concentration of pesticide methyl parathion and a heavy metal ferous sulphate," *Biomedical and Pharmacology Journal*, vol. 5, no. 2, pp. 305–312, 2012.

[46] F. Khalil, I. J. Kang, S. Undap et al., "Alterations in social behavior of Japanese medaka (Oryzias latipes) in response to sublethal chlorpyrifos exposure," *Chemosphere*, vol. 92, no. 1, pp. 125–130, 2013.

[47] H. Xing, T. Liu, Z. Zhang, X. Wang, and S. Xu, "Acute and subchronic toxic effects of atrazine and chlorpyrifos on common carp (Cyprinus carpio L.): immunotoxicity assessments," *Fish and Shellfish Immunology*, vol. 45, no. 2, pp. 327–333, 2015.

[48] A. Stalin, P. Suganthi, S. Mathivani et al., "Impact of chlorpyrifos on behavior and histopathological indices in different tissues of freshwater fish Channa punctatus (Bloch)," *Environmental Science and Pollution Research*, vol. 26, no. 17, pp. 17623–17631, 2019.

[49] A. S. Harabawy and Y. Y. Mosleh, "The role of vitamins A, C, E and selenium as antioxidants against genotoxicity and

cytotoxicity of cadmium, copper, lead and zinc on erythrocytes of Nile tilapia, Oreochromis niloticus," *Ecotoxicology and Environmental Safety*, vol. 104, pp. 28–35, 2014.

[50] M. Faheem, Z. Zahid, and N. G. C. Ferreira, "Toxicity assessment of dibutyl phthalate in grass carp: an integrated biomarker approach," *Pakistan Veterinary Journal*, vol. 41, no. 3, pp. 365–371, 2021.

[51] A. Ghaffar, R. Hussain, G. Abbas et al., "Fipronil (phenylpyrazole) induces hemato-biochemical, histological and genetic damage at low doses in common carp, Cyprinus carpio (Linnaeus, 1758)," *Ecotoxicology*, vol. 27, no. 9, pp. 1261–1271, 2018.

[52] R. Hussain, A. Khan, F. Mahmood, S. Rehan, and F. Ali, "Clinico-hematological and tissue changes induced by butachlor in male Japanese quail (Coturnix japonica)," *Pesticide Biochemistry and Physiology*, vol. 109, pp. 58–63, 2014.

[53] S. Sodhi, A. Sharma, A. P. S. Brar, and R. S. Brar, "Effect of α tocopherol and selenium on antioxidant status, lipid peroxidation and hepatopathy induced by malathion in chicks," *Pesticide Biochemistry and Physiology*, vol. 90, no. 2, pp. 82–86, 2008.

[54] F. D. Campos-Pereira, C. A. Oliveira, A. A. Pigoso et al., "Early cytotoxic and genotoxic effects of atrazine on Wistar rat liver: a morphological, immunohistochemical, biochemical, and molecular study," *Ecotoxicology and Environmental Safety*, vol. 78, pp. 170–177, 2012.

[55] S. Lim, S. Y. Ahn, I. C. Song et al., "Chronic exposure to the herbicide, atrazine, causes mitochondrial dysfunction and insulin resistance," *PLoS One*, vol. 4, no. 4, p. e5186, 2009.

[56] R. Hussain, F. Mahmood, A. Khan, M. T. Javed, S. Rehan, and T. Mehdi, "Cellular and biochemical effects induced by atrazine on blood of male Japanese quail (Coturnix japonica)," *Pesticide Biochemistry and Physiology*, vol. 103, no. 1, pp. 38–42, 2012.

[57] A. Ghaffar, R. Hussain, A. Khan, and R. Z. Abbas, "Hemato-biochemical and genetic damage caused by triazophos in fresh water fish, Labeo rohita," *International Journal of Agriculture and Biology*, vol. 17, no. 3, pp. 637–642, 2015.

[58] A. Ghaffar, R. Hussain, M. Aslam, G. Abbas, and A. Khan, "Arsenic and urea in combination alters the hematology, biochemistry and protoplasm in exposed rahu fish (Labeo rohita) (Hamilton, 1822)," *Turkish Journal of Fisheries and Aquatic Science*, vol. 16, no. 2, pp. 289–296, 2016.

[59] A. Ghaffar, R. Hussain, S. Noreen et al., "Dose and time-related pathological and genotoxic studies on thiamethoxam in fresh water fish (Labeo rohita) in Pakistan," *Pakistan Veterinary Journal*, vol. 40, no. 2, pp. 151–156, 2020.

[60] M. L. Namratha, M. Lakshman, M. Jeevanalatha, and B. A. Kumar, "Hematological alterations induced by glyphosate and ameliorative effect of ascorbic acid in Wistar rats," *Continental Veterinary Journal*, vol. 1, no. 1, pp. 32–36, 2020.

[61] I. Cervantes-Camacho, S. M. Guerrero-Estévez, M. F. López, E. Alarcón-Hernández, and E. López-López, "Effects of bisphenol a on Foxl2 gene expression and DNA damage in adult viviparous fish Goodea atripinnis," *Journal of Toxicology and Environmental Health, Part A*, vol. 83, no. 3, pp. 95–112, 2020.

[62] S. Aziz, S. Abdullah, H. Anwar, F. Latif, and W. Mustfa, "Effect of engineered nickel oxide nanoparticles on antioxidant enzymes in freshwater fish, Labeo rohita," *Pakistan Veterinary Journal*, vol. 41, no. 3, pp. 424–428, 2021.

[63] R. Meli, A. Monnolo, C. Annunziata, C. Pirozzi, and M. C. Ferrante, "Oxidative stress and BPA toxicity: an antioxidant approach for male and female reproductive dysfunction," *Antioxidants*, vol. 9, no. 5, p. 405, 2020.

[64] J. W. Lee, H. Choi, U. K. Hwang et al., "Toxic effects of lead exposure on bioaccumulation, oxidative stress, neurotoxicity, and immune responses in fish: a review," *Environmental Toxicology and Pharmacology*, vol. 68, pp. 101–108, 2019.

[65] A. Naseer, A. Hussain, B. Aslam et al., "Vitamin E and selenium attenuate hepatotoxicity, nephro-toxicity and oxidative stress induced by rifampicin in rabbits," *Pakistan Veterinary Journal*, vol. 40, no. 3, pp. 277–282, 2020.

[66] M. Ghazanfar, S. Shahid, and Z. I. Qureshi, "Vitamin C attenuates biochemical and genotoxic damage in common carp (Cyprinus carpio) upon joint exposure to combined toxic doses of fipronil and buprofezin insecticides," *Aquatic Toxicology*, vol. 196, pp. 43–52, 2018.

[67] S. Naz, R. Hussain, Q. Ullah, A. M. M. Chatha, A. Shaheen, and R. U. Khan, "Toxic effect of some heavy metals on hematology and histopathology of major carp (Catla catla)," *Environmental Science and Pollution Research*, vol. 28, no. 6, pp. 6533–6539, 2021.

[68] R. A. Phatak and S. Sinha, "Histopathological and oxidative impairment in liver and gills of Catla catla exposed to artificial seawater," *Journal of Fisheries and Life Sciences*, vol. 6, no. 1, pp. 1–6, 2021.

[69] D. Madeira, L. Narciso, H. N. Cabral, C. Vinagre, and M. S. Diniz, "Influence of temperature in thermal and oxidative stress responses in estuarine fish," *Comparative Biochemistry and Physiology Part A: Molecular and Integrative Physiology*, vol. 166, no. 2, pp. 237–243, 2013.

[70] G. Jabeen, F. Manzoor, and M. Arshad, "Effect of cadmium exposure on hematological, nuclear and morphological alterations in erythrocyte of fresh water fish (Labeo rohita)," *Continental Veterinary Journal*, vol. 1, no. 1, pp. 20–24, 2021.

[71] M. S. Al-Harbi, F. A. El-Rahman, and N. S. El-Shenawy, "The beneficial effects of ascorbic acid during chlorpyrifos-induced oxidative stress and histopathological changes in Oreochromis spilurus," *Toxicology and Environmental Health Sciences.*, vol. 6, no. 3, pp. 203–216, 2014.

[72] S. Braz-Mota, H. Sadauskas-Henrique, R. M. Duarte, A. L. Val, and V. M. Almeida-Val, "Roundup® exposure promotes gills and liver impairments, DNA damage and inhibition of brain cholinergic activity in the Amazon teleost fish Colossoma macropomum," *Chemosphere*, vol. 135, pp. 53–60, 2015.

[73] M. Latif and M. Faheem, "Study of oxidative stress and histo-biochemical biomarkers of diethyl phthalate induced toxicity in a cultureable fish, Labeo rohita," *Pakistan Veterinary Journal*, vol. 40, no. 2, pp. 202–208, 2020.

[74] J. Qiang, F. Tao, W. Bao et al., "miR-489-3p regulates the oxidative stress response in the liver and gill tissues of hybrid yellow catfish (Pelteobagrus fulvidraco♀ × P. vachelli♂) under Cu2+ exposure by targeting Cu/Zn-SOD," *Frontiers in Physiology*, vol. 10, p. 868, 2019.

[75] Y. Jin, T. Zhou, N. Li et al., "JAK and STAT members in channel catfish: identification, phylogenetic analysis and expression profiling after Edwardsiella ictaluri infection," *Developmental and Comparative Immunology*, vol. 81, pp. 334–341, 2018.

[76] J. Q. Wang, R. Hussain, A. Ghaffar et al., "Clinico-hematological, mutagenic, and oxidative stress induced by pendimethalin in freshwater fish bighead carp (Hypophthalmichthys

nobilis)," *Oxidative Medicine and Cellular Longevity*, vol. 2022, Article ID 2093822, 15 pages, 2022.

[77] G. Afzal, H. I. Ahmad, R. Hussain et al., "Bisphenol A induces histopathological, hematobiochemical alterations, oxidative stress, and genotoxicity in common carp (Cyprinus carpio L.)," *Oxidative Medicine and Cellular Longevity*, vol. 2022, Article ID 5450421, 14 pages, 2022.

[78] M. Shukry, M. F. Abd El-Kader, B. M. Hendam et al., "Dietary Aspergillus oryzae modulates serum biochemical indices, immune responses, oxidative stress, and transcription of HSP70 and cytokine genes in Nile tilapia exposed to salinity stress," *Animals*, vol. 11, no. 6, p. 1621, 2021.

[79] M. A. Dawood, A. E. Noreldin, and H. Sewilam, "Blood biochemical variables, antioxidative status, and histological features of intestinal, gill, and liver tissues of African catfish (Clarias gariepinus) exposed to high salinity and high-temperature stress," *Environmental Science and Pollution Research*, vol. 29, no. 37, pp. 56357–56369, 2022.

[80] D. Tiwari, J. Kamble, S. Chilgunde et al., "Clastogenic and mutagenic effects of bisphenol A: an endocrine disruptor," *Mutation Research/Genetic Toxicology and Environmental Mutagenesis*, vol. 743, no. 1-2, pp. 83–90, 2012.

[81] D. Ali, F. A. Falodah, B. Almutairi, S. Alkahtani, and S. Alarifi, "Assessment of DNA damage and oxidative stress in juvenile Channa punctatus (Bloch) after exposure to multi-walled carbon nanotubes," *Environmetal Toxicology*, vol. 35, no. 3, pp. 359–367, 2020.

Hindawi
Oxidative Medicine and Cellular Longevity
Volume 2022, Article ID 9354555, 23 pages
https://doi.org/10.1155/2022/9354555

Review Article

Current Insights on Bioactive Molecules, Antioxidant, Anti-Inflammatory, and Other Pharmacological Activities of Cinnamomum camphora Linn

Mohamed Joonus Aynul Fazmiya,[1] Arshiya Sultana,[1] Khaleequr Rahman,[2] Md Belal Bin Heyat,[3] Sumbul,[1] Faijan Akhtar,[4] Salabat Khan,[3] and Seth Christopher Yaw Appiah[5]

[1]*Department of Amraze Niswan wa Ilmul Qabalat, National Institute of Unani Medicine, Ministry of Ayush, Bengaluru, Karnataka, India*
[2]*Department of Ilmul Saidla, National Institute of Unani Medicine, Ministry of Ayush, Bengaluru, Karnataka, India*
[3]*IoT Research Center, College of Computer Science and Software Engineering, Shenzhen University, Shenzhen, Guangdong 518060, China*
[4]*School of Computer Science and Engineering, University of Electronic Science and Engineering, Chengdu, China*
[5]*Health and Social Care Research Group, Department of Sociology and Social Work, Kwame Nkrumah University of Science and Technology, Kumasi, Ghana*

Correspondence should be addressed to Mohamed Joonus Aynul Fazmiya; mjafazmiya@gmail.com, Arshiya Sultana; drarshiya@yahoo.com, Md Belal Bin Heyat; belalheyat@gmail.com, Faijan Akhtar; faijanakhtar98@gmail.com, and Seth Christopher Yaw Appiah; scyappiah@knust.edu.gh

Received 7 July 2022; Revised 26 August 2022; Accepted 22 September 2022; Published 7 October 2022

Academic Editor: Tarique Hussain

C. camphora is a renowned traditional Unani medicinal herb and belongs to the family Lauraceae. It has therapeutic applications in various ailments and prophylactic properties to prevent flu-like epidemic symptoms and COVID-19. This comprehensive appraisal is to familiarize the reader with the traditional, broad applications of camphor both in Unani and modern medicine and its effects on bioactive molecules. Electronic databases such as Web of Science, PubMed, Google Scholar, Scopus, and Research Gate were searched for bioactive molecules, and preclinical/clinical research and including 59 research and review papers up to 2022 were retrieved. Additionally, 21 classical Unani and English herbal pharmacopeia books with ethnomedicinal properties and therapeutic applications were explored. Oxidative stress significantly impacts aging, obesity, diabetes mellitus, depression, and neurodegenerative diseases. The polyphenolic bioactive compounds such as linalool, borneol, and nerolidol of *C. camphora* have antioxidant activity and have the potential to remove free radicals. Its other major bioactive molecules are camphor, cineole, limelol, safrole, limonene, alpha-pinene, and cineole with anti-inflammatory, antibacterial, anxiolytic, analgesic, immunomodulatory, antihyperlipidemic, and many other pharmacological properties have been established in vitro or in vivo preclinical research. Natural bioactive molecules and their mechanisms of action and applications in diseases have been highlighted, with future prospects, gaps, and priorities that need to be addressed.

1. Introduction

The WHO stated that around 80% global population uses different types of traditional medicine to treat many diseases [1]. Traditional medicine is the knowledge, skills, and procedures that indigenous peoples and other cultures have used for a long time in order to preserve health and avoid illness [2, 3]. One of the oldest forms of medicine is Unani medicine, which originated in Greek [4] and is based on seven essential factors responsible for the maintenance of health

and imbalance any one of them can lead to disease or even to death. The great physicians, Avicenna and Galan, stated that the primary elements contribute to the formation of things in nature [5]. The intermixture of primary elements forms temperament. The temperament indicates the state of equilibrium to the number of elements and the ratio of the particular compound and different combination responses to its specific nature. Hence, any changes in the quality or quantity of humor alter the equilibrium and disturb the normal temperament. Proper physiological functions are maintained by the homeostasis of temperament. Simple temperamental imbalances cause intrinsic power (immunity) to fight back and maintain body normal levels. If the body's temperament, functions are impaired owing to a change in humor, diet therapy, pharmacotherapy, regimental therapy, or surgery may be required, depending on the situation [5, 6]. Temperament (*Mizaj*) and humor, which is the principal concept in this system and disturbances in the quality and quantity of humor, cause numerous conditions. The four main modes of therapy available in Unani medicine [7] are regimental diet therapy, pharmacotherapy, and surgery. Correction through pharmacotherapy and regimental therapy helps to maintain homeostasis of the humor [4]. First-degree drugs are safer, temperamental quality is less, and second-degree drugs are also safe and have strong temperamental quality but no toxic effect. Third-degree temperamental medicine drugs are strong, the toxic effect may manifest prominently, and fourth-degree drugs are excessively strong and toxic. The drug is moderate (*Mutadil*) in temperament; it has no toxic, no temperamental quality, and the activity is only limited medicinal effect. Commonly, cold temperamental drugs are suitable for hot temperamental individuals and may produce effects on cold temperamental individuals in inappropriate doses. *Cinnamomum camphora* (L.) is a traditional Unani medicinal plant with a third-degree cold and dry temperament and hence useful in hot temperamental individuals [8].

C. camphora (L.) is a renowned Unani medicinal herb applied for several disease conditions in Unani as well as other traditional medicines. Camphor is a terpene ketone derived from *C camphora* wood or synthetically produced from turpentine. White, yellow, brown, and blue camphor oil are the four different fractions of camphor oil [9–11]. Camphor is obtained by distillation with water from the wood of trees or plants and purified by sublimation, and it occurs in translucent white crystals [12–14]. Since the ancient era in the Unani traditional system of medicine, *C. camphora* has been using its ethnomedicinal properties like antiseptic, analgesic, and rubefacient properties. Camphor has been use for very long time in various traditional systems of medicine such as Ayurveda, Unani, Siddha, and Chinese. It has been used in Unani medicine mainly in respiratory disorders *(Amrāz-i-Riyah)*, gastrointestinal (*Amrāz-i-Me'da wa Am'a*), integument disease *(Amrāz-i-Jild*), *eye diseases (Amrāz-i-Ayn)*, and nervine and cerebral disorders *(Amrāz-i- damaghi wa a'sabi*) especially in hot conditions for headache, strengthening senses and brain [15], bilious diarrhea [8], inflammation of the liver [15], and useful in bladder and kidney inflammation [16]. Furthermore, externally, it is used for various ailments such as eye diseases, ear pain, joint, muscular pain, chest congestion, and headache applications such as ear drops or gargling with or without other suitable drugs [12, 15, 16]. An overdose may result in systemic toxicity. Signs of intoxication include gastrointestinal pain, emesis, agitation, tremors, and convulsions, which are followed by CNS depression marked by apnea and coma [17]. Furthermore, it is an important ingredient of *Arq Ajeeb* used as a prophylactic medicine for COVID-19 as per AYUSH guidelines. This comprehensive appraisal is to familiarize the reader towards the extensive, well recognized, and broad applications of camphor both in Unani and contemporary applications.

To collect information on *C. camphora* for its temperament (*Mizaj*), adverse effects (*Mudir*), corrective (*Muslih*), substitute (*Badal*), ethnomedicinal properties (*Afa'l*), Unani compound formulations, and ethnomedicinal therapeutic uses, a literature survey of traditional Unani texts was conducted. Additionally, full-text paper and thorough search of electronic databases such as PubMed, Scopus, Google Scholar, and Research Gate were conducted to gather all accessible information on phytochemical, physicochemical, and pharmacological investigations relevant to *C. camphora*. All relevant articles are written in English up to 2022. The search occurred between August 2020 and May 2021. The keywords used were as follows: "*C. camphora*," "chemical component," "Unani Medicine," "*Kafoor*," "preclinical studies," "clinical trial," "phytochemical," "adverse effect," "toxicity," and "traditional." Chemical structure images were taken by PubChem. Standard Unani Medical Terminology of WHO was reviewed to define the suitable Unani terminologies. The scientific name and synonyms were authenticated and reproduced using The Plant List (http://www.theplantlist.org). A total of 464 papers and 21 books were retrieved, 386 were excluded, and we included research and review papers from the electronic database (Figure 1). Twenty-one included Unani classical manuscripts, and herbal pharmacopeial texts were consulted, including the incorporation of Urdu translation of the traditional textbooks such as *Makhzan al-Mufridat*, *Al Jami ul Mufradat Al Advia Wal Aghzia* (1197-1248 AD), *Muhit-i-A'zam* (1806–1902 AD), *Khazainul Adwiya*, (19th century), and *Bustan ul-Mufridat*, *Kitab ul Mansuri* (850-925 AD).

We collected data from traditional, classical Unani and herbal pharmacopoeia literature and up-to-date reviews and research to address a traditional and contemporary overview of the application of *C. camphora* in various ailments. We conducted this review to report most of the information on *C. camphora* therapeutic and traditional uses for several diseases. In addition, we also included a comparison between therapeutic traditional uses and its current research to prove its ethnomedicinal properties. Furthermore, the mechanism of natural bioactive molecules isolated from *C. camphora* was also highlighted. Preclinical and clinical trials were also reviewed to prove the effect of *C. camphora* in various diseases. Because no previous publications have incorporated this type of information in the review article, this review aims to overview and analyze the taxonomy, distribution, macroscopic description of the plant, various

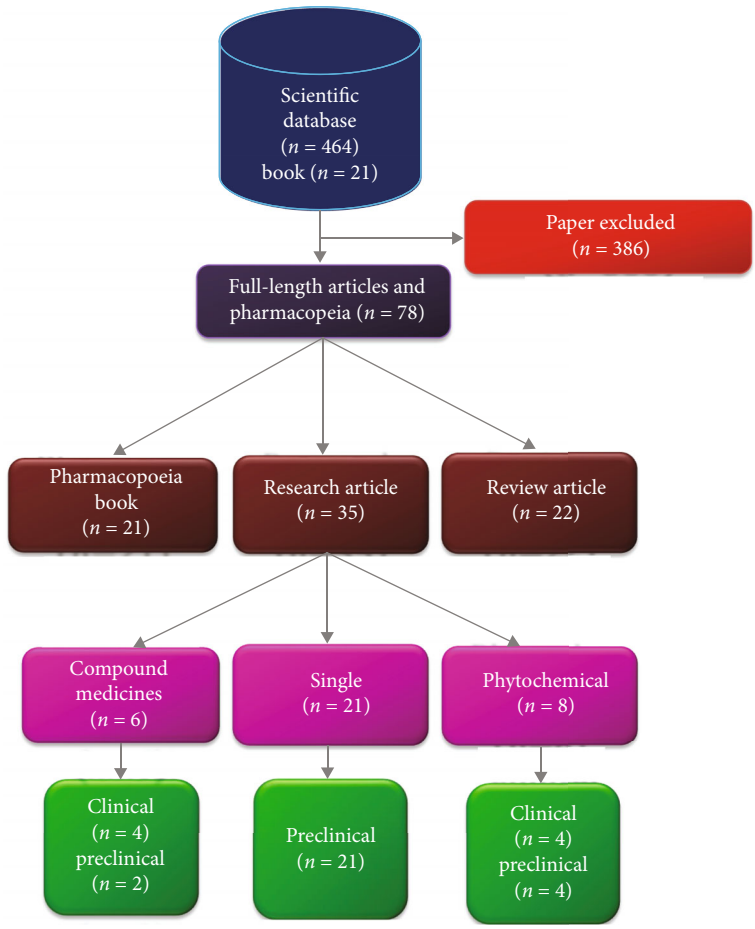

Figure 1: Flow diagram of type and inclusion and exclusion of the study.

ethnomedicinal properties, therapeutic Unani applications, natural bioactive molecules isolated from different parts of the plant, present mechanism of action of natural bioactive molecules, comparison of therapeutic Unani applications proven currently by preclinical and clinical studies, gap, and future recommendation.

Hence, the following are the primary contributions of this study:

(i) Traditional Unani overview of *C. camphora* plants such as temperament, ethnomedicinal properties, therapeutic applications in various disease conditions, adverse effects, corrective, substitute, and Unani compound formulations containing *C. camphora* with dose and therapeutic applications

(ii) Various natural bioactive molecules separated from various parts of the *C. camphora* plant with their structures and their mechanisms of action depiction such as analgesic, anti-inflammatory, antioxidant, and anti-allergic

(iii) We also highlighted current research carried out in vitro, in vivo, and silico pharmacological studies such as antioxidant, anti-inflammatory, anti-allergic, antibacterial, antifungal activity, anxiolytic and antidepressant, analgesic, anti-hyperlipidemic, antifertility, hepatoprotective, antifertility, wound healing, prostaglandin synthesis inhibition, and oestrogenic activities

(iv) We included preclinical and clinical studies of the main active biomolecules to report the significant use of C. *camphora* in day-to-day life. It also has a prophylactic effect against the SAR-CoV virus as per the study, and it is one of the main ingredients of *Arq Ajeeb* compound formulation used as a prophylactic inhaler to prevent COVID-19 infection

(v) This review also contributes toward comparative therapeutic evaluation, research gaps, future recommendations, and conclusions

2. Vernacular Name, Taxonomy, Distribution, and Types of *C. camphora*

The vernacular name summarized in Table 1. Camphor tree is a shrub or an evergreen tree [18] belonging to the family Lauraceae, Laurales order, genus Cinnamomum, and species *camphora* [14, 19]. Over 250-300 species of the genus are

Table 1: Vernacular name of *C. camphora*.

Language	Vernacular name	Ref.
Unani medicine	*Kafoor*	[14, 16, 23]
Persian	*Kafur, Kafoor*	[14, 16, 23]
English	Camphor, Bheemseni camphor (natural), Bomeo camphor	[14, 16, 23]
Arabic	*Kafoor*	[14, 16, 23]
Germany	Kampher	[14, 16, 23]
French	Camphre	[14, 16, 23]
Hindi	*Duk, Ben, Guj, Kafoof*	[14, 16, 23]
Sanskrit	*Karpoor, Ghausar, Himavaluka*	[14, 16, 23]
Tamil	Pachai Karpooram, Karpooran-Cheena, Karuppuram	[14, 16, 23]
Gujarati	Kapoor, Karpoor	[14, 16, 23]
Telugu	*Pacha Karpooram, Cheen Karpooram*	[14, 16, 23]
Siddha medicine	Karupporam	[13]
Ayurveda medicine	Karpura, Ghanasaara, Chandra, Chandra Praba, Indu, Tushaara, Gandhadravya	[13]

distributed globally [20]. Twenty-six species are found in India, and approximately 40 species are commonly used for medical conditions. Leaves and stem bark are the sources of medicinal activity. *Cinnamomum zeylanicum*, *C. camphora*, *C. burmannii*, *C. cassia*, *C. tamala*, and *C. verum* species are rice sources of aromatic oil [20, 21]. Camphor (*Kafoor*) is an exudate of a camphor tree as per the description in Unani literature. Moisture or liquid comes out from cracks or incision in the tree and freezes out as rust. It is also expelled through the hole of the tree [12], or the wood of that tree is chopped and soaked and heated in the water causing sublimation [12]. It is clear crystal white with a strong smell [8, 12]. Camphor is found naturally or artificially synthesized. The natural camphor is D-camphor, whereas the synthetic one is L-camphor [22]. Authentic Unani texts described numerous varieties of camphor. The best type is *Kaisuri* followed by *Riyahi*. *Kaisuri* is found in the city of *Qaisr* on the island of *Tarindib*, so the name has been given *Kafuri Kaisur* [8]. There are three different kinds of camphor: Formosa camphor [22], Borneo or Barus camphor, and blumea or Ngai camphor. Borneo camphor is high priced, and it is naturally formed in the stems of Dryobalanops camphor grown in Dutch Sumatra and sinks in water. This is considered the best type. Borneo Camphor is high priced, and it is naturally formed in the stems of *Dryobalanops camphor* grown in Dutch Sumatra and sinks in water, and the third type is Blumea or Ngai camphor.

3. Macroscopic Description

Its opposite, frequently three-nerved, long petiolate, oblong or ovate, 5- to 12.5-cm long, and 2.5 to 5-cm broad leaves are usually three-nerved. Its flowers are tiny and hermaphrodite or produced via polygamy or abortion. Typically, females are larger and have few components. Nine stamens are there, unless they are aborted. The ovary is sessile, free from the perianth, style is narrow, the stigma is discoid, and the style is narrow or obscurely 3-lobed [18]. The fruit is a berry with spreading, somewhat expanded perianth, completely or partially deciduous segments, and less frequently persistent seeds [18].

4. Description in Unani Literature

4.1. Temperament (Mizaj). Temperament is one of the unique features and fundamental principles of the Unani system of medicine [24]. All medicinal substance, plants, animals, and minerals have their temperament. The temperament of drugs is used as a tool to assess the actions and toxicological properties of Unani drugs. The medications were divided into four groups based on their innate nature: hot (*Hārr*), cold (*Bārid*), moist (*Ratb*), and dry (*Yābis*) in terms of their effect on a moderate human body and four degrees 1, 2, 3, or 4 in terms of increasing intensity of action. As a result, different scholars have claimed that its temperament is variable [12]. The temperament of camphor is cold and dry in the third degree [12, 14], cold second, and dry in the third-degree [8].

4.2. Ethnomedicinal Properties (Afa'l). Camphor, administered orally, has several pharmacological properties such as expectorant (Munaffith-i-Balgham) [12]; stimulant (Muharrik) [12]; brain and heart tonic (Muqawwi-i-Qalb wa Dimāgh) [12]; exhilarant of brain and heart (Mufarrih al- Qalb wa Dimāgh) [15]; antipyretic (Dāfi-i-Hummā) [12, 16]; hemostatic (Ḥābis-i-Dam); anti-pyretic for tubercular infection (Ḥummā Diqq) (a form of fever that gradually depletes the body's fluids and weakens its organs, resulting in weight loss) [12, 16]; antispasmodic (Dāfi?-i-Tashannuj) [12]; astringent (Qābiḍ) [12]; disinfectant (Mani'-i-'Ufunat) [15]; anaphrodisiac (Duf-i-Bah- [12]; constipation (Qabz) [12]; and carminative, reflux expectorant, which stimulate the heart and respiratory system and analgesic and sedative to the nervous system [13]. Additionally, the overview of ethnomedicinal properties, therapeutic applications in Unani medicine, and pharmacological activities are mentioned in Figure 2 (https://www.ayurtimes.com/cinnamomum-camphora/3/6/2022 and https://plant.ces.ncsu.edu/plants/cinnamomum-caomphora/).

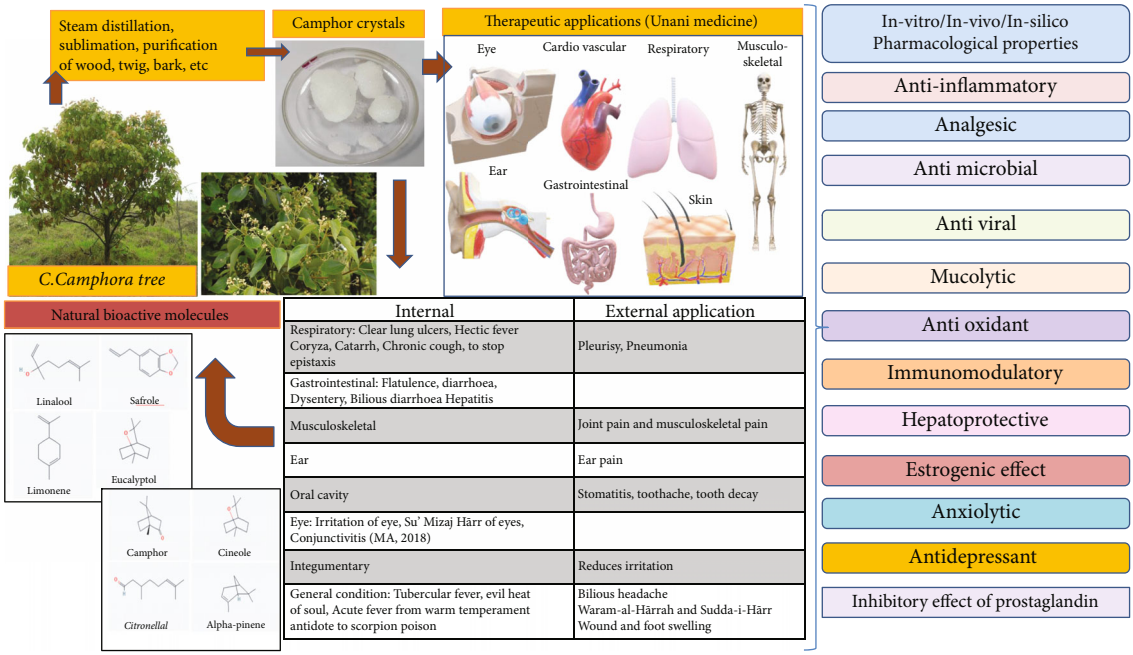

Figure 2: Overview of ethnomedicinal properties, therapeutic applications in Unani medicine, and pharmacological activities.

4.2.1. Topical Application. Topical application of camphor has antiseptic [12] and massages externally and initially; it has stimulant [12] rubefacient (Muhammir) and then anesthetic (Mukhaddir) [12] and analgesic (Musakkin-i-Alam) ethnomedicinal properties [12, 16].

4.3. Therapeutic Application as per Unani System of Medicine. As per Unani system of medicine, Camphor is useful in respiratory, gastrointestinal, musculoskeletal, integumentary, oral cavity, ear condition, eye diseases, and other general conditions (Table 2).

5. Therapeutic Dose, Adverse Effects, and Correctives of *C. camphora* in the Traditional and Contemporary Era

Unani classical texts mention doses range from minimum to 182 [12] up to 250 mg to 550 mg. According to another opinion 7 gm/week [15], the maximum dose is 364 mg to 728 mg. More than 8.75 gm reduces sexual power or may cause death [16]. The minimum dose is 182 to 364 mg and can be given for strengthening the patient [16]. The lethal dose in adult humans is 5 to 20 g. One teaspoon of camphorated oil (~1 mL of camphor) was lethal to 16 and 19-month-old children [25]. Unani scholars stated that overdose or misuse of this drug may adversely affect cold temperamental people (*Barid Mizaj)* [12, 15, 16], stagnation of sperm (*Munjamid Mani*), and weakness in individual's stomach [15, 16] that reduces sexual power and sperm quality and forms kidney stone [12, 15, 16].

Camphor is quickly absorbed by the mucous membranes, skin, and gastrointestinal tract in liquid form. Symptoms may appear 5–90 minutes after consumption. The rate of absorption is heavily reliant on the existence of food and other compounds [26]. In humans, intoxication signs are abdominal distress, emesis, tremors, excitement, seizures, and CNS depression characterized by apnea and *coma* [17, 25]. The traditional Unani medicine discusses various corrective agents (*Muslih*) and forms of simple and compound drugs that can use according to the condition internally or externally to manage or minimize the adverse effects of camphor. As camphor is cold temperament and to combat it coldness, hot and aromatic herbs such as oil of *Viola odorata* L. (*Rogan-i-Banafsha*), *oil of Narcissus tazetta* Linn (*Rogan-i-Nargis*), *Ambar*, and Castoreum (*Jundabedastar*) [15, 16] are used as corrective. Oil of *Iris ensata* Thunb (*Roghan-i-Sosan*), [12, 16] a flower of *Viola odorata* L. (*Gul-i-Banafsha*) [12], and a confection of *Rosa damascene* act as a corrective in a condition such formation of renal stone caused by camphor use [15]. *Narcissus tazetta* L. (*Banafsha*), *Nelumbo nucifera* Gaertn (*Niloufer*), *Crocus sativus*, a confection of *Rosa damescene* (*Gulkand*), *Ambar*, and *Musk* are drugs that act as corrective in headache caused by use of camphor [15].

6. Substitute (*Badal*)

The idea of drug substitution (*Abdāl-i-Adwiya*) is a significant criterion of Unani pharmacotherapy [27]. In Unani Medicine, replacing the main drug with a substitute having the same or closest pharmacological action with the first desired drug and a substitute can be chosen depending on the situation. Need for drug substitutes, Al-Razi surmised that "frequently, all drugs needed for treatment are not easily available everywhere. As a result, if a physician is uninformed of the replacements that must be used in

Table 2: *C. Camphora* effect on system, therapeutic application, dosage form and method of use.

System	Therapeutic application	Dosage form	Method of usage	Ref.
Respiratory	Pleurisy (*Dhāt al-Janb*) and pneumonia (*Dhāt al-Ri'a*) Epistaxis Lung ulcers Specific fevers (*Hummā Diqq*) Coryza, catarrh (*Nazla-o-Zukām),* and old cough	Oil	External application with suitable oil	[8, 12, 15, 16]
Gastrointestinal	Flatulence (*Riyāh-i-Miʿda)* Passing loose stools due to the predominance of yellow bile or blood (*Ishāl-i-Safrāwi* and *Damwi)* It can also be used in dysentery, bilious diarrhea, and inflammation of the liver (*Waram al-Kabid)*	—	—	[8, 12, 15, 16]
Musculoskeletal	Joint pain and accumulation of humor in the distended muscle fibers causes soreness (*Wajaʿal-Khāsira*, and *Wajaʿal-Mafāsil*)	Oil	External application camphor powder mixed with oil	[12]
Integumentary	Skin conditions and reduces irritation	Oil Cream (*Marham*)	External application with suitable oil or cream	[12]
Oral cavity	Tooth pain	Camphor sublimation	Powder or powder with rose oil on affected tooth	[12, 16]
	Stomatitis and toothache (*Qulāʿ*and *Dānton ka Dard*)	Gargle and mouth wash	Camphor along with distillate water of *Rosa bourboniana* (*Arq-i-Gulab*)	[15]
Ear condition	Ear pain	Ear drop	Camphor with fresh coriander juice (*Aāb-i-Kasneez Sabs*)	[12, 15]
Eye diseases	Eye irritation Abnormal hot temperament (*Su' Mizaj Hārr)* of eyes. Conjunctivitis and prevents eye involvement in smallpox	Fine powder (*Surma)* Fine powder (*Surma)*	Fine powder apply on eyelid Fine powder with the juice of coriander	[12, 15]
General condition	Fever due to tuberculosis Exhilarant and cardiac tonic	Powder	-	[8, 12, 15, 16]
	Bilious headache, evil heat of soul, and fever	Paste	Location application of paste prepared by mixing powdered camphor with rose oil and grapes apply on the forehead	
	Antidote to scorpion poison	Powder	Powder with rose oil	
	It works in the hot type of inflammation (*Waram-al-Hārrah)* and obstacles (*Sudda-i-Hārr*)	Oil or ointment	Camphor mixed with suitable oil	
	Epistaxis	Nasal drops	Camphor is used with *Myrtus communis* for epistaxis	
	Wound and foot swelling	Dusting powder, ointment	—	

place of the principal drug, the medical profession's objectivity will be compromised" [28]. The great physician, Avicenna states that a substitute can be used "When the initially intended medicine is unavailable" [4, 29]. In case of non-availability of Camphor, *Barbarea vulgaris* (*Tabashir Sufaida*) [12, 16, 30] or *Pterocarpus santalinus* (*Sandal*) [15, 16] or fossil resin of *Pinus succinifera* (*Kahruba*) [15] can use as a substitute.

7. Ethnomedicinal Properties and Therapeutic Applications of Unani Compound Formulations of Camphor (*Murakkabat*)

Compound medicines are pharmaceuticals that contain two or more herbs as ingredients in a variety of dose formulations and administration routes. Topical preparations include ointment, lotions, and fine powders for ocular use.

Oral preparations include pills, tablets, powder, and semi-solid confection forms. Several Unani compound formulations as per pharmacopoeia preparation possessing different ethnomedicinal properties, therapeutic applications, and dosage forms with doses acting on different body systems have been described in detail in Table 3.

8. Natural Bioactive Molecules of *C. camphora* and their Mechanism of Action

Seventy-four compounds were discovered in leaf, branch, wood, and root chromatograms of *C. camphora* tissues [35]. Phytochemical components of *C. camphora* are phenolics, flavonoids such as tannins (2.09%), saponins, alkaloids (3.85%), and carbohydrates [36]. The bioactive compound of *C. camphora* oil identifies the relevant analgesic effects β-caryophyllene, α-caryophyllene, germacrene D, bicyclogermacrene, unidentified, nerolidol, spathulenol, and unidentified (E)-α-atlantone [36]. Another study identified 96 various compounds in the essential oils by two-dimensional gas chromatography such as methyl isobutyl ketone, pinene (α and β), α-thujene, camphene, sabinene, α-phellandrene, hexanal, 3-hexanal-1-ol, 1-hexaol, and sabinene [37]. The major bioactive molecules of *C. camphora* are camphor, linalool, safrole, and cineole. The major bioactive molecules in different parts of the plant are mentioned in Table 4 and Figure 3.

The pathophysiology of respiratory diseases (sinusitis, asthma, bronchitis, and COPD) is mucociliary dysfunction, inflammation-induced edema, and hypersecretion of goblet cells that probably plays an important role. Cineole natural substance from camphor has pharmacological properties that are known to reduce inflammation, secretion of goblet cells decreases, the ciliary beat frequency is sped up, and bronchodilatory and mucolytic properties hence help in the drainage of sinuses and other respiratory organs [3]. Consequently, cineole would be therapeutically beneficial for asthma and bronchitis patients based on its proven broncho-dilating and anti-inflammatory effects. Other studies also have proven the effect on cineole [41–44].

A new elucidation for the analgesic application of camphor is the combination of transient receptor potential A1 (TRPA1) inhibition and desensitization of TRPV1. Camphor activates and then desensitizes TRPV1, thereby having an analgesic action. Linalool bioactive molecules showed pain reduction in mouse models such as inflammatory pain, acetic acid-induced writhing response, and the hot plate test. The likely mechanism perhaps is related to its regulation of NMDA receptors and suppression of pro-inflammatory cytokines [36]. In a clinical investigation, topical borneol treatment dramatically reduced pain compared to placebo. Furthermore, an in vivo study in mice that exhibited TRPM8 channels may perhaps be the molecular target of borneol [45]. *C. camphora* natural bioactive molecule menthol after topical application (skin, mucous membrane, and oral and nasal cavities) also activates TRPA1, s highly sensitive menthol receptor that contributes in counterirritants and analgesic activities. This suggests the involvement of different kinetics of channels and fast desensitization due to these sensory effects of menthol [46].

Clinical investigations and contemporary medical experiments in migraine and vascular headache demonstrated the crucial role of nitric oxide (NO). NO and nitric oxide synthase (NOS) inhibitors can significantly reduce the severity, frequency, intensity, and accompanying symptoms of migraine attacks. A protein complex known as nuclear factor-kappa β(NF-B) regulates DNA transcription, cytokine synthesis, and cell viability. NF-κB induces the expression of inducible nitric oxide synthase (iNOS), and overexpression of iNOS can catalyze L-arginine to yield nitric oxide (NO). Proinflammatory factors are also activated by NF-κB and then cause a neurogenic inflammation reaction, which sensitizes the pain center and initiates headache. In the pathogenesis of migraine, NF-κB has a significant mediating role. The essential oil of camphor leaves in the mouse model showed noteworthy analgesic action on migraine by inhibiting the nuclear factor-kappa B (NF-κB)/inducible nitric oxide synthase (iNOS) pathway and reduced neurogenic inflammation. Essential oil of *C. camphor* perhaps inhibits the iNOS and expression of NF-κB and therefore decreases NO production and neurogenic inflammatory response (Figure 4). Therefore, it could treat migraine. The main analgesic compounds recognized in the camphor's essential oil camphor leaves were nerolidol and (E)-α-atlantone [36]. Citronellol, which affects cyclooxygenase (COX) 1 and 2, is the enzymes involved in the production of prostaglandins from arachidonic acid and decreases the production of inflammatory mediators which is related to its ability to reduce cell migration and paw edema [47].

Markel et al. [48] investigated the influence of camphor on the expression of oestrogenic genes. They discussed how the UV filter 4-methyl benzylidene camphor (4-MBC) is oestrogenic and interferes with the thyroid axis. They discovered that, in rats, exposure to 4-MBC altered the mRNA levels of ER-alpha, progesterone receptor (PR), preproenkephalin (PPE), and insulin-like growth factor-I (IGF-I) in the brain in a sex- and region-specific manner. Methanolic extract of *C. camphora* contains anti-inflammatory mechanisms that limit NO and PGE2 synthesis in LPS/IFN-activated macrophages and prevent the generation of TNF IL-6 and IL-1 from RAW264.7 cell [10]. The proanthocyanidins (PAs) in the leaves of *C. camphora* inhibit tyrosinase monophenolase and hence have been proven to have anti-tyrosinase activity. The PAs also showed strong antioxidant capacity with the ferric reducing antioxidant power (FRAP), scavenging 2,2-diphenyl-1-picrylhydrazyl (DPPH) and 1,2′-azino-bis (3-ethylbenzthiazoline-6-sulphonic acid) (ABTS) assays [49].

9. Preclinical and Clinical Studies of Main Active Biomolecules

The preclinical studies of the main natural active biomolecules are summarized in Table 5. Table 6 summarizes the preclinical and clinical studies of the compound formulation of camphor.

Table 3: Unani formulations, dose, dosage form, ethnomedicinal properties, and therapeutic applications of *C. camphora* as one of the ingredients in different body systems.

Unani formulation	Dose	Dosage form	Ethnomedicinal properties	Therapeutic application	Ref.
			Respiratory system		
Habb-i-Nafs-ud-Dam Silli	5-10 gm	Pills	Hemostyptic (*Habis-i-Dam*), healing agent (*Mudammil*), Antipyretic (*Dafiʿ-i-Humma*)	Nasal bleeding (*Nafs-ud-Dam*), phthisis (*Sill*), asthma (*Diq al-Rewi*)	[31]
Habb-i-Jawahar Muwallif Khas	500 mg	Pills	Tonic (*Muqawwi*), expectorant (*Munaffis-i-Balgham*), analgesics (*Musakkin*)	Phthisis, bronchial asthma	[32]
Habb-i-Khunaq	5-10 gm	Pill	Analgesics, anti-inflammatory (*Muhallil-i-warm*)	Inflammation of bilateral pharyngeal muscle/ diphtheria (*Khunaq*), pharyngitis, and laryngitis	[32]
			Gastrointestinal system		
Habb-i-Qabid	125-250 mg	Pills	Astringent (*Qabid*), antiseptic (*Dafiʿ-i-Taʿaffun*)	Infantile diarrhoea (*Ishal al-Atfal*)	[33]
Qurs-i-Atash	5-10 gm	Tablet	Anti-bilious *(Dafiʿ-i-Safra)*	Reduce thirst, acidosis *(Humudat-i-Mi'da)*	[31]
Qurs-i-Kafoor Musik	5-10 gm	Tablet	Astringent	Diarrhea	[31]
Jawarish-i-Kafoor	5-10 gm	Semisolid confection	Stomachic (*Muqawwi-i-Mi'da*), carminative (Kāsir-i-Riyāh)	Dyspepsia (*Su' al-Hadm*) indigestion (*Tukhma*), flatulence (*Nafkh-i-Shikam*)	[31]
Habb-i-Taoon Qawi	250-500 gm	Pill	Antidote *(Dafiʿ-i-sumum)*	Plague (*Taʿun*) Food poisoning (*Hayda*)	[32]
Habb-i-Taiyub-ul-fam	5-10 gm	Pill	*Mutib-i-Dehan*	Halitosis (*Bakhr al-Fam*)	[32]
Safuf-i-kahruba	3-5gm	Powder	Digestive (*Hazim*), laxative (*Mulaiyin*), appetizer (*Mustahi*)	Indigestion *(Du'fʿ-i-hadim*), reduce thirst (*Duʿf-i-*istiha)	[23]
Habb-e-Pechish	220 mg (one pill)	Pill	Astringent and hemostyptic	Dysentery, diarrhea	[23]
Qurs-e-Zaheer	2 tab twice	Tablet	Anti-dysenteric, stomachic	Dysentery, indigestion (*Dafiʿ-i-Mi'da)*	[34]
Tiryaq-i-Pechish Jadid	3 gm twice a day	Powder	Anti-diarrhea	Useful in bilious and phlegmatic dysentery (*Zahīr Safrawi*), *Wa Balghami)*, Chronic dysentery (*Zahīr Muzmin*)	[34]
Marham-i-Bawaseer	Q.S. for external use	Ointment	Prevent piles *(Dafiʿ-Bawasīr)*	Burning sensation of hemorrhoid (*Sozish-i-Bawasīr*), painful hemorrhoid (*Waj-ul-Bawasīr*), bleeding piles (*Bawasīr Damya)*	[34]
Marham Saeeda Chob Neemwal	Q.S for external us	Ointment	Anti-inflammatory	Hemorrhoid	[31]
			Eye		
Jauhar-i-Naushadar	Q.S	Semisolid sublimation	Detergent (*Jālī*), analgesics	Keratitis (*Sabal*), corneal opacity (*Bayād*), pterygium (*Zufra*) (for ophthalmic use)	[31]
Kohal-i-Kafoor	Q.S	Finest powder (for ophthalmic use)	Resolvent (*Muhallil-i-Waram*)	Conjunctivitis, burning sensation of eye	[31]
Burood-i-Muqawwi-i-Basar	Q.S	Fine powder (for	Eye tonic (*Muqawwi-i-Basar*)	Asthenopia/amblyopia (*Dafiʿ*-al-*Basar*)	[31]

Table 3: Continued.

Unani formulation	Dose	Dosage form	Ethnomedicinal properties	Therapeutic application	Ref.
		ophthalmic use)			
Burood-i-Sozish-i-Chashm	Q.S	Fine powder (for ophthalmic use)	Refrigerant (*Mubarrid*), analgesics	Burning sensation of the eye (*Sozish-i-Chashm),* eye irritation (*Kharish-i-Chashm*)	[31]
Kohlul Jawahar	Q.S	Past	Eye tonic	Weakness eyesight *(Duf'-i-Basar*)	[31]
			Cardiovascular system		
Mufarrah Shaikh ur Rais	5 gm	Semisolid confection	Cardiac tonic (*Muqawwi-i-Qalb*)	Weakness of heart *(Du'f al Qalb*) and palpitation (*Khafqan*)	[31]
			Integumentary system		
Marham Kharish Jadeed	Q.S for external us	Ointment	Refrigerant and antibacterial (*Qatil-i-Jara'sim*)	Fungal infection (*Dād*), ringworm (*Qūbā*), irritation (*Kharish*), itching (*Hikkah*), and blood infection (*Fasad-i-dam*)	[31]
Marham Kafoor	Q.S for external us	Ointment	Refrigerant, antiseptic	Ulcer (*Qurūh)* and inflammatory wound	[31]
Marham-e-Safaida Kafoori		Ointment	Healing agent (*Mudammil*), antiseptic (*Dafi'-i-Ta'affun*), wound (*Qurooh-i-Afni*)	Wound	[31]
			Reproductive system		
Jauhar-i-Kafoor	125 mg in a capsule	Dried powder	Antiseptic, refrigerant (*Mubarrid*)	Gonorrhoea (*Sozāk*)	[31]
Halwa-i-Suparipak	10-20 gm	Semisolid preparation	Spermatogenic (*Muwalliz-i-Mani*), retentive of semen (*Mumsik*), aphrodisiac (*Muqawwi-i-Bah*)	Spermatorrhoea (*Jarayan*), nocturnal emersion (*Surat-i-Inzal*), loss of libido (*Du'f al Bah*)	[31]
			Nervous system		
Jauhar-i-kafoor kawi	For inhalation	Semisolid sublimation	Nervine tonic (*Muqawwi dimagh*)	Convulsion (*Sara*), syncope (*Ghazhi*)	[32]
			Miscellaneous		
Qurs-i-Sartan-Kafoori	3-5 gm	Tablet	Hemostyptic, antipyretic	Type of bilious fever with excessive thirst and bilious vomiting *(Hummā -i-Muharraqa*), tuberculosis (*Dīq*), cough, phthisis	[31]
Qurs i-kafoor Lulvi	2-4 gm	Tablet	Antipyretic, healing agent, expectorant, astringent	Acute fever (*Hummā al-hadda*), phthisis, hectic fever (*Hummā diq*), gastrogenic diarrhea (*Ishal mi'di*)	[32]
Habb-i-kafoor marwareed	500 mg	Pills	Antidote, antipyretic	Fever, epidemic fever (*Hummā- Waba'iyya*)	[32]
Hab-i-Tap-i-larza	150-250 mg	Pill	Antipyretic	Type of fever *(Hummā -i-Ejamia*)	[32]
Hab-i-kafoor	125-250 mg	Pill	Antipyretic	*Hummā -i-muharraqa*	[23]
Qur-i-kafoor	Four tablets (each 775 mg)	Tablet	Refrigerant	Hectic fever and bilious fever	[31]
Habb-i-Ikseer Bukhar	400 mg thrice a day with lukewarm water	Pill	Antipyretic for fever with chills (*Dafi'-tap-i-Larza*) Antipyretic for seasonal fever *(Dafi'-i-tap-i-Mausami)*	Continuous fever Seasonal fever	[34]

Q.S.: quantity as required.

Table 4: Natural bioactive molecules found in different parts of the *C. camphora* tree.

Part of the tree	Major natural bioactive molecules												
	Camphor	1,8-Cineole	Linalool	Citronellal	α-pinene	Camphene	Safrole	β-pinene	Limonene	Eucalyptol	α-Terpineol or terpineol	D-borneol	References
Leaf oil	+	+	+	+	+	+							[18]
Branch	+				+	+							[18]
Wood essential oil	+	+					+				+		[18]
Root essential oil	+						+				+		[18]
Essential oil from leaf and branch mixture	+	+			+	+		+	+		+		[18, 38]
Essential oil from wood, leaf and branch mixture	+				+				+		+		[18]
Twig essential oil	+									+			[37]
Seeds oil	+		+							+			[37]
Fruit oil	+		+				+						[37, 39]
Fresh leaves												+	[10, 40]

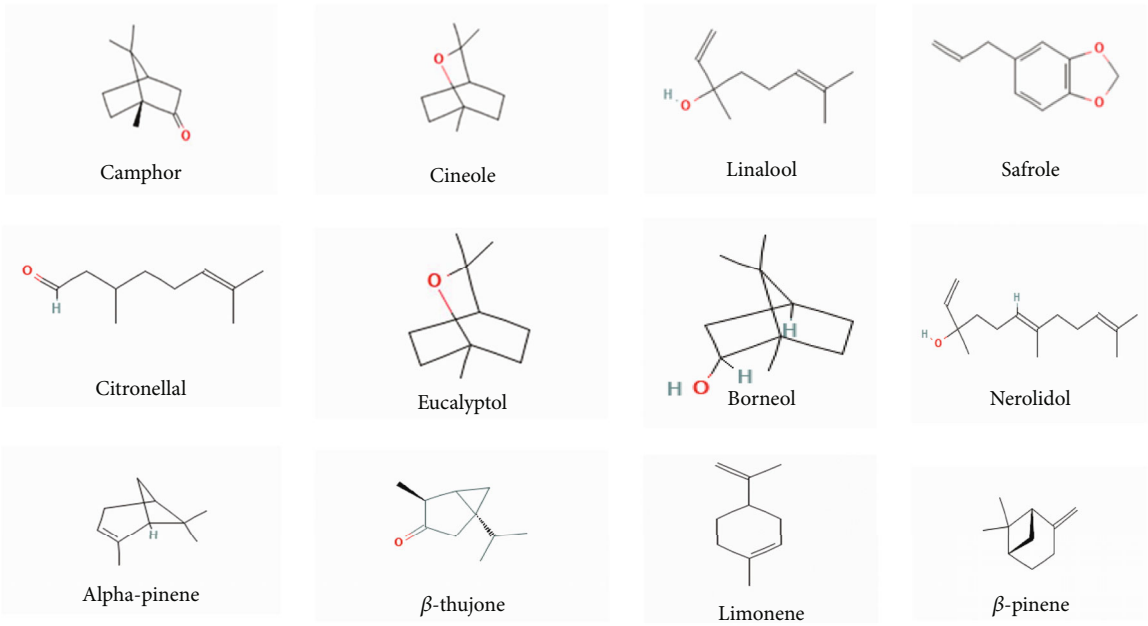

Figure 3: Bioactive molecules in *C. camphora*.

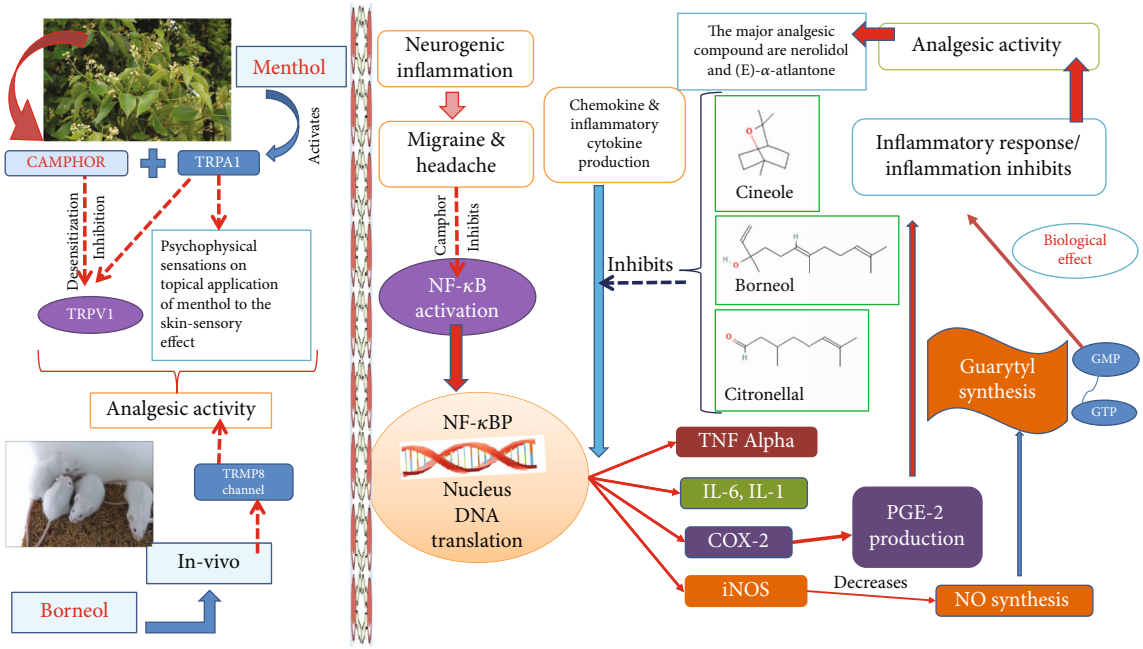

Figure 4: Anti-inflammatory and analgesic mechanisms of action of natural bioactive molecules of *C. camphora*.

9.1. In Vitro Pharmacological Properties. Numerous in vitro experimental studies show that antioxidant, antimicrobial, anti-inflammatory, and miscellaneous activities have been demonstrated by numerous research on *C. camphora*.

9.1.1. Antioxidant Activity. By interacting with biological components within the cell, the oxidation process damages cells, resulting in a variety of illnesses and chronic diseases like cancer and cardiovascular conditions. Additionally, oxidation changes the nutritional value and safety of food by producing secondary reaction products [58]. Oxidative stress is a condition when antioxidant levels are low. Antioxidant activity of polyphenols, which is influenced by their polyphenolic structure, has the effect of removing free radicals and improving antioxidant activity [59]. Due to an excess of reactive oxygen species (ROS), oxidative stress develops when the body's antioxidant system becomes depleted. Due to this, an increase in the concentration of free

Table 5: Preclinical (*in vitro*/*in vivo*/in silico) and clinical studies of *C. camphora* and its main natural bioactive molecules.

Natural bioactive molecule	Methodology	Test drug	Control	Result	Pharmacological activity /disease	Ref.
Camphor	Cell line study (male Wister rat DRG cells)	Dorsal root ganglion of adult male Wistar rats	Crt wash	Activate TRP receptor (TRPM8) and mutant channel	Analgesic by cold and heat sensitization of camphor	[50]
Citronellal	Rat module *in vivo* and *in vitro* (paw edema and peritoneal fluid leucocyte count)	50,100,200 mg/kg	Dexamethasone (2 mg/kg, s.c.),	In vitro and vivo studies of citronellal significantly ($p < 0.01$) reduce paw edema and leucocyte count	Anti-inflammatory and analgesics	[47]
Clinical trials						
Cinelol	Randomized, double-blind, clinical trial	100 mg capsule three daily for 7 days	Placebo	Symptom (headache, heaviness, secretion, and nasal obstruction) reduced	Acute non-purulent rhinosinusitis	[42]
Cineole	Randomized placebo-controlled trial (multicenter)	200 mg cineole or placebo 3 times for six months during (concomitant therapy)	Placebo	Significant improvement notes test group Improvement in dyspnea, lung function	Anti-asthmatic	[43]
Cineole (Eucalyptol)	Randomized placebo controlled clinical trial	200 mg cineole or placebo 3 times for six months during winter	Placebo	Improve lung function and health status. Reduce exacerbation and dyspnea	COPD	[44]
Cinelol	Randomized placebo-controlled clinical trial	3×200 mg of cineole, per day for 10 days	Placebo control	Significantly reduce cough $p = 0.0001$	Bronchitis	[41]

radicals inside cells is the root cause of many chronic disorders such as nonalcoholic fatty liver, type 2 diabetics, neurological conditions, and reproductive-related problems [59–61]. Reactive oxygen species (ROS) at baseline levels are necessary for basic physiological activities. Ageing, obesity, type 2 diabetes mellitus (T2DM), depression, and neurodegeneration are all conditions that are significantly impacted by oxidative stress [59] (Figure 5). Camphor has antioxidant, hepatoprotective, antidepressant, estrogenic, and anti-inflammatory qualities in addition to being an antioxidant that prevents oxidative damage and neutralizes free radicals. Camphor's antioxidant capabilities may lessen tissue damage and oxidative stress. In scavenging DPPH, ABTS, and ferric reducing antioxidant power (FRAP) assays, the phytochemical proanthocyanidins (PAs) from leaves and branches of *C. camphora* displayed significant antioxidant activity [49]. The antioxidant activity of hexane, chloroform, and ethanol extracts was determined using the DPPH (2,2-diphenyl-1-picrylhydrazyl) technique on dried camphor leaves. Another study evaluated the antioxidant activity of leaves of *C. camphora* in three different solvents and was tested by using the DPPH method, and hot extraction (Soxhlet) and cold extraction (maceration) methods were applied for the presence of components in the camphor leaves. The antioxidant activity of ethanol extracts was higher than that of other extracts. These findings show that camphor leaves, which have significant antioxidant quality, are excellent for pharmaceutical composition. Linalool, nerolidol, and borneol are the phenolic compounds extracted from the ethanolic extract. The hot extraction method by using ethanol solvent can extract antioxidant and mineral content against camphor leaves [62] (see Figure 6). Liu et al. [63] established the flavonoids extracted from C. camphora leaves' in vitro antioxidative capacity. Both the ferric reducing antioxidant power assay and the 1,1-diphenyl-2-picryl-hydrazyl (DPPH) free radical scavenging assay demonstrated a dose-dependent increase in antioxidant activity in the flavonoids, which is outstanding compared to commercial antioxidants [64].

9.1.2. Antimicrobial. Numerous disorders in the body are brought on by pathogens, which are inhibited by antimicrobial agents, which also stop the establishment of microbial colonies. One of the biggest problems in human health is the over and improper use of antibiotics. Additionally, the rapid spread of microorganisms that are resistant to antibiotics is concerning. The herbal potential of *C. camphora* is recognized to serve as an antibiotic, antiviral, and antifungal. Wang et al. [65] described that there is evidence that *C. camphora* essential oil has therapeutic properties like antibacterial effects. The obtained MICs and MBCs verified the clinical strains' significant susceptibility to CCEO. The development of E. coli biofilms is intimately associated to prolonged E. coli infection and can lead to antibiotic resistance. E. coli was significantly destroyed by CCEO, and the E. coli biofilm was also effectively destroyed. *C. camphora* essential oil (CCEO) was active against *E. coli* in suspension and biofilms, two states that are common in living organisms. Escherichia coli, one of the most frequent microbial pathogens, is mainly responsible for biofilm-associated

Table 6: Unani compound formulations with *C. camphora* and pharmacological application in preclinical (*in vitro*/*in vivo*/in silico) and clinical studies.

Unani formulation	Method/ model	Extract use/dosage form	Control/ organism tested	Result	Pharmacological application	Ref.
Preclinical studies						
Arq-Ajeeb	*In vivo* (rats)	0.07 ml and 0.14 ml/kg, p.o.	Charcoal administration	Reduce diarrhea in rats	Anti-diarrheal activity	[51]
Compound preparation of sesame oil, camphor, and honey	Animal (rat)	Daily dressing with extract	Oil Vaseline	Maximal healing was noticed in the test group	Healing effect of second-degree burn	[52]
Arq Ajīb contains methanol, camphor	In silico approach	Inhibits SARS-CoV-2 spike glycoprotein and main protease	—	Good interactions and binding affinities with 3CLpro and S glycoprotein	Inhibitory effect on SARS-CoV-2	[53]
Extract C. camphora and Ziziphora tenuior	In vitro mice liver	3, 5, 10, 25, 50, and 100 mg/ml of extracts	—	The extract exhibited dose-dependent and time-dependent antiparasitic effects	Anti-parasitic and immunomodulatory	[54]
Clinical studies						
Marham-i-Raal	Single-arm pre- and posttreatment study	2 gm on episiotomy wound	—	REEDA score decreased, and VAS score decreased	Episiotomy wound healing and pain reduction	[55]
Marham-i-Raal	Case study	External application (3 months) (ointment)	—	Completely heal foot ulcer	Chronic wound healing	[21]
Arq Ajib	Clinical study	Liquid application	—	Decrease in VAS score for pain intensity	Headache	[56]
Composition of A. indica and C. camphora	Controlled clinical trial	Oral and topical	Psoralen plus ultraviolet A (PUVA) solution	In individuals with moderate-to-severe CPP, test medications that are efficacious and well-tolerated	Chronic plaque psoriasis	[57]

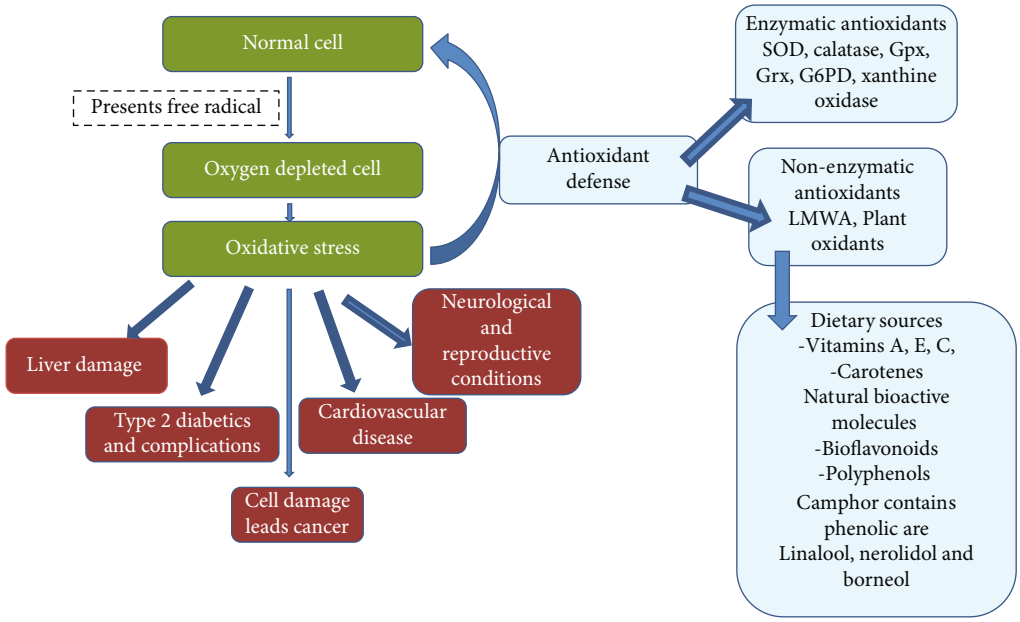

Figure 5: Oxidative stress affects various systems and antioxidant defenses including natural bioactive molecules.

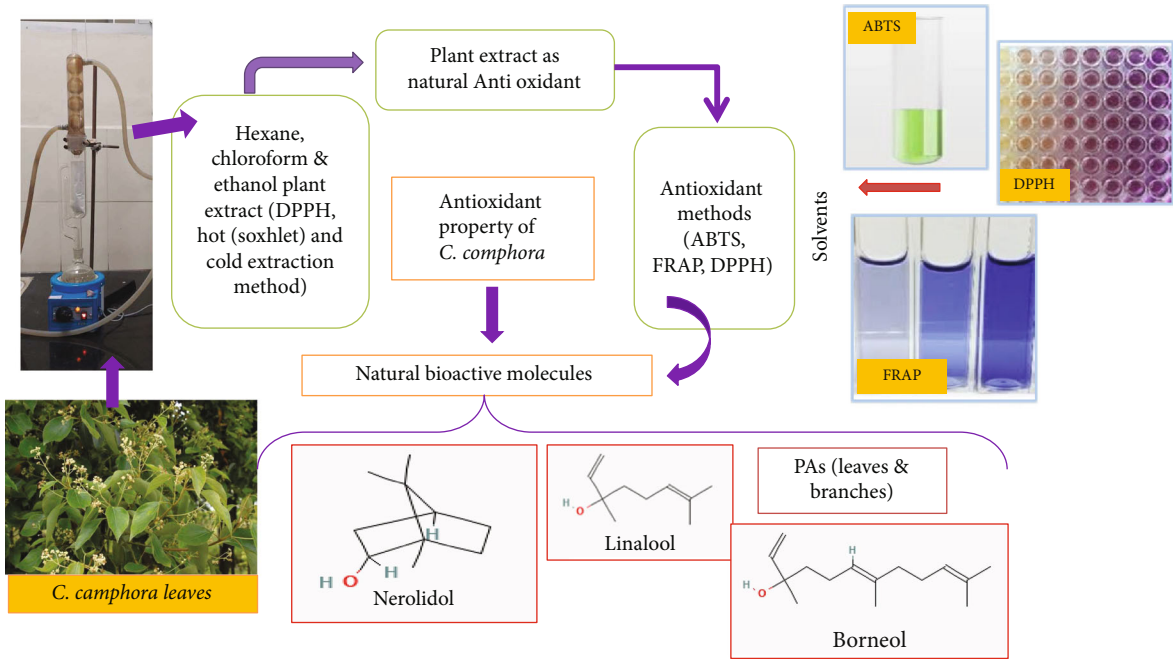

Figure 6: Antioxidant activity of natural bioactive molecules of *C. camphora*.

opportunistic illnesses like diarrhea, endometritis, and mastitis [65]. In another in vitro study of camphor ethanolic extract has been showed antibacterial action against *Escherichia coli*, *Staphylococcus aureus*, and *Pseudomonas aeruginosa* [56]. Poudel et al. [37] analyzed in vitro study of *C. camphora* essential oil against five Gram-positive bacteria, *Streptococcuspyogenes*, *Propionibacteriumacnes*, *Bacilluscereus*, *Staphylococcusepidermidis*, and *Staphylococcusaureus*, and two Gram-negative bacteria, *Pseudomonas aeruginosa* and *Serratia marcescens*, showing its antibacterial properties [37].

The phytochemical compounds found in *C. Camphora* have a wide variety of antibacterial properties against various pathogens. Leaf, branch, and wood essential oil were tested again using seven strains of fungi, *Aspergillus niger*, *Aspergillus fumigatus*, *Candida albicans*, *Microsporum canis*, *Trichophyton mentagrophytes*, *Microsporum gypseum*, and *Trichophyton rubrum*. *Serratia marcescens* responded favorably to the wood essential oil's antimicrobial properties. Camphor, 1,8-cineole, -terpineol, and safrole were the main ingredients in the wood oil; hence, the reported activity of the wood oil against *S. marcescens* may be the result of synergism between these and other constituents. Only a small amount of action was seen against S. marcescens by camphor, 1,8-cineole, -terpineol, and safrole. According to one study, camphor and 1,8-cineole work together to have a synergistic antibacterial effect [35]. All fungi were cultured on yeast malt, and studies showed good antifungal activity against *Aspergillus niger* and *Aspergillus fumigatus*, while the leaf essential oil showed good antifungal activity comparatively to other parts of the plant [35]. Kulzam is a well-known Unani liquid composition used to cure several ailments such as cough, colds, and sore throats [66]. The major components identified in Kulzam were camphor, menthol, etc. The ingredients of the formulation are *Sat-i-Pudina*, *Sat-i-Ajwain*, *camphor*, *Roghan baid majnun*, *Roghan-i-darchini*, *Roghan-i-zaitun*, and *Roghan-i-laung*. Kulzam demonstrated a significant effect on all tested microorganisms at both 100 and 150 (micro) levels of the undiluted formulation (test sample), and at 150 (micro) level, it inhibited growth more than the standard. Furthermore, it highlights the fact that gram-negative microorganisms are more vulnerable to inhibitory activity than gram-positive ones. Comparing the formulation to that of standard clotrimazole, it showed a very significant zone of inhibition against the fungus *Candida albicans* and *Aspergillus fumigatus* [66]. In an in vitro investigation, essential oil from *C. camphora* leaves, flowers, and twigs showed antifungal action again 7 strains including *Aspergillus clavatus*, *Aspergillus niger*, *Chaetomium globosum*, *Cladosporium cladosporioides*, *Myrothecium verrucaria*, *Penicillium citrinum*, and *Trichoderma viride* in 1000 μg/ml concentration [67]. In addition, when compared to other sections of the plant, the leaf oil exhibited the best antifungal efficacy [67]. Five locally gathered plant species' fresh leaves were hydro distilled using Clevenger's apparatus to separate the essential oils and stored in a glass jar. Using the poisoned food approach on a potato dextrose agar medium, the oils were evaluated for resistance to *Aspergillus flavus* at 5000 ppm. Only the oil of *C. camphora* showed absolute fungitoxicity against the test fungus among the five essential oils examined [55]. Studies showed camphor oil possesses mycostatic application against *Aspergillus flavus* [68]. According to Karashima et al. [46], CHO cell showed induce expression of TRPA1, 0.5 mg/ml tetracycline was added to the culture medium, and cells were used 5–24 h after induction and menthol used as test drug. *C. camphora* constituent menthol activates TRPA1 and inhibits it in mouse neuron in in vitro study,

suggesting the involvement of different kinetics of channel and fast desensitization due to these sensory effects of menthol, a widely used additive in counterirritants and analgesic activity.

9.1.3. Anti-Inflammatory and Prostaglandin Synthesis Inhibition. Inflammation is a healing process that is triggered by pathogen, toxins, and radiations. These factors set off the immune system and cause inflammatory reactions in the organs of the host, which may result in cell death and/or illness. Unani traditional medicine is potentially useful for the treatment of inflammation-related diseases, such as rheumatism, bronchitis, asthma, COPD, acute non-purulent rhinosinusitis, dermatitis, neurodegenerative diseases, and muscle pains. There are well-known anti-inflammatory compounds that have been extracted from plants and evaluated in human clinical trials. Cinelol, cineole, citronellal, and camphor make up the majority of them [41–44]. Numerous investigations have revealed that *C. camphora* has an anti-inflammatory activity in vitro. An *in vitro* investigation of *C. camphora* leaf extract indicated that it reduced the generation of inflammatory chemokines. Its leaves had a significant impact on 2,4-dinitrochlorobenzene-induced atrophic dermatitis in mice. An *in vitro* investigation of *C. camphora* leaf ethanolic extract indicated that it reduced the generation of inflammatory chemokines. Its leaves had a significant impact on 2,4-dinitrochlorobenzene-induced atrophic dermatitis in mice. Lee et al. examined the inhibitory impact of CCex on IFN- (10 ng/mL) stimulated HaCaT keratinocytes' ability to produce the inflammatory chemokine (MDC). The outcomes demonstrated that CCex inhibited MDC formation by IFN- in a concentration-dependent manner. The MeOH extract of *C. Camphora* inhibited prostaglandin E2 (PGE2) production in LPS/IFN-activated macrophages by up to 70%. To further understand *C. camphora's* anti-inflammatory activity, researchers looked at macrophage-mediated inflammatory events like cytokine production, NO release, PGE2 release, functional activation of adhesion molecules, and oxidative stress. It can have a strong immunomodulatory influence on numerous inflammatory responses at the transcriptional level, according to the findings of the study [10]. Methanolic extract of *C. camphora* contains anti-inflammatory mechanisms that limit NO and PGE2 synthesis in LPS/IFN-activated macrophages and prevent the generation of IL-1, IL-6, and TNF- from RAW264.7 cells [10].

By interacting with biological components within the cell, the oxidation process damages cells, resulting in a variety of illnesses and chronic diseases like cancer and cardiovascular conditions. Additionally, oxidation changes the nutritional value and safety of food by producing secondary reaction products [64]. The effectiveness of EOC derived from leaves in treating allergic inflammation, such as atopic dermatitis, was described by Kang [69]. The extract significantly reduced inflammation in low-calcium, high-temperature human adult keratinocytes and improved 2,4-dinitrochlorobenzene-induced atopic dermatitis in mice. These results will make it easier to create EOC as a novel, all-natural treatment for inflammatory skin disorders [69].

9.1.4. Anti-Hyperlipidemic Activity. Camphor compound was examined in rats with experimental dyslipoproteinemia for its pharmacotherapeutic efficacy, antioxidant, and anticoagulant action. The positive results of the study allowed this substance to be recommended for the prevention of atherosclerotic damage to the vascular endothelium and the prevention of thrombogenesis [70].

9.1.5. Antifertility Activity. In order to understand the impact of camphor as a male local contraceptive, in-vitro effect of camphor on human sperm vialbility and motility was examined. A decrease in sperm motility and viability in an in vitro investigation where camphor was used indicates that fertilization efficacy is reduced. Camphor may work as a contraceptive effect. The sperm motility and viability decrease are probably because of a fall in fructose levels or denaturation of protein and cholesterol, which are the energy sources for sperm motility [71].

9.2. In Vivo Pharmacological Studies

9.2.1. Wound Healing Activity. Camphor, a potent wound healing and ant wrinkle drug, reduced MMP1 expression but increased collagen and elastin expression in UV-exposed mouse skin after 4 weeks of therapy. Camphor might prevent the loss of elastin and help it recover after UV-induced damage to retain skin suppleness [60]. It also decreased the depths of the epidermis and subcutaneous fat layer in UV-exposed mouse skin. The ethyl acetate soluble fraction of an ethanolic extract of C. camphora leaves in Wister rats showed improvement in wound healing and increased wound contraction due to enhance and accelerated activity of fibroblast and epithelial cell migration to the wound site and early dermal and epidermal regeneration. Furthermore, the treated group also showed a considerable increase in collagen content [75].

9.2.2. Anti-Testosterone Activity. Jugular vein samples were taken for hormonal analysis from Awassi lambs and rams fed *C. camphora* at a dose of 20 mg/kg/animal, and semen samples were collected from the animals using artificial vagina in the control group. The study found that the testosterone hormone concentration in the treatment group was much lower than in the control group, which could be attributed to camphor's oestrogenic impact, which reduces testosterone hormone levels. Camphor may suppress catecholamine secretion by inhibiting nicotine acetylcholine receptors, which has an influence on male sexual behavior and reproductively via its effect on blood testosterone levels and/or the sympathetic nervous system. During the second and fourth weeks of the experimental study, mass activity in the camphor group was significantly ($P < 0.05$) lower than in the control group, whereas the individual sperm motility percentage showed no significant differences between the camphor and control groups throughout the entire experimental period, i.e., over the final three weeks of the trial, the camphor group displayed lower levels testosterone [73].

9.2.3. Oestrogenic Effect. Maerkel et al. [48] evaluated the estrogenic effect on the brain and reproductive organs both

prenatal and postnatal exposure to UV filter 4-methylbenzylidene camphor (4-MBC) in rats. Following pre- and postnatal exposure to the UV filter 4-MBC, the current study found alterations in the expression level and estrogen sensitivity of target genes as well as in the steroid receptor coactivator SRC-1 in sexually dimorphic brain areas of adult rat offspring. They discussed how the UV filter 4-methyl benzylidene camphor (4-MBC) is oestrogenic and interferes with the thyroid axis. They found that 4-MBC exposure changed the mRNA levels of ER-alpha, progesterone receptor (PR), preproenkephalin (PPE), and insulin-like growth factor-I (IGF-I) at the brain level in rats in a sex- and region-specific manner [48].

9.2.4. Anti-Allergic Activity. Edema, a dysfunctional skin barrier, and the invasion of several inflammatory cell types are the hallmarks of allergic skin inflammation, such as atopic dermatitis (AD). *In vivo*, *C. camphora* leaves (100 mg/kg) improved atopic dermatitis symptoms by lowering serum immunoglobulin E levels, reducing lymph node thickness and length, decreasing ear edema, and lowering the number of inflammatory cells infiltrating the ears. Atrophic dermatitis is an allergic inflammatory disorder that can be treated with the leaves of *C. camphora*. IFN-γ, an important mediator of immunity and inflammation, induces the Janus tyrosine kinases- signal transducer and activator of transcription (JAK-STAT) signal pathway. The investigators reported that in skin inflammation lesions, leaf extract inhibited macrophage-derived chemokine (MDC/CCL22) production via the downregulation of (STAT) 1 and extracellular signal-regulated kinase 1/2 (ERK1/2) pathways and, hence, improved several symptoms (ear edema and lymph node size) change in blood parameter (serum IgE) and histological changes in mice with allergic dermatitis. By administering DNCB to mice, we established experimental AD in order to research the effects of CCex on AD in vivo. IgE levels are correlated with the severity of AD and are linked to defective skin barrier, making IgE a key therapeutic target for AD. When compared to the induction group in this investigation, the CCex-treated group had considerably lower serum IgE levels (p 0.001). Comparing the cutaneous edema in the CCex-treated mice to that in the induction mice on day 29, the difference was significant (p 0.001). Additionally, the CCex-treated group showed considerably less epidermal thickness and inflammatory cell infiltration than the induction group [69].

9.2.5. Anxiolytic and Antidepressant Activity. Antidepressant and anxiolytic medications are used to treat depression and anxiety. Albino mice weighing 18-30 gm were used for the study CCO given three different doses 250 mg/kg CCO orally, 500 mg/kg, and 750 mg/kg CCO orally in each group. and imipramine15mg/kg given intra peritoneal as a standard control. *C. camphora* oil (CCO) showed significant anti-anxiety and antidepressant effects compared to the control group in rat models. Numerous monoterpenoid compounds in the essential oil of *C. camphora* are confirmed by phytochemical studies. β-thujone, β-pinene, linalool, and limonene are monoterpenoids that are testified to have antidepressant applications. Furthermore, recent research has proposed the antidepressant action of β-pinene, which increases dopamine level and inhibits MAO activity in rabbits. Additionally, few studies showed that numerous biologically active molecules, including monoterpenoids, are potent inhibitors of MAO-A and MAO-B [9] (Figure 8).

9.2.6. Antioxidant Activity. As previously mentioned, *C. camphora* seed kernel oil increased the concentrations of superoxide dismutase and catalase in diet-induced rats, which consequently boosted antioxidant activity and reduced malondialdehyde concentration (a biomarker of lipid peroxidation and oxidative stress) [64].

9.2.7. Analgesic Activity. C. camphora leaf essential oils showed a significant analgesic effect against nitroglycerin-induced experimental migraine in mice models and inhibited the nuclear factor-kappa Beta, inducible nitric oxide synthase, and nitric oxide pathway [36].

9.2.8. Hepatoprotective Activity. According to Johari et al. [74], camphor powder solution given female rats by intraperitoneal injection for 14 days showed hepatoprotective activity in the treatment of a deferent type of liver conditions. On the liver enzymes, it is proven to have a stimulating impact. However, the researchers recommended that camphor use in a higher dosage uninterruptedly probably leads to a substantial increase in the concentration of liver enzymes [74].

10. Toxicity Studies

C. camphora essential oil from seeds, twigs, and leaves showed robust contact toxicity against cotton aphids with median lethal concentration (LC50) values of 146.78, 274.99, and 245.79, mg/L after 48 h of treatment, respectively [37]. Camphor is quickly absorbed by the mucous membranes, skin, and gastrointestinal tract in liquid form. Symptoms may appear 5–90 minutes after consumption [26]. In humans, indications of intoxication include nausea, vomiting, trembling, and convulsions, which are followed by CNS depression characterized by apnea and coma [17, 75].

11. Discussion and Comparative Therapeutic Evaluation

Unlike petroleum products, camphor is a botanical hydrocarbon, very inexpensive, and can be easily cultivated without any shortages. Therefore, camphor is an exceptional carbon source for the production of high purity, high yield, and high efficiency [76]. According to Unani physicians, seven factors are responsible for the maintenance of health, and loss of any one of these can lead to disease or even death. Dietotherapy and pharmacotherapy are mainly used to maintain the equilibrium of humors to maintain health and treat disease conditions. All single drugs have specific and many ethnopharmacological properties according to their active principles and temperament. *C. camphora* (L.) is a traditional Unani medicinal plant with a third-degree cold and dry temperament and hence useful in hot

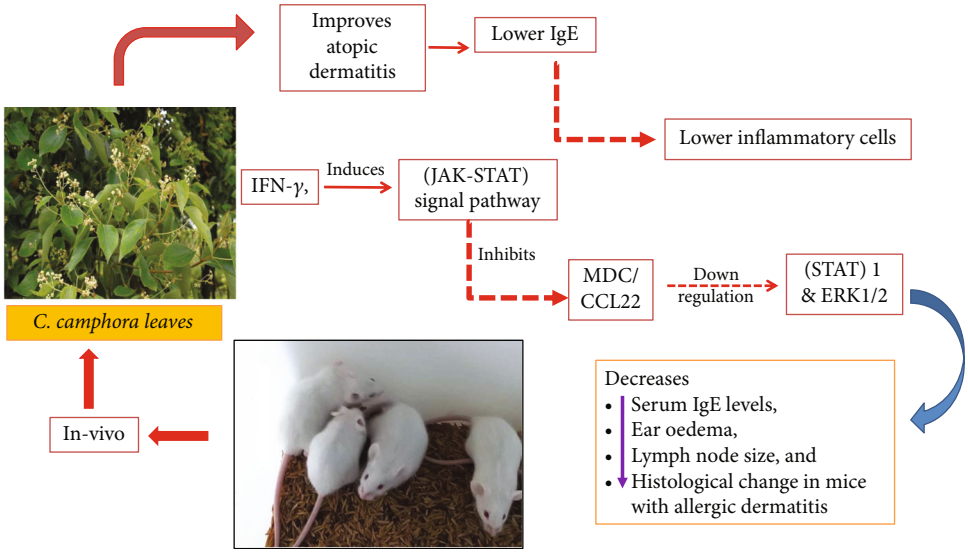

Figure 7: Anti-allergic activity of natural bioactive molecules of *C. camphora* in allergic dermatitis.

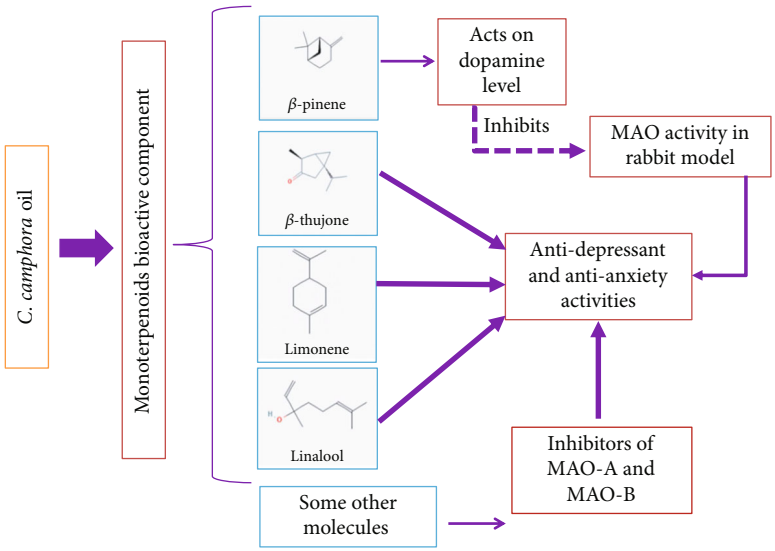

Figure 8: Anti-anxiety and antidepressant activity of natural bioactive molecules of *C. camphora*.

temperamental individuals [8] used since ancient times. Nowadays, natural and artificial camphor is also used for medicinal conditions and commercial purposes. A review of Unani and other conventional literature realized that *C. camphora* has prophylactic and several pharmacological properties for treating medical conditions and strengthening mental and physical properties and it is effective in treating respiratory conditions, musculoskeletal, gastrointestinal, oral, eye, integumentary, and general conditions. Unani physicians evaluated ethno-pharmacological properties, usage, patient temperament, and disease condition when prescribing medications and then selected single pharmaceuticals with correctives (*Muslih*) to reduce undesirable or unwanted effects. Furthermore, to combat the adverse effect of camphor on cold temperamental people [12, 15, 16], they advised camphor with hot temperament and fragrance herbs such as *Zafran*, *Amber*, and *Misk* [15].

Camphor's distinctive aroma has led to its widespread use in ointments and inhalants, particularly as a remedy to treat respiratory ailments. Unani physicians stated that *C. camphora* is commonly used in respiratory conditions such as acute and chronic cough, fever, common cold, lung ulcers, pleurisy, pneumonia, coryza, and catarrh in various forms as a single drug or with another herbal, mineral, or animal origin drug as a compound formula as it possesses expectorant, antipyretics, deobstruent, and mucolytic properties [8, 12, 15, 16]. *C. camphora* has been a useful remedy in symptoms of COVID-19 and inhibits SARS CoV-2 spike glycoprotein CoV [53]. Furthermore, one of the ingredients of many compounds, Unani formulation, is useful in viral infections

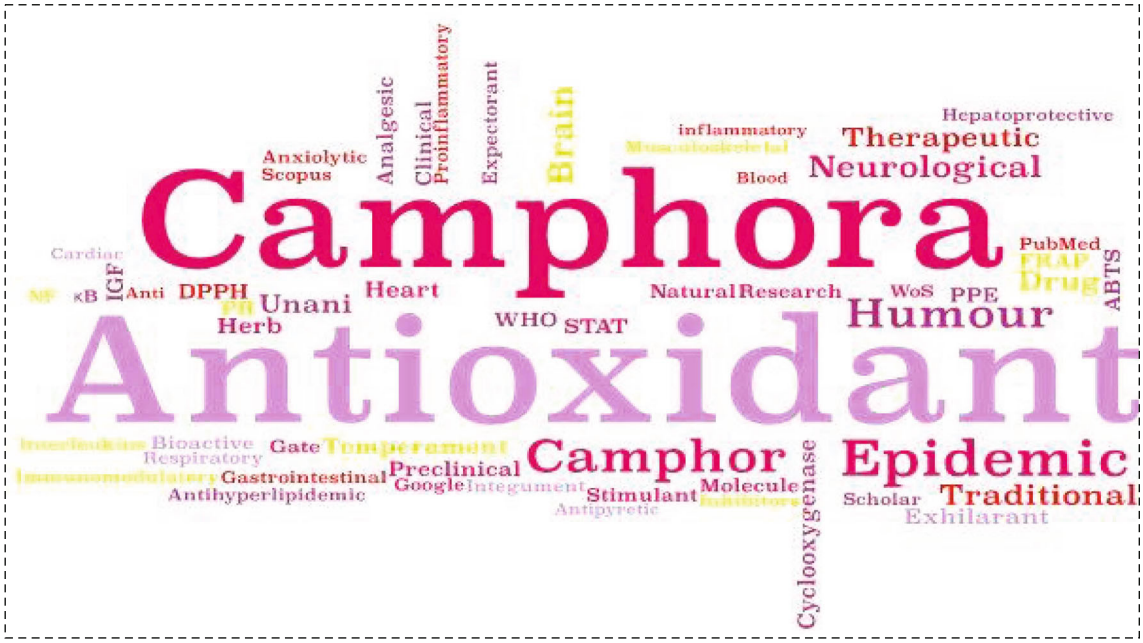

Figure 9: Word cloud of the current study.

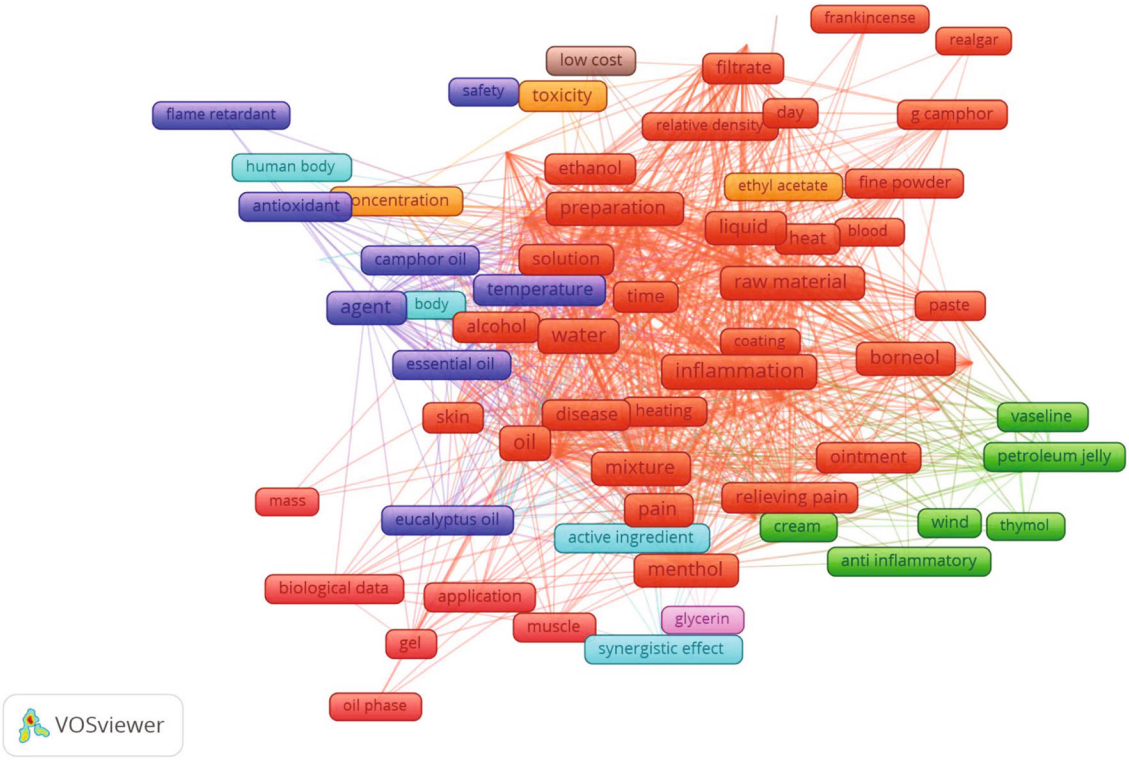

Figure 10: Network visualization of the Camphor based on previously published data in the Web of Science.

and respiratory diseases (Table 3). In vitro, in vivo, and clinical, recent studies have proven its antibacterial [35, 56, 77], anti-inflammatory [10, 37, 69], analgesics [36], and immunomodulatory properties. Hence, it is beneficial in conditions such as acute non-purulent rhinosinusitis, asthma, COPD, bronchitis, and the inhibitory effect of SARS-CoV [53]. It is used as a nasal decongestant and a cough suppressant [78]. Anti-asthmatic, cough suppressant, mucolytic, bronchodilator control, airway mucus hypersecretion, and anti-asthmatic qualities are found in camphor, cineole, linalool, and safrole [76].

Compound drugs of *C. camphora* and external medication used for the suitable medicament in musculoskeletal conditions such as arthritis and muscular pain with

ethnomedicinal properties such as stimulant, rubefacient, anastatic, and analgesics [12]. Camphor is a major active ingredient in liniments and balms used as a topical analgesic, and it is a natural compound [78]. Lee et al. [10] in their in vitro study confirmed anti-inflammatory and antioxidant properties of camphor. They hypothesize that the anti-inflammatory actions of C. camphora is perhaps due to the modulation of cytokine, NO, and PGE(2) production. TRPM8, TRPV3, and TRPV1 (transient receptor potential) channels are activated, and TRPA1 is inhibited by camphor leading to excitation, warm sensation, and desensitization of sensory nerves, itch, relieving pain, and irritation in the applied area [76, 78].

We have designed the word cloud in the current study based on the closest terms used in this study (Figure 9). It would be helpful for the researchers, scientists, doctors, students, and academicians to work in this area. Previously, many researchers are used word cloud in the field of stress [79, 80], motor imagery [81], augmented reality [82], blockchain technology [83], and premenstrual syndrome with oxidative stress [84]. In addition, we also designed the network visualization based on previous published studies mentioned in Figure 10. This network visualization may also be helpful to the researchers, scientists, doctors, students, and academicians to work in this area. Previously, many researchers are used network visualization in the field of premenstrual syndrome, insomnia [85], bruxism [86], motor imagery, augmented reality, stress [87], and blockchain technology.

Camphor is a cardiac and nervine tonic in proper dose and dosage forms. It acts as an exhilarant, tonic, stimulant innate faculty of soul and nerves. The Unani formulation such as Jauhar-i-Kafoor is used for inhalation as nervine and exhilarant for vital organs and useful in convulsion. *Jauhar-i-Kafoor* is also useful as cardiac tonic for conditions such as a syncope, weakness of heart functions, and palpitation. Overdose or misused of camphor can cause adverse effects such as abdominal discomfort, tremor, apnea, coma, and CNS depression. Hence, a proper dose stimulates and enhances nervine and cardiac activity, while an overdose can disrupt the system. However, more research is required to confirm. According to the findings, a proper dose stimulates and enhances nervine and cardiac activity, while an overdose can disrupt the system. However, more research is required to confirm. Studies have shown that *C. camphora* or some of its components might find some applications in the future for the treatment of memory disorders or for improving brain functions in patients [76].

12. Research Gaps, Future Recommendations, and Concluding Remark

Strength includes authenticity and research articles showed that *C. camphora* has therapeutic applications in various diseases, proven in few recent preclinical and clinical studies. However, other ethnopharmacological activities with eye applications and gastrointestinal and cardiovascular diseases require additional modern pharmacological interpretations to explicate its basic mechanism. The review showed that isolated compounds, extract dose range, route of administration, and dose frequency are clarified in the existing recent research. However, more preclinical and clinical trials are recommended to explore its therapeutic applications in other diseases. Furthermore, it has been normally combined with other single drugs in Unani medicine; hence, drug interactions should be researched further in conventional therapies. There are no studies that have revealed interactions between conventional medicine and camphor, and additional research is needed to determine the safety and efficacy of camphor. Nonetheless, prospective clinical studies are recommended to validate the herb's healing effect. In humans, indications of intoxication include gastrointestinal like nausea, vomiting, and nervous system trembling and convulsions, which are followed by CNS depression characterized by apnea and coma.

The comprehensive review concludes that it is a drug that has been effectively used in Unani medicine for centuries to treat several ailments, particularly respiratory, nervous, musculoskeletal, and eye disorders. Camphor has been related to a variety of biological activities, including antibacterial, antifungal, anti-inflammatory, analgesics, antitussive, and antioxidant. However, bioactivity was often determined using an essential oil rich in camphor rather than pure camphor, and clinical studies of pure camphor have not been found. Moreover, sparse preclinical and clinical researches are available. However, more studies are needed to explore the pharmacological activities. This review has demonstrated that camphor is a medication with many wide ranges of applications.

Abbreviations

ABTS:	2,2′-Azino-Bis 3-ethylbenzothiazoline-6-sulfonic acid
BC:	Before Christ
COPD,:	Chronic obstructive pulmonary disease
COX:	Cyclooxygenase
DPPH:	2,2-diphenyl-1-picryl-hydrazyl hydrate
DM:	Diabetes mellitus
CNS:	Central nervous system
CCEO:	*C. camphora* essential oil
FRAP:	Ferric reducing antioxidant power
IGF-I:	Insulin-like growth factor-I
IL-1:	Interleukin-I
IL-6:	Interleukin-6
iNOS:	Inducible nitric oxide synthase
LPG/IFN:	Interferons
MAO-A:	Monoamine oxidase a
MeOH:	Methanol
MBC:	Methyl benzylidene camphor
mRNA:	Messenger RNA
MMP1:	Matrix metalloproteinase-1
MSP:	*M. oleifera* seed preparation
NIUM:	National Institute of Unani medicine
NO:	Nitric oxide
NOS,:	Nitric oxide synthase
NF-Kb:	Nuclear factor-kappa B
PGE2:	Prostaglandin E2

PPE: Preproenkephalin
PR: Progesterone receptor
PUVA: Psoralen plus ultraviolet a
REEDA: Redness, edema, ecchymosis, discharge, approximation
TRPV1: Transient receptor potential A1
TRPM8: Transient receptor potential cation channel subfamily M (melastatin), member 8
TNF-α: Tumor necrotic factor alpha
UV: Ultra violet
VAS: Visual analogue scale
JAK-STAT: Janus kinase signal transducer and activator of transcription
MDC/CCL22: Macrophage-derived chemokine
GMP: Guanosine triphosphate
GTP: Guanosine-5′-triphosphate.

Data Availability

The data will be available with the first author.

Conflicts of Interest

The authors declare that they have no conflicts of interest.

Authors' Contributions

M.J.A.F., A.S., and M.B.B.H have contributed to drafting, conceptualization, design, validation, critically reviewing, revision, and proofreading. K.R., and S. have contributed to guidance and proofreading. F.A, S.K., and S.C.Y.A. have contributed to critical reviewing, revision, and proofreading. M.J.A.F, A.S., M.B.B.H., S., and F.A., contributed equally. All authors have read and agreed to the published version of the manuscript.

Acknowledgments

The authors are grateful to the Prof. Wu, Prof. Abdul Wahab, Dr. Renu Rana, and Dr. Ijaz Gul for the useful discussion to improve this study. This publication work was supported by the China NSFC (U2001207 and 61872248), Guangdong NSF (2017A030312008), Shenzhen Science and Technology Foundation (ZDSYS20190902092853047 and R2020A045), the Project of DEGP (2019KCXTD005), and the Guangdong "Pearl River Talent Recruitment Program" (2019ZT08X603).

References

[1] WHO, *WHO Global report on traditional and complementary medicine 2019*, WHO, Geneva, 2019, https://apps.who.int/iris/bitstream/handle/10665/312342/9789241515436-eng.pdf?ua=1.

[2] S. Mehdi, A. Sultana, M. B. B. Heyat et al., "A review of amenorrhea toward Unani to modern system with emerging technology: current advancements, research gap, and future direction," in *Computational Intelligence in Healthcare Applications*, pp. 121–135, Elsevier, 2022.

[3] A. Sultana, S. Mehdi, K. Rahman et al., "Recent advancements of pelvic inflammatory disease: A review on evidence-based medicine," in *Computational Intelligence in Healthcare Applications*, pp. 101–120, Elsevier, 2022.

[4] S. Ansari, Q. A. Khan, R. Anjum, A. Siddiqui, and K. Sultana, "Fundamentals of Unani system of medicine - a review," *European Journal of Biomedical and Pharmaceutical Science*, vol. 4, pp. 219–223, 2017.

[5] S. I. Ahmed, *Introduction to Al-Umoor Al-Tabiyah*, Hkm Nuzhat Ishtiyaq, Aligarh, 1st ed. edition, 1980.

[6] R. M. Z. Kitab, *Ul-Mansoori (Urdu Translation)*, Central Council of Research of Unani Medicine, New Delhi, 2001.

[7] A. Sultana, Baig, Rahman et al., "Contemporary overview of bacterial vaginosis in conventional and complementary and alternative medicine," in *Computational Intelligence in Healthcare Applications*, pp. 33–53, Elsevier, 2022.

[8] H. Baghdadi, *Kitab ul-Mukhtarat Fi'l Tibb*, vol. I, Central Council of Research of Unani Medicine, New Delhi, 2005.

[9] N. V. Jay Rabadia, S. Satish, and J. Ramanjaneyulu, "An investigation of anti-depressant activity of Cinnamomum Camphora oil in experimental mice," *Asian Journal of Biomedical and Pharmaceutical Sciences*, vol. 3, pp. 44–48, 2013.

[10] H. J. Lee, E. A. Hyun, W. J. Yoon et al., "In vitro anti-inflammatory and anti-oxidative effects of Cinnamomum camphora extracts," *Journal of Ethnopharmacology*, vol. 103, no. 2, pp. 208–216, 2006.

[11] R. Singh and T. Jawaid, "Cinnamomum camphora (Kapur): review," *Pharmacognosy Journal*, vol. 4, no. 28, pp. 1–5, 2012.

[12] M. Kabir al-Din, *Makhzan al-Mufradat*, Idarae Kitabus Shifa, New Delhi, 2007.

[13] C. P. Khare, *Indian Medicinal Plants: An Illustrated Dictionary (Google eBook)*, Heidelberg Springer, Berlin, 2007.

[14] K. M. Nadkarni, *Indian Plants and Drugs*, Srishti Book Distributors, New Delhi, 2010.

[15] M. Khan, *Muhit-i-A'zam*, vol. IV, Central Council of Research of Unani Medicine, New Delhi, 2018.

[16] M. H. Abdul Hakim, *Bustan ul-Mufridat*, Idarae Kitabus Shifa, New Delhi, 2002.

[17] E. A. Hausner and R. H. Poppenga, *Hazards Associated with the Use of Herbal and Other Natural Products*, Elsevier Inc., Third Edit, 2013.

[18] B. Kirtikar and Basu, *Indian Medicinal Plants*, vol. I, International Book Distributors, Dehradun, 2nd ed, 2nd ed. edition, 2012.

[19] N. Garg and A. Jain, "Therapeutic and medicinal uses of Karpura-a review," *International Journal of Science and Research*, vol. 6, pp. 2319–7064, 2015, http://www.ijsr.net.

[20] G. Tewari, "A review on aroma profile of Cinnamomum species in North and North East India," *World Journal of Pharmaceutical Reseaech*, vol. 6, no. 11, pp. 1–22, 2017.

[21] S. S. Alam, W. Ahmad, M. Rizwanullah, and M. Muzammil, "Healing of a traumatic wound with herbo-medicinal ointment; Marham-E-Raal: a case study," *Journal of Pharmaceutical and Scientific Innovation*, vol. 9, no. 6, pp. 152–155, 2020.

[22] P. Zuccarini and G. Soldani, "Camphor: benefits and risks of a widely used natural product," *Acta Biologica Szegediensis*, vol. 53, pp. 77–82, 2009.

[23] Anonymus, *National Formulary of Unani Medicine. th Part 6 ., Part IV*, Central Council of Research of Unani Medicine, New Delhi, 2011.

[24] A. Sultana, W. Begum, R. Saeedi et al., "Experimental and computational approaches for the classification and correlation of temperament (Mizaj) and uterine dystemperament (Su'-I-Mizaj Al-Rahim) in abnormal vaginal discharge (Sayalan Al-Rahim) based on clinical analysis using support vector Mach," *Complexity*, vol. 2022, Article ID 5718501, 2022.

[25] S. Narayan and N. Singh, "Camphor poisoning-an unusual cause of seizure," *Medical Journal, Armed Forces India*, vol. 68, no. 3, pp. 252-253, 2012.

[26] F. Barrueto, *Camphor*, Elsevier, USA, 2nd ed. edition, 2005.

[27] A. P. Ansari, S. H. Sana, and H. Ansari, "The concept of Abd ā l-i-Adwiya (drug substitution / therapeutic interchange) in Unani medicine: a critical appraisal," *Journal of Advanced Research in Pharmaceutical Sciences and Pharmacology Interventions*, vol. 3, pp. 1–11, 2020, https://www.researchgate.net/publication/343047047_The_Concept_of_Abdal-i-Adwiya_Drug_Substitution_Therapeutic_Interchange_in_Unani_Medicine_A_Critical_Appraisal.

[28] A. Razi, *Kitab al-Abdāl*, Central Council of Research of Unani Medicine, New Delhi, 1st ed. edition, 1999.

[29] I. Sina, *Al-Qanun fi'l Tibb*, Idarae Kitab-us-Shifa, New Delh, 2010.

[30] N. Ghani, *Khazainul Advia Vol. I-IV*, Idarae Kitabus Shifa, New Delhi, 2001.

[31] Anonymus, *National Formulary of Unani Medicine. th Part 6., Part II*, Central Council of Research of Unani Medicine, New Delhi, 2011.

[32] Anonymus, *National Formulary of Unani Medicine. th Part 6 ., Part III.V*, Central Council of Research of Unani Medicine, New Delhi, 2011.

[33] Anonymus, *National Formulary of Unani Medicine. th Part 6 ., Part VI*, Central Council of Research of Unani Medicine, New Delhi, 2011.

[34] Anonymus, *National Formulary of Unani Medicine. th Part 6 ., Part I*, Central Council of Research of Unani Medicine, New Delhi, 2011.

[35] D. K. Poudel, A. Rokaya, P. K. Ojha et al., "The chemical profiling of essential oils from different tissues of *Cinnamomum camphora* L. and their antimicrobial activities," *Molecules*, vol. 26, no. 17, p. 5132, 2021.

[36] L. Y. Fan, Q. Lin, N. Y. Yang, and L. H. Chen, "Analgesic effects of the essential oil from *Cinnamomum camphora* against nitroglycerin-induced migraine in mice," *Indian Journal of Pharmaceutical Sciences*, vol. 82, pp. 166–170, 2020.

[37] H. Jiang, J. Wang, L. Song et al., "Gc×Gc-tofms analysis of essential oils composition from leaves, twigs and seeds of *Cinnamomum camphora* l. presl and their insecticidal and repellent activities," *Molecules*, vol. 21, no. 4, p. 423, 2016.

[38] S. C. Joshi, R. C. Padalia, D. S. Bisht, and C. S. Mathela, "Terpenoid diversity in the leaf essential oils of Himalayan Lauraceae species," *Chemistry & Biodiversity*, vol. 6, no. 9, pp. 1364–1373, 2009.

[39] S. Jianyu, "Composition and biological activities of the essential oil extracted from a novel plant of *Cinnamomum camphora* Chvar. Borneol," *Journal of Medicinal Plant Research*, vol. 6, pp. 3487–3494, 2012.

[40] S. H. Lee, D. S. Kim, S. H. Park, and H. Park, "Phytochemistry and applications of *Cinnamomum camphora* essential oils," *Molecules*, vol. 27, no. 9, p. 2695, 2022.

[41] J. Fischer and U. Dethlefsen, "Efficacy of cineole in patients suffering from acute bronchitis: a placebo-controlled double-blind trial," *Cough*, vol. 9, pp. 1–5, 2013.

[42] W. Kehrl, U. Sonnemann, and U. Dethlefsen, "Therapy for acute nonpurulent rhinosinusitis with cineole: results of a double-blind, randomized, placebo-controlled trial," *The Laryngoscope*, vol. 114, no. 4, pp. 738–742, 2004.

[43] H. Worth and U. Dethlefsen, "Patients with asthma benefit from concomitant therapy with cineole: a placebo-controlled, double-blind trial," *The Journal of Asthma*, vol. 49, no. 8, pp. 849–853, 2012.

[44] H. Worth, C. Schacher, and U. Dethlefsen, "Concomitant therapy with cineole (Eucalyptole) reduces exacerbations in COPD: a placebo-controlled double-blind trial," *Respiratory Research*, vol. 10, no. 1, 2009.

[45] S. Wang, D. Zhang, J. Hu et al., "A clinical and mechanistic study of topical borneol-induced analgesia," *EMBO Molecular Medicine*, vol. 9, no. 6, pp. 802–815, 2017.

[46] Y. Karashima, N. Damann, J. Prenen et al., "Bimodal action of menthol on the transient receptor potential channel TRPA1," *The Journal of Neuroscience*, vol. 27, no. 37, pp. 9874–9884, 2007.

[47] M. S. Melo, A. G. Guimarães, M. F. Santana et al., "Anti-inflammatory and redox-protective activities of citronellal," *Biological Research*, vol. 44, no. 4, pp. 363–368, 2011.

[48] K. Maerkel, S. Durrer, M. Henseler, M. Schlumpf, and W. Lichtensteiger, "Sexually dimorphic gene regulation in brain as a target for endocrine disrupters: developmental exposure of rats to 4-methylbenzylidene camphor," *Toxicology and Applied Pharmacology*, vol. 218, no. 2, pp. 152–165, 2007.

[49] H. Yang, P. Xu, W. Song, and X. Zhai, "Anti-tyrosinase and antioxidant activity of proanthocyanidins from *Cinnamomum camphora*," *International Journal of Food Properties*, vol. 24, no. 1, pp. 1265–1278, 2021.

[50] T. Selescu, A. C. Ciobanu, C. Dobre, G. Reid, and A. Babes, "Camphor activates and sensitizes transient receptor potential melastatin 8 (TRPM8) to cooling and icilin," *Chemical Senses*, vol. 38, no. 7, pp. 563–575, 2013.

[51] M. A. Khan, N. A. Khan, I. A. Qasmi, G. Ahmad, and S. Zafar, "Antidiarrhoeal activity of Arque-Ajeeb, a compound formulation of Unani medicine in rats," *Oriental Pharmacy and Experimental Medicine*, vol. 4, no. 2, pp. 87–90, 2004.

[52] R. Vaghardoost, S. G. Majd, H. Tebyanian et al., "The healing effect of sesame oil, camphor and honey on second degree burn wounds in rat," *World Journal of Plastic Surgery*, vol. 7, pp. 67–71, 2018, http://www.ncbi.nlm.nih.gov/pubmed/29651394.

[53] N. Z. Ahmed, G. D. John Davis, A. A. Khan et al., "Arq Ajīb - a wonder Unani formulation for inhibiting SARS-CoV-2 spike glycoprotein and main protease - an *in silico* approach," *Journal of Complementary and Integrative Medicine*, vol. 9, no. 6, pp. 152–155, 2022.

[54] M. H. G. Kanaan, S. A. Anah, G. A. Jasim, and A. Ghasemian, "In-vitro protoscolicidal and immunomodulatory effects of *Cinnamomum camphora* and Ziziphora tenuior against Echinococcus granulosus protoscolices," *Reviews in Medical Microbiology*, vol. 32, no. 1, pp. 45–50, 2021.

[55] A. Sultana, A. F. Joonus, and K. Rahman, "Effect of Marham-i-Raal on episiotomy wound healing: a single-arm pre-and post-treatment study," *Cellmed Orthocellular Medicine and Pharmaceutical Association*, vol. 11, pp. 17.1–17.4, 2021.

[56] M. M. I. Zafar, F. Hassan, S. B. S. Naqvi et al., "Evaluation of antibacterial activity of camphor, benzoin, cubebs, fenugreek, apricot and cinnamon leaf against standard cultures and clinical isolates of an array of organisms, Pakistan," *Journal de Pharmacologie*, vol. 36, pp. 69–75, 2019.

[57] N. Khanna, T. Nazli, K. M. Siddiqui, M. Kalaivani, and Raisur-Rahman, "A non-inferiority randomized controlled clinical trial comparing unani formulation & psoralen plus ultraviolet a sol in chronic plaque psoriasis," *The Indian Journal of Medical Research*, vol. 147, no. 1, pp. 66–72, 2018.

[58] I. Mahdi, W. B. Bakrim, G. T. M. Bitchagno, H. Annaz, M. F. Mahmoud, and M. Sobeh, "Unraveling the phytochemistry, traditional uses, and biological and pharmacological activities of Thymus algeriensis Boiss. & Reut," *Oxidative Medicine and Cellular Longevity*, vol. 2022, Article ID 6487430, 2022.

[59] Q. Guo, F. Li, Y. Duan et al., "Oxidative stress, nutritional antioxidants and beyond," *Science China. Life Sciences*, vol. 63, no. 6, pp. 866–874, 2020.

[60] T. Hussain, G. Murtaza, E. Metwally et al., "The role of oxidative stress and antioxidant balance in pregnancy," *Mediators of Inflammation*, vol. 2021, Article ID 9962860, 2021.

[61] T. Hussain, B. Tan, G. Murtaza et al., "Flavonoids and type 2 diabetes: Evidence of efficacy in clinical and animal studies and delivery strategies to enhance their therapeutic efficacy," *Pharmacological Research*, vol. 152, article 104629, 2020.

[62] S. H. A. Muhamad, S. On, S. N. A. Sanusi, A. A. Hashim, and M. H. Addinna Zai, "Antioxidant activity of camphor leaves extract based on variation solvent," *Journal of Physics Conference Series*, vol. 1349, no. 1, article 012102, 2019.

[63] Z. Liu, L. Kong, S. Lu, and Z. Zou, "Application of a combined homogenate and ultrasonic cavitation system for the efficient extraction of flavonoids from *Cinnamomum camphora* leaves and evaluation of their antioxidant activity in vitro," *Journal of Analytical Methods in Chemistry*, vol. 2019, Article ID 4892635, 2019.

[64] J. Fu, C. Zeng, Z. Zeng, B. Wang, and D. Gong, "*Cinnamomum camphora* seed kernel oil ameliorates oxidative stress and inflammation in diet-induced obese rats," *Journal of Food Science*, vol. 81, no. 5, pp. H1295–H1300, 2016.

[65] L. Wang, K. Zhang, K. Zhang et al., "Antibacterial activity of Cinnamomum camphora essential oil on Escherichia coli during planktonic growth and biofilm formation," *Frontiers in Microbiology*, vol. 11, pp. 1–11, 2020.

[66] K. A. Kumar, R. K. Choudhary, B. Joshi, V. Ramya, V. Sahithi, and P. Veena, "Determination of antibacterial, antifungal activity and chemical composition of essential oil portion of unani formulation kulzam," *International Journal of Green Pharmacy*, vol. 5, no. 1, pp. 28–33, 2011.

[67] C. Ho and E. I. Wang, "Essential Oil Compositions and Bioactivities of the Various Parts of *Cinnamomum camphora* Sieb. var. linaloolifera Fujuta," *Forestry Research Quarterly*, vol. 31, pp. 77–96, 2009.

[68] A. K. Mishra, S. K. Dwivedi, N. Kishore, and N. K. Dubey, "Fungistatic properties of essential oil of Cinnamomum camphora," *Pharmaceutical Biology*, vol. 29, pp. 259–262, 1991.

[69] N. J. Kang, S. C. Han, S. H. Yoon et al., "Cinnamomum camphora leaves alleviate allergic skin inflammatory responses in vitro and in vivo," *Toxicology Research*, vol. 35, no. 3, pp. 279–285, 2019.

[70] T. A. Azhunova, S. M. Nikolaev, L. B. Buraeva, D. B. Dashiev, and S. A. Banzaraksheeva, "Hypolipidemic, anti-oxidant and anticoagulant action of camphor-25 compound," *Patologicheskaia Fiziologiia i Èksperimental'naia Terapiia*, vol. 2, pp. 16–19, 2009.

[71] M. V. Jadhav, R. C. Sharma, R. Mansee, and A. K. Gangawane, "Effect of Cinnamomum camphora on human sperm motility and sperm viability," *Journal of Clinical Research Letters*, vol. 1, pp. 1–10, 2010.

[72] P. K. Sen and S. Garg, "Wound repair and regenerating effect of ethyl acetate soluble fraction of ethanolic extract of Cinnamomum camphora leaves in wistar albino rats," *Journal of Drug Delivery and Therapeutics*, vol. 9, pp. 1173–1176, 2019.

[73] T. Dawood, "Effect of adding Cinnamomum camphora on the testosterone hormone and reproductive traits of the Awassi rams," *Kufa Journal For Veterinary Medical Sciences*, vol. 5, pp. 36–45, 2016.

[74] H. Johari, M. Abedini, and S. Fallahi, "The effect of camphor (Cinnamomum camphora) on concentration of liver enzymes in female rats," *International Journal of Latest Research in Science and Technology*, vol. 4, pp. 111–113, 2015.

[75] R. H. Poppenga, *Hazards Associated with the Use of Herbal and Other Natural Products*, Elsevier Inc., Second Edi, 2006.

[76] R. Hamidpour, S. Hamidpour, M. Hamidpour, and R. Hamidpour, "The Effect of Camphor Discovery for Treating Asthma," *Advances in Bioengineering and Biomedical Science Research*, vol. 2, no. 1, pp. 1–4, 2019.

[77] Y. Li, Q. Y. Zhang, B. F. Sun et al., "Single-cell transcriptome profiling of the vaginal wall in women with severe anterior vaginal prolapse," *Nature Communications*, vol. 12, article 87, 2021.

[78] H. Xu, N. T. Blair, and D. E. Clapham, "Camphor activates and strongly desensitizes the transient receptor potential vanilloid subtype 1 channel in a vanilloid-independent mechanism," *The Journal of Neuroscience*, vol. 25, no. 39, pp. 8924–8937, 2005.

[79] F. Akhtar, P. K. Patel, M. B. B. Heyat et al., "Smartphone addiction among students and its harmful effects on mental health, oxidative stress, and neurodegeneration towards future modulation of anti-addiction therapies: a comprehensive survey based on SLR, research questions, and network visualization," *CNS & Neurological Disorders - Drug Targets*, vol. 21, 2022.

[80] B. N. Teelhawod, F. Akhtar, M. B. B. Heyat et al., "Machine learning in E-health: a comprehensive survey of anxiety," in *2021 International Conference on Data Analytics for Business and Industry (ICDABI)*, pp. 167–172, Sakheer, Bahrain, 2021.

[81] B. Guragai, O. AlShorman, M. Masadeh, and M. B. B. Heyat, "A Survey on Deep Learning Classification Algorithms for Motor Imagery," in *2020 32nd International Conference on Microelectronics (ICM)*, pp. 1–4, Aqaba, Jordan, 2020.

[82] S. Sheikh, M. B. Heyat, O. AlShorman, M. Masadeh, and F. Alkahatni, "A review of usability evaluation techniques for augmented reality systems in education," in *2021 Innovation and New Trends in Engineering, Science and Technology Education Conference (IETSEC)*, pp. 1–6, Amman, Jordan, 2021.

[83] F. Akhtar, J. P. Li, M. B. Heyat et al., "Potential of blockchain technology in digital currency: a review," in *2019 16th International Computer Conference on Wavelet Active Media Technology and Information Processing*, pp. 85–91, Chengdu, Sichuan, China, 2019.

[84] A. Sultana, K. Rahman, M. B. Heyat, F. Akhtar, and A. Y. Muaad, "Role of inflammation, oxidative stress, and mitochondrial changes in premenstrual psychosomatic behavioral

symptoms with anti-inflammatory, antioxidant herbs, and nutritional supplements," *Oxidative Medicine and Cellular Longevity*, vol. 2022, Article ID 3599246, 2022.

[85] M. B. Bin Heyat, F. Akhtar, M. A. Ansari et al., "Progress in detection of insomnia sleep disorder: a comprehensive review," *Current Drug Targets*, vol. 22, pp. 672–684, 2021.

[86] M. B. Heyat, F. Akhtar, M. H. Khan et al., "Detection, treatment planning, and genetic predisposition of bruxism: a systematic mapping process and network visualization technique," *CNS & Neurological Disorders Drug Targets*, vol. 20, pp. 755–775, 2021.

[87] F. Akhtar, M. B. Heyat, J. P. Li, P. K. Patel, and B. Guragai, "Role of machine learning in human stress: a review," in *2020 17th International Computer Conference on Wavelet Active Media Technology and Information Processing (ICCWAMTIP)*, pp. 170–174, Chengdu, China, 2020.

Hindawi
Oxidative Medicine and Cellular Longevity
Volume 2022, Article ID 7585406, 14 pages
https://doi.org/10.1155/2022/7585406

Research Article

Bio-Functional Potential and Biochemical Properties of Propolis Collected from Different Regions of Balochistan Province of Pakistan

Ali Akbar,[1] Zareen Gul,[2] Saliha Aziz,[1] Muhammad Bilal Sadiq,[3] Jahangir Khan Achakzai,[4] Shazia Saeed,[2] Su Hlaing Chein,[5] and Hassan Sher[6]

[1]*Department of Microbiology, University of Balochistan, Quetta Balochistan, Pakistan*
[2]*Department of Botany, University of Balochistan, Quetta Balochistan, Pakistan*
[3]*School of Life Sciences, Forman Christian College (A Chartered University), Lahore, Pakistan*
[4]*Disipline of Biochemistry, Department of Natural and Basic Sciences, University of Turbat Kech, 92600 Balochistan, Pakistan*
[5]*Spectrum-Sustainable Development Knowledge, Yangon 11111, Myanmar*
[6]*Centre for Plant Sciences and Biodiversity, University of Swat, Charbagh, 19120 Khyber Pakhtunkhwa, Pakistan*

Correspondence should be addressed to Ali Akbar; aliakbar.uob@gmail.com and Su Hlaing Chein; suhlaing.shc08@gmail.com

Received 29 July 2022; Accepted 22 September 2022; Published 5 October 2022

Academic Editor: Tarique Hussain

Propolis is a well-known resinous natural substance collected by honeybees (*Apis mellifera* L.) from plants exudations. Variations in chemical composition of propolis are due to different sources from which it is collected and change in climate and geographical location. In this study, different propolis samples were collected from different regions of Balochistan and examined for its chemical composition, total phenolics and total flavonoid contents, and antioxidant potential by using DPPH radical scavenging assay and antimicrobial activity. Bioactive components analysis revealed the presence of steroids, carbohydrates, flavonoids, coumarins, cardiac glycosides, quinones, anthraquinones, terpenoids, tannins, and phlobatannins at different levels. The total phenolics contents were ranged from 2.9343 ± 1.247 to 6.0216 ± 2.873 mg GAE g^{-1}, and flavonoid contents were found to be 0.1546 ± 0.087 to 0.6586 ± 0.329 mg QE $g^{-1,}$ respectively. The antioxidant ability of each extract was analyzed by their concentration having 50% inhibition (IC_{50}). The propolis sample P3 possessed lower $IC_{50} 27.07 \pm 0.73$ mg mL^{-1} with higher % inhibition of DPPH radical, and P8 showed lower % inhibition by having $IC_{50} 84.43 \pm 2.07$ mg mL^{-1}. The antibacterial activity of all samples was analyzed against a wide group of bacteria including *Escherichia coli*, *Staphylococcus aureus*, *Pseudomonas aeruginosa*, and *Klebsiella pneumonia* and propolis extract (P4) was highly active against *Klebsiella pneumoniae* with the maximum diameter of zone of inhibition 20.33 ± 1.52 mm, and propolis extract (P3) showed maximum zone of inhibition against *Escherichia coli* 19.06 ± 1.90, while propolis extract (P2) was found less active with minimum diameter of zone of inhibition 7.46 ± 1.50 mm. The antifungal activity of extract was considered as active against the fungal species. Propolis extract (P3) showed 82% of zone of inhibition against *Aspergillus Niger*, and propolis extract (P1) was highly active against *Aspergillus parasiticus* with 80% of zone of inhibition. By comparing the vibration frequencies in wave numbers of the sample spectrograph acquired from an FTIR spectrophotometer, the functional groups present in the extracts were identified. The presence of seven elements (Fe, Zn, Mn, Ni, Pb, Cd, and Cr) was analyzed through atomic absorption spectrophotometer. The obtained concentrations were within the permissible ranges established by the World Health Organization. The GC-MS analysis revealed the presence of 80 different compounds belonged to different classes. The obtained results confirmed the imperative potential of propolis which can be used in various biological applications.

1. Introduction

Honeybees like Apis mellifera L. collect propolis, a sticky adhesive natural substance, from the buds, leaves, and other parts of plants and trees [1]. Propolis is rich in natural compounds which mainly depend on the type of plant accessible to the bees, geographical origin, and collection season. Propolis contains phenolic compounds (flavonoids, phenolic acids, and their esters) that have promising biological actions such as antibacterial, anti-inflammatory, and antioxidant potential [2]. Propolis usually comprises of 50% resin and plant balm, 30% wax, 10% volatile oils, 5% pollen, and 5% other organic residues [3]. More than 300 chemicals have been found in propolis samples from various geographical origins, according to current investigations [4]. Both volatile and nonvolatile fractions of propolis from various botanical and geographic origins were discovered to contain a wide range of chemical compounds, including aldehydes, organic acids, esters, hydrocarbons, cyclic compounds, terpenes, flavonoid aglycones, phenolic acids and their esters, phenolic aldehydes, alcohols, ketones, sesquiterpenes, quinones, and coumarins [5].

The widespread use of propolis in modern and traditional medicine has heightened interest in its chemical composition. Because of the presence of numerous components, propolis is becoming more popular as a natural medication and additional food. Propolis' chemical ingredients defend against oxidative stress-related chronic diseases such as cancer and metabolic disorders [4]. It serves as a body defense agent against free radicals; propolis as a natural substance has promising antioxidant potential [2]. Previous studies reported the antibacterial potential of propolis extract against *Mycobacterium tuberculosis*; moreover, the extract synergized the effect of established anti tubercular drugs such as isoniazid [6]. Propolis and its components were also reported with promising anti-*Helicobacter pylori* activity. Propolis is used in a wide range of cosmetic products such as creams, shampoos, and lotions [7]. Propolis composition may vary with botanical and geographical origins. In this study, propolis collected from different regions of Balochistan province of Pakistan was analyzed for chemical composition and bioactive potential.

2. Materials and Methods

2.1. Sample Collection. The propolis samples were collected from different regions of Balochistan province: Ziarat (P1), Kalat (P2), Sibi (P3), Kohlu (P4), Hub (P5), Bela (P6), Musa Khail (P7), and Jaffar Abad (P8).

2.2. Sample Preparation. To avoid direct sun exposure, all propolis samples were dried for 2-3 weeks at room temperature in dark containers. The dried samples were grounded by mechanical grinder to particle size of about 10–80 μm [8].

2.3. Maceration Extraction. Dried propolis sample (10 g) was extracted with 100 mL ethanol as extraction solvent following standard procedures described by Akbar et al. [9]. The flask was intermittently shaken for 24 h followed by filtration through Whatman No. 1 filter. The extracts were concentrated with the help of rotary evaporator followed by freeze drying to obtained powdered extract.

2.4. Phytochemical Analysis. The presence of phytochemicals such as alkaloids, tannins, cardiac glycosides, anthraquinones, saponins, flavonoids, coumarins, quinones, steroids, terpenoids, and phlobatannins in propolis extracts was determined by using standard protocols [9, 10].

2.5. Total Phenolic and Flavonoid Contents. TPC and TFC were determined using colorimetric methods as described by Sadiq et al. [11]. Gallic as was used as a reference standard for TPC, and quercetin was used as reference standard for TFC. Results were expressed as mg of gallic acid equivalent per gram for TPC and mg of quercetin equivalent per gram for TFC.

2.6. DPPH Free Radical Scavenging Activity. Antioxidant activity of propolis extract was evaluated by DPPH free radical scavenging ability. Propolis extract (50 μl) was treated with 5 mL of DPPH (40 PPM produced in ethanol), and the reaction mixture was held at room temperature and in the dark for 30 minutes. At 517 nm, the absorbance of the resulting combination was measured. DPPH solution was used as control. DPPH inhibition (%) was calculated by Equation (1):

$$\text{DPPH inhibition}(\%) = [(\text{A1} - \text{A2})/\text{A1}] \times 100. \quad (1)$$

In above equation, $A1$ is the control (DPPH) absorbance, while $A2$ is absorbance of extract. The IC_{50} value expresses the antioxidant ability of the extract. The IC_{50} value required for 50% DPPH inhibition was estimated from the relationship curve of scavenging activities against different concentrations of propolis sample.

2.7. Fourier Transform Infrared Analysis (FTIR). The extract was chemically characterized by FTIR spectrometer (Nicolet, Avatar 360). The sample (5 μL) was placed in FTIR and spectrum was recorded in the range of 4000-500 cm^{-1} with resolution of 4 cm^{-1}.

2.8. Total Protein Analysis by Lowry's Method. The protein content of propolis extract was determined by using the Lowry's method [12]. Briefly, 4.5 mL of reagent 1 (48 mL of 2% sodium carbonate in 0.1 N NaOH +1 mL of 1% $KNaC_4H_4O_6.4H_2O$+1 mL of 0.5% $CuSO_4.5H_2O$) was added to 0.5 mL of each extract and incubated for 15 min at room temperature. After that 0.5 mL of freshly prepared reagent 2 (2 mL Folin Ciocalteu reagent, 2 mL distilled water) was mixed rapidly into the mixture and incubated for 30 min in dark. Bovine serum albumin (BSA) was used as a standard for the procedure, and deionized water was used as blank. Subsequently, the absorbance of the standard solutions and sample extract was measured at 660 nm. The quantification was performed in triplicate, and the amount of protein was expressed as mg BSAE g^{-1} of sample [13].

2.9. Carbohydrate Analysis. Carbohydrates were estimated by phenol sulfuric reagent method. 0.5 mL of extract was treated with 0.05 mL of 80% phenol followed by 5 mL of concentrated sulfuric acid and allowed to stand for 10 min. The mixture was shaken and placed for 10 to 20 min in a

water bath at 25 to 30 °C, and change in characteristic yellow orange color was observed before readings were taken. The absorbance was measured at 510 nm with glucose, used as standard, and deionized water was used as blank. The results were expressed as mg GE g^{-1} [13].

2.10. Antibacterial Activity. The propolis extract was evaluated against different bacterial strains (*Escherichia coli*, *Staphylococcus aureus*, *Pseudomonas aeruginosa*, and *Klebsiella pneumoniae*) by agar well diffusion assay. Mueller Hinton Agar (Oxoid, UK) plates were prepared, and the bacterial culture (10^7 CFU/ml) was spread over the agar plates. Wells were made by 6-mm cork borer in agar plates, and 170 μL of three concentrations (25, 50, and 100 mg mL^{-1}) of each extract were introduced into the agar wells. Doxycycline was used as positive control, whereas dimethyl sulfoxide (DMSO) was used as negative control. Incubation was carried out for 24 h at 37 °C. The results were expressed in terms of diameter of inhibition zone around the wells [14].

2.11. Antifungal Activity. For antifungal activity, 2 g of propolis extract and 1 mL DMSO were added to freshly prepared Sabouraud dextrose agar (Oxoid, UK), and after homogenization, 25 mL of the agar was added into each petri plate. After solidification, 6-mm diameter wells were made in agar by cork borer and fungal plugs (*Aspergillus parasiticus*, *Aspergillus niger*, and *Aspergillus flavus)* of same size were inoculated into wells. The antifungal drug fluconazole was used as a reference. Plates were incubated at 37 °C for 72 h, and the diameter of inhibition zone around the well was recorded [14]. Results are calculated by the following equation:

$$\%\text{Inhibition} = 100 - \text{linear growth in test(mm)/linear growth in control(mm)} \times 100. \quad (2)$$

2.12. Antileishmanial Assay. The antileishmanial activity of propolis extracts was evaluated by following the method [14] with slight variations. Propolis extracts were analyzed against *L. major* (promastigotes) in culture by 96-well plate. Simply, 1×10^7 cells/mL of promastigotes at log phase was used. The promastigotes were grown in NNN biphasic medium, and 1 mg mL^{-1} of the stock solution was prepared in DMSO. A twofold serial dilution of each sample was carried out, and 10 μL of each dilution with 50 μL of the promastigotes log-phase culture was dispensed to each well of a 96-well plate. Glucantime were used as a standard drug. Plates were incubated at 37 °C for 72 hours, after which 1 mL of DMSO was added to each well, and 20 mL of NBT solution (5 mg/mL in phosphate buffer, pH 7.2) was used to confirm the mortality of the test and standard drugs. The IC_{50} values were computed using the linear regression approach, and the absorbance was measured using a Microplate Reader (RT-6000) at 630 nm. The percent of cell viability is calculated by using the following equations:

$$\%\text{cell viability} = \text{Absorbance of test sample/Absorbance of control} \times 100, \quad (3)$$

$$\%\text{inhibition} = 100 - \%\text{viability}, \quad (4)$$

2.13. MTT Cell Assay. The cytotoxic effect of propolis extracts against HeLa cell line (cervical cancer carcinoma) was determined by using MTT 3-(4,5-dimethylthiazol-2-yl)-2,5-diphenyltetrazolium bromide colorimetric assay as described by Javed et al. [15]. HeLa cell line was cultured at 37 °C in a humidified atmosphere with 5% CO_2 in minimal essential medium supplemented with 10% FBS, 100 mg mL^{-1} streptomycin and 100 units mL^{-1} penicillin. After that, 180 mL of cell suspensions (1×106 cell mL^{-1}) were added in 96-well plates and treated with 100 mg mL^{-1} of each extract and incubated for 48 h. By dissolving MTT in phosphate-buffered saline (PBS, pH 7.2), 20 mL (5 mg mL^{-1} in phosphate buffer) of 0.5 percent 3-(4,5-dimethylthiazol-2-yl)-2,5-diphenyltetrazolium bromide (MTT solution) was added, and the mixture was then incubated for 3 hours at 37 °C to determine the viability of the cells. After the incubation period, the supernatant in each well was carefully removed, and 1 mL of DMSO was then added to each well. Utilizing a UV spectrophotometer, absorbance at 570 nm was used to calculate the amount of formazan produced. Doxorubicin (100 mg mL^{-1}) served as the standard medication, and DMSO served as the negative control. Measurements were made to determine the concentration necessary for 50% inhibition (IC_{50}). The percent of cell viability was calculated by using the following equation:

$$\%\text{cell viability} = \text{Absorbance of test sample/Absorbance of control} \times 100. \quad (5)$$

2.14. Atomic Absorption Spectrophotometry for Trace Elements. Trace elements Fe, Zn, Mn, Ni, Pb, Cd, and Cr analyses were carried out through atomic absorption Perkin Elmer 3110 spectrophotometer with hollow cathode lamps as radiation source operated at 5 mA at 393 and 279 nm wavelengths and acetylene air flame as fuel. Digestion of each sample was done according to a previously reported protocol [14, 16]. Briefly, 0.5 g powder of each sample was taken, and 8 mL mixture of acids (5 mL nitric acid, 2 mL sulfuric acid, and 1 mL perchloric acid) was added. After 24 h, the mixture was heated for 30 min at 60 °C at 150 °C, further heated at 150 °C for 15 min, and allowed the solution to settle. The digested mixture was then transferred to a 50-mL volumetric flask and filled with distilled water before being filtered through Whatman No. 1 filter paper. After wet digestion, these produced solutions were tested for element detection, and the findings were given in μg g^{-1}.

2.15. Gas Chromatography-Mass Spectrometry Analysis. The propolis sample was analyzed using a Shimadzu (TQ-8040) series GC-MS system (Tokyo, Japan) equipped with an AOC-20i auto sampler supplied with experimental

Table 1: Phytochemical analysis of propolis collected from different sites.

S. no	Phytochemical test	P1	P2	P3	P4	P5	P6	P7	P8
1.	Carbohydrates	+	+	+	+	+	+	−	+
2.	Cardiac glycosides	−	−	+	+	+	+	+	+
3.	Tannins	−	+	+	−	+	+	−	+
4.	Steroids	+	+	+	+	+	+	+	+
5.	Terpenoids	−	+	+	+	+	−	+	+
6.	Flavonoids	+	+	+	+	+	+	−	−
7.	Saponins	+	+	−	+	−	+	+	+
8.	Coumarin	+	+	+	+	+	−	+	−
9.	Quinones	+	+	−	+	+	+	+	+
10.	Anthraquinones	−	+	+	+	+	−	+	+
11.	Phlobatannins	+	+	+	+	+	+	−	+

Note: (+) sign indicates the presence of phytochemicals, while (−) sign indicates the absence.

conditions for the Rxi-5 MS capillary column length = 30 m, id = 0.25 mm, and film thickness = 0.25 mm (Bellefonte PA, USA). A sample of 2 μL was injected with an auto sampler in a split ratio of 10 : 1 and the carrier gas helium at a flow rate of 1 ml/min. The mass spectrum was obtained by electron ionization at 70 eV with a mass scan mode range of 45-500 amu (atomic mass units). The injector temperature was set at 280 °C, and the oven temperature was programmed from 50 °C for 3 min and then increased at the rate of 175 °C at 3 °C/min for 5 min and finally to 200 °C for 5 °C/min for 25 min. The solvent cut time was 2.00 min, and the end GC–MS time was 74 min. By comparing the mass spectrum records of the discovered compounds with those of the NIST 14 and 14s (National Institute of Standards and Technology) Libraries, the identification and composition of the compounds were confirmed. The components of propolis were identified by mass spectrometry using their names, molecular formulas, molecular weights, and structures.

2.16. Statistical Analysis. The results of all analyses were carried out in triplicate and the data were presented as the mean ± standard deviation (SD). The inhibitory concentrations (IC_{50}) were measured by the linear regression method.

3. Result

3.1. Phytochemical Analysis. Phytochemical analysis of propolis extracts indicated the presence of various phytochemicals such as steroids, carbohydrates, flavonoids, coumarins, cardiac glycosides, quinones, anthraquinones, terpenoids, tannins, and phlobatannins at different levels. In sample P1, all phytochemical constituents were present except tannins, anthraquinones, terpenoids, and cardiac glycosides. Cardiac glycosides were found absent in sample P2. Steroids, carbohydrates, flavonoids, coumarins, cardiac glycosides, quinones, anthraquinones, terpenoids, tannins, and phlobatannins were abundant in P3 and P5, but saponins were lacking in P4, which contained all phytochemicals except tannins. Terpenoids, coumarins, and anthraquinones were not found in P6, although carbohydrates, tannins, flavonoids, and phlobatannins were P7, while P8 was rich in all phytochemicals except flavonoids and coumarins in the current study as presented in Table 1.

3.2. Total Flavonoid and Phenolic Contents. In present study TFC was ranged between 0.1546 ± 0.087 and 0.6586 ± 0.329 mg of quercetin g^{-1} of propolis extract. The propolis extract (P1) collected from Ziarat region expressed maximum flavonoid content (0.6586 ± 0.329) and the extract (P6) from Bela region have the lowest content (0.1546 ± 0.087) mg of quercetin g^{-1} of propolis extract presented in (Table 2).

In present study, TPC varied between 2.9343 ± 1.247 and 6.0216 ± 2.873 mg of gallic acid g^{-1} of propolis extract. The propolis extract (P3) collected from Sibi was with maximum phenolic content (6.0216 ± 2.873), and the sample (P5) from Hub region showed lowest content (2.9343 ± 1.247) mg of gallic acid g^{-1}, respectively as shown in (Table 2).

3.3. DPPH Free Radicals Scavenging Activity. DPPH scavenging ability of propolis extracts was evaluated by their concentrations having 50% inhibition (IC_{50}) that is the concentration of extract required to scavenge 50% DPPH free radicals. The lower IC_{50} values indicated higher antioxidant potential and same for radical scavenging activity. In the present study, an inverse relation between DPPH scavenging activity and IC_{50} was found. The extract (P3) from Sibi was seen to have greatest antioxidant activity with smallest IC_{50} value of (27.07 ± 0.73 mg mL^{-1}), and the sample (P8) collected from Jaffar Abad with highest IC_{50} value (84.43 ± 2.07 mg mL^{-1}) showed lowest antioxidant potential as presented in (Table 3).

3.4. FTIR Analysis. FTIR was used to determine the presence of functional groups in propolis extract. Functional groups were examined according to the peaks in spectra [17]. The most stable peaks in the spectrum were at 3734-3648 cm^{-1}, and designated to elongation of O-H of hydroxyl bonds and N-H of amino acids, the peaks at 3338-3334 cm^{-1} were given to the O-H stretching of phenolic compounds, and peaks at 3000-3200 cm^{-1} were assigned to the C-H stretching of flavonoids and aromatic rings. Peaks at 2973-2833 cm^{-1} were associated with methylene asymmetric stretching, and the peaks at approximately 2721-2075 cm^{-1} designated to the hydrocarbons' symmetric stretching. The peaks at 1683-1636 cm^{-1} were assigned to C=O, C=C stretching vibrations of flavonoids and designated to the N-H asymmetric stretching of amino acids. In addition, there was a high correspondence of the signals at 1558-1506 cm^{-1}; ascribed to elongation of flavonoids and aromatic rings, the peak at 1456-1400 cm^{-1} were associated with bending vibrations C-H, CH_2, and CH_3 of flavonoid and aromatic rings. The main characteristics of extract was explained from the signals of stretching vibrations and bending at 1399-1310 cm^{-1} and 1230-1203 cm^{-1} attributed to asymmetrical O-H and C-CO bending of hydrocarbons and phenol groups. The peaks at 1198-1000 cm^{-1} were designated to stretching vibrations of C-C of flavonoids and

Table 2: Total flavonoid content and total phenolic content of different propolis extracts.

Sample	Total flavonoid content $(\text{mg QE g}^{-1}) \pm \text{SD}$	Total phenolic content $(\text{mg GAE g}^{-1}) \pm \text{SD}$
P1	0.6586 ± 0.329	5.9209 ± 2.880
P2	0.6025 ± 0.339	4.1074 ± 3.445
P3	0.3873 ± 0.543	6.0216 ± 2.873
P4	0.5923 ± 0.297	5.7347 ± 4.099
P5	0.4291 ± 0.449	2.9343 ± 1.247
P6	0.1546 ± 0.087	5.9194 ± 3.247
P7	0.5636 ± 0.399	5.0588 ± 1.005
P8	0.6467 ± 0.305	4.9128 ± 2.589

Results are expressed as mean of three determinations ± standard deviation.

Table 3: DPPH free radicals scavenging activity of propolis extracts and IC_{50} (mg mL^{-1}).

Samples	DPPH% scavenging activity	IC_{50} mg mL^{-1}
P1	56.81 ± 3.08	79.09 ± 0.91
P2	66.43 ± 4.37	41.04 ± 1.28
P3	68.39 ± 1.02	27.07 ± 0.73
P4	64.19 ± 09.5	54.75 ± 0.97
P5	64.44 ± 3.26	52.53 ± 1.16
P6	61.64 ± 2.13	60.81 ± 0.65
P7	58.52 ± 2.08	77.03 ± 1.04
P8	52.79 ± 1.09	84.43 ± 2.07

Results are expressed as mean of three determinations ± standard deviation.

secondary alcohol groups. Specifically, a symmetrical stretching at 945-881 cm^{-1} linked to C-C-O, primary, and secondary alcohols. The FTIR results confirmed the presence of hydrocarbons, flavonoids, aromatic compounds, phenolic compounds, primary and secondary alcohols, and amino acids as presented in (Table 4).

3.5. Total Protein Content. Protein content in propolis extract was determined by using Lowery's method. The total proteins content ranged from 0.018 ± 0.020 to 0.834 ± 0.282 mg of BSAE g^{-1} of propolis extract. Sample P3 showed maximum protein content 0.834 ± 0.282, whereas the minimum protein content was found in P8 as 0.018 ± 0.020 mg of BSA g^{-1} of propolis extract as presented in (Table 5).

3.6. Total Carbohydrates Content. The results of carbohydrate content in propolis extract ranged from 0.356 ± 0.066 to 3.616 ± 0.802 mg of glucose g^{-1} of propolis extract. The highest content of carbohydrate found in (P1) as 3.616 ± 0.802 mg/g, whereas the lowest content was found in P5 as 0.356 ± 0.066 mg/g, respectively. Results are shown in (Table 5).

3.7. Antibacterial Activity. Propolis extract (P3) showed maximum zone of inhibition against *E. coli* (19.06 ± 1.90 mm) followed by *S. aureus* with the diameter of inhibition zone of 16.73 ± 2.01 mm, *P. aeruginosa* 15.73 ± 1.41 mm, and *K. pneumoniae* 14.66 ± 2.51 mm, respectively. The propolis extract (P4) collected from Kohlu was highly active against *K. pneumoniae* than other gram-positive and gram-negative bacteria with the maximum diameter of zone of inhibition 20.33 ± 1.52 mm. Propolis extract (P2) was found less active against S. *aureus* and *E. coli* with the diameter of inhibition zone of 7.44 and 8.66 mm, respectively (Table 6).

3.8. Antifungal Activity. The antifungal activity of propolis extracts was analyzed against three fungal species *A. parasiticus*, *A. niger*, and *A. flavus*. *A. niger* was highly sensitive to propolis extract (P3) with inhibition of 82% followed by *A.s flavus* with 81%, while *A. parasiticus* showed the 79% inhibition, respectively. Among other samples, propolis extract (P1) was highly active against *A. parasiticus* with 80% of inhibition (Table 7).

3.9. Antileishmanial Assay. For formative antileishmanial activity of promastigotes (*L. major*), antileishmanial assay was performed against two propolis samples P3 and P5. A twofold serial dilution of each sample (1 mg mL^{-1}) was carried out. The standard drug Glucantime ($IC_{50} = 7.31 \pm 0.64\ \text{mg mL}^{-1}$) was used to compare the parasite inhibition with each extract. The IC_{50} value was observed for both extract against *L. major*, and P5 showed good potential ($IC_{50} = 11.25 \pm 1.09\ \text{mg mL}^{-1}$), followed by the P3 ($IC_{50} = 16.35 \pm 0.26\ \text{mg mL}^{-1}$) by comparing the values of each extract with the standard. The results revealed that all concentrations showed highest % inhibition and the viability increased with a decrease in concentration, as presented in Figure 1.

3.10. MTT Cell Assay. Evaluation of the anticancer activity of propolis extracts was carried out through MTT cell assay against HeLa cell line. The assay was performed at 100 mg mL^{-1} for each extract by using doxorubicin as a standard drug. According to the obtained results, each extract exhibited anticancer activity, and % inhibition was expressed in terms of IC_{50}. Comparing the results to the standard (IC_{50} 11 ± 0.32 mg mL^{-1}), it was revealed that the propolis extract (P3) showed the highest anticancer activity with lowest IC_{50} (15 ± 0.26 mg mL^{-1}) followed by P5 having IC_{50} value of 19 ± 0.12 mg mL^{-1}, respectively, (Figure 2).

Table 4: Fourier Transform infrared analysis of propolis extract.

Range (cm^{-1})	Type of signal	Type of link	Main attribution
3740-3550	Elongation	O-H and N-H	Hydroxyls and amino acids
3366-3333	Stretching	O-H	Phenolic groups
3000-3200	Stretching	C-H, aromatics	Flavonoids and aromatic rings
2971-2830 and 2730-2066	Elongation symmetric and asymmetric	C-H	Hydrocarbons
1699-1610	Asymmetric bending vibrations	C=O	Lipids, flavonoids and amino acids
1560-1505	Elongation	C=C, aromatics	Flavonoids and aromatic rings
1450-1415	Bending vibrations	C-H, $C-H_2$ and $C-H_3$	Flavonoids and aromatic rings
1399-1310	Bending vibration	C-H	CH3 group of flavonoids
1232-1200	Bending vibration (O-H) and asymmetrically bending (C-CO)	O-H and C-CO	Hydrocarbons
1198-1000	Stretching vibration (C-C) and bending (C-OH)	C-C and C-OH	Flavonoids and secondary alcohol groups

Table 5: Estimation of total protein content and total carbohydrate content.

Samples	Total proteins $(mg\,BSAE\,g^{-1}) \pm SD$	Total carbohydrate $(mg\,GE\,g^{-1}) \pm SD$
P1	0.478 ± 0.143	3.616 ± 0.802
P2	0.316 ± 0.184	0.377 ± 0.124
P3	0.834 ± 0.282	0.554 ± 0.080
P4	0.765 ± 0.266	0.498 ± 0.787
P5	0.282 ± 0.363	0.356 ± 0.066
P6	0.663 ± 0.220	0.629 ± 0.106
P7	0.442 ± 0.112	0.598 ± 0.063
P8	0.018 ± 0.020	0.504 ± 0.068

Results are expressed as mean ± SD for three readings.

Table 6: Antibacterial activity of propolis extract against pathogenic bacteria.

Samples	Diameter of zone of inhibition against pathogen			
	E. coli	*S. aureus*	*K. pneumoniae*	*P. aeruginosa*
P1	14.3 ± 1.50	13.8 ± 1.25	13.8 ± 3.01	16.5 ± 1.80
P2	8.66 ± 0.28	7.46 ± 1.50	12.83 ± 2.25	12.73 ± 1.55
P3	19.06 ± 1.90	16.73 ± 2.01	14.66 ± 2.51	15.73 ± 1.41
P4	12.5 ± 1.32	13.66 ± 2.51	20.33 ± 1.52	11.83 ± 2.84
P5	10.83 ± 1.25	12.1 ± 0.85	11.5 ± 1.5	12.5 ± 1.5
P6	18.5 ± 1.5	14.83 ± 2.56	17.5 ± 1.5	10.15 ± 1.32
P7	10.5 ± 2.29	11.76 ± 1.36	16.76 ± 2.54	10.86 ± 1.20
P8	13.6 ± 1.50	13.83 ± 1.25	12.73 ± 2.96	15.1 ± 0.85
Doxycycline	20.4 ± 1.51	23.8 ± 1.73	23.4 ± 2.14	23.5 ± 1.53

Note. Inhibitory zones in mm as mean ± standard deviation of three replicates.

3.11. Atomic Absorption Spectrophotometer of Trace Elements. For the determination of trace elements, different propolis samples P1-P8 were analyzed by atomic absorption Perkin Elmer 3110 spectrophotometer. According to the obtained results, Fe was $443.38 \pm 0.3\,\mu g\,g^{-1}$ in P1, $534.67 \pm 0.2\,\mu g\,g^{-1}$ in P2, $823.84 \pm 0.1\,\mu g\,g^{-1}$ in P3, $355.17 \pm 0.7\,\mu g\,g^{-}$ in P4, $528.96 \pm 0.1\,\mu g\,g^{-1}$ in P5, $1331.46 \pm 0.5\,\mu g\,g^{-1}$ in P6, $1079.68 \pm 0.1\,\mu g\,g^{-1}$ in P7, and $663.31 \pm 0.4\,\mu g\,g^{-1}$ in P8, respectively. Concentration of Zn was in range of $0.257 \pm 0.5\,\mu g\,g^{-1}$ in P1 to $0.472 \pm 1.2\,\mu g\,g^{-1}$ in P2.

Table 7: Antifungal activity (% inhibition) of propolis extracts against pathogenic fungi.

Samples	*A. parasiticus*	*A. niger*	*A. flavus*
P1	80	65	69
P2	75	71	74
P3	79	82	81
P4	34	50	65
P5	38	46	52
P6	71	69	73
P7	64	67	63
P8	76	52	68
Fluconazole	92	89	94

Results are expressed as % age of inhibition zone against *Aspergillus parasiticus*, *Aspergillus niger*, and *Aspergillus flavus*.

Concentration of Mn varied in the range of 040.86 ± 0.8 $\mu g\,g^{-1}$ in P5 to 077.44 ± 0.6 $\mu g\,g^{-1}$in P3. Among all samples, lower Ni concentration was 1.25 ± 0.16 $\mu g\,g^{-1}$ in P2, and higher was 64.23 ± 0.4 $\mu g\,g^{-1}$ in P7. Pb was 4.58 ± 1.2 $\mu g\,g^{-1}$ in P6 to 10.50 ± 0.6 $\mu g\,g^{-1}$ in P7, respectively. Higher concentration of Cd was 0.412 ± 0.5 $\mu g\,g^{-1}$ in P4, and lower concentration was 0.010 ± 0.2 $\mu g\,g^{-1}$ present in P7. Cr was present in very less amount in all evaluated samples. Minimum concentration was 0.001 ± 0.4 $\mu g\,g^{-1}$ in P5, and maximum concentration was 0.115 ± 0.3 $\mu g\,g^{-1}$ in P1, respectively, as presented in (Table 8).

3.12. GC-MS Analysis. The results of the GC-MS analysis showed that a total of 80 different compounds were identified. These compounds belonged to various chemical classes. Results of identified compounds were presented in terms of their retention time, concentration (area %), molecular formula, and molecular weight as shown in Table 9. The identified compound belonged to ethers, alcohols, terpenes, phenolics, acids, and other aromatic compounds.

4. Discussion

The current study was aimed to analyze the bioactive components, antimicrobial activity, and the presence of trace elements of propolis samples collected from different areas of Balochistan. Phytochemical analysis is critical for identifying bioactive molecules that may lead to medication development and discovery. Propolis contains a wide variety of secondary metabolites such as steroids, flavonoids, tannins, alkaloids, and terpenoids, which have antibacterial, antitumor, anthelmintic, anti-inflammatory, and antiradical activities [18]. The ethanolic extract of propolis obtained from different parts of Balochistan contained almost all the components, tannins, cardiac glycosides, saponins, terpenoids, flavonoids, coumarin, quinones, phlobatannins, and anthraquinones. The intensity of the color may indicate a higher concentration of these compounds in propolis extract. The ethanolic extract of Malaysian propolis has been found to contain flavonoids, alkaloids, cardiac glycosides, tannins, saponins, phenol, xanthoproteins, terpenoids, and resins [19]. Variations in propolis composition are highly influenced due to phytogeographical diversity, climate change, seasonal variations, and specie of the queen bee [1].

Polyphenols are leading group of phytochemicals and deemed as active component of propolis. These compounds comprise are good reducing agents due to which they act as good antioxidants. The results concerning TPC indicated variations among all extracts. The highest TPC value 6.0216 ± 2.873 mg of gallic acid g^{-1} was found in P3 extract whereas minimum value 2.9343 ± 1.247 mg of gallic acid g^{-1} was obtained in the sample P5 as shown in (Table 2). The results of total phenolic contents of ethanolic extracts were comparatively minimum than other reported studies [3] and supported by the previously observations of [1] who evaluated the total phenolic contents of propolis collected from peripheral region of Faisalabad Pakistan. Results are also in accordance with [20] in propolis samples collected from different regions of Korea.

Flavonoid contents are known to have antimicrobial, antioxidant, anti-inflammatory, and antidepressant potential. These contents are good antioxidants having strong reducing potentials. In present study, total flavonoid content was ranged between 0.1546 ± 0.087 and 0.6586 ± 0.329 mg of quercetin g^{-1} of propolis extract. The propolis extract (P1) collected from Ziarat region expressed maximum flavonoid content (0.6586 ± 0.329) and the extract (P6) from Bela region have the lowest content (0.1546 ± 0.087) mg of quercetin g^{-1} of propolis extract presented in (Table 2). Results of current study are minimum than other reported studies from different location in Turkey [3], Pakistan [1], China [21], and Iran [22]. According to Choi et al. [20], the variations in total phenolic and total flavonoids of propolis samples depend on their geographic origin.

The DPPH assay for analyzing free radical scavenging activity is widely accepted feature for the evaluation of antioxidant potential of natural extracts. The antioxidant ability of propolis extracts of different regions of Balochistan were analyzed by their concentrations having 50% inhibition (IC_{50}) that is the concentration of extract required to scavenge 50% DPPH free radicals. The lower IC_{50} values indicated higher antioxidant potential and same for radical scavenging activity. In present study, an inverse relation between DPPH scavenging activity and IC_{50} was found. The extract (P3) from Sibi was seen to have greatest antioxidant activity with smallest IC_{50} value of (27.07 ± 0.73 $mg\,mL^{-1}$), and the sample (P8) collected from Jaffar Abad with highest IC_{50} value (94.43 ± 2.07 $mg\,mL^{-1}$) showed lowest antioxidant potential as presented in (Table 3). According to Zehra, Yildiz, Şahin, Asadov, and Kolayli [23], the antioxidant potential of propolis extracts have a positive correlation with their phenolic, flavonoids, and other bioactive contents. Recentlym Shahbaz et al. [1] reported the DPPH free radical scavenging activity of propolis up to 70% which is in accord to the findings of current study. In a similar way Choi et al. [20] concluded that propolis extract from Korea exhibits higher antioxidant activity as compared to

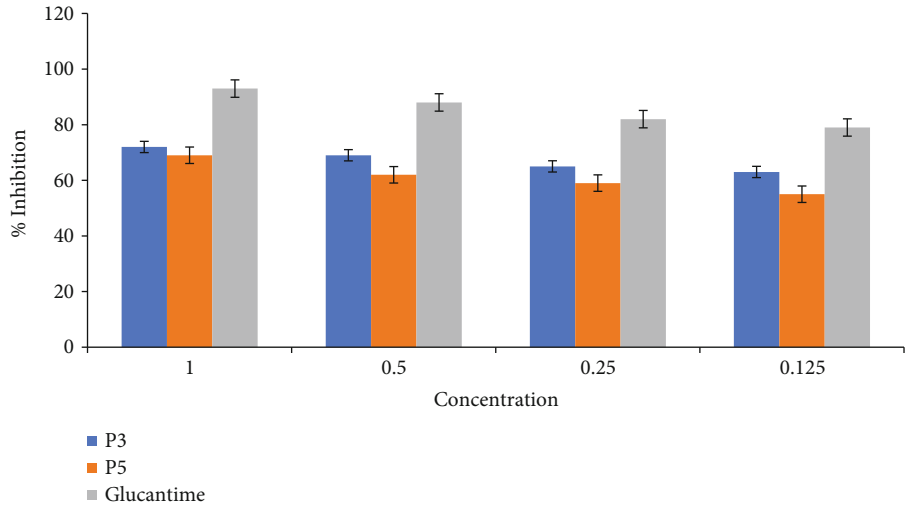

Figure 1: Efficiency of ethanolic extracts of propolis P3 and P5 against promastigotes (*Leishmania major*).

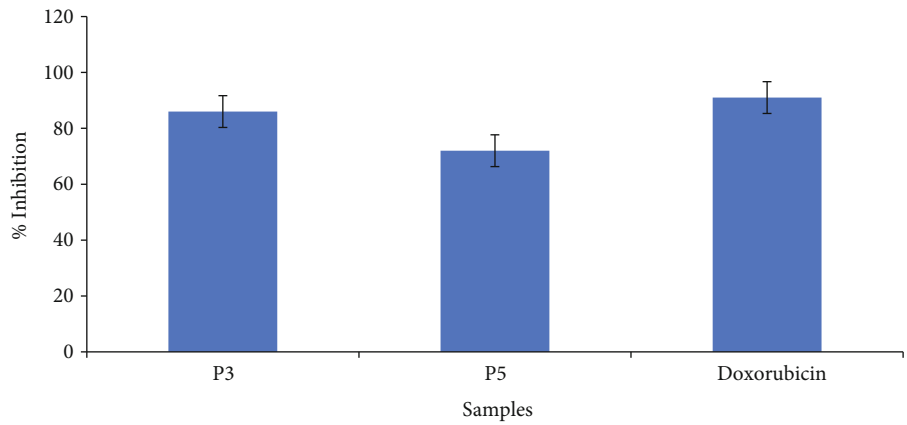

Figure 2: Anticancer activity of propolis extracts P3 and P5 against HeLa cell line. Bars represent the standard deviation of the mean.

Table 8: Atomic absorption spectrophotometry of trace elements found in propolis extract.

Elements	P1 ($\mu g\, g^{-1}$)	P2 ($\mu g\, g^{-1}$)	P3 ($\mu g\, g^{-1}$)	P4 ($\mu g\, g^{-1}$)	P5 ($\mu g\, g^{-1}$)	P6 ($\mu g\, g^{-1}$)	P7 ($\mu g\, g^{-1}$)	P8 ($\mu g\, g^{-1}$)
Fe	443.38 ± 0.3	534.61 ± 0.2	823.84 ± 0.1	355.17 ± 0.7	528.96 ± 0.1	1331.46 ± 0.5	1079.68 ± 0.1	663.31 ± 0.4
Zn	0.257 ± 0.5	0.472 ± 1.2	0.445 ± 0.3	0.290 ± 0.12	0.450 ± 0.8	0.378 ± 1	0.462 ± 0.12	0.297 ± 0.1
Mn	042.91 ± 0.12	055.96 ± 0.13	077.44 ± 0.6	044.53 ± 0.1	040.86 ± 0.8	052.28 ± 0.3	070.60 ± 0.3	052.17 ± 0.2
Ni	5.92 ± 0.13	1.25 ± 0.16	7.97 ± 0.3	7.93 ± 0.1	13.19 ± 0.5	23.14 ± 0.2	64.23 ± 0.4	26.23 ± 0.7
Pb	6.57 ± 0.12	7.37 ± 0.8	5.78 ± 0.12	9.62 ± 0.8	5.42 ± 0.12	4.58 ± 1.2	10.50 ± 0.6	8.66 ± 0.7
Cd	0.312 ± 0.7	0.217 ± 0.1	0.108 ± 0.1	0.412 ± 0.5	0.112 ± 0.5	0.023 ± 1	0.010 ± 0.2	0.221 ± 0.6
Cr	0.015 ± 0.3	0.007 ± 0.13	0.009 ± 0.5	0.013 ± 0.3	0.001 ± 0.4	0.002 ± 0.6	0.002 ± 0.1	0.006 ± 0.6

Note. Fe = iron; Zn = zinc; Mn = manganese; Ni = nickel; Pb = lead; Cd = cadmium; and Cr = chromium.

Brazilian propolis due to higher concentration of flavonoids and phenolic contents. Furthermore, Al-Juhaimi et al. [3] concluded that DPPH inhibition is the direct function of phenolic contents present in samples. Current results for the percent inhibition of DPPH were in agreement with their findings.

The FTIR analysis of different propolis extract was carried out to characterize functional groups present in samples. The FTIR results confirmed the presence of hydrocarbons, flavonoids, aromatic compounds, phenolic compounds, primary and secondary alcohols, and amino acids. According to Ahmed, Amirat, Aissat, Aissa, and Khiati

Table 9: The major compounds analyzed in ethanolic extract of propolis by GCMS analysis.

S. #	Retention time (min)	Area (%)	Name of the compound	Mol. Formula	Mol. Weight
1.	3.035	0.00	2-Chloroethyl methyl sulfoxide	C_3H_7ClOS	126
2.	3.083	0.01	Carbonochloridic acid, ethyl ester	$C_3H_5ClO_2$	108
3.	3.145	0.02	Acetic acid, mercapto-, methyl ester	$C_3H_6O_2S$	106
4.	3.175	0.01	Propyl mercaptan	C_3H_8S	76
5.	3.305	0.01	Dimethyl sulfoxide	C_2H_6OS	78
6.	3.401	0.02	Cyclohexan-1,4,5-triol-3-one-1-carboxylic acid	$C_7H_{10}O_6$	190
7.	3.425	0.03	S-methyl methanethiosulfonate	$C_2H_6OS_2$	110
8.	3.469	0.02	o,S,S′-Trimethyl phosphorotrithioate	$C_3H_9OPS_3$	188
9.	3.579	0.10	Dichloromethylpho sphonic acid	$CH_3Cl_2O_3P$	164
10.	3.706	0.10	Sulfide, ethyl propyl	$C_5H_{12}S$	104
11.	3.810	0.05	Carbamimidoylsulfanylacetic acid	$C_3H_6N_2O_2S$	134
12.	3.860	0.09	Ethane, 1-chloro-1-fluoro-	C_2H_4ClF	82
13.	3.905	0.05	Propane, 1,1,1,2-tetrachloro-	$C_3H_4Cl_4$	180
14.	3.990	0.06	1,6-Dideoxy-l-mannitol	$C_6H_{14}O_4$	150
15.	4.100	0.14	1,3-Difluoro-2-propanol	$C_3H_6F_2O$	96
16.	4.195	0.10	Diethoxymethyl acetate	$C_7H_{14}O_4$	162
17.	4.361	0.16	Silane, bis(fluoromethyl)dimethyl-	$C_4H_{10}F_2Si$	142
18.	4.400	0.12	Methoxyacetaldehyde diethyl acetal	$C_7H_{16}O_3$	148
19.	4.510	0.12	2-propanol, 1-methoxy-	$C_4H_{10}O_2$	90
20.	4.560	0.21	Diethyl pyrocarbonate	$C_6H_{10}O_5$	162
21.	6.717	5.87	Ethyl fluoroformate	$C_3H_5FO_2$	92
22.	7.214	0.21	Glycerin	$C_3H_8O_3$	92
23.	7.592	0.01	1,2-Propanediol, 1-acetate	$C_5H_{10}O_3$	118
24.	7.908	0.03	p-Dioxane-2,3-diol	$C_4H_8O_4$	120
25.	7.950	0.10	Fluoroacetic acid	$C_2H_3FO_2$	78
26.	7.987	0.05	Propanoic acid, 2-hydroxy-, methyl ester,	$C_4H_8O_3$	104
27.	8.071	0.03	1-butanol, 2-nitro-	$C_4H_9NO_3$	119
28.	8.216	0.05	2-Butenal, 2-methyl-, (E)-	C_5H_8O	84
29.	8.366	0.13	Butyl lactate	$C_7H_{14}O_3$	146
30.	8.424	0.04	2,3-Butanediol, [R-(R∗,R∗)]-	$C_4H_{10}O_2$	90
31.	8.685	0.01	2-Mercaptopropanoic acid	$C_3H_6O_2S$	106
32.	8.712	0.01	Ethanethiol, 2-(diethylboryloxy)-	$C_6H_{15}BOS$	146
33.	8.750	0.01	Butanoic acid, 4-chloro-3-oxo-, methyl ester	$C_5H_7ClO_3$	150
34.	8.853	0.05	3-Cyclopentene-1-acetaldehyde, 2-oxo-	$C_7H_8O_2$	124
35.	8.970	0.01	1-Nitro-2-acetamido-1,2-dideoxy-d-glucitol	$C_8H_{16}N_2O_7$	252
36.	9.156	0.04	2-Furanmethanol	$C_5H_6O_2$	98
37.	9.325	0.02	4,5-Dihydro-2-methylimidazole-4-one	$C_4H_6N_2O$	98
38.	9.535	0.09	Cyclopent-4-ene-1,3-dione	$C_5H_4O_2$	96
39.	9.595	0.01	1-(4-Methoxy-2-nitroanilino)-1- a-d arabinofuranose	$C_{12}H_{16}N_2O_7$	300
40.	9.685	0.01	Butanoic acid, heptafluoro-, 4-butoxy-4-oxobutyl ester	$C_{12}H_{15}F_7O_4$	356
41.	9.998	0.31	2(5H)-Furanone	$C_4H_4O_2$	84
42.	10.297	0.12	6-Oxa-bicyclo[3.1.0]hexan-3-one	$C_5H_6O_2$	98
43.	11.215	0.01	11-Bromo-1-undecanol, TMS derivative	$C_{14}H_{31}BrOSi$	322
44.	11.479	0.01	2,4-Dihydroxy-2,5-dimethyl-3(2H)-furan-3-one	$C_6H_8O_4$	144
45.	11.295	0.01	Decane, 3,4-dimethyl-	$C_{12}H_{26}$	170
46.	12.265	0.01	Cyclohexanone, 2-ethyl-4-methoxy-	$C_9H_{16}O_2$	156
47.	12.360	0.02	Cyclotetrasiloxane, octamethyl-	$C_8H_{24}O_4Si_4$	296
48.	13.845	0.02	2,4-Di-tert-butylthiophenol	$C_{14}H_{22}S$	222

Table 9: Continued.

S. #	Retention time (min)	Area (%)	Name of the compound	Mol. Formula	Mol. Weight
49.	14.075	0.05	Silane, 2-butenylmethoxymethylph	$C_{12}H_{18}OSi$	206
50.	14.155	0.07	Arsenous acid, tris(trimethylsilyl) ester	$C_9H_{27}AsO_3Si_3$	342
51.	14.250	0.02	2,2′-(Methylenedithio)bispropanoic acid	$C_7H_{12}O_4S_2$	224
52.	14.310	0.01	Benzene, 4-ethyl-1,2-dimethoxy-	$C_{10}H_{14}O_2$	166
53.	14.840	0.01	1H-Pyrrole-2-ethanamine, 1-methyl-	$C_7H_{12}N_2$	124
54.	14.965	0.02	1,2-Bis(dimethylphosphino)ethane	$C_6H_{16}P_2$	150
55.	16.175	0.01	Zidovudine	$C_{10}H_{13}N_5O_4$	276
56.	17.715	0.02	l-Gala-l-ido-octose	$C_8H_{16}O_8$	240
57.	20.125	0.01	DL-phenylalanine	$C_9H_{11}NO_2$	165
58.	21.935	0.01	Fumaric acid, 2-chlorophenyl decyl ester	$C_{20}H_{27}ClO_4$	366
59.	22.555	0.01	2-Methoxy-4-vinylphenol	$C_9H_{10}O_2$	150
60.	24.350	0.01	Methyl abietate isomer	$C_{21}H_{32}O_2$	316
61.	24.440	0.01	Isovanillic acid, 2TMS derivative	$C_{14}H_{24}O_4Si_2$	312
62.	24.762	0.20	Methyl 4-methoxysalicylate, TMS derivative	$C_{12}H_{18}O_4Si$	254
63.	24.795	0.10	Resorcinol, 2TMS derivative	$C_{12}H_{22}O_2Si_2$	254
64.	25.145	0.02	3,5-Dinitrobenzyl alcohol, benzyldimethylsilyl ether	$C_{16}H_{18}N_2O_5Si$	346
65.	25.695	0.01	Cyclotetrasiloxane, 2,4,6,8-tetrame	$C_4H_{16}O_4Si_4$	240
66.	25.795	0.01	2-Furanone, 3,4-dihydroxytetrahydro	$C_4H_6O_4$	118
67.	28.296	0.05	1,3-Benzenedimethanethiol	$C_{14}H_{26}S_2Si_2$	314
68.	29.740	0.01	Epimethendiol-diOTMS	$C_{26}H_{48}O_2Si_2$	448
69.	31.995	0.02	Ethyl-1-thio-.beta.-d-glucopyranosi	$C_8H_{16}O_5S$	224
70.	32.500	0.06	6-Desoxy-l-gulitol	$C_6H_{14}O_5$	166
71.	38.351	0.01	Ethyl iso-allocholate	$C_{26}H_{44}O_5$	436
72.	39.620	0.01	d-mannitol, 1-decylsulfonyl-	$C_{16}H_{34}O_7S$	370
73.	40.154	0.12	Hexadecanoic acid, methyl ester	$C_{17}H_{34}O_2$	270
74.	44.621	0.03	1,1′-Bicyclopentyl, 2-hexadecyl-	$C_{26}H_{50}$	362
75.	47.395	0.02	Bicyclo[2.2.1]heptane, 2,2-dimethyl-5-methylene-	$C_{10}H_{16}$	136
76.	47.787	0.01	Oleic acid	$C_{18}H_{34}O_2$	282
77.	48.545	0.01	Thiazolidine, 2-methyl-2-(4-nitrophenyl)-	$C_{10}H_{12}N_2O_2S$	224
78.	48.726	0.04	Methyl stearate	$C_{19}H_{38}O_2$	298
79.	48.888	0.01	9,12-Octadecadienoic acid (Z,Z)-, methyl ester	$C_{19}H_{34}O_2$	294
80.	49.202	0.18	cis-Vaccenic acid	$C_{18}H_{34}O_2$	282

[24], the propolis' FTIR data revealed the presence of O-H stretch and C-H bound for alcohol at frequencies between 2848 cm^{-1} and 2915 cm^{-1}, as well as O-H and C=O at 1168 cm^{-1} and C-O and C-C at 1000 cm^{-1}, respectively. The OH group can be seen in FTIR spectra between 3550 and 3540 cm^{1}, and an asymmetric CH2 methyl group can be seen at 2900 cm^{1}, according to a recent publication [17]. The geochemistry of the soil where propolis is grown may have a significant impact on the content and components of propolis.

Protein content in propolis extract was determined by using Lowery's method. The total proteins content was ranged from 0.018 ± 0.020 to 0.834 ± 0.282 mg of BSAE g^{-1} of propolis extract. Sample P3 showed maximum protein content 0.834 ± 0.282, whereas the minimum protein content was found in P8 as 0.018 ± 0.020 mg of BSAg^{-1} of propolis extract. Total protein contents were in agreement with the values reported by Laaroussi et al. [25] with revealed values of 1.65% to 6.18%, respectively. Current results were also in accordance with findings of [26] for propolis from different geographic regions. The presence of protein in propolis is mostly related to the pollen fraction added by bees for bee glue production.

Carbohydrates are one of the three macronutrients used in diet, along with protein. The total carbohydrates in propolis extract were estimated using the phenol sulfuric technique. The carbohydrate content of propolis extract in our study ranged from 0.356 ± 0.066 mg of glucose g^{-1} to 3.616 ± 0.802 mg of glucose g^{-1}. The highest carbohydrate content was identified in P1 at 3.616 ± 0.802, while the lowest was found in P5 at 0.356 ± 0.066. Current findings are in agreement with the values reported by Laaroussi et al. [25]. According to Fikri, Popova, Sulaeman, and Bankova [27],

the harvesting techniques of propolis may influence the carbohydrate contents due to sugar residues from honey. Additionally, buds are the potential sources of carbohydrates in propolis.

Rich in polyphenols and flavonoids, propolis has excellent antibacterial power against pathogenic germs without having any negative effects. Propolis antimicrobial properties are extremely significant for the bee colony. By interfering with the enzymatic activity of bacteria, propolis prevents the growth of bacteria. Propolis can harm both gram-positive and gram-negative bacteria. The propolis' primary ingredients, phenols, flavonoids, phenolic acids, and their esters, are what give it its potent antibacterial activity [28]. In current study propolis showed antibacterial activity against *S. aureus*, *E. coli*, *K. pneumonia*, and *P. aeruginosa*. Propolis extract (P3) showed maximum zone of inhibition against *E. coli* 19.06 ± 1.90 followed by *S. aureus* with the diameter of inhibition zone of 16.73 ± 2.01, *P. aeruginosa* 15.73 ± 1.41, and *K. pneumoniae* 14.66 ± 2.51 mm, respectively. The propolis extract (P4) collected from Sibi was highly active against *K. pneumoniae* than other gram-positive and gram-negative bacteria with the maximum diameter of zone of inhibition 20.33 ± 1.52 mm, while propolis extract (P2) was found less active with minimum diameter of zone of inhibition 7.46 ± 1.50 mm followed by *E. coli* with the diameter of inhibition zone of 8.66 ± 0.28 mm, respectively. The antibacterial effects of propolis results on *S. aureus* and *Escherichia coli* are in agreement with Shahbaz et al. [1] and relatively higher than Afata et al. [18]. Studies have linked propolis from Brazil, Egypt, Mangolia, and Albania to antibacterial activity against *S. aureus*, with zones of inhibition of 24, 21.8, 24.3, and 21.8 mm, respectively [1]. Different extraction techniques very certainly produce different chemical components, which could ultimately cause variations in the antibacterial activity [29]. It is unclear if the antibacterial effect is brought on by a single active component or by the combination of several active elements found in propolis extracts. However, Al-Juhaimi et al. [3] concluded that propolis strength against bacterial strains may be due to the strong effect of phenolics, flavonoids ,and other components present in propolis extracts.

The antifungal activity of propolis extracts was tested in terms of the % age of inhibition zone against three filamentous fungal species *A. parasiticus*, *A. niger*, and *A. flavus*. All extracts were found highly active against all three fungi. *Aspergillus Niger* was highly sensitive to propolis extract (P3) with the percentage of zone of inhibition 82% followed by *A. flavus* with 81%, while *A. parasiticus* showed the percentage of zone of inhibition 79%, respectively. Among other samples, propolis extract (P1) was highly active against *A. parasiticus* with 80% of zone of inhibition. The great potential for antifungal activity and trend was found in consistent with the literature [30, 31]. However, the present findings were relatively higher than Afata et al. [18], where extracts showed minimum results against *Aspergillus niger*. The antifungal activity of each extract may be due to the presence of antifungal compounds that include linalool and other phenolic and flavonoid compounds reported in different propolis extracts [32].

Efficiency of ethanolic extracts of propolis P3 and P5 against promastigotes (*Leishmania major*) was determined by antileishmanial assay. A twofold serial dilution of ($1\,\mathrm{mg\,mL^{-1}}$) sample was carried out, and the activity was checked at different concentrations (1, 0.5, 0.25, and $0.125\,\mathrm{mg\,mL^{-1}}$) against standard drug Glucantime proven by IC_{50} values (IC_{50} $7.31 \pm 0.64\,\mathrm{mg\,mL^{-1}}$). The activity was carried out under an incubation period of 48 h at 22 °C. Moreover, 50% inhibitory concentration was observed for each extract and the P5 showed good potential (IC_{50} $11.25 \pm 1.09\,\mathrm{mg\,mL^{-1}}$), followed by P3 ($IC_{50}$ $16.35 \pm 0.26\,\mathrm{mg\,mL^{-1}}$). The results revealed that the highest activity was observed in the concentration of ($1\,\mathrm{mg\,mL^{-1}}$) and the viability increased with a decrease in concentration and the %inhibition decreased. Propolis extracts have been evaluated against leishmanial parasites from different part of the world and have proven with significant leishmanicidal potentials. According to Do Nascimento et al. [33], the ethanolic extract of Brazilian red propolis showed IC_{50} of $37.9\,\mu\mathrm{g\,mL^{-1}}$ and nanoparticles of red propolis extract IC_{50} of $31.34\,\mu\mathrm{g\,mL^{-1}}$. Previously, Duran, Muz, Culha, Duran, and Ozer [34] analyzed antileishmanial activity of Turkey propolis with excellent leishmanicidal effect IC_{50} of 250 and $500\,\mu\mathrm{g\,mL^{-1}}$. In another study, Brazilian propolis extract showed IC_{50} $49\,\mu\mathrm{g\,mL^{-1}}$ against *L. major* species, while the Bulgarian propolis extract showed leishmanicidal activity for *L. chagasi* and *L. major* species with IC_{50} 2.8 to $41.3\,\mu\mathrm{g\,mL^{-1}}$. According to scientific literature, excellent leishmanicidal activity of propolis can be explained by the presence of various flavonoids, such as quercetin, fisetin, and luteolin, and some phenolic acids and phenolic acid esters in the extracts [33]. Description of the literature demonstrated that some flavonoids have leishmanicidal effects with IC_{50} values from 0.6 to $0.8\,\mu\mathrm{g\,mL^{-1}}$.

Cancer is one of the major diseases that are enlightened by increasing the human body cells in with the failure to be controlled. Therefore, various studies have been reported to develop new therapeutic treatments for cancer. Propolis is a rich source of biologically potent compounds regulating several cellular processes. The anticancer activity of propolis from various regions of Balochistan Pakistan have not been reported and published by other researchers until date, but researchers from different parts of the world reported propolis to have in cytotoxic effects against different destructive cell lines. According to Forma and Bryś [4], both propolis extracts and active chemicals can decrease cancer cell growth, angiogenesis, and metastasis while also stimulating apoptosis. It may potentially have an impact on cancer multidrug resistance. Few studies reported the strong cytotoxic activity of galangin, syringic acid, caffeic acid, and ferulic acid against different cancer cell lines [35]. In vitro, an ethanolic extract of Algerian propolis and galangin reduced the number of B16F1 melanoma cells compared to a reference [36]. Recently, Fang, Xiong, Xu, Yin, and Luo [37] reported the proapoptotic activity of polyphenolic compounds such as ferulic acid and caffeic acid on human tongue squamous carcinoma cells (CAL-27). Current results were higher than the findings of Dastan et al. [22] who reported propolis methanolic extracts with (IC_{50}) 702.5 and $177.7\,\mu\mathrm{g\,mL^{-1}}$ after 24 and 48 hours.

The AAS is a method of analysis that provides the estimated concentration of different elements. Different samples P1, P2, P3, P4, P5, P6, P7, and P8 were examined for the content of two nonessentials (lead and cadmium) and five essential elements (iron, zinc, nickel, chromium, and manganese).

The human body requires iron for the synthesis of oxygen to produce red blood cells. Anemia is brought on by Fe deficiency, but excessive amounts harm body tissues. In general, iron is not thought to have negative health effects unless it is consumed in excessively high doses [14, 16]. The currents findings were ranged from 355.17 $\mu g\,g^{-1}$ in P11 to 1331.46 $\mu g\,g^{-1}$ in P13, relatively higher than previous findings [38].

Zinc is second most prevailing transition metal in organisms after iron. It promotes the carbon incorporation and terpene consumption and antioxidant enzyme activation. The concentration of Zn was in range of $0.257 \pm 0.5\ \mu g\,g^{-1}$ in P1 to $0.472 \pm 1.2\ \mu g\,g^{-1}$ in P2. Manganese is good antioxidant and important for plant and animal growth. It is a low toxic element with considerable biological application, and its deficiency causes reproductive problems in mammals, and excessive amount leads to different lungs and brain diseases [14, 16]. It helps in the synthesis and activation of many enzymes. The Mn concentration in present work varied in the range of 40.86 $\mu g\,g^{-1}$ in P10 to 77.44 $\mu g\,g^{-1}$ in P12. Current results were relatively higher than previous findings [38]. Nickel is an important element that controls different metabolic processes in plants. Nickel is present in RNA and DNA of human body where it functions in association with nucleic acids. Nickel shows carcinogenic side effects when taken in higher concentrations; however, its deficiency causes heart and liver problems [14, 16]. Among all samples, lower Ni concentration was $-5.92 \pm 0.13\ \mu g\,g^{-1}$ in P1 and higher was $64.23 \pm 0.4\ \mu g\,g^{-1}$ in P7, respectively. Current results were in accordance with previous findings [38] and higher than Zeb et al. [39]. Cadmium concentration may occur in bee products from air and mineral fertilizers, and its presence in certain concentrations in organisms can have adverse effects [40]. This toxic element can damage the brain, kidney, liver, and heart. In present work the concentration of Cd varied from $0.010 \pm 0.2\ \mu g\,g^{-1}$ present in P7 to $0.412 \pm 0.5\ \mu g\,g^{-1}$ in P4. Various studies conducted have shown Cd concentration in propolis samples [38]. However, present results were relatively higher than the permissible limit and those found in literature [39]. Long term exposure to Pb can cause severe health effects such as chronic pain, blood pressure alteration, and change in blood composition, anxiety, passivity disorders, and cancer. According to the current findings Pb was ranged from $4.58 \pm 1.2\ \mu g\,g^{-1}$ in P6 to $10.50 \pm 0.6\ \mu g\,g^{-1}$ in P7, respectively. Vehicular emission on the nearby roadway and use of fertilizers are the most important explanation for the high Pb concentration. Various studies conducted have shown Pb concentration in various propolis samples [38, 40]. Chromium was present in very less amount in all evaluated samples. Minimum concentration of Cr was $0.001 \pm 0.4\ \mu g\,g^{-1}$ in P5, and maximum concentration was $0.115 \pm 0.3\ \mu g\,g^{-1}$ in P1. Chromium concentration in all evaluated samples was less than the permissible limit. Current findings were in agreement with Achudume and Nwafor [41] and lower than the results of Ullah et al. [38].

The results of the GC-MS (gas chromatography-mass spectrometry) analysis showed that a total of 80 different compounds were present in propolis. These compounds belonged to various chemical classes such as aromatic acids, esters, alcohols, flavonoids, and terpenes. Accordingly, it is believed that the presence of flavonoids [42] may cause the antibacterial and cytotoxic effects. The compounds, hexadecanoic acid, methyl ester, 9,12-Octadecadienoic acid (Z,Z)-, and methyl ester are previously been reported for their antioxidant, anti-inflammatory, cytotoxic, and antibacterial potentials (Fahad et al., 2021).

5. Conclusion

Present study represents the data about chemical composition of propolis collected from different regions of Balochistan. Overall, the results of this report show that propolis is rich in phenolic and flavonoid contents with high antioxidant potentials. The use of propolis as an active agent for the treatment of various infectious diseases could also be supported by the strength of broad spectrum antibacterial and antifungal activities. Moreover, all analyzed samples revealed a great variation in their trace elements. However, more research is necessary to publicize the biological activity of the identified bioactive components and their therapeutic potential.

Data Availability

Major part of the data is already included in the manuscript; the remaining data will be made available on reasonable request.

Conflicts of Interest

The authors declare that they have no conflicts of interest.

Acknowledgments

We acknowledge the financial support of Higher Education Commission (HEC) Pakistan for this study under NRPU 2016 Project No. 6470-Balochistan.

References

[1] M. Shahbaz, T. Zahoor, R. Arshad et al., "Chemical profiling, HPLC characterization and in-vitro antioxidant potential of Pakistani propolis collected from peripheral region of Faisalabad," *Cellular and Molecular Biology*, vol. 67, no. 1, pp. 40–44, 2021.

[2] Y. Kara, Z. Can, and S. Kolaylı, "What should be the ideal solvent percentage and solvent-Propolis ratio in the preparation of Ethanolic Propolis extract?," *Food Analytical Methods*, vol. 15, no. 6, pp. 1707–1719, 2022.

[3] F. Y. Al-Juhaimi, M. M. Özcan, I. A. Mohamed Ahmed et al., "Bioactive compounds, antioxidant activity, fatty acid composition, and antimicrobial activity of propolis from different locations in Turkey," *Journal of Apicultural Research*, vol. 61, no. 2, pp. 246–254, 2022.

[4] E. Forma and M. Bryś, "Anticancer activity of propolis and its compounds," *Nutrients*, vol. 13, no. 8, p. 2594, 2021.

[5] A. Jihene, I. J. Karoui, A. Ameni, M. Hammami, and M. Abderrabba, "Volatile compounds analysis of Tunisian propolis and its antifungal activity," *Journal of Biosciences and Medicines*, vol. 6, no. 6, pp. 115–131, 2018.

[6] M. Romero, J. Freire, E. Pastene, A. García, M. Aranda, and C. González, "Propolis polyphenolic compounds affect the viability and structure of Helicobacter pylori in vitro," *Revista Brasileira de Farmacognosia*, vol. 29, no. 3, pp. 325–332, 2019.

[7] E. Jung, J. B. Weon, H. Ji et al., "Comparative study of the biological activity of Propolis extracts with various countries of origin as cosmetic materials," *Journal of the Society of Cosmetic Scientists of Korea*, vol. 46, no. 2, pp. 159–166, 2020.

[8] I. Al-Ani, S. Zimmermann, J. Reichling, and M. Wink, "Antimicrobial activities of European propolis collected from various geographic origins alone and in combination with antibiotics," *Medicine*, vol. 5, no. 1, p. 2, 2018.

[9] A. Akbar, I. Ali, N. U. Samiullah, S. A. Khan, Z. I. Rehman, and S. U. Rehman, "Functional, antioxidant, antimicrobial potential and food safety applications of curcuma longa and cuminum cyminum," *Pakistan Journal of Botany*, vol. 51, no. 3, pp. 1129–1135, 2019.

[10] F. Behlil, K. N. Samiullah, A. Akbar et al., "Phytochemical screening and antioxidant activity determination of some medicinally important plants of Balochistan," *Pakistan Journal of Botany*, vol. 51, no. 2, pp. 1–8, 2019.

[11] M. B. Sadiq, W. Hanpithakpong, J. Tarning, and A. K. Anal, "Screening of phytochemicals and in vitro evaluation of antibacterial and antioxidant activities of leaves, pods and bark extracts of acacia nilotica (l.) del," *Industrial Crops and Products*, vol. 77, pp. 873–882, 2015.

[12] O. H. Lowry, N. J. Rosebrough, A. L. Farr, and R. J. Randall, "Protein measurement with the Folin phenol reagent," *Journal of Biological Chemistry*, vol. 193, no. 1, pp. 265–275, 1951.

[13] F. I. Fahad, N. Barua, M. S. Islam et al., "Investigation of the pharmacological properties of Lepidagathis hyalina nees through experimental approaches," *Life*, vol. 11, no. 3, p. 180, 2021.

[14] Z. Gul, A. Akbar, and S. K. Leghari, "Elucidating therapeutic and biological potential of Berberis baluchistanica Ahrendt bark, leaf, and root extracts," *Frontiers in Microbiology*, vol. 13, article 823673, 2022.

[15] T. Javed, S. A. Raja, K. Ur Rehman, S. Khalid, N. Khalid, and S. Riaz, "In silico bimolecular characterization of anticancer phytochemicals from Fagonia indica," *Pakistan Journal of Pharmaceutical Sciences*, vol. 34, no. 3, pp. 883–889, 2021.

[16] Z. Gul, A. Akbar, S. K. Leghari et al., "Daily dose standardization based on essential and nonessential trace element presence in Berberis baluchistanica Ahrendt bark, leaf, and root," *BioMed Research International*, vol. 2022, Article ID 6811613, 9 pages, 2022.

[17] P. Mustafa, M. B. Niazi, Z. Jahan et al., "PVA/starch/propolis/anthocyanins rosemary extract composite films as active and intelligent food packaging materials," *Journal of Food Safety*, vol. 40, no. 1, article e12725, 2020.

[18] T. N. Afata, R. Nemo, N. Ishete, G. Terefe, and A. Dekebo, "Phytochemical investigation, physicochemical characterization, and antimicrobial activities of Ethiopian Propolis," *Arabian Journal of Chemistry*, vol. 15, no. 7, article 103931, 2022.

[19] U. Z. Usman, A. A. Bakar, and M. Mohamed, "Phytochemical screening and comparison of antioxidant activity of water and ethanol extract propolis from Malaysia," *International Journal of Pharmacy and Pharmaceutical Sciences*, vol. 8, no. 5, pp. 413–415, 2016.

[20] Y. Choi, D. Noh, S. Cho, H. J. Suh, K. Kim, and J. Kim, "Antioxidant and antimicrobial activities of propolis from several regions of Korea," *LWT-Food Science and Technology*, vol. 39, no. 7, pp. 756–761, 2006.

[21] Q. Ding, A. R. Sheikh, X. Gu et al., "Chinese Propolis: ultrasound-assisted enhanced ethanolic extraction, volatile components analysis, antioxidant and antibacterial activity comparison," *Food Science & Nutrition*, vol. 9, no. 1, pp. 313–330, 2021.

[22] D. Dastan, R. Mahmoudi, M. Saidijam, S. Gholamzadeh Khoei, M. Hasan Abdali, and S. Afshar, "Evaluation of chemical composition of Hamadan Propolis as a potential anticancer agent," *Jentashapir Journal of Cellular and Molecular Biology*, vol. 12, no. 2, 2021.

[23] C. Zehra, O. Yildiz, H. Şahin, A. Asadov, and S. Kolayli, "Phenolic profile and antioxidant potential of propolis from Azerbaijan," *Mellifera*, vol. 15, no. 1, pp. 16–28, 2015.

[24] M. Ahmed, M. Amirat, S. Aissat, M. A. Aissa, and B. Khiati, "FTIR characterization of Sahara honey and propolis and evaluation of its anticandidal potentials," *Acta Scientifica Naturalis*, vol. 7, no. 3, pp. 46–57, 2020.

[25] H. Laaroussi, P. Ferreira-Santos, Z. Genisheva et al., "Unraveling the chemical composition, antioxidant, α-amylase and α-glucosidase inhibition of Moroccan propolis," *Food Bioscience*, vol. 42, article 101160, 2021.

[26] N. A. Abdullah, N. Zullkiflee, S. N. Z. Zaini, H. Taha, F. Hashim, and A. Usman, "Phytochemicals, mineral contents, antioxidants, and antimicrobial activities of propolis produced by Brunei stingless bees Geniotrigona thoracica, Heterotrigona itama, and Tetrigona binghami," *Saudi Journal of Biological Sciences*, vol. 27, no. 11, pp. 2902–2911, 2020.

[27] A. M. Fikri, M. Popova, A. Sulaeman, and V. Bankova, "Stingless bees and Mangifera indica: a close relationship?," *Indian Journal of Natural Products and Resources (IJNPR) [Formerly Natural Product Radiance (NPR)]*, vol. 11, no. 2, pp. 130–134, 2020.

[28] J. Iqbal, B. A. Abbasi, R. Ahmad et al., "Phytogenic synthesis of nickel oxide nanoparticles (NiO) using fresh leaves extract of Rhamnus triquetra (wall.) and investigation of its multiple in vitro biological potentials," *Biomedicine*, vol. 8, no. 5, p. 117, 2020.

[29] M. M. Rahman, A. Richardson, and M. Sofian-Azirun, "Antibacterial activity of propolis and honey against Staphylococcus aureus and Escherichia coli," *African Journal of Microbiology Research*, vol. 4, no. 18, pp. 1872–1878, 2010.

[30] S. Ghahari, H. Alinezhad, G. A. Nematzadeh, M. Tajbakhsh, and R. Baharfar, "Biochemical composition, antioxidant and biological activities of the essential oil and fruit extract of Xanthium strumarium Linn. From Northern Iran. Journal of agricultural," *Science and Technology*, vol. 19, no. 7, pp. 1603–1616, 2017.

[31] S. Aziz, A. Akbar, Z. Gul et al., "Functional potential and chemical profile analysis of propolis oil extracted from propolis of balochistan," *Journal of Food Quality*, Article ID 4782813, 2022.

[32] M. M. Nichitoi, A. M. Josceanu, R. D. Isopescu et al., "Polyphenolics profile effects upon the antioxidant and antimicrobial activity of propolis extracts," *Scientific Reports*, vol. 11, no. 1, pp. 1–12, 2021.

[33] T. G. Do Nascimento, P. F. Da Silva, L. F. Azevedo et al., "Polymeric nanoparticles of Brazilian red propolis extract: preparation, characterization, antioxidant and leishmanicidal activity," *Nanoscale Research Letters*, vol. 11, no. 1, pp. 1–16, 2016.

[34] N. Duran, M. Muz, G. Culha, G. Duran, and B. Ozer, "GC-MS analysis and antileishmanial activities of two Turkish propolis types," *Parasitology Research*, vol. 108, no. 1, pp. 95–105, 2011.

[35] J. F. Rivero-Cruz, J. Granados-Pineda, J. Pedraza-Chaverri et al., "Phytochemical constituents, antioxidant, cytotoxic, and antimicrobial activities of the ethanolic extract of Mexican brown propolis," *Antioxidants*, vol. 9, no. 1, p. 70, 2020.

[36] L. Benguedouar, M. Lahouel, S. C. Gangloff et al., "Ethanolic extract of Algerian propolis and galangin decreased murine melanoma tumor progression in mice," *Anti-Cancer Agents in Medicinal Chemistry (Formerly Current Medicinal Chemistry-Anti-Cancer Agents)*, vol. 16, no. 9, pp. 1172–1183, 2016.

[37] D. Fang, Z. Xiong, J. Xu, J. Yin, and R. Luo, "Chemopreventive mechanisms of galangin against hepatocellular carcinoma: A review," *Biomedicine & Pharmacotherapy*, vol. 109, pp. 2054–2061, 2019.

[38] R. Ullah, F. A. Jan, H. Gulab, S. Saleem, N. Ullah, and Wajidullah, "Metals Contents in Honey, Beeswax and Bees and Human Health Risk Assessment Due to Consumption of Honey: A Case Study from Selected Districts in Khyber Pakhtunkhwa, Pakistan," *Archives of Environmental Contamination and Toxicology*, vol. 82, no. 3, pp. 341–354, 2022.

[39] J. Zeb, H. Tahir, A. Othman et al., "Geo-environmental approach to assess heavy metals around auto-body refinishing shops using bio-monitors," *Heliyon*, vol. 8, no. 1, article e08809, 2022.

[40] G. Yasin, S. Ur Rahman, M. T. B. Yousaf et al., "Phytoremediation potential of E. camaldulensis and M. alba for copper, cadmium, and lead absorption in urban areas of Faisalabad City, Pakistan. International," *Journal of Environmental Research*, vol. 15, no. 4, pp. 597–612, 2021.

[41] A. Achudume and B. Nwafor, "The ecological assessment of metals in local brands of honey in Southwest Nigeria," *African Journal of Agricultural Research*, vol. 5, no. 18, pp. 2608–2610, 2010.

[42] F. Asgharpour, A. A. Moghadamnia, S. Kazemi, H. R. Nouri, and M. Motallebnejad, "Applying GC-MS analysis to identify chemical composition of Iranian propolis prepared with different solvent and evaluation of its biological activity," *Caspian Journal of Internal Medicine*, vol. 11, no. 2, pp. 191–198, 2020.

[43] S. N. A. Syed Salleh, N. A. Mohd Hanapiah, H. Ahmad, W. L. Wan Johari, N. H. Osman, and M. R. Mamat, "Determination of total phenolics, flavonoids, and antioxidant activity and GC-MS analysis of Malaysian stingless bee Propolis water extracts," *Scientifica*, vol. 2021, Article ID 3789351, 11 pages, 2021.

[44] S. Ezzat, A. Khattaby, S. Abdelmageed, and M. A. Abd Elaal, "Cytotoxicity, antioxidant, anti-inflammatory activity, and GC-MS analysis of Egyptian propolis," *Comparative Clinical Pathology*, vol. 28, no. 6, pp. 1589–1598, 2019.

Hindawi
Oxidative Medicine and Cellular Longevity
Volume 2022, Article ID 4122253, 16 pages
https://doi.org/10.1155/2022/4122253

Research Article

A Comparison of the Antiosteoporotic Effects of Cornelian Cherry (*Cornus mas* L.) Extracts from Red and Yellow Fruits Containing Different Constituents of Polyphenols and Iridoids in Osteoblasts and Osteoclasts

Eunkuk Park,[1] **Tomasz Sozański**,[2] **Chang-Gun Lee**,[1,3] **Alicja Z. Kucharska**,[4] **Dominika Przybylska**,[4] **Narcyz Piórecki**,[5,6] **and Seon-Yong Jeong**[1]

[1]*Department of Medical Genetics, Ajou University School of Medicine, Suwon 16499, Republic of Korea*
[2]*Department of Pharmacology, Wroclaw Medical University, ul. J. Mikulicza-Radeckiego 2, 50-345 Wroclaw, Poland*
[3]*AI-Superconvergence KIURI Translational Research Center, Ajou University School of Medicine, Suwon 16499, Republic of Korea*
[4]*Department of Fruit, Vegetable and Plant Nutraceutical Technology, Wroclaw University of Environmental and Life Sciences, J. Chełmońskiego 37, 51-630 Wroclaw, Poland*
[5]*Bolestraszyce Arboretum and Institute of Physiography, Bolestraszyce 130, 37-722 Wyszatyce, Poland*
[6]*Institute of Physical Culture Sciences, Medical College, University of Rzeszów, Cicha 2A, 35-326 Rzeszów, Poland*

Correspondence should be addressed to Tomasz Sozański; tomasz.sozanski@umw.edu.pl
and Seon-Yong Jeong; jeongsy@ajou.ac.kr

Received 19 June 2022; Revised 16 August 2022; Accepted 12 September 2022; Published 3 October 2022

Academic Editor: Tarique Hussain

Background and aims. Bone remodeling in which old or damaged bone cells are removed by osteoclasts, and new bone cells are developed by osteoblasts is a key target for antiosteoporotic agents. These processes can also be modulated by nutrients. In this study, we have compared the antiosteoporotic effects of three extracts from cornelian cherry (*Cornus mas* L.) fruits: RED EXT1 extracts from red fruits, and YL EXT2 and YL EXT3 extract from yellow fruits. *Methods.* Polyphenolic and iridoid constituents of extracts were analyzed qualitatively and quantitatively using the ultraperformance liquid chromatography system coupled with a quadrupole-time of flight mass spectrometry. Primary cultured osteoblasts isolated from mouse calvarias and osteoclast-lineage primary cultured monocytes isolated from mouse bone marrow were used for the assessment of osteoblast and osteoclast differentiation. In the osteoblast culture, cellular viability, alkaline phosphatase (ALP) activity, ALP staining, and mRNA expression of Alpl and Runx2 were examined. In the osteoclast culture, the examined parameters were cellular viability, tartrate-resistant acid phosphatase (TRAP) activity and staining, and mRNA expression of Nfatc1, Ctsk, and Acp. *Results.* A total of 41 main compounds of iridoids, anthocyanins, hydrolysable tannins, phenolic acids, and flavonols were identified in the three extracts. RED EXT1 contained most of the tested polyphenols and iridoids and was the only extract containing anthocyanins. YL EXT2 contained only one iridoid, loganic acid and gallic acid. YL EXT3 comprised a mixture of iridoids and polyphenols. RED EXT1, YL EXT 2, and to a lesser extent YL EXT3 promoted osteoblast differentiation increasing significantly ALP activity and the amount of ALP-positive stained cells. All extracts upregulated mRNA expression of Alpl and Runx2. RED EXT1 caused the most significant decrease in TRAP activity and the numbers of TRAP-positive multinucleated cells. RED EXT1 caused also the most significant downregulation of mRNA expression of osteoclast related genes Nfatc1, Ctsk, and Acp5. Extracts from yellow fruits, mostly YL EXT2 caused lower, but still significant inhibitory effect on TRAP and osteoclast related genes. *Conclusions.* The main conclusion of our study is that all three extracts, especially RED EXT1 from red cornelian cherry fruits, possess the antiosteoporotic potential and may be a promising phytomedicine candidate for the prevention and treatment of osteoporosis.

1. Introduction

Osteoporosis is a common systemic bone disease characterized by the loss of bone mass and deterioration of the bone microstructure, leading to fractures and subsequent complications. An increased life expectancy in developed countries combined with comorbidities and drugs causing bone loss has resulted in osteoporosis, becoming more prominent in the last few decades. Moreover, increased levels of physical activity in elderly populations, offering several benefits but leading to a higher risk of pathological fractures, makes osteoporosis an increasingly greater medical, social, and economic challenge.

Bone remodeling is regulated by homeostasis between osteoclasts resorbing old or damaged bone cells and osteoblasts developing new bone structures [1]. The differentiation and function of osteoclasts and osteoblasts are key target areas for antiosteoporotic agents. It has been proven that bone metabolism can be modulated by nutrients [2, 3]. Recently published studies have reported that polyphenols, especially anthocyanins [4, 5], phenolic acids [6], and flavonols [7], as well as iridoids [8] and hydrolysable tannins [9] can prevent bone loss through different mechanisms. All these substances are present in cornelian cherries, in varying amounts, making their extracts promising candidates for antiosteoporotic agents.

A previous *in vitro* study demonstrated that *Cornus officinalis* Sieb. et Zucc. shared a few similar iridoid and polyphenol constituents with the cornelian cherry (*Cornus mas* L.), and it inhibits the receptor activator of nuclear factor-kappaB ligand (RANKL)-induced osteoclast differentiation [10]. Our previous studies showed that red cornelian cherries, rich in polyphenols and iridoids, prevented both cholesterol-induced dyslipidemia and atherosclerosis via the upregulation of peroxisome proliferator-activated receptors (PPARs) expression [11–14] and prevented bone loss in osteoporotic animals by inhibiting bone resorption and increasing bone formation [15]. Another study demonstrated that the pulp of cornelian cherries partially reversed impaired microarchitecture bone quality in Zucker diabetic fatty rats [16].

In the present study, we have compared the antiosteoporotic effects of three different extracts from cornelian cherry fruits: RED EXT1 from red fruits containing exceptionally anthocyanins and substantial amounts of various other polyphenols and iridoids, YL EXT2 from yellow fruits containing a single iridoid, loganic acid and gallic acid, and YL EXT3 from yellow fruits comprising substantial amounts of various iridoids and polyphenols. To investigate the effects of extracts on bone remodeling, we used an *in vitro* model of mouse primary cultured osteoblasts isolated from mouse calvarias and osteoclasts isolated from mouse bone marrow monocytes. In the osteoblast culture, the analyzed parameters were cellular viability, alkaline phosphatase (ALP) activity and amount of ALP-positive stained cells, and mRNA expression of a gene (Alpl) and transcription factor (Runx2) involved in osteoblastic bone remodeling. In osteoclast culture, the analysis pertained to cellular viability, tartrate-resistant acid phosphatase (TRAP) activity, the number of TRAP-positive multinucleated cells, and mRNA expression of transcriptional factor (Ctsk), as well as genes (Nfatc1, Acp5) involved in osteoclast differentiation and activity.

2. Materials and Methods

2.1. Reagents and Standards. All reagents and organic solvents were of analytical grade. Authentic standards of loganic acid, loganin, sweroside, cyanidin 3-*O*-glucoside, *p*-coumaric acid, ellagic acid, quercetin 3-*O*-glucoside, and kaempferol 3-*O*-glucoside were purchased from Extrasynthese (Genay, France). *Trans*-caftaric acid was purchased from the Cayman Chemical Company (Michigan, EUA, Ann Arbor, MI, USA). *Trans*-coutaric acid was purchased from Merck (Darmstadt, Germany). Methanol, acetonitrile, and formic acid were obtained from POCH (Gliwice, Poland).

2.2. Extraction, Purification, and Fractionation of Extracts. Red ('Podolski') and yellow ('Yantarnyi' and 'Flava') cornelian cherries were harvested in the Arboretum in Bolestraszyce, near Przemyśl, Poland. The plant materials were authenticated by Elżbieta Żygała, M.Sc. (Arboretum and Institute of Physiography in Bolestraszyce, Przemyśl, Poland), and adequate voucher specimens ('Yantarnyi' – BDPA 14131; 'Flava' – BDPA 8795; 'Podolski' – BDPA 10462) were deposited at the Herbariums of Arboretum in Bolestraszyce, Poland. After harvesting, the fruits were immediately frozen at −20°C.

Extracts were prepared as previously described by Lewandowski et al. [17] with some modifications. Frozen ripe cornelian cherries were shredded and heated for 5 min at 95°C using a Thermomix (Vorwerk, Wuppertal, Germany). The pulp was subsequently cooled to 50°C and depectinized at this temperature for 2 h by adding 0.5 mL/kg of Pectinex BE XXL (Novozymes A/S, Denmark). After depectinization, the pulp was pressed in a laboratory hydraulic press (SRSE, Warsaw, Poland). The pressed juice was filtered and run through an Amberlite XAD-16 resin column (Rohm and Haas, Chauny Cedex, France). Impurities were washed off with distilled water. RED EXT1 (red fruits) and YL EXT3 (yellow fruits) were eluted with 80% ethanol while YL EXT2 (yellow fruits) was eluted with up to 50% ethanol (v/v in water). The eluents were concentrated at 40°C under vacuum. The solvent was evaporated using a Rotavapor (Unipan, Warsaw, Poland) and freeze-dried (Alpha 1–4 LSC, Christ, Osterode am Harz, Germany). As a result, we have obtained three extracts from cornelian cherry fruits: RED EXT1 from red fruits containing substantial amounts of various anthocyanins, iridoids, and hydrolysable tannins with moderate or small amounts of phenolic acids and flavonols, YL EXT2 from yellow fruits containing a single iridoid, loganic acid and small amounts of phenolic acids, and YL EXT3 from yellow fruits comprising substantial amounts of various iridoids and hydrolysable tannins, and moderate or small amounts of phenolic acids and flavonols.

2.3. Qualitative Identification of Compounds by Liquid Chromatography-Mass Spectrometry (LC-MS). This method was previously described by Przybylska et al. [18]. Compounds were identified using the Acquity ultraperformance liquid chromatography (UPLC) system, coupled with a quadrupole-time of flight (Q-TOF) MS instrument (UPLC/Synapt Q-TOF MS, Waters Corp., Milford, MA, USA), with an electrospray ionization source. Separation was achieved using an Acquity UPLC BEH C18 column (100 × 2.1 mm i.d., 1.7 μm; Waters Corp., Milford, MA, USA). The mobile phase was a mixture of 2.0% aq. formic acid v/v (a) and acetonitrile (b). The gradient program is as follows: initial conditions: 1% B in A, 12 min; 25% B in A, 12.5 min; 100% B, 13.5 min; 1% B in A. The flow rate was 0.45 mL/min, and the injection volume was 5 μL. The column was operated at 30°C. The UV-Vis absorption spectra were recorded online during the UPLC analysis, and the spectra were measured in the wavelength range of 200–600 nm, in steps of 2 nm. The major operating parameters of the Q-TOF MS were set as follows: capillary voltage of 2.0 kV, cone voltage of 40 V, cone gas flow of 11 L/h, collision energy of 28–30 eV, source temperature of 100°C, desolvation temperature of 250°C, argon as the collision gas, desolvation gas (nitrogen) flow rate of 600 L/h, and data acquisition range (m/z) of 100–2500 Da. The compounds were monitored at 245, 280, 320, 360, and 520 nm and explored in the negative and positive (only anthocyanins) modes before and after fragmentation. The data was collected with the MassLynx V 4.1 software (Waters Corp., Milford, MA, USA).

2.4. Quantitative Determination of Anthocyanins, Flavonols, Phenolic Acids, and Iridoids Using HPLC-PDA. The HPLC analysis was performed as described by Spychaj et al. [19] using the Dionex (Germering, Germany) system equipped with an Ultimate 3000 diode array detector, LPG-3400A quaternary pump, EWPS-3000SI autosampler, TCC-3000SD thermostated column compartment, and controlled with the Chromeleon v.7.2 software. Separation was achieved using a Cadenza Imtakt column CD-C18 (75 × 4.6 mm, 5 μm). The mobile phase was composed of solvent A (4.5% aq. formic acid, v/v) and solvent B (100% acetonitrile). The gradient profile is as follows: 5% B in A, 0–1 min; 25% B in A, 1–20 min; 100% B, 20–26 min; 5% B in A, 26–30 min. The flow rate of the mobile phase was 1 mL/min, and the injection volume was 20 μL. The column was operated at 30°C. Anthocyanins were detected at 520 nm, flavonols at 360 nm, phenolic acids at 320 nm, gallic acid at 280 nm, ellagic acid at 254 nm, and iridoids at 245 nm. Calibration curves at concentrations ranging from 0.02 to 0.3 mg/mL ($R^2 \geq 0.9998$) were determined experimentally for cyanidin 3-*O*-glucoside, quercetin 3-*O*-glucoside, kaempferol 3-glucoside, caffeic acid, *trans*-caftaric acid, trans-coutaric acid, *p*-coumaric acid, ellagic acid, and gallic acid. The results were expressed as mg/100 g of the dried extract. Results were provided as the mean ± standard deviation of three replications and expressed as mg/100 g dw (dry weight) of the extract.

2.5. Quantitative Determination of Hydrolysable Tannins by HPLC-PDA. The HPLC analysis was performed as described by Przybylska et al. [18] using the Dionex (Germering, Germany) system equipped with an Ultimate 3000 diode array detector, LPG-3400A quaternary pump, EWPS-3000SI autosampler, TCC-3000SD thermostated column compartment, and controlled using the Chromeleon v.7.2 software. Separation was achieved using a Hypersil GOLD C18-column (250 × 4.6 mm, 5 μm; Thermo Fisher Scientific Inc., UK). The following mixtures were used as eluents: (a), water-FA (98.5 : 1.5, v/v) and (b), acetonitrile-FA (98.5 : 1.5, v/v). The gradient profile is as follows: initial conditions: 100% A, 30 min; 30% B, 33 min; 70% B, 45 min; 70% B in A, 48 min; 100% B, 55–60 min; 100% A. The flow rate of the mobile phase was 1.2 mL/min, and the injection volume was 20 μL. The column was operated at 22°C. Hydrolysable tannins were detected at 280 nm. A calibration curve at concentrations ranging from 0.02 to 0.3 mg/mL ($R^2 \geq 0.9996$) was determined experimentally for gallic acid. Results are provided as the total of individual isomers of three replications and expressed as mg/100 g of the extract.

2.6. Primary Osteoblast Culture and Induction of Osteoblast Differentiation. Primary cell cultures of the mice were conducted using a protocol approved by the Institutional Animal Care and Use Committee (IACUC) of Ajou University School of Medicine (2016-0062). Primary osteoblasts of the mice were isolated from neonatal C57BL/6 mice (4–5 pups), as previously described [20]. The calvarias of the mice were dissected and digested with collagenase II (Sigma, St. Louis, MO, USA) at 37°C for 2 h. The digestive solution was filtered through a 40 μm cell strainer, and the cells were incubated with an α-modified minimal essential medium (α-MEM; Gibco) supplemented with 10% fetal bovine serum (FBS; Gibco) and 1% penicillin/streptomycin (Gibco) for 2–3 days. After 70–80% of confluency was reached, the cells were incubated with 10 mM β-glycerophosphate (Sigma) and 50 μg/mL ascorbic acid (Sigma) for 3 days.

2.7. Isolation of Primary Monocytes and Induction of Osteoclast Differentiation. To isolate osteoclast-lineage primary-cultured monocytes, bone marrow (BM) cells from nine-week-old C57BL/6 mice were isolated as previously described [21]. The femoral bones of the mice were flushed using warm phosphate-buffered saline (Gibco), and the cellular suspension was subsequently filtered through a 40 μm cell strainer to remove the debris. BM cells were then incubated with an α-MEM (Gibco) containing 10% FBS (Gibco) and 50 ng/mL of macrophage colony-stimulating factor (M-CSF) (Peprotech, Cranbury, NJ, USA) without penicillin/streptomycin (Gibco) for 3 days in a petri dish. For osteoclast differentiation, the cells were seeded in a 96-well plate and incubated with a growth medium supplemented with M-CSF (50 ng/mL; Peprotech) and RANKL (50 ng/mL; Peprotech) for 5 days.

2.8. Cell Viability Assay. The cells were incubated in 96-well plates and treated with different concentrations of *Cornus mas* L. extracts (2, 5, and 10 μg/mL) during differentiation. The cells were then incubated with D-Plus™ cell counting kit (CCK) cell viability assay reagent (Dongin Biotech, Seoul, Korea) at 37°C, and the cell viability was measured using a

microplate reader (Bio-Rad, Hercules, CA, USA) at an absorbance of 450 nm.

2.9. ALP/TRAP Activity Assay and Staining. The cells were collected using a lysis buffer (0.5 M Tris-hydrogen chloride (HCL), pH 8.8, containing 0.9% sodium chloride, 1% Triton X-100, and 200 mM ethylenediaminetetraacetic acid (EDTA)), and ALP activity was measured using 1-Step™ p-nitrophenyl phosphate (Sigma) according to the manufacturer's recommendations. ALP-positive cells were stained with 5-bromo-4-chloro-3-indolyl phosphate/nitro blue tetrazolium (BCIP/NBT; Sigma) at room temperature. TRAP activity and staining were processed using an Acid Phosphatase Kit (Sigma) in accordance with the manufacturer's instructions.

2.10. Quantitative Reverse-Transcriptase Polymerase Chain Reaction (qRT-PCR). The total RNA was isolated using the TRIzol reagent (Invitrogen, Carlsbad, CA, USA) according to the manufacturer's instruction, and the complementary DNA (cDNA) was synthesized using a RevertAid™ H Minus First Strand cDNA Synthesis Kit (Fermentas, Hanover, NH, USA). qRT-PCR was processed using a SYBR Green I qPCR Kit (TaKaRa, Shiga, Japan), via the CFX Connect™ Real-Time System (Bio-Rad). The gene-specific primers used in this study were as follows: forward 5′-TCC CAC GTT TTC ACA TTC GG-3′ and reverse 5′-CCC GTT ACC ATA TAG GAT AGC C-3′ for mouse Alpl, forward 5′-TAA AGT GAC AGT GGA CGG TCC C-3′ and reverse 5′-AAT GCG CCC TAA ATC ACT GAG G-3′ for mouse Runx2, forward 5′-AAT ACC TCC CTC TCG ATC CTA CA-3′ and reverse 5′-TGG TTC TTG ACT GGA GTA ACG TA-3′ for mouse Ctsk, forward 5′-TGG TAT GTG CTG GCT GGA AAC-3′ and reverse 5′-AGT TGC CAC ACA GCA TCA CTG-3′ for mouse Acp5, forward 5′-AGG TCG GTG TGA ACG GAT TTG-3′ and reverse 5′-TGT AGA CCA TGT AGT TGA GGT CA-3′ for mouse Gapdh, forward 5′-GAG GAG TCC TGT TGA TGT TGC CAG-3′ and reverse 5′-GGC TGG CCT ATA GGC TCA TAG TGC-3′ for mouse Hprt. All gene expression levels were normalized using mouse Gapdh (osteoblast) and mouse Hprt (osteoclast), and relative expression levels were calculated using the $2^{-\Delta\Delta Ct}$ method ($\Delta\Delta Ct = \Delta Ct_{Treatment} - \Delta Ct -_{Induction}$).

2.11. Statistical Analysis. The data in the bar graphs is presented as the mean ± standard error of the mean (SEM) using the GraphPad Prism 9.0 software (GraphPad Software, San Diego, CA, USA). Statistical analysis was performed in multiple groups using a one-way analysis of variance with Tukey's honest significant difference post hoc test. A probability value below 0.05 ($p < 0.05$) was considered statistically significant.

3. Results and Discussion

3.1. A Comparison of the Chemical Composition of Cornelian Cherry (Cornus mas L.) Extracts from Red and Yellow Fruits. The polyphenols and iridoids were analyzed via LC-MS and HPLC in the three extracts. The results of qualitative and quantitative identification of the compounds of cornelian cherry extracts are presented in Table 1.

Phenolic and iridoid compounds, as well as hydrolysable tannins, were identified by their elution order, retention times, spectra of individual peaks (MS, MS/MS), and by comparison with data in the literature [22–24]. A total of 41 main compounds were identified: 4 iridoids (loganic acid and cornuside with pseudomolecular ions $[M - H]^-$ at *m/z* 375 and 541, respectively, and sweroside and loganin with $[M - H + 46]^-$ at *m/z* 403 and 435, respectively), 7 anthocyanins (5 glycosides: delphinidin 3-*O*-galactoside, cyanidin 3-*O*-galactoside, cyanidin 3-*O*-robinobioside, pelargonidin 3-*O*-galactoside, and pelargonidin 3-*O*-robinobioside with $[M + H]^+$ at *m/z* 463, 449, 595, 433, and 579, respectively, and 2 aglycons: cyanidin and pelargonidin with $[M + H]^+$ at *m/z* 287 and 271, respectively), 6 phenolic acids (gallic acid, 2 isomers of caftaric acid, coutaric acid, *p*-coumaric acid, and ellagic acid with $[M - H]^-$ at *m/z* 169, 311, 295, 163, and 301, respectively), 4 flavonols (quercetin 3-*O*-glucuronide, quercetin 3-*O*-glucoside, kaempferol 3-*O*-galactoside, and kaempferol 3-*O*-glucuronide with $[M - H]^-$ at *m/z* 477, 463, 447, and 461, respectively), and 20 hydrolysable tannins, including their spatial isomers. Among the hydrolysable tannins, the main compounds were one trimeric ellagitannin (cornusiin C, which gave two ions, $[M - 2H]^{-2}$ at *m/z* 1176 and $[M - H]^-$ at *m/z* 2353), two dimeric ellagitannins (camptothin A, which displayed two ions $[M - 2H]^{-2}$ at *m/z* 708 and $[M - H]^-$ at *m/z* 1417 and cornusiin A with two ions, $[M - 2H]^{-2}$ at *m/z* 784 and $[M - H]^-$ at *m/z* 1569), as well as gemin D – the simplest among the ellagitannin molecules with ion $[M - H]^-$ at *m/z* = 633 and its two derivatives (tellimagrandin I with $[M - H]^-$ at *m/z* 785 and tellimagrandin II with $[M - H]^-$ at *m/z* 937).

RED EXT1 contained most of the identified compounds (40 compounds), namely 16.9% iridoids, 3.5% anthocyanins, 1.2% phenolic acids, 0.6% flavonols, and 16.8% hydrolysable tannins. The quantitative and qualitative composition of iridoids and phenolic compounds in RED EXT1 is comparable to the composition of the red fruit extract described by Dzydzan et al. [23]. Extracts from yellow fruits (YL EXT2 and YL EXT3) did not contain anthocyanins but were richer in iridoids. YL EXT2 contained only one iridoid, 22.1% of loganic acid, whereas YL EXT3 contained four iridoids, which made up a quantity of 27.7% in total and included 17% of loganic acid. YL EXT2 contained four phenolic acids which made up a quantity of only 0.9% in total. As compared to the other extracts, YL EXT3 was the richest in phenolic acids, making up a quantity of 3.5% in total. The flavonols found in YL EXT3 were comparable to those present in RED EXT1, whereas YL EXT2 did not contain any of these compounds. A comparison between the two yellow fruit extracts showed that YL EXT2 mainly contained loganic acid and small amounts of phenolic acids, but no flavonols or tannins, whereas YL EXT3 was more abundant in various iridoids, phenolic acids, and hydrolysable tannins. Collectively, the three extracts contained different constituents of iridoids, anthocyanins, hydrolysable tannins, phenolic acids, and flavonols.

Table 1: Identification and content (mg/100 g dw) of main compounds of extracts from red (RED EXT1) and yellow (YL EXT2 and YL EXT3) cornelian cherry fruits by using LC-MS and HPLC.

Compound	UV λ_{max} (nm)	MS^1 $[M-H]^-/[M-H]^+$ (*m/z*)	MS^2 Other ions (*m/z*)	RED EXT1	YL EXT2	YL EXT3
					Mg/100 g DW	
			IRIDOIDS			
Loganic acid	245	375	213	12913.51 ± 159.09	22052.09 ± 206.67	17986.41 ± 190.37
Sweroside	245	403 $[M-H+46]^-$	195	533.64 ± 14.71	0.00	1135.86 ± 15.95
Loganin	245	435 $[M-H+46]^-$	227	1285.98 ± 35.44	0.00	2205.69 ± 30.97
Cornuside	245/273	541	169	2140.49 ± 17.96	0.00	6364.23 ± 50.54
Total iridoids				**16873.62**	**22052.09**	**27692.19**
			ANTHOCYANINS			
Delphinidin 3-*O*-galactoside	524	463+	303+	663.84 ± 7.42	0.00	0.00
Cyanidin 3-*O*-galactoside	515	449+	287+	203.43 ± 8.49	0.00	0.00
Cyanidin 3-*O*-robinobioside	516	595+	287+	301.25 ± 3.26	0.00	0.00
Pelargonidin 3-*O*-galactoside	501	433+	271+	1509.59 ± 23.75	0.00	0.00
Pelargonidin 3-*O*-robinobioside	501	579+	271+	268.22 ± 7.44	0.00	0.00
Cyanidin	523	287+		231.34 ± 6.01	0.00	0.00
Pelargonidin	509	271+		300.75 ± 5.47	0.00	0.00
Total anthocyanins				**3478.42**	**0.00**	**0.00**
			PHENOLIC ACIDS			
Gallic acid	272	169		0.00	263.59 ± 9.94	0.00
Trans-caftaric acid	326	311	179/149	101.03 ± 5.76	252.58 ± 4.47	43.63 ± 3.42
Caftaric acid isomer	326	311	179/149	562.26 ± 9.56	360.82 ± 13.68	1102.77 ± 27, 14
Coutaric acid isomer	312	295	163/149	333.07 ± 8.82	36.08 ± 2.19	1475.38 ± 36.47
p-Coumaric acid	310	163		33.58 ± 1.70	0.00	565.88 ± 12.78
Ellagic acid	254	301		146.24 ± 1.06	0.00	338,53 ± 7.92
Total phenolic acids				**1176.18**	**913.07**	**3526.19**
			FLAVONOLS			
Quercetin 3-*O*-glucuronide	354	477	301	306.24 ± 10.42	0.00	816.52 ± 13.52
Quercetin 3-*O*-glucoside	353	463	301	23.69 ± 2.07	0.00	0.00
Kaempferol 3-*O*-galactoside	348	447	285	235.32 ± 9.97	0.00	0.00
Kaempferol 3-*O*-glucuronide	351	461	285	27.93 ± 2.76	0.00	0.00
Total flavonols				**593.18**	**0.00**	**816.52**

Table 1: Continued.

Compound	UV λ_{max} (nm)	MS^1 $[M-H]^-/[M-H]^+$ (*m*/*z*)	MS^2 Other ions (*m*/*z*)	RED EXT1	YL EXT2	YL EXT3
					Mg/100 g DW	
			HYDROLYSABLE TANNINS			
Total gemin D isomers	265	633	301/275/249/169	903.33	0.00	1024.41
Tellimagrandin I	267	785	633/301/275/249/169	276.11	0.00	437.58
Tellimagrandin II	271	937	785/633/301/275/249/169	595.47	0.00	0.00
Total camptothin A isomers	264	708^{-2}, 1417	1247/783/633/301	2294.22	0.00	2699.29
Total cornusiin A isomers	273	784^{-2}, 1569	935/633/313/301	8503.24	0.00	3385.07
Total cornusiin C isomers	268	1176^{-2}, 2353	786/633/451/301	4249.05	0.00	1551.42
Total hydrolysable tannins				**16821.42**	**0.00**	**9097.77**

Abbreviations: (dw): dry weight; (HPLC): high-performance liquid chromatography; (LC-MS): liquid chromatography-mass spectrometry; (*m*/*z*): mass-to-charge ratio.

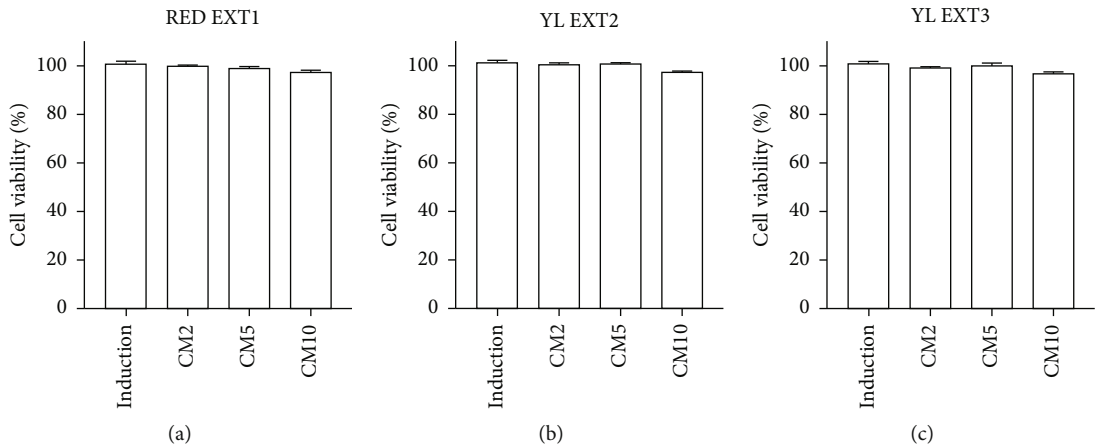

Figure 1: The effect of *Cornus mas* L. extracts on the cellular viability of primary osteoblasts in mice. Primary osteoblasts were incubated with ascorbic acid (50 μg/mL), β-glycerophosphate (10 mM), and cotreated with RED EXT1 (a), YL EXT2 (b), and YL EXT3 (c) at three different concentrations (2, 5, and 10 μg/mL) for 3 days. CM, *Cornus mas* L. extract. Cell viability was assessed using a water-soluble tetrazolium assay.

3.2. The Effects of Extracts from Cornelian Cherry Fruits on Osteoblast Differentiation. Further, we investigated the effects of the three cornelian cherries (*Cornus mas* L.) extracts (RED EXT1, YL EXT2, and YL EXT3) on osteoblast differentiation. Primary osteoblasts isolated from neonatal mouse calvarias were cultured in an osteoblastic induction media containing β-glycerophosphate and ascorbic acid and cotreated with different concentrations of *Cornus mas* L. extracts (2, 5, and 10 μg/mL) for three days. Treatment with the extracts did not influence the cell viability of primary-cultured osteoblasts, proving that there is no risk of cytotoxicity from these three extracts for primary osteoblasts (Figure 1).

Osteoblast differentiation was evaluated using an ALP activity assay and ALP staining. ALP plays a major role in the regulation of bone formation and mineralization during osteoblast differentiation [25]. Treatment with two of the three extracts, RED EXT1 and YL EXT2, significantly increased ALP activity at a concentration of 5 and 10 μg/mL. EXT3 increased ALP activity only at a concentration of 10 μg/mL (Figure 2). In addition, ALP staining results also showed an increase in ALP staining-positive cells in all three extracts (Figure 3). Although all three cornelian cherry extracts augmented osteoblast differentiation by increasing ALP activity, RED EXT1 and YL EXT2, compared to the YL EXT3, exhibited better efficacy on both ALP activity and staining, probably due to differences in the contents of the bioactive compounds. RED EXT1 consisted of abundant amounts of anthocyanins, a mixture of iridoids and hydrolyzable tannins, moderate amounts of phenolic acids, and small amounts of flavonols. Notably, despite YL EXT2 containing only a single iridoid, loganic acid, and a few phenolic acids, it showed better efficacy than YL EXT3 containing various iridoids and polyphenols. Among the three extracts, only YL EXT2 consisted of gallic acid and the highest amount of loganic acid, suggesting that these two compounds may be responsible for the better effect of YL EXT2 on the augmentation of osteoblast differentiation.

Next, we further investigated the effect of the three extracts on the mRNA expression changes of osteoblastogenesis biomarker genes: Alpl and runt-related transcription factor 2 (Runx2). Alpl is a bone-specific isoform localized on the surface of osteoblasts and is a sensitive indicator of bone metabolism [26]. Runx2 is an essential transcription factor for osteoblast differentiation during the early stages of bone formation [27]. These factors play an important role in the transcriptional regulation of bone formation and mineralization [28]. Primary cultured preosteoblasts were treated with the three extracts (RED EXT1, YL EXT2, and YL EXT3) at 10 μg/mL for 3 days, and thereafter the mRNA expression levels were analyzed using quantitative reverse transcriptase-polymerase chain reaction (qRT-PCR). All three extracts increased the mRNA expression levels of Alpl and Runx2 compared to that in the osteoblast-induced controls (Figure 4). These results suggest that *Cornus mas* L. extracts may enhance osteoblast differentiation by upregulating the expression of the Alpl and Runx2 genes at the transcription level. There was no difference in the augmentation efficacy of the three extracts for the expression of Alpl and Runx2. Taken together, these results showed that the three extracts from the *Cornus mas* L. fruits exhibited bone formation effects.

3.3. The Effects of Cornelian Cherry Fruits Extracts on Osteoclast Differentiation. Imbalanced homeostasis between bone resorption and bone formation results in weak and fragile bones associated with the risk of developing bone diseases [1, 29]. Dysregulation of osteoclast differentiation is a key factor causing abnormal bone metabolism and leading to osteoporosis [30–33]. Previous studies have suggested that a decrease in osteoclast differentiation is one of the main strategies for the prevention and treatment of osteoporosis [34–37]. Therefore, we investigated the effects of the three *Cornus mas* L. extracts (RED EXT1, YL EXT2, and YL EXT3) on osteoclast differentiation. Mouse bone marrow-derived osteoclast-lineage primary-cultured monocytes were isolated from the femoral bone. To induce osteoclast

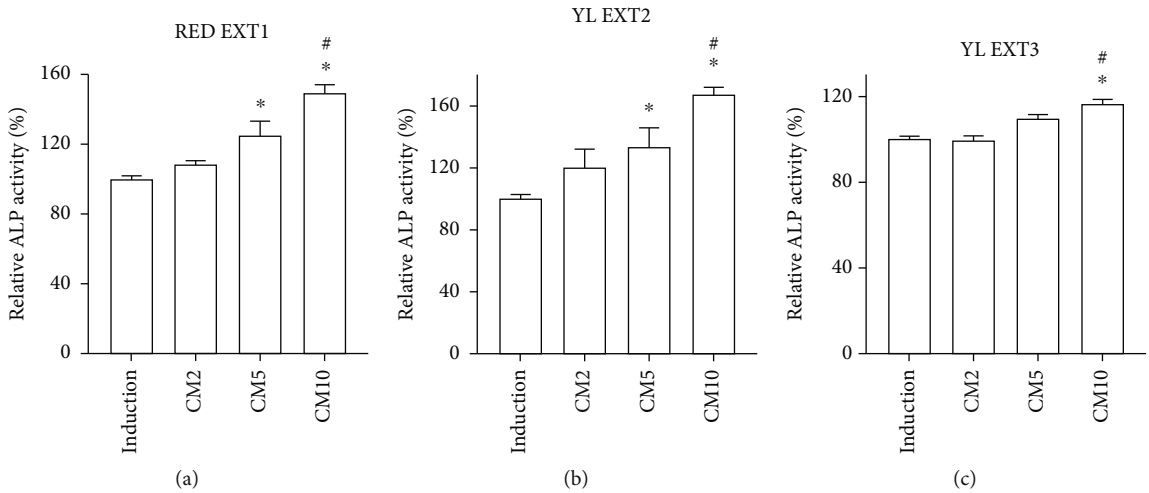

Figure 2: The effect of *Cornus mas* L. extracts on the alkaline phosphatase (ALP) activity in the primary osteoblasts of mice. The primary osteoblasts were incubated with ascorbic acid (50 μg/mL), β-glycerophosphate (10 mM), and cotreated with RED EXT1 (a), YL EXT2 (b), and YL EXT3 (c) at three different concentrations (2, 5, and 10 μg/mL) for three days. ALP activity was measured using p-nitrophenyl phosphate at an absorbance of 405 nm. CM, *Cornus mas* L. extract. $^{*}p < 0.05$ vs. induction, $^{\#}p < 0.05$ vs. CM2 (one-way analysis of variance (ANOVA) with Tukey's honest significant difference post hoc test).

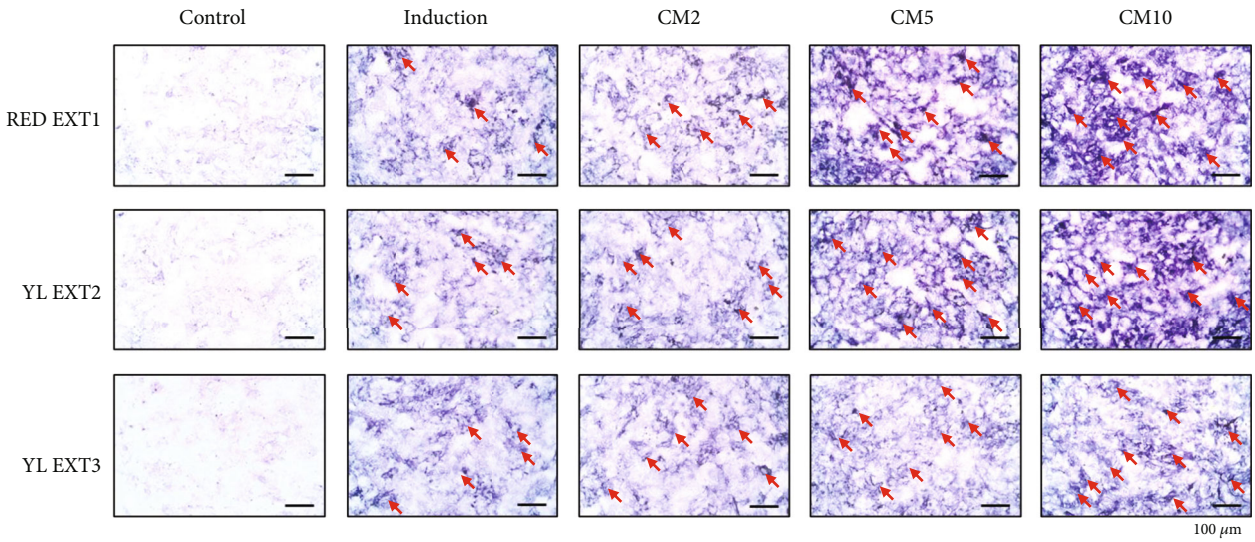

Figure 3: The effects of *Cornus mas* L. extracts on alkaline phosphatase (ALP) staining in the primary osteoblasts of mice. The primary osteoblasts were incubated with ascorbic acid (50 μg/mL) and β-glycerophosphate (10 mM) and cotreated with RED EXT1, YL EXT2, and YL EXT3 at three different concentrations (2, 5, and 10 μg/mL) for 3 days. ALP-positive cells were visualized using a light microscope and indicated with arrows. CM, *Cornus mas* L. extract.

differentiation, the monocytes were treated with M-CSF and RANKL [38]. Treatment with the three extracts at three different concentrations (2, 5, and 10 μg/mL) for 5 days did not affect cell viability, indicating that there is no risk of cytotoxicity for primary monocytes from these three extracts (Figure 5).

During osteoclast differentiation, TRAP stimulates the migration of osteoclasts into the bone resorption region [39]. TRAP is considered to be an important osteoclast histochemical indicator during skeletal development [40]. To assess osteoclast differentiation, TRAP activity assays and TRAP staining were used in this study. All three *Cornus mas* L. extracts showed a significant decrease in TRAP activity in the primary monocytes of mice at 10 μg/mL, and RED EXT1 and YL EXT2 also showed a significant decrease at 2 and 5 μg/mL (Figure 6). Among the three extracts, RED EXT1 exhibited the best efficacy, higher as compared to extracts from yellow fruits (Figure 6(a)). The results of the TRAP staining further revealed that the number of TRAP-positive multinuclear cells was significantly decreased after treatment with the three extracts (Figure 7). These results indicate that the *Cornus mas* L. extracts prevented osteoclast differentiation by decreasing TRAP activity, resulting in the attenuation of osteoclastic bone resorption. The best inhibitions of TRAP activity and TRAP staining were observed

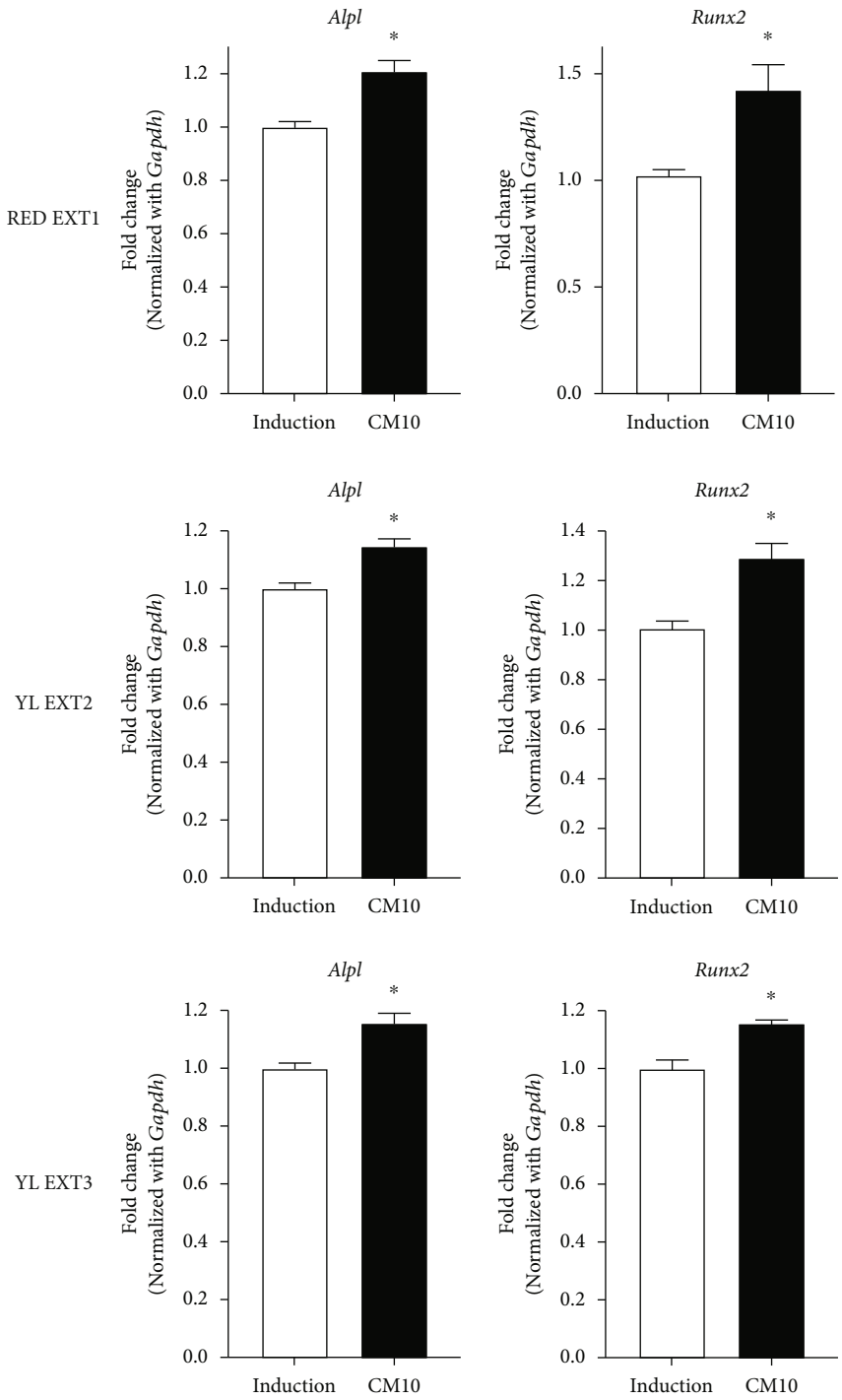

Figure 4: The effects of the *Cornus mas* L. extracts on the expression changes of osteoblast-specific genes in the primary osteoblasts of mice. The primary osteoblasts were incubated with ascorbic acid (50 μg/mL) and β-glycerophosphate (10 mM) with or without 10 μg/mL of *Cornus mas* L. extracts for 3 days. Osteoblast-specific genes including Alpl and Runx2 were measured by qRT-PCR using gene-specific primers. CM, *Cornus mas* L. extract treatment. $^{*}p < 0.05$ vs. induction (Student's t-test).

from the RED EXT1. Anthocyanins were only detected in RED EXT1, suggesting that the pronounce inhibitory effect of RED EXT1 on TRAP activity and staining could be attributed to the anthocyanins.

Bone resorption resulting from osteoclast differentiation is regulated by osteoclast-related enzymes, such as tartrate-resistant acid phosphatase 5 (Acp5) and cathepsin K (Ctsk) [41]. The transcription factor, nuclear factor of activated T cells 1 (Nfatc1), is known to promote osteoclast differentiation [42]. To confirm the inhibitory effects of *Cornus mas* L. extracts on osteoclast differentiation, the mRNA expression changes of osteoclastogenesis-related genes (Nfatc1,

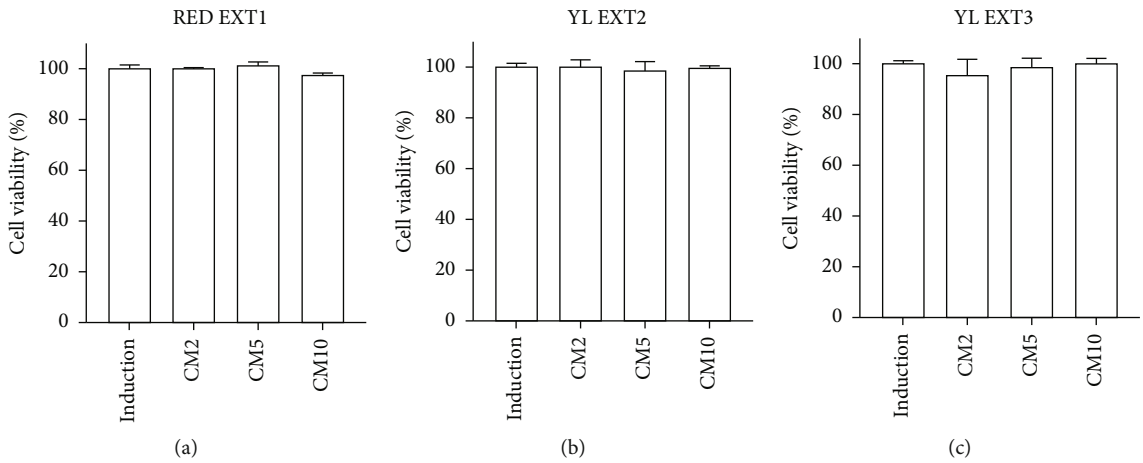

Figure 5: The effect of *Cornus mas* L. extracts on the cellular viability of primary osteoclasts in mice. The primary monocytes were incubated with macrophage colony-stimulating factor (M-CSF) (50 ng/mL) and receptor activator of nuclear factor-kappa B ligand (RANKL) (50 ng/mL) and cotreated with RED EXT1 (a), YL EXT2 (b), and YL EXT3 (c) at three different concentrations (2, 5, and 10 μg/mL) for 5 days. Cell viability was assessed using a WST assay. CM, *Cornus mas* L. extract.

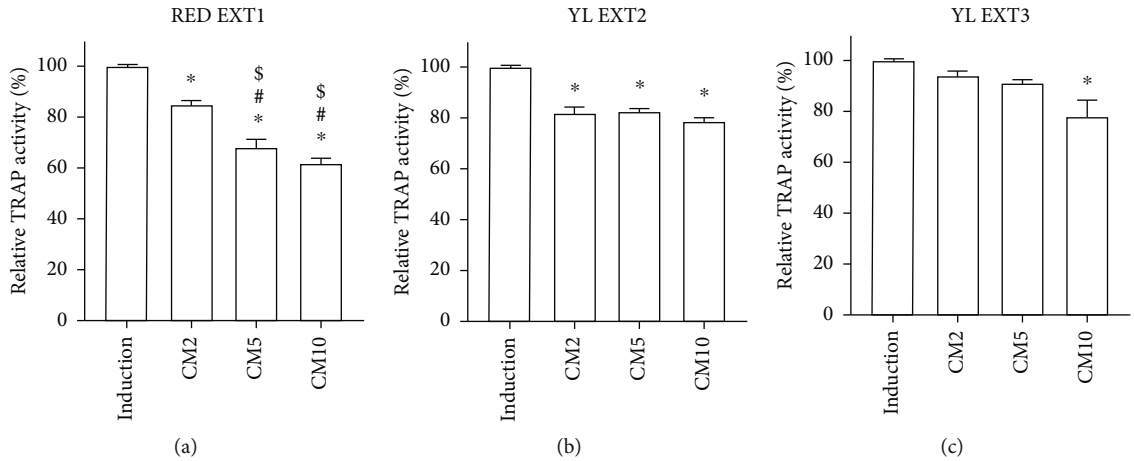

Figure 6: The effect of *Cornus mas* L. extracts on tartrate-resistant acid phosphatase (TRAP) activity in the primary osteoclasts of mice. The primary monocytes were incubated with M-CSF (50 ng/mL) and RANKL (50 ng/mL) and cotreated with RED EXT1 (a), YL EXT2 (b), and YL EXT3 (c) at three different concentrations (2, 5, and 10 μg/mL) for 5 days. TRAP activity was measured using acid-phosphatase at an absorbance of 405 nm. CM, *Cornus mas* L. extract. $^{*}p < 0.05$ vs. induction, $^{\#}p < 0.05$ vs. CM2, $^{\$}p < 0.05$ vs. CM5 (one-way ANOVA with Tukey's honest significant difference post hoc test).

Ctsk, and Acp5) were investigated. The results showed that treatment with all three extracts significantly decreased the mRNA expression levels of Nfatc1, Ctsk, and Acp5 at a concentration of 10 μg/mL (Figure 8). This finding indicates that *Cornus mas* L. extracts inhibit osteoclast differentiation through the decreased expression of these osteoclastogenic genes. Being consistent with the results from TRAP activity assays and staining, RED EXT1 was more effective than YL EXT2 and YL EXT3 in this experiment. These results suggest that the anthocyanins contained in RED EXT1 play a crucial role in the osteoclastogenesis reduction effects of *Cornus mas* L. extracts.

We analyzed and compared the constituents in a total of 41 compounds of iridoids, phenolic acids, flavonols, anthocyanins, and tannins in the three extracts obtained from red (RED EXT1) and yellow (YL EXT2 and YL EXT3) *Cornus mas* L. fruits using LC-MS and HPLC (Table 1). Although we did not examine the identified compounds directly, comparing the antiosteoporotic efficacies of the three extracts and reviewing the literature, it is possible to interpret which compounds are responsible for the antiosteoporotic effects of the extracts.

Our results are consistent with our recently published studies showing the antiosteoporotic effects of the cornelian cherry extract containing loganic acid. Park et al. [8] found that loganic acid isolated from *Gentiana lutea* L. roots extract significantly stimulated osteoblast differentiation by increasing ALP activity and upregulating the mRNA expression of Alpl, Bglap, and Sp7. In animal experiments, extracts from the cornelian cherry ameliorated the harmful changes in the bone turnover markers and bone mineral density (BMD) of hypercholesterolemic-diet rabbits [15] and

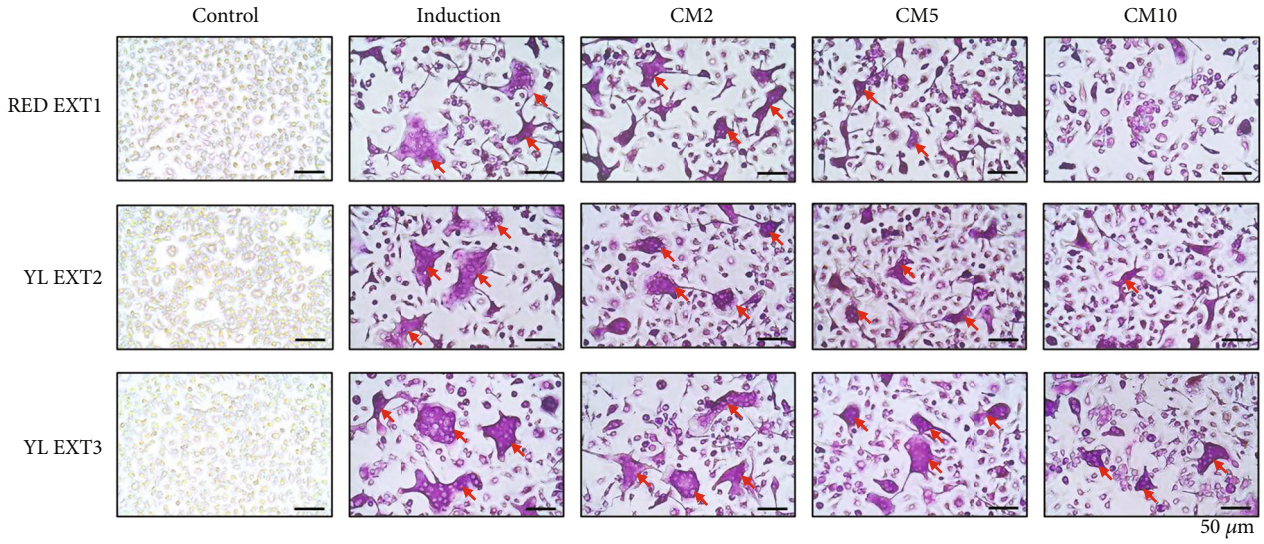

Figure 7: The effects of *Cornus mas* L. extracts on the tartrate-resistant acid phosphatase (TRAP) staining of primary osteoclasts in mice. The primary monocytes were incubated with ascorbic acid (50 μg/mL) and β-glycerophosphate (10 mM) and cotreated with RED EXT1, YL EXT2, and YL EXT3 at three different concentrations (2, 5, and 10 μg/mL) for 5 days. TRAP-positive cells were visualized using a light microscope and indicated with arrows. CM, *Cornus mas* L. extract.

counteracted the decrease in BMD and bone flexural strength of ovariectomized mice [8, 43]. In addition, phenolic acids, such as gallic acid and ellagic acid, were also revealed to have antiosteoporotic effects through the RANKL-related pathway [6, 44]. Unexpectedly, the antiosteoporotic effects of the YL EXT2 extract, containing only a single iridoid, loganic acid, were better than that of the YL EXT3 extract containing various iridoids including loganic acid, loganin, cornuside, and sweroside. Loganin and sweroside are known to have beneficial bone remodeling roles from previous studies [45, 46], and cornuside also reportedly has an antiosteoporotic effect [47]. We may try to explain the better antiosteoporotic effect of YL EXT2 because it contains uniquely gallic acid and a higher amount of loganic acid than YL EXT3. The exact molecular mechanism of the antiosteoporotic effect proposed for loganic acid requires further investigation, although anti-inflammatory activity and impact on described transcription factors and genes seem to be involved.

Regarding anthocyanins, although previous studies proved their possible inhibitory effect on osteoclast differentiation through the RANKL-mediated pathway [48, 49], only a few recently published studies suggest their possible enhanced effect on osteoblast differentiation and osteoblast-related mineralization through the ERK1/2 signaling pathway [50] or the inhibition of GSK-3β and subsequent activation of β-catenin [4]. Other proposed antiosteoporotic mechanisms of action of anthocyanins include their anti-inflammatory and antioxidant properties [50]. Inflammatory factors, glutathione depletion, and redox stress can inhibit the synthesis and differentiation of osteoblasts and bone mineralization. Polyphenols, especially anthocyanins can reduce these processes by the activation of sirtuin type 1 deacetylase expression with subsequent upregulation of ALP and Runx2 [51].

Phenolic acids, such as gallic acid or ellagic acid showed in other studies an antiosteoporotic effect through the RANKL-related pathway [6, 44]. Nevertheless, in our study, gallic acid was found only in small amounts in YL EXT2 and ellagic acid was present in small amounts in RED EXT1, and moderate amounts of it were found in YL EXT3. Cornelian cherry extracts, especially YL EXT3, contained more caftaric acid and coumaric acid but we did not find information about their potential impact on bone metabolism in the available data. Moreover, YL EXT3 proved the weakest antiosteoporotic activity in tests conducted as part of this study.

In previous studies, flavonols such as kaempferol and quercetin proved to have an antiosteoporotic effect. They decreased osteoclastogenesis, mainly through RANKL-related pathways, and promoted osteoblast differentiation [7, 52]. Proposed mechanisms responsible for the benefits of kaempferol in senile osteoporosis include also anti-inflammatory and antioxidative properties and regulation of osteoblasts' and osteoclasts' apoptosis [53]. Kaempferol and quercetin in the forms of 3-*O*-glucuronide, 3-*O*-galactoside, or *O*-glucoside were found in small amounts in RED EXT1, but their potential contribution to the antiosteoporotic effect is difficult to elucidate. YL EXT3 contained moderate amounts of quercetin 3-*O*-glucuronide but had the lowest antiosteoporotic potency. YL EXT2 did not contain flavonols. An accurate assessment of possible synergism between anthocyanin or iridoids and flavonols would require additional studies using different compositions of extracts and higher doses of flavonols.

Hydrolysable tannins were most abundant in RED EXT1, but substantial amounts were also found in YL EXT3; they were not present at all in YL EXT2. Previous studies have shown the antiosteoporotic potential of hydrolysable tannins. Corilagin inhibited osteoclastogenesis via downregulation of the NF-κB and PI3K/AKT signaling

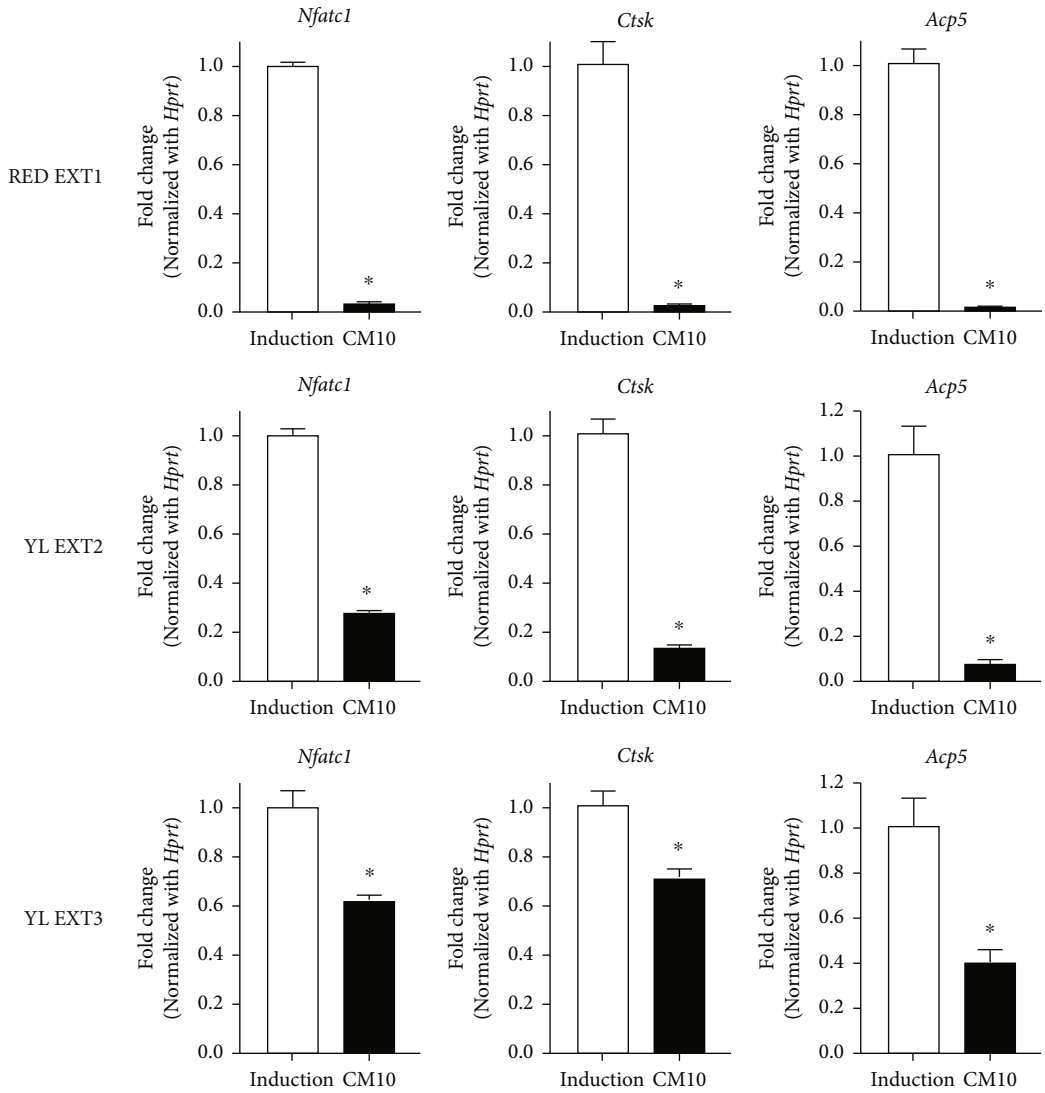

Figure 8: The effects of *Cornus mas* L. extracts on the expression changes of osteoclast-specific genes in the primary osteoclasts of mice. The primary monocytes were incubated with M-CSF (50 ng/mL) and RANKL (50 ng/mL) with or without 10 μg/mL of *Cornus mas* L. extracts for 5 days. Osteoclast-specific genes including Nfatc1, Ctsk, and Acp5 were measured with qRT-PCR using gene-specific primers. CM; *Cornus mas* L. extract. $^*p < 0.05$ vs. induction (Student's t-test).

pathways in murine bone marrow macrophage cells (BMMs) [54]. Other studies have proven that geraniin enhanced proliferation and osteoblastic differentiation of bone marrow-derived stem cells (BMSCs) in both normal and osteoporotic rats through the activation of Wnt/β-catenin signaling [55]; it also reduced bone turnover marker levels, increased osteoprotegerin (OPG), decreased RANKL, and increased the OPG/RANKL ratio in rats with ovariectomy-induced osteoporosis [9]. Hydrolysable tannins can also hydrolyze to phenolic acids, such as gallic acid and ellagic acid, and potentially exert an effect through these substances. Both RED EXT1 and YL EXT3 extracts were found to contain gemin, tellimagrandin, camptothin, and cornusiin isomers. It is worth emphasizing that cornusiin isomers were about 3 times more abundant in RED EXT1 than in YL EXT3. Although RED EXT1 proved to have strong antiosteoporotic effects, it is difficult to understand why YL EXT3 showed a lower efficacy than even YL EXT2, which did not contain any hydrolysable tannins at all. It is difficult to explain this finding, especially that we investigated mixtures of substances; contribution of hydrolysable tannins to antiosteoporotic effects may depend on its different structures and doses, and interactions with other extracts' constituents. It seems that among hydrolysable tannins detected in our study, the most promising substance is cornusiin, but further investigations with isolated compounds are needed.

Collectively, this study demonstrated that *Cornus mas L.* extracts enhanced osteoblastogenesis and reduced osteoclastogenesis. Comparison of the antiosteoporotic efficacy of the three extracts and analysis of the constituents in the polyphenols and iridoids, may help elucidate the molecular mechanisms responsible for the antiosteoporotic effects. Among the three extracts, the RED EXT1 extract uniquely

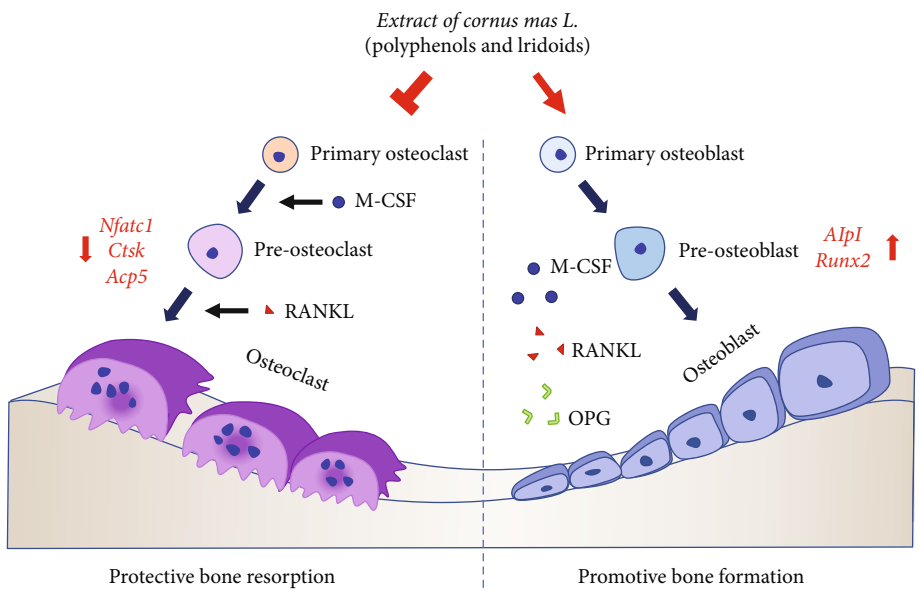

Figure 9: A suggested molecular mechanism for *Cornus mas* L. extracts in the regulation of osteoblast and osteoclast differentiation. Abbreviations: M-CSF, macrophage colony-stimulating factor; OPG, osteoprotegerin; RANKL, receptor activator of nuclear factor-kappa B ligand.

comprised several anthocyanins and the highest variety of polyphenols and iridoids; the YL EXT2 extract uniquely contained gallic acid and the highest amount of an irodoid, loganic acid (Table 1). RED EXT1, and YL EXT2 showed similar efficacy to each other, and better efficacy than YL EXT3, in the augmentation of osteoblast differentiation (Figures 2–4). These results strongly suggest that the iridoids, such as loganic acid, present in the extracts, may be responsible for the increase in osteoblast differentiation via the upregulation of Alpl and Runx2 expressions at the transcription level. Meanwhile, RED EXT1 showed the best efficacy in inhibiting osteoclast differentiation (Figures 6–8), strongly suggesting that the anthocyanins present in the extracts may be responsible for the decrease in osteoclast differentiation via the downregulation of Nfatc1, Ctsk, and Acp5 expressions at the transcription level. A suggested molecular mechanism for *Cornus mas L.* extracts in the regulation of osteoblast and osteoclast differentiation is described in Figure 9.

4. Conclusions

The main conclusions of our study were that three extracts from red and yellow *Cornus mas* L. fruits containing different constituents of iridoids and polyphenols such as anthocyanins, hydrolysable tannins, phenolic acids, and flavonols had antiosteoporotic effects. All these extracts significantly enhanced osteoblast differentiation and significantly reduced osteoclast differentiation. The antiosteoporotic effects of the RED EXT1 extract, containing several anthocyanins and iridoids, exerted via reduction of osteoclast differentiation, were better than that of YL EXT2 and YL EXT3. These results suggest that the red *Cornus mas* L. extract could be a promising phytomedicine candidate for the prevention and treatment of osteoporosis.

Abbreviations

Acp5:	Tartrate-resistant acid phosphatase 5
ALP:	Alkaline phosphatase
Alpl:	Alkaline phosphatase, biomineralization associated
Bglap:	Bone gamma-carboxyglutamic acid-producing protein
CM:	*Cornus mas*
CtsK:	Cathepsin K
Dw:	Dry weight
ESI:	Electrospray ionization
ERK 1/2:	Extracellular signal-regulated protein kinase 1/2
GSK-3β:	Glycogen synthase kinase 3 beta
HPLC–PDA:	High-performance liquid chromatography–photodiode array detection
LC-MS:	Liquid chromatography mass spectrometry
M-CSF:	Macrophage colony-stimulating factor
M/*z*:	Mass-to-charge ratio
Nfatc1:	Nuclear factor of activated T cells 1
NF-κB:	Nuclear factor kappa-light-chain-enhancer of activated B cells
OPG:	Osteoprotegerin
PI3K/AKT:	Phosphatidylinositol 3-kinase/protein kinase B
PPARs:	Peroxisome proliferator-activated receptors
RANKL:	Receptor activator of nuclear factor-kappa B ligand
qRT-PCR:	Quantitative reverse transcriptase-polymerase chain reaction
Q-TOF:	Quadruple time of flight
Runx2:	Runt-related transcription factor 2
TRAP:	Tartrate-resistant acid phosphatase
UPLC:	Ultra-performance liquid chromatography.

Data Availability

All the data generated or analyzed during this study are included in this article. Further inquiries can be directed to the corresponding authors.

Conflicts of Interest

We confirm that there are no known conflicts of interest associated with this publication and there has been no significant financial support for this work that could have influenced its outcome.

Authors' Contributions

Eunkuk Park contributed in drafting of the article, literature search and project administration, and critical revision of manuscript and its approval to be submitted. Alicja Z. Kucharska worked on the plant materials and samples preparation of cornelian cherry extracts, acquisition of laboratory data – identification and determination of compounds by LC-MS and HPLC-PDA, drafting in manuscript part of the methods section concerning plant materials, samples preparation and LC-MS and HPLC-PDA, and critical revision of manuscript and its approval to be submitted. Chang-Gun Lee was assigned in analysis, validation, interpretation of data collected, investigation, methodology development, and critical revision of manuscript and its approval to be submitted. Dominika Przybylska worked on the plant materials and samples preparation of cornelian cherry extracts, acquisition of laboratory data – identification and determination of compounds by LC-MS and HPLC-PDA, and critical revision of manuscript and its approval to be submitted. Narcyz Piórecki contributed in providing cornelian cherry fruits, preparation specimens of fruits to be deposited at the Herbariums of Arboretum in Bolestraszyce, and critical revision of manuscript and its approval to be submitted. Tomasz Sozański was assigned in the main conception of the study, participation in acquisition of laboratory data, literature search, analysis and interpretation of data collected, major contribution in drafting of the article, and critical revision of manuscript and its approval to be submitted. Seon-Yong Jeong worked on the conceptualization and design of the work, writing and editing of manuscript, and critical revision of manuscript and its approval to be submitted. Eunkuk Park, Tomasz Sozański, and Chang-Gun Lee contributed equally to this work.

Acknowledgments

This study was supported by the Korea Initiative for fostering the University of Research and Innovation Program of the National Research Foundation (NRF) funded by the Korean government (Ministry of Science and ICT, South Korea) (No. NRF2021M3H1A104892211) by Korea Health Technology R&D Project through the Korea Health Industry Development Institute (KHIDI), funded by the Ministry of Health and Welfare (No. HR22C1734), and the statutory means of the Wroclaw Medical University (SUBZ.A080.22.076). The APC/BPC is cofinanced by Wroclaw University of Environmental and Life Sciences, University of Rzeszow, and Wroclaw Medical University.

References

[1] J. M. Kim, C. Lin, Z. Stavre, M. B. Greenblatt, and J. H. Shim, "Osteoblast-osteoclast communication and bone homeostasis," *Cell*, vol. 9, no. 9, p. 2073, 2020.

[2] M. Rondanelli, M. A. Faliva, G. C. Barrile et al., "Nutrition, physical activity, and dietary supplementation to prevent bone mineral density loss: a food pyramid," *Nutrients*, vol. 14, no. 1, p. 74, 2022.

[3] B. Xia, R. Zhu, H. Zhang et al., "Lycopene improves bone quality and regulates AGE/RAGE/NF-κB signaling pathway in high-fat diet-induced obese mice," *Oxidative Medicine and Cellular Longevity*, vol. 2022, Article ID 3697067, 14 pages, 2022.

[4] W. A. H. M. Karunarathne, I. M. N. Molagoda, K. T. Lee, Y. H. Choi, C. Y. Jin, and G. Y. Kim, "Anthocyanin-enriched polyphenols from *Hibiscus syriacus* L. (Malvaceae) exert anti-osteoporosis effects by inhibiting GSK-3 β and subsequently activating β-catenin," *Phytomedicine*, vol. 91, article 153721, 14 pages, 2021.

[5] Z. Ren, N. A. Raut, T. O. Lawal, S. R. Patel, S. M. Lee, and G. B. Mahady, "Peonidin-3-O-glucoside and cyanidin increase osteoblast differentiation and reduce RANKL-induced bone resorption in transgenic medaka," *Phytotherapy Research*, vol. 35, no. 11, pp. 6255–6269, 2021.

[6] X. Lin, G. Yuan, Z. Li et al., "Ellagic acid protects ovariectomy-induced bone loss in mice by inhibiting osteoclast differentiation and bone resorption," *Journal of Cellular Physiology*, vol. 235, no. 9, pp. 5951–5961, 2020.

[7] M. Martiniakova, M. Babikova, V. Mondockova, J. Blahova, V. Kovacova, and R. Omelka, "The role of macronutrients, micronutrients and flavonoid polyphenols in the prevention and treatment of osteoporosis," *Nutrients*, vol. 14, no. 3, p. 523, 2022.

[8] E. Park, C. G. Lee, E. Lim et al., "Osteoprotective effects of loganic acid on osteoblastic and osteoclastic cells and osteoporosis-induced mice," *International Journal of Molecular Sciences*, vol. 22, no. 1, p. 233, 2020.

[9] X. Wang, M. Wang, X. Cui et al., "Antiosteoporosis effect of geraniin on ovariectomy-induced osteoporosis in experimental rats," *Journal of Biochemical and Molecular Toxicology*, vol. 35, no. 6, pp. 1–8, 2021.

[10] J. Y. Kim, Y.-K. Kim, M. K. Choi, J. Oh, H. B. Kwak, and J.-J. Kim, "Effect of *Cornus officinalis* on receptor activator of nuclear factor-kappaB ligand (RANKL)-induced osteoclast differentiation," *Journal of Bone Metabolism*, vol. 19, no. 2, pp. 121–127, 2012.

[11] T. Sozański, A. Z. Kucharska, A. Szumny et al., "The protective effect of the *Cornus mas* fruits (cornelian cherry) on hypertriglyceridemia and atherosclerosis through PPAR α activation in hypercholesterolemic rabbits," *Phytomedicine: International Journal of Phytotherapy and Phytopharmacology*, vol. 21, no. 13, pp. 1774–1784, 2014.

[12] T. Sozański, A. Z. Kucharska, A. Rapak et al., "Iridoid-loganic acid *versus* anthocyanins from the *Cornus mas* fruits (cornelian cherry): common and different effects on diet-induced atherosclerosis, PPARs expression and inflammation," *Atherosclerosis*, vol. 254, pp. 151–160, 2016.

[13] T. Sozański, A. Z. Kucharska, J. Wiśniewski et al., "The iridoid loganic acid and anthocyanins from the cornelian cherry (*Cornus mas* L.) fruit increase the plasma l-arginine/ADMA ratio and decrease levels of ADMA in rabbits fed a high-cholesterol diet," *Phytomedicine: International Journal of Phytotherapy and Phytopharmacology*, vol. 52, pp. 1–11, 2019.

[14] T. Sozański, A. Z. Kucharska, S. Dzimira et al., "Loganic acid and anthocyanins from cornelian cherry (Cornus mas L.) fruits modulate diet-induced atherosclerosis and redox status in rabbits," *Advances in Clinical Experimental Medicine*, vol. 27, no. 11, pp. 1505–1513, 2018.

[15] B. Nowak, A. Matuszewska, M. Tomanik et al., "Cornelian cherry extract ameliorates osteoporosis associated with hypercholesterolemia in New Zealand rabbits," *Advances in Clinical Experimental Medicine*, vol. 29, no. 12, pp. 1389–1397, 2020.

[16] R. Omelka, J. Blahova, V. Kovacova et al., "Cornelian cherry pulp has beneficial impact on dyslipidemia and reduced bone quality in Zucker diabetic fatty rats," *Animals*, vol. 10, no. 12, p. 2435, 2020.

[17] Ł. Lewandowski, I. Bednarz-Misa, A. Z. Kucharska et al., "Cornelian cherry (*Cornus mas* L.) extracts exert cytotoxicity in two selected melanoma cell lines-a factorial analysis of time-dependent alterations in values obtained with SRB and MTT assays," *Molecules*, vol. 27, no. 13, p. 4193, 2022.

[18] D. Przybylska, A. Z. Kucharska, I. Cybulska, T. Sozański, N. Piórecki, and I. Fecka, "*Cornus mas* L. stones: a valuable by-product as an ellagitannin source with high antioxidant potential," *Molecules*, vol. 25, no. 20, p. 4646, 2020.

[19] R. Spychaj, A. Z. Kucharska, A. Szumny, D. Przybylska, E. Pejcz, and N. Piórecki, "Potential valorization of Cornelian cherry (*Cornus mas* L.) stones: Roasting and extraction of bioactive and volatile compounds," *Food Chemistry*, vol. 358, article 129802, 12 pages, 2021.

[20] M. L. Doolittle, C. L. Ackert-Bicknell, and J. H. Jonason, "Isolation and culture of neonatal mouse calvarial osteoblasts," *Methods in Molecular Biology*, vol. 2230, pp. 425–436, 2021.

[21] M. J. Oliva-Martin, L. I. Sánchez-Abarca, A. Carrillo-Jiménez, J. A. Pérez-Simón, and J. L. Venero, "Evaluation of a method for murine monocyte isolation by bone marrow depletion," *Analytical Biochemistry*, vol. 480, pp. 42–48, 2015.

[22] A. Z. Kucharska, A. Szumny, A. Sokół-Łętowska, N. Piórecki, and S. V. Klymenko, "Iridoids and anthocyanins in cornelian cherry (*Cornus mas* L.) cultivars," *Journal of Food Composition and Analysis*, vol. 40, pp. 95–102, 2015.

[23] O. Dzydzan, I. Bila, A. Z. Kucharska, I. Brodyak, and N. Sybirna, "Antidiabetic effects of extracts of red and yellow fruits of cornelian cherries (*Cornus mas* L.) on rats with streptozotocin-induced diabetes mellitus," *Food & Function*, vol. 10, no. 10, pp. 6459–6472, 2019.

[24] M. Szandruk-Bender, M. Rutkowska, A. Merwid-Ląd et al., "Cornelian cherry iridoid-polyphenolic extract improves mucosal epithelial barrier integrity in rat experimental colitis and exerts antimicrobial and antiadhesive activities *In Vitro*," *Oxidative Medicine and Cellular Longevity*, vol. 2020, Article ID 7697851, 19 pages, 2020.

[25] Y. Sugawara, K. Suzuki, M. Koshikawa, M. Ando, and J. Iida, "Necessity of enzymatic activity of alkaline phosphatase for mineralization of osteoblastic cells," *The Japanese Journal of Pharmacology*, vol. 88, no. 3, pp. 262–269, 2002.

[26] J. Masrour Roudsari and S. Mahjoub, "Quantification and comparison of bone-specific alkaline phosphatase with two methods in normal and Paget's specimens," *Caspian Journal of Internal Medicine*, vol. 3, no. 3, pp. 478–483, 2012.

[27] T. Komori, "Regulation of proliferation, differentiation and functions of osteoblasts by RUNx2," *International Journal of Molecular Sciences*, vol. 20, no. 7, p. 1694, 2019.

[28] W. Huang, S. Yang, J. Shao, and Y.-P. Li, "Signaling and transcriptional regulation in osteoblast commitment and differentiation," *Frontiers in Bioscience-Landmark*, vol. 12, no. 8-12, pp. 3068–3092, 2007.

[29] K. A. Abulfadle, R. R. A. Atia, H. O. Mohammed, R. S. Ramadan, and N. A. Mohammed, "The potential anti-osteoporotic effect of exercise—induced increased preptin level in ovariectomized rats," *Anatomical Science International*, pp. 1–14, 2022.

[30] J. F. Charles and A. O. Aliprantis, "Osteoclasts: more than 'bone eaters'," *Trends in Molecular Medicine*, vol. 20, no. 8, pp. 449–459, 2014.

[31] H. Kitaura, A. Marahleh, F. Ohori et al., "Osteocyte-related cytokines regulate osteoclast formation and bone resorption," *International Journal of Molecular Sciences*, vol. 21, no. 14, p. 5169, 2020.

[32] Y. Kohara, R. Haraguchi, R. Kitazawa, and S. Kitazawa, "Knockdown of *Lrp1* in RAW264 cells inhibits osteoclast differentiation and osteoclast-osteoblast interactions *in vitro*," *Biochemical and Biophysical Research Communications*, vol. 523, no. 4, pp. 961–965, 2020.

[33] Y.-H. Hwang, S.-A. Jang, A. Lee et al., "Polysaccharides isolated from lotus leaves (LLEP) exert anti-osteoporotic effects by inhibiting osteoclastogenesis," *International Journal of Biological Macromolecules*, vol. 161, pp. 449–456, 2020.

[34] Y. Yang and B. Yang, "Anti-osteoporosis effect of *Ganoderma* (lingzhi) by inhibition of osteoclastogenesis," *Advances in Experimental Medicine and Biology*, vol. 1182, pp. 263–269, 2019.

[35] Y. Nara, H. Kitaura, S. Ogawa et al., "Anti-c-fms antibody prevents osteoclast formation and bone resorption in co-culture of osteoblasts and osteoclast precursors i*n vitro* and in ovariectomized mice," *International Journal of Molecular Sciences*, vol. 21, no. 17, p. 6120, 2020.

[36] Y. Zhuang, X. Sun, B. Liu, H. Hou, and Y. Sun, "Effects of rambutan peel (*Nephelium lappaceum*) phenolicextract on RANKL-induced differentiation of RAW264.7 cells into osteoclasts and retinoic acid-induced osteoporosis in rats," *Nutrients*, vol. 12, no. 4, p. 883, 2020.

[37] C. G. Lee, J. Kim, S. H. Yun et al., "Anti-osteoporotic effect of morroniside on osteoblast and osteoclast differentiation in vitro and ovariectomized mice in vivo," *International Journal of Molecular Sciences*, vol. 22, no. 19, article 10642, 2021.

[38] D. S. Győri and A. Mócsai, "Osteoclast signal transduction during bone metastasis formation," *Frontiers in Cell and Developmental Biology*, vol. 8, pp. 507–515, 2020.

[39] H. Drissi and A. Sanjay, "The multifaceted osteoclast; far and beyond bone resorption," *Journal of Cellular Biochemistry*, vol. 117, no. 8, pp. 1753–1756, 2016.

[40] A. R. Hayman, "Tartrate-resistant acid phosphatase (TRAP) and the osteoclast/immune cell dichotomy," *Autoimmunity*, vol. 41, no. 3, pp. 218–223, 2008.

[41] L. Zhu, Y. Tang, X.-Y. Li et al., "Osteoclast-mediated bone resorption is controlled by a compensatory network of secreted and membrane-tethered metalloproteinases," *Science Translational Medicine*, vol. 12, no. 529, article eaaw6143, p. 16, 2020.

[42] Q. Zhao, X. Wang, Y. Liu, A. He, and R. Jia, "NFATc1: functions in osteoclasts," *International Journal of Biochemistry & Cell Biology*, vol. 42, no. 5, pp. 576–579, 2010.

[43] B. Nowak, A. Matuszewska, A. Szeląg et al., "Cornelian cherry (*Cornus mas* L.) extract reduces cardiovascular risk and prevents bone loss in ovariectomized Wistar rats," *Journal of Functional Foods*, vol. 90, article 104974, p. 9, 2022.

[44] S. Chauhan, A. Sharma, N. K. Upadhyay, G. Singh, U. R. Lal, and R. Goyal, "In-vitro osteoblast proliferation and in-vivo anti-osteoporotic activity of *Bombax ceiba* with quantification of lupeol, gallic acid and β-sitosterol by HPTLC and HPLC," *BMC Complementary and Alternative Medicine*, vol. 18, no. 1, p. 233, 2018.

[45] L. Y. Choi, M. H. Kim, and W. M. Yang, "Promotion of osteogenesis by sweroside via BMP2-involved signaling in postmenopausal osteoporosis," *Phytotherapy Research*, vol. 35, no. 12, pp. 7050–7063, 2021.

[46] M. Li, W. Wang, P. Wang, K. Yang, H. Sun, and X. Wang, "The pharmacological effects of morroniside and loganin isolated from Liuweidihuang Wan, on MC3T3-E1 cells," *Molecules*, vol. 15, no. 10, pp. 7403–7414, 2010.

[47] F. Gao, S.-L. Xia, X.-H. Wang, X. X. Zhou, and J. Wang, "Cornuside I promoted osteogenic differentiation of bone mesenchymal stem cells through PI3K/Akt signaling pathway," *Journal of Orthopaedic Surgery and Research*, vol. 16, no. 1, p. 397, 2021.

[48] J. Cheng, L. Zhou, Q. Liu et al., "Cyanidin chloride inhibits ovariectomy-induced osteoporosis by suppressing RANKL-mediated osteoclastogenesis and associated signaling pathways," *Journal of Cellular Physiology*, vol. 233, no. 3, pp. 2502–2512, 2018.

[49] N. Imangali, Q. T. Phan, G. Mahady, and C. Winkler, "The dietary anthocyanin delphinidin prevents bone resorption by inhibiting RANKL-induced differentiation of osteoclasts in a medaka (*Oryzias latipes*) model of osteoporosis," *Journal of Fish Biology*, vol. 98, no. 4, pp. 1018–1030, 2021.

[50] B. Hu, L. Chen, Y. Chen, Z. Zhang, X. Wang, and B. Zhou, "Cyanidin-3-glucoside regulates osteoblast differentiation via the ERK1/2 signaling pathway," *ACS Omega*, vol. 6, no. 7, pp. 4759–4766, 2021.

[51] V. Domazetovic, G. Marcucci, I. Falsetti et al., "Blueberry juice antioxidants protect osteogenic activity against oxidative stress and improve long-term activation of the mineralization process in human osteoblast-like SaOS-2 cells: involvement of SIRT1," *Antioxidants*, vol. 9, no. 2, p. 125, 2020.

[52] B. Nowak, A. Matuszewska, A. Nikodem et al., "Oral administration of kaempferol inhibits bone loss in rat model of ovariectomy-induced osteopenia," *Pharmacolgical Reports*, vol. 69, no. 5, pp. 1113–1119, 2017.

[53] F. Tang, P. Zhang, W. Zhao et al., "Research on the mechanism of kaempferol for treating senile osteoporosis by network pharmacology and molecular docking," *Evidence-Based Complementary and Alternative Medicine*, vol. 2022, Article ID 6741995, 12 pages, 2022.

[54] J. Lu, C. Ye, Y. Huang et al., "Corilagin suppresses RANKL-induced osteoclastogenesis and inhibits oestrogen deficiency-induced bone loss via the NF-κB and PI3K/AKT signalling pathways," *Journal of Cellular and Molecular Medicine*, vol. 24, no. 18, pp. 10444–10457, 2020.

[55] J. Mo, R. Yang, F. Li et al., "Geraniin promotes osteogenic differentiation of bone marrow mesenchymal stem cells (BMSCs) via activating β-catenin: a comparative study between BMSCs from normal and osteoporotic rats," *Journal of Natural Medicines*, vol. 73, no. 1, pp. 262–272, 2019.

Hindawi
Oxidative Medicine and Cellular Longevity
Volume 2022, Article ID 4229981, 11 pages
https://doi.org/10.1155/2022/4229981

Research Article

Mineral and Phenolic Composition of *Erodium guttatum* Extracts and Investigation of Their Antioxidant Properties in Diabetic Mice

Kaoutar Benrahou,[1] Hanae Naceiri Mrabti,[1] Saad Fettach,[1] Mohamed Reda Kachmar,[2] Mostafa Kouach,[3] Jean-François Goossens,[3] Latifa Doudach,[4] Shafi Mahmud,[5] Mohammed Merae Alshahrani,[6] Ahmed Abdullah Al Awadh,[6] Abdelhakim Bouyahya,[7] and My El Abbes Faouzi[1]

[1]*Laboratory of Pharmacology and Toxicology, Bio Pharmaceutical and Toxicological Analysis Research Team, Faculty of Medicine and Pharmacy, Mohammed V University in Rabat, BP 6203, Rabat, Morocco*
[2]*Faculty of Sciences, Health and Environment Laboratory, Plant Protection Team, Moulay Ismail University, BP 11201, Zitoune, Meknes, Morocco*
[3]*Univ. Lille, CHU Lille, ULR 7365-GRITA-Groupe de Recherche sur les formes Injectables et les Technologies Associées, F-59000 Lille, France*
[4]*Department of Biomedical Engineering Medical Physiology, Higher School of Technical Education of Rabat, Mohammed V University in Rabat, BP 6203, Rabat, Morocco*
[5]*Division of Genome Sciences and Cancer, The John Curtin School of Medical Research and The Shine-Dalgarno Centre for RNA Innovation, The Australian National University, Canberra, ACT 2601, Australia*
[6]*Department of Clinical Laboratory Sciences, Faculty of Applied Medical Sciences, Najran University, 1988, Najran 61441, Saudi Arabia*
[7]*Laboratory of Human Pathologies Biology, Faculty of Sciences, Mohammed V University in Rabat, Morocco*

Correspondence should be addressed to Abdelhakim Bouyahya; boyahyaa-90@hotmail.fr

Received 11 July 2022; Accepted 2 September 2022; Published 19 September 2022

Academic Editor: Muhammad Saleem Kalhoro

Erodium guttatum is widely used in folk medicine in many countries to treat various ailments such as urinary inflammation, diabetes, constipation, and eczema. The aim of this study is the determination of mineral and phenolic compounds of *E. guttatum* extracts as well as the investigation of their antidiabetic and antioxidant properties. The mineral composition was determined by the methods of inductively coupled plasma atomic emission spectroscopy analysis. Phytochemical contents of total polyphenols, total flavonoids, and catechic tannins were estimated by colorimetric dosages. The phenolic composition was identified by high-resolution mass spectrometry (HRMS) analysis. The antioxidant activity of *E. guttatum* extracts was measured *in vitro* by five methods (DPPH, ABTS, FRAP, H_2O_2, and xanthine oxidase) and *in vivo* by assaying the malondialdehyde marker (MDA), superoxide dismutase (SOD), catalase (CAT), and glutathione (GSH). The obtained results showed that the root plant material is rich in minerals such as k, Ca, and Mg. The methanolic extract of *E. guttatum* is the richest in polyphenols (389.20 ± 1.55 mg EAG/gE), tannins (289.70 ± 3.57 mg EC/gE), and flavonoids (432.5 ± 3.21 mg ER/gE). Concerning the ESI-HRMS analysis, it showed the presence of numerous bioactive compounds, including shikimic acid, rottlerine, gallic acid, and vanillic acid. Moreover, the aqueous and alcoholic extracts of *E. guttatum* exhibited antiradical and antioxidant activity in five tests used, with the best effect of the methanolic extract. Moreover, findings showed that *in vivo* investigations confirmed those obtained *in vitro*. On the other hand, *E. guttatum* showed important antidiabetic effects *in vivo*. Indeed, diabetic mice treated with extracts of *E. guttatum* were able to significantly reduce MDA levels and increase the secretion of enzymatic and nonenzymatic antioxidants (SOD, CAT, and GSH, respectively). However, the antioxidant activity of the extracts might be attributed to the abundance of bioactive molecules; as results, this work serves as a foundation for additional pharmacological research.

1. Introduction

Oxidative stress is a consequence results from the oxidative balance deregulation between the production and the release of free radicals, which can cause certain damage at the tissue level by the oxidation of bimolecular such as enzymes, proteins, DNA, and lipids [1]. Excessive production of reactive oxygen species (ROS) is considered as a major risk factor of several diseases such as aging, atherosclerosis, diabetes, rheumatoid arthritis, carcinogenesis, and neurodegenerative diseases [2]. Interestingly, cells can produce many antioxidant defense enzymes to trap and neutralize ROS, including catalase, superoxide dismutase, glutathione reductase, glutathione peroxidase, and some antioxidant molecules (uric acid, glutathione, albumin, protein-SH groups, bilirubin), as well as some vitamins such as ascorbic acid, α-tocopherol, and carotenoids [3].

Most organisms have evolved antioxidant defense and repair systems to protect them against oxidative damage. However, these systems are insufficient to completely prevent the damage [4]. Therefore, it is necessary to develop natural nontoxic antioxidants to protect the human body from free radicals and delay the progression of many chronic diseases [5–7]. For a long time, medicinal plants have been proven to be very rich in antioxidant molecules other than vitamin C, vitamin E, and carotenoids. The antioxidant effect is due to their richness in phenolic components, such as flavonoids, phenolic acids, and phenolic diterpenes [7].

Morocco is endowed with a great climatic and biological variety in which plants can be cultivated or grown spontaneously. Morocco is very popular due to its large and very diverse flora; out of 4200 spontaneous species, about 1500 introduced species have been recorded, some of them listed in Moroccan pharmacopoeia [8]. Plants always had a crucial role, especially for their important therapeutic role in treatment. Modern medicine has made great strides throughout the last century. Traditional medicine is still important in the lives of many people around the world. Indeed, the pharmacopoeia contains approximately 25,000 herbs, and approximately 50% of all pharmaceutical products on the market are of natural origin [9].

Numerous studies show that medicinal plants are frequently used, including those from the Geraniaceae family. Ethnopharmacological data indicated that several species of *Erodium* are traditionally used in Turkey to treat various diseases such as urinary inflammation, diabetes, constipation, and eczema [10]. In other countries, it is used as an astringent and antiseptic tea [11]. The genus *Erodium* exists on all continents, and it is especially very widespread in the Mediterranean region, and more than 60 species can be found. *Erodium* contains annual or perennial herbaceous beds and it is characterized by five fertile stamens and five staminodes. The leaves are pinnate or undivided into pinnatifid to pinnatisect. Leaf size and shape can vary between populations, and variation within populations is generally evident [12].

Among the species of the genus *Erodium*, we found *Erodium guttatum*, which is used in traditional medicine, while it is less explored for its biological and pharmacological properties. Indeed, antioxidant studies have not been performed on *E. guttatum*. In addition, *in vitro* antioxidant and antimicrobial activities are the only studies performed on *E. guttatum* [13]. Additionally, this work is aimed at determining the mineral and phenolic compounds of *E. guttatum* root extracts as well as the investigation of their *in vitro* and *in vivo* antioxidant and antidiabetic effects.

2. Materials and Methods

2.1. Plant Material and Preparation of Extracts. The fresh roots of *E. guttatum* were harvested in February 2018 in the northeast regions of Oujda, Morocco. After being identified by botanist Professor Mohammed Fennan, the specimen was deposited at the Herbarium of Botany of the Scientific Institute of Rabat under the reference number 110970. The roots of *E. guttatum* were dried in the shade at room temperature and then ground using an electric grinder. The ground material obtained was stored in a dry place and protected from moisture and light until its use.

To prepare the ethanolic and methanolic extracts, 30 g of plant material (powder) was macerated successively with 300 mL of ethanol and methanol for 48 h with mechanical stirring. The aqueous extract was infused with boiling water for 1 hour and allowed to cool. The extracts were then filtered, and the filtrate obtained was evaporated using a rotary evaporator and then lyophilized.

2.2. Mineral Composition. The mineral composition (Ca, Mg, Mn, Fe, Zn, K, Na, and P) was determined using an inductively coupled plasma atomic emission spectroscopy (ICP AES, JobinYvonUltima 2). The 150 mg of the plant and leaf powders were washed with a 2 mL of HNO_3 acid (70%) mixture in a Teflon beaker, before being incinerated at 110°C. Then, 0.5 mL of hydrofluoric acid (HF) was added, and the covered beaker was placed on a sand bath. The sample mixture was heated until a clear solution was obtained. After removing the cover, the mixture evaporated to dryness. Finally, 2 mL of HCl acid was added and the residue was extracted with 25 mL of 2.0 M HCl.

2.3. Determination of Total Phenols. Quantification of the total polyphenol is performed using the Folin Ciocalteu (phosphotungstic and phosphomolybdic) reagent described in the literature [14]. Indeed, 0.25 mL of each concentration extract (1 mg/mL) was mixed with 2.5 mL of Folin Ciocalteu reagent (10 times diluted in distilled water). The reaction mixture was stirred vigorously, and then, 4 mL of 7.5% (W/V) Na_2CO_3 sodium carbonate was added. The mixture was incubated in a water bath at 45°C for 30 minutes, and the absorbance was recorded by a spectrophotometer at 765 nm. Under the same operating conditions, the standard range of gallic acid was carried out at different concentrations (1.95, 3.9, 7.81, 15.625, and 31.25 μg/mL), and the results were expressed in milligrams of gallic acid equivalent in grams of extract (mg EAG/1 g extract).

2.4. Total Flavonoid Determination. The flavonoid content was estimated using the colorimetric method with aluminum trichloride ($AlCl_3$) and sodium hydroxide (NaOH) as

described by Dewanto et al. [15]. In brief, 0.5 mL of each 1 mg/mL concentration sample was mixed with 3.2 mL of distilled water and 0.15 mL of 5% (*w*/*v*) $NaNO_2$ sodium nitrite solution. The reaction mixture was incubated for 5 minutes. 0.15 mL of aluminum trichloride ($AlCl_3$) was added, followed by a second additional incubation for 6 minutes. Finally, 1 mL of sodium hydroxide NaOH (1 M) was added, and the mixture was incubated at room temperature for 30 minutes while shaded. The absorbance was measured at a wavelength of 510 nm. As a standard range, rutin was used at different final concentrations (50, 100, 150, 200, 250, 300, 350, and 400 μg/mL), and results were expressed in milligrams of gallic acid equivalent per gram of extract (mg ER/1 g Ex).

2.5. Dosage of Condensed Tannins. The tannin content was estimated by the method of vanillin as described by Julkunen-Tiitto [16]. However, 50 μL of each 1 mg/mL concentration extract was mixed with 1.5 mL of 4% vanillin (prepared with methanol), and then, 750 μL of concentrated HCl hydrochloric acid was added. The reaction medium is stirred vigorously and incubated at room temperature and in the dark for 20 minutes. The absorbance was read at a wavelength of 500 nm, and the calibration curve was established with catechin at concentrations of (50, 100, 200, 300, 400, 500, 600, 800, and 1000 μg/mL) under the same conditions.

2.6. Determination of Chemical Composition by HRMS Analysis. HRMS analysis was performed by ionization (ESI) mass spectrometry (MS). The extracts were dissolved to a final concentration of 1-2 pmol/μL in methanol. Compounds were measured in negative and positive modes by full mass scanning (*m*/*z* 50 to 1000) using a Thermo Scientific Orbitrap Exactive mass spectrometer equipped with a heated electrospray ionization source (HESI-II). The instrument parameter settings are as follows: sheath gas 10 in positive mode and 20 in negative mode (arbitrary units), spray voltage 3.5 kV and 3 kV in positive and negative mode, respectively, with a 275°C capillary temperature. Mass spectra were collected at a resolution of 100,000. Data processing was performed using the associated software, Xcalibur 2.2 and Exactive 1.1.

2.7. Antioxidant Activity

2.7.1. Radical Scavenging Assay with DPPH. DPPH (2,2-diphenyl-1-pierylhydrazyl) is a synthetic free radical of intense violet color. In the presence of free radical scavengers, purple DPPH is reduced to yellow DPPHH (2,2-diphenyl-1-picryl-hydrazine) [17]. In brief, 1.25 mL of each extract was mixed with 0.25 mL of methanol prepared DPPH solution and incubated in the dark at room temperature for 30 minutes, and the absorbance was recorded at 517 nm against a control sample. The percentage of antiradical activity is calculated according to the following formula:

$$I\% = \left[\frac{(\text{Absorbance Negative Control} - \text{Absorbance Sample})}{\text{Absorbance Negative Control}}\right] * 100. \quad (1)$$

2.7.2. Ferric Reducing Power Assay (FRAP). FRAP is an antioxidant test that measures the power of reducing ferric iron to ferrous iron [18]. However, the measure of the reducing power was determined by mixing 0.5 mL of each extract at a concentration of 1 mg/mL with 1.25 mL of phosphate buffer solution (0.2 M, pH 6.6) and 1.25 mL of aqueous solution of potassium ferricyanide [K_3Fe (CN) $_6$] at 1%. The mixture was incubated in a water bath at 50°C for 20 minutes, then 1.25 mL of trichloroacetic acid (10%) was added to stop the reaction. The tubes are centrifuged at 3000 rpm for 10 minutes. An aliquot (1.25 mL) of supernatant is combined with 1.25 mL of distilled water and 0.25 mL of a 0.1% aqueous $FeCl_3$ (ferric chloride) solution. Ascorbic acid is used as a standard, and the final results are expressed in milligram equivalents of ascorbic acid per gram of extract.

2.7.3. Trolox Equivalent Antioxidant Capacity (TEAC) Assay. For the ABTS test (2,2′-Azino-bis (3-ethylbenzothiazoline-6-sulfonic acid)), the cationic radical ABTS was generated by mixing 10 mL of the solution of ABTS (2 mM) in H_2O and 100 μL of the potassium persulfate solution (70 mM). The mixture is preserved for 16 hours. The resulting solution was diluted with methanol to obtain an absorbance of 0.70 to 734 nm. From this solution, 2 mL of diluted ABTS were mixed with 200 μL of each extract at a concentration of 1 mg/mL and allowed to react for 1 minute. The absorbance was measured at 734 nm. Trolox is used as a standard, and the final results are expressed in milligram equivalents of Trolox per gram of extract [19].

2.7.4. H_2O_2 Test. The activity of scavenging H_2O_2 was determined by the Muruhan et al. [20] method. A solution of H_2O_2 (40 mmol/L) was prepared in phosphate buffer (pH 7.4). The concentration of H_2O_2 was determined spectrophotometrically from the absorption at 230 nm. Indeed, 1 mL of the extract or of the standard (ascorbic acid) at different concentrations was added to the H_20_2 solution (0.6 mL, 40 mmol/L). After 10 min of incubation, the absorbance of H_2O_2 was determined at 230 nm against a blank solution containing a phosphate buffer without H_2O_2. The scavenging percentage of H_2O_2 for the extract and ascorbic acid was calculated using the following equation:

$$\% = \left[\frac{(A_0 - A_1)}{A_0}\right] \times 100, \quad (2)$$

where A_0 was the absorbance of the control and A_1 was the absorbance in the presence of the sample or standard.

2.7.5. Xanthine Inhibition Assay. Inhibition of xanthine oxidase (xo) was determined by Umamaheswari et al. [21]. However, 1 mL of the extract or standard (allopurinol) was mixed with 1.9 mL of phosphate buffer (pH 7.5), 0.1 mL of enzyme solution (0.2 units/mL), and 1.0 mL of 0.5 mM xanthine solution. The reaction mixture was incubated for 15 minutes at 25°C. Subsequently, the enzymatic reaction was stopped with 1 mL of 1 M HCl, and the absorbance of the reaction mixture was measured at 295 nm against a control

solution prepared in the same manner without adding any enzyme solution. The percentage of XO inhibition was calculated as follows:

$$I(\%) = \left[\left(\frac{(\mathrm{Ac} - \mathrm{Acb}) - (\mathrm{As} - \mathrm{Asb})}{(\mathrm{Ac} - \mathrm{Acb})}\right) \times 100\right], \quad (3)$$

where Ac denoted the absorbance of the control, Acb the absorbance of the control blank, As the absorbance of the sample, and Asb the absorbance of the sample blank.

2.7.6. Animals. Healthy male mice (20–25 g) were used in the experiments. Animals were kept in cages at the Rabat Faculty of Medicine and Pharmacy (Morocco) and maintained in a controlled room at 22 ± 02°C with a 12 h light–dark cycle with free access to water and standard food.

2.7.7. Ethics Approval. The study was conducted in accordance with the principles described in the "Guide for the Care and Use of Laboratory Animals", 8th edition, prepared by the National Academy of Sciences (National Research Council of the National Academies, 2011). Every effort was made to minimize animal suffering and the number of animals used. Mohammed V University in Rabat granted ethics approval.

2.7.8. Experimental Design

(1) (1) Development of Type 2 Diabetes. The antihyperglycemic effect of *E. guttatum* extract was studied in hyperglycemic mice induced by HFD. Indeed, after 15 days of accommodation, excluding normal control with a normal diet, the other mice were fed a high-fat diet. The diet was prepared daily as described in the literature [22]. It consists of standard diet carbohydrates at 50%, protein at 18%, fat at 30%, and salt and vitamins at 2%. After 4 weeks, the mice received an intraperitoneal injection of 100 mg/kg of streptozotocin dissolved in a citrate buffer (0.1 M, pH 4.5). Five days later, blood samples were taken from the tail vein of the fasting mice after the induction of STZ. Mice with a fasting blood sugar level greater than 126 mg/dL were considered T2DM and included in the study.

(2) (2) Experimental Design. After induction of diabetes, the thirty diabetic mice were divided into five groups of six mice each. The untreated diabetic group (negative control); the diabetic group treated with metformin at a dose of 300 mg/kg (positive control); and the aqueous, ethanol, and methanol extracts were given to the other three diabetic groups at a dose of 200 mg/kg [23, 24]. The normal group containing the six nondiabetic mice was allowed free access to a normal diet and treated with saline.

2.7.9. Preparation of Homogenates. At the end of the treatment, we extracted the organs (liver, kidney, and pancreas) for the determination of the markers of oxidative stress. Initially, we cut and ground the organs with 10% phosphate buffer (0.05 M, pH 7.4). Subsequently, the homogenate was centrifuged at 10,000 rpm for 10 min at 4°C. In the last step, we collected the supernatant and stored it as an aliquot at -20°C for analysis of oxidative stress parameters.

2.7.10. Determination of Malondialdehyde (MDA). The determination of malondialdehyde is based on the measurement in acidic and hot media of the MDA-TBA complex according to the Ohkawa et al.'s technique [25]. 100 μL of the homogenate or MDA was mixed with 300 μL of 0.6% thiobarbituric acid and 700 μL of 1% phosphoric acid. The reaction mixture was then heated to 95°C for 30 minutes. After cooling, 2 mL of n-butanol was added and then centrifuged at 3000 rpm for 10 minutes. The absorbance of the MDA-TBA complex was determined spectrophotometrically at 535 nm.

2.7.11. Superoxide Dismutase Assay. Superoxide dismutase (SOD) constitutes the enzymes of the first lines of defense against free radicals. They disproportionate the superoxide anion into hydrogen peroxide and oxygen. The assay is carried out according to the method of Beauchamp and Fridovich [26]. A reaction mixture was prepared by adding 50 mM phosphate buffer (pH 7.2), 0.25% triton x-100, 10 mM EDTA (pH 8), 120 mM L-methionine, 0.75 mM NBT, and at the end, 10 μM of riboflavin. The reaction was performed at 25°C under a 15 W lamp for 10 min to induce the photoreaction of riboflavin and O_2. The absorption is read at 560 nm, and the SOD (superoxide dismutase) activity is calculated according to the following equation:

$$\text{Inhibition\%} = \left(\frac{\text{Absorbance Blank} - \text{Absorbance sample}}{\text{Absorbance blank}}\right) \times 100. \quad (4)$$

The SOD unit is the amount of enzyme that causes 50% inhibition of NBT reduction.

2.7.12. Catalase Activity. Catalase activity was determined by the Aebi [27] method, measuring the disappearance of hydrogen peroxide (H_2O_2). The catalytic activity was expressed in μmol of H_2O_2 per minute and per mg of protein. 780 μL of phosphate buffer (100 mM, pH 7.5) was mixed with 20 μL of homogenate. Then, the reaction was initiated by adding 200 μL of hydrogen peroxide (H_2O_2) (500 mM). The decrease in optical density due to the decomposition of hydrogen peroxide after 1 min was measured against the blank without homogenate at 240 nm.

2.7.13. Glutathione (GSH) Activity Assay. The glutathione level was measured according to the Maron method [28]. The assay is based on the reduction of 5.5-dithio-bis-2-nitrobenzoic acid (Ellman's reagent) by the (-SH) groups of glutathione. Indeed, the reaction mixture contained 200 μL of TCA (5%) and 400 μL of homogenate and was centrifuged at 12,000 g for 10 min, then 50 μL of the supernatant was taken and added to 100 μL of DTNB (6 mM) and 850 μL of 50 mM phosphate buffer. The absorbance was read after 5 min at 412 nm.

3. Results

3.1. Mineral Composition. The mineral composition of *E. guttatum* roots is summarized in Table 1. Five macroelements (calcium (Ca^{2+}), potassium (K^{+}), magnesium (Mg), sodium (Na^{+}), and phosphorus (P)) and fourteen microelements (boron (B), manganese (Mn), copper (Cu), iron (Fe^{2+}), zinc (Zn), molybdenum (Mo), nickel (Ni), cobalt (Co), chromium (Cr), selenium (Se), lead (Pb), vanadium (V), arsenic (AS), and cadmium (Cd)) were analyzed. As can be seen, roots contain significantly more Ca^{2+} (28300.88 mg/kg), K^{+} (8861.61 mg/kg), Mg (2421.03 mg/kg), and P (1421.74 mg/kg), with minor content in Zn (334. 74 mg/kg), Na (228.26 mg/kg), Fe^{2+} (170.54 mg/kg), B (19.54 mg/kg), Mn (18.15 mg/kg), and Cu (15.64 mg/kg) and trace amounts of Se (0.01 mg/kg), Cd (0.12 mg/kg), and Mo (0.5 mg/kg).

3.2. Phenolic, Flavonoids, and Tannin Contents. The quantification of polyphenols, condensed tannins, and total flavonoids of *E. guttatum* extracts is presented in Table 2. In fact, the quantity of phenols is greater in the methanolic extract (389.20 ± 1.55 mg of GAE/g of extract), followed by the ethanol extract (348.1 ± 2.3 mg of GAE/g of extract), and aqueous (248.17 ± 1.81 mg of GAE/g of extract). The condensed tannins are also much more concentrated in the methanolic extract (289.70 ± 3.57 mg EC/g of extract) than in the ethanolic extract (243.3 ± 2.21 mg EC/g of extract) and aqueous (114.95 ± 2.60 mg EC/g of extract). The same observations were recorded for flavonoids, the methanolic extract (432.5 ± 3.21 of ER/g of extract), the ethanolic extract (417.5 ± 1.42 of ER/g of extract), and the aqueous extract (315.5 ± 4.50 of ER/g of extract).

3.3. Chemical Bioactive Compounds. The compounds identified by the ESI-HRMS experiment are summarized in Table 3, the selectivity of HRMS (Figure 1) as well as molecular formulas, RDB (Rings and Double Bond Equivalents) unsaturation values, and mass accuracy. Direct analysis by electrospray ionization (ESI) in both negative and positive mode in full mass scanning (m/z 50 to 1000 amu) identified 10 compounds, summarized as follows: shikimic acid, rottlerin, rugulosin, and procyanidin C1 in EGA at m/z of (174, 516, 542, and 866). Sucrose, tiliroside, and vanillic acid have m/z values of 342, 594.13, and 168 in EGE, respectively; the presence of gallic acid at m/z; 170 and catechin (m/z; 290) in EGA, EGM, and EGE.

3.4. Antioxidant Activity

3.4.1. In Vitro Studies

(1) (1) Scavenging of the Free Radical DPPH. The antiradical activity profile of each extract tested against the DPPH radical is presented in Figure 2. Indeed, these curves reveal that the antiradical power is proportional to the concentration of the extracts. We found that the percentage of inhibition increased as the concentration of the extracts increases.

Table 1: Mineral composition of *Erodium guttatum* roots.

Mineral composition (mg/kg)	*E. guttatum*
B	19.54
Ca	28300.88
Cu	15.64
Fe	170.54
K	8861.61
Mg	2421.03
Mn	18.15
Na	228.26
P	1421.74
Zn	334.74
As	4.12
Cd	0.12
Co	3.45
Cr	5.12
Mo	0.5
Ni	7.14
Pb	5.87
Se	0.01
V	7.14

From these data, the IC_{50} inhibitory concentration was determined by GraphPad prism 6 software, and it is shown in Table 4. The results obtained show that each extract tested has an interesting antifree radical power. Indeed, by comparing the IC_{50} values, it is observed that the methanolic extract has a significantly higher activity than aqueous and ethanolic extracts ($p < 0.05$). Thus, the ethanolic extract of *E. guttatum* has a significantly higher antiradical activity than the aqueous extract ($p < 0.05$).

(2) (2) Iron-Reducing Power (FRAP). Ferric reducing power can serve as a significant indicator of antioxidant potential. The methanol extract showed better antioxidant activity. In addition, the methanolic extract has a reducing power of 540.2 ± 1.40 mg EAA/gE, which is significantly ($p < 0.05$) higher than that of the ethanolic extract (220.72 ± 1.05 mg EAA/gE). Thus, the aqueous extract showed significantly ($p < 0.05$) higher antioxidant activity than the ethanolic extract (Table 4). Furthermore, if we rank our extracts according to iron reduction potency with respect to ascorbic acid, we will obtain the following order: methanolic extract of *E. guttatum*, aqueous extract of *E. guttatum*, and ethanolic extract of *E. guttatum*.

(3) (3) Antioxidant Power by ABTS. The antioxidant activity of three tested extracts was evaluated using the ABTS method. The results of the extracts are presented in Table 4 and are expressed as TEAC (TROLOX Equivalent Antioxidant Capacity). Indeed, the results showed that methanolic extract has a significantly ($p < 0.05$) powerful activity of 228.68 ± 2.93 mg of Trolox ET/gE, while aqueous extract has an antioxidant power of 218.52 ± 1.34 mg of

Table 2: Total phenolic, flavonoid, and condensed tannin contents of *E. guttatum*.

		Phenolic content[(1)]	Flavonoids content[(2)]	Tannin content[(3)]
Erodium guttatum	Aqueous extract	248.17 ± 1.81	315.5 ± 4.50	114.95 ± 2.60
	Methanol extract	389.20 ± 1.55	432.5 ± 3.21	289.70 ± 3.57
	Ethanol extract	348.1 ± 2.3	417.5 ± 1.42	243.3 ± 2.21

The results are expressed as [(1)] mg of gallic acid equivalent, [(2)] mg of rutin equivalent, and [(3)] mg of catechin equivalent.

Table 3: Data from aqueous, ethanolic, and methanolic extracts of *E. guttatum* root by ESI-HRMS experiments.

m/z	Name	Formula	RDB equiv
170	Gallic acid	$C_6H_6O_5$	5.5
290	Catechin	$C_{15}H_{14}O_6$	9.5
516	Rottlerin	$C_{30}H_{28}O_8$	17.5
866	Procyanidine C1	$C_{45}H_{38}O_{18}$	27.5
120	Purine	$C_5H_4N_4$	6.5
174	Shikimic acid	$C_7H_{10}O_5$	3.5
542	Rugulosin	$C_{30}H_{22}O_{10}$	19.5
168	Vannilic acid	$C_8H_8O_4$	5.5
342	Sucrose	$C_{12}H_{22}O_{11}$	2.5
594	Tilirozide	$C_{30}H_{26}O_{13}$	17.5

Trolox ET/gE, and ethanolic extract shows an activity of 189.13 ± 1.41 mg of Trolox ET/gE.

(4) (4) Hydrogen Peroxide Trapping Test H_2O_2. The scavenging effects of aqueous and alcoholic extracts of *E. guttatum* and ascorbic acid on the H_2O_2 radicals expressed by IC_{50} are shown in Table 4. The hydrogen peroxide H_2O_2 scavenging test showed that the aqueous extract exhibited the best antioxidant effect. By comparing the IC_{50} values, the aqueous extract ($IC_{50} = 4.65 \pm 0.7\ \mu g/mL$) presented an activity that was significantly ($p < 0.05$) higher than that of ascorbic acid ($IC_{50} = 5.98 \pm 0.47\ \mu g/mL$). Moreover, the ethanolic extract showed significantly ($p < 0.05$) higher activity than the methanolic extract.

(5) (5) Xanthine Oxidase Test. Xanthine oxidase is a flavoprotein that catalyzes the oxidation of hypoxanthine to xanthine and generates superoxide and uric acid. Indeed, the results obtained indicate that the methanolic extract presented the best inhibitory activity of 4.85 ± 0.80 μg/mL. Similarly, the methanolic extract has a significantly ($p < 0.05$) higher activity than the ethanolic (7.80 ± 1.5 μg/mL) and aqueous (7.83 ± 1.21 μg/mL) extracts. On the other hand, there is no difference in inhibitory activity between the aqueous and ethanolic extracts (Table 4).

3.4.2. In Vivo Studies

(1) (1) Lipid Peroxidation. The effect of aqueous and alcoholic extracts of *E. guttatum* on lipid peroxidation in hepatic, renal, and pancreatic tissues in mice rendered diabetic by HFD-STZ is summarized in Table 5. Indeed, we found an elevation of MDA in the liver, kidneys, and pancreas of untreated diabetic mice (0.961 ± 0.07 nM/g liver; 0.813 ± 0.08 nM/g liver; 0.861 ± 0.09 nM/g liver), respectively, compared to the nondiabetic control group (0.36 ± 0.03 nM/g liver; 0.24 ± 0.02 nM/g liver; 0.402 ± 0.02 nM/g liver). Likewise, *E. guttatum* extracts reduced MDA levels compared to the control (nondiabetic) group. The diabetic group treated with the methanolic extract showed a better reduction in MDA. In addition, in the liver and kidney, there was a significant difference between the group treated with methanol extract (0.188 ± 0.03 nM/g liver; 0.195 ± 0.03 nM/g kidney) and the group treated with metformin (0.55 ± 0.06 nM/g liver; 0.42 ± 0.03 nM/g kidney) ($p < 0.05$). The control (nondiabetic) group was significantly inferior to the metformin-treated group ($p < 0.05$) in the liver and kidney.

(2) (2) Superoxide Dismutase (SOD), Catalase (CAT), and Glutathione (GSH) Activity. The extracts of *E. guttatum* enhanced the production of enzymatic and nonenzymatic antioxidants (SOD, CAT, and GSH, respectively). The results are presented in Tables 6, 7, and 8. For three tests, we found that the groups of mice treated with the methanolic extract showed better secretion of enzymatic and nonenzymatic antioxidants. Also, we noticed a better increase in SOD secretion in the groups of diabetic mice treated with the methanolic extract and metformin compared to the normal control group ($p < 0.05$). Similarly, the enzymatic activity of SOD on hepatic, renal, and pancreatic tissues was significantly reduced in untreated diabetic mice compared to that measured in normal controls ($p < 0.05$). On the other hand, diabetic mice treated with ethanolic and aqueous extracts caused an increase in SOD levels in the kidneys and pancreas, indeed, for ethanolic extract (799 ± 8.38 units/g of the kidney; 616.3 ± 1.44 units/g of the pancreas) and for the aqueous extract (768.2 ± 3.1 units/g of the kidney; 565.9 ± 1.92 units/g of pancreas).

In addition, in the three organs (liver, kidney, and pancreas), the level of CAT was increased in the groups of diabetic mice treated with the aqueous, ethanolic, and methanolic extracts. Similarly, the treatment of diabetic mice with extracts of *E. guttatum* caused an increase in the level of CAT compared to the groups of mice treated with metformin ($p < 0.05$). Thus, there was no significant difference between the normal (nondiabetic) control group and the metformin-treated group ($p < 0.05$). Similarly, there was no significant difference between the groups of diabetic mice treated with the methanolic extract (0.46 ± 0.23 U/mg of protein) and the ethanolic extract (0.46 ± 0.11 U/mg protein) ($p > 0.05$) in the liver.

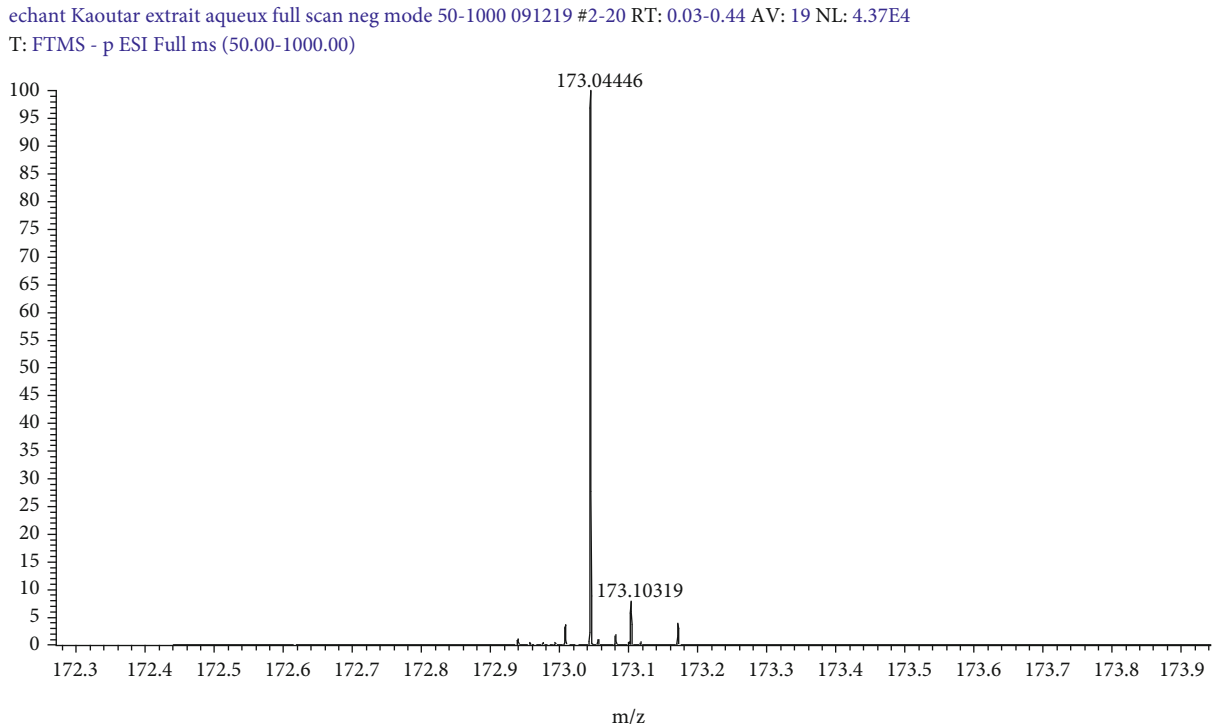

Figure 1: HRMS mass spectrum obtained in negative mode for shikimic acid in aqueous extract.

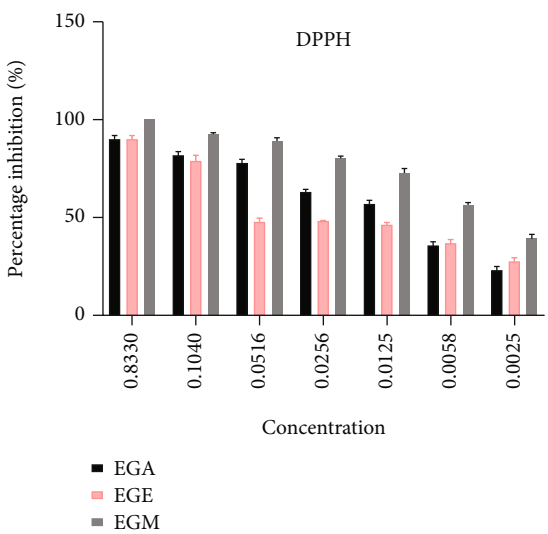

Figure 2: Percentage of DPPH radical inhibition by extracts of *E. guttatum*. EGA: *Erodium guttatum* aqueous extract; EGM: *Erodium guttatum* methanolic extract; EGE: *Erodium guttatum* ethanolic extract.

Similarly, in the liver and kidney, the GSH level was significantly increased in the groups of diabetic mice treated with the three extracts. In the pancreas, the level of GSH in the groups of mice treated with the aqueous extract ($77.0 \pm 0.05\,\mu$mol/mg of protein) is significantly higher than that of the groups treated with the methanolic extract ($67.4 \pm 0.0305\,\mu$mol/mg of protein) and ethanol ($62.2 \pm 0.0305\,\mu$mol/mg of protein) as well as the group treated with metformin ($63.3 \pm 0.0505\,\mu$mol/min/mg protein) and the untreated group ($65.6 \pm 0.0305\,\mu$mol/mg protein) ($p < 0.05$).

4. Discussion

Here, we reported mineral and phenolic composition of *E. guttatum* root extracts as well as their antioxidant and antidiabetic activities. Mineral composition analysis showed that *E. guttatum* roots are rich in Ca^{2+} (28300.88 mg/kg), K^{+} (8861.61 mg/kg), Mg (2421.03 mg/kg), and P (1421.74 mg/kg) with minor content of Se (0.01 mg/kg), Cd (0.12 mg/kg), and Mo (0.5 mg/kg). Indeed, these minerals are essential for restoring solid tissues in bones and teeth, as well as regenerating blood cells and maintaining osmotic balance [29]. K^{+} maintains the ionic balance and excitability of tissues, Ca^{2+} is an anticoagulant and necessary for the functioning of the myocardium, and Fe^{2+} plays an important role. It is involved in the binding of oxygen to hemoglobin and acts as a catalyst for several enzymes such as cytochrome oxidase. Magnesium protects muscle cells from degeneration, growth retardation, cardiomyopathy, immunological dysfunction, impaired spermatogenesis, and bleeding disorders [28, 29]. Chromium is one of the indispensable metals in the human body and animals. It is involved in the regulation of glucose tolerance [30–32]. For Pd, it has been reported that the permissible and accepted daily intake by WHO is 10 mg/kg. Thus, the roots of *E. guttatum* have a concentration lower than the allowed concentration [33]. The abundance of Ca^{2+}, K^{+}, and Mg is similar to other previous studies in plants [32–35].

Table 4: Antioxidant activity by DPPH, FRAP, ABTS, H_2O_2, and xanthine oxidase (XO) methods of *Erodium guttatum*; average of three replicates.

		DPPH test[(1)]	ABTS test[(2)]	FRAP test[(3)]	H_2O_2 test[(1)]	Xanthine oxidase (XO)[(1)]
Erodium guttatum	Aqueous extract	$7 \pm 3.78^{**}$	$218.52 \pm 1.34^{**}$	$338.7 \pm 0.56^{*}$	$4.65 \pm 0.7^{****}$	$7.83 \pm 1.21^{****}$
	Methanol extract	$3 \pm 1.45^{***}$	$228.68 \pm 2.93^{****}$	540.2 ± 1.40^{ns}	$7.43 \pm 1.58^{**}$	$4.85 \pm 0.80^{**}$
	Ethanol extract	$4 \pm 1.24^{***}$	$189.13 \pm 1.41^{****}$	220.72 ± 1.05^{ns}	$5.21 \pm 0.68^{****}$	$7.80 \pm 1.5^{****}$
BHT		3.28 ± 0.79	—	—	—	—
Ascorbic acid		—	—	—	5.98 ± 0.47	—
Allopurinol		—	—	—	—	0.78 ± 0.01

The results are expressed as [(1)] IC_{50} (μg/mL), [(2)] mg of Trolox equivalent, and [(3)] mg of ascorbic acid equivalent per gram of extracts. Data are the mean ± standard deviation. Values are mean ± SEM. ****Highly significant statistical difference ($p < 0.0001$), *** ($p < 0{,}001$), ** ($p < 0.01$), * ($p < 0.5$); ns: statistically insignificant difference.

Table 5: Malondialdehyde (MDA) levels in the liver, kidney, and pancreas in diabetic mice treated with extracts of *E. guttatum* (200 mg/kg) and metformin (300 mg/kg) (nM/mg tissue).

	EGA	EGM	EGE	DT	ND	DTM
Liver	$0.259 \pm 0.03^{a,c}$	0.188 ± 0.03^{a}	0.216 ± 0.03^{a}	0.961 ± 0.07^{b}	0.36 ± 0.03^{c}	0.55 ± 0.06^{d}
Kidney	$0.325 \pm 0.05^{e,h,i}$	0.195 ± 0.03^{f}	$0.251 \pm 0.04^{e,f}$	0.813 ± 0.08^{g}	$0.24 \pm 0.02^{f,h}$	0.42 ± 0.03^{i}
Pancreas	0.211 ± 0.01^{j}	0.180 ± 0.02^{j}	0.209 ± 0.02^{j}	0.861 ± 0.09^{k}	$0.402 \pm 0.02^{j,l}$	0.410 ± 0.04^{l}

Data represent the mean ± standard deviation of six independent experiments. Values in the same line with different superscript letters indicate significant differences (p value < 0.0001). Abbreviations: EGA: aqueous extract of *E. guttatum*; EGM: methanolic extract of *E. guttatum*; EGE: ethanolic extract of *E. guttatum*. DT: diabetic group; ND: nondiabetic group; DTM: metformin-treated diabetic group.

Table 6: Level of the antioxidant superoxide dismutase enzyme (SOD) in the liver, kidney, and pancreas in diabetic mice treated with extracts of *E. guttatum* (200 mg/kg) and metformin (300 mg/kg) (unit/g tissue).

	EGA	EGM	EGE	DT	ND	DTM
Liver	638.7 ± 6.21^{a}	793.1 ± 0.85^{b}	702.5 ± 0.95^{c}	532.3 ± 2.86^{d}	732.2 ± 11.7^{e}	904.3 ± 7.8^{f}
Kidney	768.2 ± 3.1^{g}	$811.4 \pm 2.17^{h,i}$	799 ± 8.38^{h}	420.5 ± 10.2^{j}	$830.0 \pm 3.06^{i,k}$	832.1 ± 9.2^{k}
Pancreas	565.9 ± 1.92^{l}	632.4 ± 3.75^{m}	616.3 ± 1.44^{m}	480.2 ± 22.5^{n}	540.6 ± 12.5^{l}	724.2 ± 6.3^{o}

Data represent the mean ± standard deviation of six independent experiments. Values in the same line with different superscript letters indicate significant differences (p value < 0.0001). Abbreviations: EGA: aqueous extract of *E. guttatum*; EGM: methanolic extract of *E. guttatum*; EGE: ethanolic extract of *E. guttatum*. DT: diabetic group; ND: nondiabetic group; DTM: metformin-treated diabetic group.

Table 7: Catalase (CAT) levels in the liver, kidney, and pancreas in diabetic mice treated with extracts of *E. guttatum* (200 mg/kg) and metformin (300 mg/kg) (U/mg protein).

	EGA	EGM	EGE	DT	ND	DTM
Liver	0.43 ± 0.05	0.46 ± 0.23	0.46 ± 0.11	0.18 ± 0.06	0.48 ± 0.04	0.47 ± 0.04
Kidney	0.46 ± 0.02	0.54 ± 0.02	0.49 ± 0.02	0.14 ± 0.03	0.56 ± 0.02	0.5 ± 0.06
Pancreas	0.51 ± 0.02	0.59 ± 0.01	0.54 ± 0.03	0.17 ± 0.08	0.43 ± 0.04	0.42 ± 0.02

Values are mean ± SD. Values are mean ± SEM. ns: statistically insignificant difference. EGA: aqueous extract of *E. guttatum*; EGM: methanolic extract of *E. guttatum*; EGE: ethanolic extract of *E. guttatum*; DT: diabetic group; ND: nondiabetic group; DTM: diabetic group treated with metformin.

The phytochemical assay reveals that methanolic extract is the richest in polyphenols, tannins, and flavonoids, with a content of 389.20 ± 1.55 mg of EAG/g of extract, 289.70 ± 3.57 mg EC/g of the extract, and 432.5 ± 3.21 mg of RE/g of the extract. However, these results can be explained by the difference in polarity of the solvents used to extract the phenolic molecules. These values are higher than those obtained by Hamza et al. [13] who worked on the same species from a different region. It was reported that *E. guttatum* hydromethanolic extract contains 124 ± 6 mg GAE/g extract of total polyphenols, 52 ± 2.3 d ER/g extract of flavonoids, and 20 ± 0.5 mg EC/g extract of tannins. Additionally, phenols and phenolic compounds, including flavonoids, have been reported to be widely present in plant sources and to promote antioxidant potency [36].

Table 8: Glutathione (GSH) levels in the liver, kidney, and pancreas in diabetic mice treated with extracts of *E. guttatum* (200 mg/kg) and metformin (300 mg/kg) (μmol/min/mg of proteins).

	EGA	EGM	EGE	DT	ND	DTM
Liver	79.1 ± 0.06^{a}	81.5 ± 0.02^{b}	71.3 ± 0.07^{c}	41.7 ± 0.03^{d}	89.0 ± 0.03^{e}	85.4 ± 0.05^{f}
Kidney	70.3 ± 0.05^{g}	79.6 ± 0.05^{h}	77.0 ± 0.04^{i}	35.2 ± 0.05^{j}	84.3 ± 0.05^{k}	87.0 ± 0.02^{l}
Pancreas	77.0 ± 0.05^{m}	67.4 ± 0.03^{n}	62.2 ± 0.03^{o}	33.2 ± 0.09^{p}	65.6 ± 0.03^{q}	63.3 ± 0.05^{r}

Data represent the mean ± standard deviation of six dependent experiments. Values in the same line with different superscript letters indicate significant differences (p value < 0.0001). Abbreviations: EGA: aqueous extract of *E. guttatum*; EGM: methanolic extract of *E. guttatum*; EGE: ethanolic extract of *E. guttatum*. DT: diabetic group; ND: nondiabetic group; DTM: metformin-treated diabetic group.

Chemical analysis by ESI-HRMS identified certain bioactive compounds such as shikimic acid, rottlerin, rugulosin, procyanidin C1, and vanillic acid. In addition, several scientific studies demonstrate the antidiabetic power of natural resources [37]. For example, shikimic acid is an intermediate metabolite synthesized from tryptophan that induces specific anabolic effects on bone, decreases oxidative stress, and reduces the expression of antioxidant genes in the diabetic retina of rats. Also, it decreases the formation of advanced glycation end products derived from glucose [38]. Gallic acid has antihyperglycemic, antilipid peroxidative, and antioxidant effects. It regulates mitochondrial function *via* the activation of the alpha receptor which are activated by the coactivator1 alpha peroxisome proliferators (PGC1 alpha) and increases the translocation of GLUT4 and therefore the activity of glucose absorption in an independent manner. Gallic acid prevents the damage caused by oxidative stress in the diabetic state [39]. Catechin maintains a low level of hemoglobin A (1c) in type 2 diabetics, improves the level of glucokinase, glucose-6 phosphatase, glycogen synthase, and glycogen phosphorylase, decreases the level of cholesterol and triglycerides, and induces the restoration of the structure of the artery wall and cerebral blood flow [40]. Moreover, other studies have also reported the antidiabetic effect of vanillic acid [39, 40].

The results obtained about antiradical activity *E. guttatum* root extracts show that methanolic extract has the strongest DPPH radical inhibitory activity, with an IC_{50} of 3 ± 1.45 μg /mL. This same extract has the most powerful iron-reducing power (540.2 ± 1.40 mg EAA/gE), which was observed with the FRAP test. This extract also has the ability to stabilize the highest ABTS cationic radical (228.68 ± 2.93 mg ET/gE). Also, the same result was observed by the xanthine oxidase test. On the other hand, the study of the antioxidant activity with H_2O_2 trapping test indicated that aqueous extract has the strongest inhibiting activity of the H_2O_2 radical with an IC_{50} of 4.65 ± 0.7 μg/mL. These different tests revealed that *E. guttatum* extracts have significant antioxidant effects, with minor differences between aqueous and alcoholic extracts. Moreover, these differences between these three extracts could be explained by the number of phenolic compounds such as polyphenols and flavonoids as well as the type of active ingredient present in each extract [41–44]. Moreover, by comparing our results with other results obtained for the same species, we found that the antioxidant activities of the root extracts of *E. guttatum* are more potent than those obtained by Hamza et al. [13].

In order to confirm the antioxidant effect *in vitro*, we studied the antioxidant effect *in vivo* on hepatic, renal, and pancreatic tissue in mice rendered diabetic by HFD-STZ. We found that the methanolic extract was the best extract that reduced MDA levels and therefore can inhibit lipid peroxidation, with a statistically insignificant difference compared to metformin. Similarly, we noticed an increase in the production of the MDA marker in untreated diabetic mice.

For the determination of enzymatic and nonenzymatic antioxidants (SOD, CAT, and GSH, respectively), we noticed an increase in antioxidant enzymes in diabetic mice treated with *E. guttatum* extracts with better secretion obtained by the methanolic extract. Indeed, lipid peroxidation is promoted by the generation of free radicals, which in turn produce end products such as malondialdehyde [45]. During oxidative stress, the level of peroxidation end products such as aldehydes increases, and the production of this biomarker is used in the measurement of oxidative stress [44, 45]. Thus, several modes of action of lipid peroxidation have been reported in the literature [46, 47]. These results obtained are similar to previous studies demonstrating the lipid peroxidation inhibitory effect of different plant extracts [48, 49]. Likewise, it has been reported that this activity can be attributed to the phenol content, which correlates with their chemical structures.

Superoxide dismutase (SOD) is one of the important enzymes of the antioxidant defense system. It removes by converting superoxide anions into hydrogen peroxide, thereby reducing toxicity caused by reactive oxygen species [50, 51]. Catalase is another antioxidant enzyme that catalyzes hydrogen peroxide into water and oxygen, protecting tissues from the deleterious effects of hydroxyl radicals. Glutathione (GSH) is a nonenzymatic tripeptide that hydrolyzes free radicals directly and protects proteins against free radicals [52, 53]. Treatment of diabetic mice with *E. guttatum* extracts showed an increase in the content of these enzymes in animal tissues. The extracts also increased the content of GSH protein. This indicates that these extracts may improve enzymatic activities by increasing the content of CAT, SOD, and GSH. In addition, it has been reported in several studies that medicinal plants can restore and activate the content of antioxidant enzymes in streptozotocin-induced diabetic animals [32, 54–56].

5. Conclusion

The phytochemical assay and the evaluation of the mineral composition of *E. guttatum* aqueous and alcoholic extracts

showed their richness in phenolic compounds (polyphenols, flavonoids, and tannins) and minerals. Similarly, the study of *in vitro* antioxidant activity using five methods (DPPH, ABTS, FRAP, H_2O_2, and xanthine oxidase) and *in vivo* (by the dosage of MDA, SOD, CAT, and GSH) showed that plant extracts, particularly the methanolic extract, exhibit remarkable antioxidant activity. Moreover, the results indicate a positive correlation between the antioxidant activity and the content of phenolic compounds. Moreover, the reducing and antiradical activities are well correlated; this means that the substances present in the plant extracts studied have the property of reducing oxidants and trapping free radicals. Therefore, the obtained data provides a basis for further toxicological and pharmacological studies.

Data Availability

The data used to support the findings of this study are included within the article.

Conflicts of Interest

The authors declare that they have no conflicts of interest.

References

[1] S. E. Lee, H. J. Hwang, J. S. Ha, H. S. Jeong, and J. H. Kim, "Screening of medicinal plant extracts for antioxidant activity," *Life Sciences*, vol. 73, no. 2, pp. 167–179, 2003.

[2] E. M. Jeong, M. Liu, M. Sturdy et al., "Metabolic stress, reactive oxygen species, and arrhythmia," *Journal of Molecular and Cellular Cardiology*, vol. 52, no. 2, pp. 454–463, 2012.

[3] B. Halliwell and J. M. C. Gutteridge, "The antioxidants of human extracellular fluids," *Archives of Biochemistry and Biophysics*, vol. 280, no. 1, pp. 1–8, 1990.

[4] H. C. Grice, "Safety evaluation of butylated hydroxyanisole from the perspective of effects on forestomach and oesophageal squamous epithelium," *Food and Chemical Toxicology*, vol. 26, no. 8, pp. 717–723, 1988.

[5] M. Y. Kim, P. Seguin, J. K. Ahn et al., "Phenolic compound concentration and antioxidant activities of edible and medicinal mushrooms from Korea," *Journal of Agricultural and Food Chemistry*, vol. 56, no. 16, pp. 7265–7270, 2008.

[6] K. Sayah, I. Marmouzi, H. Naceiri Mrabti, Y. Cherrah, and M. E. A. Faouzi, "Antioxidant activity and inhibitory potential ofCistus salviifolius(L.) andCistus monspeliensis(L.) aerial parts extracts against key enzymes linked to hyperglycemia," *BioMed Research International*, vol. 2017, Article ID 2789482, 7 pages, 2017.

[7] F. Shahidi, P. K. Janitha, and P. D. Wanasundara, "Phenolic antioxidants," *Critical Reviews in Food Science and Nutrition*, vol. 32, no. 1, pp. 67–103, 1992.

[8] J. El-Hilaly, M. Hmammouchi, and B. Lyoussi, "Ethnobotanical studies and economic evaluation of medicinal plants in Taounate province (Northern Morocco)," *Journal of Ethnopharmacology*, vol. 86, no. 2–3, pp. 149–158, 2003.

[9] M. Eddouks, M. Ajebli, and M. Hebi, "Ethnopharmacological survey of medicinal plants used in Daraa-Tafilalet region (province of Errachidia), Morocco," *Journal of Ethnopharmacology*, vol. 198, pp. 516–530, 2017.

[10] P. E. S. Munekata, C. Alcántara, M. C. Collado et al., "Ethnopharmacology, phytochemistry and biological activity of _Erodium_ species: A review," *Food Research International*, vol. 126, p. 108659, 2019.

[11] I. Fecka and W. Cisowski, "TLC determination of tannins and flavonoids in extracts from some Erodium species using chemically modified stationary phases," *Journal of Planar Chromatography - Modern TLC*, vol. 15, no. 6, pp. 429–432, 2002.

[12] R. L. Verhoeven and H. J. T. Venter, "Pollen morphology of Erodium in southern Africa," *South African J. Bot.*, vol. 53, no. 4, pp. 279–283, 1987.

[13] G. Hamza, B. H. Emna, W. Yeddes, Z. Dhouafli, T. S. Moufida, and H. El Akrem, "Chemical composition, antimicrobial and antioxidant activities data of three plants from Tunisia region: Erodium glaucophyllum, Erodium hirtum and Erodium guttatum," *Data Br.*, vol. 19, pp. 2352–2355, 2018.

[14] G. A. Spanos and R. E. Wrolstad, "Influence of processing and storage on the phenolic composition of Thompson seedless grape juice," *Journal of Agricultural and Food Chemistry*, vol. 38, no. 7, pp. 1565–1571, 1990.

[15] V. Dewanto, X. Wu, and R. H. Liu, "Processed sweet corn has higher antioxidant activity," *Journal of Agricultural and Food Chemistry*, vol. 50, no. 17, pp. 4959–4964, 2002.

[16] R. Julkunen-Tiitto, "Phenolic constituents in the leaves of northern willows: methods for the analysis of certain phenolics," *Nutr. Toxicol. Asp. Food Saf.*, vol. 33, no. 2, pp. 213–217, 1985.

[17] B. Huang, H. Ke, J. He, X. Ban, H. Zeng, and Y. Wang, "Extracts of Halenia elliptica exhibit antioxidant properties in vitro and in vivo," *Food and Chemical Toxicology*, vol. 49, no. 1, pp. 185–190, 2011.

[18] R. Amarowicz, R. B. Pegg, P. Rahimi-Moghaddam, B. Barl, and J. A. Weil, "Free-radical scavenging capacity and antioxidant activity of selected plant species from the Canadian prairies," *Food Chemistry*, vol. 84, no. 4, pp. 551–562, 2004.

[19] C. I. G. Tuberoso, M. Boban, E. Bifulco, D. Budimir, and F. M. Pirisi, "Antioxidant capacity and vasodilatory properties of Mediterranean food: the case of Cannonau wine, myrtle berries liqueur and strawberry-tree honey," *Food Chemistry*, vol. 140, no. 4, pp. 686–691, 2013.

[20] S. Muruhan, S. Selvaraj, and P. K. Viswanathan, "In vitro antioxidant activities of Solanum surattense leaf extract," *Asian Pacific Journal of Tropical Biomedicine*, vol. 3, no. 1, pp. 28–34, 2013.

[21] M. Umamaheswari, K. AsokKumar, A. Somasundaram, T. Sivashanmugam, V. Subhadradevi, and T. K. Ravi, "Xanthine oxidase inhibitory activity of some Indian medical plants," *Journal of Ethnopharmacology*, vol. 109, no. 3, pp. 547–551, 2007.

[22] P. S. Kanthe, B. S. Patil, S. C. Bagali, R. C. Reddy, M. R. Aithala, and K. K. Das, "Protective effects of ethanolic extract of Emblica officinalis (amla) on cardiovascular pathophysiology of rats, fed with high fat diet," *Journal of Clinical and Diagnostic Research*, vol. 11, p. 9, 2017.

[23] A. M. da Cunha, S. Menon, R. Menon, A. G. Couto, C. Bürger, and M. W. Biavatti, "Hypoglycemic activity of dried extracts of Bauhinia forficata link," *Phytomedicine*, vol. 17, no. 1, pp. 37–41, 2010.

[24] U. Sharma, R. K. Sahu, A. Roy, and D. K. Golwala, "In vivo antidiabetic and antioxidant potential of Stephania hernandifolia in streptozotocin-induced-diabetic rats," *Journal of Young Pharmacists*, vol. 2, no. 3, pp. 255–260, 2010.

[25] H. Ohkawa, N. Ohishi, and K. Yagi, "Assay for lipid peroxides in animal tissues by thiobarbituric acid reaction," *Analytical Biochemistry*, vol. 95, no. 2, pp. 351–358, 1979.

[26] C. Beauchamp and I. Fridovich, "Superoxide dismutase: improved assays and an assay applicable to acrylamide gels," *Analytical Biochemistry*, vol. 44, no. 1, pp. 276–287, 1971.

[27] H. Aebi, "[13] Catalase _in vitro_," *Methods in Enzymology*, vol. 105, no. C, pp. 121–126, 1984.

[28] M. Maron, J. W. Defierre, and B. Mannervik, "Levels of glutathione, glutathione reductase and glutathione _S_ -transferase activities in rat lung and liver," *Liver lung kidnet Biochem Biophys Acta*, vol. 582, no. 1, pp. 67–78, 1979.

[29] U. Usunobun and I. V. Chinwe, "Phytochemical screening, mineral composition and in vitro antioxidant activities of Pterocarpus mildbraedii leaves," *Int. J. Sci. World*, vol. 4, no. 1, p. 23, 2016.

[30] S. Datta, B. K. Sinha, S. Bhattacharjee, and T. Seal, "Nutritional composition, mineral content, antioxidant activity and quantitative estimation of water soluble vitamins and phenolics by RP-HPLC in some lesser used wild edible plants," *Heliyon*, vol. 5, no. 3, p. e01431, 2019.

[31] T. Seal, "Determination of nutritive value, mineral contents and antioxidant activity of some wild edible plants from Meghalaya state, India," *Asian Journal of Applied Sciences*, vol. 4, no. 3, pp. 238–246, 2011.

[32] R. Bhat, K. Kiran, A. B. Arun, and A. A. Karim, "Determination of mineral composition and heavy metal content of some nutraceutically valued plant products," *Food Analytical Methods*, vol. 3, no. 3, pp. 181–187, 2010.

[33] N. Boroomand, M. Sadat-Hosseini, M. Moghbeli, and M. Farajpour, "Phytochemical components, total phenol and mineral contents and antioxidant activity of six major medicinal plants from Rayen, Iran," *Natural Product Research*, vol. 32, no. 5, pp. 564–567, 2018.

[34] H. N. Mrabti, I. Marmouzi, K. Sayah et al., "Arbutus unedo L aqueous extract is associated with in vitro and in vivo antioxidant activity," *J. Mater. Environ. Sci.*, vol. 8, no. 1, pp. 217–224, 2017.

[35] L. Ferrara, D. Montesano, and A. Senatore, "The distribution of minerals and flavonoids in the tea plant (Camellia sinensis)," *Farmaco*, vol. 56, no. 5–7, pp. 397–401, 2001.

[36] S. A. Van Acker, M. N. Tromp, D. H. Griffioen, W. P. Van Bennekom, W. J. Van Der Vijgh, and A. Bast, "Structural aspects of antioxidant activity of flavonoids," *Free Radical Biology & Medicine*, vol. 20, no. 3, pp. 331–342, 1996.

[37] S. S. Zinjarde, S. Y. Bhargava, and A. R. Kumar, "Potent α-amylase inhibitory activity of Indian Ayurvedic medicinal plants," *BMC Complementary and Alternative Medicine*, vol. 11, 2011.

[38] A. L. Al-Malki, "Shikimic acid from Artemisia absinthium inhibits protein glycation in diabetic rats," *International Journal of Biological Macromolecules*, vol. 122, pp. 1212–1216, 2019.

[39] S. Manish Pal, G. Avneet, and S. S. Siddhraj, "Gallic acid: pharmacogical promising lead molecule: a review," *Int. J. Pharmacogn. Phytochem. Res.*, vol. 10, no. 4, pp. 132–138, 2018.

[40] A. Ganeshpurkar and A. Saluja, "The pharmacological potential of catechin," *Indian Journal of Biochemistry & Biophysics*, vol. 57, no. 5, pp. 505–511, 2020.

[41] N. Sharma, N. Tiwari, M. Vyas, N. Khurana, A. Muthuraman, and P. Utreja, "An overview of therapeutic effects of vanillic acid," *Plant Arch.*, vol. 20, pp. 3053–3059, 2020.

[42] A. Ingole, M. P. Kadam, A. P. Dalu et al., "A review of the pharmacological characteristics of vanillic acid," *J. Drug Deliv. Ther.*, vol. 11, pp. 200–204, 2021.

[43] S. Cai, C. Huang, B. Ji et al., "In vitro antioxidant activity and inhibitory effect, on oleic acid-induced hepatic steatosis, of fractions and subfractions from oat (Avena sativa L.) ethanol extract," *Food Chemistry*, vol. 124, no. 3, pp. 900–905, 2011.

[44] Y. Cai, Q. Luo, M. Sun, and H. Corke, "Antioxidant activity and phenolic compounds of 112 traditional Chinese medicinal plants associated with anticancer," *Life Sciences*, vol. 74, no. 17, pp. 2157–2184, 2004.

[45] M. A. Ghani, C. Barril, D. R. Bedgood, and P. D. Prenzler, "Measurement of antioxidant activity with the thiobarbituric acid reactive substances assay," *Food Chemistry*, vol. 230, pp. 195–207, 2017.

[46] L. M. Sayre, G. Perry, and M. A. Smith, "Oxidative stress and neurotoxicity," *Chemical Research in Toxicology*, vol. 21, no. 1, pp. 172–188, 2008.

[47] M. N. Alam, N. J. Bristi, and M. Rafiquzzaman, "Review on in vivo and in vitro methods evaluation of antioxidant activity," *Saudi Pharm. J.*, vol. 21, no. 2, pp. 143–152, 2013.

[48] E. E. Farmer and M. J. Mueller, "ROS-mediated lipid peroxidation and RES-activated signaling," *Annual Review of Plant Biology*, vol. 64, pp. 429–450, 2013.

[49] D. A. Butterfield, A. Castegna, C. B. Pocernich, J. Drake, G. Scapagnini, and V. Calabrese, "Nutritional approaches to combat oxidative stress in Alzheimer's disease," *The Journal of Nutritional Biochemistry*, vol. 13, no. 8, pp. 444–461, 2002.

[50] E. A. Irondi, G. Oboh, S. O. Agboola, A. A. Boligon, and M. L. Athayde, "Phenolics extract of Tetrapleura tetraptera fruit inhibits xanthine oxidase and Fe2+-induced lipid peroxidation in the kidney, liver, and lungs tissues of rats in vitro," *Food Science and Human Wellness*, vol. 5, no. 1, pp. 17–23, 2016.

[51] H. T. Abdul and I. Mohammed, "In vivo antioxidant and lipid peroxidation effect of various extracts from aerial parts of Chomelia asiatica (Linn) in rat fed with high fat diet," *African Journal of Pharmacy and Pharmacology*, vol. 10, no. 38, pp. 810–816, 2016.

[52] J. Eliza, P. Daisy, and S. Ignacimuthu, "Antioxidant activity of costunolide and eremanthin isolated from Costus speciosus (Koen ex. Retz) Sm," *Chemico-Biological Interactions*, vol. 188, no. 3, pp. 467–472, 2010.

[53] D. Yao, W. Shi, Y. Gou et al., "Fatty acid-mediated intracellular iron translocation: a synergistic mechanism of oxidative injury," *Free Radical Biology & Medicine*, vol. 39, no. 10, pp. 1385–1398, 2005.

[54] T. Livingston, K. Rich, S. MacKenzie, and J. D. Godkin, "Glutathione content and antioxidant enzyme expression of in vivo matured sheep oocytes," *Animal Reproduction Science*, vol. 116, no. 3–4, pp. 265–273, 2009.

[55] S. Arivazhagan, S. Balasenthil, and S. Nagini, "Garlic and neem leaf extracts enhance hepatic glutathione and glutathione dependent enzymes during N-methyl-N'-nitro-N-nitrosoguanidine (MNNG)-induced gastric carcinogenesis in rats," *Phyther. Res.*, vol. 14, no. 4, pp. 291–293, 2000.

[56] K. Bouabid, F. Lamchouri, H. Toufik, and M. E. A. Faouzi, "Phytochemical investigation, in vitro and in vivo antioxidant properties of aqueous and organic extracts of toxic plant: Atractylis gummifera L," *Journal of Ethnopharmacology*, vol. 253, 2020.

Hindawi
Oxidative Medicine and Cellular Longevity
Volume 2022, Article ID 4509019, 10 pages
https://doi.org/10.1155/2022/4509019

Research Article

Overexpression of hsa_circ_0061817 Can Inhibit the Proliferation and Invasion of Lung Cancer Cells Based on Active Compounds

Longping Ye,[1,2,3] Youqing Zhong,[1] Lihua Hu,[1] Ya Huang,[1,3] Xiang Tang,[1] Shanjun Yu,[1] Jianxin Huang,[1] Ziyuan Wang,[1] Qi Li,[1,2,3] and Xiangdong Zhou[1,2,3]

[1]*Department of Respiratory Medicine, The First Affiliated Hospital of Hainan Medical University, Haikou, Hainan 570102, China*
[2]*NHC Key Laboratory of Tropical Disease Control, Hainan Medical University, Haikou 571199, China*
[3]*Key Laboratory of Emergency and Trauma of Ministry of Education, Hainan Medical University, Haikou 571199, China*

Correspondence should be addressed to Qi Li; lqlq198210@sina.com

Received 12 July 2022; Revised 27 July 2022; Accepted 2 August 2022; Published 16 September 2022

Academic Editor: Tarique Hussain

Objective. This study was aimed at investigating the expression level of hsa_circ_0061817 in lung adenocarcinoma cells and its effect on cell proliferation and invasion and the possible mechanism of hsa_circ_0061817 in lung adenocarcinoma. *Methods.* The overexpression plasmids of hsa_circ_0061817 (OE-hsacirc_0061817) were transfected into human lung A549 cells and mouse LLC-LUC cells, respectively. The cell viability was detected by CCK-8, and the cell proliferation was detected by cell clone formation assay and EdU assay. Transwell test was used to detect the ability of cell invasion, and apoptosis was detected by flow cytometry. WB was applied to determine the expression of apoptosis and epithelial mesenchymal transition- (EMT-) related proteins and also target proteins for observation the effect of OE-hsa_circ_0061817 on the growth of A549 cells in nude mice. Bioinformatics method was used to predict the binding microRNA (miRNA) of hsa_circ_0061817 and construct the regulatory network of competitive endogenous RNA (ceRNA) and functional analysis of miRNA target genes. *Results.* Compared with PLO-ciR group, the cell viability, proliferation, and invasive ability of A549 and LLC-LUC were significantly reduced in OE-hsa_circ_00061817 group, while the apoptosis increased in OE-hsa_circ_00061817 group compared to PLO-ciR group. WB results showed that the expression of caspase 3, caspase 7, caspase 9, and E-cadherin increased significantly, while the expression levels of vimentin and N-cadherin decreased severely. Most importantly, OE-hsa_circ_00061817 inhibited the growth of A549 tumor-bearing nude mice. According to TargetScan and mirBase databases, hsa_circ_0061817 may competitively bind hsa_mir-181b-3p, hsa-mir-337-3p, hsa-mir-421, and hsa-mir-548d-3p. The results of functional enrichment showed that miRNA target genes were involved in many cancer-related biological processes, including negative regulation of apoptosis, gene expression, transcriptional imbalance in cancer, transforming growth factor-β, and P53 signal pathway. *Conclusions.* Over expression of hsa_circ_0061817 inhibits the proliferation of lung adenocarcinoma A549 and LLC-LUC cells and may reduce the invasive ability of lung adenocarcinoma cells by weakening the process of EMT, which provides a new target for the prevention and treatment of lung adenocarcinoma.

1. Introduction

Lung adenocarcinoma is one of the most common malignant tumors, and the mortality rate ranks first in all malignant tumors [1]. Among them, the incidence rate in East Asian countries is about half, and the mortality rate is higher than that in other countries [2, 3]. Most patients with lung adenocarcinoma are often in an advanced stage with distant metastasis and poor prognosis. The 5-year survival rate is only 20%~30% [4, 5]. If early lung adenocarcinoma can be found and treated in time, the 5-year survival rate can reach 90% [6]. The occurrence and development of lung adenocarcinoma are affected by many factors [7], but its exact etiological mechanism is still unclear, which greatly limits its further treatment.

Circular RNA (circRNA) is a kind of noncoding RNA molecule with 5′ and 3′ ends covalently bound to form a circular structure [8, 9]. It has the characteristics of abundant

expression, stable structure, evolutionary conservation, and competitive endogenous and has become a research hotspot in the field of RNA [10, 11]. A large number of studies have found that lncRNA has the functions of regulating genes, interfering with transcription, regulating protein function, intranuclear transport, and so on [12]. Further studies have found that lncRNA is involved in the occurrence and progression of many diseases, especially in the process of tumorigenesis and evolution. It has the function of protocancer or tumor suppressor. lncRNAs are aberrantly expressed in many tumors by regulating gene expression [13]. Moreover, circRNAs play a variety of important roles in cell biology by binding with miRNAs and RNA binding proteins, or act as protein translation templates and immune regulators in cells [14, 15], thereby participating in the occurrence and development of human tumors. In addition, circRNA can be stably expressed in tissue, blood, urine, and saliva, which makes it a great potential to become a biomarker in the clinic [16]. circRNAs are thought to affect carcinogenesis through sponging miRNAs, binding with protein, influencing splicing events or transcription of genes, and even by translation into proteins or small peptides [17]. Abnormal expression patterns of circRNAs have been associated with pathogenesis of human cancers including lung cancer. Therefore, it is of great significance to find specific circRNAs related to lung adenocarcinoma and explore their mechanism in the occurrence and development of lung adenocarcinoma.

It has been reported that lncRNAs play an important role in regulating tumor progression and tumor biological behaviors such as gene expression, cell proliferation, cell differentiation, immune responses, and apoptosis, among which the most crucial process is the regulation of competing endogenous RNAs (ceRNAs) [18, 19]. The ceRNA hypothesis, first proposed by Salmena et al. in 2011, has gained a lot of attention in terms of tumorigenesis [20]. Basically, the hypothesis states that, in the ceRNA gene interaction network, which consists of lncRNAs, miRNAs, and mRNAs, lncRNAs can act as miRNA sponges and inhibit miRNA functions by sharing miRNA response elements (MRE), thereby indirectly regulating mRNA expression levels [21]. Hence, the idea that lncRNAs could serve as promising biomarkers for multiple diseases has gained increasing attention. Currently, the importance of the lncRNA-miRNA-mRNA-ceRNA regulatory network has been confirmed in various types of cancers [22–24]. However, only few studies on the roles of lncRNAs have been conducted in lung cancer. Moreover, lncRNA-related ceRNA network remains unelucidated in lung cancer.

The previous study of our research group found that hsa_circ_0061817 showed significantly low expression only in lung adenocarcinoma tissues, especially in early lung adenocarcinoma tissues, showing good lung adenocarcinoma tissue specificity. However, it is relatively lacking of relevant studies of hsa_circ_0061817 on regulating lung cancer cells. Therefore, this study was aimed at further exploring the important regulatory role of hsa_circ_0061817 on the proliferation and invasion of lung adenocarcinoma cells and its key molecular mechanism, in order to provide new ideas for the treatment of lung adenocarcinoma.

2. Materials and Methods

2.1. Materials. Human lung adenocarcinoma cell lines A549 and LLC-LUC were purchased from the Cell Bank of Shanghai Chinese Academy of Sciences. 6-week-old male BALB/c nude mice were purchased from Shanghai Slaker Experimental Animal Co., Ltd. with animal production license No. SCXK (Shanghai) 2017-0015 and raised in the animal center of Hainan Medical College, with animal use license No. 2022-0013 (Hainan Medical College). Fetal bovine serum (No. 42Q1782K), RPMI1640 medium (No. 31870082), and ham's F-12K medium (No. 21127022) were purchased from GIBCO company in the United States. CCK-8 Kit (No. C0037), Ripa lysate (No. P0013K), BCA protein concentration determination kit (No. P0012), Beyoclick™ EdU-555 cell proliferation detection kit (No. C0075S), ECL color development kit (No. P0018FS), and Annexin V/PI apoptosis detection kits (No. 4136994) were purchased from BD company in the United States. TRIzol reagent (No. 15596026) was purchased from Invitrogen company in the United States. PrimeScript™ RT master mix (No. RR036A) and SYBR® Premix EX Taq™ (No. RR820A) were purchased from Takara company in Japan. Caspase 3 (No. ab2302), caspase 7 (No. ab255818), caspase 9 (No. ab32539), E-cadherin (No. ab235682), vimentin (No. ab137321), N-cadherin (No. ab76011), and GAPDH (No. ab8245) were purchased from American Abcam company. Horseradish peroxidase-labeled donkey anti-rabbit IgG antibody (No. 1534671) was purchased from Life Technologies in the United States. Goat anti-mouse IgG antibody labeled with horseradish peroxidase (No. ab1501115) was purchased from Abcam company in the United States. hsa_circ_0067582 overexpression (OE-circ 0067582) plasmid and its negative control were purchased from Gemma gene (Shanghai Co., Ltd). Lipofectamine 2000 (No. 11668019) was purchased from Invitrogen company in the United States.

2.2. Cell Culture. Human lung adenocarcinoma cell lines A549 and LLC-LUC were treated with 10% fetal bovine serum and 1% double antibody (100 U/ml penicillin and 100 U/ml penicillin, respectively), F-12K medium, and RPMI1640 medium and cultured in 37°C and 5% CO_2 cell incubator. The cells were subcultured when the degree of cell fusion reached 80%.

Real-time fluorescence quantitative PCR (qRT-PCR) was used to detect the expression level of hsa_circ_0061817 in A549 and LLC-LUC cells. GAPDH was used as internal reference for relative quantification. The total RNA of cells was extracted by TRIzol method, and the RNA concentration was detected by spectrophotometer when A260/A280 value was between 1.8 and 2.0. RNA reverse transcription was further performed. has_circ_0061817 reverse transcription was performed by PrimeScript™ RT master mix reverse transcription kit. SYBR® Premix Ex Taq™ kit was applied for qRT-PCR amplification with CFX96 real-time quantitative

PCR instrument (Bio-Rad company in the United States), using $2^{-\Delta\Delta Ct}$. The relative expression of has_circ_0061817 was calculated by CT method. Three multiple wells were set for each sample, and the experiment was repeated three times. Primer sequence is as follows: hsa_circ_0061817 upstream primer: 5′ CACAGTGGCAAAAGAAACTTGGT 3′, downstream primer: 5′ TGT GGGGTCCAAGATAT GGC 3′, and GAPDH upstream primer: 5′ ACCCAC TCCTCCCCTTTGAC 3′, downstream primer: 5′ TGTT GCTGTAGCCAAATTCGTT 3′.

2.3. Cell Transfection. The full-length coding sequence of hsa_circ_0061817 was cloned into PLO-ciR vector, and the blank PLO-ciR vector was used as negative control. A549 and LLC-LUC cells were inoculated into 6-well plates (1×10^5/well), when the cell fusion degree reaches 60%; the serum-free medium containing OE-circ 0061817 plasmids and PLO-ciR vector was added to the 6-well plate according to the operation steps of the transfection reagent Lipofectamine 2000. After 48 h transfection, the cells were collected, and qRT-PCR was used to detect the overexpression efficiency of plasmid.

2.4. Cell Viability Was Detected by CCK-8 Method. A549 and LLC-LUC cells transfected with OE-circ 0067582 plasmid were treated with 5×10^3 pieces/well evenly spread in 96 well plates, cultured at 37°C and 5% CO_2 for 24, 48, 72, and 96 hours, respectively, and then added to each well 10 ml mix of CCK-8 solution evenly. The culture plate was incubated in the incubator for 4 hours, and the absorbance value of each well at 450 nm was measured with an enzyme labeling instrument. Each group was set 6 multiple wells.

2.5. Clone Formation Experiment. After transfection, A549 and LLC-LUC cells (5×10^2 cells/well) were collected and inoculated into a 24 well plate and incubated in an incubator. The culture medium was changed every three days. After 14 days, the formation of cell clone was visible to the naked eye. The culture medium was sucked and discarded. PBS was used for washing three times and stained with 0.5% crystal violet for 15 min, then washed with pure sterilized water, and observed the number of cell clones.

2.6. EdU Assay Was Used to Detect Cell Proliferation. A549 and LLC-LUC cells inoculated into 24 well plates were transfected for 48 hours, fixed with 4% paraformaldehyde for 30 minutes, decolorized with 2 mg/ml glycine, and incubated in shaking table for 5 minutes; 5% TritonX-100 decolorizing shaker was incubated for 10 min; and the cells were stained with Apollo and DAPI according to the instructions of Beyoclick™ EdU-555 kit. After being sealed with antifluorescence quencher, the cells were photographed under fluorescence inverted microscope.

2.7. Transwell Assay Was Used to Detect Cell Invasion. A549 and LLC-LUC cells were transfected with OE-ciR 0061817 plasmids and blank PLO-ciR vectors, respectively. After being cultured in the cell incubator for 48 hours, the cells were collected after routine digestion with 25% trypsin. After PBS cleaning, they were resuspended with serum-free medium to make a single cell suspension. The cell concentration was adjusted to 1×10^5/ml. Then, 100 μl cells were inoculated into the Transwell chamber covered with matrix glue and hydrated with serum-free medium, and 600 μl conditioned medium containing 20% FBS was added to each well in the lower chamber. After incubation in 37°C and 5% CO_2 cell incubator for 48 h, the plate was taken out, and the Transwell cells were washed with PBS once, fixed with 4% paraformaldehyde for 15 min, dyed with crystal violet for 10 min, and then washed with PBS twice. After wiping the cells on the surface above the basement membrane of the cell with cotton ball, the cells were observed and taken photos under the microscope to count the number of cells passing through the small hole.

2.8. Apoptosis Was Observed by Flow Cytometry. A549 and LLC-LUC cells transfected with OE-ciR-0061817 plasmids and blank PLO-ciR vectors were cultured for 24 hours. After digesting the cells with trypsin without EDTA, the medium was added to terminate the digestion, and the cells were collected. After being washed with PBS twice, the collected cells were adjusted to 1×10^9 cells/ml, and 100 μl cell suspension was added to each Falcon tube, and then, add 5 ml PI and 5 μl Annexin V-FITC, incubated in dark for 15 min, add binding buffer, and the apoptosis was detected by flow cytometry within 1 h.

2.9. The Expression of Apoptosis- and Epithelial Mesenchymal Transition-Related Proteins Were Detected by Western Blot. A549 and LLC-LUC cells were collected 48 hours after transfection. The total protein was extracted by Ripa lysate kit, and the cell protein concentration was measured by BCA protein quantitative kit. The same amount of protein of each sample was separated by 10% SDS-PAGE and transferred to PVDF membrane by constant current 350 mA wet method. The membranes were blocked with 5% skimmed milk for 2 h at room temperature. After TBST cleaning, the membranes were incubated, respectively, with the primary antibodies including caspase3 (1: 2000), caspase 7 (1 : 1000), caspase 9 (1 : 1000), E-cadherin (1 : 2000), vimentin (1 : 2000), N-cadherin (1 : 1000), and GAPDH (1 : 5000) at 4°C overnight. The membranes were washed with TBST buffer for 3 times, and each time was 5 min. Then, the secondary antibodies were added and incubated at room temperature for 2 h. The images were collected by chemiluminescence and gel imaging system, and the gray value of protein strip was analyzed by ImageJ software.

2.10. Xenograft Tumor Experiment. Six nude mice were randomly divided into OE-ciR 0061817 group and PLO-ciR group, with 3 mice in each group. A549 cells transfected with OE-ciR 0067582 plasmids and blank PLO-ciR vectors were prepared into single cell suspension with serum-free medium. The cells with the concentration of 1×10^6 (100 μl) were injected into the left axillary skin of nude mice. The general condition and tumor growth of nude mice were observed every day. The long diameter and short diameter of

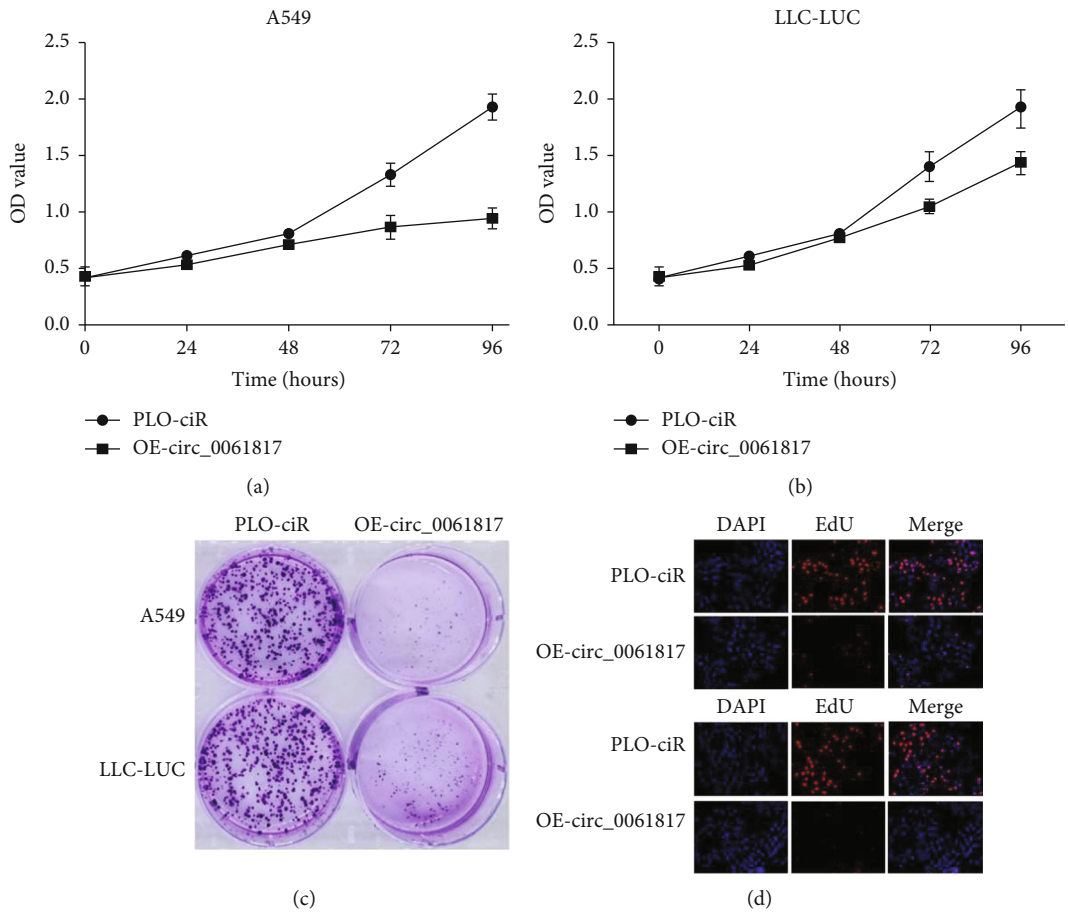

Figure 1: Effects of overexpression of hsa_circ_0061817 on the cell viability and proliferation of A549 and LLC-LUC cells. (a and b) CCK-8 assay: the effect of OE-circ 0061817 plasmids on the viability of A549 and LLC-LUC cells. (c) Cell cloning assay to examine the effect of OE-circ 0061817 plasmids on the proliferation of A549 and LLC-LUC cells. (d) EdU staining was performed to determine the DNA replication activity of the OE-circ 0061817 plasmid in A549 and LLC-LUC cells (×200).

the tumor with Vernier caliper were measured every 5 days until 30 days. The relevant data was recorded, and the tumor growth curve was drawn. The tumor-bearing mice were sacrificed at the 30th day, and the subcutaneous tumors were separated, weighed, and taken photos.

2.11. Construction and Functional Enrichment Analysis of Competitive Endogenous RNA Network. The miRNAs that may interact with hsa_circ_0061817 were predicted by TargetScan (http://www.targetscan.org/vert72) and miRnada (http://www.microrna.org/). Construct miRnada miRNA relationship pair. TarBase (http://www.tarbase.com/) database was used to predict the downstream targets of miRNA and construct the regulatory relationship of miRNA-mRNA. Integrating the relationship between hsa_circ_0061817 miRNA and miRNA mRNA, the regulatory network of circRNA-miRNA-mRNA competitive endogenous RNA (ceRNA) was constructed by circBase (http://www.circbase.org/), and the regulatory network was visualized by Cytoscape software. Further, Diana miRpath software (http://SNF 515788. VM. Okeanos. Grnet. Gr/) was used to analyze the GO and KEGG signal pathways of miRNA target genes to explore the biological functions of target genes.

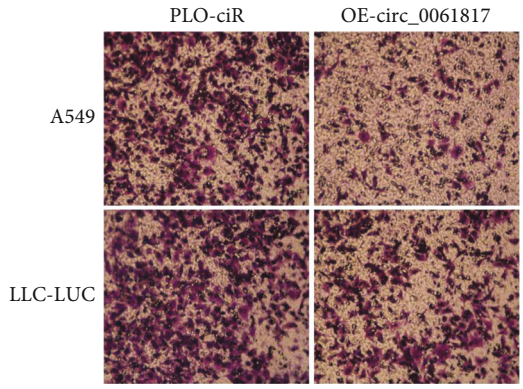

Figure 2: The effect of OE-circ 0061817 plasmids on the invasion ability of A549 and LLC-LUC cells was evaluated by Transwell assay (0.1% crystal violet staining, ×200).

3. Results

3.1. The Effects of Overexpression of hsa_circ_0061817 on the Viability and Proliferation of A549 and LLC-LUC Cells. Compared with those in PLO-circ group, the expression levels of hsa_circ_0061817 in OE-ciR 0061817 group were

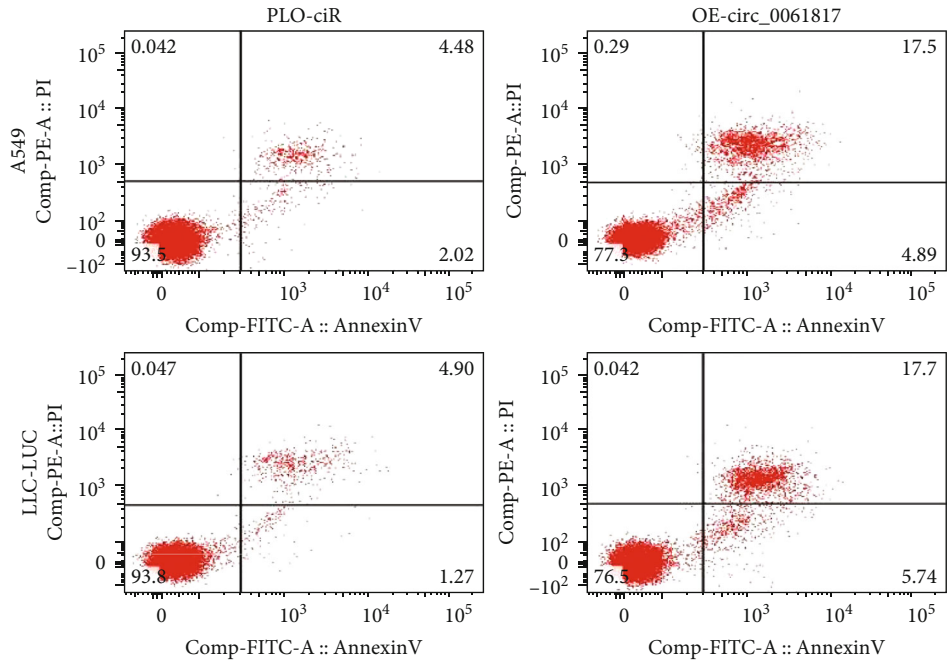

Figure 3: Effect of OE-circ 0061817 plasmids on A549 and LLC_LUC cells by flow cytometry.

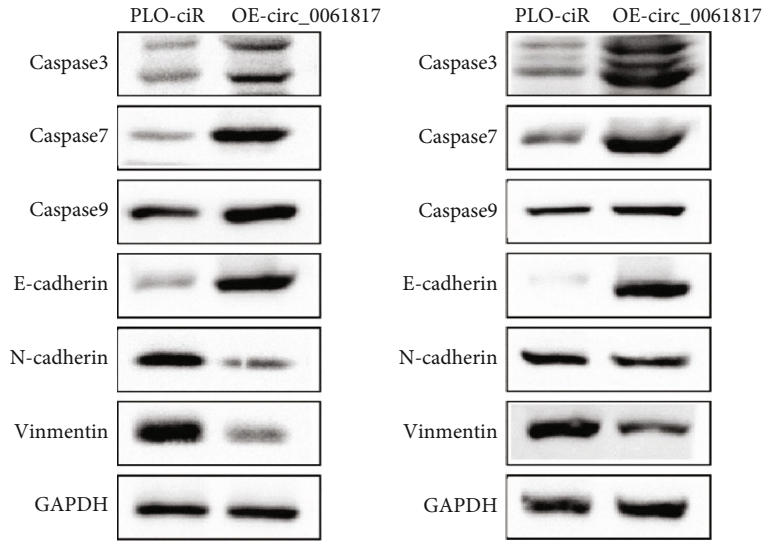

Figure 4: Effect of OE-circ 0067582 on the expression levels of caspase 3, caspase 7, caspase 9, E-cadherin, vimentin, and N-cadherin in A549 and LLC-LUC cells by western blot.

significantly increased in A549 (17.28 ± 1.24 vs. 1.08 ± 0.24; $t = 7.986$, $P = 0.003$) and LLC-LUC cells (12.47 ± 1.15 vs. 1.04 ± 0.35; $t = 5.581$, $P = 0.008$). Compared with PLO-ciR group, the cell viability was significantly lower in the A549 cells in OE-ciR 0061817 group transfected with hsa_circ_0061817 plasmids for 48 hours (0.61 ± 0.13 vs. 0.86 ± 0.14; $t = 3.765$, $P = 0.030$) (Figure 1(a)). The cell viability of LLC-LUC cells decreased significantly at 72 h (0.82 ± 0.12 vs. 1.15 ± 0.18; $t = 4.584$, $P = 0.010$) and 96 h (1.16 ± 0.18 vs. 1.72 ± 0.25; $t = 5.679$, $P = 0.005$) (Figure 1(b)). The results of cell clone formation and EdU staining showed that compared with PLO-circ group, in OE-ciR 0061817 group, the number of clones formed by A549 cells (15.33 ± 2.51 vs. 37.66 ± 4.72; $t = 6.709$, $P = 0.003$) and LLC-LUC cells (22.41 ± 3.05 vs. 53.42 ± 6.50; $t = 5.857$, $P = 0.003$) decreased significantly (Figure 1(c)). The DNA replication activity of A549 (35.60 ± 3.49 vs. 60.00 ± 5.89; $t = 4.528$, $P = 0.01$) and LLC-LUC (28.48 ± 5.27 vs. 71.60 ± 7.54; $t = 9.847$, $P = 0.001$) decreased significantly (Figure 1(d)).

3.2. Effect of Overexpression of hsa_circ_0061817 on the Invasive Ability of A549 and LLC-LUC Cells. The results of Transwell experiment showed that compared with the PLO-ciR group, the number of A549 (72.67 ± 9.29 vs.

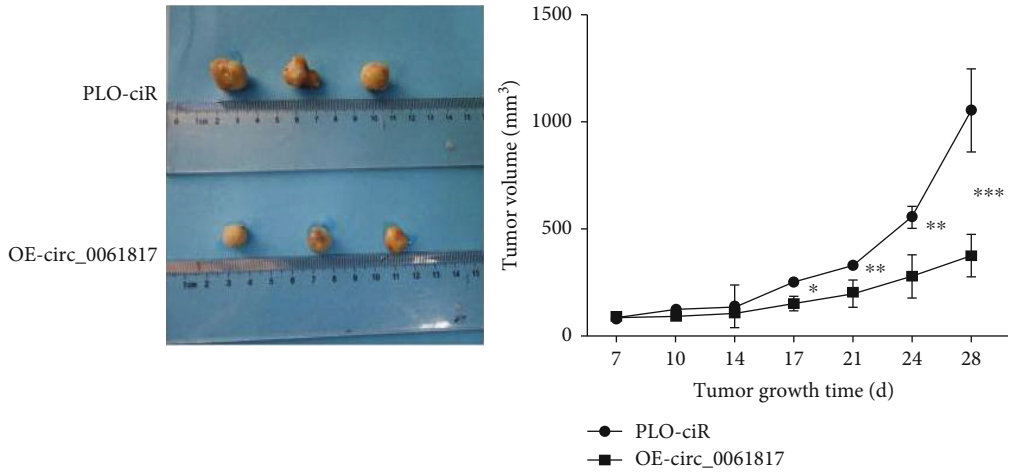

Figure 5: Effect of OE-circ 0061817 plasmid on tumor growth in A549 tumor-bearing nude mice.

149.78 ± 16.26; $t = 7.782$, $P = 0.002$) and LLC-LUC cells (114.35 ± 14.64 vs. 184.65 ± 19.50; $t = 6.342$, $P = 0.003$) passing through the chamber decreased significantly in OE-ciR 0061817 group (Figure 2).

3.3. Effects of Overexpression of hsa_circ_0061817 on Apoptosis and Epithelial Mesenchymal Transition of A549 and LLC-LUC Cells. The results of flow cytometry showed that the percentage of apoptosis in the A549 (19.92 ± 1.13 % ratio of OE-ciR 0061817 group compared with PLO-ciR group 7.82 ± 1.05%; $t = 7.225$, $P < 0.001$) and LLC-LUC (22.44 ± 1.18% ratio of OE-ciR 0061817 group compared with PLO-ciR group 5.67 ± 1.07%; $t = 11.509$, $P = 0.0025$) increased significantly in OE-ciR 0061817 group compared to PLO-ciR group (Figure 3). Western blot showed that compared with the PLO-ciR group, the protein expression level of caspase 3 of A549 and LLC-LUC cells in OE-ciR 0061817 group (3.83 ± 0.24 vs. 1.00 ± 0.09; $t = 6.863$, $P = 0.002$ and 4.68 ± 0.27 vs. 1.00 ± 0.09; $t = 7.024$, $P = 0.001$), caspase 7 (1.84 ± 0.22 vs. 1.00 ± 0.11; $t = 3.295$, $P = 0.04$ and 2.44 ± 0.12 vs. 1.00 ± 0.10; $t = 6.008$, $P = 0.004$), caspase 9 (1.40 ± 0.07 vs. 1.00 ± 0.06; $t = 4.408$, $P = 0.012$ and 1.46 ± 0.11 vs. 1.00 ± 0.09; $t = 6.278$, $P = 0.004$), E-cadherin (3.11 ± 0.20 vs. 1.00 ± 0.09; $t = 12.453$, $P = 0.002$ and 4.36 ± 0.22 vs. 1.00 ± 0.15; $t = 10.867$, $P = 0.001$), vimentin (0.28 ± 0.02 vs. 1.00 ± 0.09; $t = 7.242$, $P = 0.002$ and 0.38 ± 0.04 vs. 1.00 ± 0.10; $t = 5.694$, $P = 0.004$), and N-cadherin (0.23 ± 0.03 vs. 1.00 ± 0.08; $t = 6.480$, $P = 0.003$ and 0.33 ± 0.04 vs. 1.00 ± 0.10; $t = 7.446$, $P = 0.001$) decreased significantly (Figure 4).

3.4. Effect of Overexpression of hsa_circ_0061817 on the Growth of LLC-LUC Cells in Nude Mice. The results of subcutaneous tumorigenesis experiment in nude mice showed that the subcutaneous tumor volume of OE-ciR 0061817 group increased slowly from the 20th day compared with PLO-ciR group, and the difference was statistically significant (0.41 ± 0.12 cm^3 vs. 0.64 ± 0.07 cm^3; $t = 7.682$, $P = 0.002$) (Figure 5). On the 30th day, the subcutaneous tumor weight of mice in OE-circ 0067582 group was significantly lower than that in PLO-ciR group (0.48 ± 0.25 g vs. 1.36 ± 0.13 g; $t = 3.526$, $P = 0.0125$).

3.5. Construction of ceRNA Network and Functional Enrichment Analysis. Through the prediction of TargetScan and miRnada database, it was found that hsa_circ_0067582 can match has-mir-181b-3P, has-mir-337-3P, has-mir-421, and has-mir-548d-3P through seed sequence (Figure 6(a)). The downstream targets of the above miRNAs were obtained from the TarBase database, and the hsa_circ_0061817 miRNA mRNA network was constructed by Cytoscape software (Figure 6(b)). Venny2 1 software construction Wayne diagram results show that different miRNAs connect multiple common downstream targets (Figure 6(c)). The results of functional enrichment analysis showed that the predicted targets of miRNA were involved in a variety of biological functional processes, such as negative regulation of apoptosis, RNA binding, and gene expression (Figure 6(d)) and were associated with a variety of cancer-related pathways, such as proteoglycan, mRNA monitoring pathway, transcriptional imbalance in cancer, transforming growth factor-β (TGF-β), and P53 signaling pathway (Figure 6(e)).

4. Discussion

circRNA is a new type of noncoding RNA member composed of one or more spliced exons or introns, which has the characteristics of conservation, richness, and tissue specificity, so it may play a special molecular marker role in some diseases (such as tumors) [25]. circRNA can regulate gene expression by alternative splicing, regulating the expression of parental genes, and acting as a scaffold for protein complex assembly and RNA protein interaction and affect the occurrence and development of tumors [26, 27].

Previous studies have found that hsa_circ_0061817 is closely related to nonsmall lung adenocarcinoma and has the potential as a biomarker for the prevention and diagnosis of nonsmall lung adenocarcinoma [28, 29]. Li et al. showed that hsa_circ_0061817 partially inhibited NSCLC cell cancer partly by degrading IGF2BPs [30]. Our research

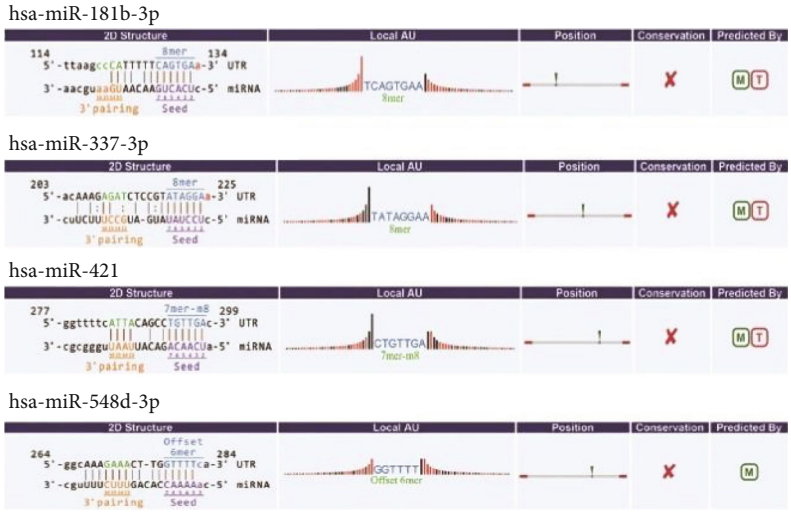

(a)

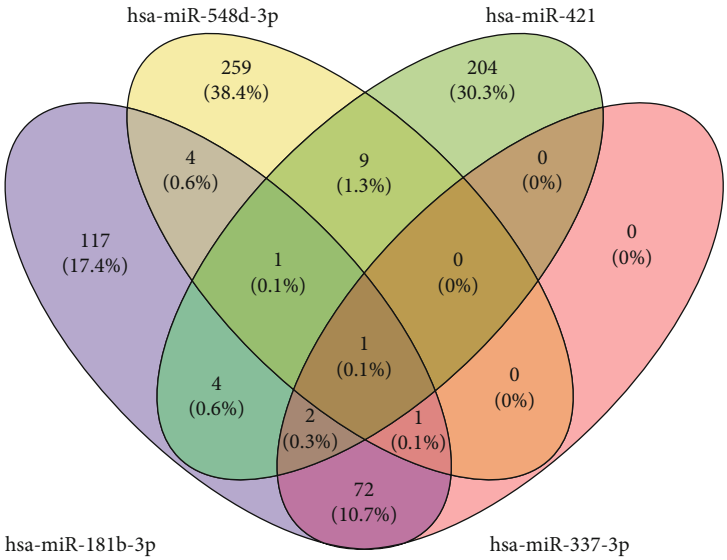

(b)

Figure 6: Continued.

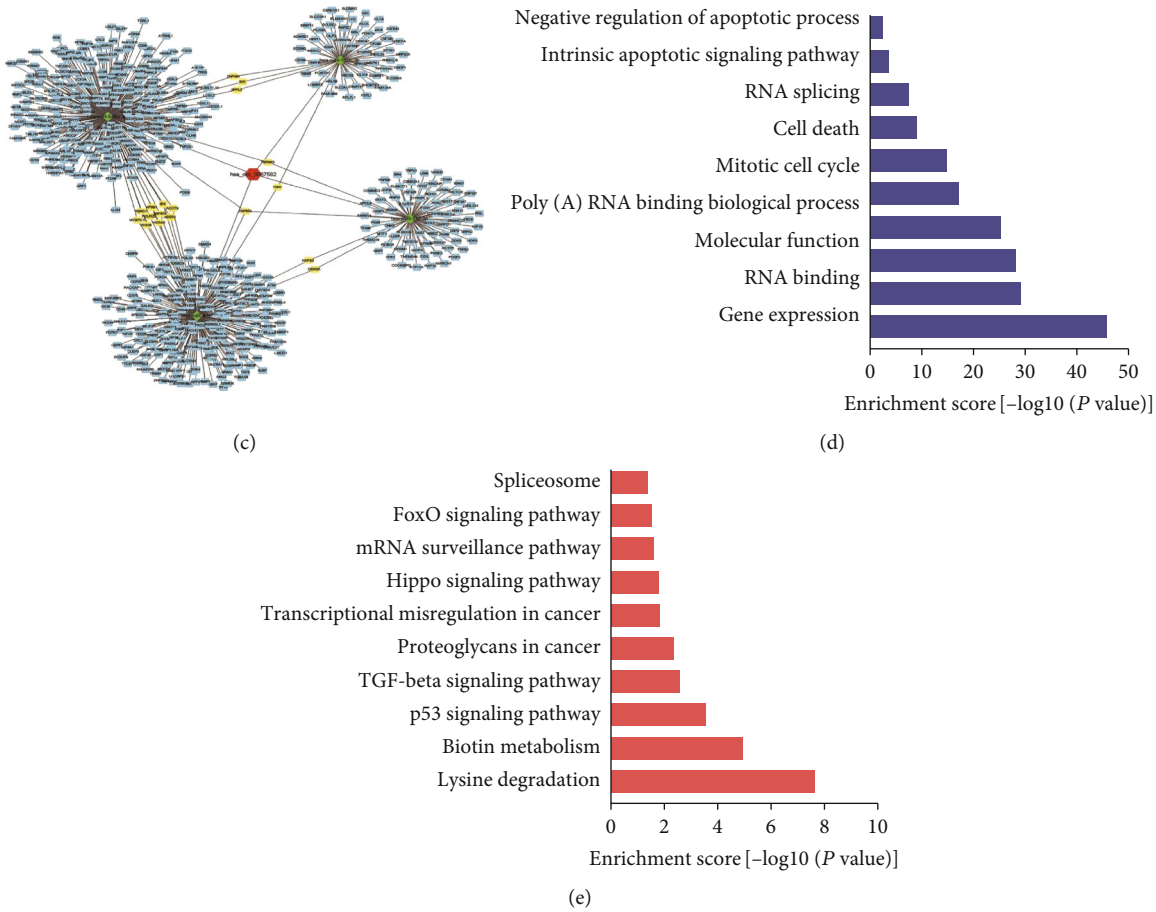

Figure 6: The competing endogenous RNA network mediated by has_circ_0061817 in lung adenocarcinoma and the functional enrichment map of target genes. (a) The TargetScan and miRnada databases predicted has_circ_0061817 interacting microRNAs; (b) Venn diagram of hsa-mir-181b-3P, hsa-mir-337-3P, hsa-mir-421, and hsa-mir-548d-3P target genes; (c) hsa_circ_0061817-miRNA-mRNA regulatory network, with red hexagons representing hsa_circ_0061817, green prisms representing miRNAs, blue rectangles representing miRNA target genes, and yellow rectangles representing miRNA coregulated target genes; (d) GO functional enrichment plots of target genes; (e) KEGG functional enrichment plots of target genes.

showed that overexpression of hsa_circ_0061817 could inhibit the cell viability, proliferation, and invasion of A549 and LLC-LUC cells and promote the apoptosis of A549 and LLC-LUC cells. In addition, overexpression of hsa_circ_0061817 in A549 and LLC-LUC cells was accompanied by the increase of the expression levels of the apoptosis-related proteins like caspase 3, caspase 7, and caspase 9. Additionally, Kong et al. found that hsa through KEGG and GO analyses of mir path_circ_0061817 may be involved in galactose metabolism, intercellular junctions, N-glycoside synthesis, stem cell pluripotency, and TGF by binding with hsa-mir-148a-5p-β signal and other related signal pathways to regulate the development of lung adenocarcinoma [31]. Epithelial mesenchymal transition (EMT) is a phenomenon that epithelial cells transform into mesenchymal cells. It is not only involved in embryonic development and normal physiology but also involved in many pathological processes. EMT is also involved in the occurrence and development of tumors, especially in promoting tumor invasion and metastasis. Studies have shown that tumor cells enhance the ability of tumor cell migration and movement by means of EMT and promote tumor invasion and metastasis [32]. More and more studies have shown that EMT is an important link in tumor invasion and metastasis [33, 34] and promotes the invasion and migration ability of lung cells [35]. Its main characteristics are the increase of vimentin expression and the decrease of E-cadherin expression. The latest review by Patel et al. clarified that the identity and plasticity of cancer cells are required for transitional states such as epithelial mesenchymal transition (EMT) and mesenchymal epithelial transition (MET) in the occurrence, development, and metastasis of primary tumors. The functional roles of EMT, MET, and partial state (called PEMT) may vary depending on tumor type, spreading state, and degree of metastatic colonization [36]. Our study found that the overexpression of hsa_circ_0061817 significantly increased the expression level of E-cadherin in A549 and LLC-LUC cells and significantly decreased the expression level of vimentin and N-cadherin, suggesting that the overexpression of hsa_circ_0061817 may inhibit the invasion of A549 and LLC-LUC cells by inhibiting the process of EMT. At the same time, LLC-LUC cells overexpressing hsa_circ_0061817 slowed down the growth of subcutaneous transplanted tumors in nude mice. These results suggested that hsa_circ_0061817

may play an important role in the occurrence and development of lung adenocarcinoma, and hsa_circ_0061817 was expected to become a new therapeutic target for lung adenocarcinoma.

Studies have shown that circRNA can play an important role in the occurrence and development of tumors directly or indirectly [37]. In addition, ceRNA has greatly expanded the functional genetic information in the human genome and enriched the understanding of the potential mechanisms of tumorigenesis. According to the prediction of TargetScan and miRnada database, hsa_circ_0061817 may competitively bind multiple miRNAs, namely, has-mir-181b-3P, has-mir-337-3P, has-mir-421, and has-mir-548d-3p. It has been reported that has-mir-421 is closely related to lung adenocarcinoma. The results of Chen et al. [38] showed that the increased expression level of has-mir-421 in plasma can significantly distinguish normal people, especially in early lung adenocarcinoma. However, has-mir-181b-3P, has-mir-337-3P, and has-mir-548d-3P have not been reported in lung adenocarcinoma, which is worthy of further study on their interaction with hsa_circ_0061817. Through the functional enrichment analysis of miRNA target genes, it was found that the target genes were significantly enriched in negative regulation of apoptosis, RNA binding, gene expression, mRNA monitoring pathway, transcriptional imbalance in cancer and TGF-β, P53 signaling pathway, etc. Among them, most pathways have been supported to be closely related to the mechanism of tumorigenesis, such as TGF-β signal pathway mediates EMT of lung adenocarcinoma cells and promotes the migration and invasion of lung adenocarcinoma cells [39]. These results suggest that the ceRNA network mediated by hsa_circ_0061817 is involved in many biological processes of the occurrence and development of lung adenocarcinoma.

In conclusion, the results showed that overexpression of hsa_circ_0061817 could significantly inhibit the proliferation and invasion of A549 and LLC-LUC cells and promote apoptosis. This study further revealed the role of hsa_circ_0061817 in lung adenocarcinoma and its potential molecular mechanism in its occurrence and development and provided a new direction for exploring new targets for the prevention and treatment of lung adenocarcinoma.

Data Availability

The datasets used and/or analyzed during the current study are available from the corresponding author on reasonable request.

Conflicts of Interest

The authors declare that the research was conducted in the absence of any commercial or financial relationships that could be construed as a potential conflict of interest.

Authors' Contributions

All authors participated in the present study. Longping Ye, Youqing Zhong, and Lihua Hu contributed equally to this work. Conception and design were carried out by Longping Ye and Youqing Zhong, data collection by Lihua Hu, data analysis by Ya Huang, drafting the article or critical revision by Xiangdong Zhou and Qi Li, and study supervision by Qi Li. All authors have read and approved the final version submitted. Longping Ye, Youqing Zhong, and Lihua Hu are the co-first authors.

Acknowledgments

This work was supported by the Hainan Innovation Team Project (820CXTD448), Key R&D Project of Hainan Province (ZDYF20223), National Natural Science Foundation of China (81860001, 82011530049, and 82160012), and Postgraduate Innovation and Scientific Research Project of Hainan Medical University (HYYB2021A06). This work was also the project supported by the Hainan Province Clinical Medical Center. We are also grateful to the contributors to the public databases used in this study.

References

[1] H. Li, D. Han, L. Zhang et al., "PD-1/L1 inhibitors may increase the risk of pericardial disease in non-small-cell lung cancer patients: a meta-analysis and systematic review," *Immunotherapy*, vol. 14, no. 7, pp. 577–592, 2022.

[2] N. Heersche, G. D. M. Veerman, M. de With et al., "Clinical implications of germline variations for treatment outcome and drug resistance for small molecule kinase inhibitors in patients with non-small cell lung cancer," *Drug Resistance Updates*, vol. 62, article 100832, 2022.

[3] E. Göker, A. Altwairgi, A. Al-Omair et al., "Multi-disciplinary approach for the management of non-metastatic non-small cell lung cancer in the Middle East and Africa: expert panel recommendations," *Lung Cancer*, vol. 158, pp. 60–73, 2021.

[4] Z. Baumann, P. A. der Maur, and M. Bentires-Alj, "Feed-forward loops between metastatic cancer cells and their microenvironment-the stage of escalation," *EMBO Molecular Medicine*, vol. 14, no. 6, article e14283, 2022.

[5] J. Liang, G. Bi, G. Shan, X. Jin, Y. Bian, and Q. Wang, "Tumor-associated regulatory T cells in non-small-cell lung cancer: current advances and future perspectives," *Journal of Immunology Research*, vol. 2022, Article ID 4355386, 8 pages, 2022.

[6] N. Iwamoto, J. Ichinose, R. Hoshi et al., "Positive bag lavage cytology during thoracoscopic surgery for lung cancer is a significant predictor of locoregional recurrence," *General Thoracic and Cardiovascular Surgery*, vol. 70, no. 4, pp. 366–371, 2022.

[7] M. Entezari, M. Ghanbarirad, A. Taheriazam et al., "Long non-coding RNAs and exosomal lncRNAs: potential functions in lung cancer progression, drug resistance and tumor microenvironment remodeling," *Biomedicine & Pharmacotherapy*, vol. 150, article 112963, 2022.

[8] S. X. Zhang, A. Hanineva, K. S. Park, J. J. Wang, M. M. DeAngelis, and M. H. Farkas, "Emerging roles of circular RNAs in retinal diseases," *Neural Regeneration Research*, vol. 17, no. 9, pp. 1875–1880, 2022.

[9] A. R. Sharma, S. Banerjee, M. Bhattacharya, A. Saha, S. S. Lee, and C. Chakraborty, "Recent progress of circular RNAs in different types of human cancer: technological landscape, clinical

opportunities and challenges (review)," *International Journal of Oncology*, vol. 60, no. 5, 2022.

[10] Y. L. Zheng, J. B. Guo, G. Song et al., "The role of circular RNAs in neuropathic pain," *Neuroscience and Biobehavioral Reviews*, vol. 132, pp. 968–975, 2022.

[11] C. Chen, C. Xia, H. Tang et al., "Circular RNAs involve in immunity of digestive cancers from bench to bedside: a review," *Frontiers in Immunology*, vol. 13, article 833058, 2022.

[12] Z. Xu, B. Peng, Q. Liang et al., "Construction of a ferroptosis-related nine-lncRNA signature for predicting prognosis and immune response in hepatocellular carcinoma," *Frontiers in Immunology*, vol. 12, article 719175, 2021.

[13] E. T. Fok, L. Davignon, S. Fanucchi, and M. M. Mhlanga, "The lncRNA connection between cellular metabolism and epigenetics in trained immunity," *Frontiers in Immunology*, vol. 9, p. 3184, 2019.

[14] O. Beylerli, I. Gareev, A. Sufianov, T. Ilyasova, and F. Zhang, "The role of microRNA in the pathogenesis of glial brain tumors," *Non-coding RNA Research*, vol. 7, no. 2, pp. 71–76, 2022.

[15] S. Bidula, "Analysis of putative G-quadruplex forming sequences in inflammatory mediators and their potential as targets for treating inflammatory disorders," *Cytokine*, vol. 142, article 155493, 2021.

[16] L. Wei, Y. Yang, W. Wang, and R. Xu, "Circular RNAs in the pathogenesis of sepsis and their clinical implications: a narrative review," *Annals of the Academy of Medicine, Singapore*, vol. 51, no. 4, pp. 221–227, 2022.

[17] S. Ghafouri-Fard, M. E. Dinger, P. Maleki, M. Taheri, and M. Hajiesmaeili, "Emerging role of circular RNAs in the pathobiology of lung cancer," *Biomedicine & Pharmacotherapy*, vol. 141, article 111805, 2021.

[18] F. Wang, J.-H. Yuan, S.-B. Wang et al., "Oncofetal long non-coding RNA PVT1 promotes proliferation and stem cell-like property of hepatocellular carcinoma cells by stabilizing NOP2," *Hepatology*, vol. 60, no. 4, pp. 1278–1290, 2014.

[19] M. Su, Y. Xiao, J. Ma et al., "Long non-coding RNAs in esophageal cancer: molecular mechanisms, functions, and potential applications," *Journal of Hematology & Oncology*, vol. 11, no. 1, p. 118, 2018.

[20] L. Salmena, L. Poliseno, Y. Tay, L. Kats, and P. P. Pandolfi, "A ceRNA hypothesis: the Rosetta Stone of a hidden RNA language?," *Cell*, vol. 146, no. 3, pp. 353–358, 2011.

[21] P. Wang, H. Zhi, Y. Zhang et al., "miRSponge: a manually curated database for experimentally supported miRNA sponges and ceRNAs," *Database: The Journal of Biological Databases and Curation*, vol. 2015, article bav098, 2015.

[22] J. Liu, H. Li, B. Zheng, L. Sun, Y. Yuan, and C. Xing, "Competitive endogenous RNA (ceRNA) regulation network of lncRNA-miRNA-mRNA in colorectal carcinogenesis," *Digestive Diseases and Sciences*, vol. 64, no. 7, pp. 1868–1877, 2019.

[23] A. Chu, J. Liu, Y. Yuan, and Y. Gong, "Comprehensive Analysis of Aberrantly Expressed ceRNA network in gastric cancer with and without H.pylori infection," *Journal of Cancer*, vol. 10, no. 4, pp. 853–863, 2019.

[24] Y. Bai, J. Long, Z. Liu et al., "Comprehensive analysis of a ceRNA network reveals potential prognostic cytoplasmic lncRNAs involved in HCC progression," *Journal of Cellular Physiology*, vol. 234, no. 10, pp. 18837–18848, 2019.

[25] C. Xue, G. Li, Q. Zheng et al., "The functional roles of the circRNA/Wnt axis in cancer," *Molecular Cancer*, vol. 21, no. 1, p. 108, 2022.

[26] S. S. Choi, S. E. Kim, S. Y. Oh, and Y. H. Ahn, "Clinical implications of circulating circular RNAs in lung Cancer," *Biomedicines*, vol. 10, no. 4, p. 871, 2022.

[27] Y. Gao, S. Shang, S. Guo et al., "Lnc2Cancer 3.0: an updated resource for experimentally supported lncRNA/circRNA cancer associations and web tools based on RNA-seq and scRNA-seq data," *Nucleic Acids Research*, vol. 49, no. D1, pp. D1251–D1258, 2021.

[28] P. Ge, J. Zhang, L. Zhou et al., "CircRNA expression profile and functional analysis in testicular tissue of patients with non-obstructive azoospermia," *Reproductive Biology and Endocrinology*, vol. 17, no. 1, p. 100, 2019.

[29] H. Xie, J. Yao, Y. Wang, and B. Ni, "Exosome-transmitted circVMP1 facilitates the progression and cisplatin resistance of non-small cell lung cancer by targeting miR-524-5p-METTL3/SOX2 axis," *Drug Delivery*, vol. 29, no. 1, pp. 1257–1271, 2022.

[30] B. Li, L. Zhu, C. Lu et al., "circNDUFB2 inhibits non-small cell lung cancer progression via destabilizing IGF2BPs and activating anti-tumor immunity," *Nature Communications*, vol. 12, no. 1, p. 295, 2021.

[31] M. Kong, H. Li, W. Yuan, L. Mao, and J. Chen, "The role of Circ_PRKCI/miR-24-3p in the metastasis of prostate cancer," *Journal of BUON*, vol. 26, no. 3, pp. 949–955, 2021.

[32] D. Fu, S. Senouthai, J. Wang, and Y. You, "FKN facilitates HK-2 cell EMT and tubulointerstitial lesions via the Wnt/β-catenin pathway in a murine model of lupus nephritis," *Frontiers in Immunology*, vol. 10, p. 784, 2019.

[33] X. Liu, X. Huang, J. Ma et al., "3'untranslated regions (3'UTR) of *Gelsolin* mRNA displays anticancer effects in non-small cell lung cancer (NSCLC) cells," *American Journal of Cancer Research*, vol. 11, no. 8, pp. 3857–3876, 2021.

[34] S. Shao, L. Piao, L. Guo et al., "Tetraspanin 7 promotes osteosarcoma cell invasion and metastasis by inducing EMT and activating the FAK-Src-Ras-ERK1/2 signaling pathway," *Cancer Cell International*, vol. 22, no. 1, p. 183, 2022.

[35] Y. Hu, J. Bai, D. Zhou et al., "The miR-4732-5p/XPR1 axis suppresses the invasion, metastasis, and epithelial-mesenchymal transition of lung adenocarcinomaviathe PI3K/Akt/GSK3β/Snail pathway," *Molecular Omics*, vol. 18, no. 5, pp. 417–429, 2022.

[36] S. Patel, A. Alam, R. Pant, and S. Chattopadhyay, "Wnt signaling and its significance within the tumor microenvironment: novel therapeutic insights," *Frontiers in Immunology*, vol. 10, p. 2872, 2019.

[37] J. Xu, N. Sang, J. Zhao, W. He, N. Zhang, and X. Li, "Knockdown of circ_0067934 inhibits gastric cancer cell proliferation, migration and invasion via the miR-1301-3p/KIF23 axis," *Molecular Medicine Reports*, vol. 25, no. 6, 2022.

[38] J. Chen, L. Xu, M. Fang, Y. Xue, Y. Cheng, and X. Tang, "Hsa_circ_0060927 participates in the regulation of Caudatin on colorectal cancer malignant progression by sponging miR-421/miR-195-5p," *Journal of Clinical Laboratory Analysis*, vol. 36, no. 5, article e24393, 2022.

[39] G. Han, Y. Wang, T. Liu et al., "Salvianolic acid B acts against non-small cell lung cancer A549 cells via inactivation of the MAPK and Smad2/3 signaling pathways," *Molecular Medicine Reports*, vol. 25, no. 5, 2022.

Hindawi
Oxidative Medicine and Cellular Longevity
Volume 2022, Article ID 7138194, 17 pages
https://doi.org/10.1155/2022/7138194

Research Article

Exploration of the Protective Mechanism of Naringin in the Acetaminophen-Induced Hepatic Injury by Metabolomics

Zihan Lin,[1] Guanzhen Wang,[1,2] Wei Gu,[1] Shengchao Zhao,[1,2] Ziyi Shen,[1] Wei Liu,[2] Guodong Zheng,[3] Baizhong Chen,[4] Yi Cai,[3] Mingxi Li,[5] Chunpeng (Craig) Wan,[5] and Tingdong Yan[1]

[1]*School of Life Sciences, Shanghai University, 99 Shangda Road, Shanghai 200444, China*
[2]*University and College Key Lab of Natural Product Chemistry and Application in Xinjiang, School of Chemistry and Environmental Science, Yili Normal University, Yining 835000, China*
[3]*Guangzhou Municipal and Guangdong Provincial Key Laboratory of Molecular Target & Clinical Pharmacology, the NMPA and State Key Laboratory of Respiratory Disease, School of Pharmaceutical Sciences and the Fifth Affiliated Hospital, Guangzhou Medical University, Guangzhou 511436, China*
[4]*Guangdong Xinbaotang Biological Technology Co., Ltd., Guangdong, Jiangmen 529000, China*
[5]*Research Center of Tea and Tea Culture, College of Agronomy, Jiangxi Agricultural University, Nanchang 330045, China*

Correspondence should be addressed to Yi Cai; yicaisysu@163.com, Chunpeng (Craig) Wan; chunpengwan@jxau.edu.cn, and Tingdong Yan; yantdntu2018@163.com

Received 15 June 2022; Revised 23 July 2022; Accepted 22 August 2022; Published 16 September 2022

Academic Editor: Tarique Hussain

Naringin is a dihydroflavone which was found in citrus fruits. Previous studies have indicated the antiapoptotic, antioxidative stress, and anti-inflammatory effects of naringin. It can improve many common diseases, including fibrosis or hepatotoxicity, cardiovascular disease, and diabetes. Acetaminophen (APAP) is a frequently used painkiller, and hepatotoxic side effects limit its use. The purpose of the current examination is to find the impact of naringin on APAP-induced hepatic injury. Firstly, we pretreated mice model groups with naringin. Then, the liver injury model was established by injecting intraperitoneally into mice with APAP. After the mice were euthanized, we obtained serum and liver tissue samples from the mice. Finally, these samples were analyzed using a metabolomics approach to find the underlying mechanism of the effects of naringin on APAP-induced liver injury and provide a new treatment strategy for APAP-induced liver injury. Our data indicate that naringin significantly improves APAP-induced liver injury in mice and reduces the expression levels of liver injury markers in a dose-dependent manner. Furthermore, analysis of differential metabolites in mice with liver injury showed that naringin reduced APAP-induced hepatotoxicity due to reversing multiple metabolite expression levels and the rescue of energy, amino acid, and purine metabolism.

1. Introduction

Natural products are small molecular compounds extracted from fruits, vegetables, and Traditional Chinese medicine. Unlike traditional drugs, they generally have the characteristics of multiple efficacy and low toxicity and have potential therapeutic value for various complex diseases. Naringin, a naturally occurring and pharmacologically active flavonoid, was found in citrus fruits [1–5] such as lemons, grapefruits, sorbs, and vegetables [5]. Several studies have shown that this natural substance has a wide range of functions [2–4, 6], such as antioxidant, anti-inflammatory, and antiapoptotic roles. Further research has demonstrated that naringin can alleviate or improve a variety of common diseases, including fibrosis or hepatotoxicity [4, 6–9], cardiovascular diseases (CVD) [3, 10], diabetes [11], and neurodegenerative disease [12–14].

Some drugs have not been widely used in treating diseases because of severe side effects, including methotrexate

(MTX) [4], and cyclophosphamide (CTX) [9]. Therefore, it is of great significance to find natural products that can alleviate the side effects of drugs. Elsawy et al. employed MTX to induce acute liver injury in rats and subsequently treated these rats with naringin. They found that naringin significantly reduced the upregulation of markers of MTX-induced liver injury and reduced oxidative stress, protecting hepatocytes from MTX-induced damage [4]. In another study on cyclophosphamide, naringin also alleviated CTX-induced oxidant production, hepatocyte dysfunction, and inflammation [9].

Acetaminophen (APAP) is frequently used as an analgesic agent whose hepatotoxic side effects are primarily involved in acute liver failure [15–17]. At safe doses, once ingested, APAP is quickly absorbed in the small intestine and immediately reaches inside liver cells. Enzymes catalyze the majority (about 80-90%) of APAP from the UDP-glucuronic acid transferase (UGT) 1A subfamily or sulfonate transferases. Then, it binds to glucuronic acid, forming non-toxic metabolites and excreting from the body in urine. Finally, this process does not damage liver cells [15, 16, 18, 19]. Whereas once the accumulation of APAP exceeds the tolerable dose for the human body, the glucuronidation and sulfonation pathways tend to saturate, and excessive APAP will be metabolized to form a large number N-acetyl-para-benzoquinoneimine (NAPQI). Unfortunately, NAPQI will deplete glutathione (GSH) stored by liver cells. Subsequently, redundant NAPQI react with biomacromolecules such as proteins, DNA, and unsaturated lipids in the cell, raising downstream events. For instance, reactive oxygen species (ROS) production, mitochondrial dysfunction, cell necrosis, apoptosis, autophagy, etc. cells will die in the end [15, 16, 18–20]. Hence, we can ameliorate the liver injury caused by APAP by targeting its metabolism.

Several previous studies have shown that naringin protects hepatocytes from liver injury by exerting antioxidant and anti-inflammatory effects [21–26]. Therefore, based on APAP metabolism, we are convinced that naringin may also be beneficial in improving APAP metabolism to reduce APAP-induced hepatotoxicity. Herein, a pretreated APAP-mediated liver injury mice model was exposed to naringin and then analyzed liver tissue and serum with metabolomic approaches to find whether naringin reduces APAP-induced hepatotoxicity and possible molecular mechanisms involved.

2. Materials and Methods

2.1. Ethical Statement. All procedures were performed by the current Chinese legislation on the care and use of laboratory animals and approved by the Department of Scientific Management of Guangzhou Medical University.

2.2. Naringin and Other Chemicals. All solvents mentioned in this article are LC-MS grade and purchased from Sigma-Aldrich. Ultrapure H_2O was obtained from Milli-Q pure water system. The commercially available kits of alanine aminotransferase (ALT), aspartate aminotransferase (AST), glutathione peroxidase (GSH-Px), and malondialdehyde (MDA) are purchased from the Nanjing Jiancheng Bioengineering Institute (Jiancheng Bioengineering Institute, Nanjing, China). Naringin was bought from Shanghai Weihuan Biotechnology Co., Ltd. (Weihuan Biotechnology, Shanghai, China).

2.3. Centrifugal Operation. All centrifuge operations are performed by Dynamica centrifuges, purchased from the Shanghai Miaosheng Technology & Trade Co., Ltd. The model is Velocity 14R.

2.4. Animal Treatment. A total of 24 male C57BL/6J mice (age, 6 weeks) were obtained from Guangdong Medical Laboratory Animal Center (Guangzhou, China). Mice were randomly assigned into the following four groups: (1) vehicle control ($n = 8$), (2) APAP ($n = 8$), (3) APAP+50 mg/kg/d naringin ($n = 8$), and (4) APAP+100 mg/kg/d naringin ($n = 8$). Initially, naringin suspension was prepared from 0.5% carboxymethyl cellulose solution, and APAP was dissolved in normal saline at a concentration of 20 mg/ml and dissolved by heating at 55°C for animal experiment. The control group of these animal experiments was given the same volume of liquid but composed solely of the vehicle solution (0.5% carboxymethylcellulose). Naringin is a single treatment, and the mice were orally given naringin. Then, APAP (300 mg/kg) was injected intraperitoneally at 3 h following naringin treatment. About 48 h post-APAP exposure, mice were anaesthetized with pentobarbital (50 mg/kg, dissolved in saline with a concentration of 2%) via intraperitoneal injection. After that, the mice were sacrificed; tissue and serum samples were collected according to the instructions provided with commercial kits for subsequent experiments.

2.5. Serum ALT/AST Activity Analysis. The collected blood samples were placed at room temperature for about 2 h, centrifuge for 15 min at 840xg and separated serum stored at -20°C for later analysis. The serum alanine transaminase (ALT) and aspartate transaminase (AST) assays in each group were performed following the manufacturer's instructions.

2.6. Histopathology. The left liver lobe of the mice was fixed using paraformaldehyde (4%), dehydrated, and embedded in paraffin. The liver sections (5 μm) were prepared and stained using hematoxylin and eosin (H&E), and then, microscopy was done. The cell necrotic boundaries were manually counted in three random fields per sample.

2.7. Glutathione Peroxidase and Malondialdehyde Measurement. The contents of glutathione peroxidase (GSH-Px) and malondialdehyde (MDA) in the liver tissues were assayed using commercial kits following the manual instructions provided by the manufacturers.

2.8. ^{1}H NMR Analysis. The collected tissue samples were cut and weighed and consequently homogenized with 50% acetonitrile. The mixture was centrifuged at 12000xg for 10 min to remove the precipitate at 4°C. The supernatant was lyophilized under nitrogen, placed overnight in a -80°C refrigerator, and freeze-dried. The samples were placed in 550 μl 99.8% D_2O phosphate buffer (0.2 M, containing 0.05%

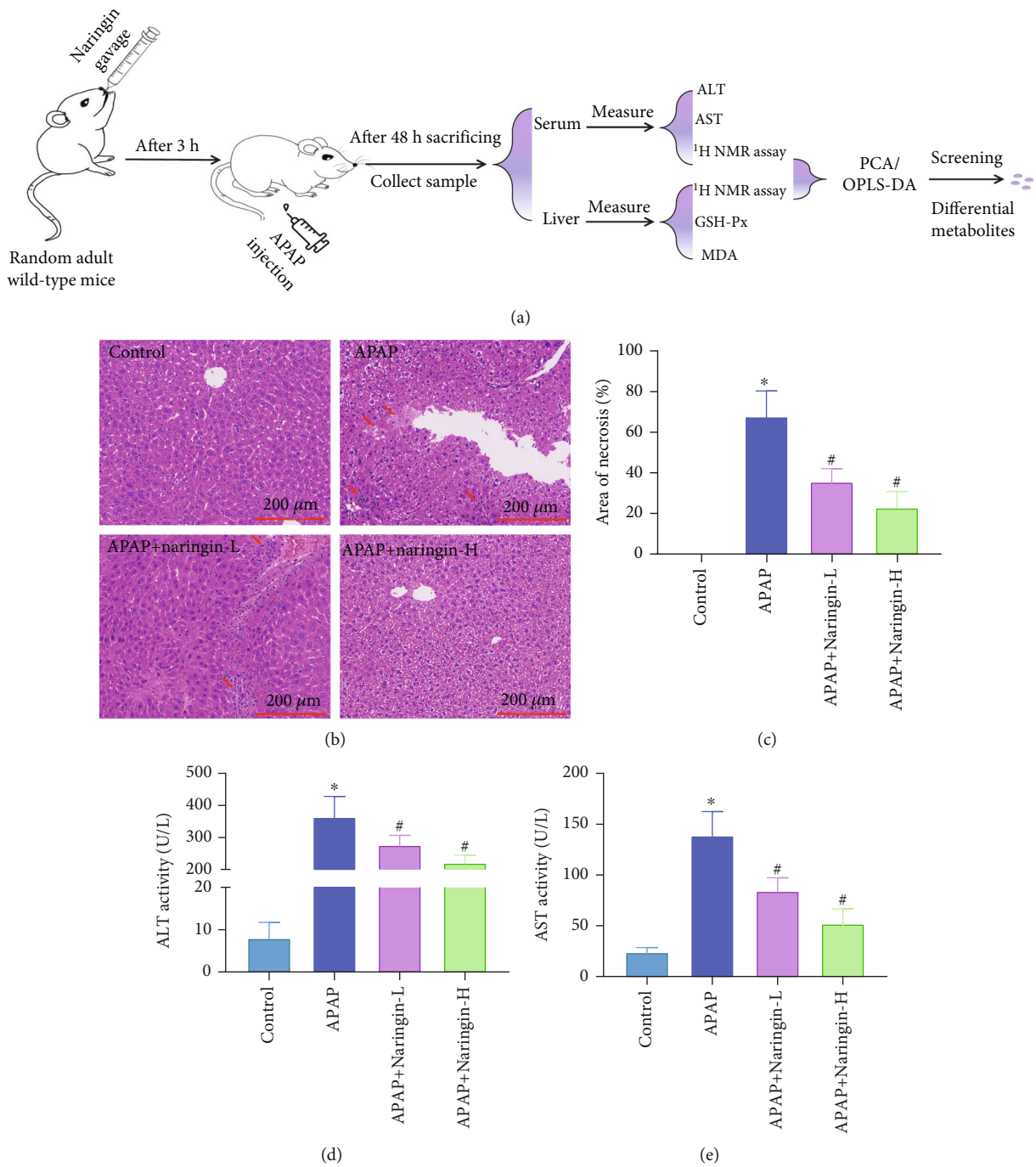

Figure 1: Continued.

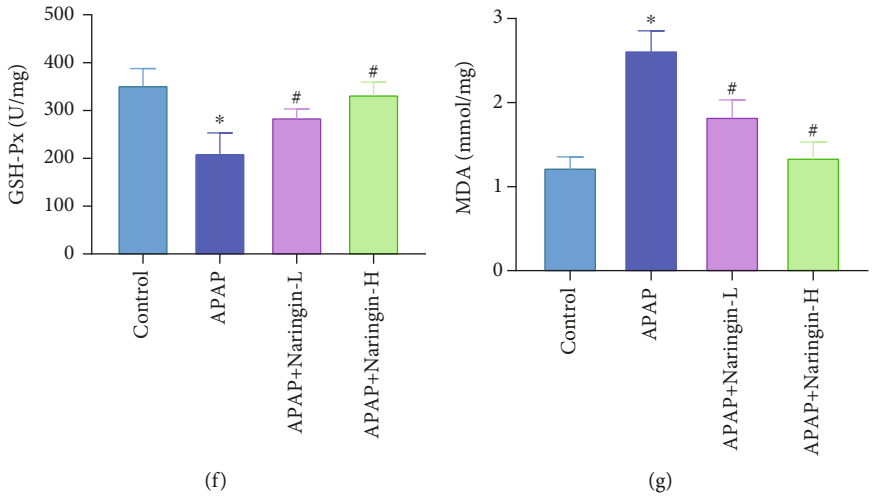

Figure 1: Naringin alleviates acetaminophen-induced hepatic injury in mice. (a) The design scheme of mouse experiment. (b) Hematoxylin-eosin (H&E) staining of mouse liver in control, APAP, APAP+naringin low-dose, and APAP+naringin high-dose groups. (c) Area of necrosis (%) in control, APAP, APAP+naringin low-dose, and APAP+naringin high-dose groups. (d-g) Histogram of changes of liver injury markers in control, APAP, APAP+naringin low-dose, and APAP+naringin high-dose groups. $^{*}P < 0.05$ vs. control, $^{\#}P < 0.05$ vs. APAP, $n = 8$.

sodium 3-(trimethylsilyl) propionate-2, 2, 3, 3-d4 (TSP), pH 7.4) and mixed with oscillation. The precipitation was removed by centrifugation. The supernatant was put on the machine for NMR analysis.

2.9. Data Preprocessing and Software. The TopSpin software (Bruker Biospin, Germany) version V3.0 was used to perform Fourier transform (FT), phase adjustment, baseline correction, and calibration. All spectra were multiplied by an exponential window function with a widening factor of 1 Hz when the Fourier transform was performed to improve SNR. The single-peak calibration of TSP at 0.00 ppm was used to remove the residual water peak, and the integral interval was 0.650-4.550 and 5.175-9.700 ppm. The integral interval was 0.015 ppm for data analysis.

The displacement range of finger-recognized compounds was imported into R software to calculate the integral area of each compound, and the fold value was obtained by intergroup comparison. Combined with a one-way analysis of variance, 0.05 was set as the threshold to screen differentially expressed metabolites.

2.10. Statistical Analysis. Data are presented as mean ± SEM. Statistical analysis was performed with the use of SPSS statistic software 15.0. Differences among groups were tested by one-way analysis of variance (ANOVA) with Tukey's post hoc test. In all cases, differences were considered statistically significant with $P < 0.05$.

3. Results

3.1. Naringin Pretreatment Repaired Liver Injury and Reversed the Level of Liver Injury Markers in the Samples. We established a mouse model of liver injury using APAP and measured the extent of liver injury, including the proportion of liver cell necrosis and the production of liver injury markers. The proportion of liver injury and necrosis can be intuitively revealed by H&E staining results, whereas various markers can indirectly reflect APAP-induced endogenous metabolite changes. For this purpose, we selected four classic biomarkers for liver injuries, such as ALT, AST, MDA, and GSH-Px. The design scheme of the animal experiment is well elucidated (Figure 1(a)). Compared with the control, histopathology results of the liver tissue samples of mice in the model group showed that the liver tissue was significantly damaged after intraperitoneal injection of APAP (Figure 1(b)). In addition, statistics on the proportion of necrotic area showed that about 70% of the tissue was necrotic in the model group. After low-dose (50 mg/kg/d) naringin treatment, the necrotic area was reduced by about half, while high-dose (100 mg/kg/d) naringin treatment showed only about 20% necrotic area (Figure 1(c), $P < 0.05$). These results indicated that naringin repaired APAP-induced liver tissue damage and showed extremely significant therapeutic effects at high doses.

Furthermore, ALT and AST levels in serum and GSH-Px and MDA in liver tissue were measured. The results showed that naringin pretreatment reversed the levels of these markers of liver injury in the model group. To be specific, the levels of ALT, AST, and MDA in samples of model mice were significantly increased compared to the control group. Nevertheless, following pretreatment with naringin, ALT, AST, and MDA levels downregulated considerably in a dose-dependent fashion (Figures 1(d), 1(e), and 1(g), $P < 0.05$). Instead, although GSH-Px levels in the liver of model mice were significantly downregulated, naringin treatment reversed them (Figure 1(f), $P < 0.05$).

3.2. Identification of Major Metabolites in the Serum and Liver of Mice by NMR Spectroscopy. After ^{1}H, NMR experiments were conducted on the serum and liver samples of the four groups of mice (control group, marked as N; APAP

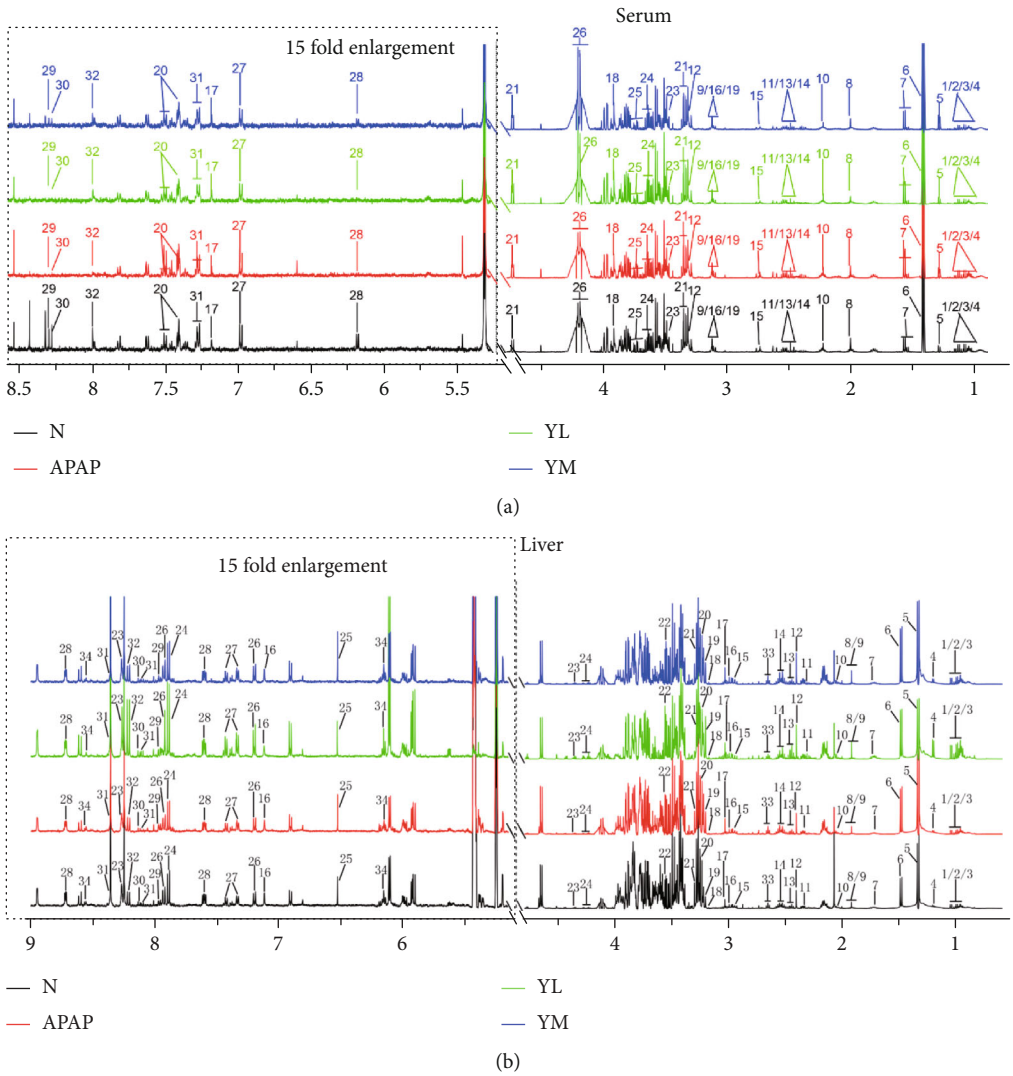

Figure 2: Typical 500 MHz CPMG ^{1}H NMR spectra for serum (a) and liver (b) samples of the four groups of mice. N: control; APAP; YL: APAP+low-dose therapy; YM: APAP+high-dose therapy. Keys: 1. isoleucine; 2. leucine; 3. valine; 4. 3-hydroxyisobutyrate; 5. 3-hydroxybutyrate; 6. lactate; 7. alanine; 8. acetate; 9. lysine; 10. homoserine; 11. glutamine; 12. O-acetylcarnitine; 13. pyruvate; 14. succinate; 15. citrate; 16. N, N-dimethylglycine; 17. histamine; 18. creatine; 19. ornithine; 20. phenylalanine; 21. glucose; 22. taurine; 23. methanol; 24. glycerol; 25. threonine; 26. 1,3-dihydroxyacetone; 27. tyrosine; 28. inosine; 29. formate; 30. hypoxanthine; 31. tryptophan; 32. xanthine.

group, marked as APAP; APAP+low-dose naringin therapy group, marked as YL; APAP+high-dose naringin therapy group, marked as YM), the typical hydrogen spectra as shown in Figure 2 were obtained. The names are identified by querying public metabolomics databases, such as HMDB (http://www.hmdb.ca/) and MMCD (http://mmcd.nmrfam.wisc.edu/), and annotated in legends.

29 and 28 metabolites were identified in extracts of serum (Figure 2(a)) and liver (Figure 2(b)), respectively. To visualize the identification results, different colors and numbers represent different groups of spectra and identified metabolites, respectively. In addition, based on the low metabolite concentrations in the low-field region (2.175-9.700 ppm), the spectra were magnified by a factor of 15 to align with the high-field region.

3.3. Naringin Can Reverse the Level of Small Molecule Metabolites in Serum and Liver Tissue Induced by APAP in Mice

3.3.1. PCA. We used R software to carry out pattern recognition multivariable analysis for the normalized spectral data. We used the mean centre scaling method to obtain the PCA (principal component analysis) graph, shown in Figure 3, to describe the weight of principal components. These graphics can help us analyze the changes of small molecule metabolites in serum and liver of APAP-induced mice compared to the control group. PCA patterns based on the NMR spectra of mouse serum are shown in Figure 3(a). The APAP-administered group and the control group mostly overlapped, indicating that APAP did not

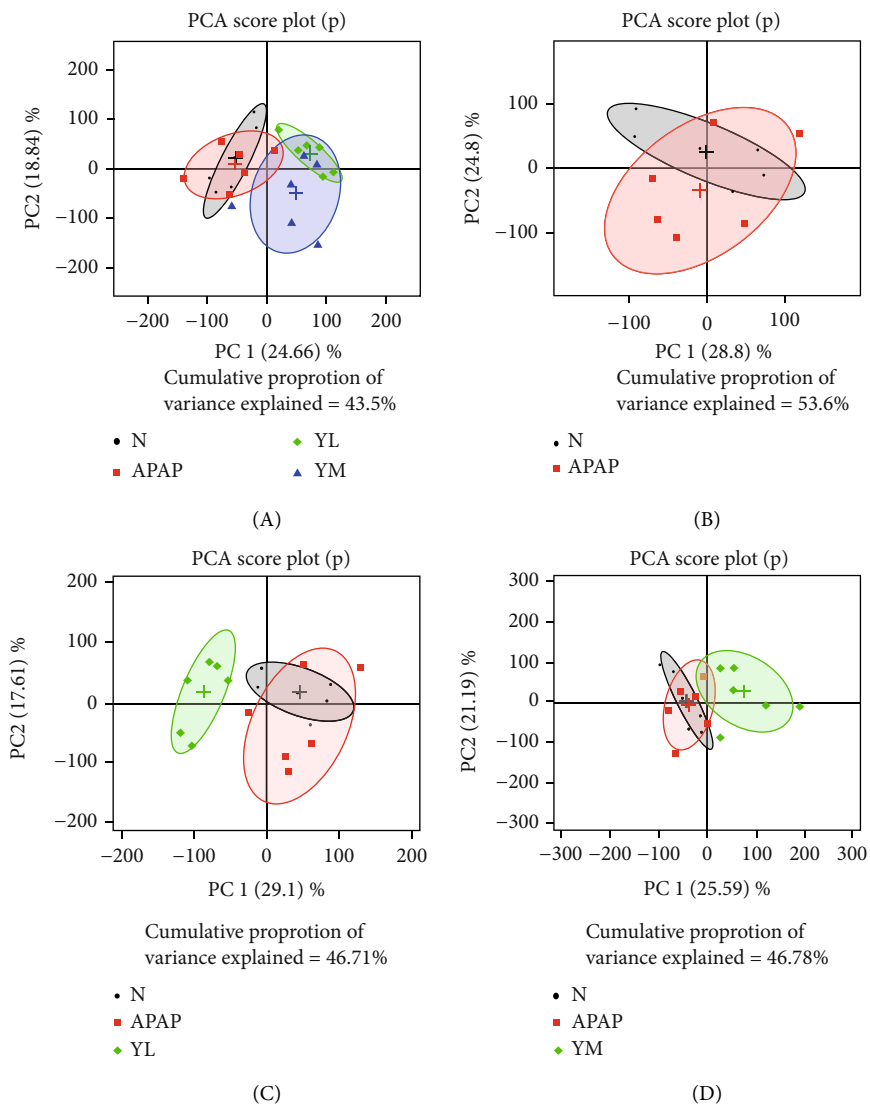

(a)

Figure 3: Continued.

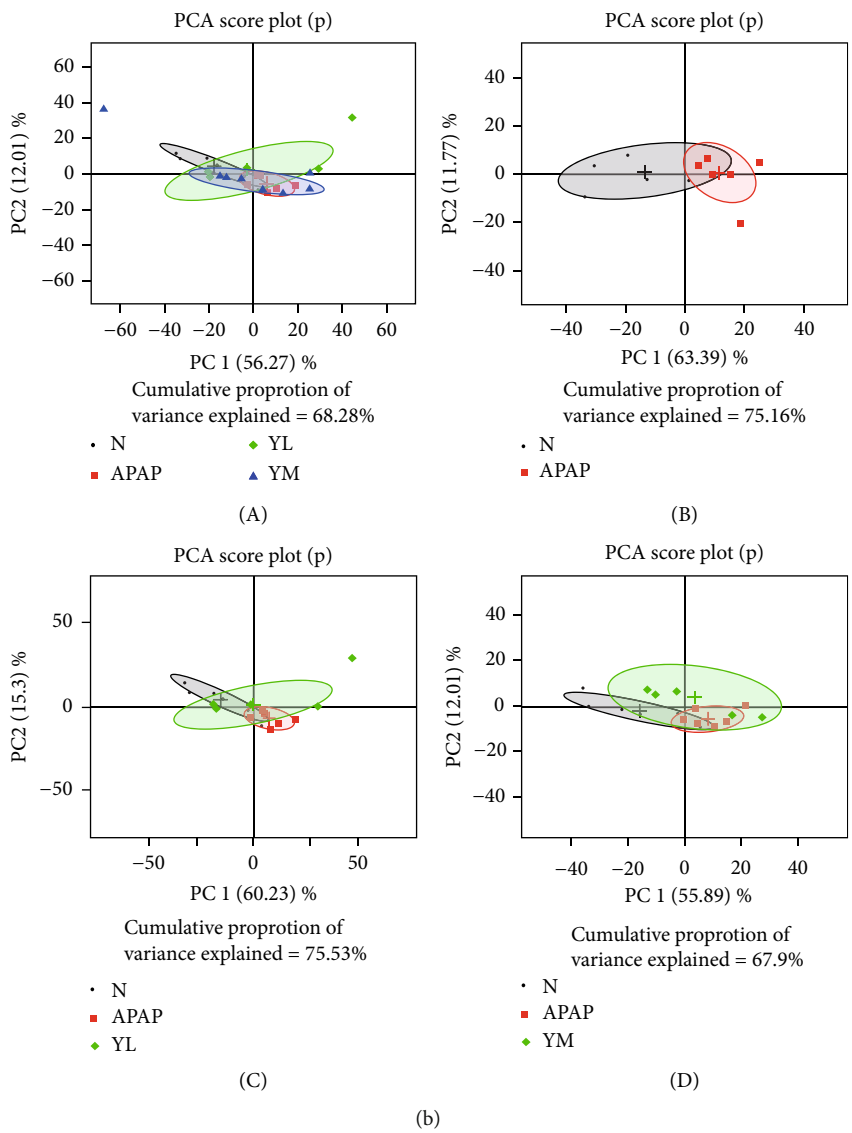

Figure 3: PCA score plots. (a) PCA score plot based on ^{1}H CPMG NMR spectra of serum obtained from four groups. (b) PCA score plot based on ^{1}H CPMG NMR spectra of liver obtained from four groups. N: control; APAP; YL: APAP+low-dose therapy; YM: APAP+high-dose therapy.

change the overall metabolic level of the mouse serum (Figure 3(a)-A and B). However, the drug-treated groups (YL/YM) showed a separation trend with the control group, suggesting that naringin changed metabolites levels in serum(Figures 3(a)-A, C, and D, the green figure has no overlap with the grey figure). In the liver, both APAP and drug-treated groups overlapped completely with the control group, indicating that neither APAP nor drugs caused liver metabolite disturbances (Figure 3(b)). However, PCA is an unsupervised analytical method, and to further differentiate metabolic levels between groups, we used the supervised OPLS-DA to filter out irrelevant factors.

3.3.2. OPLS-DA. The OPLS-DA score chart is shown in Figure 4. Based on the complete separation of APAP and control groups, metabolic disturbances in serum were caused by APAP (Figure 4(a)-B). However, compared with the APAP group, the administration group was closer to the control group, especially the YM group, indicating that the metabolic disturbance caused by APAP was reversed in a dose-dependent manner (Figure 4(a)-A). Consistent with the serum results, the APAP group was completely separated from the control group (Figure 4(b)-B). In contrast, the drug and control groups overlapped completely (Figure 4(a)-A, C, D). The results indicated that APAP caused the disturbance of the overall metabolic level of the liver, but was improved by the drug.

3.4. Screening Small Molecule Metabolites with Significant Differences. To further identify the differential metabolites, the loading value of the first principal component of the OSC-OPLS-DA model was adopted to plot the loading plot, as shown in Figures 5 and 6. Orthogonal signal correction

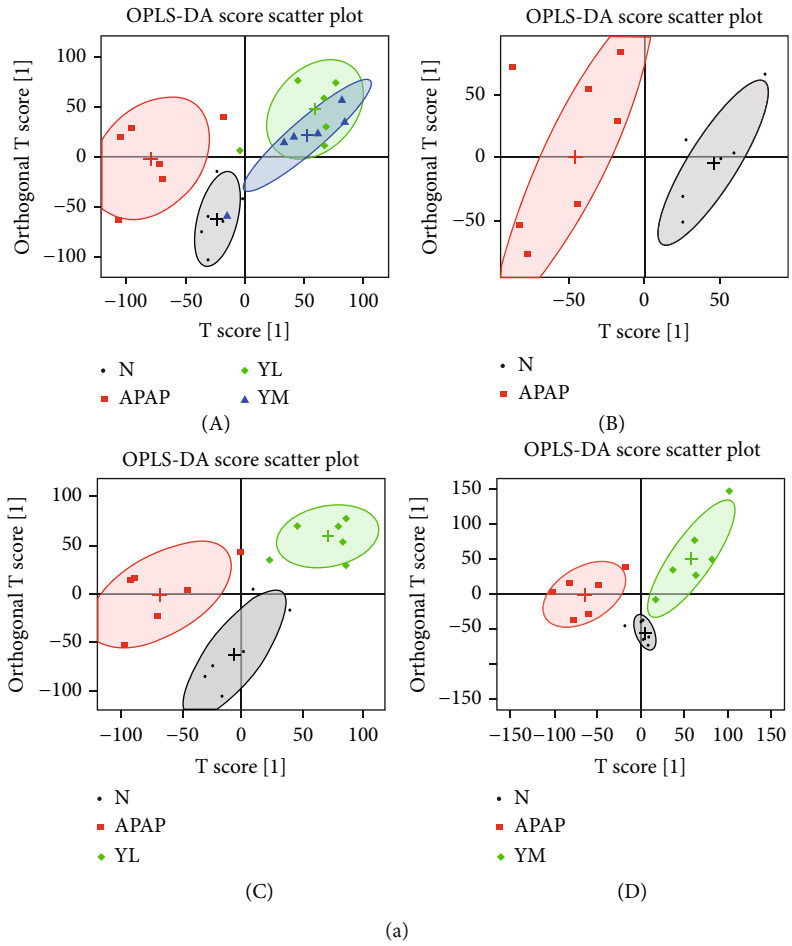

(a)

Figure 4: Continued.

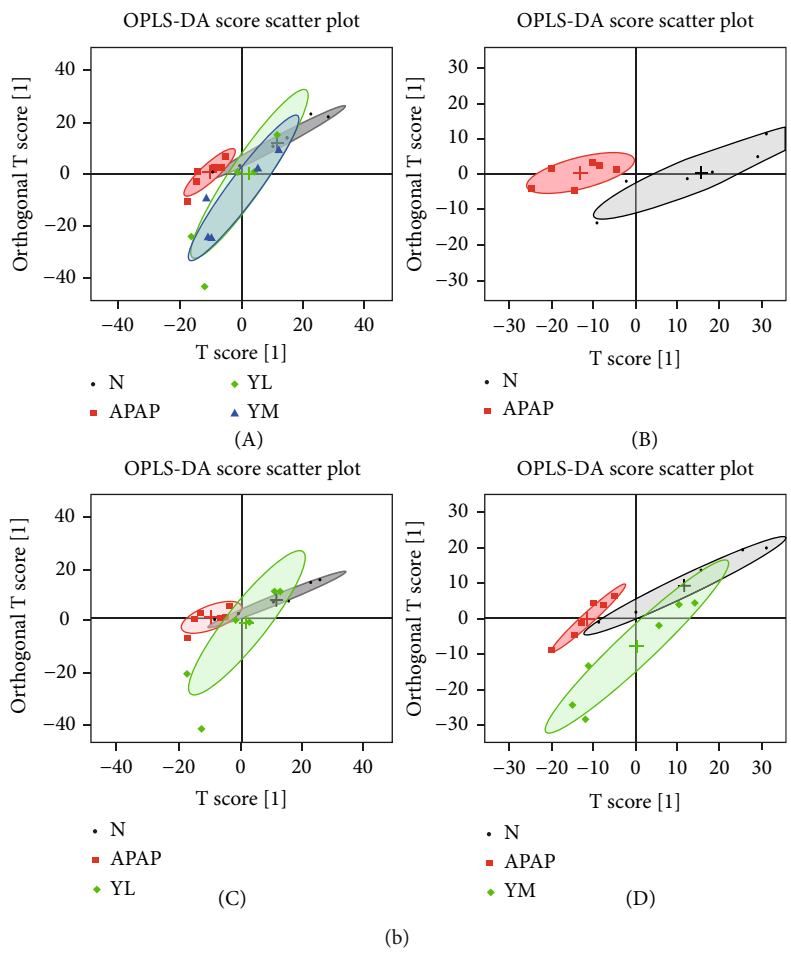

Figure 4: OPLS-DA score plots. (a) OPLS-DA score plots (a, b, c, and d), respectively, are derived from ^{1}H NMR spectra of serum from different groups. (b) OPLS-DA score plots (a, b, c, and d), respectively, are derived from ^{1}H NMR spectra of liver from different groups. N: control; APAP; YL: APAP+low-dose therapy; YM: APAP+high-dose therapy.

(OSC) was performed on the PLS-DA model. OSC could remove the variables that were not meaningful to the grouping to maximize the differences between groups. To find the differential metabolites contributing to group separation, the redder the peak, the more significant difference between the two groups, and the bluer the peak, there is no significant difference. The peak above the loading plot has a higher content in the group on the right side of the OPLS-DA score, while the peak below the loading plot has a higher content on the left side OPLS-DA score. The displacement range of finger-recognized compounds was imported into R software to calculate the integral area of each compound, and the fold value was obtained by intergroup comparison. Combined with a one-way analysis of variance, 0.05 was set as the threshold to screen differentially expressed metabolites. Please refer to Tables 1 and 2 for details.

According to the information on differential metabolites, the reduced metabolites (isoleucine, valine, 3-hydroxyisobutyrate, acetate, pyruvate, histamine, inosine, hypoxanthine, and xanthine) can be observed in model groups compared to control groups in serum samples. Metabolites with elevated expression levels include leucine, 3-hydroxybutyrate, alanine, homoserine, glutamine, taurine, glycerol, threonine and 1, 3-dihydroxyacetone. The significant decrease in pyruvate, inosine, hypoxanthine, and xanthine, while 3-hydroxybutyrate, alanine, homoserine, taurine, and threonine is significantly increased. However, although APAP treatment caused this change in metabolites, there is a certain degree of reversal effect after naringin treatment and presented the characteristics of dose-dependence.

Similarly, there were reduced metabolites in the APAP model group in liver tissue samples compared to the control group, including 3-hydroxyisobutyrate, ethanolamine, and ATP. The significantly increased metabolites are leucine, lactate, alanine, glutamate, isocitrate, creatine, choline, and fumarate. Naringin treatment also reversed the expression levels of some metabolites, including ATP, leucine, alanine, and fumarate, in a dose-dependent manner. However, most metabolite changes did not improve with medium doses of naringin, suggesting that further research is needed to determine the therapeutic dose of naringin to achieve the best protective effect.

3.5. Summary of Pathway Analysis. In addition, to reveal metabolic pathways that may be involved in naringin improving liver injury, metabolic pathway analysis of

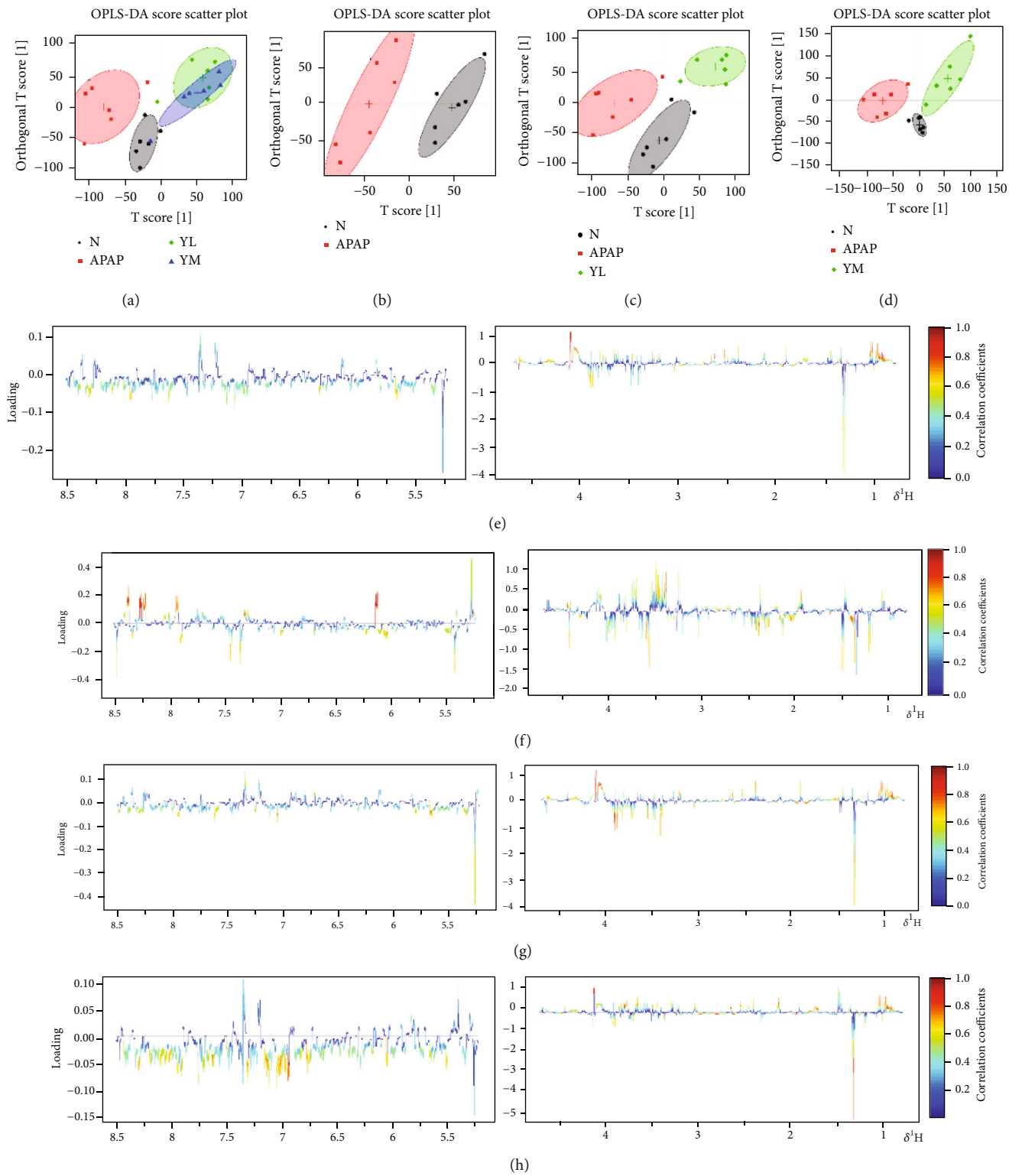

Figure 5: OSC-PLS-DA score plots (a–d) derived from the ^{1}H NMR spectra of serum and corresponding coefficient color-coded loading plots (e–h) obtained from different groups. The color map shows the significance of metabolite variations between the two classes. The color bar corresponds to the weight of the corresponding variable in the discrimination of statistically significant (red) or no significant (blue). Positive and negative peaks indicate a relatively decreased and increased metabolite level in different groups. Peaks in the positive direction indicate metabolites that are more abundant in the groups in the positive direction of the first principal component. Consequently, metabolites that are more abundant in the groups in the negative direction of the first primary component are presented as peaks in the negative direction. Keys of the assignments were shown in Figure 2(a). N: control; APAP; YL: APAP+low-dose therapy; YM: APAP +high-dose therapy.

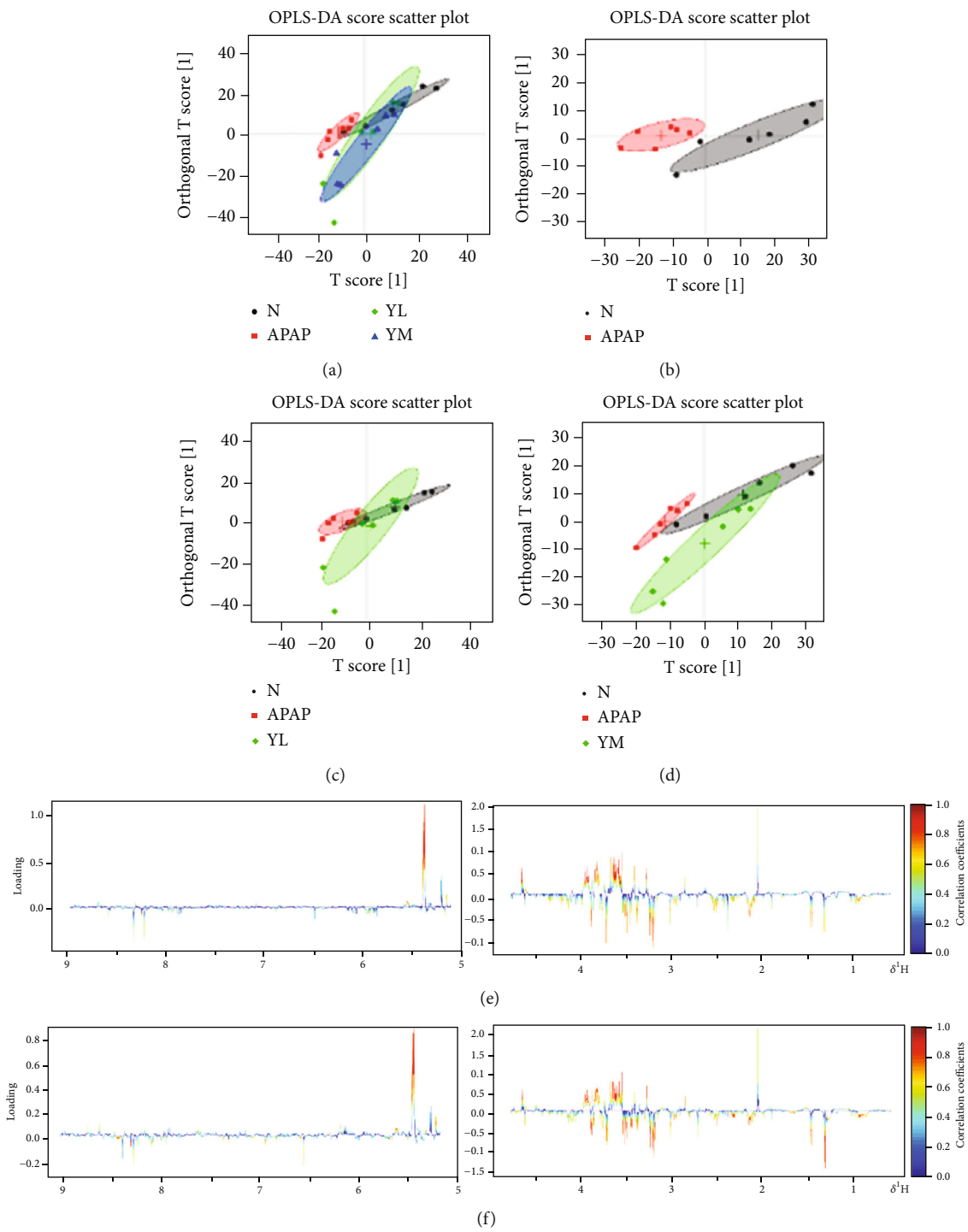

Figure 6: Continued.

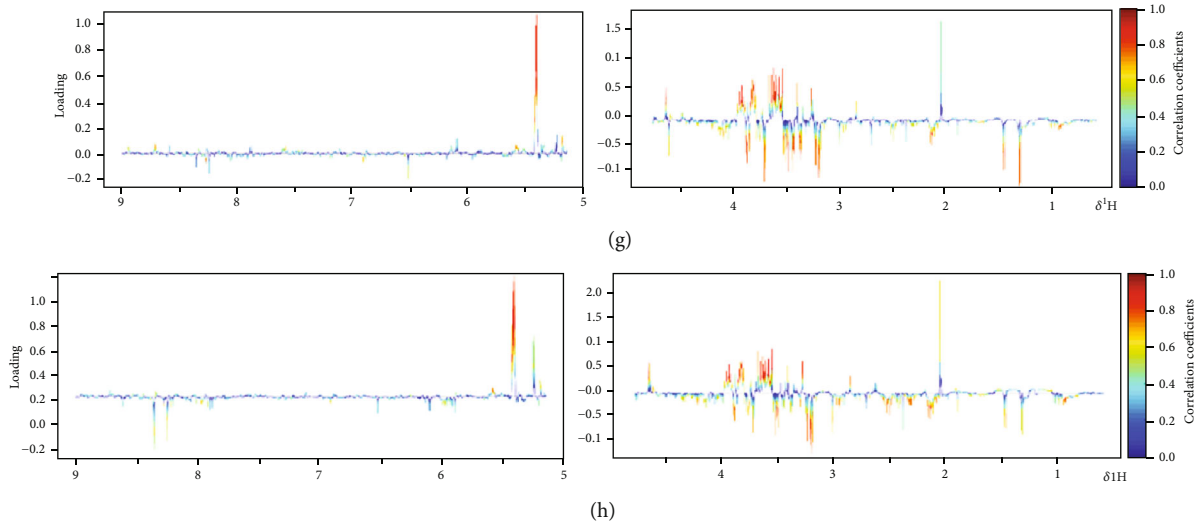

Figure 6: OSC-PLS-DA score plots (a–d) derived from the ^{1}H NMR spectra of liver and corresponding coefficient color-coded loading plots (e–h) obtained from different groups. The color map shows the significance of metabolite variations between the two classes. The color bar corresponds to the weight of the corresponding variable in the discrimination of statistically significant (red) or no significant (blue). Positive and negative peaks indicate a relatively decreased and increased metabolite level in different groups. Peaks in the positive direction indicate more abundant metabolites in the groups in the positive direction of the first principal component. Consequently, metabolites that are more abundant in the groups in the negative direction of the first primary component are presented as peaks in the negative direction. Keys to the assignments are shown in Figure 2(b). N:control; APAP; YL: APAP+low-dose therapy; YM: APAP+high-dose therapy.

differential metabolites of serum and liver between normal and liver-injured mice was performed using MetaboAnalyst 5.0. The results are shown in Figure 7. In general, pathways with an impact value of >0.1 was considered potentially targeted metabolic pathways. As shown in Figure 7, naringin treatment significantly affected the metabolism of various amino acids, TCA cycle, and gluconeogenesis pathways in serum and liver. These data suggest that naringin may play its role in protecting liver cells by targeting these metabolic pathways.

4. Discussion

Naringin has antioxidant, antiapoptotic, and anti-inflammatory effects in several studies. It is found that naringin protects endothelial cells from ox-LDL-induced apoptosis and injury in an in vitro model of atherosclerosis [3].

In this study, we were interested in whether naringin could affect APAP-mediated liver injury, providing new ideas for the treatment or remission of this hepatotoxicity. APAP is an essential factor in the cause of acute liver failure, and this nature has seriously affected the use of this drug. Therefore, people should explore a new substance to alleviate this side effect. There have been some studies on APAP metabolism, but there is no way to avoid this side effect altogether. The challenge is that APAP metabolism involves a wide range of pathways. To this end, we investigated the impact of naringin on APAP-induced hepatotoxicity and the possible molecular mechanisms engaged by analyzing the degree of metabolite changes induced by APAP.

The liver is the chief organ controlling and managing the metabolism in the body, equipped with a variety of metabolic enzymes, including AST and ALT, primarily involved in catalyzing the transfer of amino acids between amino acids and ketone acids [27]. However, liver cells damage caused by external stimulation may disturb the integrity of the cellular membranes and enhance the permeability. This increased permeability enhances ALT and AST release into the blood to raise blood serum levels of ALT and AST. Therefore, the detection of blood ALT and AST levels indirectly reflects the degree of liver injury. The liver serves as a major site for biological oxidation; when aerobic cells are metabolized, a burst of reactive oxygen species (ROS) is generated that results in lipid peroxidation of cell membranes and damage to surrounding cells in the liver tissues. ROS-mediated lipid peroxidation elevated MDA levels, and fluctuating levels of MDA may reflect the degree of lipid peroxidation in liver cells [28].

On the contrary, the primary function of GSH-Px is to decompose peroxides. Therefore, when liver cells are damaged, the activity of GSH-Px is reduced, and the peroxides cannot be decomposed, and the antioxidant capacity of the liver is reduced [29]. Our results have demonstrated that, compared with normal mouse samples, model mice have significantly increased areas of liver necrosis and significantly increased levels of ALT and AST in serum and MDA in the liver, which naringin treatment successfully reversed in a dose-dependent manner. As expected, APAP-induced liver injury decreased GSH-Px activity, whereas high-dose naringin significantly enhanced GSH-Px activity. On the other hand, R software was used to perform orthogonal partial least squares (OPLS) on normalized data to find the correlation between NMR data (the x variable) and other variables (Y variable, grouping information). Partial least

Table 1: Differential expression of metabolites between each two groups in serum.

Compound	APAP vs N $\log_2$ (FC)	P	YL vs N $\log_2$ (FC)	P	YM vs N $\log_2$ (FC)	P
Isoleucine	−0.10		0.06		0.27	
Leucine	0.17		−0.45	*	−0.50	***
Valine	−0.16		−0.59	**	−0.70	***
3-Hydroxyisobutyrate	−0.32	*	−0.81	***	−0.49	*
3-Hydroxybutyrate	0.66	*	−0.14		1.16	***
Lactate	0.15		0.34		0.39	*
Alanine	0.60	*	0.44	*	0.20	
Acetate	−0.37	*	−0.8	*	−0.44	*
Lysine	0.09		−0.18		−0.28	*
Homoserine	0.46	*	0.32	*	0.15	
Glutamine	0.51	*	0.20		0.28	
O-Acetylcarnitine	0.15		−0.10		−0.19	*
Pyruvate	−1.02	***	−0.52	*	−0.34	
Succinate	0.15		−0.45	*	−0.21	
Citrate	−0.01		−0.46	**	−0.37	*
N.N-Dimethylglycine	0.13		−0.05		0.22	
Histamine	−0.29	*	0.16		0.42	*
Creatine	0.13		0.09		0.06	
Ornithine	−0.17		0.49	*	0.45	*
Phenylalanine	0.12		−0.16		−0.05	
Glucose	−0.12		0.19		−0.16	
Taurine	0.74	*	0.28		0.72	***
Methanol	−0.13		0.11		−0.08	
Glycerol	0.38	*	002		−0.05	
Threonine	0.76	**	0.48	*	0.16	
1.3-Dihydroxyacetone	0.42	*	−0.05		0.16	
Tyrosine	−0.14		−0.06		−0.02	
Inosine	−1.84	***	−1.47	***	−0.72	**
Formate	005	*	0.23		0.48	
Hypoxanthine	−1.37	**	−0.96	**	−0.57	**
Tryptophan	−0.12		−0.23		0.14	
Xanthine	−1.05	**	−0.22		−0.22	

Color bar −1 −0.5 0 0.5 1

[a]Color coded according to the logarithmic transformation of fold change ($\log_2$(FC)), warm color (red) shows the degree of increase in identified metabolites, and blue the decrease in APAP vs. N, YL vs. N, and YM vs. N groups. [b]P values corrected by Benjamini Hochberg methods were calculated based on a parametric Student's t-test or a nonparametric Mann–Whitney test. $^{*}P < 0.05$, $^{**}P < 0.01$, $^{***}P < 0.001$.

squares discriminant analysis (PLS-DA) uses the data scale scaling method of unit variance scaling. The PLS-DA was used to test the quality of the model with the two-fold cross-validation method, and the R2X and Q2 obtained after the cross-validation were used to evaluate the validity of the model (representing the variables that could be explained by the model and the predictability of the model, respectively). After that, the model's effectiveness was further tested by changing the order of the classification variable Y randomly several times ($n = 2000$) to obtain the corresponding random $Q2$ value. OPLS-DA filtered out irrelevant orthogonal signals to obtain more reliable differential metabolites. PCA graph and OPLS-DA score plots were used to analyze the experimental results of ^{1}H NMR, which showed that induction of APAP did change the level of small molecule metabolites in the samples, and the expression was more evident in liver samples. However, treatment with naringin saved the levels of metabolites in the model samples, suggesting that naringin has the potential to treat APAP-induced liver injury.

The levels of succinate in serum and fumarate in the liver of the APAP model group were significantly increased, while ATP (Adenosine triphosphate) level was significantly decreased. Both succinate and fumarate are important intermediates of TCA circulation and the respiratory chain. Thus, their increase indicates that the APAP group mice have damaged mitochondria, disrupted TCA circulation, and disrupted the respiratory chain, and reduced efficiency of

Table 2: Differential expression of metabolites between each two groups in liver.

Compound	APAP vs N $\log_2$ (FC)	P	YL vs N $\log_2$ (FC)	P	YM vs N $\log_2$ (FC)	P
Isoleucine	0.18		−0.01		0.01	
Leucine	0.54	*	0.31		0.43	
Valine	0.24		0.02		0.21	
3-Hydroxyisobutyrate	−0.70	**	−0.53	*	−0.63	**
Lactate	0.53	*	0.33	*	0.24	
Alanine	0.60	**	0.44	*	004	
Lysine	−0.17		0.08		001	
Arginine	0.03		0.04		−0.21	
Acetate	0.19		−0.08		0.49	
Homoserine	0.16		0.37		0.19	
Glutamate	0.55	*	006	**	0.75	**
Succinate	−0.06		0.23		009	***
Glutamine	−0.03		0.25		003	
Isocitrate	0.59	*	−0.01		005	**
Glutathione	0.04		0.24		0.61	**
Histamine	0.26		0.08		001	
Creatine	0.74	**	0.37		1.01	***
Ethanolamine	−0.43	*	0.10		−0.19	
Choline	0.90	**	007		0.92	***
Betaine	0.02		0.09		001	
Taurine	0.01		−0.01		0.03	
Glycine	0.36		0.39		0.37	
Inosine	0.01		0.19		0.38	
Uridine	−0.03		0.07		0.27	
Fumarate	0.64	**	0.31		0.22	
Histidine	0.01		0.03		−0.10	
Phenylalanine	0.15		0.15		0.17	
Nicotinurate	−0.09		0.02		−0.12	
Xanthine	0.11		0.21		0.21	
NAD.	−0.10		0.02		−0.14	
NADP.	0.10		0.23		0.24	
Hypoxanthine	0.17		0.25		0.15	
5.6.Dihydrouracil	0.08		0.29		−0.47	**
ATP	−0.30	*	0.15		0.74	**

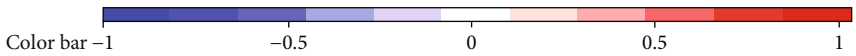

[a]Color coded according to the logarithmic transformation of fold change ($\log_2$(FC)), warm color (red) shows the degree of increase in identified metabolites, and blue the decrease in APAP vs. N, YL vs. N, and YM vs. N groups. [b]P values corrected by Benjamini Hochberg methods were calculated based on a parametric Student's t-test or a nonparametric Mann–Whitney test. $^{*}P < 0.05$, $^{**}P < 0.01$, $^{***}P < 0.001$.

energy generation [30]. ATP is the main molecule that drives the cellular reaction process. Glucose is converted to pyruvate, and two ATP molecules are produced through glycolysis. Subsequently, when oxygen is sufficient, pyruvate is directed into the tricarboxylic acid cycle, where a reaction involving substrate-level phosphorylation can have a certain amount of ATP. The respiration chains can also phosphorylate the intermediate to produce large amounts of ATP [31]. In contrast, when oxygen is scarce, pyruvate is converted to lactate, a process that produces little ATP. Consistent with this, there was a significant increase in lactate in serum and liver in the APAP group, indicating an enhanced anaerobic glycolysis pathway that ultimately leads to inadequate ATP supply. Therefore, to cope with this energy crisis, the body needs to use other ways to produce energy. Fatty acid oxidation can release a large amount of energy. As a product

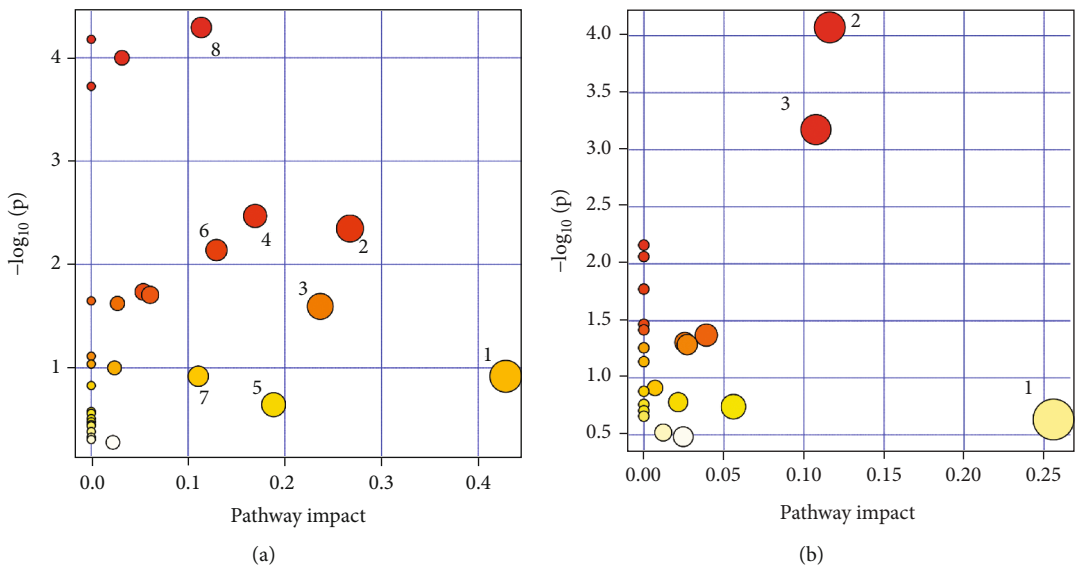

Figure 7: Summary of pathway analysis of serum and liver. (a) Serum: (1) taurine and hypotaurine metabolism; (2) pyruvate metabolism; (3) glycerolipid metabolism; (4) histidine metabolism; (5) citrate cycle (TCA cycle); (6) glycolysis/gluconeogenesis; (7) alanine, aspartate, and glutamate metabolism; (8) arginine and proline metabolism. (b) Liver: (1) glutathione metabolism; (2) alanine, aspartate, and glutamate metabolism; (3) citrate cycle (TCA cycle).

of fatty acid oxidation [32], acetate was significantly upregulated in the liver of the APAP model group, indicating that the fatty acid oxidation process was enhanced.

Gluconeogenesis is another energy-saving pathway in which enzymes gradually convert pyruvate into glucose, providing the body with more glucose for energy production. A precursor of gluconeogenesis [33], alanine, is a key link between carbohydrate and amino acid metabolism. In this cycle, the ammonia produced by the breakdown of proteins is converted to L-alanine by transamination, which is then transported to the liver. Catalyzed by alanine aminotransferase, the amino group is transferred to α-ketoglutarate to form glutamate and pyruvate, which can be further converted to glucose [34]. However, our data showed that alanine levels in serum and liver of the APAP model group were significantly increased, while pyruvate and glucose levels were not significantly increased, indicating that the gluconeogenesis pathway was impaired. Therefore, fatty acid oxidation may be the leading energy supplement for APAP-induced stimulation in mice in the model group.

Furthermore, liver samples from the APAP model group showed significantly elevated leucine, isoleucine, and valine levels. They are commonly known as branched-chain amino acids essential for protein synthesis [35–37]. As previously mentioned, induction of APAP produces ROS, which further destroys proteins in the cytoplasm and membranes of liver cells [38]. The elevated levels of these three essential amino acids indicate enhanced hepatic catabolism and damage to some proteins. Our results suggest that low-dose naringin therapy salvages the increased levels of branched amino acids preventing ROS damage to proteins.

A purine catabolic pathway can be performed to save the body from oxidative damage. In this process, inosine goes through the first step of metabolism to produce hypoxanthine, which is then converted to xanthine by the catalysis of xanthine oxidoreductase and finally converted from xanthine to uric acid, which is an effective free radical scavenger with antioxidant effect [30, 39]. Therefore, the significant reduction of inosine, hypoxanthine, and xanthne in the APAP model group may be attributed to a self-protection mechanism of hepatocytes.

In conclusion, our study demonstrates the potential value of naringin in the treatment of APAP-induced liver injury in mice. The underlying mechanisms include antioxidants, salvage, glucose metabolism, regulation of amino acids, and purine metabolism. Our study focused on the changes of endogenous metabolites in mice with liver injury and explored the therapeutic effects of naringin based on them. Using metabolomics analysis based on NMR, we identified small molecule metabolites that changed significantly before and after drug treatment and explored the metabolic pathways involved, providing a new strategy for alleviating the liver toxicity and side effects of APAP drugs.

Data Availability

The original contributions presented in the study are included in the article. Further inquiries can be directed to the corresponding authors.

Conflicts of Interest

The authors declare that they have no conflicts of interest.

Authors' Contributions

ZL is responsible for the investigation, data analysis, and writing—original draft; GW, WG, SZ, ZS, and ML for the resources and investigation; WL for the investigation; YC for the funding acquisition, resources, and supervision; GZ

and BC for the writing—review and editing; and CW and TY for the funding acquisition, conceptualization, supervision, resources, and writing—review and editing. All authors have read and agreed to the final manuscript draft. Zihan Lin and Guanzhen Wang contributed equally to this work.

Acknowledgments

This work was supported by grants from the National Natural Science Foundation of China (no. 31972899), by the Program for Professor of Special Appointment (Eastern Scholar) at Shanghai Institutions of Higher Learning, and Shanghai Overseas Talents Introduction Program.

References

[1] M. A. Alam, N. Subhan, M. M. Rahman, S. J. Uddin, H. M. Reza, and S. D. Sarker, "Effect of citrus flavonoids, naringin and naringenin, on metabolic syndrome and their mechanisms of action," *Advances in Nutrition*, vol. 5, no. 4, pp. 404–417, 2014.

[2] R. Chen, Q. L. Qi, M. T. Wang, and Q. Y. Li, "Therapeutic potential of naringin: an overview," *Pharmaceutical Biology*, vol. 54, no. 12, pp. 3203–3210, 2016.

[3] H. Zhao, M. Liu, H. Liu, R. Suo, and C. Lu, "Naringin protects endothelial cells from apoptosis and inflammation by regulating the Hippo-YAP pathway," *Bioscience Reports*, vol. 40, no. 3, p. BSR20193431, 2020.

[4] H. Elsawy, A. I. Algefare, M. Alfwuaires et al., "Naringin alleviates methotrexate-induced liver injury in male albino rats and enhances its antitumor efficacy in HepG2 cells," *Bioscience Reports*, vol. 40, no. 6, article BSR20193686, 2020.

[5] M. Vabeiryureilai, K. Lalrinzuali, and G. C. Jagetia, "NF-κB and COX-2 repression with topical application of hesperidin and naringin hydrogels augments repair and regeneration of deep dermal wounds," *Burns*, vol. 48, no. 1, pp. 132–145, 2022.

[6] O. F. Koroglu, M. Gunata, N. Vardi et al., "Protective effects of naringin on valproic acid-induced hepatotoxicity in rats," *Tissue & Cell*, vol. 72, article 101526, 2021.

[7] C. Zhou, Y. Lai, P. Huang et al., "Naringin attenuates alcoholic liver injury by reducing lipid accumulation and oxidative stress," *Life Sciences*, vol. 216, pp. 305–312, 2019.

[8] K. A. El-Mihi, H. I. Kenawy, A. El-Karef, N. M. Elsherbiny, and L. A. Eissa, "Naringin attenuates thioacetamide-induced liver fibrosis in rats through modulation of the PI3K/Akt pathway," *Life Sciences*, vol. 187, pp. 50–57, 2017.

[9] A. J. Akamo, S. O. Rotimi, D. I. Akinloye et al., "Naringin prevents cyclophosphamide-induced hepatotoxicity in rats by attenuating oxidative stress, fibrosis, and inflammation," *Food and Chemical Toxicology*, vol. 153, article 112266, 2021.

[10] K. D. Croft, "The chemistry and biological effects of flavonoids and phenolic acids[a]," *Annals of the New York Academy of Sciences*, vol. 854, no. 1 TOWARDS PROLO, pp. 435–442, 1998.

[11] H. A. Al-Aubaidy, A. Dayan, M. A. Deseo et al., "Twelve-week Mediterranean diet intervention increases citrus bioflavonoid levels and reduces inflammation in people with type 2 diabetes mellitus," *Nutrients*, vol. 13, no. 4, p. 1133, 2021.

[12] X. Meng, M. Fu, S. Wang, W. Chen, J. Wang, and N. Zhang, "Naringin ameliorates memory deficits and exerts neuroprotective effects in a mouse model of Alzheimer´s disease by regulating multiple metabolic pathways," *Molecular Medicine Reports*, vol. 23, no. 5, p. 332, 2021.

[13] M. H. Wang, C. C. Yang, H. C. Tseng, C. H. Fang, Y. W. Lin, and H. S. Soung, "Naringin ameliorates haloperidol-induced neurotoxicity and orofacial dyskinesia in a rat model of human tardive dyskinesia," *Neurotoxicity Research*, vol. 39, no. 3, pp. 774–786, 2021.

[14] V. Varshney and D. Garabadu, "Naringin exhibits mas receptor-mediated neuroprotection against amyloid beta-induced cognitive deficits and mitochondrial toxicity in rat brain," *Neurotoxicity Research*, vol. 39, no. 4, pp. 1023–1043, 2021.

[15] C. Bunchorntavakul and K. R. Reddy, "Acetaminophen (APAP or N-acetyl-p-aminophenol) and acute liver failure," *Clinics in Liver Disease*, vol. 22, no. 2, pp. 325–346, 2018.

[16] A. M. Larson, "Acetaminophen hepatotoxicity," *Clinics in Liver Disease*, vol. 11, no. 3, pp. 525–548, 2007.

[17] A. Iorga and L. Dara, "Cell death in drug-induced liver injury," *Advances in Pharmacology*, vol. 85, pp. 31–74, 2019.

[18] X. Chao, H. Wang, H. Jaeschke, and W. X. Ding, "Role and mechanisms of autophagy in acetaminophen-induced liver injury," *Liver International*, vol. 38, no. 8, pp. 1363–1374, 2018.

[19] C. I. Ghanem, M. J. Pérez, J. E. Manautou, and A. D. Mottino, "Acetaminophen from liver to brain: new insights into drug pharmacological action and toxicity," *Pharmacological Research*, vol. 109, pp. 119–131, 2016.

[20] M. Dönmez, B. Uysal, Y. Poyrazoğlu et al., "PARP inhibition prevents acetaminophen-induced liver injury and increases survival rate in rats," *Turkish Journal of Medical Sciences*, vol. 45, no. 1, pp. 18–26, 2015.

[21] V. Rodríguez, L. Plavnik, and N. Tolosa de Talamoni, "Naringin attenuates liver damage in streptozotocin-induced diabetic rats," *Biomedicine & Pharmacotherapy*, vol. 105, pp. 95–102, 2018.

[22] C. Caglayan, Y. Temel, F. M. Kandemir, S. Yildirim, and S. Kucukler, "Naringin protects against cyclophosphamide-induced hepatotoxicity and nephrotoxicity through modulation of oxidative stress, inflammation, apoptosis, autophagy, and DNA damage," *Environmental Science and Pollution Research International*, vol. 25, no. 21, pp. 20968–20984, 2018.

[23] M. Mahdavinia, L. Khorsandi, S. Alboghobeish, A. Samimi, M. A. Dehghani, and L. Zeidooni, "Liver histopathological alteration and dysfunction after bisphenol A administration in male rats and protective effects of naringin," *Avicenna J Phytomed.*, vol. 11, no. 4, pp. 394–406, 2021.

[24] Z. Lv, W. Wu, S. Ge et al., "Naringin protects against perfluorooctane sulfonate-induced liver injury by modulating NRF2 and NF-κB in mice," *International Immunopharmacology*, vol. 65, pp. 140–147, 2018.

[25] R. A. Hassan, W. G. Hozayen, H. T. Abo Sree, H. M. Al-Muzafar, K. A. Amin, and O. M. Ahmed, "Naringin and hesperidin counteract diclofenac-induced hepatotoxicity in male Wistar rats *via* their antioxidant, anti-inflammatory, and antiapoptotic activities," *Oxidative Medicine and Cellular Longevity*, vol. 2021, Article ID 9990091, 14 pages, 2021.

[26] V. K. Rathi, S. Das, A. Parampalli Raghavendra, and B. S. S. Rao, "Naringin abates adverse effects of cadmium-mediated hepatotoxicity: an experimental study using HepG2 cells," *Journal of Biochemical and Molecular Toxicology*, vol. 31, no. 8, p. 10.1002/jbt.21915, 2017.

[27] L. Xu, Y. Yu, R. Sang, J. Li, B. Ge, and X. Zhang, "Protective effects of taraxasterol against ethanol-induced liver injury by regulating CYP2E1/Nrf2/HO-1 and NF-κB signaling pathways in mice," *Oxidative Medicine and Cellular Longevity*, vol. 2018, Article ID 8284107, 11 pages, 2018.

[28] C. Han, Y. Wei, X. Wang, C. Ba, and W. Shi, "Protective effect of *Salvia miltiorrhiza* polysaccharides on liver injury in chickens," *Poultry Science*, vol. 98, no. 9, pp. 3496–3503, 2019.

[29] J. Wang, Q. Kan, J. Li, X. Zhang, and Y. Qi, "Effect of neferine on liver ischemia-reperfusion injury in rats," *Transplantation Proceedings*, vol. 43, no. 7, pp. 2536–2539, 2011.

[30] M. H. Li, X. Feng, D. J. Deng Ba et al., "Hepatoprotection of *Herpetospermum caudigerum* Wall. against CCl_4-induced liver fibrosis on rats," *Journal of Ethnopharmacology*, vol. 229, pp. 1–14, 2019.

[31] W. G. Kaelin Jr. and C. B. Thompson, "Clues from cell metabolism," *Nature*, vol. 465, no. 7298, pp. 562–564, 2010.

[32] S. M. Bernson and D. G. Nicholls, "Acetate, a major end product of fatty-acid oxidation in hamster brown-adipose-tissue mitochondria," *European Journal of Biochemistry*, vol. 47, no. 3, pp. 517–525, 1974.

[33] G. Martin, N. Vincent, J. Combet, and G. Baverel, "A simple model for alanine metabolism in isolated rat hepatocytes," *Biochimica et Biophysica Acta*, vol. 1175, no. 2, pp. 161–173, 1993.

[34] K. F. Petersen, S. Dufour, G. W. Cline, and G. I. Shulman, "Regulation of hepatic mitochondrial oxidation by glucose-alanine cycling during starvation in humans," *The Journal of Clinical Investigation*, vol. 129, no. 11, pp. 4671–4675, 2019.

[35] T. Kawaguchi, N. Izumi, M. R. Charlton, and M. Sata, "Branched-chain amino acids as pharmacological nutrients in chronic liver disease," *Hepatology*, vol. 54, no. 3, pp. 1063–1070, 2011.

[36] Y. Muto, S. Sato, A. Watanabe et al., "Effects of oral branched-chain amino acid granules on event-free survival in patients with liver cirrhosis," *Clinical Gastroenterology and Hepatology*, vol. 3, no. 7, pp. 705–713, 2005.

[37] Y. Nakaya, K. Okita, K. Suzuki et al., "BCAA-enriched snack improves nutritional state of cirrhosis," *Nutrition*, vol. 23, no. 2, pp. 113–120, 2007.

[38] L. Y. Ruan, M. H. Li, Y. X. Xing et al., "Hepatotoxicity and hepatoprotection of Polygonum multiflorum Thund. as two sides of the same biological coin," *Journal of Ethnopharmacology*, vol. 230, pp. 81–94, 2019.

[39] X. Fu, J. Wang, S. Liao et al., "^{1}H NMR-based metabolomics reveals refined-Huang-Lian-Jie-Du-decoction (BBG) as a potential ischemic stroke treatment drug with efficacy and a favorable therapeutic window," *Frontiers in Pharmacology*, vol. 10, p. 337, 2019.

Hindawi
Oxidative Medicine and Cellular Longevity
Volume 2022, Article ID 3914408, 13 pages
https://doi.org/10.1155/2022/3914408

Research Article

Phytotherapeutic Approach in the Management of Cisplatin Induced Vomiting; Neurochemical Considerations in Pigeon Vomit Model

Ihsan Ullah,[1] Fazal Subhan,[2] Muhammad Shahid,[2] Nisar Ahmad,[3,4] Rehmat Shah,[5] Javaid Alam,[6] Ikram Ul Haq,[7] Rahim Ullah,[8] Muhammad Ayaz,[9] and H. C. Ananda Murthy[10,11]

[1]*Department of Pharmacy, University of Swabi, Swabi, Pakistan*
[2]*Department of Pharmacy, Institute of Integrative Biosciences, CECOS University of IT and Emerging Sciences, Peshawar, KP, Pakistan*
[3]*Department of Pharmacy, University of Peshawar, Peshawar, Pakistan*
[4]*Department of Pharmacy, Islamia College of Pharmacy, Sialkot, Pakistan*
[5]*Pharmacist, Health Department, Khyber Pakhtunkhwa, Pakistan*
[6]*Drug and Herbal Research Center, Faculty of Pharmacy, University Kebangsan, Malaysia*
[7]*National Institute of Health, Islamabad, Pakistan*
[8]*Sarhad University of Science and Information Technology, Peshawar, Pakistan*
[9]*Department of Pharmacy, Faculty of Biological Sciences, University of Malakand, Chakdara, 18000 Dir (L), KP, Pakistan*
[10]*Department of Applied Chemistry, School of Applied Natural Science, Adama Science and Technology University, P O Box 1888, Adama, Ethiopia*
[11]*Department of Prosthodontics, Saveetha Dental College & Hospital, Saveetha Institute of Medical and Technical Science (SIMATS), Saveetha University, Chennai 600 077, Tamil Nadu, India*

Correspondence should be addressed to Ihsan Ullah; ihsanmkd@gmail.com, Muhammad Ayaz; ayazuop@gmail.com, and H. C. Ananda Murthy; anandkps350@gmail.com

Received 11 July 2022; Revised 29 August 2022; Accepted 2 September 2022; Published 13 September 2022

Academic Editor: Tarique Hussain

Cisplatin induced vomiting involves multiple mechanisms in its genesis and a single antiemetic agent do not cover both the phases (acute & delayed) of vomiting in clinics; necessitating the use of antiemetics in combination. *Cannabis sativa* and other selected plants have ethnopharmacological significance in relieving emesis. The aim of the present study was to investigate the intrinsic antiemetic profile of *Cannabis sativa* (*CS*), *Bacopa monniera (BM,* family *Scrophulariaceae)*, and *Zingiber officinale* (*ZO*, family *Zingiberaceae*) in combinations against vomiting induced by highly emetogenic anticancer drug-cisplatin in pigeons. We have analysed the neurotransmitters which trigger the vomiting response centrally and peripherally. Electrochemical detector (ECD) was used for the quantification of neurotransmitters and their respective metabolites by high performance liquid chromatography in the brain stem (BS) and area postrema (AP) while peripherally in the small intestine. Cisplatin (7 mg/kg i.v.) induced reliable vomiting throughout the observation period (24 hrs). *CS*-HexFr (10 mg) + *BM*-MetFr (10 mg)–Combination 1, *BM*-ButFr (5 mg) + *ZO*-ActFr (25 mg)–Combination 2, *ZO*-ActFr (25 mg) + *CS*-HexFr (10 mg)–Combination 3, and *CS*-HexFr (10 mg) + *BM*-ButFr (5 mg)–Combination 4; provided ~30% (30 ± 1.1), 70% (12 ± 0.4; $P < 0.01$), 60% (19 ± 0.2; $P < 0.05$) and 90% (05 ± 0.1; $P < 0.001$) protection, respectively, against cisplatin induced vomiting as compared to cisplatin control. Standard MCP (30 mg) provided ~50% (23 ± 0.3) protection ($P > 0.05$). *CS* Hexane fraction (10 mg/kg), *BM* methanolic (10 mg/kg) and bacoside rich *n*-butanol fraction (5 mg/kg) and *ZO* acetone fraction (25 mg/kg) alone provided ~62%, 36%, 71%, and 44% protection, respectively, as compared to cisplatin control. The most effective and synergistic combination 4 was found to reduce 5HT and 5HIAA ($P < 0.05 – 0.001$) in all the brain areas area postrema (AP)+brain stem (BS) and intestine at the 3rd hour of cisplatin administration. In continuation, at the

18th of cisplatin administration reduction in dopamine ($P < 0.001$) in the AP and 5HT in the brain stem and intestine ($P < 0.001$) was observed. The said combination did not change the neurotransmitters basal levels and their respective metabolites any significantly. In conclusion, all the tested combinations offered protection against cisplatin induced vomiting to variable degrees, where combination 4 provided enhanced attenuation by antiserotonergic mechanism at the 3rd hour while a blended antidopaminergic and antiserotonergic mechanism at the 18th hour after cisplatin administration.

1. Introduction

Nausea and vomiting are the two important adverse effects faced by the patients undergoing cancer chemotherapy [1, 2]. These adverse effects may often result in noncompliance to the chemotherapy but it may result to the refusal of patients to undergo emetogenic chemotherapy cycles. It is known that the cancer is second in the United States which resulted in more deaths; and the studies advocate the increase in the number of cancer patients and, more importantly, breast, lungs, head and neck, colorectal, and stomach carcinomas [3–5].

The emetogenecity of antineoplastics varies and that is why they are also classified based on its emetogenic propensity. The high emetogenic class contains all the platinum analogues including cisplatin. Cisplatin has the unique aspect that induces vomiting in two phases; the first phase which stays up to 24 hours is known as acute phase while the phase after 24 hours is called delayed phase and it is believed today that it remains up to 7 days after the initiation of chemotherapy cycle. Mechanistically, the vomiting caused by cisplatin is multifactorial with respect to acute and delayed phases. The acute phase is triggered by serotonin; the primary neurotransmitter to be considered while neuropeptide "Substance P" is the mediator for delayed phase [6, 7]. Keeping in view the aforementioned mediators to trigger the vomiting response, the pharmacotherapy also varies in the management of this biphasic vomiting response. For the management of acute phase serotonin receptor blockers e.g. Ondansetron etc. are proved beneficial while the same has shown no significant control over the delayed phase of vomiting; being controlled by neurokinin 1 receptor antagonists (Apprepitant) in combination with dexamethasone. In clinical setups, the combination of antiemetics is used to control both the phases of vomiting induced by cisplatin by following the international guidelines, but still this is a clinical challenge, as the considerable proportion of patients undergoing cancer chemotherapy faces the problem of vomiting [8, 9] making it a need for a time to look for new antiemetic having a broad spectrum so it has the capability to control both the phases of vomiting.

The natural plants and the phytochemicals isolated from them are proved to be very important for ailing community and also provide structural templates for the new compounds to be developed [10–15]. The drugs like Quinine etc. have their source from plants and have still significance in the management of various diseases [16–22]. The scientific community is still involving in the isolation and characterization of active phytochemicals against various pathologies [23–25]. Recently, the standardization of extracts/fractions/isolates is getting much more attention to identify the active moiety responsible for the therapeutic response [26–30]. Keeping in view the biphasic vomiting response and the multimechanisms behind the two phases established the use of antiemetics in combination and provides the platform to search for a cost effective combination of herbal origin which may provide good control over the acute and delayed phases of vomiting in clinics. The current study is focusing on *Bacopa monniera* (*BM*), *Cannabis sativa* (*CS*), and *Zingiber officinale* (*ZO*) to see their impact on cisplatin induced vomiting either alone or in combination in the pigeon emesis model. Pigeon emesis model is good for preliminary screening of chemical entities/compounds/extracts/fractions for the antiemetic potential and has been used by the scientific community for the said purpose. Pigeon demonstrates a robust and very clear vomiting response as compared to *Suncus murinus* to almost all the emetogenics.

The literature is rich enough to advocate the antiemetic effect of *Cannabis sativa* and *Zingiber officinale* as antiemetic, while the antiemetic activity of *Bacopa monniera* is reported by our laboratory for the first time. The major chemical moiety of Cannabis extract i.e. Δ^9-tetrahydocannabinal (Δ^9-THC) has been shown to be antiemetic and also shown promising results in clinics [31, 32]. Furthermore, the *cannabis* preparations have shown superior antiemetic activity as compared to Dopamine receptor blockers [33]. The identification of endocannabinoids and cannabinoid receptors [34, 35] revolutionized the research in cannabinoids for the two decades.

Zingiber officinale is well known for its use as spice and flavouring agent and also been used for the treatment for vomiting and anorexia [36]. Gingirol is reported as the active component responsible for its activities along with some other moieties as well [36, 37]. Sharma and his coworkers have reported the antiemetic activity of ginger against cisplatin induced vomiting in dogs [38] and against cyclophosphamide induced vomiting in the *Suncus murinus* [39].

Bacopa monniera is well known for its significance in the management of memory impairments [40] and cognitive disorders [41]. The literature is indicating bacosides as the major and important chemical constituent responsible for its activities. The plant extracts are standardized by the prompittayarat in 2007 [42] and our laboratory also did the HPLC fingerprinting of *bacopa* extracts [43] indicating the bacosides as major constituents. Our studies also provided evidences for the mechanisms behind the antiemetic activity of bacosides against cisplatin induced vomiting in pigeon. Based on the previous reports as its antidopaminergic aspect and our findings the bacoside rich fraction is included in the current study.

The antiemetic activity of *CS*, *ZO*, and *BM* is well investigated alone. Keeping in view the mechanistically multifactorial phenomenon associated with cisplatin induced vomiting, we hypothesize that the combinations of these safe and tolerable plant extracts may exhibit a broad spectrum antiemetic activity which may be helpful to cover all the phase of vomiting caused by cisplatin in clinics.

2. Materials and Methods

2.1. Animals. Pigeons of both gender (male and female) and of all species (mix breed at the breeding facility of the Department) having weight in range of 250–350 g were used ($n = 8$). The light/dark cycle was kept as 12 hours and the food and water was available as usual. All the procedures to be done on experimental animals were first approved by the Ethical committee of the Department having the reference No 5/pharm and are according to the animal scientific procedure ACT, 1986 (UK).

2.2. Drugs and Chemicals. Methanol, acetonitrile, 1-octane suphonic acid (HPLC grade, Fisher scientific), EDTA, and sodium dihydrogen orthophosphate (Merck), Metoclopramide (GSK, Pakistan). The neurotransmitter standards (noradrenaline, dopamine, and serotonin) and their metabolites (DOPAC, 5HIAA, and HVA) were purchased from Acros Organics (Belgium). Cisplatin was gifted by the Korea United Pharm (Korea). Bacosides were gifted by the University of Mississippi USA. *N*-butanol, *n*-hexane, and acetone were from Haq Chemicals Pakistan.

2.3. Extraction and Fractionation of Bacopa monniera. Bacopa monniera (*BM*) was carefully collected near the locality of Quid-e-Azam University, Islamabad. A specimen was identified by taxonomist Prof. Dr. Muhammad Ibrar from University of Peshawar and the same was submitted to the Department of Botany herbarium for future reference (V # 7421). The plant required parts were collected, shade dried, and grinded. One kilogram plant material was first treated with *n*-hexane with solvent to crude drug ratio of 03 : 01 to remove all nonpolar components and then treated with acetone (01 : 0.9) for the purpose to remove fats and chlorophyll, then extracted using commercial grade methanol (03 : 0.7) using soxhelet apparatus and the yield was 28 grams. The product was further processed with *n*-butanol and the 1.6 grams of the fraction was obtained; which is the bacoside rich fraction [44, 45]. All the fractions were dissolved in distilled water for administration.

2.4. Extraction of Cannabis sativa. Cannabis sativa (*CS*) was collected at District Malakand KP, Pakistan at its flowering stage and later on authenticated by Prof. Dr. Muhammad Ibrar and a specimen was submitted to the Department herbarium with voucher number 8717. The required plant parts were collected, dried under shade, and then grinded. The grinded material was extracted as reported by our lab [46–48].

2.5. Extraction of Zingiber officinale. 500 grams of the ginger rhizomes were purchased from local market at Mardan, Pakistan. A specimen was identified and the same is submitted to the herbarium with voucher number 20017–pup. The rhizomes were washed and crushed in a way to expose its inner part. Maceration procedure was used for extraction of active phytochemicals (yield 4.72%) [49].

2.6. Drug Formulation. The emetogenic drug cisplatin was dissolved in normal saline by gentle heating up to 60°C. The *n*-butanol (bacoside rich fraction) was dissolved in distilled water for administration. The *n*-hexane fraction of *CS* was dissolved in mixer of ethanol, emulsifier, and distilled water in ratio of 5: 5: 90, respectively [50, 51]. Ginger acetone fraction was dissolved in distilled water and sonicated for complete dissolution.

2.7. Drug Administration. Intramuscular route (Chest muscle) was used for administration of test extracts, standard, and vehicle, while intravenous route was used for administration of cisplatin. After cisplatin administration the animals were put back in confining cages and the behaviour was observed up to 24 hours. Standard antiemetic–metoclopramide, respective vehicles, and test extract combinations were administered 30 minutes before the administration of cisplatin. At the end of the experiment the body weight was noted to calculate body weight loss and the animals were euthanized.

2.8. Antiemetic Assay. Cisplatin was administered (7 mg/kg) and the behaviour of the animals was recoded for 24 hours [48, 52]. Food and water were available to the experimental animals as usual. The one vomiting episode was considered with or without the expulsion of stomach contents and the relaxed posture among the two episodes was considered the separation marker [53]. Further in the studies, cisplatin was used at the dose of 7 mg/kg to induce vomiting and to evaluate the antiemetic effects of various extracts alone or in combination.

2.9. Tissue Sampling for Neurotransmitters Analysis. The brain areas: (1). Area postrema and (2). Brain stem were collected at the end of experiment by following the Atlas [54, 55], which were later on processed for quantification of neurotransmitters and their metabolites. Intestinal samples were also collected 10 cm from the pylorus for HPLC-ECD analysis.

2.10. Determination of Neurotransmitters and Their Metabolites. The brain and intestinal samples were first cleared using cold saline and then homogenized in cold 0.2% perchloric acid at 5000 rpm using Teflon glass homogenizer, centrifuged at 12000 g/minute (4°C), filtered using 0.45 μ filter. High performance liquid chromatography was used along with electrochemical detector for quantification of neurotransmitter and their metabolites in brain areas and intestine as reported in our previous studies [56].

2.11. Statistical Analysis. One-way analysis of variance was applied as a tool for group comparison and Student *t*-test/tukey's multiple comparison test/Dunnett's test was used as post hoc tests by using GraphPad Prism (Version 8). *P* value less than 0.05 was considered as statistically significant. The animal which showed no vomiting response is excluded from latency calculations.

3. Results

3.1. Antiemetic Effect of CS Hexane Fraction (10 mg/kg), BM Methanolic (10 mg/kg), and Bacoside Rich N-Butanol Fraction (5 mg/kg), and ZO Acetone Fraction (25 mg/kg) Alone and in Combinations. To see for any possible

synergistic combination among the selected plant extracts against cisplatin induced vomiting. The combinations tested were

(1) *CS*-HexFr+*BM*-MetFr

(2) *BM*-ButFr+*ZO*-ActFr

(3) *ZO*-ActFr+*CS*-HexFr

(4) *CS*-HexFr+*BM*-ButFr

Furthermore, all the fractions of *CS*, *BM*, and *ZO* most effective doses were also tested for their antiemetic effects alone as well.

The vomiting response of ~45 episodes with latency of ~66 minutes was recorded for cisplatin control, where all the animals showed reliable vomiting response up to the observation period (Table 1). Standard antiemetic metoclopramide suppressed the vomiting response to ~23 episodes (50%) and increased the latency up to 248 min ($P > 0.05$) as compared to cisplatin control. Combination 4 proved to be a synergistic combination as calculated by limpel equation [57] and it provided protection up to 89% ($P < 0.001$, Table 1) against the vomiting induced by cisplatin during the observation period. Combination 4 significantly increased the latency to first vomit as well ($P < 0.01$). Combination 2 reduced the vomiting episodes up to 12 (73%), while combination 3 provided up to 58% protection (~19 episodes) against cisplatin induced vomiting ($P < 0.05$, Table 1). Furthermore, Combination 1 also attenuated the vomiting response but nonsignificantly. Only combination 4 significantly ($P < 0.01$) increased the latency to first vomit while others failed to do so. The combination 4 provided enhanced protection and proved to be synergistic where it provided complete remission of vomiting response in one animal, although it attenuated the vomiting response to a maximum degree and increased the latency as well. Combination 4 in comparison to other combinations lowered the vomiting episodes but the difference was found to be statistically nonsignificant (Table 1, Figures 1–3). The most effective doses of the *CS* (10 mg/kg), *BM* methanolic (10 mg/kg), *BM n*-butanolic (5 mg/kg), and *ZO* (25 mg/kg) alone provided up to 62%, 36%, 71%, and 44% attenuation of vomiting as compared to cisplatin control (Table 1, Figures 1–3).

3.2. Effect of CS Hexane Fraction (10 mg/kg), BM Methanolic (10 mg/kg) and Bacoside Rich N-Butanol Fraction (5 mg/kg), and ZO Acetone Fraction (25 mg/kg) Alone and Combination 1, 2, 3, and 4 on Cisplatin-Induced Jerks and Weight Loss. Animals in control group (cisplatin treated) lost their body weight up to 15%, while the combination 1 and 3 showed the reduction in weight loss significantly (P <0.05–0.01, Table 1). In continuation, combination 2, 4, and standard metoclopramide failed to do so. No combination reduced the jerking episodes any significantly.

3.3. Effect of Standard MCP and Combination 4 on Basal Neurotransmitters Cum Metabolites in the Brain Areas and Intestine. Metoclopramide significantly reduced the concentration of 5 hydroxy indole acetic acid (5HIAA) in the area postrema and brain stem significantly ($P < 0.05$ and $P < 0.001$, respectively) as compared to basal level. Furthermore, the homovanillic acid (HVA) was also decreased significantly when compared with basal HVA concentration (Table 2). Combination 4 only reduced the concentration of 5HIAA in the brain stem as compared to basal level ($P < 0.05$, Table 2).

3.4. Effect of Metoclopramide and Combination 4 on Neurotransmitters Cum Metabolites in the Brain Areas and Intestine at 3rd Hour of Cisplatin Treatment. The concentration of 5-hydroxy tryptamine was significantly increased ($P < 0.001$) in the brain stem and at the level of intestine as compared to vehicle treated, while in the area postrema a nonsignificant increase was observed (Table 3). Metoclopramide (30 mg/kg) did not changed the concentration of all the neurotransmitters and their metabolites in the brain areas and intestine but only reduced the concentration of 5-hydroxy tryptamine in the brain stem and intestine ($P < 0.001$) as compared to cisplatin control (Table 3). In continuation, metoclopramide also decreased the concentration of 5HIAA in the brain stem, area postrema, and intestine ($P < 0.01 - 0.001$, Table 3).

Combination 4 significantly (P <0.05–0.001) decreased the concentration of 5HT and its metabolite 5-hydroxy indole acetic acid (5HIAA) in the brain stem, area postrema, and intestine (Table 3). However, no significant effects were observed on the other neurotransmitters in the brain areas and intestine except dihydroxy pheny acetic acid (DOPAC) which was found significantly increased in intestine ($P < 0.05$, Table 3).

3.5. Effect of Metoclopramide or Combination 4 on Neurotransmitters Cum Metabolites in the Brain Areas and Intestine at 18th Hour of Cisplatin Treatment. The concentration of neurotransmitter–Dopamine was significantly ($P < 0.001$) increased in the area postrema while a nonsignificant trend was observed in the brain stem and intestine (Table 4). 5HT concentrations were also noted to be increased in area postrema, brain stem, and intestine with significance of $P < 0.01$, $P < 0.001$, and $P < 0.001$, respectively, and did not affect the levels of others (DOPAC, HVA, 5HIAA, and NA) (Table 4). Metoclopramide decreased the dopamine surge significantly in area postrema ($P < 0.001$). In addition, the decrease in the concentration of 5HT was also observed in the area postrema ($P < 0.01$), brain stem ($P < 0.001$), and intestine ($P < 0.001$) as compared to cisplatin control (Table 4). Furthermore, 5HIAA concentration was also decreased in area postrema ($P < 0.01$). Combination 4 significantly ($P < 0.001$) decreased the upsurge of dopamine in the area postrema and 5HT in the brain stem and intestine (Table 4) as compared to cisplatin control. No significant changes were noted by Combination 4 on any of the neurotransmitter and their metabolites (Table 4).

4. Discussion

The current study is expedited to investigate the antiemetic effects of *Cannabis sativa* (*CS*), *Zingiber officinale* (*ZO*), and *Bacopa monniera* (*BM*) alone or in combination against

Table 1: Effect of *CS* Hexane fraction (10 mg/kg), *BM* methanolic (10 mg/kg) and bacoside rich *n*-butanol fraction (5 mg/kg) and *ZO* acetone fraction (25 mg/kg) alone and in combinations on cisplatin induced *R*+*V* in pigeons.

Drug treatment	Dose & route	Pigeons n/vomited	*R* + *V* Mean ± sem	Latency (min) mean ± sem	Jerks Mean ± sem	Wt loss (%) mean ± sem
Saline+cisplatin	02 ml/kg i.m. +7 mg/kg i.v.	6/6	45 ± 1.9	66 ± 8.4	542 ± 84	15.5 ± 1.8
MCP+cisplatin	30 mg/kg i.m. +7 mg/kg i.v.	7/7	23.5 ± 0.3	248 ± 95	411 ± 112	10.8 ± 1.6
CS-HexFr+cisplatin	10 mg/kg i.m. +07 mg/kg i.v.	6/6	16.5 ± 2.7 **	258 ± 113	226 ± 84	7.5 ± 1.8
BM-MetFr+cisplatin	10 mg/kg i.m. +7 mg/kg iv	6/6	29 ± 4.3	243 ± 172	570 ± 138	8.9 ± 1.3
BM-ButFr + cisplatin	5 mg/kg i.m. +7 mg/kg iv	8/8	13 ± 2.1 ***	137 ± 24	330 ± 95	9.1 ± 2.1 *
ZO-ActFr + cisplatin	25 mg/kg i.m. +07 mg/kg i.v.	8/8	25 ± 1.8	139 ± 21	223 ± 81	8.7 ± 1.4 *
(CS-HexFr + BM-MetFr) + cisplatin	(10+10 mg/kg i.m.) +7 mg/kg i.v.	6/6	30 ± 1.1	131 ± 16	672 ± 124	5.1 ± 2.5 **
(BM-ButFr + *ZO*-ActFr) + cisplatin	(5 + 25 mg/kg i.m.) +7 mg/kg i.v.	6/6	12 ± 0.4 **	69 ± 21	598 ± 194	9.6 ± 2.4
(*ZO*-ActFr + CS-HexFr) + cisplatin	(25+10 mg/kg i.m.) +7 mg/kg i.v.	7/7	19 ± 0.2 *	85 ± 12	415 ± 108	7.3 ± 1.9 *
(CS-HexFr + BM-ButFr) + cisplatin	(10+ 5 mg/kg i.m.) +7 mg/kg i.v.	6/5	05 ± 0.1 ***	369 ± 123 **	99 ± 47	10.6 ± 1.7

Effect of *CS* Hexane fraction (CS-HexFr), *BM* methanolic fraction (BM-MetFr), bacoside rich *n*-butanol fraction (BM-ButFr), and *ZO* acetone fraction (*ZO*-ActFr) alone and in combinations on cisplatin induced vomiting and jerking during a 24 hr observation period. Standard metoclopramide (MCP; 30 mg/kg) is also shown. Values significantly different compared to cisplatin control are indicated as $*P < 0.05$, $**P < 0.01$, and $***P < 0.001$ (ANOVA followed by Tukey post hoc test). Combination 1 (CS-HexFr 10 mg + BM-MetFr 10 mg), Combination 2 (BM-ButFr 5 mg + *ZO*-ActFr 25 mg), Combination 3 (*ZO*-ActFr 25 mg + CS-HexFr 10 mg), and Combination 4 (CS-HexFr 10 mg + BM-ButFr 5 mg).

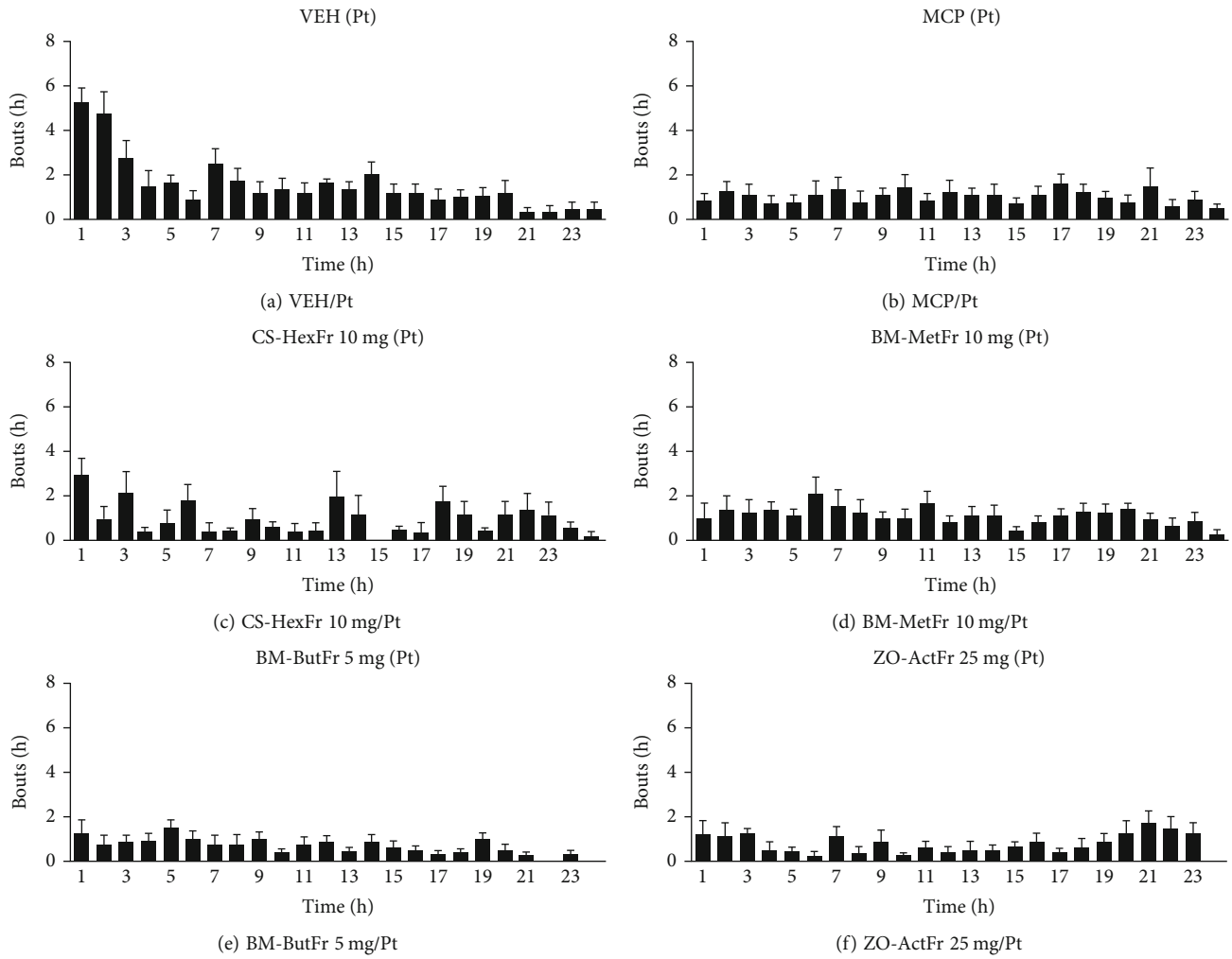

Figure 1: Antiemetic effect of *CS* Hexane fraction (10 mg/kg), *BM* methanolic (10 mg/kg) and bacoside rich *n*-butanol fraction (5 mg/kg) and *ZO* acetone fraction (25 mg/kg) alone.

cisplatin induced vomiting in pigeon. *CS*, *ZO*, and *BM* extracts exhibited prominent antiemetic activity. Preparations containing the active phytochemical from *CS* were found effective against cisplatin induced vomiting (7 mg/kg) [58]. In continuation, our previous study reported *CS* antiemetic activity in pigeons where the hexane fraction proved to be very effective against cisplatin induced vomiting at the dose of 10 mg/kg single and twice daily dosing provided up to 58.5% (17 ± 3.4 episodes) and 65.6% (14.1 ± 2.9 episodes) protection, respectively [47]. In the current study, *CS*-HexFr 10 mg provided up to 62.2% (17 ± 2.7 episodes) protection against cisplatin induced vomiting (Table 1). The hexane fraction of *CS* extract contains all the nonpolar compounds and the active component-Δ^9-THC. The *CS* major component Δ^9-THC has been reported to have its clinical significance in the management of cisplatin induced vomiting [59]. CB_1 receptors which are present presynaptically are involved in the mediation of antiemetic effect of THC, whose stimulation results in the inhibition of neurotransmitters which trigger the act of vomiting [60, 61]. The dose of 7 mg/kg was selected based on our previous study [45] which produced reliable vomiting response during the observation period and also not resulted in mortality.

BM belongs to family Scrophulariaceae and is present abundantly in Pakistan [62]. *BM* extracts are subjected to standardization in previous studies and our laboratory also did the standardization of plant extracts for quantification of bacosides by HPLC finger printing. The findings authenticate that the butanolic fraction contains the highest concentration of bacosides [43]. Clinical trials on bacosides for the management of memory enhancement establish the safety and tolerability of these phytochemicals and available currently in various herbal preparations alone or in combination. *BM* exhibit prominent antioxidant activity [63] and attenuate the dopamine receptor mediated hyperactivity [64]. The reports by our lab advocate that bacosides in a potent manner (~700 μg/kg) suppress the vomiting induced by cisplatin up to 24 hours in pigeons [51] so it will be a good candidate to be used alone or in combination for the CIV management in clinics.

In this study, *BM*-MetFr 10 mg and *BM*-ButFr 5 mg attenuated cisplatin induced vomiting up to 35.6%

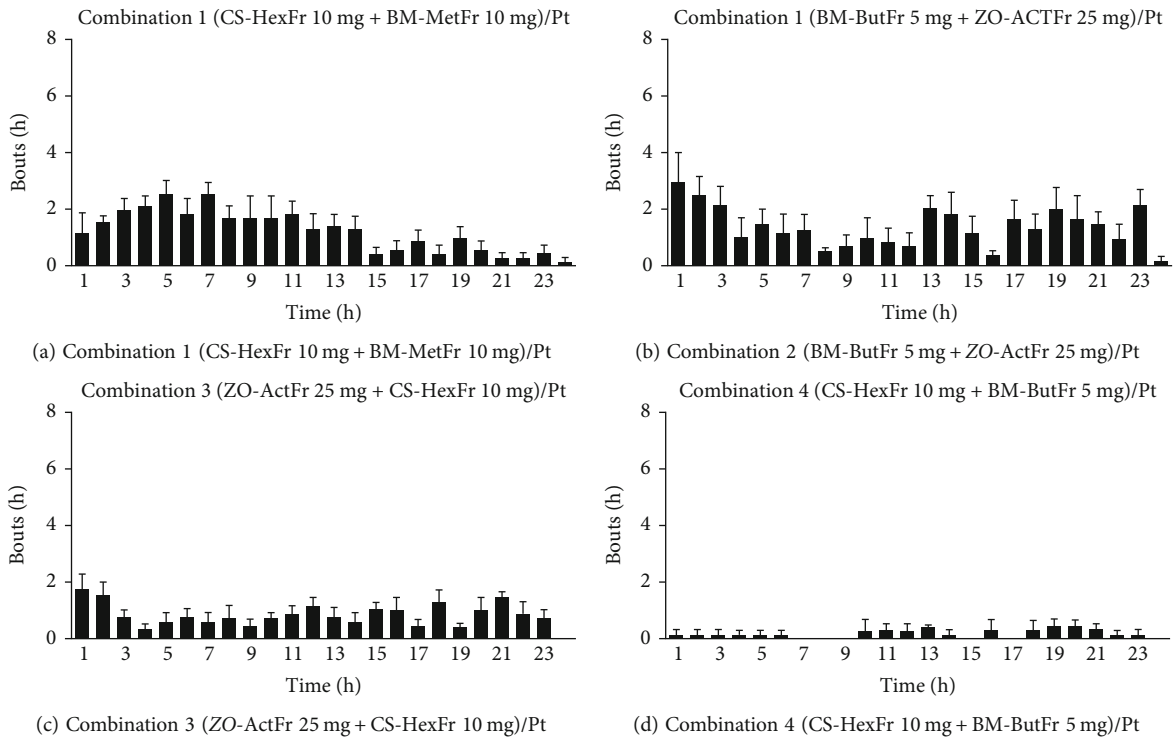

(a) Combination 1 (CS-HexFr 10 mg + BM-MetFr 10 mg)/Pt

(b) Combination 2 (BM-ButFr 5 mg + *ZO*-ActFr 25 mg)/Pt

(c) Combination 3 (*ZO*-ActFr 25 mg + CS-HexFr 10 mg)/Pt

(d) Combination 4 (CS-HexFr 10 mg + BM-ButFr 5 mg)/Pt

Figure 2: Antiemetic effect of combination of *CS* Hexane fraction (10 mg/kg), *BM* methanolic (10 mg/kg) and bacoside rich *n*-butanol fraction (5 mg/kg) and *ZO* acetone fraction (25 mg/kg).

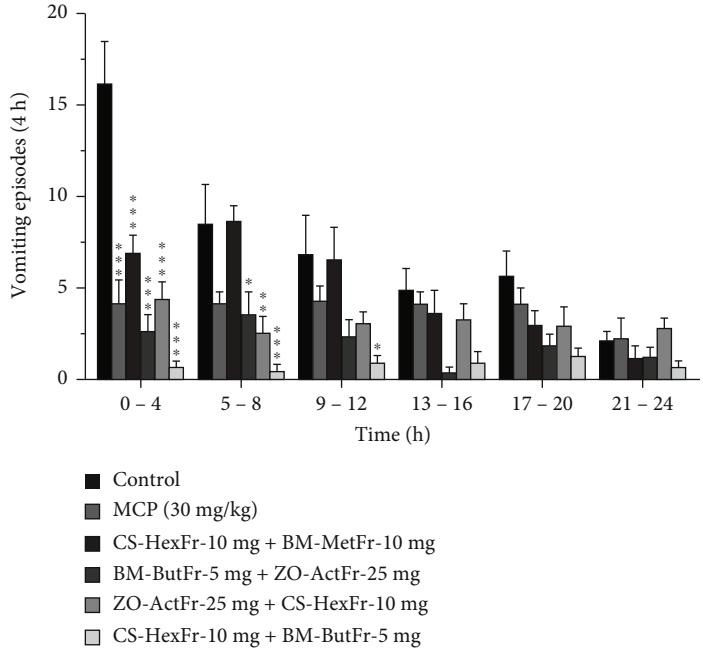

Figure 3: Number of vomiting episodes observed after treatment with combination of *CS* Hexane fraction (10 mg/kg), *BM* methanolic (10 mg/kg) and bacoside rich *n*-butanol fraction (5 mg/kg) and *ZO* acetone fraction (25 mg/kg). Each column represents mean vomiting episodes after every 4 h ± S.E.M. $^{*}P < 0.05$, $^{**}P < 0.01$, $^{***}P < 0.001$ as compared to control, two-way repeated measures ANOVA followed by Tukey's *post hoc* test.

Table 2: Effect of metoclopramide (MCP) or combination (CS-HexFr 10 mg + BM-ButFr 5 mg) on basal level of neurotransmitters and their metabolites at the brain level of Area postrema (AP), Brain stem (BS), and intestine in pigeons.

Treatment	NA	DOPAC	DA	5HIAA	HVA	5HT
Area Postrema						
Saline	0.590 ± 0.011	0.470 ± 0.011	0.610 ± 0.139	0.175 ± 0.106	0.887 ± 0.083	0.059 ± 0.041
MCP 30 mg	0.031 ± 0.004	0.020 ± 0.010	0.032 ± 0.021	0.006 ± 0.011 *	0.120 ± 0.056 *	0.041 ± 0.002
(CS-HexFr 10 mg + BM-ButFr 5 mg)	1.491 ± 1.382	0.408 ± 0.276	0.225 ± 0.088	0.100 ± 0.044	1.096 ± 0.507	0.147 ± 0.095
Brain stem						
Saline	0.089 ± 0.021	0.063 ± 0.070	0.193 ± 0.067	0.071 ± 0.031	0.059 ± 0.020	0.012 ± 0.001
MCP 30 mg	0.120 ± 0.041	0.034 ± 0.004	0.050 ± 0.019	0.006 ± 0.010 ***	0.073 ± 0.040	0.020 ± 0.020
(CS-HexFr 10 mg + BM-ButFr 5 mg)	0.160 ± 0.115	0.031 ± 0.000	0.428 ± 0.157	0.012 ± 0.003 *	0.104 ± 0.042	0.020 ± 0.006
Intestine						
Saline	0.187 ± 0.063	0.074 ± 0.010	0.087 ± 0.056	0.083 ± 0.049	0.071 ± 0.031	0.054 ± 0.013
MCP 30 mg	0.129 ± 0.047	0.063 ± 0.014	0.063 ± 0.021	0.012 ± 0.010	0.207 ± 0.012	0.071 ± 0.010
(CS-HexFr 10 mg + BM-ButFr 5 mg)	0.248 ± 0.040	0.123 ± 0.045	0.056 ± 0.001	0.029 ± 0.010	0.119 ± 0.115	0.063 ± 0.021

Effect of combination of CS-HexFr (10 mg) with BM-ButFr (5 mg) administered 30 minutes before saline administration, on the basal level of neurotransmitters and their metabolites (ng/mg tissue wet weight) at the brain level of AP and BS and Intestine in pigeons at $t = 3$ hr ($n = 6 - 8$). Standard MCP is also shown. Values significantly different compared to basal level are indicated as $*P < 0.05$, $**P < 0.01$, $***P < 0.001$ (ANOVA followed by Tukey post hoc analysis).

Table 3: Effect of standard metoclopramide (MCP), or combination of CS-HexFr (10 mg) with BM-ButFr (5 mg) on neurotransmitters and their metabolites at the brain level of area postrema (AP) and brain stem (BS) and intestine at 3rd hour of cisplatin treatment.

Treatment	NA	Dopac	DA	5HIAA	HVA	5HT
Area Postrema						
Saline	0.701 ± 0.271	0.199 ± 0.010	0.763 ± 0.200	0.091 ± 0.040	0.900 ± 0.173	0.131 ± 0.050
Cisplatin	1.704 ± 1.401	0.408 ± 0.170	0.091 ± 0.270	0.379 ± 0.001#	0.607 ± 0.109	0.314 ± 0.110
MCP 30 mg	0.116 ± 0.078	0.142 ± 0.050	0.310 ± 0.137	0.026 ± 0.006 **	0.040 ± 0.021	0.030 ± 0.005 *
(CS-HexFr 10 mg + BM-ButFr 5 mg)	0.166 ± 0.139	0.192 ± 0.088	0.339 ± 0.144	0.046 ± 0.019 **	0.443 ± 0.181	0.048 ± 0.022 *
Brain stem						
Saline	0.117 ± 0.031	0.041 ± 0.020	0.260 ± 0.130	0.020 ± 0.010	0.070 ± 0.023	0.016 ± 0.001
Cisplatin	0.113 ± 0.040	0.185 ± 0.046	0.040 ± 0.010	0.057 ± 0.001###	0.032 ± 0.002	0.153 ± 0.011###
MCP 30 mg	0.041 ± 0.021	0.039 ± 0.003	0.013 ± 0.002	0.021 ± 0.001 ***	0.023 ± 0.001	0.008 ± 0.000 ***
(CS-HexFr 10 mg + BM-ButFr 5 mg)	0.089 ± 0.007	0.011 ± 0.001	0.119 ± 0.069	0.003 ± 0.002 ***	0.018 ± 0.003	0.006 ± 0.002 ***
Intestine						
Saline	0.416 ± 0.037	0.092 ± 0.010	0.129 ± 0.024	0.041 ± 0.000	0.107 ± 0.052	0.051 ± 0.001
Cisplatin	0.301 ± 0.047	0.024 ± 0.002	0.037 ± 0.004	0.304 ± 0.030###	0.043 ± 0.005	0.689 ± 0.104###
MCP 30 mg	0.109 ± 0.040 *	0.029 ± 0.001	0.246 ± 0.183	0.031 ± 0.006 ***	0.067 ± 0.030	0.041 ± 0.005 ***
(CS-HexFr 10 mg + BM-ButFr 5 mg)	0.266 ± 0.104	0.047 ± 0.275 *	0.399 ± 0.232	0.003 ± 0.001 ***	0.004 ± 0.002	0.007 ± 0.006 ***

Effect of combination of CS-HexFr (10 mg) with BM-ButFr (5 mg) administered 30 mins before cisplatin challenge, on the level of neurotransmitters and their metabolites (ng/mg tissue wet weight) at the brain level of AP and BS and Intestine of pigeons at $t = 3$ hr of cisplatin administration ($n = 6 - 8$). Standard MCP is also shown. Values significantly different compared to cisplatin control are indicated as $*P < 0.05$, $**P < 0.01***P < 0.001$, while values significantly different compared to basal level are indicated as $\#P < 0.05$, $\#\#\#P < 0.001$ (ANOVA followed by Tukey post hoc analysis).

Table 4: Effect of standard metoclopramide (MCP) or combination of CS-HexFr (10 mg) with BM-ButFr (5 mg) on neurotransmitters and their metabolites at the brain level of area postrema (AP) and brain stem (BS) and intestine at 18th hour of cisplatin treatment.

Treatment	NA	Dopac	DA	5HIAA	HVA	5HT
Area Postrema						
Saline	0.507 ± 0.054	0.299 ± 0.129	0.520 ± 0.117	0.207 ± 0.020	0.863 ± 0.130	0.012 ± 0.011
Cisplatin	0.307 ± 0.056	0.021 ± 0.001	6.898 ± 1.300###	0.205 ± 0.048	0.584 ± 0.106	0.153 ± 0.040##
MCP 30 mg	0.250 ± 0.081	0.076 ± 0.041	0.125 ± 0.030 ***	0.020 ± 0.010 **	0.383 ± 0.129	0.005 ± 0.002 **
(CS-HexFr 10 mg + BM-ButFr 5 mg)	0.471 ± 0.174	0.166 ± 0.066	0.504 ± 0.362 ***	0.072 ± 0.012	1.388 ± 0.370	0.107 ± 0.029
Brain stem						
Saline	0.091 ± 0.004	0.083 ± 0.013	0.081 ± 0.041	0.193 ± 0.037	0.032 ± 0.020	0.010 ± 0.000
Cisplatin	0.090 ± 0.003	0.011 ± 0.001	0.192 ± 0.037	0.047 ± 0.002	0.008 ± 0.010	0.172 ± 0.001###
MCP 30 mg	0.012 ± 0.002	0.005 ± 0.001	0.021 ± 0.028	0.015 ± 0.003	0.097 ± 0.048	0.020 ± 0.001 ***
(CS-HexFr 10 mg + BM-ButFr 5 mg)	0.277 ± 0.094 ***	0.007 ± 0.002	0.074 ± 0.074	0.014 ± 0.002	0.022 ± 0.020	0.022 ± 0.004 ***
Intestine						
Saline	0.317 ± 0.160	0.120 ± 0.060	0.193 ± 0.050	0.010 ± 0.001	0.041 ± 0.010	0.062 ± 0.013
Cisplatin	0.265 ± 0.029	0.013 ± 0.001	0.230 ± 0.031	0.340 ± 0.054	0.073 ± 0.005	0.506 ± 0.107###
MCP 30 mg	0.184 ± 0.059	0.021 ± 0.010	0.030 ± 0.010	0.031 ± 0.008	0.527 ± 0.435	0.037 ± 0.004 ***
(CS-HexFr 10 mg + BM-ButFr 5 mg)	0.464 ± 0.060	0.001 ± 0.001	1.308 ± 0.240	0.020 ± 0.011	0.113 ± 0.112	0.047 ± 0.027 ***

Effect of combination of CS-HexFr (10 mg) with *BM*-ButFr (5 mg) administered 30 mins before cisplatin challenge, on the level of neurotransmitters and their metabolites (ng/mg tissue wet weight) at the brain level of AP and BS and Intestine of pigeons at $t = 18$ hr of cisplatin administration ($n = 6 - 8$). Standard MCP is also shown. Values significantly different compared to cisplatin control are indicated as $**P < 0.01$ $***P < 0.001$, while values significantly different compared to basal level are indicated as $##P < 0.01$ $###P < 0.001$ (ANOVA followed by Tukey post hoc analysis).

(29 ± 4.3, $P > 0.05$) and 71.1% (13 ± 2.1) where *BM*-ButFr 5 mg provided more pronounced suppression ($P < 0.001$) as compared to *BM*-MetFr 10 mg and standard MCP. *BM* has proved to be better than the dopamine receptor antagonist – metoclopramide; which may reside in its ability to scavenge free radicals [63], suppression of dopaminergic, and serotonergic activity [43, 65].

ZO belonging to family *Zingiberaceae* having common name–Ginger. Ginger rhizome is cultivated throughout the Asian countries and is used as spice. The use of *ZO* for medicinal purposes is reported since long and is been added to Indian and Chinese pharmacopoeias. The acetone fraction which is reported to be gingerol rich fraction was screened for its antiemetic activity against cisplatin induced vomiting and provided up to 44.4% (25 ± 1.8) protection. The standardization of ginger extracts has the findings that up to 60 mg/g of gingerols are present in extract [66]. Postoperative nausea and vomiting is well managed by Ginger and the antiemetic results are almost equal to the antiemetic response by metoclopramide [67]. Our lab studies have reported the dose of 50 mg to be very effective in suppression of vomiting induced by cisplatin while the longer protection was observed with the dose of 25 mg [49]. There are so many reasons to support the antiemetic activity of ginger including the enhancement of gastroprokinetic activity, antiserotonergic effect [37], inhibitory action of substance P, and expression of NK_1 receptors [68]. Our previous study [49] and current results (Table 1) supports the claim that ginger acetone fraction is having antiemetic activity.

Metoclopramide is dopamine receptor antagonist and also shares serotonin (5HT3) receptor blocking at high doses [69]; both the properties contribute in its antiemetic property. In the present study the dose of Metoclopramide used is based on a previous study [70]. Serotonin receptor blockers have showed intrinsic emetic activity in pigeons (Unpublished data) so the $5HT_3$ antagonist drugs were not used as standard antiemetic.

The multimechanisms behind the vomiting induced by cisplatin resulted in the use of antiemetics in combination and a single antiemetic fails for control both the phases of vomiting. The international guidelines also recommend the use of $5HT_3$ blockers, NK_1 receptor antagonists, and dexamethasone in the management of both the phases of vomiting. Various combinations of plant extracts were tested in this study and one combination (No 4) was found to be synergistic and provided very nice remission of vomiting response (Table 1).

In continuation, the protection observed for *CS*-HexFr 10 mg alone was ~62.2% (Current study) and 55.45% in our previous published work [48] while for *BM*-ButFr 5 mg the protection observed was 71.1% (Current study) and 68.08% protection in our previous study [65]. Combination 2 was also found to be effective though less significant ($P < 0.01$) to combination 4 (Table 1).

In the current study, treatments with combination 4 do not changed basal neurotransmitters level and their metabolites any significantly. Furthermore, the decrease in the concentration of 5HIAA by MCP (30 mg) and combination 4 was observed at the brain stem (Table 2). The combination of *CS*-HexFr (10 mg) with *BM*-ButFr (5 mg) reduced 5HT and 5HIAA in the brain areas (AP and BS) and intestine (Table 3, $P < 0.05 - 0.001$). These findings are supportive for the antiemetic activity of Combination 4 for the 3rd hour (at the acute vomiting response). Similar effect was also observed by metoclopramide. Combination of *CS*-HexFr 10 mg with *BM*-ButFr 5 mg suppressed the dopamine concentration in the brain area of AP as compared to cisplatin control while no significant dopaminergic suppression was seen in the BS and intestine (Table 4) at 18th hour of cisplatin treatment. In continuation, Combination 4 (CS-HexFr 10 mg + *BM*-ButFr 5 mg) significantly ($P < 0.001$) reduced 5HT concentration at the level of BS and intestine (Table 4). The standard MCP (30 mg) also presented almost the same picture of neurotransmitter suppression in the brain area of AP, BS, and intestine. The antiserotonergic along with antidopaminergic effects noted of combination 4 in the current study is supporting the synergistic and prolongs protection provided against the vomiting induced by cisplatin in pigeons as compared to metoclopramide (Table 1).

5. Conclusions

In conclusion, the combination 4 provided a synergistic protection and our neurotransmitter quantification supports the involvement of antiserotonergic and antidopaminergic effects in an overlapping mode at the two different time points. At the acute time point (3rd hour), dominantly the antiserotonergic effects were observed. Moreover, antidopaminergic and antiserotonergic effects were observed at the 18th of cisplatin administration. These neurochemical findings advocate the promising antiemetic effect of combination 4 against cisplatin induced vomiting in pigeon. The combination may be useful alone or as adjunct in the management of cisplatin induced vomiting in clinics as *cannabis* preparations (Nabilone etc.) and preparations of *bacopa* (Bacomind®) are already available in the market and have safety and tolerability profile.

Abbreviations

CS: *Cannabis sativa*
BM: *Bacopa monniera*
ZO: *Zingiber officinale*
HPLC: High performance liquid chromatography
ECD: Electrochemical detector
5HT: 5-Hydroxy tryptamine
DA: Dopamine
HVA: Homovanillic acid
Dopac: Dihydroxy phenyl acetic acid
5HIAA: 5 Hydroxy indole acetic acid
CS-HexFr: *Cannabis sativa* (hexane fraction)
ZO-ActFr: *Zingiber officinale* (acetone fraction)
BM-ButFr: *Bacopa monniera* butanolic fraction
AP: Area Postrema
BS: Brain stem
HEC: Highly emetogenic chemotherapy
5HT3: 5 hydroxy tryptamine type 3
NK1: Neurokinin type 1
CIV: Chemotherapy induced vomiting
THC: Tetrahydrocannabinol
MCP: Metoclopramide
R+V: Retching+vomiting.

Data Availability

Data presented in the current manuscript belongs to the PhD work of Dr Ihsan Ullah and is not published anywhere. Data is available to researchers upon request.

Ethical Approval

All the experimental procedures were approved by the Ethical committee, Department of Pharmacy, University of Peshawar (Ref. No 5/pharm) and are in accordance with the animal scientific procedure ACT, 1986 (United Kingdom).

Conflicts of Interest

The authors declare to have no conflict of interest.

Authors' Contributions

Ihsan Ullah (IU) is responsible for the data creation, analysis, and manuscript writing. Fazal Subhan (FS) is responsible for the project design, supervision, and data analysis. Muhammad Shahid (MS) is responsible for the data analysis and manuscript writing. Nisar Ahmad (NA) is responsible for the data analysis and for revising manuscript draft. Rehmat Shah (RS) is responsible for the manuscript write up and revision. Javaid Alam (JA) is responsible for the data creation, project design, and manuscript write up. Ikram Ul Haq (IUH) is responsible for the project design, analysis, and manuscript write up. Rahim Ullah (RU) is responsible for the manuscript write up, and Muhammad Ayaz (MA) and Hanabe Chowdappa Ananda Murthy (HCAM) is responsible for the manuscript write up, data analysis, and revision of the manuscript draft. Dr. Ihsan Ullah, PhD scholar at the Department of Pharmacy, University of Peshawar conducted the research work there.

Acknowledgments

Authors are grateful to Department of Pharmacy, University of Peshawar for providing laboratory facilities to conduct the research.

References

[1] R. Navari, "Management of chemotherapy-induced nausea and vomiting," *Drugs*, vol. 73, no. 3, pp. 249–262, 2013.

[2] A. T. Khalil, M. Ovais, J. Iqbal et al., "Microbes-mediated synthesis strategies of metal nanoparticles and their potential role

in cancer therapeutics," in *Seminars in cancer biology*, Academic Press, 2021.

[3] D. M. Parkin, "Global cancer statistics in the year 2000," *The Lancet Oncology*, vol. 2, no. 9, pp. 533–543, 2001.

[4] M. H. Mahnashi, Y. S. Alqahtani, B. A. Alyami et al., "Phytochemical analysis, α-glucosidase and amylase inhibitory, and molecular docking studies on Persicaria hydropiper L. Leaves essential oils," *Leaves Essential Oils. Evidence-Based Complementary and Alternative Medicine*, vol. 2022, article 7924171, 11 pages, 2022.

[5] C. Patra, I. Ahmad, M. Ayaz, A. T. Khalil, S. Mukherjee, and M. Ovais, *Biogenic Nanoparticles for Cancer Theranostics*, Elsevier, 1st edition, 2021.

[6] G. Higgins, G. Kilpatrick, K. Bunce, B. Jones, and M. Tyers, "$5HT_3$ receptor antagonists injected into the area postrema inhibit cisplatin induced emesis in the ferret," *British Journal of Pharmacology*, vol. 97, no. 1, pp. 247–255, 1989.

[7] L. Grélot, J. Dapzol, E. Estève et al., "Potent inhibition of both the acute and delayed emetic responses to cisplatin in piglets treated with GR205171, a novel highly selective tachykinin NK_1 receptor antagonist," *British Journal of Pharmacology*, vol. 124, no. 8, pp. 1643–1650, 1998.

[8] M. Markman, "Progress in preventing chemotherapy-induced nausea and vomiting," *Cleveland Clinic Journal of Medicine*, vol. 69, no. 8, pp. 609-610, 2002.

[9] D. G. Pfister, D. H. Johnson, C. G. Azzoli et al., "American society of clinical oncology treatment of unresectable non–small-cell lung cancer guideline: update 2003," *Journal of Clinical Oncology*, vol. 22, no. 2, pp. 330–353, 2004.

[10] M. Ovais, M. Z. Hoque, A. T. Khalil, M. Ayaz, and I. Ahmad, "Mechanisms underlying the anticancer applications of biosynthesized nanoparticles," in *Biogenic Nanoparticles for Cancer Theranostics*, pp. 229–248, Elsevier, 2021.

[11] N. T. Mir, U. Saleem, F. Anwar et al., "Lawsonia inermis markedly improves cognitive functions in animal models and modulate oxidative stress markers in the brain," *Medicina*, vol. 55, no. 5, p. 192, 2019.

[12] M. H. Mahnashi, Y. S. Alqahtani, B. A. Alyami et al., "Cytotoxicity, anti-angiogenic, anti-tumor and molecular docking studies on phytochemicals isolated from Polygonum hydropiper L," *BMC Complementary Medicine and Therapies*, vol. 21, no. 1, pp. 1–14, 2021.

[13] A. Sani, D. Hassan, A. T. Khalil et al., "Floral extracts-mediated green synthesis of NiO nanoparticles and their diverse pharmacological evaluations," *Journal of Biomolecular Structure and Dynamics*, vol. 39, no. 11, pp. 4133–4147, 2021.

[14] M. F. Akhtar, M. O. Mehal, A. Saleem et al., "Attenuating effect of Prosopis cineraria against paraquat-induced toxicity in prepubertal mice, Mus musculus," *Environmental Science and Pollution Research*, vol. 29, no. 10, pp. 15215–15231, 2022.

[15] M. Ayaz, A. Nawaz, F. Naz, F. Ullah, A. Sadiq, and Z. U. Islam, "Phytochemicals-based therapeutics against Alzheimer's disease: an update," *Current Topics in Medicinal Chemistry*, vol. 27, 2022.

[16] D. J. Newman, G. M. Cragg, and K. M. Snader, "The influence of natural products upon drug discovery," *Natural Product Reports*, vol. 17, no. 3, pp. 215–234, 2000.

[17] M. S. Butler, "The role of natural product chemistry in drug discovery," *Journal of Natural Products*, vol. 67, no. 12, pp. 2141–2153, 2004.

[18] T. Zohra, A. T. Khalil, F. Saeed et al., "Green nano-biotechnology: a new sustainable paradigm to control dengue infection," *Bioinorganic Chemistry and Applications*, vol. 2022, Article ID 3994340, 21 pages, 2022.

[19] M. Q. Nasar, M. Shah, A. T. Khalil et al., "Ephedra intermedia mediated synthesis of biogenic silver nanoparticles and their antimicrobial, cytotoxic and hemocompatability evaluations," *Inorganic Chemistry Communications*, vol. 137, article 109252, 2022.

[20] M. Ayaz, F. Subhan, A. Sadiq, F. Ullah, J. Ahmed, and R. D. E. Sewell, "Cellular efflux transporters and the potential role of natural products in combating efflux mediated drug resistance," *Frontiers in Bioscience*, vol. 22, no. 4, pp. 732–756, 2017.

[21] S. Ahmad, F. Ullah, M. Ayaz, A. Ahmad, A. Sadiq, and S. N.-U.-H. Mohani, "Nutritional and medicinal aspects of Rumex hastatus D. Don along within vitroanti-diabetic activity," *International Journal of Food Properties*, vol. 22, no. 1, pp. 1733–1748, 2019.

[22] A. T. Khalil, M. D. Khan, S. Razzaque et al., "Single precursor-based synthesis of transition metal sulfide nanoparticles and evaluation of their antimicrobial, antioxidant and cytotoxic potentials," *Applied Nanoscience*, vol. 11, no. 9, pp. 2489–2502, 2021.

[23] M. Ayaz, A. Nawaz, S. Ahmad et al., "Underlying anticancer mechanisms and synergistic combinations of phytochemicals with cancer chemotherapeutics: potential benefits and risks," *Journal of Food Quality*, vol. 2022, Article ID 1189034, 15 pages, 2022.

[24] M. Mukim, A. Kabra, C. Hano et al., "Rivea hypocrateriformis (desr.) choisy: an overview of its ethnomedicinal uses, phytochemistry, and biological activities and prospective research directions," *Journal of Chemistry*, vol. 2022, Article ID 9099672, 11 pages, 2022.

[25] F. A. Khan, G. Ali, K. Rahman et al., "Efficacy of 2-Hydroxyflavanone in rodent models of pain and inflammation: involvement of opioidergic and GABAergic antinociceptive mechanisms," *Molecules*, vol. 27, no. 17, p. 5431, 2022.

[26] M. Ayaz, M. Junaid, F. Ullah et al., "GC-MS analysis and gastroprotective evaluations of crude extracts, isolated saponins, and essential oil from Polygonum hydropiper L," *Frontiers in Chemistry*, vol. 5, p. 58, 2017.

[27] M. Ovais, M. Ayaz, A. T. Khalil et al., "HPLC-DAD finger printing, antioxidant, cholinesterase, and α-glucosidase inhibitory potentials of a novel plant Olax nana," *BMC Complementary and Alternative Medicine*, vol. 18, no. 1, pp. 1–13, 2018.

[28] T. Zohra, M. Ovais, A. T. Khalil et al., "Bio-guided profiling and HPLC-DAD finger printing of Atriplex lasiantha Boiss," *BMC Complementary and Alternative Medicine*, vol. 19, no. 1, pp. 1–14, 2019.

[29] A. Zeb, "A reversed phase HPLC-DAD method for the determination of phenolic compounds in plant leaves," *Analytical Methods*, vol. 7, no. 18, pp. 7753–7757, 2015.

[30] M. S. Islam, A. M. Al-Majid, E. N. Sholkamy et al., "Synthesis, molecular docking and enzyme inhibitory approaches of some new chalcones engrafted pyrazole as potential antialzheimer, antidiabetic and antioxidant agents," *Journal of Molecular Structure*, vol. 1269, article 133843, 2022.

[31] M. Ware, P. Daeninck, and V. Maida, "A review of nabilone in the treatment of chemotherapy-induced nausea and vomiting," *Therapeutics and Clinical Risk Management*, vol. 4, no. 1, pp. 99–107, 2008.

[32] P. Stark, "The pharmacologic profile of nabilone: a new anti-emetic agent," *Cancer Treatment Reviews*, vol. 9, pp. 11–16, 1982.

[33] E. Russo, "Journal of Cannabis Therapeutics: An Editorial Introduction," *Journal of Cannabis Therapeutics*, vol. 1, no. 1, pp. 1–4, 2001.

[34] R. Abalo, P. Cabezos, G. Vera, V. López-miranda, E. Herradón, and M. I. Martín-fontelles, "Cannabinoid-induced delayed gastric emptying is selectively increased upon intermittent administration in the rat: role of CB_1 receptors," *Neurogastroenterology & Motility*, vol. 23, no. 5, p. 457, 2011.

[35] M. D. Van Sickle, L. D. Oland, K. Mackie, J. S. Davison, and K. A. Sharkey, "*Δ*9-tetrahydrocannabinol selectively acts on CB1receptors in specific regions of dorsal vagal complex to inhibit emesis in ferrets," *American Journal of Physiology-Gastrointestinal and Liver Physiology*, vol. 285, no. 3, pp. G566–G576, 2003.

[36] V. E. Tyler, L. R. Brady, and J. E. Robbers, *Phrmacognosy*, Lea and Febiger, Philadelphia, 9th edition, 1988.

[37] H. Abdel-Aziz, T. Windeck, M. Ploch, and E. J. Verspohl, "Mode of action of gingerols and shogaols on 5-HT_3 receptors: binding studies, cation uptake by the receptor channel and contraction of isolated guinea-pig ileum," *European Journal of Pharmacology*, vol. 530, no. 1-2, pp. 136–143, 2006.

[38] S. Sharma, V. Kochupillai, S. Gupta, S. Seth, and Y. Gupta, "Antiemetic efficacy of ginger (Zingiber officinale) against cisplatin- induced emesis in dogs," *Journal of Ethnopharmacology*, vol. 57, no. 2, pp. 93–96, 1997.

[39] J. Yamahara, H. Q. Rong, M. Iwamoto, G. Kobayashi, H. Matsuda, and H. Fujimura, "Active components of ginger exhibiting anti-serotonergic action," *Phytotherapy Research*, vol. 3, no. 2, pp. 70-71, 1989.

[40] N. Limpeanchob, S. Jaipan, S. Rattanakaruna, W. Phrompittayarat, and K. Ingkaninan, "Neuroprotective effect of Bacopa monnieri on beta-amyloid-induced cell death in primary cortical culture," *Journal of Ethnopharmacology*, vol. 120, no. 1, pp. 112–117, 2008.

[41] C. Calabrese, W. Gregory, M. Leo, D. Kraemer, K. Bone, and B. Oken, "Effects of a standardized Bacopa monnieri extract on cognitive performance, anxiety, and depression in the elderly: a randomized, double-blind, placebo-controlled trial," *The Journal of Alternative and Complementary Medicine*, vol. 14, no. 6, pp. 707–713, 2008.

[42] W. Phrompittayarat, W. Putalun, H. Tanaka, K. Jetiyanon, S. Wittaya-areekul, and K. Ingkaninan, "Comparison of various extraction methods of Bacopa monnieri," *Naresuan University Journal: Science and Technology (NUJST)*, vol. 15, no. 1, pp. 29–34, 2007.

[43] K. Rauf, F. Subhan, and R. D. E. Sewell, "A bacoside containing Bacopa monnieri extract reduces both morphine hyperactivity plus the elevated striatal dopamine and serotonin turnover," *Phytotherapy Research*, vol. 26, no. 5, pp. 758–763, 2011.

[44] A. Kahol, T. Singh, S. Tandon, M. Gupta, and S. Khanuja, "Process for the preparation of a extract rich in bacosides from the herb Bacopa monniera," 2004, U.S. Patent No. 6,833,143.

[45] I. Ullah, F. Subhan, Z. Lu, S. W. Chan, and J. A. Rudd, "Action of _Bacopa monnieri_ to antagonize cisplatin-induced emesis in _Suncus murinus_ (house musk shrew)," *Journal of Pharmacological Sciences*, vol. 133, no. 4, pp. 232–239, 2017.

[46] N. Doorenbos, P. Fetterman, M. Quimby, and C. Turner, "Cultivation, extraction, and analysis of Cannabis sativa L," *Annals of the New York Academy of Sciences*, vol. 191, no. 1, pp. 3–14, 1971.

[47] I. Ullah, F. Subhan, J. Alam, M. Shahid, and M. Ayaz, "Suppression of cisplatin-induced vomiting by Cannabis sativa in pigeons: neurochemical evidences," *Frontiers in Pharmacology*, vol. 9, p. 231, 2018.

[48] I. Ullah, F. Subhan, K. Rauf, A. Badshah, and G. Ali, "Role of gastrointestinal motility/gastric emptying in cisplatin-induced vomiting in pigeon," *African Journal of Pharmacy and Pharmacology*, vol. 6, no. 35, pp. 2592–2599, 2012.

[49] I. Ullah, F. Subhan, M. Ayaz et al., "Anti-emetic mechanisms of Zingiber officinale against cisplatin induced emesis in the pigeon; behavioral and neurochemical correlates," *BMC Complementary and Alternative Medicine*, vol. 15, no. 1, pp. 34–42, 2015.

[50] J. Feigenbaum, S. Richmond, Y. Weissman, and R. Mechoulam, "Inhibition of cisplatin-induced emesis in the pigeon by a non-psychotropic synthetic cannabinoid," *European Journal of Pharmacology*, vol. 169, no. 1, pp. 159–165, 1989.

[51] I. Ullah, *Evaluation of some selected medicinal plants and their combinations in cisplatin induced vomiting in vomit model (s); behavioral neurochemical correlates*, (Dissertation), University of Peshawar, 2013.

[52] S. Tanihata, H. Igarashi, M. Suzuki, and T. Uchiyama, "Cisplatin-induced early and delayed emesis in the pigeon," *British Journal of Pharmacology*, vol. 130, no. 1, pp. 132–138, 2000.

[53] P. Preziosi, M. D'Amato, R. Del Carmine, M. Martire, G. Pozzoli, and P. Navarra, "The effects of 5-HT3 receptor antagonists on cisplatin-induced emesis in the pigeon," *European Journal of Pharmacology*, vol. 221, no. 2-3, pp. 343–350, 1992.

[54] H. J. Karten and W. Hodos, *A stereotaxic atlas of the brain of the pigeon: (Columba Livia), vol. 696*, Johns Hopkins University Press Baltimore, MD, 1967.

[55] H. M. Duvernoy and P.-Y. Risold, "The circumventricular organs: an atlas of comparative anatomy and vascularization," *Brain Research Reviews*, vol. 56, no. 1, pp. 119–147, 2007.

[56] K. Rauf, F. Subhan, G. Ali, and M. Ayaz, "Effect of acute and sub chronic use of Bacopa monnieri on dopamine and serotonin turnover in mice whole brain Khalid Rauf1," *African Journal of Pharmacy and Pharmacology*, vol. 6, no. 39, pp. 2767–2774, 2012.

[57] L. Limpel, P. Schuldt, and D. Lamont, "Weed control by dimethyl tetrachloroterephthalate alone and in certain combinations," *In: Proceedings of 27th Northeast Weed Control Conference*, vol. 16, pp. 48–53, 1962.

[58] R. Mechoulam and J. Feigenbaum, "5 towards cannabinoid drugs," *Progress in Medicinal Chemistry*, vol. 24, pp. 159–207, 1987.

[59] S. Sallan, N. Zinberg, and E. Frei, "Antiemetic effect of delta-9-tetrahydrocannabinol in patients receiving cancer chemotherapy," *New England Journal of Medicine*, vol. 293, no. 16, pp. 795–797, 1975.

[60] N. Darmani, "Δ^9-tetrahydrocannabinol and synthetic cannabinoids prevent emesis produced by the cannabinoid CB_1 receptor antagonist/inverse agonist SR 141716A," *Neuropsychopharmacology*, vol. 24, no. 2, pp. 198–203, 2001.

[61] N. Darmani, J. Janoyan, N. Kumar, and J. Crim, "Behaviorally active doses of the CB1 receptor antagonist SR 141716A increase brain serotonin and dopamine levels and turnover," *Pharmacology Biochemistry and Behavior*, vol. 75, no. 4, p. 777, 2003.

[62] R. Qureshi and G. Raza Bhatti, "Ethnobotany of plants used by the Thari people of Nara Desert, Pakistan," *Fitoterapia*, vol. 79, no. 6, pp. 468–473, 2008.

[63] S. Bhattacharya, A. Bhattacharya, A. Kumar, and S. Ghosal, "Antioxidant activity of Bacopa monniera in rat frontal cortex, striatum and hippocampus," *Phytotherapy Research*, vol. 14, no. 3, pp. 174–179, 2000.

[64] K. Balakrishna, G. Veluchamy, S. N. Devaraj, and T. Sumathi, "Inhibitory effect of Bacopa monniera on morphine induced pharmacological effects in mice," *Natural Product Sciences*, vol. 13, no. 1, pp. 46–53, 2007.

[65] I. Ullah, F. Subhan, J. A. Rudd et al., "Attenuation of cisplatin-induced emetogenesis by standardized Bacopa monnieri extracts in the pigeon: behavioral and neurochemical correlations," *Planta Medica*, vol. 80, no. 17, pp. 1569–1579, 2014.

[66] S. Rai, K. Mukherjee, M. Mal, A. Wahile, B. P. Saha, and P. K. Mukherjee, "Determination of 6-gingerol in ginger (Zingiber officinale) using high-performance thin-layer chromatography," *Journal of Separation Science*, vol. 29, no. 15, pp. 2292–2295, 2006.

[67] E. Ernst and M. Pittler, "Efficacy of ginger for nausea and vomiting: a systematic review of randomized clinical trials," *British Journal of Anaesthesia*, vol. 84, no. 3, pp. 367–371, 2000.

[68] Q. Qiu-hai, Y. Wang, C. Wen-hui, Y. Zhi-hong, L. Zhan-tao, and W. Yao-xia, "Effect of gingerol on substance P and NK_1 receptor expression in a vomiting model of mink," *Chinese Medical Journal*, vol. 123, no. 4, pp. 478–484, 2010.

[69] M. H. Al-Zubaidy and F. K. Mohammad, "Metoclopramide-induced central nervous system depression in the chicken," *BMC Veterinary Research*, vol. 1, no. 1, pp. 2–6, 2005.

[70] R. Coronas, L. Pitarch, and J. Mallol, "Blockade of reserpine emesis in pigeons by metoclopramide," *European Journal of Pharmacology*, vol. 32, no. 2, pp. 380–382, 1975.

Hindawi
Oxidative Medicine and Cellular Longevity
Volume 2022, Article ID 7627759, 10 pages
https://doi.org/10.1155/2022/7627759

Research Article

Evaluation of Sodium Alginate Stabilized Nanoparticles and Antibiotics against Drug Resistant *Escherichia coli* Isolated from Gut of Houbara Bustard Bird

Afshan Muneer,[1] Santosh Kumar,[1] Amjad Islam Aqib,[2] Shanza Rauf Khan,[3] Syed Qaswar Ali Shah,[1] Iqra Zaheer,[4] Tauseef ur Rehman,[5] Asghar Abbas,[6] Kashif Hussain,[6] Atif Rehman,[6] Muhammad Nadeem,[7] Maheen Murtaza,[1] and Ahmad Waseem[8]

[1]*Department of Zoology, Cholistan University of Veterinary and Animal Sciences, Bahawalpur 63100, Pakistan*
[2]*Department of Medicine, Cholistan University of Veterinary and Animal Sciences, Bahawalpur 63100, Pakistan*
[3]*Department of Chemistry, University of Agriculture Faisalabad, 38000, Pakistan*
[4]*Department of Pathology, University of Agriculture Faisalabad, 38000, Pakistan*
[5]*Department of Parasitology, The Islamia University of Bahawalpur, Pakistan*
[6]*Faculty of Veterinary and Animal Sciences, Muhammad Nawaz Sharif University of Agriculture, Multan, Pakistan*
[7]*Department of Pathology, PMAS-Arid Agriculture University Rawalpindi Sub Campus Khushab, Pakistan*
[8]*Houbara Foundation International, Lal Sohanra Park, Bahawalpur 63100, Pakistan*

Correspondence should be addressed to Amjad Islam Aqib; amjadislamaqib@cuvas.edu.pk

Received 17 June 2022; Revised 12 August 2022; Accepted 27 August 2022; Published 12 September 2022

Academic Editor: Muhammad Saleem Kalhoro

Alternative approaches and/or modified approaches to tackle resistance in gut microbes are need of the hour. The current study was planned to find the resistance modulation and toxicity potential of sodium alginate stabilized MgO nanoparticles and antibiotics against *Escherichia coli* (*E. coli*) isolated from the gut of Houbara bustard bird ($n = 105$ fecal samples). The preparations consisted of gel stabilized ampicillin (G+A), gel stabilized MgO and ampicillin (G+M+A), gel stabilized MgO and cefoxitin (G+M+C), gel stabilized tylosin (G+T), gel stabilized MgO and tylosin (G+M+T), and gel stabilized MgO (M+G). The fecal samples showed 53% (56/105) prevalence of *E. coli* which was found to be significantly ($p < 0.05$) associated with most of the assumed factors and resistant to multiple drugs. G+M+T showed the lowest (4.883 ± 0.00 μg/mL) minimum inhibitory concentration (MIC) followed G+M+C, G+M+A, G+A, M+G, and G+T. Significant reduction ($p < 0.05$) in MIC with respect to incubation interval found at the 16th hr for G+M+A, G+A, and G+M+C that further remained nonsignificant ($p > 0.05$) onwards until the 24th hr of incubation. In the case of G+T and M+G, significant reduction in MIC was found at the 20th hr and 24th hr of incubation. Ecotoxicology and histopathology trials on snails showed mild changes in MICs of the preparations. The study thus concluded increasing drug resistance in *E. coli* of houbara bird while sodium alginate stabilized MgO nanoparticles and antibiotics were effective alternative antibacterial composites with mild toxicity.

1. Introduction

Escherichia coli is the main bacteria carried by migratory birds which exist as infectious microorganisms in the intestine of avian species [1]. These bacteria are equally becoming major pathogens same as Salmonella from poultry [2]. Infectious *E. coli* can cause wider range of diseases in calves [3] and deterioration of products like meat [4] in addition to intestinal disorders. Migratory birds on the other hand have a big impact on the spread of antibiotic-resistant bacteria and ARGs (antibiotic resistance genes) [5]. Among several other factors that contribute to the antibiotic resistance are the continued and improper antimicrobial use of the drugs [6] giving rise to multiple drug resistance in *E.coli* which

has also been reported in migratory birds worldwide [7]. The Houbara bustard (*Chlamydotis undulate*) or Tiloor (local name in Pakistan) is one of these migratory birds which are considered threatened species red listed by IUCN (International Union for Conservation of Nature) at risk [8]. Population of Houbara bustard ranged between 78960 and 97000 in the year 2014 whereas there are reports in its declining population at the rate of 30-49% [9].

Alternative approaches to tackle pathogens include, however are not limited to conventional plants [10], nanoparticles, peptides, prebiotics, and probiotics. Control of gut microbes and improved health are achievable milestones for better health and production of birds [11] and nanoparticles. Currently, nanotechnology plays an important role in advances in medicine and pharmaceuticals [12]. In addition to higher reactivity, greater surface-to-volume ratios, stability, bioactivity, bioavailability, controlled particle sizes, and controlled release of drugs make these particles unique in physicochemical properties [13]. The combination of nanoparticles with antibiotics, antimicrobial peptides, and essential oils has shown to reduce possible toxic effects of nanoparticles on mammalian cells in recent studies [14, 15].

It is however important to find modified approaches to enhance antibacterial activity with minimized toxicity. Stabilization of preparations is one of the appreciable approaches for an extended period. Sodium alginate gel has many uses in biomedical sciences as an excipient of drug delivery systems, tissue engineering, preservative in food products, and nanomedicines in various forms [16]. The gel itself has shown antibacterial potential in various previous studies while its uses also have been found beneficial in various wound dressings to avoid secondary bacterial infection [17]. In nanomedicines, the gel has been used as dendrimers, emulsions, lipids, nanocrystals, nanoparticles, polymeric nanoparticles, and micelles [18]. The biodegradability and biocompatibility along with very mild toxicity make its application in broader phases of various industries. Thus, there is a dire need to enhance the activity of antibiotics and non-antibiotic alternatives with reduced dosage and negligible toxicity [19]. This study focused on the evaluation of antibacterial activity of MgO nanoparticles and antibiotics stabilized in sodium alginate gel along with investigation of toxicity parameters.

2. Materials and Methodology

2.1. Preparation of Sodium Alginate Stabilized MgO Nanoparticles and Antibiotics. A hydrothermal method was used to synthesize MgO nanoparticles in the presence of a surfactant. $MgCL_2.6H_2O$ (4 grams) was dissolved in 40 mL of distilled water which was further kept at constant magnetic stirring for 4 hrs at room temperature. Sodium dodecyl sulphate (4 g) was further added in $MgCl_2$ solution. It was required to maintain 12 pH which was executed by adding 20 mL of 2.5 M NaOH drop by drop to the reaction mixture [20]. After stirring (4 hrs), the white suspension was obtained which was further heated for 6 hrs at 140°C. The white precipitate was washed and centrifuged and subsequently dried for 24 hours at 60°C in a thermoelectric oven. The ground precipitates obtained were further calcined at 450°C/3 hrs [21]. A 2% (m/v) Na-alginate solution and 2% (m/v) gelatin solutions were prepared in water. Both solutions were mixed in 80 : 20 ratio (sodium alginate: gelatin) at 500 rpm for 2 hrs by using a mechanical stirrer to yield sodium alginate gel (abbreviated in the manuscript as G). To stabilize MgO within gel, 1.5 g of MgO nanoparticles were incorporated in 20 mL of gel and stirred for 4 hrs at 500 rpm. The drug (0.035 grams) was dissolved in distilled water to finally prepare a 20 mL solution. A mixture of 20 mL of gel (sodium alginate) and 20 mL of ampicillin solution was mixed and stirred at 500 rpm for 4 hrs. The mixture was stirred at 500 rpm for 4 hrs which was then dried and ground.

Energy Dispersive X-ray Spectroscopy (EDX) of nanoparticles was carried out. A 30 kV Quanta 250 was operated to find SEM (Scanning electron microscopy) images for MgO nanoparticles. The composites were formulated in powder form and were checked through instruments as final judgment. The products finally prepared were M + G = MgO stabilized in gel, G + M + T = MgO and tylosin stabilized in gel, G + M + C = MgO and cefoxitin both stabilized in gel, G + M + A = MgO and ampicillin stabilized in gel, G + T = tylosin stabilized in gel, G + A = ampicillin stabilized in the gel.

2.2. Toxicity of Sodium Alginate Stabilized Nanoparticles and Antibiotics. For toxicity evaluation, $n = 65$ healthy and active land snails were taken from a garden where chemicals and pesticides were not used previously. There were 07 groups of snails including the control negative group. Each treatment group was further divided into two groups: (1) Group receiving dose at 1 × MIC and (2) Group receiving 10 × MIC . Each group was having $n = 05$ snails allocated on random basis (Table 1). A 50 μL of the solution was poured on the anterior side of the snail's mouth portion. Snails were kept off feed for 05 days and dead were immediately processed for histopathology [20].

2.3. Histopathology. The snails were dissected while digestive glands were collected in Bouin's fluid until further used. After deparaffinizing of the fixed sections, the 5 mm thick sections were hydrated and stained in hematoxylin for 15 minutes. It was counter stained with a 1% Eosin solution for two minutes after washing with water. Dehydration was accomplished with alcohol, which was then cleaned in xylene before being mounted on clean microscope glass with Canada balsam and lastly covered with thin cover slides Cell disintegration, unusual nuclei ranging from karyolysis to severe karyorrhexis, full pyknosis, abundant vacuolation, and frequent dark granulation were considered main pathological alterations [22].

2.4. Gut (Fecal) Sample Collection. To carry out sampling from the bird, prior consent was taken from the Houbara International Foundation Lal Suhanra Park, Bahwalpur, Pakistan while ethical consideration was observed as per standard protocols. A total of $n = 105$ fecal samples from cloaca were aseptically collected ($n = 70$ male, $n = 35$ female)

Table 1: Mortality percentages in snails at various concentrations of preparations.

Product name	Concentration used 1 × MIC (M1) (μg/mL)	10 × MIC (M2) (μg/mL)	Mortality at 1 × MIC (M1)	Mortality at 10 × MIC (M2)	% Difference in mortality % (M2-M1)
G+M+A	13.02	130.2	(2/5) 40%	(2/5) 40%	0
G+A	13.02	130.2	(2/5) 40%	(3/5) 60%	20
G+T	26.04	260.4	(3/5) 60%	(4/5) 80%	20
G+M+C	6.51	65.1	(2/5) 40%	(2/5) 40%	0
G+M+T	4.883	48.83	(1/5) 20%	(1/5) 20%	0
M+G	16.28	162.8	(2/5) 40%	(3/5) 60%	20
Control negative	Placebo		(1/5) 20%		

MIC: Minimum inhibitory concentration; values in brackets shows ratio of died from total tested, M1: mortality at 1 × MIC concentration, M2: mortality at 10 × MIC, M + G = MgO stabilized in gel, G + M + T = MgO and tylosin both stabilized in gel, G + M + C = MgO and cefoxitin both stabilized in gel, G + M + A = MgO and ampicillin both stabilized in gel, G + T = tylosin stabilized in gel, G + A = ampicillin stabilized in gel.

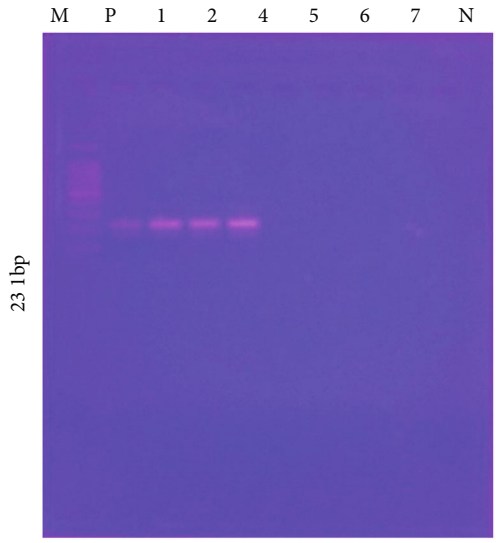

Figure 1: Agarose gel picture of amplicons of polymerase chain reaction used for identification of *E. coli* isolated from cloaca of the Houbara bustard. M: marker 1000 bp, wells 1–7 sample at 231 bp, +ve: positive control, −ve: negative control.

at different time intervals [23]. A sterile cotton swab moistened with normal saline was inserted into the cloacae of the Houbara bustard bird. Once the cloaca swabs were collected, the birds were released [24]. The samples were immediately shifted to the laboratory of Houbara Foundation International, Lal Suhanra Park, Bahawalpur, Pakistan which was situated at a few yards from the sampling area. The samples were preserved in an ice box maintaining 4°C which were finally shifted to the Central Diagnostic Laboratory (CDL), Cholistan University of Veterinary and Animal Sciences, Bahawalpur. A questionnaire was also filled in with necessary information about bird and its housing to analyze the association of assumed risk factors with prevalence of *E. coli*.

2.5. Isolation of E. Coli. Fecal samples were incubated in sterile nutrient broth overnight at 37°C. The incubated samples were homogenized on a stirrer, and sterile swabs were dipped in homogenized material. These swabs were gently spread on blood agar and incubated at 37°C/24 hrs. The colonies obtained were further streaked on MacConkey agar and incubated for 24 hrs at 37°C. A series of biochemical tests were performed to identify *E.coli* [25] following standard protocols described in Bergey's Manual of determinative bacteriology.

2.6. Molecular Identification of E. Coli. The isolates identified by biochemical methods were also subjected to molecular confirmation using PCR. The specific primers for 23S rRNA gene of 231 bp (E23S-F: ATCAACCGATTCCCCAGT; E23S-R: TCACTATCGGTCAGTCAGGAG) were used in PCR to target *E. coli* from biochemically identified bacterial cultures. During the temperature cycling, a short period of 95°C was set for 3 minutes, followed by a longer period of 95°C for 1 minute for 335 cycles, followed by a final extension stage of 72°C for 7 minutes. The amplicons were run on 2% agarose gel kept at 100 volts for 1 hr through electrophoresis equipment, and finally the gel was visualized in UV light [26] (Figure 1).

2.7. Antibiotic Susceptibility of E. Coli. A total of $n = 10$ antibiotics (enrofloxacin, fusidic acid, ciprofloxacin, sulfamethoxazole-trimethoprim, levofloxacin, chloramphenicol, vancomycin, gentamicin, linezolid, and cefoxitin) were tested against *E. coli* to find the status of its susceptibility. Kirby Bauer disc diffusion method was applied following guidelines of the Clinical and Laboratory Standard Institute (CLSI). Briefly, fresh growth of *E. coli* adjusted at $1 - 1.5 \times 10^8$ CFU/mL was spread over sterile Mueller Hinton agar. The antibiotic discs were aseptically and gently punched at equal distances from each other. Following incubation at 37°C for 20-24 hrs, zones of inhibitions were measured and compared with standards provided in CLSI, [27].

2.8. In Vitro Antibacterial Activity of Sodium Alginate Stabilized Products. To assess the potential of sodium alginate stabilized products, well diffusion method was applied as an empirical method for estimation of antibacterial activity. The broth microdilution method was applied to find a minimum inhibitory concentration (MIC) of different preparations.

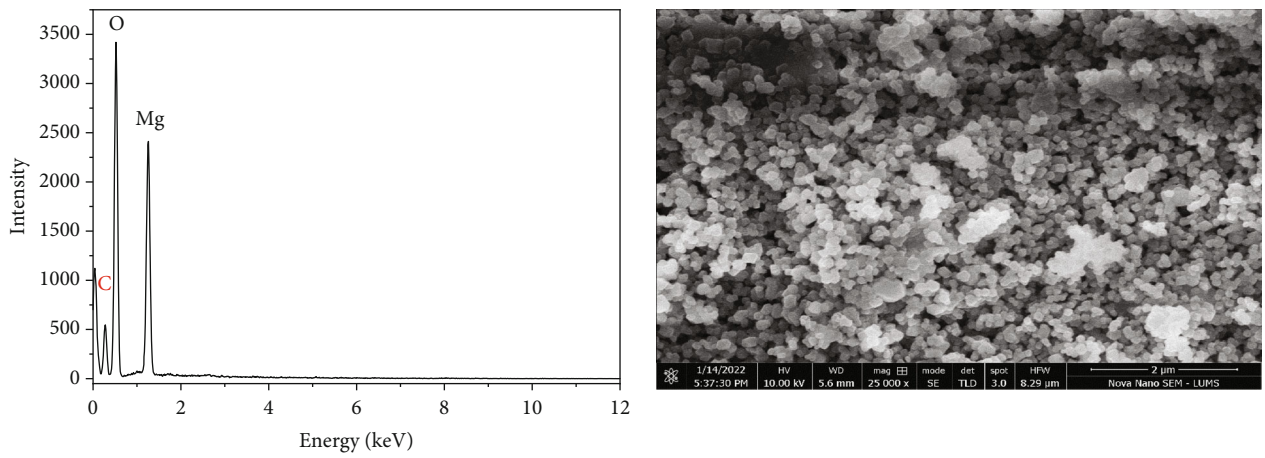

Figure 2: Characterization of MgO nanoparticles: (a) SEM images of MgO nanoparticles synthesized by the hydrothermal method and (b) XRD pattern of synthesis of MgO nanoparticles.

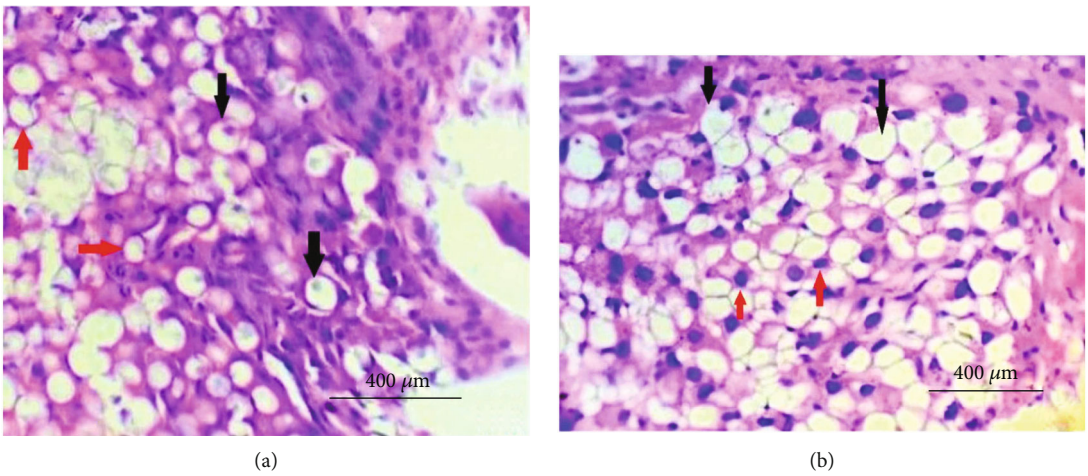

Figure 3: Microscopic lesions produced by sodium alginate stabilized composites in digestive glands of snail (stained by H&E staining method). (a) Treatment level 4.883-26.04 μg/mL of sodium alginate stabilized nanoparticles and antibiotics (at 400 X): shows vacuolar degeneration of digestive gland cells marked by the marginal nucleus (red arrows) while there are some normal cells presented with central and lighter and bigger nucleus (black arrows). (b) 10 Times the MIC of products (48.83-260.4 μg/mL). Sodium alginate stabilized composites treated digestive gland (at400 X): shows vacuolar degeneration (black arrows) and pyknotic nuclei indicating cellular degeneration (red arrows).

2.8.1. Agar Well Diffusion Method. Sterile Mueller Hinton agar was dug up 6-8 mm wide using a well borer. A fresh culture of *E. coli* adjusted at $1-1.5\times10^{8}$ CFU/mL was spread over Mueller Hinton agar. A 50 μL of 0.01 gm/mL of sodium alginate stabilized products were poured. Following 24 hrs incubation at 37°C, zones of inhibitions (ZOIs) produced by the products against *E. coli* were measured by vernier calipers [28].

2.8.2. Minimum Inhibitory Concentration (MIC). Two-dimensional outcomes were intended on this section: (1) comparison of MIC among different preparations and (2) comparison of incubation periods within each preparation. For this purpose, 96 well titration plates were filled in with Mueller Hinton broth. The preparations were serially diluted by the two-fold dilution method. Finally, the fresh growth of *E. coli* set at 10^{5} CFU/mL was poured into each well except for negative control. The well designated as negative control consisted of only broth while that of positive control contained broth and culture. Optical density values were taken at 695 nm wavelength through an ELISA reader at 0 hr, 4 hrs, 8 hrs, 12 hrs, 16 hrs, 20 hrs, and 24 hrs. The values taken were compared with 0 hr incubation to find the net OD value. Net OD value was considered to find inhibition of growth at various concentrations. The minimum concentration of preparation that inhibited the growth of bacteria was declared as MIC [27, 28].

2.9. Statistical Analysis. Univariate analysis was carried out for data on prevalence while chi-Square analysis was done

Table 2: Risk factors analysis of *E. coli* isolated from the gut of the Houbara bustard.

Variable	Levels	Screened	Positive	Prevalence (%)	*P* value	CI 95%	
						Lower	Upper
Gender	Male	35	20	57.14	0.105	40.85	72.01
	Female	70	51	72.85		61.46	81.88
Age	0-6 M	15	10	66.66	0.253	41.72	84.83
	7-12 M	36	28	77.77		61.92	88.29
	Above 1 Y	54	33	61.11		47.79	72.96
Housing system	Natural environment provision	67	41	61.19	0.062	49.22	71.95
	Pen	38	30	78.94		63.66	88.93
Feeding system	Poultry feed	38	16	42.10	<0.01	27.86	57.81
	Poultry feed plus scavenger	67	55	82.08		63.66	89.45
Season	Spring	40	25	62.5	0.016	47.03	75.78
	Winter	30	28	93.33		78.67	98.15
	Summer	35	18	51.42		35.57	67.01
GI parasites	Yes	44	35	79.54	<0.01	65.50	88.85
	No	61	26	42.62		31.01	55.10
Use of antibiotics	Frequent	25	17	68	0.688	48.41	82.79
	Occasional	30	22	73.33		55.55	85.81
	No use	50	32	64		50.14	75.86

CI: Confidence interval, $p < 0.05$ indicate significant association.

Table 3: Antibiotic susceptibility pattern of *E. coli* against different antibiotics.

Antibiotic name (abbreviation and potency)	Resistant (%)	Intermediate (%)	Sensitive (%)
Enrofloxacin (ENR 5 μg)	0	25	75
Fusidic acid (FA 10 μg)	40	10	50
Ciprofloxacin (CIP 5 μg)	30	20	60
Septran (S*T 25 μg)	20	25	25
Levofloxacin (LEV 5 μg)	25	50	25
Chloramphenicol (C 30 μg)	25	25	50
Vancomycin (VAN 30 μg)	30	30	30
Gentamicin (CN 10 μg)	10	30	60
Linezolid (LNZ 30 μg)	20	30	50
Cefoxitin (C*T 30 μg)	40	20	40

to find the association of assumed risk factors with the prevalence of *E. coli*. Parametric tests like analysis of variance (ANOVA) coupled with Tukey's test were applied at 5% probability to compare means of the zones of inhibition and MIC values of sodium alginate stabilized products. SPSS version 22 of the statistical computer program was applied to analyze data. Prevalence was calculated as per the formula [23]:

$$\text{Prevalence percentage}\,(\%) = \frac{\text{No of sample positive for } E.coli}{\text{Total No of samples}} \times 100. \quad (1)$$

3. Results

3.1. Characterization of Nanoparticles. Three peaks situated at 1.26, 0.52, and 0.28 keV were identified in pattern. Two peaks located at 1.26 and 0.52 keV matched with Mg and O, respectively. One extra peak of carbon was identified at 0.28 keV. This peak was due to carbon based sample stacking tape. Both of the peaks (1.26 and 0.52 keV) were due to Kα transitions in Mg and O, respectively. Kα transition was happened when electrons were dropped from L ($n = 2$) to K ($n = 1$) shell. The analysis of EDX data showed that Mg and O were successfully incorporated, and MgO was synthesized (Figure 2(a)). Overall morphology of product is monodisperse because nearly spherical shaped nanoparticles were observed from this figure. The boundaries of nanoparticles were defined. Nanoparticles were not agglomerated but found in dispersed form. The size of nanoparticles was ranged from 80 to 150 nm.

3.2. Ecotoxicity Analysis. The sodium alginate stabilized antibiotics and MgO nanoparticles showed direct proportion of mortality with increasing concentration of products (Table 1). There was a 20% difference in mortality of all products except those having nanoparticles and antibiotics simultaneously stabilized in sodium alginate (G+M+A, G +M+C, G+M+T). Highest mortality was noted in gel stabilized antibiotics (G+A, G+T) and gel stabilized nanoparticle (M+G) at both of 1 × MIC and 10 × MIC concentrations for these products.

3.3. Histopathology. Snails treated with 1×MIC of different concentrations of sodium alginate stabilized products were

Table 4: Minimum Inhibitory concentrations (μg/mL) of different preparations against *E. coli*.

Preparations	Time intervals of incubation					
	4 hrs (mean ± SD)	8 hrs (mean ± SD)	12 hrs (mean ± SD)	16 hrs (mean ± SD)	20 hrs (mean ± SD)	24 hrs (mean ± SD)
G+M+A	65.1 ± 22.6^{a}	52.1 ± 22.6^{a}	52.1 ± 22.6^{a}	16.28 ± 5.64^{a}	13.02 ± 5.64^{a}	13.02 ± 5.64^{a}
G+A	52.1 ± 22.6^{a}	39.06 ± 0.00^{a}	32.55 ± 11.28^{a}	22.79 ± 14.92^{a}	16.28 ± 5.64^{a}	13.02 ± 5.64^{ab}
G+T	78.13 ± 0.00^{a}	65.1 ± 2.6^{a}	52.1 ± 22.6^{a}	39.06 ± 0.00^{ab}	26.04 ± 11.28^{a}	26.04 ± 11.28^{ab}
G+M+C	78.13 ± 0.00^{a}	65.1 ± 22.6^{a}	52.1 ± 22.6^{a}	13.02 ± 5.64^{b}	8.14 ± 2.82^{a}	6.51 ± 2.82^{ab}
G+M+T	39.06 ± 0.00^{a}	32.55 ± 11.28^{a}	26.04 ± 11.28^{a}	13.02 ± 5.64^{b}	6.51 ± 2.82^{a}	4.883 ± 0.000^{b}
M+G	65.1 ± 22.6^{a}	52.1 ± 22.6^{a}	52.1 ± 22.6^{a}	39.06 ± 0.00^{b}	26.04 ± 11.28^{a}	16.28 ± 5.64^{b}

Different superscripts within a column indicate a significant difference ($p < 0.05$), SD = standard deviation; M + G = MgO stabilized in gel, G + M + T = MgO and tylosin simultaneously stabilized in gel, G + M + C = MgO and cefoxitin both stabilized in gel, G + M + A = MgO and ampicillin simultaneously stabilized in gel, G + T = tylosin stabilized in gel, G + A = ampicillin stabilized in gel.

observed to have induced microscopic alterations at several locations of the digestive tract (Figure 3(a)). The digestive glands located in the region appeared degenerated marked by the development of excretory cells. Vacuolation, and the release of secretory granules. The basophilic infiltration was evident through the parenchyma of the digestive glands. Surrounding connective tissue also seemed disintegrated, and the lumen appeared irregular and fluid filled. Pyknotic nuclei were observed in the parenchyma and interstitial tissue (Figure 3(b)).

3.4. Prevalence of E. Coli and Its Associated Risk Factors. The current study found 53% (56/105) prevalence of *E. coli* from fecal samples of the Houbara bustard bird. Female birds presented 72.85% while male birds showed a 57.14% prevalence of *E. coli* (Table 2). Association of risk factors with prevalence of *E. coli* was found significant ($p < 0.05$) with feeding system, season, and gastrointestinal parasites. On the other hand, age, gender, housing system, use of antibiotics, and types of antibiotics showed nonsignificant ($p > 0.05$) associations.

3.5. Antibiogram. The study found increasing trends of antibiotic resistance in *E. coli* (Table 3). The antibiogram showed 40% of *E. coli* resistant to fusidic acid and cefoxitin while 30% showed resistance against ciprofloxacin and vancomycin. Levofloxacin, chloramphenicol, linezolid, and sulfamethoxazole-trimethoprim faced 20-25% resistance while against gentamicin there were only 10% resistant isolates. None of the isolates were found resistant to enrofloxacin in this study. On the other hand, considerable intermediate susceptible isolates were noted against different antibiotics in that there were 50% of isolates intermediate susceptible against levofloxacin, while 30% showed the same response against vancomycin, gentamicin, and linezolid. The study also noted 20-25% of isolates falling in intermediate susceptible category against enrofloxacin, ciprofloxacin, sulfamethoxazole-trimethoprim, chloramphenicol, and cefoxitin.

3.6. Comparison of Different Preparations for Minimum Inhibitory Concentration (μg/mL). The study showed a significant difference ($p < 0.05$) in MIC values among different treatments following 24 hrs incubation (Table 4). G+M+T showed lowest MIC (4.883 ± 0.000 μg/mL) followed by G+M+C (6.51 ± 2.82 μg/mL), G+M+A (13.02 ± 5.64 μg/mL), G+A (13.02 ± 5.64 μg/mL), M+G (16.28 ± 5.64 μg/mL) and G+T (26.04 ± 11.28 μg/mL). G+M+A showed a nonsignificant difference ($p < 0.05$) in MIC compared to those of G+A, G+T, and G+M+A while a significant difference ($p < 0.05$) was noted in comparison with the MICs of G+M+T and M+G. However, all other preparations did not show a significant difference ($p < 0.05$) among each other. There was a higher standard deviation in some preparations, a possible reason for a nonsignificant difference. It was also noted from this study that comparison of MICs among different preparations remained variable at different time intervals of incubation.

The maximum antibacterial activity at earlier incubation with minimum concentrations was found promising in this study. The current study showed that the response of G+M+A, G+A, M+G, and G+T against *E. coli* remained similar for maximum antibacterial activity at the earliest among incubation periods (Figure 4). A significant reduction ($p < 0.05$) in MIC was noted at the 8th hr of incubation when compared with that of 4th hr incubation. On the other hand, G+M+T and G+M+C showed a significant reduction in MIC at the 12th hr incubation. Moreover, further significant reduction in MIC was noted only in the case of G+M+T at 16th hr of incubation. This fact indicated that depending upon the availability of time, maximum antibacterial activity at the lowest concentration could be achieved.

4. Discussion

4.1. Characterization of Nanoparticles. The preparation method of MgO nanoparticles using the hydrogel method in the current was in line with the findings of Duong et al. [29]. Moreover, the findings of SEM analysis in the current study were in line with those of Radhi and Jasim [30]. The findings of XRD and SEM of current study were also in line with those of Zaheer et al. [20] who reported 30-80 nm size, without any aggression and proved to be compact. In addition, miller indices in XRD findings of Zaheer et al. [20] were like those in current study while the sharp peaks indicated synthesized product as crystalline.

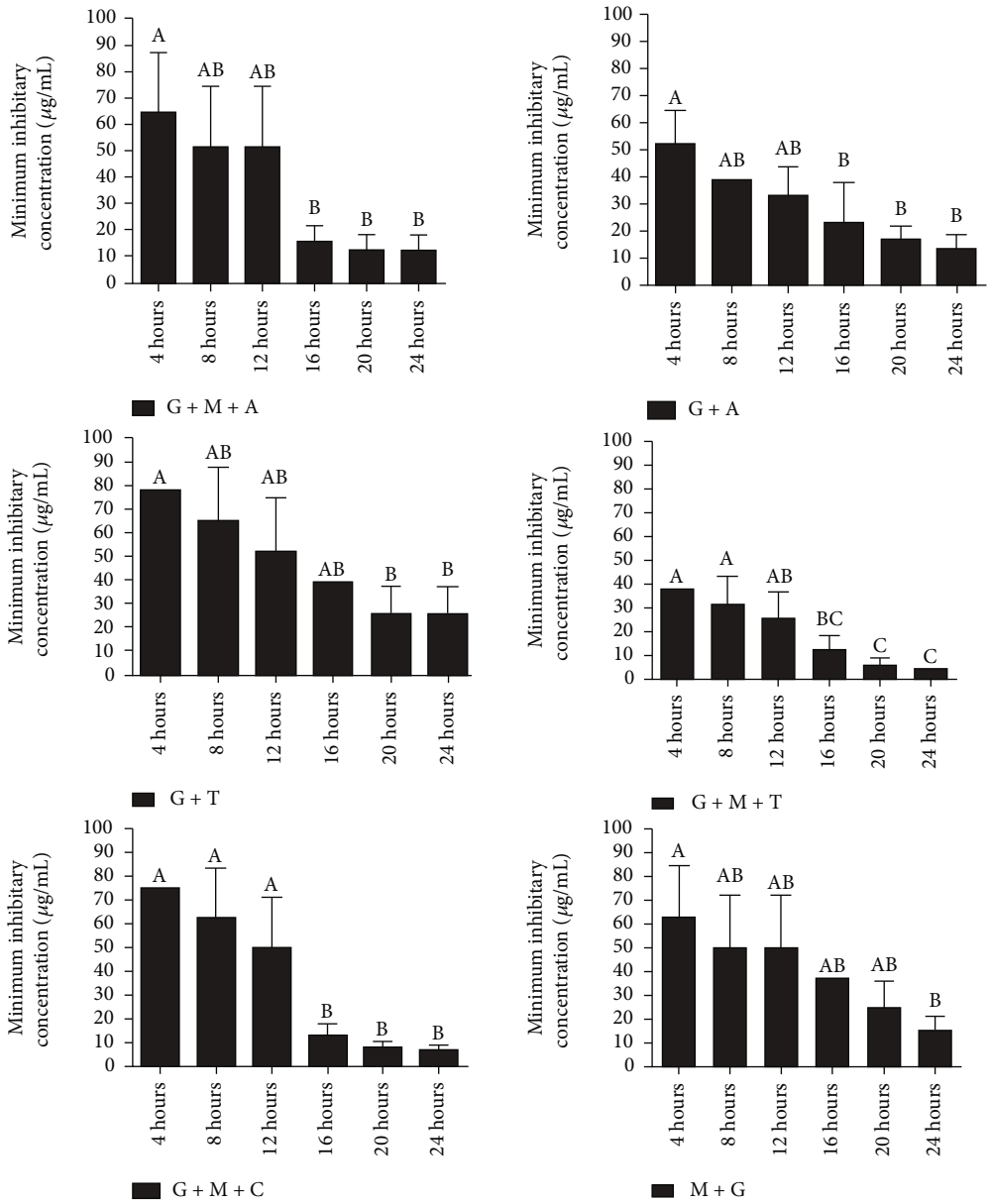

Figure 4: Minimum inhibitory concentration of different treatments/s at different time intervals G + M + A = MgO and ampicillin stabilized in sodium alginate gel; G + A = ampicillin stabilized in sodium alginate gel; G + T = Tylosine stabilized in sodium alginate gel; G + M + T = MgO and tylosin stabilized in sodium alginate gel; and M + G = MgO stabilized in sodium alginate gel.

4.2. Ecotoxicity Evaluation. The toxicity analysis of our study was in line with the findings of Zaheer et al. [20] who conducted a trial using similarly snail as the experimental animal. Caixeta et al. [31] also reported results similar to the findings of the current study. A limited number of studies evaluate the hazards of iron oxide nanoparticle treatment to terrestrial invertebrates [32, 33]. Additionally, MgO nanoparticles are listed among FDA-approved materials for safer use. The mechanism of toxicity in insects is yet to be fully understood while the known attribute so far is the production of reactive oxygen species that lead to DNA damage and eventually death of the cell due to higher alkalinity [34]. Some studies also report toxicity due to the slowdown of cellular functions of host cells leading to the death of cells [35].

The fact that snails have a propensity to bioaccumulate nanomaterials, as well as the fact that they are an important element of land and aquatic ecosystems, makes them an excellent model for assessing the ecotoxicity of nanomaterials [20]. Otludil and Ayaz [36] confered increase in the concentration of CuSO4 and the exposure times as directly proportion to the potential of the lesions and their severity in the tissue. The physical properties and chemical composition of nanomaterials determine their molluscicide activity against snails as well as their environmental transformation [31]. Based on biochemical analyses of animal sera, ZnO nanoparticles were shown to be safe during *in vivo* testing [37]. The same results were obtained in humans post 5 days exposure of ZnO nanoparticles to the dermal layers [38].

4.3. Prevalence and Associated Risk Factors. The prevalence of *E.coli* found in the current study was in line with those of Literak et al. [39] who reported 57.9% prevalence but contrary to the current study lower prevalence was noted by Zurfluh et al. [40] and higher was reported by Shobrak and Abo-Amer [41]. Similarly, higher prevalence, i.e., 85.7% in Portugal was reported by Rashid et al. [42]. Meanwhile, the prevalence of *E.coli* lower than that of current study was reported by Dotto et al. [43] and Foti et al. [44] who reported 24.31% of positive cases in Italy. The difference in the prevalence of various regions may be described based on the risk factors at various sampling areas like hygienic conditions and prevention measures. Contrary to the findings of our study, Nguyen et al. [45] reported significant ($p < 0.05$) association of use antibiotics with *E.coli*. However, Sarba et al. [46] showed age, health status, and diarrhea to be significantly associated ($p < 0.05$) risk factors. Majhi et al. [47] concluded season as a significant influencing factor for health of the birds. They reported 57% prevalence during the rainy season, 39% during summer, and 19% during the winter season. Rahman et al. [48] recorded colibacillosis cases across all seasons of the year with the highest rate occurring during the summer season at the BRAC Poultry Disease Diagnostic Centre, Gazipur, Bangladesh. Hermans and Morgan [49] reported high disease prevalence in the United Kingdom from October to February. Contradictions in results of current study with those of the previous studies might be due to different locations and seasons.

4.4. Antibiogram of E. Coli and Response of Different Preparations. Findings of the current study were found in line with those of Anwar et al. [50] and Yu et al. [51]. Infectious *E.coli* of human and animal origin showing resistance to enrofloxacin, ampicillin, gentamicin, penicillin, and ciprofloxacin has also been reported by Hemmatinezhad et al. [52]; Ranjbar et al. [53]. Response against chloramphenicol was found to be 19.2% [54] while there were 100, 91.67, 100, 100, 66.67, and 66.67% of *E. coli* resistant against vancomycin, cefotaxime, tetracycline, ciprofloxacin, amoxicillin, and gentamicin, respectively, [4].

Nano-antibiotics were supposed to possess antimicrobial properties on their own or may enhance the efficacy of conventional antibiotics, both of which have the capability of controlling bacterial infections both *in vitro* and *in vivo* [55]. Different studies have shown that metal nanoparticles combined with antibiotics have enhanced antibacterial activity and anti-MRSA (methicillin-resistant *S. aureus*) activities than nonpolymerized penicillin or N-methylthio β-lactams [56]. Similarly, Allahverdiyev et al. [57] reported a combination of amoxicillin with silver nanoparticles as an effective resistance modulator for drug-resistant *E.coli*. Similar findings were reported by Li et al. [15] who noticed high potency against *E.coli*. In another study, superparamagnetic iron oxide nanoparticles (SIONPs) at 5 mg/mL presented potential anti-biofilm expressions on biofilms produced by both Gram-negative and Gram-positive bacteria [58].

5. Conclusion

This study concluded that multiple drug resistant *E. coli* from gut of the Houbara bustard was a prevalent pathogen along with a significant association of most of the assumed risk factors. Pathogens demonstrated an increasing trend of resistance to the antibiotics. However, the resistance modulation was found prominent upon the use of sodium alginate stabilized MgO nanoparticles and antibiotics. The preparations showed significant antibacterial activity at the earliest hours of incubation that can be considered in case of outbreaks. Histopathology parameters concluded mild toxicities thus presenting safer use of the composites. This study thus proposes further *in-vivo* trials on composites and documentation of their efficacy, safety, and stability parameters.

Data Availability

No data is used.

Conflicts of Interest

The authors declare that they have no conflicts of interest.

Authors' Contributions

Afshan Muneer did research,collected data, formal analysis and prepared initial draft; Santosh Kumar conceived idea and prepared initial draft; Amjad Islam Aqib conceived idea, did research, analyzed data, and revised manuscript; Shanza Rauf Khan did research and prepared revised manuscript; Syed Qaswar Ali Shah supervised research and revised draft; Iqra Zaheer did research and analyzed data; Tauseef ur Rehman analyzed data and prepared initial draft; Asghar Abbas formalized data and initial draft; Kashif Hussain edited initial draft, analyzed data; Atif Rehman did resourcing and methodology; Muhammad Nadeem edited initial draft and revised final version; Maheen Murtaza did research, analyze data; Ahmad Waseem did resourcing, formal analysis, and collection of data.

References

[1] M. S. Islam, M. M. H. Nayeem, M. A. Sobur et al., "Virulence determinants and multidrug resistance of Escherichia coli isolated from migratory birds," *Antibiotics*, vol. 10, no. 2, p. 190, 2021.

[2] A. M. E. Sulieman, F. E. Dafallah, E. H. Abdel-Rahman, N. I. Alshammari, S. A. Shommo, and S. E. Ibrahim, "Isolation, identification and characterization of salmonella spp. from chicken purchased at Wad Madani City, Gezira state, Sudan," *Advancements in Life Sciences*, vol. 8, no. 1, pp. 98–102, 2020.

[3] N. M. Bakry, W. S. Awad, and S. A. Ahmed, "Virulence genes, antibiotic resistance and phylotyping of *Escherichia coli* O157 recovered from diarrheic calves," *International Journal of Veterinary Science*, vol. 10, no. 1, pp. 1–7, 2021.

[4] Z. Nawaz, B. Aslam, M. A. Zahoor et al., "Frequency of extended spectrum beta lactamase producing *Escherichia coli* in fresh and frozen meat," *Pakistan Veterinary Journal*, vol. 41, no. 1, pp. 102–106, 2021.

[5] S. Hernando-Amado, T. M. Coque, F. Baquero, and J. L. Martínez, "Defining and combating antibiotic resistance from one health and global health perspectives," *Nature Microbiology*, vol. 4, no. 9, pp. 1432–1442, 2019.

[6] B. Aslam, W. Wang, M. I. Arshad et al., "Antibiotic resistance: a rundown of a global crisis," *Infection and Drug Resistance*, vol. 11, pp. 1645–1658, 2018.

[7] J. Bonnedahl and J. D. Järhult, "Antibiotic resistance in wild birds," *Upsala Journal of Medical Sciences*, vol. 119, no. 2, pp. 113–116, 2014.

[8] O. Combreau, S. Riou, J. Judas, M. Lawrence, and F. Launay, "Migratory pathways and connectivity in Asian houbara bustards: evidence from 15 years of satellite tracking," *PLoS One*, vol. 6, no. 6, article e20570, 2011.

[9] G. Nabi, R. Ullah, S. Khan, M. Amin, and N. Rauf, "The Asian houbara bustard (*Chlamydotis macqueenii*): on an accelerating path to extinction?," *Biodiversity and Conservation*, vol. 28, no. 5, pp. 1301-1302, 2019.

[10] F. M. Al-Sarraj, "A review on the impacts of Azadirachta indica on multi-drug resistant extended spectrum beta lactamase-positive of *Escherichia coli* and *Klebsiella pneumonia*," *Advancements in Life Sciences*, vol. 8, no. 3, pp. 228–232, 2021.

[11] A. M. Tammam, S. A. Ibrahim, A. A. Hemid, F. Abdel-Azeem, and W. Salem, "Effect of nanoparticles supplementation in broiler diets on performance, microbial population and digestive tract measurements," *International Journal of Veterinary Science*, vol. 9, no. 3, pp. 373–378, 2020.

[12] S. Bayda, M. Adeel, T. Tuccinardi, M. Cordani, and F. Rizzolio, "The history of nanoscience and nanotechnology: from chemical–physical applications to nanomedicine," *Molecules*, vol. 25, no. 1, p. 112, 2020.

[13] M. Z. Troncarelli, H. M. Brandão, J. C. Gern, A. S. Guimarães, and H. Langoni, "Nanotechnology and antimicrobials in veterinary medicine," *Formatex*, vol. 13, pp. 543–556, 2013.

[14] A. M. Allahverdiyev, K. V. Kon, E. S. Abamor, M. Bagirova, and M. Rafailovich, "Coping with antibiotic resistance: combining nanoparticles with antibiotics and other antimicrobial agents," *Expert review of anti-infective therapy*, vol. 9, no. 11, pp. 1035–1052, 2011.

[15] P. Li, J. Li, C. Wu, Q. Wu, and J. Li, "Synergistic antibacterial effects of β-lactam antibiotic combined with silver nanoparticles," *Nanotechnology*, vol. 16, no. 9, pp. 1912–1917, 2005.

[16] H. Zhang, Y. Fu, Y. Xu et al., "One-step assembly of zein/caseinate/alginate nanoparticles for encapsulation and improved bioaccessibility of propolis," *Food & Function*, vol. 10, no. 2, pp. 635–645, 2019.

[17] D. Thomas, M. S. Nath, N. Mathew, R. Reshmy, E. Philip, and M. S. Latha, "Alginate film modified with aloevera gel and cellulose nanocrystals for wound dressing application: preparation, characterization and *in vitro* evaluation," *Journal of Drug Delivery Science and Technology*, vol. 59, article 101894, 2020.

[18] Y. H. Choi and H. K. Han, "Nanomedicines: current status and future perspectives in aspect of drug delivery and pharmacokinetics," *Journal of Pharmaceutical Investigation*, vol. 48, no. 1, pp. 43–60, 2018.

[19] R. G. Puscaselu, A. Lobiuc, and M. D. Polymers, "Alginate: From Food Industry to Biomedical Applications and Management of Metabolic Disorders. Mdpi.Com," 2020, https://www.mdpi.com/863690.

[20] T. Zaheer, M. Kandeel, R. Z. Abbas, S. R. Khan, and A. I. Aqib, "Acaricidal potential and ecotoxicity of metallic nanopesticides used against the major life stages of Hyalomma ticks," *Life*, vol. 12, no. 7, p. 977, 2022.

[21] Z. X. Tang and B. F. Lv, "MgO nanoparticles as antibacterial agent: preparation and activity," *Brazilian Journal of Chemical Engineering*, vol. 31, no. 3, pp. 591–601, 2014.

[22] H. M. Sharaf, M. A. Salama, and M. S. Abd El-Att, "Biochemical and histological alterations in the digestive gland of the land snail Helicella vestalis (Locard, 1882) exposed to methiocarb and chlorpyrifos in the laboratory," *Journal of Cytology & Histology*, vol. 6, no. 3, p. 327, 2015.

[23] M. Thrusfield, R. Christley, H. Brown et al., *Veterinary Epidemiology*, John Wiley & Sons, 2018.

[24] I. El-Shahawy and E. F. Abou, "Enteric parasites of Egyptian captive birds: a general coprological survey with new records of the species," *Tropical Biomedicine*, vol. 32, p. 6508, 2015.

[25] M. A. Sobur, A. A. M. Sabuj, R. Sarker, A. T. Rahman, S. L. Kabir, and M. T. Rahman, "Antibiotic-resistant Escherichia coli and salmonella spp. associated with dairy cattle and farm environment having public health significance," *Veterinary World*, vol. 12, no. 7, pp. 984–993, 2019.

[26] H. S. Khalefa, Z. S. Ahmed, F. Abdel-Kader, E. M. Ismail, and E. A. Elshafiee, "Sequencing and phylogenetic analysis of the *stn* gene of salmonella species isolated from different environmental sources at Lake Qarun protectorate: the role of migratory birds and public health importance," *Veterinary World*, vol. 14, no. 10, pp. 2764–2772, 2021.

[27] Clinical and Laboratory Standards Institute, *Methods for dilution antimicrobial susceptibility tests for bacteria that grow aerobically; approved standard*, M07-A11. Clinical and Laboratory Standards Institute, Wayne, PA, 10th edition, 2018.

[28] M. A. Anwar, A. I. Aqib, K. Ashfaq et al., "Antimicrobial resistance modulation of MDR *E. coli* by antibiotic coated ZnO nanoparticles," *Microbial Pathogenesis*, vol. 148, article 104450, 2020.

[29] T. H. Y. Duong, T. N. Nguyen, H. T. Oanh et al., "Synthesis of magnesium oxide nanoplates and their application in nitrogen dioxide and sulfur dioxide adsorption," *Journal of Chemistry*, vol. 2019, Article ID 4376429, 9 pages, 2019.

[30] Z. E. Radhi and N. O. Jasim, "Synthesis, characterization and antimicrobial activity of MgO nanoparticles," *IOP Conference Series: Earth and Environmental Science*, vol. 790, no. 1, article 012089, 2021.

[31] M. B. Caixeta, P. S. Araújo, B. B. Gonçalves, L. D. Silva, M. I. Grano-Maldonado, and T. L. Rocha, "Toxicity of engineered nanomaterials to aquatic and land snails: a scientometric and systematic review," *Chemosphere*, vol. 260, article 127654, 2020.

[32] H. Chen, B. Wang, W. Feng et al., "Oral magnetite nanoparticles disturb the development of *Drosophila melanogaster* from oogenesis to adult emergence," *Nanotoxicology*, vol. 9, no. 3, pp. 302–312, 2015.

[33] S. Vega-Alvarez, A. Herrera, C. Rinaldi, and F. A. Carrero-Martínez, "Tissue-specific direct microtransfer of nanomaterials into *drosophila* embryos as a versatile in vivo test bed for nanomaterial toxicity assessment," *International Journal of Nanomedicine*, vol. 9, article 2031, 2014.

[34] O. Yamamoto, T. Ohira, K. Alvarez, and M. Fukuda, "Antibacterial characteristics of $CaCO_3$-MgO composites," *Materials Science and Engineering B*, vol. 173, no. 1-3, pp. 208–212, 2010.

[35] A. Elsaesser and C. V. Howard, "Toxicology of nanoparticles," *Advanced Drug Delivery Reviews*, vol. 64, no. 2, pp. 129–137, 2012.

[36] B. Otludil and S. Ayaz, "Effect of copper sulphate (CuSO4) on freshwater snail, Physa acuta Draparnaud, 1805: a histopathological evaluation," *Bulletin of Environmental Contamination and Toxicology*, vol. 104, no. 6, pp. 738–747, 2020.

[37] W. M. Arafa, A. N. Mohammed, and F. I. A. El-Ela, "Acaricidal efficacy of deltamethrin-zinc oxide nanocomposite on *Rhipicephalus* (*Boophilus*) *annulatus* tick," *Veterinary Parasitology*, vol. 268, pp. 36–45, 2019.

[38] Y. H. Mohammed, A. Holmes, I. N. Haridass et al., "Support for the safe use of zinc oxide nanoparticle sunscreens: lack of skin penetration or cellular toxicity after repeated application in volunteers," *Journal of Investigative Dermatology*, vol. 139, no. 2, pp. 308–315, 2019.

[39] I. Literak, R. Vanko, M. Dolejska, A. Čížek, and R. Karpíšková, "Antibiotic resistant Escherichia coli and salmonella in Russian rooks (Corvus frugilegus) wintering in the Czech Republic," *Letters in Applied Microbiology*, vol. 45, no. 6, pp. 616–621, 2007.

[40] K. Zurfluh, S. Albini, P. Mattmann et al., "Antimicrobial resistant and extended-spectrum β-lactamase producing *Escherichia coli* in common wild bird species in Switzerland," *MicrobiologyOpen*, vol. 8, no. 11, p. e845, 2019.

[41] M. Y. Shobrak and A. E. Abo-Amer, "Role of wild birds as carriers of multi-drug resistant *Escherichia coli* and *Escherichia vulneris*," *Brazilian Journal of Microbiology*, vol. 45, no. 4, pp. 1199–1209, 2014.

[42] M. Rashid, M. M. Rakib, and B. Hasan, "Antimicrobial-resistant and ESBL-producing *Escherichia coli* in different ecological niches in Bangladesh," *Infection Ecology & Epidemiology*, vol. 5, no. 1, article 26712, 2015.

[43] G. Dotto, M. L. Menandro, A. Mondin, M. Martini, F. R. Tonellato, and D. Pasotto, "Wild birds as carriers of antimicrobial-resistant and ESBL-producing *Enterobacteriaceae*," *International Journal of Infectious Diseases*, vol. 53, p. 59, 2016.

[44] M. Foti, D. Rinaldo, A. Guercio et al., "Pathogenic microorganisms carried by migratory birds passing through the territory of the island of Ustica, Sicily (Italy)," *Avian Pathology*, vol. 40, no. 4, pp. 405–409, 2011.

[45] V. T. Nguyen, J. J. Carrique-Mas, T. H. Ngo et al., "Prevalence and risk factors for carriage of antimicrobial-resistant *Escherichia coli* on household and small-scale chicken farms in the Mekong Delta of Vietnam," *Journal of Antimicrobial Chemotherapy*, vol. 70, no. 7, pp. 2144–2152, 2015.

[46] E. J. Sarba, K. A. Kelbesa, M. D. Bayu, E. Z. Gebremedhin, B. M. Borena, and A. Teshale, "Identification and antimicrobial susceptibility profile of Escherichia coli isolated from backyard chicken in and around ambo, Central Ethiopia," *BMC Veterinary Research*, vol. 15, no. 1, pp. 1–8, 2019.

[47] M. Majhi, J. Pamia, S. K. Panda, L. Samal, and R. Mishra, "Effect of age and season on enteritis and antibiotic sensitivity test of *E. coli* isolated from infected chickens in Odisha, India," *International Journal of Current Microbiology and Applied Sciences*, vol. 7, no. 3, pp. 2037–2045, 2018.

[48] M. A. Rahman, M. A. Samad, M. B. Rahman, and S. M. L. Kabir, "Bacterio-pathological studies on salmonellosis, colibacillosis and pasteurellosis in natural and experimental infections in chickens," *Bangladesh Journal of Veterinary Medicine*, vol. 2, no. 1, pp. 1–8, 2009.

[49] P. G. Hermans and K. L. Morgan, "Prevalence and associated risk factors of necrotic enteritis on broiler farms in the United Kingdom; a cross-sectional survey," *Avian Pathology*, vol. 36, no. 1, pp. 43–51, 2007.

[50] M. A. Anwar, S. Aziz, K. Ashfaq et al., "Trends in frequency, potential risks, and antibiogram of *E. coli* isolated from semi-intensive dairy systems," *Pakistan Veterinary Journal*, vol. 42, no. 2, p. 167, 2022.

[51] Z. Yu, J. Wang, H. Ho, Y. T. Wang, S. N. Huang, and R. W. Han, "Prevalence and antimicrobial-resistance phenotypes and genotypes of *Escherichia coli* isolated from raw milk samples from mastitis cases in four regions of China," *Journal of Global Antimicrobial Resistance*, vol. 22, pp. 94–101, 2020.

[52] B. Hemmatinezhad, F. Khamesipour, M. Mohammadi, F. Safarpoor Dehkordi, and Z. Mashak, "Microbiological investigation of O-serogroups, virulence factors and antimicrobial resistance properties of Shiga toxin-producing Escherichia coli isolated from ostrich, turkey and quail meats," *Journal of Food Safety*, vol. 35, no. 4, pp. 491–500, 2015.

[53] R. Ranjbar, F. Safarpoor Dehkordi, M. H. Sakhaei Shahreza, and E. Rahimi, "Prevalence, identification of virulence factors, O-serogroups and antibiotic resistance properties of Shiga-toxin producing Escherichia coli strains isolated from raw milk and traditional dairy products," *Antimicrobial Resistance & Infection Control*, vol. 7, no. 1, p. 53, 2018.

[54] K. H. Ong, W. C. Khor, J. Y. Quek et al., "Occurrence and antimicrobial resistance traits of Escherichia coli from wild birds and rodents in Singapore," *International Journal of Environmental Research and Public Health*, vol. 17, no. 15, p. 5606, 2020.

[55] J. S. Kim, E. Kuk, K. N. Yu et al., "Antimicrobial effects of silver nanoparticles," *Nanomedicine: Nanotechnology, Biology and Medicine*, vol. 3, no. 1, pp. 95–101, 2007.

[56] P. Dibrov, J. Dzioba, K. K. Gosink, and C. C. Häse, "Chemiosmotic mechanism of antimicrobial activity of Ag+ in Vibrio cholerae," *Antimicrobial Agents and Chemotherapy*, vol. 46, no. 8, pp. 2668–2670, 2002.

[57] A. M. Allahverdiyev, K. V. Kon, E. S. Abamor, M. Bagirova, and M. Rafailovich, "Coping with antibiotic resistance: combining nanoparticles with antibiotics and other antimicrobial agents," *Expert Review of Anti-Infective Therapy*, vol. 9, no. 11, pp. 1035–1052, 2011.

[58] M. Huo, L. Wang, H. Zhang, L. Zhang, Y. Chen, and J. Shi, "Construction of single-iron-atom nanocatalysts for highly efficient catalytic antibiotics," *Small*, vol. 15, no. 31, article 1901834, 2019.

Hindawi
Oxidative Medicine and Cellular Longevity
Volume 2022, Article ID 6570879, 17 pages
https://doi.org/10.1155/2022/6570879

Research Article

IPO5 Mediates EMT and Promotes Esophageal Cancer Development through the RAS-ERK Pathway

Meiyu Li, Xiaofei Li, Shujia Chen, Tianai Zhang, Liaoyuan Song, Jiayue Pei, Guoyan Sun, and Lianyi Guo

The First Affiliated Hospital of Jinzhou Medical University, Jinzhou, China

Correspondence should be addressed to Xiaofei Li; doctorlixiaofei@163.com and Lianyi Guo; angel_gly@163.com

Received 20 June 2022; Revised 7 July 2022; Accepted 31 July 2022; Published 9 September 2022

Academic Editor: Tarique Hussain

Objective. In the development of many tumors, IPO5, as a member of the nuclear transporter family, exerts a significant function. Also, IPO5 is used as a therapeutic target for tumors based on some reports. By studying IPO5 expression in esophageal cancer tissues, the mechanism associated with IPO5 improving esophageal cancer development was explored in this study. *Methods*. To gain differentially expressed genes, this study utilized mRNA microarray and TCGA database for comprehensive analysis of esophageal cancer tissues and normal esophageal cancer tissues, and then the differentially expressed gene IPO5 was screened by us. To assess esophageal cancer patients' prognosis, this study also applied the Kaplan-Meier analysis, and we also conducted the GSEA enrichment analysis to investigate IPO5-related signaling pathways. This study performed TISIDB and TIMER online analysis tools to study the correlation between IPO5 and immune regulation and infiltration. We took specimens of esophageal cancer from patients and detected the expression of IPO5 in tumor and normal tissues by immunohistochemistry. The IPO5 gene-silenced esophageal cancer cell model was constructed by lentivirus transfection. Through the Transwell invasion assay, CCK-8 assay, and cell scratch assay, this study investigated the effects of IPO5 on cell propagation, invasion, and transfer. What is more, we identified the influences of IPO5 on the cell cycle through flow cytometry and established a subcutaneous tumor-forming model in nude mice. Immunohistochemistry was used to verify the expression of KI-67, and this study detected the modifications of cell pathway-related proteins using Western blot and applied EMT-related proteins to explain the mechanism of esophageal cancer induced by IPO5. *Results*. According to database survival analysis, IPO5 high-expression patients had shorter disease-free survival than IPO5 low-expression patients. Compared to normal tissues, the IPO5 expression in cancer tissues was significantly higher in clinical trials ($P < 0.05$). Through TISIDB and TIMER database studies, we found that IPO5 could affect immune regulation, and the age of IPO5 expression grows with the increase of immune infiltration level. The IPO5 expression in esophageal cancer cells was higher than normal, especially in ECA109 and OE33 cells ($P < 0.01$). After knocking out IPO5 gene expression, cell proliferation capacity and invasion capacity were reduced ($P < 0.05$) and decreased ($P < 0.01$) in the IPO5-interfered group rather than the negative control group. The growth cycle of esophageal carcinoma cells was arrested in the G2/M phase after IPO5 gene silencing ($P < 0.01$). Tumor-forming experiments in nude mice confirmed that after IPO5 deletion, the tumor shrank, the expression of KI67 decreased, the downstream protein expression level of the RAS pathway decreased after sh-IPO5 interference ($P < 0.01$), and the level of EMT marker delined ($P < 0.05$). *Conclusion*. In esophageal cancer, IPO5 is highly expressed and correlates with survival rate. Esophageal cancer cell growth and migration were significantly affected by the inhibition of IPO5 in vitro and in vivo. IPO5 mediates EMT using the RAS-ERK signaling pathway activation and promotes esophageal cancer cell development in vivo and in vitro.

1. Introduction

Presently, esophageal cancer (EC) is the sixth dominant inducement of death resulting from cancer [1] and is the 8th most common cancer in the world [2]. One of the countries with a high incidence of esophageal cancer includes China [2]. EC patients have no symptoms in the early stage, but when a series of symptoms such as swallowing difficulty

and wasting appear, they have quietly entered the middle and late stage. In China, patients' 5-year survival rate in the middle and advanced stages is only 15%-25% [3, 4]. Therefore, to reduce the incidence of EC and the main cause of death in China, going deeper into the biological mechanism of the early occurrence and rapid progression of esophageal cancer, studying more excellent gene-targeted treatment, and available, and effective methods will exert a more profound and great influence.

One of the most fundamental pathways for cell metabolism and survival is nuclear plasma transport. Its transport dysfunction leads to many diseases including cancer [5]. Nuclear transporters (karyopherins) are key regulatory molecules of nuclear plasma transport, including input protein and output protein5. The protein constructed by the IPO5 gene comes from the import protein β family, which is a type of nuclear transporter and is located in the region of chromosome 13q32, which is involved in the process of transporter protein [6]. Current studies on IPO5 are limited and are mainly focused on the following fields: Wnt pathway activity is involved in the development of various benign and malignant cancers, IPO5 interacts with IQGAP1, a regulatory factor of β -catenin, and loss of IPO5 reduces the expression of Wnt target genes during early embryogenesis [7]; human herpes virus 8 (HHV-8) can bind to IPO5mRNA, and the mechanism may be to induce the production of miRNA, leading to the pathogenesis of Kaposi's sarcoma [8]. IPO5 mediates RASAl2 nuclear transport to enhance the propagation and shift [9]. There are currently two reported examples of preliminary studies on molecular inhibitors of nuclear import proteins. Intraperitoneal administration of INI-43 significantly inhibited the growth of subcutaneous xenograft esophageal and cervical neoplasms by targeting Kpnβ1 [10]. SINE of CRM1/XPO1, a target of chronic lymphocytic leukemia, could effectively covalently bind cysteine residues in XPO1 cargo binding tank to treat the disease and is being tested in clinical trials targeting a wide range of malignancies [11]. However, the study and treatment of IPO5 in malignant tumors are still few.

The RAS-ERK pathway exerts a significant function when adjusting pivotal cellular activities, covering proliferation, survival, differentiation, and motility, and is a cascade that translates the extracellular environment into intracellular signaling, encompassing a range of biochemical processes [12, 13]. It has been suggested that the biological effects of GTPase activator protein 1 (IQGAP1) on tumor cells can be induced by regulating the response of the RAS signaling pathway [14] and binding to actin is contained in diverse processes like cell binding, propagation, circulate, and transfer [15–20]. Therefore, it is inferred that, through adjusting the RAS-ERK signaling pathway, IPO5 may promote esophageal cancer development.

We screened the gene database in the early stage of the experiment, for differentially expressed genes in esophageal cancer. Meanwhile, immunohistochemistry confirmed that in esophageal carcinoma tissues, IPO5 was expressed highly. The results showed that the changes in the esophageal cancer cell cycle could be significantly affected by the low expression of IPO5, and the growth of esophageal cancer was inhibited, possibly through the activation of the RAS-ERK pathway, which leads to epithelial-mesenchymal transformation and thus causes the occurrence of esophageal cancer. We may discover a new biomarker of esophageal cancer, providing a new molecular mechanism for further related development.

2. Materials and Methods

2.1. Main Materials. The First Affiliated Hospital of Jinzhou Medical University provided cancerous and normal tissues for six patients with esophageal cancer. All patients did not have preoperative radiation therapy or chemotherapy, and paraffin embedding was performed after the cancer tissue was removed. The ethics committee of the affiliated hospital approved all clinical specimen collection, and the patients themselves gave their consent. Esophageal cancer cells ECA109 were purchased from the Chinese Typical Culture Treasure Center. We purchased 8 BALB/C nude mice from Weitonglihua, Beijing. They were 4 weeks old and cultivated in the SPF Animal Experimental Center of Jinzhou Medical University. From Shanghai Enzyme Institute, this study purchased OE33, OE19, TE-1, and normal esophageal epithelial cells HEEC purchased from Mingzhou Biology, Ningbo. Transfection control sequence (sh-NC) and IPO5-interfering lentivirus sequence (sh-IPO5) were purchased from Shanghai Jima Biological Company. The Takara reverse transcription kit was purchased from Japan; ABI Real-time Fluorescence quantitative kit was purchased from the USA. The qRT-PCR primer sequences of IPO5 and GAPDH were obtained from the NCBI database, and the primers were synthesized by the Invitrogen Company. RPMI1640 medium and the freezer-storage solution were purchased from the Wako Company. This study bought fetal bovine serum and 0.25% trypsin-EDTA solution from the Sigma Company. And BD matrix glue and Transwell chamber were purchased from Corning, USA; the CCK-8 kit and BCA kit were purchased from Biyuntian; the cell cycle kit was purchased from Fuyuan Biology; efficient RIPA lysate was purchased from Beijing Solebao; 5 × loading buffer, GAPDH antibody, and CDK6 antibody were purchased from Beijing Bairuji; IPO5 antibodies were purchased from Santa Company; CKD4, CyclinD1, MEK, P-MEK, ERK, P-ERK, and anti-rabbit, and anti-rat antibodies were purchased from Boolsen in Beijing; AKT, P-AKT, N-Cad, Slug, and Vimentin were purchased from Wanlei Biological. The immunohistochemistry kit is available from ZSGB-BIO.

2.2. Methods

2.2.1. Data Collection. From the National Center for Biotechnology Information comprehensive gene expression database (GEO) (https://www.ncbi.cn), we obtained the expression profiles of GSE104958 and GSE131027. The raw data of both groups were preprocessed using the multiarray averaging and SVA packages to eliminate batch effects. SVA package preprocessing and multiarray averaging were utilized to eliminate batch influences and combine both sets of unprocessed data. To compare esophageal cancer tissue

samples with normal esophageal cancer tissue samples, we applied TCGA database R programming language limma package, with $P < 0.05$ and $|\log FC| 1$ or 1 as the threshold values and with the intersection of genetic variants, and finally identified 15 DCGs (differentially expressed genes).

2.2.2. R2 Database. R2 (https://hgserver1.amc.nl/cgi-bin/r2/main.cgi), which is a gene function prediction database, discusses the expression differences in these two esophageal cancer tissues.

2.2.3. GEPIA Database. Gene Expression Profile Interaction Analysis covers 33 cancers (GEPIA Analysis) (http://gepia.cancer-pku.cn/index.html). It is a network-based tool used to deanalyze RNA sequencing expression data with 8,587 normal samples and 9,736 tumor samples from TCGA and GTEx covered. This database was used to explore the expression differences between esophageal carcinoma and normal tissues.

2.2.4. Gene Set Enrichment Analysis (GSEA) Molecular Characterization Database. Available genes were collected from (http://software.broadinstitute.org/gsea/msigdb). GSEA was used to deexamine the correlation between signaling pathways and IPO5 expression.

2.2.5. The TIMER Database. Web server updates, analysis, and visualization of tumor immunity to its association with other tumor's molecular and clinical traits were used as TIMER 2.0 (http://timer.cistrome.org/). TIMER can well evaluate the level of immune aggression in TCGA cohort and find correlations between immune aggression, gene expression, mutations, and survival traits. In other words, extensive analysis and tumor-infiltrating immune cells visualization are empowered by the TIMER 2.0 web server.

2.2.6. Cell Culture. We placed HEEC, ECA109, TE-1, OE33, and OE19 in an RPMI1640 medium containing 10% fetal bovine serum and incubated the cells in a cell culture incubator at 37°C with 5% CO2.

2.2.7. Cell Transfection. We placed ECA109 and OE33 cells in 24-well plates and shifted them to the infected venom after 1 day. Cells were cultured for 2 days after transfection according to the transfection instructions and observed. When the cells grew well and the number of plate layers reached 90% or more, the cells were collected for subsequent experiments.

2.2.8. The Expression of IPO5 RNA in the Collected Samples Was Detected by QRT-PCR. Total RNA was extracted with TRIzol lysis reagent, and we synthesized cDNA with a cDNA reverse transcription kit. We assayed QRT-PCR through the ABI real-time fluorescence quantification kit. We used the $2^{-\Delta\Delta Ct}$ method to calculate GAPDH as an internal reference for mRNA. The upstream primer of IPO5 is 5′-GAGAAGCCTTTCCAGGACCC-3′, and the downstream primer sequence is 5′-AGTGTTGTTGCTGGTTCCCA-3′. The upstream primer sequence of GAPDH is 5′-AATGGGCAGCCGTTAGGAAA-3′, and the downstream primer sequence is 5′-GCGCCCAATACGACCAAATC-3′.

2.2.9. Cell Scratch Experiment. The back of the petri dish was evenly marked with a marker pen. After the cells were covered with the bottom of the 6-well plate, three vertical lines were evenly marked with the head of a gun. After gently rinsing with PBS, RPMI1640 was added for culture and incubated in a cell incubator. The ImageJ software was used for analysis.

2.2.10. Transwell Invasion Experiment. We cultured the cells for 48 h after digestion and then diluted them to 5×10^4 cells/ml and set them aside. A 24-well plate was taken to wrap the cells with matrix glue and place them in the incubator for 1 hour. After glue fixation, 200 μl of diluted cell suspension was added. We added 600 μl of 20% PBS medium to each lower chamber. We gently swabbed the upper luminal cells with a cotton swab after 32 h of incubation. We counted the number of cells invading and crossing the lumen after fixation staining under the microscope.

2.2.11. CCK-8 Cell Proliferation. First, ECA109 cells and OE33 cells were inoculated into 96-well plates at an inoculation density of 3000 cells/well. The transfection was detected at 1, 2, 3, 4, and 5 days after transfection. Add CCK-8 reagent to each well, and incubate it in a cell culture box for 1 hour. Keep it out of the light. Then the absorbance at 450 nm was measured by a microplate reader, and the cell growth curve was drawn.

2.2.12. Flow Cytometry Detection Cell Cycle. We added 70% precooled ethanol after cell digestion, PBS washing, and rehanging and placed it overnight in a 4°C refrigerator. Ethanol attached to the cell surface was washed with PBS, and PI solution containing RNA enzyme was used to stain for half an hour (incubators at 37°C were kept away from light). Flow cytometry was used for detection.

2.2.13. Tumorigenesis Experiment in Nude Mice. We split the nude rats randomly into 2 groups of 4 rats each. ECA109 cell control group and positive group with good growth after treatment were selected to make single-cell suspension and counted. RPMI1640 and matrix glue were mixed in a ratio of 1 : 2, and cells were diluted and inoculated in the right axilla of nude mice, with the inoculation amount of about 5×10^6 cells. After the subcutaneous nodules were observed to be visible to the naked eyes, we estimated the tumor size weekly over approximately 41 days. We exfoliated subcutaneous tumors and photographed them after the death of nude mice. We performed Western blot to measure the EMT-related protein expression.

2.2.14. The Expression of KI67 and IPO5 Was Detected by Immunohistochemistry. According to the steps of dewaxing, rehydration, antigen repair, sealing, incubation of primary antibody, incubation of secondary antibody, DAB color, nuclear redyeing, dehydration, sealing, and finally observation and statistics under the microscope, the nuclei of KI67

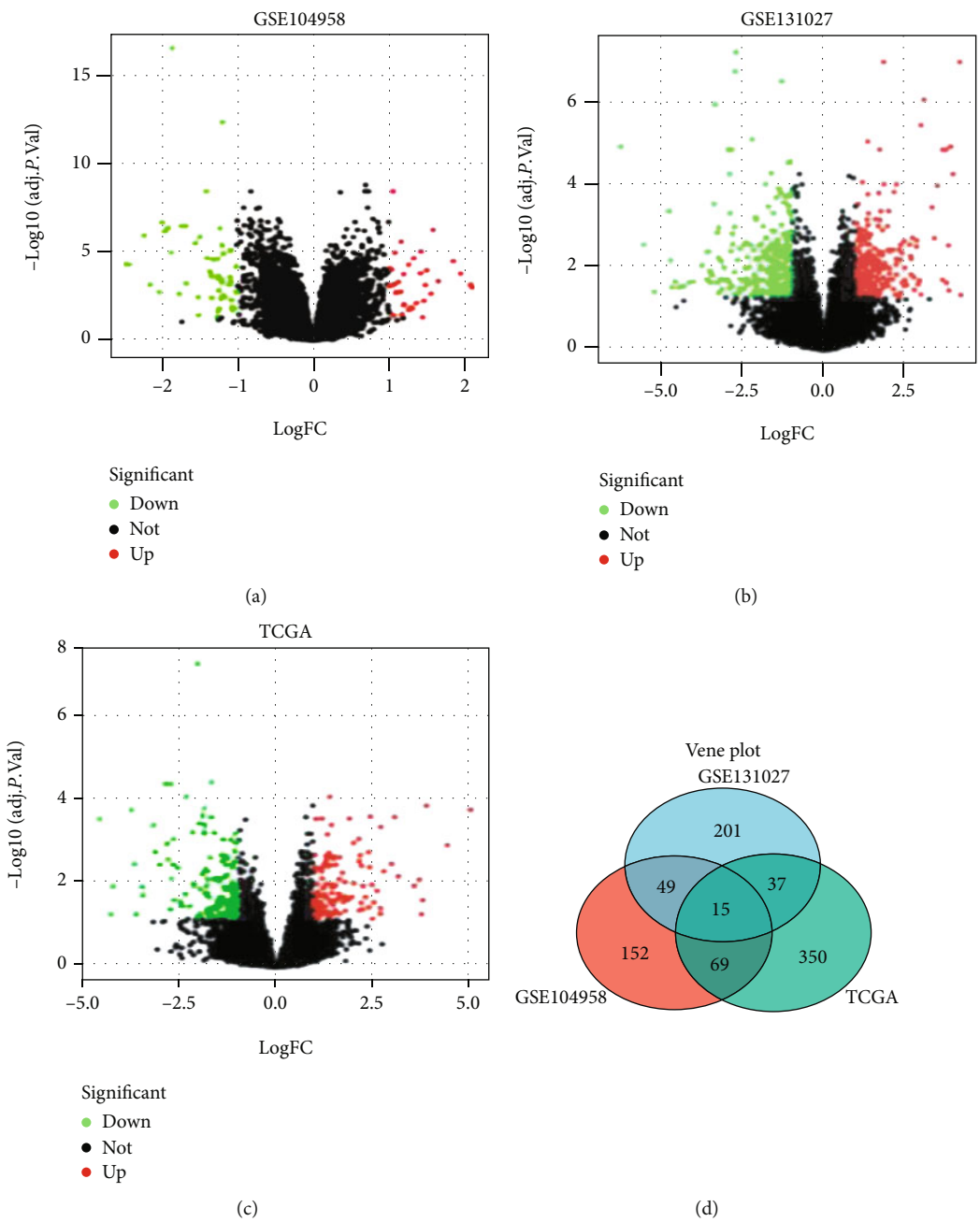

Figure 1: Differentially expressed genes between esophageal cancer and normal tissues. (a–c) Volcanic map of differentially expressed genes between esophageal cancer tissues and normal esophageal tissues. IPO5 is highly expressed in esophageal cancer tissues. (d) Venn diagram distribution of differentially expressed genes from GSE104958 and GSE131027 arrays and TCGA database. As shown in the figure, a total of 15 genes showed specific differential expression in three datasets.

were brown granules. Four fields were randomly selected under the microscope, and the positive rate of each field = number of positive cells/total cells × 100%. The statistical index of IPO5 was that the proportion of positive staining tissues was <10%, 10%-30%, 30%-50%, and >50%, and then 0-3 points were counted successively. According to the intensity of staining, the tissues were divided into no staining, light yellow, dark yellow, and dark brown, and 0-3 points were counted successively. The two scores were multiplied to obtain the total score.

2.2.15. Western Blot Test. With the total protein concentration, the protein test cell loading buffer diluted the protein. After electrophoresis, transferring, and closing operations, the primary antibody was manually diluted according to the primary antibody at 4 degrees in the freezer overnight. PBS was repeatedly added and shaken on a shaker for 10 minutes and washed three times. Secondary antibody was added, incubated in a shaker for 1 hour according to the instructions, and enhanced with three more washes of PBS at room temperature.

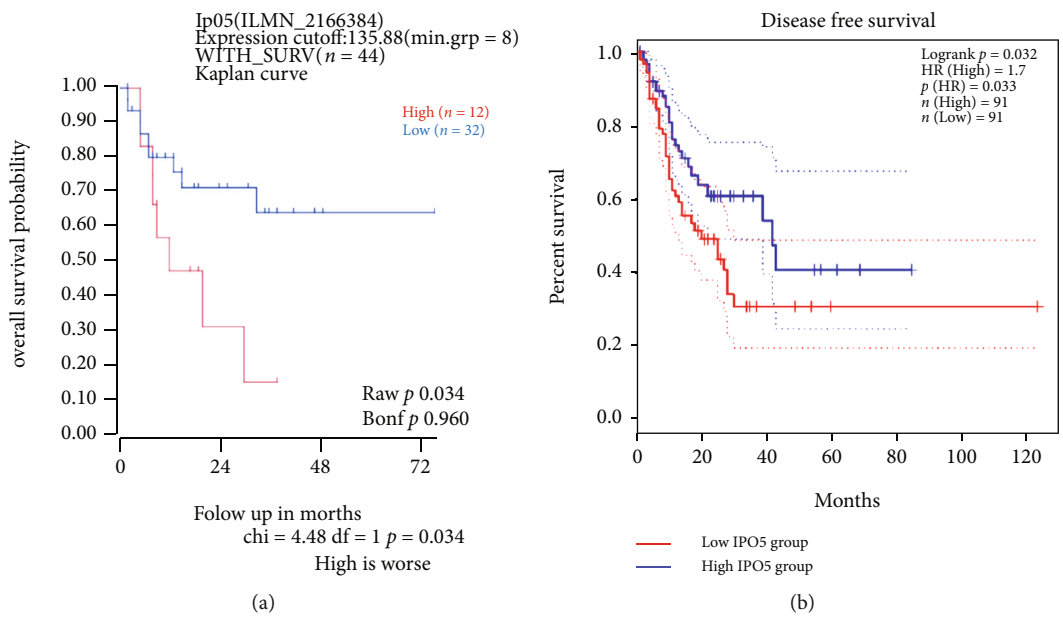

Figure 2: The prognostic value of IPO5 in esophageal cancer. (a) There was a great difference in survival between the two groups with high and low IPO5 expression ($P = 0.034$). (b) The high IPO5 expression group had worse disease-free survival than the low IPO5 expression group ($P = 0.032$).

2.3. Statistical Analysis. We analyzed the statistics using the R (V.3.5.1) and SPSS software. We drew pictures going with GraphPad Prism 7. Through an independent t-test, we compared continuous data between the two groups. $P < 0.05$ was used as the difference was statistically significant. One-way ANOVA was applied to compare data between multiple groups. Chi-square was applied to test for declassified information.

3. Results

3.1. Screening of Differential Genes (DEGs). DEG (i.e., GSE104958 and GSE131027) was analyzed using the limma software package after pretreatment and elimination of batch impact. Fifteen DEGs were obtained with $P < 0.05$ and $|\log FC|$ 1 or 1 as the threshold and intersected with TCGA database DCG (Figure 1(d)). According to $|\log FC|$, the values of the volcano show a rise in red marker genes and green marker genes (Figures 1(a)–1(c)). Ultimately, the IPO5 gene was screened and found to be differentially expressed, in esophageal cancer tissue versus normal tissue.

3.2. IPO5 Is a Prognostic Predictor of Esophageal Cancer. In the prognosis prediction of esophageal cancer, R2 and GEPIA databases were used to go for survival analysis for determining the functions of IPO5 expression. Compared to patients with low IPO5 expression, this result showed that disease-free survival in high IPO5 patients was shorter with a statistically significant difference (Figure 2). It is indicated that IPO5 may be related to a bad prognosis.

Based on the analysis of enrichment of MSigDB (c2. Cp. Kegg. V6.2. Symbols. GMT), GSEA results show the distinction between the two groups was statistically significant. The 4 most significantly enriched signaling pathways are in the IPO5 high group. By contrast, in the low-expression group of IPO5, the four most significantly enriched signaling pathways were oxidative phosphorylation, Parkinson's disease, phenylalanine metabolism, and arachidonic acid metabolism (Figure 3).

3.3. IPO5 Expression Is Related to the Immune System. Based on earlier research, there is a great correlation between the tumorigenesis and immune system.

As a result, the PO5 effect on immune factors needs to be further investigated. It was discovered a great negative relationship between IPO5 and tumor immune lymphocytes, immunosuppressants, immune activators, and chemokines ($P < 0.001$) (Figure 4).

3.4. IPO5 Is Upregulated in Esophageal Carcinoma Cells. In our previous experiment, through applying the database, IPO5 was analyzed as the differentially expressed gene between these two esophageal tissues. Subsequently, we collected postoperative specimens of clinical esophageal cancer patients for immunohistochemical experiments to further verify the above conclusions. Compared with normal esophageal normal tissues next to cancer, based on IPO5 expression in 6 pairs of esophageal cancer tissues and normal tissues, there was a significant upregulation of the expression level of IPO5 in tumor tissues, and cytoplasmic staining was primarily used to detect IPO5 ($P < 0.05$) (Figure 5).

3.5. Expression of IPO5 in Various Esophageal Cancer Cells. IPO5 expression was measured by QRT-PCR. In esophageal cancer cells, the IPO5 expression was greatly higher than in normal human esophageal epithelial cells (HEEC),

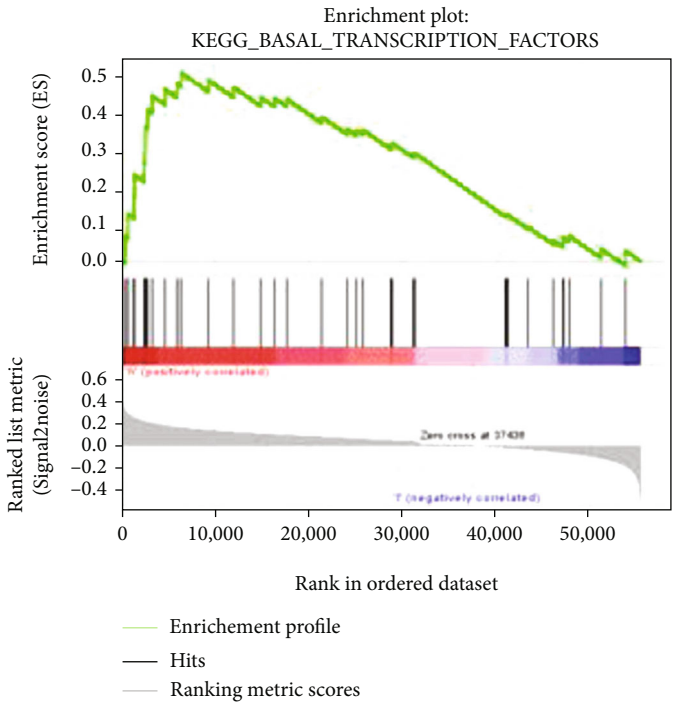

(a)

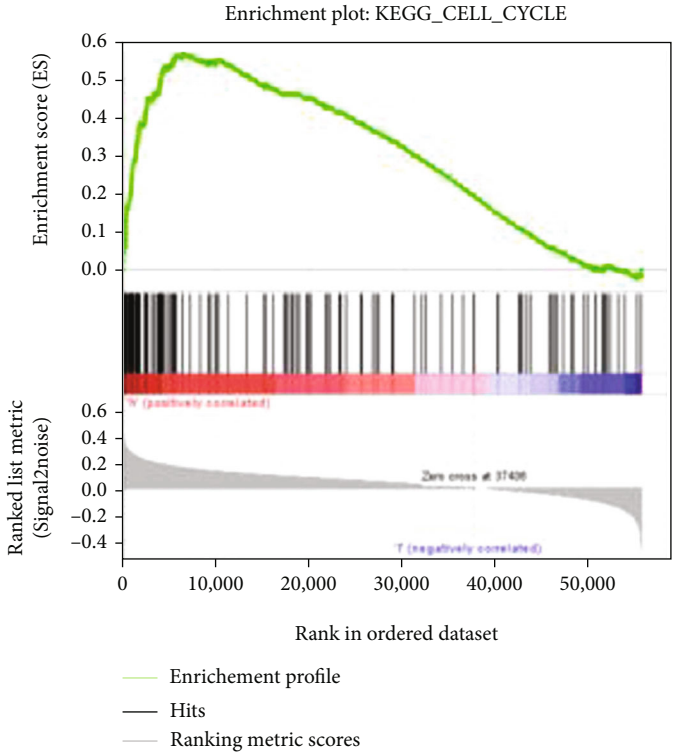

(b)

Figure 3: Continued.

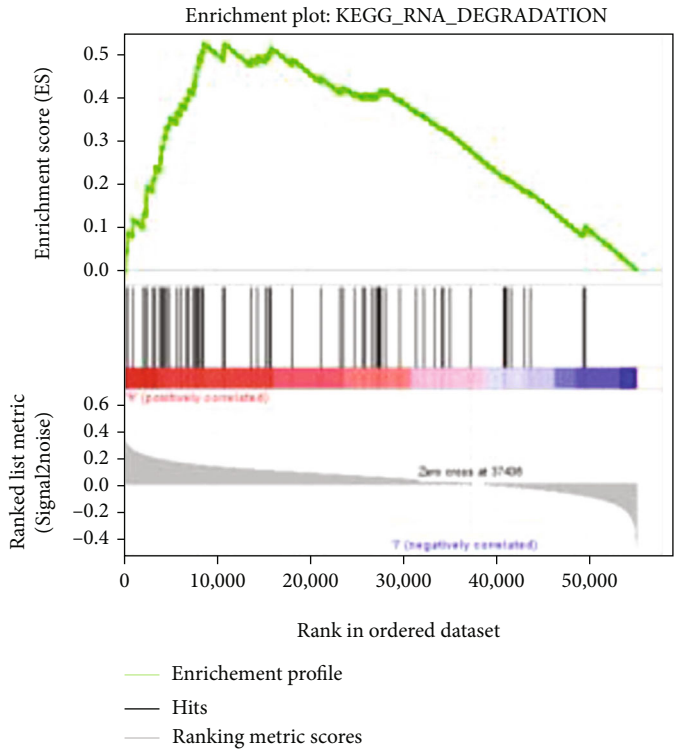

(c)

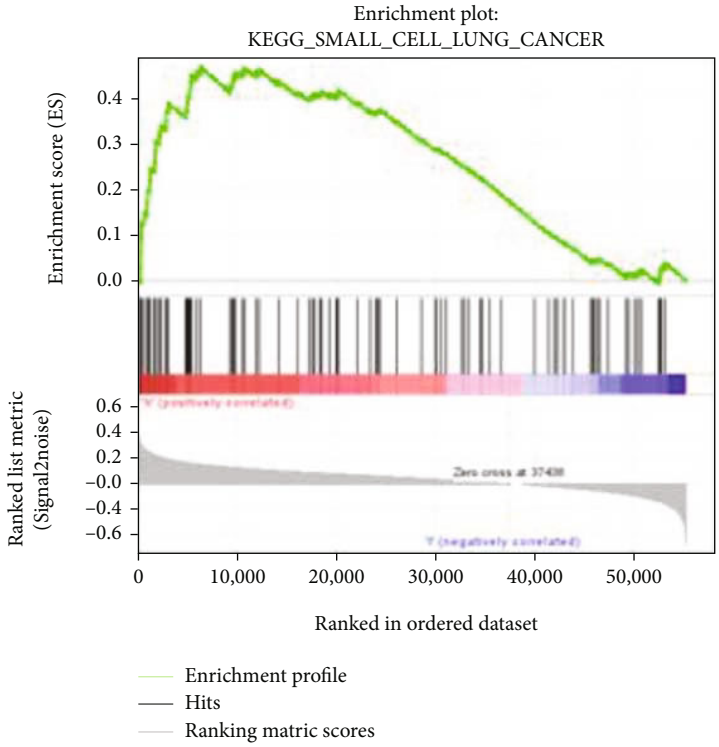

(d)

Figure 3: Continued.

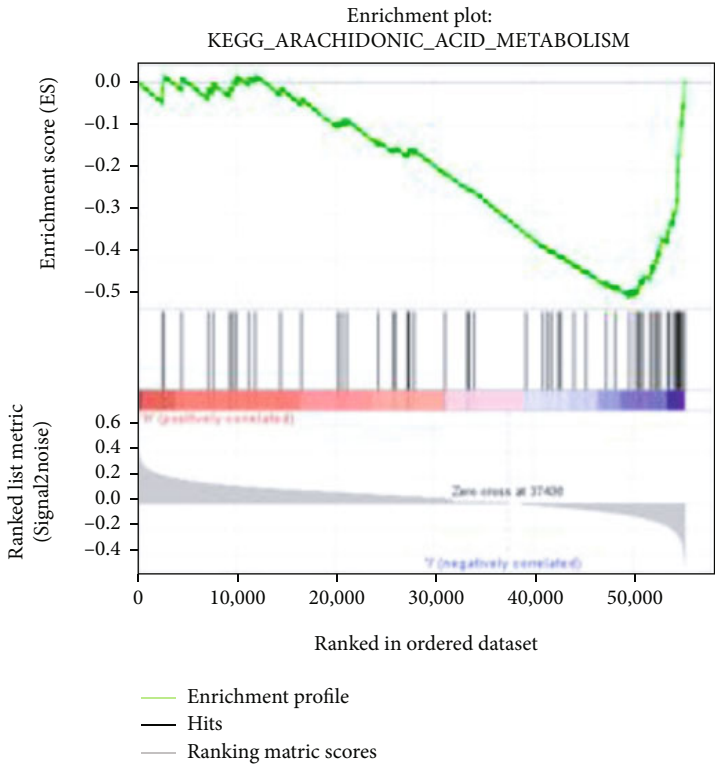

(e)

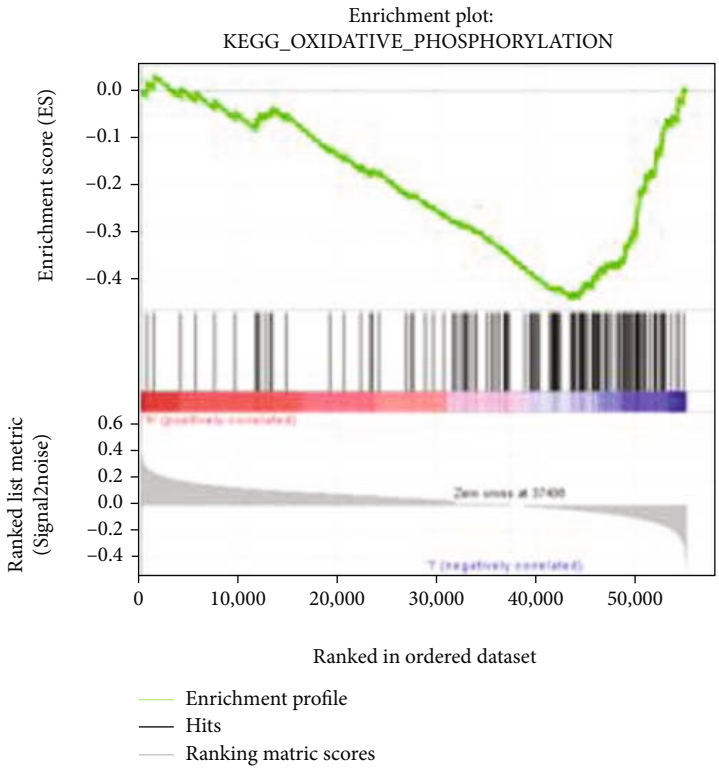

(f)

Figure 3: Continued.

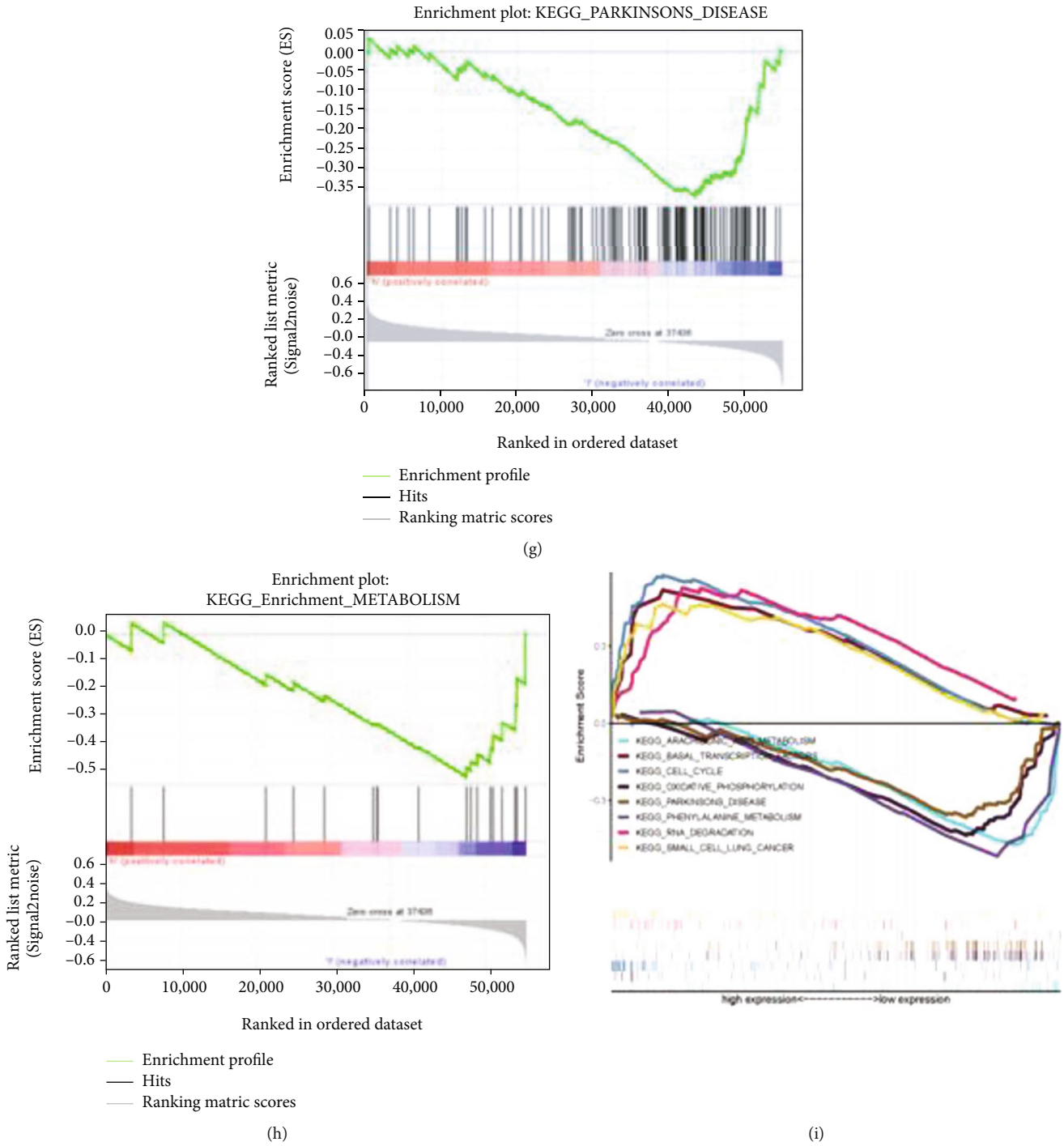

Figure 3: IPO5 enrichment analysis diagram based on GSEA. GSEA presented both group's expression was mainly enriched in (a) basic transcription factors, (b) cell cycle, (c) RNA degradation, (d) small cell lung cancer, (e) oxidative phosphorylation, (f) Parkinson's disease, (g) phenylalanine metabolism, and (h) arachidonic acid metabolism, in 8 pathways. NES: normalized enrichment score; ES: concentration score; FDR: error detection rate.

especially in ECA-109 and OE33 cells ($P < 0.01$) (Figure 6(a)). Subsequently, Western blot was applied to ECA109 and OE33 cells to verify the transfection effect of IPO5, and it was found that the expression of IPO5 decreased after interference. Therefore, ECA109 and OE33 cell lines were used for the following experiments. This study split cancer cells into sh-IPO5 and sh-NC groups based on whether they were transfected with IPO5 lentivirus or not (Figure 6(b)).

3.6. Interference with IPO5 Inhibits the Invasion, Migration, and Proliferation of Esophageal Cancer Cells. Figure 7(a) presents that in the scratch test of ECA109 cells and OE33

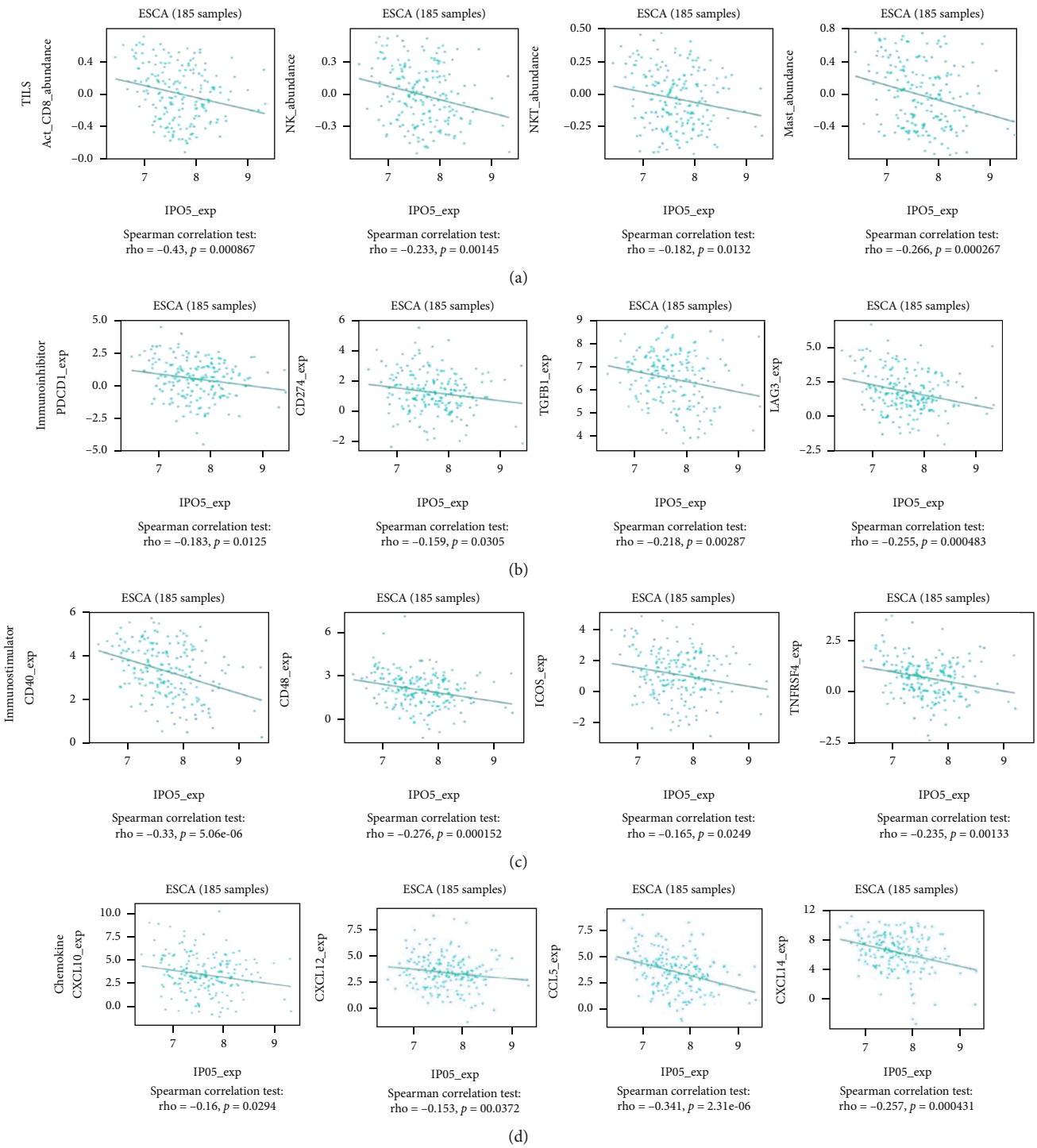

Figure 4: The expression of IPO5 is related to the immune system. IPO5 was significantly correlated with tumor immune lymphocytes, immunosuppressants, immune activators, and chemokines ($P < 0.001$).

cells, we found that the ability of the sh-IPO5-positive group to transfer had a declined ground migration capacity ($P < 0.01$) than the control group. As shown in Figure 7(b), it was found that the positive group in the Transwell invasion test has a weaker invasive capacity ($P < 0.01$). Figure 7(c) presents the CCK-8 experiment, compared with the control group, and we found that with the increase of days, the positive group had a weaker cell proliferation ability ($P < 0.05$). In summary, esophageal cancer cells' reduced migration, invasion, and proliferation can be affected by reduced IPO5 gene expression.

3.7. Cell Growth Cycle Was Inhibited after IPO5 Interference. We utilized flow cytometry to measure changes in the cell cycle before and after IPO5 gene silencing. It was discovered that compared with the control group, ECA109 and OE33

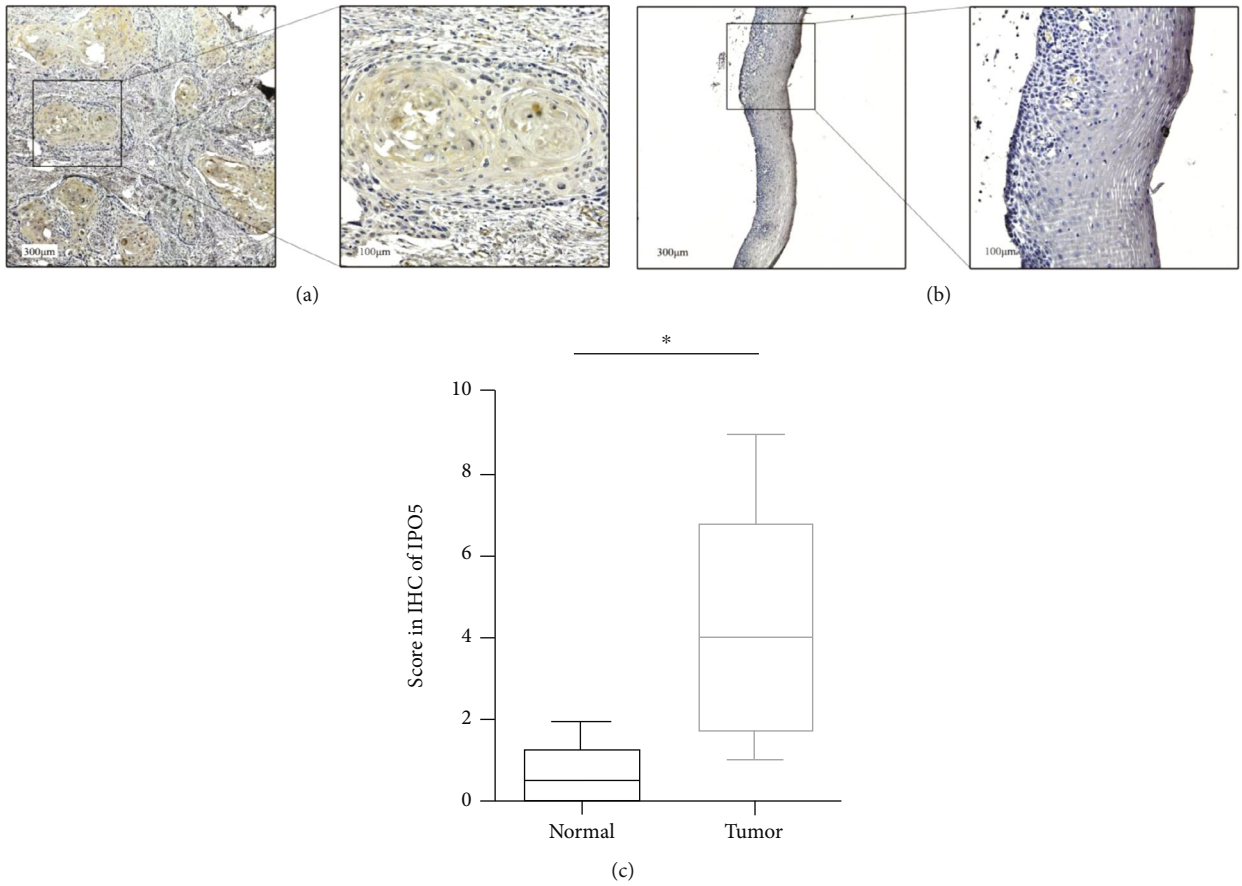

Figure 5: IPO5 expression in 6 patients with esophageal cancer was higher in cancer tissues than in adjacent tissues. (a) Esophageal cancer tissues showed high IPO5 expression. (b) Low expression of IPO5 in normal tissues of esophageal cancer. (c) Increased expression of IPO5 in cancer tissues was calculated by the immunohistochemical score in 6 patients with esophageal cancer (note: $^{*}P < 0.05$).

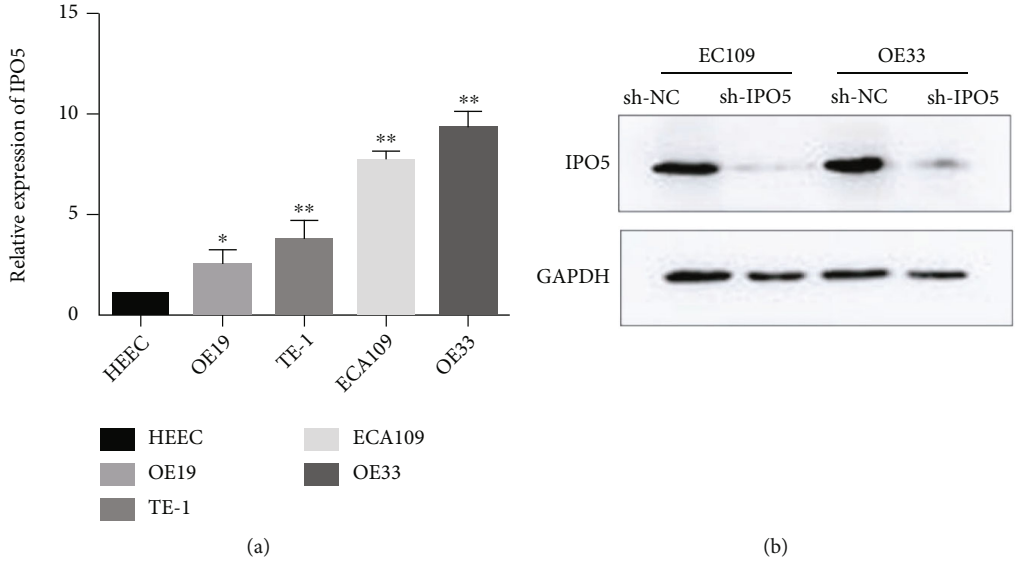

Figure 6: (a) QRT-PCR analysis presented that IPO5 expression in esophageal cancer cell lines was higher than that in normal HEEC esophageal cells, and the highest expression was found in OE33 and ECA109 cells. (b) Western blot assay showed that the expression of IPO5 was significantly downregulated after interference with IPO5 lentivirus by esophageal carcinoma cells (note: $^{*}P < 0.05$; $^{**}P < 0.01$).

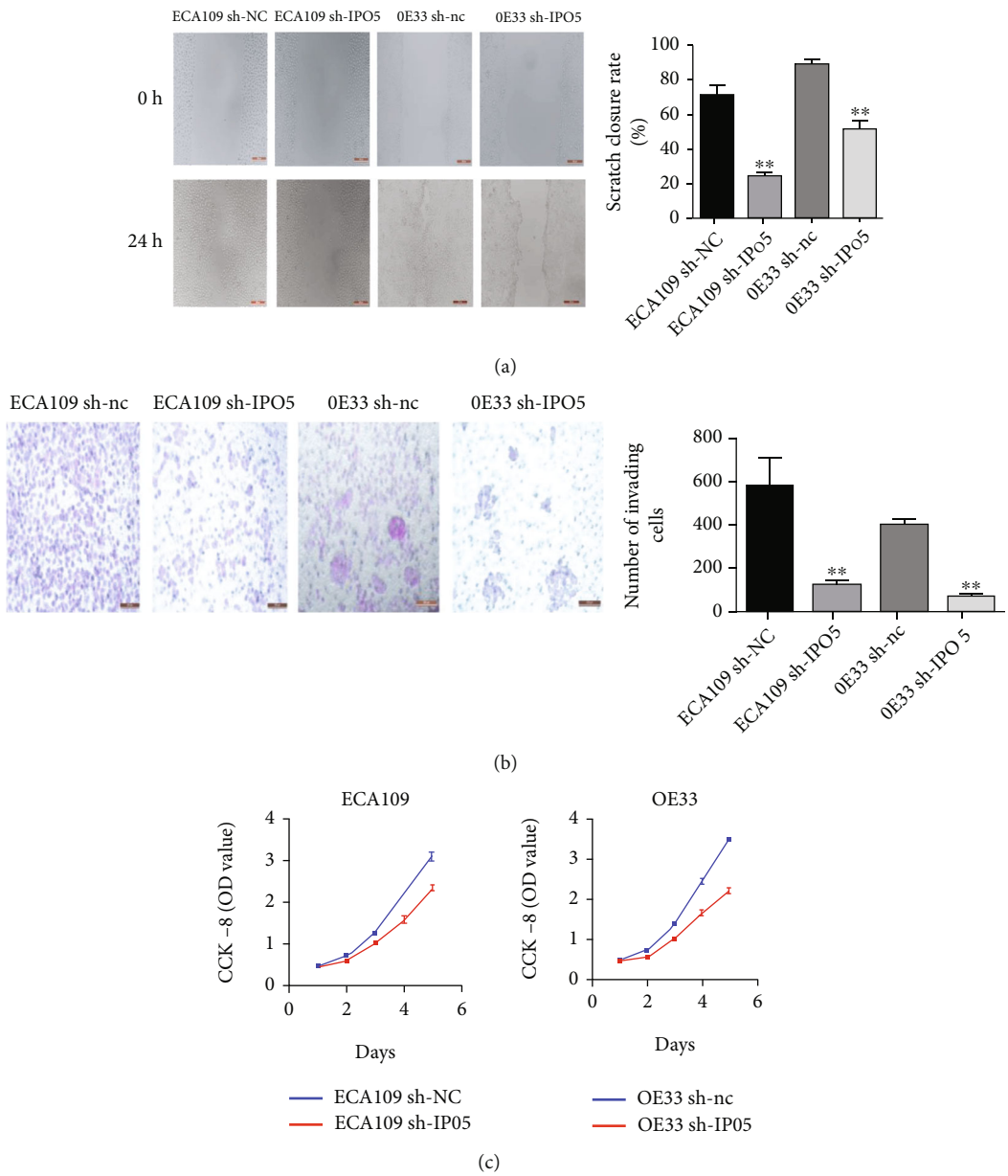

Figure 7: (a) Cell scratch test presented that the closure rate of the sh-IPO5 group was lower than that of the sh-NC group at 24 h. (b) Transwell invasion test presented the number of cells crossing the chamber was increased in the sh-NC group compared with the sh-IPO5 group. (c) CCK-8 analysis of sh-IPO5 reduced the viability of ECA109 and OE33 cells (note: $^{*}P < 0.05$; $^{**}P < 0.01$).

cell proportion in the G2/M stage was greatly aggrandized in the sh-IPO5 group.

The changes in the cell cycle before and after IPO5 gene silencing were detected by flow cytometry. It was found the ratio of ECA109 and OE33 cells in the G2/M phase was greatly aggrandized in the sh-IPO5 group ($P < 0.01$), indicating interference with IPO5 can promote G2/M phase arrest of esophageal cancer cells (Figure 8).

3.8. Tumorigenesis Experiment in Nude Mice. The nude mouse model was established and tumor sizes were documented weekly to deeply validate the IPO5 gene role in esophageal cancer. It was observed that tumor growth was greatly slower in the IPO5 knockout group compared to the negative control group ($P < 0.01$) (Figure 9(a)). Subsequently, the KI67expression was verified by immunohistochemistry, and the KI67expression level was found to be significantly reduced in the IPO5 gene silencing group ($P < 0.01$) (Figure 9(b)), suggesting IPO5 had an accelerating effect on esophageal cancer development.

3.9. Interference with IPO5 Inhibits Ras Signaling Pathway. In the sh-NC and sh-IPO5 groups of nude mouse tumors, we examined the expression of RAS pathway-related proteins MEK, P-MEK, ERK, P-ERK, AKT, and P-AKT by Western blot. The findings revealed there was a big down-regulation of P-MEK, P-ERK, and P-AKT expressions after interference by IPO5. There were no obvious modifications

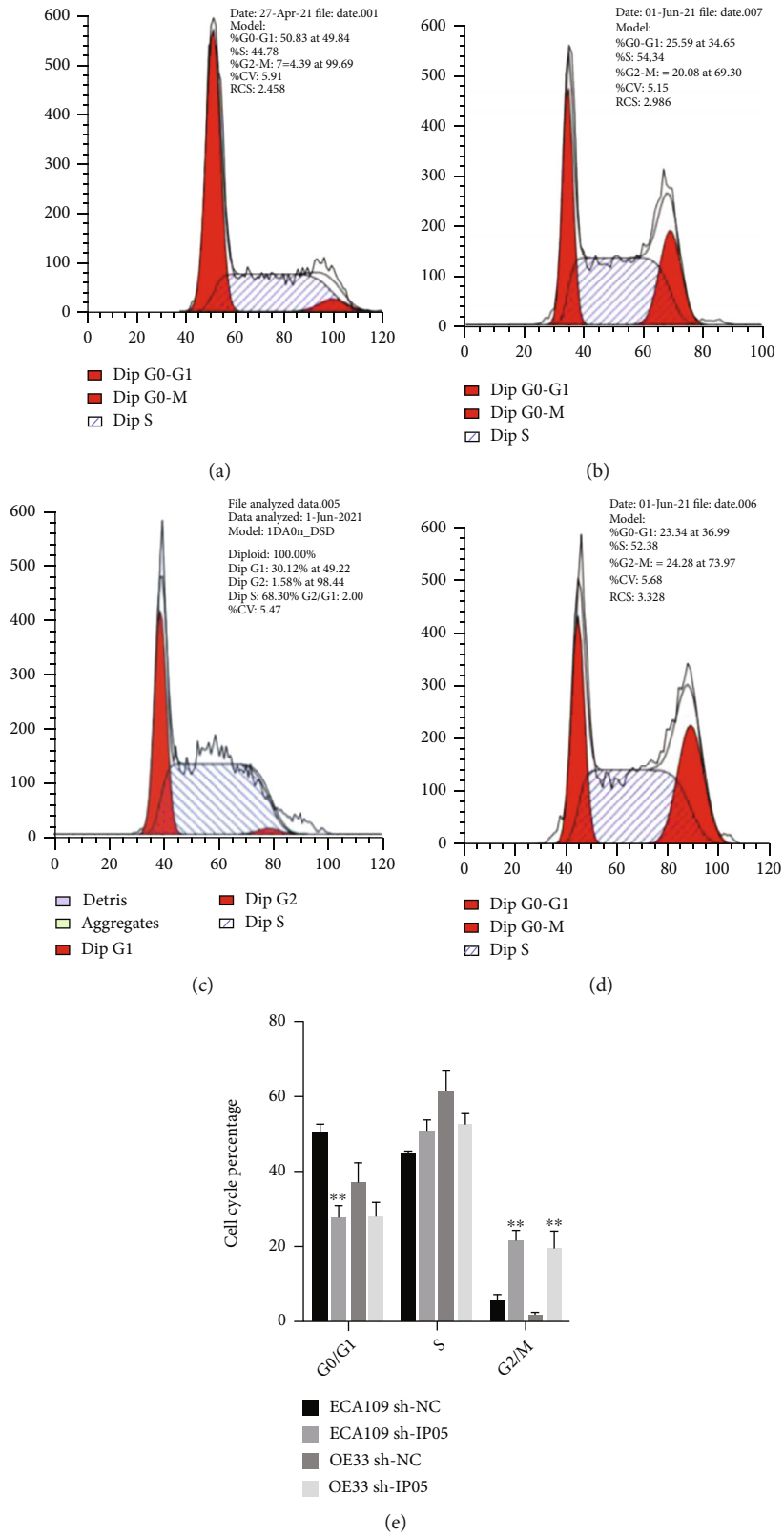

Figure 8: Cell cycle changes before and after IPO5 gene silencing detected by flow cytometry. (a, b) The proportion of G2/M phase increased before and after transfection of ECA109 cells. (c, d) The proportion of G2/M phase in OE33 cells increased before and after transfection. (e) The proportion of ECA109 and OE33 cells in the sh-IPO5 group was significantly higher than that in the sh-NC group in the G2/M phase (note: $^{**}P < 0.01$).

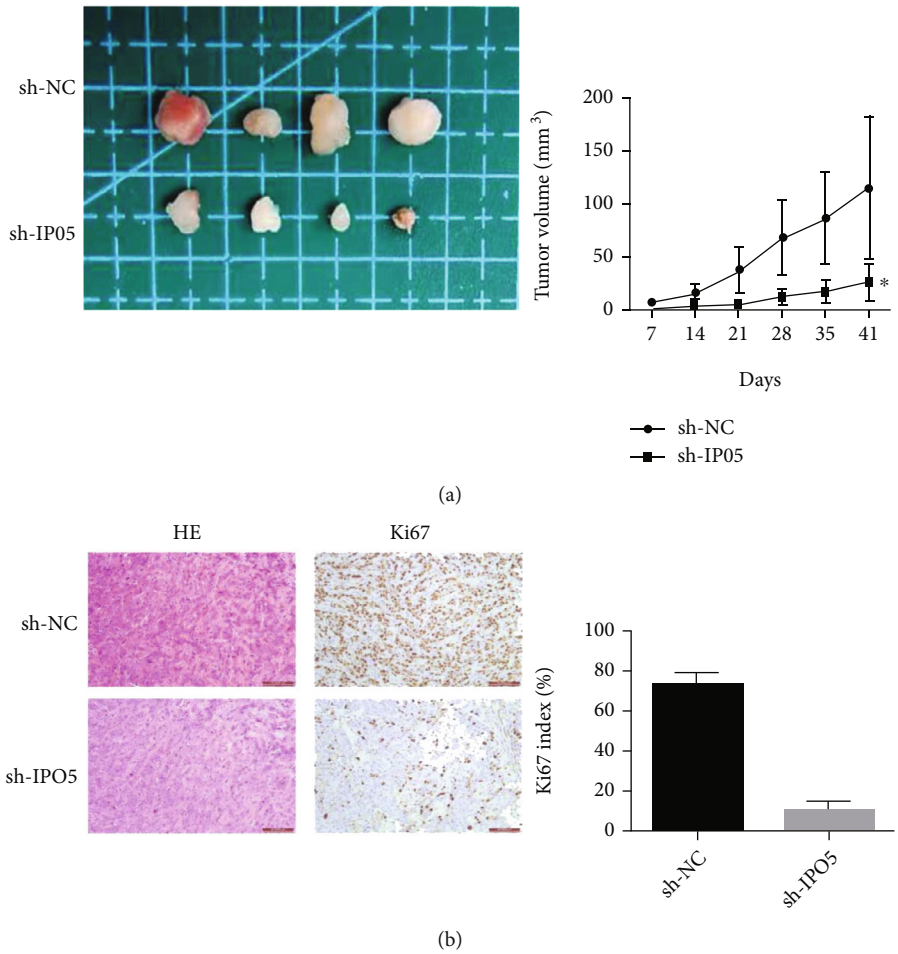

Figure 9: (a) Tumor formation experiment in nude mice presented that the growth rate of nude mice in the positive group was significantly lower than that in the negative control group. (b) Immunohistochemical test presented that KI67 expression in the positive group was significantly lower than that in the negative control group (note: $^{**}P < 0.01$).

in total protein expression ($P < 0.01$) (Figure 10), indicating that progression into esophageal cancer can be promoted by IPO5 through the RAS signaling pathway.

3.10. Interference with IPO5 Inhibits Epithelial-Mesenchymal Transformation. The IPO5 impact on epithelial transformation-related protein expression was identified by Western blot. Compared with the control group, the outcomes revealed that N-cad, Vimentin, and Slug protein expression levels were remarkably reduced in the IPO5 gene silencing group ($P < 0.05$) (Figure 11), suggesting that IPO5 promotes the occurrence of EMT-induced esophageal cancer.

4. Discussion

Nowadays, one of the world's deadliest tumors includes malignant tumors of the esophagus. Statistics show that Asia accounts for 80% of the total global incidence of disease about 21 incidence of esophageal cancer, and the symptoms are hardly found at the early stage [21]. Moreover, the advanced cancer patient's quality of life plummeted, and the survival rate is extremely low. However, people now more and more realize the importance of screening in ordinary times, and early diagnosis of esophageal cancer detection index is imminent.

In the process of nuclear plasma transport, karyopherins play an essential role as transport officers, including nuclear input proteins and export proteins [22]. Currently, nuclear transporters have been implicated in cancer progression. XPO-t overexpression is associated with poor outcomes in breast, ovarian, and mesothelioma [23, 24]. According to previous research, there was a relationship between cancer staging and prognosis CAS and overexpression in cancer cells [25]. IPO5 overexpression may occur in bladder cancer, thyroid cancer, breast cancer, malignant melanoma, colorectal cancer, etc. [26, 27]. It has been reported that DDX56 can inhibit the introduction of IRF3 nuclei by destroying the assembly of IRF3-IPO5, thereby inhibiting type I interferon, and thereby regulating antiviral innate immunity [28]. Relevant studies have shown that the expression level of IPO5 is significantly correlated with tumor immune lymphocytes, immunosuppressants, immune activators, and chemokines, which indicates that IPO5 can participate in tumor immune

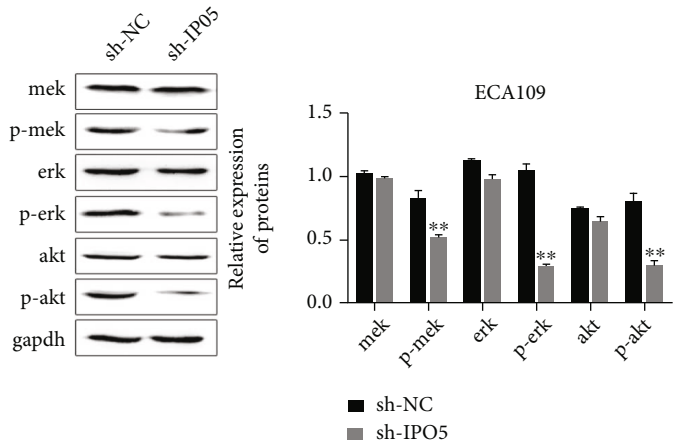

Figure 10: Western blot analysis showed that knockdown of IPO5 gene significantly reduced the expressions of P-MEK, P-ERK, and P-AKT but had no significant effect on the expressions of MEK, ERK, and AKT (note: $^{**}P < 0.01$).

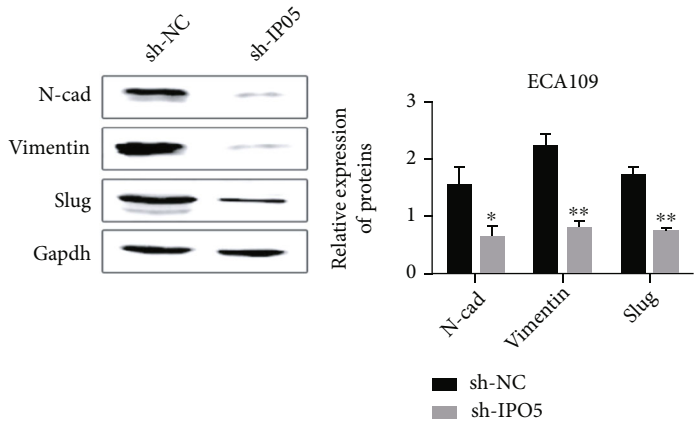

Figure 11: Western blot analysis showed that knockdown of IPO5 gene significantly reduced the expression of N-cad, Vimentin, and Slug (note: $^{*}P < 0.05$; $^{**}P < 0.01$).

microenvironment and mediate tumor immune response [29, 28]. The reduction of Wnt target genes expression involved in the development of various benign and malignant tumors can be achieved by the deletion of IPO5. Human herpetic virus 8 (HHV-8) binds to IPO5mRNA, leading to Kaposi's sarcoma [8]; IPO5 mediates RASAl2 nuclear transport to accelerate the colorectal cancer cells proliferation and migration [9]. Cell scratching, invasion and proliferation experiments, flow cytometry, and tumorigenesis experiments in nude mice in this study were used to fully demonstrate that the IPO5 gene can improve esophageal cancer proliferation, differentiation, and occurrence. Through a certain pathway, we speculated that IPO5 may accelerate cancer cell propagation.

Activation of the Wnt/β-catenin pathway has been considered related to EMT. The classical Wnt pathway inhibits GSK-3β-mediated β-catenin and plays a role in phosphorylation and degradation. Ning et al. proposed that the Wnt/GSK-3β/β-catenin pathway explored the change process of S100A4-induced mesenchymal transformation of nasal mucosal epithelial cells from molecular mechanism to cell morphology, which laid a foundation for the systematic analysis of the mechanism of nasal mucosal tissue remodeling and the search for new targets for treatment [30]. The activated AS-ERK signaling pathway is present in many cancers. RAS protein acts as a molecular switch. In the inactive state, and the conversion of GTP to GDP results in the activation of GTPase in RAS genes [31]. Activated GTP-binding RAS further transmits the signal to the downstream RAF-MEK-ERK signal cascade. In turn, various transcription factors in the nucleus are activated, thus affecting cell proliferation and differentiation, promoting cancer invasion and metastasis, etc. [32]. The RAS-ERK pathway is involved in many cancer developments. Research on the RAS-ERK signaling pathway has been increasing in recent years. For example, tumorigenic Sergi-mediated transcription in prostate cells could be adjusted by RAS-ERK and PI3K-AKT signaling pathways differentially [33]. Vemurafenib significantly reduced the proliferation of melanocyte nevus by targeting the RAS-ERK pathway [34]. Modulators of the

RAS-ERK pathway can be used as therapeutic targets for thyroid cancer [35]. Inhibition of the RAS-ERK pathway provides a novel therapeutic strategy for gemcitabine-resistant pancreatic cancer [36]. Related literature has shown that GTPase activator protein 1 (IQGAP1) can induce tumor biology based on the regulation of the RAS pathway and participates in diverse cell processes involving cell transfer, propagation, and cycle after binding with actin. At the same time, IPO5 can regulate the transcription of IQGAP1 protein, so we speculated that IPO5 can promote the progression of esophageal cancer through the RAS pathway. To verify this hypothesis, we measured low IPO5 expression influence on RAS pathway-related proteins through Western blot, and it was found that when IPO5 was knocked down, the expression of phosphorylated proteins P-ERK, P-MEK, and P-AKT was significantly reduced, while the total expression of ERK, MEK, and AKT was not significantly changed, hence the above corollary.

Epithelial-mesenchymal transition (EMT) is a process in which epithelial cells acquire mesenchymal characteristics. In cancer, EMT is related to tumor occurrence, invasion, metastasis, and drug resistance. Recently, it has been proved that EMT is not a binary process but occurs through different cell states, and different EMT states have different regulatory mechanisms for cancer. Proliferation, plasticity, invasion, and metastasis are related to different EMT states. We summarized the role of transcriptional and epigenetic landscapes, gene regulatory networks, and their surrounding niches in controlling the transition through different EMT states [37, 38]. A growing body of literature highlights the link between cancer-related EMT, which stimulates cancer cells to produce proinflammatory factors, and chronic inflammation. In contrast, the getting of EMT-like features in cancer cells can be facilitated by inflammatory mediators such as oxidative stress, soluble factors, or hypoxia. Therefore, the two phenomena may reinforce each other, making the body more prone to the formation of metastatic lesions [39]. In our experiment, we found that IPO5 was significantly negatively correlated with tumor immune lymphocytes, immunosuppressants, immune activators, and chemokines. Western blot also confirmed that IPO5 could promote the epithelial-mesenchymal transformation of esophageal cancer. It can be concluded from the above discussion that IPO5 can be used as a new biological marker to give a novel perspective for future cancer diagnosis and therapy. However, as a kind of nuclear transporter, IPO5 can cooperate with related proteins to enter the nucleus to regulate cancer-related signaling pathways, and our research mechanism in this aspect is limited. As a result of the small sample size collected clinically, some errors might exist, which we will continue to improve in future experiments.

5. Conclusion

In conclusion, the gene that triggers esophageal cancer is IPO5, and EMT mediated through the RAS pathway accelerated the progression of esophageal cancer and may be a promising targeted therapy to eradicate early-stage esophageal cancer.

Data Availability

The datasets used and/or analyzed during the current study are available from the corresponding authors on reasonable request.

Conflicts of Interest

The authors declared no potential conflicts of interest with respect to the research, authorship, and/or publication of this article.

Authors' Contributions

Meiyu Li and Shujia Chen contributed equally as co-first author.

References

[1] D. J. Uhlenhopp, E. O. Then, T. Sunkara, and V. Gaduputi, "Epidemiology of esophageal cancer: update in global trends, etiology and risk factors," *Clinical Journal of Gastroenterology*, vol. 13, no. 6, pp. 1010–1021, 2020.

[2] W. Chen, R. Zheng, P. D. Baade et al., "Cancer statistics in China, 2015," *CA: a Cancer Journal for Clinicians*, vol. 66, no. 2, pp. 115–132, 2016.

[3] F. L. Huang and S. J. Yu, "Esophageal cancer: risk factors, genetic association, and treatment," *Asian Journal of Surgery*, vol. 41, no. 3, pp. 210–215, 2018.

[4] M. J. Domper Arnal, Á. Ferrández Arenas, and Á. Lanas Arbeloa, "Esophageal cancer: risk factors, screening and endoscopic treatment in Western and Eastern countries," *World Journal of Gastroenterology*, vol. 21, no. 26, pp. 7933–7943, 2015.

[5] T. Çağatay and Y. M. Chook, "Karyopherins in cancer," *Current Opinion in Cell Biology*, vol. 52, pp. 30–42, 2018.

[6] R. Patouret, "The nuclear transport protein Importin-5: a promising target in oncology and virology," *Chimia*, vol. 75, no. 4, pp. 319–322, 2021.

[7] T. Goto, A. Sato, S. Adachi, S. Iemura, T. Natsume, and H. Shibuya, "IQGAP1 protein regulates nuclear localization of β-catenin via importin-β5 protein in Wnt signaling," *The Journal of Biological Chemistry*, vol. 288, no. 51, pp. 36351–36360, 2013.

[8] L. Quan, T. Qiu, J. Liang, M. Li, Y. Zhang, and K. Tao, "Identification of target genes regulated by KSHV miRNAs in KSHV-infected lymphoma cells," *Pathology Oncology Research*, vol. 21, no. 4, pp. 875–880, 2015.

[9] W. Zhang, Y. Lu, X. Li et al., "IPO5 promotes the proliferation and tumourigenicity of colorectal cancer cells by mediating RASAL2 nuclear transportation," *Journal of Experimental & Clinical Cancer Research*, vol. 38, no. 1, p. 296, 2019.

[10] P. J. van der Watt, A. Chi, T. Stelma et al., "Targeting the nuclear import receptor Kpnβ1 as an anticancer therapeutic," *Molecular Cancer Therapeutics*, vol. 15, no. 4, pp. 560–573, 2016.

[11] R. Lapalombella, Q. Sun, K. Williams et al., "Selective inhibitors of nuclear export show that CRM1/XPO1 is a target in chronic lymphocytic leukemia," *Blood*, vol. 120, no. 23, pp. 4621–4634, 2012.

[12] A. Herrero and P. Crespo, "RAS dimers: the novice couple at the RAS-ERK pathway ball," *Genes*, vol. 12, no. 10, p. 1556, 2021.

[13] S. Choi and R. A. Anderson, "And Akt-ion! IQGAP1 in control of signaling pathways," *The EMBO Journal*, vol. 36, no. 8, pp. 967–969, 2017.

[14] K. M. Zoheir, A. A. Abd-Rabou, G. I. Harisa et al., "IQGAP1 gene silencing induces apoptosis and decreases the invasive capacity of human hepatocellular carcinoma cells," *Tumour Biology*, vol. 37, no. 10, pp. 13927–13939, 2016.

[15] J. S. Turner, "A new cytoskeletal connection for APC: linked to actin through IQGAP," *Developmental Cell*, vol. 7, no. 6, pp. 778–780, 2004.

[16] D. Zhou, Z. Wei, S. Deng et al., "SASH1 regulates melanocyte transepithelial migration through a novel Gαs- SASH1-IQGAP1-E-Cadherin dependent pathway," *Cellular Signalling*, vol. 25, no. 6, pp. 1526–1538, 2013.

[17] M. A. Johnson, M. Sharma, M. T. Mok, and B. R. Henderson, "Stimulation of in vivo nuclear transport dynamics of actin and its co-factors IQGAP1 and Rac1 in response to DNA replication stress," *Biochimica et Biophysica Acta*, vol. 1833, no. 10, pp. 2334–2347, 2013.

[18] H. H. Erdemir, Z. Li, and D. B. Sacks, "IQGAP1 binds to estrogen receptor-α and modulates its function," *The Journal of Biological Chemistry*, vol. 289, no. 13, pp. 9100–9112, 2014.

[19] F. Zeng, W. Jiang, W. Zhao, Y. Fan, Y. Zhu, and H. Zhang, "Ras GTPase-activating-like protein IQGAP1 (IQGAP1) promotes breast cancer proliferation and invasion and correlates with poor clinical outcomes," *Medical Science Monitor*, vol. 20, no. 24, pp. 3315–3323, 2018.

[20] X. Peng, T. Wang, H. Gao et al., "The interplay between IQGAP1 and small GTPases in cancer metastasis," *Biomedicine & Pharmacotherapy*, vol. 135, article 111243, 2021.

[21] H. Sung, J. Ferlay, R. L. Siegel et al., "Global Cancer Statistics 2020: GLOBOCAN estimates of incidence and mortality worldwide for 36 cancers in 185 countries," *CA: a Cancer Journal for Clinicians*, vol. 71, no. 3, pp. 209–249, 2021.

[22] R. A. Pumroy and G. Cingolani, "Diversification of importin-α isoforms in cellular trafficking and disease states," *The Biochemical Journal*, vol. 466, no. 1, pp. 13–28, 2015.

[23] S. Vaidyanathan, P. U. Thangavelu, and P. H. Duijf, "Overexpression of ran GTPase components regulating nuclear export, but not mitotic spindle assembly, marks chromosome instability and poor prognosis in breast cancer," *Targeted Oncology*, vol. 11, no. 5, pp. 677–686, 2016.

[24] O. Melaiu, E. Melissari, L. Mutti et al., "Expression status of candidate genes in mesothelioma tissues and cell lines," *Mutation Research*, vol. 771, pp. 6–12, 2015.

[25] M. C. Jiang, "CAS (CSE1L) signaling pathway in tumor progression and its potential as a biomarker and target for targeted therapy," *Tumour Biology*, vol. 37, no. 10, pp. 13077–13090, 2016.

[26] C. A. Ott, L. Linck, E. Kremmer, G. Meister, and A. K. Bosserhoff, "Induction of exportin-5 expression during melanoma development supports the cellular behavior of human malignant melanoma cells," *Oncotarget*, vol. 7, no. 38, pp. 62292–62304, 2016.

[27] K. Shigeyasu, Y. Okugawa, S. Toden, C. R. Boland, and A. Goel, "Exportin-5 functions as an oncogene and a potential therapeutic target in colorectal cancer," *Clinical Cancer Research*, vol. 23, no. 5, pp. 1312–1322, 2017.

[28] D. Li, S. Fu, Z. Wu et al., "DDX56 inhibits type I interferon by disrupting assembly of IRF3-IPO5 to inhibit IRF3 nucleus import," *Journal of Cell Science*, vol. 133, no. 5, 2019.

[29] H. W. Chao, Y. T. Lai, Y. L. Lu, C. L. Lin, W. Mai, and Y. S. Huang, "NMDAR signaling facilitates the IPO5-mediated nuclear import of CPEB3," *Nucleic Acids Research*, vol. 40, no. 17, pp. 8484–8498, 2012.

[30] N. Gong, L. Shi, X. Bing et al., "S100A4/TCF complex transcription regulation drives epithelial-mesenchymal transition in chronic sinusitis through Wnt/GSK-3β/β-catenin signaling," *Frontiers in Immunology*, vol. 13, no. 13, pp. 835–888, 2022.

[31] J. Downward, "Targeting RAS signalling pathways in cancer therapy," *Nature Reviews Cancer*, vol. 3, no. 1, pp. 11–22, 2003.

[32] U. Degirmenci, M. Wang, and J. Hu, "Targeting aberrant RAS/RAF/MEK/ERK signaling for cancer therapy," *Cell*, vol. 9, no. 1, p. 198, 2020.

[33] B. G. Strittmatter, T. J. Jerde, and P. C. Hollenhorst, "Ras/ERK and PI3K/AKT signaling differentially regulate oncogenic ERG mediated transcription in prostate cells," *PLoS Genetics*, vol. 17, no. 7, article e1009708, 2021.

[34] Q. Yu, M. Wu, L. Sheng, Q. Li, and F. Xie, "Therapeutic effects of targeting RAS-ERK signaling in giant congenital melanocytic nevi," *American Journal of Translational Research*, vol. 10, no. 4, pp. 1184–1194, 2018.

[35] M. A. Zaballos, A. Acuña-Ruiz, M. Morante, P. Crespo, and P. Santisteban, "Regulators of the RAS-ERK pathway as therapeutic targets in thyroid cancer," *Endocrine-Related Cancer*, vol. 26, no. 6, pp. 319–344, 2019.

[36] W. J. Ryu, G. Han, S. H. Lee, and K. Y. Choi, "Suppression of Wnt/β-catenin and RAS/ERK pathways provides a therapeutic strategy for gemcitabine-resistant pancreatic cancer," *Biochemical and Biophysical Research Communications*, vol. 549, pp. 40–46, 2021.

[37] A. Dongre, S. Ortiz-Cuaran, and H. Korkaya, "Editorial: the role of the EMT program in regulating the immune response in carcinoma," *Frontiers in Immunology*, vol. 13, pp. 940–946, 2022.

[38] I. Pastushenko and C. Blanpain, "EMT Transition States during Tumor Progression and Metastasis," *Trends in Cell Biology*, vol. 29, no. 3, pp. 212–226, 2019.

[39] M. Suarez-Carmona, J. Lesage, D. Cataldo, and C. Gilles, "EMT and inflammation: inseparable actors of cancer progression," *Molecular Oncology*, vol. 11, no. 7, pp. 805–823, 2017.

Hindawi
Oxidative Medicine and Cellular Longevity
Volume 2022, Article ID 5628601, 23 pages
https://doi.org/10.1155/2022/5628601

Review Article

Artemisia spp.: An Update on Its Chemical Composition, Pharmacological and Toxicological Profiles

Javad Sharifi-Rad,[1] Jesús Herrera-Bravo,[2,3] Prabhakar Semwal,[4] Sakshi Painuli,[5] Himani Badoni,[6] Shahira M. Ezzat,[7,8] Mai M. Farid,[9] Rana M. Merghany,[10] Nora M. Aborehab,[11] Mohamed A. Salem,[12] Surjit Sen,[13,14] Krishnendu Acharya,[13] Natallia Lapava,[15] Miquel Martorell,[16,17] Bekzat Tynybekov,[18] Daniela Calina,[19] and William C. Cho[20]

[1]*Facultad de Medicina, Universidad del Azuay, Cuenca, Ecuador*
[2]*Departamento de Ciencias Básicas, Facultad de Ciencias, Universidad Santo Tomas, Chile*
[3]*Center of Molecular Biology and Pharmacogenetics, Scientific and Technological Bioresource Nucleus, Universidad de La Frontera, Temuco 4811230, Chile*
[4]*Department of Life Sciences, Graphic Era Deemed To Be University, Dehradun, 248002, Uttarakhand, India*
[5]*Uttarakhand Council for Biotechnology (UCB), Prem Nagar, Dehradun, 248007 Uttarakhand, India*
[6]*Department of Biotechnology, School of Applied and Life Sciences, Uttaranchal University, Prem Nagar, Dehradun, 248007, Uttarakhand, India*
[7]*Department of Pharmacognosy, Faculty of Pharmacy, Cairo University, Cairo 11562, Egypt*
[8]*Department of Pharmacognosy, Faculty of Pharmacy, October University for Modern Sciences and Arts (MSA), Giza 12451, Egypt*
[9]*Department of Phytochemistry and Plant Systematics, National Research Centre, 33 El Bohouth St., Dokki, P. O. 12622, Giza, Egypt*
[10]*Pharmacognosy Department, Pharmaceutical and Drug Industries Research Institute, National Research Centre (NRC), 33 El-Bohouth street, Dokki, Giza, Egypt*
[11]*Department of Biochemistry, Faculty of Pharmacy, October University for Modern Sciences and Arts (MSA), Giza 12451, Egypt*
[12]*Department of Pharmacognosy, Faculty of Pharmacy, Menoufia University, Gamal Abd El Nasr St., Shibin El Kom, 32511 Menoufia, Egypt*
[13]*Molecular and Applied Mycology and Plant Pathology Laboratory, Department of Botany, University of Calcutta, Kolkata 700019, India*
[14]*Department of Botany, Fakir Chand College, Diamond Harbour, West Bengal 743331, India*
[15]*Medicine Standardization Department, Vitebsk State Medical University, Belarus*
[16]*Department of Nutrition and Dietetics, Faculty of Pharmacy, And Centre for Healthy Living, University of Concepción, Concepción, Chile*
[17]*Universidad de Concepción, Unidad de Desarrollo Tecnológico (UDT), 4070386 Concepción, Chile*
[18]*Department of Biodiversity of Bioresources, Al-Farabi Kazakh National University, Almaty, Kazakhstan*
[19]*Department of Clinical Pharmacy, University of Medicine and Pharmacy of Craiova, 200349 Craiova, Romania*
[20]*Department of Clinical Oncology, Queen Elizabeth Hospital, Kowloon, Hong Kong*

Correspondence should be addressed to Javad Sharifi-Rad; javad.sharifirad@gmail.com, Natallia Lapava; natallia_karazhan@tut.by, Miquel Martorell; mmartorell@udec.cl, Daniela Calina; calinadaniela@gmail.com, and William C. Cho; chocs@ha.org.hk

Received 27 June 2022; Revised 7 August 2022; Accepted 12 August 2022; Published 5 September 2022

Academic Editor: Muhammad Saleem Kalhoro

Artemisia plants are traditional and ethnopharmacologically used to treat several diseases and in addition in food, spices, and beverages. The genus is widely distributed in all continents except the Antarctica, and traditional medicine has been used as antimalarial, antioxidant, anticancer, antinociceptive, anti-inflammatory, and antiviral agents. This review is aimed at systematizing scientific data on the geographical distribution, chemical composition, and pharmacological and toxicological profiles of the *Artemisia* genus. Data from the literature on *Artemisia* plants were taken using electronic databases such as PubMed/MEDLINE, Scopus, and Web of Science. Selected papers for this updated study included data about phytochemicals, preclinical pharmacological experimental studies with molecular mechanisms included, clinical studies, and toxicological and safety data. In addition, ancient texts and books were consulted. The essential oils and phytochemicals of the *Artemisia* genus have reported important biological activities, among them the artemisinin, a sesquiterpene lactone, with antimalarial activity. *Artemisia absinthium* L. is one of the most famous *Artemisia* spp. due to its use in the production of the absinthe drink which is restricted in most countries because of neurotoxicity. The analyzed studies confirmed that *Artemisia* plants have many traditional and pharmacological applications. However, scientific data are limited to clinical and toxicological research. Therefore, further research is needed on these aspects to understand the full therapeutic potential and molecular pharmacological mechanisms of this medicinal species.

1. Introduction

The search and development of medicines from plant raw materials have been one of the important areas of human science for centuries [1]. A new breath of this scientific direction was given by the discovery of unique antimalarial agent artemisinin by the Chinese scientist Youyou Tu, for which she received the Nobel Prize in Physiology or Medicine in 2015. The source of this medicine was the *Artemisia annua* L., which has long been known in Chinese folk medicine [2]. This plant is not the only one of the well-known representatives of the *Artemisia* L. genus. *Artemisia* genus (*Asteraceae*), named after the Greek goddess of the hunt and fertility Artemis, is considered one of the most widely distributed genera all over the world [3] and unites more than 400 species of plants of various life forms (grasses, shrubs, and less often trees) [4]. Many of them are weeds, some are invasive in certain regions of the planet, and at the same time, some species are listed in the Red Book. Wide distribution, a variety of component composition, and the resulting wide range of pharmacological effects made plants of the *Artemisia* genus popular remedies of traditional medicine and ensured their study and subsequent introduction into official medicine [5–7].

The medicinal and aromatic applications of *Artemisia* are well known for a long time as it produces volatile oil which has applications in medicine, cosmetics, and food production [8]. Some species of *Artemisia* are edible [9], and others especially those grown in Korea have been traditionally applied in treating inflammations and ulcers. The most famous species around the world are *A. annua* and *A. absinthium* L. which are known for their uses in traditional medicine [10, 11]. In South Africa, *Artemisia afra* Jacq. ex Willd. is commonly used for treating inflammation, coughs, colds, malaria, fever, influenza, and diabetes [12], while, in North America, *Artemisia dracunculus* L. is widely used for the treatment of wounds and possesses antioxidant and antidiabetic activities [13, 14]. Furthermore, *Artemisia vulgaris* L. is used in traditional medicine and has several activities such as anticancer, hepatoprotective, antiepileptic, antimalarial, and insecticidal properties [15–19]. Other various species such as *Artemisia nilagirica* (C.B.Clarke) Pamp., *A. dracunculus*, *Artemisia herba-alba* Asso, *A. armeniaca* Lam., and *Artemisia scoparia* Waldst. & Kitam. possess significant therapeutic properties [20]. *A. scoparia* also has a long history in medicine, and it has been in clinics as a diuretic, choleretic, and hepatoprotective [21]. *A. scoparia* was used to treat hepatitis, jaundice, sores, pruritus, asthma, gastritis, and expel parasites and to treat spiders' bites. A combination of *A. scoparia*, *Gardenia jasminoides* J. Ellis, and rhubarb (*Rheum rhabarbarum* L.) was reported to be a classical prescription for curing jaundice [21]. Currently, several biopharmaceutical products containing *Artemisia* extracts are available nowadays in the local markets to treat various diseases [22]. The purpose of the review is to systematize updated scientific data on the chemical composition and new insights in the pharmacological mechanisms of action and discusses the toxicological profiles of the *Artemisia* genus.

2. Methodology

Two biomedical literature databases were searched for this review: PubMed/MEDLINE and Web of Science using the following MeSH search terms: "Artemisia/chemistry," "Phytochemicals," "Artemisinins/pharmacology,, "Artemisinins/therapeutic use," "Medicine, Traditional," "Phytotherapy/methods," "Plant Extracts/pharmacology," "Plant Extracts/therapeutic use," "Plant Oils /pharmacology," "Plant Oils/therapeutic use," "Structure-Activity Relationship," "Animals," and "Humans." Inclusion criteria are as follows: preclinical and clinical studies on the sources, acquisition approaches, experimental pharmacology, toxicology, and safety data regarding *Artemisia* spp. were included. Both in vivo and in vitro pharmacological studies which underlie the molecular mechanism of action were included. Exclusion criteria are as follows: studies with data not relevant for the aim of this updated review, or poor quality of studies, duplicate studies. The taxonomy of plant species has been validated using the World Flora Online [23].

3. Geographical Distribution of *Artemisia* spp.

The genus *Artemisia* is widely cosmopolitan and distributed worldwide except the Antarctica [24–26]. The genus is heterogeneous and inhabits from the sea level to high altitudes

of around 4000 masl (meters above *sea level*) [27]. The species of *Artemisia* grows abundant in the Northern Hemisphere, and a low degree of colonization has been reported in the Southern Hemisphere [27, 28]. The main centre of species diversity of *Artemisia* is located in Central Asia consisting the region of Uzbekistan, Tadzhikistan, Turkmenistan, Kazakhstan, Kyrgyzstan, parts of Russia, China, and Mongolia. Other relevant centres of diversity include the territory of Iran-Turanian and Mediterranean regions and in western North America [29–33]. *Artemisia* has been spread beyond its native origin and successfully distributed and colonized in most of the arctic-alpine, temperate, and subtropical zones of the Northern Hemisphere. The distribution of the genus from Northern Asia primarily follows the main three routes: (1) in the West, it migrates into Europe, Western Asia, Mediterranean Basin, and Africa; (2) Siberia and into western North America; and (3) further south into Asia [34, 35]. Only a few number of species, not exceeding 25 taxa, have been reported from the Southern Hemisphere although a small diversity centre occurs in South America and it is found in Oceania as allochthonous taxa [32] (Figure 1).

4. Phytochemical Composition

4.1. Essential Oils. The essential oils (EOs) present in botanicals have been used for centuries in the form of spices, medicines, and their pleasant odour [36]. It has been possible only due to the development of distillation techniques in the middle ages and is used in their ancient applications in food, drugs, or cosmetics [37]. While, in the last decades, the EO industry entered different sectors with new dimensions and targets due to its various therapeutic applications. The chemical composition of *Artemisia* genus EOs has been reported by several authors around the world. The composition of EOs varies depending on several factors including the plant part, growing season, age of the plant, location, extraction techniques, solvent, and timing [38]. The detailed investigations on the EO composition of the *Artemisia* genus from different geographical regions have been presented in Table 1.

4.2. Other Bioactive Compounds. The phytochemical diversity assessment of the *Artemisia* genus exhibited the presence of different types of secondary metabolites reported by several authors around the world (Table 2).

5. Pharmacological Effects of *Artemisia* spp. Extracts and Its Bioactives: Underlying Molecular Mechanisms

Artemisia spp. have a broad range of pharmacological activities such as antiulcer, anticancer, hepatoprotective, antidiabetic, antioxidant, and antimicrobial. Some of the preclinical studies of these species' activities are summarized in Table 3 and Figure 2.

One of the available famous drugs derived from *Artemisia* species is artemisinin which exists in the leaves and flowers of *A. annua*. Other species which are known free of artemisinin were found to be active against malaria as *A. vulgaris*, *A. absinthium*, *A. dracunculus*, and *A. scoparia*; this activity was attributed to EOs and other sesquiterpenes [89]. Moreover, other studies also mentioned that artemisinin was not the only antimalarial substance in *A. annua* extracts [90–92].

5.1. Antioxidant. Antioxidants are a group of compounds that can help support the integrity of cells in the face of free radicals, unstable molecules that our body inevitably produces [93–95]. Natural antioxidants are thus essential for the proper functioning of the body [96–98]. Several studies have been reported the antioxidant activity of *A. absinthium*. Phenolic compounds (gallic acid, coumaric acid, vanillic acid, syringic acid, and chlorogenic salicylic acid) and flavonoids (quercetin and rutin) present in *A. absinthium* showed the potential of this plant against diseases related to oxidative stress [99–101]. These compounds reduce lipid peroxidation (thiobarbituric acid-reactive substances (TBARS) and recover endogenous antioxidant (e.g., superoxide dismutase (SOD) and glutathione (GSH)).

5.2. Anti-inflammatory. Inflammation is the body's natural response to protecting itself and recovering from an injury [102, 103]. It has the function of protecting the body from harmful substances and regenerating the damaged tissue [1, 104, 105]. *A. absinthium* extracts exhibit anti-inflammatory properties which may be linked to its secondary metabolites including flavonoids and sesquiterpene-type compounds and their role in inflammatory regulator inhibition such as bradykinins, histamine, prostaglandins, and serotonin [106] and through suppression of proinflammatory mediator expression such as inducible nitric oxide synthase (iNOS), prostaglandin E-2 (PGE2), cyclooxygenase-2 (COX-2), factor nuclear factor-kappa-B (NF-κB), and tumor necrosis factor-α (TNF-α) [11].

5.3. Anticancer. Cancer is a disease in which the body's cells grow uncontrollably, forming a tumor that can spread to different parts of the body [107–111]. The mechanism of the anticancer effect *A. absinthium* extract was due to the activation of the mitogen-activated protein kinase/extracellular signal-regulated kinase MEK/ERK signaling pathway, which in turn stimulates the mitochondrial pathway of caspase activation and regulates Bad and Bcl-2 family proteins, resulting in the apoptotic death of MCF-7 and MDA-MB231 human cancer cells [108].

5.4. Neuroprotective. Neurocerebral disorders, especially neurodegenerative ones, refer to several progressive brain syndromes that affect memory, thinking ability, behavior, and emotions [112–115]. *A. absinthium* has been shown to have neuroprotective effects on cerebral damage caused by reperfusion through its nicotinic and muscarinic action. The protective mechanism of ethanolic extract of *A. absinthium* may be due to its anticholinesterase activity as well as the ability to change the behavior of rats by restoring acetylcholinesterase (AChE) and monoamine oxidase (MAO) enzymes to near-normal activity [11]. The sesquiterpenoid dimer—caruifolin D—found in *A. absinthium* may

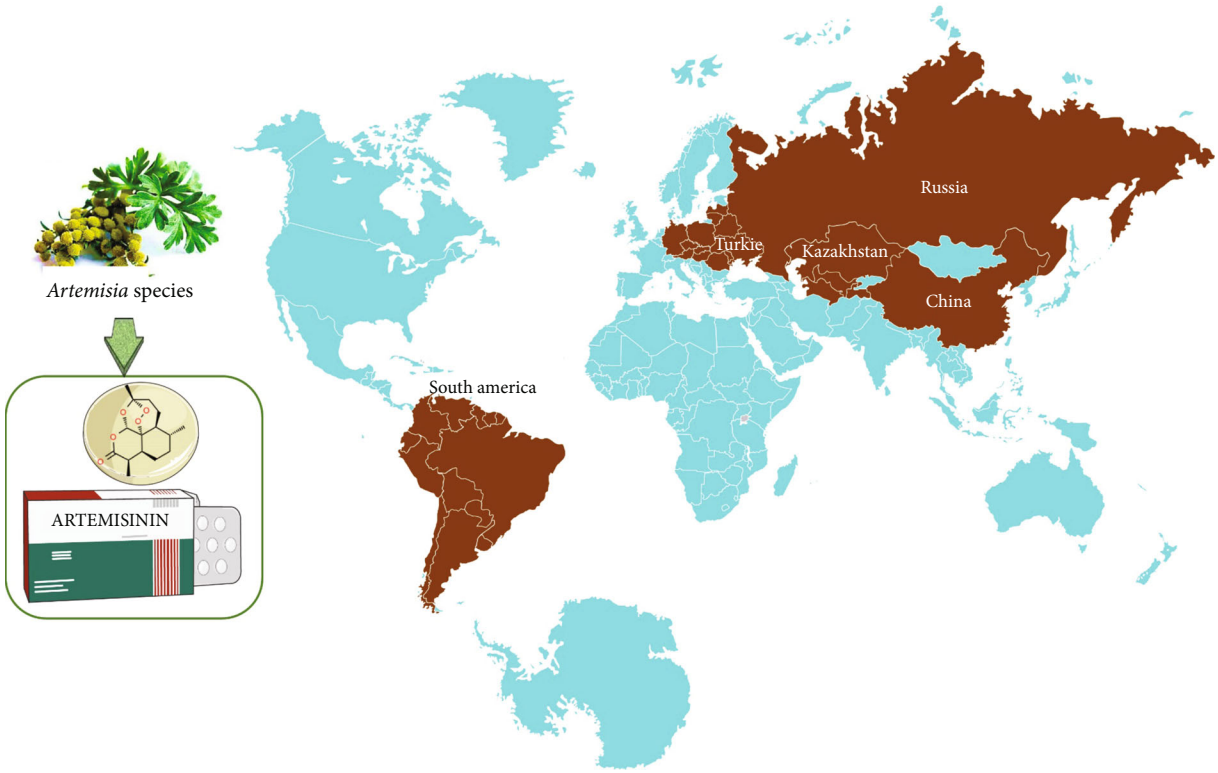

Figure 1: Geographical distribution of *Artemisia* species.

be used for the treatment of neurodegenerative diseases such as Alzheimer's or Parkinson's due to its inhibitory action on the production of neuroinflammatory mediators in BV2 microglial cells and the reactive oxygen species (ROS) production; leading to inhibitory effects on the activations of protein kinase C (PKC) and c-Jun N-terminal kinase (JNK) [116].

5.5. Hepatoprotective. *A. absinthium* hydroalcoholic extract improves hepatic function and lowers oxidative stress indicators and consistently stimulates and preserves the structural morphology of the hepatocellular membrane, resulting in lower serum aspartate (ASAT) and alanine aminotransferase (ALAT) activity. The proposed hepatoprotective mechanisms include liver microsomal drug-metabolizing enzyme suppression, free radical scavenging activity, and calcium channel blockage [117].

5.6. Antidiabetic. Diabetes is a metabolic disease that causes excess blood glucose (hyperglycemia) [118]. This disease is incurable and once diagnosed requires lifelong treatment [119]. *A. absinthium* extracts showed an insulin-sensitizing action due to their role in adenosine monophosphate-activated protein kinase (AMPK) stimulation and glucose transporter type 4 (GLUT4) translocation to the cell surface of the muscle [120]. In diabetic rats treated with *A. absinthium*, the metabolic pathway shifted towards carbohydrate as a source of energy, preserving proteins and lipids while increasing their production, leading to preventing body weight loss [121].

5.7. Antimalarial. A sesquiterpene lactone, artemisinin, which is the main active ingredient in *A. annua* is used for the treatment of *Plasmodium* parasites; these parasites are characterized by their substantial hemoglobin uptake and digestion. This produces large quantities of free redox-active heme and free ferrous iron (Fe^{2+}), which are assumed to be responsible for artemisinin's parasite specificity. Infected erythrocytes convert excess heme to hematin, which is toxic to the parasite due to oxidative damage and direct cell membrane rupture; but malarial parasites have evolved a detoxification mechanism that uses a biocrystallization process to convert hematin to the less toxic and inert crystallized hemozoin. Activated artemisinin has been shown to inhibit the development of hemozoin by alkylating heme. As a result, artemisinin's activator and target are both free heme from hemoglobin breakdown [122].

6. Clinical Studies

Long traditional usage and functional preclinical studies of different *Artemisia* species for the treatment of several diseases encouraged their clinical evaluation to support the evidence of their potential as antimalarial, antioxidant, anticancer, antinociceptive, anti-inflammatory, and antiviral agents [4].

6.1. Anti-inflammatory Activity. In a randomized double-blind clinical trial, oral treatments of 42 patients by Arthrem (supercritical CO_2-extracted *A. annua*) at doses 150 mg and 300 mg or placebo twice daily for 12 weeks were tested for

Table 1: Essential oil composition of the *Artemisia* genus from different geographical regions (2017–2021).

Plant species	Parts used	Chemical composition	Region/ country	References
Artemisia absinthium L.	L	Camphor; E-caryophyllene; eucalyptol; germacrene D; α-cadinol	Brazil	[39]
Artemisia anethoides Mattf.	AP	1,8-Cineole; terpinen-4-ol; 2-isopropyltoluene; pinocarveol	China	[40]
Artemisia annua L.	AP	Artemisia ketone; α-caryophyllene; germacrene D	China	[41]
	AP, F, L	(E)-β-Farnesene; germacra-4(15),5,10(14)-trien-1-ol; *Artemisia* alcohol 3-methyl butanoate; yomogi alcohol; *Artemisia* alcohol 3-phenylpropionate; *Artemisia* alcohol 2-methyl butanoate; α-copaene; artemisia alcohol; 1,8-cineol	Russia	[42]
Artemisia arborescens (Vaill.) L.	F, L	β-Thujone, camphor, terpinen-4-ol, germacrene D, chamazulene	Italy	[43]
Artemisia argyi H. Lév. & Vaniot	L	α-Thujone; bornanone; terpinen-4-ol; cis-2-menthenol; borneol; cis-sabino; α-terpineol; β-caryophyllene; caryophyllene oxide; neointermedeol	China	[44]
Artemisia campestris L.	—	β-Pinene; cadin-4-en-7-ol; Z-β-ocimene; γ-terpinene	Portugal	[45]
	AP	β-Pinene; α-pinene; myrcene; germacrene D; (Z)-β-ocimene; γ-curcumene	Algeria	[46]
	AP	β-Pinene; spathulenol; α-pinene; limonene; o-cymene	Morocco	[47]
	L, S	β-Pinene; 2-undecanone; limonene; benzene; α-pinene; 1,4-cyclohexadiene; β-myrcene; 2-naphthalenemethnol; 2-decanone	Tunisia	[48]
Artemisia dracunculus L.	AP	p-Allylanisole; ocimene (e)-β; ocimene (z)-β; limonene	Iran	[49]
	L	Methyl eugenol; elemicin; isoelemicin; (*Z*)-methyl isoeugenol	Poland	[50]
Artemisia gmelinii Weber ex Stechm.	—	γ-Amorphene; isohumbertiol B; caryophyllene oxide; caryophylla-4 (12), 8(13)-diene-5α-ol; ylangenol; caryophyllene; cabrevia oxide B	Russia	[51]
	AP	Cyclobutane ethanol; endo-borneol; germacrene D; eucalyptol; selin-6-en-4α-ol; bisabolone oxide A; caryophyllene; terpinen-4-ol	China	[52]
Artemisia herba-alba Asso	AP	Phellandrene; ascaridole; α-terpinolene; isoascaridole; benzyl isovalerate	India	[53]
	AP	cis-Thujone; trans-thujone; vanillyl alcohol; nordavanone; cis, threo-davanafuran	Morocco	[54]
	AP	3-Thujanone a; 3-thujanone b; camphor	Sweden	[55]
	L	α-Thujone; germacrene D; 1,8-cineole; β-thujone	Tunisia	[56]
Artemisia jordanica Danin	L	2,3-Dehydro-1,8-Cineole; camphene; endo-borneol; bornyl acetate; geranyl isovalerate	Palestine	[57]
Artemisia judaica L.	AP	Methyl pentanoate; (E)-salvene; santolina triene; allyl isovalerate; α-pinene; β-citronellene; camphene; benzaldehyde; myrcene; mesitylene; yomogi alcohol; 1,4-cineol; α-terpinene; artemisia ketone; 2,6-dimethyl phenol; chrysanthenone; camphor; artemisyl acetate; piperitone; (Z)-ethyl cinnamate; (E)-ethyl cinnamate; germacrene D; davanone	Jordan	[58]
	AP	Butanoic acid; β-linalool; 2-cyclohexen-1-one, 3-methyl-6-(1-methylethyl); acenaphthene; davana ether	Saudi Arabia	[59]
Artemisia magellanica Sch.Bip.	AP	γ-Costol; (Z)-en-yn-dicycloether; α-selinene; selina-4,11-diene (eudesma-4,11-diene); (E)-β-farnesene; 2-methylbutyl 2-methylbutyrate; (Z)-β-ocimene	Argentina	[60]
Artemisia monosperma Delile	AP	Spathulenol; cloven; β-linalool; α-citral; geranyl acetate; isohomogenol; benzene, 1,2-dimethoxy-4-(1-propenyl); caryophyllene; aristolene; 2-propenoic acid, 3-phenyl-ethyl ester	Saudi Arabia	[59]
	L	β-Pinene; limonene; cis-β-ocimene; α-terpinolene; cis-sabinene hydrate; bornyl acetate	Saudi Arabia	[61]
Artemisia nilagirica (C.B.Clarke) Pamp.	AP	β-Thujone; germacrene-D; β-thujone; caryophyllene; caryophyllene oxide; borneol	India	[62]
Artemisia pedemontana Balb.	F, L	α-Pinene; camphene; p-cymene; 1,8-cineole; linalool; camphor; borneol; terpinen-4-ol; viridiflorol; 1-α-terpineol	Spain	[63]
Artemisia persica Boiss.	AP	Laciniata furanone E; artedouglasia oxide C; pinocarvone; trans-pinocarveol; α-pinene; 1,8-cineole; artedouglasia oxide B and D	Iran	[64]
Artemisia sieversiana Ehrh.	AP	Santolina triene; α-thujone; eucalyptol; α-sabinene; trans-2-menthen-1-ol; α-selinene, caryophyllene epoxide	China	[65]

Table 1: Continued.

Plant species	Parts used	Chemical composition	Region/ country	References
Artemisia tournefortiana Rchb.	—	cis-Spiroether; Z-β-farnesene; trans-nerolidol; camphor	India	[66]
Artemisia scoparia Waldst. & Kitam.	AP	Spathulenol; acenaphthene; davana ether; 2-propenoic acid, 3-phenyl-ethyl ester	Saudi Arabia	[59]
Artemisia sieberi Besser	AP	Acenaphthene; 2-cyclohexen-1-one, 3-methyl-6-(1-methylethyl)	Saudi Arabia	[59]
Artemisia vulgaris L.	AP	Caryophyllene; humulene; germacrene D; borneol; caryophyllene oxide	Brazil	[67]
	AP	Germacrene D; 1,8-cineole; β-pinene; sabinene; cis-thujone; β-caryophyllene; caryophyllene oxide; α-humulene; davanone	Lithuania	[68]

AP: areal part; L: leaves; F: flowers; —: not reported.

their efficacy on stiffness, pain, and functional limitations in osteoarthritis of the hip and knees. Results showed a significant decrease in visual analogue scale (VAS) score and improvement in WOMAC (Western Ontario and McMaster Universities Osteoarthritis) total score only at the low dose of 150 mg [154]. Afterwards, an open-label 6 month extension trial was proceeded to examine the safety of Arthrem in the long run (6 months). Results showed that Arthrem could be a safe and effective agent for osteoarthritis management [155]. In a similar study, 90 patients diagnosed with osteoarthritis applied 3% *A. absinthium* ointment, 3% *A. absinthium* liniment, or piroxicam gel (PG) on their knees for 4 weeks. Results showed that *A. absinthium* ointment revealed significant improvement in all parameters except for WTSS (total stiffness score), where *A. absinthium* liniment only reduced VAS and WTPS (total pain score) in week 4 with recurrence in week 6 when compared to PG that improved all the parameters with no recurrence [156]. Furthermore, in a randomized controlled clinical trial, 10 patients with Crohn's disease administrated dried *A. absinthium* powder (750 mg three times daily) along with their basic therapy for 6 weeks, where another ten patients served as the control group. Results showed a significant reduction in serum TNF-α level and Crohn's disease activity index (CDAI) scores as well as remission of symptoms in eight patients [157].

In a further clinical study, a nasal spray containing an extract of *A. abrotanum* mainly composed of EO (4 mg/mL) and flavonols (2.5 μg/mL) was established for treating 12 patients with allergic rhinitis. The EO fraction is composed of 1,8-cineole, linalool, and davanone, while the flavonol fraction contained centauredin, casticin, and quercetin dimethyl-ethers, which are well known for their anti-inflammatory effect. Most of the patients exhibited a significant reduction in nasal congestion, sneezing, and rhinorrhea as well as relief of eye symptoms when compared to the effect of anti-histamines [158].

In the sight of cosmetics, twenty-five sensitive skin patients were selected for investigating the efficacy of *A. annua* extract on skin reliving. Results showed that consuming cosmetics having *A. annua* extract for 4 weeks could improve the hydration degree of the cheek cuticle by 63.90%, reduce the transepidermal water loss by 21.51%, reduce the sensitized area by 77.47%, repair skin damage, and reduce redness [159].

6.2. Anticancer Activity. Interestingly, artemisinin and its derivatives were reported as potent antitumor compounds with high selectivity on cancer cells without any side effects on normal cells [160]. Their mechanism of action is based on the cleavage of their endoperoxide bridge by Fe^{2+} in cancerous cells and the production of ROS involved in apoptosis, DNA damage, autophagy, and cell cycle arrest G0/G1 of the cancerous cells. Additionally, they can suppress angiogenesis by inhibiting the secretion of vascular endothelial growth factor (VEGF), vascular endothelial growth factor receptor 2 (VEGFR2), and kinase insert domain receptor (KDR)/flk-1 in tumors, as well as affecting different signaling pathways and transcription factors related to tumor growth [161, 162]. Besides the antitumor effect of artemisinin and its derivatives against human cancer cell lines *in vitro* [160, 163, 164], different clinical studies were established to ensure their potency. For instance, in a pilot clinical trial at phase II, the anti-tumor effect of dihydroartemisinin (200 mg/day) was tested against advanced cervical carcinoma for 3 weeks in ten women. Results showed a significant reduction in vaginal discharge and pain, with no sign of severe toxicity, as well as improvement in overall signs and symptoms. These patients also exhibited a lower expression of epidermal growth factor receptor (EGFR) and Ki-67 oncogenes [165].

Further, in a randomized, controlled clinical trial, artesunate (120 mg, once daily, IV) was combined with vinorelbine (25 mg/m^2, once daily, IV) and cisplatin (25 mg/m^2, once daily, IV) to treat patients with the advanced lung cancer stage. Results showed significant improvement in the survival rate and hindering of the progression time of the cancerous cell, devoid of extra side effects [166]. In a case report conducted by Singh and Verma [167], artesunate (50 mg) proved to reduce the tumor size of the larynx of a patient with stage II cancer by 70% following 2 weeks of treatment [167]. As well in another case report conducted by Berger et al. [168], the combination of artesunate (50 mg twice/day) with standard chemotherapy showed a significant reduction in death risk and stabilization of the disease case in 2 patients with metastatic uveal melanoma stage IV, when compared to the chemotherapy alone [168].

Table 2: Chemical composition of *Artemisia* genus from different geographical regions.

Plant species	Chemical composition	Region/ country	References
Artemisia abrotanum L.	Caffeic acid; chlorogenic acid; isochlorogenic acid; protocatechuic acid; rosmarinic acid; quercitrin	Saudi Arabia	[69]
Artemisia absinthium L.	Artemisinin; α-thujone; β-thujone; bornyl acetate; 4-terpineol; camphene; chamazulene; cadinene; myrcene; guaiazulene; linalool; γ-terpinene	-	[11]
Artemisia annua L.	Arteannuin B; artemisinin; artemisinic acid; scopoletin	China	[70]
Artemisia campestris L.	Catechin; vanillic acid; caffeic acid; syringic acid; p-coumaric acid; gallic acid	Morocco	[71]
Artemisia capillaris Thunb.	Neochlorogenic acid; chlorogenic acid; cryptochlorogenic acid; caffeic acid; 1,3-dicaffeoylquinic acid; 3,4-dicaffeoylquinic acid; 3,5-dicaffeoylquinic acid; 4,5-dicaffeoylquinic acid	China	[72]
Artemisia dubia L. ex B.D.Jacks.	Calotropoleanyl ester; α-amyrin; nonacosanoic acid; docosanoic acid; tetracosanoic acid; 1-(O-tricosanoyl) glycerol; 1-(O-pentacosanoyl) glycerol; β-sitosterol	Pakistan	[73]
Artemisia gmelinii Weber ex Stechm.	Coumarins; phenolics; flavonoids; caffeoylquinic acids; diterpene glycosides	Korea	[74]
Artemisia herba-alba Asso	Camphor; hanphillin; alkhanin; terpinen-4-ol; α-santonin; α-thujone; β-thujone; 2,5-bornanedione	Morocco	[75]
Artemisia indica Willd.	5-Hydroxy-3,7,4′-trimethoxyflavone; ludartin; maackiain; lupeol; cis-matricaria ester; trans-matricaria ester; 6-methoxy-7,8-methylenedioxy coumarin	China	[76]
Artemisia lactiflora Wall. ex DC.	β-Sitosterol; daucosterol; umbelliferone; isofraxidin; scopoletin; fraxidin; mandshurin; fraxin-8-O-β-D-glucopyranoside; euoniside; scopolin; 5,8-dihydroxy-7,4′-dimethoxy-flavone; syringing; chrysoeriol; tricin; luteolin; acacetin; apigenin; 5,7-dihydroxy-3,6,4′-trimethoxy-flavone; tectorigenin; eicosyl/docosyl-*p*-coumarate; isoferulic acid; ferulaldehyde; ethyl caffeate; caffeic acid; (−)-syringaresinol; (+)-diasyringaresinol; *p*-hydroxybenzoic acid; *p*-methylbenzaldehyde; cleomiscosin C; cleomiscosin A or B; biisofraxidin	China	[77]
Artemisia mongolica (Fisch. ex Besser) Fisch. ex Nakai	1-(3-Hydroxyphenyl)-2-(5-hydroxy-3-methoxyphenyl)ethane; 1-(3-hydroxyphenyl)-2-(3,5-dihydroxyphenyl)ethane	China	[78]
Artemisia myriantha Wall. ex Besser	Blumenol A; (+)-dehydrovomifoliol; (+)-3-hydroxy-β-ionone; (3R, 6R, 7E)-3-hydroxy-4, 7-megastigmadien-9-one; (−)-10-oxo-isodauc-3-en-15-oic acid; isoerivanin; eudesmafraglaucolide; artanomalide A; 13-acetoxy-3β-hydroxy-germacra-1(10) E,4E,7(11)-trien-12,6α-olide; 13-acetoxy-3β-tigloyl-germacra-1(10) E, 4E, 7(11)-trien-12, 6α-olide (10),13-acetoxy-3β-(3-methylbutanoyl)-germacra-1(10)E, 4E, 7(11)-trien-12, 6α-olide (11),3,9-diacetoxy-13-hydroxy-1(10), 4, 7(11)-germacratrien-12,6α-olide; 8α-angeloyloxycostunolide	China	[79]
Artemisia pontica L.	n-Hexadecanoic acid; 9,12,15-(Z,Z,Z)-octadecatrienoic acid; 2-(4a,8-dimethyl-7-oxo-1,2,3,4,4a,7-hexahydronaphthalen-2-yl)-propionic acid; 8-nitro-(1H)quinolin-4-ol-2-one; neophytadiene	Ukraine	[80]
Artemisia rupestris L.	Citrusin A; alaschanioside A; coniferin; citrusin B; syringaresinol-β-D-glucoside; (6R,9S)-3-carbonyl-α-ionol glucopyranoside; byzantionoside B	China	[81]
Artemisia scoparia Waldst. & Kitam.	Eugenol; capillene; spathulenol; capillin; scoparone; tricosane; heptacosane; nonacosane; stigmasterol; tritriacontane	Serbia	[82]
	4-Pyridone glucoside; polyacetylene glucosides	China	[83]
	Quercetin-3-O-β-d-glucoside; 3,4-dihydroxy-5-methoxycinnamic acid; caffeic acid; 6,7 dimethoxycoumarin	China	[84]
Artemisia splendens Willd.	Narcisin; quercetin; luteolin; kaempferol; genkwanin; astragalin; isorhamnetin-3-O-β-D-glucoside	Iran	[85]
Artemisia turanica Krasch.	3,5-Dicaffeoylquinic acid; 4,5-dicaffeoylquinic acid; 3,5,3′,4′-tetrahydroxy; 7,5′-methoxy flavones	Iran	[86, 87]
Artemisia vulgaris L.	Artanoic acid; luteolin; 6-methoxyluteolin; eupatilin; o-coumaric acid; vanillic acid; protocatechuic acid; 4-hydroxyphenyl acetate; vulgarin	Vietnam	[88]

Table 3: Preclinical pharmacological studies of different *Artemisia* species.

Extract/compound	Doses	*In vitro*/*in vivo*	Route of administration/ assay	Model/cells	Activity	Potential effect	Reference
A. nilagirica/ethanolic extracts	500 mg/kg	*In vivo*	Orally	Rats	Antiulcer	Gastroprotective, ↑proteins of mucus content	[123, 124]
A. nilagirica/ methanolic extract	150–250 mg/kg	*In vivo*	Orally	Swiss albino mice		Gastroprotective compared to standard drug vincristine	[125]
A. absinthium, A. vulgaris/*flowers*/ methanolic extract	62.5, 125, 250, 500 μg/mL	*In vitro*	MTT	MCF7 cells	Anticancer	↑cytotoxicity IC_{50} = 221–500 μg/mL	[126]
A. nilagirica/ethyl acetate, hexane fractions	100 μg/mL	*In vitro*	SRB	DLD-1 cells		↑cytotoxicity IC_{50} = 15.42–23.4 μg/mL	[127]
A. vulgaris/*leaves*/ methanolic extract	0.01–1.0 mg /mL	*In vitro*	MTT	Hepatocellular carcinoma cells		↑apoptosis IC_{50} = 0.1 mg/mL	[15]
A. absinthium/ methanolic extract	20, 25 g/mL	*In vitro*	MTT	MCF-7 MDA-MB231		↑cancer cells suppression	[108, 128]
A. armeniaca/CH_2Cl_2 fraction	6.25–200 μg/mL	*In vitro*	MTS	Apoptosis-proficient HL60 apoptosis-resistant K562		HL-60: IC_{50} = 75 μg/mL, K562: IC_{50} = 130 μg/mL	[129]
A. dracunculus/aerial parts, roots/ethanol, aqueous extracts	250 mg/kg	*In vivo*	Orally	STZ-induced diabetic rats	Antidiabetic	↓TGL, ↓LDL, ↓HDL	[14]
A. dracunculus L. (PMI 5011)/ethanolic extract	PMI 5011 (1%)	*In vivo*	Diet	KK-A^y mice		↑sensitivity of insulin, ↑insulin receptor signaling	[130, 131]
A. sieberi (*A. herba-alba*)/aqueous extracts	0.39 g/kg	*In vivo*	Orally	Alloxan-induced diabetic rats		↓blood glucose, ↑RBC, ↑WBC, ↑PCV, ↑ESR, ↑neutrophils, ↓heart rate	[132]
A. persica/aqueous, methanolic extracts	300, 400, 500 mg/kg	*In vivo*	Orally	Sprague-Dawley rats	Antihypertensive	↓systolic blood pressure in normotensive/hypertensive rats	[133]
A. absinthium/ aqueous extract	50, 100, 200 mg/kg	*In vivo*	Orally	Kunming mice, NIH mice	Hepatoprotective	↓inflammatory cells, ↓liver lipid peroxidation, ↑SOD, ↑GPx	[134]
A. vulgaris/aerial parts/crude extract	150, 300, 600 mg/kg	*In vivo*	i.p.	Balb-C mice		↑liver structure, ↓parenchyma congestion, ↓cellular swelling, ↓apoptotic cells	[16]
A. nilagirica/leaf extracts	32–512 μg/mL	*In vitro*	Agar disk diffusion method	15 bacterial strains	Antibacterial	Methanol, hexane extracts, ↑inhibition against phytopathogens	[135]
A. herba- alba, *A. judaica*, *A. monosperma*/EO	10.0, 5.0, 2.5, 1.0, 0.5 μL/ disc	*In vitro*	Agar disc diffusion method.	*Staphylococcus aureus* ATCC29213, *Escherichia coli* ATCC 25922		IC_{50} = 0.5 – 2.5 μL *A. judaica*, A. *monosperma* plants had the highest MIC	[136]

Table 3: Continued.

Extract/compound	Doses	*In vitro*/*in vivo*	Route of administration/assay	Model/cells	Activity	Potential effect	Reference
A. judaica/ethanol extract	250, 500, 1000, 2000, 4000 μg/mL	*In vitro*	(mic90) growth inhibition	Protozoan parasite (blastocystis)	Antiprotozoal	IC_5 = 4000 μg/mL, ↓growth, ↑destruction of blastocystis	[137]
A. nilagirica/EO	0.33 μL/mL	*In vitro*	Inverted petri plate technique	*A. flavus*, *A. niger*, *A. ochraceus*	Antifungal	IC_{50} = 1.6 μL/mL, ↓fungal growth, ↓mycotoxin secretion, ↓aflatoxigenic, ↓ochratoxigenic strains	[138]
A. annua/leaves/EO ethanolic extract	EO = 470 mg/kg ethanol extract = 450 mg/kg	*In vivo*	i.p.	Wistar rats	Antidepressant	↑immobility time in the FST, ↓other activities in the OFT depressors of SNC	[139]
A. absinthium/aerial parts/methanolic extract	125, 250, 500, 1000 mg/kg	*In vivo*	i.p.	Swiss albino mice		↓immobility period in the fst and tst.dose-dependent antidepressant activity	[140, 141]
A. vulgaris/leaves/methanolic extract	50, 100, 300 mg/kg	*In vivo*	i.p.	Swiss albino mice	Antiepileptic	Anticonvulsant activities were noticed using EPM and MBT	[18]
A. capillaris/herba/ethanolic extract	50, 100, 200, 400 mg/kg	*In vivo*	Orally	Mice		Anticonvulsivant effect through the GABA-ergic neuron	[142]
A. nilagirica/leaves/ethanolic, aqueous extracts	100, 200 mg/kg	*In vivo*	i.p.	Swiss albino mice	Anti-Alzheimer	Confirmation of the anti-Alzheimer's activity of ethanol extract after object recognition and y-maze tests	[143]
A. nilagirica/leaves/ethanolic, aqueous extracts	100, 200 mg/kg	*In vivo*	i.p.	Swiss albino mice	Anti-Parkinson	↓catalepsy score in animals treated with ethanolic extract, ↑locomotor activity, ↑rotarod readings	[143]
A. annua/aqueous, ethanolic extracts	2 g/L	*In vitro*	ABTS, ORAC, FRAP	—	Antioxidant	↑protection against the oxidative deterioration of oil-in-water emulsion	[144]
A. dracunculus L./leaves/methanolic extract	20 μL	*In vitro*	DPPH	—		↑antioxidant activity by phenolics	[13]
A. nilagirica/leaves/ethanolic, aqueous extracts	50–250 μg/mL	*In vitro*	DPPH	—		Antioxidant activity of ethanolic extract > aqueous extract	[143]
A. scoparia, *A. spicigera*/methanolic extracts	0.25; 0.125; 0.0625; 0.0312; 0.0156; 0.0078; 0.0039; 0.0019; 0.0009; 0.00048 mg/mL	*In vitro*	DPPH	—		↑free radical scavenging activity RC_{50} = 0.03157, 0.0456 mg/mL	[145]
A. nilagirica/EO	10; 8.6; 6.5; 6.5; 3.3; 2.5; 2 μg/mL	*In vitro*	Method recommended by WHO	*Aedes albopictus* mosquito	Insecticidal	LC_{50} = 5 μg/mL	[146]
A. nilagirica/EO, chloroform, petroleum ether methanolic extracts	—	*In vitro*	Method recommended by WHO	*Aedes aegypti*, *Anopheles stephensi*, *Culex quinquefasciatus* mosquito larvae		The EO of *A. nilagirica* was the most effective larvicide against *A. stephensi* larvae	[147]

Table 3: Continued.

Extract/compound	Doses	*In vitro*/*in vivo*	Route of administration/assay	Model/cells	Activity	Potential effect	Reference
A. aucheri/methanolic extract	25, 50, 100 mg/mL	*In vitro*	Scolicidal tests	*Echinococcus granulosus*		↓effect on the protoscolices of hydatid cysts	[148]
A. vulgaris/ethanolic extract	1, 5, 10, 50, 100, 500, 1000 ppm	*In vitro*	Method recommended by WHO	*Aedes aegypti*		LC_{50} = 65.8 ppm in 1 h and 18.6 ppm in 24 h, ↓ *A. aegypti* in various stages of its lifecycle	[19]
A. scoparia, *A. spicigera*/n-hexane, DCM, MeOH extracts	20, 40, 80 mg/mL	*In vitro*	Toxicity bioassay	*Tribolium castaneum* (red flour beetle)		Insecticidal properties, ↑activity of DCM extract	[145]
A. scoparia/butanol fraction	20 mg/site	*In vivo*	Topically	BALB/C mice	Antiatopic dermatitis	↓clinical symptoms in a DNFB mouse model that induced lesions, ↓inflammatory cytokines	[149]
A. scoparia/aerial parts/methanolic extract	150, 300 mg/kg	*In vivo*	—	Sprague-Dawley rats	Nephroprotective	↓DNA damages, dose = 300 mg/kg, ↓oxidative stress	[150]
A. capillaris Thunb/extract	10 mg/mouse/day	*In vivo*	Topically	Dermatophagoides farinae-sensitized NC/NGA mice	Anti-inflammatory, anti-atopic dermatitis	↓dermatitis scores, ↓bleeding, ↓hyperkeratosis, ↓hypertrophy in the dorsal skin and ear of the epidermis, ↓histamine	[151]
A. pallens/aerial parts/methanolic extract	200, 400 mg/kg	*In vivo*	Orally	Wistar rats	Anti-inflammatory, antioxidative	↓level of hepatic enzymes, ↑renal antioxidant enzymes	[152]
A. vulgaris/leaf/ethanolic extract	250, 500, 750, 1000 mg/kg	*In vivo*	Orally	ICR mice infected with *P. berghei*		↓*P. berghei*, nontoxic	[17]
A. scoparia, *A. spicigera*/dichloromethane extracts	0–2 mg/mL 10% DMSO	*In vitro*	Heme biocrystallization and inhibition assay		Antimalarial	IC_{50} = 0.778 mg/mL, IC_{50} = 0.998 mg/mL	[145]
A. annua/aqueous, hydro alcoholic extracts	—	*In vitro*	Parasite lactate dehydrogenase (pLDH)	*Plasmodium falciparum*		IC_{50} = 3.27 nM, IC_{50} = 4.95 nM	[153]
A. annua/aqueous hydro alcoholic extracts	Aqueous extract 1000 mg/kg/day, hydro alcoholic extract 500 mg/kg/day	*In vivo*	-	*Plasmodium berghei* NK173-infected m ice		↑activity on malaria of artemisinin, both extracts of *A. annua* are effective on malaria	[153]

↑: increase; ↓: decrease; MTT: 3-(4,5-dimethylthiazol-2-yl)-2,5-diphenyl-2H-tetrazolium bromide; DCM: dichloromethane; DNFB: 2,4-*dinitrofluorobenzene*; EPM: elevated plus maze; ESR: erythrocyte sedimentation rate; EO: essential oil; FST: forced swimming test; HDL: high-density lipoprotein; LDL: low-density lipoprotein; MBT: marble-burying test; MIC: minimum inhibitory concentration; OFT: open-field test; PCV: packed cell volume; RBC: red blood cell; SRB: sulforhodamine B; TC: total cholesterol; TGL: triglycerides; WBC: white blood cell; WHO: World Health Organization: i.p.: intraperitoneally; FRAP: ferric-reducing ability of plasma; ABTS: 2,2′-azino-bis(3-ethylbenzothiazoline-6-sulfonic acid; ORAC: oxygen radical absorbance capacity.

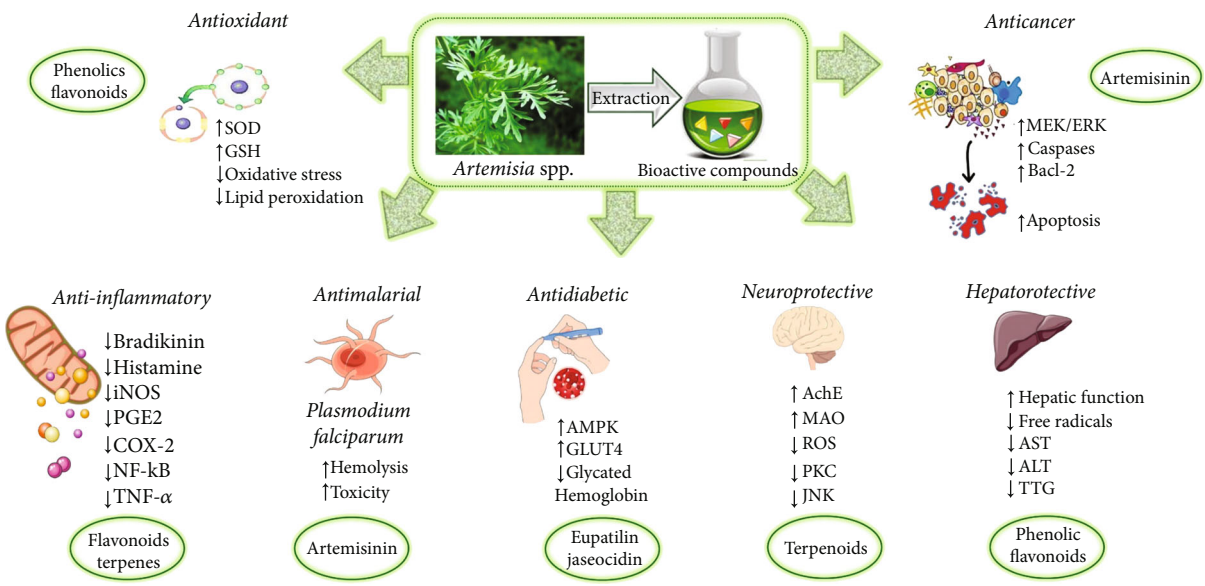

Figure 2: Illustrative scheme with the most representative pharmacological properties of bioactives of *Artemisia* spp. and their potential mechanisms of action. ↑: increase; ↓: decrease; SOD: superoxide dismutase; GSH: glutathione; MEK/ERK: mitogen-activated extracellular signal-regulated kinase/extracellular signal-regulated protein kinase; Bcl-2: B-cell lymphoma 2; *iNOS*: inducible *nitric oxide* synthase; PGE2: prostaglandin E2; *COX-2*: cyclooxygenase-2; NF-κB: nuclear factor kappa *B*; TNF-α: tumor necrosis factor α; AMPK: adenosine monophosphate-activated protein kinase; AST: aspartate aminotransferase; GLUT4: glucose transporter type 4; AchE: acetylcholinesterase; *MAO*: monoamine oxidase; ROS: reactive oxygen species; PKC: protein kinase C; JNK: Jun N-terminal kinase; ALT: alanine transaminase; TTG: tissue transglutaminase antibody.

Furthermore, artemether (40 mg once/day) proved to exhibit a significant improvement in the computed tomography scan of a 75-year-old patient with pituitary macroadenoma. Results showed a decrease in the tumor's density as well as an improvement in the overall clinical signs and symptoms [169].

6.3. Antidiabetic Activity. In a randomized double-blind clinical study, 24 patients with impaired glucose tolerance (IGT) administrated *A. dracunculus* (1000 mg) or placebo before breakfast and dinner for 90 days. Results showed a significant decrease in systolic blood pressure, glycated hemoglobin, and total insulin secretion as well as a significant increase in the high-density lipoprotein cholesterol level [170].

In a dose-response clinical study, ethanolic extract of *Artemisia princeps* Pamp. containing eupatilin and jaseocidin was investigated for its antidiabetic effect in 81 patients with hyperglycemia. Patients were randomized into four groups: negative control (lactose 2000 mg/day), positive control (pinitol 1140 mg/day), low-dose extract (2000 mg/day), and high-dose extract (4000 mg/day). Both doses significantly reduced glycated hemoglobin level, where the free fatty acid level in plasma was only lowered in patients administrated the high dose of the extract [171]. In a similar clinical trial, *A. absinthium* capsules (1 g/twice daily for 30 days) or placebo were administrated to 16 patients with type II diabetes. Results showed that *A. absinthium* reduced the glucose level by 32%, triglycerides by 10%, total cholesterol by 5%, and LDL level by 6% [172].

6.4. Antimalarial Activity. Malaria is considered the most common tropical disease that is provoked by certain parasites of the genus *Plasmodium* such as *P. malariae*, *P. viva*, *P. falciparum*, and *P. ovale* [173]. *Artemisia* species are famous for their content of sesquiterpene lactones that are responsible for the high therapeutic potential of the genus [173, 174]. For instance, artemisinin and its derivatives are the most common sesquiterpene lactones among the genus. Dihydroartemisinin (the active form inside the biological systems) is produced by reducing the lactone of artemisinin. While, alkylation of the hemiacetal group yields arteether and artemether, where artesunate is produced by acylation of the hemiacetal group with succinic acid [175]. Inside *in vivo* systems, all these derivatives are converted to dihydroartemisinin, where it possesses the highest activity, oral bioavailability, and tolerability with minimal side effects. These compounds are well known for their powerful activity against different species of *Plasmodium* as they contain the 1,2,4-trioxane moiety that may be responsible for the mechanism of action of the drugs [122]. The antimalarial activity of these compounds outcomes from the presence of Fe^{2+} after the *Plasmodium* hemolysis. This Fe^{2+} is utilized as a catalyst to open the peroxide bridge of the compound, leading to the formation of free radicals, alkylating *Plasmodium* proteins, and finally causing parasite death. Artemisinin also can perform its antimalarial activity by inhibiting PfATP6, an enzyme for the delivery of Ca^{2+} into vesicles of the parasite, which is critical for its development [122]. In a cluster-randomized clinical trial performed in different African countries, it was determined that rectal artesunate could take

from 4 to 6 h to reduce parasite load, progression of the disease, and risk of death, so it can be a good choice for patients who cannot be treated orally [176]. Moreover, the WHO reviewed different clinical trials performed by the African Quinine Artesunate Malaria Trial multicentre on 5400 children under the age of 15 years with multidrug-resistant severe malaria and suggested IV artesunate (2.4 mg/kg once daily) as a choice to treat malaria [177].

A meta-analysis study using single-patient data from different randomized, controlled trials was conducted to compare artemether and quinine in treating severe *P. falciparum* infection. Results showed that the death rate was significantly reduced with patients treated with artemether (14%) when compared to patients treated with quinine (17%). On the other hand, there was no difference between the 2 treatments in coma recovery, fever clearance, or the progress of neurological toxicity. However, the overall adverse outcomes of either death or neurological toxicity were significantly fewer in the artemether-treated group [178].

In a double-blind, randomized, placebo-controlled clinical trial, artesunate was combined with sulfadoxine-pyrimethamine to test their efficacy in reducing the timing of malaria exposure during the infancy stage. Results showed that innate cells produced a balanced level of pro-inflammatory and regulatory cytokines around 2 years of age, which was accompanied by a lower risk of clinical malaria [179]. Further, it was reported that patients with uncomplicated malaria who administrated this combination therapy exhibited an 84.1% cure rate [180].

Despite the potency of artesunate as an antimalarial drug, there are also two main antimalarial regimen options: dihydroartemisinin–piperaquine (DHA–PPQ) and artemether-lumefantrine (AL), which are considered as the first option for treating uncomplicated *P. falciparum* malaria globally [181]. For instance, DHA–PPQ was reported to have high benefits in children with uncomplicated malaria in endemic countries [182]. On the other hand, the AL therapy (marketed as "Coartem") could exert its antimalarial effect through opposing the erythrocytic stages of the parasite and so reducing the number of parasites. In addition, lumefantrine had a much-extended half-life time when combined with artemether and was supposed to clear residuals of the parasites [183].

As malaria causes severe maternal and fetal problems, the Centers for Disease Control and Prevention (CDC) suggested AL therapy for treating pregnant women with uncomplicated malaria in the United States throughout the second and third trimesters of pregnancy, at the same doses assigned for nonpregnant women [184]. In a case report implemented by Daddy et al. [185], dried leaves of *A. annua* were investigated for their efficacy as an antimalarial agent in patients (with *P. falciparum* infection) not responding to artemisinin combination therapy (ACT) or artesunate (IV). After oral administration of dried leaves of *A. annua* at a dose (0.5 g/twice daily/5 days), these patients exhibited a subside in clinical symptoms and the parasites were undetected microscopically [185]. In a large-scale double-blind, randomized clinical trial, the antimalarial effect of *A. annua* and *A. afra* infusions (1 L/day of dry leaf/twig infusion for 7 days) was compared to artesunate-amodiaquine (ASAQ) by 957 patients with malaria (with *P. falciparum* infection). Results showed that patients treated with both *Artemisia* infusions exhibited trophozoites clearance after 24 h when compared to ASAQ which took up to 14 days. Moreover, fever clearance took up to 48 h for ASAQ, but only 24 h for both *Artemisia* infusions. From days 14–28, gametocytes were undetectable for patients treated with *Artemisia* infusions, whereas on day 28, ASAQ-treated patients stayed carriers for gametocytes. These results proved that *Artemisia* infusions could break the life cycle of malaria by eliminating gametocytes with better outcomes than ASAQ [186]. In a questionnaire performed in Kenya and Uganda (2011) to study the antimalarial effect of *A. annua* teas, results showed prosperous outcomes after treating about 3000 cases including 250 children and 54 women in the first trimester of pregnancy with malaria [187].

6.5. Antiviral Activity as an Approach for Treating COVID-19 Infection. Recently, transposing of medications already in clinical use is the therapeutic strategy for controlling SARS-CoV-2 (COVID-19) infection [188, 189]. The WHO has recommended *A. annua* as a promising remedy for the treatment of COVID-19; however efficacy and side effects are not determined yet [190] (www.ClinicalTrials.gov, Identifier: NCT04530617). Moreover, *A. annua* is one of the ingredients of Jinhua Qinggan granule (one of the remedies suggested in the therapeutic regimen of COVID-19 in China) [191]. Currently, a phase II clinical study is under its way to evaluate the efficacy of *A. annua* in inhibiting the replication of the SARS-CoV-2 virus in patients with high-risk factors such as diabetes and hypertension (www.ClinicalTrials.gov Identifier: NCT04530617). As well, researchers from Saudi Arabia have established a placebo-controlled trial for evaluating the effect of artesunate in patients with mild symptoms of COVID-19 (www.ClinicalTrials.gov Identifier: NCT04387240).

Scientific evidence of this strategy might be due to the promising anti-inflammatory, immunomodulatory, and antiviral properties of the bioactive compounds in different *Artemisia* species, either among the preclinical or the clinical levels [4]. For instance, 85 patients with SARS were selected for a clinical study and 62 patients received the consigned treatment combined with the traditional Chinese medicine (TCM) (one of its components is herba *Artemisia*), while 23 patients were assigned in the control group. Results showed that patients who received the combined TCM regimen daily for 3 weeks showed a significant decrease in the total score of symptoms, as well as improvement of the lung X-rays, hepatic function, quality of life, and total score of mental sentiment factors [192].

Recently, it was reported that 1250 medical staff in Tongxu County Hospital take one or more decoctions of TCM daily as well as burn *Artemisia argyi* H.Lév. & Vaniot in the hospital corridor to cut off the route of transmitting infection, where *A. argyi* was stated as one of the herbs that can be used for contagion prevention by aromatherapy [193]. Artemisinin and its derivatives proved to have promising activities as antiviral agents. For instance, artesunate (100 mg/day) was examined for its efficacy to treat a 12-

year patient with human cytomegalovirus (HCMV) infection who exhibited resistance against assigned antiviral drugs (foscarnet and ganciclovir) after stem cell transplantation. Results showed a significant reduction in viral load at day 7, with a virus half-life of 0.9–1.9 days, representing an effective stopover in viral replication [194].

7. Safety Issues of Artemisi*a* Species

Various reports have been published regarding toxicity related to the overdosing in humans with extracts of *Artemisia*; *A. absinthium* (wormwood) was used in the formulation of the absinthe drink and currently has been restricted in most countries because of neurotoxicity [195, 196]; it was reported that few cups of sage tea or wormwood would be essential to reach the suitable daily intakes [195]. Preclinical studies of the toxicity of *Artemisia* species were examined in many reports and the most important results were summarized in Table 4. Regarding *Artemisia* spp. toxicity, different parts of *Artemisia spicigera* K. Koch and *Artemisia fragrans* Willd. significantly increased the number of MCF7 and HEK293 cell proliferation [126]. Moreover, the toxicological study of *Artemisia judaica* L. has been studied by Nofal et al. [197] and observed acute and chronic toxicity. Furthermore, *Artemisia parviflora* Roxb. ex D. Don showed no significant toxic effect on Swiss albino mice [198] as shown in Table 4. In addition, there is only one report on the toxicity of *A. vulgaris* [199] while different studies of *A. annua* demonstrated that it is considered safe and nontoxic up to 5000 mg/kg of the extract [200]. Artemether and the closely related compound arteether are hydrophobic derivatives of dihydroartemisinin reported to have neurotoxicity action [201].

8. Limitations, Therapeutic Perspectives, and Clinical Gaps

Although *Artemisia* spp. and its constituents show great potential as functional foods, dietary supplements, and safe medicines, some adverse effects have been described in the literature [206]. *A. absinthium*, grand wormwood, has been included traditionally as a major component of the highly anise-flavoured alcoholic spirit, "Absinthe," which was the most popular alcoholic beverage of the late 19th century in Europe [207]. Absinthe was prohibited at the beginning of the 20th century as a consequence of adverse symptoms called absinthism [208]. Absinthism symptoms included hallucinations, blindness, mental deterioration, and convulsions. The prebanned Absinthe was probably related to chronic alcoholism [207]. Several drugs can interact with the effects produced by Artemisinin, and therefore, the specialist should be consulted before taking it. *A. absinthium* is permitted nowadays in foods and alcoholic beverages. The consumption of thujone from *Artemisia* must not exceed 10 mg/kg according to the European Food Safety Authority (EFSA) and 3 mg/day/person according to European Medicines Agency (EMA) [206].

Some *Artemisia* species are used in regulating fertility and thus should be avoided in pregnancy due to the possible risk of embryotoxicity at higher doses. For instance, the consumption of *A. herba-alba* to pregnant mice significantly decreased the fertility ratio of offspring mice [209]. Additionally, consumption of *A. kopetdaghensis* "Krasch., Popov & Lincz. ex Poljakov" hydroalcoholic extract in pregnancy increases the risk of abortion [210].

Skin contact dermatitis has been reported upon exposure to different *Artemisia* species [211, 212]. Skin prick testing showed that the majority of patients with allergic rhinitis and asthma have positive reactions to *A. vulgaris*. Therefore, patients with *Compositae* sensitization are routinely warned against exposure to *Artemisia* species [213]. Artemisia-induced dermatitis is attributed to the content of sesquiterpene lactones [214].

Pollens from *Artemisia* species can cause serious pollinosis [206]. Nasal challenge and bronchial provocation tests verified that pollens, leaves, and stems from *Artemisia* are serious allergens causing allergic rhinitis and/or asthma [215, 216]. For instance, pollens from mugwort, *A. vulgaris*, contained allergenic substances such as profiling as well as other crossreactive allergens with immunoglobulin E (IgE) reactivity causing immediate type I allergic reactions [217]. Type I hypersensitivity involves mast cell degranulation and the release of inflammatory mediators such as histamine, causing allergic reactions such as anaphylactic shock [218]. Additionally, *A. vulgaris* pollens showed the highest levels of endotoxin among other collected plants across 100 locations in Europe [219]. Pollen extracts of six different *Artemisia* species, *A. annua*, *A. scoparia*, *A. vulgaris*, *A. princeps*, *Artemisia campestris* L., and *Artemisia tridentata* Nutt. exhibited an extensive degree of similarity and crossreactivity [220]. This study also showed that Korean and Norwegian patient sera had the same pattern of reactivity towards *A. vulgaris* and *A. princeps* [220].

Clinically, administration of the sesquiterpene lactone artemisinin as well as its derivatives such as arteether, artesunate, and artemether in appropriate therapeutic doses for short periods did not show serious side effects [221, 222]. In the liver, artemisinin is converted to various inactive metabolites, such as deoxy artemisinin, deoxyhydroartemisinin, crystal 7, and 9,10-dihydrodeoxyarthemisinin. The reaction is catalyzed by a CYP2B6 enzyme, while another CYP3A4 enzyme acts as a secondary catalyst. These enzymes belong to the cytochrome P450 group present in the smooth endoplasmic reticulum. Artemisinin derivatives are metabolized differently. They are first converted to dihydroartemisinin (DHA). DHA itself is a powerful antimalarial molecule and is active in the bloodstream for two to three hours [223]. The antimalarial activity of artesunate is actually only through DHA [224]. Artesunate is converted to DHA within one minute of absorption. About 90% of all DHA is normally bound to blood plasma. In the liver, the cytochrome P450 enzyme system (including CYP2A6, CYP3A4, and CYP3A5) converts DHA into inactive metabolites [225]. All metabolites are subject to glucuronidation and are excreted in the urine or faeces. UDP-glucuronosyltransferases, especially UGT1A9 and UGT2B7, are responsible for the process [226]. DHA is also excreted in the bile as minor glucuronides, such as tetrahydrofuran acetate. Due to its rapid metabolism, artemisinin is a relatively safe

Table 4: Toxicological studies of *Artemisia* species.

Extract/compound	Doses	*In vitro*/*in vivo*	Route of administration	Model	Effect	Ref
A. annua /leaf/hexane extract	1000, 2000, 2500 mg/kg	*In vivo*	i.p.	Wistar albino rats	↓carbohydrate, protein, lipid metabolisms, unfavourable effect on nutritional benefits, ↓hematological parameters, ↓toxicity when used acutely in rats	[202]
A. annua/hydroethanolic extract	300, 2000, 5000 mg/kg	*In vivo*	Orally	Swiss albino mice	No toxic or lethal reactions of all the doses	[200]
A. parviflora/aerial parts/ethanolic extract	0.10, 0.50, 1.0 g/kg	*In vivo*	Orally	Swiss albino mice	No significant toxic effect $LD_{50} > 1$ g/kg BW	[198]
A. abyssinica, *A. inculta*/aerial parts/ethanolic extracts	500 mg/kg, 1 and 3 g/kg	*In vivo*	Orally	Swiss albino mice	*A. inculta*, dose = 3 g/kg: CNS stimulation, *A. abyssinica*, dose = 3 g/kg: ↓locomotor activity	[203]
A. vulgaris/oils	—	*In vivo*	—	Brine shrimp *Artemia* sp. (larvae)	$LC_{50} = 10.4–23.3$ μg/mL germacrene D, camphor, 1,8-cineol, davanone: ↑toxicity	[199]
A. afra/aqueous extract	1.5–5.5 g/kg i.t., 2–24 g/kg o.p.	*In vivo*	i.p., orally	BALB/C mice, Wistar rats	Nontoxic when given acutely, low chronic toxicity, hepatoprotective effect in high doses	[204]
Artemether	0, 20, 40, 80 mg/kg i.m., 0, 50, 150, 600 mg/kg p.o.	*In vivo*	i.m., orally	Beagle dogs	High i.m. doses: neurological damage, dose = 20 mg/kg: minimal effects occurred	[201]
Artemether, artesunate	30–100 mg/kg/day	*In vivo*	i.m.	Swiss albino mice	Artemether neurotoxicity is significantly more neurotoxic than i.m. artesunate	[205]

bioactive compound [227]. Because artemisinin interactions with other drugs are not fully known, future clinical studies are needed to establish their potential interaction mechanisms.

Other limitations derive from the amounts of active ingredients in plants, depending on the area of cultivation and climate [228–230]. Also, the absorption of bioactive compounds rapidly and in variable quantities requires the future development of pharmaceutical nanoformulations that will improve the bioavailability and implicitly an increased therapeutic efficacy [231, 232].

9. Overall Conclusion

Artemisia spp. have been traditionally used for pharmacological purposes and as an edible plant used in food, spices, and beverages. *A. annua* and *A. absinthium* are the most famous *Artemisia* species. This genus distributed worldwide presents diverse chemical constituents mainly EOs and polyphenols. These species contain sesquiterpene lactones that are largely responsible for the therapeutical potential of *Artemisia* genus. The most studied biological activities of this genus are antioxidant, anti-inflammatory, antitumor, antidiabetic, antimalarial, neuroprotective, and hepatoprotective activities through preclinical and clinical evidence. *Artemisia* spp. and their constituents show great potential as dietary supplements, functional foods, and safe medicines as antimalarial, antioxidant, anticancer, antinociceptive, anti-inflammatory, and antiviral agents. The antiviral activity for treating COVID-19 infection is a hope for the current pandemic. However, it is really important and necessary for further research investigations for discovering safer *Artemisia* plant-derived drugs for curing several kinds of diseases.

Data Availability

The data supporting this review are from previously reported studies and datasets, which have been cited. The processed data are available from the corresponding author upon request.

Conflicts of Interest

The authors have no relevant affiliations or financial involvement with any organization or entity with a financial interest in or financial conflict with the subject matter or materials discussed in the manuscript. This includes employment, consultancies, honoraria, stock ownership or options, expert testimony, grants or patents received or pending, or royalties.

Authors' Contributions

All authors made a significant contribution to the work reported, whether that is in the conception, study design, execution, acquisition of data, analysis, and interpretation or in all these areas, that is, revising or critically reviewing the article, giving final approval of the version to be published, and agreeing on the journal to which the article has been submitted and confirm to be accountable for all aspects of the work.

Acknowledgments

MM wants to thank ANID Centros Basales, ACE210012.

References

[1] J. Sharifi-Rad, C. Quispe, M. Kumar et al., "*Hyssopus* essential oil: an update of its phytochemistry, biological activities, and safety profile," *Oxidative Medicine and Cellular Longevity*, vol. 2022, Article ID 8442734, 10 pages, 2022.

[2] X. Z. Su and L. H. Miller, "The discovery of artemisinin and the Nobel Prize in Physiology or Medicine," *Science China Life Sciences*, vol. 58, pp. 1175–1179, 2015.

[3] A. Ahuja, Y.-S. Yi, M.-Y. Kim, and J. Y. Cho, "Ethnopharmacological properties of *Artemisia asiatica*: a comprehensive review," *Journal of Ethnopharmacology*, vol. 220, pp. 117–128, 2018.

[4] K. S. Bora and A. Sharma, "The genus *Artemisia*: a comprehensive review," *Pharmaceutical Biology*, vol. 49, no. 1, pp. 101–109, 2011.

[5] M. Nigam, M. Atanassova, A. P. Mishra et al., "Bioactive compounds and health benefits of *Artemisia* species," *Natural Product Communications*, vol. 14, no. 7, 2019.

[6] International Union for Conservation of Nature, "Global Species Programme Red List Unit," https://www.iucnredlist.org/search/list?taxonomies=115307&searchType=species.

[7] J. Ahuja, J. Suresh, N. Paramakrishnan, K. Mruthunjaya, and M. N. Naganandhini, "An ethnomedical, phytochemical and pharmacological profile of *Artemisiaparviflora* Roxb," *Journal of Essential Oil Bearing Plants*, vol. 14, no. 6, pp. 647–657, 2011.

[8] J. A. T. da Silva, "Mining the essential oils of the Anthemideae," *African Journal of Biotechnology*, vol. 3, no. 12, pp. 706–720, 2004.

[9] B. K. Ryu, B. O. Ahn, T. Y. Oh, S. H. Kim, W. B. Kim, and E. B. Lee, "Studies on protective effect of DA-9601, *Artemisia asiatica* extract, on acetaminophen-and CCI 4-induced liver damage in rats," *Archives of Pharmacal Research*, vol. 21, no. 5, pp. 508–513, 1998.

[10] X. Feng, S. Cao, F. Qiu, and B. Zhang, "Traditional application and modern pharmacological research of *Artemisia annua* L," *Pharmacology & Therapeutics*, vol. 216, article 107650, 2020.

[11] G. E.-S. Batiha, A. Olatunde, A. El-Mleeh et al., "Bioactive compounds, pharmacological actions, and pharmacokinetics of wormwood (*Artemisia absinthium*)," *Antibiotics*, vol. 9, no. 6, 2020.

[12] N. Liu, F. Van der Kooy, and R. Verpoorte, "*Artemisia afra*: a potential flagship for African medicinal plants?," *South African Journal of Botany*, vol. 75, no. 2, pp. 185–195, 2009.

[13] B. J. Khezrilu and R. Heidari, "The evaluation of antioxidant activities and phenolic compounds in leaves and inflorescence of *Artemisia dracunculus* L. by HPLC," *Journal Of Medicinal Plants*, vol. 13, no. 51, pp. 41–50, 2014.

[14] M. Samyal, H. Kumar, S. Khokra, B. Parashar, R. Sahu, and Z. Ahmed, "Evaluation of antidiabetic and antihyperlipidemic effects of *Artemisia dracunculus* extracts in

streptozotocin-induced-diabetic rats," *Pharmacologyonline*, vol. 2, pp. 1230–1237, 2011.

[15] K. Sharmila and P. Padma, "Anticancer activity of *Artemisia vulgaris* on hepatocellular carcinoma (HepG2) cells," *International Journal of Pharmacy and Pharmaceutical Sciences*, vol. 5, pp. 479–483, 2013.

[16] A. H. Gilani, S. Yaeesh, Q. Jamal, and M. N. Ghayur, "Hepatoprotective activity of aqueous–methanol extract of *Artemisia vulgaris*," *Phytotherapy Research: An International Journal Devoted to Pharmacological and Toxicological Evaluation of Natural Product Derivatives*, vol. 19, no. 2, pp. 170–172, 2005.

[17] G. S. Bamunuarachchi, W. D. Ratnasooriya, S. Premakumara, and P. V. Udagama, "Antimalarial properties of *Artemisia vulgaris* L. ethanolic leaf extract in a Plasmodium berghei murine malaria model," *Journal Vector-Borne Disease*, vol. 50, pp. 278–284, 2013.

[18] E. R. de Almeida, A. R. da Silva, A. C. Aragatilde et al., "Anticonvulsant and anxiolytic assessment of leaves from *Artemisia vulgaris* L. in mice," *Journal of Medicinal Plants Research*, vol. 7, no. 45, pp. 3325–3331, 2013.

[19] V. I. Ninditya, E. Purwati, A. T. Utami et al., "*Artemisia vulgaris* efficacies against various stages of Aedes aegypti," *Veterinary World*, vol. 13, no. 7, pp. 1423–1429, 2020.

[20] D. Bisht, D. Kumar, D. Kumar, K. Dua, and D. K. Chellappan, "Phytochemistry and pharmacological activity of the genus *Artemisia*," *Archives of Pharmacal Research*, vol. 44, no. 5, pp. 439–474, 2021.

[21] J. Ding, L. Wang, C. He, J. Zhao, L. Si, and H. Huang, "Artemisia scoparia: traditional uses, active constituents and pharmacological effects," *Journal of Ethnopharmacology*, vol. 273, article 113960, 2021.

[22] O. A. Adewumi, V. Singh, and G. Singh, "Chemical composition, traditional uses and biological activities of *Artemisia* species," *Journal of Pharmacognosy and Phytochemistry*, vol. 9, no. 5, pp. 1124–1140, 2020.

[23] World Flora OnlineWFO The World Flora Online. Availabe online: http://www.worldfloraonline.org/.

[24] M. Sanz, R. Vilatersana, O. Hidalgo et al., "Molecular phylogeny and evolution of floral characters of *Artemisia* and allies (Anthemideae, Asteraceae): evidence from nrDNA ETS and ITS sequences," *Taxon*, vol. 57, no. 1, pp. 66–78, 2008.

[25] M. J. Abad, L. M. Bedoya, L. Apaza, and P. Bermejo, "The *artemisia* L. Genus: a review of bioactive essential oils," *Molecules*, vol. 17, no. 3, pp. 2542–2566, 2012.

[26] A. Septembre-Malaterre, M. Lalarizo Rakoto, C. Marodon et al., "*Artemisia annua*, a traditional plant brought to light," *International Journal of Molecular Sciences*, vol. 21, no. 14, p. 4986, 2020.

[27] V. A. Funk, R. J. Bayer, S. C. Keeley et al., "Everywhere but Antarctica: using a supertree to understand the diversity and distribution of the compositae," *Plant Diversity and Complexity Patterns: Local, Regional, and Global Dimensions*, vol. 55, pp. 343–374, 2005.

[28] S. Alesaeidi and S. Miraj, "A systematic review of anti-malarial properties, immunosuppressive properties, anti-inflammatory properties, and anti-cancer properties of *Artemisia annua*," *Electron Physician*, vol. 8, no. 10, pp. 3150–3155, 2016.

[29] M. Sanz, G. M. Schneeweiss, R. Vilatersana, and J. Vallès, "Temporal origins and diversification of *Artemisia* and allies (Anthemideae, Asteraceae)," *Collectanea Botanica*, vol. 30, pp. 7–15, 2011.

[30] J. Valles and E. D. McArthur, "*Artemisia* systematics and phylogeny: cytogenetic and molecular insights," in *Shrubland ecosystem genetics and biodiversity: proceedings*, E. D. Mcarthur and D. J. Fairbanks, Eds., pp. 67–74, U.S. Department of Agriculture, Forest Service, Rocky Mountain Research Station, Ogden, UT, 2001.

[31] J. Valles and T. Garnatje, "*Artemisia* and its allies: genome organization and evolution and their biosystematic, taxonomic and phylogenetic implications in the Artemisiinae and related subtribes (Asteraceae, Anthemideae)," in *Plant Genome: Biodiversity and Evolution*, A. Sharma, Ed., vol. 1B, pp. 225–285, Science Publishers, Enfield, 2005.

[32] J. Pellicer, T. Garnatje, J. Molero, F. Pustahija, S. Siljak-Yakovlev, and J. Valles, "Origin and evolution of the South American endemic *Artemisia* species (Asteraceae): evidence from molecular phylogeny, ribosomal DNA and genome size data," *Australian Journal of Botany*, vol. 58, no. 7, pp. 605–616, 2010.

[33] S. Garcia, E. D. McArthur, J. Pellicer, S. C. Sanderson, J. Vallès, and T. Garnatje, "A molecular phylogenetic approach to western North America endemic *Artemisia* and allies (Asteraceae): untangling the sagebrushes," *American Journal of Botany*, vol. 98, no. 4, pp. 638–653, 2011.

[34] Y. R. Ling, "The Old World Seriphidium (Compositae)," *Bulletin of Botanical Research*, vol. 11, pp. 1–40, 1991.

[35] Y. R. Ling, "The genera *Artemisia* L. and *Seriphidium* (Bess.) Poljak. in the world," *Compositae Newslett*, vol. 25, pp. 39–45, 1994.

[36] C. De Clerck, M. Genva, M. H. Jijakli, and M.-L. Fauconnier, "Use of essential oils and volatile compounds as biological control agents," *Foods*, vol. 10, no. 5, p. 1062, 2021.

[37] K. Başer and G. Buchbauer, "Handbook of Essential Oils: Science," in *Technology and Applications*, p. 994, CRC Pres, Boca Raton, London, New York, 2010.

[38] P. N. Kaul, A. K. Bhattacharya, B. R. Rajeswara Rao, K. V. Syamasundar, and S. Ramesh, "Volatile constituents of essential oils isolated from different parts of cinnamon (*Cinnamomum zeylanicum Blume*)," *Journal of the Science of Food and Agriculture*, vol. 83, no. 1, pp. 53–55, 2003.

[39] T. M. Vieira, H. J. Dias, T. C. Medeiros et al., "Chemical composition and antimicrobial activity of the essential oil of *Artemisia absinthium* Asteraceae leaves," *Journal of Essential Oil Bearing Plants*, vol. 20, no. 1, pp. 123–131, 2017.

[40] J.-y. Liang, W.-t. Wang, Y.-f. Zheng et al., "Bioactivities and chemical constituents of essential oil extracted from *Artemisia anethoides* against two stored product insects," *Journal of Oleo Science*, vol. 66, no. 1, pp. 71–76, 2017.

[41] H. Liu, S. S. Guo, L. Lu et al., "Essential oil from *Artemisia annua* aerial parts: composition and repellent activity against two storage pests," *Natural Product Research*, vol. 35, no. 5, pp. 822–825, 2021.

[42] S. V. Zhigzhitzhapova, E. P. Dylenova, S. M. Gulyaev et al., "Composition and antioxidant activity of the essential oil of *Artemisia annuaL*," *Natural Product Research*, vol. 34, no. 18, pp. 2668–2671, 2020.

[43] A. Russo, M. Bruno, R. Avola, V. Cardile, and D. Rigano, "Chamazulene-rich *Artemisia arborescens* essential oils affect the cell growth of human melanoma cells," *Plants*, vol. 9, no. 8, p. 1000, 2020.

[44] X. Guan, D. Ge, S. Li, K. Huang, J. Liu, and F. Li, "Chemical composition and antimicrobial activities of *Artemisia argyi* Lévl. et Vant essential oils extracted by simultaneous distillation-extraction, subcritical extraction and hydrodistillation," *Molecules*, vol. 24, no. 3, p. 483, 2019.

[45] M. I. Rocha, M. J. Gonçalves, C. Cavaleiro et al., "Chemical characterization and bioactive potential of *Artemisia campestris* L. subsp. *maritima* (DC) Arcang. essential oil and hydrodistillation residual water," *Journal of Ethnopharmacology*, vol. 276, article 114146, 2021.

[46] S. Ammar, H. Noui, S. Djamel et al., "Essential oils from three Algerian medicinal plants (*Artemisia campestris*, *Pulicaria arabica*, and *Saccocalyx satureioides*) as new botanical insecticides?," *Environmental Science and Pollution Research*, vol. 27, no. 21, pp. 26594–26604, 2020.

[47] A. Al Jahid, A. Elamrani, F. A. Lahlou et al., "Chemical composition and antibacterial activity of the essential oil isolated from the seeds of Moroccan *Artemisia campestrisL*," *Journal of Essential Oil Bearing Plants*, vol. 20, no. 2, pp. 375–384, 2017.

[48] A. Abidi, E. Sebai, M. Dhibi et al., "Chemical analyses and anthelmintic effects of *Artemisia campestris* essential oil," *Veterinary Parasitology*, vol. 263, pp. 59–65, 2018.

[49] B. A. Behbahani, F. Shahidi, F. T. Yazdi, S. A. Mortazavi, and M. Mohebbi, "Antioxidant activity and antimicrobial effect of tarragon (*Artemisia dracunculus*) extract and chemical composition of its essential oil," *Journal of Food Measurement and Characterization*, vol. 11, no. 2, pp. 847–863, 2017.

[50] M. Szczepanik, M. Walczak, B. Zawitowska et al., "Chemical composition, antimicromicrobial activity and insecticidal activity against the lesser mealworm *Alphitobius diaperinus* (Panzer)(Coleoptera: Tenebrionidae) of *Origanum vulgare* L. ssp. hirtum (Link) and Artemisia dracunculus L. essential oils," *Journal of the Science of Food and Agriculture*, vol. 98, no. 2, pp. 767–774, 2018.

[51] S. V. Zhigzhitzhapova, B. T. B. Namzalov, and L. D. Radnaeva, "Composition of Essential Oil of *Artemisia gmelinii* Web. ex Stechm. of Priolkhonian Flora (Lake Baikal)," *Ecology*, vol. 14, no. 1, pp. 71–78, 2021.

[52] Q. Xu, L. Zhang, S. Yu, G. Xia, J. Zhu, and H. Zang, "Chemical composition and biological activities of an essential oil from the aerial parts of *Artemisia Gmelinii* weber ex Stechm," *Natural Product Research*, vol. 35, pp. 346–349, 2021.

[53] M. Qadir, A. K. Maurya, A. A. Waza, V. K. Agnihotri, and W. A. Shah, "Chemical composition, antioxidant and cytotoxic activity ofArtemisia gmeliniiessential oil growing wild in Kashmir valley," *Natural Product Research*, vol. 34, no. 22, pp. 3289–3294, 2020.

[54] G. Amor, L. Caputo, A. La Storia, V. De Feo, G. Mauriello, and T. Fechtali, "Chemical composition and antimicrobial activity of Artemisia herba-alba and *Origanum majorana* essential oils from Morocco," *Molecules*, vol. 24, no. 22, p. 4021, 2019.

[55] F. Elmhalli, S. S. Garboui, A. K. B. Karlson, R. Mozūraitis, S. L. Baldauf, and G. Grandi, "Acaricidal activity against *Ixodes ricinus* nymphs of essential oils from the Libyan plants *Artemisia herba alba*, *Origanum majorana* and *Juniperus phoenicea*," *Veterinary Parasitology: Regional Studies and Reports*, vol. 24, article 100575, 2021.

[56] S. Bellili, S. Jazi, M. Y. Hrira et al., "Phytochemical identification of volatile fraction, essential oil and screening of antioxidant, antibacterial, allelopathic and insecticidal potential from *Artemisia herba-alba* leaves," *Main Group Chemistry*, vol. 16, no. 2, pp. 95–109, 2017.

[57] N. Jaradat, "Phytochemical profile and in vitro antioxidant, antimicrobial, vital physiological enzymes inhibitory and cytotoxic effects of *Artemisia jordanica* leaves essential oil from palestine," *Molecules*, vol. 26, no. 9, p. 2831, 2021.

[58] M. A. Al-Qudah, M. A. Onizat, A. K. Alshamari et al., "Chemical composition and antioxidant activity of Jordanian *Artemisia judaica* L. as affected by different drying methods," *International Journal of Food Properties*, vol. 24, no. 1, pp. 482–492, 2021.

[59] A. Guetat, F. A. Al-Ghamdi, and A. K. Osman, "The genus *Artemisia* L. in the northern region of Saudi Arabia: essential oil variability and antibacterial activities," *Natural Product Research*, vol. 31, no. 5, pp. 598–603, 2017.

[60] S. B. González, B. Gastaldi, C. Catalán et al., "Artemisia magellanica. Chemical composition of the essential oil from an unexplored endemic species of Patagonia," *Chemistry & Biodiversity*, vol. 16, no. 7, article e1900125, 2019.

[61] R. M. Romeilah, H. S. El-Beltagi, E. A. Shalaby et al., "Antioxidant and cytotoxic activities of Artemisia monosperma L. and *Tamarix aphylla* L. essential oils," *Notulae Botanicae Horti Agrobotanici Cluj-Napoca*, vol. 49, no. 1, pp. 12233–12233, 2021.

[62] T. Mishra, M. Srivastava, A. Kumar, M. Pal, and S. Tewari, "Chemical composition and termiticidal activity of *Artemisia nilagirica* Essential oil growing in Southern Hilly regions of India," *Journal of Essential Oil Bearing Plants*, vol. 20, no. 1, pp. 247–252, 2017.

[63] P. Sainz, M. F. Andrés, R. A. Martínez-Díaz et al., "Chemical composition and biological activities of *Artemisia pedemontana* subsp. assoana essential oils and hydrolate," *Biomolecules*, vol. 9, no. 10, p. 558, 2019.

[64] R. Dehghani Bidgoli, "Chemical composition of essential oil and antifungal activity of *Artemisia persica* Boiss. from Iran," *Journal of Food Science and Technology*, vol. 58, no. 4, pp. 1313–1318, 2021.

[65] C.-Y. Jiang, S.-X. Zhou, Z. Toshmatov et al., "Chemical composition and phytotoxic activity of the essential oil of *Artemisia sieversiana* growing in Xinjiang, China," *Natural Product Research*, vol. 36, no. 9, pp. 2434–2439, 2022.

[66] M. Qadir, A. K. Maurya, V. K. Agnihotri, and W. A. Shah, "Volatile composition, antibacterial and antioxidant activities of *Artemisia tourne fortiana* Reichb. from Kashmir, India," *Natural Product Research*, vol. 35, no. 1, pp. 152–156, 2021.

[67] S. Malik, L. S. S. de Mesquita, C. R. Silva et al., "Chemical profile and biological activities of essential oil from Artemisia vulgaris L. cultivated in Brazil," *Pharmaceuticals*, vol. 12, no. 2, p. 49, 2019.

[68] A. Judžentienė and J. Būdienė, "Mugwort (*Artemisia vulgaris* L.) essential oils rich in germacrene D, and their toxic activity," *Journal of Essential Oil Research*, vol. 33, no. 3, pp. 256–264, 2021.

[69] H. O. Elansary, A. Szopa, P. Kubica, H. Ekiert, D. O. El-Ansary, and A. Al-Mana, "Polyphenol content and biological activities of Ruta graveolens L. and *Artemisia abrotanum* L. in Northern Saudi Arabia," *Processes*, vol. 8, no. 5, p. 531, 2020.

[70] X. Zhang, Y. Zhao, L. Guo, Z. Qiu, L. Huang, and X. Qu, "Differences in chemical constituents of *Artemisia annua* L from different geographical regions in China," *Plos ONE*, vol. 12, no. 9, article e0183047, 2017.

[71] A. Al Jahid, S. Essabaq, A. Elamrani, M. Blaghen, and J. Jamal Eddine, "Chemical composition, antimicrobial and antioxidant activities of the essential oil and the hydro-alcoholic extract of *Artemisia campestris* L. leaves from southeastern Morocco," *Journal of Biologically Active Products from Nature*, vol. 6, no. 5-6, pp. 393–405, 2016.

[72] F. Yu, H. Qian, J. Zhang, J. Sun, and Z. Ma, "Simultaneous quantification of eight organic acid components in *Artemisia capillaris* Thunb (Yinchen) extract using high-performance liquid chromatography coupled with diode array detection and high-resolution mass spectrometry," *Journal of Food and Drug Analysis*, vol. 26, no. 2, pp. 788–795, 2018.

[73] B. H. Kiani, N. Ullah, and B. Mirza, "Transgenic *Artemisia dubia* WALL showed altered phytochemistry and pharmacology," *Arabian Journal of Chemistry*, vol. 12, no. 8, pp. 2644–2654, 2019.

[74] Y. K. Lee, E. Y. Hong, and W. K. Whang, "Inhibitory effect of chemical constituents isolated from *Artemisia iwayomogi* on polyol pathway and simultaneous quantification of major bioactive compounds," *BioMed Research International*, vol. 2017, Article ID 7375615, 12 pages, 2017.

[75] S. Amkiss, A. Dalouh, and M. Idaomar, "Chemical composition, genotoxicity and antigenotoxicity study of *Artemisia herba-alba* using the eye and wing SMART assay of *Drosophila melanogaster*," *Arabian Journal of Chemistry*, vol. 14, no. 3, article 102976, 2021.

[76] Y. T. Zeng, J. M. Jiang, H. Y. Lao, J. W. Guo, Y. N. Lun, and M. Yang, "Antitumor and apoptotic activities of the chemical constituents from the ethyl acetate extract of *Artemisia indica*," *Molecular Medicine Reports*, vol. 11, no. 3, pp. 2234–2240, 2015.

[77] Z.-Z. He, J.-F. Yan, Z.-J. Song et al., "Chemical constituents from the aerial parts of *Artemisia minor*," *Journal of Natural Products*, vol. 72, no. 6, pp. 1198–1201, 2009.

[78] Q. Wang, M. L. Wang, X. He, and Q. Wang, "Structural elucidation of two new diphenylethanes from *Artemisia mongolica*," *Chemistry of Natural Compounds*, vol. 57, no. 3, pp. 448–450, 2021.

[79] K. Zan, X.-Q. Chen, M.-B. Zhao, and P.-F. Tu, "Sesquiterpenoids from aerial parts of *Artemisia myriantha*," *China Journal of Chinese Materia Medica*, vol. 41, no. 15, pp. 2833–2837, 2016.

[80] O. Panasenko, V. Mozul, O. Denysenko, I. Aksonova, and T. Oberemko, *Characteristic of the Chemical Composition of Artemisia Pontica L*, 2021.

[81] T. Wu, F. He, Q. L. Ma, J. Chen, and H. A. Aisa, "Chemical constituents of *Artemisia rupestris*," *Chemistry of Natural Compounds*, vol. 53, no. 5, pp. 991–993, 2017.

[82] G. S. Stojanović, J. D. Ickovski, A. S. Đorđević et al., "The first report on chemical composition and antimicrobial activity of *Artemisia scoparia* Waldst. et Kit. extracts," *Natural Product Communications*, vol. 15, no. 3, article 1934578X2091503, 2020.

[83] C. A. Geng, X. Y. Huang, X. L. Chen et al., "Three new anti-HBV active constituents from the traditional Chinese herb of Yin-Chen (*Artemisia scoparia*)," *Journal of Ethnopharmacology*, vol. 176, pp. 109–117, 2015.

[84] Z. Suzhang and Y. Wei, "Study on the chemical constituents of *Artemisia scoparia*," *Journal of Xinjiang Medical University*, vol. 39, pp. 408–410, 2016.

[85] F. Heshmati Afshar, M. Zadehkamand, Z. Rezaei, A. Delazar, V. Tarhriz, and P. Asgharian, "Chemical compositions, antimicrobial effects, and cytotoxicity of Asia minor wormwood (*Artemisia splendens* Willd) growing in Iran," *BMC Chemistry*, vol. 15, no. 1, p. 33, 2021.

[86] M. Mojarrab, G. Saremi, and S. A. Emami, "Evaluation of antioxidant activity and identification of main compounds of various extracts of *Artemisia turanica* aerial parts," *Research Journal of Pharmacognosy*, vol. 4, pp. 36–36, 2017.

[87] S. Safari and M. Taherkhani, "Extraction and Identification of flavon from *Artemisia turanica* Krasch the extractwhich has been collected from Esfarayen, Khorasan province," *Eco-phytochemical Journal of Medicinal Plants*, vol. 6, no. 1, pp. 44–55, 2018.

[88] T. Van Nguyen Thien, L. T. K. Tran, N. T. T. Nhu et al., "A new eudesmane-type sesquiterpene from the leaves of Artemisia vulgaris," *Chemistry of Natural Compounds*, vol. 54, no. 1, pp. 66–68, 2018.

[89] A. Ramazani, S. Sardari, S. Zakeri, and B. Vaziri, "In vitro antiplasmodial and phytochemical study of five *Artemisia* species from Iran and in vivo activity of two species," *Parasitology Research*, vol. 107, no. 3, pp. 593–599, 2010.

[90] A. R. Bilia, D. Lazari, L. Messori, V. Taglioli, C. Temperini, and F. F. Vincieri, "Simple and rapid physico-chemical methods to examine action of antimalarial drugs with hemin:," *Life Sciences*, vol. 70, no. 7, pp. 769–778, 2002.

[91] K. C.-S. C. Liu, S.-L. Yang, M. Roberts, B. Elford, and J. Phillipson, "Antimalarial activity of *Artemisia annua* flavonoids from whole plants and cell cultures," *Plant Cell Reports*, vol. 11, no. 12, pp. 637–640, 1992.

[92] A. R. Bilia, A. R. Sannella, F. F. Vincieri et al., "Antiplasmodial effects of a few selected natural flavonoids and their modulation of artemisinin activity," *Natural Product Communications*, vol. 3, no. 12, 2008.

[93] B. Salehi, J. Sharifi-Rad, E. Capanoglu et al., "*Cucurbita* plants: from farm to industry," *Applied Sciences*, vol. 9, no. 16, p. 3387, 2019.

[94] B. Salehi, M. S. Shetty, N. V. A. Kumar et al., "*Veronica* plants-drifting from farm to traditional healing, food application, and phytopharmacology," *Molecules*, vol. 24, no. 13, p. 2454, 2019.

[95] P. Semwal, S. Painuli, T. Abu-Izneid et al., "Diosgenin: an updated pharmacological review and therapeutic perspectives," *Oxidative Medicine and Cellular Longevity*, vol. 2022, Article ID 1035441, 17 pages, 2022.

[96] B. Salehi, C. Quispe, I. Chamkhi et al., "Pharmacological properties of chalcones: a review of preclinical including molecular mechanisms and clinical evidence," *Frontiers in Pharmacology*, vol. 11, pp. 592654–592654, 2021.

[97] C. Scheau, C. Caruntu, I. A. Badarau et al., "Cannabinoids and inflammations of the gut-lung-skin barrier," *Journal of Personalized Medicine*, vol. 11, no. 6, p. 494, 2021.

[98] G. Georgiadis, I. E. Zisis, A. O. Docea et al., "Current concepts on the reno-protective effects of phosphodiesterase 5 inhibitors in acute kidney injury: systematic search and review," *Journal of Clinical Medicine*, vol. 9, no. 5, p. 1284, 2020.

[99] M. Ali and B. H. Abbasi, "Production of commercially important secondary metabolites and antioxidant activity in cell suspension cultures of *Artemisia absinthium* L," *Industrial Crops and Products*, vol. 49, pp. 400–406, 2013.

[100] K. S. Bora and A. Sharma, "Evaluation of antioxidant and free-radical scavenging potential of *Artemisia absinthium*," *Pharmaceutical Biology*, vol. 49, no. 12, pp. 1216–1223, 2011.

[101] O. Craciunescu, D. Constantin, A. Gaspar, L. Toma, E. Utoiu, and L. J. C. C. J. Moldovan, "Evaluation of antioxidant and cytoprotective activities of *Arnica montana* L. and *Artemisia absinthium* L," *Ethanolic Extracts*, vol. 6, pp. 1–11, 2012.

[102] B. Salehi, A. Prakash Mishra, M. Nigam et al., "*Ficus* plants: state of the art from a phytochemical, pharmacological, and toxicological perspective," *Phytotherapy Research*, vol. 35, no. 3, pp. 1187–1217, 2021.

[103] J. Sharifi-Rad, A. Dey, N. Koirala et al., "*Cinnamomum* species: bridging phytochemistry knowledge, pharmacological properties and toxicological safety for health benefits," *Frontiers in Pharmacology*, vol. 12, pp. 600139–600139, 2021.

[104] S. Painuli, C. Quispe, J. Herrera-Bravo et al., "Nutraceutical profiling, bioactive composition, and biological applications of *Lepidium sativum* L," *Oxidative Medicine and Cellular Longevity*, vol. 2022, Article ID 2910411, 20 pages, 2022.

[105] M. S. Islam, C. Quispe, R. Hossain et al., "Neuropharmacological effects of quercetin: a literature-based review," *Frontiers in Pharmacology*, vol. 12, 2021.

[106] A. Hadi, N. Hossein, P. Shirin, N. Najmeh, and M. J. I. J. P. S. R. R. Abolfazl, "Anti-inflammatory and analgesic activities of *Artemisia absinthium* and chemical composition of its essential oil," *International Journal of Pharmaceutical Sciences Review and Research*, vol. 38, pp. 237–244, 2014.

[107] J. Sharifi-Rad, C. Quispe, J. K. Patra et al., "Paclitaxel: application in modern oncology and nanomedicine-based cancer therapy," *Oxidative Medicine and Cellular Longevity*, vol. 2021, Article ID 3687700, 24 pages, 2021.

[108] G. Shafi, T. N. Hasan, N. A. Syed et al., "*Artemisia absinthium* (AA): a novel potential complementary and alternative medicine for breast cancer," *Molecular Biology Reports*, vol. 39, no. 7, pp. 7373–7379, 2012.

[109] J. Sharifi-Rad, A. Bahukhandi, P. Dhyani et al., "Therapeutic potential of neoechinulins and their derivatives: an overview of the molecular mechanisms behind pharmacological activities," *Frontiers in Nutrition*, vol. 8, article 664197, 2021.

[110] A. O. Docea, P. Mitrut, D. Grigore, D. Pirici, D. C. Calina, and E. Gofita, "Immunohistochemical expression of TGF beta (TGF-β), TGF beta receptor 1 (TGFBR1), and Ki67 in intestinal variant of gastric adenocarcinomas," *Romanian Journal of Morphology and Embryology*, vol. 53, 3 Supplement, pp. 683–692, 2012.

[111] P. Dhyani, C. Quispe, E. Sharma et al., "Anticancer potential of alkaloids: a key emphasis to colchicine, vinblastine, vincristine, vindesine, vinorelbine and vincamine," *Cancer Cell International*, vol. 22, no. 1, 2022.

[112] R. Amin, C. Quispe, A. O. Docea et al., "The role of tumour necrosis factor in neuroinflammation associated with Parkinson's disease and targeted therapies," *Neurochemistry International*, vol. 158, article 105376, 2022.

[113] D. Calina, A. M. Buga, M. Mitroi et al., "The treatment of cognitive, behavioural and motor impairments from brain injury and neurodegenerative diseases through cannabinoid system modulation-evidence from in vivo studies," *Journal of Clinical Medicine*, vol. 9, no. 8, p. 2395, 2020.

[114] A. M. Buga, A. O. Docea, C. Albu et al., "Molecular and cellular stratagem of brain metastases associated with melanoma," *Oncology Letters*, vol. 17, no. 5, pp. 4170–4175, 2019.

[115] B. Salehi, S. Sestito, S. Rapposelli et al., "Epibatidine: a promising natural alkaloid in health," *Biomolecules*, vol. 9, no. 1, p. 6, 2019.

[116] K.-W. Zeng, L.-X. Liao, X.-M. Song et al., "Caruifolin D from *Artemisia absinthium* L. inhibits neuroinflammation via reactive oxygen species-dependent c-jun N-terminal kinase and protein kinase c/NF-κB signaling pathways," *European Journal of Pharmacology*, vol. 767, pp. 82–93, 2015.

[117] A. Mohammadian, S. Moradkhani, S. Ataei et al., "Antioxidative and hepatoprotective effects of hydroalcoholic extract of *Artemisia absinthium* L. in rat," *Journal of Herbmed Pharmacology*, vol. 5, no. 1, pp. 29–32, 2016.

[118] J. Sharifi-Rad, C. Quispe, J. Herrera-Bravo et al., "Phytochemical constituents, biological activities, and health-promoting effects of the *Melissa officinalis*," *Oxidative Medicine and Cellular Longevity*, vol. 2021, Article ID 6584693, 20 pages, 2021.

[119] R. Hossain, C. Quispe, J. Herrera-Bravo et al., "*Lasia spinosa* chemical composition and therapeutic potential: a literature-based review," *Oxidative Medicine and Cellular Longevity*, vol. 2021, Article ID 1602437, 12 pages, 2021.

[120] A. Kartikadewi, A. Prasetyo, L. Budipradigdo, H. Nugroho, K. Tjahjono, and A. J. T. I. B. J. Lelono, "*Artemisia annua* leaf extract increases GLUT-4 expression in type 2 diabetes mellitus rat," *The Indonesian Biomedical Journal*, vol. 11, no. 1, pp. 78–84, 2019.

[121] H. M. Daradka, M. M. Abas, M. A. Mohammad, and M. M. J. C. C. P. Jaffar, "Antidiabetic effect of *Artemisia absinthium* extracts on alloxan-induced diabetic rats," *Comparative Clinical Pathology*, vol. 23, no. 6, pp. 1733–1742, 2014.

[122] J. Wang, C. Xu, Y. K. Wong et al., "Artemisinin, the magic drug discovered from traditional Chinese medicine," *Engineering*, vol. 5, no. 1, pp. 32–39, 2019.

[123] J. Suresh, N. Mahesh, J. Ahuja, and K. Santilna, "Review on *Artemisia nilagirica* (Clarke) pamp," *Journal of Biologically Active Products from Nature*, vol. 1, no. 2, pp. 97–104, 2011.

[124] F. D. Oliveira, L. N. Andrade, É. B. De Sousa, and D. P. De Sousa, "Anti-ulcer activity of essential oil constituents," *Molecules*, vol. 19, no. 5, pp. 5717–5747, 2014.

[125] V. Devmurari and N. Jivani, "Anticancer Evaluation of *Artemisia Nilagirica*," *International Journal of Pharmtech Research*, vol. 2, no. 2, pp. 1603–1608, 2010.

[126] B. Gordanian, M. Behbahani, J. Carapetian, and M. Fazilati, "In vitro evaluation of cytotoxic activity of flower, leaf, stem and root extracts of five *Artemisia* species," *Research in Pharmaceutical Sciences*, vol. 9, no. 2, p. 91, 2014.

[127] N. Sahu, S. Meena, V. Shukla et al., "Extraction, fractionation and re-fractionation of *Artemisia nilagirica* for anticancer activity and HPLC-ESI-QTOF-MS/MS determination," *Journal of Ethnopharmacology*, vol. 213, pp. 72–80, 2018.

[128] J. Ahamad, S. Mir, and S. Amin, "A pharmacognostic review on *Artemisia absinthium*," *International Research Journal of Pharmacy*, vol. 10, no. 1, pp. 25–31, 2019.

[129] M. Mojarrab, M.-S. Lagzian, S. A. Emami, J. Asili, and Z. Tayarani-Najaran, "*In vitro* anti-proliferative and apoptotic activity of different fractions of *Artemisia armeniaca*," *Revista Brasileira de Farmacognosia*, vol. 23, no. 5, pp. 783–788, 2013.

[130] Z. Q. Wang, D. Ribnicky, X. H. Zhang et al., "An extract of *Artemisia dracunculus* L. enhances insulin receptor signaling and modulates gene expression in skeletal muscle in KK- A^y mice," *The Journal of Nutritional Biochemistry*, vol. 22, no. 1, pp. 71–78, 2011.

[131] D. M. Ribnicky, P. Kuhn, A. Poulev et al., "Improved absorption and bioactivity of active compounds from an anti-diabetic extract of *Artemisia dracunculus* L," *International Journal of Pharmaceutics*, vol. 370, no. 1-2, pp. 87–92, 2009.

[132] K. Mansi and J. Lahham, "Effects of *Artemisia sieberi* Besser (a. herba-alba) on heart rate and some hematological values in normal and alloxan-induced diabetic rats," *Journal of Basic and Applied Sciences*, vol. 4, no. 2, pp. 57–62, 2008.

[133] F. Esmaeili, G. Sepehri, G.-R. Moshtaghi-Kashanian, M. Khaksari, N. Salari, and E. Sepehri, "The effect of acute administration of *Artemisia Persia* extracts on arterial blood pressure and heart rate in rats," *American Journal of Applied Sciences*, vol. 6, no. 5, pp. 843–847, 2009.

[134] N. Amat, H. Upur, and B. Blažeković, "In vivo hepatoprotective activity of the aqueous extract of *Artemisia absinthium* L. against chemically and immunologically induced liver injuries in mice," *Journal of Ethnopharmacology*, vol. 131, no. 2, pp. 478–484, 2010.

[135] A. R. Ahameethunisa and W. Hopper, "Antibacterial activity of *Artemisia nilagirica* leaf extracts against clinical and phytopathogenic bacteria," *BMC Complementary and Alternative Medicine*, vol. 10, pp. 1–6, 2010.

[136] S. M. Amin, H. M. Hassan, A. E. N. G. El Gendy et al., "Comparative chemical study and antimicrobial activity of essential oils of three *Artemisia* species from Egypt and Saudi Arabia," *Flavour and Fragrance Journal*, vol. 34, no. 6, pp. 450–459, 2019.

[137] A. B. Mokhtar, S. A. Ahmed, E. E. Eltamany, and P. Karanis, "Anti-blastocystis activity *in vitro* of Egyptian herbal extracts (Family: Asteraceae) with emphasis on Artemisia judaica," *International Journal of Environmental Research and Public Health*, vol. 16, no. 9, p. 1555, 2019.

[138] N. Sonker, A. K. Pandey, and P. Singh, "Efficiency of *Artemisia nilagirica* (Clarke) Pamp. essential oil as a mycotoxicant against postharvest mycobiota of table grapes," *Journal of the Science of Food and Agriculture*, vol. 95, no. 9, pp. 1932–1939, 2015.

[139] F. F. Perazzo, L. M. Lima, E. L. Maistro, J. E. Carvalho, V. L. Rehder, and J. C. Carvalho, "Effect of *Artemisia annua* L. leaves essential oil and ethanol extract on behavioral assays," *Farmacognosia*, vol. 18, pp. 686–689, 2008.

[140] M. Mahmoudi, M. Ebrahimzadeh, F. Ansaroudi, S. Nabavi, and S. Nabavi, "Antidepressant and antioxidant activities of *Artemisia absinthium* L. at flowering stage," *African Journal of Biotechnology*, vol. 8, 2009.

[141] M. Rahman, M. Ali, M. Sharif, and A. Tajmim, "A review study on the traditional plants has potential antidepressant property," *MOJ Cell Science & Report*, vol. 4, no. 5, 2017.

[142] T.-S. Woo, S.-Y. Yoon, I. C. D. Pena et al., "Anticonvulsant effect of *Artemisia capillaris* Herba in mice," *Biomolecules & Therapeutics*, vol. 19, no. 3, pp. 342–347, 2011.

[143] P. Pal and A. Ghosh, "Antioxidant, anti-Alzheimer and anti-Parkinson activity of *Artemisia nilagirica* leaves with flowering tops," *Pharmaceutical and Biosciences Journal*, vol. 6, no. 2, pp. 12–23, 2018.

[144] M. Skowyra, M. G. Gallego, F. Segovia, and M. P. Almajano, "Antioxidant properties of *Artemisia annua* extracts in model food emulsions," *Antioxidants*, vol. 3, no. 1, pp. 116–128, 2014.

[145] F. H. Afshar, A. Delazar, O. Janneh et al., "Evaluation of antimalarial, free-radical-scavenging and insecticidal activities of *Artemisia scoparia* and *A. spicigera*, Asteraceae," *Revista Brasileira De Farmacognosia*, vol. 21, no. 6, pp. 986–990, 2011.

[146] L. Leeja and E. J. Thoppil, "Essential oil composition and mosquito larvicidal activity of *Artemisia nilagirica* (CB Clarke) Pamp. from South India," *Journal of Phytological Research*, vol. 17, pp. 155–158, 2004.

[147] R. V. Prashant, R. Subburaju, and N. Balakrishnan, "Larvicidal activity of *Artemisia nilagirica* (Clarke) Pamp. and *Ocimum sanctum* L. A preliminary study," *Journal of Natural Remedies*, vol. 6, pp. 157–161, 2006.

[148] F. Faizei, A. H. Maghsood, F. Parandin, M. Matini, S. Moradkhani, and M. Fallah, "Antiprotoscolices effect of methanolic extract of *Zingiber officinale*, *Artemisia aucheri* and *Eucalyp-tus globulus* against Echinococcus granulosus in vitro," *Iranian Journal of Pharmacology and Therapeutics*, vol. 14, pp. 7–11, 2015.

[149] K. Ryu, M. Yoou, Y. Seo, K. Yoon, H. Kim, and H. Jeong, "Therapeutic effects of *Artemisia scoparia* Waldst. et Kitaib in a murine model of atopic dermatitis," *Clinical and Experimental Dermatology*, vol. 43, no. 7, pp. 798–805, 2018.

[150] M. Sajid, M. R. Khan, N. A. Shah et al., "Proficiencies of *Artemisia scoparia* against CCl 4 induced DNA damages and renal toxicity in rat," *BMC Complementary and Alternative Medicine*, vol. 16, pp. 1–10, 2016.

[151] H. Ha, H. Lee, C. S. Seo et al., "*Artemisia capillaris* inhibits atopic dermatitis-like skin lesions in Dermatophagoides farinae-sensitized Nc/Nga mice," *BMC Complementary and Alternative Medicine*, vol. 14, pp. 1–10, 2014.

[152] V. Honmore, A. Kandhare, A. A. Zanwar, S. Rojatkar, S. Bodhankar, and A. Natu, "*Artemisia pallens*alleviates acetaminophen induced toxicity via modulation of endogenous biomarkers," *Pharmaceutical Biology*, vol. 53, no. 4, pp. 571–581, 2015.

[153] H. Zime-Diawara, H. Ganfon, F. Gbaguidi et al., "The antimalarial action of aqueous and hydro alcoholic extracts of *Artemisia annua* L. cultivated in Benin: *In vitro* and *in vivo* studies," *Journal of Chemical and Pharmaceutical Research*, vol. 7, pp. 817–823, 2015.

[154] S. Stebbings, E. Beattie, D. McNamara, and S. Hunt, "A pilot randomized, placebo-controlled clinical trial to investigate the efficacy and safety of an extract of *Artemisia annua* administered over 12 weeks, for managing pain, stiffness, and functional limitation associated with osteoarthritis of the hip and knee," *Clinical Rheumatology*, vol. 35, no. 7, pp. 1829–1836, 2016.

[155] S. Hunt, S. Stebbings, and D. McNamara, "An open-label six-month extension study to investigate the safety and efficacy of an extract of *Artemisia annua* for managing pain, stiffness and functional limitation associated with osteoarthritis of the hip and knee," *The New Zealand Medical Journal*, vol. 129, pp. 97–102, 2016.

[156] Z. Basiri, F. Zeraati, F. Esna-Ashari et al., "Topical effects of *Artemisia Absinthium* ointment and liniment in comparison with piroxicam gel in patients with knee joint osteoarthritis: a randomized double-blind controlled trial," *Iranian Journal of Medical Sciences*, vol. 42, no. 6, pp. 524–531, 2017.

[157] S. Krebs, T. N. Omer, and B. Omer, "Wormwood (*Artemisia absinthium*) suppresses tumour necrosis factor alpha and accelerates healing in patients with Crohn's disease - A controlled clinical trial," *Phytomedicine*, vol. 17, no. 5, pp. 305–309, 2010.

[158] P. Remberg, L. Björk, T. Hedner, and O. Sterner, "Characteristics, clinical effect profile and tolerability of a nasal spray preparation of *Artemisia abrotanum* L. for allergic rhinitis," *Phytomedicine*, vol. 11, no. 1, pp. 36–42, 2004.

[159] J. Yu, G. Wang, and N. Jiang, "Study on the Repairing Effect of Cosmetics Containing *Artemisia* annua on Sensitive Skin," *Journal of Cosmetics, Dermatological Sciences and Applications*, vol. 10, no. 1, 2020.

[160] E. Konstat-Korzenny, J. A. Ascencio-Aragón, S. Niezen-Lugo, and R. Vázquez-López, "Artemisinin and its synthetic derivatives as a possible therapy for cancer," *Medical Sciences*, vol. 6, no. 1, 2018.

[161] S. Slezáková and J. Ruda-Kucerova, "Anticancer activity of artemisinin and its derivatives," *Anticancer Research*, vol. 37, no. 11, pp. 5995–6003, 2017.

[162] R. Dell'Eva, U. Pfeffer, R. Vené et al., "Inhibition of angiogenesis in vivo and growth of Kaposi's sarcoma xenograft tumors by the anti-malarial artesunate," *Biochemical Pharmacology*, vol. 68, no. 12, pp. 2359–2366, 2004.

[163] Y. Zhang, G. Xu, S. Zhang, D. Wang, P. S. Prabha, and Z. Zuo, "Antitumor research on artemisinin and its bioactive derivatives," *Natural Products and Bioprospecting*, vol. 8, no. 4, pp. 303–319, 2018.

[164] M. P. Crespo-Ortiz and M. Q. Wei, "Antitumor activity of artemisinin and its derivatives: from a well-known antimalarial agent to a potential anticancer drug," *Journal of Biomedicine and Biotechnology*, vol. 2012, Article ID 247597, 18 pages, 2012.

[165] F. H. Jansen, I. Adoubi, T. de Cnodder, N. Jansen, A. Tschulakow, and T. Efferth, "First study of oral Artenimol-R in advanced cervical cancer: clinical benefit, tolerability and tumor markers," *Anticancer Research*, vol. 31, no. 12, pp. 4417–4422, 2011.

[166] Z.-Y. Zhang, S.-Q. Yu, L.-Y. Miao et al., "Artesunate combined with vinorelbine plus cisplatin in treatment of advanced non-small cell lung cancer: a randomized controlled trial," *Journal of Chinese Integrative Medicine*, vol. 6, no. 2, pp. 134–138, 2008.

[167] N. Singh and K. Verma, "Case report of a laryngeal squamous cell carcinoma treated with artesunate," *Archive of Oncology*, vol. 10, no. 4, pp. 279-280, 2002.

[168] T. G. Berger, D. Dieckmann, T. Efferth et al., "Artesunate in the treatment of metastatic uveal melanoma-first experiences," *Oncology Reports*, vol. 14, no. 6, pp. 1599–1603, 2005.

[169] N. P. Singh and V. K. Panwar, "Case report of a pituitary macroadenoma treated with artemether," *Integrative Cancer Therapies*, vol. 5, no. 4, pp. 391–394, 2006.

[170] M. Mendez-del Villar, A. M. Puebla-Pérez, M. J. Sanchez-Pena, L. J. González-Ortiz, E. Martinez-Abundis, and M. González-Ortiz, "Effect of *Artemisia dracunculus* administration on glycemic control, insulin sensitivity, and insulin secretion in patients with impaired glucose tolerance," *Journal of Medicinal Food*, vol. 19, no. 5, pp. 481–485, 2016.

[171] J.-Y. Choi, S.-K. Shin, S.-M. Jeon et al., "Dose–response study of sajabalssuk ethanol extract from *Artemisia princeps* Pampanini on blood glucose in subjects with impaired fasting glucose or mild type 2 diabetes," *Journal of Medicinal Food*, vol. 14, no. 1-2, pp. 101–107, 2011.

[172] Y. Li, M. Zheng, X. Zhai et al., "Effect OF-GYMNEMA sylvestre, Citrullus colocynthis and *Artemisia absinthium* on blood glucose and lipid profile in diabetic human," *Acta Poloniae Pharmaceutica*, vol. 72, no. 5, pp. 981–985, 2015.

[173] S. Mohammadi, B. Jafari, P. Asgharian, M. Martorell, and J. Sharifi-Rad, "Medicinal plants used in the treatment of Malaria: a key emphasis to *Artemisia, Cinchona*, Cryptolepis, and *Tabebuia genera*," *Phytotherapy Research*, vol. 34, no. 7, pp. 1556–1569, 2020.

[174] M. J. A. Martínez, L. M. B. Del Olmo, and L. A. Ticona, "Genus: a review of bioactive sesquiterpene lactones," *Studies in Natural Products Chemistry*, vol. 37, pp. 43–65, 2012.

[175] Y. Li, "Qinghaosu (artemisinin): chemistry and pharmacology," *Acta Pharmacologica Sinica*, vol. 33, no. 9, pp. 1141–1146, 2012.

[176] M. Warsame, M. Gyapong, B. Mpeka et al., "Pre-referral rectal artesunate treatment by community-based treatment providers in Ghana, Guinea-Bissau, Tanzania, and Uganda (study 18): a cluster-randomized trial," *Clinical Infectious Diseases*, vol. 63, supplement 5, pp. S312–S321, 2016.

[177] A. M. Dondorp, C. I. Fanello, I. C. Hendriksen et al., "Artesunate versus quinine in the treatment of severe falciparum malaria in African children (AQUAMAT): an open-label, randomised trial," *The Lancet*, vol. 376, no. 9753, pp. 1647–1657, 2010.

[178] Group, A, "A meta-analysis using individual patient data of trials comparing artemether with quinine in the treatment of severe falciparum malaria," *Transactions of the Royal Society of Tropical Medicine and Hygiene*, vol. 95, no. 6, pp. 637–650, 2001.

[179] C. Dobaño, A. J. Nhabomba, M. N. Manaca et al., "A balanced Proinflammatory and regulatory cytokine signature in young African children is associated with lower risk of clinical malaria," *Clinical Infectious Diseases*, vol. 69, no. 5, pp. 820–828, 2019.

[180] S. Das, S. Manna, B. Saha, A. K. Hati, and S. Roy, "Novel pfkelch13 gene polymorphism associates with artemisinin resistance in eastern India," *Clinical Infectious Diseases*, vol. 69, no. 7, pp. 1144–1152, 2019.

[181] R. T. Eastman and D. A. Fidock, "Artemisinin-based combination therapies: a vital tool in efforts to eliminate malaria," *Nature Reviews Microbiology*, vol. 7, no. 12, pp. 864–874, 2009.

[182] L. Pull, J.-M. Lupoglazoff, M. Beardmore et al., "Artenimol–piperaquine in children with uncomplicated imported falciparum malaria: experience from a prospective cohort," *Malaria Journal*, vol. 18, pp. 1–5, 2019.

[183] C. Leblanc, C. Vasse, P. Minodier et al., "Prise en charge et prevention du paludisme d'importation de l'enfant. Mise a jour des recommandations pour la pratique clinique 2007," *Medecine et Maladies Infectieuses*, vol. 50, no. 2, pp. 127–140, 2020.

[184] S.-B. Ballard, A. Salinger, M. Desai, and K. R. Tan, "Updated CDC recommendations for using artemether-lumefantrine for the treatment of uncomplicated malaria in pregnant women in the United States," *Morbidity and Mortality Weekly Report*, vol. 67, no. 14, pp. 424–431, 2018.

[185] N. B. Daddy, L. M. Kalisya, P. G. Bagire, R. L. Watt, M. J. Towler, and P. J. Weathers, "*Artemisia annua* dried leaf tablets treated malaria resistant to ACT and i.v. artesunate: Case reports," *Phytomedicine*, vol. 32, pp. 37–40, 2017.

[186] J. Munyangi, L. Cornet-Vernet, M. Idumbo et al., "RETRACTED: *Artemisia annua* and *Artemisia afra* tea

infusions *vs*. artesunate-amodiaquine (ASAQ) in treating *Plasmodium falciparum* malaria in a large scale, double blind, randomized clinical trial," *Phytomedicine*, vol. 57, pp. 49–56, 2019.

[187] M. L. Willcox, S. Burton, R. Oyweka, R. Namyalo, S. Challand, and K. Lindsey, "Evaluation and pharmacovigilance of projects promoting cultivation and local use of *Artemisia annua* for malaria," *Malaria Journal*, vol. 10, pp. 1–7, 2011.

[188] D. Calina, C. Sarkar, A. L. Arsene et al., "Recent advances, approaches and challenges in targeting pathways for potential COVID-19 vaccines development," *Immunologic Research*, vol. 68, pp. 315–324, 2020.

[189] D. Calina, T. Hartung, A. O. Docea et al., "COVID-19 vaccines: ethical framework concerning human challenge studies," *DARU Journal of Pharmaceutical Sciences*, vol. 28, no. 2, pp. 807–812, 2020.

[190] C. Sohrabi, Z. Alsafi, N. O'Neill et al., "World Health Organization declares global emergency: a review of the 2019 novel coronavirus (COVID-19)," *International Journal of Surgery*, vol. 76, pp. 71–76, 2020.

[191] W. Zhuang, Z. Fan, Y. Chu et al., "Chinese patent medicines in the treatment of coronavirus disease 2019 (COVID-19) in China," *Frontiers in Pharmacology*, vol. 11, p. 1066, 2020.

[192] World Health Organization, "SARS: Clinical Trials on Treatment Using a Combination of Traditional Chinese Medicine and Western Medicine," in *Report of the WHO International Expert Meeting to Review and Analyse Clinical Reports on Combination Treatment for SARS, 8-10 October 2003*, Beijing, People's Republic of China, 2004.

[193] Z. Zhao, Y. Li, L. Zhou et al., "Prevention and treatment of COVID-19 using traditional Chinese medicine: a review," *Phytomedicine*, vol. 85, article 153308, 2021.

[194] M. Y. Shapira, I. B. Resnick, S. Chou et al., "Artesunate as a potent antiviral agent in a patient with late drug-resistant cytomegalovirus infection after hematopoietic stem cell transplantation," *Clinical Infectious Diseases*, vol. 46, no. 9, pp. 1455–1457, 2008.

[195] D. W. Lachenmeier and M. Uebelacker, "Risk assessment of thujone in foods and medicines containing sage and wormwood - Evidence for a need of regulatory changes?," *Regulatory Toxicology and Pharmacology*, vol. 58, no. 3, pp. 437–443, 2010.

[196] D. W. Lachenmeier, "Wormwood (*Artemisia absinthium* L.) –A curious plant with both neurotoxic and neuroprotective properties?," *Journal of Ethnopharmacology*, vol. 131, no. 1, pp. 224–227, 2010.

[197] S. M. Nofal, S. S. Mahmoud, A. Ramadan, G. Soliman, and R. Fawzy, "Anti-diabetic effect of *Artemisia judaica* extracts," *Research Journal of Medicine and Medical Sciences*, vol. 4, pp. 42–48, 2009.

[198] N. Paramakrishnan, J. Ahuja, J. Suresh, M. Khan, and M. Sebastian, "Evaluation of acute oral toxicity of aerial parts of *Artemisia parviflora* Roxb," *Der Pharmacia Sinica*, vol. 3, pp. 99–103, 2012.

[199] A. Judzentiene and R. Garjonyte, "Compositional variability and toxic activity of Mugwort (*Artemisia vulgaris*) essential oils," *Natural Product Communications*, vol. 11, no. 9, 2016.

[200] M. Siddiqui, S. Waghmare, S. Hajare, R. I. S. Deshmukh, and S. C. S. A. Ali, "Phytochemical analysis and acute toxicity studies of *Artemisia annua* in Swiss albino mice," *Journal of Pharmacognosy and Phytochemistry*, vol. 7, pp. 1893–1895, 2018.

[201] W. Classen, B. Altmann, P. Gretener, C. Souppart, P. Skelton-Stroud, and G. Krinke, "Differential effects of orally versus parenterally administered qinghaosu derivative artemether in dogs," *Experimental and Toxicologic pathology*, vol. 51, no. 6, pp. 507–516, 1999.

[202] E. Ogbole, I. Isaiah, T. Ogundeko, A. Asalu, B. Modupe, and J. Aguiyi, "Acute toxicity studies of locally cultivated Artemisia annua leaf extract in Rats," *World Journal of Pharmaceutical Sciences*, vol. 2, no. 12, pp. 1864–1870, 2014.

[203] S. Qureshi, A. Ageel, M. Al-Yahya, M. Tariq, J. Mossa, and A. Shah, "Preliminary toxicity studies on ethanol extracts of the aerial parts of *Artemisia abyssinica* and *A. inculta* in mice," *Journal of Ethnopharmacology*, vol. 28, no. 2, pp. 157–162, 1990.

[204] J. T. Mukinda and J. A. Syce, "Acute and chronic toxicity of the aqueous extract of *Artemisia afra* in rodents," *Journal of Ethnopharmacology*, vol. 112, no. 1, pp. 138–144, 2007.

[205] A. Nontprasert, M. Nosten-Bertrand, S. Pukrittayakamee, S. Vanijanonta, B. J. Angus, and N. J. White, "Assessment of the neurotoxicity of parenteral artemisinin derivatives in mice," *The American Journal of Tropical Medicine and Hygiene*, vol. 59, no. 4, pp. 519–522, 1998.

[206] A. Trendafilova, L. M. Moujir, P. M. C. Sousa, and A. M. L. Seca, "Research advances on health effects of edible *Artemisia* species and some sesquiterpene lactones constituents," *Foods*, vol. 10, 2021.

[207] S. A. Padosch, D. W. Lachenmeier, and L. U. Kröner, "Absinthism: a fictitious 19th century syndrome with present impact," *Substance Abuse Treatment, Prevention, and Policy*, vol. 1, no. 1, 2006.

[208] D. W. Lachenmeier, S. G. Walch, S. A. Padosch, and L. U. Kröner, "Absinthe—a review," *Critical Reviews in Food Science and Nutrition*, vol. 46, no. 5, pp. 365–377, 2006.

[209] J. Laadraoui, R. Aboufatima, Z. El Gabbas et al., "Effect of *Artemisia herba-alba* consumption during pregnancy on fertility, morphological and behaviors of mice offspring," *Journal of Ethnopharmacology*, vol. 226, pp. 105–110, 2018.

[210] D. Oliaee, M. T. Boroushaki, N. Oliaee, and A. Ghorbani, "Evaluation of cytotoxicity and antifertility effect of *Artemisia kopet daghensis*," *Advances in Pharmacological Sciences*, vol. 2014, Article ID 745760, 5 pages, 2014.

[211] E. Paulsen, "Systemic allergic dermatitis caused by sesquiterpene lactones," *Contact Dermatitis*, vol. 76, no. 1, pp. 1–10, 2017.

[212] P. Wu, Y. He, Z. Zeng, Z. Yang, and Y. Li, "Allergic contact dermatitis by *Artemisia*: report of two cases," *Contact Dermatitis*, vol. 83, pp. 31-32, 2020.

[213] I. Pablos, M. Egger, E. Vejvar et al., "Similar allergenicity to different *Artemisia* species is a consequence of highly cross-reactive Art v 1-like molecules," *Medicina*, vol. 55, no. 8, p. 504, 2019.

[214] M. Denisow-Pietrzyk, Ł. Pietrzyk, and B. Denisow, "Asteraceae species as potential environmental factors of allergy," *Environmental Science and Pollution Research International*, vol. 26, no. 7, pp. 6290–6300, 2019.

[215] R. Tang, J. L. Sun, J. Yin, and Z. Li, "*Artemisia* allergy research in China," *BioMed Research International*, vol. 2015, Article ID 179426, 9 pages, 2015.

[216] Z. Gao, W.-Y. Fu, Y. Sun et al., "*Artemisia* pollen allergy in China: component-resolved diagnosis reveals allergic asthma patients have significant multiple allergen sensitization," *Allergy*, vol. 74, no. 2, pp. 284–293, 2019.

[217] R. Hirschwehr, C. Heppner, S. Spitzauer et al., "Identification of common allergenic structures in mugwort and ragweed pollen," *Journal of Allergy and Clinical Immunology*, vol. 101, no. 2, pp. 196–206, 1998.

[218] C. Zhou, "Mechanism of type I hypersensitivity," in *Multidisciplinary Approaches to Allergies*, Z.-S. Gao, M. Zheng, L. J. W. J. Gilissen, H.-H. Shen, and L. J. Frewer, Eds., pp. 19–32, Springer Berlin Heidelberg, Berlin, Heidelberg, 2012.

[219] J. Oteros, E. Bartusel, F. Alessandrini et al., "*Artemisia* pollen is the main vector for airborne endotoxin," *Journal of Allergy and Clinical Immunology*, vol. 143, no. 1, pp. 369–377.e365, 2019.

[220] J. Brandys, A. Grimsøen, B. M. Nilsen, B. S. Paulsen, H. S. Park, and C. S. Hong, "Cross-reactivity between pollen extracts from six *Artemisia* species," *Planta Medica*, vol. 59, no. 3, pp. 221–228, 1993.

[221] T. Efferth and B. Kaina, "Toxicity of the antimalarial artemisinin and its dervatives," *Critical Reviews in Toxicology*, vol. 40, no. 5, pp. 405–421, 2010.

[222] M. Xia, D. Liu, Y. Liu, and H. Liu, "The therapeutic effect of Artemisinin and its derivatives in kidney disease," *Frontiers in Pharmacology*, vol. 11, p. 380, 2020.

[223] X. Dai, X. Zhang, W. Chen et al., "Dihydroartemisinin: a potential natural anticancer drug," *International Journal of Biological Sciences*, vol. 17, pp. 603–622, 2021.

[224] C. X. Anh, M. Chavchich, G. W. Birrell et al., "Pharmacokinetics and ex vivo antimalarial activity of artesunate-amodiaquine plus methylene blue in healthy volunteers," *Antimicrobial Agents and Chemotherapy*, vol. 64, no. 3, article e01441, 2020.

[225] C. Fu, H. Shi, H. Chen, K. Zhang, M. Wang, and F. Qiu, "Oral bioavailability comparison of artemisinin, deoxyartemisinin, and 10-deoxoartemisinin based on computer simulations and pharmacokinetics in rats," *ACS Omega*, vol. 6, pp. 889–899, 2021.

[226] X. Li, J. Hu, Y. Yuan et al., "Pharmacokinetics and toxicokinetics of artemisinin-hydroxychloroquine sulfate tablets in rats and dogs," *Evidence-Based Complementary and Alternative Medicine : eCAM*, vol. 2021, article 6830459, 12 pages, 2021.

[227] R. I. Mancuso, M. A. Foglio, and S. T. Olalla Saad, "Artemisinin-type drugs for the treatment of hematological malignancies," *Cancer Chemotherapy and Pharmacology*, vol. 87, no. 1, pp. 1–22, 2021.

[228] D. Kitic, B. Miladinovic, M. Randjelovic et al., "Anticancer potential and other pharmacological properties of *Prunus armeniaca* L.: an updated overview," *Plants*, vol. 11, no. 14, p. 1885, 2022.

[229] D. Tsoukalas, O. Zlatian, M. Mitroi et al., "A novel nutraceutical formulation can improve motor activity and decrease the stress level in a murine model of middle-age animals," *Journal of Clinical Medicine*, vol. 10, no. 4, p. 624, 2021.

[230] M. M. Alshehri, C. Quispe, J. Herrera-Bravo et al., "A review of recent studies on the antioxidant and anti-infectious properties of *senna* plants," *Oxidative Medicine and Cellular Longevity*, vol. 2022, Article ID 6025900, 38 pages, 2022.

[231] C. Quispe, J. Herrera-Bravo, K. Khan et al., "Therapeutic applications of curcumin nanomedicine formulations in cystic fibrosis," *Progress in Biomaterials*, 2022.

[232] A. O. Docea, D. Calina, A. M. Buga et al., "The effect of silver nanoparticles on antioxidant/pro-oxidant balance in a murine model," *International Journal of Molecular Sciences*, vol. 21, no. 4, 2020.

Hindawi
Oxidative Medicine and Cellular Longevity
Volume 2022, Article ID 3472179, 29 pages
https://doi.org/10.1155/2022/3472179

Research Article

Identification of Warning Transition Points from Hepatitis B to Hepatocellular Carcinoma Based on Mutation Accumulation for the Early Diagnosis and Potential Drug Treatment of HBV-HCC

Fei Xu,[1] Qingkang Meng,[1] Feng Wu,[2] Yakun Wang,[1] Wenjun Yang,[1] Yun Tong,[1] Lei Liu,[1] and Xiujie Chen[1]

[1]*Department of Pharmacogenomics, College of Bioinformatics Science and Technology, Harbin Medical University, Harbin 150081, China*
[2]*Department of Orthopedic Surgery, The 2nd Affiliated Hospital of Harbin Medical University, Harbin 150001, China*

Correspondence should be addressed to Lei Liu; liulei@ems.hrbmu.edu.cn and Xiujie Chen; chenxiujie@ems.hrbmu.edu.cn

Received 25 July 2022; Accepted 9 August 2022; Published 5 September 2022

Academic Editor: Tarique Hussain

The accumulation of multiple genetic mutations is essential during the occurrence and development of hepatocellular carcinoma induced by hepatitis B (HBV-HCC), but understanding their cooperative effects and identifying the warning transition point from hepatitis B to HCC are challenges. In the genomic analysis of somatic mutations of the patient with HBV-HCC in a patient-specific protein-protein interaction (ps-PPI) network, we find mutation influence can propagate along the ps-PPI network. Therefore, in the article, we got the mutation cluster as a new research unit using the Random Walks with Restarts algorithm that is used to describe the efficient boundary of mutation influences. The connection of mutation cluster leads to dysregulation of signaling pathways corresponding to HCC, while dysregulated signaling pathways accumulate gradually and experience a process from quantitative to qualitative changes including a critical mutation cluster called transition point (TP) from hepatitis B to HCC. Moreover, two subtypes of HCC patients with different prognosis and their corresponding biological and clinical characteristics were identified according to TP. The poor prognosis HCC subtype was associated with significant metabolic pathway dysregulation and lower immune cell infiltration, while we also identified several preventive drugs to block the transformation of hepatitis B to hepatocellular carcinoma. The network-level study integrated multiomics data not only showed the sequence of multiple somatic mutations and their cooperative effect but also identified the warning transition point in HCC tumorigenesis for each patient. Our study provides new insight into exploring the cooperative molecular mechanism of chronic inflammatory malignancy in the liver and lays the foundation for the development of new approaches for early prediction and diagnosis of hepatocellular carcinoma and personalized targeted therapy.

1. Introduction

Hepatocellular carcinoma (HCC) is a leading cause of cancer-related deaths worldwide, with a 5-year survival rate of 18% [1]. Hepatitis B virus (HBV) infection is a major risk factor for HCC tumorigenesis [2]. Although several studies have described the molecular mechanisms that hepatitis B drives hepatocellular carcinoma (HBV-HCC) and proposed some therapeutic strategies [3–6], the identification of transition point for early diagnosis of inflammatory-to-cancer transformation in HBV-HCC is an open question.

HCC tumorigenesis is usually accompanied by the accumulation of somatic mutations; these somatic mutations regulate different signaling pathways such as cell cycle, signal transduction, and stress response [7, 8], and different signaling pathway dysfunctions frequently occur simultaneously in cancer [9], so we can infer that these signaling pathway dysfunctions provide an advantage to the growth of cancer cells. Changing analysis of these signaling pathways from quantitative to qualitative views supplies an insight into HCC tumorigenesis, which should be essential in evaluating the transition point of tumorigenesis for the early diagnosis

of HCC. To investigate the transformation mechanism of hepatitis B to HCC, Chen et al. identified dynamic network biomarkers to detect the critical states (meaning the transition point) of many disease progression using nonlinear dynamic theory [10], and Liu et al. explored a novel landscape dynamic network biomarker methodology to identify early-warning signals of complex diseases on a single-sample basis [11]. These efforts have provided new ideas for the early detection of tumors and focus more on gene expression rather than the biological processes regulated by genes; however, the biological processes regulated by genes better represent the evolution of tumors. To understand the transformation mechanism of hepatitis B driving HCC, our study researched the transition points from quantitative changes to qualitative changes during the accumulation of somatic mutations and their associated signaling pathways in a complex PPI network of HCC patients; this overcomes the bias of individual gene expression. Our work not only describes the synergistic effects of mutated genes during uncontrollable inflammatory progression but also demonstrates the interplay of signaling pathways during tumor evolution.

Studies have shown that the progression of many complex diseases has an unstable predisease state, which can be reversed back to a normal state if treated appropriately [12]. Here, to further explore the unstable predisease state of HBV-HCC, the percolation theory is used to simulate the process of tumorigenesis. The percolation theory is a physical concept describing random propagation and flow of fluid in random porous disordered media and there is a sudden transition point with the change of the random plugging degree of the pores, which is often called percolation transition [13]. We used the PPI network as the random porous disordered media, the somatic mutations as the events of blocked pores, and a sudden transition point as the percolation transition of tumorigenesis.

In our study, we used a mutation cluster as the basic research unit to identify each patient's transition point (TP) rather than single dominance of somatic mutations, which not only reflected the synergism between these genes but was also more consistent with the HCC tumorigenesis. We constructed patient-specific protein-protein interaction (ps-PPI) networks and extracted more representative largest connected clusters (LCCs). And then, we calculated the HCC propensity score (HCC-PS) of genes in LCCs, while HCC-PS included the biological functions of genes, considered the cooperation mechanism between genes, and found the TP of each patient from hepatitis B to HCC. Finally, we proposed a novel subtype model based on the TPs; the patients in subtype 1 had metabolic dysregulation and low immune levels and had a worse prognosis. Our finding is crucial for early detection, prevention, and treatment of HBV-HCC.

2. Material and Methods

2.1. Obtaining and Processing Data. The information of 89 stage I HBV-HCC patients in China (CHCC-HBV) was obtained from the published research, including gene expression profile and proteomic data, somatic mutation profile, and clinical profile of patients with HCC and hepatitis B [14]. 68 advanced-stage patients in CHCC-HBV and 102 HBV-HCC patients in TCGA were selected for validation [14].

The human protein-protein interaction relationships with a combined score greater than 700 in the STRING database were obtained [15], which maximizes patient information retention while maintaining high confidence in protein-protein interactions (nodes = 14805, edges = 361152). 218 HCC-associated driver genes were obtained from the DriverDBv3 [16]. There are 529 pathways, including 14851 genes in the Kyoto Encyclopedia of Genes and Genomes (KEGG) database [17]. We downloaded information on 519 pathways, including 28 cancer-related pathways and 1 hepatocellular carcinoma-related pathway. The CERES scores of genome-scale CRISPR-Cas9 knockout for 18333 genes in 20 HCC cell lines were acquired from the Dependency Map (DepMap) portal [18]. CERES score is used to measure the dependency of the mutations in cancer cell lines (CCLs), and a lower score indicates that the gene is more essential in cell growth and survival of a given CCL. Differentially expressed genes (DEGs) between hepatitis B and HCC were identified using the R package "limma" [19]; adj p value < 0.05 and $|\log 2\mathrm{FC}| > 1$ were set as the threshold. Combined with gene expression profiles and clinical profiles, the univariate Cox proportional hazard regression model was used to screen overall survival- (OS-) associated genes (p value < 0.05). For each patient, the protein-protein interactions in which two gene expression values were greater than 0 in hepatitis B and HCC were extracted and the maximal interconnected network was defined as ps-PPI.

2.2. Mining Mutation Cluster and Connected Clusters (CC) in ps-PPI. It has been found that genes causing the same or similar diseases are usually close to each other in PPI [20]. Set genes with mutations as seeds separately to model their influence over the nonmutated neighbor genes in each ps-PPI using the Random Walks with Restarts (RWR) algorithm [21]. According to the RWR algorithm, the score of each nonmutated neighbor gene around the mutated gene was calculated according to the following formula:

$$P_{t+1} = (1 - r)MP_t + rP_0. \quad (1)$$

In the formula, r is the probability of one gene transferring to its neighboring gene, while the probability of one gene transferring to itself is $1 - r$. According to previous studies, $r = 0.7$ is suitable for RWR algorithm [22, 23]. The vector P_0 is a binary matrix $(0, 1)$, 0 indicates a nonmutated gene and 1 indicates a mutated gene. M is the adjacency matrix of ps-PPI, and the mutated gene seeks its affected neighborhood along with M. P_t eventually converges, and P_{t+1} reaches a steady state when the value of P_t and P_{t+1} difference is less than $1e - 10$ in this study [23–25].

X-cluster was a series of genes centered on a gene X with mutation and spread the influence of X over the nonmutated neighbor genes in the ps-PPI. The closer the nonmutated neighbor gene was to X, the higher the score was. A series of mutation clusters are scattered in the ps-PPI and

connected by nonmutated genes; therefore, the connected cluster (CC) is some connected mutation clusters in the ps-PPI.

2.3. Exploring the Order of Mutation Clusters in the Largest Connected Cluster (LCC). Each mutation cluster is a small subnet, while each connected cluster is a bigger subnet; the largest connected cluster (LCC) is the biggest subnet in the ps-PPI that is formed by some connecting CCs. This study is based on the idea of continuous somatic mutation during carcinogenesis. Shin et al. proposed the mutation-select-rule to choose the next mutation cluster, minimizing the size of the subnet on the premise that there was overlap among the previous mutation clusters [26]. We simulated the sequence of clusters during LCC formation. In each patient, a cluster centered on passenger mutation was first selected as the start, and the next cluster was added according to the mutation-select-rule until all clusters were in the LCC. Then, repeating the above steps to each cluster centered on passenger mutation, sequences of clusters were obtained with an equal number of passenger mutations. The order of any two clusters in all sequences was counted, and each patient got a unique sequence of clusters during the formation of LCC eventually.

To test the synergistic effect among the clusters in the patient's LCC to expand the effective boundary of mutation in the ps-PPI, we selected test genes randomly equal to the number of mutations in each ps-PPI, and the clusters of test genes were calculated and concatenated into LCC (test) and repeated 500 times. Finally, we compared the size of LCC (test) and that of intrinsic mutations.

2.4. Identify the Transition Point (TP) of Each Patient. The unique sequence of clusters during the formation of LCC was obtained for each patient, and most passenger mutation clusters have no obvious oncogenic effect. However, the accumulation of these passenger mutation clusters with one or several driver mutation clusters will alter the biological process and induce cancer. According to the sequence of clusters, the HCC propensity score (HCC-PS) was calculated for each cluster joined in the subnet to form the LCC. The HCC-PS was completely specific by using KEGG pathway information and each patient's gene expression profile in subnet according to the following equation. HCC-PS value represented the likelihood that the patients transform from hepatitis B to HCC, and the cluster with the largest HCC-PS was selected as the TP from hepatitis B to HCC.

$$\text{HCC-PS} = \sum_{1}^{p} P_i. \tag{2}$$

In the equation, p is the number of KEGG pathways in which genes of subnet enriched in $p < 0.01$, and P_i is the propensity score of pathway i. The formula of P_i is as follows:

$$P_i = G \sum_{j=1}^{g} W \times R_j, \tag{3}$$

$$G = \frac{G_h}{G_i}, \tag{4}$$

$$W = \frac{w_j}{W_j}. \tag{5}$$

Here, g denotes the number of genes in the subnet that are enriched in pathway i. G is the correlation coefficient between pathway i and the HCC pathway. W is the oncogenicity coefficient of gene j. R_j is the difference in gene j expression between HCC and hepatitis B. G_h is the number of intersection genes in pathway i with genes in the HCC pathway, and G_i is the number of genes in pathway i. w_j is the number of cancer pathways containing gene j, and W_j is the number of KEGG pathways containing gene j.

2.5. Selection of Candidate Genes and Establishing Subtype Model. Patients were classified into two subtypes according to the TPs, including subtype 1 with TP53 cluster as a TP and subtype 2 with no fixed biomarker cluster as TP. The subtype model was constructed in two steps. Firstly, subtype-related genes were the intersection of the following three datasets: (1) DEGs of HCC in two subtypes (adj p value < 0.05, $|\log 2\text{FC}| > 1$); (2) DEGs of hepatitis B in two subtypes (adj p value < 0.05, $|\log 2\text{FC}| > 1$); and (3) receiver operating characteristic (ROC) curves were plotted using the R package "pROC," and the area under the curve (AUC) was calculated to assess the accuracy of the model [27]; the ROC curves of two subtypes in HCC and hepatitis B were plotted, respectively, the genes with both AUC greater than 0.6. Secondly, the least absolute shrinkage and selection operator (LASSO) logistic regression model was used to extract the feature genes and their coefficient from subtype-related genes. The formula of the subtype model is as follows, and i is feature genes:

$$\text{subtype model} = \sum_{\text{i}} \text{coefficient}\,(\text{gene}_i) * \text{expression}\,(\text{gene}_i). \tag{6}$$

To validate the accuracy of the subtype model, 68 advanced-stage patients from CHCC-HBV and 102 HBV-HCC patients in TCGA were used. The TPs were identified for each patient according to the HCC-PS, and the AUC was calculated by plotting the ROC curve based on the subtype model.

2.6. Functional Enrichment Analysis Based on Multiomics Data. The differences in biological processes between hepatitis B and HCC in subtype 1 patients were analyzed. The "c2.cp.kegg.v7.4.entrez.gmt" gene set was downloaded from the MSigDB database [28]. And the R package "clusterProfiler" [29] was used for gene set enrichment analysis (GSEA) (adj p value < 0.01). Gene set variance analysis (GSVA) was performed using the R package "GSVA" [30]. The difference in the pathway between hepatitis B and HCC in subtype 1 patients was identified by "limma" algorithm (adj p value < 0.01). The results of transcriptome-based

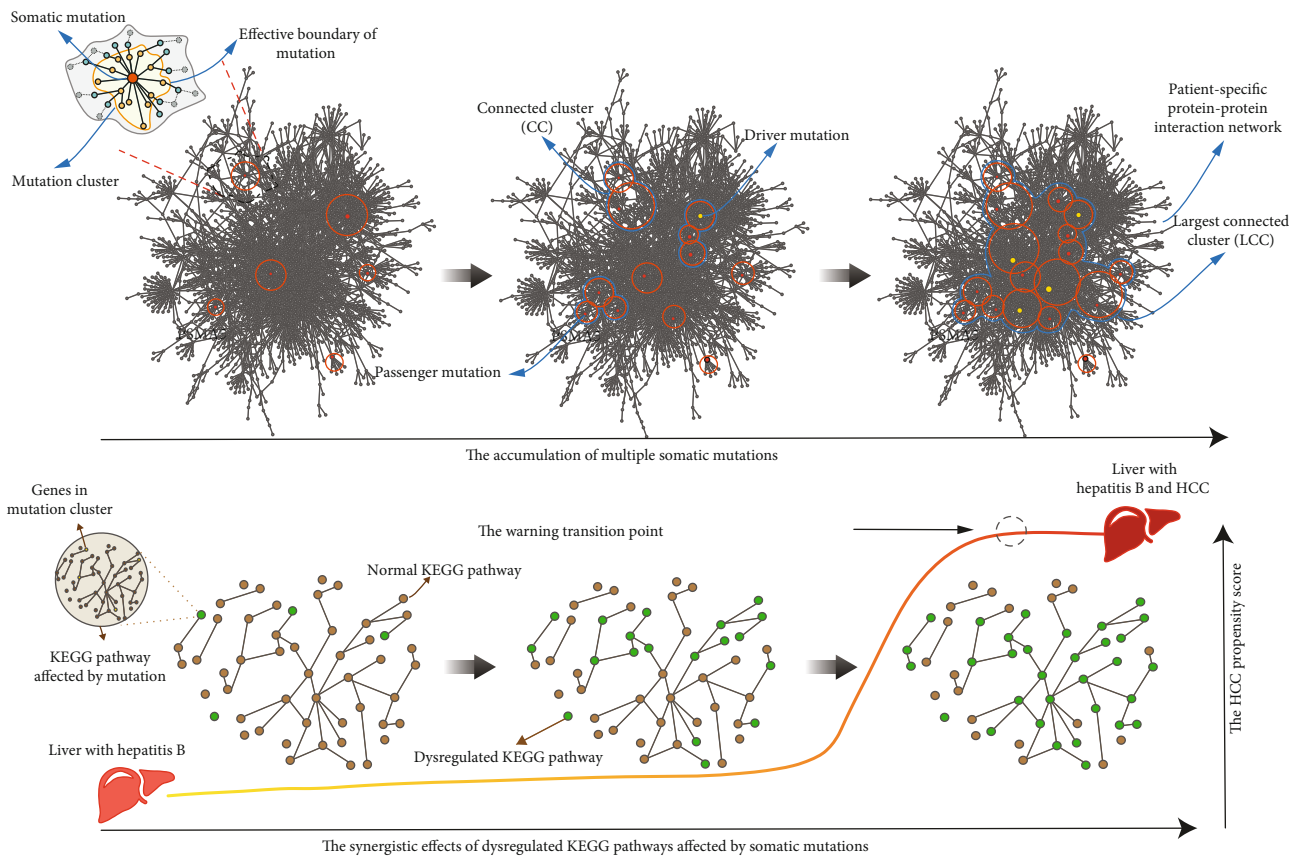

Figure 1: The accumulation of multiple somatic mutations and the synergistic effects of dysregulated pathway affected by somatic mutation in the HCC tumorigenesis.

GSEA and proteome-based GSVA were intersected to obtain the differential pathways between hepatitis B and HCC.

Single-sample gene set enrichment analysis (ssGSEA) was implemented to analyze the enrichment level of 29 immune signatures via invoking the R package "GSVA" [31, 32], combined with the "limma" for differential immune signatures between hepatitis B and HCC in the patients of subtype 1 (adj p value < 0.01).

2.7. Core Target Screening and Drug Identification. TP is defined as the threshold for the transformation from hepatitis B to HCC. The genes before TP during the formation of LCC can be used as drug targets to block cancer progression. A three-step analysis was performed to find candidate drug targets in subtype 1 patients. Firstly, DEGs between hepatitis B and HCC in subtype 1 patients were selected (adj p value < 0.05, $|\log 2FC| > 1$). DEGs with AUC > 0.9 were used to construct a transformation model from hepatitis B to HCC. Secondly, the genes before TP were identified for 51 patients separately, and the shared genes were defined as the intersection of the above 51 gene sets. The Pearson correlation coefficients (PCC) of shared genes expression with the transformation model were calculated ($|r| > 0.5$, $p < 0.05$). In the third step, the PCC of the CERES score and transformation model in HCC cell lines were calculated to screen for the poor-prognosis genes associated with HCC ($|r| > 0.5$, $p < 0.05$). The approved drugs of available drug targets in subtype 1 patients were obtained from the DrugBank database [33].

We screened 16 HCC cell lines with 95 compounds, and the drug response data and genomic markers of sensitivity were obtained from the Genomics of Drug Sensitivity in Cancer database [34], and the R package "oncoPredict" [35] was used to predict drug sensitivity of HCC patients in subtype 1.

3. Results

3.1. Unique ps-PPI. To explore the timing of transition point (TP) onset more accurately, we only chose phase I HCC patients. To simulate the accumulation of multiple somatic mutations and the synergistic effects of dysregulated pathways affected by somatic mutation during the HCC tumorigenesis, we constructed a ps-PPI for each HCC patient in this study (Figure 1). The number of interactions in each ps-PPI was counted (maximum 360830 and minimum 355666), and the number of genes in ps-PPIs was similar (minimum 14742 and maximum 14801), but the genes are different. Patients had a wide range of mutated genes from 30 to 610 and a few driver mutations from 1 to 20, while the ps-PPI preserved at least 80% of the mutated genes for each patient.

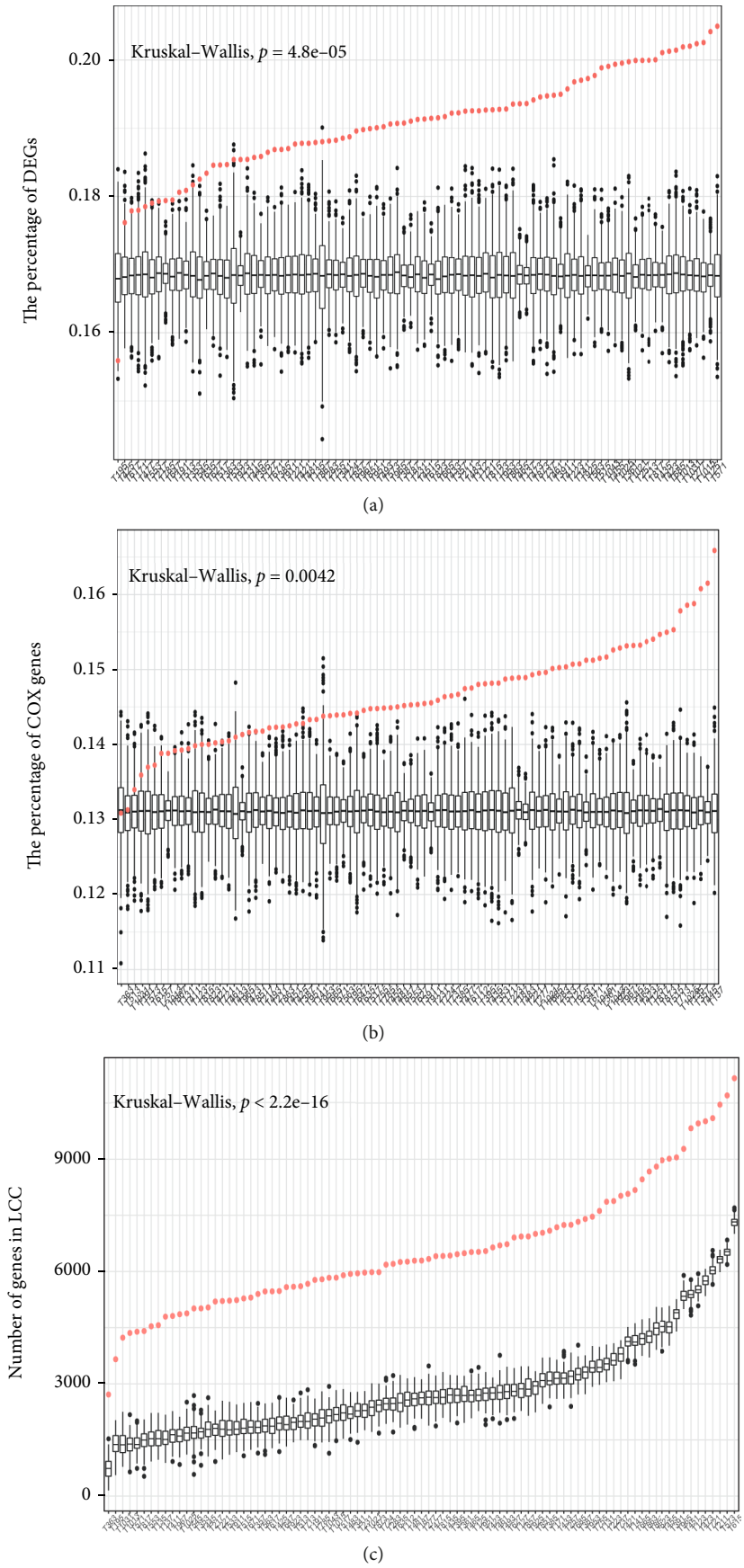

Figure 2: Continued.

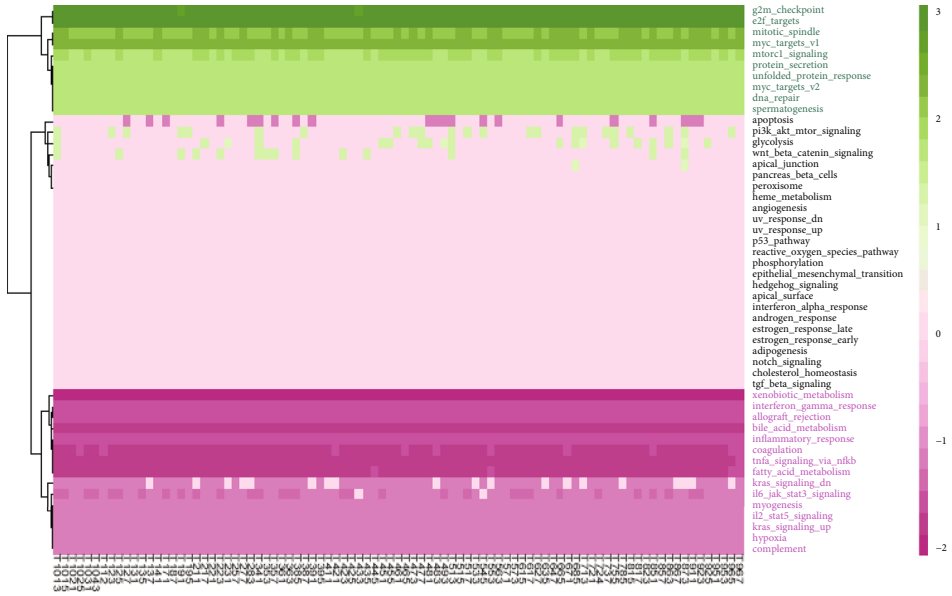

(d)

(e)

Figure 2: Analysis of LCCs. (a, b) The proportion of DEG/OS-associated genes in LCCs vs. that in LCCs (test), red dots represent LCCs and black dots represent LCCs (test). (c) The size of LCCs and the size of LCCs (test) in each patient, red dots represent LCCs and black dots represent LCCs (test). (d, e) In the biological processes of genes in LCCs and ps-PPIs, green indicates that the hallmark is activated, and pink indicates that the hallmark is suppressed.

In short, the number of genes and interactions in ps-PPIs was similar; however, mutated genes and gene expression values in each patient differed significantly. So ps-PPIs were high specificity and reflected the necessity of personalized treatment.

3.2. The Mutation Clusters as Research Units. In the ps-PPIs, we found that the genes with mutation scattered in various positions and were closely related to the nonmutated genes. We set the mutation cluster as a research unit, which consisted of a gene with mutation and its nonmutated neighbors. RWR algorithm was used to find the mutation cluster in the ps-PPIs; a score threshold of 0.001 was set to ensure a high correlation between genes in each mutation cluster while keeping the number of genes in each mutation cluster from being 0. The average size of the mutation cluster was 324, with the largest mutation cluster having 1095 genes and the smallest mutation cluster having 2 genes; it can be seen that the influence of different mutations on the network varies widely. At the same time, there are connections

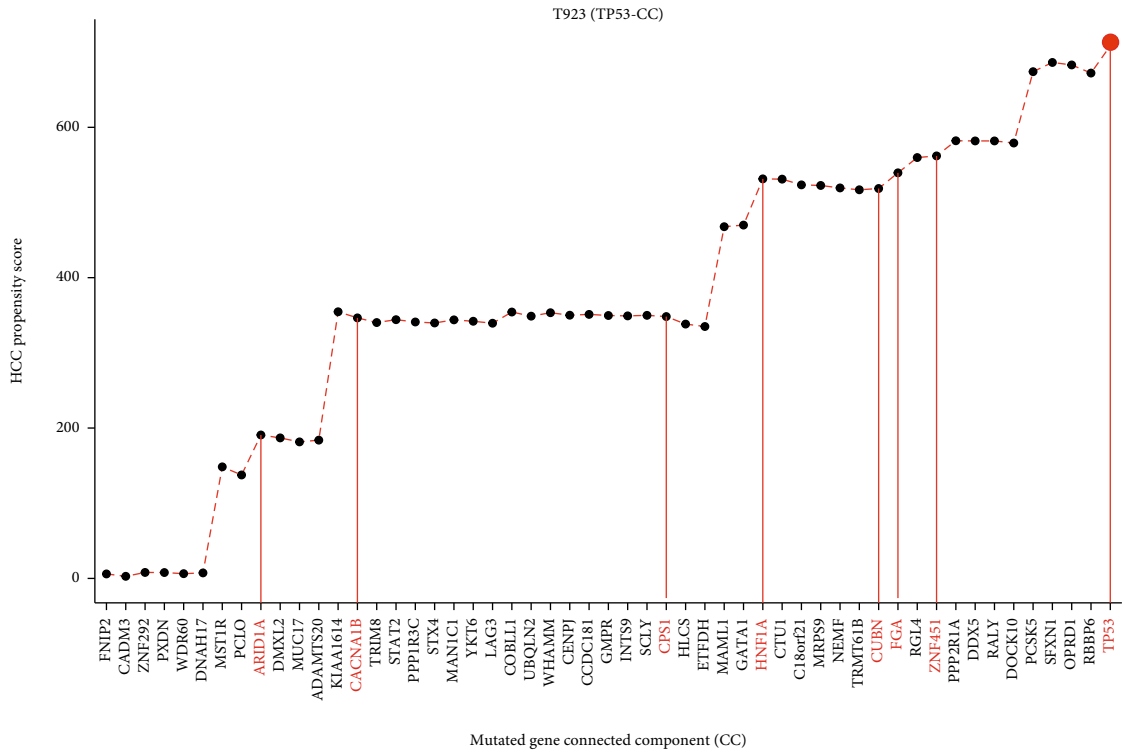

(a)

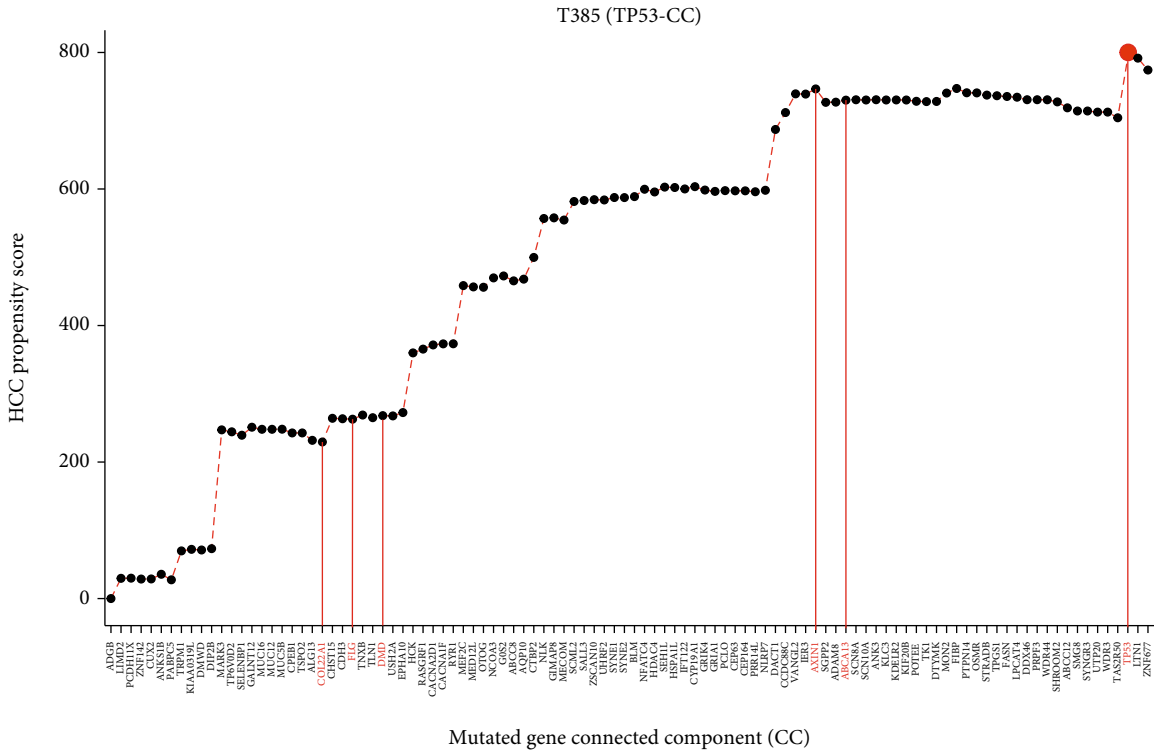

(b)

Figure 3: Continued.

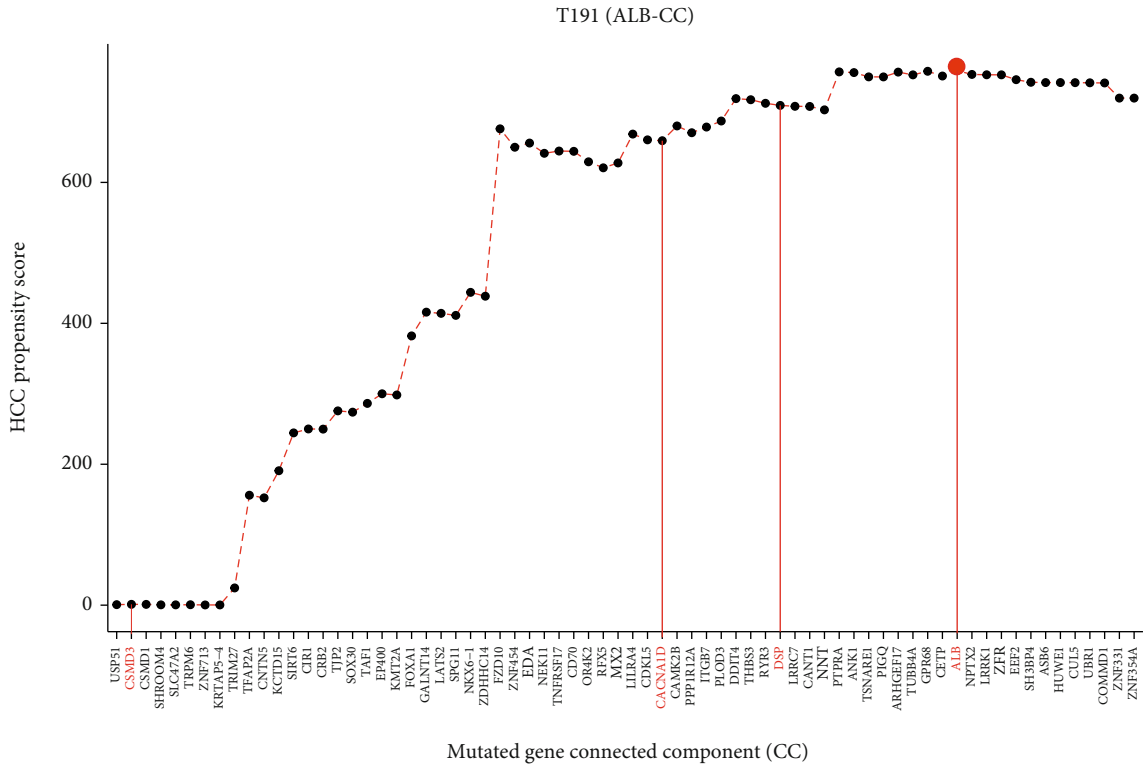

(c)

(d)

Figure 3: Continued.

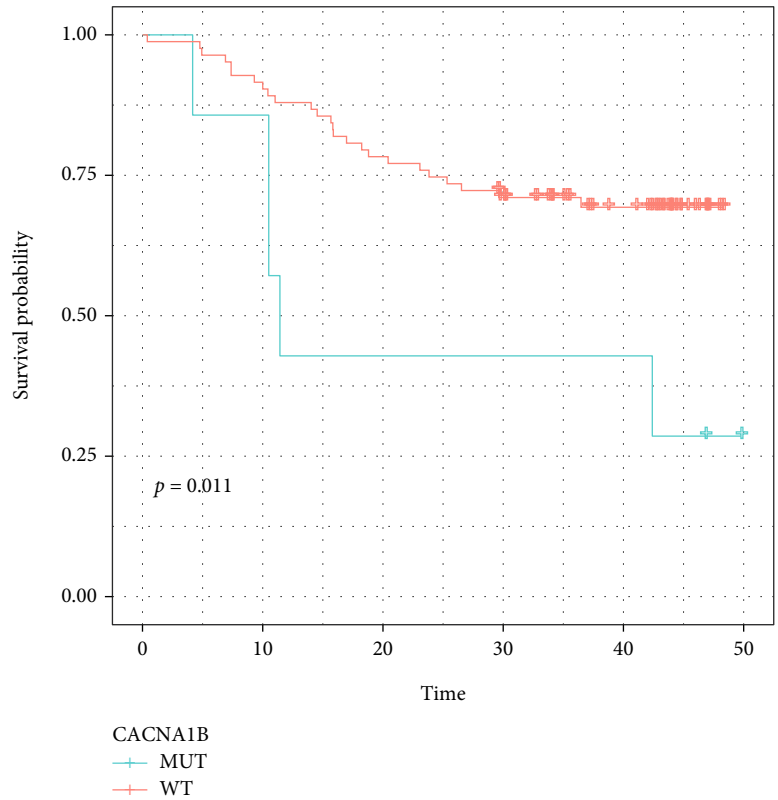

(e)

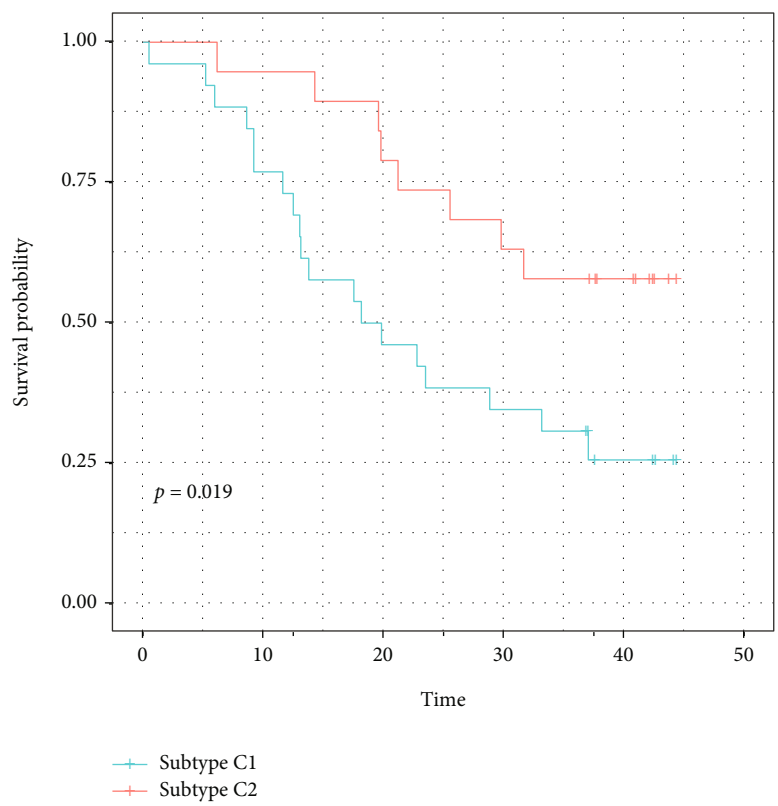

(f)

Figure 3: Continued.

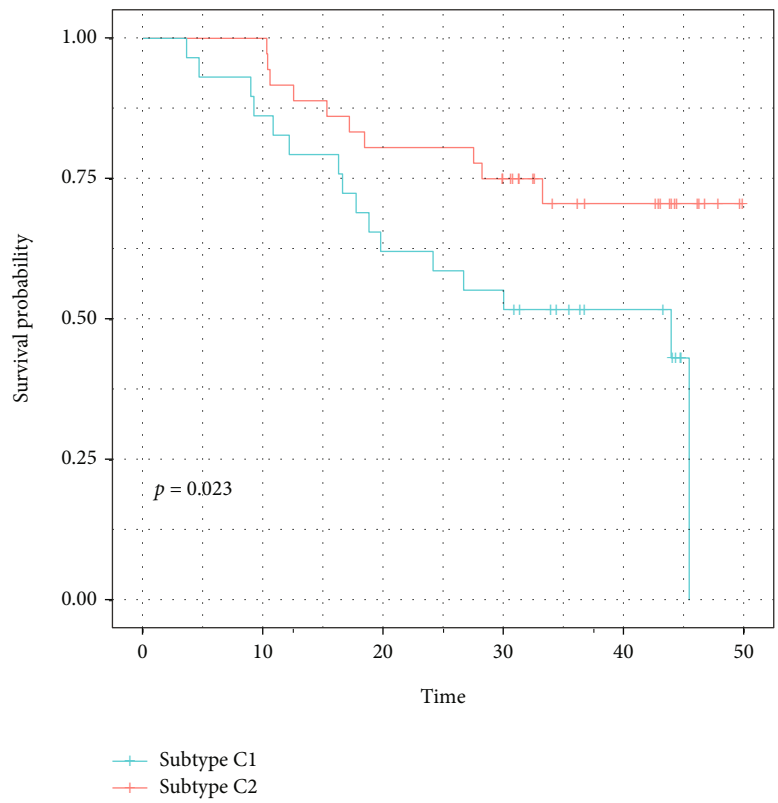

(g)

Figure 3: HCC-PS curve and patient subtypes. (a–d) Examples of HCC-PS curve. The horizontal axis is the order of mutations which means the cluster sequence, and the vertical axis is the HCC-PS. The red indicates the driver gene. (e) Kaplan-Meier plot showing different prognoses of CACNA1B-mutated patients vs. CACNA1B-WT patients. (f, g) Kaplan-Meier plot showing different prognoses of subtype 1 vs. subtype 2 in stage I CHCC-HBV patients and advanced-stage CHCC-HBV patients.

between clusters to form CCs in the ps-PPIs, and the largest CC is called LCC (Figure 1).

The number of genes in each patient's LCC was determined by the overlap and synergistic effect of CCs. Although there were only 106 somatic mutations in ps-PPIs on average (1% genes of the ps-PPIs), the size of LCCs affected by somatic mutations covered 50% of the ps-PPIs. The number of driver mutations in LCCs ranged from 1 to 16, but the number of nonmutated driver genes affected by passenger mutations in LCCs ranged from 68 to 162, which means a few mutations could have a greater impact. Moreover, 3573 DEGs between HCC and hepatitis B were identified, including 1533 upregulated and 2040 downregulated. The univariate Cox proportional hazard regression model was performed, and 2275 OS-associated genes of HCC patients were identified. The proportion of DEG/OS-associated genes in LCCs showed significant differences because of strong individualization. The proportion of DEG/OS-associated genes in LCCs with that in LCCs (test) was compared; LCCs contained more DEGs ($p = 4.8e - 5$, Figure 2(a)) and more OS-associated genes ($p = 0.0042$, Figure 2(b)). The result showed that there was not only an overlapping effect but also a synergistic effect between CCs. The size of LCCs composed of intrinsic mutations was significantly larger than the size of LCCs (test) ($p < 2.2e - 16$, Figure 2(c)). Thus, the synergistic cooperation between somatic mutations in cancer cannot be attributed to random selection; it could be determined by the topological properties of somatic mutations in the ps-PPIs.

To assess whether LCCs can represent ps-PPIs, we compared the differences in the biological processes of genes involved in ps-PPIs and LCCs; the gene set "h.all.v7.4.symbols.gmt" from MSigDB database was used for GSVA. The result showed that the genes in LCCs and the genes in ps-PPIs activated the same biological processes, such as E2F targets, G2M checkpoint, mitotic spindle, and MYC target proliferation processes while suppressing the xenobiotic metabolism, allograft rejection, bile acid metabolism, and inflammatory response, which were highly correlated with HCC tumorigenesis. LCCs could represent the patient's biological function while more fully presenting personalized information (Figures 2(d) and 2(e)).

3.3. TP Identified for Each HCC Patient. From the above results, the formation of LCCs resulted from the collaborative effect of CCs and the genes in LCCs were closely related to the cancer-related function. Then, identifying the CC development sequence in LCCs was important for cancer prevention, early diagnosis, and treatment. According to the mutation-select-rule [26], a sequence of mutation clusters was obtained for each patient, and most driver

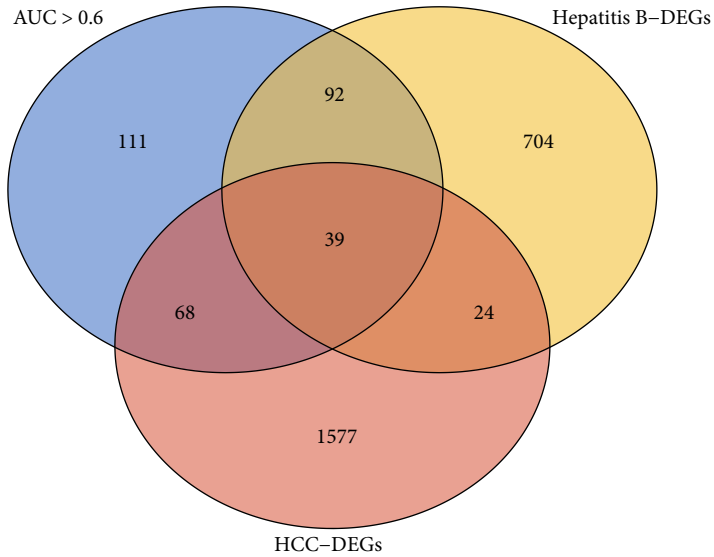

(a)

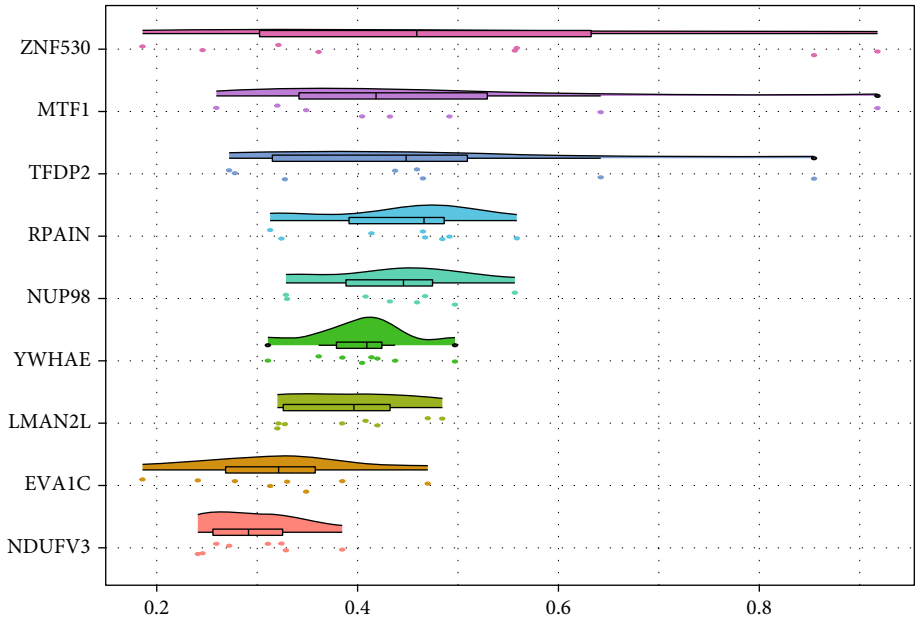

(b)

Figure 4: Continued.

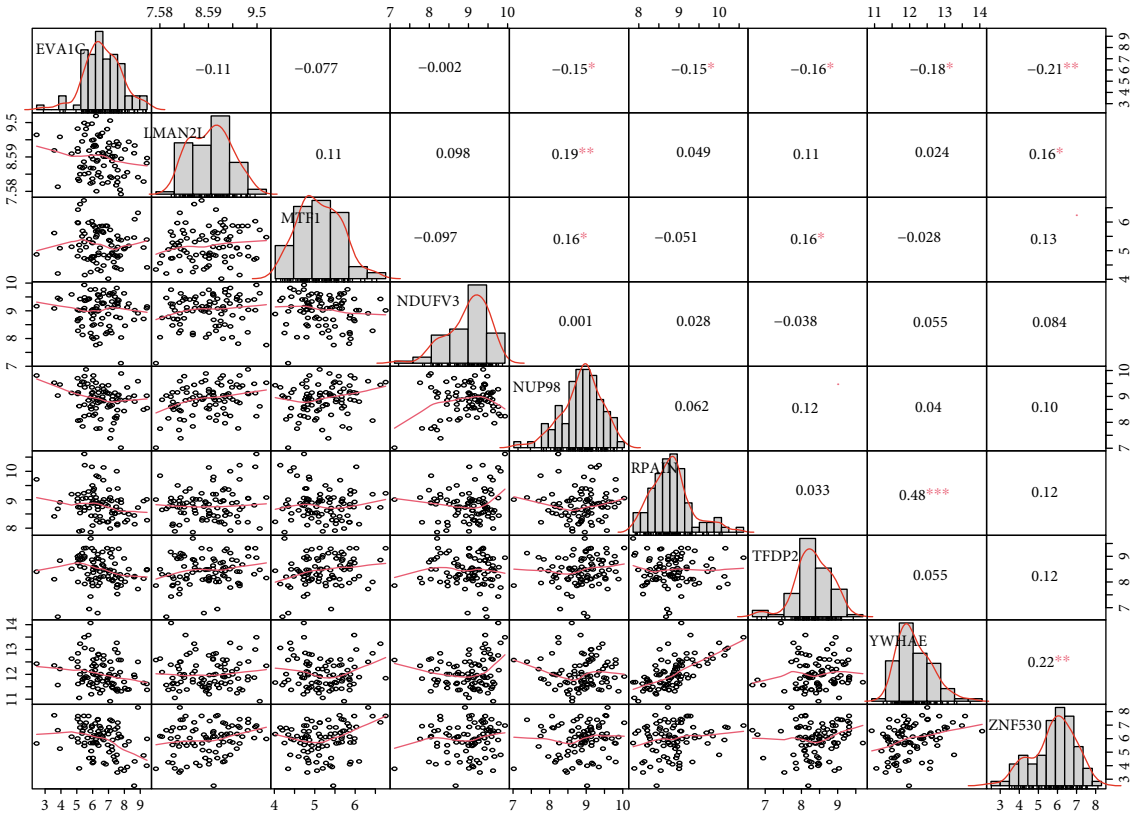

(c)

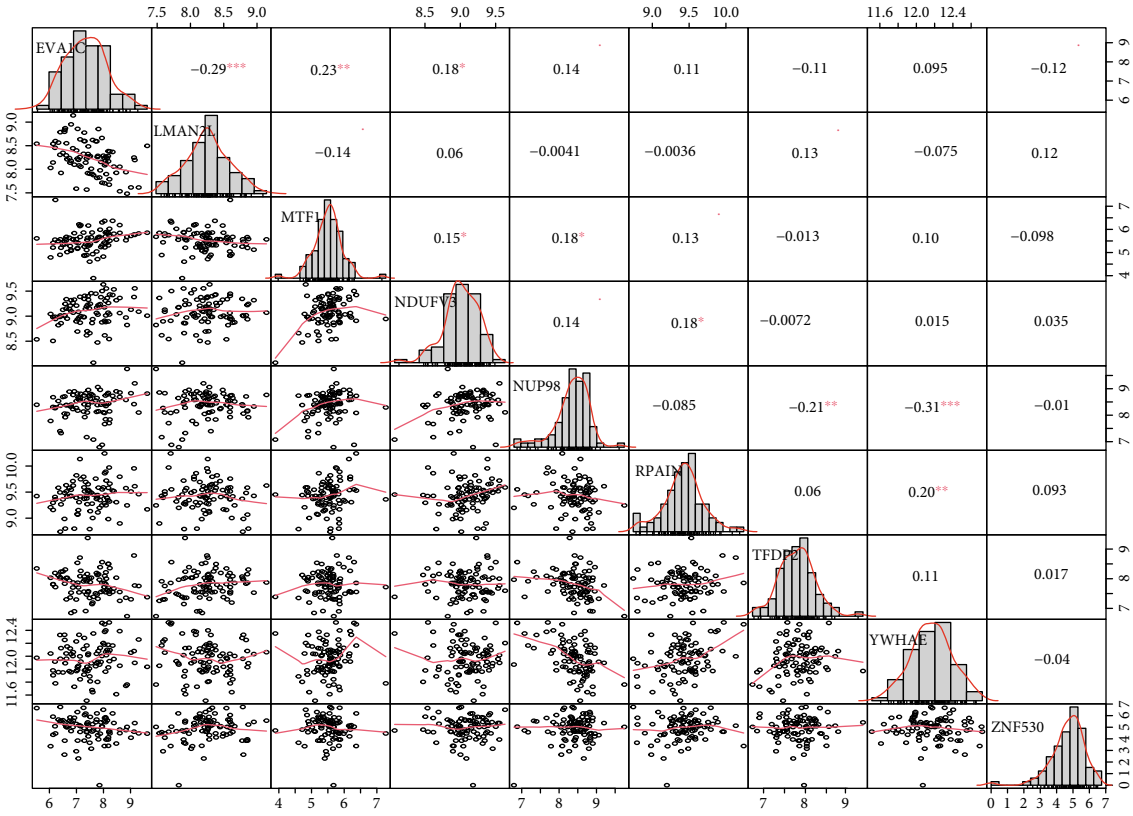

(d)

Figure 4: Continued.

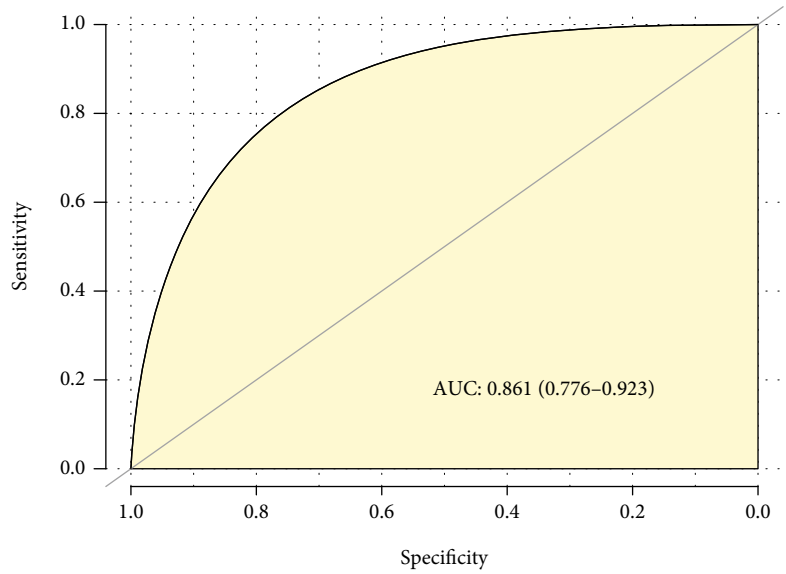

(e)

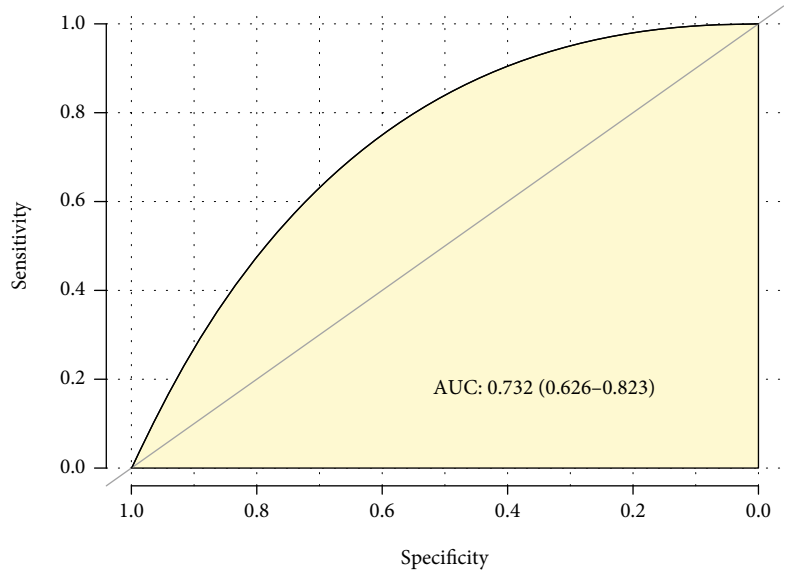

(f)

Figure 4: Continued.

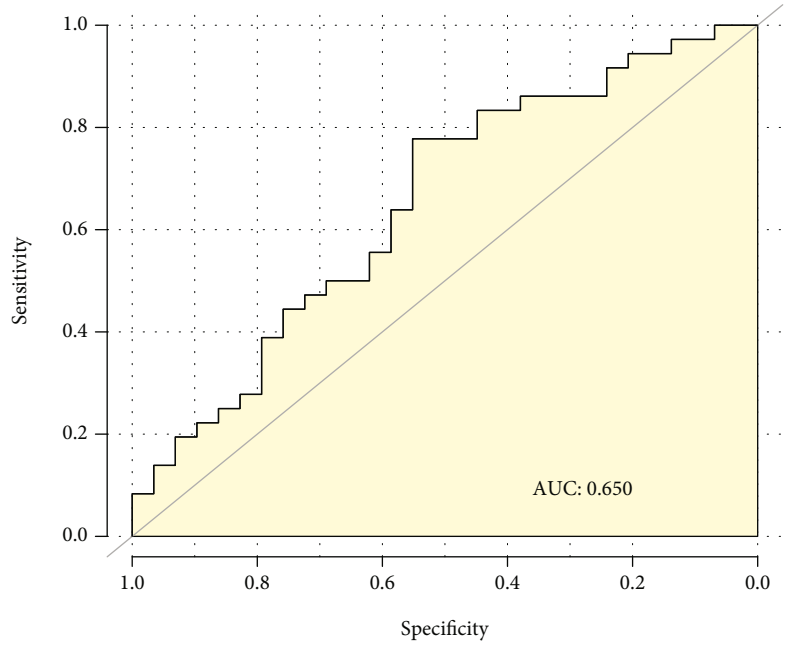

(g)

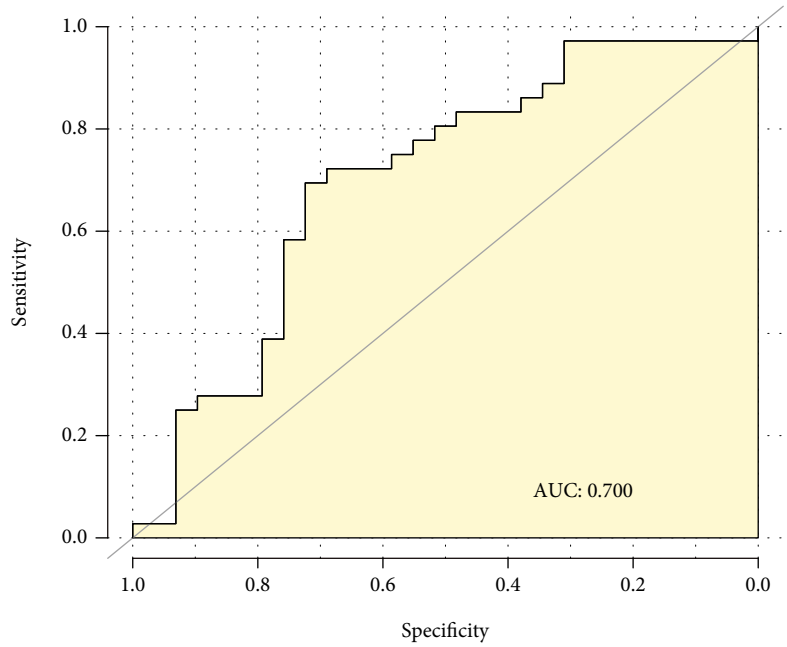

(h)

Figure 4: Continued.

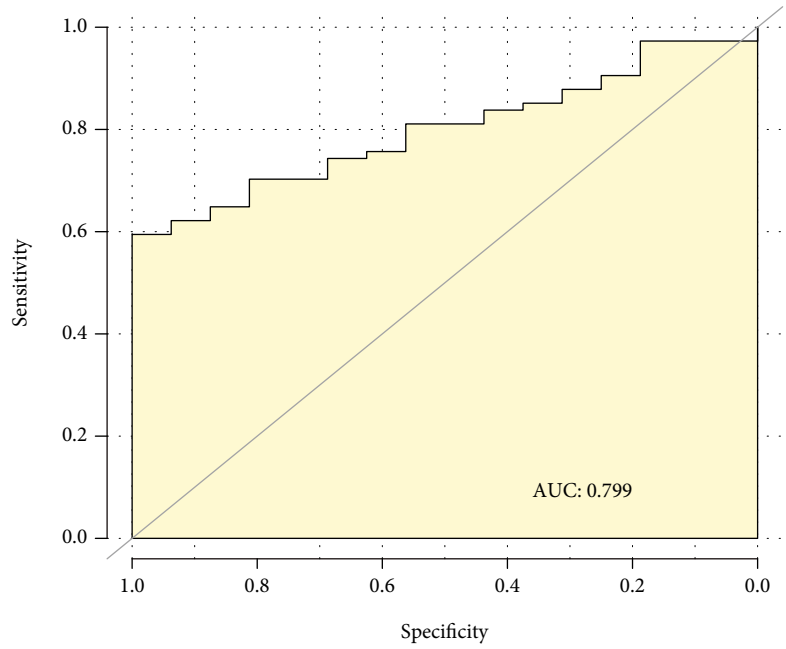

(i)

Figure 4: Construction and validation of patient subtype model. (a) Venn diagram of subtype-associated genes. (b) Semantic similarity of subtype-associated genes. (c, d) The PCCs for gene expression levels of the 9 signature genes in HCC and hepatitis B. (e, f) The ROC curve of patient subtype model in HCC and hepatitis B. The ROC curve of the subtype model in HCC of CHCC-HBV patients with advanced stages (g), hepatitis B of CHCC-HBV patients with advanced stages (h), and HCC of TCGA-HBV patients (i).

mutations observed in HCC have been optimized to maximize the transition from hepatitis B to HCC after some passenger mutations.

To identify the TP in the transformation from hepatitis B to HCC, the biological function of genes in the subnet at the time cluster joined in following the sequence of the clusters was assessed according to the HCC-PS, and the HCC-PS curve was plotted (Figures 3(a)–3(d)). The results showed that the HCC-PS increased slowly with the addition of the clusters of the passenger mutations; the HCC-PS underwent a sudden increase abruptly when a cluster of the driver mutation was added. And after that, the HCC-PS reverted to steady again until the next driver mutation and its CC were added. The HCC-PS reached the highest point, which was defined as TP, and the patient completed the transformation from hepatitis B to HCC.

Taking patient T923 as an example (Figure 3(a)), the patient has 55 genes with mutation, including 8 driver mutations. The LCC of patient T923 consisting of 5593 genes was obtained from ps-PPI; there were 53 mutations including 8 driver mutations (8 driver mutations were ARID1A, CACNA1B, CPS, HNF1A, CUBN, FGA, ZNF451, and TP53). The 53 HCC-PSs were calculated during the gradual joining of the 53 mutation clusters. It was found that the clusters of driver mutations ARID1A, HNF1A, and TP53 led to HCC-PS dramatic increase; the clusters of passenger mutations kept the HCC-PS stable due to the homeostasis. ARID1A was an important tumor suppressor gene, and it played a key role in the proliferation, differentiation, and apoptosis processes [36]. CACNA1B mutation type led to a lower survival rate compared with wild type in HBV-HCC patients ($p < 0.05$, Figure 3(e)). HNF1A was a novel oncogene that regulates the stem cell properties of human pancreatic cancer [37], and the key role of HNF1A in HCC was yet to be discovered. Under the synergistic influence of preceding mutations and their clusters, the HCC-PS of the subnet became progressively larger and reached its maximum until the TP53 cluster joined into the LCC, and the patient completed the transformation from hepatitis B to HCC.

The TPs of patients were counted; the TP53 cluster appeared as the TP in 51 patients, while 38 patients had other driver mutations as TPs, including AXIN1 cluster, CTNNB1 cluster, and other low-frequency genes. Therefore, patients were divided into two subtypes, subtype 1 composed of 51 patients with TP53 cluster as TPs and subtype 2 of 38 patients with no fixed gene as TPs. The survival time of patients in subtype 1 was significantly shorter ($p = 0.019$, Figure 3(f)), and the patients with advanced stages of CHCC-HBV in subtype 1 had a shorter survival time than patients in subtype 2 ($p = 0.023$, Figure 3(g)).

3.4. Validation of Patient Subtype Model. A three-step analysis was performed, 39 subtype-related genes were selected in subtype 1 patients (Figure 4(a)), and 9 signature genes and their coefficients were obtained using the LASSO regression (EVA1C: 0.065, LMAN2L: 0.184, MTF1: 0.051, NDUFV3: 0.237, NUP98: 0.054, RPAIN: 0.168, TFDP2: -0.067, YWHAE: 0.183, and ZNF530: -0.122). The semantic similarity among GO terms between 9 genes was less than 0.5 calculated by the R package "GOSemSim" [38] (Figure 4(b)). The PCCs

for gene expression levels of the 9 signature genes also showed a weak correlation in HCC and hepatitis B; the highest PCC was 0.48 in HCC and 0.31 in hepatitis B separately (Figures 4(c) and 4(d)); the results showed that 9 signature genes had a wide range of biological function.

The subtype model showed an AUC of 0.861 in HCC (Figure 4(e)) and 0.732 in hepatitis B (Figure 4(f)). So, the patient subtype model showed good classification efficacy in both HCC and hepatitis B. Validation of the subtype model using the CHCC-HBV patients with advanced stages showed an AUC value of 0.650 in HCC (Figure 4(g)) and 0.700 in hepatitis B (Figure 4(h)). The subtype model was also further validated in TCGA dataset with an AUC of 0.799 (Figure 4(i)). The above results indicated that the subtype model could well identify the patient with TP53 cluster as the TP.

3.5. Characteristic Changes between Hepatitis B and HCC in Subtype 1 Patients. To investigate the biological processes altered between hepatitis B and HCC in subtype 1 patients, we conducted transcriptome-based GSEA and proteome-based GSVA. The GSEA results showed that 21 KEGG pathways were activated and 48 KEGG pathways were suppressed in HCC (Figure 5(a)). The GSVA results showed that 13 KEGG pathways were promoted and 41 KEGG pathways were inhibited in HCC compared to HBV (Figure 5(b)). It is consistent with previous studies that cell-cycle, DNA damage repair pathways are activated in GSEA and GSVA results (Figure 5(c)) [14]. HBV infection can produce immune-mediated inflammation, which causes DNA damage in hepatocytes, and the DNA of HBV can randomly integrate into the chromosomal DNA of hepatocytes to further cause DNA damage, which plays a role in the development of HCC [39]. Taking the intersection of GSEA result and GSVA result yielded 28 metabolism-related and immunity-related KEGG pathways that were suppressed (Figure 5(d)). Some studies have shown that metabolism and immunity-related pathways play an important role in the development of HCC [40]. This suggests that patients in subtype 1 with HBV-HCC are more likely to have DNA damage as well as metabolic disturbances.

Emerging immunotherapeutic approaches are helpful in the treatment of HCC [41]. In this study, immune cell infiltration was analyzed in subtype 1 patients. 21 immune cells had a lower infiltration score in HCC ($p < 0.01$, Figure 5(e)). It was suggested that the HCC of subtype 1 was a "cold tumor," and the effect of single immunotherapy might not be significant [42]. The correlation between immune cells in HCC was significantly weaker than that in hepatitis B ($p < 0.05$, Figures 5(f) and 5(g)). The result revealed that combined treatment was essential for HCC patients in subtype 1.

3.6. Potential Drugs for the Patients of Subtype 1. To find the warning biomarkers for early detection and potential drug to prevent the transformation of patients in subtype 1 from hepatitis B to hepatocellular carcinoma, we constructed a translational model from hepatitis B to HCC, combining the model with TP can more accurately identify precancerous states. And it had the AUC value of 0.989 in the training dataset of stage I patients in CHCC-HBV (Figure 6(a)), the AUC value of 0.858 in the test dataset of advanced-stage patients in CHCC-HBV (Figure 6(b)), and the AUC value of 0.935 in the test dataset of patients in TCGA-LIHC (Figure 6(c)). Genes that were highly correlated with the transformation model may have potential therapeutic implications for the patients in subtype 1. 4112 genes highly associated with the HBV-HCC transformation model were identified ($|r| > 0.5$, $p < 0.05$), and 293 genes whose CERES scores closely associated with the HBV-HCC transformation model were identified ($r < -0.5$, $p < 0.05$), and 907 shared genes before TP53 cluster during the formation of LCC in subtype 1 patients were identified. Finally, 10 potential drug targets were obtained by taking intersections of shared genes before TPs and transformation model-related genes, named SNRPE, AURKB, RHOT1, NRAS, CDK2, CDC5L, TRIM28, RFC2, TAF6, and HAMP (Figure 6(d)). The correlation of 10 genes with the transformation model was found to be greater than 0.5 (Figure 6(e)). The CERES scores of 10 genes were less than 0, which indicated that 10 genes were essential for the survival of HCC CCLs (Figure 6(f)). Kaplan-Meier plot showed that the gene expression levels of 7 genes were significantly associated with patient prognosis in subtype 1 patients (Figures 6(g) and 6(h)). Therefore, we think these genes can be used as potential drug targets to block the transformation from hepatitis B to HCC, inhibiting the function of these genes in subtype 1 patients may have great preventative efficiency.

Next, drugs corresponding to the potential drug targets were screened in the DrugBank database. There were 8 approved drugs for AURKB, CDK2, and HAMP. For example, hesperidin, which targeted AURKB, has the function of hepatoprotective, therapeutic drug-related liver injury, improving inflammatory response, and preventing HCC formation in rats [43, 44]; it could illustrate the accuracy of the drug targets identified in our study. The study also provided a more accurate population classification for hesperidin to prevent and treat HCC. Higher gene expression of AURKB and CDK2 led to a poorer prognosis for HCC patients. Bosutinib is an inhibitor of CDK2 for chronic granulomatous leukemia treatment [45], and fostamatinib is an inhibitor of AURKB for persistent/chronic adult immune thrombocytopenia treatment [46]. So, inhibiting the expression of AURKB and CDK2 may prolong HCC patients' survival time.

"Cold tumors" were often associated with a poor prognosis. Targeted activation of specific kinases can promote the content of immune cells to form an inflammatory tumor environment and then convert "cold tumors" to "hot tumors," thereby enhancing the efficacy of immune checkpoint inhibitors [47]. To analyze whether potential targeted drugs have this effect, we studied the correlation between 10 genes and immune cells. The results showed that the HAMP gene expression level in HCC was positively correlated with multiple immune cells ($p < 0.01$, Figure 7(a)), whereas it was negatively correlated with multiple immune cells in hepatitis B ($p < 0.01$, Figure 7(b)). Meanwhile, the lower expression level of HAMP leads to a poorer prognosis

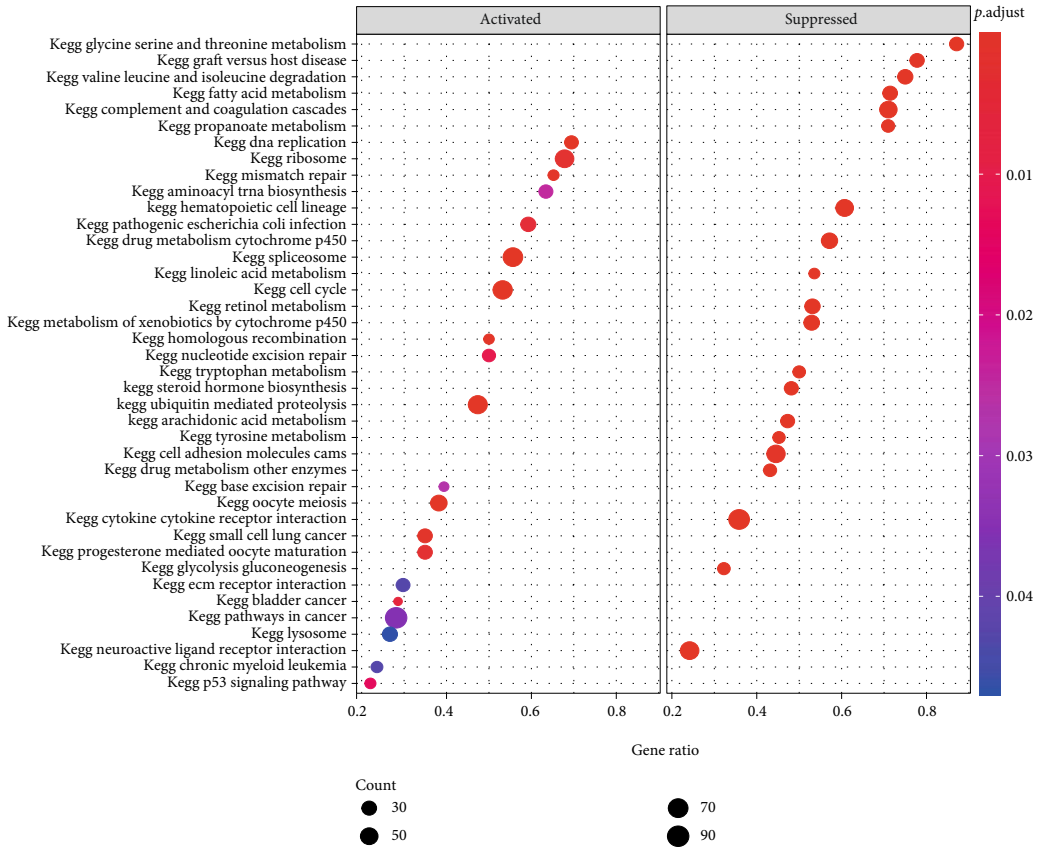

(a)

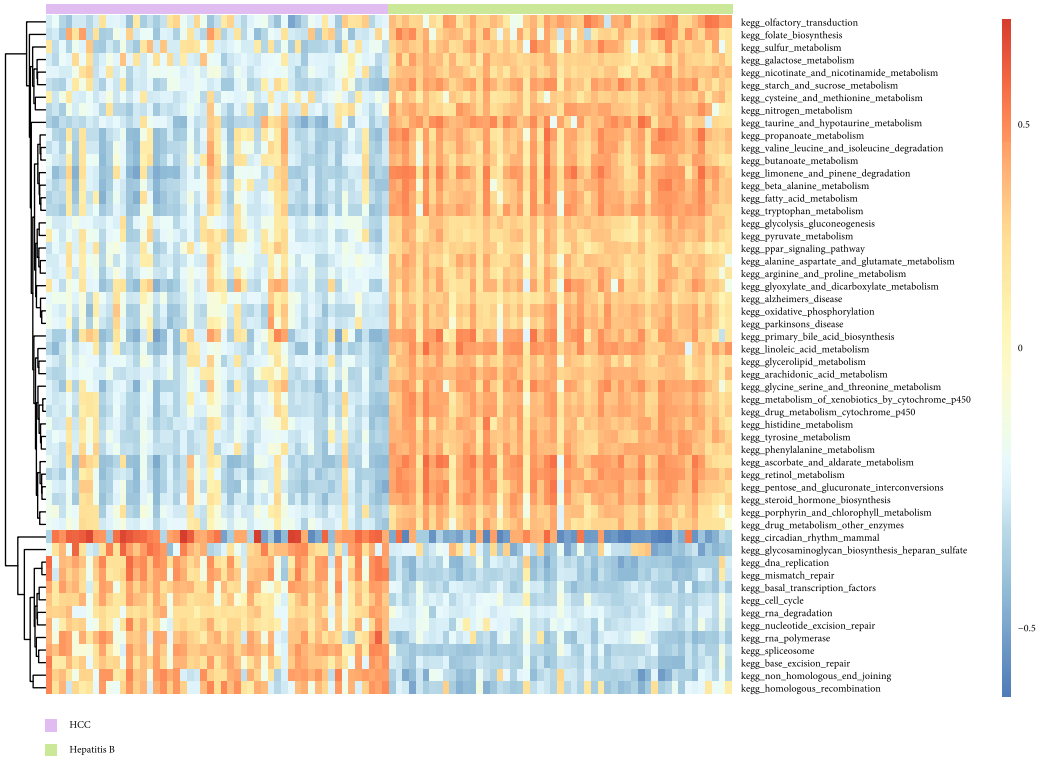

(b)

Figure 5: Continued.

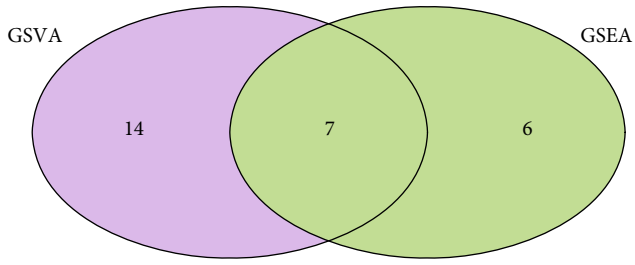

Activated KEGG pathways

Spliceosome
Base excision repair
Cell cycle
Mismatch repair
Dna replication
Nucleotide excision repair
Homologous recombination

(c)

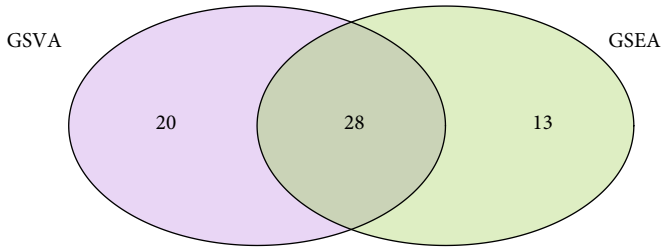

Suppressed KEGG pathways

Arachidonic acid metabolism	Steroid hormone biosynthesis
Tyrosine metabolism	Fatty acid metabolism
Drug metabolism cytochrome p450	Beta alanine metabolism
Retinol metabolism	Cysteine and methionine metabolism
Linoleic acid metabolism	Ascorbate and aldarate metabolism
Starch and sucrose metabolism	Alanine aspartate and glutamate metabolism
Histidine metabolism	Valine leucine and isoleucine degradation
Glycolysis gluconeogenesis	Propanoate metabolism
Metabolism of xenobiotics by cytochrome p450	Taurine and hypotaurine metabolism
Phenylalanine metabolism	Drug metabolism other enzymes
Tryptophan metabolism	Ppar signaling pathway
Pentose and glucuronate interconversions	Pyruvate metabolism
Arginine and proline metabolism	Butanoate metabolism
Glycine serine and threonine metabolism	Primary bile acid biosynthesis

(d)

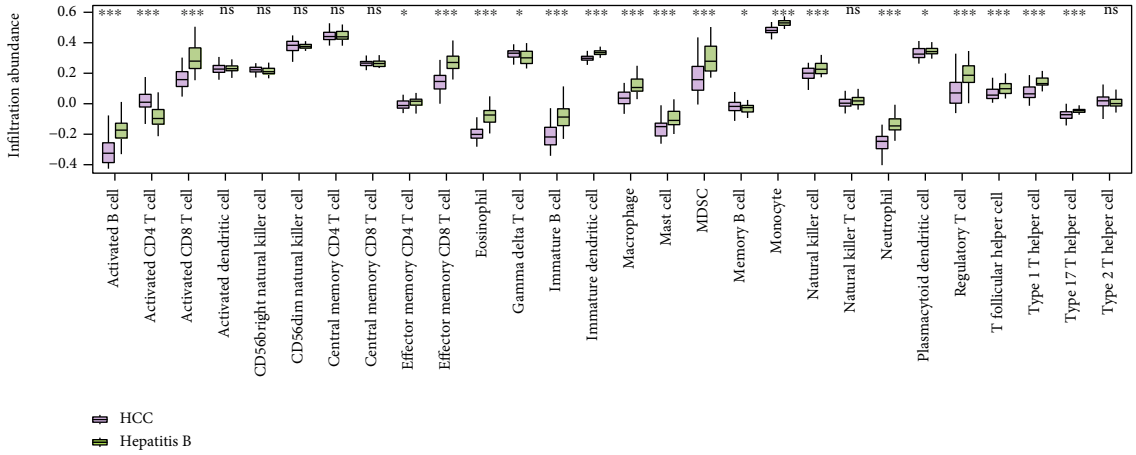

(e)

Figure 5: Continued.

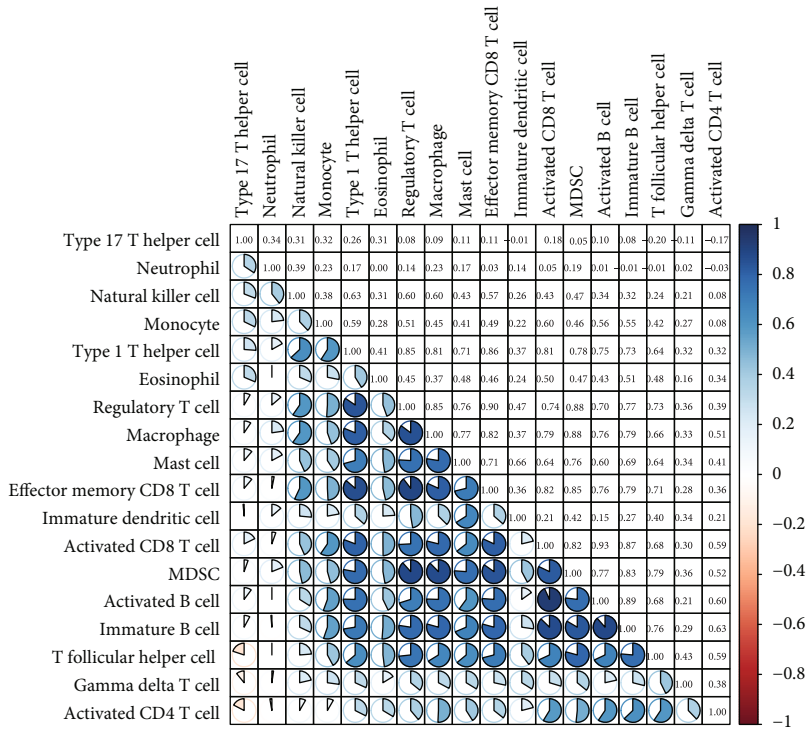

(f)

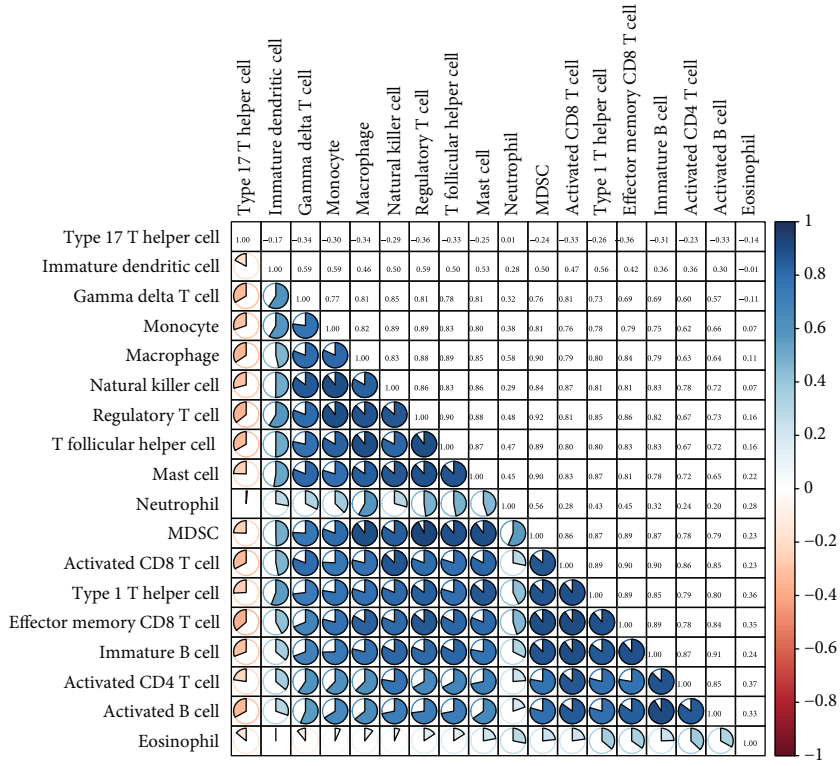

(g)

Figure 5: Enrichment analysis and immune infiltration analysis in subtype 1 patients. (a) Transcriptome-based GSEA, node size indicates the number of genes in the current pathway and node color indicates the significance of the results. (b) Proteome-based GSVA, purple represents HCC and green represents hepatitis B, red indicates that the pathway is activated, and blue indicates that it is suppressed. The Venn plot of (c) activated and (d) suppressed KEGG pathways in GSEA and GSVA. (e) Immune cell infiltration in HCC and hepatitis B, green indicates hepatitis B and purple indicates HCC. $*$ is p value < 0.05, $**$ is p value < 0.01, and $***$ is p value < 0.001. Correlation analysis of immune cells in (f) HCC and (g) hepatitis B.

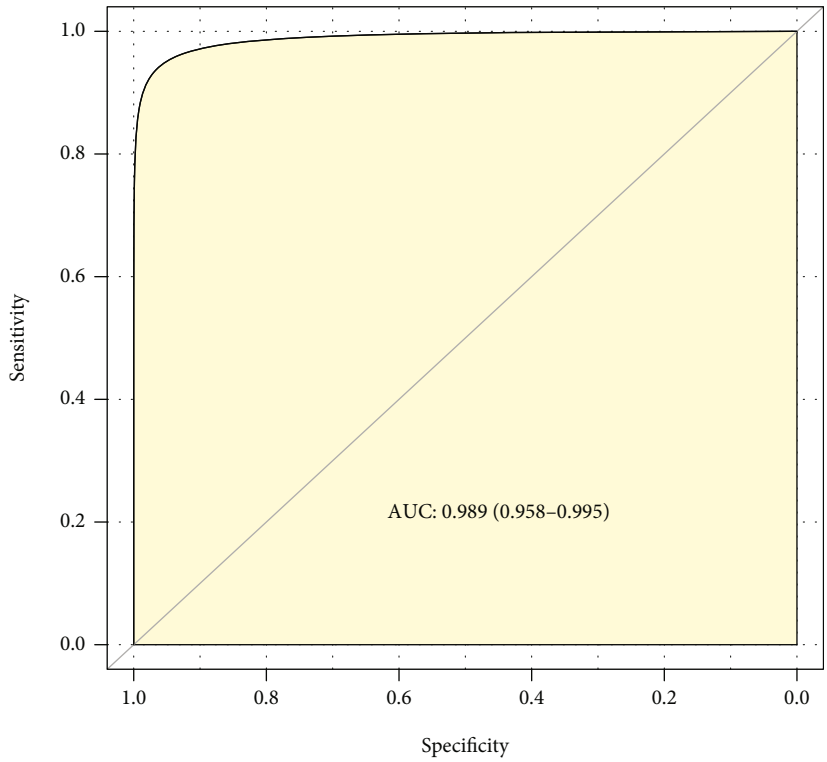

(a)

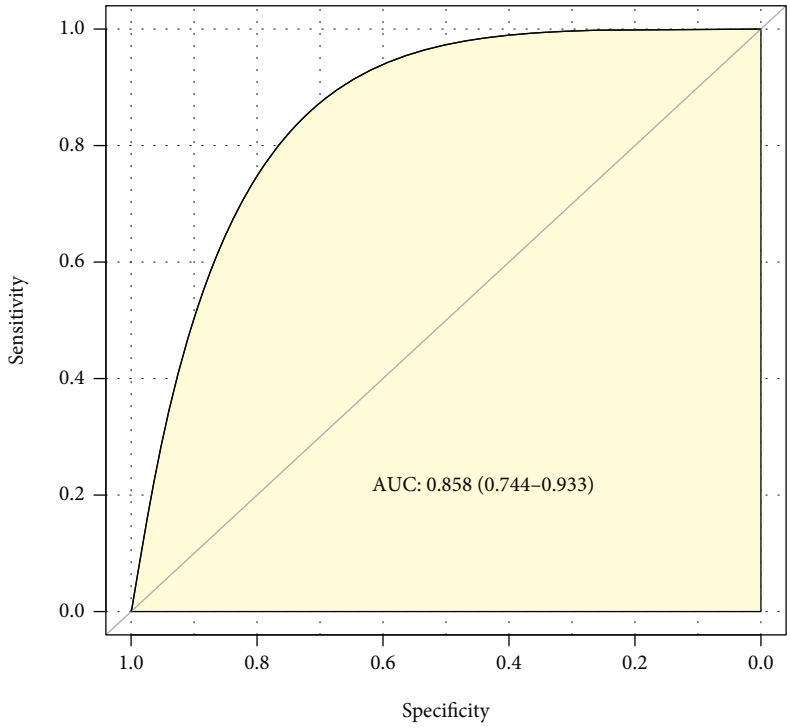

(b)

Figure 6: Continued.

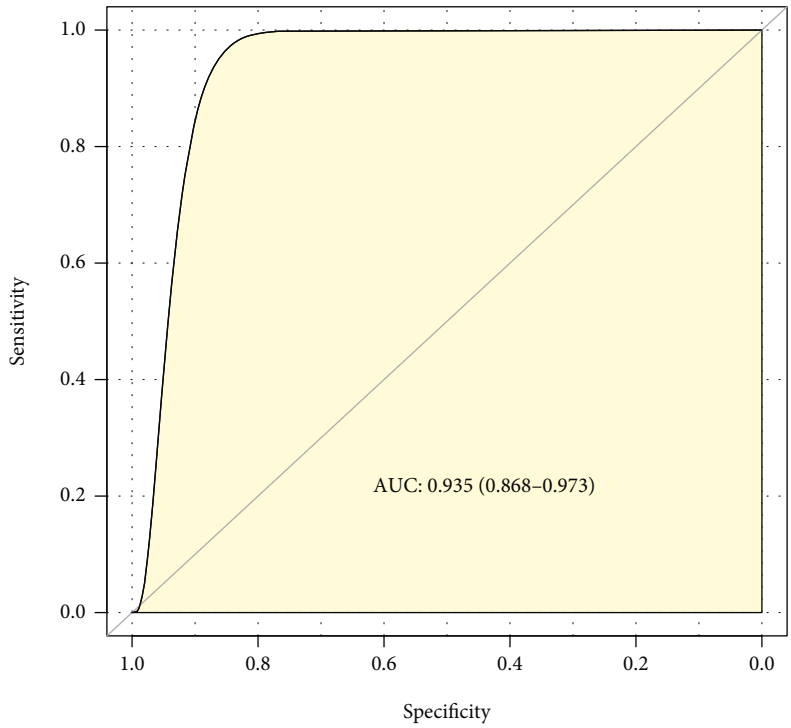

(c)

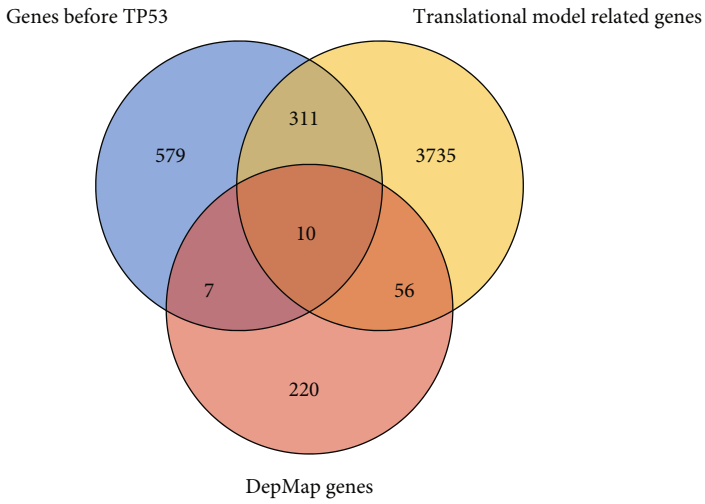

(d)

Figure 6: Continued.

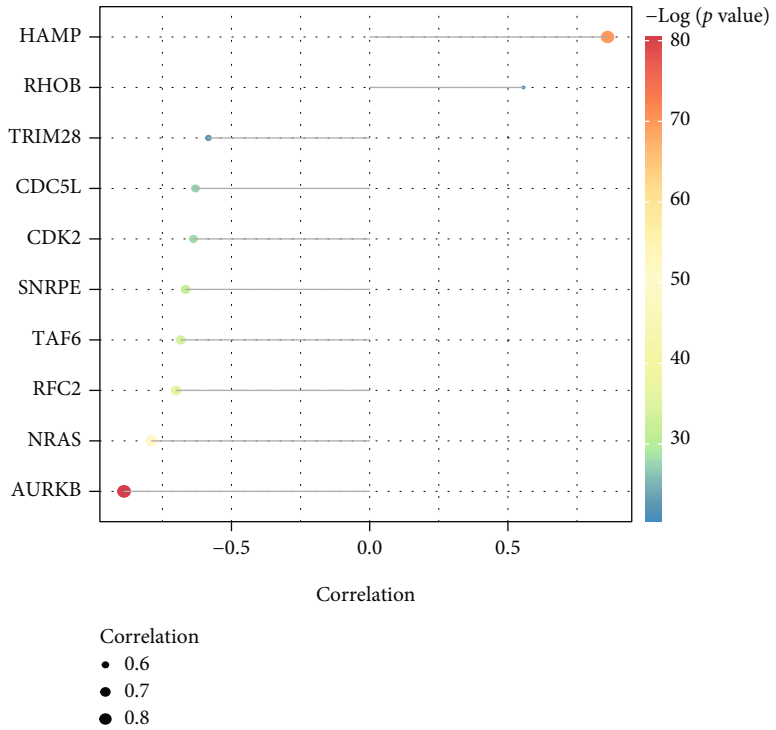

(e)

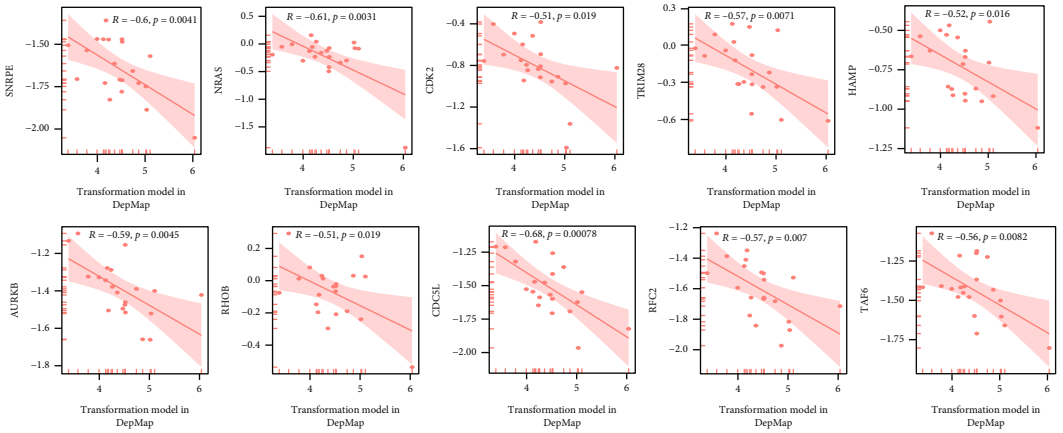

(f)

Figure 6: Continued.

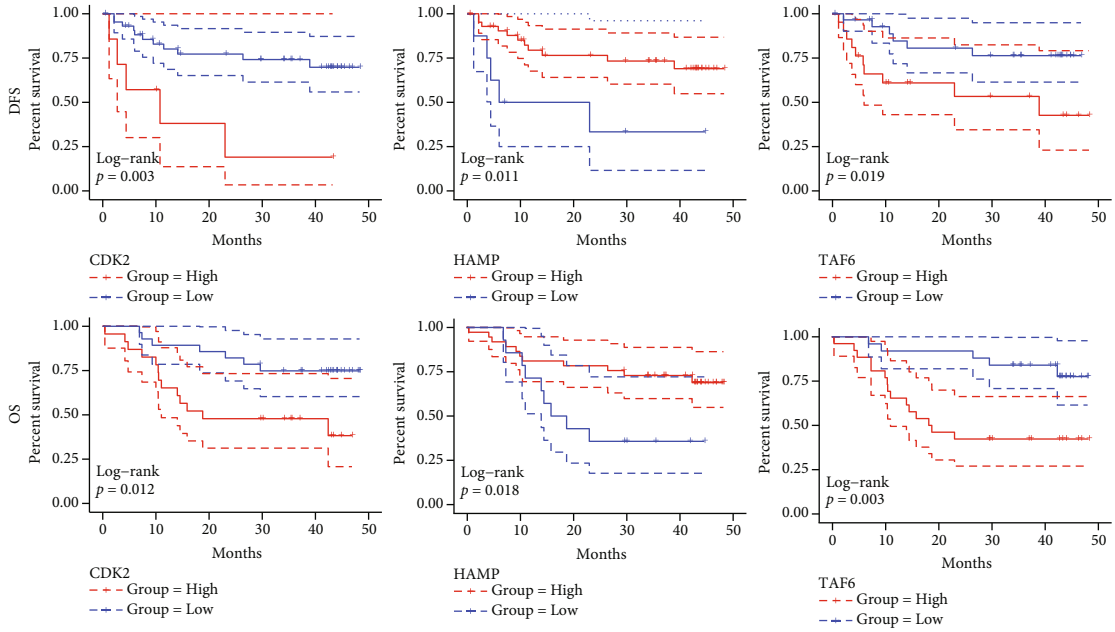

(g)

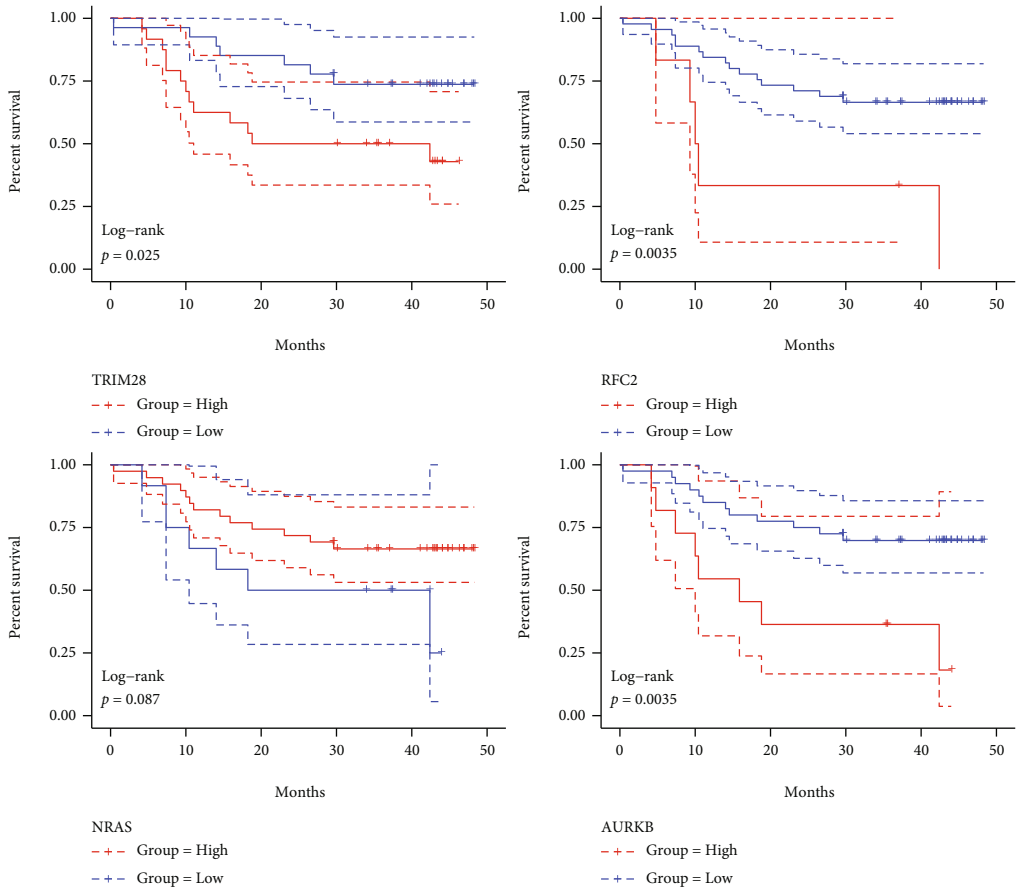

(h)

Figure 6: Identification of potential drugs in subtype 1 patients. (a–c) The ROC curve of the transformation model in the training set of stage I patients in CHCC-HBV, advanced-stage patients in CHCC-HBV, and patients in TCGA-LIHC. (d) Venn for potential drug targets. (e) The correlation between the expression level of 10 potential drug targets and the transformation model and CERES score. (f) The correlation between the CERES score of 10 potential drug targets and the transformation model. (g, h) Kaplan-Meier plot of 7 potential drug targets.

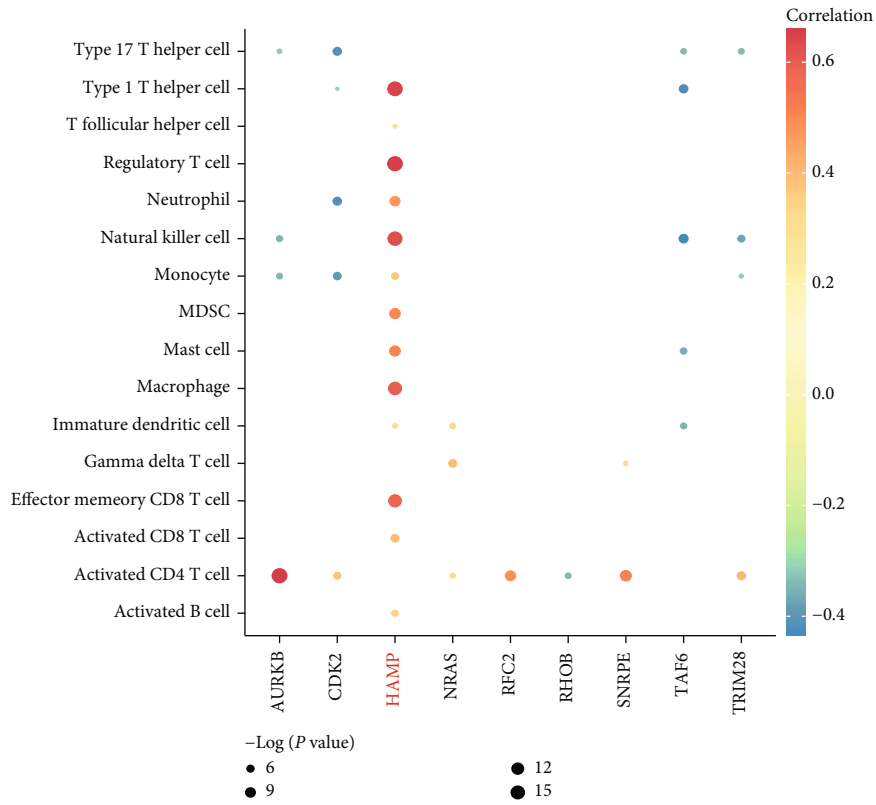

(a)

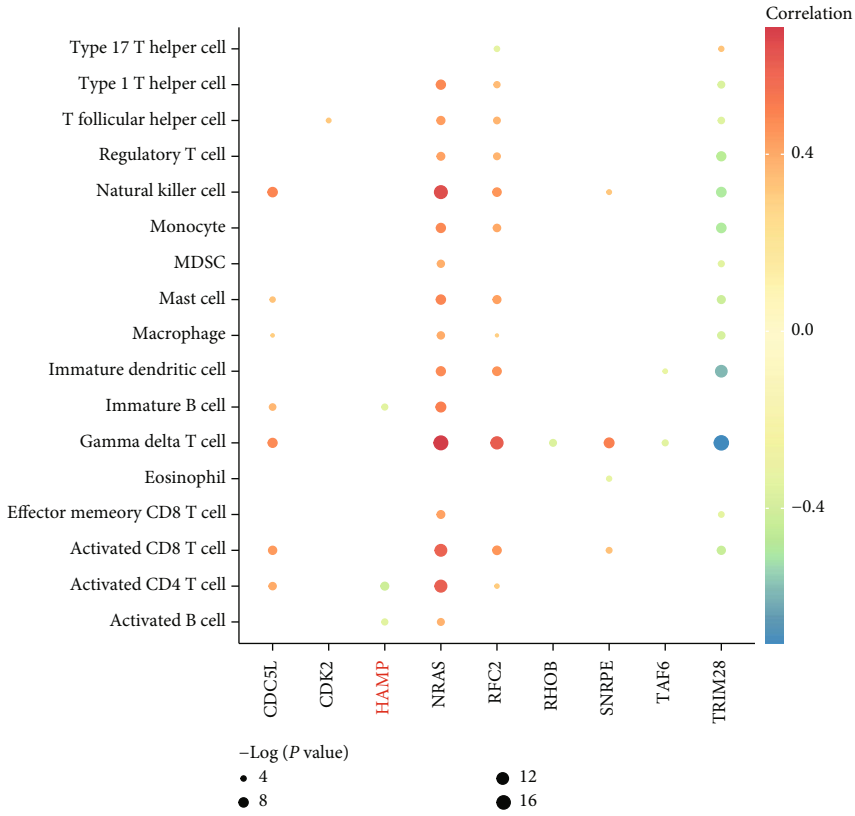

(b)

Figure 7: Continued.

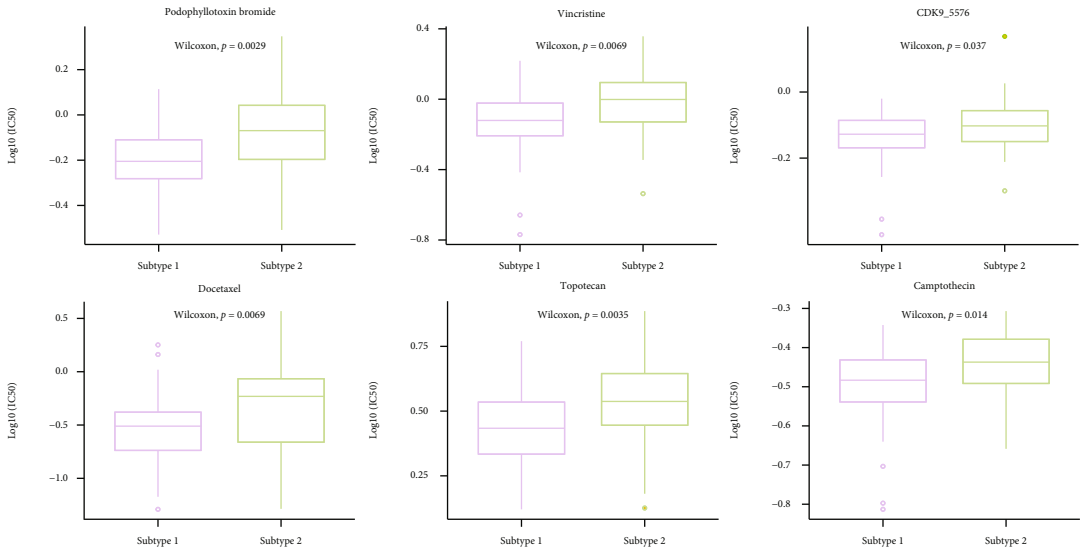

(c)

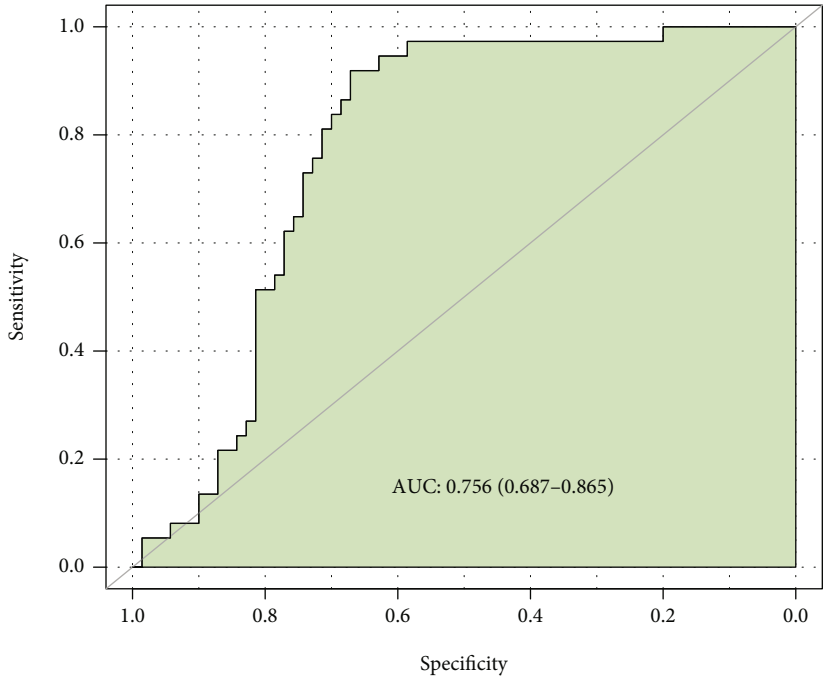

(d)

Figure 7: Continued.

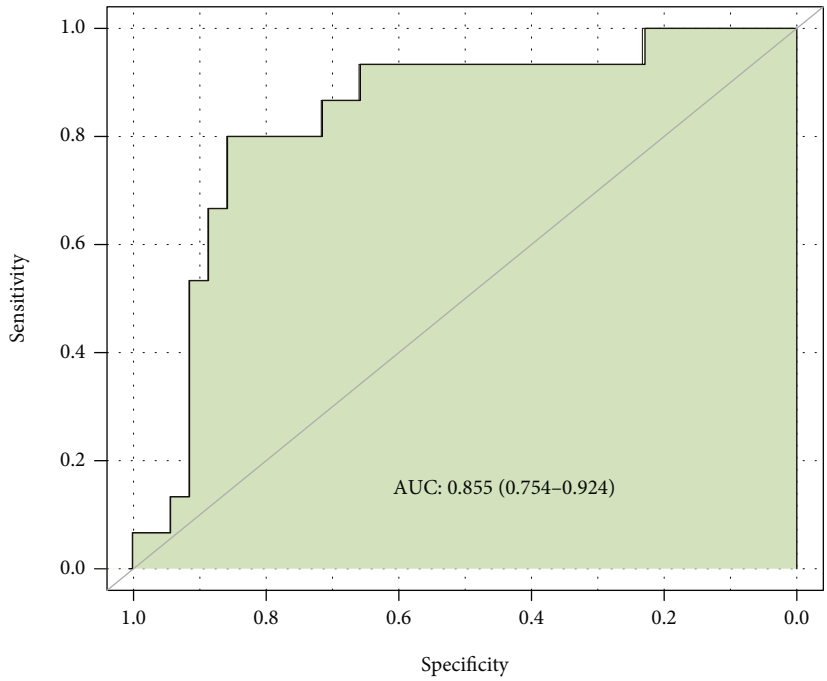

(e)

Figure 7: Identification of immunotherapy targets. (a, b) Correlation of 10 potential drug targets with immune cells in HCC and HBV. Node size indicates the significance, and node color indicates the PCCs. (c) Drugs for patients in subtype 1 who have completed the transformation from hepatitis B to HCC. (d, e) ROC curve of the transformation model in GSE121248.

in HCC patients, so HAMP may be a key target for immunotherapy in HCC patients of subtype 1. This study suggests that HAMP as a kinase may have the function to activate immune cells and prevent the transformation from hepatitis B to HCC.

We identified the potential drugs for personalized prevention from hepatitis B to HCC. And for HCC patients in subtype 1 who have completed the transformation from hepatitis B to HCC, we screened more sensitive drugs for these patients compared to patients in subtype 2; the results show that podophyllotoxin, bromide, docetaxel, vincristine, topotecan, CDK9_5576, and camptothecin may have a better therapeutic effect for patients in subtype 1 (Figure 7(c)).

4. Discussion

The transition from normal cells to cancerous cells results from the accumulation of somatic mutations [48]. During this process, the TP can lead to the inflammatory cellular transition toward cancer cells. We used percolation theory to model this transition and propose a research flow based on the accumulation mechanism of signaling pathway affected by mutant genes in the PPI network to identify transition points and to type HCC. First, we defined a new study unit, cluster, which is centered on a mutant gene and the nonmutated gene neighbors affected by it in a patient-specific protein-protein interaction (ps-PPI) network. Then, the HCC propensity score was created to describe the dynamical properties of signaling pathway accumulation during the growing process of the ps-PPI; the HCC patients with different transition points and their corresponding biological and clinical characteristics were identified and analyzed. Finally, we proposed a novel subtype model based on the TPs; the patients in subtype 1 had metabolic dysregulation and low immune levels and had a worse prognosis. Different therapeutic strategies for hepatitis B patients and HCC patients of subtype 1 were absent. For hepatitis B patients, we found the therapeutic targets and their drugs to block the further progression from hepatitis B to HCC. And for HCC patients, we demonstrated more sensitive anti-oncology drugs relative to HCC patients of subtype 2.

In previous research, using data from REVEAL-HBV, 17 risk genes were developed to predict the development of HBV-HCC [49]. Nevertheless, most prognostic markers have been developed for all HCC patients without focusing on individualized management and treatment, which exhibits a deficiency in precision treatment and preemptive prevention before HCC. In this study, 89 ps-PPIs were constructed, and the unique somatic mutations and gene expression levels of each patient make the ps-PPI an accurate and highly personalized basis for subsequent studies. The ps-PPI provides more personalized medical guidance for patients with the same cancer type and stage. Our approach identified predisease states and biomarkers to diagnose and interfere with disease onset early. 10 potential drug targets and their 8 approved drugs for patients in subtype 1 were also further identified. The majority of the 8 approved drugs we identified were related to oncology treatment, demonstrating the potential for drug repositioning.

These results are important for reducing the incidence and mortality of HBV-induced HCC, which provide important value for the early diagnosis and preventive treatment of HBV-HCC especially. As for patients in subtype 1 who have completed the transformation from hepatitis B to HCC, we also provide more sensitive drugs which may have a better therapeutic effect.

Mutated TP53 is one of the most common genomic alterations in human tumors. TP53 encodes p53, a transcription factor that regulates many gene expressions involved in numerous cellular processes [50]. HBV can bind and inactivate p53 in vitro [51]. And recombinant adenovirus human p53 (rAd-p53, gendicine), approved by CFDA in 2013, was used to repair the mutated P53 gene in head and neck squamous cell carcinoma (HNSCC) [52]. In this study, we found TP53 mutated and formed TP53 cluster in the precancerous state in some patients, guiding the transition from hepatitis B to HCC. The AUC of the transformation model for all HBV-HCC patients in an independent test dataset GSE121248 is 0.756 (Figure 7(d)), and the AUC for patients in subtype 1 is 0.855 (Figure 7(e)). The result shows that the translational model is more accurate in diagnosis for patients in subtype 1.

5. Conclusion

In conclusion, this study showed the sequence of multiple somatic mutations and their cooperative effect. And it fully identified the warning transition point in HCC tumorigenesis for each patient, which reflects the individualized analysis. However, there are a few patients who have gene expression profiles, gene mutation profiles, and clinical data of both hepatitis B and HCC at the same time. Therefore, the constructed model may not broadly represent the transformation process of HBV-HCC, but the idea and method may provide a reference for others to conduct in-depth studies. And we will collect more data to expand the sample of our study for improving the reliability.

Data Availability

The data achieved and analyzed in the current study are available in the TCGA repository (https://portal.gdc.cancer.gov/), ICGC database (https://icgc.org/), and GEO database (https://www.ncbi.nlm.nih.gov/geo/).

Conflicts of Interest

The authors have no conflicts of interest to declare.

Acknowledgments

This work was supported by the National Natural Science Foundation of China (Grant Nos. 61971166 and 61802090).

Supplementary Materials

Supplementary Table 1 and Supplementary Table 2 can be checked in the supplementary files in the submission system. *(Supplementary Materials)*

References

[1] K. Sartorius, B. Sartorius, C. Aldous, P. S. Govender, and T. E. Madiba, "Global and country underestimation of hepatocellular carcinoma (HCC) in 2012 and its implications," *Cancer Epidemiology*, vol. 39, no. 3, pp. 284–290, 2015.

[2] T. Akinyemiju, S. Abera, M. Ahmed et al., "The burden of primary liver cancer and underlying etiologies from 1990 to 2015 at the global, regional, and national level: results from the global burden of disease study 2015," *JAMA Oncology*, vol. 3, no. 12, pp. 1683–1691, 2017.

[3] E. G. Álvarez, J. Demeulemeester, P. Otero et al., "Aberrant integration of hepatitis B virus DNA promotes major restructuring of human hepatocellular carcinoma genome architecture," *Nature Communications*, vol. 12, no. 1, p. 6910, 2021.

[4] S. H. Wang, S. H. Yeh, and P. J. Chen, "Unique features of hepatitis B virus-related hepatocellular carcinoma in pathogenesis and clinical significance," *Cancers (Basel)*, vol. 13, no. 10, p. 2454, 2021.

[5] Y. Jiang, Q. Han, H. Zhao, and J. Zhang, "The mechanisms of HBV-induced hepatocellular carcinoma," *Journal of Hepatocellular Carcinoma*, vol. 8, pp. 435–450, 2021.

[6] M. Levrero and J. Zucman-Rossi, "Mechanisms of HBV-induced hepatocellular carcinoma," *Journal of Hepatology*, vol. 64, no. 1, pp. S84–S101, 2016.

[7] F. Vandin, E. Upfal, and B. J. Raphael, "De novo discovery of mutated driver pathways in cancer," *Genome Research*, vol. 22, no. 2, pp. 375–385, 2012.

[8] C. H. Yeang, F. McCormick, and A. Levine, "Combinatorial patterns of somatic gene mutations in cancer," *The FASEB Journal*, vol. 22, no. 8, pp. 2605–2622, 2008.

[9] S. Nisar, S. Hashem, M. A. Macha et al., "Exploring dysregulated signaling pathways in cancer," *Current Pharmaceutical Design*, vol. 26, no. 4, pp. 429–445, 2020.

[10] L. Chen, R. Liu, Z. P. Liu, M. Li, and K. Aihara, "Detecting early-warning signals for sudden deterioration of complex diseases by dynamical network biomarkers," *Scientific Reports*, vol. 2, no. 1, p. 342, 2012.

[11] X. Liu, X. Chang, S. Leng, H. Tang, K. Aihara, and L. Chen, "Detection for disease tipping points by landscape dynamic network biomarkers," *National Science Review*, vol. 6, no. 4, pp. 775–785, 2019.

[12] A. Achiron, I. Grotto, R. Balicer, D. Magalashvili, A. Feldman, and M. Gurevich, "Microarray analysis identifies altered regulation of nuclear receptor family members in the pre-disease state of multiple sclerosis," *Neurobiology of Disease*, vol. 38, no. 2, pp. 201–209, 2010.

[13] J. H. Zhao, H. J. Zhou, and Y. Y. Liu, "Inducing effect on the percolation transition in complex networks," *Nature Communications*, vol. 4, no. 1, p. 2412, 2013.

[14] Q. Gao, H. Zhu, L. Dong et al., "Integrated proteogenomic characterization of HBV-related hepatocellular carcinoma," *Cell*, vol. 179, no. 2, pp. 561–577.e22, 2019.

[15] D. Szklarczyk, A. L. Gable, D. Lyon et al., "STRING v11: protein-protein association networks with increased coverage, supporting functional discovery in genome-wide experimental datasets," *Nucleic Acids Research*, vol. 47, no. D1, pp. D607–D613, 2019.

[16] S. H. Liu, P. C. Shen, C. Y. Chen et al., "DriverDBv3: a multi-omics database for cancer driver gene research," *Nucleic Acids Research*, vol. 48, no. D1, pp. D863–D870, 2020.

[17] M. Kanehisa and S. Goto, "KEGG: Kyoto encyclopedia of genes and genomes," *Nucleic Acids Research*, vol. 28, no. 1, pp. 27–30, 2000.

[18] A. Tsherniak, F. Vazquez, P. G. Montgomery et al., "Defining a cancer dependency map," *Cell*, vol. 170, no. 3, pp. 564–576.e16, 2017.

[19] M. E. Ritchie, B. Phipson, D. Wu et al., "Limma powers differential expression analyses for RNA-sequencing and microarray studies," *Nucleic Acids Research*, vol. 43, no. 7, p. e47, 2015.

[20] L. Franke, H. . Bakel, L. Fokkens, E. D. de Jong, M. Egmont-Petersen, and C. Wijmenga, "Reconstruction of a functional human gene network, with an application for prioritizing positional candidate genes," *American Journal of Human Genetics*, vol. 78, no. 6, pp. 1011–1025, 2006.

[21] A. Valdeolivas, L. Tichit, C. Navarro et al., "Random walk with restart on multiplex and heterogeneous biological networks," *Bioinformatics*, vol. 35, no. 3, pp. 497–505, 2019.

[22] S. Köhler, S. Bauer, D. Horn, and P. N. Robinson, "Walking the interactome for prioritization of candidate disease genes," *American Journal of Human Genetics*, vol. 82, no. 4, pp. 949–958, 2008.

[23] Z. Q. Zhao, G. S. Han, Z. G. Yu, and J. Li, "Laplacian normalization and random walk on heterogeneous networks for disease- gene prioritization," *Computational Biology and Chemistry*, vol. 57, pp. 21–28, 2015.

[24] S. Erten, G. Bebek, R. M. Ewing, and M. Koyutürk, "DADA: degree-aware algorithms for network-based disease gene prioritization," *BioData Mining*, vol. 4, no. 1, p. 19, 2011.

[25] Y. Li and J. C. Patra, "Genome-wide inferring gene-phenotype relationship by walking on the heterogeneous network," *Bioinformatics*, vol. 26, no. 9, pp. 1219–1224, 2010.

[26] D. Shin, J. Lee, J. R. Gong, and K. H. Cho, "Percolation transition of cooperative mutational effects in colorectal tumorigenesis," *Nature Communications*, vol. 8, no. 1, p. 1270, 2017.

[27] X. Robin, N. Turck, A. Hainard et al., "pROC: an open-source package for R and S+ to analyze and compare ROC curves," *BMC Bioinformatics*, vol. 12, no. 1, p. 77, 2011.

[28] A. Liberzon, C. Birger, H. Thorvaldsdóttir, M. Ghandi, J. P. Mesirov, and P. Tamayo, "The molecular signatures database hallmark gene set collection," *Cell Systems*, vol. 1, no. 6, pp. 417–425, 2015.

[29] G. Yu, L. G. Wang, Y. Han, and Q. Y. He, "clusterProfiler: an R package for comparing biological themes among gene clusters," *Omics: a Journal of Integrative Biology*, vol. 16, no. 5, pp. 284–287, 2012.

[30] S. Hanzelmann, R. Castelo, and J. Guinney, "GSVA: gene set variation analysis for microarray and RNA-seq data," *BMC Bioinformatics*, vol. 14, no. 1, p. 7, 2013.

[31] D. A. Barbie, P. Tamayo, J. S. Boehm et al., "Systematic RNA interference reveals that oncogenic KRAS -driven cancers require TBK1," *Nature*, vol. 462, no. 7269, pp. 108–112, 2009.

[32] P. Charoentong, F. Finotello, M. Angelova et al., "Pan-cancer immunogenomic analyses reveal genotype-immunophenotype relationships and predictors of response to checkpoint blockade," *Cell Reports*, vol. 18, no. 1, pp. 248–262, 2017.

[33] D. S. Wishart, Y. D. Feunang, A. C. Guo et al., "DrugBank 5.0: a major update to the DrugBank database for 2018," *Nucleic Acids Research*, vol. 46, no. D1, pp. D1074–D1082, 2018.

[34] W. Yang, J. Soares, P. Greninger et al., "Genomics of Drug Sensitivity in Cancer (GDSC): a resource for therapeutic biomarker discovery in cancer cells," *Nucleic Acids Research*, vol. 41, pp. D955–D961, 2013.

[35] D. Maeser, R. F. Gruener, and R. S. Huang, "oncoPredict: an R package for predicting in vivo or cancer patient drug response and biomarkers from cell line screening data," *Briefings in Bioinformatics*, vol. 22, no. 6, 2021.

[36] J. N. Wu and C. W. Roberts, "ARID1A mutations in cancer: another epigenetic tumor suppressor?," *Cancer Discovery*, vol. 3, no. 1, pp. 35–43, 2013.

[37] E. V. Abel, M. Goto, B. Magnuson et al., "HNF1A is a novel oncogene that regulates human pancreatic cancer stem cell properties," *eLife*, vol. 7, 2018.

[38] G. Yu, "Gene ontology semantic similarity analysis using GOSemSim," *Methods in Molecular Biology*, vol. 2117, pp. 207–215, 2020.

[39] W. S. Mason, A. R. Jilbert, and S. Litwin, "Hepatitis B virus DNA integration and clonal expansion of hepatocytes in the chronically infected liver," *Viruses*, vol. 13, no. 2, p. 210, 2021.

[40] M. Stepien, P. Keski-Rahkonen, A. Kiss et al., "Metabolic perturbations prior to hepatocellular carcinoma diagnosis: findings from a prospective observational cohort study," *International Journal of Cancer*, vol. 148, no. 3, pp. 609–625, 2021.

[41] B. Sangro, P. Sarobe, S. Hervás-Stubbs, and I. Melero, "Advances in immunotherapy for hepatocellular carcinoma," *Nature Reviews. Gastroenterology & Hepatology*, vol. 18, no. 8, pp. 525–543, 2021.

[42] J. Galon and D. Bruni, "Approaches to treat immune hot, altered and cold tumours with combination immunotherapies," *Nature Reviews. Drug Discovery*, vol. 18, no. 3, pp. 197–218, 2019.

[43] Y. S. Mo'men, R. M. Hussein, and M. A. Kandeil, "Involvement of PI3K/Akt pathway in the protective effect of hesperidin against a chemically induced liver cancer in rats," *Journal of Biochemical and Molecular Toxicology*, vol. 33, no. 6, article e22305, 2019.

[44] S. T. Ahmad, W. Arjumand, S. Nafees et al., "Hesperidin alleviates acetaminophen induced toxicity in Wistar rats by abrogation of oxidative stress, apoptosis and inflammation," *Toxicology Letters*, vol. 208, no. 2, pp. 149–161, 2012.

[45] J. E. Cortes, C. Gambacorti-Passerini, M. W. Deininger et al., "Bosutinib versus imatinib for newly diagnosed chronic myeloid leukemia: results from the randomized BFORE trial," *Journal of Clinical Oncology*, vol. 36, no. 3, pp. 231–237, 2018.

[46] A. Newland, E. J. Lee, V. McDonald, and J. B. Bussel, "Fostamatinib for persistent/chronic adult immune thrombocytopenia," *Immunotherapy*, vol. 10, no. 1, pp. 9–25, 2018.

[47] S. Maleki Vareki, "High and low mutational burden tumors versus immunologically hot and cold tumors and response to immune checkpoint inhibitors," *Journal for Immunotherapy of Cancer*, vol. 6, no. 1, p. 157, 2018.

[48] J. S. Welch, T. J. Ley, D. C. Link et al., "The origin and evolution of mutations in acute myeloid leukemia," *Cell*, vol. 150, no. 2, pp. 264–278, 2012.

[49] H. I. Yang, M. F. Yuen, H. L. Chan et al., "Risk estimation for hepatocellular carcinoma in chronic hepatitis B (REACH-B): development and validation of a predictive score," *The Lancet Oncology*, vol. 12, no. 6, pp. 568–574, 2011.

[50] L. N. Redman-Rivera, T. M. Shaver, H. Jin et al., "Acquisition of aneuploidy drives mutant p53-associated gain-of-function phenotypes," *Nature Communications*, vol. 12, no. 1, p. 5184, 2021.

[51] P. A. Farazi and R. A. DePinho, "Hepatocellular carcinoma pathogenesis: from genes to environment," *Nature Reviews. Cancer*, vol. 6, no. 9, pp. 674–687, 2006.

[52] Y. Li, W. Guo, X. Li et al., "Expert consensus on the clinical application of recombinant adenovirus human p53 for head and neck cancers," *International Journal of Oral Science*, vol. 13, no. 1, p. 38, 2021.

Hindawi
Oxidative Medicine and Cellular Longevity
Volume 2022, Article ID 8543720, 18 pages
https://doi.org/10.1155/2022/8543720

Research Article

Interleukin-22 Ameliorates Dextran Sulfate Sodium-Induced Colitis through the Upregulation of lncRNA-UCL to Accelerate Claudin-1 Expression via Sequestering miR-568 in Mice

Chonghua He,[1] Zehan Chen,[1] Jialan Huang,[1] Riyun Gan,[1] Jianyao Wang,[2] Lisheng Wang,[1] Defeng Li,[1] and Jun Yao[1]

[1]*Department of Gastroenterology, Shenzhen People's Hospital, Jinan University of Second Clinical Medical Sciences, No. 1017 East Gate Road, Luohu District, Shenzhen, 518020, Guangdong Province, China*
[2]*Department of General Surgery, Shenzhen Children's Hospital, Shenzhen 518026, Guangdong Province, China*

Correspondence should be addressed to Defeng Li; ldf730712@163.com and Jun Yao; yj_1108@126.com

Received 27 July 2022; Revised 3 August 2022; Accepted 5 August 2022; Published 31 August 2022

Academic Editor: Tarique Hussain

Background. Bioactive compound such as interleukin-22 (IL-22) treatment is regarded as a sufficient treatment for ulcerative colitis (UC). It has been found that long noncoding RNAs (lncRNAs) expressed in many inflammatory diseases, including UC. We aimed to verify the treatment effect of bioactive compounds including IL-22 and lncRNAs in UC on colitis mice. *Methods*. UC mice were induced using DSS, followed by IL-22 or PBS intraperitoneally (i.p.) injection. Then, the histopathological parameters of the mice were determined. Then, RNA sequencing was performed to screen the differential lncRNAs. Quantitative real-time PCR (qRT-PCR) and lentivirus identified lncRNA-Ulcerative Colitis lncRNA (lncRNA-UCL) were regarded as the molecular regulator of the colitis mice. The correlation with lncRNA-UCL and mmu-miR-568 was validated using RNA-pulldown. Meanwhile, claudin-1 was predicted and confirmed as the target molecule of mmu-miR-568 using dual-luciferase assay. *Results*. IL-22 could significantly improve the histopathological features and decrease proinflammatory cytokine production in UC mice induced by DSS. It also can stimulate intestinal epithelial cell (IEC) reproduction and prevention of apoptosis. lncRNA-UCL was significantly downregulated in UC mice caused by DSS, while IL-22 treatment effectively reversed this effect. In terms of mechanism, lncRNA-UCL regulates intestinal epithelial homeostasis by sequestering mmu-miR-568 and maintaining close integrated protein expression, such as claudin-1. *Conclusions*. We have demonstrated the incredible role of bioactive compound, such as IL-22, in alleviating DSS-induced colitis symptoms via enhancing lncRNA-UCL expression. It can be regulated using tight junction (TJ) protein.

1. Introduction

UC is a major type of inflammatory bowel disease (IBD), which is a chronically recurring and relatively intractable IBD. The typical symptom of UC patients includes bloody diarrhea, mucus discharge, abdominal pain, and weight loss, which greatly impair the patient's life quality and has become a health challenge worldwide [1–3]. Many studies have suggested that hereditary factors, immunological dysregulation and environmental aspect, may be causative factors for UC [4–6]. However, pathogenesis of UC remains largely unknown [7]. The frequency of UC has increased rapidly in Asia over the past few decades [1, 8]. The number of medical approaches available for UC is limited [9–12]. Accordingly, it is highly needed to develop new and effective treatment options for UC patients.

Bioactive compound has been universally used in many diseases such as UC. IL-22 is a kind of bioactive compound vest in IL-10, which is characterized by their intestinal homeostasis maintenance and IEC barrier functions [13–15]. IL-22 is primarily generated by immune cells on mucosal surfaces. IL-22 plays crucial roles in maintaining the epithelial integrity of the intestinal tract and protection of the intestine from toxic stress and pathogens, by activating of signal transducer and

activator of transcription 3 (STAT3) signaling [16–19]. It has been well documented that IL-22 can increase IEC viability and reversal of IEC damage, as a result of IBD and graft-versus-host disease (GVHD) [20, 21]. However, controlling the dosage is quite important. Studies have found IL-22 can promote IBD development and tumorigenesis in mouse models if IL-22 is not properly controlled [22, 23], implying that IL-22 signaling should be correctively regulated to facilitate the maintenance of IEC integrity.

Long noncoding RNAs (lncRNAs) with a length of about 200 nucleotides could extensively involve in many types of crucial biological and physiological processes such as cell proliferation, metabolism, differentiation, and immunity. The upregulation and downregulation of lncRNAs are both closely related to the occurrence and metastasis of tumors, cardiovascular disorder, nervous diseases, gastrointestinal diseases, and some other diseases. Therefore, the usage of lncRNAs as markers or targets of various diseases can provide new solutions into the diagnosis and treatment. Numerous studies have shown that lncRNA dysregulation is highly relevant with the onset and advancement of many diseases, including IBD [24–26]. It has been found that the upregulation of H19 is required for IEC multiplication and mucosal healing in cell cultures and inflammatory mouse models [27]. Another study demonstrated that lncRNA uc.173 could contribute to intestinal mucosa regulation and reproduction [28]. lncRNA metastasis-associated lung adenocarcinoma transcript 1 (MALAT1) showed important function in intestinal mucosa equilibrium. If *MALAT1* downregulated, they contributed to IBD pathogenesis by disrupting TJs in DSS-induced experimental colitis [29]. These findings demonstrated the incredible function of lncRNAs in IBD pathogenesis.

Nonetheless, the lncRNA mechanism of IL-22-induced inflammation in UC remains unknown. Therefore, there is an urgent need to explore the features of lncRNAs on the intestinal epithelium in colitis under the effect of IL-22. Accordingly, we first estimated the therapeutic effect of IL-22 on DSS-induced colitis in mice. In addition, the potential mechanisms were explored in DSS-induced colitis mice, mainly at the UC-affected sites.

2. Materials and Methods

2.1. Ethics Statement. This study strictly implements the principles of the China Laboratory Animal Guideline for Ethical Review of Animal Welfare (GB/T 35892-2018), and all experiments performed on animals got approval from the Medical Ethics Committee of China Shenzhen People's Hospital.

2.2. DSS-Induced Colitis Model and IL-22 Treatment. 10-week male C57BL/6J mice were used in our study. All the mice were kept in specific pathogen-free environment. The mice were randomly divided into three groups with 9 mice in the control group (fed using water for 12 days), and 15 mice were treated by DSS with PBS, while other 15 mice were treated using DSS and IL-22. The other two groups were firstly administrated with 3% DSS (36-50 kDa; MP Biomedicals, USA) for 8 days to establish the colitis model. Then, the DSS+PBS group was fed with PBS for 9 days at the 4th day of model establishment. The DSS+IL22 group was treated using recombinant IL-22 (rIL-22, PeproTech) daily for 9 days using i.p. injection.

2.3. Mouse Tissue Processing and Histopathological Evaluation. We recorded weight loss, change in consistency of stool, and severe bleeding parameters to determine the disease activity index (DAI). DAI was determined by the degree of diarrhea and visible fecal blood, together with the severity of colitis, which was evaluated daily through the determination of weight loss and DAI [30]. After euthanasia, the entire colon, containing caecum to anus, and small intestine were excised from each of the mice. The colon was collected to measure their length and separated for other tests, including immunohistochemistry (IHC), cytokine quantitation, identification of RNA and protein, and IEC isolation. On day 8, we also collected intestinal tissue for IEC isolation and further analysis.

2.4. RNA Extraction and Quantitative Reverse Transcription PCR (qRT-PCR). TRIzol reagent (Thermo Fisher Scientific, USA) was chosen to extract RNA from tissues according to the protocol. Complementary DNA (cDNA) was synthesized using RNeasy Mini Kit (TakaRa). SYBR Green Master Mix (TaKaRa) was utilized to execute qRT-PCR on a LightCycler480 system (Roche). Target gene expression was normalized by glyceraldehyde-3-phosphate dehydrogenase (GADPH). The primer sequences we selected are recorded in Table 1.

2.5. Isolation and Culture of Mouse Colonic ECs. Colons tissues were removed from the mice and cleared by flushing using a syringe of cold PBS. Then, the colons were longitudinally opened and cut into small pieces less than 0.5 cm. The mixtures were incubated in a dissociation buffer at pH = 7.4 (10 mM EDTA, 1 mM DTT, 150 mM NaCl, and 10 mM HEPES) and 10% heat inactivated FBS at 37°C for 30 min. Thereafter, continuously shake the tubes to release of ECs, and the EC suspension was washed using cold PBS. Then, the ECs were collected through centrifugation and were used for further analysis [31].

2.6. Enzyme-Linked Immunosorbent Assay (ELISA). ELISA kit (R&D Systems, USA) was used to measure the cytokine expression in colonic tissues. The cytokine consists of IL-1β, TNF-α, IL-17A, and IL-6. Total protein concentration can be used to normalize the cytokine value.

2.7. IHC and Immunofluorescence (IF). All tissues were first embedded in paraffin. Paraffin slides were dewaxed, dehydrated, and then subjected to antigen retrieval. After blocking with 5% bovine serum albumin (BSA), it was followed by incubating with primary antibody at 4°C overnight. After incubation, an EnVision™ Detection Kit (DAKO, Denmark) was used for staining. Briefly, 3,3′-diaminobenzidine tetrahydrochloride (DAB) staining and hematoxylin were performed to counterstain the nuclei.

For the IF analysis, the procedures were the same until primary antibody incubation. After it, secondary antibodies

Table 1: The primer sequences.

Genes	Sequences
mTNF-α forward	5′-TTCTGTCTACTGAACTTC-3′
mTNF-α reverse	5′-CCATAGAACTGATGAGAG-3′
mIL-1β forward	5′-CAATGGACAGAATATCAAC-3′
mIL-1β reverse	5′-ACAGGACAGGTATAGATT-3′
mIL-6 forward	5′-TAGTCCTTCCTACCCCAATTTCC-3′
mIL-6 reverse	5′-TTGGTCCTTAGCCACTCCTTC-3′
mIFN-γ forward	5′-AGGCAGTATCACTCATTGT-3′
mIFN-γ reverse	5′-CAGCAGGTTATCATCATCATC-3′
mIL-18 forward	5′-GACTCTTGCGTCAACTTCAAGG-3′
mIL-18 reverse	5′-CAGGCTGTCTTTTGTCAACGA-3′
mIL-17A forward	5′-TCCAGAAGGCCCTCAGACTA-3′
mIL-17A reverse	5′-CTCGACCCTGAAAGTGAAGG-3′
mCXCL1 forward	5′-GCCTATCGCCAATGAGCTG-3′
mCXCL1 reverse	5′-TCTGAACCAAGGGAGCTTCA-3′
mCCL2 forward	5′-ATGAGATCAGAACCTACAACT-3′
mCCL2 reverse	5′-TCCTACAGAAGTGCTTGAG-3′
mClaudin-1 forward	5′-CATCAATGCCAGGTATGAATT-3′
mClaudin-1 reverse	5′-TGTTGGGTAAGAGGTTGTTT-3′
mZO-1 forward	5′-CACAAGGAGCCATTCCTGAAG-3′
mZO-1 reverse	5′-ATCACTAGGGGGCTCAGCAG-3′
mE-cadherin forward	5′-ATGGGGCACCACCATCAC-3′
mE-cadherin reverse	5′-CTGGGTACACGCTGGGAAAC-3′
mOccludin forward	5′-TTGAAAGTCCACCTCCTTACAGA-3′
mOccludin reverse	5′-CCGGATAAAAAGAGTACGCTGG-3′
mGAPDH forward	5′-TCTCCACACCTATGGTGCAA-3′
mGAPDH reverse	5′-CAAGAAACAGGGGAGCTGAG-3′

(Alex Fluor 488 and 594) were incubated at room temperature one more hour. Then, DAPI was used to stain the nuclei, and pictures were captured under a microscope (LSM760, Zeiss).

2.8. RNA Sequencing (RNA-seq). RNA extraction was finished, and its integrity and concentration were assessed. Then, the RNA library was constructed using a TruSeq RNA Sample Preparation Kit V2 (Illumina, San Diego, CA, USA). RNA-seq was performed on Illumina HiSeq 2500 machines (Illumina), followed by filtration of cleaning of the values. Then, the reads were illustrated on the Mus musculus reference genome (mm10). The fragments per kilobase of transcripts per million mapped (FPKM) values were used to calculate transcript expression levels. Differentially expressed genes (DEGs) among the different treatment groups were analyzed using CuffDiff in the Cufflinks package ($P < 0.05$ and $\log_2$foldchange > 2). Kyoto Encyclopedia of Genes and Genomes (KEGG) were figured out by the Database for Annotation, Visualization and Integrated Discovery (DAVID) v.6.8. The R software was used (http://www.r-project.org) to classify and draw the heatmap.

2.9. Western Blotting Analysis. Radio Immunoprecipitation Assay (RIPA) buffer was used with protease and phosphatase inhibitor cocktails (Roche) added to extract proteins. 10% SDS-PAGE was applied to isolate protein and then transferred onto polyvinylidene fluoride (PVDF) membranes (Millipore, USA). 5% nonfat milk was used to block the membranes. Primary antibody incubation and horseradish peroxidase-conjugated secondary antibody (1 : 3000) incubation were followed. ECL Enhanced Kit (Pierce Chemical Co., Rockford, IL, USA) was used to amplify signals, and then, the signals were captured by an ChemiDoc Touch Imaging System (BioRad, USA).

2.10. Cell Culture. MODE-K and HEK-293T cells were got from Chinese Academy of Science (Shanghai, China). Medium for MODE-K cells was Dulbecco's modified Eagle's medium/F12 (DMEM/F12, GIBCO), and for HEK-293T cells, it was DMEM. All cells were cultured with medium plus 10% FBS and 1% antibiotics.

2.11. Lentivirus Construction. Lentiviral vectors of sh-UCL and sh-NC containing an EGFP expression cassette were constructed and used to infect MODE-K cells. The lentiviral infected stable cell clones were selected using 5 μg/ml polybrene (Sigma). GFP-positive cells can be visualized using fluorescence microscope (Axio Observer Z1, Zeiss, Germany).

2.12. Cytoplasmic/Nuclear Fractionation. Cytoplasmic and Nuclear RNA Purification Kit (Norgen Biotek, Canada) was selected to fractionate cytoplasmic and nuclear. Firstly, extract MODE-K cell RNA, and then, nuclear and cytoplasmic RNA was analyzed using qRT-PCR. U6 and GAPDH were used as the controls for the two parts, respectively.

2.13. RNA-Pulldown. MODE-K cells were lysed on ice by protecting protease and RNase (Thermo Fisher Scientific) for 30 min. Then, streptavidin agarose beads were added into total lysate at 4°C lasting 4 h while being centrifuged. After adding biotin-labeled lncRNA-UCL probes or negative control (NC) probes, the same procedure was executed in them. After washing with a lysis buffer, qRT-PCR was utilized to know miR-568 enrichment.

2.14. Transfection. The miR-568 mimic or inhibitor (GenePharma, China) was inserted into MODE-K cells by Lipofectamine 3000 (Invitrogen) system. 48 h after transfection, the efficiency of transfection was determined and the transfected cells were used in further experiments.

2.15. miRNA Target Prediction. The potential target genes of miR-568 were predicted using TargetScan (http://www.targetscan.org/) and miRDB (http://mirdb.org/mirdb/).

2.16. Dual Luciferase. HEK-293 T cells were cotransfected with pmirGLO (NC, wt or mut) (RiboBio) and miR-568

mimics or NC using a Lipofectamine 3000. The firefly luciferase gene pmirGLO-control (Promega) in vector was used as internal control to detect transfection efficiency. After 48 h of transfection, firefly and Renilla luciferase values were figured out using a Dual-Luciferase Reporter System (Promega). Renilla luciferase activity was used to normalize the results.

2.17. 5-Ethynyl-2′-Deoxyuridine (EDU) Assay. After treatment, the MODE-K cells were cultured and incubated with EDU at concentration of 10 μM at 37°C lasting 3 h. First of all, fix the cells using 4% paraformaldehyde at 25°C half an hour. The cells were then washed and visualized using a Cell-Light EdU Apollo 567 In Vitro Kit (RioBio, Guangdong, China). Finally, EDU-positive cells could be visualized and captured under a confocal laser microscope (LSM760, Zeiss).

2.18. Statistical Analysis. Data were presented as mean ± SEM, and Graph Prism 7 (GraphPad Software, San Diego, CA, USA) was utilized for further analysis. Student's *t*-test or Mann-Whitney *U* test was chosen to distinguish whether there exist differences in all the groups. The aforementioned experiments were all duplicated three times. Statistical analysis was performed using the SPSS17.0 software (SPSS, Chicago, IL, USA). *P* value less than 0.05 was regarded to have a significant difference.

3. Results

3.1. IL-22 Decreases Clinical Disease Severity of DSS-Induced UC. First, an UC mouse model was induced by using 3% DSS. DSS was administered in mice for 8 days to construct the model. IL-22 or PBS was i.p. injected into mice from the 4th day of the model establishment. A significant body weight loss was recorded (Figure 1(a)). We captured the photos of colon to compare the colon morphology and colon length after DSS stimulation to know the IL-22 effect for colon inflammation. Our results showed that the colons were shortened significantly when induced using DSS compared to normal mice. While when DSS-induced mice got IL-22 administration, their colon length was much longer compared to those without treatment ($P < 0.001$; Figure 1(b)). If mice were injected with DSS, they will meet a higher death rate. However, IL-22 treating will reverse the results, meaning longer survival rate after IL-22 treatment (Figure 1(c)). As the same time, DSS induced a body weight loss. IL-22 can keep mice at weight even after DSS injection. IL-22 treatment even will lead to an increasing trend for body weight ($P < 0.001$; Figure 1(d)). It has been reported that DAI will increase after inducing using DSS [31]. It was found that IL-22 treatment can reverse the DAI result, indicating without rectal bleeding and kept in normal stool harness (Figure 1(e)).

3.2. IL-22 Suppressed Proinflammatory Cytokine Production in DSS-Induced UC Mice. Whether IL-22 could affect the proinflammatory activities in DSS-induced UC mice is still unknown, qPCR and ELISA were carried out. In the DSS-induced UC group, the gene expression levels of major proinflammatory cytokines, including *TNF-α*, *IL-1β*, *IL-6*, interferon-gamma (*IFN-γ*), IL-18, *IL-17A*, CXCL1, and CCL2, were elevated, compared with control group mice, while this phenomena was changed if treated with IL-22 (Figure 2(a)). In addition, the results of TNF-α, IL-1β, IL-6, and IL-17A detected by ELISA increased significantly when induced by DSS, while IL-22 treatment could reduce the cytokine levels that for proinflammation (Figure 2(b)). Taken together, we demonstrated that IL-22 could secrete proinflammatory cytokines and gene expression. UC induced by DSS could be treated by IL-22 via stop proinflammation.

3.3. IL-22 Ameliorated Intestinal Barrier Integrity. It is known that impairment and interruption of epithelial integrity are characteristics of colitis [32]. It has also been reported that DSS could induce severe impairment of mouse colon morphology, while IL-22 treatment significantly enhanced the histological changes induced by DSS. The representative images are shown in Figure 3(a), which showed the beneficial effects of IL-22 treatment. Since TJ and adhesion junction (AJ) proteins play crucial roles in maintenance of intestinal balance and epithelial barrier function, IF and qRT-PCR analyses were carried out to determine the TJ and AJ molecule expression level after IL-22 treatment. As it is shown in Figure 3(b), the expression levels of claudin-1 and STAT3 protein reduced greatly in the DSS-induced colitis group, while IL-22 treatment was able to reverse this effect (Figure 3(b)). Next, TJ protein and E-cadherin levels were examined, as they are also essential for the regulation of epithelial integrity. We found that claudin-1, ZO-1, E-cadherin, and occludin-1 gene expression levels were all significantly downregulated by DSS, whereas treatment with IL-22 reversed this effect, leading to an increased expression of claudin-1, ZO-1, and E-cadherin (Figures 3(c)–3(f)).

As we all known from the previous research, IEC apoptosis or cell death induced by DSS contributed to disruption of intestinal integrity [30, 33]. The cleaved caspase-3 and PCNA results in IHC analysis showed that DSS induced the apoptosis and suppressed the proliferation of intestinal epithelial cells. However, treatment with IL-22 downregulated the cleaved caspase-3 level while upregulated PCNA expression (Figures 3(g)–3(i)). Western blotting analysis results also showed that E-cadherin and occludin-1 protein expressed less after DSS induction, while treatment with IL-22 reversed this effect, which is similar with the previous experiment presented results (Figure 3(j)). Taken together, we further demonstrate IL-22 can alleviate DSS-induced damage by protecting damaged colon tissue by upregulating intestinal barrier-related molecule expression.

3.4. IL-22 Induced a Transcriptome Turnaround UC Mouse Colon. Numerous studies have shown that lncRNA is highly relevant with the onset of many diseases, including inflammation [34, 35]. To have a good command of knowledge of regulatory mechanism of IL-22 in DSS-induced UC mice, RNA-seq was performed to screen the differential lncRNA expression profiles in the mouse colon tissues obtained from the three groups of mice. Thousands of lncRNAs showed different expression analyzed by hierarchical clustering. We set the thresholds of $\log_2$foldchange > 2.0, P value < 0.05,

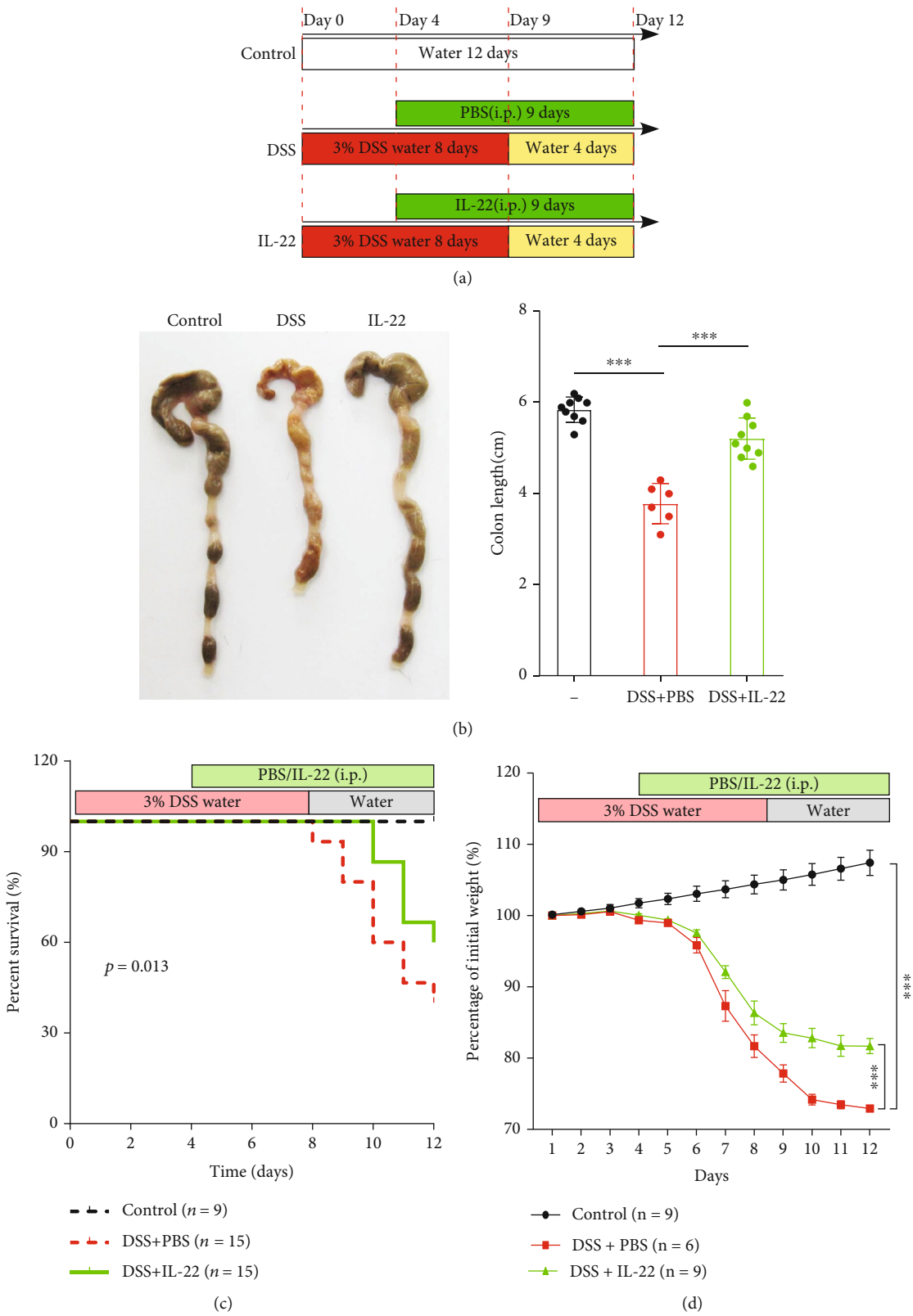

Figure 1: Continued.

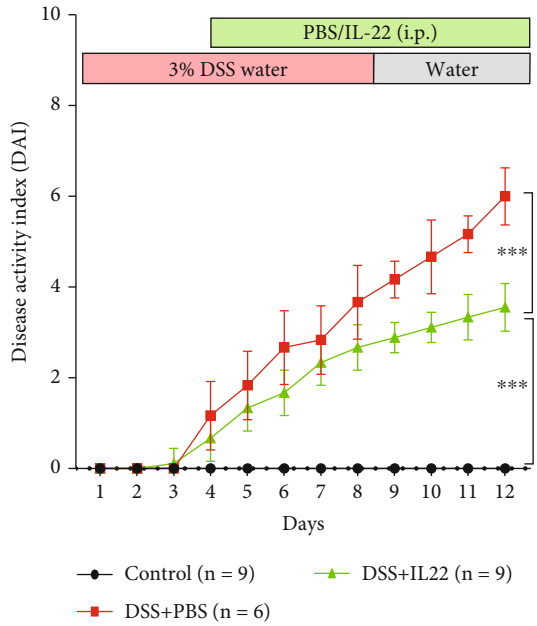

(e)

Figure 1: IL-22 ameliorates clinical symptoms in DSS-induced colitis mice. The mice used in our study were divided into three groups: control, DSS+PBS and DSS+IL-22. (a) The schematic diagram demonstrates the experimental mouse design. (b) Representative images show the differences in colon length among groups. (c) The Kaplan-Meier survival analysis shows the survival time span. (d) Change in body weight presented as percentages. (e) Disease activity index (DAI) was determined by assessing the change in body weight, bleeding, and stool. Data are presented as mean ± SEM. $^{***}P < 0.001$, using one-way ANOVA with *post hoc* analysis and *t*-test.

and P ADJ < 0.05. According to the results, 62 lncRNAs were elevated and 128 lncRNAs were denticulated in DSS group mice compared to controls. Meanwhile, we found 22 lncRNA upregulation and 30 lncRNA deregulation when comparing DSS groups with or without IL-22 treatment, which is shown on a heatmap (Figure 4(a)). KEGG pathway analysis was conducted to predict the signaling pathway that the differentially expressed genes were possible involved in (Figure 4(b)). The results showed that 5 lncRNAs were significantly downregulated in the DSS+PBS group mouse colon tissues comparing with those in control group mice but remarkably had recovered in DSS+IL-22 groups. Therefore, these 5 lncRNAs were chosen for further validation using mouse colon tissue obtained from the three group mice using qRT-PCR. We found that the expression of lncRNA NONMMUG038140 was almost the same with RNA-seq results. As a consequence, we named lncRNA NONMMUG038140 as Ulcerative Colitis lncRNA (lncRNA-UCL) and conducted further research on it in our study (Figure 4(c)).

3.5. lncRNA-UCL Located in the Cytoplasm and Interacts with mmu-miR-568. To learn more about the function and role of lncRNA-UCL in the regulation of DSS-induced colitis, the lentiviral vector containing its interfering sequence was constructed and its inhibitory efficiency was determined using qRT-PCR. As shown in Figure 5(a), the lentivirus could remarkably silence lncRNA-UCL expression, compared with lentiviral NC. It has been well established that lncRNAs regulate expression of genes through competitive endogenous RNA that is dependent on its location [36, 37]. Therefore, the subcellular location of lncRNA-UCL was determined using a cytoplasmic/nuclear isolation kit and analyzed using qRT-PCR. The results show that most lncRNA-UCL is localized in the cytoplasm while was in nucleus (Figure 5(b)). Next, microRNAs (miRNAs) that may potentially bind to lncRNA-UCL were predicted using bioinformatics tools (Figure 5(c)) and validated using qRT-PCR. As shown in Figure 5(d), lncRNA-UCL expression was inhibited by transfecting the lentivirus into MODE-K cells, and miR-568 was found to be significantly upregulated ($P < 0.01$). To further confirm the interaction between lncRNA-UCL and miR-568, the results of the RNA-pulldown assays confirmed that lncRNA-UCL could directly bind to miR-568 in MODE-K cells (Figure 5(e)). Next, miR-568 expression was examined in mouse colon tissues obtained from the three groups. The results showed that miR-568 was upregulated during DSS induction, while its levels decreased after IL-22 treatment (Figure 5(f)), suggesting lncRNA-UCL and miR-568 were negative correlated.

3.6. Identification of the Target Gene of miR-568. To determine potential target genes of miR-568, two online databases (TargetScan and miRDB) were searched, and it was found that claudin-1 may be the gene targeting ability for miR-568 (Figure 6(a)). To verify the hypothesis, miR-568 mimics and inhibitors were synthesized and transfected into MODE-K cells. Western blotting analysis results showed that the miR-568 mimics downregulated claudin-1 protein expression, whereas the miR-568 inhibitor upregulated

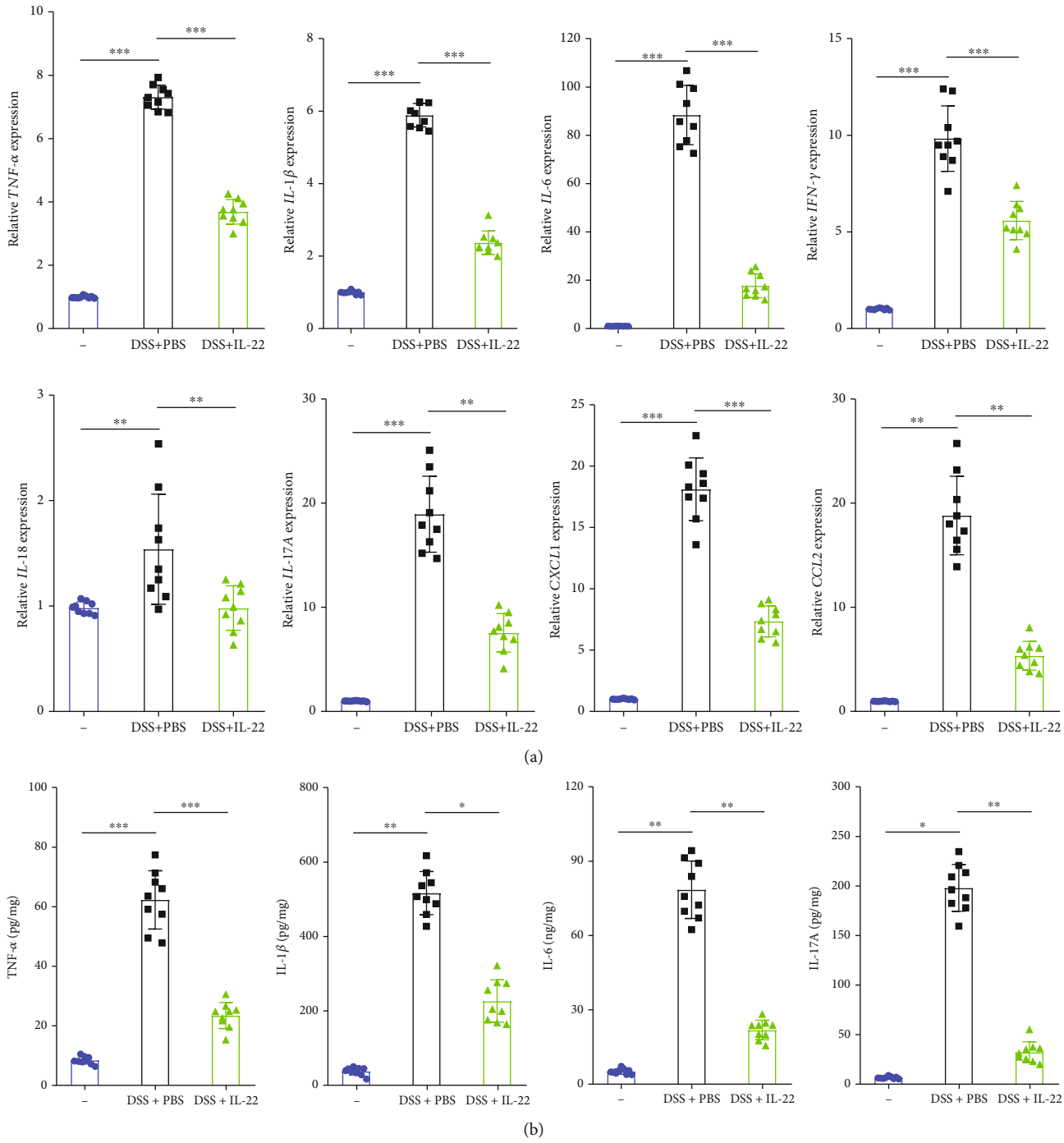

Figure 2: IL-22 inhibited the expression of proinflammatory cytokines in DSS-induced colitis mice colons. qRT-PCR was performed to determine proinflammatory cytokine mRNA expression levels (TNF-α, IL-6, IL-1β, IFN-γ, IL-18, IL-17A, CXCL1, and CCL2) in colon tissue. (b) ELISA assay was used to detect levels of soluble TNF-α, IL-6, IL-1β, and IL-17 in the medium of the colon tissues. Data are presented as mean ± SEM. $^{***}P < 0.001$; $^{**}P < 0.01$; $^{*}P < 0.05$ using Student's t-test.

claudin-1 protein expression, compared with miRNA-NC (Figure 6(b)). Then, targeting ability of claudin-1 for miR-568 was double confirmed using dual-luciferase assays. The results exhibited that miR-568 could suppress the fluorescence intensity of cells transfected with wild-type 3′-UTR of claudin-1 plasmids, compared with mutant 3′-UTR of claudin-1 plasmids (Figure 6(c)). We also detected changes in claudin-1 gene and protein expression situation in mouse colon tissues among the three groups using qRT-PCR, western blotting, and IHC analyses. The results showed that claudin-1 gene and protein expression significantly downregulated by DSS, and all the results exhibited the same

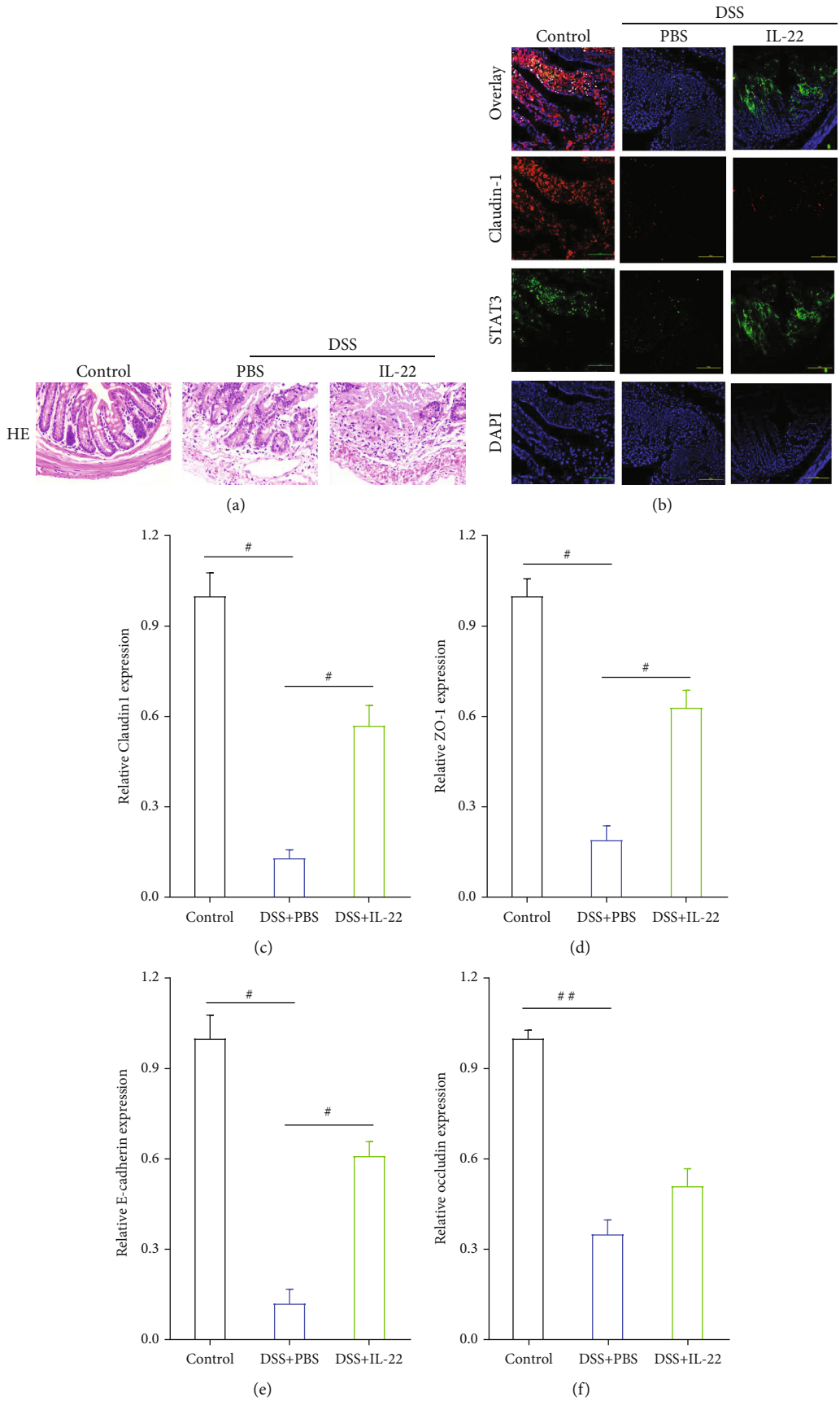

Figure 3: Continued.

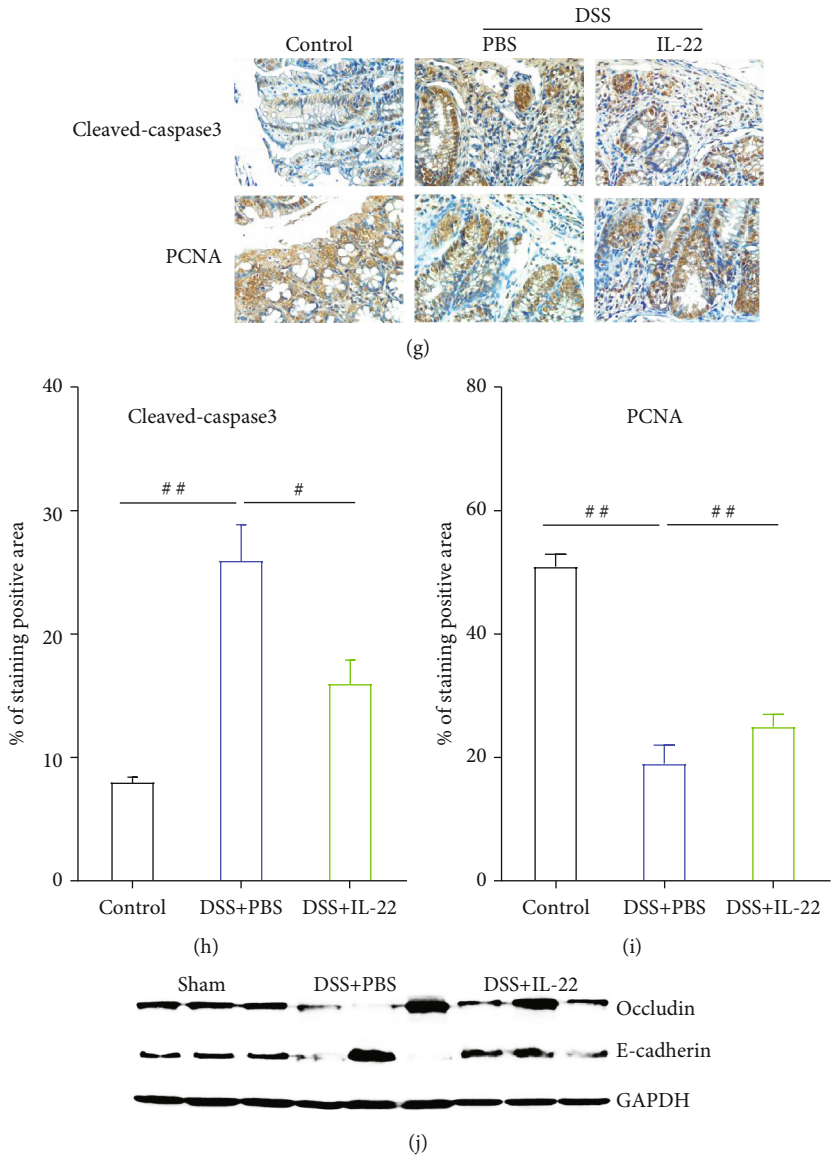

Figure 3: IL-22 enhances the expression of intestinal epithelial apical junction proteins. (a) HE staining demonstrated pathological changes of the colon tissue. (b) Immunofluorescent staining results compared changes in the expression levels of tight junction (claudin-1) and STAT3 proteins in colon tissues obtained from the control, DSS+PBS, and DSS+IL-22 groups of mice. (c–f) qRT-PCR was conducted to determine the expression of apical junction markers (E-cadherin, claudin-1, ZO-1, and occludin-1) at gene level in colon tissue. (g–i) Immunohistochemistry analysis examined the protein expression levels of intestinal apoptosis marker (cleaved caspase-3) and proliferation marker (PCNA). (j) Western blotting analysis was conducted to detect the expression levels of apical junction proteins (E-cadherin and occludin-1) in colon tissue. Data are presented as mean ± SEM. $^{\#\#}P < 0.01$; $^{\#}P < 0.05$ using Student's t-test.

trend [38]. However, IL-22 treatment significantly alleviated and reversed this effect both on claudin-1 mRNA and protein expression (Figures 6(d)–6(f)).

3.7. Upregulation of lncRNA-UCL Induced by IL-22 Sequestered miR-568 by Enhancing Claudin-1 Expression. To learn more about the function and role of IL-22 and lncRNA-UCL in IECs, qRT-PCR was performed on MODE-K cells and the results showed that IL-22 could enhance lncRNA-UCL expression obviously. Meanwhile, knockdown of lncRNA-UCL expression could enhance pro-inflammatory cytokine expression, including TNF-α, IL-1β, and IL-6 at mRNA level. However, this effect was significantly inhibited by IL-22 (Figure 7(a)). The expression levels of intestinal epithelial marker proteins under the effect of IL-22 treatment were also explored. The results of western blotting and EDU analyses show that the knockdown of lncRNA-UCL downregulated the expression of claudin-1, ZO-1, E-cadherin, and phosphorylated STAT3 protein and inhibited MODE-K cell proliferation, while IL-22 produced an opposite effect: upregulation of claudin-1, ZO-1, E-cadherin, and phosphorylated STAT3 protein and increased proliferation of MODE-K cells (Figures 7(b) and 7(c)). To elucidate the role of miR-568 on the intestinal epithelial

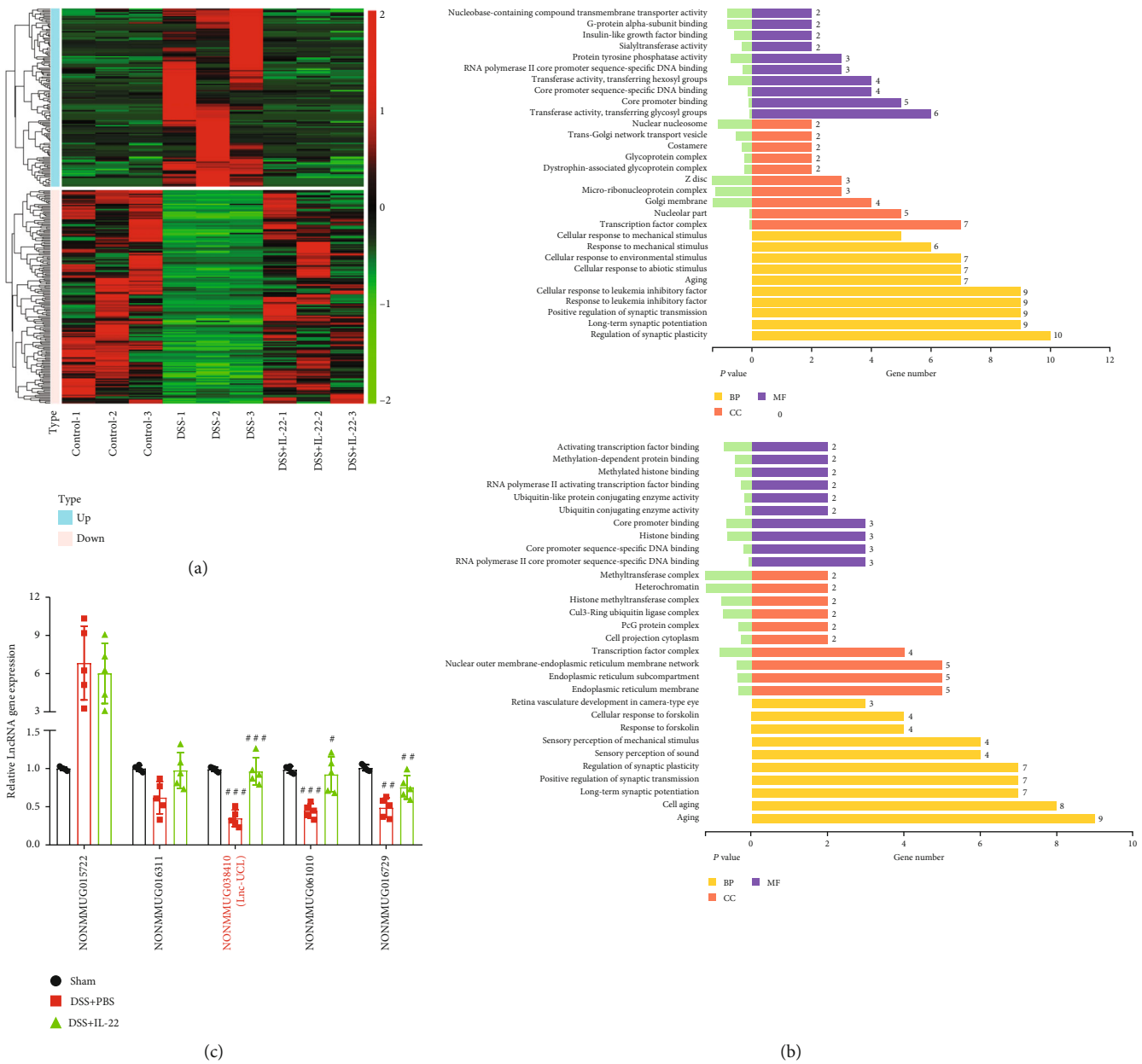

Figure 4: RNA sequencing was used to screen the differentially expressed lncRNAs in DSS-induced colitis mouse colon tissue. (a) Heatmap showing the differentially expressed lncRNAs between the colon tissues of the control, DSS+PBS, and DSS+IL-22 groups of mice. Red color is used to show the upregulated genes, and green color is used to show the downregulated genes. (b) KEGG pathway analysis showed the possible signaling pathway that may be involved in the differentially expressed lncRNA regulatory network. (c) qRT-PCR was performed to validate the identity of the top 5 lncRNAs, which were most differentially expressed in colon tissues between all groups of mice. lncRNA NONMMUG038140 (lncRNA-UCL) was selected as the target and to be used in further studies. Data are presented as mean ± SEM. $^{###}P < 0.001$; $^{##}P < 0.01$; $^{#}P < 0.05$ using Student's t-test.

integrity, miR-568 mimics were used and the results showed that miR-568 significantly suppressed the expression of claudin-1, ZO-1, E-cadherin, and phosphorylated STAT3 protein and inhibited MODE-K cell proliferation, compared to the mimics-NC (Figures 7(d) and 7(e)). Furthermore, our results also showed that the inhibition of miR-568 expression could upregulate the expression of claudin-1, ZO-1, E-cadherin, and phosphorylated STAT3 protein and promote MODE-K cell proliferation. However, the knockdown of lncRNA-UCL could simultaneously inhibit miR-568 expression and can partially release the inhibitory effect induced by the silencing of lncRNA-UCL, including recovery of the claudin-1, ZO-1, E-cadherin, and phosphorylated STAT3 protein expression and MODE-K cell proliferation

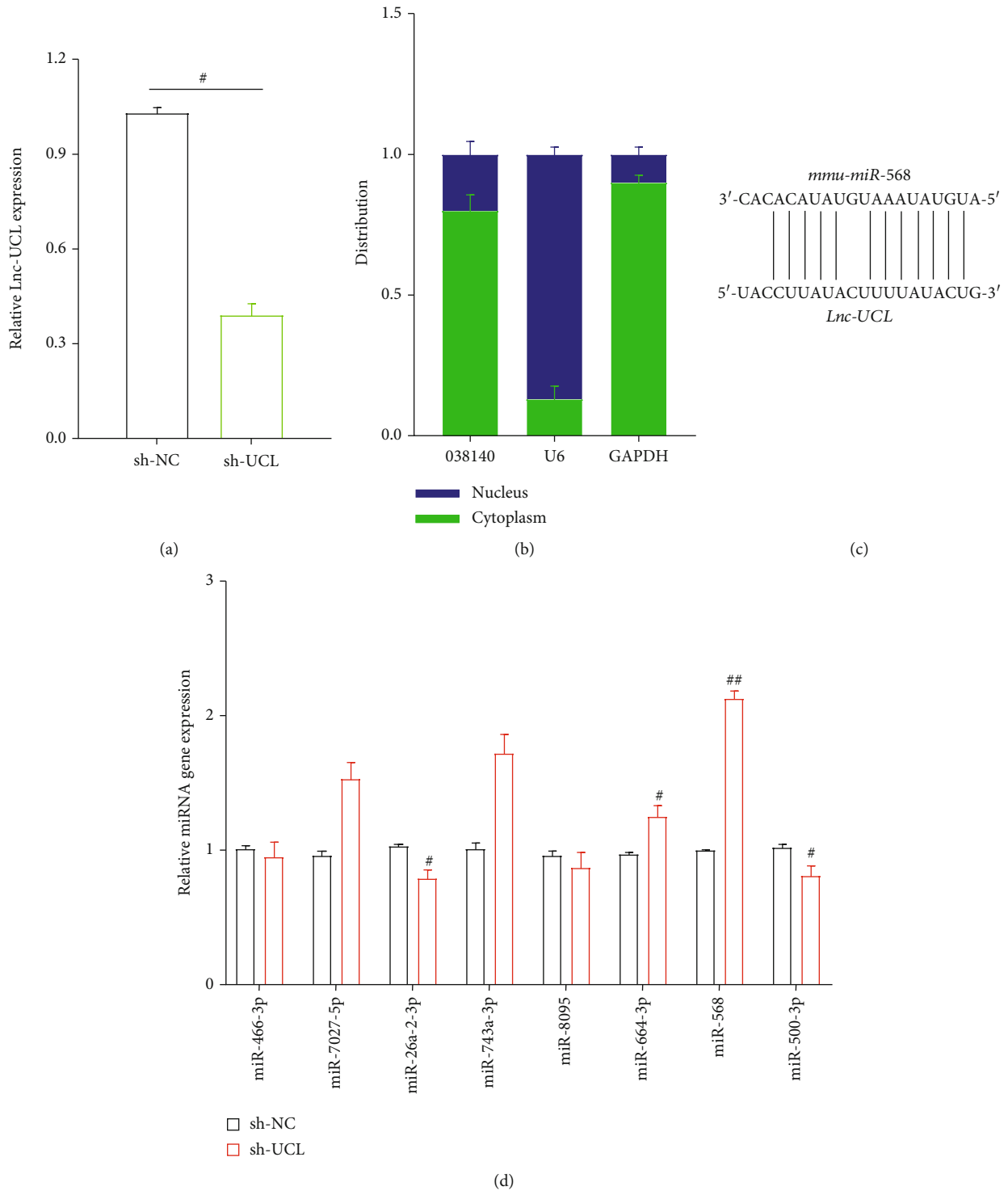

Figure 5: Continued.

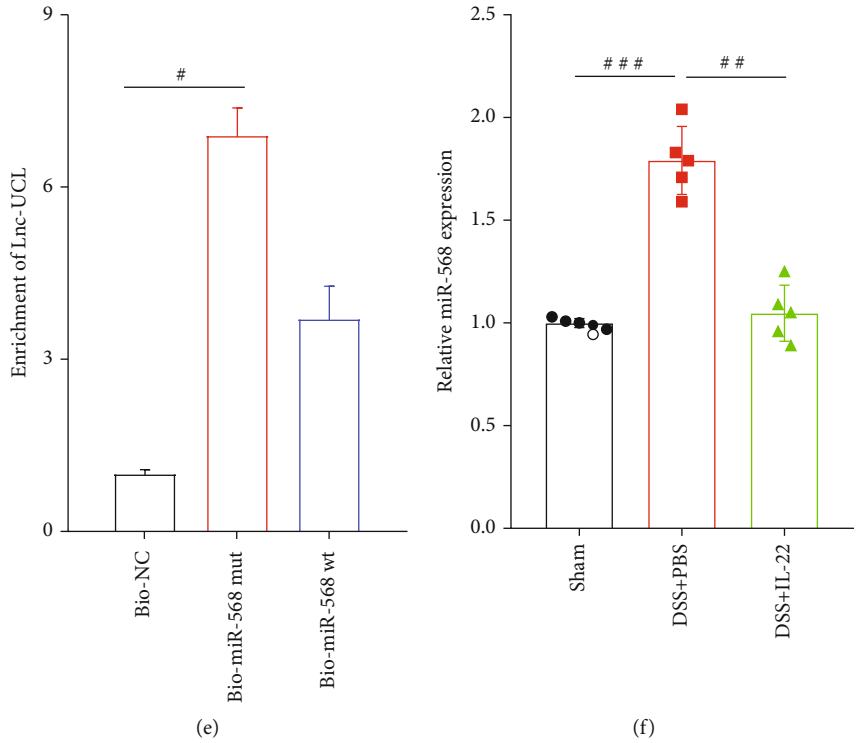

Figure 5: lncRNA-UCL is predominantly located in the cytoplasm and binds to miR-568 in intestinal epithelial cells. (a) The interfering sequence that could specifically target lncRNA-UCL was inserted into the vector, and the lentivirus was constructed to detect interfering efficiency. (b) qRT-PCR analysis of lncRNA-UCL expression in the nuclear and cytosolic components of MODE-K cells. (c) Sequence alignment showing the binding sites between miR-568 and lncRNA-UCL. (d) After the silencing of lncRNA-UCL expression, qRT-PCR analyzed the changes in miRNA expression, to identify miRNAs that may bind to lncRNA-UCL in MODE-K cells. (e) RNA-pulldown assay was conducted to detect interactions between miR-568 and lncRNA-UCL. (f) qRT-PCR was performed to measure miR-568 expression in colon tissues among all groups of mice. Data are presented as mean ± SEM. $^{###}P < 0.001$; $^{##}P < 0.01$; $^{#}P < 0.05$ using Student's t-test.

(Figures 7(f) and 7(g)). Taken together, our results indicate that lncRNA-UCL regulates IEC homeostasis via sequestering miR-568 through the targeting of claudin-1.

4. Discussion

Intestinal homeostasis is maintained by both the intestinal epithelial barrier and the mucosal immune system [39]. The intestinal epithelial barrier is a footstone in intestinal homeostasis by providing a physical barrier to defend against bacteria and pathogens, while maintaining appropriate immune responses [40]. Dysfunction of the epithelial barrier may trigger an excessive inflammatory response, resulting in abnormal elevation of proinflammatory cytokine levels, especially IL-1β, TNF-α, and IL-6, caused by intestinal epithelial injury and impaired epithelial regeneration and repair. Maintenance of epithelial integrity is dependent on the apical junction complex (AJC), which includes the expression of TJ and AJ protein expression, which form a functional and physical barrier to prevent antigenic penetration [29]. Previous studies have reported that the disruption of epithelial cell barrier integrity is a result of the decrease in TJ protein expression, including claudin-1, ZO-1, and occluding-1, is a common characteristic of patients with UC and other IBDs [38]. Thus, repair of injured epithelial barrier and reversal of unanticipated inflammation are effective strategies for UC treatment.

Previous studies have demonstrated that IL-22 is involved in immune diseases, such as psoriasis, systemic erythema, hepatitis and rheumatoid arthritis, and colitis [14, 21]. IL-22 was able to upregulate tight junction protein claudin-2 expression to promote pathogen clearance in an infectious enterocolitis mouse model [41]. Similarly, the knockdown of IL-22 resulted in aggravation of IEC injury in a *Citrobacter rodentium* infection mouse model [42]. Meanwhile, it has been suggested that IL-22 exhibited protective ability in regulation of gut inflammation by stimulating colon epithelial cell lines to produce IL-10 and SOCS3 to ameliorate DSS-induced colitis via upregulating claudin-2 expression [43].

It has been reported that bioactive compounds for colitis treatment have many advantages including reducing weight loss, exerting anti-inflammatory reaction, and colon histological damage. For example, it has been reported that thymoquinone, a bioactive compound from Dietary, had profound anti-inflammatory effects to colitis as it could stimulate the expression of the epithelial transcription factor PPAR-γ. Study had also shown that the bioactive compounds from Pale Ale Beer Powder attenuate experimental colitis in mice. Therefore, bioactive compounds for colitis

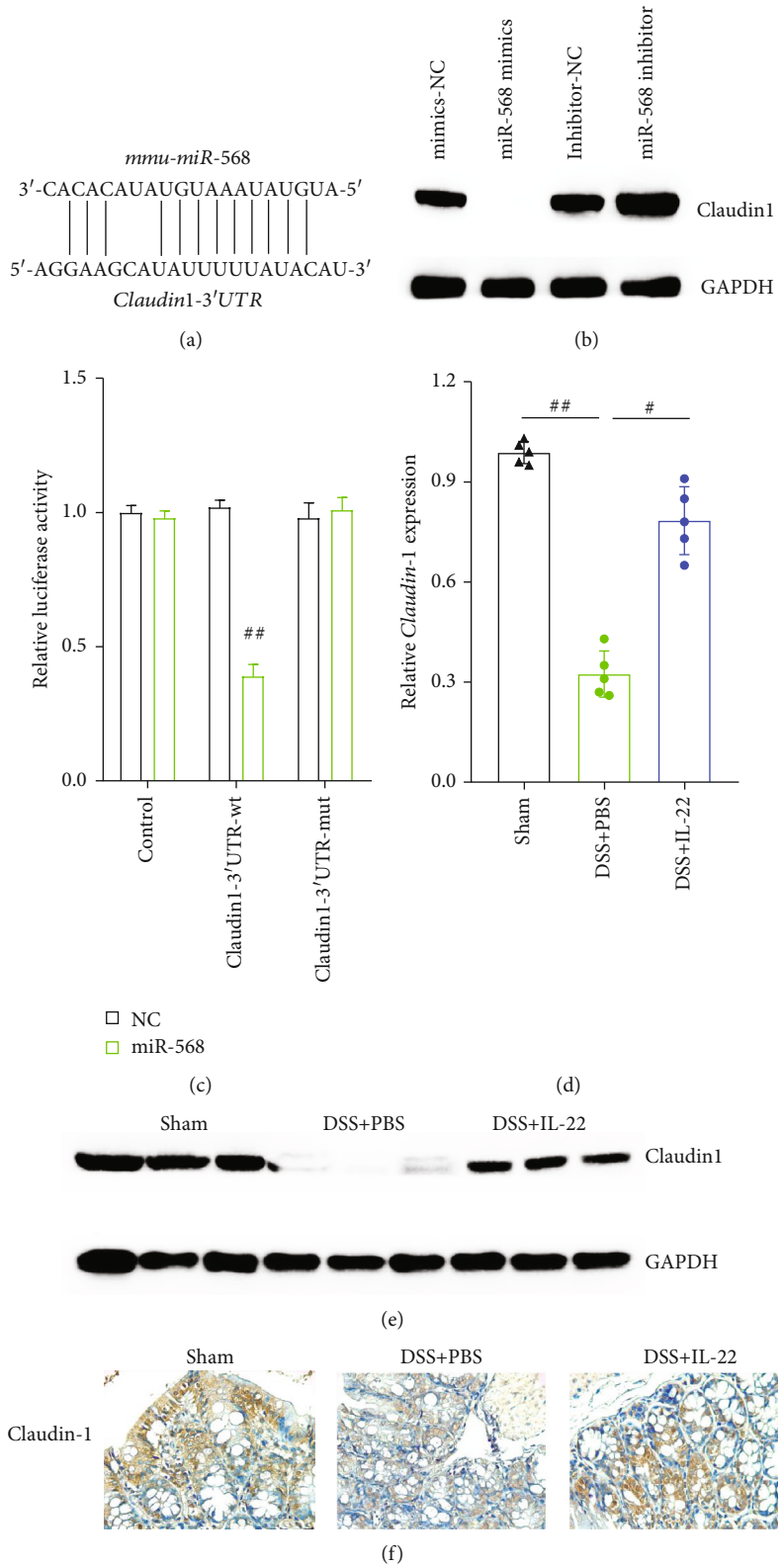

Figure 6: Claudin-1 is the direct target of miR-568 in intestinal epithelial cells. Sequence alignment showing the binding sites between miR-568 and the 3′-UTR of claudin-1 mRNA. (b) Western blot analysis was used to detect changes in claudin-1 protein expression under the effect of miR-568 mimics and inhibitor in MODE-K cells. (c) Luciferase assay of HEK-293T cells cotransfected with miR-568 mimics and wild-type or mutant 3′-UTR of the claudin-1 mRNA sequence. (d–f) qRT-PCR, western blotting, and immunohistochemistry analyses were conducted to determine claudin-1 expression levels in the colon tissues of all groups of mice. Data are presented as mean ± SEM. $^{##}P < 0.01$; $^{#}P < 0.05$ using Student's t-test.

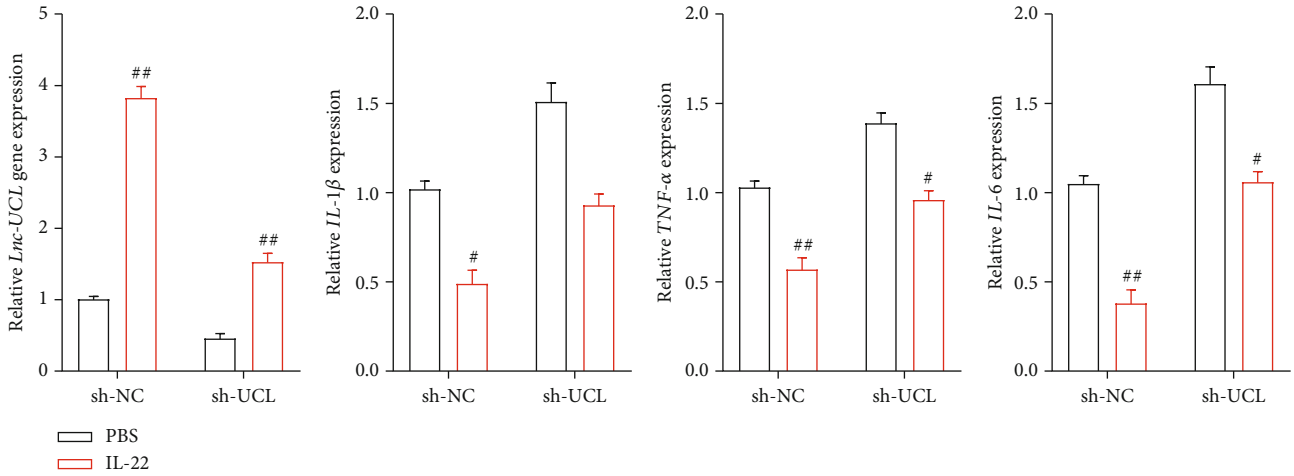

(a)

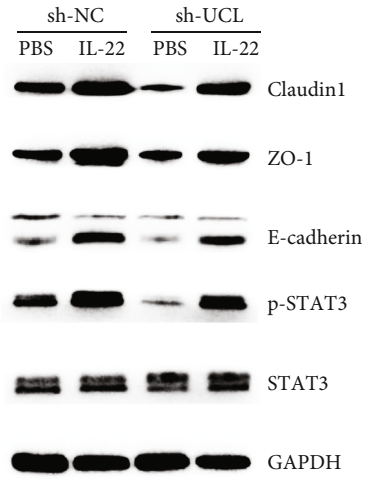

(b)

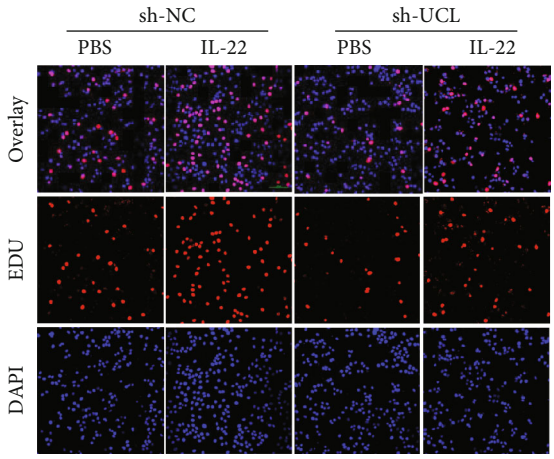

(c)

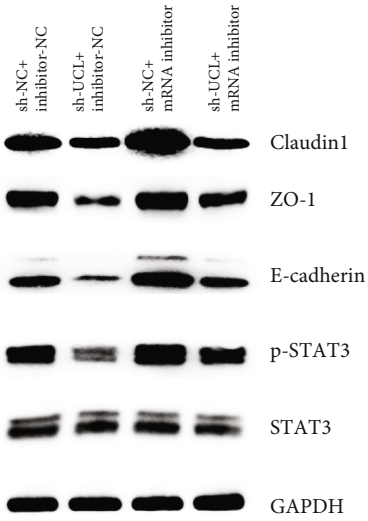

(d)

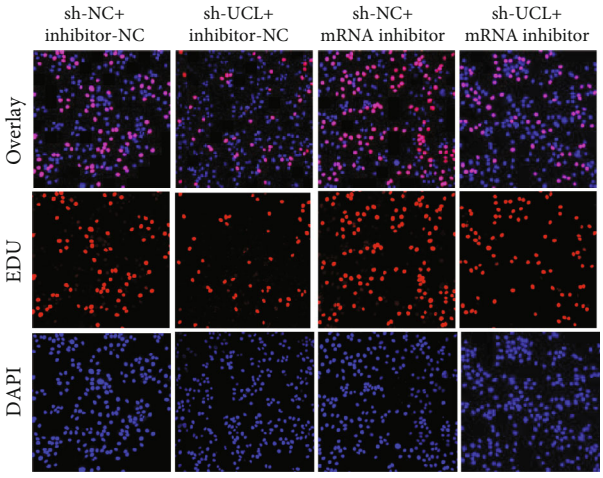

(e)

Figure 7: Continued.

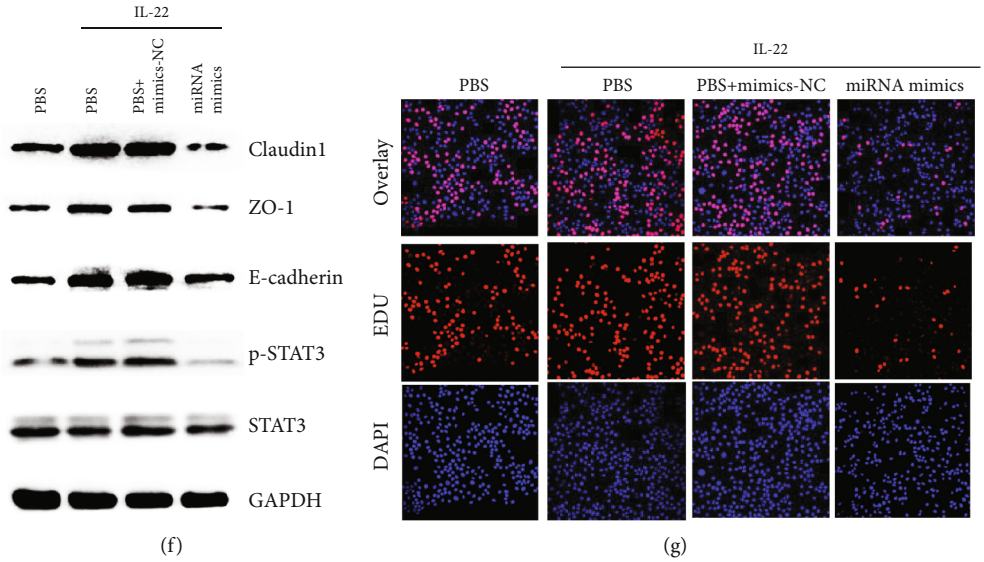

Figure 7: Elevation of lncRNA-UCL sequestered by miR-568 enhanced claudin-1 expression to maintain intestinal epithelial integrity induced by IL-22. (a) qRT-PCR was performed to determine the change in the expression of lncRNA-UCL and proinflammatory cytokines (TNF-α, IL-6, and IL-1β) at gene level after the knockdown of lncRNA-UCL and after IL-22 treatment in MODE-K cells. (b) In MODE-K cells, after the silencing of lncRNA-UCL expression and IL-22 treatment, changes in the expression of claudin-1, ZO-1, E-cadherin, and phosphorylated STAT3 protein were shown using western blotting analysis (c) while EDU assay was used to measure proliferation. (d) In MODE-K cells transfected with miR-568 mimics and treated with IL-22, western blot analysis was used to demonstrate changes in claudin-1, ZO-1, E-cadherin and phosphorylated STAT3 protein expression. (e) EDU assay was used to measure levels of proliferation. (f) In MODE-K cells, knockdown of lncRNA-UCL or interfering of miR-568 or simultaneously silencing both of lncRNA-UCL and miR-568, western blot analysis was used to show expression level changes of claudin-1, ZO-1, E-cadherin, and phosphorylated STAT3 protein. (g) EDU assay was used to measure proliferation. Data are presented as mean ± SEM. $^{###}P < 0.001$; $^{##}P < 0.01$; $^{#}P < 0.05$ using Student's t-test.

treatment have great application potential and broad application space. Here we investigated the function and role of bioactive compound, IL-22, in a DSS-induced UC mouse model. We aimed to identify its underlying potential mechanism of action in intestinal epithelial barrier regulation. RNA-seq and bioinformatics analysis were used to validate lncRNA-UCL as potential novel target molecule, which was significantly downregulated in DSS-induced mice and upregulated in IL-22-treated mice. *In vitro* experiments exhibited that that silencing of lncRNA-UCL blocked IEC proliferation, suppressed TJ protein expression (claudin-1, occludin-1, ZO-1, and E-cadherin) and enhanced proinflammatory cytokines (TNF-α, IL-1β, and IL-6) expression. Previous studies have demonstrated that IL-22 can enhance epithelial growth, tissue regeneration, mucosal defense, and elimination of inflammation by activation of the STAT3 [17, 44]. In our study, we found that the phosphorylation level of STAT3 was decreased by DSS. However, IL-22 treatment could somehow rescue activated STAT3. Meanwhile, knockdown of lncRNA-UCL expression was also able to downregulate the phosphorylation of STAT3 *in vitro*. In terms of a molecular mechanism, we proposed that lncRNA-UCL regulated the epithelial integrity by regulating the expression of TJ proteins via interacting with miR-568, as lncRNA-UCL is predominantly located in the cytoplasmic, which was shown using subcellular fraction assays. Our results verified that DSS caused the upregulation of miR-568 in colitis mice, while treatment with IL-22 attenuated the increase in miR-568 expression. Furthermore, we further confirmed that miR-568 regulated TJ protein expression by directly targeting the 3′-UTR of claudin-1 mRNA. Thus, we can conclude that IL-22 induced lncRNA-UCL upregulation to maintain the claudin-1 mRNA levels by sequestering miR-568, leading to raising intestinal TJ protein expression levels.

Recently, many studies have shown that lncRNAs are incorporated in pre- and posttranscriptional regulation of gene expression. However, very few lncRNAs have been investigated to have a relationship in the regulation of UC or IBD development and progression. DQ786243 was the first reported CD-associated lncRNA, which may cause CD patients' peripheral blood mononuclear cell upregulation [45]. Elevated expression of H19 in inflamed tissues promoted IEC proliferation, regeneration, and mucosal healing by inhibiting p53 protein, miR-34a, and let-7 gene expression in mice and human patients [27]. Another investigation conducted on mice, human tissue, and a primary organoid model found that H19 suppressed Paneth and goblet cell function and stopped autophagy, resulting in intestinal pathologies [46]. MALAT1 kept intestinal balance by sequestering miR-146b-5p that targeted the AJC proteins, CLDN11, and NUMB [29]. lncRNA-NAIL regulated colitis initiation and progression via sequestering and inactivating Wip1, thereby enhancing NF-κB and p38 activity, which led to inflammation. Additionally, NAIL could be a probable target biomarker for IBD treatment [47].

At present, various kinds of lncRNAs have been discovered and identified through sequencing, and some of them have been confirmed to have the ability of gene expression regulation. In this study, we identified the novel lncRNA-UCL, which was downregulated in DSS-treated mouse colon tissues. However, its expression was elevated by IL-22 treatment. It has been well established that lncRNAs can regulate gene expression through a ceRNA-related mechanism that is located in the cytoplasm. Our data showed that lncRNA-UCL was mainly expressed in cytoplasm of IECs. Subsequently, a RNA pulldown assay was used to verify that lncRNA-UCL could bind to miR-568 in intestinal epithelial cells. Our results confirmed that lncRNA-UCL regulated intestinal epithelial cell apoptosis and proliferation via sequestering miR-568, thereby upregulating the target protein, claudin-1, and other AJC proteins, including occludin-1, ZO-1, and E-cadherin. However, we failed to identify the homolog of lncRNA-UCL in the human genome, which limits the clinical value of our study to some extent. Moreover, miR-568 has rarely been studied. It was found that human miR-568 targets AKT3/mTORC to regulate hepatocellular carcinoma stemness and response to chemotherapy [48]. It was also found that human miR-568 regulated acute respiratory distress syndrome and ventilator-induced lung injury inflammatory syndromes via targeting pre-B-cell colony-enhancing factor PBEF/NAMPT, implying potential clinical application value [49].

5. Conclusion

We have demonstrated the incredible role of bioactive compound, such as IL-22, in alleviating DSS-induced colitis symptoms via enhancing lncRNA-UCL expression. It can be regulated using TJ protein, and the lncRNA/miR-568/claudin-1 axis is important for intestinal epithelial cell normal growth.

Data Availability

Data in this study are available from the corresponding author if anyone has reasonable request.

Ethical Approval

This study was conducted in accordance with Declaration of Helsinki principles, and all experiments performed on animals were approved by the Medical Ethics Committee of Shenzhen People's Hospital, Shenzhen, China.

Conflicts of Interest

The authors declare that they have no conflicts of interest.

Authors' Contributions

Jun Yao conceived the study and revised the manuscript. Chonghua He and Zehan Chen performed the experiments and analyzed the data. Chonghua He wrote the manuscript. Jialan Huang and Riyun performed the animal experiments and analyzed the data. Jianyao Wang and Lisheng Wang revised the manuscript. Defeng Li performed the sequencing data analysis. All authors read and approved the final version. Chonghua He and Zehan Chen contributed equally to this work.

Acknowledgments

This study was supported by the National Natural Science Foundation of China (No. 81800489) and Technical Research and Development Project of Shenzhen (No. JCYJ2021 0324113215040). We are grateful to the collaboration of all fellows at Department of Gastroenterology, Shenzhen People's Hospital, Jinan University.

References

[1] S. C. Ng, H. Y. Shi, N. Hamidi et al., "Worldwide incidence and prevalence of inflammatory bowel disease in the 21st century: a systematic review of population-based studies," *Lancet*, vol. 390, no. 10114, pp. 2769–2778, 2017.

[2] G. R. D'Haens and S. van Deventer, "25 years of anti-TNF treatment for inflammatory bowel disease: lessons from the past and a look to the future," *Gut*, vol. 70, no. 7, pp. 1396–1405, 2021.

[3] B. Shen, G. S. Kochhar, U. Navaneethan et al., "Endoscopic evaluation of surgically altered bowel in inflammatory bowel disease: a consensus guideline from the Global Interventional Inflammatory Bowel Disease Group," *The Lancet Gastroenterology & Hepatology*, vol. 6, no. 6, pp. 482–497, 2021.

[4] E. E. Nyström, B. Martinez-Abad, L. Arike et al., "An intercrypt subpopulation of goblet cells is essential for colonic mucus barrier function," *Science*, vol. 372, no. 6539, article eabb1590, 2021.

[5] A. Kurilshikov, C. Medina-Gomez, R. Bacigalupe et al., "Large-scale association analyses identify host factors influencing human gut microbiome composition," *Nature Genetics*, vol. 53, no. 2, pp. 156–165, 2021.

[6] D. Corridoni, A. Antanaviciute, T. Gupta et al., "Single-cell atlas of colonic CD8(+) T cells in ulcerative colitis," *Nature Medicine*, vol. 26, no. 9, pp. 1480–1490, 2020.

[7] H. S. De Souza, C. Fiocchi, and D. Iliopoulos, "The IBD interactome: an integrated view of aetiology, pathogenesis and therapy," *Nature Reviews Gastroenterology & Hepatology*, vol. 14, no. 12, pp. 739–749, 2017.

[8] A. N. Ananthakrishnan, G. G. Kaplan, and S. C. Ng, "Changing global epidemiology of inflammatory bowel diseases: sustaining health care delivery into the 21st century," *Clinical Gastroenterology and Hepatology*, vol. 18, no. 6, pp. 1252–1260, 2020.

[9] S. W. Syversen, G. L. Goll, K. K. Jørgensen et al., "Effect of therapeutic drug monitoring vs standard therapy during infliximab induction on disease remission in patients with chronic immune-mediated inflammatory diseases: a randomized clinical trial," *JAMA*, vol. 325, no. 17, pp. 1744–1754, 2021.

[10] A. Salas, C. Hernandez-Rocha, M. Duijvestein et al., "JAK-STAT pathway targeting for the treatment of inflammatory bowel disease," *Nature Reviews Gastroenterology & Hepatology*, vol. 17, no. 6, pp. 323–337, 2020.

[11] X. Tong, Y. Zheng, Y. Li, Y. Xiong, and D. Chen, "Soluble ligands as drug targets for treatment of inflammatory bowel

disease," *Pharmacology & Therapeutics*, vol. 226, article 107859, 2021.

[12] M. R. Spalinger, A. Sayoc-Becerra, C. Ordookhanian et al., "The JAK inhibitor tofacitinib rescues intestinal barrier defects caused by disrupted epithelial-macrophage interactions," *Journal of Crohn's and Colitis*, vol. 15, no. 3, pp. 471–484, 2021.

[13] B. Bernshtein, C. Curato, M. Ioannou et al., "IL-23-producing IL-10Ralpha-deficient gut macrophages elicit an IL-22-driven proinflammatory epithelial cell response," *Science Immunology*, vol. 4, no. 36, article eaau6571, 2019.

[14] J. A. Dudakov, A. M. Hanash, and M. R. van den Brink, "Interleukin-22: immunobiology and pathology," *Annual Review of Immunology*, vol. 33, pp. 747–785, 2015.

[15] W. Ouyang, S. Rutz, N. K. Crellin, P. A. Valdez, and S. G. Hymowitz, "Regulation and functions of the IL-10 family of cytokines in inflammation and disease," *Annual Review of Immunology*, vol. 29, pp. 71–109, 2011.

[16] Q. Hou, L. Ye, H. Liu et al., "Lactobacillus accelerates ISCs regeneration to protect the integrity of intestinal mucosa through activation of STAT3 signaling pathway induced by LPLs secretion of IL-22," *Cell Death & Differentiation*, vol. 25, no. 9, pp. 1657–1670, 2018.

[17] G. Pickert, C. Neufert, M. Leppkes et al., "STAT3 links IL-22 signaling in intestinal epithelial cells to mucosal wound healing," *Journal of Experimental Medicine*, vol. 206, no. 7, pp. 1465–1472, 2009.

[18] K. Sugimoto, A. Ogawa, E. Mizoguchi et al., "IL-22 ameliorates intestinal inflammation in a mouse model of ulcerative colitis," *The Journal of Clinical Investigation*, vol. 118, no. 2, pp. 534–544, 2008.

[19] C. L. Zindl, J. F. Lai, Y. K. Lee et al., "IL-22-producing neutrophils contribute to antimicrobial defense and restitution of colonic epithelial integrity during colitis," *Proceedings of the National Academy of Sciences*, vol. 110, no. 31, pp. 12768–12773, 2013.

[20] M. E. Keir, T. Yi, T. T. Lu, and N. Ghilardi, "The role of IL-22 in intestinal health and disease," *Journal of Experimental Medicine*, vol. 217, no. 3, article e20192195, 2020.

[21] B. Pan, D. Wang, L. Li et al., "IL-22 accelerates thymus regeneration via Stat3/Mcl-1 and decreases chronic graft-versus-host disease in mice after allotransplants," *Biology of Blood and Marrow Transplantation*, vol. 25, no. 10, pp. 1911–1919, 2019.

[22] Y. Zhu, T. Shi, X. Lu et al., "Fungal-induced glycolysis in macrophages promotes colon cancer by enhancing innate lymphoid cell secretion of IL-22," *The EMBO Journal*, vol. 40, no. 11, article e105320, 2021.

[23] T. Arshad, F. Mansur, R. Palek, S. Manzoor, and V. Liska, "A double edged sword role of interleukin-22 in wound healing and tissue regeneration," *Frontiers in Immunology*, vol. 11, article 2148, 2020.

[24] A. H. Mirza, C. H. Berthelsen, S. E. Seemann et al., "Transcriptomic landscape of lncRNAs in inflammatory bowel disease," *Genome Medicine*, vol. 7, no. 1, pp. 1–22, 2015.

[25] X. Han, S. Huang, P. Xue et al., "LncRNA PTPRE-AS1 modulates M2 macrophage activation and inflammatory diseases by epigenetic promotion of PTPRE," *Science Advances*, vol. 5, no. 12, article eaax9230, 2019.

[26] Q. Zhang, T. C. Chao, V. S. Patil et al., "The long noncoding RNA ROCKI regulates inflammatory gene expression," *The EMBO Journal*, vol. 38, no. 8, article e100041, 2019.

[27] H. Geng, H. F. Bu, F. Liu et al., "In inflamed intestinal tissues and epithelial cells, interleukin 22 signaling increases expression of H19 long noncoding rna, which promotes mucosal regeneration," *Gastroenterology*, vol. 155, no. 1, pp. 144–155, 2018.

[28] L. Xiao, J. Wu, J. Y. Wang et al., "Long noncoding RNA uc.173 promotes renewal of the intestinal mucosa by inducing degradation of microRNA 195," *Gastroenterology*, vol. 154, no. 3, pp. 599–611, 2018.

[29] Y. Li, L. Zhu, P. Chen et al., "MALAT1 maintains the intestinal mucosal homeostasis in Crohn's disease via the miR-146b-5p-CLDN11/NUMB pathway," *Journal of Crohn's and Colitis*, vol. 15, no. 9, pp. 1542–1557, 2021.

[30] H. Lee, Y. S. Son, M. O. Lee et al., "Low-dose interleukin-2 alleviates dextran sodium sulfate-induced colitis in mice by recovering intestinal integrity and inhibiting AKT-dependent pathways," *Theranostics*, vol. 10, no. 11, pp. 5048–5063, 2020.

[31] C. Li, Y. Zhou, P. Rychahou et al., "SIRT2 contributes to the regulation of intestinal cell proliferation and differentiation," *Cellular and Molecular Gastroenterology and Hepatology*, vol. 10, no. 1, pp. 43–57, 2020.

[32] K. Parikh, A. Antanaviciute, D. Fawkner-Corbett et al., "Colonic epithelial cell diversity in health and inflammatory bowel disease," *Nature*, vol. 567, no. 7746, pp. 49–55, 2019.

[33] E. Mennillo, X. Yang, M. Paszek, J. Auwerx, C. Benner, and S. Chen, "NCoR1 protects mice from dextran sodium sulfate-induced colitis by guarding colonic crypt cells from luminal insult," *Cellular and Molecular Gastroenterology and Hepatology*, vol. 10, no. 1, pp. 133–147, 2020.

[34] Z. Cai, J. J. Kotzin, B. Ramdas et al., "Inhibition of inflammatory signaling in Tet2 mutant preleukemic cells mitigates stress-induced abnormalities and clonal hematopoiesis," *Cell Stem Cell*, vol. 23, no. 6, pp. 833–849, 2018.

[35] M. K. Atianand, W. Hu, A. T. Satpathy et al., "A long noncoding RNA lincRNA-EPS acts as a transcriptional brake to restrain inflammation," *Cell*, vol. 165, no. 7, pp. 1672–1685, 2016.

[36] D. W. Thomson and M. E. Dinger, "Endogenous microRNA sponges: evidence and controversy," *Nature Reviews Genetics*, vol. 17, no. 5, pp. 272–283, 2016.

[37] F. Rashid, A. Shah, and G. Shan, "Long non-coding RNAs in the cytoplasm," *Genomics Proteomics Bioinformatics*, vol. 14, no. 2, pp. 73–80, 2016.

[38] S. Devriese, V. Eeckhaut, A. Geirnaert et al., "Reduced mucosa-associated Butyricicoccus activity in patients with ulcerative colitis correlates with aberrant claudin-1 expression," *Journal of Crohn's and Colitis*, vol. 11, no. 2, pp. 229–236, 2017.

[39] E. C. Martens, M. Neumann, and M. S. Desai, "Interactions of commensal and pathogenic microorganisms with the intestinal mucosal barrier," *Nature Reviews Microbiology*, vol. 16, no. 8, pp. 457–470, 2018.

[40] J. M. Allaire, S. M. Crowley, H. T. Law, S. Y. Chang, H. J. Ko, and B. A. Vallance, "The intestinal epithelium: central coordinator of mucosal immunity," *Trends in Immunology*, vol. 39, no. 9, pp. 677–696, 2018.

[41] P. Y. Tsai, B. Zhang, W. Q. He et al., "IL-22 upregulates epithelial claudin-2 to drive diarrhea and enteric pathogen clearance," *Cell Host Microbe*, vol. 21, no. 6, pp. 671–681, 2017.

[42] B. Wang, J. H. Lim, T. Kajikawa et al., "Macrophage beta2-integrins regulate IL-22 by ILC3s and protect from lethal

Citrobacter rodentium-induced colitis," *Cell Reports*, vol. 26, no. 6, pp. 1614–1626, 2019.

[43] Y. Wang, J. B. Mumm, R. Herbst, R. Kolbeck, and Y. Wang, "IL-22 increases permeability of intestinal epithelial tight junctions by enhancing claudin-2 expression," *The Journal of Immunology*, vol. 199, no. 9, pp. 3316–3325, 2017.

[44] C. A. Lindemans, M. Calafiore, A. M. Mertelsmann et al., "Interleukin-22 promotes intestinal-stem-cell-mediated epithelial regeneration," *Nature*, vol. 528, no. 7583, pp. 560–564, 2015.

[45] Y. Q. Qiao, M. L. Huang, A. T. Xu, D. Zhao, Z. H. Ran, and J. Shen, "LncRNA DQ786243 affects Treg related CREB and Foxp3 expression in Crohn's disease," *Journal of Biomedical Science*, vol. 20, pp. 1–7, 2013.

[46] T. X. Yu, H. K. Chung, L. Xiao et al., "Long noncoding RNA H19 impairs the intestinal barrier by suppressing autophagy and lowering Paneth and goblet cell function," *Cellular and Molecular Gastroenterology and Hepatology*, vol. 9, no. 4, pp. 611–625, 2020.

[47] S. C. Akıncılar, L. Wu, Q. F. Ng et al., "NAIL: an evolutionarily conserved lncRNA essential for licensing coordinated activation of p38 and NFkappaB in colitis," *Gut*, vol. 70, no. 10, pp. 1857–1871, 2020.

[48] G. Shu, H. Su, Z. Wang et al., "LINC00680 enhances hepatocellular carcinoma stemness behavior and chemoresistance by sponging miR-568 to upregulate AKT3," *Journal of Experimental & Clinical Cancer Research*, vol. 40, no. 1, pp. 1–13, 2021.

[49] D. M. Adyshev, V. R. Elangovan, N. Moldobaeva, B. Mapes, X. Sun, and J. G. N. Garcia, "Mechanical stress induces pre-B-cell colony-enhancing factor/*NAMPT* expression via epigenetic regulation by *miR-374a* and *miR-568* in human lung endothelium," *American Journal of Respiratory Cell and Molecular Biology*, vol. 50, no. 2, pp. 409–418, 2014.

Hindawi
Oxidative Medicine and Cellular Longevity
Volume 2022, Article ID 7078787, 19 pages
https://doi.org/10.1155/2022/7078787

Research Article

Investigation of Transcript Variant 6 of *TPD52L2* as a Prognostic and Predictive Biomarker in Basal-Like MDA-MB-231 and MDA-MB-453 Cell Lines for Breast Cancer

Xin Zhang,[1,2] **Daniel O'Brien**,[3] **and Xiaohui Zhang**[4]

[1]*Department of Spine Surgery, Weifang People's Hospital, Weifang, Shandong 261000, China*
[2]*Key Laboratory of Human Spine Biomechanics of Weifang City, Weifang, Shandong 261000, China*
[3]*Bioinformatics Core, Mayo Clinic, Rochester, MN 55905, USA*
[4]*Department of Breast Surgery, Peking Union Medical College Hospital, Chinese Academy of Medical Science, Beijing 100730, China*

Correspondence should be addressed to Xin Zhang; zhangxin07@stu.cpu.edu.cn

Received 22 July 2022; Accepted 10 August 2022; Published 29 August 2022

Academic Editor: Tarique Hussain

Background. Basal-like breast cancer (BLBC) exhibits worse pathological features than other breast cancer subtypes, and patients diagnosed with BLBC have short disease-free and overall survival times. Thus, the identification of novel biomarkers and therapeutic targets for BLBC is of upmost importance. Although TPD52L2 is upregulated in multiple cancers, little is known about its roles in BLBC. *Methods*. RNA levels were analyzed between breast cancer tissues and paired adjacent normal tissues using RNA-seq data from The Cancer Genome Atlas (TCGA). TPD52L2 stable knockdown and inducible knockout cell lines were established using basal-like MDA-MB-231 and MDA-MB-453 cell lines. Cell proliferation assays *in vitro* and tumor growth analysis *in vivo* were performed to determine the function of TPD52L2 during BLBC progression. Transwell assays were used to estimate the regulatory effect of TPD52L2 on BLBC cell migration. The expression profile of all *tpd52l2* transcripts was analyzed to assess the functional protein isoform. Association of transcript variant 6 (V6) expression with pathological parameters was carried out using the clinical data of the BRCA cohort. *Results*. We identified V6 of TPD52L2 as a novel biomarker and regulator of BLBC progression. TPD52L2 is upregulated in BLBCs and associated with patient outcomes. TPD52L2 knockdown suppresses tumor growth, and V6 correlates with cancer-related phenotypes in BLBC. Clinical data further proved that V6 is associated with different pathological features, such as pathological stage and pathological tumor status, and independently predicts patient outcomes and responses to therapies. *Conclusions*. Our findings demonstrate that V6 of TPD52L2 is a novel biomarker for BLBC patients. V6 promotes cell proliferation and migration and has marked oncogenic roles in determining the malignant phenotypes of BLBC.

1. Introduction

Breast cancer (BC) is one of the most lethal diseases and led to almost 685,000 female deaths in 2020 worldwide [1]. It is a heterogeneous disease with diverse molecular alterations and cellular components. The PAM50 signature is used to divide breast cancers into luminal A, luminal B, Her 2-enriched, basal-like, and normal-like subtypes. Compared to other subtypes, basal-like breast cancer (BLBC) exhibits worse clinical and pathological features, such as poorer differentiation, higher proliferation capacity, increased stemness and metastasis potential, and more prominent lymphocyte infiltration. Patients diagnosed with BLBC generally have short disease-free and overall survival times [2]. Most BLBC cases are triple-negative breast cancer (TNBC) (negative expression of estrogen receptor (ER), progesterone receptor (PR), and Her2 receptor). Endocrine and target molecular therapies have limited effects on this malignant subtype [3]. Genomic and transcriptomic analyses contribute to the understanding of the molecular basis and malignant phenotypes of cancers. Many biomarkers have been identified and have decreased the lethality of BLBC in recent years. A signature of 80 genes

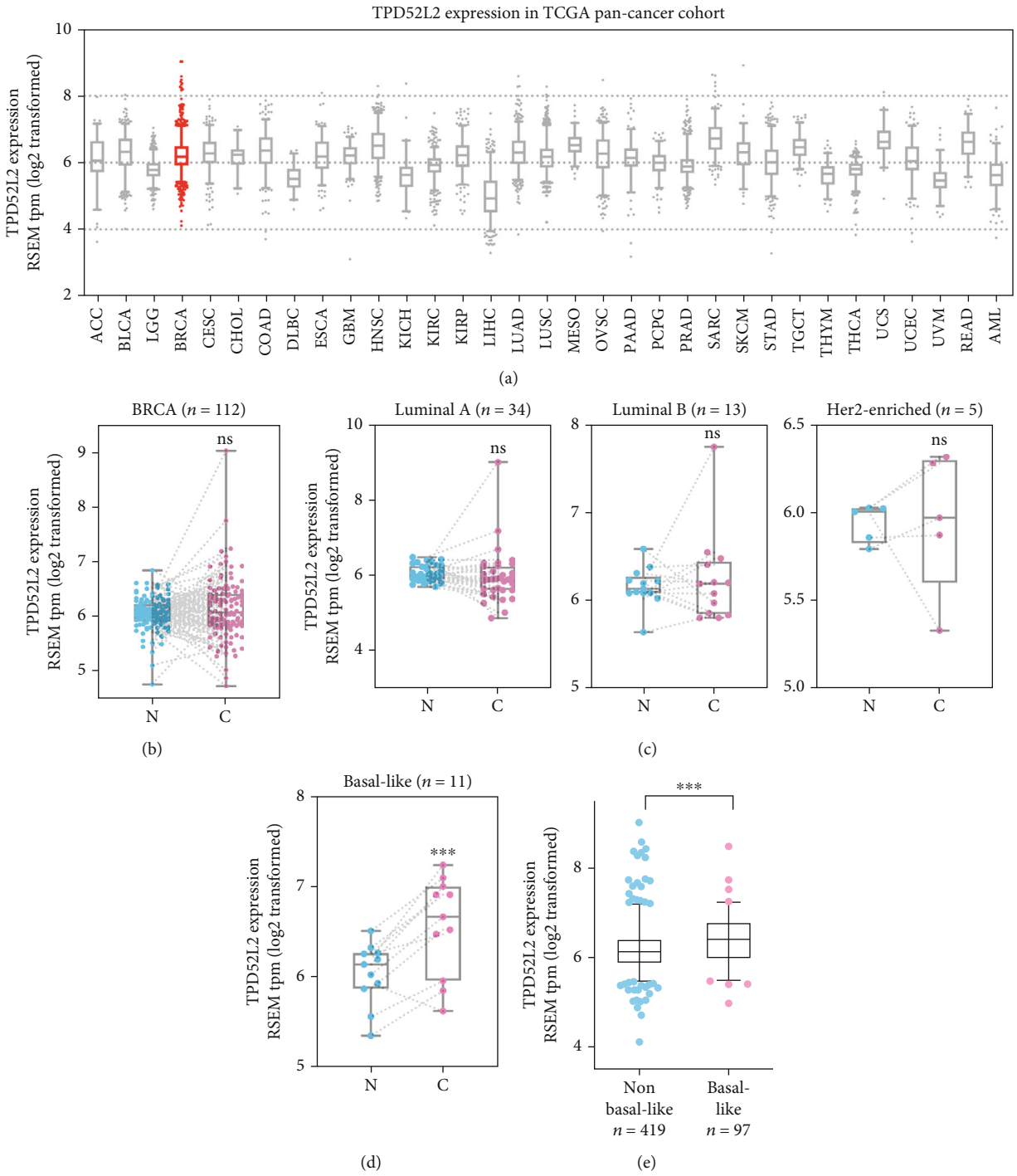

Figure 1: Continued.

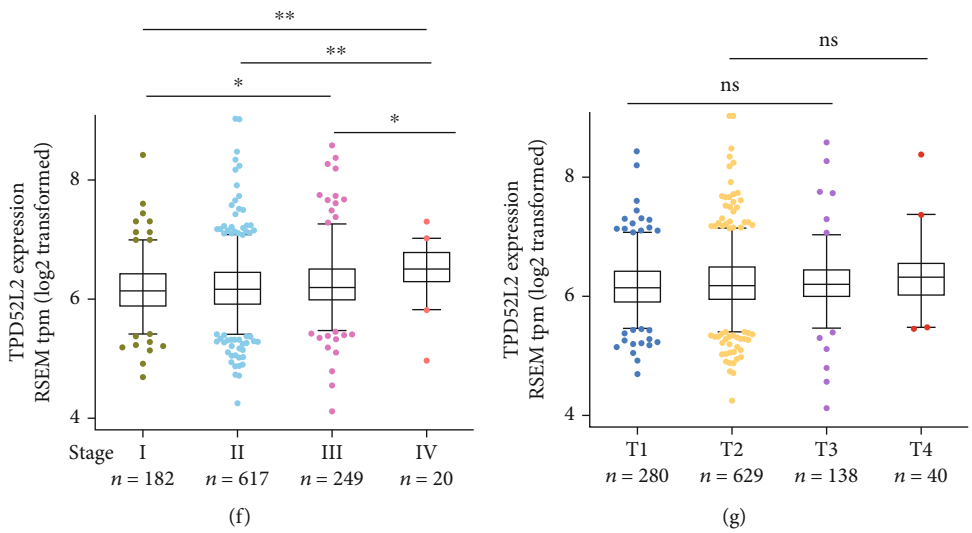

Figure 1: Expression analysis of TPD52L2 in breast cancer. (a) TPD52L2 expression in cancer tissues based on TCGA dataset. (b) Comparative analysis of TPD52L2 expression between cancer tissues and paired adjacent normal tissues from the BRCA cohort of TCGA. The difference was not significant (paired t-test). (c, d) TPD52L2 expression between cancer tissues and paired adjacent normal tissues in breast cancer patients with different PAM50 subtypes. (d) For BLBC patients, the difference between groups was significant (paired t-test, $^*p < 0.05$). (e) TPD52L2 expression between non-BLBC and BLBC patients from the BRCA cohort. The difference between groups was significant (Mann–Whitney test). (f, g) Comparative analysis of TPD52L2 expression in breast cancer patients from the BRCA cohort: (e) stages I, II, III, and IV and (f) T1, T2, T3, and T4. The differences between groups were significant (Mann–Whitney test, $^*p < 0.05$).

distinguished two basal-like subgroups with different clinical features. This signature was associated with the cancer immune response and epithelial-mesenchymal transition [4]. To date, biomarkers that are associated with pathological features and can predict clinical outcomes have been limited in BLBC. Therefore, the identification of new biomarkers and therapeutic targets for BLBCs and the demonstration of their molecular mechanisms will lead to better management of this aggressive disease.

The tumor protein D52-like family is a group of coiled coil proteins. This family consists of TPD52, TPD52L1 (TPD53), TPD52L2 (TPD54), and TPD52L3 (TPD55), which are highly expressed in multiple cancers. TPD52 was shown to be overexpressed in breast cancer and prostate cancer and identified as a candidate oncogene [5, 6]. TPD52 overexpression increased the storage of fatty acids in triglycerides in cultured cells and formed more lipid droplets after oleic acid supplementation [7]. In oral squamous cell carcinoma (OSCC), TPD52 was elevated under hypoxic conditions in a HIF-independent manner and promoted cell proliferation and survival [8]. It was recently validated that immunohistochemistry (IHC) of TPD52 had important prognostic values for group 3/4 medulloblastomas [9]. These data suggested that inhibition of TPD52 could contribute to cancer treatment.

TPD52L2 is another abundant member of the tumor protein D52-like family. Proteomic analysis revealed that TPD52L2 was one of the most abundant proteins in HeLa cells, ranking 180th out of 8,804 proteins, with an estimated 3.3×10^6 copies per cell [10]. TPD52L2 is involved in a new class of intracellular transport vesicles: intracellular nanovesicles (INVs). It can interact with Rab GTPases and bind directly to INVs to regulate the trafficking of specific cargos with dileucine sorting motifs [11]. However, there are limited studies on its cellular functions, molecular mechanisms, and clinical significance in different types of cancers. In this study, we evaluated TPD52L2 expression and its impact on patient outcomes in a breast cancer cohort from The Cancer Genome Atlas (TCGA) dataset. We found that TPD52L2 is upregulated in BLBC and is notably associated with the outcomes of patients with BLBC and lymph node-positive BLBC. TPD52L2 knockdown had an inhibitory effect on the growth of BLBC cells, and transcript variant 6 (V6) was identified to be translated into the oncogenic protein isoform. Clinical data further validated that V6 is linked to pathological features and predicts patient outcomes and therapy response. Our results established TPD52L2 as a novel biomarker in BLBCs and a potential therapeutic target.

2. Materials and Methods

2.1. TPD52L2 Expression Analysis in Tumors and Normal Tissues. Data for TCGA cohorts were downloaded from the UCSC Xena browser and analyzed [12]. The TPD52L2 expression data and patient survival data for 33 cancer types were obtained from TCGA. All the clinical parameters of breast cancer patients were downloaded from the BRCA cohort (http://xena.ucsc.edu/). Normal (GTEx samples) and tumor (TCGA samples) tissues were compared using resources from TCGA TARGET GTEx dataset in UCSC Xena [12, 13]. The overall survival of patients in the GSE96058 dataset was analyzed using the published resource Kaplan–Meier plotter (http://kmplot.com/) [14].

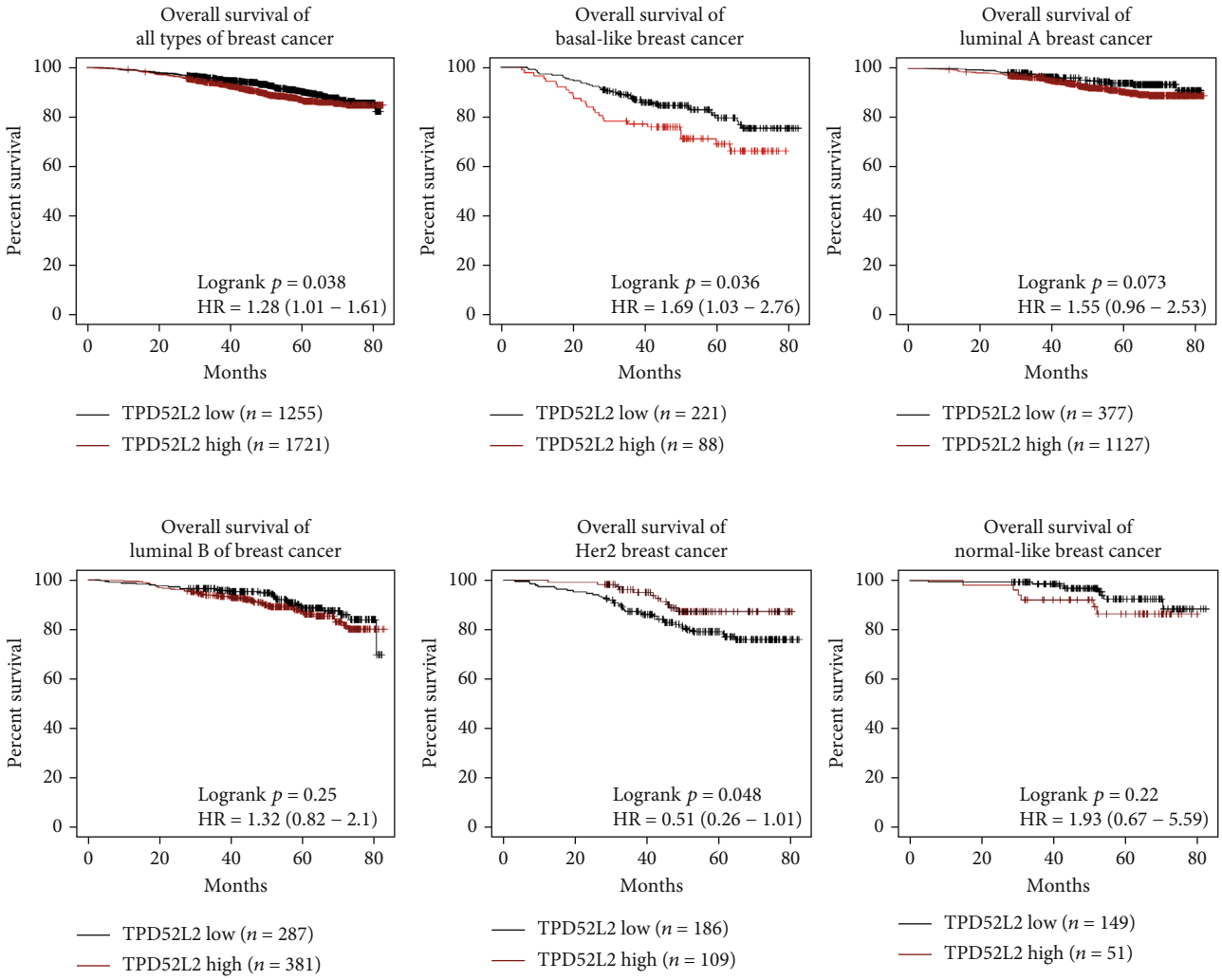

(a)

Figure 2: Continued.

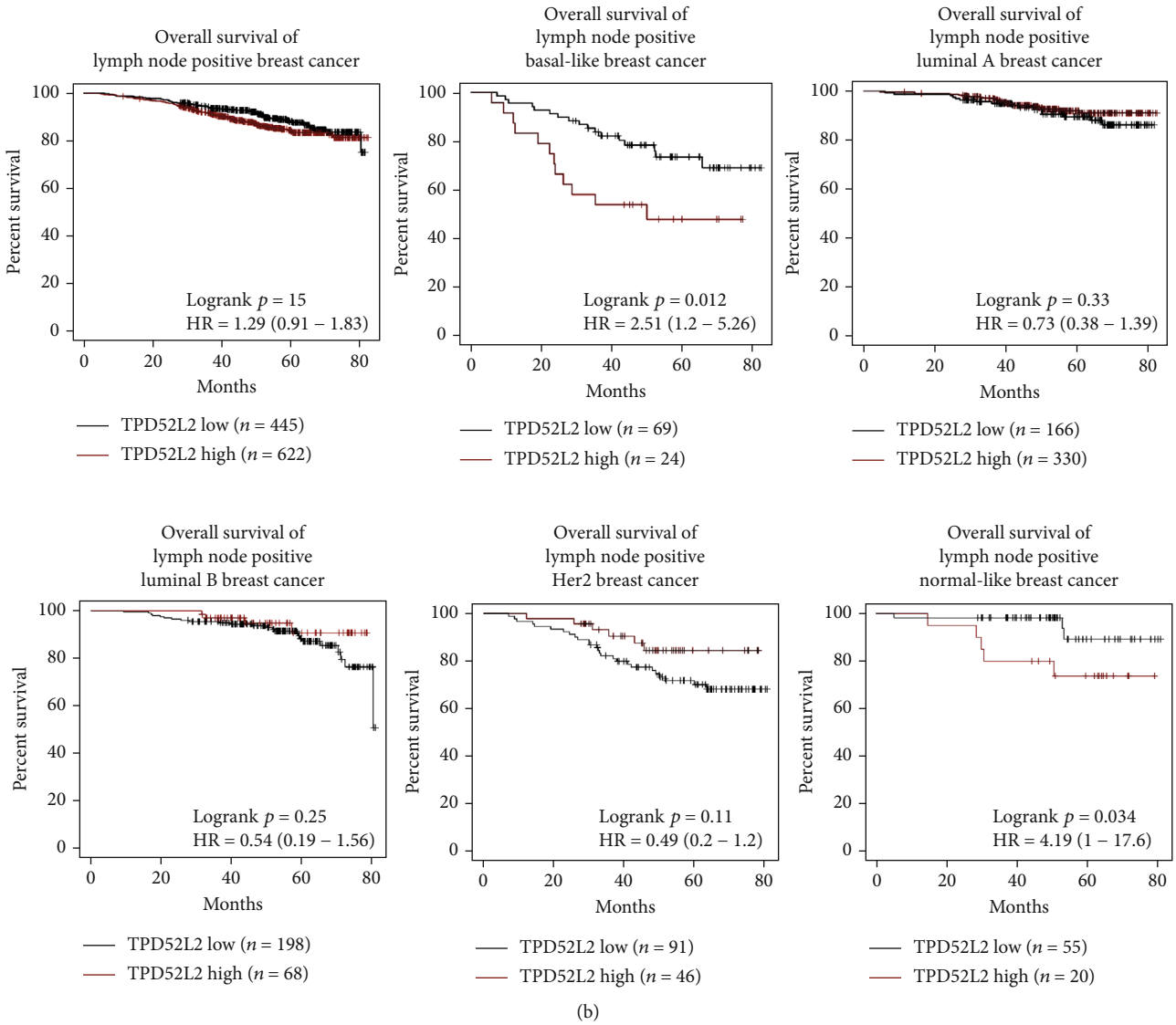

Figure 2: Kaplan–Meier curves indicating the OS of breast cancer patients with low and high TPD52L2 levels from the GSE96058 dataset [14]. (a) Kaplan–Meier curves of the OS of all breast cancer patients and patients with different PAM50 subtypes, including basal-like, luminal A, luminal B, Her2, and normal-like subtypes. (b) Kaplan–Meier curves of the OS of all lymph node-positive breast cancer patients and lymph node-positive patients with different PAM50 subtypes, including basal-like, luminal A, luminal B, Her2, and normal-like subtypes (log-rank test, $^*p < 0.05$).

2.2. Cell Culture and Expression Plasmids. MDA-MB-231 and MDA-MB-453 cells were cultured in Dulbecco's modified Eagle's medium (DMEM, HyClone; Thermo Scientific) with 10% fetal bovine serum (FBS), 100 U/mL penicillin, and 100 μg/mL streptomycin in 5% CO_2-humidified incubators at 37°C. All cell lines were purchased from the American Type Culture Collection (ATCC) and free of mycoplasma contamination (tested by the vendor). Expression plasmids of ten transcript variants of *tpd52l2* were purchased from GenScript. Briefly, the cDNAs of ten transcript variants of *tpd52l2* were cloned into vector pcDNA3.1 with an HA tag linked to the C-terminus of the protein sequence. All constructs were confirmed by DNA sequencing.

2.3. TPD52L2 Stable Knockdown Cell Lines. TPD52L2 short hairpin RNA (shRNA) plasmids were purchased from OriGene. The target sequences of shRNAs used in this study included GGAAGGGAGGTTGTCACTG, AGAAAGGTG CGGGATCCGA, and TGGCGCAGAGTGACAATTT. MDA-MB-231 cells were transfected with shRNA plasmids using Lipofectamine 2000 transfection reagents purchased from Invitrogen. The transfected cells were selected with 2 μg/mL puromycin 36 h after transfection for 5 days. Clones were isolated and validated by Western blotting and sequencing of genomic DNA.

2.4. Cell Viability Assay. Viable cells were measured using Cell Counting Kit-8 (CCK-8, Dojindo) as previously described [15]. Briefly, 3000 cells per well were seeded in 96-well plates, and the medium was replaced every 3 days. Ten microliters of CCK-8 solution were added to each well containing 100 μL of culture medium and incubated for 2 h

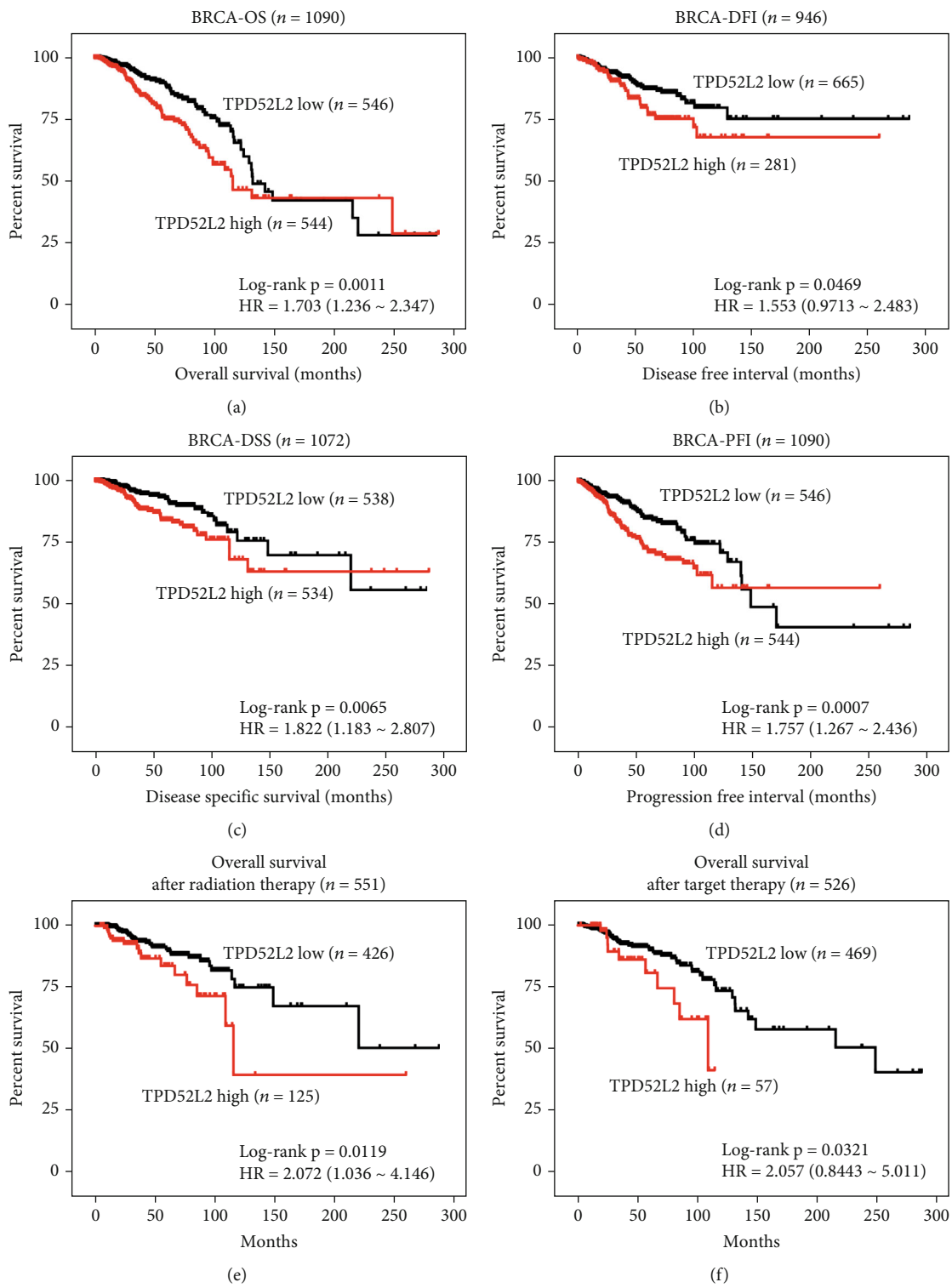

Figure 3: TPD52L2 impact on breast cancer patient survival and therapy response. (a–d) Kaplan–Meier curves indicate the OS, DFI, DSS, and PFI of breast cancer patients with low and high TPD52L2 levels from the BRCA cohort. (e, f) Kaplan–Meier curves indicate the OS of breast cancer patients with low and high TPD52L2 levels after treatment with radiation therapy or targeted therapy from the BRCA cohort (log-rank test, $^*p < 0.05$).

at 37°C. The absorbance was measured at 450 nm using an ELISA plate reader. Cell proliferation was measured once per day for seven days.

2.5. Colony Formation Assays. In total, 1000 MDA-MB-231 cells or 2000 MDA-MB-453 cells per well were seeded in 6-well plates. The cells were cultured for 14 days, and visible

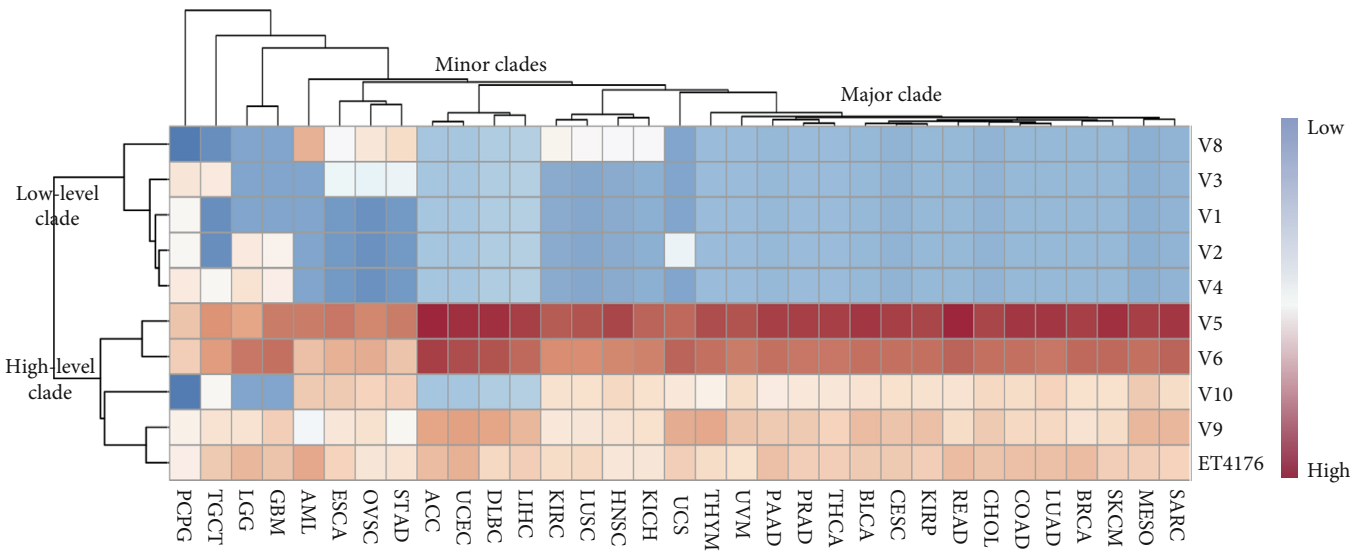

(a)

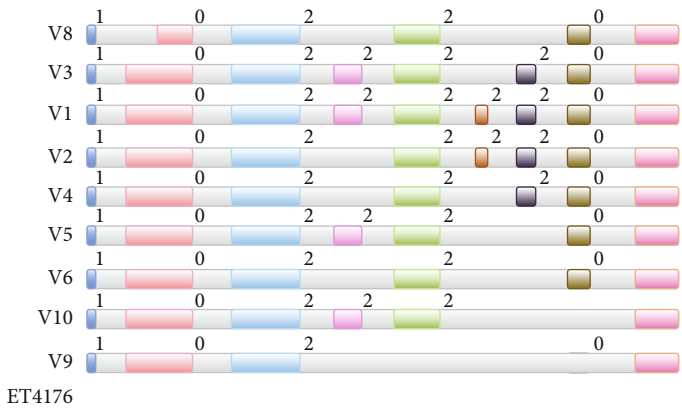

(b)

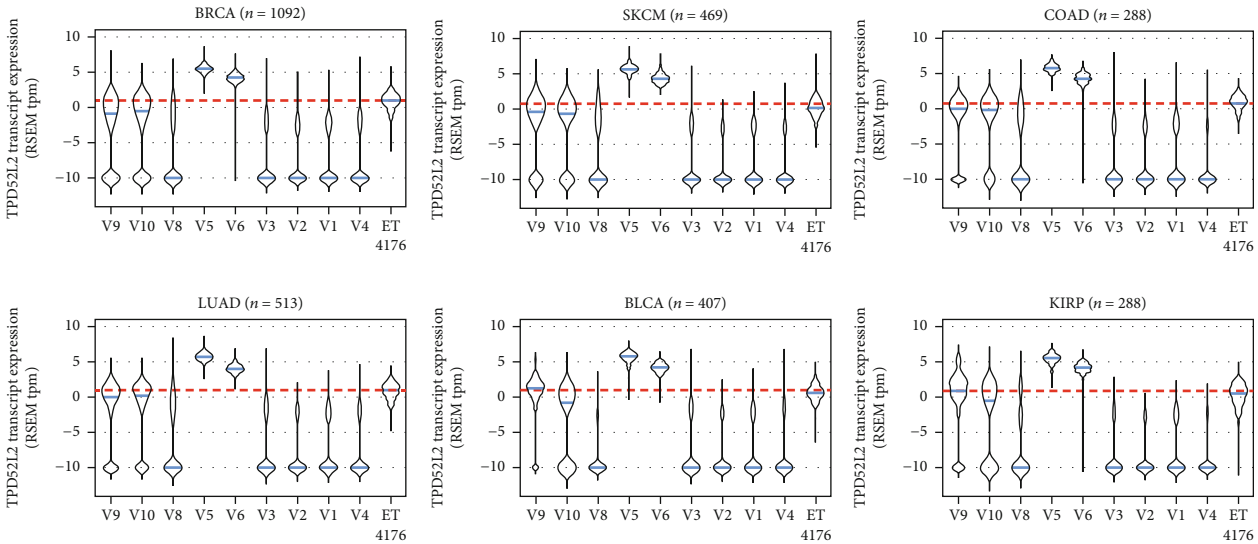

(c)

Figure 4: Continued.

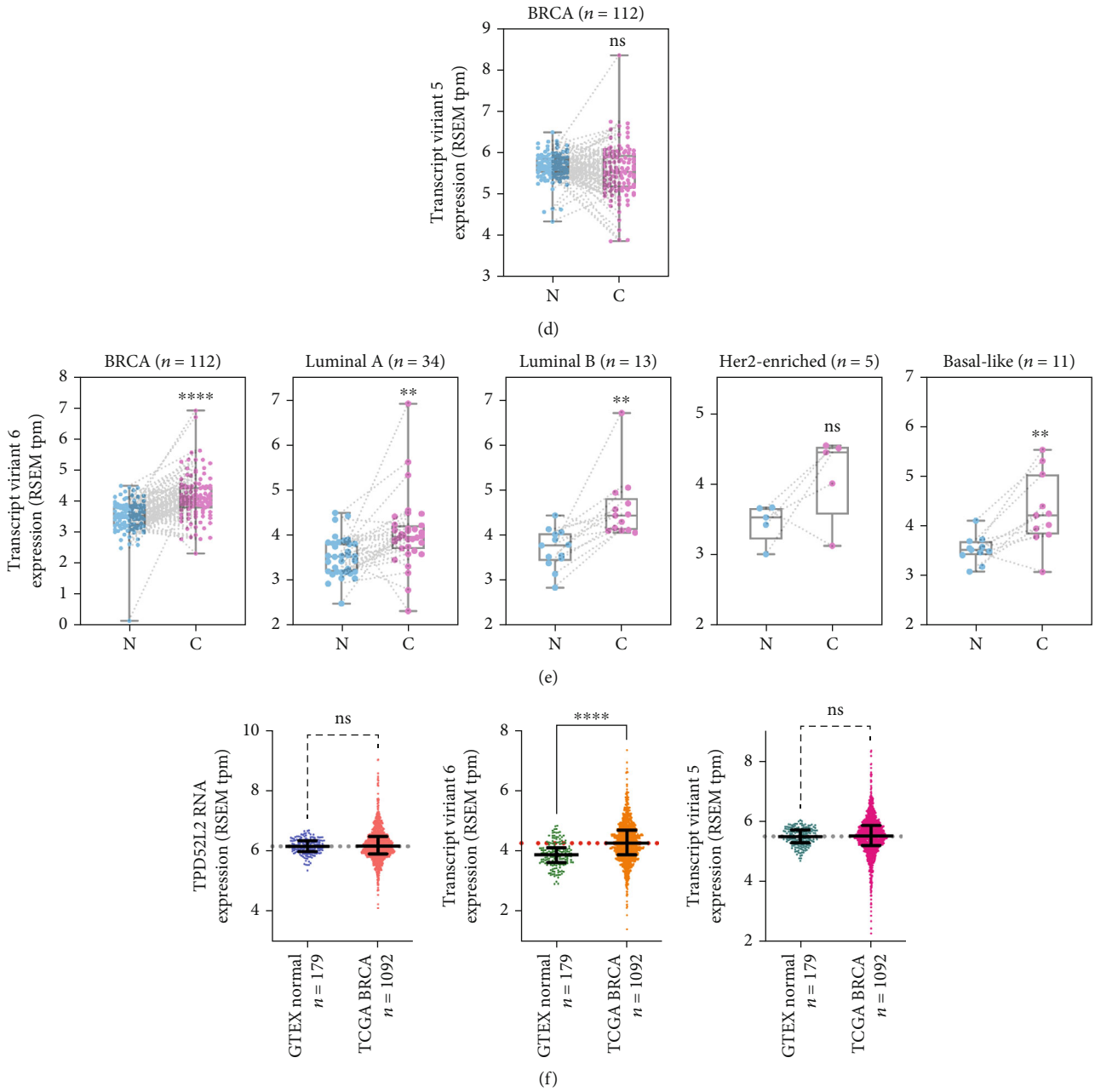

Figure 4: Expression profiles of *tpd52l2* transcript variants. (a) Heatmap of the expression of the ten transcript variants of the *tpd52l2* gene in patients from 33 cohorts of TCGA dataset (including 469 patients with primary and metastatic cancers from SKCM and 9083 patients with primary cancers from the other 32 cohorts). Cohorts were arranged by unsupervised clustering of median transcript expression. (b) Intron and exon distributions of each transcript variant of the *tpd52l2* gene. Colored bars represent exons, and white-gray bars represent introns. 0/1/2 represent the intron/exon phase. (c) Comparative analysis of *tpd52l2* transcript expression in patients with primary cancers from the BRCA, COAD, LUAD, BLCA, and KIRP cohorts and in patients with primary and metastatic cancers from the SKCM cohort of TCGA dataset. Blue lines are the median expression of each transcript. Red dashed lines indicate the cutoff value of one. (d) Expression of transcript variant 5 of *tpd52l2* between breast cancer tissues and paired adjacent normal tissues from the BRCA cohort of TCGA dataset. $n = 112$, no significant difference, paired t-test. (e) Expression analysis of transcript variant 6 of *tpd52l2* between breast cancer tissues and paired adjacent normal tissues grouped by PAM50 in the BRCA cohort (paired t-test, $^{*}p < 0.05$). (f) Comparative analysis of the mRNA expression level of *tpd52l2* and the transcript expression levels of V5 and V6 between cancer tissues in the BRCA cohort and normal breast tissues in GTEx (Mann–Whitney test, $^{*}p < 0.05$).

colonies were formed. The cells were fixed with 4% paraformaldehyde solution and visualized by staining with 1% crystal violet. The colonies were counted. Each assay was performed in triplicate and repeated three times.

2.6. Migration Assay. Migration assays were performed on Transwell plates (Millipore). MDA-MB-231 cells (1×10^5) and MDA-MB-453 cells (2×10^5) were seeded on a polycarbonate membrane insert placed in a Transwell plate and

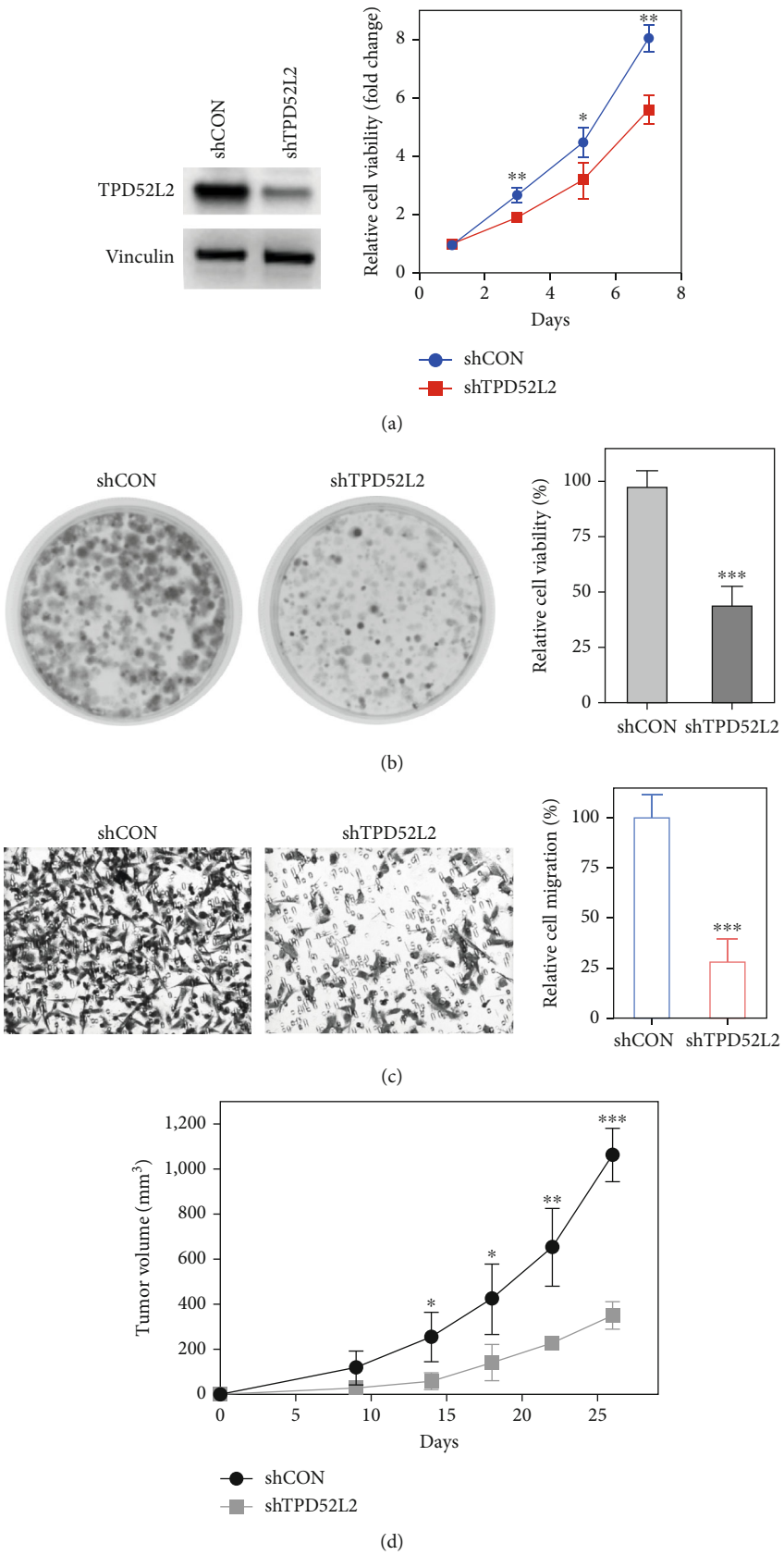

Figure 5: Continued.

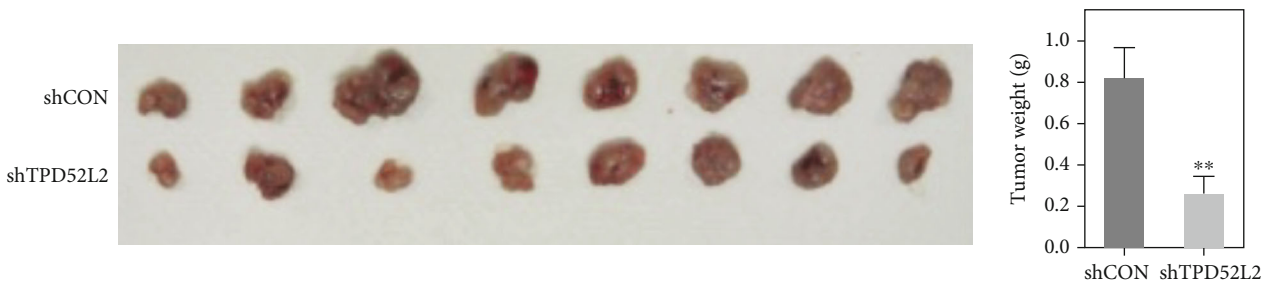

(e)

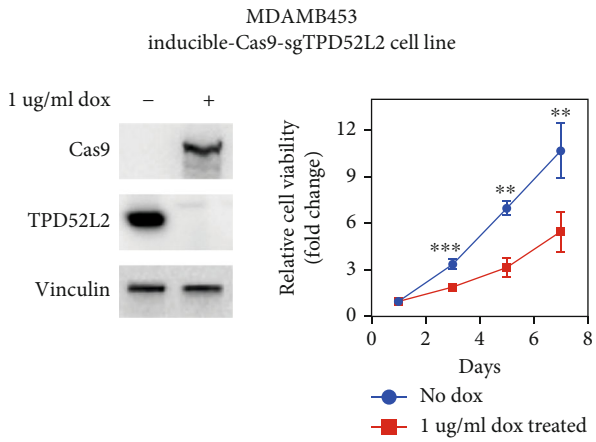

(f)

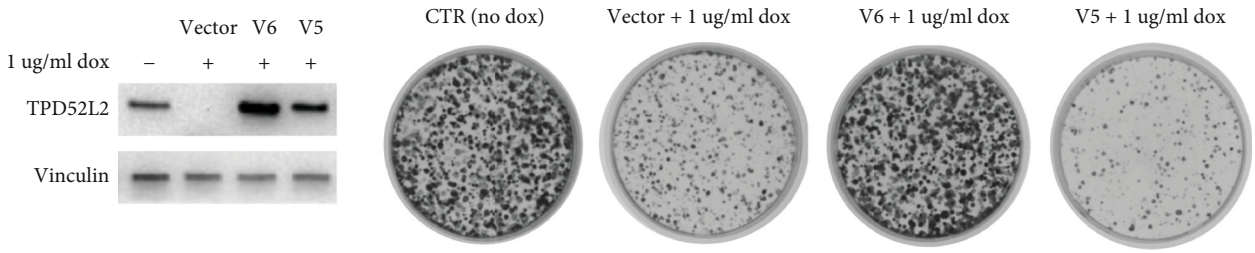

(g)

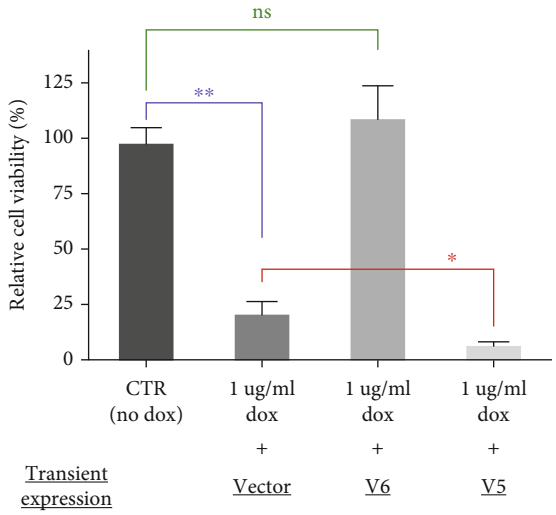

(h)

Figure 5: Continued.

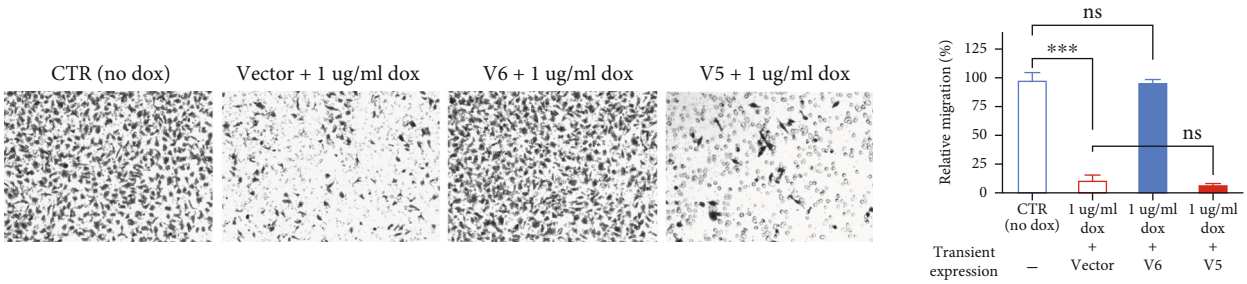

(i)

Figure 5: The effect of TPD52L2 on the tumorigenesis of BLBC cells *in vitro* and *in vivo*. (a–e) The MDA-MB-231 cell line was transfected with either shCON or 3 different shRNAs targeting TPD52L2. After puromycin selection and positive colony enrichment, MDA-MB-231 cell lines with stable knockdown were established. (a) Cell viability assays. The samples were assayed in triplicate. Each point represents the mean value from three independent samples. (b) Colony formation assays. (c) Cell migration assays. Representative photographs and bar graphs were from three independent experiments (mean ± SD, $n = 3$, t-test, $^*p < 0.05$). (d) Growth curves of xenograft tumors obtained upon subcutaneous implantation of shCON or shTPD52L2 cells. Tumor volumes were monitored every 3 days by measuring tumor diameters (mean ± SD, $n = 10$, $^*p < 0.05$). (e) Images and weights of xenograft tumors. The 5tumors were removed, photographed, and weighed (mean ± SD, $n = 10$, t-test, $^*p < 0.05$). (f–i) MDA-MB-453 cells were infected with lentiviruses expressing CAS9 under the control of a doxycycline-inducible promoter and lentiviruses expressing a sgRNA targeting TPD52L2 (sgTPD52L2). Stable inducible Cas9-sgTPD52L2 cell lines were established after two rounds of selection using blasticidin and puromycin. (f) Cell viability assays of inducible Cas9-sgTPD52L2 cell lines. The samples were assayed in triplicate. Each point represents the mean value from three independent samples. (g) The stable cell lines were treated with doxycycline for 48 h and then washed and transfected with plasmids containing the cDNAs of V5 or V6 tagged with HA. Forty-eight hours after transfection, the cells were lysed and immunoblotted as indicated. (h) Colony formation assays. (i) Cell migration assays. Representative photographs and bar graphs are from three independent experiments. The data are presented as the mean ± SD ($n = 3$, t-test, $^*p < 0.05$).

cultured in DMEM without serum; then, DMEM containing 10% FBS was added to the wells of the plates [15]. After incubation at 37°C in a CO_2 incubator for 18 h, the membrane was washed with phosphate-buffered saline (PBS), and the cells at the top of the membrane were wiped with cotton swabs. Cells that migrated to the bottom of the membrane were fixed with methanol, stained with 1% crystal violet, and counted in nine random fields at 200x magnification. Each assay was performed in triplicate and repeated three times.

2.7. Western Blotting. Proteins were extracted with SDS lysis buffer (50 mM Tris-HCl (pH 6.8), 10% glycerol, and 2% SDS) and quantified using the BCA protein assay reagent (Thermo Fisher). Extracts were loaded on a 12% SDS-PAGE gel, separated, and then electrophoretically transferred to a PVDF membrane (GE Healthcare) [15]. The membrane was blocked in 2% skim milk for 0.5 h at room temperature and then incubated overnight with the indicated antibodies at 4°C. The membrane was incubated with an HRP-IgG (Santa Cruz) secondary antibody for 1 h at room temperature. Chemiluminescence was detected using an ECL blot detection system (Santa Cruz). Vinculin (13901) and HA-tagged (3724) antibodies were purchased from Cell Signaling Technology Company. The TPD52L2 (11795-1-AP) antibody was purchased from Proteintech Company.

2.8. Hierarchical Clustering and Transcript Expression Analysis. The expression of ten *TPD52L2* transcript variants of 33 cancer types from TCGA dataset, which included information for a total of 9552 cancer tissues (containing 9185 primary cancers and 366 metastatic cancers of the SKCM cohort) (additional files), was downloaded from the UCSC Xena browser and analyzed by unsupervised hierarchical clustering (median value of transcript expression) using ClustVis at http://biit.cs.ut.ee/clustvis/ [12, 16].

2.9. Gene Structure and Protein Sequence Analyses. The exon/intron distributions were analyzed using GSDS software [17]. The mRNA, cDNA, and gene sequences of *TPD52L2* are listed in additional files. The amino acid sequences of ten protein isoforms of TPD52L2 were compared using Clustal Omega2 software with default parameters [18]. Protein sequences are listed in additional files.

2.10. TPD52L2 Inducible Knockout Cell Lines. Tetracycline-inducible lentiviral hEF1α-Blast-Cas9 nuclease particles and Edit-R lentiviral sgRNA particles were obtained from Dharmacon. The target sequence of the sgRNA was GCTC AGGGCTGAGCTTACCA. MDA-MB-453 cells were infected at an MOI of 5 according to the manufacturer's instructions. Briefly, MDA-MB-453 cells were infected with inducible Cas9 lentivirus, and 36 h after infection, cells were cultured in DMEM containing 10% tetracycline-free serum (HyClone) with 8 μg/mL blasticidin S (Fisher Scientific) to select for stably expressing cells. Cells were passaged every 3 days for two weeks, and then, single clones were isolated and validated by Western blotting. Next, the inducible Cas9 clones were expanded and infected with sgRNA lentivirus. Cells were cultured in 2 μg/mL puromycin (Fisher Scientific) for 5 days to obtain stable cell lines, and then, single clones were isolated and expanded. Dox (1 μg/mL) hyclate (Fisher Scientific) was added to Tet-free medium for 2 days, and stably expressing cells were examined and selected by Western blotting.

Table 1: Association between the transcript expression of V6 and clinicopathological parameters in breast cancer patients of the BRCA cohort.

Clinicopathological parameters	n	TPD52L2 expression High (>median)	Low (<median)	p value
Age				
≥60	370	169	201	0.8141
≤60	443	206	237	
Her2				
Positive	113	59	54	0.1575
Negative	647	288	359	
PR				
Positive	518	226	292	0.05107
Negative	253	130	123	
ER				
Positive	597	269	328	0.3822
Negative	177	87	90	
Pathologic_M				
M0	906	435	471	0.008415*
M1	22	17	5	
Pathologic_N				
N0	513	244	269	0.05549
N1	361	171	190	
N2	119	71	48	
N3	77	43	34	
Pathologic_T				
T1	280	114	166	0.000301*
T2	629	319	310	
T3	138	85	53	
T4	40	24	16	
Pathologic_stage				
Stage I	182	76	106	0.0006917*
Stage II	617	297	320	
Stage III	249	144	105	
Stage IV	20	15	5	

Age: at initial pathological diagnosis; pTNM: pathological tumor node metastasis; pT: pathological tumor; pN: pathological node. The median expression value was 4.251. *The significance of correlations between V6 expression and clinicopathological parameters was calculated by the χ^2 test, and Fisher's exact test was used when the patient number had an expected count < 5.

2.11. In Vivo Tumorigenesis. Animal experiments were performed in accordance with a protocol approved by the animal care and use committees of Weifang People's Hospital. Five million tumor cells were resuspended in 0.1 mL phosphate-buffered saline and inoculated into the flanks of 6-week-old female athymic nude mice. Ten mice were injected in each group. Tumor growth was monitored every 3 days by measuring tumor diameters. Tumor width (W) and length (L) were measured, and tumor volume was calculated using the following formula: volume $= (W \times L)^2/2$. Mice were sacrificed 28 days after inoculation. The tumors were removed, photographed, and weighed, and the average weight of the tumors was calculated ($^*p < 0.01$).

2.12. Statistical Analysis. Statistical analysis was performed using GraphPad Prism 9. The results were statistically evaluated, and $p < 0.05$ was considered statistically significant. The Mann–Whitney test was used to compare the expression of TPD52L2 between cancer tissues and unpaired normal tissues, as well as in different subgroups. A paired t-test was used to analyze the difference in expression between cancer tissues and paired adjacent normal tissues. Fisher's exact test and Pearson's chi-squared test were used to determine the association between TPD52L2 (or transcript V6) expression and clinical parameters of breast cancer patients [19]. Survival data were analyzed using the Kaplan–Meier method with the log-rank test [19, 20].

3. Results

3.1. TPD52L2 Expression Is Upregulated in BLBC. We found that TPD52L2 was highly expressed in the 1092 patients with primary breast cancer from TCGA BRCA cohort, with a median expression value of 6.177 (Figure 1(a)). However, no remarkable difference could be detected between 112 breast cancer tissues and paired adjacent normal tissues (Figure 1(b)). To expand our analysis, we investigated TPD52L2 expression in patients with luminal A, luminal B, and Her 2-enriched, and BLBCs (Figures 1(c) and 1(d)). As shown in Figure 1(d), TPD52L2 was upregulated in BLBCs, with a median value of 6.67, which was significantly higher than that in paired adjacent normal tissues, with a median value of 6.14 ($n = 11$, $p < 0.001$). For other subtypes, including luminal A, luminal B, and Her 2-enriched, TPD52L2 expression showed no difference between cancer tissues and paired adjacent normal tissues.

Importantly, TPD52L2 expression in 97 patients with BLBCs was much higher than that in 419 patients with non-BLBCs (Mann–Whitney test, $p < 0.001$) (Figure 1(e)). We further examined whether TPD52L2 expression was correlated with pathological stage and pathological tumor (pT) status. TPD52L2 expression increased significantly for patients with higher pathological stages compared to those with lower stages (Mann–Whitney test, stage IV *vs.* stage I: $p = 0.0014$; stage IV *vs.* stage II: $p = 0.0048$) (Figure 1(f)). The median expression value was 6.13 in patients with stage I disease and 6.51 in patients with stage IV disease. No significant correlation was found between TPD52L2 expression and tumor size (T1 *vs.* greater) (Figure 1(g)).

3.2. TPD52L2 Predicted the Prognosis of BLBC. We analyzed the OS of patients from another breast cancer dataset, GSE96058 [14]. Patients with BLBC showed better overall survival in the TPD52L2 low-expression group than in the TPD52L2 high-expression group (Kaplan–Meier survival analysis with log-rank test, basal-like: $n = 309$, $p = 0.036$) (Figure 2(a)). Among the lymph node-positive BLBC patients, those in the TPD52L2 low-expression group lived longer than those in the TPD52L2 high-expression group

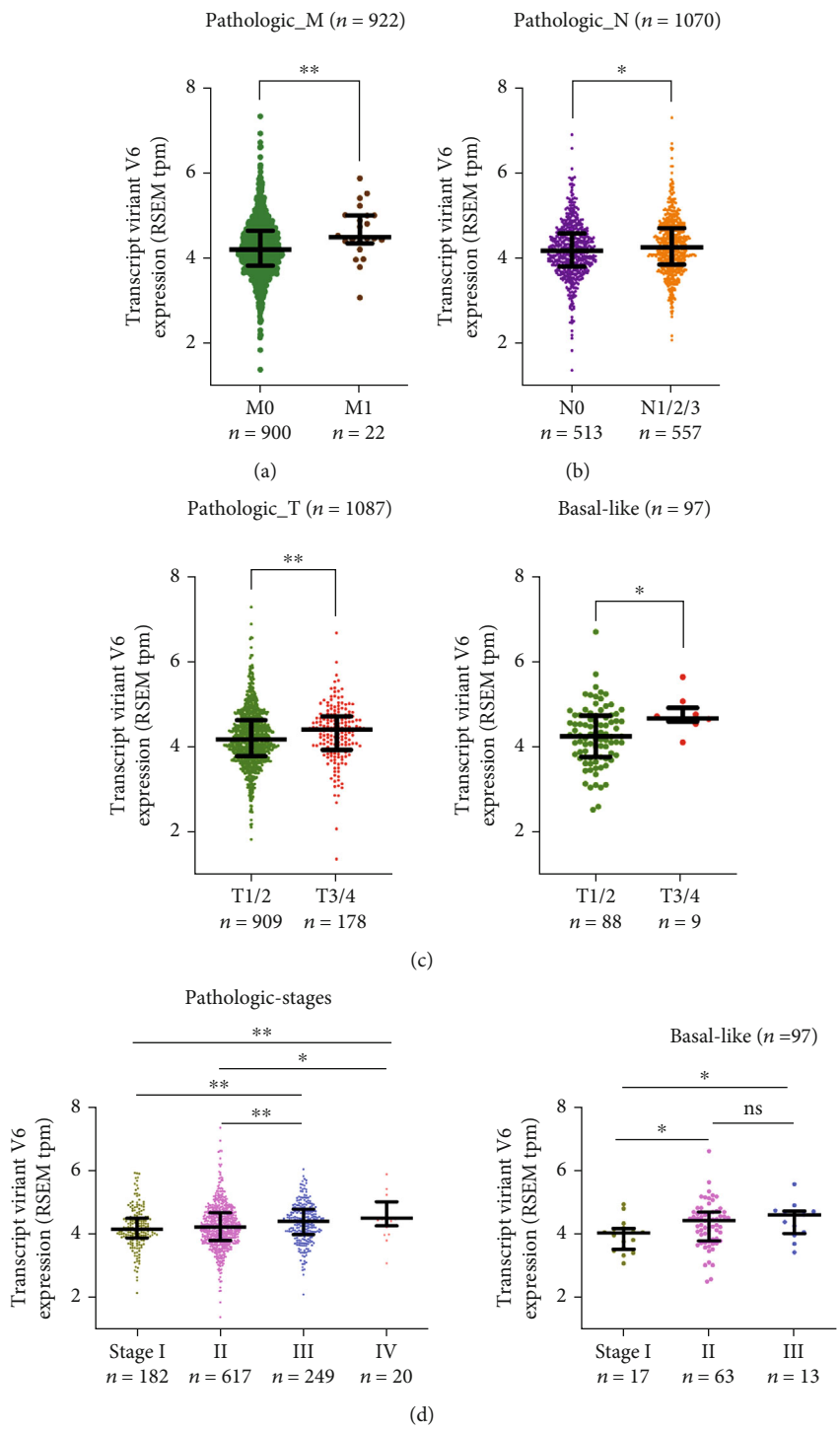

Figure 6: Continued.

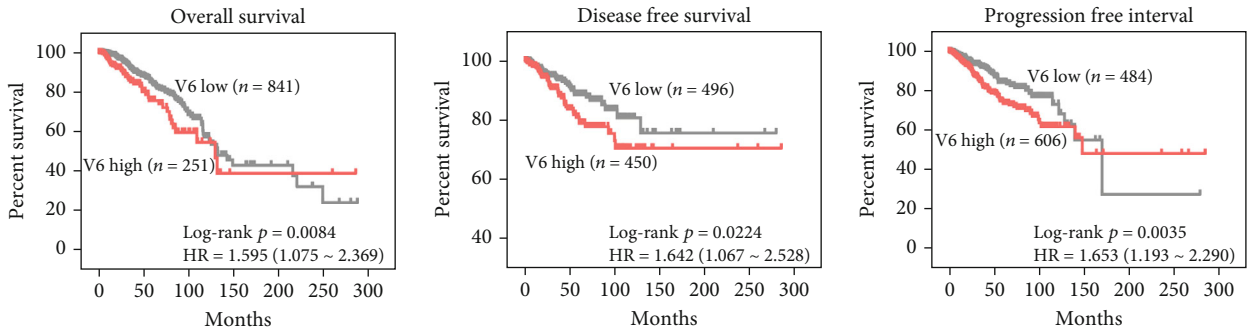

(e)

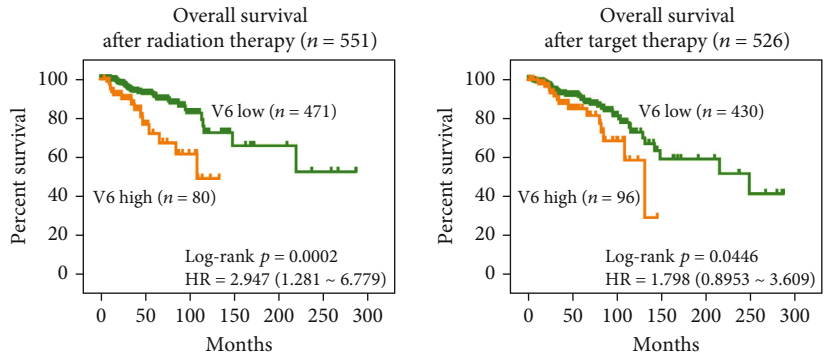

(f)

Figure 6: Expression of V6 of *tpd52l2* in patients with different pathological characteristics and its impact on survival and therapy response. (a) Comparative analysis of transcript expression of V6 in breast cancer patients with pathological_M0 status and pathological_M1 status. (b) Comparative analysis of transcript expression of V6 in breast cancer patients with pathological_N0 status and higher status (N1, N2, and N3). (c) Comparative analysis of transcript expression of V6 in breast cancer patients or BLBC patients with lower pathological T stage (T1 and T2) and higher pathological T stage (T3 and T4). (d) Comparative analysis of transcript expression of V6 in breast cancer patients or BLBC patients with different pathological stages (stages I, II, III, and IV). (e) Kaplan–Meier curves indicating the OS, DFS, and PFI of breast cancer patients in the BRCA cohort. (f) Kaplan–Meier curves indicating the OS of breast cancer patients who received radiation therapy or targeted therapy in the BRCA cohort (Kaplan–Meier analysis with log-rank test for survival analysis, Mann–Whitney test for expression analysis, $^*p < 0.05$).

(Kaplan–Meier survival analysis with log-rank test, basal-like: $n = 93$, $p = 0.012$) (Figure 2(b)). As for other PAM50 subtypes, the OS time of lymph node-positive patients was not different between the low-expression group and the high-expression group (Figures 2(a) and 2(b)).

We then analyzed whether TPD52L2 expression was correlated with the prognosis of breast cancer patients in the BRCA cohort. As shown in Figure 3(a), the median survival was 132 months for patients in the TPD52L2 low-expression group and 115 months for patients in the TPD52L2 high-expression group (Kaplan–Meier survival analysis with log-rank test, $n = 1090$, $p = 0.0011$) (Figure 3(a)). TPD52L2 expression was also correlated with disease-free interval (DFI), disease-specific survival (DSS), and progression-free interval (PFI). The outcomes were better for patients with low TPD52L2 expression than for patients with high TPD52L2 expression (Kaplan–Meier survival analysis with log-rank test, DFI: $n = 946$, $p = 0.0469$; DSS: $n = 1072$, $p = 0.0065$; and PFI: $n = 1090$, $p = 0.0007$) (Figures 3(b)–3(d)). Furthermore, we observed significant impacts of TPD52L2 on the overall survival of patients who received radiation therapy, and OS time decreased dramatically in the high TPD52L2 expression group (Kaplan–Meier survival analysis with log-rank test, $p = 0.0119$) (Figure 3(e)). Similarly, for patients who received targeted molecular therapy, those with low TPD52L2 levels received a greater survival benefit (median time: ~248 months) than those with high TPD52L2 levels (median time: ~109 months) (Kaplan–Meier survival analysis with log-rank test, $p = 0.0321$) (Figure 3(f)).

3.3. The Expression Profile of tpd52l2 Transcript Variants in Breast Cancer. The *tpd52l2* gene has at least ten transcript variants yet one protein isoform according to previous works [21, 22]. To assess which transcript was translated into protein, we first examined the expression of all ten transcript variants in cancer patients from 33 cohorts of TCGA datasets. Unsupervised clustering analyses classified 16 cancer types as a major clade, including BLCA, LUAD, READ, COAD, BRCA, and SKCM (Figure 4(a)). These cancer types displayed lower expression of transcript variants 8, 3, 1, 2, and 4 (V8, V3, V1, V2, and V4) and higher expression of transcript variants 5, 6, 10, and 9 (V5, V6, V10, and V9) than those of other cohorts. BRCA and SKCM were clustered into one subclade, indicating that breast carcinoma had the closest relationship with skin cutaneous melanoma in this

Table 2: Association between the transcript expression of V6 and clinicopathological parameters in patients with BLBC.

Clinicopathological parameters	n	TPD52L2 expression High (>median)	Low (<median)	p value
Pathologic_T				
T1	22	6	16	0.0099*
T2	65	35	30	
T3	8	7	1	
T4	1	1	0	
Pathologic_M				
M0	94	48	46	1
M1	3	2	1	
Pathologic_stage				
Stage I	17	3	14	0.0101*
Stage II	63	35	28	
Stage III	13	9	4	
Stage IV	2	1	1	
Pathologic_N				
N0	61	29	32	0.6541
N1	24	13	11	
N2	8	5	3	
N3	4	3	1	

Age: at initial pathological diagnosis; pTNM: pathological tumor-node-metastasis; pT: pathological tumor; pN: pathological node. The median expression value was 4.251. *The significance of correlations between V6 expression and clinicopathological parameters was calculated by the χ^2 test, and Fisher's exact test was used when the patient number had an expected count < 5.

analysis. There were several minor clades, including one minor clade with higher expression of V8 in KICH, HNSC, LUSC, and KIRC and another minor clade with lower expression of V10 in LIHC, DLBC, UCEC, and ACC, when compared to other cancer types (Figure 4(a)). Gene structures of the transcripts, excluding the 3′-UTR and 5′-UTR, are shown in Figure 4(b), and the predicted intron/exon phases are marked. The transcripts in the same subclades exhibited highly conserved gene structural patterns.

We identified that V5 and V6 were the top two enriched transcripts in patients using the median value of one as the expression cutoff value (Figure 4(c)). Due to the higher abundance of V5 and V6 in BRCA patients, we hypothesized that one of the two transcripts could be translated into the functional protein TPD52L2 in BLBCs. We compared the expression of V5 and V6 in breast cancer tissues and paired adjacent normal tissues according to the PAM50 classification. V5 expression showed no difference between breast cancer tissues and paired adjacent normal tissues in any subtype. In contrast, V6 expression was markedly elevated in breast cancer tissues compared with paired adjacent normal tissues in all PAM50 subtypes, except the Her2-enriched subtype (Figures 4(d) and 4(e)). We also examined the expression of each transcript between breast cancer tissues and normal breast tissues of the GTEx dataset. V6 expression was markedly elevated in tumor tissues compared with normal tissues, whereas V5 and other transcripts showed no significant difference (Figure 4(f)). These clinical results suggested that V6 is most likely to be the functional transcript of the TPD52L2 protein.

3.4. TPD52L2 Knockdown Suppressed the Proliferation and Migration of BLBC Cells. Based on the clinical data, we hypothesized that TPD52L2 could help to maintain the malignant phenotypes of BLBC cells. We selected highly aggressive basal-like MDA-MB-231 cells and established a stable knockdown cell line via lentiviral infection of TPD52L2 shRNA (Figure 5(a)) [23]. We detected a dramatic decrease in cell proliferation via the CCK-8 assay and further observed that the ability to form colonies was remarkably suppressed in TPD52L2 stable knockdown cells (Figures 5(a) and 5(b)). The colony number of knockdown cells was less than 50% of that of the control cells (Figure 5(b)). Moreover, cell migration decreased significantly after TPD52L2 knockdown (Figure 5(c)). The migration rate of control cells was approximately 4-fold higher than that of knockdown cells. No change in cell apoptosis was detected using annexin V staining and flow cytometry (data not shown).

To determine the effect of TPD52L2 on tumorigenesis *in vivo*, we subcutaneously injected control and stable knockdown cells into nude mice and monitored tumor growth. As shown in Figure 5(d), the potential to form tumors was markedly decreased in the TPD52L2 stable knockdown line when compared to the control line at the same time. Tumor volumes of the control line reached over 1100 mm^3 in 28 days, whereas tumor volumes of the knockdown line were less than 400 mm^3 on the 27th day. The tumor weights of the knockdown line decreased more than 3-fold compared to those of the control line (Figure 5(e)).

Taken together, our findings revealed the impact of TPD52L2 on breast cancer patient survival and responses to radiation and targeted therapies, its association with pathological stages and lymph node metastasis, its enriched expression in BLBCs, and its important roles in maintaining malignant phenotypes and promoting tumor growth, establishing TPD52L2 as a novel biomarker in BLBC.

3.5. V6 Was Identified as the Functional TPD52L2 Protein in BLBC. We compared the amino acid sequences of ten protein isoforms of TPD52L2. V6 had the same molecular weight as the endogenous TPD52L2 protein, further supporting our hypothesis. To corroborate and expand the results, we investigated whether V5 or V6 was required to rescue the functional loss of TPD52L2 and to maintain the cancer-related phenotypes. We produced TPD52L2 inducible knockout cells using sgRNA with doxycycline-induced CAS9 according to CRISPR-Cas9 knockout techniques (Figure 5(f)). Our attempts to produce stable TPD52L2 knockout cells were not successful, suggesting that the BLBC cell lines we tested failed to survive without TPD52L2 function. All experiments were performed with the BLBC cell line MDA-MB-453 [23].

Consistent with the results of MDA-MB-231 stable knockdown cells, inducible depletion of TPD52L2 caused a dramatic decrease in MDA-MB-453 cell proliferation and migration, the levels of which were approximately 25% and 15% of those of the uninduced control line, respectively (Figures 5(g)–5(i)). V6 markedly increased cell proliferation in the colony formation assay in TPD52L2 inducible knockout cells, which had nearly the same number and size of colonies as the control line, and there was an increasing but nonsignificant trend (Figure 5(g)). V5 exerted an inhibitory effect on cell proliferation, with an approximately 2-fold decrease compared to that in the control cells (Figures 5(g) and 5(h)). Similarly, we observed a significant increase in cell migration upon expression of V6 in TPD52L2 inducible knockout cells, and the migration rate was restored to the same level as that in uninduced control cells (Figure 5(i)). V5 had no detectable effect on migration (Figure 5(i)). Therefore, V6 was proven to be the functional isoform of the TPD52L2 protein that positively regulates the oncogenesis phenotypes of BLBC.

3.6. Expression of V6 Is Closely Associated with the Clinicopathological Parameters of Breast Cancer. Finally, we analyzed the correlation between the expression of V6 and the clinicopathological parameters of patients in the BRCA cohort. As shown in Table 1, elevated V6 expression was strongly associated with higher pathological metastasis (pM) stage ($n = 928$, Fisher's exact test, $p = 0.008415$), higher pT stage ($n = 1087$, the χ^2 test, $p < 0.001$), and worse pathological stage ($n = 1068$, Fisher's exact test, $p < 0.001$). V6 expression was significantly higher in patients with pathological_M1 stage disease than in patients with pathological_M0 stage disease (Mann–Whitney test, $p = 0.0039$) (Figure 6(a)). The median expression value of 4.506 in patients with pathological_M1 stage was significantly higher than the median expression value of 4.218 in patients with pathological_M0 stage. V6 expression was slightly lower in patients with pathological_N0 status than in those with pathological_N1/2/3 status (Mann–Whitney test, $p < 0.05$) (Figure 6(b)). Additionally, patients with high V6 expression were more likely to develop advanced pathological T stage disease (Figure 6(c)). Breast cancer patients with pathological stage III/IV disease had higher V6 transcript expression than those with stage I/II (Figure 6(d)). No significant correlation was found between V6 expression and other clinical parameters, such as age, pathological node status (pN), ER expression, PR expression, and HER2 expression (Table 1).

More importantly, in BLBC, patients with high V6 expression were more likely to exhibit advanced pathological stage and worse pT stage disease than those with luminal A, luminal B, and Her 2-enriched subtypes (Figures 6(c) and 6(d)). V6 was increased in patients with pT3/4 stage disease compared with those with pT1/2 stage disease (Mann–Whitney test, $p = 0.0145$) (Figure 6(c), Table 2) and increased in parallel with pathological stage (stage I *vs.* stage II and stage III) (Figure 6(d), Table 2).

Furthermore, V6 was found to be a prognostic indicator for BRCA patients. Its elevated expression was closely associated with poor survival (Figure 6(e)). The overall survival of BRCA patients who received radiation therapy or targeted molecular therapy was closely correlated with V6 expression. Patients in the high V6 group had worse outcomes after radiation therapy or target molecular therapy than patients in the low V6 group (Kaplan–Meier survival analysis with log-rank test, radiation therapy: $p = 0.0002$; target therapy: $p = 0.046$) (Figure 6(f)).

4. Discussion

The well-known characteristics of BLBC include poor differentiation, squamous metaplasia (skin-like differentiation with or without sebaceous elements), lack of hormone receptor expression, high proliferation capacity, and expression of basal CKs [24]. More effective treatments and methods for identifying earlier-stage disease are urgently needed for this subtype. In the present study, we provided new clinical evidence that TPD52L2 is significantly upregulated in BLBCs versus non-BLBCs and that its high expression is closely associated with a poor prognosis in patients with BLBC. The finding that high TPD52L2 expression is closely related to advanced pathological stage may imply a relationship between TPD52L2 and tumorigenesis (Figure 1(f)). Generally, tumors of higher pathological stages grow and metastasize more rapidly than tumors of lower pathological stages. Therefore, the correlation between TPD52L2 expression and tumor pathological stage supports our study on the growth- and metastasis-promoting effects of TPD52L2 in BLBC cell lines. Furthermore, higher TPD52L2 expression was significantly predictive of worse clinical outcome in lymph node-positive patients with BLBC, indicating a potential relationship between TPD52L2 and malignancies with lymph node metastasis. A previous study reported that TPD52 was a radiation response biomarker in several cancer cell lines [3]. In our study, TPD52L2 gene expression was also proven to be closely associated with the efficacy and outcome of radiation therapy, as breast cancer patients with low TPD52L2 levels had longer survival times after radiation therapy, as well as target therapy, than those with high TPD52L2 levels (Figures 3(e) and 3(f)). Since our study mainly investigated the RNA level of TPD52L2 in patients with BLBC, a detailed clinical study of patients' TPD52L2 protein level by IHC staining is required to verify the relationship between TPD52L2 and tumorigenesis, and further studies are needed if that is the case. Overall, our clinical analyses demonstrated for the first time that TPD52L2 is closely associated with the development and progression of BLBC and suggests that TPD52L2 is a biomarker for BLBC patients.

Zhuang et al. showed that TPD52L2 overexpression inhibited colony formation and cell proliferation in luminal-type MCF7 cells [23]. Here, we presented new clinical evidence that TPD52L2 had no correlation with the prognosis of patients with luminal A and luminal B breast cancers and failed to predict the clinical outcomes of lymph node-positive patients with luminal subtype breast cancers (Figures 2(a) and 2(b)). Therefore, based on the positive correlation between TPD52L2 and the clinical parameters of BLBC, in our study, we examined the effects of TPD52L2

on the tumorigenesis of MDA-MB-231 and MDA-MB-453 cells and tumors derived from these cells. We found that decreased TPD52L2 expression by knockdown or knockout significantly inhibited cell growth *in vitro* and *in vivo*, and this inhibitory effect could be mainly attributed to TPD52L2-mediated positive regulation of cell proliferation. A currently accepted model for TPD52L2 cellular function involves its recognition of binding partners, including TPD52, TPD53, and several Rab GTPases, as well as its involvement in multiple membrane trafficking pathways: anterograde traffic, recycling, and Golgi integrity [11]. It is possible that TPD52L2 promotes BLBC progression partially due to its important roles in intracellular transport vesicles. However, the detailed molecular mechanisms in BLBC still need to be investigated in depth. Most recently, TPD52L2 was reported to be involved in cell migration, as it is a core protein of intracellular nanovesicles, in which it was proven to mediate $\alpha 5\beta 1$ integrin trafficking during the migration process [25]. Consistently, in the present study, we not only provided clinical evidence that patients with BLBC with high TPD52L2 levels had a significantly poorer prognosis than those with low levels but also provided novel experimental results that depletion of TPD52L2 inhibited cell migration, while overexpression of V6 reversed this inhibition in BLBC cells. This finding further supports that TPD52L2 is involved in the malignant phenotypes of human cancers.

Over the years, increasing evidence has shown that TPD52 family members have many transcript variants due to alternative splicing [22, 23, 26]. Different transcripts of a gene generated by alternative splicing are often translated into proteins with altered domains of composition, thus affecting their biological functions. The well-known transcription factor SREBP1, which mainly controls fatty acid synthesis, has two protein isoforms, SREBP1-a and SREBP1-c. They were generated from the same gene, *srebf1*, by posttranscriptional alternative splicing [27]. TPD52L2 has at least 10 transcript variants in human tissues [24]. To date, there is no compelling evidence about the transcript variant of TPD52L2 that plays the most important role in BLBC. In the present study, we utilized a two-step process to investigate the functional protein isoform of TPD52L2 in breast cancer. First, we analyzed the expression profile of ten transcript variants of *tpd52l2* in different cancer types from 33 cohorts of TCGA dataset via hierarchical clustering and verified two predominantly expressed transcript variants, V5 and V6, in breast cancer and several other cancer types (Figure 4(a)). Interestingly, in the present study, BRCA and SKCM were clustered into one subclade, proving that the expression profile of *tpd52l2* is associated with the squamous metaplasia characteristics of BLBCs. Moreover, a previous study proved that BRCA and SKCM have the most similar RNA expression patterns of all metastasis-associated genes among 11 cancer types in TCGA dataset [28]. We can infer that, to some extent, BRCA and SKCM share similarities in metastasis-related phenotypes and mechanisms. Next, we identified cancer-specific transcripts according to relative transcript levels between normal and cancer tissues and corroborated that V6 was the breast cancer-specific transcript. The specificity of V6 was further confirmed by comparing the molecular weights and amino acid sequences of all protein isoforms encoded by the ten transcript variants of the *tpd52l2* gene. Moreover, we overexpressed V5 and V6 in TPD52L2-depleted BLBC cells and excluded the possibility of V5, which failed to promote cell proliferation and migration (Figures 5(g) and 5(i)). Accordingly, using the clinical data from the BRCA cohort, we observed that the V6 transcript was remarkably upregulated in cancer tissues compared with paired adjacent normal tissues, and its high level was significantly associated with higher pathological T stage and pathological stage in BLBCs. These data further support the potential impact of TPD52L2 on cancer-related phenotypes (Figures 6(a)–6(d)). We also found that V6 expression could predict the prognosis of patients with SKCM and patients with MESO receiving radiation therapy or targeted therapy (data not shown). This result further supported the close relationship of BRCA and SKCM or MESO in the hierarchical clustering generated by the transcript expression profile of *tpd52l2* and provided solid evidence that V6 plays oncogenic roles in SKCM and MESO. Most recently, a detailed bioinformatic analysis revealed the oncogenic role of TPD52L2 in lung adenocarcinoma and demonstrated that its high expression is associated with immune infiltration and tumor immunosuppressive status, further supporting our results [29].

In summary, our current findings demonstrated that V6 of TPD52L2 is a novel biomarker for the prediction of clinical outcomes in BLBCs. V6 promotes cell proliferation and migration and has a close association with malignant phenotypes in BLBCs. Due to the association of V6 expression and patient prognosis after radiation therapy or targeted therapy in SKCM and MESO datasets, we recommend that further studies address whether TPD52L2 plays a similar malignancy-related role in other cancer types. More importantly, since the coiled-coil domain has been identified as an effective drug target for several severe disease treatments [30], our data indicated that TPD52L2 can be used as an effective biomarker and a therapeutic target for BLBC. Further investigations are required to achieve the clinical application, relieve patients' suffering, and overcome those incurable diseases.

Abbreviations

BC: Breast cancer
BLBC: Basal-like breast cancer
TCGA: The Cancer Genome Atlas
ACC: Adrenocortical carcinoma
BLCA: Bladder urothelial carcinoma
BRCA: Breast invasive carcinoma
CESC: Cervical squamous cell carcinoma
CHOL: Cholangiocarcinoma
COAD: Colon adenocarcinoma
READ: Rectum adenocarcinoma
DLBC: Diffuse large B-cell lymphoma
ESCA: Esophageal carcinoma
GBM: Glioblastoma multiforme
HNSC: Head and neck squamous cell carcinoma
KICH: Kidney chromophobe
KIRC: Kidney renal clear cell carcinoma
KIRP: Kidney renal papillary cell carcinoma

AML: Acute myeloid leukemia
LGG: Brain lower grade glioma
LIHC: Liver hepatocellular carcinoma
LUAD: Lung adenocarcinoma
LUSC: Lung squamous cell carcinoma
MESO: Mesothelioma
OVSC: Ovarian serous cystadenocarcinoma
PAAD: Pancreatic adenocarcinoma
PCPG: Pheochromocytoma and paraganglioma
PRAD: Prostate adenocarcinoma
SARC: Sarcoma
SKCM: Skin cutaneous melanoma
STAD: Stomach adenocarcinoma
TGCT: Testicular germ cell tumor
THCA: Thyroid carcinoma
THYM: Thymoma
UCEC: Uterine corpus endometrial carcinoma
UCS: Uterine carcinosarcoma
UVM: Uveal melanoma
SREBP1: Sterol regulatory element binding protein 1
INVs: Intracellular nanovesicles.

Data Availability

TCGA data is openly available in the public repository: https://xenabrowser.net. Kaplan–Meier data of the GSE96058 dataset is openly available in the published resource: http://kmplot.com/. Other data will be available on reasonable request from the authors.

Conflicts of Interest

The authors declare that they have no competing interests.

Acknowledgments

This work is financially supported by the Talent Research Fund of Weifang People's Hospital.

References

[1] L. Wilkinson and T. Gathani, "Understanding breast cancer as a global health concern," *The British Journal of Radiology*, vol. 95, no. 1130, 2022.

[2] S. Banerjee, J. S. Reis-Filho, S. Ashley et al., "Basal-like breast carcinomas: clinical outcome and response to chemotherapy," *Journal of Clinical Pathology*, vol. 59, no. 7, pp. 729–735, 2006.

[3] B. Gusterson and C. J. Eaves, "Basal-like breast cancers: from pathology to biology and back again," *Stem Cell Reports*, vol. 10, no. 6, pp. 1676–1686, 2018.

[4] H. H. Milioli, I. Tishchenko, C. Riveros, R. Berretta, and P. Moscato, "Basal-like breast cancer: molecular profiles, clinical features and survival outcomes," *BMC Medical Genomics*, vol. 10, no. 1, p. 19, 2017.

[5] J. R. Pollack, T. Sørlie, C. M. Perou et al., "Microarray analysis reveals a major direct role of DNA copy number alteration in the transcriptional program of human breast tumors," *Proceedings of the National Academy of Sciences of the United States of America*, vol. 99, no. 20, pp. 12963–12968, 2002.

[6] M. A. Rubin, S. Varambally, R. Beroukhim et al., "Overexpression, amplification, and androgen regulation of TPD52 in prostate cancer," *Cancer Research*, vol. 64, no. 11, pp. 3814–3822, 2004.

[7] A. Kamili, N. Roslan, S. Frost et al., "TPD52 expression increases neutral lipid storage within cultured cells," *Journal of Cell Science*, vol. 128, no. 17, pp. 3223–3238, 2015.

[8] Y. Abe, Y. Mukudai, M. Kurihara et al., "Tumor protein D52 is upregulated in oral squamous carcinoma cells under hypoxia in a hypoxia-inducible-factor-independent manner and is involved in cell death resistance," *Cell & Bioscience*, vol. 11, no. 1, p. 122, 2021.

[9] A. Delaidelli, C. Dunham, M. Santi et al., "Clinically tractable outcome prediction of non-WNT/non-SHH medulloblastoma based on TPD52 IHC in a multicohort study," *Clinical Cancer Research*, vol. 28, no. 1, pp. 116–128, 2022.

[10] M. Y. Hein, N. C. Hubner, I. Poser et al., "A human interactome in three quantitative dimensions organized by stoichiometries and abundances," *Cell*, vol. 163, no. 3, pp. 712–723, 2015.

[11] G. Larocque, P. J. La-Borde, N. I. Clarke, N. J. Carter, and S. J. Royle, "Tumor protein D54 defines a new class of intracellular transport vesicles," *The Journal of Cell Biology*, vol. 219, no. 1, article e201812044, 2020.

[12] M. J. Goldman, B. Craft, M. Hastie et al., "Visualizing and interpreting cancer genomics data via the Xena platform," *Nature Biotechnology*, vol. 38, no. 6, pp. 675–678, 2020.

[13] J. Vivian, A. A. Rao, F. A. Nothaft et al., "Toil enables reproducible, open source, big biomedical data analyses," *Nature Biotechnology*, vol. 35, no. 4, pp. 314–316, 2017.

[14] A. Lánczky and B. Győrffy, "Web-based survival analysis tool tailored for medical research (KMplot): development and implementation," *Journal of Medical Internet Research*, vol. 23, no. 7, article e27633, 2021.

[15] X. Zhang, Y. Zhao, C. Wang et al., "Rhomboid domain-containing protein 1 promotes breast cancer progression by regulating the p-Akt and CDK2 levels," *Cell Communication and Signaling: CCS*, vol. 16, no. 1, p. 65, 2018.

[16] T. Metsalu and J. Vilo, "ClustVis: a web tool for visualizing clustering of multivariate data using principal component analysis and heatmap," *Nucleic Acids Research*, vol. 43, no. W1, pp. W566–W570, 2015.

[17] B. Hu, J. Jin, A. Y. Guo, H. Zhang, J. Luo, and G. Gao, "GSDS 2.0: an upgraded gene feature visualization server," *Bioinformatics*, vol. 31, no. 8, pp. 1296-1297, 2015.

[18] F. Sievers, A. Wilm, D. Dineen et al., "Fast, scalable generation of high-quality protein multiple sequence alignments using Clustal Omega," *Molecular Systems Biology*, vol. 7, no. 1, p. 539, 2011.

[19] M. M. Saleh, M. Scheffler, S. Merkelbach-Bruse et al., "Comprehensive analysis of TP53 and KEAP1 mutations and their impact on survival in localized- and advanced-stage NSCLC," *Journal of Thoracic Oncology*, vol. 17, no. 1, pp. 76–88, 2022.

[20] J. S. Parker, M. Mullins, M. C. Cheang et al., "Supervised risk predictor of breast cancer based on intrinsic subtypes," *Journal of Clinical Oncology*, vol. 27, no. 8, pp. 1160–1167, 2009.

[21] Z. Qiang, L. Jun-Jie, W. Hai et al., "TPD52L2 impacts proliferation, invasiveness and apoptosis of glioblastoma cells via modulation of wnt/β-catenin/snail signaling," *Carcinogenesis*, vol. 39, no. 2, pp. 214–224, 2018.

[22] Y. Zhuang, R. C. Ly, C. V. Frazier et al., "The novel function of tumor protein D54 in regulating pyruvate dehydrogenase and metformin cytotoxicity in breast cancer," *Cancer & Metabolism*, vol. 7, no. 1, p. 1, 2019.

[23] R. M. Neve, K. Chin, J. Fridlyand et al., "A collection of breast cancer cell lines for the study of functionally distinct cancer subtypes," *Cancer Cell*, vol. 10, no. 6, pp. 515–527, 2006.

[24] F. Cunningham, J. E. Allen, J. Allen et al., "Ensembl 2022," *Nucleic Acids Research*, vol. 50, no. D1, pp. D988–D995, 2022.

[25] N. Niu, Y. Qin, B. L. Fridley et al., "Radiation pharmacogenomics: a genome-wide association approach to identify radiation response biomarkers using human lymphoblastoid cell lines," *Genome Research*, vol. 20, no. 11, pp. 1482–1492, 2010.

[26] Y. Fan, T. Hou, Y. Gao et al., "Acetylation-dependent regulation of TPD52 isoform 1 modulates chaperone-mediated autophagy in prostate cancer," *Autophagy*, vol. 17, no. 12, pp. 4386–4400, 2021.

[27] J. D. Horton, J. L. Goldstein, and M. S. Brown, "SREBPs: activators of the complete program of cholesterol and fatty acid synthesis in the liver," *The Journal of Clinical Investigation*, vol. 109, no. 9, pp. 1125–1131, 2002.

[28] F. Chen, Y. Zhang, S. Varambally, and C. J. Creighton, "Molecular correlates of metastasis by systematic pan-cancer analysis across The Cancer Genome Atlas," *Molecular Cancer Research*, vol. 17, no. 2, pp. 476–487, 2019.

[29] A. Zhong, T. Chen, T. Zhou, Z. Zhang, and M. Shi, "TPD52L2 is a prognostic biomarker and correlated with immune infiltration in lung adenocarcinoma," *Frontiers in Pharmacology*, vol. 12, article 728420, 2021.

[30] H. M. Strauss and S. Keller, "Pharmacological interference with protein-protein interactions mediated by coiled-coil motifs," *Handbook of Experimental Pharmacology*, vol. 186, pp. 461–482, 2008.

Hindawi
Oxidative Medicine and Cellular Longevity
Volume 2022, Article ID 2312784, 19 pages
https://doi.org/10.1155/2022/2312784

Research Article

Adjunctive Use of Active Compounds such as Chlorhexidine in the Nonsurgical Treatment of Peri-Implant Mucositis for Oral Health: A Systematic Review and Meta-Analysis

Rui Zhao,[1] **Sixin Liu**,[2] **Yiming Liu**,[1] **and Shuxia Cui**[1]

[1]*Department of Stomatology, The First Affiliated Hospital of Zhengzhou University, Zhengzhou, 450052 Henan, China*
[2]*University of Michigan School of Dentistry, 1011 N University Ave, Ann Arbor, MI 48109, USA*

Correspondence should be addressed to Rui Zhao; zhaorui37@163.com and Sixin Liu; lsx5859@163.com

Received 4 July 2022; Accepted 9 August 2022; Published 27 August 2022

Academic Editor: Tarique Hussain

Background. Peri-implant mucositis (PiM) is characterized as a reversible inflammatory change of the peri-implant soft tissues without alveolar bone loss or continuing marginal bone loss. Without proper control of PiM, the reversible inflammation may advance to peri-implantitis (PI). Mechanical debridement (MD) by the implant surface is the most common and conventional nonsurgical approach to treat PiM but with limitations in complete resolution of diseases. For more than a decade, chlorhexidine (CHX) and active compounds has been investigated in the treatment of PiM. Therefore, the aim of this systematic review and meta-analysis was to evaluate the efficacy of CHX treatment in combination with MD versus MD alone or MD+placebo in patients with PiM on their oral health problems. *Methods*. A search using electronic databases (Ovid MEDLINE, EMBASE, Science Direct databases, and Cochrane Central Register of Controlled Trials) and a manual search up to May 2022 were performed independently by 2 reviewers and included eligible randomized controlled trials (RCTs) comparing MD+CHX versus MD alone or MD+placebo. The assessment of quality for all the selected RCTs was conducted according to the Cochrane Handbook for Systematic Reviews of Interventions. Disease resolution of PiM (absence of BOP), IPPD reduction, IBOP% reduction, and PI% reduction after treatment as primary outcomes were selected as the primary outcomes. Weighted mean differences (WMD) and 95% confidence interval (CI) were for continuous outcomes, and odds ratio (OR) and 95% CI was for dichotomous outcomes using random effect models. This review is registered on the PROSPERO database (CRD42020221989). *Results*. After independent screening, nine eligible studies were included in this systematic review and meta-analysis. Meta-analysis showed OR of disease resolution between test and control groups amounted to 1.41 (95% CI (0.43, 4.65), $P = 0.57$, $I^2 = 65\%$) not favoring adjunctive CHX treatment over MD alone. Through subgroup analysis, the results indicated that oral irrigation of CHX may have more benefits on the resolution of PiM. Similarly, CHX did not significantly improve IPPD reduction at both short-, medium-, and long-term follow-up. Only a short-term effect has been observed at IBOP% reduction (WMD = 13.88, 95% CI (10.94, 16.81), $P < 0.00001$, $I^2 = 9\%$), IPI reduction (WMD = 0.12, 95% CI (0.09, 0.14), $P < 0.00001$, $I^2 = 0\%$), and FMPPD reduction (WMD = 0.19 mm, 95% CI (0.03, 0.35), $P = 0.02$, $I^2 = 0\%$) with adjunctive CHX application. *Conclusion*. Adjunctive CHX application may have some benefits to improve the efficacy of MD in PiM treatment by reducing IBOP%, IPI, and FMPPD in short-term. But these benefits disappeared at medium- and long-term follow-up. In order to achieve better disease resolution of PiM, adjunctive CHX irrigation with MD may be suggested and has positive potential. Well-designed large clinical trials are needed in future.

1. Introduction

Long-term success of dental implants supported fixed prostheses depends on healthy situation of soft and hard tissues surrounding implants [1]. Many complications such as biological complication including PiM and PI may affect the tissues surrounding implants and cause dental implant failure. PiM is characterized as a reversible inflammatory change of the peri-implant soft tissues without alveolar bone loss or continuing marginal bone loss, while peri-implatitis (PI) is

a chronic inflammation result in progressive loss of supporting bone [2, 3]. According to recent meta-analysis and systematic review, PiM occurred in approximately 21%–88% of subjects with implants and 9%–51% of the inserted implant sites, and weighted mean prevalence was 46.8% and 29.5%, respectively [4]. Moreover, without proper control of PiM, the reversible inflammation may advance to PI causing irreversible bone loss which is still a challenging complication because of the absence of predictable, evidence-based protocol [5]. Therefore, the management of PiM has critical clinical significance. It has been shown that the absence of signs of clinical inflammation is necessary for concluding healthy condition of peri-implant [6].

The basic treatment of PiM is to eliminate or suppress of bacterial biofilm and periodontal pathogens [7]. The mechanical debridement (MD) by implant surface using curettes is the most common and conventional nonsurgical approach [2]. However, limitations of this protocol still exist in the complete resolution of PiM due to the complex abutment connection geometry and the implant neck morphology [8]. Besides MD, many adjunctive therapies have been applied to increase the inflammation control and antimicrobial effect, such as air polishing, photodynamic treatment, local use of systemic antibiotics, and probiotics [9–12]. Among all peri-implant therapy adjuvants, chlorhexidine (CHX), a broad-spectrum bacteriostatic and bactericidal agent has been commonly used since 1950s and proved in dental plaque control and prevention of bacterial biofilm [13–16]. The use of CHX in dentistry and oral healthcare continues to be widespread and common usage includes (but is not limited to): the management of oral hygiene, dental plaque, and caries; gingivitis, periodontitis, and peri-implant disease; root canal therapy, oral surgery, and associated complications; oral mucosal disease and as a prerinse to reduce aerosolisation of microbes during dental procedures [14]. For example, CHX as a mouthwash applied in dentistry, not only have antimicrobial effect on local part but also have full-mouth effect on bacteria, fungus, and virus causative for various of different oral infectious disease [17]. For more than a decade, several studies have been conducted to investigate the adjunctive effectiveness of CHX in the nonsurgical treatment of PiM but with inconclusive results[13, 18–24]. Three factors may be explained to the heterogeneity in outcomes: (1) different case definitions of PiM in clinical studies; (2) the wide range of CHX concentration, frequency, and treatment duration applied in studies; and (3) different delivery systems of CHX, such as mouthwash, spray, and gel formulations. To date, only one systematic review included 4 studies to 2016 with weak quality of evidence suggested that the adjunctive CHX therapy may not improve outcomes with nonsurgical management of PiM [25].

Therefore, the purpose of this systematic review was to analyze the available scientific literature and conduct meta-analysis to evaluate whether adjunctive CHX therapy is effective in improving outcomes when compared with MD alone or combination with placebo in the nonsurgical treatment of PiM in humans.

2. Methods

2.1. Protocol. This systematic review was registered in PROSPERO (CRD42020221989) and conducted in accordance with the guidelines of the PRISMA statement (Preferred Reporting Items for Systematic Reviews and the principles of PRISMA statement) [26] and Cochrane Handbook for Systematic Reviews of Intervention [27].

2.2. Focused Question. The focused question of this systematic review was addressed according to the population, intervention, comparison, outcome (PICO), and principle [28]: "What is the effect of adjunctive CHX therapy in patients undergoing nonsurgical treatment of PiM when compared with MD alone or MD + placebo?"

Population: patients diagnosed with PiM based on similar case definitions in the publications.

Intervention: the use of CHX as adjuncts in nonsurgical treatment.

Comparison: the nonsurgical treatment without the use of CHX or combined with placebo.

Outcomes: the changes of signs of peri-implant mucosal inflammation, such as pocket probing depth (PPD), bleeding on probing (BOP), plaque index (PI), microorganism load, and species.

2.3. Search Strategy. Two reviewers (RZ and SX Liu) independently executed search and review of the literature to retrieve all relevant articles published up to and including May 2022. The following databases were included as electronic databases: Ovid MEDLINE, EMBASE, ScienceDirect databases, and Cochrane Central Register of Controlled Trials. A broad hand search was supplemented from the following journals: *Journal of Dental Research*; *Clinical Oral Implants Research*, *Clinical Implant Dentistry and Related Research*, *International Journal of Oral and Maxillofacial Implants*, *Journal of Periodontology*, and *Journal of Clinical Periodontology*. Finally, checking the references of all selected articles and related systematic reviews was comprised. If required, the corresponding authors were contacted and requested to provide missing data or information. In case there was any gray literature, we also searched the database System for Information on Grey literature in Europe (http://www.opengrey.eu) as recommended by high standards for systematic reviews. A commercially available software (Endnote X7; Thomson, London, UK) was used for electronic title management. Any disagreement concerning eligibility between the two reviewers during the first and second stage of the study selection was resolved by discussion or arbitration through a third reviewer (YM Liu) to reach a definitive decision.

The combination of key words from the Medical Subject Headings (MeSH) identified by an asterisk symbol (*) and free text terms included: Intervention OR Therapy OR Treatment OR Mechanical debridement OR MD Professionally administered plaque removal OR PARR OR non- surgical periodontal therapy OR non-surgical therapy OR Periodontal treatment OR Periodontal therapy AND Chlorhexidine OR Chlorhexidine* OR Chlorhexidine phosphanilate OR

Chlorhexidine gluconate OR zinc-Chlorhexidine OR chlorhexidine gluconate lidocaine hydrochloride OR CHX OR CHX formulations Probiotic treatment OR anti-microbial OR anti-infective AND Peri-implant diseases OR Peri-implant mucositis OR Mucositis* OR Peri-implant

The study inclusion and exclusion criteria are as follows:

During the first stage of the study selection, the titles and abstracts were screened and evaluated according to the following inclusion criteria: (1) English language; (2) randomized controlled clinical trial (RCT) in adult patients (>18 years); (3) assessed treatment of patients with a primary diagnosis of PiM according to standard diagnostic criteria [3]; (4) comparison of MD+CHX versus MD+placebo or MD alone; and (5) reported data in terms of clinical parameters about peri-implant mucosal inflammation (i.e., PPD, BOP, and PI) or microbial outcome.

At the second stage of the selection, all full-text articles selected in the first stage were identified according to the following exclusion criteria: (1) not RCT study design; (2) inadequate case definition; (3) inclusion of less than 10 patients; (4) received surgical treatment or other active interventions (e.g., air abrasive therapy, antibiotics therapy); (5) a follow-up assessment less than 8 weeks; (6) reported without clinical data of PiM inflammation; and (7) *in vitro* and animal model studies, case report, letters to the editor, opinion articles, review articles, interviews, and monographs.

2.4. Risk of Bias (Quality) Assessment. Risk of bias assessment for all the selected RCTs using the *Cochrane Handbook for Systematic Reviews of Interventions* [27] from seven criteria (random sequence generation; allocation concealment; blinding of participants and personnel; blinding of outcome assessment; incomplete outcome data; selective reporting; and other bias) was performed by two reviewers (RZ and SX Liu) independently. In general, studies were rated as "high risk of bias" (high), "low risk of bias" (low), or "unclear risk of bias" (?). Both reviewers discussed and resolved any disagreements.

2.4.1. Data Items. The meta-analysis estimated diseases resolution of PiM (absence of BOP), IPPD, IBOP%, and PI% reduction after treatment as primary outcomes. Secondary outcomes included reduction of FMPPD, FMBOP%, FMPI, and changes in microorganism number and species.

2.4.2. Data Synthesis. Data extraction was conducted by two blinded reviewers (RZ and SX Liu) from the included articles into predesigned data extraction template on Microsoft Excel: (1) study identification: first author's name, year of publication, journal's name and country; (2) study design (RCTs); (3) number of dental implants (4) population (subjects): sample size, gender, mean, and age range in years; (5) PiM diagnostic criteria; (6) group assessed; (7) intervention: details of CHX administration including dose, concentration, frequency, duration, any pre-treatment (mechanical or chemical disinfection) and vehicle, and oral hygiene instruction; (8) smoking habits; (9) follow-up; and (10) primary and secondary outcomes and observation period. Electronic mails were sent to respective authors in order to retrieve any relevant unpublished data that we could not extract. Any discrepancies were resolved by discussion with a third examiner (YM Liu).

2.4.3. Analysis Method. Heterogeneity between RCT's meta-analysis was tested and evaluated through Q and I^2 test. Q test was used to estimate the between-studies variation. When a P value of Q statistic was <0.1, it was defined as an indicator of heterogeneity. The threshold for the interpretation of I^2 values was also used to estimate the heterogeneity as follows: 0–30% (low heterogeneity), 30–60% (moderate heterogeneity), >60% (substantial heterogeneity). Differences between the MD+CHX and MD alone or MD +placebo groups were expressed as weighted mean differences (WMD) and 95% confidence interval (CI) for continuous outcomes, and odds ratio (OR) and 95% CI for dichotomous outcomes, using random effect models. For continuous data, mean differences and standard errors were entered for each study. If data were not reported in terms of mean differences, the mean difference was calculated and the standard deviation was estimated using the $r_d = \text{sqrt}(r_1{}^2/n_1 + r_2{}^2/n_2)$ formula. The meta-analysis was performed using Review Manager software (RevMan, version 5.3 for Windows).

3. Results

3.1. Study Selection. The flow diagram of the screening process is described in Figure 1. A total of 104 potentially relevant titles and abstracts were identified through the electronic and manual search. Among them, 88 articles were excluded based on the title and abstract after removing the duplicates. Therefore, 15 remaining articles were assessed for complete evaluation, but among them four were further excluded at this stage because they did not fulfill the inclusion criteria. One study conducted at the same center and on the same date was reported in two separate papers which provided clinical data of implant [23] and full mouth [29]. Similarly, Philip et al. conducted a study at Academic Centre for Dentistry Amsterdam and published two articles, respectively, about clinical changes[21] and microbiome[30]. Therefore, we combined the data of two articles and analyzed as one study for this review [21, 23].

Finally, nine studies met the inclusion criteria and were included in this systematic review [18, 20–23, 29–31].

3.2. Study Characteristics. Table 1 reports the general characteristics and conclusions of the 9 included studies. All of them were RCTs conducted at a single center with a parallel design and published in the English language from 2002 to 2021, spanning 19 years. The average number of participants per study was 38.5 with a minimum of 13 [24] and a maximum of 89 [21]. The average ages of patients involved in studies were range from 41.5 to 70 years old. The follow-up period of included studies ranged from 3 months [13, 18, 19, 21, 22, 31] to 12 months [23].

3.3. Treatment Modalities. Oral hygiene instructions were provided in all the studies. Nonsurgical mechanical therapy was performed with ultrasonic devices and polishing at

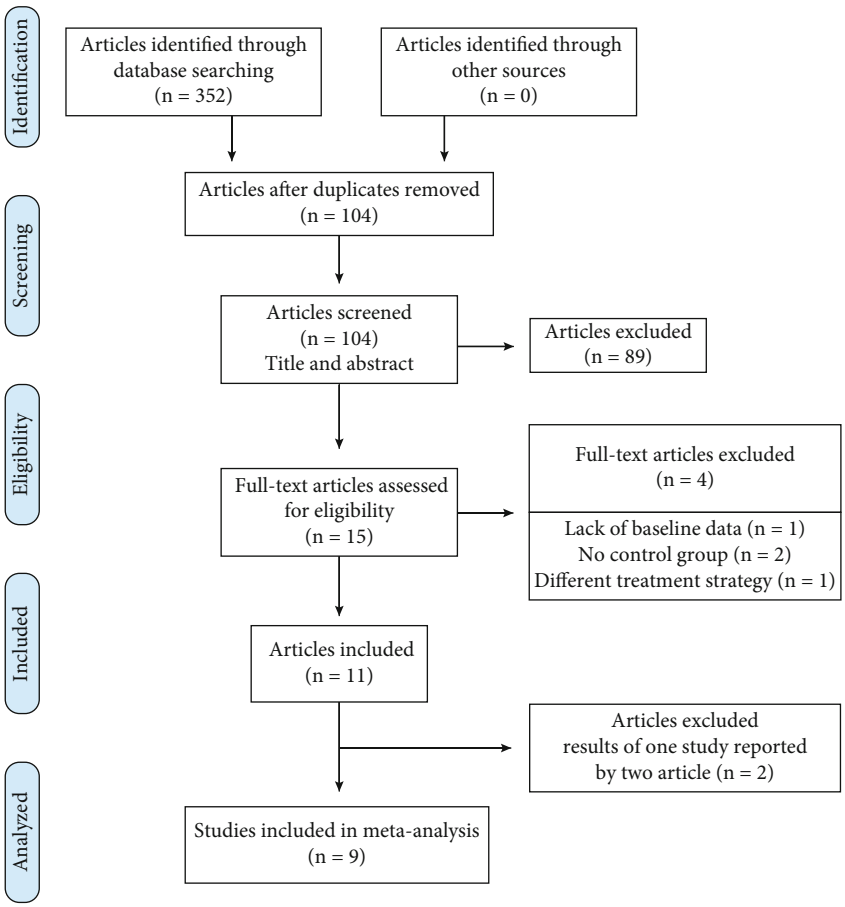

Figure 1: Flow chart of literature search and inclusion.

baseline. Prescribed CHX varied in types (mouth rinses, gels, spray, and irrigation devices), concentration (0.03%, 0.06%, 0.12%, 0.2%, 0.5%, and 1%), frequency (once or twice a day), and period of intake (10 or 14 days, 4 or 12 weeks, and 1 year). As the application of CHX gel was always combined with CHX mouth rinse [24], we did the subgroup analysis according to oral irrigation and mouth rinse/gel in meta-analysis. The types of administration were as follows: three trials used mouth rinse [13, 21, 23], two trails used gel [19, 31], one trail used irrigation [18], and three trails used both irrigations and mouth rinse [20, 22, 24]. All studies were placebo-controlled except one study [22].

Four studies included only nonsmokers or former smokers [13, 18, 20, 22], and five studies included both nonsmokers and smokers and reported the constituents of different smoking types [19, 21, 23, 24, 31]. Number of subjects, six distribution, and mean age in each group were always reported (Table 1).

3.4. Risk of Bias. The results of the risk of bias assessment within studies are depicted in Figure 2. Though we tried our best to contact corresponding authors of included studies to seek information according to the advice in Section 16.1.2 of the Cochrane Handbook, no response was obtained. Only one study did not describe the process of randomization and allocation concealment [22]. Porras et al. [22] did not use placebo in the control group; thus, the blinding to the participants cannot be achieved. Two studies did not explain the binding of outcome assessment [18, 24]. The study of Alzoman et al. [13], Hallstrom et al. [31], and Bunk et al. [18] did not report the mean and standard deviation of IPPD or IBOP%, which lead to an incomplete outcome data. Three studies included in this systematic review were considered with a low risk of bias.

3.5. Study Outcomes. In detail, the main outcomes and statistical differences between the test group (MD+CHX) and control group (MD+placebo/MD alone) were described and summarized in Table 1.

3.6. Disease Resolution. Absence of BOP-positive site around implant was the sign of achieving complete disease resolution [21], and there were four studies reported the results of diseases resolution at final visit. Bunk et al. reported more percentage of disease resolution in the CHX group (95%) than the control group (50%) at 12 weeks ($P < 0.05$). On the contrary, three studies [21, 23, 24] found similar disease resolution percentage between two groups. Overall diseases resolution rates of PiM were 62.92% with CHX and 55.95% with control, which did not differ significantly (OR = 1.41 (95% CI (0.43, 4.65), $P = 0.57$)). Interstudy heterogeneity appeared significant regarding disease resolution

Table 1: Characteristics of the included studies.

Study journal region	Type	Number of implants	Clinical parameters	Subjects M/F age	Peri-implant mucositis definition	Treatment	CHX administration	Smoking	Follow-up	Mean (SD) outcome
Porras et al. [22] *J Periodontol* American	RCT single-blind parallel	28	IPPD, ICAL, microbiological parameters	16 NG 58.9	BOP + plaque + PD ≤ 5 mm + incipient radiographic lesion	With OHI, MD alone (control), MD + CHX (test)	Local irrigation with 0.12% CHX and topical application of CHX gel were conducted after MD. 0.12% CHX mouthrinse twice a day for 10 days.	No	3 months (days 30, 90)	Test: IPPD: 3.27 (SD:0.81) (BL) to 2.71 (SD: 0.7) (3 months) (sign.) ICAL: 2.63 (SD:1.6) (BL) to 2.3 (SD:1.5) (3 months) Control: IPPD: 3.48 (SD: 0.61) (BL) to 2.55 (SD: 0.72) (3 months) (sign.) ICAL: 3.08 (SD: 1.27) (BL) to 2.01 (SD: 1.23) (3 months) (sign.)
Thone-Muhling et al. [24] *Clin Oral Impl Res* Germany	RCT single-blind parallel	36	IPPD, FMPPD, IGR, FMGR, ICAL, FMCAL, IBOP%, FMBOP%, IGI, FMGI, IPI, FMPI	13 8 : 5 51.5	BOP and/or GI ≥ *I* + no evidence of radiographic bone loss	With OHI, MD alone (control), MD +CHX (test)	Topical application of I% CHX gel once and brush at dorsal of tongue; tonsil was sprayed with 0.2% CHX spray once day and 0.2% CHX mouthrinse twice daily for 14 days.	38%	8 months (days 30, 60, 120, 240)	Test: IPPD: 3.49 (SD: 0.78) (BL) to 3.03 (SD: 0.46) (4 months) FMPPD: 2.4 (SD: 0.48) (BL) to 2.28 (SD: 0.4) (4 months) IGR: 0.21 (SD: 0.25) (BL) to 0.25 (SD: 0.37) (4 months) FMGR: 0.78 (SD: 0.55) (BL) to 0.81 (SD: 0.57) (4 months) ICAL: 3.7 (SD: 0.72) (BL) to 3.29 (SD: 0.38) (4 months) FMCAL: 3.19 (SD: 0.72) (BL) to 3.08 (SD: 0.49) (4 months) IBOP%: 22 (SD: 11) (BL) to 8 (SD: 9) (4 months) (sign.) FMBOP%: 9 (SD: 9) (BL) to 7 (SD: 7) (4 months) IGI: 0.6 (SD: 0.24) (BL) to 0.23 (SD: 0.23) (4 months) FMGI: 0.33 (SD: 0.19) (BL) to 0.18 (SD: 0.13) (4 months) (sign.) IPI: 0.02 (SD: 0.04) (BL) to 0.02 (SD: 0.04) (4 months) FMPI: 0.18 (SD: 0.07) (BL) to 0.17 (SD: 0.09) (4 months) Control: IPPD: 3.4 (SD: 0.62) (BL) to 2.92 (SD: 0.63) (4 months) (sign.) FMPPD: 2.36 (SD: 0.39) (BL) to 2.19

Table 1: Continued.

Study journal region	Type	Number of implants	Clinical parameters	Subjects M/F age	Peri-implant mucositis definition	Treatment	CHX administration	Smoking	Follow-up	Mean (SD) outcome
										(SD: 0.34) (4 months) IGR: 0.33 (SD: 0.42) (BL) to 0.36 (SD: 0.47) (4 months) FMGR: 1.13 (SD: 0.5) (BL) to 1.26 (SD: 0.55) (4 months) ICAL: 3.73 (SD: 0.38) (BL) to 3.28 (SD: 0.38) (4 months) (sign.) FMCAL: 3.48 (SD: 0.31) (BL) to 3.45 (SD: 0.49) (4 months) IBOP%: 17 (SD: 19) (BL) to 8 (SD: 9) (4 months) FMBOP%: 5 (SD: 4) (BL) to 5 (SD: 4) (4 months) IGI: 0.62 (SD: 0.36) (BL) to 0.34 (SD: 0.24) (4 months) FMGI: 0.29 (SD: 0.11) (BL) to 0.18 (SD: 0.08) (4 months) (sign.) IPI: 0.01 (SD: 0.02) (BL) to 0.13 (SD: 0.3) (4 months) FMPI: 0.15 (SD: 0.07) (BL) to 0.2 (SD: 0.13) (4 months)
Heitz-Mayfield et al. [19] *Clin Oral Impl Res* Australia	RCT placebo double-blind parallel	29	IBOP-positive sites, IPPD, total DNA count	29 14 : 15 69	BOP+no evidence of radiographic bone loss	With OHI, MD+placebo (control), MD +CHX (test)	Dental gel containing 0.5% CHX for 4 weeks	50%/ 33%	3 months (days 30.90)	Test: IPPD: 3.67 (SD: 0.92) (BL) to 3.12 (SD: 0.92) (3 months) Total DNA count: 5.24 (SD: 0.5) (BL) to 5.31 (SD: 0.48) (3 months) Control: IPPD: 3.6 (SD: 0.95) (BL) to 2.97 (SD: 0.85) (3 months) Total DNA count: 5.44 (SD: 0.37) (BL) to 5.09 (SD: 0.53) (3 months)
Menezes et al. [20] *J Periodontal* Brazil	RCT placebo double-blind parallel	119	IPI%, IGBI%, IPPD, IBOP%, IKM width	50 42/58 55.96/ 61.16	BOP+no radiographic signs of bone loss	With OHI, MD+placebo (control), MD +CHX (test)	CHX solutions applied to brush dorsum of tongue, subgingival irrigation and rinsing twice daily for 14 days.	No	6 months (days 30, 90, 180)	Test: IPI%:38.52 (SD: 34.02) (BL) to 10.24 (SD: 20.09) (3 months) (sign.) IGBI%: 36.88 (SD: 32.47) (BL) to 10.24 (SD: 22.07) (3 months) (sign.) IPPD: 2.85 (SD: 0.6) (BL) to 2.34 (SD: 0.54) (3 months) (sign.) IBOP%: 75.82 (SD: 33.98) (BL) to

Table 1: Continued.

Study journal region	Type	Number of implants	Clinical parameters	Subjects M/F age	Peri-implant mucositis definition	Treatment	CHX administration	Smoking	Follow-up	Mean (SD) outcome
										40.44 (SD: 35.64) (3 months) (sign.) IKM width: 1.61 (SD: 1.76) (BL) to 1.29 (SD: 1.71) (3 months) (sign.) Control: IPI%: 52.15 (SD: 32.2) (BL) to 13.79 (SD: 25.72) (3 months) (sign.) IGBI%: 28.01 (SD: 32.47) (BL) to 9.48 (SD: 14.68) (3 months) (sign.) IPPD: 2.72 (SD: 0.68) (BL) to 2.37 (SD: 0.6) (3 months) (sign.) IBOP%: 67.54 (SD: 34.38) (BL) to 44.59 (SD: 36.1) (3 months) (sign.) IKM width: 1.68 (SD: 1.61) (BL) to 1.74 (SD: 1.56) (3 months) (sign.)
Hallstrom et al. [31] *Int J Dent Hygiene* Sweden	RCT placebo double-blind parallel	37	FMPI%, FMBOP%, FMPPD%, IPPD%	37 20 : 17 69	PD ≥ 4 mm and/or BOP + CBL < 2 mm	With OHI, MD+placebo (control), MD +CHX (test)	Dental gel containing 0.2% CHX digluconate, once daily for 12 weeks	65%	3 months (days 28, 84)	Test: FMPI%: 27 (BL) to 20 (3 months) (sign.) FMBOP%: 18 (BL) to 14 (3 months) FMPPD%: 5 (BL) to 4 (3 months) IPPD%: 69 (BL) to 33 (3 months) (sign.) Control: FMPI%: 23 (BL) to 20 (3 months) (sign.) FMBOP%: 18 (BL) to 14 (3 months) FMPPD%: 6 (BL) to 4 (3 months) IPPD%: 70 (BL) to 55 (3 months)
Pulcini et al. [23] *J Clin Periodontol/ Bollain et al. [29] Clin Oral Invest* Spain	RCT placebo double-blind parallel	One or more per subject	PI, IBOP%, IPPD, CLI, microbiological parameters, FMPI, FMBOP%, FMPPD, staining	54 27 : 27 61.15	BOP and/or suppuration +no evidence of radiographic bone loss	With OHI +airpolishing, MD+placebo (control), MD +CHX (test)	0.03% CHX and 0.05% CPC mouthrinse, twice daily for 1 year	7.4%/ 14.8%	12 months (6, 12 months)	Test: IBOP%: 58.64 (SD: 27.49) (BL) to 10.42 (SD: 13.74) (12 months) (sign.) IPI: 0.48 (SD: 0.26) (BL) to 0.18 (SD: 0.22) (12 months) (sign.) IPPD: 3.36 (SD: 0.78) (BL) to 2.5 (SD: 0.43) (12 months) (sign.) CLI: 8.63 (SD: 1.97) (BL) to 9.1 (SD: 1.86) (12 months) FMPI: 0.52 (SD: 0.3) (BL) to 0.178 (SD: 0.14) (12 months) (sign.) FMBOP%: 29.95 (SD: 12.3) (BL) to 5.5 (SD: 5.75) (12 months) (sign.) FMPPD: 2.45 (SD: 0.56) (BL) to 2.41 (SD: 0.4) (3 months) Control: IBOP%:46.3 (SD: 24.17) (BL) to 14.39 (SD: 18.04) (12 months) (sign.) PI: 0.54 (SD: 0.3)

Table 1: Continued.

Study journal region	Type	Number of implants	Clinical parameters	Subjects M/F age	Peri-implant mucositis definition	Treatment	CHX administration	Smoking	Follow-up	Mean (SD) outcome
										(BL) to 0.25 (SD: 0.29) (3 months) (sign.) IPPD: 3.38 (SD: 0.6) (BL) to 2.57 (SD: 0.57) (12 months) (sign.) CLI: 9.45 (SD: 2.19) (BL) to 10.09 (SD: 2.15) (12 months) FMPI: 0.48 (SD: 0.3) (BL) to 0.23 (SD: 0.21) (12 months) (sign.) FMBOP%: 27.65 (SD: 9.6) (BL) to 7.98 (SD: 7.55) (12 months) (sign.) FMPPD: 2.63 (SD: 0.26) (BL) to 2.54 (SD: 0.32) (3 months)
Bunk et al. [18] *Clin Oral Impl Res* Germany	RCT placebo single-blind parallel	40	IPI, IBOP-positive sites, prevalence of PiM, mucositis Severity score	40 17 : 23 70	BOP and/or suppuration +no evidence of radiographic bone loss	With OHI, MD alone (control), MD +CHX (test)	0.06% CHX oral irrigation, once daily for 12 weeks	No	3 months (days 28, 56, 84)	Test: IBOP-positive sites: 2.4 (SD: 0.88) (BL) to 0.1 (SD: 0.45) (3 months) (sign.) mucositis severity score: 9.05 (SD: 1.79) (BL) to 2.1 (SD: 2.22) (3 months) (sign.) IPI: 1.26 (SD: 0.4) (BL) to 0.79 (SD: 0.6) (3 months) (sign.) prevalence of PiM: 100% (BL) to 5% (3 months) (sign.) Control: IBOP-positive sites: 2.35 (SD:0.99) (BL) to 0.85 (SD: 1.09) (3 months) (sign.) mucositis severity score: 9.05 (SD: 2.54) (BL) to 4.5 (SD: 3.27) (3 months) (sign.) IPI: 1.33 (SD: 0.52) (BL) to 0.83 (SD: 0.63) (3 months) (sign.) Prevalence of PiM: 100% (BL) to 50% (3 months, implant level) (sign.)
Alzoman et al. [13] *Oral Hlth Prev dent* Saudi Arabia	RCT placebo double-blind parallel	32		32 20 : 12 41.25	BOP and/or erythema, swelling, suppuration pus+CBL < 2 mm	With OHI MD+placebo (control), MD +CHX (test)	0.12% CHX mouthrinse, twice daily for 2 weeks	No	3 months (days 21, 42, 84)	Test: IPI: 0.42 (SD: 0.02) (BL) to 0.07 (SD: 0.04) (3 months) (sign.) IBOP%: 51.1 (SD: 0.5) (BL) to 9.42 (SD: 4.84) (3 months) (sign.) IPPD:4.2 (SD: 0.3) (BL) to 2.09 (SD: 0.32) (3 months) (sign.) Control: IPI: 0.43 (SD: 0.04) (BL) to 0.33 (SD: 0.04) (3 months) IBOP%: 48.7 (SD: 1.3) (BL) to 36.4 (SD: 4.84) (3 months) IPPD:4.1 (SD: 0.3) (BL) to 3.37 (SD: 0.5) (3 months)

Table 1: Continued.

Study journal region	Type	Number of implants	Clinical parameters	Subjects M/F age	Peri-implant mucositis definition	Treatment	CHX administration	Smoking	Follow-up	Mean (SD) outcome
Philip et al. [21] J Clin Periodontol/ Philip et al. [30] J Clin Periodontol Netherlands	RCT placebo double-blind parallel	One or more per subject	IPI, IBI, IBOP%, IPPD, FMPI, FMGI, FMBOP%, FMPPD, percentages of completed patients, microbiological parameters	89 48/41 61.87	BOP and/or erythema, swelling, suppuration pus +CBL < 2 mm	With OHI, MD+placebo (control), MD +CHX (test)	0.2% CHX mouthrinse, twice daily for 1 month	13%/ 11%	3 months (days 30, 90)	Test: IPI: 0.61 (SD: 0.54) (BL) to 0.52 (SD: 0.41) (3 months) IBI: 1.03 (SD: 0.44) (BL) to 0.28 (SD: 0.3) (3 months) (sign.) IBOP%: 43.88 (SD: 22.52) (BL) to 8.88 (SD: 12.17) (3 months) (sign.) IPPD: 3.44 (SD: 0.6) (BL) to 2.76 (SD: 0.47) (3 months) (sign.) FMPI: 0.5 (SD: 0.23) (BL) to 0.08 (SD: 0.07) (3 months) (sign.) FMGI: 0.32 (SD: 0.33) (BL) to 0.36 (SD: 0.23) (3 months) FMBOP%: 10.27 (SD: 8.82) (BL) to 2.26 (SD: 2.14) (3 months) (sign.) FMPPD: 2.67 (SD: 0.31) (BL) to 2.62 (SD: 0.3) (3 months) Control: IPI: 0.6 (SD: 0.5) (BL) to 0.33 (SD: 0.25) (3 months) (sign.) IBI: 1.08 (SD: 0.52) (BL) to 0.19 (SD: 0.32) (3 months) (sign.) IBOP%: 47.02 (SD: 24.45) (BL) to 7.73 (SD: 13.96) (3 month) (sign.) IPPD: 3.17 (SD: 0.78) (BL) to 2.4 (SD: 0.67) (3 month) (sign.) FMPI: 0.61 (SD: 0.27) (BL) to 0.06 (SD: 0.08) (3 months) (sign.) FMGI: 0.3 (SD: 0.41) (BL) to 0.29 (SD: 0.19) (3 months) FMBOP%: 8.64 (SD: 6.89) (BL) to 1.86 (SD: 2.98) (3 months) (sign.) FMPPD: 2.46 (SD: 0.38) (BL) to 2.5 (SD: 0.47) (3 months)

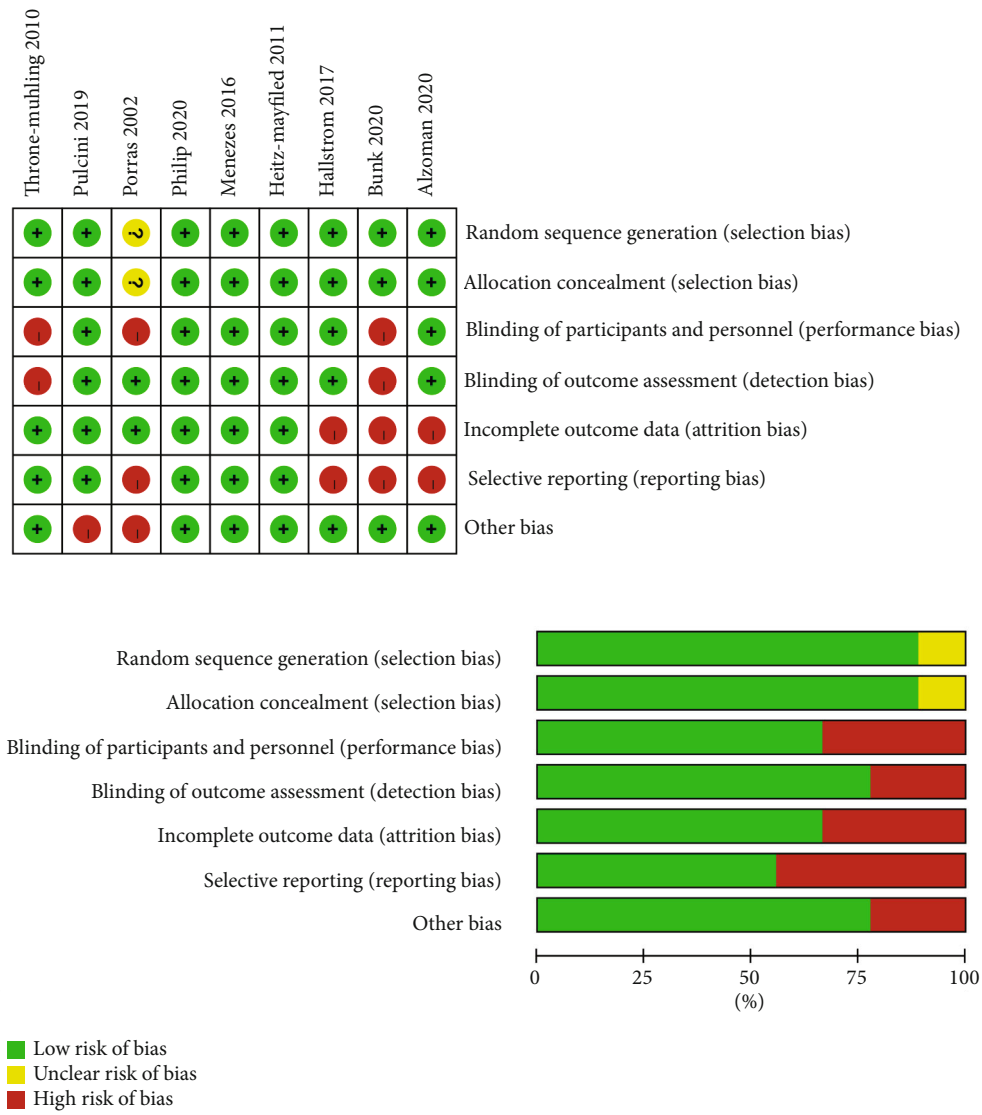

Figure 2: Quality assessment of the selected studies (The Cochrane Collaboration tool for assessing risk of bias).

($P < 0.05$, $I^2 = 65\%$). Hence, subgroup analysis was conducted and could explain heterogeneity based on variation in CHX types (Figure 3). The results indicated that oral irrigation of CHX may have more benefits on the resolution of PiM.

3.7. PPD Reduction. Pocket probing depth around the implant was evaluated by seven studies at different time intervals. In the study of Porras et al., as the control group showed greater IPPD than the test group at the baseline, so the reduction of IPPD of the control group was significantly greater compared to the test group at 3 months. Five studies showed a significant reduction of IPPD in both the test and control groups and did not highlight the differences between them [19–21, 23, 24]. Only one study reported the IPPD of the test group was significantly lower than control group at both 3, 6, and 12 weeks of follow-up [13]. Mean IPPD reduction regarding MD+CHX treatment at the end of observation period ranged from 0.36 (±0.6) [20] to 2.11 (±0.31) mm [13], while this reduction ranged from 0.23 (±0.68) [20] to 2.17 (±0.24) mm [13] for control.

Four studies [19, 21, 22, 24] reported IPPD reduction at 1 month after treatment and the WMD in IPPD reduction between the experimental and control groups amounted to -0.07 mm (95% CI (-0.25, 0.11), $P = 0.43$) not favoring the additional CHX therapy (P value for heterogeneity: 0.67, $I^2 = 0\%$ = low heterogeneity) (Figure 4(a)). Similar results were found at longer term and the WMD of -0.02 mm (95% CI (-0.26, 0.22), $P = 0.84$) (P value for heterogeneity: 0.46, $I^2 = 0\%$ = low heterogeneity) for 2-4 months and the WMD of 0.09 mm (95% CI (-0.07, 0.25), $P = 0.26$) (P value for heterogeneity: 0.88, $I^2 = 0\%$ = low heterogeneity) for more than 6 months follow-up.

At full mouth level, the full mouth pocket probing depth (FMPPD) were recorded by three studies [21, 24, 29] and meta-analysis were conducted at different time points. More FMPPD reduction was observed following CHX adjunctive therapy at 1 month with the WMD of 0.19 mm (95% CI (0.03, 0.35, $P = 0.02$) (P value for heterogeneity: 0.94, $I^2 = 0\%$ = low heterogeneity) (Figure 4(b)), whereas no significant difference was found at 2-4 months (0.02, 95% CI

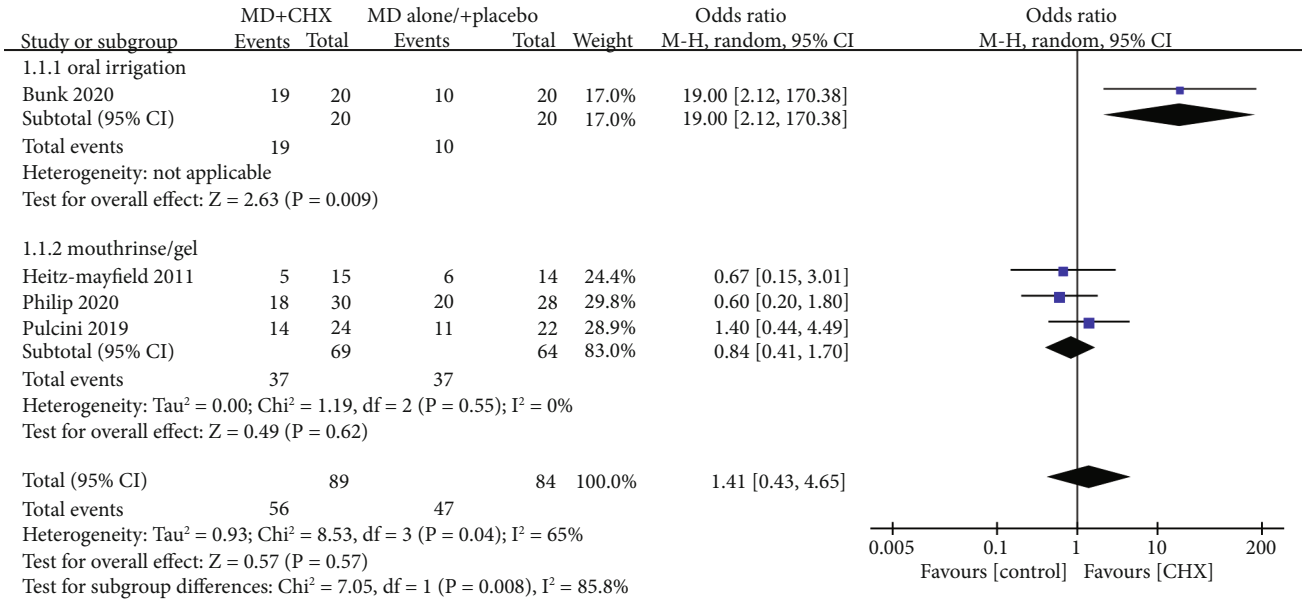

Figure 3: Forest plot of disease resolution of PiM.

(-0.16,0.21), $P = 0.8$) and ≥6 months (-0.02, 95% CI (-0.23,0.19), $P = 0.85$) between the experimental and control groups. The interstudy heterogeneity was both low, given an I^2 of 0%.

3.8. BOP Changes. Implant bleeding on probing sites (IBOP%) were expressed as percentage of sites with bleeding of the total number of available sites and evaluated by eight studies [13, 18–21, 23, 24, 31]. Three studies [13, 22, 23] showed a significant difference of IBOP% reduction in favor of the MD+CHX treatment. However, the other studies did not report differences between groups. Mean IBOP% reduction regarding the MD+CHX treatment at the end of observation period ranged from 6 (±10) [24] to 57.5 (±25.75) [18], while this reduction ranged from 0 (±21) [24] to 45 (±28.75) [18] for control.

At 1-month follow-up, four studies were included to conduct meta-analysis and the WMD in IBOP% reduction between the experimental and control groups amounted to 13.88 (95% CI (10.94, 16.81), $P < 0.00001$) (P value for heterogeneity: 0.35, $I^2 = 9\%$ = low heterogeneity) (Figure 5(a)). So, there was greater IBOP% reduction with MD+CHX indicating adjunctive CHX treatment was effective at 1 month. However, at 2-4 months (1.32, 95% CI (-1.55, 4.18), $P = 0.37$) and ≥6 months (4. 6, 95% CI (-4.36, 13.55), $P = 0.31$) of follow-up, the experimented group presented similar IBOP% changes with control group. The interstudy heterogeneity was both low, given an I^2 of 0%.

At full mouth level, the full mouth bleeding on probing sites (FMBOP%) were recorded by three studies[21, 24, 29] and meta-analysis were conducted at different time points. The meta-analysis failed to show a significant FMBOP% reduction at both 1 month (2.07, 95% CI (-1.16, 5.3), $P = 0.21$), 2-4 months (1.18, 95% CI (-2.02, 4.38), $P = 0.47$) and ≥6 months (4.95% CI (-2.33, 10.33), $P = 0.22$) follow-up between MD+CHX and control (Figure 5(b)). The interstudy heterogeneity was both low, given an I^2 of 0%.

3.9. PI Changes. Six studies performed the measurement of the implant plaque index (IPI) around the selected implants [13, 18, 20, 21, 23, 24]. Bunk et al. found the change of IPI seems to be highly dependent upon IPI measured at baseline. But, in the studies of Menezes et al. and Pulcini et al., the IPI of the control group were higher than the test group at baseline. Mean IPI reduction regarding MD+CHX treatment at the end of observation period ranged from 0.01 (±0.03)[24] to 0.46 (±0.48)[18], while this reduction ranged from 0.1 (±0.16)[13] to 0.4 (±0.28) [20] for control.

At 1-month follow-up, based on four studies, the WMD in IPI reduction between the experimental and control groups amounted to 0.12 (95% CI (0.09, 0.14), $P < 0.00001$) favoring the additional CHX therapy (P value for heterogeneity: 0.63, $I^2 = 0\%$ = low heterogeneity) (Figure 6(a)). But no significant difference was observed at 2-4 months (0.08, 95% CI (-0.1,0.25), $P = 0.38$) (P value for heterogeneity: 0.002, $I^2 = 80\%$ = substantial heterogeneity). Conversely, when evaluating IPI reduction at ≥6 months follow-up, control group demonstrated a significant greater IPI reduction than MD+CHX group(-0.12, 95% CI (-0.22,-0.02), $P = 0.02$) (P value for heterogeneity: 0.15, $I^2 = 47\%$ = moderate heterogeneity).

At full mouth level, the full mouth plaque index (FMPI) was recorded by three studies [21, 24, 29] and meta-analysis were conducted at different time points. The heterogeneity between trials was high except for at ≥6 months follow-up ($P = 0.71$, $I^2 = 0\%$ = low heterogeneity) (Figure 6(b)). The meta-analysis failed to show a significant difference regarding FMPI reduction between the MD+CHX and control groups at all time points.

3.10. Microbiological Outcomes. Five studies [19, 22–24, 30] performed the collection of the biological samples in the deepest peri-implant pockets (Table 2). The plaque samples

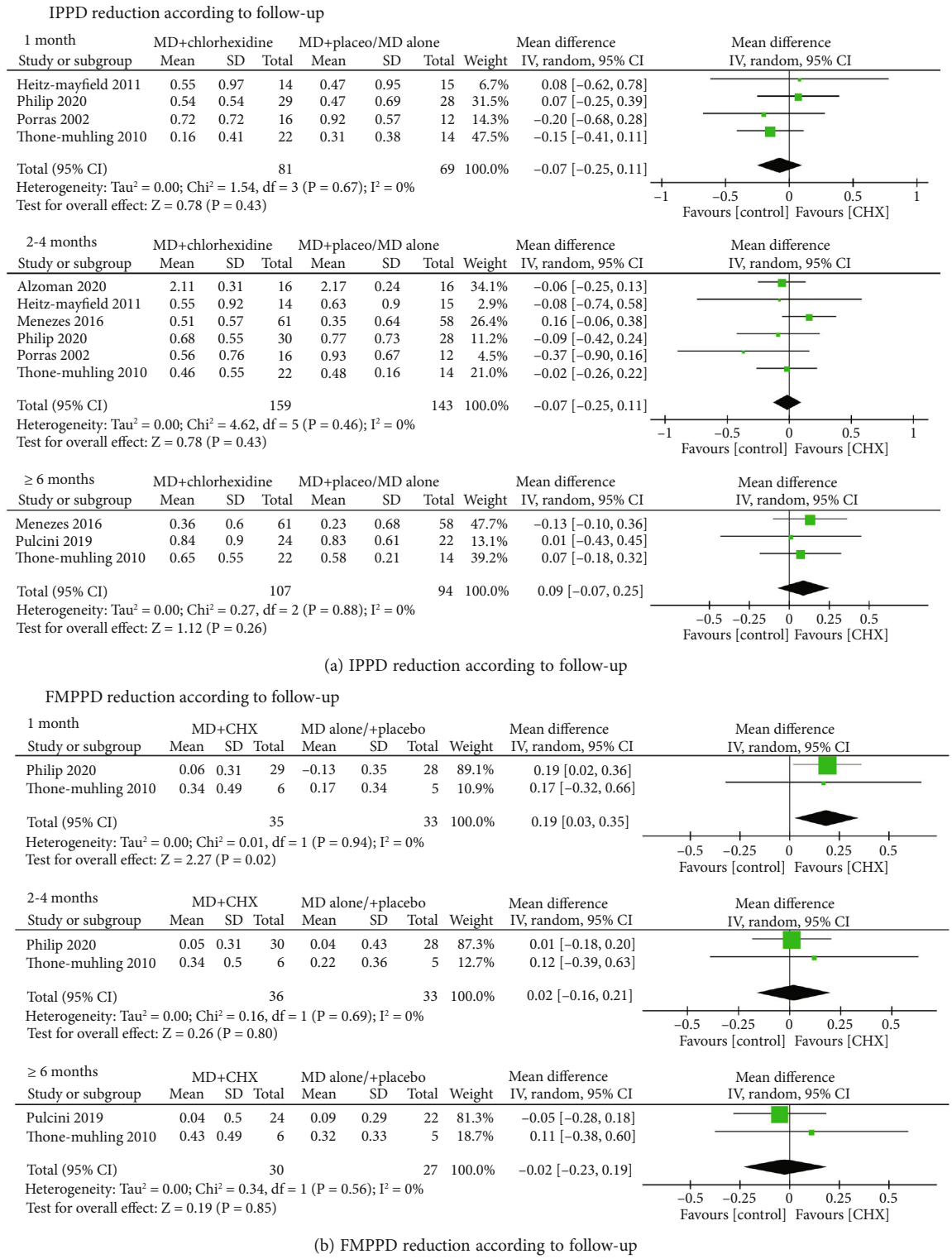

Figure 4: Forest plot of PD reduction (a) at implant level and (b) at full-mouth level.

were all collected from subgingival plaque except for Porras et al. [22] which collected from supragingival plaque. Studies used sterile paper points for 10 s [22, 23] and 20 s [24] in the peri-implant pocket. Only Pulcini et al. [23] reported the time between the collection and processing of the samples.

Among five studies, different techniques were applied to investigate the microbiological outcomes, including DNA probes, RT-qPCR, DNA-DNA hybridization, quantitative (CFU), and16S rRNA sequencing. So, a meta-analysis could not be performed due to the different types of microbiological results. Thone-Muhling et al. [24] and Heitz-Mayfield

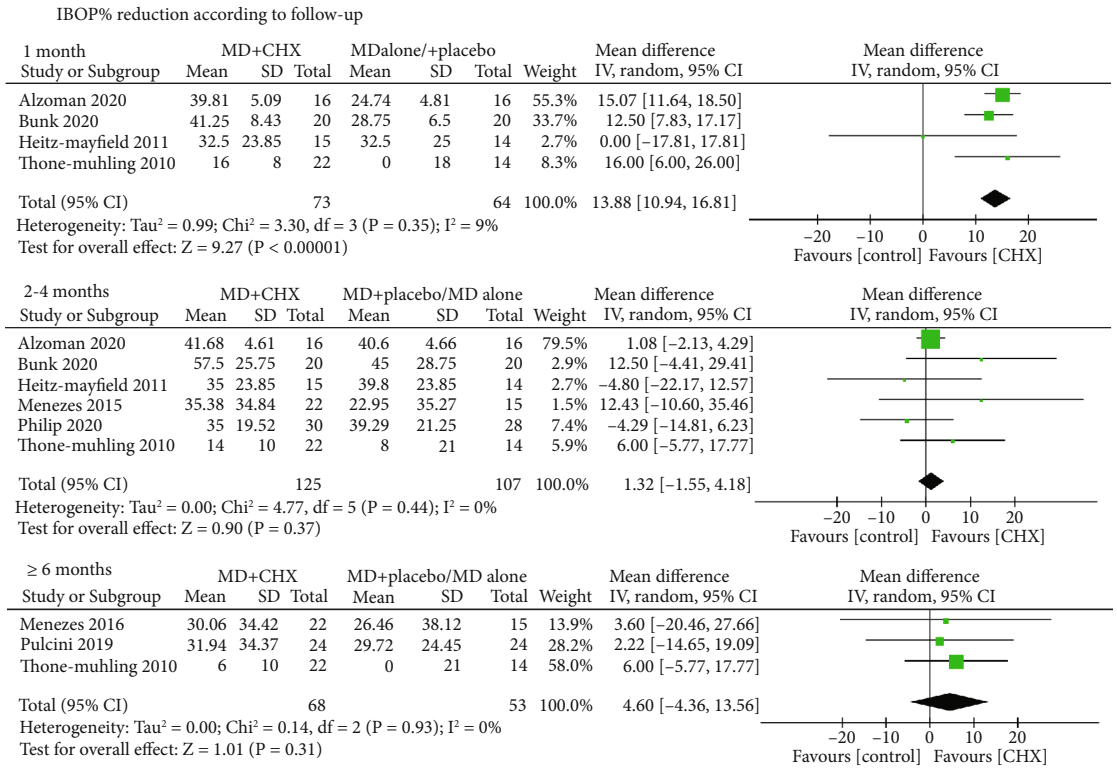

(a) IBOP% reduction according to follow-up

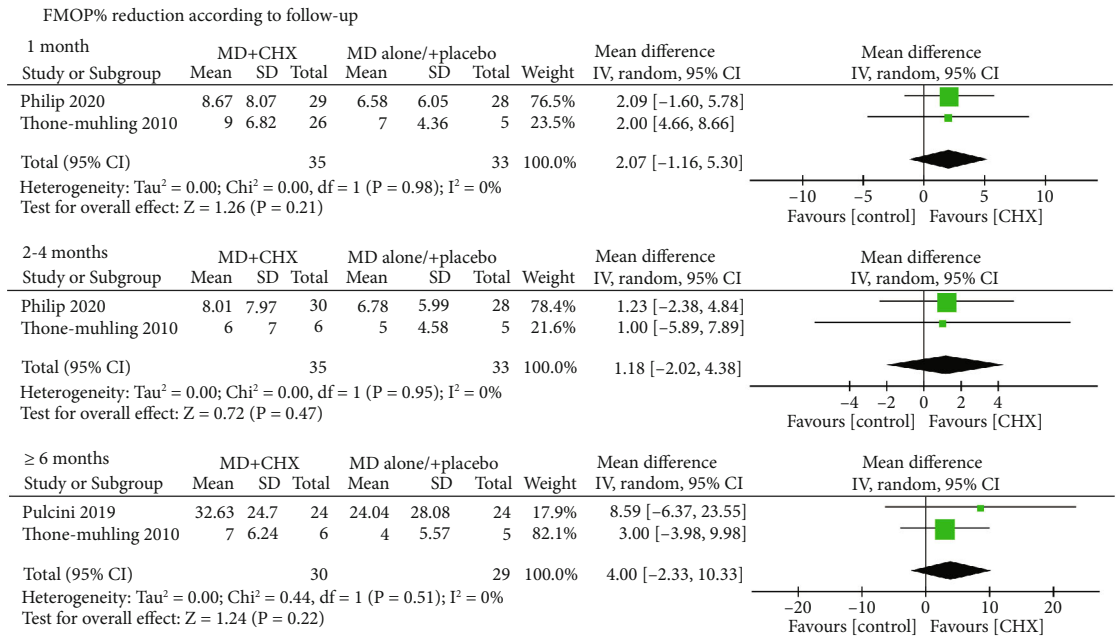

(b) FMBOP% reduction according to follow-up

Figure 5: Forest plot of BOP% reduction (a) at implant level and (b) at full-mouth level.

et al. [19] found there were no significant differences in mean total DNA counts between test and control groups ($P > 0.1$).

3.11. Adverse Events. Any side effects or adverse events during adjunctive CHX application were recorded in four studies [19, 21, 24, 31]. No adverse events were reported except one study. Philip et al. reported staining of the teeth or tongue and taste alteration in the CHX group [21].

4. Discussion

CHX was always regularly considered and recommended for individuals who are at several different stages during dental

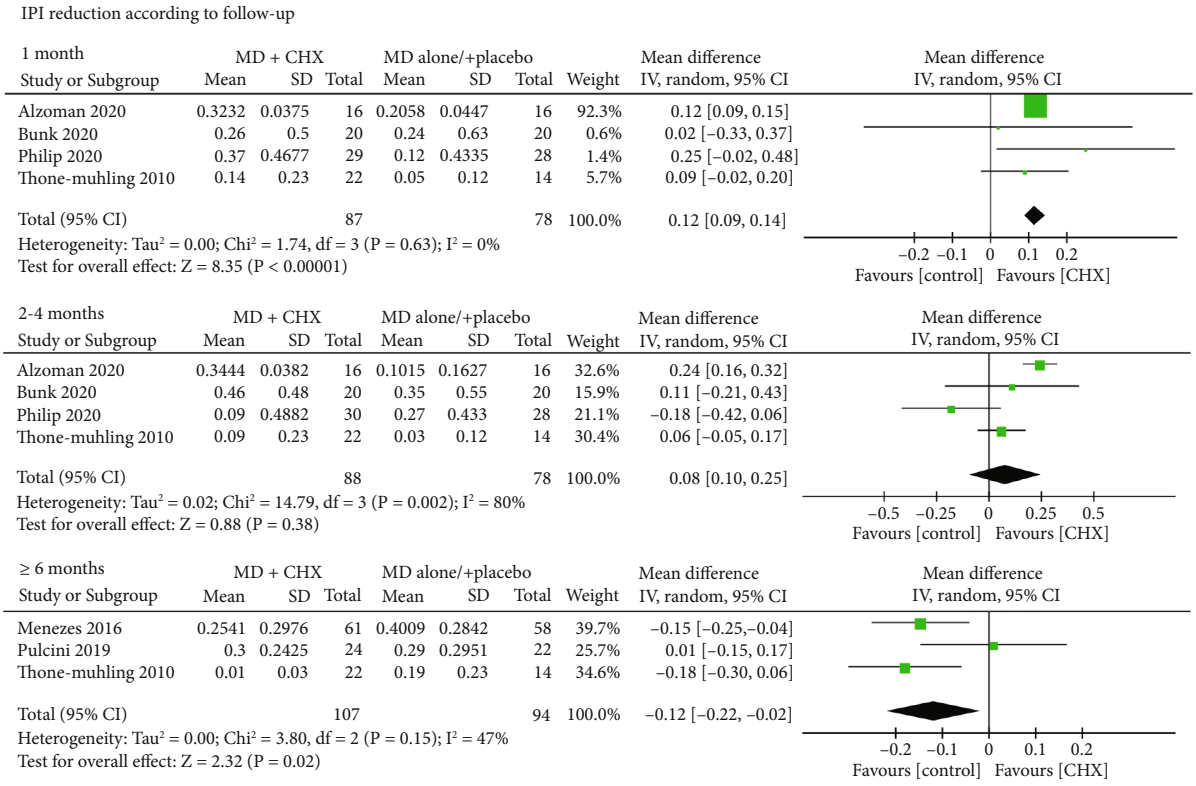

(a) IPI reduction according to follow-up

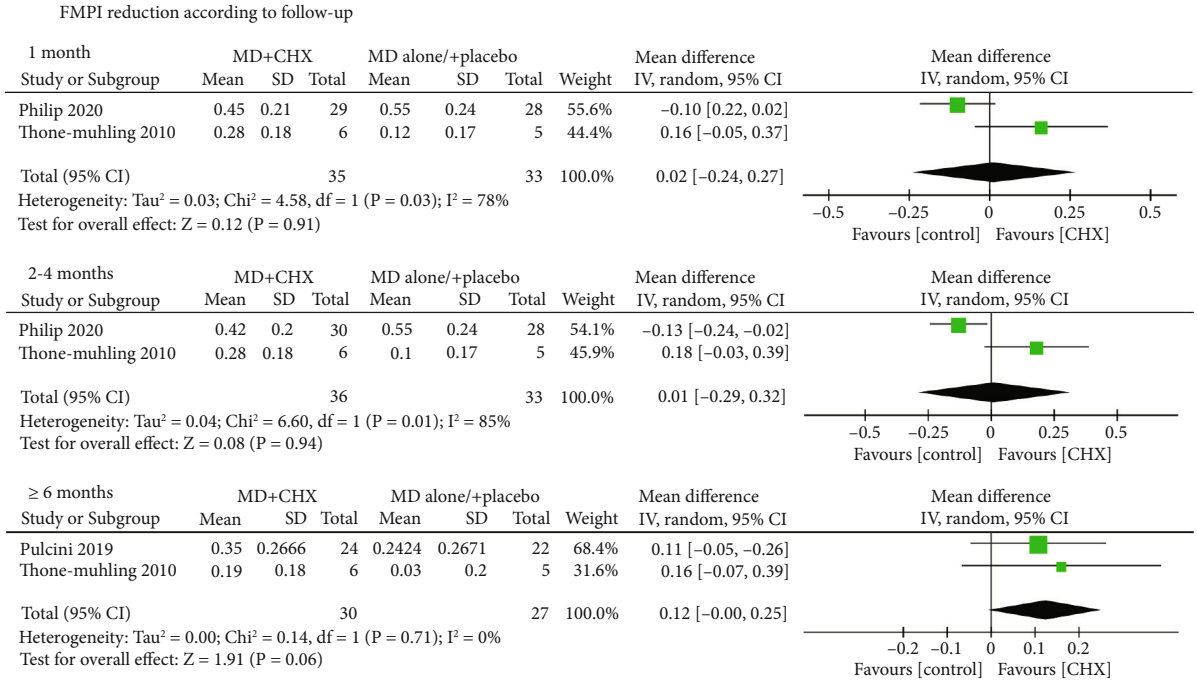

(b) FMPI reduction according to follow-up

Figure 6: Forest plot of PI reduction (a) at implant level and (b) at full-mouth level.

implant treatment, including presurgical mouth rinse, postoperative protocols, and during implant maintenance [14]. CHX could damage the cellular membranes which was a broad-spectrum antimicrobial agent [17]. Therefore, many dentists recommended the regular CHX application during implant inflammation. Currently, the guidelines even suggest that management of peri-implant diseases could include nonsurgical debridement with carbon fiber or plastic curettes and irrigate the pocket with 0.2% CHX [32]. However, some relatives RCTs indicated no adjunctive benefits

Table 2: Microbiological methods of the selected studies.

Study	Sampling type	Instrument collection	Load implant collection	Time	Transport media/ processing	Technique	Targeted oral bacteria	Major findings
Porras et al. [22]	Supragingival plaque	Sterile paper points	Deepest PPD	10s	In a sterile plastic container/ WD	DNA probes	*A. actinomycetemcomitans, P. intermedia, P. gingivalis, E. corrodens, C. retus, B. forsythus, T. denticola, F. nucleatum*	Most of the sites were free of pathogens with the exception of *E. corrodens* after both treatment at 3 months.
Thone-Muhling et al. [24]	Subgingival plaque	Sterile paper points	Deepest PPD	20s	In a sterile Eppendorf tube/WD	RT-qPCR	*A. actinomycetemcomitans, P. intermedia, P. gingivalis, D. pneumosintes, C. retus, P. micra*	The microbiological outcomes showed no significant reductions for implants and teeth in the total bacterial load after 8 months. In both groups, a decrease in the bacterial counts was detected after 24 h, although not significant for all bacteria and for all groups.
Heitz-Mayfield et al. [19]	Subgingival plaque	Sterile paper points	Deepest PPD	WD	In a sterile Eppendorf tube/WD	DNA-DNA hybridization	40 subgingival species with the additional of *Staphylococcus aureus*	There were no significant differences in mean total DNA counts between test and control group. ($P > 0.1$)
Pulcini et al. [23]	Subgingival plaque	Sterile paper points	Deepest PPD	10s	In a screw-capped vial/within 2 h	Quantiative (CFU)	*P. gingivalis, P. intermedia, T. forsythia, P. micra, C. retus, F. nucleatum, Capnocytophaga* spp., *E. corrodens*	No significant differences between groups were observed at any time point in regards to the frequency of detection of target species. For proportions of target species, the test group showed statistically significant reductions in the proportions of *Porphyromonas gingivalis* after 3 months and of *Prevotella intermedia*, *F. nucleatum* and *P. micra* up to 6 months ($P < 0.05$). In the control group, significant reductions were only observed for *F. nucleatum* after 6 months ($P = 0.02$).
Philip et al. [21]	Subgingival plaque	Sterile implant deplaquer	Deepest PPD	WD	In a sterile Eppendorf tube/WD	16S rRNA sequencing	Subgingival microbiota	The sites with peri-implant mucositis presented with a less diverse and less anaerobic microbiome. Exposure to CHX, resulted in microbial changes after both 1 and 3 months.

of CHX in the treatment of PiM. Therefore, the primary aim of this study was to evaluate whether supplementation of CHX with nonsurgical therapy resulted in improved outcomes in the management of peri-implant mucositis.

Our results of this meta-analysis support the no adjunctive clinical benefits in terms of disease resolution and IPPD reduction at both short-, medium-, and long-term of follow-up evaluation. It has been clearly demonstrated that the CHX could confer some clinical benefit in the managing of gingivitis [33, 34]. However, the efficacy of adjunctive CHX treatment seems dispensable as the cure rate of PiM did not improve. Based on our data, the resolution of inflammation was not achieved in all patients with PiM. Compared with periodontal tissue, the peri-implant tissue seems more susceptible by many factors, such as absence of keratinized gingival, the lack of periodontal ligament and Sharpey's fibers, and the presence of residual cement [35], which may limit the access to oral hygiene control and plaque control [23]. Moreover, both animal and human experiments have demonstrated the significant quantitative and qualitative differences of supracrestal connective tissue compartment around the teeth and dental implants in regard to the number of collagen fiber orientation, fibroblasts, and vascular supply [29]. A systematic review focusing on whether CHX improves outcomes in the management of peri-implant diseases was conducted by Liu et al., and only four studies (reported from 2002 to 2016) were included [25]. In addition, the previous meta-analysis only analyzed the outcomes of IPPD changes and did not find a significant difference between CHX+MD and placebo+MD/MD alone which was consistent with our results of meta-analysis.

Interestingly, our subgroup analysis indicated that oral irrigation of CHX may have more benefits than CHX mouth rinse or CHX gel on the resolution of PiM. The ideal treatment of PiM was achieving the complete resolution of diseases. However, based on the results of the present systematic review, the oral irrigation with CHX seems achieved a higher PiM resolution rate (95%) compared with rinsing with CHX solution or CHX gel (53.62%). Oral irrigator, also known as dental water jet or water flosser, an electric device which has been available for just over fifty years and delivers pulsating fluid through controlled pressure to provide the compression and decompression of gingival tissue, removing supragingival plaque and flushing out subgingival bacteria and other debris [36, 37]. Oral irrigators have often been used in addition to tooth brushing and shown to be effective in reducing oral biofilm, clinical periodontal indexes, and host inflammatory mediators by reducing pro-inflammatory cytokines (IL-1β and PGE2) in the gingival crevicular fluid [38, 39]. Tutuncuoglu et al. assessed the efficacy of oral irrigation in PiM patients and concluded that the use of an oral irrigator can be as effective as an interdental brush in interdental cleaning [40]. Consistent with our meta-analysis, oral irrigation of CHX would result in better plaque control and better resolution of PiM, compared with other types such as CHX mouth-rinse or CHX gel.

In term of other primary outcomes, the magnitude of the reduction in IPPD varied among the included studies. Five studies revealed a decrease in IPPD that was generally <1 mm and only one study reported a IPPD reduction to 2 mm in both the test and control groups. Data synthesis of the included studies evaluated that WMD in IPPD reduction at different time points and were both not in favor of the additional CHX therapy over MD alone. And regarding the BOP changes, greater IBOP% reduction of the test group was only found at 1-month follow-up, indicating adjunctive CHX treatment was effective on the inflammation control of peri-implant tissue at short term. Similar changes were also found of PI reduction around peri-implants. Conversely, the control group demonstrated a significant greater IPI reduction at ≥6 months follow-up. Evidences indicated that significant short-term improvements of plaque control around implants by adjunctive CHX treatment. CHX is also often advised for short-term use only (2-4 weeks).

As an antiseptic mouthwash or irrigation, CHX solution has a full-mouth antimicrobial effect on bacteria, fungus, and virus causative for various of different oral infectious diseases, such as gingivitis, periodontitis, and caries [17]. In our study, more FMPPD reduction were observed following CHX adjunctive therapy at 1 month compared with the control group. Other benefits of full-month parameters failed to observed. Regarding the small number of included studies, limited data available. and the variability of CHX application, these factors may be explained by these limitations. The microbiological outcomes of oral bacteria were reported in five studies but meta-analysis could not be performed due to the variability and different types of microbiological results [19, 21–24]. Three studies showed no significant differences of microbial outcomes between groups [19, 23, 24]. Philip et al. used 16S V4 rRNA gene amplicon sequencing to analyzed bioinformatically and found peri-implant sites with mucositis harbor ecologically less complex and less anaerobic biofilms with lower biomass than patient-matched dental sites with gingivitis while they elicit an equal inflammatory response [30]. So distinct from gingivitis, more aerobic bacteria such as Neisseria and Haemophilu were survived in PiM-related plaque community. They also found that the inflamed implant sites had a lower plaque index than the dental sites with gingivitis, indicating the inflammatory response around the implants is triggered by the presence and characteristics of the implant (both its structure and material) and not the oral microflora. These aspects of PiM may help to explain the minor microbiocidal changes of locally delivered CHX as an adjunct to MD compared to the control.

In recent years, several adjunctive or alternative therapies (such as antiseptic and antibiotic therapy, probiotics, photodynamic treatment) to MD have already been applied and evaluated in order to gain better control of the progression of the PiM. However, no beneficial effect in resolving peri-implant mucositis was found of these therapies [41, 42]. Therefore, the primary aim of this study was to evaluate whether supplementation of CHX with nonsurgical therapy resulted in improved outcomes in the management of PiM. Additionally, according to what we know, this is the first systematic review that discusses the preexisting criteria of CHX application (oral irrigator and mouth rinse/gel) for PiM. Our results also support that CHX adjunctive therapy cannot

bring evident clinical benefits compared to MD alone in the treatment of PiM. In contrast to the gingivitis, up to now, there was no evidence for the primary prevention, plaque control or complete of PiM [43]. It seems the vital item of peri-implant health was the prevention and control of inflammation. Therefore, any risk factors for the development of PiM should be given attention. An environmental, behavioral, or biological factor that if present directly increases the probability of PiM should be avoided if possible, such as excess cement, smoking, ideal design, and surface characteristics of transmucosal portion of implants.

However, owing to the inevitably differences between included studies, the present study has a few limitations. At first, included studies demonstrated some variability in the type of CHX used, dose, and method of administration. We only conducted subgroup analysis between oral irrigator and mouth rinse/gel of CHX. For other clinical variables, subgroup analysis was not performed because they not have enough power to detect a true effect with fewer studies. Considering these may increase the clinical heterogeneity of the study, we used random-effects model to minimize the statistical error. I^2 statistics showed a low level of heterogeneity in terms of PPD reduction, and BOP% changes, suggesting the heterogeneity of the data was acceptable. However, the heterogeneity of disease resolution was high. Hence, subgroup analysis was conducted and could explain heterogeneity based on variation in CHX types. Well-designed large clinical trials are needed in future to directly investigate the effects of additional CHX application on PiM. Second, as smoking was demonstrated a risk factor of peri-implant diseases, only four studies included only nonsmokers or former smokers [13, 18, 20, 22]. The other five studies included both nonsmokers and smokers, and reported the constituents of different smoking. Third, some included studies reported the primary outcomes with different parameters and measuring method, such as the information about BOP, plaque control, or microbiological load. In order to obtain more useful and adequate data, Alzoman, Bunk, and Heitz-Mayfield were contacted, but none of them replied. Finally, because of the high heterogeneity, the limited available data of the included studies, and the small size of the studies analyzed in our review, the quality of the evidence might be decreased, and the impact of the conclusions of this meta-analysis could be reduced.

5. Conclusion

Adjunctive CHX application may have some benefits to improve the efficacy of MD in PiM treatment by reducing IBOP%, IPI, and FMPPD in short-term. But these benefits were disappeared at medium- and long-term follow-up. In order to achieve better disease resolution of PiM, adjunctive CHX irrigation with MD may be suggested and has positive potential. Well-designed large clinical trials are needed in future.

Data Availability

The datasets used and/or analyzed during the current study are available from the corresponding author on reasonable request.

Conflicts of Interest

The authors have no conflicts of interest to declare.

Acknowledgments

This study was supported by grants from the National Natural Science Foundation of China (U1904145)and the Joint Project of Medical Science and Technology of Henan Province (LHGJ20220365).

References

[1] F. Schwarz, J. Derks, A. Monje, and H. L. Wang, "Peri-implantitis," *Journal of Clinical Periodontology*, vol. 45, pp. S246–S266, 2018.

[2] T. Berglundh, G. Armitage, M. G. Araujo et al., "Peri-implant diseases and conditions: consensus report of workgroup 4 of the 2017 world workshop on the classification of periodontal and peri-implant diseases and conditions," *Journal of Periodontology*, vol. 89, Supplement 1, pp. S313–S318, 2018.

[3] J. Lindhe, J. Meyle, and on behalf of Group D of the European Workshop on Periodontology, "Peri-implant diseases: consensus report of the Sixth European Workshop on Periodontology," *Journal of Clinical Periodontology*, vol. 35, 8 Supplement, pp. 282–285, 2008.

[4] C.-T. Lee, Y.-W. Huang, L. Zhu, and R. Weltman, "Prevalences of peri-implantitis and peri-implant mucositis: systematic review and meta-analysis," *Journal of Dentistry*, vol. 62, pp. 1–12, 2017.

[5] I. Kormas, C. Pedercini, A. Pedercini, M. Raptopoulos, H. Alassy, and L. F. Wolff, "Peri-implant diseases: diagnosis, clinical, histological, microbiological characteristics and treatment strategies. A narrative review," *Antibiotics*, vol. 9, no. 11, p. 835, 2020.

[6] M. G. Araujo and J. Lindhe, "Peri-implant health," *Journal of Periodontology*, vol. 89, Supplement 1, pp. S249–S256, 2018.

[7] S. Renvert and I. Polyzois, "Treatment of pathologic peri-implant pockets," *Periodontology 2000*, vol. 76, no. 1, pp. 180–190, 2018.

[8] A. Al-Jadaa, T. Attin, T. Peltomäki, and P. R. Schmidlin, "Comparison of three in vitro implant leakage testing methods," *Clinical Oral Implants Research*, vol. 26, no. 4, pp. e1–e7, 2015.

[9] H. Hallström, G. R. Persson, S. Lindgren, M. Olofsson, and S. Renvert, "Systemic antibiotics and debridement of peri-implant mucositis. a randomized clinical trial," *Journal of Clinical Periodontology*, vol. 39, no. 6, pp. 574–581, 2012.

[10] G.-H. Lin, F. Suárez López Del Amo, and H.-L. Wang, "Laser therapy for treatment of peri-implant mucositis and peri-implantitis: an American Academy of Periodontology best evidence review," *Journal of Periodontology*, vol. 89, no. 7, pp. 766–782, 2018.

[11] M. Pena, L. Barallat, J. Vilarrasa, M. Vicario, D. Violant, and J. Nart, "Evaluation of the effect of probiotics in the treatment of peri-implant mucositis: a triple-blind randomized clinical trial," *Clinical Oral Investigations*, vol. 23, no. 4, pp. 1673–1683, 2019.

[12] F. Schwarz, K. Becker, and S. Renvert, "Efficacy of air polishing for the non-surgical treatment of peri-implant diseases: a systematic review," *Journal of Clinical Periodontology*, vol. 42, no. 10, pp. 951–959, 2015.

[13] H. Alzoman, T. G. Alojaym, S. N. Chalikkandy, A. Mehmood, F. Rashed, and D. D. Divakar, "Comparison of an herbal- and a 0.12% chlorhexidine-based oral rinse as adjuncts to nonsurgical mechanical debridement in the management of peri-implant mucositis: a randomised controlled trial," *Oral Health & Preventive Dentistry*, vol. 18, no. 1, pp. 645–651, 2020.

[14] Z. L. S. Brookes, R. Bescos, L. A. Belfield, K. Ali, and A. Roberts, "Current uses of chlorhexidine for management of oral disease: a narrative review," *Journal of Dentistry*, vol. 103, article 103497, 2020.

[15] N. P. Lang, P. Hotz, H. Graf et al., "Effects of supervised chlorhexidine mouthrinses in children," *Journal of Periodontal Research*, vol. 17, no. 1, pp. 101–111, 1982.

[16] S. C. Supranoto, D. E. Slot, M. Addy, and G. A. Van der Weijden, "The effect of chlorhexidine dentifrice or gel versus chlorhexidine mouthwash on plaque, gingivitis, bleeding and tooth discoloration: a systematic review," *International Journal of Dental Hygiene*, vol. 13, no. 2, pp. 83–92, 2015.

[17] E. Varoni, M. Tarce, G. Lodi, and A. Carrassi, "Chlorhexidine (CHX) in dentistry: state of the art," *Minerva Stomatologica*, vol. 61, no. 9, pp. 399–419, 2012.

[18] D. Bunk, M. Eisenburger, S. Hackl, J. Eberhard, M. Stiesch, and J. Grischke, "The effect of adjuvant oral irrigation on self-administered oral care in the management of peri-implant mucositis: a randomized controlled clinical trial," *Clinical Oral Implants Research*, vol. 31, no. 10, pp. 946–958, 2020.

[19] L. J. Heitz-Mayfield, G. E. Salvi, D. Botticelli et al., "Anti-infective treatment of peri-implant mucositis: a randomised controlled clinical trial," *Clinical Oral Implants Research*, vol. 22, no. 3, pp. 237–241, 2011.

[20] K. M. Menezes, A. N. Fernandes-Costa, R. D. Silva-Neto, P. S. Calderon, and B. C. Gurgel, "Efficacy of 0.12% chlorhexidine gluconate for non-surgical treatment of peri-implant mucositis," *Journal of Periodontology*, vol. 87, no. 11, pp. 1305–1313, 2016.

[21] J. Philip, M. L. Laine, and D. Wismeijer, "Adjunctive effect of mouthrinse on treatment of peri-implant mucositis using mechanical debridement: a randomized clinical trial," *Journal of Clinical Periodontology*, vol. 47, no. 7, pp. 883–891, 2020.

[22] R. Porras, G. B. Anderson, R. Caffesse, S. Narendran, and P. M. Trejo, "Clinical response to 2 different therapeutic regimens to treat peri-implant mucositis," *Journal of Periodontology*, vol. 73, no. 10, pp. 1118–1125, 2002.

[23] A. Pulcini, J. Bollaín, I. Sanz-Sánchez et al., "Clinical effects of the adjunctive use of a 0.03% chlorhexidine and 0.05% cetylpyridinium chloride mouth rinse in the management of peri-implant diseases: a randomized clinical trial," *Journal of Clinical Periodontology*, vol. 46, no. 3, pp. 342–353, 2019.

[24] M. Thöne-Mühling, K. Swierkot, C. Nonnenmacher, R. Mutters, L. Flores-de-Jacoby, and R. Mengel, "Comparison of two full-mouth approaches in the treatment of peri-implant mucositis: a pilot study," *Clinical Oral Implants Research*, vol. 21, no. 5, pp. 504–512, 2010.

[25] S. Liu, M. Li, and J. Yu, "Does chlorhexidine improve outcomes in non-surgical management of peri-implant mucositis or peri-implantitis?: a systematic review and meta-analysis," *Medicina Oral, Patología Oral y Cirugía Bucal*, vol. 25, no. 5, pp. e608–e615, 2020.

[26] D. Moher, A. Liberati, J. Tetzlaff, D. G. Altman, and The PRISMA Group, "Preferred reporting items for systematic reviews and meta-analyses: the PRISMA statement," *PLoS Medicine*, vol. 6, no. 7, article e1000097, 2009.

[27] J. P. T. Higgins, J. Thomas, J. Chandler et al., *Cochrane Handbook for Systematic Reviews of Interventions*, John Wiley & Sons, 2019.

[28] S. A. Miller and J. L. Forrest, "Enhancing your practice through evidence-based decision making: PICO, learning how to ask good questions," *Journal of Evidence Based Dental Practice*, vol. 1, no. 2, pp. 136–141, 2001.

[29] J. Bollain, A. Pulcini, I. Sanz-Sánchez et al., "Efficacy of a 0.03% chlorhexidine and 0.05% cetylpyridinium chloride mouth rinse in reducing inflammation around the teeth and implants: a randomized clinical trial," *Clinical Oral Investigations*, vol. 25, no. 4, pp. 1729–1741, 2020.

[30] J. Philip, M. J. Buijs, V. Y. Pappalardo, W. Crielaard, B. W. Brandt, and E. Zaura, "The microbiome of dental and peri-implant subgingival plaque during peri-implant mucositis therapy: a randomized clinical trial," *Journal of Clinical Periodontology*, vol. 49, no. 1, pp. 28–38, 2021.

[31] H. Hallstrom, S. Lindgren, and S. Twetman, "Effect of a chlorhexidine-containing brush-on gel on peri-implant mucositis," *International Journal of Dental Hygiene*, vol. 15, no. 2, pp. 149–153, 2017.

[32] D. C. Matthews, "Prevention and treatment of periodontal diseases in primary care," *Evidence-Based Dentistry*, vol. 15, no. 3, pp. 68-69, 2014.

[33] J. Serrano, M. Escribano, S. Roldan, C. Martin, and D. Herrera, "Efficacy of adjunctive anti-plaque chemical agents in managing gingivitis: a systematic review and meta-analysis," *Journal of Clinical Periodontology*, vol. 42, Supplement 16, pp. S106–S138, 2015.

[34] Y. Zhang, Y. Zhao, C. Xu et al., "Chlorhexidine exposure of clinical *Klebsiella pneumoniae* strains leads to acquired resistance to this disinfectant and to colistin," *International Journal of Antimicrobial Agents*, vol. 53, no. 6, pp. 864–867, 2019.

[35] S. Jepsen, T. Berglundh, R. Genco et al., "Primary prevention of peri-implantitis: managing peri-implant mucositis," *Journal of Clinical Periodontology*, vol. 42, Supplement 16, pp. S152–S157, 2015.

[36] S. N. Bhaskar, D. E. Cutright, A. Gross, J. Frisch, J. D. Beasley 3rd, and B. Perez, "Water jet devices in dental practice," *Journal of Periodontology*, vol. 42, no. 10, pp. 658–664, 1971.

[37] N. A. Rosema, N. L. Hennequin-Hoenderdos, C. E. Berchier, D. E. Slot, D. M. Lyle, and G. A. van der Weijden, "The effect of different interdental cleaning devices on gingival bleeding," *Journal of the International Academy of Periodontology*, vol. 13, no. 1, pp. 2–10, 2011.

[38] C. W. Cutler, T. W. Stanford, C. Abraham, R. A. Cederberg, T. J. Boardman, and C. Ross, "Clinical benefits of oral irrigation for periodontitis are related to reduction of pro-inflammatory cytokine levels and plaque," *Journal of Clinical Periodontology*, vol. 27, no. 2, pp. 134–143, 2000.

[39] E. Ng and L. P. Lim, "An overview of different interdental cleaning aids and their effectiveness," *Dentistry Journal*, vol. 7, no. 2, 2019.

[40] S. Tütüncüoğlu, B. O. Cetinkaya, F. Pamuk et al., "Clinical and biochemical evaluation of oral irrigation in patients with peri-implant mucositis: a randomized clinical trial," *Clinical Oral Investigations*, vol. 26, no. 1, pp. 659–671, 2022.

[41] A. Ramanauskaite, T. Fretwurst, and F. Schwarz, "Efficacy of alternative or adjunctive measures to conventional non-surgical and surgical treatment of peri-implant mucositis and

peri-implantitis: a systematic review and meta-analysis," *International Journal of Implant Dentistry*, vol. 7, no. 1, p. 112, 2021.

[42] R. Zhao, H. Hu, Y. Wang, W. Lai, and F. Jian, "Efficacy of probiotics as adjunctive therapy to nonsurgical treatment of peri-implant mucositis: a systematic review and meta-analysis," *Frontiers in Pharmacology*, vol. 11, article 541752, 2020.

[43] N. P. Lang, B. R. Cumming, and H. Loe, "Toothbrushing frequency as it relates to plaque development and gingival health," *Journal of Periodontology*, vol. 44, no. 7, pp. 396–405, 1973.

Hindawi
Oxidative Medicine and Cellular Longevity
Volume 2022, Article ID 2710607, 19 pages
https://doi.org/10.1155/2022/2710607

Research Article

Rutin and Quercetin Counter Doxorubicin-Induced Liver Toxicity in Wistar Rats *via* Their Modulatory Effects on Inflammation, Oxidative Stress, Apoptosis, and Nrf2

Osama M. Ahmed,[1] **Mohammed H. Elkomy**,[2] **Hanaa I. Fahim**,[1] **Mohamed B. Ashour**,[1] **Ibrahim A. Naguib**,[3] **Badrah S. Alghamdi**,[4,5] **Heba Uallah R. Mahmoud**,[1] **and Noha A. Ahmed**[1]

[1]*Physiology Division, Zoology Department, Faculty of Science, Beni-Suef University, P.O. Box 62521, Beni-Suef, Egypt*
[2]*Department of Pharmaceutics, College of Pharmacy, Jouf University, Sakaka 72341, Saudi Arabia*
[3]*Department of Pharmaceutical Chemistry, College of Pharmacy, Taif University, P.O. Box 11099 Taif 21944, Saudi Arabia*
[4]*Department of Physiology, Neuroscience Unit, Faculty of Medicine, King Abdulaziz University, Jeddah 22252, Saudi Arabia*
[5]*Pre-Clinical Research Unit, King Fahd Medical Research Center, King Abdulaziz University, Jeddah, Saudi Arabia*

Correspondence should be addressed to Osama M. Ahmed; osamamoha@yahoo.com
and Mohammed H. Elkomy; mhalkomy@ju.edu.sa

Received 14 June 2022; Accepted 14 July 2022; Published 27 July 2022

Academic Editor: Tarique Hussain

The presented study was performed to verify whether rutin and/or quercetin can inhibit liver injury induced by doxorubicin (DXR) in male Wistar rats. In this study, male Wistar rats were treated via the oral route with rutin and quercetin (50 mg/kg) either alone or in combination every other day for five weeks concomitant with receiving intraperitoneal DXR (2 mg/kg) two times a week for five successive weeks. Quercetin, rutin, and their combination significantly improved the deteriorated serum AST, ALT, and ALP activities and total bilirubin level, as well as albumin, AFP, and CA 19.9 levels in DXR-injected rats. Treatments of the DXR-injected group with quercetin and rutin prevented the elevation in liver lipid peroxidation and the reduction in superoxide dismutase, glutathione-S-transferase and glutathione peroxidase activities, and glutathione content. Treatments with quercetin and rutin significantly repressed the elevated expression of liver p53 and TNF-α and enhanced Nrf2 expression. Furthermore, the treatments significantly reduced DXR-induced liver histological changes. In conclusion, rutin and quercetin either alone or in combination may have potential preventive effects against DXR-induced hepatotoxicity through inhibiting oxidative stress, inflammation, and apoptosis as well as modulating the Nrf2 expression.

1. Introduction

Doxorubicin (DXR) is an anthracycline antibiotic with broad spectrum activity and is considered one of the most effective chemotherapeutics against cancer [1]. It is used alone or in combination to treat a variety of hematological and solid malignancies, including breast cancer [2]. Despite its therapeutic efficacy, DXR is accompanied by notable liver toxicity and other organ toxicities [3–9], which may limit the scope of its clinical applications in the treatment of cancer. Additionally, DXR counters cell proliferation, activates oxidative stress, attenuates antioxidant defense system, suppresses topoisomerase type II, and eventually results in cells' death due to necrosis or apoptosis [10–12]. Although inflammation, apoptosis, deoxyribonucleic acid (DNA) damage, calcium metabolism impairment, and excessive free radical production may have a direct effect in the degeneration of organ function to varying degrees, the specific mechanism of DXR-mediated multiple organ toxicity has not yet been fully investigated [13]. DXR accumulates in the mitochondria, causing structural and functional alterations. Nevertheless, elevation of reactive oxygen species (ROS) and

reactive nitrogen species (RNS) to substantial levels within the cell, which finally leads to cell damage and programmed cell death (PCD), is regarded as one of the main reasons of DXR-induced adverse effects in humans and animals [14, 15]. When the amount of ROS produced within a cell surpasses its defense requirement, the cell is declared in "oxidative stress" state. Induction of protein oxidation and lipid peroxidation (LPO), inhibition of antioxidant enzymes, nucleic acid injury, PCD pathway stimulation, and eventual cell death or damage are among the hazards created by increased liberation of ROS evoked by environmental conditions [16, 17]. Connection between oxidative stress and DXR-induced toxicity has been established in various body organs [7, 18]. As a result, using antioxidants [7, 8] such as natural flavonoids together with DXR may help decrease or prevent DXR-induced adverse effects.

Plant constituents with aromatic ring in their core structure and one or more hydroxyl groups are known as flavonoids beside other phenolic substances. Of these constituents, >8000 phenolic compounds have been identified [19, 20]; of which, 50% are flavonoids (glycosides, aglycones, and methylation derivatives) [21]. These phytochemical compounds can be found in foods and herbal medications. The flavonoids and various other reported phenolic components were found to exhibit excellent antioxidative, cardioprotective, anticancer, antibacterial, antidiabetic, antihypertensive, anti-inflammatory, and immune response boosting effects and provide skin protection from hazardous ultraviolet radiation (UV) radiation, making them outstanding drugs for pharmaceutical and medical use [22–24]. The flavonoid quercetin has a glycoside known as rutin (quercetin rutinoside). It works as an antioxidant in humans by connecting to the ferrous iron (Fe^{+2}), thus preventing generation of highly reactive free radicals which might harm cells [4]. Rutin has also been shown to produce anti-inflammatory effect *in vitro* and in animal models [25]. Moreover, renocardioprotective, antidiabetic, and anticancer properties have been reported for rutin [8, 24, 26]. Quercetin, which is known as a natural plant-derived aglycone of rutin, is frequently used as a dietary supplement and was recently shown to be effective in the treatment of several diseases. Cardiovascular protective, renocardioprotective, anticancer, antiulcer, antiallergy, anti-inflammatory, antiviral, antidiabetic, antihypertensive, gastroprotective, immunomodulatory, and anti-infective qualities are only a few of quercetin beneficial effects [8, 24, 27, 28]. In our previous publication, rutin and quercetin, *via* suppressing oxidative stress and boosting antioxidant defense system, were labeled as chemopreventive agents against nephrocardiotoxicity induced by doxorubicin [8]. Most of other publications investigated the effects of rutin and quercetin on DXR-induced cardiotoxicity [29–33], but rare published studies assessed their effects on DXR-induced hepatotoxicity [34, 35]. However, the mechanisms of actions were not entirely delineated by these studies. Furthermore, no published studies have revealed the combinatory effects of rutin and quercetin on DXR-induced hepatotoxicity.

Therefore, the presented study was designed to determine whether rutin and quercetin, as well as their combination, could help to prevent DXR-induced liver damage and toxicity in a male Wistar rat animal model.

2. Materials and Methods

2.1. Experimental Animals. In the presented study, 50 male Wistar rats weighing approximately 120-145 g (about 10 weeks old) were selected as experimental animals. They were obtained from the "National Research Center's Animal House in Giza, Egypt." The experimental animals were adapted to laboratory set conditions for 10 days prior to experiments. The rats were accommodated in polyethylene cages withheld under room temperature set to $25 \pm 1^{\circ}C$ and relative humidity set to 20%-30% with cyclic daylight (12 h/day). The animals were granted free full access to drinking water and were supplemented balanced commercial pelleted diet. The Ethics Committee of the Care and Use of Experimental Animals, Faculty of Science, Beni-Suef University, Egypt, has approved the experimental study (ethical approval number: BSU/FS/2015/22). All attempts have been made to reduce pain and discomfort.

2.2. Chemicals and Drugs. Pharmacia Italia (Milan, Italy) provided the DXR in the form of Adriamycin hydrochloride. Sigma Chemical Company (St. Louis, MO, USA) provided the rutin and quercetin. All of the other chemicals were ultrapure and available at market.

2.3. Doses and Treatment. DXR was administered intraperitoneally to the animals. The dose of DXR was adjusted to 2 mg/1 mL sterile isotonic saline/kg bw (kilogram body weight) [7, 8] and given twice a week for 5 weeks. The doses of quercetin and rutin were modified to 50 mg/kg bw [36, 37] and given orally every other day for 5 successive weeks *via* oral gavage. Drug solutions in carboxymethyl cellulose (CMC) were prepared by solvating rutin or quercetin (50 mg) in 1% CMC (5 mL).

2.4. Animal Grouping. In this experiment, the rats were categorized into five separate groups (10 rats for each) as indicated in Scheme 1:

Group 1 (normal group): for 5 successive weeks, this group was intraperitoneally injected with sterile isotonic saline (1 mL/kg) every other day. During the same period on every other day, the group was also given 5 mL/kg of 1% CMC by oral administration

Group 2 (DXR-injected control group): for 2 days per week for 5 successive weeks, DXR (2 mg/kg) was given to this group intraperitoneally [7, 8]. Moreover, for 5 successive weeks on every other day, this group was also given 5 mL/kg of 1% CMC by oral administration

Group 3 (DXR-injected group supplemented with rutin): similar to the DXR-injected control group, this group was given DXR intraperitoneally. Moreover, for 5 successive weeks, this group was given rutin (50 mg/kg bw) orally every other day [36]

Group 4 (DXR-injected group supplemented with quercetin): similar to the DXR-injected control group, this group was given DXR intraperitoneally. Moreover, for 5 successive

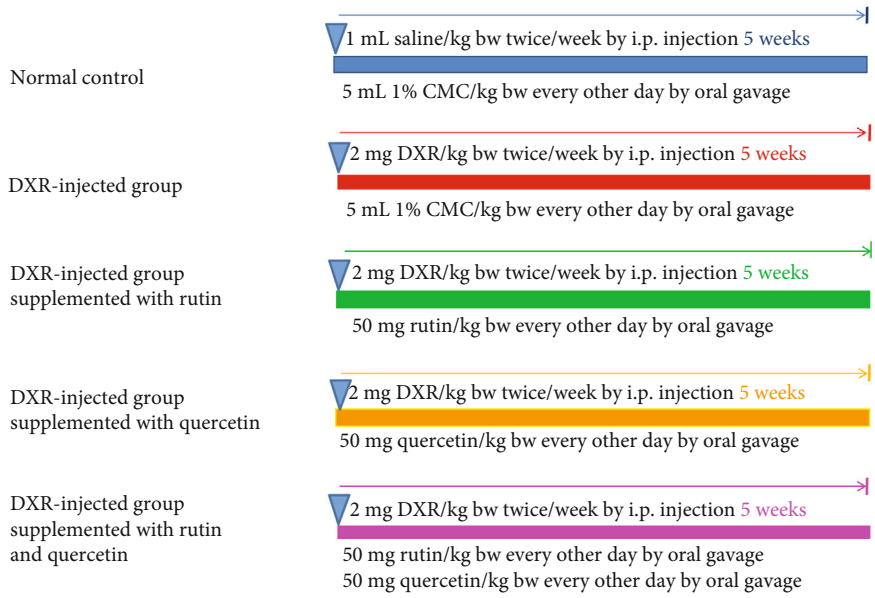

Scheme 1: Schematic diagram of animal groups and employed experimental design.

weeks, this group was given quercetin (50 mg/kg bw) orally every other day [37]

Group 5 (DXR-injected group supplemented with rutin and quercetin): similar to the DXR-injected control group, this group was given DXR intraperitoneally. Moreover, for 5 successive weeks, this group was orally coadministered with rutin (50 mg/kg bw) and quercetin (50 mg/kg bw) every other day

2.5. Tissue and Blood Sampling. Blood samples were taken from each rat's jugular vein at the end of the experiment after induction of anesthesia *via* diethyl ether inhalation. The samples were then stored in centrifuge tubes and let to coagulate for 45 minutes (min) at ambient temperature before being centrifuged for 15 min at 3000 rpm. For every animal, the collected sera (clear, nonhemolyzed supernatant) were split into 4 sections and stored at -30°C for subsequent biochemical analysis. The animals were then sacrificed and dissected for isolation of the liver. The isolated levers were homogenized separately in 10% *w*/*v* phosphate-buffered saline solution (pH 7.2) using a Telfon homogenizer (Glas-Col, Terre Haute, USA). After centrifugation of the collected homogenates at 3000 rpm (round per min), the obtained supernatants were then extracted and fractionated into 3 sections, which were maintained in a deep freezer (at -30°C) till utilized for measurement of antioxidant defense markers and oxidative stress.

2.6. Biochemical Studies. The method of Murray was adopted to assess serum alanine transaminase (ALT) and aspartate transaminase (AST) [38] utilizing the reagent kits acquired from Spinreact (Spinreact, S.A./S.A.U. Ctra.Santa Coloma, 7 E-17176 Sant Esteve De Bas (Gi) Spain). Serum alkaline phosphatase (ALP) was measured according to the method of Schumann et al. [39] utilizing the reagent kits acquired from Spectrum Diagnostics (Al-Obour City, Cairo, Egypt). The total bilirubin in the serum was measured through a colorimetric process using Spectrum Diagnostics kits according to Balistreri and Shaw [40]. According to Gendler [41], serum albumin was tested using a colorimetric method utilizing the kits acquired from Diamond Diagnostics (24 El Mon-tazah St., Heliopolis, Cairo, Egypt). The serum tumor markers, alpha fetoprotein (AFP), and carbohydrate antigen 19.9 (CA19.9), were quantitatively measured employing the enzyme immunosorbent assay (ELISA) and using kits acquired, respectively, from R&D Systems, Inc. (614 McKinley Place NE, Minneapolis, MN 55413, USA) and RayBiotech, Inc. (3607 Parkway Lane, Suite 100 Norcross, GA 30092) in accordance with the instructions supplied with each kit.

The levels of malondialdehyde (MDA) as an indicator of LPO [42], glutathione peroxidase (GPx) [43], glutathione (GSH) [44], superoxide dismutase (SOD) [45], and gluathione-S-transferase (GST) [46] of the liver were assessed according to published methods.

2.7. Immunohistochemical Investigation. For immunohistochemical detection of apoptotic protein (p53), tumor necrosis factor-α (TNF-α), and nuclear factor erythroid 2–related factor 2 (Nrf2), pieces of liver (3 mm^3) were fixed in 10% NBF (neutral-buffered formalin). The fixed liver samples were processed, blocked, and sectioned into 5 μm thick sections that were then mounted onto positive-charged slides (Fisher Scientific, Pittsburgh, PA, USA) in the Department of Pathology, National Cancer Institute (NCI), Cairo University, Egypt. The reactivity of p53 and Nrf2 was investigated using the methods of previous publications [47–52]. Dilution of the primary antibody was 1 : 100 in phosphate buffer saline (PBS) and dilutions of the secondary biotinylated antibodies of p53 and Nrf2 were, respectively, 1 : 100 and 1 : 200 in PBS. ImageJ, a free software program, was used to examine and analyze the labeling (1.51 d) [53]. The integrated intensities (in pixels) of the positive reaction of p53 and Nrf2 were measured using ImageJ software.

Table 1: Serum parameters related to liver function in normal rats and in rats injected with DXR (without and with the supplementation of rutin and/or quercetin).

Parameter Groups	ALT (U/L)	AST (U/L)	ALP (U/L)	Bilirubin (mg/dL)	Albumin (g/dL)
Normal control	57.50 ± 4.06	152.25 ± 5.68	180.50 ± 0.12	0.35 ± 6.40	3.12 ± 0.04
DXR-injected control group	$101.00 \pm 16.69^{++}$	$261.33 \pm 18.18^{++}$	$276.50 \pm 19.23^{++}$	$0.53 \pm 5.16^{++}$	$2.48 \pm 0.18^{++}$
DXR-injected group supplemented with rutin	$65.50 \pm 4.52^{**}$	$162.00 \pm 1.80^{**}$	$131.00 \pm 5.39^{**\$}$	$0.40 \pm 4.93^{**}$	2.65 ± 0.14
DXR-injected group supplemented with quercetin	$48.00 \pm 4.28^{**}$	$183.00 \pm 9.12^{**}$	$79.66 \pm 2.44^{**}$	$0.56 \pm 2.84^{\$\$}$	$2.96 \pm 0.09^{**}$
DXR-injected group supplemented with rutin and quercetin	$49.00 \pm 4.75^{**}$	$176.83 \pm 15.61^{**}$	$102.66 \pm 7.18^{**}$	$0.43 \pm 0.10^{*}$	$2.92 \pm 0.02^{*}$
F-probability	$P < 0.001$	$P < 0.001$	$P < 0.001$	$P < 0.001$	$P < 0.001$

Values are $M \pm$ SE ($n = 6$). $^{+}P < 0.05$, $^{++}P < 0.01$: the DXR-injected control group versus (vs.) normal control. $^{*}P < 0.05$, $^{**}P < 0.01$: the DXR-injected groups treated with rutin and/or quercetin vs. DXR-injected control group. $^{\$}P < 0.05$, $^{\$\$}P < 0.01$: the DXR-injected groups treated with rutin or quercetin alone vs. DXR-injected group treated with rutin and quercetin mixture.

Table 2: Serum AFP and CA19.9 levels in normal rats and in rats injected with DXR (without and with the supplementation of rutin and/or quercetin).

Parameter Group	AFP (ng/mL)	CA19.9 (U/L)
Normal control	0.46 ± 0.04	119.17 ± 2.36
DXR-injected control group	$1.17 \pm 0.03^{++}$	$270.37 \pm 36.93^{++}$
DXR-injected group supplemented with rutin	$1.19 \pm 0.05^{\$\$}$	$199.9 \pm 0.72^{**\$\$}$
DXR-injected group supplemented with quercetin	$0.92 \pm 0.16^{*\$}$	$174.8 \pm 4.92^{**\$}$
DXR-injected group supplemented with rutin and quercetin	$0.63 \pm 0.05^{**}$	$125.3 \pm 1.74^{**}$
F-probability	$P < 0.001$	$P < 0.001$

Values are $M \pm$ SE ($n = 6$). $^{+}P < 0.05$, $^{++}P < 0.01$: the DXR-injected control group vs. normal control. $^{*}P < 0.05$, $^{**}P < 0.01$: the DXR-injected groups treated with rutin and/or quercetin vs. DXR-injected control group. $^{\$}P < 0.05$, $^{\$\$}P < 0.01$: the DXR-injected groups treated with rutin or quercetin alone vs. DXR-injected group treated with rutin and quercetin mixture.

Table 3: Liver GSH content and LPO in normal rats and in rats injected with DXR (without and with the supplementation of rutin and/or quercetin).

Parameter Group	GSH (nmole/100 mg tissue)	LPO (nmole MDA/100 mg tissue/hr)
Normal control	118.91 ± 5.11	17.55 ± 1.05
DXR-injected control group	$64.32 \pm 6.54^{++}$	$28.11 \pm 0.87^{++}$
DXR-injected group supplemented with rutin	$106.95 \pm 14.40^{**\$\$}$	$20.41 \pm 1.57^{**}$
DXR-injected group supplemented with quercetin	79.13 ± 8.04	$18.25 \pm 1.40^{**}$
DXR-injected group supplemented with rutin and quercetin	70.80 ± 4.65	$20.35 \pm 0.87^{**}$
F-probability	$P < 0.001$	$P < 0.001$

Values are $M \pm$ SE ($n = 6$). $^{+}P < 0.05$, $^{++}P < 0.01$: the DXR-injected control group vs. normal control. $^{*}P < 0.05$, $^{**}P < 0.01$: the DXR-injected groups treated with rutin and/or quercetin vs. DXR-injected control group. $^{\$}P < 0.05$, $^{\$\$}P < 0.01$: the DXR-injected groups treated with rutin or quercetin alone vs. DXR-injected group treated with rutin and quercetin mixture.

2.8. Histopathological Studies. Pieces of the liver (3 mm^3) from each tested animal were transported to the "Pathology Department, NCI, Cairo University, Egypt" after preserving in 10% NBF. The samples were processed and stained with hematoxylin and eosin (H&E) based on the technique revealed by Banchroft et al. [54]. The stained liver sections were then inspected by a histopathologist to detect histopathological lesions. Lesions were scored and graded 0 (absence of lesion), I (mild), II (moderate), or III (severe).

2.9. Statistical Analysis. The obtained data were represented as mean ± standard error of mean ($M \pm$ SEM). One-way

Table 4: GPx, GST, and SOD activities in the liver of normal rats and rats injected with DXR (without and with the supplementation of rutin and/or quercetin).

Parameter Groups	GPx (mU/100 mg tissue)	GST (mU/100 mg tissue)	SOD (mU/100 mg tissue)
Normal control	101.91 ± 8.61	105.40 ± 4.72	112.91 ± 1.68
DXR-injected control group	$70.10 \pm 2.32^{++}$	$69.03 \pm 4.63^{++}$	111.29 ± 1.35
DXR-injected group supplemented with rutin	$85.28 \pm 5.29^{*}$	$79.98 \pm 5.24^{\$}$	$137.89 \pm 2.63^{**\$\$}$
DXR-injected group supplemented with quercetin	75.60 ± 5.30	$99.10 \pm 14.26^{*}$	$126.74 \pm 4.77^{**}$
DXR-injected group supplemented with rutin and quercetin	79.56 ± 1.51	$108.72 \pm 6.64^{*}$	$123.51 \pm 3.35^{**}$
F-probability	$P < 0.001$	$P < 0.01$	$P < 0.001$

Values are $M \pm$ SE ($n = 6$). $^{+}P < 0.05$, $^{++}P < 0.01$: the DXR-injected control group vs. normal control. $^{*}P < 0.05$, $^{**}P < 0.01$: the DXR-injected groups treated with rutin and/or quercetin vs. DXR-injected control group. $^{\$}P < 0.05$, $^{\$\$}P < 0.01$: the DXR-injected groups treated with rutin or quercetin alone vs. DXR-injected group treated with rutin and quercetin mixture.

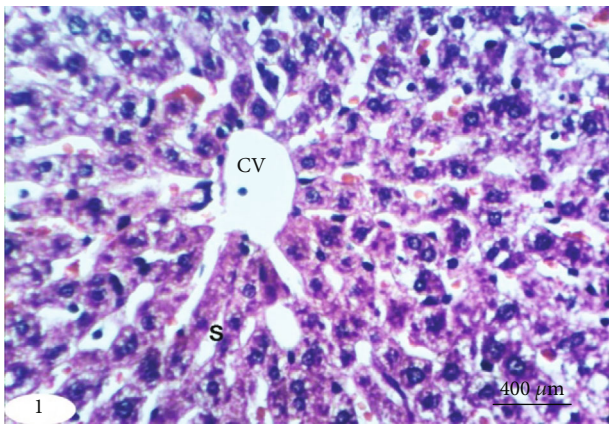

Figure 1: Photomicrograph of liver section in an untreated rat indicating normal liver architecture composed of a central vein (CV) with thin walls and normal hepatocytes with narrow intercellular sinusoids (S) (H&E; ×400).

analysis of variance (ANOVA) was employed for data analysis using PC-STAT statistical program [55]. For each variable, pairwise comparisons of different groups were achieved by employing the least significant difference (LSD) post hoc test at $P < 0.05$ and $P < 0.01$.

3. Results

3.1. Effect on Liver Function Relevant Serum Parameters. The data representing the effect on serum ALT, AST, and ALP activities as well as on the albumin levels and total bilirubin by quercetin and/or rutin is shown in Table 1. The intraperitoneal administration of DXR to rats resulted in a significant elevation ($P < 0.01$) in the activities of serum ALT (75.65%), AST (71.64%), and ALP (53.18%) in addition to total bilirubin level (50.99%). On the other isle, albumin activity was significantly decreased ($P < 0.01$) by -20.32% relative to the normal control.

The oral supplementation of rutin to DXR-injected animals was associated with a significant drop ($P < 0.01$) in the activities of serum ALT (-35.14%), AST (-38.00%), and ALP (-52.62%) and in the total bilirubin level (-24.95%) without influencing ($P > 0.05$) the serum albumin level (6.79%). Similarly, the oral supplementation of quercetin to DXR-injected rats significantly dropped ($P < 0.01$) the activities of ALT, AST, and ALP recording percent changes of -52.47%, -29.97%, and -71.17%, respectively, while it significantly elevated ($P < 0.01$) the level of albumin (19.10%). The oral supplementation of a combination of rutin and quercetin to DXR-injected rats was associated with a significant drop ($P < 0.01$) in the activities of serum ALT, AST, and ALP by -51.48%, -32.33%, and -62.86%, respectively, and with a significant elevation ($P < 0.05$) in the level of albumin (17.69%). The oral supplementation of a mixture of quercetin and rutin also produced an outstanding decrease in bilirubin level (-18.57%). Quercetin proved to be the most potent in reducing the high ALT and ALP activities by -52.47% and -71.18%, respectively, as well as in increasing the lowered albumin level by 19.10%. Rutin proved to be the most potent in decreasing the high AST activity and bilirubin level by -38.00% and -24.95%, respectively.

3.2. Effect on Serum Tumor Marker Level. Data reflecting the influence on serum AFP and CA 19.9 levels by rutin and/or querctin are shown in Table 2. Serum AFP and CA19.9 levels significantly increased ($P < 0.01$) by 154.34% and 126.88%, respectively, in response to the intraperitoneal administration of DXR in Wistar rats. A nonsignificant elevation ($P > 0.05$) in serum AFP by 1.71% and a significant drop ($P < 0.01$) in serum CA19.9 by -26.06% were spotted when the DXR-injected rats were supplemented with rutin. A significant decrease ($P < 0.05$) in AFP level by -21.36% and a highly significant drop ($P < 0.01$) in CA19.9 level by -35.3% were recording after supplementing the DXR-injected rats with quercetin. On other hand, the levels of both AFP and CA19.9 were significantly downregulated ($P < 0.01$) by -46.15% and -53.65%, respectively, upon supplementing the DXR-injected rats with the combination of quercetin and rutin. The general between-group effect on serum levels of AFP and CA19.9 was very significant ($P < 0.001$) as revealed by the one-way ANOVA.

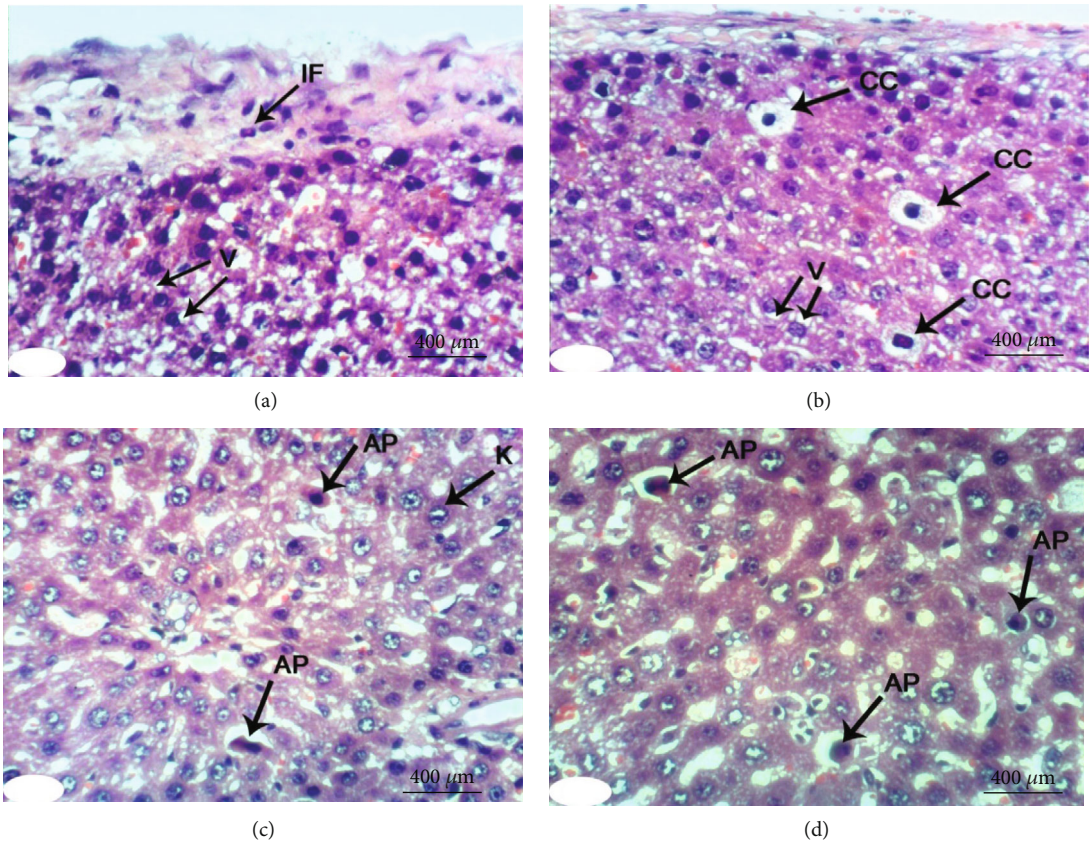

Figure 2: Photomicrographs of liver sections in rats injected with DXR indicating inflammation (IF) of hepatic capsule (a), cytoplasmic vacuolization (V) of subcapsular hepatocytes (a, b), clear cells of hepatocytes (CC) (b), apoptosis (AP) of hepatocytes (c, d), and karyomegally (K) of hepatocytic nuclei (c) (H&E; ×400).

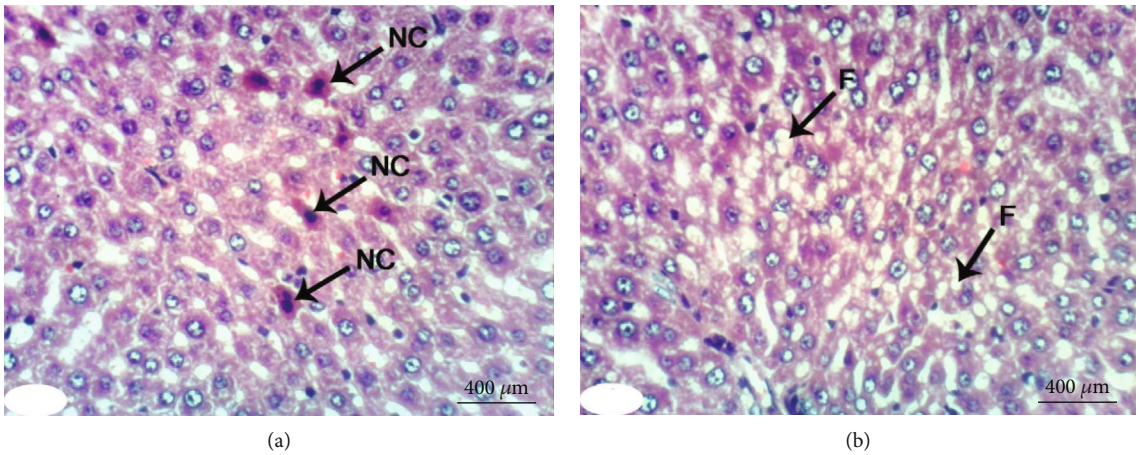

Figure 3: Photomicrographs of liver sections in rats injected with DXR after supplementing with rutin indicating necrosis (NC) of spaoradic hepatocytes (a) and fatty change (F) of hepatocytes (b) (H&E; ×400).

3.3. Influence of the Treatments on Liver Antioxidant Defense System and Oxidative Stress. Liver GSH content was significantly downregulated ($P < 0.01$) by -45.90% relative to normal control when DXR was administered intraperitoneally to rats. This effect was reversed by supplementing rutin to DXR-injected rats where a significant upregulation ($P < 0.01$) of GSH content by 66.25% was produced. On the other hand, the supplementation of quercetin alone or together with rutin to the DXR-injected group was associated with a nonsignificant elevation ($P > 0.05$) in the GSH content by 23.01% and 10.06%, respectively.

Liver LPO level was significantly upregulated ($P < 0.01$) upon intraperitoneal administration of DXR to Wistar rats where the recorded percentage change was 60.17% relative

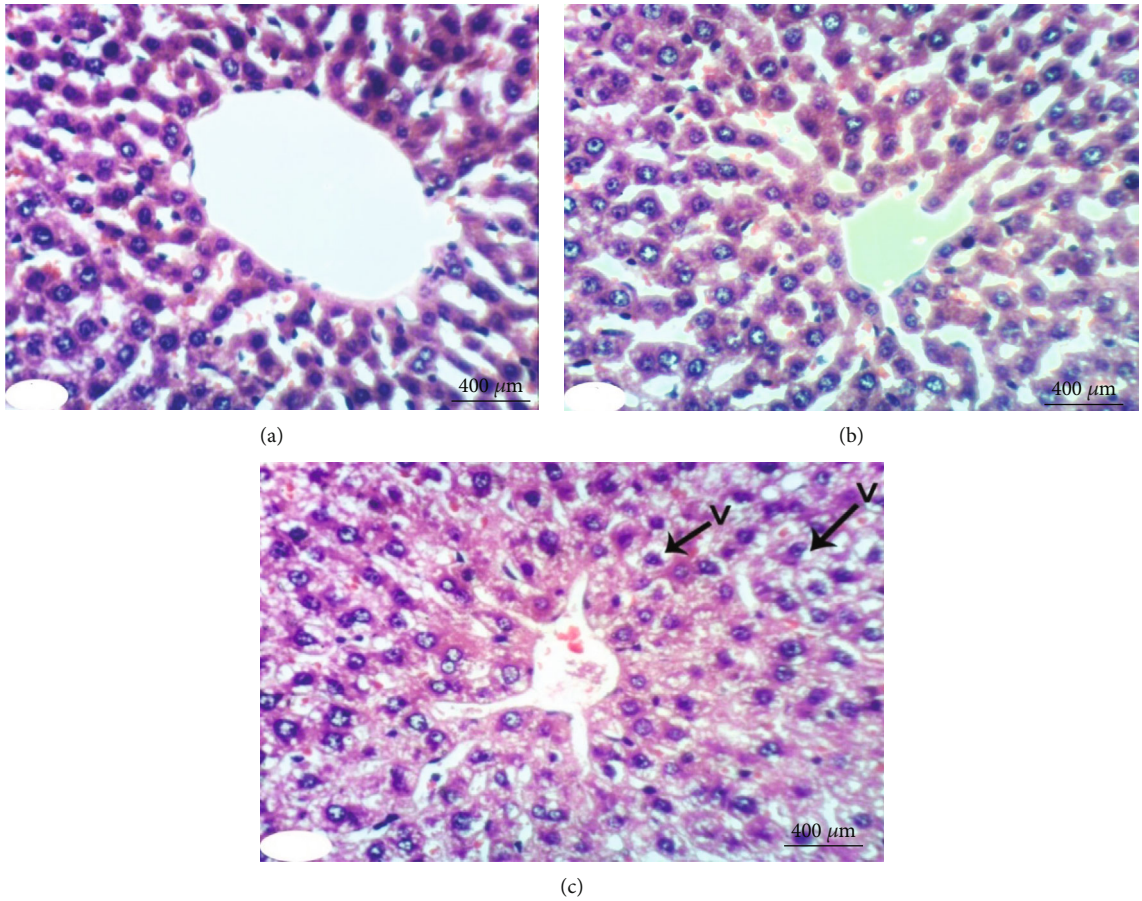

Figure 4: Photomicrographs of liver sections in rats injected with DXR after supplementing with quercetin indicating nearly normal structure of liver tissue with no histological changes (a, b) and slight vacuolization (V) of hepatocytes (c) (H&E; ×400).

to control rats. The supplementation with either rutin or quercetin or their combination caused liver LPO to drop significantly ($P < 0.05$) with quercetin being the most efficient in reducing the elevated LPO by -35.08% (Table 3).

3.4. Effect on the Activities of Diverse Antioxidant Enzymes in the Liver of DXR-Injected Rats. Liver GPx activity was highly suppressed ($P < 0.01$) following intraperitoneal administration of DXR to Wistar rats, where the documented percentage change was -31.20%. The oral supplementation of rutin to DXR-injected rats significantly elevated ($P < 0.01$) liver GPx activity by 21.64%. On the other isle, liver GPx activity increased marginally ($P > 0.05$) by 6.98% following oral supplementation of quercetin to DXR-injected rats. A similar marginal increase ($P > 0.05$) in liver GPx activity by 13.48% was observed when rutin and quercetin were co-supplemented to DXR-injected rats (Table 4).

Upon administration of DXR intraperitoneally to Wistar rats, liver GST activity was significantly reduced ($P < 0.01$), where the reported percentage change was -34.50%. The oral supplementation of rutin to DXR-injected rats failed to significantly alter the activity of liver GST ($P > 0.05$) with 15.86% being reported as the percentage change. However, the oral supplementation of quercetin to DXR-injected rats managed to elevate the activity of liver GST in a significant manner ($P < 0.01$) by 43.42%. Further elevation in the percentage change ($P < 0.01$) to 57.50% was observed upon oral cosupplementation of quercetin and rutin (Table 4).

A non-significant impact ($P > 0.05$) was spotted on the activity of liver SOD, with reported percentage change -1.43%, when DXR was intraperitoneally injected to Wistar rats. The oral supplementation of rutin was tied to a significant elevation ($P < 0.01$) in liver SOD activity by 23.90%. Likewise, the activity was significantly upregulated ($P < 0.01$) by 13.88% upon treatment with quercetin. Administering a mixture of quercetin and rutin significantly raised ($P < 0.01$) liver SOD activity by 10.98% (Table 4).

3.5. Histopathological Investigations. Normal liver architecture composed of hepatic lobules was presented when normal control rats were given equivalent volumes of vehicles (Figure 1). Each of them has a thin-walled central vein from which the hepatic trabeculae radiate in the direction of the lobule periphery and alternate interchanges with sinusoids around the periphery of each lobule branches of hepatic artery, in addition to hepatic portal vein and bile ductules (Figure 1). Conversely, the liver of DXR-injected rats showed significant changes. Hepatic capsule inflammation and subcapsular hepatocyte cytoplasmic vacuolization (Figures 2(a) and 2(b)), clear cells of hepatocytes (Figure 2(b)),

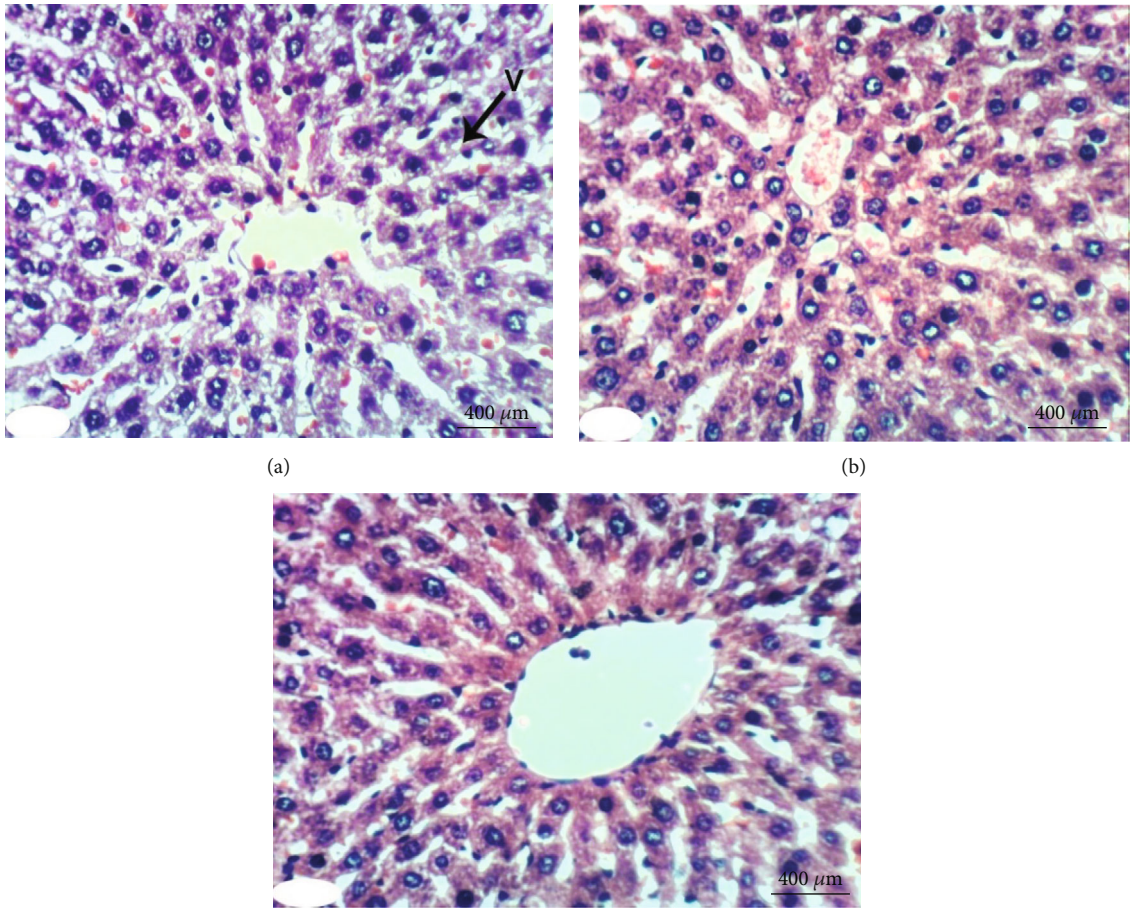

(a) (b) (c)

Figure 5: Photomicrographs of liver sections in rats injected with DXR after supplementing with a combination of quercetin and rutin indicating slight vacuolization (V) of hepatocytes (a) and almost normal structure of the liver tissue with no histological changes (b, c) (H&E; ×400).

karyomegaly of hepatocytic nuclei (Figure 2(c)), and apoptosis of hepatocytes (Figures 2(c) and 2(d)) are examples of such changes.

When treated with rutin, liver sections of DXR-injected rats manifested the necrosis of sporadic hepatocytes (Figure 3(a)) and fatty change of hepatocytes (Figure 3(b)). Quercetin treatment, on the other hand, resulted in some improvement in the liver histological features if compared to the control rats injected with DXR. Apparently, histopathological changes were lacking (Figures 4(a) and 4(b)) and slight vacuolization of hepatocytes was exhibited (Figure 4(c)). The same outcomes were noticed when the DXR-injected rats were treated with the mixture of quercetin and rutin (Figures 5(a)–5(c)).

The liver histological lesion scores presented in Table 5 depicted that inflammation, necrosis, activated apoptosis, vascularization of hepatocytes, clear cells of hepatocytes, and karyomegaly of hepatocytic nuclei exhibited less scores in quercetin and rutin treated rats than in control rats injected with DXR; the combinatory effect was the most potent. All histological scores exhibited significant effects ($P < 0.01$) when the group injected with DXR was contrasted with the normal control group. With the exception of the effect of rutin on vascularization of hepatocytes, all treated DXR-injected group showed significant improvements of all lesions when compared with the DXR-injected control (Table 6).

3.6. Immunohistochemical Investigations. Immunohistochemical staining of p53 showed a weak expression of p53 in the liver of normal rats (Figure 6(a)). On the contrary, the liver of DXR-injected rats exhibited a very high activated expression of p53 illustrated by a dense cytoplasmic brownish color (Figure 6(b)). Conversely, DXR-injected rats treated with rutin (Figure 6(c)) exhibited a weak expression of p53, whereas the DXR-injected rats treated with quercetin showed a weak expression of p53 (Figure 6(d)). Treatment with the mixture of quercetin and rutin demonstrated a moderate expression of p53 in the liver of DXR-injected rats (Figure 6(e)).

Immunohistochemical staining of TNF-α demonstrated a weak expression of TNF-α in the liver of normal rats (Figure 7(a)). In contrast, a strong activated expression of TNF-α (represented by a dense cytoplasmic brownish color) in the liver of DXR-injected rats was demonstrated (Figure 7(b)). However, DXR-injected rats exhibited a weak

Table 5: Histological lesion scores of liver in normal rats and in rats injected with DXR (without and with the supplementation of rutin and/or quercetin).

Histopathological changes	Score	Normal control	DXR-injected control	DXR-injected group treated with rutin	DXR-injected group treated with quercetin	DXR-injected group treated with rutin and quercetin
Inflammation	0	6 (100.00%)	2 (33.33%)	4 (66.66%)	5 (83.33%)	6 (100.00%)
	I	—	2 (33.33%)	2 (33.33%)	1 (16.66%)	—
	II	—	2 (33.33%)	—	—	—
	III	—	—	—	—	—
Necrosis	0	6 (100.00%)	—	4 (66.66)	6 (100.00%)	6 (100.00%)
	I	—	3 (50.00%)	2 (33.33%)	—	—
	II	—	1 (16.66%)	—	—	—
	III	—	2 (33.33%)	—	—	—
Activated apoptosis	0	6 (100.00%)	2 (33.33%)	5 (83.33%)	6 (100.00%)	6 (100.00%)
	I	—	2 (33.33%)	1 (16.66%)	—	—
	II	—	2 (33.33%)	—	—	—
	III	—	—	—	—	—
Vacuolization of hepaocytes	0	6 (100.00%)	—	2 (33.33%)	4 (66.66)	5 (83.33%)
	I	—	1 (16.7%)	—	1 (16.66%)	—
	II	—	1 (16.7%)	2 (33.33%)	—	1 (16.66%)
	III	—	4 (66.66)	2 (33.33%)	1 (16.66%)	—
Clear cells of hepatocytes	0	6 (100.00%)	2 (33.33%)	6 (100.00%)	6 (100.00%)	6 (100.00%)
	I	—	2 (33.33%)	—	—	—
	II	—	2 (33.33%)	—	—	—
	III	—	—	—	—	—
Karyomegaly of hepatocytic nuclei	0	6 (100.00%)	2 (33.33%)	5 (83.33%)	6 (100.00%)	6 (100.00%)
	I	—	1 (16.66%)	1 (16.66%)	—	—
	II	—	1 (16.66%)	—	—	—
	III	—	2 (33.33%)	—	—	—

Number of animals in each group is 6. 0: means absence of lesion; I: means mild; II: means moderate; and III: means severe. The % in brackets is the percentage of animals in every assigned grade.

(Figure 7(c)), moderate (Figure 7(d)), and negative (Figure 7(e)) expression of TNF-α when treated with rutin, quercetin, and rutin/quercetin mixture, respectively.

Immunohistochemical staining of Nrf2 demonstrated a mild expression of Nrf2 in the liver of normal rats (Figure 8(a)). Activated expression of Nrf2 was negative in the liver of DXR-injected rats (Figure 8(b)). On the contrary, DXR-injected rats treated with rutin demonstrated strong expression illustrated by dense cytoplasmic brownish color (Figure 8(c)). The liver of DXR-injected rats treated with quercetin demonstrated a mild activated expression of Nrf2 (Figure 8(d)). The liver of DXR-injected rats treated with the mixture presented negative expression of Nrf2 (Figure 8(e)).

Image analysis of immunohistochemical sections indicated a significant increase ($P < 0.01$) of liver p53 expression recording percentage change of 998.41% on injection of DXR. All DXR-injected groups supplemented with rutin or quercetin or their mixture demonstrated a significant drop ($P < 0.01$) in liver p53 reporting percentage changes of -92.47%, -66.37%, and -64.58%, respectively (Table 7).

A significant rise ($P < 0.01$) of liver TNF-α expression was induced by the injection of DXR reporting percentage change of 659.36%. All DXR-injected groups supplemented with quercetin and/or rutin exhibited significant drops ($P < 0.01$) in TNF-α expression recording percentage changes of -80.70%, -78.59%, and -97.57%, respectively (Table 7).

In contrast to p53 and TNF-α, the injection of DXR significantly reduced ($P < 0.01$) liver Nrf2 expression recording percentage of -98.76%. The DXR-injected group supplemented with either rutin or quercetin exhibited a sharp rise ($P < 0.01$) in liver Nrf2 expression recording percentage of 73620% and 14360%, respectively. However, supplementing with both rutin and quercetin failed to elevate liver Nrf2 content in a significant way ($P > 0.05$) although a percentage change of 214% was recorded (Table 7).

4. Discussion

While DXR is effective against a range of human malignancies, its toxicity precludes it from being used as a cancer chemotherapeutic agent [18, 56, 57]. Additionally, one of the most serious drawbacks of the anticancer therapy with DXR on the long term is resistance to the chemotherapeutic agent [18].

As demonstrated in this research, DXR enhanced the activities of the cytoplasmic enzyme ALT, the cytoplasmic

Table 6: Effect on histological lesion scores of liver in normal rats and in rats injected with DXR (without and with the supplementation of rutin and/or quercetin).

Lesion score Groups	Inflammation	Necrosis	Activated apoptosis	Vascularization of hepatocytes	Clear cells of hepatocytes	Karyomegaly of hepatocytic nuclei
Normal control	0.000 ± 0.000	0.000 ± 0.000	0.000 ± 0.000	0.000 ± 0.000	0.000 ± 0.000	0.000 ± 0.000
DXR-injected control group	$1.000 \pm 0.365^{++}$	$1.333 \pm 0421^{++}$	$1.000 \pm 0.365^{++}$	$2.500 \pm 0.341^{++}$	$1.000 \pm 0.365^{++}$	$1.500 \pm 0.562^{++}$
DXR-injected group supplemented with rutin	$0.333 \pm 0.210^{*}$	$0.333 \pm 0.210^{**}$	$0.161 \pm 0.166^{**}$	$1.666 \pm 0.557^{\$}$	$0.000 \pm 0.000^{**}$	$0.166 \pm 0167^{**}$
DXR-injected group supplemented with quercetin	$0.000 \pm 0.000^{**}$	$0.000 \pm 0.000^{**}$	$0.000 \pm 0.000^{**}$	$0.666 \pm 0.494^{**}$	$0.000 \pm 0.000^{**}$	$0.000 \pm 0.000^{**}$
DXR-injected group supplemented with rutin and quercetin	$0.000 \pm 0.000^{**}$	$0.000 \pm 0.000^{**}$	$0.000 \pm 0.000^{**}$	$0.333 \pm 0.333^{**}$	$0.000 \pm 0.000^{**}$	$0.000 \pm 0.000^{**}$
F-probability	$P < 0.01$	$P < 0.001$	$P < 0.01$	$P < 0.001$	$P < 0.001$	$P < 0.01$

Values are $M \pm$ SE ($n = 6$). $^{+}P < 0.05$, $^{++}P < 0.01$: the DXR-injected control group vs. normal control. $^{*}P < 0.05$, $^{**}P < 0.01$: the DXR-injected groups treated with rutin and/or quercetin vs. DXR-injected control group. $^{\$}P < 0.05$: the DXR-injected groups treated with rutin or quercetin alone vs. DXR-injected group treated with rutin and quercetin mixture.

and mitochondrial enzyme AST, and the membrane-bound enzyme ALP, as well as total bilirubin level. Reduced liver functioning and hepatocellular damage are responsible for these increases. In a DXR-induced hepatotoxicity model, similar high levels of serum indices for hepatocellular damage as well as hepatobiliary deterioration were previously reported [58–61]. The current data are also consistent with those previously published elsewhere [60, 62–65] as elevation of the activities of ALT, AST, and ALP in the serum of rats injected with DXR has been reported. Sathesh et al. [66] also stated that DXR treatment caused tissue damage as well as an increase in enzyme membrane leakage. Thus, our results in accordance with previous publications confirmed that a significant increase of liver cytoplasmic enzymes in the serum takes place as considerable amounts of these enzymes leak to blood stream from necrotic hepatocytes, as a result of DXR-induced toxicity. In addition, the increase in serum ALP activity reflects the damage in bile ductular cells and release of this membrane bound enzyme into blood. The damaging effects of DXR on liver cells may attributed to the stimulation of oxidative stress and inflammation. Both increased levels of LPO and TNF-α have important implications of necrosis and damage of liver cells [67–69] (Scheme 2). The current investigation showed that employing rutin and quercetin for the treatment of DXR-injected rats remarkably decreased the raised activities of serum ALT, AST, and ALP and the level of total bilirubin as well. The decrease in these serum biomarkers provides evidence that both rutin and quercetin treatments have profound positive effects on the function and integrity of the liver. In addition, the decrease in ALT, AST, and ALP activities may be secondary to the improvements in liver structural integrity as demonstrated by the results of the histological investigation conducted herein. Oxidative stress, inflammation, and apoptosis suppression by treatments with rutin and quercetin attribute to the amelioration of liver function and structural integrity (Scheme 2).

The present investigation found that DXR-injected animals exhibited elevated levels of serum total bilirubin, which is similar with the results of Liss et al. [70], Ahmed [71], Hozayen et al. [60], Hassan et al. [67], Ahmed et al. [68], and Ahmed et al. [72]. These researchers argued that it is a clear indicator of liver disease and may be caused by bile ductile occlusion induced by portal triad inflammation and fibrosis and/or conjugated bilirubin reflux from necrotic hepatocytes to sinusoids. When DXR-injected rats in the present investigation were treated with rutin or rutin/quercetin mixture, a substantial drop in the elevated serum bilirubin levels resulted; this reflects an improvement in the hepatobiliary system.

According to the current findings, the DXR-injected rats were with significantly reduced levels of serum albumin. Relative to control rats injected with DXR, quercetin and quercetin/rutin-treated rats were with significantly increased albumin level, which is similar to the observations by Hozayen et al. [60] and Ahmed et al. [73]. These investigators documented ameliorative effects of various flavonoids on serum albumin levels in drug- and chemicals-intoxicated rats. The decrease in the concentration of serum albumin herein in DXR-injected rats could be assigned to the impaired synthesis of albumin in the affected hepatic tissue under the oxidative stress and the damaging effects of DXR. The amelioration of serum albumin level, however, could indicate the protecting role of quercetin and quercetin/rutin mixture on the liver maintaining albumin synthesis near normal.

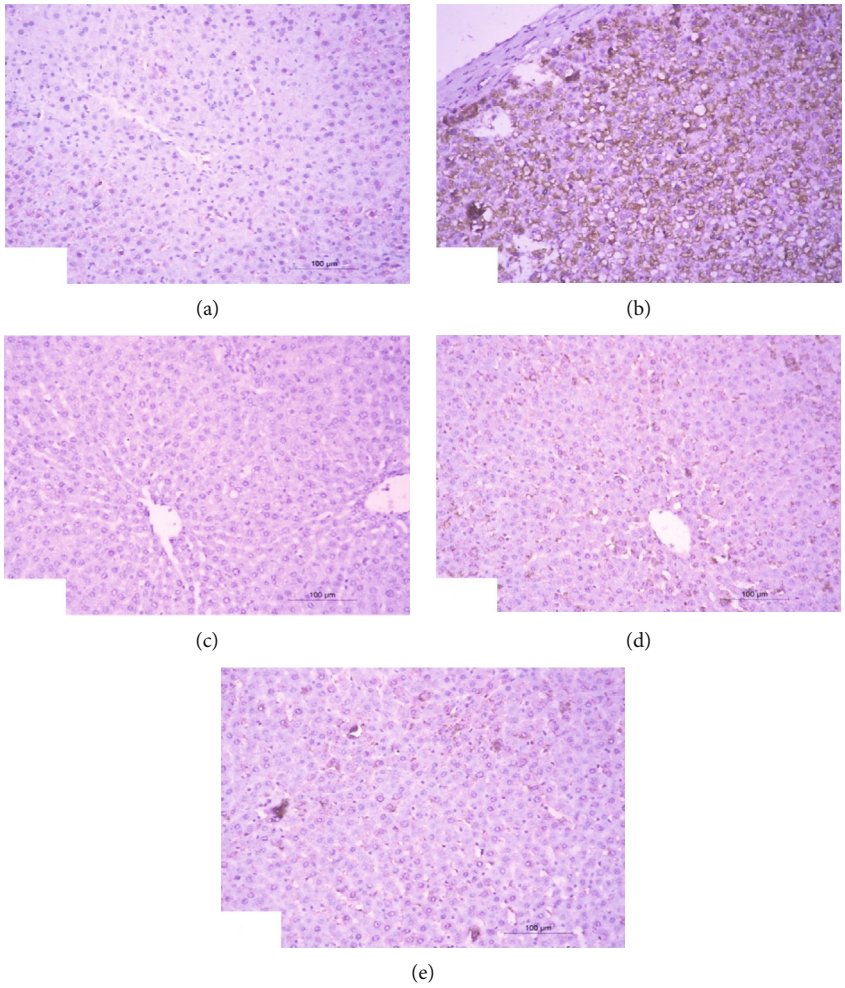

Figure 6: Photomicrographs of immunohistochemical sections of liver for detection of p53 showing weak expression in normal rats (a), very strong staining expression (immunopositivity indicated by brownish color) in DXR administered rats (b), weak expression in DXR administered rats treated with rutin (c), and moderate expression in DXR administered rats treated with quercetin (d) and its combination with rutin (6e) (×100).

The amelioration of liver function biomarkers in serum resulting from treatment with rutin and quercetin was linked to the enhancement of liver histological architecture and integrity. This synchronization was evidenced by the present results, which indicated less values of histopathological scores including inflammation, necrosis, apoptosis, vacuolization of hepatocytes, clear cells of hepatocytes, and karyomegaly of hepatocytic nuclei when rats injected with DXR were supplemented with rutin and quercetin. With the exception of vascularization of hepatocytes, the effects of rutin and quercetin were quite similar. This can be explained by the elucidation that after the rutin and quercetin administration, sulfates and glucuronides of quercetin were exclusively present in the bloodstream, whereas rutin and quercetin were not detected [74–77]. Because the administration of both rutin and quercetin results in the production of the same metabolites, i.e., sulfates and glucuronides of quercetin, this may attribute the nonsignificant effects between these two treatments.

Returning to our data, DXR-injected rats had higher levels of the tumor indicators CA19.9 and AFP in serum which is in line with the observations by Hozayn et al. [60] but differ from those by Attallah et al. [77] who found that serum AFP and CA 19.9 indicators were nonsignificantly altered by all tested dosages of the hepatotoxin, furfural, in the early identification of hepatocellular carcinoma (HCC).

The elevated level of AFP in serum could have resulted from the greater leakage of newly synthesized AFP from injured hepatocytes into the circulating blood. Additionally, this could be due to increased susceptibility of rats to HCC, as a result of DXR administration [78]. AFP synthesis is restored in moderately differentiated hepatomas in murine regenerative cells, and AFP reexpression occurs in the perinecrotic cell layer in the liver poisoned by various hepatotoxins, according to Abelev [79] and Fahim et al. [78]. Furthermore, increased CA 19.9 levels have been linked to impaired liver function [80]. Nonmalignant conditions such as pancreatitis, cholelithiasis, cholestasis, certain lung disorders, and liver cirrhosis have also been linked to elevated serum CA 19.9 [81]. Additionally, Schlick et al. [82] indicated that the elevated levels of serum CA 19.9 were caused by toxicity associated with Folfirinox treatment of pancreatic

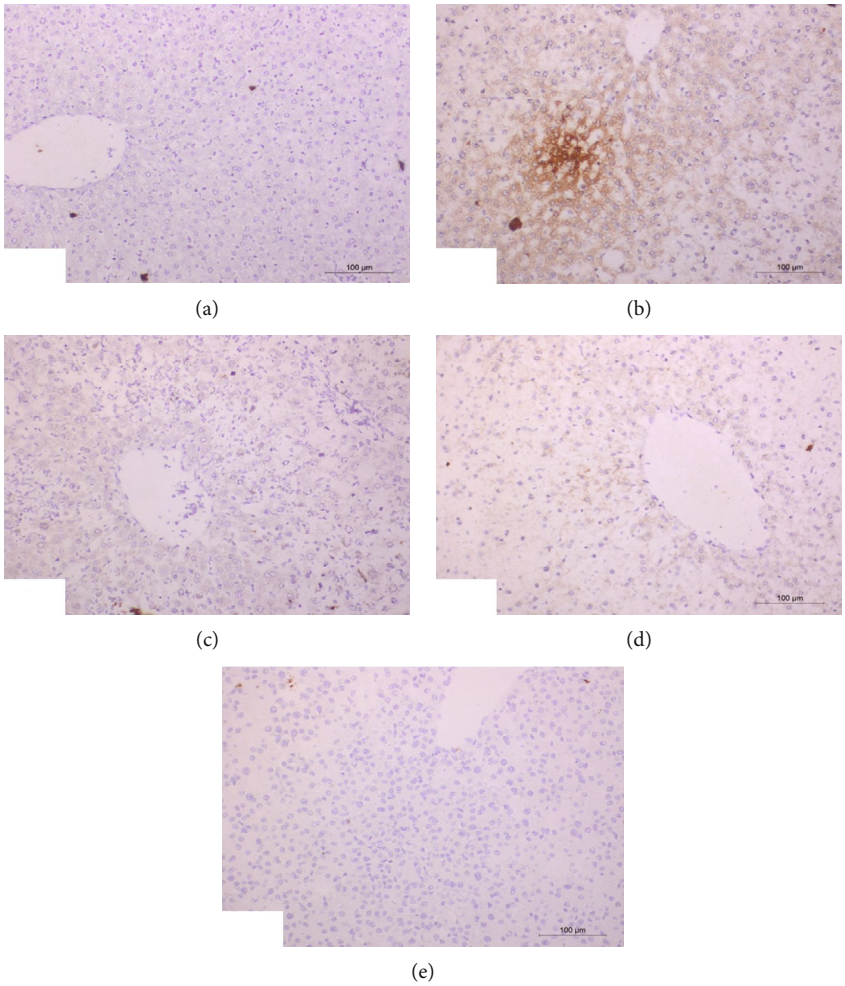

Figure 7: Photomicrographs of immunohistochemical sections of liver for detection of TNF-α showing weak expression of in normal rats (a), strong expression (immunopositivity indicated by brownish color) in DXR-injected rats (b), weak expression in DXR-injected rats treated with rutin (c) and quercetin (d), and negative expression in DXR-injected rats treated with mixture of rutin and quercetin (e) (×100).

cancer. The DXR-treated rats had a marginal increase in serum AFP, which contradicts to the findings of Hozayn et al. [60] who claimed that serum AFP levels were significantly increased after DXR administration alone but were significantly improved when the DXR-injected animals received either rutin or hesperidin.

Supplementing DXR-injected rats with rutin significantly spiked the level of serum CA19.9. The quercetin treatment of DXR-injected rats significantly lowered AFP and CA19.9 values in serum. Baker et al. [83] reported similar findings and indicated that estrogen binding to AFP was prohibited by the flavonols quercetin and kaempferol with an apparent equilibrium dissociation constant of approximately 5×10^{-7} M. In a N-nitrosodiethylamine-induced hepatocarcinogenesis model, remodeling of preneoplastic foci was expedited and HCC cells, hyperplastic nodules, in addition to the number of persistent foci were greatly reduced by quercetin treatment [84]. Despite these positive findings, other researchers discovered that in a rat model of heterocyclic amine-induced hepatocarcinogenesis dietary quercetin was able to increase the formation of GST-P-positive foci. Conversely, this investigation focused on GST-P foci rather than on tumor formation as a replacement endpoint [85, 86]. In human HCC cells, quercetin suppresses proliferation and promotes apoptosis in *vitro* [87]. Quercetin was also reported to enhance human HCC cell death induced by radiation [88].

In contrast, supplementing rutin and quercetin to rats injected with DXR significantly reduced both AFP and CA19.9 levels. These results may indicate that rutin and quercetin may have potent effects to improve the levels of these tumor markers and decrease the probability of liver cancer.

The deleterious biochemical and histological changes demonstrated in the DXR-injected rats were linked to a significant rise in the level of liver LPO, as well as to a significant drop in the liver content of GSH and in the activities of antioxidant enzymes (GST, GPx, and SOD).

DXR-induced cellular damage is mediated by the induction of ROS production and attenuation of the antioxidant defense system by DXR as hypothesized by many investigators [60, 89–92]. Those investigators also reported that

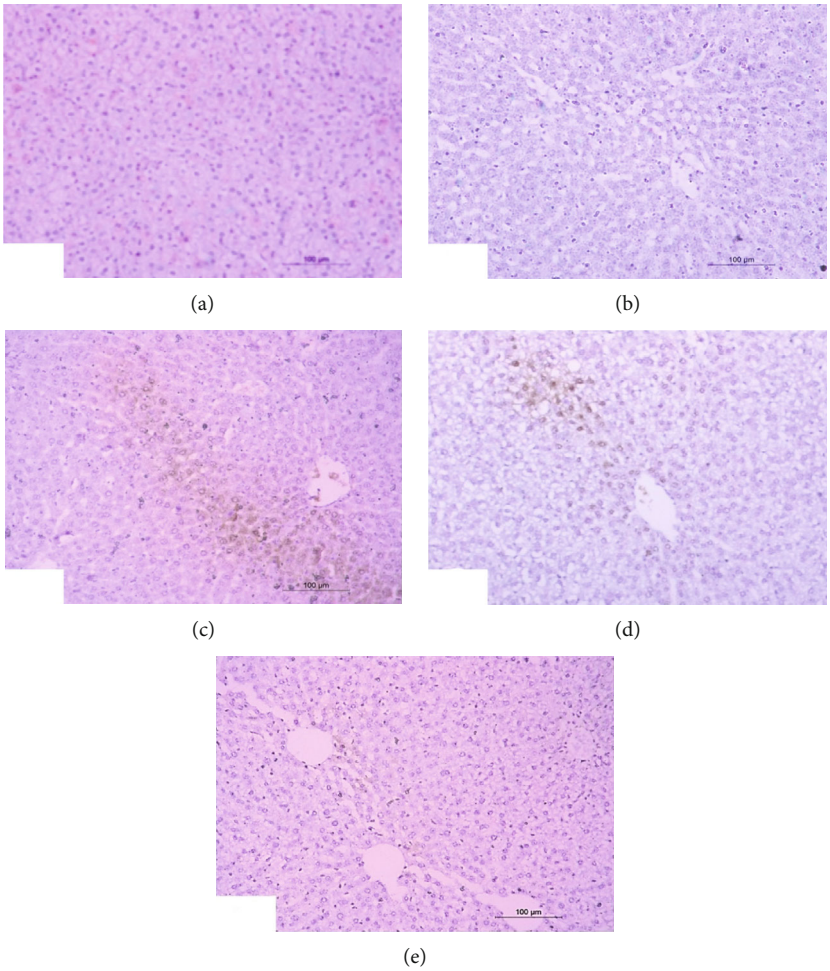

Figure 8: Photomicrographs of immunohistochemical sections of liver for detection of Nrf2 showing weak expression of Nrf2 in normal rats (a), very weak expression in DXR-injected rats (b), strong expression (immunopositivity indicated by brownish color) in DXR-injected rats treated with rutin (c), mild expression (immunopositivity indicated by brownish color) in DXR-injected rats treated with quercetin (d), and very weak expression in DXR-injected rats treated with a mixture of rutin and quercetin (e) (×100).

Table 7: Liver p53, TNF-α, and Nrf2 in normal rats and in rats injected with DXR (without and with the supplementation of rutin and/or quercetin).

Parameter Group	p53 (% area)	TNF-α (% area)	Nrf2 (% area)
Normal control	7.56 ± 0.74	3.74 ± 0.83	4.02 ± 0.002
DXR-injected control group	$83.04 \pm 5.61^{++}$	$28.40 \pm 5.93^{++}$	$0.05 \pm 0.0002^{++}$
DXR-injected group supplemented with rutin	$6.25 \pm 1.06^{**\$\$}$	$5.48 \pm 0.68^{**}$	$36.86 \pm 1.67^{**\$\$}$
DXR-injected group supplemented with quercetin	$27.93 \pm 3.89^{**}$	$6.08 \pm 0.08^{**}$	$7.23 \pm 0.001^{**\$\$}$
DXR-injected group treated with rutin and quercetin	$29.41 \pm 4.38^{**}$	$0.69 \pm 0.15^{**}$	0.157 ± 0.001
F probability	$P < 0.001$	$P < 0.001$	$P < 0.001$

Values are $M \pm$ SE ($n = 6$). $^{+}P < 0.05$, $^{++}P < 0.01$: the DXR-injected control group vs. normal control. $^{*}P < 0.05$, $^{**}P < 0.01$: the DXR-injected groups treated with rutin and/or quercetin vs. DXR-injected control group. $^{\$}P < 0.05$, $^{\$\$}P < 0.01$: the DXR-injected groups treated with rutin or quercetin alone vs. DXR-injected group treated with rutin and quercetin mixture.

higher LPO level is linked to liver damage. In the same line, Jagetia and Lalrinengi [93] revealed that DXR's enhanced toxicity in the liver could be attributed to its capacity to deplete GST and to elevate LPO. It was also indicated by the same authors that DXR administration produced time and dose-dependent reduction in the activity of GST. The

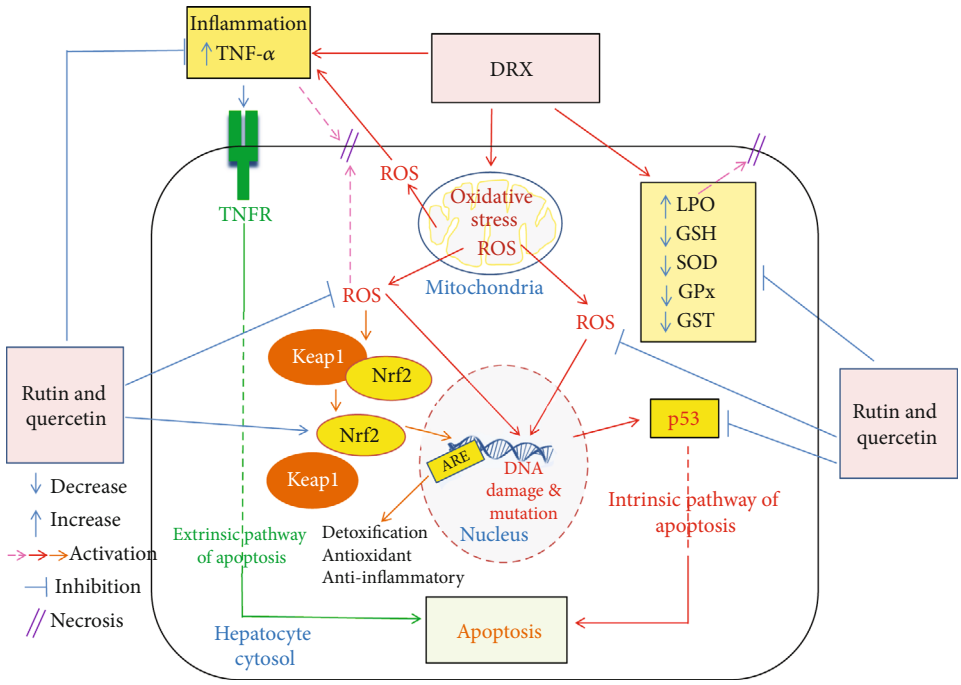

Scheme 2: Schematic figure showing the mechanisms of action of rutin and quercetin to counter DXR hepatotoxicity via oxidative stress, inflammation and apoptosis suppression and antioxidant defense mechanism promotion through the Nrf2 signaling pathway. DXR: doxorubicin; Keap1: Kelch-like ECH-associated protein 1; ARE: antioxidant response element; Nrf2: nuclear factor E2-related factor 2; ROS: reactive oxygen species; TNFR: tumor necrosis factor-α receptor.

activity increased when naringin was administered before and after DXR treatment. These results are in consistent with those of Jagetia and Lalnuntluangi [94].

According to Chen et al. [95], rutin at a dose of 1.0 μg/kg bw remarkably inhibit LPO in rat liver and effectively restored GSH content and SOD activity in alcohol-treated rat livers. These results indicate that rutin have a favorable effect in reducing the adverse effect of alcohol and could be used to treat liver injury as a potent antialcoholic agent.

Found in nonedible and edible plants, polyphenolic substances have been shown to have antioxidant activities among other biological effects. Antioxidants, such as flavonoids, behave as reducing agents that act by neutralizing superoxide ($O_2^{\cdot-}$) and hydroxyl radicals ($^{\cdot}OH$) among other oxidizing free radicals. Besides, flavonoids and phenolic compounds have been shown to be powerful suppressors of LPO and thus acting as effective scavengers of peroxyl radicals ($ROO^{\cdot}$). The constituents of orange, including phenols and flavonoids, have the potential to lower oxidative damage by direct and indirect inhibition of free radical excessive production [96].

The preventive effects of rutin and quercetin against liver toxicity were accompanied by a reduction in liver LPO and an increase in GSH concentration, as well as increased GPx, GST, and SOD activities. This is consistent with the findings of Umarani et al. [97], Kebiechc et al. [98], and our previous publications [23, 24]. It is worth mentioning here that apoptosis, *via* an intrinsic pathway, and necrosis, *via* increased membrane lipid peroxidation, are activated by the state of oxidative stress and the excessive liberation of ROS. Thus, employing rutin, quercetin and their combination to relieve the state of oxidative stress and promote the antioxidant defense system may be a key player in suppressing both apoptosis and necrosis (Scheme 2).

The intrinsic pathway leading to apoptosis is essentially mediated by the proapoptotic protein, p53 (Scheme 2). The administration of DXR, in the current study, resulted in high levels of liver p53, which is improved when quercetin or a combination of rutin and quercetin is administered as a treatment. These results are consistent with those of Porteiro et al. [99] and Wang et al. [100] who revealed that antitumor drugs like DXR promote the apoptosis of tumor cells by implementing a mechanism that is mediated through activated p53. Attempting to understand the role of p53 protein in the ability of quercetin to potentiate liver cancer cell apoptosis induced by DXR, Wang et al. examined p53 protein expression in control, quercetin-treated, and quercetin/DXR cotreated cells. The fact that no measurable levels of p53 protein expression were detected in the quercetin-treated cells and that remarkable levels were detected in the quercetin/DXR cotreated cells ruled out the involvement of p53 protein expression. The presented results in this study are also in concurrence with the study of Hassan et al. [67] who found that the two flavonoids naringin and hesperidin have antiapoptotic effects. Accordingly, it can be stated that the antiapoptotic actions of rutin and quercetin may abate the deteriorating effects of DXR on liver function and integrity (Scheme 2).

TNF-α (a proinflammatory cytokine) level increased significantly in the serum of rats injected with DXR in the current study. These findings are consistent with those of Shankar et al. [101] and Ahmed et al. [28] who reported

augmented levels of cytokine TNF-α upon DXR injection, which triggers multiple inflammatory pathways and apoptosis *via* an extrinsic pathway through binding to tumor necrosis factor receptor (TNFR) (Scheme 2). Tangpong et al. [102] demonstrated that TNF-α causes mitochondrial dysfunction as a result of its downstream effects, which include increased oxidative stress, TUNEL-positive cell death, cytochrome C release, and caspase 3 activity; all of which have been linked to DXR-induced apoptosis. Nevertheless, cell death induced by TNF-α is mainly apoptotic although necrosis may also take part [67, 103] (Scheme 2). When DXR-injected rats were treated with rutin and quercetin in the present study, the elevated TNF-α expression in the liver dropped significantly. Thus, it can be suggested that the anti-inflammatory, antiapoptotic and antinecrotic effects of rutin and quercetin in DXR-injected rats may be attributed at least in part to the suppressing effects on TNF-α.

Nrf2 is an emerging regulator of cellular resistance to ROS (Scheme 2). It activates the basal as well as induced expressions of antioxidant response element- (ARE-) dependent genes to control the physiological and pathophysiological outcomes of oxidant exposure [104]. In the present study, liver Nrf2 expression was significantly decreased in the DXR-injected group as compared to the normal control and was significantly increased following administration of rutin and quercetin in rats injected with DXR-injected rats. There is accumulating evidence from previous publications that the expression of antioxidant ARE genes, which also exert anti-inflammatory actions, is regulated mainly by the transcription factor Nrf2 [105] (Scheme 2). Thus, the increase in liver Nrf2 expression may be a key player in mediating the antioxidant and anti-inflammatory effects exerted by rutin and quercetin in Wistar rats with DXR-induced hepatotoxicity (Scheme 2).

5. Conclusions

In conclusion, quercetin and/or rutin was proved to provide potential chemopreventive effects against hepatotoxicity induced by DXR through suppressing oxidative stress, inflammation, and apoptosis, as well as through modulating effects of Nrf2.

Abbreviations

AFP: Alpha fetoprotein
ALP: Alkaline phosphatase
ALT: Alanine transaminase
ANOVA: Analysis of variance
AST: Aspartate transaminase
ARE: Antioxidant response element
CA19.9: Carbohydrate antigen 19.9
CMC: Carboxymethyl cellulose
DNA: Deoxyribonucleic acid
DXR: Doxorubicin
ELISA: Enzyme-linked immunosorbent assay
Fe^{+2}: Ferrous iron
GPx: Glutathione peroxidase
GSH: Glutathione
GST: Gluathione-S-transferase
H&E: Hematoxylin and eosin
Keap1: Kelch-like ECH-associated protein 1
kg bw: Kilogram body weight
LPO: Lipid peroxidation
LSD: Least significant difference
$M \pm$ SEM: Mean ± standard error of mean
MDA: Malondialdehyde
min: Minutes
NCI: National Cancer Institute
Nrf2: Nuclear factor erythroid 2–related factor 2
p53: Apoptotic protein 53
PBS: Phosphate buffer saline
PCD: Programmed cell death
RNS: Reactive nitrogen species
ROS: Reactive oxygen species
rpm: Round per min
SOD: Superoxide dismutase
TNF-α: Tumor necrosis factor-α
TNFR: Tumor necrosis factor-α receptor
UV: Ultraviolet radiation
vs: Versus.

Data Availability

All data are available from the corresponding author under reasonable request.

Conflicts of Interest

The authors declare that they have no conflict of interest.

Acknowledgments

This research work was funded by the Institutional Fund Projects under grant no. (IFFPP-17-22). Therefore, authors gratefully acknowledge technical and financial support from Ministry of Education and King Abdulaziz University, DSR, Jeddah, Saudi Arabia. The authors also, deeply thank Prof. Dr. K. A. Ahmed, Professor of Histopathology, Pathology Department, Faculty of Veterinary Medicine, Cairo University, Giza, Egypt, for his help in examining and reading the histological and immunohistochemical stained sections.

References

[1] K. Coldwell, S. M. Cutts, T. J. Ognibene, P. T. Henderson, and D. R. Phillips, "Detection of adriamycin-DNA adducts by accelerator mass spectrometry," in *Drug-DNA Interaction Protocols*, pp. 103–118, Humana Press, United States, 2010.

[2] A. Jabłońska-Trypuć, G. Świderski, R. Krętowski, and W. Lewandowski, "Newly synthesized doxorubicin complexes with selected metals-synthesis, structure and anti-breast cancer activity," *Molecules*, vol. 22, no. 7, article 1106, 2017.

[3] A. V. Kuznetsova, R. Margreiter, A. Amberger, V. Saks, and M. Grimm, "Changes in mitochondrial redox state, membrane potential and calcium precede mitochondrial dysfunction in doxorubicin-induced cell death," *Biochimica et*

Biophysica Acta (BBA) – Molecular cell Research, vol. 1813, no. 6, pp. 1144–1152, 2011.

[4] N. Patel, C. Joseph, G. B. Corcoran, and S. D. Ray, "Silymarin modulates doxorubicin-induced oxidative stress, Bcl-xL and p53 expression while preventing apoptotic and necrotic cell death in the liver," *Toxicology and Applied Pharmacology*, vol. 245, no. 2, pp. 143–152, 2010.

[5] M. Mohan, S. Kamble, P. Gadhi, and S. Kasture, "Protective effect of _Solanum torvum_ on doxorubicin-induced nephrotoxicity in rats," *Food and Chemical Toxicology*, vol. 48, no. 1, pp. 436–440, 2010.

[6] P. P. Trivedi, S. Kushwaha, D. N. Tripathi, and G. B. Jena, "Cardioprotective effects of Hesperetin against doxorubicin-induced oxidative stress and DNA damage in rat," *Food and Chemical Toxicology*, vol. 11, no. 3, pp. 215–225, 2011.

[7] O. M. Ahmed, M. B. Ashour, and A. S. Abd El-Fattah, "The preventive effects of navel orange peel ethanolic extract and naringin on doxorubicin-induced nephrocardiotoxicity in male albino rats," *Indo American Journal of Pharmaceutical Research*, vol. 7, no. 7, pp. 109–125, 2017.

[8] H. U. R. Mahmoud, O. M. Ahmed, H. I. Fahim, N. A. Ahmed, and M. B. Ashour, "Effects of rutin and quercetin on doxorubicin-induced renocardiotoxicity in male Wistar rats," *Advances in Animal and Veterinary Sciences*, vol. 8, no. 4, pp. 370–384, 2020.

[9] A. M. Mahmoud, O. M. Ahmed, I. B. Mohamed, H. A. Soliman, and B. M. Mohamed, "The preventive effects and mode of actions of Ulva fasciata synthesized silver nanoparticles in doxorubicin-induced hepatotoxicity in Wistar rats," *Journal of Pharmaceutical Research International*, vol. 33, no. 24A, pp. 24–48, 2021.

[10] H. Q. Ta, K. S. Thomas, R. S. Schrecengost, and A. H. Bouton, "A novel association between p130Cas and resistance to the chemotherapeutic drug adriamycin in human breast cancer cells," *Cancer Research*, vol. 68, no. 21, pp. 8796–8804, 2008.

[11] K. V. Sathesh, S. Sharmila, T. Premkumar et al., "ZAK is required for doxorubicin, a novel ribotoxic stressor, to induce SAPK activation and apoptosis in HaCaT cells," *Cancer Biology & Therapy*, vol. 10, no. 3, pp. 258–266, 2010.

[12] B. Cao, M. Li, W. Zha et al., "Metabolomic approach to evaluating adriamycin pharmacodynamics and resistance in breast cancer cells," *Metabolomics*, vol. 9, no. 5, pp. 960–973, 2013.

[13] M. Gharanei, A. Hussain, R. S. James, O. Janneh, and H. Maddock, "Investigation into the cardiotoxic effects of doxorubicin on contractile function and the protection afforded by cyclosporin A using the work-loop assay," *Toxicology In Vitro*, vol. 28, no. 5, pp. 722–731, 2014.

[14] W. G. Hozayen, O. M. Ahmed, and H. T. Abo Sree, "Effects of purslane shoot and seed ethanolic extracts on doxorubicin-induced testicular toxicity in albino rats," *Life Science J*, vol. 10, no. 3, pp. 2550–2558, 2013.

[15] H. Yapislar, E. Taskin, S. Ozdas, D. Akin, and E. Sonmez, "Counteraction of apoptotic and inflammatory effects of adriamycin in the liver cell culture by clinopitolite," *Biological Trace Element Research*, vol. 170, no. 2, pp. 373–381, 2016.

[16] S. Mishra, A. B. Jha, and R. S. Dubey, "Arsenite treatment induces oxidative stress, upregulates antioxidant system, and causes phytochelatin synthesis in rice seedlings," *Protoplasma, Protoplasma*, vol. 248, no. 3, pp. 565–577, 2011.

[17] S. Srivastava and R. S. Dubey, "Manganese-excess induces oxidative stress, lowers the pool of antioxidants and elevates activities of key antioxidative enzymes in rice seedlings," *Plant Growth Regulation*, vol. 64, no. 1, pp. 1–16, 2011.

[18] O. M. Ahmed, M. M. Abdul-Hamid, A. M. El-Bakry, H. M. Mohamed, and F. S. Abdel Rahman, "Effects of green tea infusion and epicatechin on doxorubicin-induced renocardiotoxicity in male albino rats," *IJPSR*, vol. 10, no. 5, pp. 1000–1014, 2019.

[19] S. Kumar and A. K. Pandey, "Chemistry and biological activities of flavonoids: an overview," *The Scientific World Journal*, vol. 2013, Article ID 162750, 16 pages, 2013.

[20] S. I. Ahmed, M. Q. Hayat, M. Tahir et al., "Pharmacologically active flavonoids from the anticancer, antioxidant and antimicrobial extracts of Cassia angustifolia Vahl.BMC complement," *Bmc Complementary and Alternative Medicine*, vol. 16, pp. 1–9, 2016.

[21] S. Kumar and A. K. Pandey, "Phenolic content, reducing power and membrane protective activities of Solanum xanthocarpum root extracts," *Vegetos*, vol. 26, no. 1, pp. 301–307, 2013.

[22] M. Działo, J. Mierziak, U. Korzun, M. Preisner, J. Szopa, and A. Kulma, "The potential of plant phenolics in prevention and therapy of skin disorders," *International Journal of Molecular Sciences*, vol. 17, no. 2, p. 160, 2016.

[23] O. M. Ahmed, "Natural flavonoids: chemistry, therapeutic potentials, therapeutic targets and mechanisms of actions," *Current Pharmaceutical Design*, vol. 27, no. 4, article 537, 2021.

[24] O. M. Ahmed, S. F. AbouZid, N. A. Ahmed, M. Y. Zaky, and H. Liu, "An up-to-date review on citrus flavonoids: chemistry and benefits in health and diseases," *Current Pharmaceutical Design*, vol. 27, no. 4, pp. 513–530, 2021.

[25] T. Guardia, A. E. Rotelli, A. O. Juarez, and L. E. Pelzer, "Anti-inflammatory properties of plant flavonoids. Effects of rutin, quercetin and hesperidin on adjuvant arthritis in rat," *Farmaco*, vol. 56, no. 9, pp. 683–687, 2001.

[26] O. M. Ahmed, A. Abdel Moneim, A. Yazid, and A. M. Mahmoud, "Antihyperglycemic, antihyperlipidemic and antioxidant effects and the probable mechanisms of action of Ruta graveolens infusion and rutin in nicotinamide-streptozotocin-induced diabetic rats," *Diabetologia Croatica*, vol. 39, no. 1, article 15, 2010.

[27] P. Lakhanpal and D. K. Rai, "Quercetin A versatile flavonoid," *Internet Journal of Medical Update*, vol. 2, pp. 22–37, 2007.

[28] O. M. Ahmed, M. M. Abdul-Hamid, A. M. El-Bakry, H. M. Mohamed, and F. S. Abdel Rahman, "Camellia sinensis and epicatechin abate doxorubicin-induced hepatotoxicity in male Wistar rats via their modulatory effects on oxidative stress, inflammation, and apoptosis," *Journal of Applied Pharmaceutical Science*, vol. 9, no. 4, pp. 30–44, 2019.

[29] R. K. Parabathina, E. Muralinath, P. Lakshmana Swamy, V. V. Hari Krishna, and R. G. Srinivasa, "Studies on protective effects of flavonoids morin, rutin, quercetin and vitamin-E against the doxorubicin-induced cardiomyopathy in rabbits," *International Journal of Genetic Engineering and Biotechnology*, vol. 2, no. 2, pp. 173–189, 2011.

[30] K. Ferenczyova, B. Kalocayova, and M. Bartekova, "Potential implications of quercetin and its derivatives in cardioprotection," *International Journal of Molecular Sciences.*, vol. 21, no. 5, p. 1585, 2020.

[31] R. A. Syahputra, U. Harahap, A. Dalimunthe, M. P. Nasution, and D. Satria, "The role of flavonoids as a cardioprotective strategy against doxorubicin-induced cardiotoxicity: a review," *Molecules*, vol. 27, no. 4, p. 1320, 2022.

[32] Y. Ma, L. Yang, J. Ma et al., "Rutin attenuates doxorubicin-induced cardiotoxicity via regulating autophagy and apoptosis," *Biochimica et Biophysica Acta - Molecular Basis of Disease*, vol. 1863, no. 8, pp. 1904–1911, 2017.

[33] X.-L. Meng, M.-M. Yu, Y.-C. Liu et al., "Rutin inhibits cardiac apoptosis and prevents sepsis-induced cardiomyopathy," *Frontiers in Physiology*, vol. 13, article 834077, 2022.

[34] R. K. Parabathina, P. L. Swamy, V. V. S. N. Harikrishna, G. SrinivasaRao, and K. S. Rao, "Vitamin-E, Morin, Rutin, Quercetin prevents tissue biochemical changes induced by Doxorubicin in oxidative stress conditions: Effect on heart, liver and kidney homogenates," *Journal of Chemical and Pharmaceutical Research*, vol. 2, no. 4, pp. 826–834, 2010.

[35] F. Rahmani, P. Najafizadeh, Z. Mousavi, T. Rastegar, and E. Barzegar, "The protective effect of quercetin against hepatotoxicity induced by doxorubicin in male rats. Iranian," *Iranian Journal of Pharmacology and Therapeutics*, vol. 16, pp. 1–8, 2018.

[36] S. N. Suganya and T. Sumathi, "Rutin a dietary flavonoid protects against altered neurobehavioral, membrane bound enzymes and striatal damage induced by 3-nitropropionic acid in male Wistar rats," *International Journal of Pharmacognosy and Phytochemical Research*, vol. 8, no. 7, pp. 1191–1199, 2016.

[37] L. Bo, Y. Liu, S. Jia, Y. Liu, and C. Sun, "Metabonomics analysis of quercetin against the nephrotoxicity of acrylamide in rats," *Food & Function*, vol. 9, no. 11, pp. 5965–5974, 2018.

[38] R. Murray and A. Kaplan, "Alanine aminotransferase," in *Clinical Chemistry. Theory, analysis and correlation*, pp. 1088–1090, Kaplan LA, Pesce AJ, Louis. Toronto. Princeton, 1984.

[39] G. Schumann, R. Klauke, F. Canalias et al., "IFCC primary reference procedures for the measurement of catalytic activity concentrations of enzymes at 37 C. Part 9: Reference procedure for the measurement of catalytic concentration of alkaline phosphatase," *Clinical Chemistry and Laboratory Medicine*, vol. 49, no. 9, pp. 1439–1446, 2011.

[40] W. F. Balistreri and N. W. Tietz, "Shaw LM Liver function," in *Fundamentals of Clinical Chemistry*, pp. 729–761, W.B. Saunders, Philadelphia, 1987.

[41] S. Gendler and A. Kaplan, *Uric acid*, Clinical Chemistry, St Louis, Toronto, 1984.

[42] H. G. Preuss, S. T. Jarrel, R. Scheckenbach, S. Lieberman, and R. A. Anderson, "Comparative effects of chromium, vanadium and Gymnema sylvestre on sugar-induced blood pressure elevations in SHR," *Journal of American Collage of Nutrition*, vol. 17, no. 2, pp. 116–123, 1998.

[43] E. Beutler, O. Duren, and B. M. Kelly, "Improved method for the determination of blood glutathione," *The Journal of Laboratory and Clinical Medicine*, vol. 61, pp. 882–888, 1963.

[44] B. Matkovics, M. Kotorman, I. S. Varga, D. Q. Hai, and C. Varga, "Oxidative stress in experimental diabetes induced by streptozotocin," *Acta Physiologica Hungarica*, vol. 85, pp. 29–38, 1998.

[45] B. Mannervik and C. Guthenberg, "[28] Glutathione transferase (human placenta)," *Methods in Enzymology*, vol. 77, pp. 231–235, 1981.

[46] S. Marklund and G. Marklund, "Involvement of the superoxide anion radical in the autoxidation of pyrogallol and a convenient assay for superoxide dismutase," *European Journal of Biochemistry*, vol. 47, no. 3, pp. 469–474, 1974.

[47] A. M. Hussein and O. M. Ahmed, "Regioselective one-pot synthesis and anti-proliferative and apoptotic effects of some novel tetrazolo[1,5- _a_]pyrimidine derivatives," *Bioorganic & Medicinal Chemistry*, vol. 18, no. 7, pp. 2639–2644, 2010.

[48] S. R. Galaly, O. M. Ahmed, and A. M. Mahmoud, "Thymoquinone and curcumin prevent gentamicin-induced liver injury by attenuating oxidative stress, inflammation and apoptosis," *Journal of Physiology and Pharmacology*, vol. 65, no. 6, pp. 823–832, 2014.

[49] O. M. Ahmed and R. R. Ahmed, "Anti-proliferative and apoptotic efficacies of ulvan polysaccharides against different types of carcinoma cells in vitro and in vivo," *Journal of Cancer Science & Therapy*, vol. 6, no. 6, pp. 202–208, 2014.

[50] O. M. Ahmed and R. R. Ahmed, "Anti-proliferative and apoptotic efficacy of diallyl disulfide on Ehrlich ascites carcinoma," *Hepatoma Research*, vol. 1, no. 2, pp. 67–74, 2015.

[51] N. G. Tawfik, W. R. Mohamed, H. S. Mahmoud et al., "Isatin counteracts diethylnitrosamine/2-acetylaminofluorene-induced hepatocarcinogenesis in male Wistar rats by upregulating anti-inflammatory, antioxidant, and detoxification pathways," *Antioxidants*, vol. 11, no. 4, article 699, 2022.

[52] N. Y. S. Yassin, S. F. AbouZid, A. M. El-Kalaawy, T. M. Ali, M. M. Almehmadi, and O. M. Ahmed, "Silybum marianum total extract, silymarin and silibinin abate hepatocarcinogenesis and hepatocellular carcinoma growth via modulation of the HGF/c-Met, Wnt/β-catenin, and PI3K/Akt/mTOR signaling pathways," *Biomedicine & Pharmacotherapy*, vol. 145, article 112409, 2022.

[53] F. Varghese, A. B. Bukhari, R. Malhotra, and A. De, "IHC profiler: an open source plugin for the quantitative evaluation and automated scoring of immunohistochemistry images of human tissue samples," *PLoS One*, vol. 9, no. 5, article 96801, 2014.

[54] J. Banchroft, A. Stevens, and D. Turner, *Theory and Practice of Histological Techniques*, Elsevier health sciences, Churchillivingstone, New York, London, San Francisco, 1996.

[55] M. Rao, K. Blane, and M. Zonneberg, *One-Way Analysis of Variance. Version 1A (C) copyright.The University of Georgia*, University of Georgia, USA, 1985.

[56] S. Lv, M. Li, Z. Tang et al., "Doxorubicin-loaded amphiphilic polypeptide-based nanoparticles as an efficient drug delivery system for cancer therapy," *Acta Biomaterialia*, vol. 9, no. 12, pp. 9330–9342, 2013.

[57] Z. Xin, S. Jiang, P. Jiang et al., "Melatonin as a treatment for gastrointestinal cancer: a review," *Journal of Pineal Research*, vol. 58, no. 4, pp. 375–387, 2015.

[58] I. Andreadou, F. Sigala, E. K. Iliodromitis et al., "Acute doxorubicin cardiotoxicity is successfully treated with the phytochemical oleuropein through suppression of oxidative and nitrosative stress," *Journal of Molecular and Cellular Cardiology*, vol. 42, no. 3, pp. 549–558, 2007.

[59] D. Cosan, A. Basaran, H. Gunes, I. Degirmenci, and E. Aral, "The effect of doxorubicin on rats that received toxic and carcinogenic benzo (a) pyrene," *Folia Histochemica et Cytobiologica*, vol. 46, no. 3, pp. 367–372, 2008.

[60] W. G. Hozayen, H. S. Abou Seif, and S. Amin, "Protective effects of ruitn and / or hesperidin against doxorubicin-

induced hepatotoxicity," *International Journal of Clinical Nutrition*, vol. 2, no. 1, pp. 11–17, 2014.

[61] Z. Anber, "Effect of doxorubicin and cyclophosphamide regimen versus taxane on liver enzymes in Iraqi women with breast cancer," *Biomedical Research*, vol. 29, no. 21, pp. 3869–3873, 2018.

[62] S. F. Llesuy and S. L. Arnaiz, "Hepatotoxicity of mitoxantrone and doxorubicin," *Toxicology*, vol. 63, article 18, 1990.

[63] K. Ito, H. Ozasa, Y. Nagashima, K. Hagiwara, and S. Horikawa, "Pharmacological preconditioning with doxorubicin:," *Biochemical Pharmacology*, vol. 62, no. 9, pp. 1249–1255, 2001.

[64] R. Injac, M. Perse, N. Obermajer et al., "Potential hepatoprotective effects of fullerenol $C_{60}(OH)_{24}$ in doxorubicin-induced hepatotoxicity in rats with mammary carcinomas," *Biomaterials*, vol. 29, no. 24-25, pp. 3451–3460, 2008.

[65] B. Sahu, J. Kumar, M. Kuncha, R. Borkar, R. Srinivasc, and R. Sistla, "Baicalein alleviates doxorubicin-induced cardiotoxicity via suppression of myocardial oxidative stress and apoptosis in mice," *Life Sciences*, vol. 144, pp. 8–18, 2016.

[66] K. Sathesh, S. Sharmila, T. Premkumar, K. Palanisamy, S. Jagan, and T. Devaki, "Protective effect of umbelliferone against doxorubicin induced cardiotoxicity in Wistar albino rats," *Science and Technology*, vol. 2, pp. 90–98, 2016.

[67] R. A. Hassan, W. G. Hozayen, H. T. Abo Sree, H. M. Al-Muzafar, K. A. Amin, and O. M. Ahmed, "Naringin and hesperidin counteract diclofenac-induced hepatotoxicity in male wistar rats via their antioxidant, anti-inflammatory, and antiapoptotic activities," *Oxidative Medicine and Cellular Longevity*, vol. 2021, Article ID 9990091, 14 pages, 2021.

[68] O. M. Ahmed, S. A. Galaly, M. M. A. Mostafa et al., "Thyme oil and thymol counter doxorubicin-induced hepatotoxicity via modulation of inflammation, apoptosis, and oxidative stress," *Oxidative Medicine and Cellular Longevity*, vol. 2022, Article ID 6702773, 19 pages, 2022.

[69] O. M. Ahmed, H. I. Fahim, H. Y. Ahmed et al., "The preventive effects and the mechanisms of action of navel orange peel hydroethanolic extract, naringin, and naringenin in N-acetyl-p-aminophenol-induced liver injury in Wistar rats," *Oxidative Medicine and Cellular Longevity*, vol. 2019, Article ID 2745352, 19 pages, 2019.

[70] G. M. Liss, R. A. Greenberg, and C. H. Tamburro, "Use of serum bile acids in the identification of vinyl chloride hepatotoxicity," *The American Journal of Medicine*, vol. 78, no. 1, pp. 68–76, 1985.

[71] O. Ahmed, "Histopathological and biochemical evaluation of liver and kidney lesions in streptozotocin diabetic rats treated with glimepiride and various plant extracts," *Journal of Union Arabian Biology*, vol. 16, pp. 585–625, 2001.

[72] O. M. Ahmed, H. I. Fahim, E. E. Mohamed, and A. Abdel-Moneim, "Protective effects of Persea americana fruit and seed extracts against chemically induced liver cancer in rats by enhancing their antioxidant, anti-inflammatory, and apoptotic activities," *Environmental Science and Pollution Research*, vol. 29, no. 29, pp. 43858–43873, 2022.

[73] O. M. Ahmed, A. A. Ahmed, H. I. Fahim, and M. Y. Zaky, "Quercetin and naringenin abate diethylnitrosamine/acetylaminofluorene-induced hepatocarcinogenesis in Wistar rats: the roles of oxidative stress, inflammation and cell apoptosis," *Drug and Chemical Toxicology*, vol. 45, no. 1, pp. 262–273, 2022.

[74] C. Manacha, C. Moranda, C. Demignéa, O. Texierb, F. Régératb, and C. Rémésya, "Bioavailability of rutin and quercetin in rats," *FEBS Letters*, vol. 409, no. 1, pp. 12–16, 1997.

[75] C.-Y. Yang, S.-L. Hsiu, K.-C. Wen et al., "Bioavailability and metabolic pharmacokinetics of rutin and quercetin in rats," *Journal of Food and Drug Analysis*, vol. 13, no. 3, p. Article 5, 2005.

[76] M. K. Piskula and J. Terao, "Quercetin's solubility affects its accumulation in rat plasma after oral administration," *Journal of Agricultural and Food Chemistry*, vol. 46, no. 10, pp. 4313–4317, 1998.

[77] A. M. Attallah, N. A. Al-Ghawalby, A. A. Abdel Aziz, E. A. El-Sayed, A. A. Tabll, and A. M. El-Waseef, "Clinical value of serum CEA, CA 19-9, CA 242 and AFP in diagnosis of gastrointestinal tract cancers," *International Journal of Cancer Research*, vol. 2, pp. 50–56, 2006.

[78] H. Fahim, O. M. Ahmed, R. Ahmed, M. Khedr, T. Mekhaeel, and S. S. Abou, "Protective effects of Ulva lactuca against acetaminophen-induced liver injury," *Journal of Egyptian German Society of Zoology*, vol. 56, pp. 377–415, 2008.

[79] G. Abelev, "fetoproyein vestn ross," *Akad Med Nauk*, vol. 9, pp. 77–83, 2021.

[80] J. Pissaia, D. Bernard, O. Scatton, O. Soubrane, F. Conti, and Y. Calmus, "Significance of serum tumor markers carcinoembryonic antigen, CA 19-9, CA 125, and CA 15-3 in preorthotopic liver transplantation evaluation," *Transplantation Proceedings*, vol. 41, no. 2, pp. 682–684, 2009.

[81] J. Rapé, X. Filella, M. Alsina-Donadeu, L. Juan-Pereira, A. Bosch-Ferrer, and R. Rigo-Bonnin, "Increasing plasma concentration of tumor markers in absence of neoplasm," *Oncol. Section Catalan Assoc. Clin. Lab. Sci.*, vol. 1, article 18125, 2011.

[82] K. Schlick, T. Magnes, L. Ratzinger et al., "Novel models for prediction of benefit and toxicity with FOLFIRINOX treatment of pancreatic cancer using clinically available parameters," *PLoS One*, vol. 13, no. 11, article 0206688, 2018.

[83] M. E. Baker, K. L. Medlock, and D. M. Sheehan, "Flavonoids inhibit estrogen binding to rat alpha-fetoprotein," *Proceedings of the Society for Experimental Biology and Medicine*, vol. 217, no. 3, pp. 317–321, 1998.

[84] Q. Tang, A. Denda, T. Tsujiuchi et al., "Inhibitory effects of inhibitors of arachidonic acid metabolism on the evolution of rat liver preneoplastic foci into nodules and hepatocellular carcinomas with or without phenobarbital exposure," *Japanese Journal of Cancer Research*, vol. 84, no. 2, pp. 120–127, 1993.

[85] M. Hirose, S. Takahashi, K. Ogawa, M. Futakuchi, and T. Shirai, "Phenolics: blocking agents for heterocyclic amine-induced carcinogenesis," *Food and Chemical Toxicology*, vol. 37, no. 9-10, pp. 985–992, 1999.

[86] M. Hirose, S. Takahashi, K. Ogawa et al., "Chemoprevention of heterocyclic amine-induced carcinogenesis by phenolic compounds in rats," *Cancer Letters*, vol. 143, no. 2, pp. 173–178, 1999.

[87] S. Ramos, M. Alia, L. Bravo, and L. Goya, "Comparative effects of food-derived polyphenols on the viability and apoptosis of a human hepatoma cell line (HepG2)," *Journal of Agricultural and Food Chemistry*, vol. 53, no. 4, pp. 1271–1280, 2005.

[88] J. Van-Rijn and J. Van-den-Berg, "Flavonoids as enhancers of X-ray induced cell damage in hepatoma cells," *Clinical Cancer Research*, vol. 3, no. 10, pp. 1775–1779, 1997.

[89] M. A. Abd El-Aziz, A. I. Othman, M. Amer, and M. A. El-Missiry, "Potential protective role of angiotensin-converting enzyme inhibitors captopril and enalapril against adriamycin-induced acute cardiac and hepatic toxicity in rats," *Journal of Applied Toxicology*, vol. 21, no. 6, pp. 469–473, 2001.

[90] Y. Kalender, M. Yel, and S. Kalender, "Doxorubicin hepatotoxicity and hepatic free radical metabolism in rats: the effects of vitamin E and catechin," *Toxicology*, vol. 209, no. 1, pp. 39–45, 2005.

[91] M. Yagmurca, O. Bas, H. Mollaoglu et al., "Protective effects of erdosteine on doxorubicin-induced hepatotoxicity in rats," *Archives of Medical Research*, vol. 38, no. 4, pp. 380–385, 2007.

[92] Y. QuanJun, Y. GenJin, W. LiLi et al., "Protective effects of dexrazoxane against doxorubicin-induced cardiotoxicity: a metabolomic study," *PLoS One*, vol. 12, no. 1, article 0169567, 2017.

[93] G. C. Jagetia and C. Lalrinengi, "Treatment of mice with naringin alleviates the doxorubicin-induced oxidative stress in the liver of Swiss albino mice," *MOJ Anatomy and Physiology*, vol. 4, no. 2, pp. 267–278, 2017.

[94] G. Jagetia and V. Lalnuntluangi, "The citrus flavanone naringin enhances antioxidant status in the albino rat liver treated with doxorubicin," *Biochemistry & Molecular Biology Journal*, vol. 2, no. 2, pp. 1–9, 2016.

[95] S. Chen, C. Chu, C. Chyau, Z. Fu, and P. Duh, "Effect of water extract of djulis (Chenopodium formosaneum) and its bioactive compounds on alcohol-induced liver damage in rats," *International Journal of Food Science and Nutrition*, vol. 5, no. 1, pp. 55–63, 2018.

[96] A. E. Abdel Moneim, "Citrus peel extract attenuates acute cyanide poisoning-induced seizures and oxidative stress in rats," *CNS & Neurological Disorders Drug Targets*, vol. 13, no. 4, pp. 638–646, 2014.

[97] V. Umarani, S. Muvvala, A. Ramesh, B. Lakshmi, and N. Sravanthi, "Rutin potentially attenuates fluoride-induced oxidative stress-mediated cardiotoxicity, blood toxicity and dyslipidemia in rats," *Toxicology Mechanisms and Methods*, vol. 25, no. 2, pp. 143–149, 2015.

[98] M. Kebiechc, Z. Lakroun, M. Lahouel, J. Bouayed, and A. Meraihi, "Evaluation of epirubicin-induced acute oxidative stress toxicity in rat liver cells and mitochondria, and the prevention of toxicity through quercetin administration," *Experimental and Toxicologic Pathology*, vol. 61, no. 2, pp. 161–167, 2009.

[99] B. Porteiro, M. F. Fondevila, X. Buque et al., "Pharmacological stimulation of p53 with low-dose doxorubicin ameliorates diet- induced nonalcoholic steatosis and steatohepatitis," *Molecular Metabolism*, vol. 8, pp. 132–143, 2018.

[100] B. Wang, P. P. Van Veldhoven, C. Brees et al., "Mitochondria are targets for peroxisome-derived oxidative stress in cultured mammalian cells free radic," *Biologie et Médecine*, vol. 65, pp. 882–894, 2013.

[101] S. Shankar, Q. Chen, and R. K. Srivastava, "Inhibition of PI3K/AKT and MEK/ERK pathways act synergistically to enhance antiangiogenic effects of EGCG through activation of FOXO transcription factor," *Journal of Molecular Signaling*, vol. 3, no. 7, pp. 1–11, 2008.

[102] J. Tangpong, M. Cole, R. Sultana et al., "Adriamycin-induced, TNF-α-mediated central nervous system toxicity," *Neurobiology of Disease*, vol. 23, no. 1, pp. 127–139, 2006.

[103] B. E. Jones, C. R. Lo, H. Liu et al., "Hepatocytes sensitized to tumor necrosis factor-α cytotoxicity undergo apoptosis through caspase-dependent and caspase-independent pathways∗," *The Journal of Biological Chemistry*, vol. 275, no. 1, pp. 705–712, 2000.

[104] Q. Ma, "Role of Nrf2 in oxidative stress and toxicity," *Annual Review of Pharmacology and Toxicology*, vol. 53, no. 1, pp. 401–426, 2013.

[105] S. Saha, B. Buttari, E. Panieri, E. Profumo, and L. Saso, "An overview of Nrf2 signaling pathway and its role in inflammation," *Molecules*, vol. 25, no. 22, article 5474, 2020.